## 5.10 REFERENCES


1) Wang, C.; Cheng, T.C.; Zheng, G.; Mu, Y.D.L.; Palk, B.; and Moon, M.; "Failure analysis of composite dielectric of power capacitors in distribution systems," *IEEE Transactions on Dielect. Elect. Insul.*, vol. 5, pp. 583–588, Aug. 1998.
2) Wu, J.C.; Jou, H.L.; Wu, K.D.; and Shen, N.C.; "Power converter-based method for protecting three-phase power capacitor from harmonic destruction," *IEEE Transactions on Power Delivery*, vol. 19, issue 3, pp. 1434–1441, July 2004.
3) Fernandez, A.; Sebastian, J.; Hernando, M.M.; Villegas, P.; and Garcia, J.; "Helpful hints to select a power-factor correction solution for low- and medium-power single-phase power supplies," *IEEE Transactions on Industrial Electronics*, vol. 52, issue 1, pp. 46–55, Feb. 2005.
4) Basu, S.; and Bollen, M.H.J; "A novel common power-factor correction scheme for homes and offices," *IEEE Transactions on Power Delivery*, vol. 20, issue 3, pp. 2257–2263, July 2005.
5) Wolfle, W.H.; and Hurley, W.G.; "Quasi-active power-factor correction with a variable inductive filter: Theory, design and practice," *IEEE Transactions on Power Electronics*, vol. 18, issue 1, Part 1, pp. 248–255, Jan. 2003.
6) Grebe, T.E.; "Application of distribution system capacitor banks and their impact on power quality," *IEEE Transactions on Industry Applications*, vol. 32, issue 3, pp. 714–719, May–June 1996.
7) Simpson, R.H.; "Misapplication of power capacitors in distribution systems with nonlinear loads – three case histories," *IEEE Transactions on Industry Applications*, vol. 41, no. 1, pp. 134–143, Jan.–Feb. 2005.
8) "IEEE recommended practices and requirements for harmonic control in electric power systems," *IEEE Standard 519-1992*, New York, NY, 1993.
9) Heydt, G.T.; *Electric Power Quality*, Star in a Circle Publications, USA, 1991.
10) ANSI/IEEE Standard 18-1980.
11) VDE 0560 T1 and T4.
12) DIN 48500.
13) Hoppner, A.; *Schaltanlagen, Taschenbuch für Planung, Konstruktion und Montage von Schaltanlagen*, Brown, Boveri & Cie, Aktiengesellschaft, Mannheim, Publisher: W. Girardet, Essen, Germany, 1966.
14) Dubey, G.K.; *Power Semiconductor Controlled Drives*, Prentice Hall, Englewood Cliffs, New Jersey, 1989.


CHAPTER 6

# Lifetime Reduction of Transformers and Induction Machines

The total installed power capacity within the Eastern, Western, and Texan power pools of the United States is 900 GW with about 70 GW of spinning reserve. Approximately 60% of the 900 GW is consumed by induction motors and 100% passes through transformers. Similar percentages exist in most countries around the world. For this reason transformers and induction motors are important components of the electric power system.

The lifetime of any device is limited by the aging of the insulation material due to temperature: the higher the activation energy of any material, the faster the aging proceeds. Iron and copper/aluminum have low activation energies and for this reason their aging is negligible. Insulation material – either of the organic or inorganic type – is most susceptible to aging caused by temperature. If a device is properly designed then the rated temperature results in the rated lifetime. Temperature rises above rated temperature result in a decrease of lifetime below its rated value. There are a few mechanisms by which the rated lifetime can be reduced:

1. Temperature rises above the rated temperature can come about due to overload and voltage or current harmonics.
2. Lifetime can be also decreased by intermittent operation. It is well known that generators of pumped storage plants must be rewound every 15 years as compared to 40 years for generators which operate at a constant temperature.
3. Vibration within a machine due to load variations (e.g., piston compressor) can destroy the mechanical properties of conductor insulation.
4. Faults – such as short-circuits – can impact the lifetime due to excessive mechanical forces acting on the winding and their insulation.

In this chapter we are concerned with aging due to elevated temperatures caused by harmonics. The presence of current and voltage harmonics in today's power systems causes additional losses in electromagnetic components and appliances, creating substantial elevated temperature rises and decreasing lifetime of machines and transformers. Therefore, estimating additional losses, temperature rises, and aging of power system components and loads has become an important issue for utilities and end users alike.

Three different phases are involved in the estimation (or determination) of the lifetime of magnetic devices:

1. modeling and computation of the additional losses due to voltage or current harmonics,
2. determination of the ensuing temperature rises, and
3. estimation of the percentage decrease of lifetime as compared with rated lifetime [1].

The literature is rich in documents and papers that report the effect of poor power quality on losses and temperature rises of power system components and loads; however, a matter that still remains to be examined in more detail is the issue of device aging under nonsinusoidal operating conditions. Earlier papers were mostly concerned about magnetic device losses under sinusoidal operating conditions [2–13]. However, more recent research has expanded the scope to magnetic device derating under nonsinusoidal operation [14–17]. Only a few papers have addressed the subjects of device aging and economics issues caused by poor power quality [18–23].

In the first sections of this chapter the decrease of lifetime of power system components and loads such as universal motors, single- and three-phase transformers, and induction motors are estimated based on their terminal voltage harmonics. After a brief review of temperature relations, the concept of weighted harmonic factors is introduced. This is a quantity that relates the device terminal voltage harmonic amplitudes to its temperature rise. Additional temperature rises and losses due to harmonics are discussed, and thereafter the weighted harmonic factors are employed to determine the decrease of lifetime of electrical appliances. Toward the end of this chapter the time-varying nature of harmonics is addressed with respect to their measurement, sum-

ST. GEORGE COLLEGE OF TAFE


ISBN 978-0-12-369536-9
© Elsevier Inc. All rights reserved.

mation, and propagation. The probabilistic evaluation of the economical damage – that is, cost – due to harmonic losses in industrial energy systems is explored next, and the increase of temperature in a device as a function of time as well as intermittent operation of devices concludes this chapter.

## 6.1 RATIONALE FOR RELYING ON THE WORST-CASE CONDITIONS

Field measurements show that the harmonic voltages and currents of a distribution feeder are time-varying. This is due to

1. the changes in the loads, and
2. the varying system's configuration.

This means that steady-state harmonic spectra do not exist. However, loads such as variable-speed drives for air-conditioning, rolling mills, and arc furnaces operate during their daily operating cycle for at least a few hours at rated operation. It is for this operating condition that system components (e.g., transformers, capacitors) and loads must be designed. Most electromagnetic devices such as transformers and rotating machines have thermal time constants of 1 to 3 hours – depending on their sizes and cooling mechanisms. When these components continually operate at rated power, they are exposed to steady-state current and voltage spectra resulting at an ambient temperature of $T_{amb} = 40°C$ in the maximum temperature rise $T_{risemax}$, and the resulting temperature $T_{max} = T_{amb} + T_{risemax}$ must be less or equal to the rated temperature $T_{rat}$. The worst case is therefore when the power system components operate at rated load with their associated current or voltage spectra where individual harmonic amplitudes are maximum. It is not sufficient to limit the total harmonic distortion of either voltage ($THD_v$) or current ($THD_i$) because these parameters can be the same for different spectra – resulting in different additional temperature rises, insulation stresses, and mechanical vibrations. In Sections 6.2 to 6.10 worst-case conditions will be assumed.

## 6.2 ELEVATED TEMPERATURE RISE DUE TO VOLTAGE HARMONICS

Most electric appliances use electric motors and/or transformers. In all these cases the power system's sinusoidal voltage causes ohmic and iron-core losses resulting in a temperature rise, which approaches the rated temperature rise ($T_{riserat}$) at continuous operation:

$$T_{rat} = T_{amb} + T_{riserat}, \tag{6-1}$$

where $T_{amb} = 40°C$ is the ambient temperature. The lifetime of a magnetic device is greatly dependent on this temperature rise and the lifetime will be reduced if this rated temperature rise is exceeded over any length of time [1].

The presence of voltage harmonics in the power system's voltage causes harmonic currents in induction motors and transformers of electrical appliances, resulting in an elevated temperature rise ($T_{riserat} + \Delta T_h$) such that the device temperature is

$$T = T_{amb} + T_{riserat} + \Delta T_h, \tag{6-2}$$

where $\Delta T_h$ is the additional temperature rise due to voltage (integer, sub-, inter-) harmonics. Through a series of studies this additional temperature rise of various electric machines and transformers was calculated and measured as a function of the harmonic amplitude $V_h$ and the phase shifts of the voltage harmonics $\varphi_h$ with respect to the fundamental [18, 19].

The insulating material of electrical apparatus, as used in electrical appliances, is of either organic or inorganic origin. The deterioration of the insulation caused by the elevated temperature rise is manifested by a reduction of the mechanical strength and/or a change of the dielectric behavior of the insulation material. This thermal degradation is best represented by the reaction rate equation of Arrhenius. Plots which will be drawn based on this equation are called Arrhenius plots [24, 25]. The slopes of these plots are proportional to the activation energy $E$ of the insulation material under consideration. Knowing the rated lifetime of insulation materials at rated temperature ($T_{rat} = T_{amb} + T_{riserat}$), and the elevated temperature rise ($\Delta T_h$) due to given amplitudes $V_h$ and phase shifts $\varphi_h$ of voltage harmonics, one will be able to estimate from the Arrhenius plot the reduction of the lifetime of an electrical appliance due to $\Delta T_h$.

*Definition: The activation energy E is the energy transmitted in the form of heat to the chemical reaction of decomposition.*

## 6.3 WEIGHTED-HARMONIC FACTORS

The harmonic voltage content (order $h$, amplitude $V_h$, and phase shift $\varphi_h$) of power system voltages varies with the type and size of harmonic generators and loads as well as with the topology of the system,





and it will hardly be the same for any two networks. Since voltage harmonics result in additional losses and temperature rises ($\Delta T_h$) in electrical appliances, it would be desirable to derive one single criterion which limits – for a maximum allowable additional temperature rise – the individual amplitudes and phase shifts of the occurring harmonic voltages including their relative weight with respect to each other in contributing to the elevated temperature rise $\Delta T_h$.

Also, this criterion should be simple enough so that the additional losses, temperature rises $\Delta T_h$, and the reduction of lifetime of electrical appliances can easily be predicted as a function of the harmonic content of their terminal voltages. As most electrical appliances use transformers and motors as input devices, in this section weighted harmonic factors will be derived for single-phase and three-phase transformers and induction machines.

The ambient temperature is at the most $T_{amb} = 40°C$. The rated temperature rise depends on the class of insulation material used. $T_{riserat} = 80°C$ is a commonly permitted value so that

$$T_{rat} = T_{amb} + T_{riserat} = 40°C + 80°C = 120°C. \tag{6-3}$$

In transformers, iron-core sheets and copper (aluminum) conductors are insulated by paper, plastic material, or varnish.

The Swedish scientist Svante Arrhenius originated the so-called Arrhenius rule: a differential equation describing the speed of degradation or deterioration of any (organic, inorganic) material. This deterioration is not oxidation due to elevated temperatures.

The idea of a weighted harmonic factor for different magnetic devices [20] is based on the fact that the additional temperature rise $\Delta T_h$ is different for transformers, universal machines, and induction machines, although the harmonic content ($V_h$, $\varphi_h$) of the terminal voltages is the same.

### 6.3.1 Weighted-Harmonic Factor for Single-Phase Transformers

Figure 6.1 illustrates the equivalent circuit of a single-phase transformer for the fundamental ($h = 1$) and harmonic voltages of hth order.

The ohmic losses of the hth harmonic expressed in terms of the fundamental ohmic losses are

$$\frac{W_{ohmic,h}}{W_{ohmic,1}} = \left(\frac{V_{ph}}{V_{p1}}\right)^2 \left(\frac{R_{ph} + R'_{sh}}{R_{p1} + R'_{s1}}\right) (\text{RATIO}), \tag{6-4}$$

where

$$\text{RATIO} = \frac{(R_{p1} + R'_{s1} + R'_{load,1})^2 + \omega^2 (L_{p1} + L'_{s1} + L'_{load,1})^2}{(R_{ph} + R'_{sh} + R'_{load,h})^2 + (h\omega)^2 (L_{ph} + L'_{sh} + L'_{load,h})^2}.$$

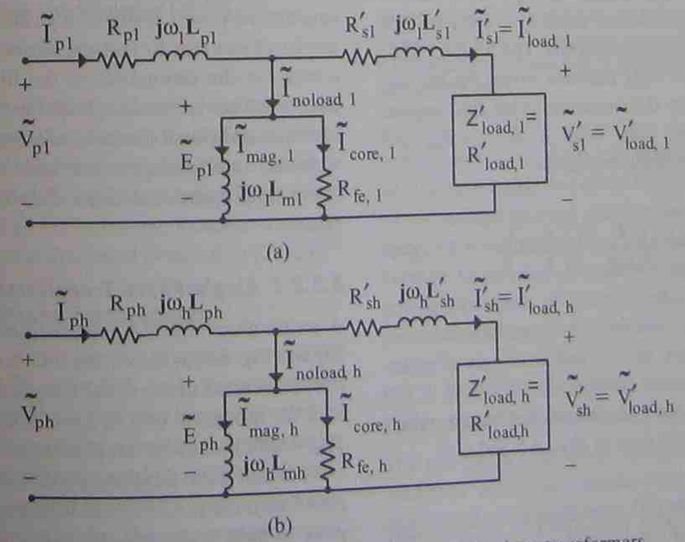



**FIGURE 6.1** Fundamental (a) and harmonic (b) equivalent circuits of single-phase transformers.

ST. GEORGE COLLEGE OF LAW

In most residential power transformers the influence of the skin effect can be neglected. However, the skin effect of an ohmic load cannot be ignored, because $R'_{load,h}$, $R'_{load,l} >> R_{ph}$, $R_{p1}$, $R'_{sh}$, $R'_{s1}$. Therefore, one obtains

$$\frac{W_{ohmic,h}}{W_{ohmic,1}} = \left(\frac{V_{ph}}{V_{p1}}\right)^2 \frac{\left(R'_{load,1}\right)^2 + \omega^2\left(L_{p1} + L'_{s1} + L'_{load,1}\right)^2}{\left(R'_{load,h}\right)^2 + (h\omega)^2\left(L_{ph} + L'_{sh} + L'_{load,h}\right)^2}. \tag{6-5}$$

Due to $L_{ph} \approx L_{p1}$, $L'_{sh} \approx L'_{s1}$, $L'_{load,h} \approx L'_{load,1}$, and the fact that the load resistance $R'_{load,h}$ increases less than linearly with frequency [18], the following simplified expression is considered:

$$\frac{W_{ohmic,h}}{W_{ohmic,1}} \approx \frac{1}{h^n}\left(\frac{V_{ph}}{V_{p1}}\right)^2, \tag{6-6}$$

where $0 < n < 2$ depends on the resistance and inductance values of the equivalent circuit of a load.

The iron-core losses of a single-phase transformer due to a voltage harmonic of order $h$ are expressed in terms of the corresponding losses caused by the fundamental as

$$\frac{W_{iron,h}}{W_{iron,1}} = \left(\frac{B_{max,h}}{B_{max,1}}\right)^2 \frac{\left\{\sigma\left(\frac{fh}{100}\right)^2 k_m^2 + \varepsilon\left(\frac{fh}{100}\right)\right\}}{\left\{\sigma\left(\frac{f}{100}\right)^2 + \varepsilon\left(\frac{f}{100}\right)\right\}}, \tag{6-7}$$

where $B_{max,1}$ and $B_{max,h}$ define fundamental and harmonic maximum flux densities, respectively, and $\sigma$ and $\varepsilon$ are [26] coefficients related to eddy-current and hysteresis losses, respectively. The term $k_m$ takes the reaction of the eddy currents within the laminations and between the laminations on the original field into account [18]. With $h$ $B_{max,h} \propto E_{ph}$ and $B_{max,1} \propto E_{p1}$, the relation becomes

$$\frac{W_{iron,h}}{W_{iron,1}} = \left(\frac{E_{ph}}{hE_{p1}}\right)^2 \left(\frac{R_{fe,1}}{R_{fe,h}}\right), \tag{6-8}$$

where $R_{fe,1}$ and $R_{fe,h}$ are the iron-core loss resistances for the fundamental ($h = 1$) and harmonic of order $h$, respectively.

The total losses for a harmonic of order $h$ are then determined from the sum of Eqs. 6-6 and 6-8:

$$\frac{W_{total,h}}{W_{total,1}} \approx \frac{1}{h^n}\left(\frac{V_{ph}}{V_{p1}}\right)^2 + \frac{1}{h^2}\left(\frac{E_{ph}}{E_{p1}}\right)^2 \left(\frac{R_{fe,1}}{R_{fe,h}}\right). \tag{6-9}$$

According to [27], the core-loss resistance ratio is $R_{fe,h}/R_{fe,1} = h^{0.6}$ and because of the leakage reactance being proportional to $h$, one obtains the inequality $(E_{ph}/E_{p1}) < (V_{ph}/V_{p1})$ or

$$\left(\frac{E_{ph}}{E_{p1}}\right)^2 = \left(\frac{V_{ph}}{V_{p1}}\right)^m, \tag{6-10}$$

where the exponent $m$ is less than 2. Therefore, for single-phase transformers Eq. 6-9 becomes

$$\frac{W_{total,h}}{W_{total,1}} \approx \frac{1}{h^n}\left(\frac{V_{ph}}{V_{p1}}\right)^2 + \frac{1}{h^{2.6}}\left(\frac{V_{ph}}{V_{p1}}\right)^m. \tag{6-11}$$

Depending on the relative sizes of the ohmic and iron-core losses at full load, Eq. 6-11 can be rewritten for all occurring harmonics and is called the weighted harmonic factor [20]:

$$\frac{W_{total,h\Sigma}}{W_{total,1}} = K_1 \sum_{h=2}^{\infty} \frac{1}{(h)^k}\left(\frac{V_{ph}}{V_{p1}}\right)^l, \tag{6-12}$$

where $W_{total,h\Sigma}$ and $W_{total,1}$ are the total harmonic losses and the total fundamental losses, respectively. Also $0 \le k \le 2.0$ and $0 \le l \le 2.0$. Average values for $k$ and $l$ are obtained from measurements as discussed in a later section.

### 6.3.2 Measured Temperature Increases of Transformers

Measured temperature rises in transformers and induction machines as they occur in a residential/commercial power system – together with calculated loss increases due to voltage harmonics – represent a base for the estimation of the lifetime reduction due to voltage harmonics. It is thereby assumed that for small additional temperature rises – as compared with the rated temperature rise – the additional losses are proportional to the additional temperature rise.

#### 6.3.2.1 *Single-Phase Transformers*

A single-phase 150 VA transformer was tested [18, 19] and Fig. 6.2a,b shows the measured temperature rises in percent of the rated temperature rises at full load for moderate (e.g., $T_{amb} = 23°C$) and high (e.g., $T_{amb} = 40°C$) ambient temperatures.

Note that if the third harmonic voltage $v_3(t)$ superposed with the fundamental voltage $v_1(t)$ produces a peak-to-peak voltage $\{v_1(t) + v_3(t)\}$ that is maximum, then the peak-to-peak flux density in the core



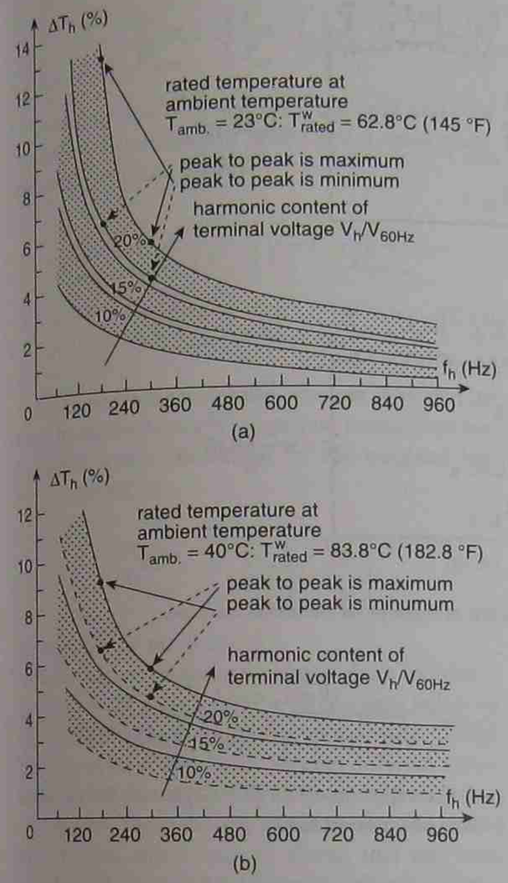



**FIGURE 6.2** Measured additional temperature rise of the 150 VA single-phase transformer winding in % of the rated temperature rise at full load at an ambient temperature of (a) 23°C and (b) 40°C as a function of the harmonic voltage amplitude, phase shift, and frequency [29, 30].

$\{B_1(t) + B_3(t)\}$ is minimum. That is, the total harmonic losses are smaller than those when the peak-to-peak voltage is minimum, resulting in a maximum peak-to-peak value of the flux density. This "alternating" behavior of the harmonic losses and associated temperatures is discussed in detail in [27, 28].

#### 6.3.2.2 *Three-Phase Transformers*

Three 150 VA single-phase transformers were assembled to Δ/Y-grounded and Y-grounded/Y-grounded configurations and they were subjected to the same harmonic voltage conditions as the single-phase transformer of the preceding section. The temperatures of the transformer windings were measured at the same location as for the single-phase transformer. The tests were limited to balanced operation. However, no phase-lock loop was available and no stable relation between fundamental and harmonic voltage systems could be maintained. Therefore, the temperature data of Fig. 6.3a,b represent average values and the alternating behavior could not be observed, although it also exists in three-phase transformers.

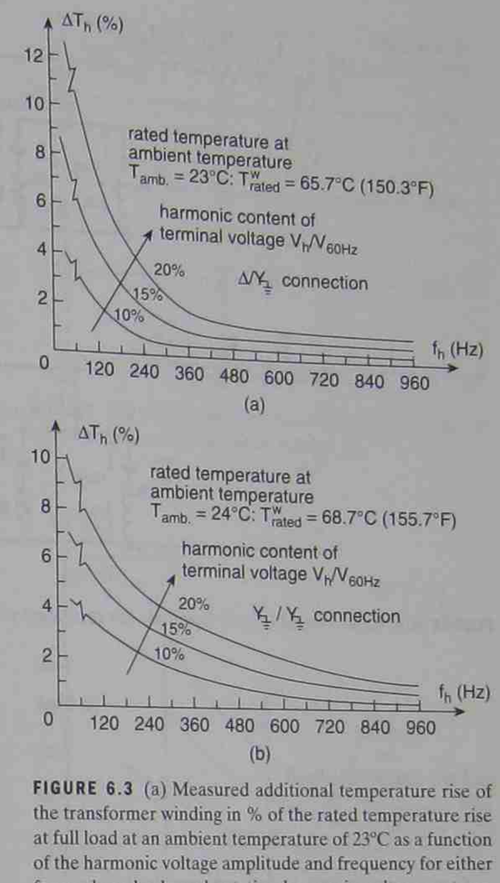



**FIGURE 6.3** (a) Measured additional temperature rise of the transformer winding in % of the rated temperature rise at full load at an ambient temperature of 23°C as a function of the harmonic voltage amplitude and frequency for either forward- or backward-rotating harmonic voltage systems, if the transformer bank is in Δ/Y-grounded connection [29, 30]. (b) Measured additional temperature rise of the transformer winding in % of the rated temperature rise at full load at an ambient temperature of 24°C as a function of the harmonic voltage amplitude and frequency for either forward- or backward-rotating harmonic voltage systems, if the transformer bank is in Y-grounded/Y-grounded connection [29, 30].

### 6.3.3 Weighted-Harmonic Factor for Three-Phase Induction Machines

The per-phase equivalent circuits of a three-phase induction motor are shown for the fundamental ($h = 1$) and a (integer, sub-, inter-) harmonic of hth order in Fig. 6.4. In Fig. 6.4 the fundamental slip is

ST. GEORGE COLLEGE OF LAKE

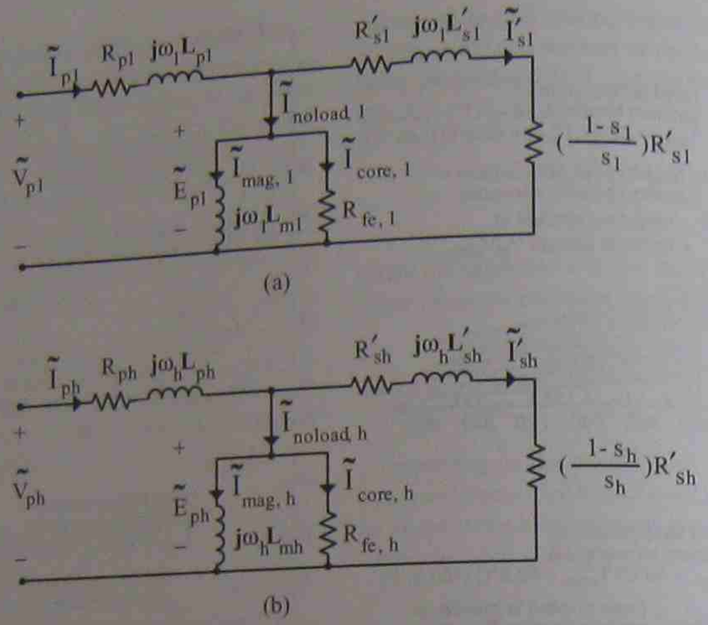



**FIGURE 6.4** Fundamental (a) and harmonic (b) equivalent circuits of three-phase induction machines.

$$s_1 = \frac{n_{s1} - n_m}{n_{s1}}, \qquad (6\text{-}13a)$$

and the harmonic slip is

$$s_h = \frac{n_{sh} - n_m}{n_{sh}}. \qquad (6\text{-}13b)$$

The ohmic losses caused by either the fundamental or a harmonic of order $h$ are proportional to the square of the respective currents. Therefore, one can write for the ohmic losses caused by voltage harmonics:

$$\frac{W_{ohmic,h}}{W_{ohmic,1}} = \left(\frac{R_{ph} + R'_{sh}}{R_{p1} + R'_{s1}}\right)\left(\frac{V_{ph}}{V_{p1}}\right)^2\left(\frac{Z_{p1}}{Z_{ph}}\right)^2, \qquad (6\text{-}14)$$

where

$$Z_{p1} = \sqrt{\left(R_{p1} + R'_{s1}/s_1\right)^2 + \left(\omega_1 L_p + \omega_1 L'_s\right)^2}$$

and

$$Z_{ph} = \sqrt{\left(R_{ph} + R'_{sh}/s_1\right)^2 + \left(h\omega_1 L_p + h\omega_1 L'_s\right)^2}.$$

For all time harmonics ($h = 2, 3, 4, \ldots$) an induction machine operating at rated speed can be considered being at standstill because $s_1 << s_h$. With $R_{ph}$, $R'_{sh}/s_h << h\omega_1 L_p$, $h\omega_1 L'_s$, the per-unit starting impedance

$$Z_{start\,pu} = \frac{\sqrt{\left(\omega_1 L_p + \omega_1 L'_s\right)^2}}{\sqrt{\left(R_{p1} + R'_{s1}/s_1\right)^2 + \left(\omega_1 L_p + \omega_1 L'_s\right)^2}}, \qquad (6\text{-}15)$$

and the slip $s_h = \{h \mp (1 - s_1)\}/h \approx (h \mp 1)/h$, Eq. 6-14 can be rewritten as

$$\frac{W_{ohmic,h}}{W_{ohmic,1}} \approx \left(\frac{R_{ph} + R'_{sh}}{R_{p1} + R'_{s1}}\right)\left(\frac{V_{ph}}{V_{p1}}\right)^2 \frac{1}{h^2 Z^2_{start\,pu}}. \qquad (6\text{-}16)$$

The additional iron-core losses due to a voltage harmonic of order $h$ referred to the iron-core losses at the fundamental frequency are (see Fig. 6.4)

$$\frac{W_{ohmic,h}}{W_{ohmic,1}} \approx \left(\frac{V_{ph}}{V_{p1}}\right)^2\left(\frac{Z_{fe,1}}{Z_{fe,h}}\right)^2 \frac{R_{fe,h}}{R_{fe,1}} = \left(\frac{E_{ph}}{E_{p1}}\right)^2 \frac{R_{fe,1}}{R_{fe,h}}, \qquad (6\text{-}17)$$

where

$$Z_{fe,1} = \frac{(j\omega_1 L_m + R_{fe,1})(R_{p1} + j\omega_1 L_p)}{j\omega_1 L_m} + R_{fe,1},$$

$$Z_{fe,h} = \frac{(jh\omega_1 L_m + R_{fe,h})(R_{ph} + jh\omega_1 L_p)}{jh\omega_1 L_m} + R_{fe,h}.$$

From [31] follows $\frac{R_{fe,h}}{R_{fe,1}} = h^{0.6}$, and therefore the iron-core losses are



$$\frac{W_{ohmic,h}}{W_{ohmic,1}} \approx \left(\frac{E_{ph}}{E_{p1}}\right)^2\left(\frac{1}{h^{0.6}}\right). \qquad (6\text{-}18)$$

Summing Eqs. 6-16 and 6-18, the total iron-core losses for a harmonic of order $h$ of a three-phase induction machine become

$$\frac{W_{ohmic,h}}{W_{ohmic,1}} = \left(\frac{R_{ph} + R'_{sh}}{R_{p1} + R'_{s1}}\right)\left(\frac{V_{ph}}{V_{p1}}\right)^2 \frac{1}{h^2 Z^2_{start\,pu}} + \left(\frac{E_{ph}}{E_{p1}}\right)^2\left(\frac{1}{h^{0.6}}\right), \qquad (6\text{-}19)$$

or for all occurring harmonics, one can show that the total harmonic losses $W_{total\,h\Sigma}$ relate to the total fundamental losses, as defined by the weighted harmonic factor [32]:

$$\frac{W_{total\,h\Sigma}}{W_{total\,1}} = K_2 \sum_{h=2}^{\infty} \frac{1}{(h)^k}\left(\frac{V_{ph}}{V_{p1}}\right)^l, \qquad (6\text{-}20)$$

where $0 \le k \le 2$ and $0 \le l \le 2$.

Note that the relations for single-phase transformers (Eq. 6-12) and that for a three-phase induction motor (Eq. 6-20) are identical in structure, though the exponents $k$ and $l$ may assume different values for single-phase transformers and three-phase induction motors. These exponents will be identified in the next section and it will be shown that the same structure of the weighted harmonic factor will also be valid for three-phase transformers and single-phase induction machines as well as universal machines.

Depending on the values of $k$ and $l$ one obtains different loss or temperature dependencies as a function of the frequency. Unfortunately, these dependencies can vary within wide ranges from constant to hyperbolic functions. This is so because the iron-core losses depend on the electric steel (e.g., conductivity, lamination thickness, permeability) used and the winding configurations in primary or stator and secondary or rotor. These can exhibit different conductivities (e.g., Cu, Al) or skin and proximity effects. In order to study these dependencies various $k$ and $l$ combinations will be assumed, as is depicted in Figs. 6.5 to 6.7:

- $k = 0$ and $l = 1$ results in a linear frequency-independent characteristic (Fig. 6.5).
- $k = 1$ and $l = 1$ results in a inverse frequency-dependent characteristic (Fig. 6.6).
- $k = 2$ and $l = 2$ results in a quadratic inverse frequency-dependent characteristic (Fig. 6.7).

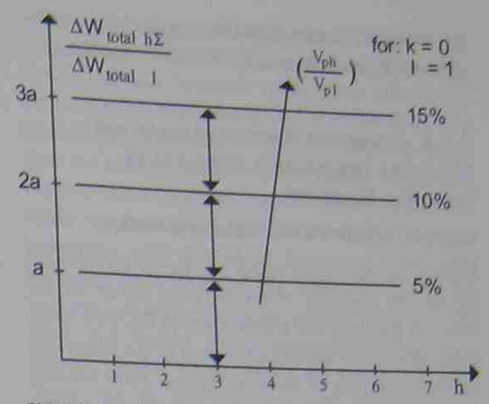



**FIGURE 6.5** Linear frequency-independent increase of harmonic losses with harmonic voltage $V_{ph}$.

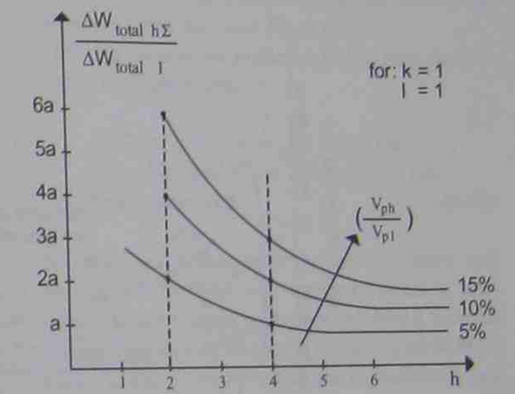



**FIGURE 6.6** Inverse frequency-dependent increase of harmonic losses with harmonic voltage $V_{ph}$.

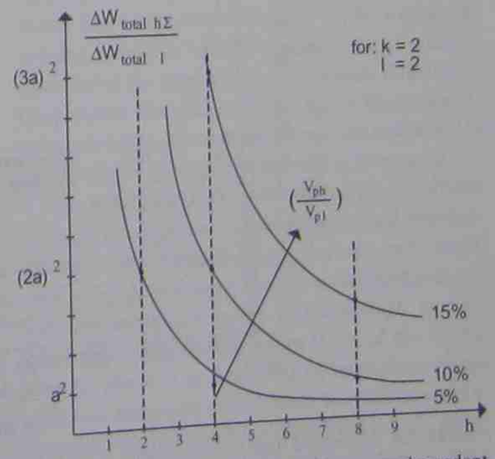



**FIGURE 6.7** Quadratic inverse frequency-dependent increase of harmonic losses with harmonic voltage $V_{ph}$.

ST. GEORGE COLLEGE OF T.A.F.E.

In real transformers and induction machines combinations of these characteristics will be possible.

### 6.3.4 Calculated Harmonic Losses and Measured Temperature Increases of Induction Machines

#### 6.3.4.1 *Single-Phase Induction Motors*

Calculated additional losses due to voltage harmonics for the machine of Eq. 6-21 are shown for the stator in Fig. 6.8a and for the rotor in Fig. 6.8b. Measured additional temperature rises of the stator end winding and that of the squirrel-cage rotor winding at full load as a function of the harmonic voltage amplitude, phase shift, and frequency for the same single-phase induction motor are depicted in Fig. 6.9a and 6.9b, respectively. Note that the maximum additional temperature rises are obtained when the peak-to-peak value of the terminal voltage is a maximum as a function of the superposed harmonic voltage with the fundamental voltage.

$$P = 2 \text{ hp},\ V_r = 115/208 \text{ V},\ I_r = 24/12 \text{ A},\ f = 60 \text{ Hz},\ \eta = 0.73,\ n_{rat} = 1725 \text{ rpm}. \quad (6\text{-}21)$$

Figure 6.8a,b shows that the additional harmonic losses due to subharmonic voltages and interharmonics below the fundamental become very large, even at low percentages and, therefore, the subharmonic voltages must be limited to below 0.5% of the fundamental. Note that at the slip frequency which corresponds to a slip of $s = 0$ the total stator losses reach a minimum (see Fig. 6.8a) because the total rotor losses are about zero (see Fig. 6.8b).

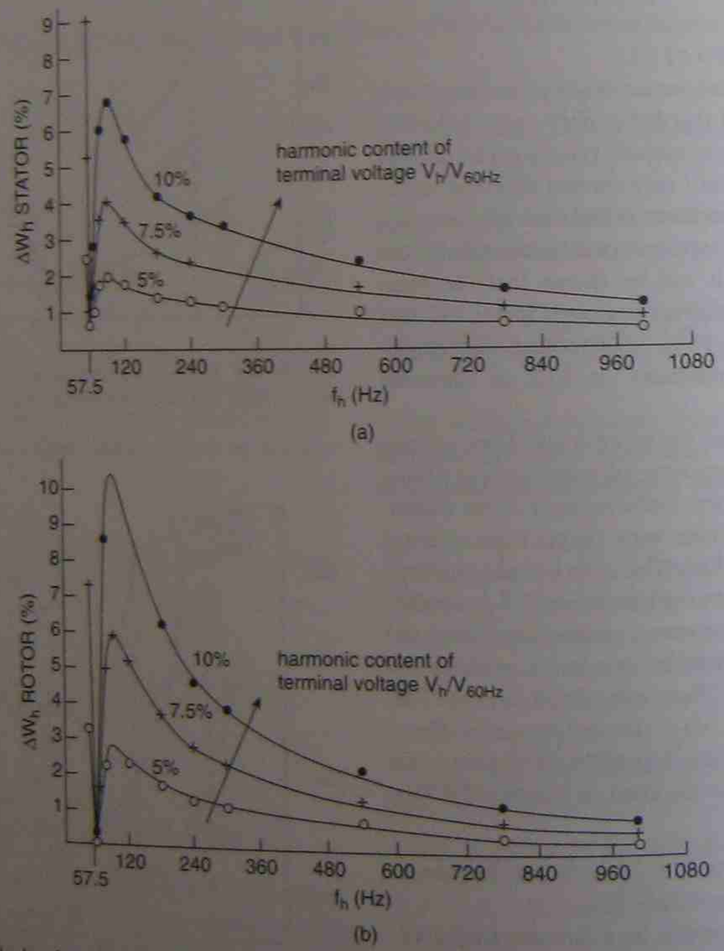



**FIGURE 6.8** Calculated total harmonic losses of (a) the stator referred to the rated losses of the stator and (b) the rotor referred to the rated losses of the rotor as a function of the harmonic frequency $h$ for the single-phase machine of Eq. 6-21 [33].



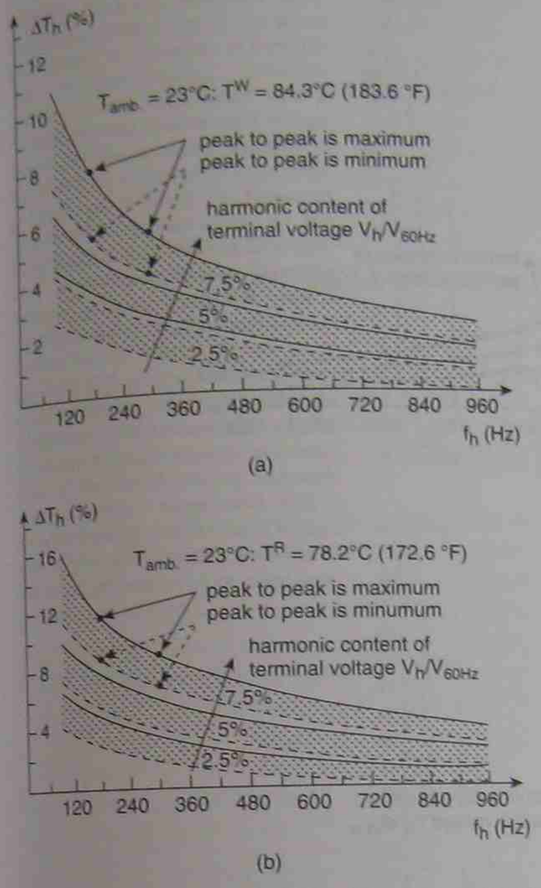



**FIGURE 6.9** (a) Measured additional temperature rise of the stator-end winding at full load as a function of the harmonic voltage amplitude, phase shift, and frequency for the single-phase machine of Eq. 6-21 [33] (referred to rated temperature rise of stator). (b) Measured additional temperature rise of the squirrel-cage rotor winding at full load as a function of the harmonic voltage amplitude, phase shift, and frequency for the single-phase machine of Eq. 6-21 [33] (referred to rated temperature rise of rotor).

#### 6.3.4.2 *Three-Phase Induction Motors*

Figure 6.4a,b illustrates the equivalent circuit of three-phase induction machines for the fundamental and time harmonics of order $h$ (integer, sub-, and interharmonics). The total harmonic losses were calculated [18, 19] for a three-phase induction machine with the following nameplate data and equivalent circuit parameters:

$$P = 800 \text{ W},\ p = 4 \text{ poles},\ n_{rat} = 1738 \text{ rpm},\ f = 60 \text{ Hz},\ V_{L\text{-}L} = 220/380 \text{ V},\ \Delta/Y \text{ connected},\ I_{ph} = 2.35 \text{ A},\ R_{s1} = 7.0\ \Omega,\ X_{s1} = 8.0\ \Omega,\ X_{m1} = 110.0\ \Omega,\ R'_{r1} = 4.65\ \Omega,\ X'_{r1} = 7.3\ \Omega. \quad (6\text{-}22)$$

Figure 6.10a shows the total harmonic stator losses referred to the total rated stator losses and Fig. 6.10b depicts the total harmonic rotor losses referred to the total rated rotor losses. In Fig. 6.10a there is a local maximum around 360 Hz; this maximum stems from the iron-core losses and its location depends on the lamination thickness of the iron-core sheets. The losses rapidly increase for subharmonics and interharmonics with decreasing frequency. The total harmonic rotor losses of Fig. 6.10b are larger for backward-rotating harmonic voltage systems (full lines) and smaller for forward-rotating harmonic systems (dashed lines). As for the stator, the rotor losses due to subharmonics and interharmonics below 60 Hz increase greatly with decreasing frequency. Note that at the slip frequency which corresponds to a slip of $s = 0$ the total stator losses reach a minimum (see Fig. 6.10a) because the total rotor losses are about zero (see Fig. 6.10b).

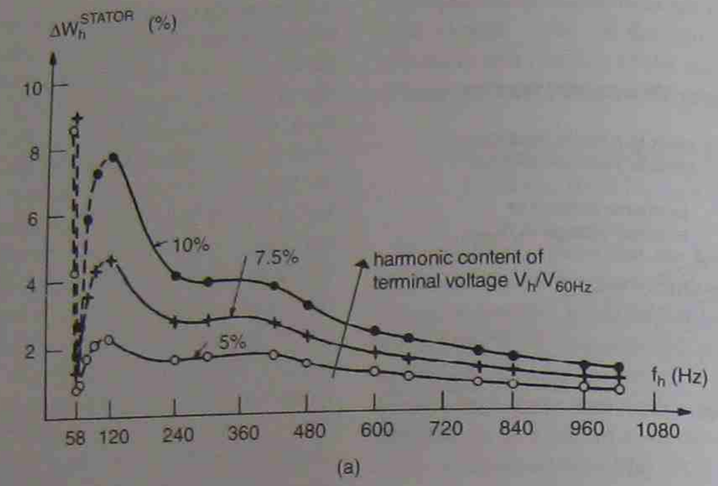
For the three-phase induction motor with the following nameplate data:

$$P = 2 \text{ hp},\ q_1 = 3;\ N_s = \text{LPF},\ f = 60 \text{ Hz},\ n_{rat} = 1725 \text{ rpm},\ V_{L\text{-}L} = 200 \text{ A},\ I_{ph} = 7.1 \text{ A},\ \text{time: continuous}. \quad (6\text{-}23)$$

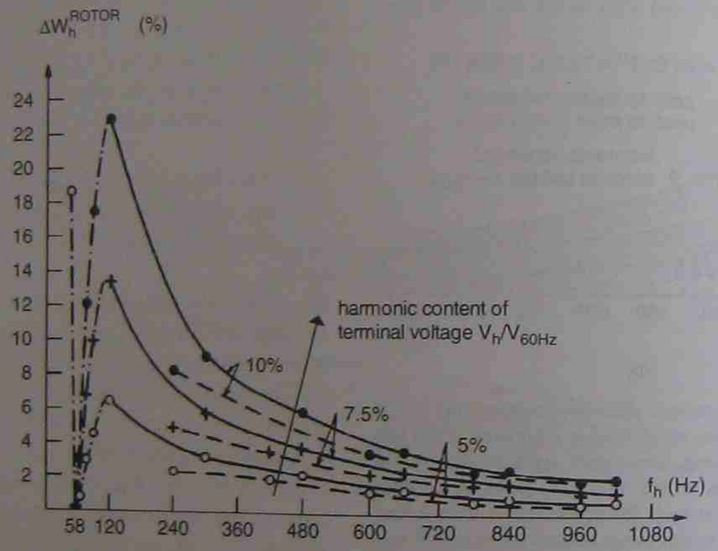
the additional temperature rise of the stator end winding for forward- and backward-rotating harmonic voltage systems superimposed with a forward voltage system of fundamental frequency of 60 Hz is shown in Fig. 6.11a. Note that for subharmonic and interharmonics below 60 Hz the stator temperature increases rapidly. The corresponding temperature rises of the squirrel-cage winding of the rotor are depicted in Fig. 6.11b and 6.11c for forward- and backward-rotating harmonic voltage systems, respectively. The temperature rise due to the backward-rotating harmonic voltage system is slightly larger than that of the forward-rotating system, if the rotor temperature rise is considered. Again, the temperature rises due to sub- and interharmonics below 60 Hz are rapidly increasing with decreasing frequency.

Figures 6.10 and 6.11 illustrate that the additional temperature rises due to subharmonic and interharmonics below 60 Hz voltages become very large, even at low percentages; therefore, the subharmonic and interharmonics below 60 Hz voltage components must be limited to below 0.5% of the fundamental voltage. The sensitivity of large three-phase induction machines with respect to additional temperature rises has also been calculated in [34], and it is recommended to limit the subharmonic voltages to 0.1%.

ST. GEORGE UNIVERSITY LAFAYETTE




(a)




(b)

**FIGURE 6.10** (a) Calculated total harmonic stator losses referred to the total rated stator losses for the machine of Eq. 6-22 [30]. (b) Calculated total harmonic rotor losses referred to the total rated rotor losses for the machine of Eq. 6-22 [30].

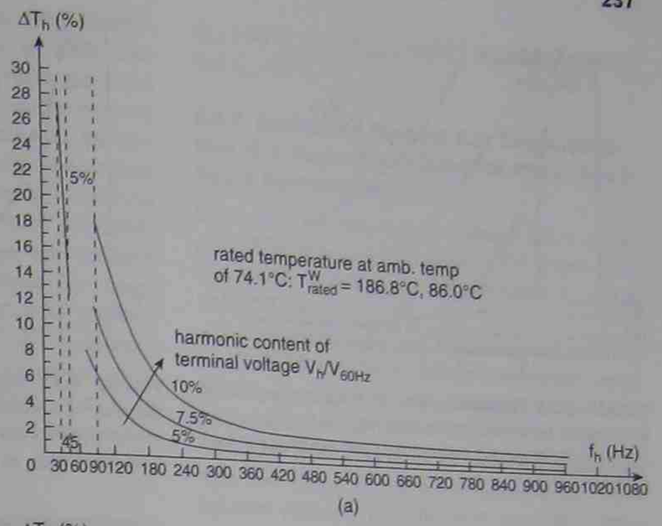
## 6.4 EXPONENTS OF WEIGHTED-HARMONIC FACTORS

In references [18, 19], the functional dependencies of the additional losses and the additional temperature rises due to harmonics of the terminal voltage are calculated for linear circuits and measured for actual machines, respectively. Thereby it is assumed that the additional temperature rise is proportional to the additional losses. Inspecting these loss and temperature functions, one notes that they can be approximated by hyperbolas for $h \geq 1.0$, as shown in Fig. 6.12.

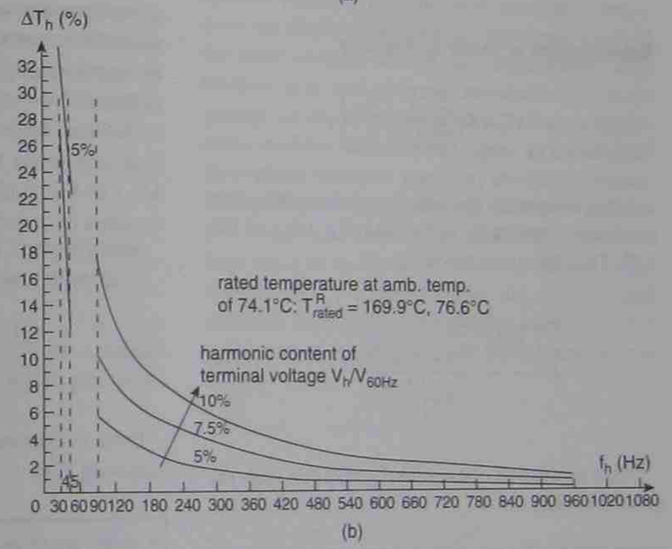
For $h < 1$ corresponding to the slip frequency where the stator field is in synchronism with the mechanical rotor no voltage $\bar{E}$ will be induced in the rotor and the rotor currents are zero; that is, the rotor loss is zero and the total motor loss is at a minimum, as is indicated in Fig. 6.12. At very low inter- or subharmonic frequencies, say, 3 Hz, the magnetizing reactance is very small and the 3 Hz current becomes very large, resulting in large total losses and harmonic torques as discussed in Chapter 3.



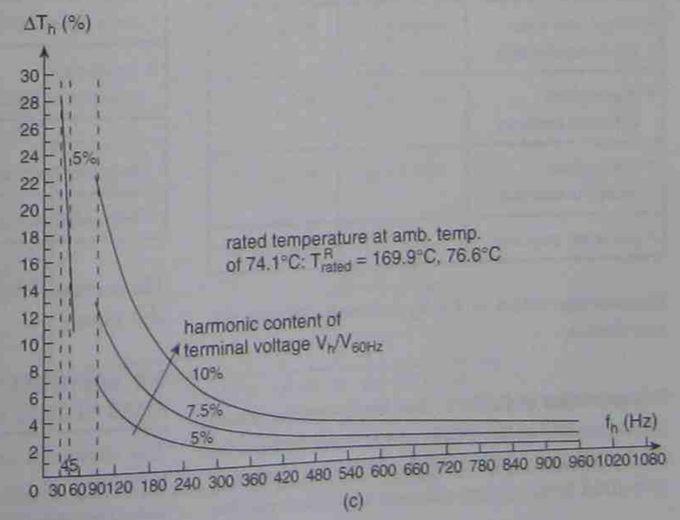
**FIGURE 6.11** (a) Measured additional temperature rise of the stator end winding as a function of forward- and backward-rotating harmonic voltage systems superposed with a forward-rotating fundamental voltage system for the induction machine of Eq. 6-23 [30] (referred to rated temperature rise of stator). (b) Measured additional temperature rise of the rotor squirrel-cage winding as a function of forward-rotating harmonic voltage systems superposed with a forward-rotating fundamental voltage system for the induction machine of Eq. 6-23 [30] (referred to rated temperature rise of rotor). (c) Measured additional temperature rise of the rotor squirrel-cage winding as a function of backward-rotating harmonic voltage systems superposed with a forward-rotating fundamental voltage system for the induction machine of Eq. 6-23 [30] (referred to rated temperature rise of rotor).




(a)




(b)




(c)

ST. GEORGE COLLEGE OF LAKE

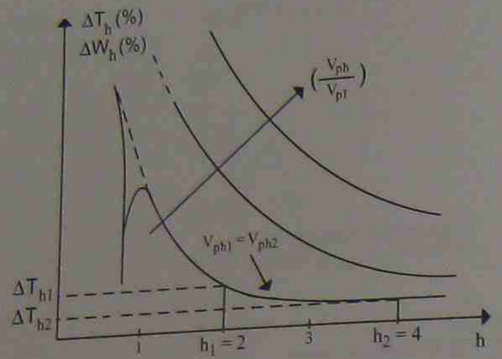



**FIGURE 6.12** Hyperbolic inverse frequency-dependent increase of harmonic losses with harmonic voltage $V_{ph}$, except at the frequency corresponding to mechanical speed (slip frequency).

**Determination of Factor k.** Knowing

$$\Delta T_h = K_1 \sum_{h=2}^{\infty} \frac{1}{(h)^k} \left( \frac{V_{ph}}{V_{p1}} \right)^l, \qquad (6\text{-}24)$$

one can determine the exponent $k$ from two given (measured) points ($h_1$, $\Delta T_{h1}$) and ($h_2$, $\Delta T_{h2}$) of Fig. 6.12. Therefore, one can write

$$k = \frac{\log\left\{ \dfrac{\Delta T_{h2}}{\Delta T_{h1}} \left( \dfrac{(V_{ph1}/V_{p1})^l}{(V_{ph2}/V_{p1})^l} \right) \right\}}{\log\left( \dfrac{h_1}{h_2} \right)}. \qquad (6\text{-}25)$$

From evaluation of measured points one finds the following [33]:

| | | |
|---|---|---|
| • Single- and three-phase transformers | $0.6 \le k \le 1.2$ | ▶ $k_{avg} = 0.90$ |
| • Single-phase induction machines | $0.5 \le k \le 1.2$ | ▶ $k_{avg} = 0.85$ |
| • Three-phase induction machines | $0.7 \le k \le 1.2$ | ▶ $k_{avg} = 0.95$ |
| • Universal machines | $0.8 \le k \le 1.2$ | ▶ $k_{avg} = 1.00$ |

The average values of $k = k_{avg}$ for each category are also shown.

**Determination of Factor *l*.** For the determination of the exponent $l$ of the weighted-harmonic factors, the functional dependencies of the additional losses and measured temperature rises on the harmonic frequencies and amplitude of references [18, 19] can be used. These calculated and measured functions can be approximated by a family of hyperbolas, as shown in Fig. 6.13.



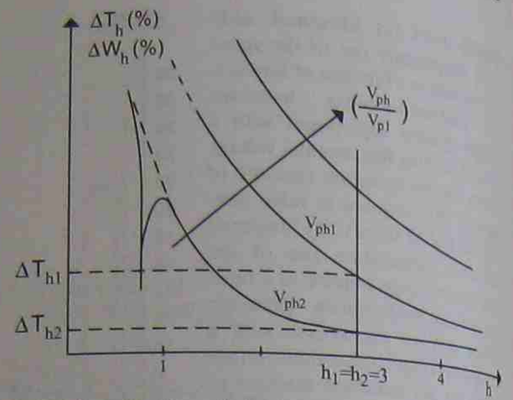



**FIGURE 6.13** Hyperbolic inverse frequency-dependent increase of harmonic losses with harmonic voltage $V_{ph}$, except at the frequency corresponding to mechanical speed (slip frequency).

One can determine the values of the exponent $l$ from any given two points ($V_{ph1}$, $\Delta T_{h1}$) and ($V_{ph2}$, $\Delta T_{h2}$) of Fig. 6.13 for any given two harmonic frequencies of order $h_1$ and $h_2$:

$$l = \frac{\log\left\{ \dfrac{\Delta T_{h2}}{\Delta T_{h1}} \left( \dfrac{h_1}{h_2} \right)^k \right\}}{\log\left( \dfrac{V_{ph1}}{V_{ph2}} \right)}. \qquad (6\text{-}26)$$

From evaluation of measured points one finds the following [33]:

| | | |
|---|---|---|
| • Single- and three-phase transformers | $1.50 \le l \le 2.0$ | ▶ $l_{avg} = 1.75$ |
| • Single-phase induction machines | $1.0 \le l \le 1.80$ | ▶ $l_{avg} = 1.40$ |
| • Three-phase induction machines | $1.2 \le l \le 2.0$ | ▶ $l_{avg} = 1.60$ |
| • Universal machines | $1.5 \le l \le 2.5$ | ▶ $l_{avg} = 2.00$ |

The average values $l = l_{avg}$ for each category are also shown.

## 6.5 ADDITIONAL LOSSES OR TEMPERATURE RISES VERSUS WEIGHTED-HARMONIC FACTORS

The additional losses and temperature rises due to harmonics of the terminal voltage of transformers, induction machines, and universal machines are calculated and measured in references [18, 19]. Provided these additional losses due to such time harmonics are small as compared with the rated losses ($W_{total\,h\Sigma} << W_{total\,1}$), a proportionality between the additional losses and the additional temperature rises can be assumed because the cooling conditions are not significantly altered. Calculations and measurements show that the previously mentioned electromagnetic devices are sensitive to voltage harmonics in the frequency range $0 \le f_h \le 1500$ Hz. Harmonics of low order generate the largest additional loss. The correspondence of a given value of the weighted-harmonic factor (to an additional loss and temperature rise) leads to the additional temperature rise (or loss) versus the harmonic-factor function [20] as shown in Fig. 6.14.

With assumed values for the average exponents $k_{avg}$ and $l_{avg}$ as they apply to transformers, induction and universal machines, one can compute for given percentages of the harmonic voltages the weighted-harmonic factor and associate with it the additional losses or temperature rises.

### 6.5.1 Application Example 6.1: Temperature Rise of a Single-Phase Transformer Due to Single Harmonic Voltage

Determine the temperature rise $\Delta T_h$ of a single-phase transformer provided $V_3 = 0.10$ pu $= 10\%$, $T_{amb} = 40°C$, and $T_{rated} = 100°C$. Assume $k_{avg} = 0.90$ and $l_{avg} = 1.75$.

### 6.5.2 Application Example 6.2: Temperature Rise of a Single-Phase Induction Motor Due to Single Harmonic Voltage

Determine the temperature rise $\Delta T_h$ of a single-phase induction motor provided $V_3 = 0.10$ pu $\equiv 10\%$, $T_{amb} = 40°C$, and $T_{rated} = 100°C$. Assume $k_{avg} = 0.85$ and $l_{avg} = 1.40$.

Transformers, induction machines, and universal machines have different loss or temperature sensitivities with respect to voltage harmonics and, therefore, the additional temperature rises are different for all five types of devices. The additional temperature rise (loss) versus weighted-harmonic factor function indicates that the most sensitive components are single-phase induction machines, whereas the least sensitive devices are transformers with resistive load and universal machines. This is so because for any harmonic terminal voltage, a single-phase machine (and to some degree an unbalanced three-phase induction machine) develops forward- and backward-rotating harmonic fields and responds like being under short-circuit conditions due to the large slip $s_h$ of the harmonic field with respect to the rotating rotor. In transformers the resistive and inductive loads can never have zero impedance due to the nature of the frequency dependency of such loads.

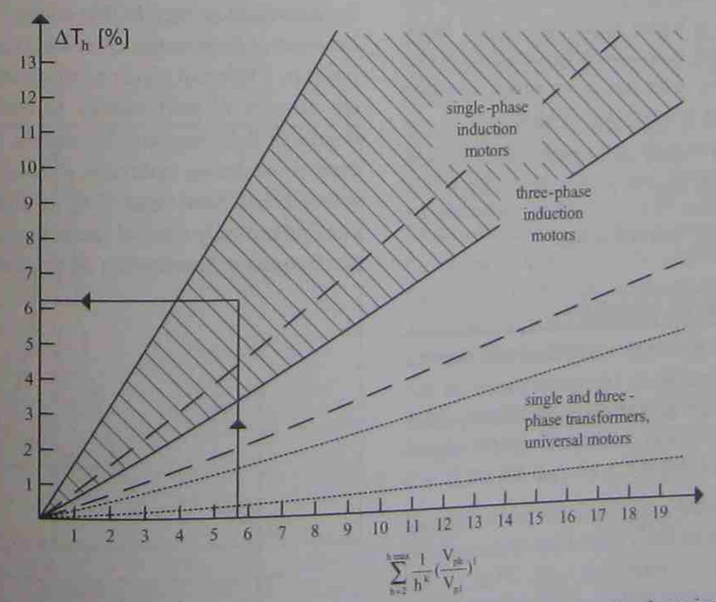



**FIGURE 6.14** Additional temperature rise (or loss) versus weighted-harmonic factor function for universal motors, single- and three-phase transformers, and induction motors [33].



ST. GEORGE COLLEGE OF LAFE

## 6.6 ARRHENIUS PLOTS

A series of studies have investigated the behavior of various electric machines and transformers as they occur in a residential distribution system and are exposed to harmonics of the terminal voltage [18, 19]. The influence of such harmonics expresses itself, among others (e.g., mechanical vibration), in an elevated (additional) temperature rise of the machine windings and iron cores. The question arises how the lifetime of the machines will be affected by such additional temperature rises.

**Thermal Aging.** The insulating material of an electric apparatus as used in electrical appliances is of organic or inorganic origin. Due to the heating of these materials, caused by the loss within the machine, a deterioration of the insulating materials will occur. This deterioration is manifested either by

- lowering of the mechanical strength, and/or
- changing of the dielectric behavior of the insulating material.

It may be mentioned that not only the heat itself, but also small motions due to expansion and contraction of the wire and iron laminations, are causing deteriorations by mechanical friction. In addition, time harmonics induce small core vibrations that may aggravate the mechanical stresses. The mechanical failure of the insulation is a result of the decrease of the tensile strength or flexibility of the insulation material. The thermal lifetime of electric machines and transformers is highly dependent on the mode of utilization; there is no doubt that machines with frequently variable load are more prone to aging from a mechanical failure point of view.

All further investigations consider machines or transformers operating at constant rated load, where the chemical changes of the insulating materials are responsible only for thermal aging.

## 6.7 REACTION RATE EQUATION

For many years it has been recognized that thermal degradation of organic or inorganic materials can be best represented by the reaction rate equation [24, 25]

$$\frac{dR}{dt} = Ae^{(-E/KT)}, \tag{6-27}$$

In this equation, $dR/dt$ is the reduction in property $R$ with respect to time, $A$ is a constant of integration,



$K$ is the gas constant or, depending on the units, the Boltzmann constant, $T$ is the absolute temperature in kelvins, and $E$ is the activation energy of the aging reaction (large $E$ leads to fast aging, small $E$ leads to slow aging).

Equation 6-27 expresses the rule of chemical reactions which was derived by Svante Arrhenius in 1880. The form of the original Arrhenius formula can be obtained from the differential equation by integration as follows:

$$dR = Ae^{-(E/KT)}dt,$$

$$\int dR = A\int e^{-(E/KT)}dt,$$

$$R = Ae^{-(E/KT)}dt,$$

$$\frac{R}{t} = Ae^{-(E/KT)},$$

$$\ln(R/t) = \ln(Ae^{-(E/KT)}),$$

$$\ln R - \ln t = \ln A - E/KT,$$

or

$$\ln t = \left(\frac{E}{K}\right)\frac{1}{T} + B. \tag{6-28}$$

The plot $\ln t$ versus $1/T$ is a straight line with the slope $E/K$, if for the lifetime $t$ a logarithmic scale is employed, as shown in Fig. 6.15.

Equation 6-28 expresses that the logarithm of the degradation (decreased life) time $t$ is proportional to the activation energy $E$: this energy is transmitted in the form of heat to the chemical reaction or decomposition. Different kinds of materials need a different amount of heat energy to arrive at the same degree of deterioration. To obtain these data in the case of insulating materials, extensive experimental research has been done [24]. In this reference, one can find not only a list of the activation energies, but the frequency distribution of the activation energies

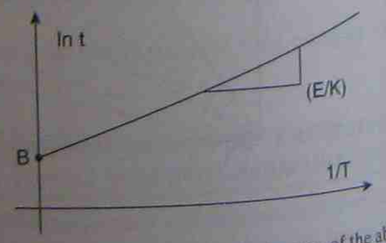



**FIGURE 6.15** Lifetime $t$ versus the inverse of the absolute temperature $T$.





of various materials. Properties monitored for these materials include flexural strength, impact strength, and dielectric strength. In Fig. 4 of [24], one notes the number of materials for each increment of 0.1 eV activation energy (see Fig. 6.16). The peak of this distribution curve occurs at about $E = 1.15$ eV.

The practical use of the Arrhenius plot and the consequences of the data of Fig. 4 of [24] will be discussed in the next section.

## 6.8 DECREASE OF LIFETIME DUE TO AN ADDITIONAL TEMPERATURE RISE

The slope of the Arrhenius plot based on

$$\ln t = \left(\frac{E}{K}\right)\frac{1}{T} + B \tag{6-29}$$

is the most important quantity (proportional to the activation energy $E$) for our investigation; this is the only quantity that determines the aging of the insulation material. Therefore, we have to use the slope of the Arrhenius plot as a measure of aging.

If one knows from experiments two (different) points of the plot belonging to temperatures $T_1$ and $T_2$ and lifetimes $t_1$ and $t_2$, respectively, that is, $(T_1, t_1)$ and $(T_2, t_2)$, then one can obtain for a given insulation material

$$\ln t_1 - \ln t_2 = \left(\frac{E}{K}\right)\left(\frac{1}{T_1} - \frac{1}{T_2}\right). \tag{6-30}$$

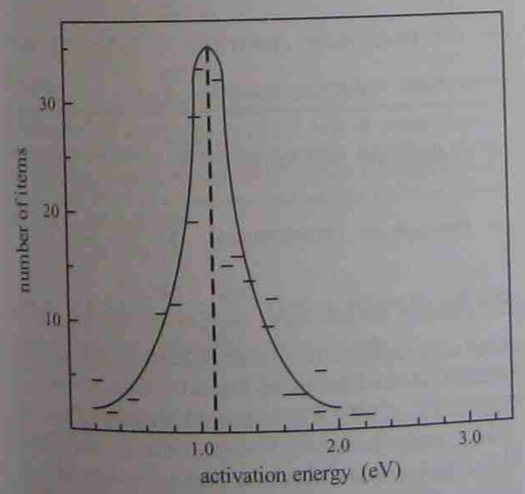



**FIGURE 6.16** Frequency distribution of activation energies of various organic and inorganic materials [24].

It must be noted that if the activation energy $E$ is measured in electron volts one has to use for $K$ the Boltzmann constant: $K = 1.38 \cdot 10^{-23}$ J/Kelvin; in case the activation energy is given in kilocalories per mole the constant $K$ will be the gas constant $K = R = 19.84 \cdot 10^{-4}$ kcal/mol. Note that $1\text{ eV} = 1.602 \cdot 10^{-19}$ J or $1\text{ J} = 0.624 \cdot 10^{19}$ eV.

Suppose one knows the rated lifetime $t_2$ of an apparatus and its rated (constant) temperature $T_2$ at which it is operating. The question arises to what extent the lifetime decreases provided the elevated temperature becomes $T_1 = T_2 + \Delta T$ where $\Delta T = \Delta T_h$. To answer this question one has to substitute in Eq. 6-30 $T_1$ by $T_2 + \Delta T$:

$$\ln t_1 - \ln t_2 = \left(\frac{E}{K}\right)\left(\frac{1}{T_2 + \Delta T} - \frac{1}{T_2}\right). \tag{6-31}$$

After some manipulations, the new decreased lifetime is

$$t_1 = t_2 e^{-\left(\frac{E}{K}\right)\frac{\Delta T}{T_2(T_2 + \Delta T)}}, \tag{6-32}$$

where $t_2$ is the rated lifetime, $T_2$ is the rated temperature in kelvins, and $\Delta T$ is the (additional) temperature rise in degrees Celsius. Several examples will illustrate the use of the above relation as applied to the calculation of the decrease of the lifetime due to the additional temperature rise caused by the additional harmonic losses. In all following examples it is assumed that the rated lifetime of the apparatus is $t_2 = 40$ years, and the steady-state rated temperature of the hottest spot is $T_2 = 100°\text{C} \equiv 273 + 100 = 373$ °Kelvin.

### 6.8.1 Application Example 6.3: Aging of a Single-Phase Induction Motor with E = 0.74 eV Due to a Single Harmonic Voltage

Determine for an activation energy of $E = 0.74$ eV the slope $E/K$ and for the additional temperature rise $\Delta T_{h=3} = 6.6°\text{C}$ (see Application Example 6.2 with $T_{amb} = 40°$, $T_2 = T_{rat} = 100°\text{C}$) the reduced lifetime of a single-phase induction motor.

### 6.8.2 Application Example 6.4: Aging of a Single-Phase Induction Motor with E = 0.51 eV Due to a Single Harmonic Voltage

Determine for an activation energy of $E = 0.51$ eV the slope $E/K$ and for the additional temperature rise $\Delta T_{h=3} = 6.6°\text{C}$ (see Application Example 6.2 with $T_{amb} = 40°$, $T_2 = T_{rat} = 100°\text{C}$) the reduced lifetime of a single-phase induction motor.

ST. GEORGE COLLEGE OF TAFE

## 6.9 REDUCTION OF LIFETIME OF COMPONENTS WITH ACTIVATION ENERGY E = 1.1 EV DUE TO HARMONICS OF THE TERMINAL VOLTAGE WITHIN RESIDENTIAL OR COMMERCIAL UTILITY SYSTEMS

Figure 6.14 shows the additional temperature rises (or losses) in percent of the rated temperature rises (or losses) as a function of the weighted-harmonic factor. These functions are obtained from calculations and measurements [18, 19]. Note that the ambient temperature has been eliminated. For the evaluation of the reduction of the lifetime one must base all calculations on an activation energy of about $E = 1.1$ eV because of Fig. 6.16, which confirms that the majority of (insulation) materials have such a distinct activation energy.

According to Fig. 6.14, a weighted harmonic-voltage factor of $\sum_{h=2}^{h\max} \frac{1}{h^k}\left(\frac{V_{ph}}{V_{p1}}\right)^l = 5.8$ corresponds to additional temperature rises (referred to the rated temperature rises) on the average of 6.2% for single-phase induction machines, 3.2% for three-phase induction machines, and 0.85% for transformers and universal machines. These percentage values confirm that single-phase machines are very sensitive to harmonic voltages due to their forward- and backward-rotating fields and their short-circuited rotor, three-phase induction machines are sensitive to voltage harmonics due to their short-circuited rotor, transformers are not very sensitive to voltage harmonics because of their resistive load, and universal machines are not sensitive as well because the commutator transforms a voltage source to a current source where the current magnitudes are limited. A weighted-harmonic voltage factor of 5.8 results for the rated temperature $T_2 = 85°C$ at $T_{amb60Hz} \approx T_{ambh} = 23°C$ in temperature increases of 3.84°C for single-phase induction machines, 1.98°C for three-phase induction machines, and 0.53°C for transformers and universal machines. With these additional temperature increases one obtains at an activation energy of $E = 1.1$ eV – with $E/K = 12{,}769$ Kelvin – the decreased lifetime (using Eq. 6-32) of 31.5% for single-phase induction machines, 18% for three-phase induction machines, and 5% for transformers and universal machines.

**Conclusion.** It is believed that the weighted-harmonic voltage factor for single-phase and three-phase induction motors in the neighborhood of 5.8 represents a compromise which on the one hand promotes the installation of solid-state circuits by choosing generous permissible harmonic voltage levels, and on the other hand avoids severe detrimental reactions on the majority of the residential or commercial power system components including loads. Harmonic spectra of the residential or commercial power system voltage that satisfy for single-phase and three-phase induction motors

$$\sum_{h=2}^{h\max} \frac{1}{h^k}\left(\frac{V_{ph}}{V_{p1}}\right)^l \approx 5.8. \tag{6-33}$$

result in acceptable temperature rises as far as induction motors, transformers, and universal machines are concerned. Thus it is recommended not to rigidly fix the harmonic voltages but rather the additional temperature rises they generate.

## 6.10 POSSIBLE LIMITS FOR HARMONIC VOLTAGES

In order to illustrate the use of Eqs. 6-33 and 6-32, the harmonic voltage spectra for a single-phase and for a three-phase feeder (see Table 6.1) are proposed [33].

With average values of $k_{avg} = 0.85$ and $l_{avg} = 1.4$ for single-phase induction motors, $k_{avg} = 0.95$ and $l_{avg} = 1.6$ for three-phase induction motors, $k_{avg} = 0.90$ and $l_{avg} = 1.75$ for single-phase and three-phase transformers, and $k_{avg} = 1.0$ and $l_{avg} = 2.0$ for universal machines, one obtains for the single-phase spectrum of Table 6.1 the weighted harmonic-voltage factor

for single-phase induction motors $\sum_{h=2}^{h\max} \frac{1}{h^k}\left(\frac{V_{ph}}{V_{p1}}\right)^l \approx 5.7$,

for the three-phase spectrum of Table 6.1 for

three-phase induction motors $\sum_{h=2}^{h\max} \frac{1}{h^k}\left(\frac{V_{ph}}{V_{p1}}\right)^l \approx 5.7$,

for single-phase transformers $\sum_{h=2}^{h\max} \frac{1}{h^k}\left(\frac{V_{ph}}{V_{p1}}\right)^l \approx 7.37$,

for three-phase transformers $\sum_{h=2}^{h\max} \frac{1}{h^k}\left(\frac{V_{ph}}{V_{p1}}\right)^l \approx 7.4$,

and for universal motors $\sum_{h=2}^{h\max} \frac{1}{h^k}\left(\frac{V_{ph}}{V_{p1}}\right)^l \approx 8.5$. Any other set of voltage harmonics is feasible if Eq. 6-33 is about satisfied. Based on Fig. 6.14 (with $T_2 = 85°C$, $T_{amb} = 23°C$, $E = 1.1$ eV, and rated lifetime of $t_2 = 40$ years), those harmonic factors result in the additional temperature rises and lifetime reductions of Table 6.2.



### 6.10.1 Application Example 6.5: Estimation of Lifetime Reduction for Given Single-Phase and Three-Phase Voltage Spectra with High Harmonic Penetration with Activation Energy E = 1.1 eV

Estimate the lifetime reductions of induction machines, transformers, and universal machines for the single- and three-phase voltage spectra of Table E6.5.1 and their associated lifetime reduction for an activation energy of $E = 1.1$ eV. The ambient temperature is $T_{amb} = 23°C$, the rated temperature is $T_2 = 85°C$, and the rated lifetime of $t_2 = 40$ years can be assumed.

**TABLE 6.1** Possible Voltage Spectra of Single-Phase and Three-Phase Feeders

| $h$ | $\left(\frac{V_h}{V_{60Hz}}\right)_{1\Phi}$ (%) | $\left(\frac{V_h}{V_{60Hz}}\right)_{3\Phi}$ (%) |
|---|---|---|
| 1 | 100 | 100 |
| 2 | 0.5 | 0.5 |
| 3 | 4.0 | 2.0[a] |
| 4 | 0.3 | 0.5 |
| 5 | 3.0 | 5.0 |
| 6 | 0.2 | 0.2 |
| 7 | 2.0 | 3.5 |
| 8 | 0.2 | 0.2 |
| 9 | 1.0 | 0.3 |
| 10 | 0.1 | 0.1 |
| 11 | 1.5 | 1.5 |
| 12 | 0.1 | 0.1 |
| 13 | 1.5 | 1.0 |
| 14 | 0.1 | 0.05 |
| 15 | 0.5 | 0.1 |
| 16 | 0.05 | 0.05 |
| 17 | 1.0 | 0.5 |
| 18 | 0.05 | 0.01 |
| 19 | 1.0 | 0.5 |
| All higher harmonics < 0.5% | | |

[a]Under certain conditions (e.g., DC bias of transformers as discussed in Chapter 2, and the harmonic generation of synchronous generators as outlined in Chapter 4) triplen harmonics are not of the zero-sequence type and can therefore exist in a three-phase system.

### 6.10.2 Application Example 6.6: Estimation of Lifetime Reduction for Given Single-Phase and Three-Phase Voltage Spectra with Moderate Harmonic Penetration with Activation Energy E = 1.1 eV

Estimate the lifetime reductions for induction machines, transformers, and universal machines for the single- and three-phase voltage spectra of Table E6.6.1 and their associated lifetime reduction for an activation energy of $E = 1.1$ eV. The ambient temperature is $T_{amb} = 23°C$, the rated temperature is $T_2 = 85°C$, and the rated lifetime of $t_2 = 40$ years can be assumed.

**TABLE E6.5.1** Possible Voltage Spectra with High-Harmonic Penetration

| $h$ | $\left(\frac{V_h}{V_{60Hz}}\right)_{1\Phi}$ (%) | $\left(\frac{V_h}{V_{60Hz}}\right)_{3\Phi}$ (%) |
|---|---|---|
| 1 | 100 | 100 |
| 2 | 2.5 | 0.5 |
| 3 | 5.71 | 1.0 |
| 4 | 1.6 | 0.5 |
| 5 | 1.25 | 7.0 |
| 6 | 0.88 | 0.2 |
| 7 | 1.25 | 5.0 |
| 8 | 0.62 | 0.2 |
| 9 | 0.96 | 0.3 |
| 10 | 0.66 | 0.1 |
| 11 | 0.30 | 2.5 |
| 12 | 0.18 | 0.1 |
| 13 | 0.57 | 2.0 |
| 14 | 0.10 | 0.05 |
| 15 | 0.10 | 0.1 |
| 16 | 0.13 | 0.05 |
| 17 | 0.23 | 1.5 |
| 18 | 0.22 | 0.01 |
| 19 | 1.03 | 1.0 |
| All higher harmonics < 0.2% | | |

**TABLE 6.2** Additional Temperature Rise and Associated Lifetime Reduction of Induction Motors, Transformers, and Universal Motors Due to the Harmonic Spectra of Table 6.1

| | Single-phase induction motors | Three-phase induction motors | Single-phase transformers | Three-phase transformers | Universal motors |
|---|---|---|---|---|---|
| $\Delta T_h$ (%) | 6.2 | 3.2 | 1.2 | 1.2 | 1.3 |
| $\Delta T_h$ (°C) | 3.84 | 1.98 | 0.74 | 0.74 | 0.81 |
| Lifetime reduction (%) | 31.5 | 17.8 | 7.1 | 7.1 | 7.7 |

ST. GEORGE COLLEGE OF I.A.E.E

**TABLE E6.6.1** Possible Voltage Spectra with Moderate-Harmonic Penetration

| $h$ | $\left(\frac{V_h}{V_{60\,Hz}}\right)_{1\phi}$ (%) | $\left(\frac{V_h}{V_{60\,Hz}}\right)_{3\phi}$ (%) |
|---|---|---|
| 1 | 100 | 100 |
| 2 | 0.5 | 0.5 |
| 3 | 3.0 | 0.5 |
| 4 | 0.3 | 3.0 |
| 5 | 2.0 | 0.2 |
| 6 | 0.2 | 2.5 |
| 7 | 1.0 | 0.2 |
| 8 | 0.2 | 0.3 |
| 9 | 0.75 | 0.1 |
| 10 | 0.1 | 1.0 |
| 11 | 1.0 | 0.1 |
| 12 | 0.1 | 0.85 |
| 13 | 0.9 | 0.05 |
| 14 | 0.1 | 0.1 |
| 15 | 0.3 | 0.05 |
| 16 | 0.05 | 0.3 |
| 17 | 0.5 | 0.01 |
| 18 | 0.05 | 0.2 |
| 19 | 0.4 | |
| All higher harmonics < 0.2% | | |

## 6.11 PROBABILISTIC AND TIME-VARYING NATURE OF HARMONICS

As mentioned in Section 6.1, the harmonic current or voltage spectra within a distribution feeder are continually changing as a function of changes in the load and the system's condition. The rationale given for using the worst-case conditions, where loads are operating for at least a few hours at rated operation generating the "rated current/voltage spectra," is the basis for the IEEE [35] and IEC [36] harmonic guidelines and standards, respectively. Nevertheless it will be worthwhile to study the time-varying nature [37, 38] of harmonic spectra. In these publications continually changing current ($THD_i$) and voltage ($THD_v$) total harmonic distortions are plotted as a function of time. They indeed change widely from 2.5% to about 9% for $THD_v$, and from 1% to about 5% for the $THD_i$ for one site, and for another site the changes are similar in magnitude. As mentioned in prior sections, the THDs are neither a good measure for temperature rises nor for vibrations; instead harmonic components should be used in any further studies. The measured THD data are characterized by statistical measures (e.g., minimum, maximum, average or mean values, standard deviation, probability distribution), histograms or probability density functions (pdf), probability distribution functions ($PX(x)$), statistical description of sub-time intervals, and combined deterministic or statistical description [41–45]. These publications address the harmonic summation and propagation by explaining the sum of random harmonic phasors via the representation of harmonic phasors, marginal pdf of x–y components, pdf of sum of projections of independent phasors, and pdf of magnitude of sum of random phasors. These papers apply the methods described to a 14-bus transmission system and provide general guidelines with respect to their applicability. The probabilistic evaluation of the economic cost due to harmonic losses in industrial energy systems is presented in the next section.

## 6.12 THE COST OF HARMONICS

The cost of harmonics can originate either in

- the complicated solid-state components necessary to maintain the current or voltage harmonics at a low level, for example, switched-mode power supplies operating at unity-power factor [39], or in
- the use of simple peak-rectifiers resulting in high harmonic amplitudes [40].

Both costs are not negligibly small and must be considered in the future. The first approach appears to be favored by the IEC [36] for low-, medium-, and high-voltage power systems, whereas the latter appears to be favored by IEEE [35] for single-phase systems only.

In references [41–45] the cost of the latter approach is discussed by defining the economic damage (cost) due to harmonic losses $D = D_w + D_a$, where $D_w$ is the operating cost and $D_a$ is the aging cost. This economic damage is a probabilistic quantity because the harmonic voltage or current spectra change in a random manner. The expected value of these costs is defined as $E(D) = E(D_w) + E(D_a)$, where $E(D_w)$ is the present-worth expected value of the operating costs due to harmonic losses and $E(D_a)$ is the present-worth expected value of the aging costs due to harmonic losses. Numerical results for a 20 kV, 150 MVA industrial feeder illustrate that the economic damage for induction motors is significant and within a lifetime of 35 years amounts to about the purchase cost ($7,625) of an induction motor.

## 6.13 TEMPERATURE AS A FUNCTION OF TIME

Rotating machines, transformers, and inductors must be designed so that their rated temperatures will not be exceeded. For rotating machines the maximum torques are not a design criterion as long as the machines continue to operate. The maximum permissible temperature (hot spot) must not be exceeded, otherwise the lifetime will be reduced. Note that any machine works most efficiently and cost-effectively if the permissible (maximum) rated temperature will be reached but not exceeded at any time. At steady state machines must be able to operate at rated torque. For a short time machines can be operated above rated torque. This leads to the concept of intermittent operation discussed in a later section.



A motor can be replaced by a radiating sphere as illustrated in Fig. 6.17. During a small time increment $dt$ one can assume that the temperature of the sphere increases by the incremental temperature $d\theta$. For this reason the change in stored heat (increase) $dQ_C$ during the time $dt$ is

$$dQ_C = C \cdot d\theta, \tag{6-34}$$

where $\theta$ is the temperature rise and $C$ is the heat-absorption capacity. Note that Eq. 6-34 is independent of time.

Due to thermal radiation a part of the stored heat will be emitted to the surrounding environment. The change of the stored heat (reduction) $dQ_A$ is time dependent:

$$dQ_A = A \cdot \theta \cdot dt, \tag{6-35}$$

where $A$ is the heat-radiation capacity.

The sum of Eqs. 6-34 and 6-35 yields the ordinary differential equation

$$dQ = dQ_C + dQ_A = C \cdot d\theta + A \cdot \theta \cdot dt = P_{loss} \cdot dt, \tag{6-36}$$

where $P_{loss} \cdot dt$ is the (loss) energy absorbed by the machine during the incremental time $dt$. Dividing Eq. 6-36 by $dt$ and $A$, one obtains the first-order ordinary differential equation

$$\frac{P_{loss}}{A} = \frac{C}{A}\cdot\frac{d\theta}{dt} + \theta = \tau_\theta \cdot \frac{d\theta}{dt} + \theta, \tag{6-37}$$

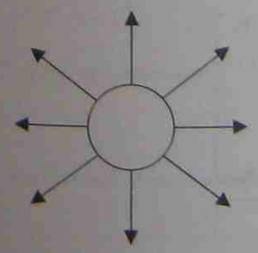


**FIGURE 6.17** Rotating machine represented by radiating sphere.

where $\tau_\theta = (C/A)$ is the thermal time constant. The solution of this first-order differential equation is

$$\theta = \frac{P_{loss}}{A} + k \cdot e^{(-t/\tau_\theta)}. \tag{6-38}$$

For $t = 0$ and $\theta = \theta_o$ (initial temperature rise) and for $t = \infty$ with $\theta = \theta_f = P_{loss}/A$ (final temperature rise) one obtains for the temperature as a function of time

$$\theta = \theta_f - (\theta_f - \theta_o) \cdot e^{(-t/\tau_\theta)}. \tag{6-39}$$

Figure 6.18 illustrates the solution of Eq. 6-39 including its time constant. The temperature transient during a load cycle is schematically depicted in Fig. 6.19 with $\theta_f = P_{loss}/A$.

### 6.13.1 Application Example 6.7: Temperature Increase of Rotating Machine with a Step Load

An enclosed fan-cooled induction motor has a thermal time constant of $\tau_\theta = 3\ h$ and a steady-state rated temperature of $\theta_f = 120°C$ at an ambient temperature of $\theta_{amb} = 40°C$. The motor has at time $t = 0_-$ a temperature of $\theta = \theta_{amb}$, and the motor is fully loaded at $t = 0_+$. Calculate the time $t_{95\%}$ when the fully loaded motor reaches 95% of its final temperature $\theta_f = 120°C$.

## 6.14 VARIOUS OPERATING MODES OF ROTATING MACHINES

Depending on their applications, rotating machines can be subjected to various operating modes such as steady-state, short-term, steady-state with short-term, intermittent, and steady-state with intermittent operating modes.

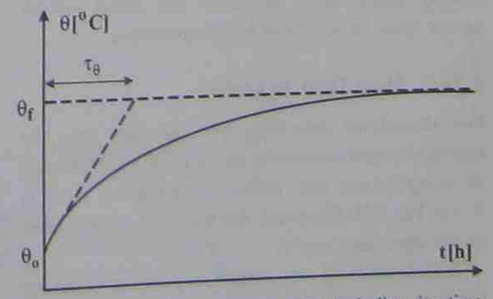



**FIGURE 6.18** Solution of Eq. 6-39 including its time constant.

ST. GEORGE COLLEGE OF LA&E

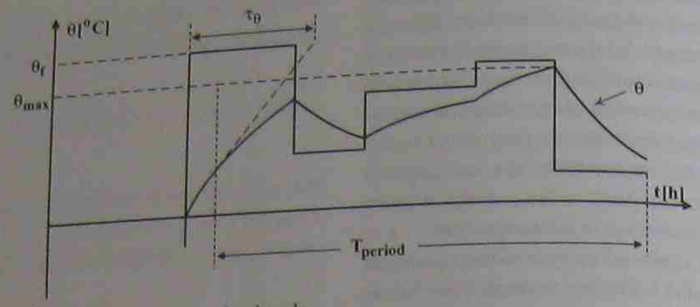



**FIGURE 6.19** Temperature transient during a load cycle.

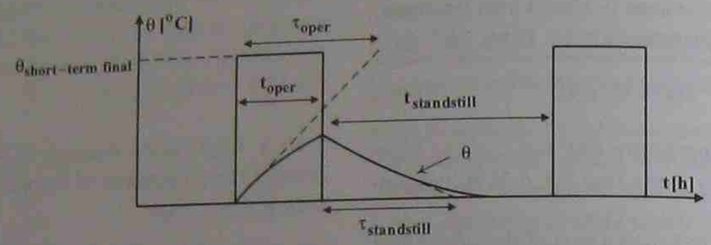



**FIGURE 6.20** Transient temperature for short-term operation.

### 6.14.1 Steady-State Operation

Steady-state temperature is reached when the operating time of the machine $t_{oper}$ is large as compared with the time constant $\tau_\theta$ of the machine. That is,

$$t_{oper} \geq (3\text{–}4) \cdot \tau_\theta. \tag{6-40}$$

According to experience the thermal time constant for openly ventilated machines is

$$\tau_\theta \approx 1 \text{ h} \tag{6-41}$$

and for enclosed but ventilated machines

$$\tau_\theta \approx (3\text{–}4) \text{ h}. \tag{6-42}$$

During steady-state operation the rated output power must be delivered by the machine.

### 6.14.2 Short-Term Operation

For short-term operation one assumes that the machine cools down to the ambient temperature and its temperature rise (initial temperature rise) is $\theta_0 = 0$. Fig. 6.20 illustrates the transient temperature of this operating mode.

The absence of any ventilation during standstill (time $t_{standstill}$) requires that the time constant during standstill be longer than that during operation (time $t_{oper}$), that is, $\tau_{standstill} > \tau_{oper}$. For short-term operation the times $t_{oper}$ and $t_{standstill}$ must relate to the time constants as follows:

$$t_{oper} < (3\text{–}4)\ \tau_{oper}, \tag{6-43}$$

$$t_{standstill} < (3\text{–}4)\ \tau_{standstill}. \tag{6-44}$$

The transient temperature is for short-term operation (see Fig. 6.20):

$$\theta_{short\text{-}term} = \theta_{rated} = \theta_{short\text{-}term_final}\left(1 - e^{\left(-\frac{t_{oper}}{\tau_{oper}}\right)}\right). \tag{6-45}$$

The final short-term temperature is obtained from Eq. 6-45:

$$\theta_{short\text{-}term_final} = \frac{\theta_{rated}}{\left(1 - e^{\left(-\frac{t_{oper}}{\tau_{oper}}\right)}\right)}. \tag{6-46}$$

with

$$\theta_{short\text{–}term_final} \propto P_{loss_short\text{–}term} \tag{6-47}$$

and

$$\theta_{rated} \propto P_{loss_rated}. \tag{6-48}$$



It follows for the losses during short-term operation:

$$P_{loss_short\text{-}term} = \frac{P_{loss_rated}}{\left(1 - e^{\left(-\frac{t_{oper}}{\tau_{oper}}\right)}\right)}. \tag{6-49}$$

For machines whose losses consist of iron-core and copper losses (e.g., induction machines) the total losses at rated operation are

$$P_{loss_rated} = p \cdot P_{rated} + q \cdot P_{rated}. \tag{6-50}$$

The first term of Eq. 6-50 pertains to the iron-core and the second term to the copper losses. The losses during short-term operation are

$$P_{loss_short\text{-}term} = p \cdot P_{rated} + q \cdot P_{rated}\left(\frac{P_{loss_short\text{-}term}}{P_{rated}}\right)^2. \tag{6-51}$$

Introducing Eqs. 6-50 and 6-51 into Eq. 6-49 yields the ratio

$$\frac{P_{loss_short\text{-}term}}{P_{rated}} = \sqrt{\left(1 + \frac{p}{q}\right)\frac{1}{1 - e^{\left(-\frac{t_{oper}}{\tau_{oper}}\right)}} - \frac{p}{q}}, \tag{6-52}$$

where the ratio $p/q$ is available from the manufacturer of the machine.

### 6.14.3 Steady State with Short-Term Operation

In this case the short-term load is superposed with the steady-state load (see Fig. 6.21). The operating time $t_{oper}$ and the pause time $t_{pause}$ relate to the time constant as follows:

$$t_{oper} < (3\text{–}4) \cdot \tau_\theta, \tag{6-53}$$

$$t_{pause} > (3\text{–}4) \cdot \tau_\theta, \tag{6-54}$$

and the ratio between the required power during steady-state with short-term load to the rated power is

$$\frac{P_{steady\text{-}state+short\text{-}time}}{P_{rated}} = \sqrt{\frac{1}{\left(1 - e^{\left(-\frac{t_{oper}}{\tau_\theta}\right)}\right)}}. \tag{6-55}$$

In Eq. 6-55 the iron-core losses are neglected ($p = 0$).

### 6.14.4 Intermittent Operation

The mode of intermittent operation occurs most frequently. One can differentiate between two cases:

- irregular load steps (see Fig. 6.22), and
- regular load steps.

The case with irregular load steps is discussed in Application Example 6.8.

The case with regular load steps can be approximated as follows based on Fig. 6.23:

$$\frac{P_{intermittent}}{P_{rated}} = \sqrt{\left(1 + \frac{p}{q}\right)\left(1 + \frac{t_{pause}}{t_{oper}} \cdot \frac{\tau_\theta}{\tau_{standstill}}\right) - \frac{p}{q}}. \tag{6-56}$$

### 6.14.5 Steady State with Intermittent Operation

Steady state with superimposed periodic intermittent operation (see Fig. 6.24) does not occur frequently. The ratio between the power required for this case and the rated power is

$$\frac{P_{steady\text{-}state+periodic\ intermittent}}{P_{rated}} = \sqrt{\left(1 + \frac{t_{pause}}{t_{oper}}\right)} \tag{6-57}$$

for $t_{oper} < (3\text{–}4)\tau\theta$ and $t_{pause} < (3\text{–}4)\tau\theta$. In summary one can state that for the motor sizing the maximum temperature (and not the torque) is important.

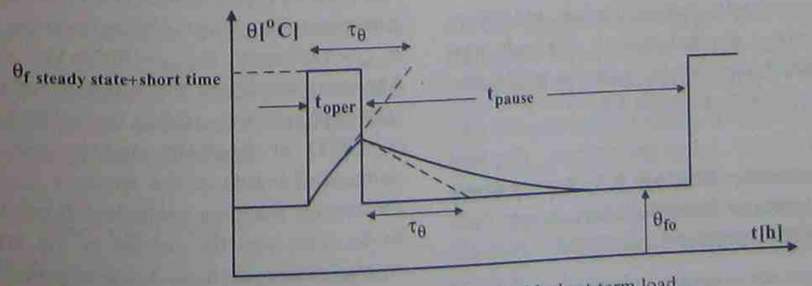



**FIGURE 6.21** Transient temperature for steady-state load superposed with short-term load.

COLLEGE OF LAFE

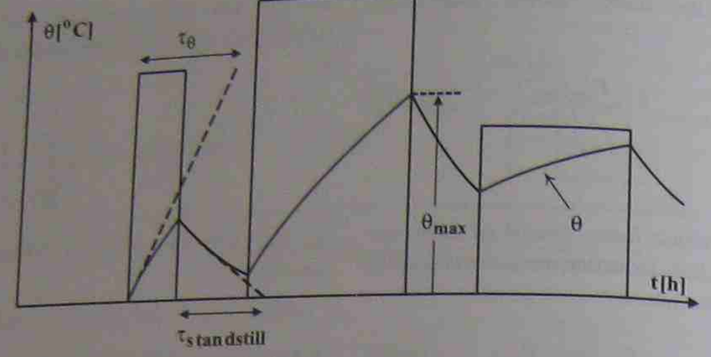



**FIGURE 6.22** Intermittent operation with irregular load steps.

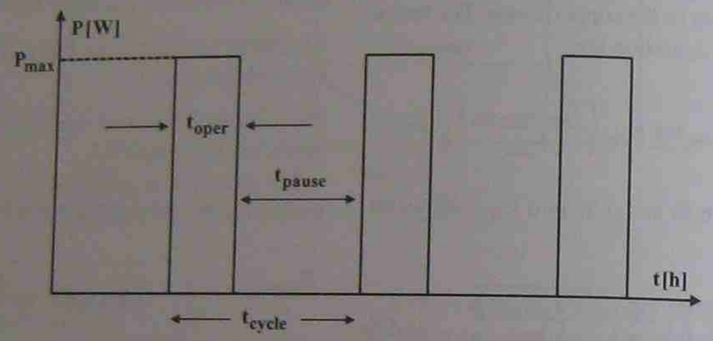



**FIGURE 6.23** Intermittent operation with regular load steps.

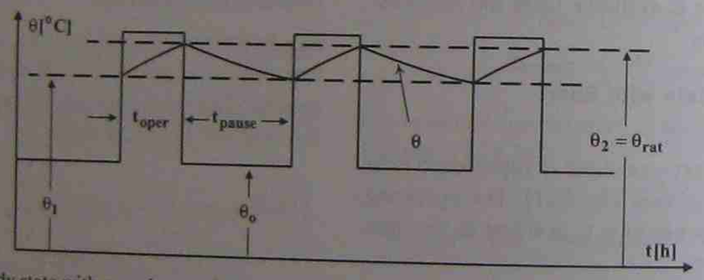



**FIGURE 6.24** Steady state with superimposed periodic intermittent operation with regular load steps.

Intermittent operation occurs in drives such as used in hybrid cars, wind-power plants, air-conditioning and refrigeration systems, and others. For this reason a detailed analysis of steady state with superposed intermittent operation will be presented in Application Example 6.8.

### 6.14.6 Application Example 6.8: Steady State with Superimposed Periodic Intermittent Operation with Irregular Load Steps

A three-phase, squirrel-cage induction motor is fed by a voltage-source inverter. The induction motor is operated at variable frequency and constant (rated) flux (that is, $|\tilde{E}|/f = \text{constant}$) and has the following nameplate data: $V_{L\text{-}L} = 460$ V, $f = 60$ Hz, $p = 4$ poles, $n_{m_rat} = 1720$ rpm, $P_{out_rat} = 29.594$ kW or 39.67 hp. The stator winding is Y-connected, and the parameters per phase are $R_s = 0.5\ \Omega, R'_r = 0.2\ \Omega, X_s = X'_r = 1\ \Omega$, $X_m = 30\ \Omega$ at $f = 60$ Hz, and $R_{fe} \to \infty$. The axial moment of inertia of the motor is $J_m = 0.234$ kgm$^2$, the viscous damping coefficient $B$ can be assumed to be zero, and the inertia of the load referred to the motor shaft is $J_{load} = 5$ kgm$^2$. The steady-state/intermittent load cycle is shown in Fig. E6.8.1.



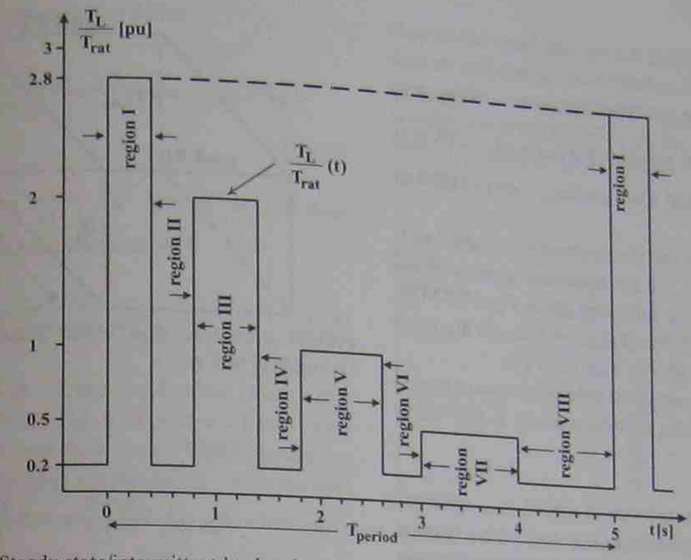



**FIGURE E6.8.1** Steady-state/intermittent load cycle.

The induction motor is operated at 60 Hz (natural torque-speed characteristic).

a) Determine the rated synchronous speed, rated synchronous angular velocity, rated angular velocity, rated slip, rated stator current $|\tilde{I}_s|$, rated rotor current $|\tilde{I}'_r|$, and rated induced voltage $|\tilde{E}|$.
b) Calculate the maximum torque $T_{max}$ at $s_m$ and the fictitious maximum torque $T_{max_fict}$ at $s = 1$.
c) Derive from the equation of motion the slip $s(t)$ as a function of the initial slip $s(0)$, the load torque $T_L(t)$, the maximum fictitious torque $T_{max_fict}$, the time constant $\tau_m$, and the time $t$.
d) Apply the solution for $s(t)$ to the different regions of Fig. E6.8.1 and plot $s(t)$ from $t = 0$ to the maximum time $t = 5$ s of the load-cycle time period of $T_{period} = 5$ s.
e) Calculate the torque $T(t)$ and plot it from $t = 0$ to $t = 5$ s.
f) Based on the slip function compute pointwise the stator current $|\tilde{I}_s(t)|$ and plot $|\tilde{I}_s(t)|$ from $t = 0$ to $t = 5$ s.
g) Plot $|\tilde{I}_s(t)|^2$ as a function of time from $t = 0$ to $t = 5$ s.
h) Determine the rms value of the motor (stator) current $i_s(t)$ for the entire load cycle as specified in Fig. E6.8.1; that is, determine

$$I_{s_rms} = \sqrt{\frac{1}{T}\int_{t}^{t+T} |\tilde{I}_s(t)|^2 dt}.$$

i) Is this induction motor over- or underdesigned? If it is underdesigned, what is the reduction of lifetime?

### 6.14.7 Reduction of Vibrations and Torque Pulsations in Electric Machines

Vibrations and torque pulsations generate electromagnetic forces that mainly act on the end turns of stator windings. As it is well known the turns residing in the stator slots are not exposed to high magnetic fields and for this reason the magnetic forces acting on the turns within the slots are relatively small. Besides increased temperatures, vibrations and torque pulsations are a major reason for the deterioration of the insulation materials. Vibrations and pulsating torques can have their origin in motor asymmetries (e.g., rotor eccentricities, interturn faults, cogging due to permanent magnets, and a poor selection of stator and rotor slotting [47]) and loads (e.g., piston compressors). For this reason it will be important to demonstrate how torque pulsations caused by loads can be reduced to an acceptable level. This will be the subject of Application Example 6.9.

### 6.14.8 Application Example 6.9: Reduction of Harmonic Torques of a Piston-Compressor Drive with Synchronous Motor as Prime Mover

The drive motor of a piston compressor is a nonsalient-pole synchronous motor with an amortisseur. To compensate for the piston stroke an eccentric shaft is employed. The load ($L$) torque at the eccentric shaft consists of an average torque and two harmonic torques:

$$T_L = T_{Lavg} + T_{L1} + T_{L4}, \qquad \text{(E6.9-1)}$$

21. LEIHKE COLLEGE LIBRARY

where

$$T_{Lavg} = 265.53 \text{ kNm}, \quad \text{(E6.9-2)}$$

$$T_{L1} = 31.04 \text{ kNm} \sin(\omega_{ms} t - \pi), \quad \text{(E6.9-3)}$$

$$T_{LA} = 50.65 \text{ kNm} \sin(4\omega_{ms} - \pi/6). \quad \text{(E6.9-4)}$$

The drive motor and the flywheel are coupled with the eccentric shaft, and the nonsalient-pole synchronous motor has the following data: $P_{rat} = 7.5$ MW, $p = 28$ poles, $f = 60$ Hz, $V_{L\text{-}Lrat} = 6$ kV, $\cos \Phi_{rat} = 0.9$ overexcited, $\eta_{rat} = 96.9\%$, $T_{max}/T_{rat} = 2.3$.

The slip of the nonsalient pole synchronous motor when operating as an induction motor is $s_{rat} = 6.8\%$ at $T_{rat}$.

a) Calculate the synchronous speed $n_{ms}$, synchronous angular velocity $\omega_{ms}$, rated stator current $\bar{I}_{a_rat}$, rated torque $T_{rat}$, the torque angle $\delta$, stator current $\bar{I}_a$ at $T_{Lavg}$ and the synchronous reactance $X_s$ (in ohms and in per unit).
b) Neglecting damping provided by induction-motor action, derive the nonlinear differential equation for the motor torque, and by linearizing this equation find an expression for the eigen angular frequency $\omega_{eigen}$ of the undamped motor.
c) Repeat part b, but do not neglect damping provided by induction motor action.
d) Solve the linearized differential equations of part b (without damping) and part c (with damping) and determine – by introducing phasors – the axial moment of inertia $J$ required so that the first harmonic motor torque will be reduced to ±4% of the average torque (Eq. E6.9-2).
e) Compare the eigen frequency $f_{eigen}$ with the pulsation frequencies occurring at the eccentric shaft.
f) State the total motor torque $T(t)$ as a function of time (neglecting damping) for one revolution of the eccentric shaft and compare it with the load torque $T_L(t)$. Why are they different?

### 6.14.9 Calculation of Steady-State Temperature Rise $\Delta T$ of Electric Apparatus Based on Thermal Networks

The losses of an electric apparatus (e.g., rotating machine, transformer, and inductor) heat up various parts of the apparatus, and the losses are dissipated via heat conduction, convection, and radiation.

**Heat Flow Related to Conduction.** Assume that the losses at end #2 with the temperature $\theta_2$ of a homogeneous body (see Fig. 6.25) are

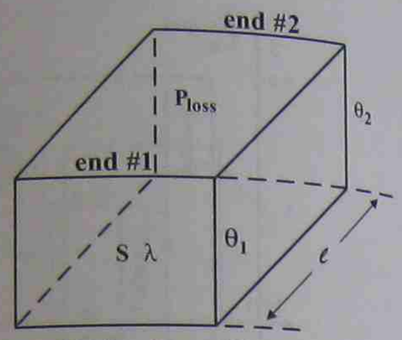



**FIGURE 6.25** Heat flow within a homogeneous body (principle of heat pipe).

$$P_{loss} = \lambda \cdot S \frac{\theta_2 - \theta_1}{\ell} = \lambda \cdot S \frac{\Delta T}{\ell}, \quad \text{(6-58)}$$

where $\lambda$ is the thermal conductivity of a homogeneous body measured in $\left[\frac{W}{m°C}\right]$, $S$ is the surface of the homogeneous body perpendicular to the heat flow measured in m$^2$, and $\ell$ is the length of the homogeneous body along the direction of the heat flow measured in $m$.

The temperature at end #1 $\theta_1$ is given by Eq. 6-58:

$$\Delta T = (\theta_2 - \theta_1) = \frac{\ell}{\lambda \cdot S} P_{loss} = R_{conduct} \cdot P_{loss}, \quad \text{(6-59)}$$

where the term $\left[\frac{\ell}{\lambda \cdot S}\right]$ is defined as the heat conduction resistance

$$R_{conduct} = \frac{\ell}{\lambda \cdot S} \quad \text{(6-60)}$$

**Heat Flow Related to Radiation and Convection.** The heat flow due to radiation and convection from the heat source to the cooling medium (e.g., ambient air) is proportional to the surface $A$ of the body (e.g., winding) on which the heat source resides and its temperature difference $\Delta T = (\theta_2 - \theta_1)$ with respect to the cooling medium:

$$P_{loss} = \alpha \cdot A(\theta_2 - \theta_1), \quad \text{(6-61a)}$$

where $\alpha$ is the thermal conductivity measured in $\left[\frac{W}{m^2°C}\right]$ between the heat source and the cooling medium.





Correspondingly, one can define

$$\Delta T = (\theta_2 - \theta_1) = \frac{1}{\alpha \cdot A} P_{loss} = R_{radiation/convection} \cdot P_{loss} \quad \text{(6-61b)}$$

where the term $\frac{1}{\alpha \cdot A}$ is defined as the heat radiation/convection resistance

$$R_{radiation/convection} = \frac{1}{\alpha \cdot A}. \quad \text{(6-62)}$$

The application of the conduction relationship (Eq. 6-59) generates Fig. 6.26, where a linear function leads to the heat flow from a high-temperature body #2 (e.g., winding) via insulation – with the heat conduction resistance $R_{conduct} = \frac{\ell}{\lambda \cdot S}$ – to a low-temperature body #1 (e.g., iron core).

The application of the radiation/convection relationship (Eq. 6-61) generates Fig. 6.27, where a step function leads to the heat flow from a high-temperature body #2 (e.g., frame) – with the heat radiation/convection resistance $R_{radiation/convection} = \frac{1}{\alpha \cdot A}$ – to a low-temperature body #1 (e.g., ambient air). An example for this case is the interface between the motor frame and the ambient air.

Figure 6.28 depicts the heat flow as it occurs from a winding via the insulation, the iron core, the small air gap between iron core and frame, and from the frame of an electrical apparatus to the ambient air serving as cooling medium. Note that the heat drop in the small air gap is a mixture between conduction and convection/radiation. The reason is that some of the iron core laminations have contact (heat transfer via conduction) with the frame and some have no contact (heat transfer via convection/radiation).

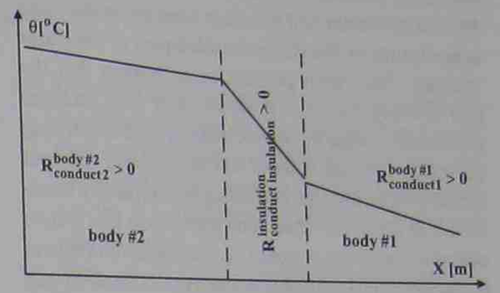



**FIGURE 6.26** Linear heat flow through conduction from a high-temperature body #2 to a low-temperature body #1 with finite thermal resistances.

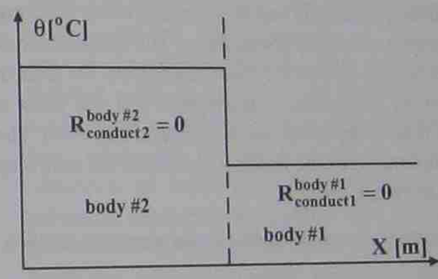



**FIGURE 6.27** Step-function heat flow through convection/radiation from a high-temperature body to a low-temperature cooling medium.

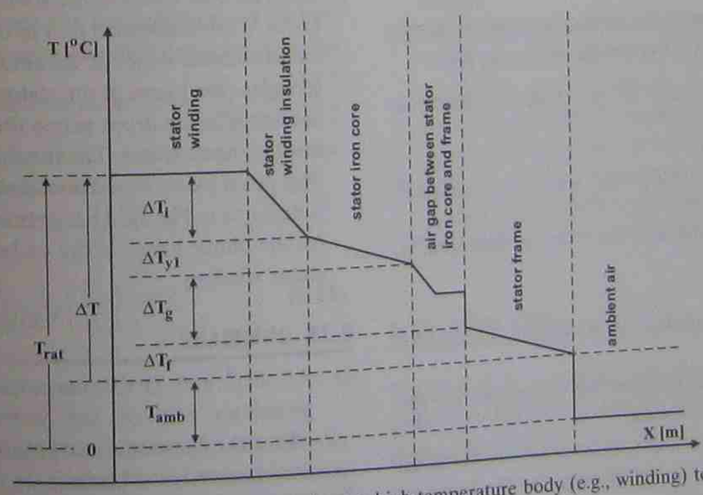



**FIGURE 6.28** Heat flow within electrical apparatus from a high-temperature body (e.g., winding) to a low-temperature cooling medium (e.g., ambient air).

### 6.14.10 Application Example 6.10: Temperature-Rise Equations for a Totally Enclosed Fan-Cooled 100 hp Motor

For a totally enclosed fan-cooled motor [48] the surface of the external frame dissipates the heat. The ribs are located along the axis of the machine where the hot air is removed by a fan. Test results show [49, 50] that the stator end windings have about the same temperature as the slot-embedded part of the stator winding. This result permits us to assume that the end winding does not dissipate heat (e.g., radiates and removes heat by convection) to the surrounding air inside the end bells of the motor, and the heat developed by the stator winding is completely transferred to the stator core. The stator iron loss is then added to the stator copper loss and the resultant heat is transferred to the stator frame via the small air gap between core and frame from which it is removed by the fan through radiation and convection. A second assumption refers to the heat of the rotor winding. It is assumed that this heat is transferred to the stator. This means that the temperature of the rotor is higher than that of the stator. The temperature of the hottest spot in the stator determines the class of winding insulation. It is assumed that this point is residing in the stator winding inside a stator slot. The temperature of the hot spot consists of the following temperature drops:

- temperature drop across stator winding insulation, $\Delta T_i$
- temperature drop across stator back iron (yoke), $\Delta T_{y1}$
- temperature drop across the small air gap between the stator back iron and the frame of the motor, $\Delta T_g$
- difference between the temperature of the frame and the ambient temperature of the air, $\Delta T_f$.

The temperature rise of the stator winding is therefore

$$\Delta T = \Delta T_i + \Delta T_{y1} + \Delta T_g + \Delta T_f \qquad \text{(E6.10-1)}$$

The thermal network of the motor is shown in Fig. E6.10.1, where

$R_i$ is the thermal conductivity resistance of the stator slot insulation

$R_{y1}$ is the thermal conductivity resistance of the stator back iron or yoke

$R_g$ is the thermal conductivity resistance of the small air gap between the stator core and the frame of the motor



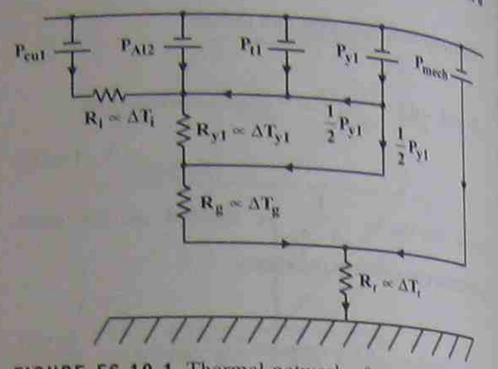



**FIGURE E6.10.1** Thermal network of a totally enclosed fan-cooled induction motor.

$R_f$ is the thermal radiation/convection resistance of the outside of the stator frame and the moving air

$P_{cu1}$ is the stator ohmic (copper) loss

$P_{Al2}$ is the rotor ohmic (aluminum) loss

$P_{t1}$ is the stator teeth (iron-core) loss

$P_{y1}$ is the stator yoke (iron-core) loss

$P_{mech}$ is the friction (bearing, windage) loss

### 6.14.11 Application Example 6.11: Temperature-Rise Equations for a Drip-Proof 5 hp Motor

The temperature rise equation is written for a drip-proof motor [48]. This equation is based on the following assumptions:

1. The ohmic losses in the embedded part of the stator winding produce a temperature drop across the slot insulation.
2. The iron-core losses of the stator teeth, the ohmic losses in the embedded part of the stator winding, and the ohmic losses of the rotor bars and half of the iron-core losses of the stator back iron generate temperature drops across the stator back iron and the motor frame. The thermal network of this drip-proof motor based on the above assumptions is depicted in Fig. E6.11.1. In this figure $P_{em}$ stands for the ohmic losses in the embedded part of the stator winding.

## 6.15 SUMMARY

1) All IEC and IEEE harmonic standards and guidelines rely on the worst-case condition where the harmonic current or voltage spectra are independent of time.
2) The weighted-harmonic voltage factor is based on the same assumption and estimates the additional temperature rise for rated operation of transformers, induction motors, and universal motors for the voltage spectrum with maximum individual harmonic voltage amplitudes.
3) The weighted-harmonic voltage factor

$$\sum_{h=2}^{\infty} \frac{1}{(h)^k}\left(\frac{V_h}{V_1}\right)^l \qquad \text{(6-63)}$$

described in this chapter is related to the square of the total harmonic distortion of the voltage

$$THD_v = \sqrt{\sum_{h=2}^{\infty}\left(\frac{V_h}{V_1}\right)^2} \qquad \text{(6-64)}$$

by introducing the weighting function $\left(\frac{1}{h}\right)^k$ and replacing the exponent 2 of the ratio by $\sum_{h=2}^{\infty}\frac{1}{(h)^k}\left(\frac{V_h}{V_1}\right)^2$ by the exponent $l$.

4) $\sum_{h=2}^{\infty}\frac{1}{(h)^k}\left(\frac{V_h}{V_1}\right)^l$ can be used as a measure for the losses and temperature rises of electromagnetic apparatus due to harmonic voltages.
5) Acceptable limits for the reduction of lifetime due to thermal aging requires limits for the value of the weighted-harmonic factor $\sum_{h=2}^{\infty}\frac{1}{(h)^k}\left(\frac{V_h}{V_1}\right)^l$ and indirectly limits the amplitude of the occurring voltage harmonics.
6) A weighted harmonic factor of

$$\sum_{h=2}^{\infty}\frac{1}{(h)^k}\left(\frac{V_h}{V_1}\right)^l = 5.8 \qquad \text{(6-65)}$$

is recommended.

7) It is evident that for a given weighted-harmonic voltage factor, single- and three-phase induction machines are more susceptible to aging than transformers and universal machines.



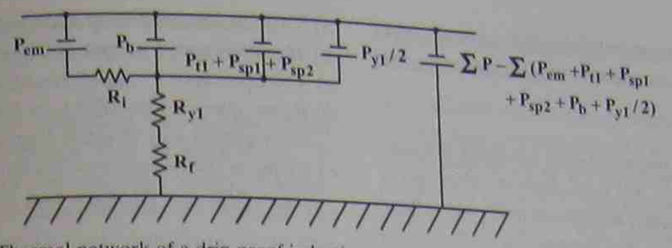



**FIGURE E6.11.1** Thermal network of a drip-proof induction motor.

8) Strictly speaking, all current or voltage harmonic spectra are continually changing as a function of time due to changing system configuration and loads, and the assumption of time-independent spectra is a simplification leading to a first-cut approach only.
9) The cost of harmonics incurs by either purchasing more expensive solid-state equipment (e.g., PWM inverters, switched-mode power supplies), which generates a reduced amount of harmonics, or by using less-sophisticated but harmonic generating equipment (e.g., six-step inverters, diode rectifiers), which generate a greater amount of harmonics than the more expensive switched-mode equipment. In the first case the losses occur in the switched-mode equipment (e.g., efficiencies ranging from 80 to 98%), whereas in the second case of less-sophisticated solid-state equipment (e.g., efficiencies ranging from 90 to 98%) the harmonic losses incur in the loads (e.g., induction motors) and their reduction of lifetime must be accounted for due to temperature increase.
10) Design considerations for intermittent operation are presented so that no lifetime reduction occurs.
11) Most drives are subjected to pulsating loads that cause vibrations within the drive motor, in particular the motor windings. To limit vibrations to a certain value the required axial moment of inertia J of a flywheel is calculated.
12) The temperature rises for totally enclosed fan-cooled and for drip-proof induction motors are derived.

## 6.16 PROBLEMS

### Problem 6.1: Aging of Transformers and Induction Machines Due to Single Harmonic Voltage

The terminal voltage of a single-phase transformer (rated resistive load) and a single-phase induction

machine (operation at rated load) contains a third-harmonic voltage component of $V_{h3}/V_{h1} = 2.5\%, 5\%,$ and 7.5%.

a) Determine for the worst-case condition the temperature rises $\Delta T$ for both devices, which occur due to the previously mentioned harmonic voltage components. You may assume for both devices a rated temperature of $T_{rat} = T_2 = 125°C$ at an ambient temperature of $T_{amb} = 40°C$.
b) Calculate for the temperature rises $\Delta T$ of part a the decrease of lifetime for both devices under the given three (not simultaneously occurring) harmonic voltage components for an activation energy of $E = 1.15$ eV.

### Problem 6.2: Operation of Induction Motor at Reduced Line-to-Line Voltage

A 100 hp, 480 $V_{L\text{-}L}$, 60 Hz, 6-pole three-phase induction motor runs at full load and rated voltage with a slip of 3%. Under conditions of stress on the power supply system, the line-to-line voltage drops to 420 $V_{L\text{-}L}$. If the load is of the constant torque type, then compute for the lower voltage

a) The slip (use small slip approximation).
b) The shaft speed in rpm.
c) The hp output.
d) The rotor copper loss ($I_2^2 r_2$) in terms of the rated rotor copper loss at rated voltage.
e) Estimate the reduction of lifetime due to reduced voltage operation provided the rated temperature is $T_{rat} = 125°C$, the ambient temperature is $T_{amb} = 40°C$, rated lifetime is $t_2 = 40$ years, and $E = 1.15$ eV.

### Problem 6.3: Operation of Induction Motor at Increased Line-to-Line Voltage

Repeat Problem 6.2 for the condition when the line-to-line voltage of the power supply system increases to 520 $V_{L\text{-}L}$, and estimate the reduction of lifetime.

### Problem 6.4: Reduced Voltage and Frequency Operation of Induction Machines

A 100 hp, 480 $V_{L\text{-}L}$, 60 Hz, 6-pole three-phase induction motor runs at full load and rated voltage and frequency with a slip of 3%. Under conditions of stress on the power supply system the terminal voltage and the frequency drops to 420 $V_{L\text{-}L}$ and 54 Hz, respectively. If the load is of the constant torque type, then compute for the lower voltage and frequency:

a) The slip (use small slip approximation).
b) The shaft speed in rpm.
c) The hp output.
d) Rotor copper loss ($I_2^2 r_2$) in terms of the rated rotor copper loss at rated frequency and voltage.
e) Estimate the reduction of lifetime for $T_{rat} = 125°C$, $T_{amb} = 40°C$, $t_2 = 40$ years, and $E = 1.15$ eV.

### Problem 6.5: Lifetime Reduction of Induction Motors and Transformers for Given Voltage Spectra

Estimate the lifetime reductions of induction machines, transformers, and universal machines for the single- and three-phase voltage spectra of Table P6.5, and their associated lifetime reductions for an activation energy of $E = 1.15$ eV. The ambient temperature is $T_{amb} = 40°C$, the rated temperature is $T_2 = 120°C$, and the rated lifetime of $t_2 = 40$ years can be assumed.

### Problem 6.6: Calculate the Stator rms Current of an Induction Motor at Steady-State Operation with Superimposed Intermittent, Irregular Load Steps

Repeat the analysis of Application Example 6.8 provided the inverter-motor drive is operated at $f = 30$ Hz with constant flux, $(E/f) = \text{constant}$, control.

**TABLE P6.5** Possible voltage spectra with high-harmonic penetration

| $h$ | $\left(\frac{V_h}{V_{60\,Hz}}\right)_{1\Phi}$ (%) | $\left(\frac{V_h}{V_{60\,Hz}}\right)_{3\Phi}$ (%) |
|---|---|---|
| 1 | 100 | 100 |
| 2 | 0.5 | 0.5 |
| 3 | 7.0 | 0.5 |
| 4 | 1.6 | 0.5 |
| 5 | 5.0 | 7.5 |
| 6 | 0.88 | 0.2 |
| 7 | 3.0 | 5.0 |
| 8 | 0.62 | 0.2 |
| 9 | 2.0 | 0.3 |
| 10 | 0.66 | 0.1 |
| 11 | 1.0 | 4.0 |
| 12 | 0.18 | 0.1 |
| 13 | 0.8 | 3.0 |
| 14 | 0.10 | 0.05 |
| 15 | 0.10 | 0.1 |
| 16 | 0.13 | 0.05 |
| 17 | 0.23 | 1.5 |
| 18 | 0.22 | 0.05 |
| 19 | 1.03 | 1.0 |
| All higher harmonics < 0.2% | | |





### Problem 6.7: Calculate the Reduction of Harmonic Synchronous Motor Torques for a Given Time-Dependent Load

The drive motor of a pulsating load is a nonsalient-pole synchronous motor with an amortisseur. To compensate for the changing load torque as a function of time a flywheel is coupled with the shaft. The load ($L$) torque at the shaft consists of an average torque and two harmonic torques:

$$T_L = T_{Lavg} + T_{L1} + T_{L3}, \qquad \text{(P6.7-1)}$$

where

$$T_{Lavg} = 260 \text{ kNm}, \qquad \text{(P6.7-2)}$$

$$T_{L1} = 30 \text{ kNm} \sin(\omega_{rm} t - \pi), \qquad \text{(P6.7-3)}$$

$$T_{L3} = 50 \text{ kNm} \sin(3\omega_{rm} - \pi/6). \qquad \text{(P6.7-4)}$$

The nonsalient-pole synchronous motor has the following data: $P_{rat} = 5$ MW, $p = 40$ poles, $f = 60$ Hz, $V_{L\text{-}L,rat} = 6$ kV, $\cos \Phi_{rat} = 0.8$ overexcited, $\eta_{rat} = 95\%$, $T_{max}/T_{rat} = 2.5$. The slip of the nonsalient pole synchronous motor when operating as an induction motor is $s_{rat} = 6\%$ at $T_{rat}$.

a) Calculate the synchronous speed $n_{rm}$, synchronous angular velocity $\omega_{rm}$, rated stator current $\tilde{I}_{s,rat}$, rated torque $T_{rat}$, the torque angle $\delta$, stator current $\tilde{I}_s$ at $T_{Lavg}$ and the synchronous reactance $X_s$ (in ohms and in per unit).
b) Neglecting damping provided by induction-motor action, derive the nonlinear differential equation for the motor torque, and by linearizing this equation find an expression for the eigen angular frequency $\omega_{eigen}$ of the undamped motor.
c) Repeat part b, but do not neglect damping provided by induction motor action.
d) Solve the linearized differential equations of part b (without damping) and part c (with damping) and determine – by introducing phasors – the axial moment of inertia J required so that the first harmonic order motor torque will be reduced to ±2% of the average torque (Eq. P6.7-2).
e) Compare the eigen frequency $f_{eigen}$ with the pulsation frequencies occurring at the eccentric shaft.
f) State the total motor torque $T(t)$ as a function of time (neglecting damping) for one revolution of the eccentric shaft and compare it with the load torque $T_L(t)$. Why are they different?

### Problem 6.8: Temperature Transient of an Induction Machine

An enclosed fan-cooled induction motor has a thermal time constant of $\tau_\theta = 4$ h and a steady-state rated temperature of $\theta_f = 140°C$ at an ambient temperature of $\theta_{amb} = 40°C$. The motor has at time $t = 0-$ a temperature of $\theta = \theta_{amb}$, and the motor is fully loaded at $t = 0+$. Calculate the time $t_{95\%}$ when the fully loaded motor reaches 95% of its final temperature $\theta_f = 140°C$.

### Problem 6.9: Calculation of the Temperature Rise of a Totally Enclosed Fan-Cooled 100 hp Induction Motor

a) Based on Application Example 6.10 calculate the temperature rise $\Delta T$ of a totally enclosed fan-cooled induction motor provided the following data are given: Input power $P_{in} = 79{,}610$ W, output power $P_{out} = 74{,}600$ W, line frequency $f = 60$ Hz, thickness of stator slot insulation $\beta_i = 9 \cdot 10^{-4}$ m, thermal conductivity of stator slot insulation $\lambda_i = 0.109$ W/m°C, total area of the stator slots $S_i = 2.006$ m$^2$, thermal conductivity of the stator laminations (iron core) $\lambda_c = 47.24$ W/m°C, radial height of stator back iron $h_{y1} = 0.049$ m, cross-sectional area of the stator core at the middle of the stator back iron (stator yoke) $S_{y1} = 0.482$ m$^2$, length of the small air gap between the stator core and the frame of the motor $\beta_\delta = 3 \cdot 10^{-5}$ m, thermal conductivity of the small air gap between stator core and frame $\lambda_\delta = 0.028$ W/m°C, outside surface area of the stator frame $S_\delta = 0.563$ m$^2$, surface thermal coefficient for dissipation of heat to stationary air $\alpha_0 = 14.30$ W/m$^2$°C, surface thermal coefficient for dissipation of heat to moving air at $v = 16$ m/s $\alpha_v = 88.66$ W/m$^2$°C, surface area in contact with stationary air $S_0 = 0.841$ m$^2$, and surface area in contact with moving air $S_v = 3.36$ m$^2$. Table P6.9 details the percentage values of the various losses of the 100 hp induction motor. Note that the iron core losses of the rotor are very small due to the low frequency in the rotor member (slip frequency).
b) Determine the rated temperature of the motor $T_{rat}$ provided the ambient temperature is $T_{amb} = 40°C$.

**TABLE P6.9** Percentage Losses of a 100 hp Three-Phase Induction Motor

| $P_{out}$ | $P_{st}$ | $P_{rt}$ | $P_{sp}$ | $P_{Ad}$ | $P_{sp2}$ | $P_{mech}$ |
|---|---|---|---|---|---|---|
| 30% | 8% | 10% | 2% | 45% | 2% | 3% |

### Problem 6.10: Calculation of the Temperature Rise of a Drip-Proof 5 hp Induction Motor

a) Based on Application Example 6.11 calculate the temperature rise $\Delta T$ of a drip-proof induction motor provided the following data are given: Input power $P_{in} = 4355$ W, output power $P_{out} = 3730$ W, line frequency $f = 60$ Hz, thickness of stator slot insulation $\beta_i = 6 \cdot 10^{-4}$ m, thermal conductivity of stator slot insulation $\lambda_i = 0.148$ W/m°C, total area of the stator slots $S_i = 0.0701$ m$^2$, thermal conductivity of the stator laminations (iron core) $\lambda_c = 47.24$ W/m°C, radial height of stator back iron $h_{y1} = 0.0399$ m, cross-sectional area of the stator core at the middle of the stator back iron (stator yoke) $S_{y1} = 0.0325$ m$^2$, length of the small air gap between the stator core and the frame of the motor $\beta_\delta = 5 \cdot 10^{-6}$ m, thermal conductivity of the small air gap between stator core and frame $\lambda_\delta = 0.236$ W/m°C, outside surface area of the stator frame $S_\delta = 0.0403$ m$^2$, surface thermal coefficient for dissipation of heat to stationary air $\alpha_o = 18.70$ W/m$^{2o}$C, surface thermal coefficient for dissipation of heat to moving air at $v = 4.6$ m/s $\alpha_v = 58.81$ W/m$^{2o}$C, surface area in contact with stationary air $S_o = 0.181$ m$^2$, and surface area in contact with moving air $S_v = 0.696$ m$^2$. Table P6.10 details the percentage values of the various losses of the 5 hp induction motor. Note that the iron-core losses of the rotor are very small due to the low frequency in the rotor member (slip frequency).

b) Determine the rated temperature of the motor $T_{rat}$ provided the ambient temperature is $T_{amb} = 40$°C.

### Problem 6.11: Solution of the Partial Differential Equation Governing Heat Conduction

The solution of the heat equation in one spatial dimension ($x$)

$$\frac{\partial T(x,t)}{\partial t} = c^2 \frac{\partial^2 T(x,t)}{\partial x^2} \qquad \text{(P6.11-1)}$$

is based on the separation of variables as was proposed by Fourier, where $T$ is the temperature and $x$ is the spatial coordinate as illustrated, for example, in Fig. P6.11, and $t$ is the time. The boundary conditions are

$$T(0, t) = 0 \text{ and } T(\ell, t) = 0 \qquad \text{(P6.11-2)}$$

for all times $t$, and the initial condition at $t = 0$ is

$$T(x, 0) = f(x), \qquad \text{(P6.11-3)}$$

where $f(x)$ is a given function of $x$.

The temperature $T(x, t)$, is assumed separable in $x$ and $t$.

$$T(x, t) = X(x) \cdot T(t) \qquad \text{(P6.11-4)}$$

so that

$$X'' \cdot T = \frac{1}{c^2} X \cdot T', \qquad \text{(P6.11-5)}$$

or after dividing by $X(x)T(t)$

$$\frac{X''}{X} = \frac{1}{c^2}\frac{T'}{T} = k, \qquad \text{(P6.11-6)}$$

where $k$ is the separation constant. We can expect $k$ to be negative as can be seen from the time equation:

$$T' = c^2 k T \qquad \text{(P6.11-7)}$$

or after integration

$$T(t) = T_O e^{c^2 k T}. \qquad \text{(P6.11-8)}$$

Thus $T(t)$ will increase in time if $k$ is positive and decrease in time if $k$ is negative. The increase of $T$ in time is not possible without any additional heating mechanism and therefore we assume that $k$ is negative. To force this we set $k = -p^2$. The spatial differential equation is now

$$X'' + p^2 X = 0, \qquad \text{(P6.11-9)}$$

which is similar to the harmonic motion equation with the trigonometric solution

$$X(x) = A \cos px + B \sin px. \qquad \text{(P6.11-10)}$$

Now, applying the boundary condition, we find that for

$$X(0) = 0, \quad X(\ell) = 0. \qquad \text{(P6.11-11)}$$

$A = 0$ and $\sin(p\ell) = 0$, resulting in $p\ell = n\pi$. We take the most general solution by adding together all possible solutions, satisfying the boundary conditions, to obtain

$$T(x, t) = \sum_{n=0}^{\infty} B_n \sin\frac{n\pi}{\ell} e^{\frac{n^2\pi^2c^2}{\ell^2}t}. \qquad \text{(P6.11-12)}$$

The final step is to apply the initial conditions

$$T(x, 0) = \sum_{n=0}^{\infty} B_n \sin\frac{n\pi}{\ell} = f(x). \qquad \text{(P6.11-13)}$$

Finding the Fourier coefficient of the above expression leads to

$$B_n = \frac{2}{\ell}\int_0^{\ell} f(x)\sin\frac{n\pi}{\ell}x\,dx \qquad \text{(P6.11-14)}$$

for all positive integers $n$.

Note that because every term in the solution for $T(x, t)$ has a negative exponential in it, the temperature must decrease in time, and the final solution will tend to $T = 0$.

a) For $c^2 = 1$, $\ell = 1$, that is, $\frac{\partial T(x,t)}{\partial t} = \frac{\partial^2 T(x,t)}{\partial x^2}$, the boundary conditions $T(0, t) = T(1, t) = 0$, and the initial condition $T(x, 0) = f(x) = -4x^2 + 4x$ find $T(x, t)$ for $0 < x < 1$. The initial conditions and boundary conditions are shown in Fig. P6.11 as a function of the spatial coordinate $x$ and the time $t$. Calculate and plot $T(x, t)$ as a function of $x$ for $t = 1$ ms; thereby it will be sufficient to take into account three terms of the Fourier series.

b) For $c^2 = 1$, $\ell = 1$, that is, $\frac{\partial T(x,t)}{\partial t} = \frac{\partial^2 T(x,t)}{\partial x^2}$, the boundary conditions $T(0, t) = T(1, t) = 0$, and the initial conditions $T(x, 0) = f(x) = x$ (for $0 < x < 1/2$) and $T(x, 0) = f(x) = 1 - x$ (for $1/2 < x < 1$) find $T(x, t)$. Calculate and plot $T(x, t)$ as a function of $x$ for $t = 1$ ms; thereby it will be sufficient to take into account three terms of the Fourier series.

**TABLE P6.10** Percentage Losses of a 5 hp Three-Phase Induction Motor

| $P_{out}$ | $P_{s1}$ | $P_{r1}$ | $P_{sp1}$ | $P_{AD}$ | $P_{sp2}$ | $P_{mech}$ |
|---|---|---|---|---|---|---|
| 30% | 8% | 10% | 2% | 42% | 2% | 6% |



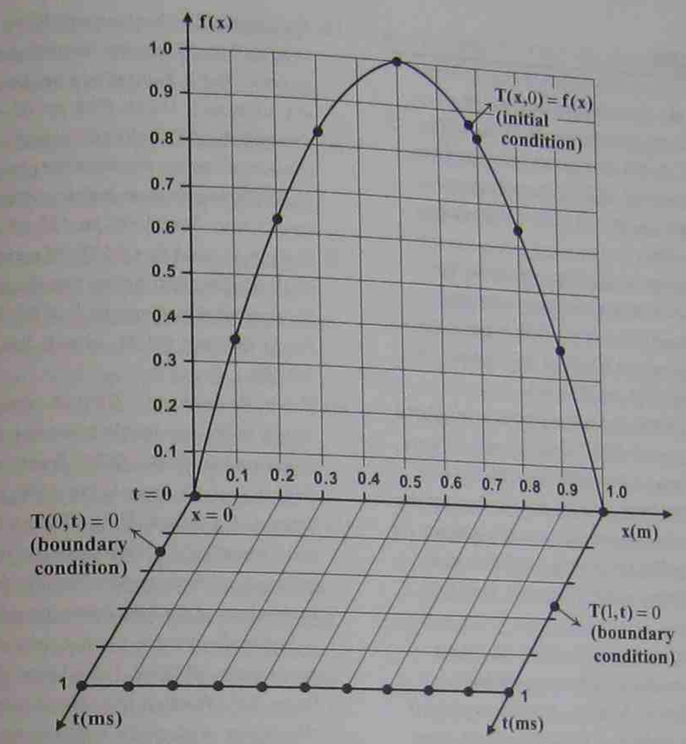



**FIGURE P6.11** Heat conduction in a homogeneous one-dimensional body of length $\ell = 1$ m.

## 6.17 REFERENCES


1) Montsinger, V.M.; "Loading transformer by temperature," *Trans. AIEE*, vol. 49, 1930, p. 776.
2) Pierce, L.W.; "Thermal considerations in specifying dry-type transformers," *IEEE Transactions on Industry Applications*, vol. 30, issue 4, July–Aug. 1994, pp. 1090–1098.
3) Yan, T.; and Zhongyan, H.; "The calculating hot-point temperature-rise of transformer windings," *ICEMS 2001, Proceedings of the Fifth International Conference on Electrical Machines and Systems 2001*, vol. 1, 18–20 Aug. 2001, pp. 220–223.
4) Pierce, L.W.; "Hottest spot temperatures in ventilated dry type transformers," *IEEE Transactions on Power Delivery*, vol. 9, issue 1, Jan. 1994, pp. 257–264.
5) Radakovic, Z.; and Feser, K.; "A new method for the calculation of the hot-spot temperature in power transformers with ONAN cooling," *IEEE Transactions on Power Delivery*, vol. 18, issue 4, Oct. 2003, pp. 1284–1292.
6) Okoro, O.I.; Weidemann, B.; and Ojo, O.; "An efficient thermal model for induction machines," 2004. 39th IAS Annual Meeting, *Conference Record of the 2004 IEEE Industry Applications Conference*, vol. 4, 3–7 Oct. 2004, pp. 2477–2484.
7) Pierce, L.W.; "Predicting liquid filled transformer loading capability," *IEEE Transactions on Industry Applications*, vol. 30, issue 1, Jan.–Feb. 1994, pp. 170–178.
8) Weekes, T.; Molinski, T.; and Swift, G.; "Transient transformer overload ratings and protection," *IEEE Electrical Insulation Magazine*, vol. 20, issue 2, Mar.–Apr. 2004, pp. 32–35.
9) Moreno, J.F.; Hidalgo, F.P.; and Martinez, M.D.; "Realisation of tests to determine the parameters of the thermal model of an induction machine," *IEEE Proceedings – Electric Power Applications*, vol. 148, issue 5, Sept. 2001, pp. 393–397.
10) Sang-Bin, L.; and Habetler, T.G.; "An online stator winding resistance estimation technique for temperature monitoring of line-connected induction machines," *IEEE Transactions on Industry Applications*, vol. 39, issue 3, May–June 2003, pp. 685–694.
11) Siyambalapitiya, D.J.T.; McLaren, P.G.; and Tavner, P.J.; "Transient thermal characteristics of induction machine rotor cage," *IEEE Transactions on Energy Conversion*, vol. 3, issue 4, Dec. 1988, pp. 849–854.
12) Duran, M.J.; and Fernandez, J.; "Lumped-parameter thermal model for induction machines," *IEEE Transactions on Energy Conversion*, vol. 19, issue 4, Dec. 2004, pp. 791–792.
13) Rajagopal, M.S.; Seetharamu, K.N.; and Ashwathnarayana, P.A.; "Transient thermal analysis of induction motors," *IEEE Transactions on Energy Conversion*, vol. 13, issue 1, March 1998, pp. 62–69.
14) Pierce, L.W.; "Transformer design and application considerations for nonsinusoidal load currents," *IEEE Transactions on Industry Applications*, vol. 32, issue 3, May–June 1996, pp. 633–645.
15) Galli, A.W.; and Cox, M.D.; "Temperature rise of small oil-filled distribution transformers supplying nonsinusoidal load current," *IEEE Transactions on Power Delivery*, vol. 11, issue 1, Jan. 1996, pp. 283–291.
16) Picher, P.; Bolduc, L.; Dutil, A.; and Pham, V.Q.; "Study of the acceptable dc current limit in core-form power transformers," *IEEE Transactions on Power Delivery*, vol. 12, issue 1, Jan. 1997, pp. 257–265.
17) Sousa, G.C.D.; Bose, B.K.; Cleland, J.; Spiegel, R.J.; and Chappell, P.J.; "Loss modeling of converter induction machine system for variable speed drive," *Proceedings of the 1992 International Conference on Industrial Electronics, Control, Instrumentation, and Automation*, 1992, vol. 1, 9–13 Nov. 1992, pp. 114–120.
18) Fuchs, E.F.; Roesler, D.J.; and Alashhab, F.S.; "Sensitivity of electrical appliances to harmonics and fractional harmonics of the power system's voltage, part I," *IEEE Transactions on Power Delivery*, April 1987, vol. TPWRD-2, no. 2, pp. 437–444.
19) Fuchs, E.F.; Roesler, D.J.; and Kovacs, K.P.; "Sensitivity of electrical appliances to harmonics and fractional harmonics of the power system's voltage, part II," *IEEE Transactions on Power Delivery*, April 1987, vol. TPWRD-2, no. 2, pp. 445–453.
20) Fuchs, E.F.; Roesler, D.J.; and Kovacs, K.P.; "Aging of electrical appliances due to harmonics of the power system's voltage," *IEEE Transactions on Power Delivery*, July 1986, vol. TPWRD-1, no. 3, pp. 301–307.
21) Fuchs, E.F.; Roesler, D.J.; and Masoum, M.A.S.; "Are harmonic recommendations according to IEEE and IEC too restrictive?" *IEEE Transactions on Power Delivery*, vol. 19, no. 4, October 2004, pp. 11775–1786.
22) Fuchs, E.F.; Lin, D.; and Martynaitis, J.; "Measurement of three-phase transformer derating and reactive power demand under nonlinear loading conditions," *IEEE Transactions on Power Delivery*, vol. 21, issue 2, April 2006, pp. 665–672.
23) Lin, D.; and Fuchs, E. F.; "Real-time monitoring of iron-core and copper losses of three-phase transformers under (non)sinusoidal operation," *IEEE Transactions on Power Delivery*, vol. 21, issue 3, July 2006, pp. 1333–1341.





24) Dixon, R.R.; "Thermal aging predictions from an Arrhenius plot with only one data point," *IEEE Transactions on Electrical Insulation*, vol. E1-15, no. 4, 1980, p. 331.
25) http://nobelprize.org/chemistry/laureates/1903/arrhenius-bio.html.
26) Richter, R.; *Elektrische Maschinen*, Springer Verlag, Berlin, 1924, p. 157.
27) Fuchs, E.F.; Masoum, M.A.S.; and Roesler, D.J.; "Large signal nonlinear model of anisotropic transformers for nonsinusoidal operation, parts I and II," *IEEE Transactions on Power Delivery*, vol. PWRD-6, January 1991, pp. 174–186, and vol. PWRD-6, October 1991, pp. 1509–1516.
28) Fuchs, E.F.; and Fei, R.; "A new computer-aided method for the efficiency measurement of low-loss transformers and inductors under nonsinusoidal operation," *IEEE Transactions on Power Delivery*, vol. PWRD-11, January 1996, pp. 292–304.
29) Fuchs, E.F.; Alashhab, F.; Hock, T.F.; and Sen, P.K; "Impact of harmonics on home appliances," Topical Report (First Draft), prepared for the U.S. Department of Energy under contract No. DOE-RA-50150-9, June 1981, University of Colorado at Boulder.
30) Fuchs, E.F.; Chang, L.H.; Appelbaum, J.; and Moghadamnia, S.; "Sensitivity of transformer and induction motor operation to power system's harmonics," Topical Report (First Draft), prepared for the U.S. Department of Energy under contract No. DOE-RA-50150-18, April 1983, University of Colorado at Boulder.
31) Fuchs, E.F.; Chang, L.H.; and Appelbaum, J.; "Magnetizing current, iron losses and forces of three-phase induction machines at sinusoidal and nonsinusoidal terminal voltages, part I: Analysis," *IEEE Transactions on Power Apparatus and Systems*, November 1984, vol. PAS-103, no. 11, pp. 3303–3312.
32) Cummings, P.G.; Private communication, January 4, 1984.
33) Fuchs, E.F.; "Investigations on the impact of voltage and current harmonics on end-use devices and their protection," Summary Report, prepared for the U.S. Department of Energy under contract No. DE-AC02-80RA 50150, January 1987, University of Colorado at Boulder.
34) de Abreu, J.P.G.; and Emanuel, A.E.; "The need to limit subharmonic injection," *Proceedings of the 9th International Conference on Harmonics and Quality of Power*, vol. I," October 1–4, 2000, pp. 251–253.
35) *IEEE Standard 519*, IEEE recommended practices and requirements for harmonic control in electric power systems, IEEE-519, 1992.
36) IEC 61000-3-2 (2001–10) Consolidated edition, electromagnetic compatibility (EMC) – part 3-2: limits for harmonic current emissions.
37) Baghzouz, Y.; Burch, R.F.; Capasso, A.; Cavallini, A.; Emanuel, A.E.; Halpin, M.; Imece, A.; Ludbrook, A.; Montanari, G.; Olejniczak, K.J.; Ribeiro, P.; Rios-Marcuello, S.; Tang, L.; Thaliam, R.; and Verde, P.; "Time-varying harmonics: I. Characterizing measured data," *IEEE Transactions on Power Delivery*, vol. 13, issue 3, July 1998, pp. 938–944.
38) Baghzouz, Y.; Burch, R.F.; Capasso, A.; Cavallini, A.; Emanuel, A.E.; Halpin, M.; Langella, R.; Montanari, G.; Olejniczak, K.J.; Ribeiro, P.; Rios-Marcuello, S.; Ruggiero, F.; Thallam, R.; Testa, A.; and Verde, P.; "Time-varying harmonics; II. Harmonic summation and propagation," *IEEE Transactions on Power Delivery*, vol. 17, issue 1, Jan. 2002, Page(s):279–285.
39) Erickson, R. W.; and Maksimovic, D.; *Fundamentals of Power Electronics*, Second Edition, Kluwer Academic Publishers, ISBN 0-7923-7270-0, 2000.
40) Fuchs, E.F.; Masoum, M.A.S.; and Ladjevardi, M.; "Effects on distribution feeders from electronic loads based on future peak-load growth, part I: measurements, " *Proceedings of the IASTED International Conference on Power and Energy Systems (EuroPES 2005)*, Paper # 468-019, Benalmadena, Spain, June 15–17, 2005.
41) Carpinelli, G.; Caramia, P.; Di Vito, E.; Losi, A.; and Verde, P.; "Probabilistic evaluation of the economical damage due to harmonic losses in industrial energy system," *IEEE Transactions on Power Delivery*, vol. 11, issue 2, April 1996, pp. 1021–1031, and Correction to "Probabilistic evaluation of the economical damage due to harmonic losses in industrial energy systems," *IEEE Transactions on Power Delivery*, vol. 11, issue 3, July 1996, p. 1692.
42) Verde, P.; "Cost of harmonic effects as meaning of standard limits," *Proceedings of the Ninth International Conference on Harmonics and Quality of Power*, vol. 1, 1–4 Oct. 2000, pp. 257–259.
43) Caramia, P.; Carpinelli, G.; Verde, P.; Mazzanti, G.; Cavallini, A.; and Montanari, G.C.; "An approach to life estimation of electrical plant components in the presence of harmonic distortion," *Proceedings of the Ninth International Conference on Harmonics and Quality of Power, 2000.* vol. 3, 1–4 Oct. 2000, pp. 887–892.
44) Caramia, P.; and Verde, P.; "Cost-related harmonic limits," *IEEE Power Engineering Society Winter Meeting, 2000.* vol. 4, 23–27 Jan. 2000, pp. 2846–2851.
45) Caramia, P.; Carpinelli, G.; Losi, A.; Russo, A.; and Verde, P.; "A simplified method for the probabilistic evaluation of the economical damage due to

harmonic losses," *Proceedings of the 8th International Conference on Harmonics And Quality of Power*, 1998. vol. 2, 14-16 Oct. 1998, Page(s): 767–776.

46) Dubey, G.K.; *Power Semiconductor Controlled Drives*, Prentice Hall, Englewood Cliffs, New Jersey, 1989.

47) Heller, B.; and Hamata,V.; *Harmonic Field Effects in Induction Machines*, Academia, Publishing House of the Czechoslovak Academy of Sciences, Prague, 1977.

48) Fuchs, E.F.; Appelbaum, J.; Khan, I.A.; Höll, J.; and Frank, U.V.; *Optimization of Induction Motor Efficiency, Volume 1: Three-Phase Induction Motors*, Final Report prepared by the University of Colorado for the Electric Power Research Institute (EPRI), Palo Alto, EL-4152-CCM, Volume 1, Research Project 1944-1, 1985.

49) Fuchs, E.F.; Huang, H.; Vandenput, A.J.; Höll, J.; Appelbaum, J.; Zak, Z.; and Ericki, M.S.; *Optimization of Induction Motor Efficiency, Volume 2: Single-Phase Induction Motors*, Final Report prepared by the University of Colorado for the Electric Power Research Institute (EPRI), Palo Alto, EL-4152-CCM, Volume 2, Research Project 1944-1, 1987.

50) Fuchs, E.F.; Höll, J.; Appelbaum, J.; Vandenput, A.J.; and Klode, H.; *Optimization of Induction Motor Efficiency, Volume 3: Experimental Comparison of Three-Phase Standard Motors with Wanlass Motors*, Final Report prepared by the University of Colorado for the Electric Power Research Institute (EPRI), Palo Alto, EL-4152-CCM, Volume 3, Research Project 1944-1, 1985.

51) http://www-solar.mcs.st-and.ac.uk/~alan/MT2003/PDE/node21.html.

# 7 CHAPTER

# Power System Modeling under Nonsinusoidal Operating Conditions

The calculation of power system harmonic voltages and currents and analyzing power quality problems can be classified into frequency- and time-domain methods. Frequency-domain techniques are widely used for harmonic problem formulation. They are a reformulation of the fundamental load flow problem in the presence of nonlinear loads and/or distorted utility voltages. This complicated, nonlinear, and harmonically coupled problem has been solved in several ways in order to reach a compromise between simplicity and reliability of the formulation. Time-domain techniques can accurately model system nonlinearities and are mostly used for power quality problems such as transient and stability issues under nonsinusoidal operating conditions. They require more computation time than frequency-domain approaches but can accurately model nonlinearities (e.g., saturation and hysteresis), transients, and stability associated with transformers, nonlinear loads, and synchronous generators. Some techniques are based on a combination of frequency- and time-domain methods. In the frequency domain, the power system is linearly modeled while nonlinear simulation of components and loads can be accurately performed in the time domain. Hybrid time- and frequency-domain techniques result in moderate computational speed and accuracy.

This chapter starts with a review of power system matrices and the fundamental Newton–Raphson load flow algorithm. In Section 7.4, the Newton–Raphson harmonic power flow formulation is presented and explained in detail. In the last part of this chapter, a survey and classification of harmonic power flow approaches are addressed. All phasors are in per unit (pu) and all phase angles are assumed to be in radians.

## 7.1 OVERVIEW OF A MODERN POWER SYSTEM

The power system of today is a complicated interconnected network consisting of the following major sections as is illustrated in Fig. 7.1:

- generation,
- transmission and subtransmission,
- distribution, and
- linear and nonlinear loads.

**Generation.** The three-phase AC synchronous generator or alternator is one of the fundamental components of a power system consisting of two synchronously rotating fields: one field is produced by the rotor driven at synchronous speed and excited by DC current. The DC current in the rotor winding is provided by an excitation system with or without slip rings. The second field is set up through the stator windings by the three-phase armature currents.

An important element of power systems are AC generators with rotating rectifiers, known as brushless excitation systems [1]. The excitation system controls the generator voltage and indirectly controls the reactive power flow within the power system together with synchronous condensers and capacitor banks. The slip ring free rotor enables the generation of high power – from 50 MVA up to 1600 MVA – at high voltages, typically in the 30–40 kV range. Hydrogen and water cooling permit the high power density of synchronous generators, which are mostly of the 2 and 4-pole types. Hydrogenerators are of the synchronous and of the induction machine types and can have up to 40 poles [2]. The source of mechanical power for AC generators may be water turbines, steam turbines (where the steam is either generated by coal, natural gas, oil, or nuclear fuel), and gas turbines for peak-power generation. Coal or natural gas fired plants have an efficiency of about 30% [3], whereas combined-cycle plants (gas turbine in series with a steam turbine) can reach efficiencies of about 60% [4]. Today's deregulated power system also relies on distributed renewable energy resources such as solar, fuel cells, and turbines driven by wind, tides, water, and biomass generated gas. In a typical power station several generators are connected to a common point called a bus and operated in parallel to provide the total required power.

**Transformers.** Another key component of a power system is the transformer. Its role is to transform power with very high efficiency (e.g., 98%) from one


ISBN 978-0-12-369536-9
© Elsevier Inc. All rights reserved.

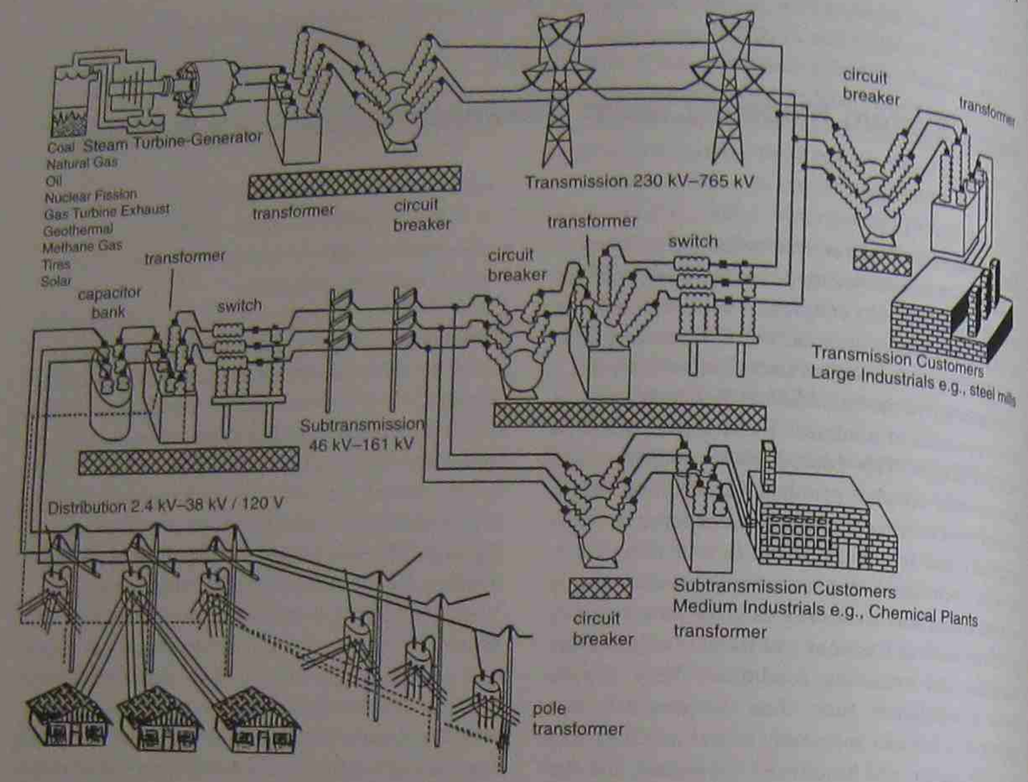



**FIGURE 7.1** Basic elements of a power system.

level of voltage to another. Using a step-up transformer of turns ratio a will reduce the secondary current by a ratio of $1/a$. This will reduce the real power loss $I^2R$ and the reactive power $I^2X$ of the transmission line, which makes the transmission of power over long distances feasible.

Due to insulation requirements and other practical design problems, terminal voltages of generators are limited to relatively low values, typically in the 30–40 kV range. Consequently, step-up transformers are used for transmission of power. At the receiving end of a transmission line, step-down transformers are employed to reduce the voltage to suitable levels for distribution or direct utilization. The power may go through several transformers between generator and the end user.

**Transmission and Subtransmission.** Overhead transmission lines permit the transfer of energy from generating units to the distribution system that serves the end users. Transmission lines also interconnect neighboring utilities to permit economic dispatch of power within regions during normal operating conditions, as well as transfer of power between regions during emergencies. Transmission-line voltage levels above 60 kV are standardized at 69 kV, 115 kV, 138 kV, 161 kV, 230 kV, 345 kV, 500 kV, and 745 kV. Transmission voltages above 230 kV are referred to as extrahigh voltage (EHV). High-voltage transmission lines are terminated at substations.

There are three types of substations: high-voltage substations, receiving substations, and primary substations. At the primary substations, the voltage is stepped down through a transformer to a value suitable for end users. For example, large industrial customers may be served directly from the transmission system.

The segment of the transmission system that connects high-voltage substations through step-down transformers to distribution substations is called the subtransmission network. There is no clear delineation between transmission and subtransmission voltage levels. Typically, the subtransmission voltage levels range from 69 kV to 138 kV. Some large industrial customers may be served from the subtransmission system. Capacitor and reactor banks are usually installed in subtransmission substations for maintaining or controlling the transmission line voltage.



It is well known that for distribution voltages higher than 15 kV ferroresonance may occur if cables instead of overhead lines are used. To avoid this problem, gas-insulated underground cables are relied on to deliver in cities the power at high voltages.

**Distribution.** The distribution system (in the range of 4 kV to 34.5 kV) connects distribution substations to end users. Some small industrial consumers may be served directly by primary feeders. The secondary distribution network reduces the voltage for utilization by commercial and residential consumers. Either overhead transmission lines or cables are employed to deliver power to consumers. Typical secondary distribution systems operate at levels of 240/120 *V* (single-phase, three-wire), 208*Y*/120 *V* (three phase, four wire), and 480*Y*/277 *V* (three-phase, four-wire). The power for residential loads in the United States are derived from transformers that reduce the primary feeder voltage to 240/120 *V* using a single-phase, three-wire line. Distribution systems are made up of both overhead and underground lines. The growth of underground distribution has been extremely rapid, especially in new residential areas.

**Linear and Nonlinear Loads.** Power systems serve linear and nonlinear loads. Loads are divided into three key categories within a power system: industrial, commercial, and residential. Industrial loads are functions of both voltage and frequency. Induction motors form a high proportion (e.g., 60%) of these loads. Commercial and residential loads consist largely of lighting, heating, and cooling (e.g., induction motors). These loads are largely independent of frequency and consume reactive power with a total power factor of larger than TPF = 80%.

The nonlinear $v$–$i$ characteristics of nonlinear loads generate both current and voltage harmonics and call for nonsinusoidal analysis and modeling of power systems. A typical power system consists of a few large industrial nonlinear loads (e.g., large rectifier bridges, large variable-speed drives); however, the number of small nonlinear loads (such as power electronic rectifiers, high-efficiency lighting, and small variable-speed drives) is rapidly increasing. This requires attention to such nonlinear loads during the design, planning, and operation of distribution systems.

## 7.2 POWER SYSTEM MATRICES

Frequency- and time-domain techniques employ vectors and matrices for mathematical modeling of power systems and for defining input and output variables. This section deals with the bus admittance and the Jacobian matrices, which are essential components of all power flow formulations.

### 7.2.1 Bus Admittance Matrix

Table 7.1 presents a review of circuit-component definitions and laws. Ohm's and Kirchhoff's laws can be used for matrix formulations that are useful for load flow analyses. This approach yields two matrices:

- Kirchhoff's current law (KCL) generates bus matrices, which result from the fact that the sum of currents entering a bus is zero.
- Kirchhoff's voltage law (KVL) results in loop matrices, which describe voltages in a circuit loop.

The bus matrix written in terms of admittance originates directly from the KCL applied to each circuit bus other than the reference (ground) bus.

#### *7.2.1.1 Application Example 7.1: A Simple Power System Configuration*

A simple power system configuration is shown in Fig. E7.1.1 where bus 1 is called the swing or

**TABLE 7.1** Review of Circuit Definitions and Laws

| Circuit-component definitions | | Circuit laws | |
|---|---|---|---|
| Resistance | $R$ | Ohm's law | $V = IZ$ |
| conductance | $G = 1/R$ | | $V = I/Y$ |
| Inductance | $L$ | Kirchhoff's voltage-loop law (KVL) | $\Sigma V = 0$, leads to loop matrix |
| reactance (inductive) | $j\omega L$ | | |
| Capacitance | $C$ | Kirchhoff's current-node law (KCL) | $\Sigma I = 0$, leads to bus matrix |
| reactance (capacitive) | $1/j\omega C = -j/\omega C$ | | |
| Impedance | $Z = R + j\omega L$ (e.g., inductor) | | |
| | $Z = R - j/\omega C$ (e.g., capacitor) | | |
| Admittance | $Y = 1/Z$ | | |
| Susceptance | $B = 1/X$ | | |

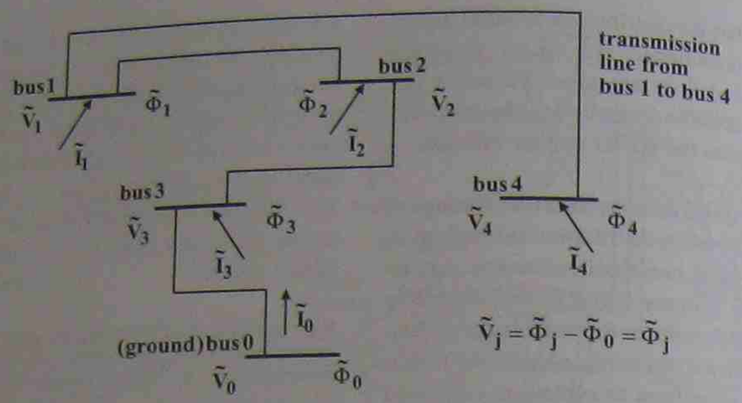



**FIGURE E7.1.1** Simple power system configuration (single-phase representation).

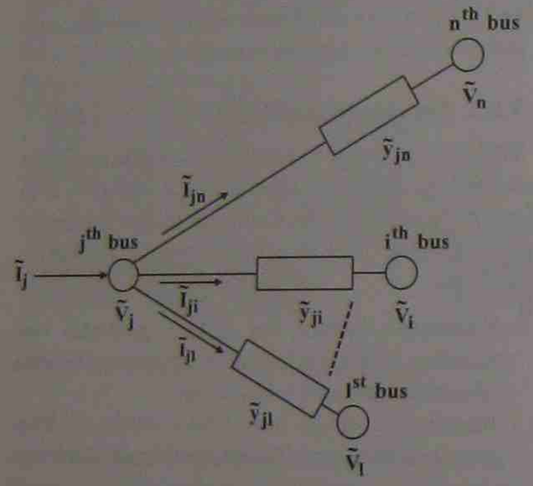



**FIGURE 7.2** Currents entering and leaving a circuit bus.

slack bus and bus 0 is called the reference or ground bus.

Let $j$ be an arbitrary circuit bus other than the reference bus (which is denoted as bus 0), as shown in Fig. 7.2. Then

$$\sum_{i=1}^{n} \tilde{I}_{ji} = \tilde{I}_j, \tag{7-1}$$

where $\tilde{I}_{ji} \equiv$ line current, which leaves bus $j$ and enters bus $i$ via a line and $\tilde{I}_j \equiv$ current injected at bus $j$ from an external source or bus injection current. The tilde (~) above $\tilde{I}_{ji}$ and $\tilde{I}_j$ denotes a complex line current and a complex bus injection current, respectively.

Application of Ohm's law (Fig. 7.3) leads to

$$\tilde{I}_{ji} = \tilde{y}_{ji}(\tilde{V}_j - \tilde{V}_i), \tag{7-2}$$

where $\tilde{y}_{ji}$ is the complex line admittance of a line from bus $j$ to bus $i$. The tilde notation in $\tilde{y}_{ji}$ indicates that it is a line admittance.

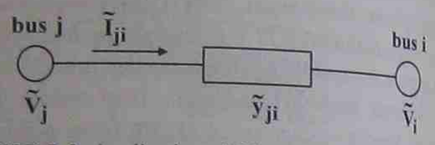



**FIGURE 7.3** Application of Ohm's law.

Certain elements of $\sum_{i=1}^{n} \tilde{I}_{ji} = \tilde{I}_j$ are zero:

- The current $\tilde{I}_{jj}$ is zero since no line joins bus $j$ with bus $j$ and this is reflected in $\tilde{I}_{jj} = \tilde{y}_{jj}(\tilde{V}_j - \tilde{V}_j)$ because it gives zero for $\tilde{I}_{jj}$ due to $(\tilde{V}_j - \tilde{V}_j) = 0$; and
- $\tilde{I}_{ji}$ will be zero if no line exists between $j$ and $i$, the "line impedance" is infinite, and the "line admittance" $\tilde{y}_{ji}$ is zero. One can write now (introducing Eq. 7-2 into Eq. 7-1)

$$\sum_{i=1}^{n} \tilde{y}_{ji}(\tilde{V}_j - \tilde{V}_i) = \tilde{I}_j. \tag{7-3}$$

Note that $\tilde{V}_j$ and $\tilde{V}_i$ are bus voltages with respect to bus 0, the reference (ground) bus. Equation 7-3 is written for $i = 1, 2, \ldots, n$ and the coefficient of voltage $\tilde{V}_j$ in the Kirchhoff equation at bus $j$ is $\sum_{i=1}^{n} \tilde{y}_{ji}$ whereas the coefficient of $\tilde{V}_i$ $(i \neq j)$ in the $j$th equation is $(-\tilde{y}_{ji})$.

All equations now read ($n \times n$ equation system)

For $j = 1$:

$$\tilde{I}_1 = \left(\sum_{\substack{i=1 \\ i\neq 1}}^{n} \tilde{y}_{1i}\right)\tilde{V}_1 + (-\tilde{y}_{12})\tilde{V}_2 + \ldots + (-\tilde{y}_{1n})\tilde{V}_n, \tag{7-4a}$$

For $j = 2$:



$$\tilde{I}_2 = (-\tilde{y}_{21})\tilde{V}_1 + \left(\sum_{\substack{i=1 \\ i\neq 2}}^{n} \tilde{y}_{2i}\right)\tilde{V}_2 + \ldots + (-\tilde{y}_{2n})\tilde{V}_n, \tag{7-4b}$$

For $j = n$:

$$\tilde{I}_n = (-\tilde{y}_{n1})\tilde{V}_1 + (-\tilde{y}_{n2})\tilde{V}_2 + \ldots + \left(\sum_{\substack{i=1 \\ i\neq n}}^{n} \tilde{y}_{ni}\right)\tilde{V}_n. \tag{7-4c}$$

Observe the pattern of the coefficients of the bus voltages on the right-hand side of the equation system. This pattern will be generalized as the rule for the formation of a matrix of coefficients of $\bar{V}_j$. These $n$ equations can be written in matrix form

$$\bar{I}_{\text{bus}} = \bar{Y}_{\text{bus}}\bar{V}_{\text{bus}}, \tag{7-5}$$

where $\bar{I}_{\text{bus}}$ is the bus injection vector representing the $n$ phasor injection currents, $\bar{Y}_{\text{bus}}$ is the bus admittance matrix (it is an $n \times n$ matrix of coefficients formed as indicated above), and $\bar{V}_{\text{bus}}$ is the bus voltage vector of $n$ phasor voltages referenced to bus 0:

$$\tilde{V}_n = \tilde{\Phi}_n - \tilde{\Phi}_0 = \tilde{\Phi}_n, \tag{7-6}$$

where $\tilde{\Phi}_n$ and $\tilde{\Phi}_0$ are the potentials at bus $n$ and bus 0, respectively, and $\tilde{\Phi}_0 = 0$.

If $\bar{Y}_{\text{bus}}$ is a nonsingular matrix then its inverse $(\bar{Y}_{\text{bus}})^{-1}$ can be found and there exists a solution to the matrix equation. If $\bar{Y}_{\text{bus}}$ is singular then $(\bar{Y}_{\text{bus}})^{-1}$ cannot be found and there exists no solution to the matrix equation.

$$\underset{\substack{\uparrow \\ n\times 1}}{\bar{I}_{\text{bus}}} = \underset{\substack{\uparrow \\ n\times n}}{\bar{Y}_{\text{bus}}}\ \underset{\substack{\uparrow \\ n\times 1}}{\bar{V}_{\text{bus}}}, \tag{7-7}$$

row column $n \times 1$

Note that the injection currents find a return path through bus 0 (ground). Also note that the Kirchhoff current law is not applied to bus 0 in these equations; however, the total current entering bus 0 is the negative sum of the currents $\tilde{I}_1, \tilde{I}_2, \ldots, \tilde{I}_n$. Therefore, the Kirchhoff current law at bus 0 is

$$-\sum_{i=1}^{n} \tilde{I}_i = -\left[\left(-\tilde{y}_{21} - \tilde{y}_{31} - \ldots - \tilde{y}_{n1} + \sum_{\substack{i=1 \\ i\neq 1}}^{n} \tilde{y}_{1i}\right)\tilde{V}_1 + \left(-\tilde{y}_{12} - \tilde{y}_{32} - \ldots - \tilde{y}_{n2} + \sum_{\substack{i=1 \\ i\neq 2}}^{n} \tilde{y}_{2i}\right)\tilde{V}_2 + \ldots\right], \tag{7-8}$$

which can be readily simplified as

$$\tilde{I}_0 = -\tilde{y}_{01}\tilde{V}_1 - \tilde{y}_{02}\tilde{V}_2 - \ldots - \tilde{y}_{0n}\tilde{V}_n, \tag{7-9}$$

where $\tilde{y}_{0k}$ is the primitive admittance joining buses 0 and $k$.

Because the relation in Eq. 7-9 is a linear combination of the previous $n$ equations, it cannot be used to obtain additional information beyond that given in the $n \times n$ equation system. Inspection of the coefficients of the $\tilde{V}$ terms in the $n \times n$ equation system reveals a rule for the formation of $\bar{Y}_{\text{bus}}$. The following rules are used to "build" the bus admittance matrix referenced to bus 0.

### The Admittance Matrix Building Algorithm

- $y_{jj}$: the diagonal entries of $\bar{Y}_{\text{bus}}$ are formed by summing the admittances of lines terminating at bus $j$. Note there is no tilde on $y_{jj}$.
- $y_{ij}$: the off-diagonal entries are the negatives of the admittances of lines between buses $i$ and $j$. If there is no line between $i$ and $j$, this term is zero. Note there is no tilde on $y_{ij}$.

Usually, bus 0 is the ground bus, but other buses may be chosen as the reference (for specialized applications). Since bus 0 is commonly chosen as the reference, the notation

$$\bar{Y}_{\text{bus}} = \bar{Y}_{\text{bus}}^{(0)} \tag{7-10}$$

is employed to denote the bus admittance matrix referenced to ground. If some other bus is used as the reference, for example bus k, the following notation is used:

$$\bar{Y}_{\text{bus}}^{(k)}. \tag{7-11}$$

#### 7.2.1.2 Application Example 7.2: Construction of Bus Admittance Matrix (Fig. E7.2.1)

$$-\sum_{j=1}^{4} \tilde{I}_j = -(\tilde{I}_1 + \tilde{I}_2 + \tilde{I}_3 + \tilde{I}_4) = \tilde{I}_0. \tag{E7.1-1}$$

Inspection of the $\bar{Y}_{\text{bus}}$ building algorithm reveals several properties of the bus matrix:

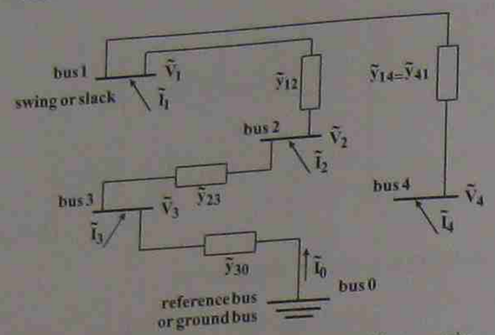



**FIGURE E7.2.1** Example for construction of bus matrix.

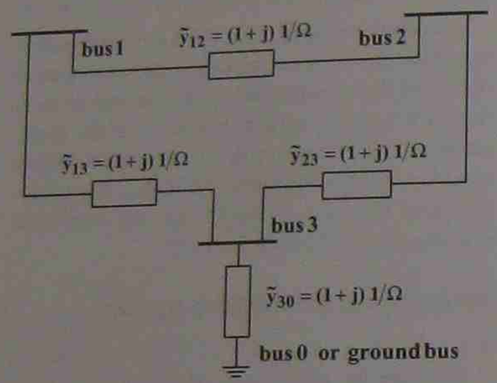



**FIGURE E7.3.1** Building of nonsingular bus admittance matrix for simple power system configuration.

- $\bar{Y}_{bus}$ is complex and symmetric;
- $\bar{Y}_{bus}$ is sparse since each bus is connected to only a few nearby buses, and this causes many $y_{ji} = 0$ entries; and
- Provided that there is a net nonzero admittance tie to the reference bus (e.g., ground), $\bar{Y}_{bus}$ is nonsingular and may be inverted to find $\bar{V}_{bus}$ from

$$\bar{I}_{bus} = \bar{Y}_{bus}\bar{V}_{bus}, \tag{7-12}$$

or

$$\bar{V}_{bus} = (\bar{Y}_{bus})^{-1}\bar{I}_{bus}. \tag{7-13}$$

If there are no ties to the reference bus, $\bar{Y}_{bus}$ is singular and cannot be inverted because no solution to the n × n equation system exists.

#### 7.2.1.3 Application Example 7.3: Building of Nonsingular Bus Admittance Matrix (Fig. E7.3.1)

Note: Off-diagonal entries = sum of negatives of the line admittances

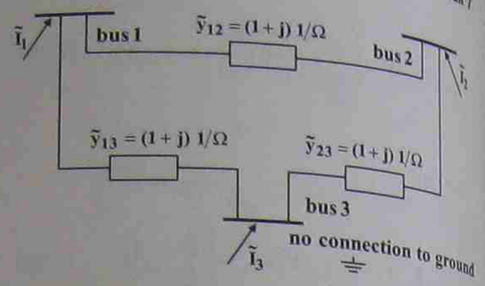



**FIGURE E7.4.1** Building of singular bus admittance matrix for simple power system configuration.

$$y_{21} = y_{12} = -(1 + j)\ 1/\Omega,$$
$$y_{31} = y_{13} = -(1 + j)\ 1/\Omega,$$
$$y_{32} = y_{23} = -(1 + j)\ 1/\Omega,$$

Main-diagonal entry for bus 1: $y_{11} = (2 + 2j)\ 1/\Omega$,
Main diagonal entry for bus 2: $y_{22} = (2 + 2j)\ 1/\Omega$,
Main-diagonal entry for bus 3: $y_{33} = (3 + 3j)\ 1/\Omega$,

Therefore,

$$\bar{Y}_{bus} = \begin{bmatrix} y_{11} & y_{12} & y_{13} \\ y_{21} & y_{22} & y_{23} \\ y_{31} & y_{32} & y_{33} \end{bmatrix} = \begin{bmatrix} (2+2j) & -(1+j) & -(1+j) \\ -(1+j) & (2+2j) & -(1+j) \\ -(1+j) & -(1+j) & (3+3j) \end{bmatrix} \tag{E7.3-1}$$

$\bar{Y}_{bus}$ is complex and symmetric, but not sparse.

#### 7.2.1.4 Application Example 7.4: Building of Singular Bus Admittance Matrix (Fig. E7.4.1)

$$\bar{I}_{bus} = \bar{Y}_{bus}\bar{V}_{bus} = \begin{bmatrix} (2+2j) & -(1+j) & -(1+j) \\ -(1+j) & (2+2j) & -(1+j) \\ -(1+j) & -(1+j) & (2+2j) \end{bmatrix} \begin{bmatrix} \tilde{V}_1 \\ \tilde{V}_2 \\ \tilde{V}_3 \end{bmatrix}, \tag{E7.4-1}$$

$$\tilde{I}_1 = (2 + 2j)\tilde{V}_1 - (1 + j)\tilde{V}_2 - (1 + j)\tilde{V}_3 \tag{E7.4-2}$$

$$\tilde{I}_2 = -(1 + j)\tilde{V}_1 + (2 + 2j)\tilde{V}_2 - (1 + j)\tilde{V}_3 \tag{E7.4-3}$$

$$\tilde{I}_3 = -(1 + j)\tilde{V}_1 - (1 + j)\tilde{V}_2 + (2 + 2j)\tilde{V}_3 \tag{E7.4-4}$$

Add Eqs. E7.4-2 and E7.4-3:

$$(\tilde{I}_1 + \tilde{I}_2) = (1 + j)\tilde{V}_1 + (1 + j)\ \tilde{V}_2 - (2 + 2j)\tilde{V}_3$$

or

$$\underbrace{-(\tilde{I}_1 + \tilde{I}_2)}_{I_3} = -(1 + j)\tilde{V}_1 - (1 + j)\tilde{V}_2 + (2 + 2j)\tilde{V}_3 \tag{E7.4-5}$$





Note that Eq. E7.4-2 + Eq. E7.4-3 = Eq. E7.4-5, which is the same as Eq. E7.4-4. That is, these equations are dependent. One concludes that the matrix is singular and no solution exists for Eqs. E7.4-2 to E7.4-4.

### 7.2.2 Triangular Factorization

In the United States there exist three power grids: the Eastern, Western, and Texan pools. Because of stability problems these pools are linked with small (100 MW range) DC buses. Nevertheless if even one of the pools is analyzed, the number of buses will be very large: a few thousand buses or more, depending on the detail of modeling. Fortunately, not all buses are mutually linked through a transmission line and for this reason the resulting bus admittance matrix is very sparse, that is, only about 1% of the entire matrix entries are nonzero. However, because of the large dimensions (few thousands) a direct solution (e.g., Gaussian elimination) of the equation system is not feasible and one uses the Newton–Raphson method together with the Jacobian matrix to arrive at the solution via iterations.

To reduce computer memory requirements, sparsity programming is used: it is a digital programming technique whereby sparse matrices are stored in compact forms. The usual basis of sparsity programming techniques is the storage of only nonzero entries. Two broad classes of sparsity programming techniques are

- the entry-row-column storage method, and
- the chained-data-structure method.

Applications of sparsity programming methods are primarily in $\bar{Y}_{bus}$ methods. In this chapter the Jacobian will be used; this matrix is as sparse as the $\bar{Y}_{bus}$ matrix and lends itself to sparsity programming.

In power engineering, as well as in many other branches of engineering, it is necessary to solve a simultaneous set of algebraic linear equations. The general form is the solution of

$$\bar{A} \cdot \bar{x} = \bar{b} \tag{7-14}$$

Given are the $n$ by $n$ matrix $\bar{A}$ and the $n$-dimensional vector $\bar{b}$. Such is the case in the solution of

$$\bar{I}_{bus} = \bar{Y}_{bus}\bar{V}_{bus} \tag{7-15}$$

or

$$\bar{V}_{bus} = [\bar{Y}_{bus}]^{-1}\ \bar{I}_{bus} \tag{7-16}$$

for $\bar{V}_{bus}$ where the injection currents and the admittance matrix are given. Using the notation of $\bar{A} \cdot \bar{x} = \bar{b}$, let $\bar{A}$ be factored into two matrices called triangular factorization:

$$\bar{A} = \bar{L} \cdot \bar{U} \tag{7-17}$$

where $\bar{L}$ is lower left triangular (e.g., $l_{rc}$ is zero for $c > r$) and $\bar{U}$ is upper right triangular (e.g., $u_{rc}$ is zero for $r > c$). Then

$$\bar{A} \cdot \bar{x} = [\bar{L} \cdot \bar{U}]\bar{x} = \bar{b} \tag{7-18}$$

Let $(\bar{U} \cdot \bar{x})$ be a new variable $\bar{w}$, which is an $n$-dimensional vector; then

$$\bar{w} = \bar{U} \cdot \bar{x} \tag{7-19}$$

$$\bar{L} \cdot \bar{w} = \bar{b} \tag{7-20}$$

where

$$\bar{w} = \begin{bmatrix} w_1 \\ w_2 \\ \vdots \\ w_n \end{bmatrix}, \quad \bar{b} = \begin{bmatrix} b_1 \\ b_2 \\ \vdots \\ b_n \end{bmatrix}, \tag{7-21a,b}$$

$$\bar{L} = \begin{bmatrix} l_{11} & 0 & 0 & . \\ l_{21} & l_{22} & . & . \\ l_{31} & l_{32} & l_{33} & . \\ . & . & . & . \end{bmatrix}, \quad \bar{U} = \begin{bmatrix} u_{11} & u_{12} & u_{13} & . \\ 0 & u_{22} & u_{13} & . \\ 0 & 0 & u_{33} & . \\ . & . & . & . \end{bmatrix}. \tag{7-22a,b}$$

Note that $\bar{x}$ and $\bar{b}$ correspond to the $\bar{V}_{bus}$ vector and the current vector $\bar{I}_{bus}$, respectively.

#### 7.2.2.1 Application Example 7.5: Matrix Multiplication

Given

$$\bar{U} = \begin{bmatrix} u_{11} & u_{12} \\ 0 & u_{22} \end{bmatrix}, \quad \bar{L} = \begin{bmatrix} l_{11} & 0 \\ l_{21} & l_{22} \end{bmatrix}. \tag{E7.5-1a,b}$$

Find entries of the matrix $\bar{L} \cdot \bar{U}$.

#### 7.2.2.2 Application Example 7.6: Triangular Factorization

Given

$$\bar{U} = \begin{bmatrix} u_{11} & u_{12} \\ 0 & u_{22} \end{bmatrix}, \quad \bar{x} = \begin{bmatrix} x_1 \\ x_2 \end{bmatrix}. \tag{E7.6-1a,b}$$

show that $\bar{w} = \bar{U} \cdot \bar{x}$ is a column ($n = 2$) vector.

$$\bar{w} = \bar{U} \cdot \bar{x} = \begin{bmatrix} u_{11} & u_{12} \\ 0 & u_{22} \end{bmatrix} \begin{bmatrix} x_1 \\ x_2 \end{bmatrix} \qquad \text{(E7.6-2)}$$

$2 \times \boxed{2 \quad 2} \times 1$

row column row column

$$\bar{w} = \begin{bmatrix} u_{11}x_1 + u_{12}x_2 \\ u_{22}x_2 \end{bmatrix}. \qquad \text{(E7.6-3)}$$

Therefore, $\bar{w}$ is a $2 \times 1$ matrix or a column vector.

**Forward Substitution.** $\bar{L} \cdot \bar{w} = \bar{b}$ is readily solved for $\bar{w}$ since the form of the equation is rather special:

$$\bar{L} = \begin{bmatrix} l_{11} & 0 & 0 & 0 & \cdot \\ l_{21} & l_{22} & 0 & 0 & \cdot \\ l_{31} & l_{32} & l_{33} & 0 & \cdot \\ \cdot & \cdot & \cdot & \cdot & \cdot \end{bmatrix} \begin{bmatrix} w_1 \\ w_2 \\ \vdots \\ w_n \end{bmatrix} = \begin{bmatrix} b_1 \\ b_2 \\ \vdots \\ b_n \end{bmatrix}. \qquad \text{(7-23)}$$

The top row of the matrix equation is solved readily for $w_1$ since the only nonzero entry on the left-hand side is $l_{11}w_1$ and therefore

$$l_{11}w_1 = b_1, \qquad \text{(7-24a)}$$

or

$$w_1 = \frac{b_1}{l_{11}}. \qquad \text{(7-24b)}$$

From row 2 one finds

$$l_{21}w_1 + l_{22}w_2 = b_2, \qquad \text{(7-24c)}$$

or

$$w_2 = \frac{b_2 - l_{21}w_1}{l_{22}}. \qquad \text{(7-24d)}$$

This process of forward substitution continues until all components of $\bar{w}$ are computed.

Having found vector $\bar{w}$, the relation $\bar{w} = \bar{U} \cdot \bar{x}$ is used to find $\bar{x}$:

$$\begin{bmatrix} w_1 \\ w_2 \\ \vdots \\ w_n \end{bmatrix} = \begin{bmatrix} u_{11} & u_{12} & u_{13} & \cdot \\ 0 & u_{22} & u_{23} & \cdot \\ 0 & 0 & u_{33} & \cdot \\ \cdot & \cdot & \cdot & \cdot \end{bmatrix} \begin{bmatrix} x_1 \\ x_2 \\ \vdots \\ x_n \end{bmatrix}. \qquad \text{(7-25)}$$

**Backward Substitution.** The bottom row is readily solved ($n = 3$) for $x_3$:



$$w_3 = u_{33}x_3, \qquad \text{(7-26a)}$$

or

$$x_3 = \frac{w_3}{u_{33}}. \qquad \text{(7-26b)}$$

The second row from the bottom yields

$$w_2 = u_{22}x_2 + u_{23}x_3 \qquad \text{(7-26c)}$$

or

$$x_2 = \frac{w_2 - u_{23}x_3}{u_{22}}. \qquad \text{(7-26d)}$$

**Rule**: The value of $x_n$ is backward substituted into the $(n-1)$st row of the above matrix equation to find $x_{n-1}$ from

$$w_{n-1} = u_{n-1\,n-1}x_{n-1} + u_{n-1\,n}x_n \qquad \text{(7-27)}$$

This process of back substitution is employed to find all other components of $\bar{x}$.

**Note**: By the process of

(*i*) triangular factorization of $\bar{A}$,
(*ii*) forward, and
(*iii*) backward substitution,

the solution of $\bar{A} \cdot \bar{x} = \bar{b}$ is found without inverting $\bar{A}$! At first glance, it may appear remarkable that the inversion of $\bar{A}$ may be avoided, but there is some information that lies uncalculated in the use of triangular factorization compared to a solution using inversion. If $\bar{A} \cdot \bar{x} = \bar{b}$ is to be solved for many different values of $\bar{b}$, inversion is readily used since a given vector $\bar{b}$ premultiplied by $\bar{A}^{-1}$ gives the required result $\bar{x} = \bar{A}^{-1} \cdot \bar{b}$. In such an application $\bar{A}^{-1}$ is calculated only once.

If triangular factorization is used, the forward/backward substitution process would have to be repeated for each different $\bar{b}$ vector. In power engineering applications, however, it is usually necessary to solve $\bar{A} \cdot \bar{x} = \bar{b}$ only once: the inverse of $\bar{A}$ is not really desired – only $\bar{x}$ is sought. The triangular factorization method is favored for most applications.

The success of the triangular factorization method depends on

- the speed of the factorization of $\bar{A}$ into $\bar{L}$ and $\bar{U}$, and
- the sparsity of $\bar{L}$ and $\bar{U}$.





A sparse $\bar{A}$ is of considerable interest because if the triangular matrices were sparse, the memory advantages of sparsity programming may be added to the speed advantages of triangular factorization.

**Formation of the Table of Factors.** Let $\bar{L}$ have unit (main) diagonal entries

$$\bar{L} = \begin{bmatrix} 1 & 0 & 0 & \cdot \\ l_{21} & 1 & 0 & \cdot \\ l_{31} & l_{32} & 1 & \cdot \\ \cdot & \cdot & \cdot & \cdot \end{bmatrix}, \quad \bar{U} = \begin{bmatrix} u_{11} & u_{12} & u_{13} & \cdot \\ 0 & u_{22} & u_{23} & \cdot \\ 0 & 0 & u_{33} & \cdot \\ \cdot & \cdot & \cdot & \cdot \end{bmatrix} \qquad \text{(7-28a,b)}$$

and let $\bar{U}$ be stored superimposed onto $\bar{L}$ (omitting the writing of the unit entries of $\bar{L}$):

$$\begin{bmatrix} u_{11} & u_{12} & u_{13} & \cdot \\ l_{21} & u_{22} & u_{23} & \cdot \\ l_{31} & l_{32} & u_{33} & \cdot \\ \cdot & \cdot & \cdot & \cdot \end{bmatrix}. \qquad \text{(7-29)}$$

This superimposed array is called the table of factors. The upper right triangle of the table is $\bar{U}$; the lower left triangle is $\bar{L}$ with the unit diagonal entries deleted.

### 7.2.3 Jacobian Matrix

The proposal to use for a partial derivative "∂" instead of "d" stems from Carl Gustav Jacob Jacobi, 1804–1851, a German mathematician. At about the same time as Jacobi, the Russian mathematician Michail Vasilevich Ostrogradski (1801–1862) also introduced the Jacobian of $n$ functions $y_1, y_2, \ldots, y_n$ and $n$ unknowns $x_1, x_2, \ldots, x_n$ as follows:

$$\bar{J} = \begin{bmatrix} \frac{\partial y_1}{\partial x_1} & \frac{\partial y_1}{\partial x_2} & \cdots & \frac{\partial y_1}{\partial x_n} \\ \frac{\partial y_2}{\partial x_1} & \frac{\partial y_2}{\partial x_2} & \cdots & \frac{\partial y_2}{\partial x_n} \\ \vdots & \vdots & \vdots & \vdots \\ \frac{\partial y_n}{\partial x_1} & \frac{\partial y_n}{\partial x_2} & \cdots & \frac{\partial y_n}{\partial x_n} \end{bmatrix}. \qquad \text{(7-30)}$$

It is possible to factorize arbitrary nonsingular matrices $\bar{J}$ into $\bar{L}$ and $\bar{U}$ without the need for new computer storage areas: in other words, $\bar{J}$ is destroyed and replaced by the table of factors. The table of factors is approximately as sparse as $\bar{J}$ and, therefore, the table of factors does not require additional storage.

Techniques that result in the destruction of the original data and the replacement of those data by the solution are known as *in situ* methods. Matrix $\bar{J}$ is factored into $\bar{L}$ and $\bar{U}$ *in situ* and $\bar{J}$ is destroyed and replaced by the table of factors.

The formulas required for the calculation of the table of factors are readily found, noting that

$$\bar{L} \cdot \bar{U} = \bar{J} \ (= \bar{A}) \qquad \text{(7-31)}$$

Write $\bar{L}$ and $\bar{U}$, and find the entries of $\bar{L}$ and $\bar{U}$, that is, the table of factors:

$$\begin{bmatrix} 1 & 0 & 0 & 0 & \cdot \\ l_{21} & 1 & 0 & 0 & \cdot \\ l_{31} & l_{32} & 1 & 0 & \cdot \\ \cdot & \cdot & \cdot & \cdot & \cdot \end{bmatrix} \begin{bmatrix} u_{11} & u_{12} & u_{13} & \cdot \\ 0 & u_{22} & u_{23} & \cdot \\ 0 & 0 & u_{33} & \cdot \\ \cdot & \cdot & \cdot & \cdot \end{bmatrix} =$$

$$\bar{J} = \begin{bmatrix} J_{11} & J_{12} & J_{13} & \cdot \\ J_{21} & J_{22} & J_{23} & \cdot \\ J_{31} & J_{32} & J_{33} & \cdot \\ \cdot & \cdot & \cdot & \cdot \end{bmatrix}. \qquad \text{(7-32)}$$

#### 7.2.3.1 Application Example 7.7: Jacobian Matrices

Given

$$\begin{bmatrix} 1 & 0 \\ l_{21} & 1 \end{bmatrix} \begin{bmatrix} u_{11} & u_{12} \\ 0 & u_{22} \end{bmatrix} = \begin{bmatrix} J_{11} & J_{12} \\ J_{21} & J_{22} \end{bmatrix}. \qquad \text{(E7.7-1)}$$

Find $u_{11}$, $u_{12}$, $u_{22}$, and $l_{21}$

$$J_{11} = u_{11} \quad \text{or} \quad u_{11} = J_{11}$$
$$J_{12} = u_{12} \quad \text{or} \quad u_{12} = J_{12}$$
$$J_{21} = l_{21}u_{11} \quad \text{or} \quad l_{21} = J_{21}/u_{11}$$
$$J_{22} = l_{21}u_{12} + u_{22} \quad \text{or} \quad u_{22} = J_{22} - l_{21}u_{12}$$

In general,

$$u_{11} = J_{11}$$
$$u_{12} = J_{12}$$
$$\vdots \quad \vdots$$
$$u_{1c} = J_{1c}$$
$$\vdots \quad \vdots$$
$$u_{1n} = J_{1n}$$

**Forward and Backward Substitution.** The solution of a simultaneous set of algebraic linear equations by triangular factorization involves two main steps:

- formation of the table of factors, and
- forward/backward substitutions.

Having found the table of factors as indicated previously, the following relations are used to complete the solution:

$$\begin{aligned} \bar{L}\cdot\bar{w} &= \bar{b} \\ \bar{U}\cdot\bar{x} &= \bar{w} \end{aligned} \qquad (7\text{-}33)$$

Vector $\bar{b}$ is destroyed in this process and converted *in situ* to vector $\bar{w}$. Since $l_{11}$ is unity, $w_1$ is simply $b_1$ as can be seen from the matrix solution

$$\begin{bmatrix} l_{11} & 0 & 0 & 0 & \cdot \\ l_{21} & l_{22} & 0 & 0 & \cdot \\ l_{31} & l_{32} & l_{33} & 0 & \cdot \\ \cdot & \cdot & \cdot & \cdot & \cdot \end{bmatrix} \begin{bmatrix} w_1 \\ w_2 \\ \vdots \\ w_n \end{bmatrix} = \begin{bmatrix} b_1 \\ b_2 \\ \vdots \\ b_n \end{bmatrix}. \qquad (7\text{-}34)$$

Subsequent rows of $\bar{w}$ are found using

$$w_r = b_r - \sum_{q=1}^{r-1} l_{rq} w_q$$

created destroyed

for $r = 1, 2, \ldots, n$

As this equation is used, $w_1$ replaces $b_1$, $w_2$ replaces $b_2$, and so on.

Having found $w_1$ a similar process is used to find $\bar{x}$:

$$\begin{bmatrix} u_{11} & u_{12} & u_{13} & \cdot \\ 0 & u_{22} & u_{23} & \cdot \\ 0 & 0 & u_{33} & \cdot \\ \cdot & \cdot & \cdot & \cdot \end{bmatrix} \begin{bmatrix} x_1 \\ x_2 \\ \vdots \\ x_n \end{bmatrix} = \begin{bmatrix} w_1 \\ w_2 \\ \vdots \\ w_n \end{bmatrix}. \qquad (7\text{-}35)$$

By inspection,

$$u_{nn} x_n = w_n \qquad (7\text{-}36)$$

or

$$x_n = \frac{w_n}{u_{nn}}. \qquad (7\text{-}37)$$

Again, *in situ* technique is used and $x_n$ replaces $w_n$.

In row $n-1$:



$$u_{n-1\,n-1} x_{n-1} + u_{n-1\,n} x_n = w_{n-1} \qquad (7\text{-}38)$$

or

$$x_{n-1} = \frac{w_{n-1} - u_{n-1\,n} x_n}{u_{n-1\,n-1}}. \qquad (7\text{-}39)$$

Element $x_{n-1}$ replaces $w_{n-1}$. The process continues for rows $n-2, n-3, \ldots, 1$. In row $r$

$$x_r = \frac{w_r - \sum_{q=r+1}^{n} u_{rq} x_q}{u_{rr}}. \qquad (7\text{-}40)$$

This completes the solution.

## 7.3 FUNDAMENTAL POWER FLOW

The electric power flow problem is the most studied and documented problem in power engineering. It is the calculation of line loading given the generation and demand levels of $P$, $Q$, and $S$ measured in kW, kVAr, kVA, respectively. The transmission network is (nearly) linear, and one might expect the power flow to be a linear problem. However, because power $p = (v \cdot i)$ is a product of voltage $v$ and current $i$, the problem formulation is nonlinear even for a linear transmission network. Additional nonlinearities arise from the specification and use of complex voltages and currents. Also, there are transmission component nonlinearities that may be considered, such as tap changing transformers, in which the tap is adjusted to hold a given bus voltage at a fixed magnitude.

The power flow formulation does not consider time variations of loads, generation, or network configuration. The sinusoidal steady state is assumed and, as a result, equations are algebraic in form rather than differential.

Prior to 1940 there were a limited number of interconnected power systems and the servicing of the load was elementary since the systems were primarily radial circuits (Fig. 7.4). In more recent years, the

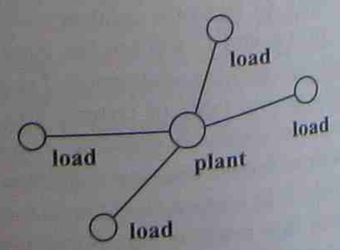



**FIGURE 7.4** Radial power systems.





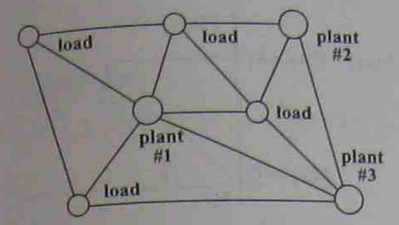



**FIGURE 7.5** Interconnected power systems.

numerous advantages of interconnection were recognized, and modern power systems are characterized by a high degree of interconnection (Fig. 7.5), for example, within the three U.S. power grids (Western, Eastern, and Texan pools). Many loop circuits with many load/generation buses and high levels of power exchange between neighboring companies exist. The latter point relates closely to interconnection advantages.

With no addition of generation capacity, it is possible to increase the generation available through interconnection. For example, in the case of an outage of a generating unit, power may be purchased from a neighboring company. The cost savings realized from lower installed capacity usually far outweigh the cost of the transmission circuits required to access neighboring companies. The analysis of large interconnected power systems generally involves the simultaneous solution of many (thousands) nonlinear algebraic equations using the Newton–Raphson approach. Like most engineering problems, the power flow problem has a set of given data and a set of quantities that must be calculated.

In this section, each complex unknown will be counted as two real unknowns, and each complex equation will be considered as two real equations. The objective of fundamental power flow is to calculate line loading for given generation and load levels ($P$, $Q$, and $S$).

### 7.3.1 Fundamental Bus Admittance Matrix

As discussed and formulated in the previous section, for an n bus system (not including the ground bus, which is the reference bus), the fundamental bus admittance matrix is an $n \times n$ matrix:

$$\bar{Y}_{\text{bus}} = \begin{bmatrix} y_{11} & y_{12} & \cdots & y_{1n} \\ y_{21} & y_{22} & \cdots & y_{2n} \\ \vdots & \vdots & \vdots & \vdots \\ y_{n1} & y_{n2} & \cdots & y_{nn} \end{bmatrix}, \qquad (7\text{-}41)$$

where $f_1 = 60$ Hz and $\omega_1 = 2\pi f_1 = 377$ rad/s.

The entries of $\bar{Y}_{\text{bus}}$ are found as follows:

Main-diagonal entries:

$y_{kk}$ = sum of line admittances connected to bus $k$ ($k = 1, 2, \ldots, n$).

Off-diagonal entries:

$y_{kj}$ = −(line admittance connected between buses $k$ and $j$).

Since $y_{kj} = y_{jk}$, the matrix $\bar{Y}_{\text{bus}}$ is symmetric.

### 7.3.2 Newton–Raphson Power Flow Formulation

The power (load) flow problem consists of calculations of power flows (real, reactive) and voltages (magnitude, phase) of a network for specified (demand and generation powers) terminal or bus conditions. All voltages and currents are assumed to have fundamental ($h = 1$, $f_1 = 60$ Hz) frequency components. A single-phase representation is considered to be adequate because power systems are approximately balanced within all three phases. Associated with each bus (e.g., bus $j$) are four quantities:

- real power P,
- reactive power Q,
- root-mean-squared (rms) voltage value $|\bar{V}|$, and
- phase angle of voltage $\delta$.

Three types of buses are represented and two of the four quantities are specified at each bus:

- **Swing bus.** It is necessary to select one reference bus (called the swing or slack bus) providing the transmission losses because these are unknown until the final solution is available. The voltage amplitude and its phase angle are given at the swing bus (usually 1.0 per unit (pu) and zero radians, respectively), and all other bus voltage angles are measured with respect to the phase angle of this reference bus. The remaining buses are either PV or PQ buses.
- **Voltage controlled (PV) buses.** The real power P and the voltage magnitude (amplitude) $|\bar{V}|$ are specified for PV buses. These are usually the generation buses at which the injected real power is specified and held fixed by turbine settings (e.g., steam entry valve). A voltage regulator holds $|\bar{V}|$ fixed at PV buses by automatically varying the generator field excitation.
- **Load (PQ) buses.** These are mostly system loads at which real and reactive powers (P and Q, respectively) are specified.

The following notations will be used:

- For a given bus (e.g., the $j$th bus):
  - $P_j$ = real power
  - $Q_j$ = reactive power
  - $|\tilde{V}_j|$ = rms value of voltage, and
  - $\delta_j$ = angle of voltage.
- For the swing or slack bus ($j = 1$):
  - $|\tilde{V}_1| = 1.0$ pu
  - $\delta_1 = 0$ radians, and
  - It will cover all transmission line losses of the system ("slack").
- For a $PV$ bus (e.g., the $j$th bus):
  - It is a generation bus
  - $P_j$ is given by turbine setting, and
  - $|\tilde{V}_j|$ is given by generator excitation.
- For a $PQ$ bus (e.g., the $j$th bus):
  - It is a load bus,
  - $P_j$ and $Q_j$ are given by the load demand,
  - because power values are given ($p = v \cdot i$) one obtains an algebraic, nonlinear system of equations.

**Fundamental Bus Voltage Vector.** For power system modeling at rated frequency, the bus voltage vector is defined as (note: the bar above the $x$ means vector, and $t$ means transpose):

$$\bar{x} = [\delta_2,\ |\tilde{V}_2|,\ \delta_3,\ |\tilde{V}_3|,\ \ldots\ \delta_n,\ |\tilde{V}_n|]^t \qquad (7\text{-}42)$$

where $\delta_j$ is the phase shift of voltage at bus $j$ with respect to the swing bus voltage phase angle and $|\tilde{V}_j|$ is the voltage rms magnitude at bus $j$. Note that if bus 1 is the swing bus, $|\tilde{V}_1|$ and $\delta_1$ are known (usually 1.0 per unit and zero radians).

Although power system components are assumed to be linear in the conventional power flow formulation, the problem is a nonlinear one because power $p$ is the product of voltage $v$ and current $i$. The load flow problem requires the solution of algebraic but nonlinear equations, which are solved using the Newton–Raphson method as will be discussed next.

i) Linear approximation, one-dimensional analysis (Fig. 7.6):

$$F(x_1) = (x_1 - x_0)\frac{dF(x_0)}{dx}, \qquad (7\text{-}43)$$

where $h = (x_1 - x_0)$, or

$$F(x_1) = h\frac{dF(x_0)}{dx}. \qquad (7\text{-}44)$$

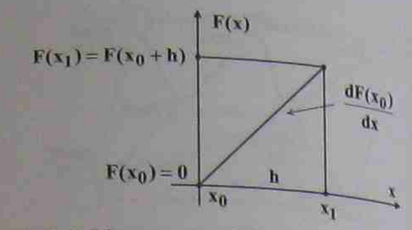



**FIGURE 7.6** Linear extrapolation from coordinate point $x_0$, $F(x_0)$ to $x_1$, $F(x_1)$.

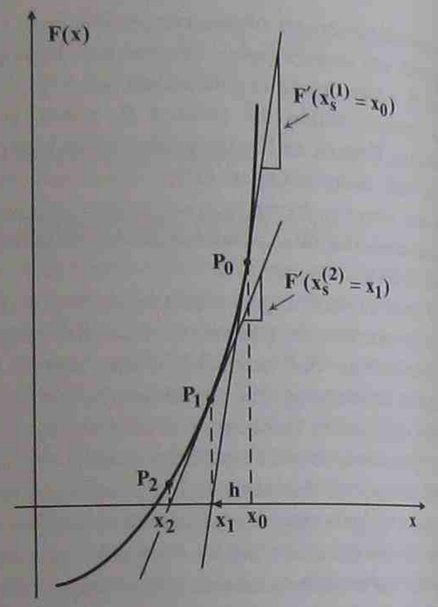



**FIGURE 7.7** Taylor series approximation for one variable, where $h = (x_1 - x_0)$.

$$\left[\frac{dF(x_0)}{dx}\right]^{-1} F(x_1) = (x_1 - x_0), \qquad (7\text{-}45)$$

$$x_1 = x_0 + \left[\frac{dF(x_0)}{dx}\right]^{-1} F(x_1), \qquad (7\text{-}46a)$$

or

$$x_1 = x_0 + \frac{F(x_1)}{\left[\frac{dF(x_0)}{dx}\right]}. \qquad (7\text{-}46b)$$

updated guess — first guess after first iteration

ii) Taylor series for one variable (Fig. 7.7):

$$F(x) = F(x_0) + \frac{(x - x_0)}{1!}F'(x_0) + \frac{(x - x_0)^2}{2!}F''(x_0) + \ldots + \frac{(x - x_0)^n}{n!}F^{(n)}(x_0) + \ldots, \qquad (7\text{-}47)$$





or

$$F(x_0 + h) = F(x_0) + \frac{h}{1!}F'(x_0) + \frac{h^2}{2!}F''(x_0) + \ldots + \frac{h^n}{n!}F^{(n)}(x_0) + \ldots, \qquad (7\text{-}48)$$

$$F(x_0 + h) \approx F(x_0) + \frac{h}{1!}F'(x_0), \qquad (7\text{-}49a)$$

$$F(x_1) \approx F(x_0) + (x_1 - x_0)F'(x_0) \qquad (7\text{-}49b)$$

$$\text{for } F(x_1) = 0 \quad x_1 = x_0 - \frac{F(x_0)}{F'(x_0)}. \qquad (7\text{-}49c)$$

iii) Taylor series for two variables (replace "$d$" by "$\partial$", Fig. 7.6):

$$F(x_0 + h, y_0 + k) = F(x_0, y_0) + \left\{\frac{\partial F(x_0, y_0)}{\partial x}h + \frac{\partial F(x_0, y_0)}{\partial y}k\right\} + \frac{1}{2}\left\{\frac{\partial^2 F(x_0, y_0)}{\partial x^2}h^2 + 2\frac{\partial^2 F(x_0, y_0)}{\partial x \partial y}hk + \frac{\partial^2 F(x_0, y_0)}{\partial y^2}k^2\right\} + \frac{1}{6}\{\ldots\} + \ldots + \frac{1}{h!}\{\ldots\} + R_n, \qquad (7\text{-}50)$$

where $R_n$ is the remainder.

Equation 7-50 can be written in matrix form neglecting higher order terms:

$$F(x_0 + h, y_0 + k) = F(x_0, y_0) + \left[\frac{\partial F(x_0, y_0)}{\partial x}\ \frac{\partial F(x_0, y_0)}{\partial y}\right]\begin{bmatrix} h \\ k \end{bmatrix}, \qquad (7\text{-}51)$$

where

$$h = (x_1 - x_0) \text{ and } k = (y_1 - y_0)$$

or, for $F(x_1, y_1) = 0$,

$$\begin{bmatrix} x_1 \\ y_1 \end{bmatrix} = \begin{bmatrix} x_0 \\ y_0 \end{bmatrix} - \frac{F(x_0, y_0)}{\left[\frac{\partial F(x_0, y_0)}{\partial x}\ \frac{\partial F(x_0, y_0)}{\partial y}\right]}, \qquad (7\text{-}52)$$

or

$$\begin{bmatrix} x_1 \\ y_1 \end{bmatrix} = \begin{bmatrix} x_0 \\ y_0 \end{bmatrix} - \left[\frac{\partial F(x_0, y_0)}{\partial x}\ \frac{\partial F(x_0, y_0)}{\partial y}\right]^{-1} F(x_0, y_0). \qquad (7\text{-}53)$$

Therefore,

$$\begin{bmatrix} x_1 \\ y_1 \end{bmatrix} = \begin{bmatrix} x_0 \\ y_0 \end{bmatrix} - (\bar{J})^{-1} F(x_0, y_0), \qquad (7\text{-}54)$$

where the two-dimensional Jacobian $\bar{J}$ is

$$\bar{J} = \left[\frac{\partial F(x_0, y_0)}{\partial x}\ \frac{\partial F(x_0, y_0)}{\partial y}\right]. \qquad (7\text{-}55)$$

**Residuals of an Equation System.** Given the equation system:

$$x_1 - 2x_2 - 4x_3 = 0$$
$$3x_1 + x_2 + 7x_3 = 0.$$
$$7x_1 - x_2 + x_3 = 0$$

The approximate (guessed) solutions are $x_{10}, x_{20}, x_{30}$. Introducing approximate solutions in the equation system:

$$x_{10} - 2x_{20} - 4x_{30} = \text{residual 1}$$
$$3x_{10} + x_{20} + 7x_{30} = \text{residual 2}$$
$$7x_{10} - x_{20} + x_{30} = \text{residual 3}$$

If $\sum_{i=1}^{3} |\text{residual } i| = 0$, then solution of the equation system has been obtained.

**Fundamental Mismatch Power.** The power flow algorithm is based on the Newton–Raphson approach forcing the mismatch powers (at system buses) to zero. The mismatch powers (real and reactive powers) correspond to the residuals of the equation system as discussed above. Specifically the term "mismatch power" at bus $i$ refers to the summation of the complex powers leaving via lines connected to bus $i$ and the specified complex load (demand) power at this bus. Note that the bus itself cannot produce or dissipate power and therefore the mismatch power for a given bus must be zero. Therefore, the mismatch power vector is

$$\Delta\bar{W} = [P_2 + F_{r,2},\ Q_2 + F_{i,2},\ \ldots\ P_n + F_{r,n},\ Q_n + F_{i,n}]^t, \qquad (7\text{-}56)$$

where $P_j$ and $Q_j$ are the real and reactive load powers at bus $j$, respectively, and $F_{r,j}$ and $F_{i,j}$ are the real and reactive line powers computed later in this section. Figure 7.8 illustrates the definition of power at a given bus. Note the following:

- $P_2 > 0$ demand (load) of real power,
- $P_2 < 0$ generation of real power,

ST. GEORGE MAIN ... UNIVERSITY OF LAGE

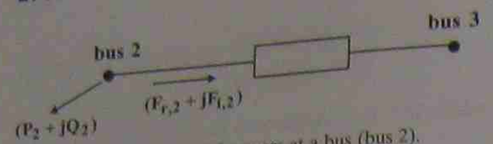



**FIGURE 7.8** Definition of powers at a bus (bus 2).

- $Q_2 > 0$ demand (inductive load) of reactive power, and
- $Q_2 < 0$ generation (capacitive load) of reactive power.

For an $n$-bus system consisting of the swing bus and PQ buses (inclusion of PV buses is considered later), the mismatch power vector has $2(n-1)$ rows corresponding to buses 2 through $n$ (bus 1 is assumed to be the swing bus). Clearly $\Delta\bar{W}$ is a function of $\bar{x}$, the bus voltage vector (Eq. 7-42).

**The Fundamental Newton-Raphson Power Flow Algorithm.** The power flow problem simplifies to finding $\bar{x}$ such that

$$\Delta\bar{W}(\bar{x}) = 0. \tag{7-57}$$

Let $\bar{x}_s$ be the bus solution vector and expand Eq. 7-57 in a Taylor series about $\bar{x} = \bar{x}$, where $\bar{x}_s$ is the (guessed) solution (see Eqs. 7-46 and 7-52):

$$\Delta\bar{W}(\bar{x}) = \Delta\bar{W}(\bar{x}_s) + \bar{J}(\bar{x} - \bar{x}_s), \tag{7-58}$$

or

$$\bar{J}^{-1}\Delta\bar{W}(\bar{x}) = \bar{J}^{-1}\Delta\bar{W}(\bar{x}_s) + (\bar{x} - \bar{x}_s), \tag{7-59}$$

where $\bar{J}$ is the Jacobian.

With $\Delta\bar{W}(\bar{x}) = 0$ because $\bar{x}$ is the (converged) solution vector,

$$\bar{x} = \bar{x}_s - \bar{J}^{-1}\Delta\bar{W}(\bar{x}_s). \tag{7-60}$$

Due to the linearization (neglect of higher order terms), the solution $\bar{x}_s$ of Eq. 7-60 is an approximation which only can be improved by iterations. Therefore,

$$\bar{x}^{\xi+1} = \bar{x}^{\xi} - \bar{J}^{-1}\Delta\bar{W}(\bar{x}^{\xi}) \tag{7-61}$$

or with

$$\Delta\bar{x}^{\xi} = \bar{J}^{-1}\Delta\bar{W}(\bar{x}^{\xi}) \tag{7-62}$$

$$\bar{x}^{\xi+1} = \bar{x}^{\xi} - \Delta\bar{x}^{\xi} \tag{7-63}$$



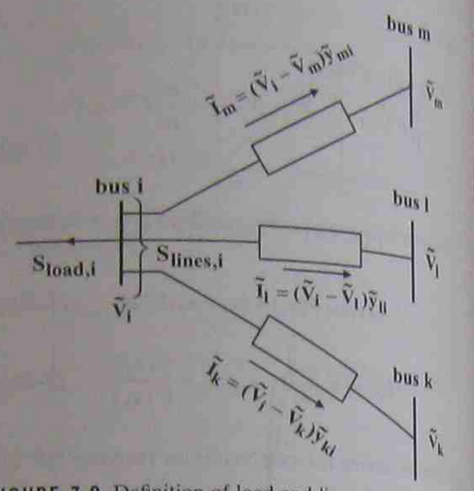



**FIGURE 7.9** Definition of load and line apparent powers as well as line currents.

where superscript $\xi$ indicates the iteration number and $\bar{J}$ is a $2(n-1) \times 2(n-1)$ matrix consisting of partial derivatives of mismatch powers with respect to the bus voltages. Note that all quantities are complex (thus the 2 in front of $(n-1)$) and the swing bus voltage (magnitude and phase angle) is known (therefore $n-1$). If $\Delta\bar{W}(\bar{x}_s) = 0$ then

$$\bar{x} = \bar{x}_s - \bar{J}^{-1}\Delta\bar{W}(\bar{x}_s) = \bar{x}_s. \tag{7-64}$$

The evaluation of Eq. 7-61 (the solution) is done by computer using triangular factorization and forward/backward substitution. This works for a few thousands of buses quite well. In case of hand calculations, where there are just a few buses, we use matrix inversion.

### 7.3.3 Fundamental Jacobian Entry Formulas

Figure 7.9 shows a typical $i$ bus of an $n$-bus system. This $i$ bus is connected to three other buses $m$, $k$, and $l$. The load connected to bus $i$ demands a complex power $S_{load,i}$.

The total complex (apparent) power leaving bus $i$ via the lines to buses $k$, $l$, $m$ is

$$S_{lines,i} = \tilde{V}_i[\tilde{I}_k + \tilde{I}_l + \tilde{I}_m]^*, \tag{7-65}$$

where * denotes the complex conjugate and $\tilde{y}_{ij}$ are the line admittances:

$$S_{lines,i} = \tilde{V}_i[(\tilde{V}_i - \tilde{V}_k)\tilde{y}_{ki} + (\tilde{V}_i - \tilde{V}_l)\tilde{y}_{li} + (\tilde{V}_i - \tilde{V}_m)\tilde{y}_{mi}]^*, \tag{7-66}$$





or

$$S_{lines,i} = \tilde{V}_i[\tilde{V}_i(\tilde{y}_{ki} + \tilde{y}_{li} + \tilde{V}_{mi}) - \tilde{y}_{ki}\tilde{V}_k - \tilde{y}_{li}\tilde{V}_l - \tilde{y}_{mi}\tilde{V}_m]^*, \tag{7-67}$$

With the entries of the admittance matrix

$$\begin{aligned} y_{ii} &= (\bar{Y}_{bus})_{ii} = \tilde{y}_{ki} + \tilde{y}_{li} + \tilde{y}_{mi}, \\ y_{ki} &= (\bar{Y}_{bus})_{ki} = -\tilde{y}_{ki}, \\ y_{li} &= (\bar{Y}_{bus})_{li} = -\tilde{y}_{li}, \\ y_{mi} &= (\bar{Y}_{bus})_{mi} = -\tilde{y}_{mi}, \end{aligned}$$

it follows

$$S_{lines,i} = [(\bar{Y}_{bus})_{ii}\tilde{V}_i + (\bar{Y}_{bus})_{ki}\tilde{V}_k + (\bar{Y}_{bus})_{li}\tilde{V}_l + (\bar{Y}_{bus})_{mi}\tilde{V}_m]^*\tilde{V}_i. \tag{7-68}$$

Using the notation

$$\bar{V}_{bus} = \begin{bmatrix} \tilde{V}_i \\ \tilde{V}_k \\ \tilde{V}_l \\ \tilde{V}_m \end{bmatrix}, \tag{7-69}$$

one can write in a condensed manner

$$S_{lines,i} = [(\text{row } i \text{ of } \bar{Y}_{bus})\bar{V}_{bus}]^*\tilde{V}_i. \tag{7-70}$$

Therefore, for the PQ buses we have the mismatch powers

$$\Delta W_i = S_{load,i} + S_{lines,i} \tag{7-71}$$

$$= S_{load,i} + [(\text{row } i \text{ of } \bar{Y}_{bus})\bar{V}_{bus}]^*\tilde{V}_i, \tag{7-72}$$

where $S_{load,i}$ is the load (demand) complex (apparent) power at bus $i$ ($S_{load,i} = P_i + jQ_i$). Breaking the mismatch power $\Delta W_i$ into a real part $\Delta P_i$ and an imaginary part $\Delta Q_i$, we have the real and reactive mismatch powers, respectively:

$$\Delta P_i = P_i + \text{Real}\{[(\text{row } i \text{ of } \bar{Y}_{bus})\bar{V}_{bus}]^*\tilde{V}_i\} \tag{7-73}$$

and

$$\Delta Q_i = Q_i + \text{Imag}\{[(\text{row } i \text{ of } \bar{Y}_{bus})\bar{V}_{bus}]^*\tilde{V}_i\} \tag{7-74}$$

with $P_i$ and $Q_i$ being the real and reactive load (demand) powers at bus $i$.

**Inspection of Matrix Expression** (Eq. 7-70). Let us inspect the expression $\tilde{V}_i$ [(row $i$ of $\bar{Y}_{bus}$)$\bar{V}_{bus}$]* (with entries of admittance matrix in terms of line admittances, note minus signs):

$$\tilde{V}_i[(\text{row } i \text{ of } \bar{Y}_{bus})\bar{V}_{bus}]^* = \tilde{V}_i[\tilde{V}_i(\tilde{y}_{ki} + \tilde{y}_{li} + \tilde{V}_{mi}) - \tilde{y}_{ki}\tilde{V}_k - \tilde{y}_{li}\tilde{V}_l - \tilde{y}_{mi}\tilde{V}_m]^* \tag{7-75}$$

with

$$\begin{aligned} \tilde{V}_i &= V_i e^{j\delta_i}, \\ \tilde{V}_k &= V_k e^{j\delta_k}, \\ \tilde{V}_l &= V_l e^{j\delta_l}, \\ \tilde{y}_{ki} &= |\tilde{y}_{ki}| e^{j\theta_{ki}}. \end{aligned} \tag{7-76}$$

Therefore, for the complex (apparent) power between buses k and $i$ one gets

$$\tilde{V}_i[(-\tilde{y}_{ki})\tilde{V}_k]^* = |\tilde{V}_i|e^{j\delta_i}(-|\tilde{y}_{ki}|)e^{-j\theta_{ki}}|\tilde{V}_k|e^{-j\delta_k} = |\tilde{V}_i||\tilde{V}_k|(-|\tilde{y}_{ki}|)e^{j(-\theta_{ki}-\delta_k+\delta_i)} = F_{r,ki} + F_{i,ki}, \tag{7-77}$$

$$F_{i,ki} = V_i V_k(-|\tilde{y}_{ki}|)\cos(-\theta_{ki} - \delta_k + \delta_i), \tag{7-78}$$

and

$$F_{r,ki} = V_i V_k(-|\tilde{y}_{ki}|)\sin(-\theta_{ki} - \delta_k + \delta_i) \tag{7-79}$$

or for all buses connected to bus $i$,

$$\Delta P_i = P_i + F_{r,i} = P_i + \sum_{j=1}^{n} y_{ij}V_jV_i\cos(-\theta_{ij} - \delta_j + \delta_i) \tag{7-80}$$

and

$$\Delta Q_i = Q_i + F_{i,i} = Q_i + \sum_{j=1}^{n} y_{ij}V_jV_i\sin(-\theta_{ij} - \delta_j + \delta_i), \tag{7-81}$$

where $y_{ij}$ and $\theta_{ij}$ are the magnitude and the phase angle of the $(i,j)$th entry of the admittance matrix, respectively, and $V_j = |\tilde{V}_j|$ and $\delta_j$ are the voltage rms magnitude and phase angle at bus $j$.

The Jacobian matrix is defined as

$$\bar{J} = \begin{bmatrix} \frac{\partial\Delta P_2}{\partial\delta_2} & \frac{\partial\Delta P_2}{\partial V_2} & \cdots & \frac{\partial\Delta P_2}{\partial\delta_n} & \frac{\partial\Delta P_2}{\partial V_n} \\ \frac{\partial\Delta Q_2}{\partial\delta_2} & \frac{\partial\Delta Q_2}{\partial V_2} & \cdots & \frac{\partial\Delta Q_2}{\partial\delta_n} & \frac{\partial\Delta Q_2}{\partial V_n} \\ \vdots & \vdots & \vdots & \vdots & \vdots \\ \frac{\partial\Delta P_n}{\partial\delta_2} & \frac{\partial\Delta P_n}{\partial V_2} & \cdots & \frac{\partial\Delta P_n}{\partial\delta_n} & \frac{\partial\Delta P_n}{\partial V_n} \\ \frac{\partial\Delta Q_n}{\partial\delta_2} & \frac{\partial\Delta Q_n}{\partial\delta_n} & \cdots & \frac{\partial\Delta Q_n}{\partial\delta_n} & \frac{\partial\Delta Q_n}{\partial V_n} \end{bmatrix}, \tag{7-82a}$$

where

- The main-diagonal entries of the Jacobian are

$$\frac{\partial \Delta P_i}{\partial \delta_i} = -\sum_{\substack{j=1 \\ j\neq i}}^{n} y_{ij} V_i V_j \sin(\delta_i - \delta_j - \theta_{ij}). \qquad (7\text{-}82b)$$

- Off-diagonal entry:

$$\frac{\partial \Delta P_i}{\partial \delta_k} = y_{ik} V_i V_k \sin(\delta_i - \delta_k - \theta_{ik}) \quad k \neq i. \qquad (7\text{-}82c)$$

(Note that the negative sign cancels with negative sign due to derivative of $-\delta_k$).

- Main-diagonal entry:

$$\frac{\partial \Delta P_i}{\partial V_i} = \sum_{\substack{j=1 \\ j\neq i}}^{n} y_{ij} V_j \cos(\delta_i - \delta_j - \theta_{ij}) + 2V_i y_{ii} \cos(-\theta_{ii}). \qquad (7\text{-}82d)$$

- Off-diagonal entry:

$$\frac{\partial \Delta P_i}{\partial V_k} = y_{ik} V_i \cos(\delta_i - \delta_k - \theta_{ik}) \quad k \neq i. \qquad (7\text{-}82e)$$

- Main-diagonal entry:

$$\frac{\partial \Delta Q_i}{\partial \delta_i} = \sum_{\substack{j=1 \\ j\neq i}}^{n} y_{ij} V_i V_j \cos(\delta_i - \delta_j - \theta_{ij}). \qquad (7\text{-}82f)$$

- Off-diagonal entry:

$$\frac{\partial \Delta Q_i}{\partial \delta_k} = -y_{ik} V_i V_k \cos(\delta_i - \delta_k - \theta_{ik}) \quad k \neq i. \qquad (7\text{-}82g)$$

- Main-diagonal entry:

$$\frac{\partial \Delta Q_i}{\partial V_j} = \sum_{\substack{j=1 \\ j\neq i}}^{n} y_{ij} V_j \sin(\delta_i - \delta j - \theta_{ij}) + 2V_i y_{ii} \sin(-\theta_{ii}). \qquad (7\text{-}82h)$$

- Off-diagonal entry:

$$\frac{\partial \Delta Q_i}{\partial V_k} = y_{ik} V_i \sin(\delta_i - \delta_k - \theta_{ik}) \quad k \neq i. \qquad (7\text{-}82i)$$

### 7.3.4 Newton–Raphson Power Flow Algorithm

Based on the equations given, the conventional fundamental power flow algorithm is the computation

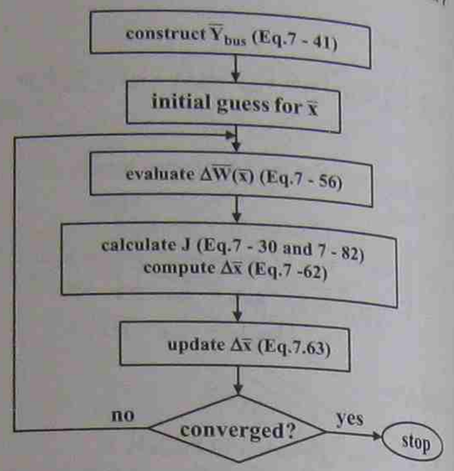



**FIGURE 7.10** Fundamental Newton–Raphson power flow algorithm.

of the bus voltage vector for a given system configuration and linear loads. The Newton–Raphson approach (Eq. 7-64) will be used to force the mismatch power to zero (Eq. 7-57). The iterative solution procedure for the fundamental Newton–Raphson power flow algorithm is as follows (Fig. 7.10):

- **Step 1:** Construct the admittance matrix $\bar{Y}_{bus}$ (Eq. 7-41).
- **Step 2:** Make an initial guess for $\bar{x}$ (e.g., 1.0 pu volts and zero radians for all bus voltages, Eq. 7-42).
- **Step 3:** Evaluate mismatch power ($\Delta\bar{W}(\bar{x})$, Eq. 7-56). If it is small enough then stop.
- **Step 4:** Establish Jacobian $\bar{J}$ (Eqs. 7-30 and 7-82) and calculate $\Delta\bar{x}^s$ (Eq. 7-62) using either matrix inversion (for problems with a few buses) or upper (lower) triangular factorization combined with backward/forward substitution.
- **Step 5:** Update the bus vector voltage (Eq. 7-63) and go to Step 3.

It is recommended to use upper (lower) triangular factorization combined with backward/forward substitution rather than matrix inversion in computing the solution because an iterative method is used where the coefficient matrix is updated from iteration to iteration.

### 7.3.5 Application Example 7.8: Computation of Fundamental Admittance Matrix

A simple (few buses) power system (Fig. E7.8.1) is used to illustrate in detail the Newton–Raphson load



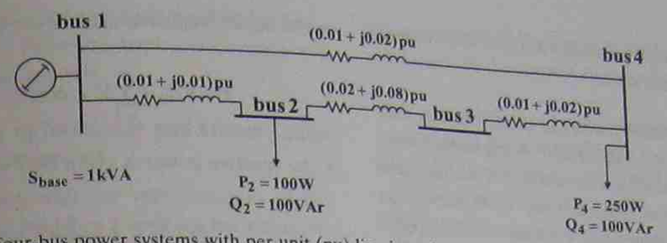



**FIGURE E7.8.1** Four-bus power systems with per unit (pu) line impedances.

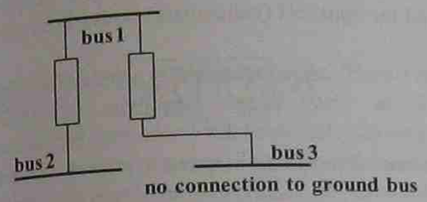



**FIGURE 7.11** No connection to ground results in singular admittance matrix.

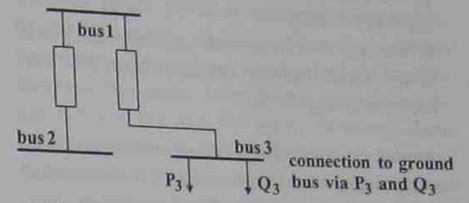



**FIGURE 7.12** PQ bus (bus 3) results in nonsingular Jacobian and load flow problem has a well-defined solution because the inverse of $\bar{J}$ exists, although $\bar{Y}_{bus}^{-1}$ is singular.

flow analysis. All impedances are in pu and the base apparent power is $S_{base} = 1$ kVA. Compute the fundamental admittance matrix for this system.

#### Comment about Singularity

- Considering

$$[\bar{I}_{bus}] = [\bar{Y}_{bus}]^{-1}[\bar{V}_{bus}],$$

without any connection (admittance) from any bus to ground (Fig. 7.11), $\bar{Y}_{bus}^{-1}$ is singular. However, if $\bar{Y}_{bus}$ contains load information (admittance to ground) then it will not be singular.

- Considering

$$[\Delta\bar{x}] = [\bar{J}]^{-1}[\Delta\bar{W}],$$

if $[\bar{J}]$ contains load information ($P_3$, $Q_3$, Fig. 7.12), then $[\bar{J}]$ is not singular.

### 7.3.6 Application Example 7.9: Evaluation of Fundamental Mismatch Vector

For the system of Fig. E7.8.1, assume bus 1 is the swing bus ($\delta_1 = 0$ and $|\tilde{V}_1| = 1.0$ pu). Then we can make an initial guess for bus voltage vector $\bar{x}^0 = (\delta_2, |\tilde{V}_2|, \delta_3, |\tilde{V}_3|, \delta_4, |\tilde{V}_4|)^t = (0, 1, 0, 1, 0, 1)^t$. Note, the superscript 0 means initial guess. Compute the mismatch power vector for this initial condition.

### 7.3.7 Application Example 7.10: Evaluation of Fundamental Jacobian Matrix

For the system of Fig. E7.8.1, compute the Jacobian matrix.

### 7.3.8 Application Example 7.11: Calculation of the Inverse of Jacobian Matrix

Compute the inverse of the Jacobian matrix (evaluated in Application Example 7.10) using the adjoint and determinant.

### 7.3.9 Application Example 7.12: Inversion of a 3 × 3 Matrix

In order to demonstrate the entire procedure for the computation of the inverse of a matrix the following 3 × 3 matrix will be used

$$\bar{A} = \begin{bmatrix} 1 & 3 & -1 \\ 2 & -4 & 2 \\ 3 & 1 & 1 \end{bmatrix}.$$

### 7.3.10 Application Example 7.13: Computation of the Correction Voltage Vector

For the system of Fig. E7.8.1, compute the correction voltage vector $\Delta\bar{x}^0$, updating the mismatch power vector, and check the convergence of the load flow algorithm (using a convergence tolerance of 0.0001).

## 7.4 NEWTON-BASED HARMONIC POWER FLOW

Classifications of solution approaches for the harmonic power (load) flow problem are summarized at the end of this chapter. In this section, the Newton-based harmonic power flow [5, 6] is selected, ana-

lyzed, and thoroughly illustrated. There are two main reasons for this selection:

- The Newton-based harmonic power flow is relatively easy to understand and to implement since it is an extension of the conventional fundamental Newton–Raphson formulation; it is based on similar terminologies and equations. It is capable of including any type of nonlinear load assuming its *v–i* characteristic is available in the frequency (or time) domain.
- It was the first proposed approach for power system modeling with nonlinear loads and harmonic couplings [5, 6].

Among the limitations of the Newton-based harmonic power flow in its present form is the assumption of balanced network and load conditions.

### 7.4.1 Harmonic Bus Admittance Matrix and Power Definitions

For nonsinusoidal operating conditions power system matrices will be defined at harmonic frequencies. These matrices include the harmonic bus admittance matrix $\bar{Y}_{bus}^{(h)}$, the harmonic bus impedance matrix $\bar{Z}_{bus}^{(h)} = 1/\bar{Y}_{bus}^{(h)}$, and the harmonic Jacobian $\bar{J}^{(h)}$ matrix.

The harmonic bus admittance matrix $\bar{Y}_{bus}^{(h)}$ is identical to the fundamental bus admittance matrix $\bar{Y}_{bus}^{(1)} = \bar{Y}_{bus}$ with the difference that line admittances are evaluated at the hth harmonic frequency $f_h = h \cdot f_1$:

$$\bar{Y}_{bus}^{(h)} = \begin{bmatrix} y_{11}^{(h)} & y_{12}^{(h)} & \cdots & y_{1n}^{(h)} \\ y_{21}^{(h)} & y_{22}^{(h)} & \cdots & y_{2n}^{(h)} \\ \cdot & \cdot & \cdots & \cdot \\ y_{n1}^{(h)} & y_{n2}^{(h)} & \cdots & y_{nn}^{(h)} \end{bmatrix}, \quad (7\text{-}83)$$

where $\omega_h = 2\pi h f_1 = h \cdot 377$ rad/s.

**Power Definitions at Harmonic Frequencies.** Consider a voltage $v(t)$ and a current $i(t)$ expressed in terms of their rms harmonic components

$$v(t) = V_0 + \sum_{h=1}^{\infty} \sqrt{2} V_h \sin(h\omega_1 t + \theta_h^v), \quad (7\text{-}84)$$

$$i(t) = I_0 + \sum_{h=1}^{\infty} \sqrt{2} I_h \sin(h\omega_1 t + \theta_h^i). \quad (7\text{-}85)$$

Then

- the active (real, average) power is given by

$$P = V_0 I_0 + \sum_{h=1}^{\infty} V_h I_h \cos(\theta_h^v - \theta_h^i), \quad (7\text{-}86)$$

- the reactive power is given by

$$Q = \sum_{h=1}^{\infty} V_h I_h \sin(\theta_h^v - \theta_h^i), \quad (7\text{-}87)$$

- and the apparent (voltampere) power is

$$S = \sqrt{\left(\sum_{h=0}^{\infty} I_h^2\right)\left(\sum_{h=0}^{\infty} V_h^2\right)}. \quad (7\text{-}88)$$

In case of sinusoidal $v(t)$ and $i(t)$ ($h = 1$ only), we have

$$S^2 = P^2 + Q^2. \quad (7\text{-}89)$$

For nonsinusoidal cases that relation does not hold and must be replaced by

$$D = \sqrt{S^2 - P^2 - Q^2}, \quad (7\text{-}90)$$

where D is called the distortion power. Other definitions have also been proposed for harmonic powers, which are not discussed here.

**Classification of Time Harmonics.** Time harmonics can be classified into three types (Table 7.2):

- positively rotating harmonics (+),
- negatively rotating harmonics (–), and
- zero-sequence harmonics (0).

Triplen (multiples of three) harmonics ($3h$, for $h = 1, 2, 3, \ldots$) in a balanced three-phase system are predominantly of the zero-sequence type. With a few exceptions (discussed in preceding chapters), zero-sequence currents cannot flow from the network into

**TABLE 7.2** Classification of Time Harmonics

| Positive (+) sequence | Negative (–) sequence | Zero (0) sequence |
|---|---|---|
| 1 | 2 | 3 |
| 4 | 5 | 6 |
| 7 | 8 | 9 |
| 10 | 11 | 12 |
| 13 | 14 | 15 |
| 16 | 17 | 18 |
| 19 | 20 | 21 |
| ⋮ | ⋮ | ⋮ |



a delta or an ungrounded wye-connected device (e.g., transformer), and therefore triplen harmonics are excluded from this analysis.

### 7.4.2 Modeling of Nonlinear and Linear Loads at Harmonic Frequencies

Before proceeding with the reformulation of the Newton–Raphson load flow to include harmonic frequencies, it is necessary to properly model linear and nonlinear loads at fundamental and harmonic frequencies.

**Harmonic Modeling of Nonlinear Loads.** The v–i relationship of nonlinear loads (such as line-commutated converters) will be modeled as coupled harmonic current sources. The injected harmonic currents of a nonlinear load ($I_{injected}^{(h)}$) at bus m will be a function of its fundamental and harmonic voltages:

$$\begin{cases} \text{Real}(I_{injected}^{(h)}) = g_{r,m}^{(h)}(\tilde{V}_m^{(1)}, \tilde{V}_m^{(5)}, \tilde{V}_m^{(7)}, \ldots, \tilde{V}_m^{(L)}, \alpha_m, \beta_m) \\ \text{Imag}(I_{injected}^{(h)}) = g_{i,m}^{(h)}(\tilde{V}_m^{(1)}, \tilde{V}_m^{(5)}, \tilde{V}_m^{(7)}, \ldots, \tilde{V}_m^{(L)}, \alpha_m, \beta_m) \end{cases}, \quad (7\text{-}91)$$

where $\alpha_m$ and $\beta_m$ are the nonlinear load control parameters and $L$ is the maximum harmonic order considered $L = h_{max}$. The currents of Eq. 7-91 are referred to the nonlinear bus m to which the nonlinear load is connected. The nonlinearity of $g_m^{(h)}$ is due to strong couplings between harmonic currents and voltages dictated by the nonlinear load. In some cases (e.g., decoupled harmonic power flow formulation), it is convenient to ignore harmonic couplings $g_m^{(h)}(\tilde{V}_m^{(h)}, \alpha_m, \beta_m)$ and simplify the problem.

As an example, for a full-wave bridge rectifier connected to bus m (shown in Fig. 7.13), $\alpha_m$ is the firing angle of semiconductor-controlled rectifiers (SCRs), and $\beta_m$ is either the commutating impedance (inductance) or the DC voltage ($E$). Note that the equivalent circuit models a three-phase full-wave rectifier/inverter with a general load, where $L_{com}$ is the commutating inductance, that is, the leakage inductance of the transformer, and

- for a passive load, only resistance $R$ and filter inductance $F$ are considered,
- for a DC motor drive, only $R$ and $E$ are considered ($E > 0$) when motoring, and
- for inverter operation with a DC generator, only $R$ and $E$ are considered ($E < 0$).

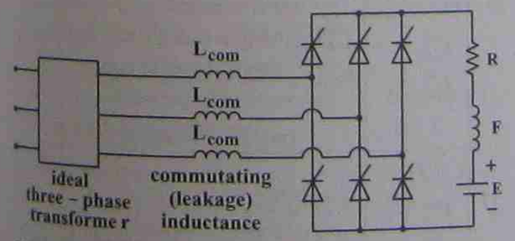



**FIGURE 7.13** Line-commutated converter with general load.

**Modeling Linear Loads at Harmonic Frequencies.** For the formulation of harmonic power flow, equivalent circuits of linear loads are required. At the fundamental frequency, linear loads are modeled as conventional PQ and PV buses. However, shunt admittances are used to model them at harmonic frequencies [7, 8]. The admittance of a linear load connected to bus $k$ at the hth harmonic is

$$y_k^{(h)} = \frac{(P_k^{(1)} - jQ_k^{(1)})/h}{|V_k^{(1)}|^2}. \quad (7\text{-}92)$$

where $j$ represents the operator $\sqrt{-1}$.

Capacitor banks are modeled as a fixed shunt reactance. Transformers are approximated by linear leakage inductances, and their nonlinearities and losses due to eddy currents, hysteresis, and saturation are neglected.

### 7.4.3 The Harmonic Power Flow Algorithm (Assembly of Equations)

Power system components, loads, and generators that produce time harmonics in an otherwise harmonic-free network are termed nonlinear. Other buses such as the standard PQ and PV buses with no converter or other nonlinear devices connected are termed linear. Consider

- Bus 1 to be the conventional swing (slack) bus with specified values for voltage magnitude $|\tilde{V}_1|$ and phase angle $\delta_1$.
- Buses 2 through $(m-1)$ to be the conventional linear PQ (or PV) buses. As with the conventional power flow problem, active $P_i^{(1)}$ and reactive $Q_i^{(1)}$ powers are assumed to be known at these linear buses.
- Buses $m$ through $n$ to be nonlinear buses. At these buses, the fundamental real power $P_i^{(1)}$ and the total apparent power $S_{i,total}$ (or the total reactive power $Q_{i,total}$) are specified.

Network voltages and currents are represented by Fourier series components, and the bus voltage vector

$\bar{x}$ of the fundamental power flow (Eq. 7-42) is redefined as

$$\bar{U} = [\delta_2^{(1)}, |\tilde{V}_2^{(1)}|, \ldots, \delta_n^{(1)}, |\tilde{V}_n^{(1)}|, \delta_1^{(5)}, |\tilde{V}_1^{(5)}|, \ldots, \delta_n^{(5)}, |\tilde{V}_n^{(5)}|, \ldots, \delta_1^{(L)}, |\tilde{V}_1^{(L)}|, \ldots, \delta_n^{(L)}, |\tilde{V}_n^{(L)}|, \alpha_m, \beta_m, \ldots, \alpha_n, \beta_n]^t = [\bar{V}^{(1)}, \bar{V}^{(5)}, \ldots, \bar{V}^{(L)}, \bar{\Phi}]^t \tag{7-93}$$

where (superscripts and subscripts denote harmonic orders and bus numbers, respectively)

Fundamental voltages are

$$\bar{V}^{(1)} = \delta_2^{(1)}, |\tilde{V}_2^{(1)}|, \ldots, \delta_n^{(1)}, |\tilde{V}_n^{(1)}|, \tag{7-94a}$$

Fifth harmonic voltages are

$$\bar{V}^{(5)} = \delta_1^{(5)}, |\tilde{V}_1^{(5)}|, \ldots, \delta_n^{(5)}, |\tilde{V}_n^{(5)}|, \tag{7-94b}$$

Lth harmonic voltages are

$$\bar{V}^{(L)} = \delta_1^{(L)}, |\tilde{V}_1^{(L)}|, \ldots, \delta_n^{(L)}, |\tilde{V}_n^{(L)}|, \tag{7-94c}$$

Nonlinear device variables vector is

$$\bar{\Phi} = \alpha_m, \beta_m, \ldots, \alpha_n, \beta_n. \tag{7-95}$$

Harmonic bus voltage magnitudes, phase angles, and the nonlinear device parameters ($\alpha_m$, $\beta_m$) are unknowns; therefore the conventional formulation (forcing the fundamental mismatch powers to zero) is not sufficient to solve the harmonic power flow problem. Three additional relations are used:

- Kirchhoff's current law for the fundamental frequency (fundamental current balance) at nonlinear buses.
- Kirchhoff's current law for each harmonic (harmonic current balance) at all buses.
- Conservation of apparent voltamperes (apparent power or voltampere balance) at nonlinear buses.

Note that Kirchhoff's current law for the fundamental frequency is not applied to linear buses since active and reactive power (mismatch power) balance has already been applied at these buses.

**Current Balance for Fundamental Frequency.** The current balance is written for fundamental frequency ($h = 1$) at the nonlinear buses as indicated in Fig. 7.14, where the nonlinear currents $g_{r,m}^{(1)}$, $g_{i,m}^{(1)}$ are referred to bus m. Therefore one obtains for the nonlinear buses (from bus m to bus n) for the fundamental current balance:

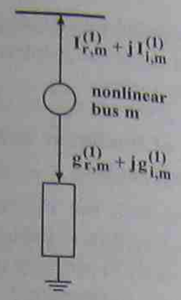



**FIGURE 7.14** Application of current balance ($I_{r,m}^{(1)} + jI_{i,m}^{(1)} + g_{r,m}^{(1)} + jg_{i,m}^{(1)} = 0$) at a nonlinear bus.

$$\begin{bmatrix} I_{r,m}^{(1)} \\ I_{i,m}^{(1)} \\ \cdot \\ \cdot \\ \cdot \\ I_{r,n}^{(1)} \\ I_{i,n}^{(1)} \end{bmatrix} = - \begin{bmatrix} g_{r,m}^{(1)}(\tilde{V}_m^{(1)}, \tilde{V}_m^{(5)}, \ldots, \tilde{V}_m^{(L)}, \alpha_m, \beta_m) \\ g_{i,m}^{(1)}(\tilde{V}_m^{(1)}, \tilde{V}_m^{(5)}, \ldots, \tilde{V}_m^{(L)}, \alpha_m, \beta_m) \\ \cdot \\ \cdot \\ \cdot \\ g_{r,n}^{(1)}(\tilde{V}_n^{(1)}, \tilde{V}_n^{(5)}, \ldots, \tilde{V}_n^{(L)}, \alpha_n, \beta_n) \\ g_{i,n}^{(1)}(\tilde{V}_n^{(1)}, \tilde{V}_n^{(5)}, \ldots, \tilde{V}_n^{(L)}, \alpha_n, \beta_n) \end{bmatrix}, \tag{7-96}$$

where $I_{r,m}^{(1)}$ and $I_{i,m}^{(1)}$ are the fundamental real and reactive line currents at the mth nonlinear bus, respectively, and $g_{r,m}^{(1)}$ and $g_{i,m}^{(1)}$ are the fundamental real and reactive injected load currents at the same bus. Note that the line and injected load currents are positive if they leave the bus.

**Current Balance at Harmonic Frequencies.** For all (linear and nonlinear) buses one can write

$$\begin{bmatrix} I_{r,1}^{(h)} \\ I_{i,1}^{(h)} \\ \cdot \\ \cdot \\ \cdot \\ I_{r,m-1}^{(h)} \\ I_{i,m-1}^{(h)} \\ \hline I_{r,m}^{(h)} \\ I_{i,m}^{(h)} \\ \cdot \\ \cdot \\ \cdot \\ I_{r,n}^{(h)} \\ I_{i,n}^{(h)} \end{bmatrix} = - \begin{bmatrix} 0 \\ \cdot \\ \cdot \\ \text{(swing bus and linear buses)} \\ \cdot \\ \cdot \\ 0 \\ \hline g_{r,m}^{(h)}(\tilde{V}_m^{(1)}, \tilde{V}_m^{(5)}, \ldots, \tilde{V}_m^{(L)}, \alpha_m, \beta_m) \\ g_{i,m}^{(h)}(\tilde{V}_m^{(1)}, \tilde{V}_m^{(5)}, \ldots, \tilde{V}_m^{(L)}, \alpha_m, \beta_m) \\ \cdot \\ \text{(nonlinear buses)} \\ \cdot \\ g_{r,n}^{(h)}(\tilde{V}_n^{(1)}, \tilde{V}_n^{(5)}, \ldots, \tilde{V}_n^{(L)}, \alpha_n, \beta_n) \\ g_{i,n}^{(h)}(\tilde{V}_n^{(1)}, \tilde{V}_n^{(5)}, \ldots, \tilde{V}_n^{(L)}, \alpha_n, \beta_n) \end{bmatrix} \tag{7-97}$$



The line currents $I_{r,m}^{(h)}$ and $I_{i,m}^{(h)}$ will be computed in the next section.

**Apparent Power or Voltampere Balance.** The third type of relation is the apparent power (voltampere) balance at each nonlinear bus $j$:

$$S_j^2 = (P_j')^2 + (Q_j')^2 + D_j^2, \tag{7-98}$$

where $j = m, \ldots, n$ and

$$(P_j')^2 = \left(\sum_h P_j^{(h)}\right)^2 = (V_j^{(1)} I_j^{(1)} \cos\theta_j^{(1)} + V_j^{(5)} I_j^{(5)} \cos\theta_j^{(5)} + V_j^{(7)} I_j^{(7)} \cos\theta_j^{(7)} + \ldots)^2 \tag{7-99a}$$

$$(Q_j')^2 = \left(\sum_h Q_j^{(h)}\right)^2 = (V_j^{(1)} I_j^{(1)} \sin\theta_j^{(1)} + V_j^{(5)} I_j^{(5)} \sin\theta_j^{(5)} + V_j^{(7)} I_j^{(7)} \sin\theta_j^{(7)} + \ldots)^2 \tag{7-99b}$$

are the total (fundamental plus harmonics) real and reactive load powers at nonlinear buses. $D_m$ to $D_n$ can be computed from $g_{r,m}, g_{i,m}, \ldots, g_{r,n}, g_{i,n}$; therefore, distortion powers are not independent variables. Equation 7-98 is used to update (between iterations) the nonlinear-device injected powers P and Q at the nonlinear buses.

The number of unknowns for the n buses are as follows ($K$ = number of harmonics considered not including fundamental, e.g., for h = 1, 5, 7, 11 we get $K = 3$):

| | |
|---|---|
| • Fundamental bus voltage magnitudes and phases for all buses but the swing bus | $2(n-1)$ |
| • Fundamental real and reactive powers at the swing bus (losses $P_1$, $Q_1$) | 2 |
| • Harmonic (not including fundamental) voltage magnitudes and phases at all (total) $n$ buses | $2nK$ |
| • Total reactive powers $Q_j'$ at each nonlinear bus, where $n$ is the number of all buses and $(m-1)$ the number of linear buses | $n-(m-1) = (n-m+1)$ |
| • Two variables ($\alpha_j$, $\beta_j$) associated with each nonlinear bus | $2(n-m+1)$ |
| • Total number of unknowns | $2n(K+1) + 3(n-m+1)$ |

The number of available equations are as follows:

| | |
|---|---|
| • Fundamental real and reactive power balance at all $(m-1)$ linear buses but the swing bus | $2(m-2)$ |
| • Fundamental voltage magnitude and phase at the swing bus ($\|\tilde{V}_1\| = 1\ pu$, $\delta_1 = 0\ radians$) | 2 |
| • Fundamental real and imaginary current balance at $n-(m-1)$ nonlinear buses (at $(m-1)$ linear buses the $P_i^{(1)}$ and $Q_i^{(1)}$ are specified) | $2(n-(m-1)) = 2(n-m+1)$ |
| • Harmonic real and reactive current (except the fundamental) balance at all $n$ buses | $2nK$ |
| • Apparent voltampere balance at $n-(m-1)$ nonlinear buses to compute reactive power (if reactive power is specified at nonlinear buses, however, this apparent voltampere balance is not required at nonlinear buses) | $(n-m+1)$ |
| • Total number of equations | $2n(K+1) + (n-m+1)$ |

There remain $2(n-m+1)$ equations to be defined. These can be the total real and reactive mismatch powers at the n – (m – 1) nonlinear buses:

$$\Delta P_j^{\text{nonlinear}} = P_j' + \sum_h F_{r,j}^{(h)}, \tag{7-100a}$$

$$\Delta Q_j^{\text{nonlinear}} = Q_j' + \sum_h F_{i,j}^{(h)}, \tag{7-100b}$$

where $j = m, \ldots, n$ and $P_j'$ and $Q_j'$ are the total (fundamental and harmonics) nonlinear load real and reactive powers at bus j, respectively. $\sum_h F_{r,j}^{(h)}$ and $\sum_h F_{i,j}^{(h)}$ (for $h = 1, 5, 7, \ldots, L$) are the total real and reactive line powers, respectively. Note that the formulas for $F_{r,j}^{(h)}$ and $F_{i,j}^{(h)}$ are identical to those for $F_{r,j}$ and $F_{i,j}$ of the fundamental power flow problem with the difference that $\bar{Y}_{\text{bus}}^{(h)}$ and the hth harmonic voltages must be used. The application of the newly defined mismatch powers at the nonlinear buses results in $2(n-m+1)$ additional equations, and the number of equations is identical to the number of unknowns.

### 7.4.4 Formulation of Newton–Raphson Approach for Harmonic Power Flow

The mismatch vector (consisting of mismatch power and mismatch currents) for harmonic power flow is defined as

ST. GEORGE COMMUNITY COLLEGE LIBRARY

$$\Delta\bar{M} = [\Delta\bar{W}, \Delta\bar{I}^{(5)}, \ldots, \Delta\bar{I}^{(L)}, \Delta\bar{I}^{(1)}]^t, \quad (7\text{-}101)$$

where $\Delta\bar{W}$ is the mismatch power vector (Eq. 7-56) and $(\Delta\bar{I}^{(5)}, \ldots, \Delta\bar{I}^{(L)}, \Delta\bar{I}^{(1)})$ is the mismatch current vector for the harmonics including the fundamental.

In Eq. 7-101,

$$\Delta\bar{W} = [P_2^{(1)} + F_{r,2}^{(1)}, Q_2^{(1)} + F_{i,2}^{(1)}, \ldots, P_{m-1}^{(1)} + F_{r,m-1}^{(1)}, Q_{m-1}^{(1)} + F_{i,m-1}^{(1)}, \Delta P_m^{\text{nonlinear}}, \Delta Q_m^{\text{nonlinear}}, \ldots, \Delta P_n^{\text{nonlinear}}, \Delta Q_n^{\text{nonlinear}}]^t \quad (7\text{-}102)$$

where $P_2^{(1)} + F_{r,2}^{(1)}$, $Q_2^{(1)} + F_{i,2}^{(1)}, \ldots, P_{m-1}^{(1)} + F_{r,m-1}^{(1)}$, $Q_{m-1}^{(1)} + F_{i,m-1}^{(1)}$ applies to linear buses, and $\Delta P_m^{\text{nonlinear}}$, $\Delta Q_m^{\text{nonlinear}}, \ldots, \Delta P_n^{\text{nonlinear}}, \Delta Q_n^{\text{nonlinear}}$ applies to nonlinear buses. $P_j^{(1)}$ and $Q_j^{(1)}$ are the real and reactive fundamental load powers for the linear bus $j$ (as defined by the fundamental load flow analysis), respectively; $F_{r,j}^{(1)}$ and $F_{i,j}^{(1)}$ are the (line) fundamental real and reactive powers at the linear bus $j$ (see fundamental load flow analysis), respectively.

The fundamental current mismatch is defined for nonlinear buses where all currents (e.g., line currents and nonlinear load currents) are referred to the swing bus:

$$\Delta\bar{I}^{(1)} = [I_{r,m}^{(1)} + G_{r,m}^{(1)}, I_{i,m}^{(1)} + G_{i,m}^{(1)}, \ldots, I_{r,n}^{(1)} + G_{r,n}^{(1)}, I_{i,n}^{(1)} + G_{i,n}^{(1)}]^t, \quad (7\text{-}103)$$

and the harmonic current mismatch is defined for linear and nonlinear buses including swing bus:

$$\Delta\bar{I}^{(h)} = [I_{r,1}^{(h)}, I_{i,1}^{(h)}, \ldots, I_{r,m-1}^{(h)}, I_{i,m-1}^{(h)}, I_{r,m}^{(h)} + G_{r,m}^{(h)}, I_{i,m}^{(h)} + G_{i,m}^{(h)}, \ldots, I_{r,n}^{(h)} + G_{r,n}^{(h)}, I_{i,n}^{(h)} + G_{i,n}^{(h)}]^t, \quad (7\text{-}104)$$

where the nonlinear load current components $G_{r,n}^{(h)}$ and $G_{i,m}^{(h)}$ are given (referred to swing bus) and the line current components $I_{r,m}^{(h)}$ and $I_{i,m}^{(h)}$ will be generated in the next section. The Newton–Raphson method is implemented by forcing the appropriate mismatches, $\Delta\bar{M}$, to zero using the Jacobian matrix $\bar{J}$ and obtaining appropriate correction terms $\Delta\bar{U}^{(\xi)} = \bar{U}^{(\xi)} - \bar{U}^{(\xi+1)}$, where $\xi$ represents the iteration number:

$$\Delta\bar{M} = \bar{J}\,\Delta\bar{U}^{(\xi)}. \quad (7\text{-}105)$$

The Jacobian $\bar{J}$ is a $2(nK+n-1)+2(n-m+1)$ by $2(nK+n-1)+2(n-m+1)$ matrix, where $n$ is the total number of buses, $(m-1)$ is the number of linear buses including the swing bus, and $K$ is the number of harmonics considered, excluding the fundamental ($h=1$):

$$\begin{bmatrix} \Delta\bar{W} \\ \Delta\bar{I}^{(5)} \\ \Delta\bar{I}^{(7)} \\ \cdot \\ \cdot \\ \cdot \\ \Delta\bar{I}^{(L)} \\ \Delta\bar{I}^{(1)} \end{bmatrix} = \begin{bmatrix} \bar{J}^{(1)} & \bar{J}^{(5)} & \cdots & \bar{J}^{(L)} & 0 \\ \overline{YG}^{(5,1)} & \overline{YG}^{(5,5)} & \cdots & \overline{YG}^{(5,L)} & \bar{H}^{(5)} \\ \overline{YG}^{(7,1)} & \overline{YG}^{(7,5)} & \cdots & \overline{YG}^{(7,L)} & \bar{H}^{(7)} \\ \vdots & \vdots & \cdots & \vdots & \vdots \\ \overline{YG}^{(L,1)} & \overline{YG}^{(L,5)} & \cdots & \overline{YG}^{(L,L)} & \bar{H}^{(L)} \\ \overline{YG}^{(1,1)} & \overline{YG}^{(1,5)} & \cdots & \overline{YG}^{(1,L)} & \bar{H}^{(1)} \end{bmatrix} \begin{bmatrix} \Delta\bar{V}^{(1)} \\ \Delta\bar{V}^{(5)} \\ \Delta\bar{V}^{(7)} \\ \cdot \\ \cdot \\ \cdot \\ \Delta\bar{V}^{(L)} \\ \Delta\bar{\Phi} \end{bmatrix}. \quad (7\text{-}106)$$

Solving the equation for the correction vector yields

$$\begin{bmatrix} \Delta\bar{V}^{(1)} \\ \Delta\bar{V}^{(5)} \\ \Delta\bar{V}^{(7)} \\ \cdot \\ \cdot \\ \cdot \\ \Delta\bar{V}^{(L)} \\ \Delta\bar{\Phi} \end{bmatrix} = \begin{bmatrix} \bar{J}^{(1)} & \bar{J}^{(5)} & \cdots & \bar{J}^{(L)} & 0 \\ \overline{YG}^{(5,1)} & \overline{YG}^{(5,5)} & \cdots & \overline{YG}^{(5,L)} & \bar{H}^{(5)} \\ \overline{YG}^{(7,1)} & \overline{YG}^{(7,5)} & \cdots & \overline{YG}^{(7,L)} & \bar{H}^{(7)} \\ \cdots & \cdots & \cdots & \cdots & \cdots \\ \overline{YG}^{(L,1)} & \overline{YG}^{(L,5)} & \cdots & \overline{YG}^{(L,L)} & \bar{H}^{(L)} \\ \overline{YG}^{(1,1)} & \overline{YG}^{(1,5)} & \cdots & \overline{YG}^{(1,L)} & \bar{H}^{(1)} \end{bmatrix}^{-1} \begin{bmatrix} \Delta\bar{W} \\ \Delta\bar{I}^{(5)} \\ \Delta\bar{I}^{(7)} \\ \cdot \\ \cdot \\ \cdot \\ \Delta\bar{I}^{(L)} \\ \Delta\bar{I}^{(1)} \end{bmatrix}, \quad (7\text{-}107)$$

where all elements in this matrix equation are subvectors and submatrices partitioned from $\Delta\bar{M}$, $\bar{J}$, and $\Delta\bar{U}^{(\xi)}$.



The subvectors are

- $(\Delta\bar{V}^{(1)}, \Delta\bar{V}^{(5)}, \ldots, \Delta\bar{\Phi})$ $t$ = correction vector,
- $\Delta\bar{W}$ = mismatch power vector at all buses except the swing bus,
- $\Delta\bar{I}^{(1)}$ = fundamental mismatch current vector at nonlinear buses, and
- $\Delta\bar{I}^{(h)}$ = hth harmonic mismatch current vector at all buses.

The submatrices are

- $\bar{J}^{(1)}$ = Jacobian $2(n-1)$ square matrix corresponding to Jacobian of fundamental power flow written for all buses except the swing bus, and
- $\bar{J}^{(h)}$ = Jacobian of harmonic $h \neq 1$ with dimensions $2(n-1) \times 2n$, whereby there are zero entries for $(m-1)$ linear buses:

$$\bar{J}^{(h)} = \left[\begin{array}{c} \bar{0}_{2(m-2)\times 2n} \\ \text{(zero entries for linear buses)} \\ \hline \text{partial derivatives of the h}^{\text{th}}\text{ harmonic mismatch (total) } P \text{ and } Q \text{ at nonlinear buses with respect to } V^{(h)} \text{ and } \delta^{(h)}. \\ \text{These are similarly formed as those for the fundamental power flow.} \end{array}\right], \quad (7\text{-}108)$$

where $\bar{0}_{2(m-2)\times 2n}$ denotes a $2(m-2)$ by $2n$ array of zeros and $\bar{J}^{(h)}$ is a $2(n-1)$ by $2n$ matrix.

The partial derivatives are found using the harmonic admittance matrix $\bar{Y}_{\text{bus}}^{(h)}$ and the harmonic voltages:

$$\overline{YG}^{(h,j)} = \begin{cases} \bar{Y}^{(h,h)} + \bar{G}^{(h,h)} & \text{for } h = j \\ \bar{0} + \bar{G}^{(h,j)} & \text{for } h \neq j \end{cases} \quad (7\text{-}109)$$

or

$$\overline{YG}^{(h,j)} = \begin{bmatrix} \bar{Y}^{(h,h)} & \bar{G}^{(h,h)} \\ \bar{Y}^{(h,j)} \equiv 0 & \bar{G}^{(h,j)} \end{bmatrix}. \quad (7\text{-}110)$$

- $\bar{Y}^{(h,h)}$ is an array of partial derivatives of the hth harmonic (linear) line currents with respect to the hth harmonic bus voltages,
- $\bar{G}^{(h,h)}$ is an array of partial derivatives of the hth (nonlinear) harmonic load currents with respect to the hth harmonic bus voltages, and
- $\bar{G}^{(h,j)}$ is an array of partial derivatives of the hth harmonic nonlinear load currents with respect to the $j$th harmonic bus voltages:

$$\bar{G}^{(h,j)} = \left[\begin{array}{c|cc|ccc} \bar{0}_{2(m-1)\times 2(m-1)} & & & \bar{0}_{2(m-1)\times 2(n-m+1)} & & \\ \hline & \frac{\partial G_{r,m}^{(h)}}{\partial \delta_m^{(j)}} & \frac{\partial G_{r,m}^{(h)}}{\partial V_m^{(j)}} & \cdots & 0 & 0 \\ & \frac{\partial G_{i,m}^{(h)}}{\partial \delta_m^{(j)}} & \frac{\partial G_{i,m}^{(h)}}{\partial V_m^{(j)}} & \cdots & 0 & 0 \\ \bar{0}_{2(n-m+1)\times 2(m-1)} & \cdots & \cdots & \cdots & \cdots & \cdots \\ & 0 & 0 & \cdots & \frac{\partial G_{r,n}^{(h)}}{\partial \delta_n^{(j)}} & \frac{\partial G_{r,n}^{(h)}}{\partial V_n^{(j)}} \\ & 0 & 0 & \cdots & \frac{\partial G_{i,n}^{(h)}}{\partial \delta_n^{(j)}} & \frac{\partial G_{i,n}^{(h)}}{\partial V_n^{(j)}} \end{array}\right], \quad (7\text{-}111)$$

where the partial derivatives of $G_{r,m}^{(h)}$ and $G_{i,m}^{(h)}$ are referred to the swing bus. Note that $\overline{YG}^{(h,j)}$ is a $2n$ square matrix; however, for $h=1$ only the last $2(n-m+1)$ rows exist because the fundamental current balance is not applied to linear buses. $\overline{YG}^{(1,j)}$ is a $2(n-m+1) \times 2n$ matrix and for $j=1$ the first two columns do not exist because $|\bar{V}|^{(1)}$ and $\delta^{(1)}$ are known, that is, $\overline{YG}^{(h,1)}$ is a $2n \times 2(n-1)$ matrix.

$\bar{H}^{(h)}$ is an array of partial derivatives of real and imaginary nonlinear load currents with respect to the firing angle $\alpha$ and the commutation impedance $\beta$:

$$\bar{H}^{(h)}=\begin{bmatrix} \bar{0}_{2(m-1)\times 2(n-m+1)} & \\ \hline \dfrac{\partial G_{r,m}^{(h)}}{\partial \alpha_m} & \dfrac{\partial G_{r,m}^{(h)}}{\partial \beta_m} \\ \dfrac{\partial G_{i,m}^{(h)}}{\partial \alpha_m} & \dfrac{\partial G_{i,m}^{(h)}}{\partial \beta_m} \\ \vdots & \vdots \\ \dfrac{\partial G_{r,n}^{(h)}}{\partial \alpha_n} & \dfrac{\partial G_{r,n}^{(h)}}{\partial \beta_n} \\ \dfrac{\partial G_{i,n}^{(h)}}{\partial \alpha_n} & \dfrac{\partial G_{i,n}^{(h)}}{\partial \beta_n} \end{bmatrix} \quad \begin{matrix} \\ \hline 0 \quad 0 \\ 0 \quad 0 \\ \vdots \quad \vdots \\ 0 \quad 0 \\ 0 \quad 0 \end{matrix} \qquad (7\text{-}112)$$

where $h = 1, 5, 7, \ldots, L$. For $h = 1$ the entries are zero.

### 7.4.5 Harmonic Jacobian Entry Formulas Related to Line Currents

Figure 7.15 shows a typical nonlinear bus $i$ of an $n$ bus system. This $i$th bus is connected to three other buses, $m$, $k$, and $l$. The nonlinear device connected to bus $i$ demands a complex load current $\tilde{g}_{\text{load},i}^{(h)}$ (referred to the nonlinear bus $i$) at the hth harmonic frequency.

The total hth harmonic complex current leaving bus $i$ via the lines is

$$\tilde{I}_{\text{lines},i}^{(h)} = \tilde{I}_k^{(h)} + \tilde{I}_l^{(h)} + \tilde{I}_m^{(h)}, \qquad (7\text{-}113a)$$

$$\tilde{I}_{\text{lines},i}^{(h)} = (\tilde{V}_i^{(h)} - \tilde{V}_k^{(h)})\tilde{y}_{ik}^{(h)} + (\tilde{V}_i^{(h)} - \tilde{V}_l^{(h)})\tilde{y}_{il}^{(h)} + (\tilde{V}_i^{(h)} - \tilde{V}_m^{(h)})\tilde{y}_{im}^{(h)}, \qquad (7\text{-}113b)$$

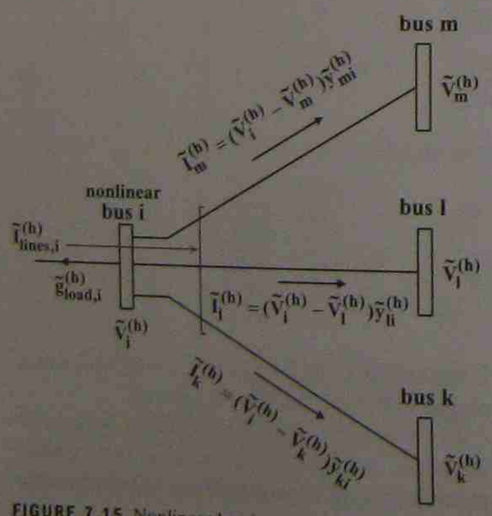



**FIGURE 7.15** Nonlinear bus $i$.

where $\tilde{y}_{ij}^{(h)}$ is the admittance of the line connecting buses $i$ and $j$ evaluated at the hth harmonic frequency. Rearranging terms gives

$$\tilde{I}_{\text{lines},i}^{(h)} = (\tilde{y}_{ik}^{(h)} + \tilde{y}_{il}^{(h)} + \tilde{y}_{im}^{(h)})\tilde{V}_i^{(h)} - \tilde{y}_{ik}^{(h)}\tilde{V}_k^{(h)} - \tilde{y}_{il}^{(h)}\tilde{V}_l^{(h)} - \tilde{y}_{im}^{(h)}\tilde{V}_m^{(h)}, \qquad (7\text{-}114a)$$

or

$$\tilde{I}_{\text{lines},i}^{(h)} = (\bar{Y}_{\text{bus}}^{(h)})_{ii}\tilde{V}_i^{(h)} + (\bar{Y}_{\text{bus}}^{(h)})_{ik}\tilde{V}_k^{(h)} + (\bar{Y}_{\text{bus}}^{(h)})_{il}\tilde{V}_l^{(h)} + (\bar{Y}_{\text{bus}}^{(h)})_{im}\tilde{V}_m^{(h)}, \qquad (7\text{-}114b)$$

where $(\bar{Y}_{\text{bus}}^{(h)})_{ij}$ is the $(i,j)$th entry of the hth harmonic admittance matrix. Because $k$, $l$, and $m$ are the only buses connected to bus $i$ (see Fig. 7.15),

$$\tilde{I}_{\text{lines},i}^{(h)} = (\text{row } i \text{ of } \bar{Y}_{\text{bus}}^{(h)})\bar{V}_{\text{bus}}^{(h)}, \qquad (7\text{-}115)$$

where $\bar{V}_{\text{bus}}^{(h)}$ is a complex vector of the hth harmonic bus voltages. Therefore, the mismatch current for the hth harmonic is based on the Kirchhoff current law at bus $i$:

$$\Delta\tilde{I}_i^{(h)} = \tilde{I}_{\text{lines},i}^{(h)} + \tilde{G}_{\text{load},i}^{(h)} = (\text{row } i \text{ of } \bar{Y}_{\text{bus}}^{(h)})\bar{V}_{\text{bus}}^{(h)} + \tilde{G}_{\text{load},i}^{(h)}, \qquad (7\text{-}116)$$

where $\tilde{G}_{\text{load},i}^{(h)}$ is the hth harmonic nonlinear complex load current (for bus $i$), referred to the swing bus:

$$\tilde{G}_{\text{load},i}^{(h)} = \tilde{G}_{r,i}^{(h)} + j\tilde{G}_{i,i}^{(h)} \qquad (7\text{-}117)$$

In this equation, the second index i pertains to bus $i$ and the first index $i$ indicates imaginary. Breaking the mismatch current $\Delta\tilde{I}_i^{(h)}$ into a real part $\Delta I_{r,i}^{(h)}$ and an imaginary part $\Delta I_{i,i}^{(h)}$, we get

$$\Delta I_{r,i}^{(h)} = \text{Real}\{(\text{row } i \text{ of } \bar{Y}_{\text{bus}}^{(h)})\bar{V}_{\text{bus}}^{(h)}\} + G_{r,i}^{(h)}, \qquad (7\text{-}118a)$$

$$\Delta I_{i,i}^{(h)} = \text{Imag}\{(\text{row } i \text{ of } \bar{Y}_{\text{bus}}^{(h)})\bar{V}_{\text{bus}}^{(h)}\} + G_{i,i}^{(h)}, \qquad (7\text{-}118b)$$

Therefore,

$$\Delta I_{r,i}^{(h)} = I_{r,i}^{(h)} + G_{r,i}^{(h)} = \sum_{j=1}^{n} y_{ij}^{(h)}|\tilde{V}_j^{(h)}|\cos(\theta_{ij}^{(h)} + \delta_j^{(h)}) + G_{r,i}^{(h)}, \qquad (7\text{-}119a)$$

$$\Delta I_{i,i}^{(h)} = I_{i,i}^{(h)} + G_{i,i}^{(h)} = \sum_{j=1}^{n} y_{ij}^{(h)}|\tilde{V}_j^{(h)}|\sin(\theta_{ij}^{(h)} + \delta_j^{(h)}) + G_{i,i}^{(h)}, \qquad (7\text{-}119b)$$

where $y_{ij}^{(h)}$ and $\theta_{ij}^{(h)}$ are the magnitude and phase angle of the $(i,j)$th entry of the hth harmonic admittance matrix, respectively, and $|\tilde{V}_j^{(h)}|$ and $\delta_j^{(h)}$ are the hth harmonic voltage magnitude and phase angle of bus $j$ with respect to swing bus.



The entries of the Jacobian matrix corresponding to line currents are submatrices $\bar{Y}^{(h,h)}$ ($h = 1, 5, \ldots, L$). These matrices are defined as

$$\bar{Y}^{(h,h)} = \frac{\partial(\bar{I}^{(h)})}{\partial(\bar{V}^{(h)})}. \qquad (7\text{-}120)$$

Note that $\bar{Y}^{(h,j)} = 0$ for $h \neq j$. The zero terms are due to the fact that the v–i characteristics of the nonlinear devices are modeled in the Jacobian matrix using submatrices $\bar{G}^{(h,j)}$.

$$\bar{Y}^{(h,h)}=\begin{bmatrix} \dfrac{\partial I_{r,1}^{(h)}}{\partial \delta_1^{(h)}} & \dfrac{\partial I_{r,1}^{(h)}}{\partial V_1^{(h)}} & \cdots & \dfrac{\partial I_{r,1}^{(h)}}{\partial \delta_n^{(h)}} & \dfrac{\partial I_{r,1}^{(h)}}{\partial V_n^{(h)}} \\ \dfrac{\partial I_{i,1}^{(h)}}{\partial \delta_1^{(h)}} & \dfrac{\partial I_{i,1}^{(h)}}{\partial V_1^{(h)}} & \cdots & \dfrac{\partial I_{i,1}^{(h)}}{\partial \delta_n^{(h)}} & \dfrac{\partial I_{i,1}^{(h)}}{\partial V_n^{(h)}} \\ \vdots & \vdots & & \vdots & \vdots \\ \dfrac{\partial I_{r,n}^{(h)}}{\partial \delta_1^{(h)}} & \dfrac{\partial I_{r,n}^{(h)}}{\partial V_1^{(h)}} & \cdots & \dfrac{\partial I_{r,n}^{(h)}}{\partial \delta_n^{(h)}} & \dfrac{\partial I_{r,n}^{(h)}}{\partial V_n^{(h)}} \\ \dfrac{\partial I_{i,n}^{(h)}}{\partial \delta_1^{(h)}} & \dfrac{\partial I_{i,n}^{(h)}}{\partial V_1^{(h)}} & \cdots & \dfrac{\partial I_{i,n}^{(h)}}{\partial \delta_n^{(h)}} & \dfrac{\partial I_{i,n}^{(h)}}{\partial V_n^{(h)}} \end{bmatrix} \qquad (7\text{-}121)$$

For $h = 1$ only the last $2(n - m + 1)$ rows exist because fundamental current balance is not performed for linear load buses. Also for $h = 1$ the first two columns of the matrix do not exist (are zero) because $|\tilde{V}_1^{(1)}|$ and $\delta_1^{(1)}$ are known and constant.

The entries of $\bar{Y}^{(h,h)}$ are computed from Eq. 7-119 by setting $G_{r,i}^{(h)}$ and $G_{i,i}^{(h)}$ to zero:

$$\frac{\partial I_{r,i}^{(h)}}{\partial \delta_j^{(h)}} = -y_{ij}^{(h)}|\tilde{V}_j^{(h)}|\sin(\theta_{ij}^{(h)} + \delta_j^{(h)}), \quad \text{for } h = 1, 5, \ldots, L, \qquad (7\text{-}122a)$$

$$\frac{\partial I_{r,i}^{(h)}}{\partial |\tilde{V}_j^{(h)}|} = y_{ij}^{(h)}\cos(\theta_{ij}^{(h)} + \delta_j^{(h)}), \quad \text{for } h = 1, 5, \ldots, L, \qquad (7\text{-}122b)$$

$$\frac{\partial I_{i,i}^{(h)}}{\partial \delta_j^{(h)}} = y_{ij}^{(h)}|\tilde{V}_j^{(h)}|\cos(\theta_{ij}^{(h)} + \delta_j^{(h)}), \quad \text{for } h = 1, 5, \ldots, L, \qquad (7\text{-}122c)$$

$$\frac{\partial I_{i,i}^{(h)}}{\partial |\tilde{V}_j^{(h)}|} = y_{ij}^{(h)}\sin(\theta_{ij}^{(h)} + \delta_j^{(h)}), \quad \text{for } h = 1, 5, \ldots, L, \qquad (7\text{-}122d)$$

where $h$ and $j$ denote harmonic order and bus number, respectively.

### 7.4.6 Newton-Based Harmonic Power Flow Algorithm

Based on the equations given, the harmonic power flow algorithm is the computation of bus voltage vector $\bar{U}$ for a given system configuration with linear and nonlinear loads. The Newton–Raphson approach (Eq. 7-107) will be used to force the mismatch vector (Eq. 7-101) to zero using the harmonic Jacobian matrix and obtaining appropriate correction terms $\Delta\bar{U}$. Therefore ($\xi$ represents the iteration number),

$$\Delta\bar{U}^{\xi} = J^{-1}\Delta\bar{M}(\bar{U}^{\xi}), \qquad (7\text{-}123)$$

$$\bar{U}^{(\xi+1)} = \bar{U}^{\xi} - \Delta\bar{U}^{\xi}. \qquad (7\text{-}124)$$

The solution procedure for the harmonic power flow algorithm is as follows (Fig. 7.16):

**Step 1:** Perform the fundamental load flow analysis (treating all nonlinear devices as linear loads) and compute an initial (approximate) value for the fundamental bus voltage magnitudes and phase angles. Make an initial guess for the harmonic bus voltage magnitudes and phase angles (e.g., 0.1 pu and 0 radians).

**Step 2:** Compute nonlinear device currents $G_{r,m}^{(h)}$ and $G_{i,m}^{(h)}$ (referred to the swing bus) for nonlinear loads.

**Step 3:** Evaluate $\Delta\bar{M}(\bar{U})$ using Eqs. 7-101, 7-102. If it is small enough then stop.

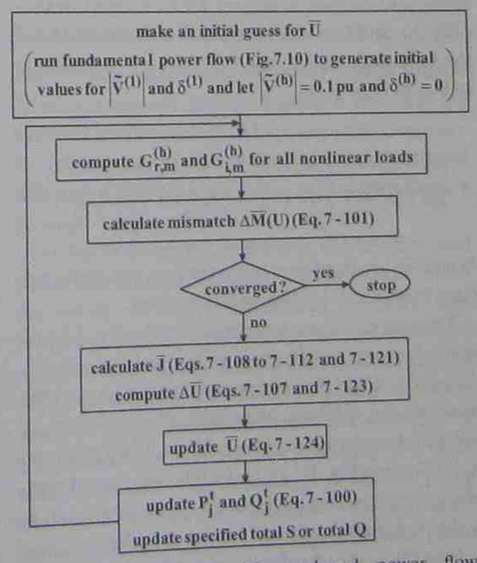



**FIGURE 7.16** Harmonic Newton-based power flow algorithm.

ST. GEORGE

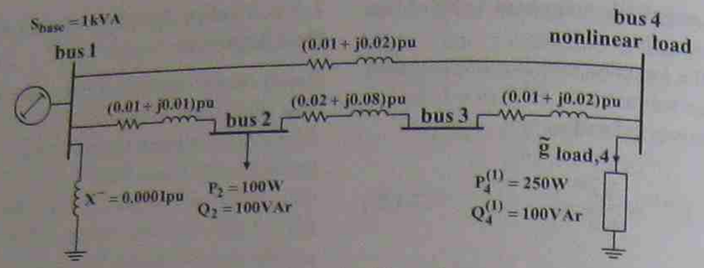



**FIGURE E7.14.1** Four-bus power system with one nonlinear load bus, where $n = m = 4$, that is, there is one nonlinear bus (bus 4), two linear buses (buses 2 and 3), and the swing bus (bus 1).

**Step 4:** Evaluate $\bar{J}$ (Eqs. 7-108 to 7-112 and 7-121) and calculate $\Delta\bar{U}$ (Eqs. 7-107 and 7-123) using matrix inversion or forward/backward substitution.

**Step 5:** Update $\bar{U}$ (Eq. 7-124).

**Step 6:** Update the total (fundamental plus harmonic) powers at nonlinear buses ($P_i$ and $Q_i$ (Eq. 7-100)), and the specified total apparent power or total reactive power (Eq. 7-98), whichever is known.

**Step 7:** Go to Step 2.

### 7.4.7 Application Example 7.14: Computation of Harmonic Admittance Matrix

The harmonic power flow algorithm will be applied to the nonlinear power system as shown in Fig. E7.14.1 where all impedances are given in pu at 60 Hz and the base is $S_{base} = 1$ kVA. In order to simplify the problem, the harmonic $v$–$i$ characteristic of the nonlinear load at bus 4 (referred to the voltage at bus 4) is given as

$$g_{4,4}^{(5)} = 0.3(V_4^{(1)})^2\cos(3\delta_4^{(1)}) + 0.3(V_4^{(5)})^2\cos(3\delta_4^{(5)}),$$
$$g_{4,4}^{(5)} = 0.3(V_4^{(1)})^2\sin(3\delta_4^{(1)}) + 0.3(V_4^{(5)})^2\sin(3\delta_4^{(5)}).$$

It will be assumed that the voltage at the swing bus (bus 1) is $|\tilde{V}_1^{(1)}| = 1.00$ pu and $\delta_1^{(1)} = 0$ rad.

The swing bus can be represented by Fig. E7.14.2 at the fundamental frequency. For the 5th harmonic, $\tilde{E}_{an}$ of Fig. E7.14.3 represents a short-circuit, and the synchronous machine impedance $Z_1$ is replaced by the (subtransient) impedance $Z_2 = jX^{-} = j0.0001$ pu at 60 Hz (see Fig. E7.14.1). In this case the subtransient reactance has been chosen to be very small in order to approximate bus 1 as an ideal bus.

Compute the fundamental and 5th harmonic admittance matrices.

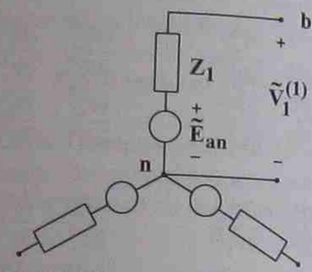



**FIGURE E7.14.2** Representation of swing bus (bus 1) for fundamental ($h = 1$) frequency.

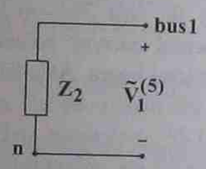



**FIGURE E7.14.3** Equivalent circuit of swing bus for the 5th harmonic ($h = 5$).

### 7.4.8 Application Example 7.15: Computation of Nonlinear Load Harmonic Currents

For the system of Fig. E7.14.1, assume an initial value for the bus vector $\bar{U}^0$ and compute the fundamental and the 5th harmonic currents injected into the system by the nonlinear load. The computation of the nonlinear load harmonic currents is the initial step of the harmonic load flow algorithm.

### 7.4.9 Application Example 7.16: Evaluation of Harmonic Mismatch Vector

Using the results of Application Example 7.15, evaluate the mismatch vector for the system of Fig. E7.14.1.



### 7.4.10 Application Example 7.17: Evaluation of Fundamental and Harmonic Jacobian Submatrices

Using the results of Application Examples 7.15 and 7.16, evaluate the Jacobian matrix for the system of Fig. E7.14.1.

### 7.4.11 Application Example 7.18: Computation of the Correction Bus Vector and Convergence of Harmonic Power Flow

Using the results of Application Examples 7.15 to 7.17, evaluate the correction bus vector $\Delta\bar{U}^0$ for the system of Fig. E7.14.1. Update the mismatch vector and comment on the convergence of the harmonic load flow.

## 7.5 CLASSIFICATION OF HARMONIC POWER FLOW TECHNIQUES

Different approaches have been proposed and implemented to solve the harmonic power flow (HPF) problem [5-29]. In this section, the following criteria will be employed to classify some of these algorithms:

- Modeling technique used to simulate power system and nonlinear loads (time domain, harmonic domain).
- System condition (single-phase, three-phase, balanced, unbalanced).
- Solution approach (coupled, decoupled).

Modeling techniques include time-domain, harmonic-domain and hybrid time/harmonic-domain approaches. Time-domain approaches are based on transient analysis and have great flexibility and high accuracy; however, they usually require long computing times (especially for large power systems containing many nonlinear loads with strong harmonic couplings). Harmonic-domain approaches calculate the frequency response of power systems and require shorter computing times; however, it is usually difficult to obtain accurate frequency models for nonlinear loads [13]. Hybrid modeling techniques use a combination of frequency-domain (to limit the computing time) and time-domain (to increase the accuracy) approaches to simulate the power system and nonlinear loads, respectively [9, 14]. Therefore, comprehensive hybrid models are employed to achieve the benefits of the accuracy of the time-domain analysis and the simplicity of frequency-domain approach.

It is sufficient to use single-phase harmonic models for single-phase and balanced three-phase systems. Unbalanced harmonic conditions are usually imposed by the system configuration, disturbances, and (non)linear loads. Unbalanced harmonic power flow solutions are relatively complicated and require long computing times and considerable memory storage.

Solution approaches may also be classified into coupled and decoupled methods [12]. Most nonlinear loads and power system components impose couplings between (time and/or space) harmonics and call for accurate coupled solution approaches. If harmonic couplings are not too strong, a decoupled approach may be implemented where separate models are used at different harmonic frequencies and superposition is employed to calculate the final solution.

Based on the above-mentioned criteria, HPF algorithms can be classified as follows:

- Newton-based coupled harmonic power flow as outlined in Section 7.4 [5, 6].
- Decoupled harmonic power flow [16, 17, 19].
- Fast harmonic power flow [17].
- Modified fast decoupled power flow [20].
- Fuzzy harmonic power flow [13].
- Probabilistic harmonic power flow [12, 22].
- Modular harmonic power flow [9, 11, 14, 23].

Table 7.3 presents a comparison of harmonic power flow algorithms. The remainder of this chapter briefly outlines the solution procedure of these algorithms.

### 7.5.1 Decoupled Harmonic Power Flow

The Newton-based harmonic power flow of Section 7.4 is very accurate because harmonic couplings are included at all frequencies. However, it might encounter convergence problems for large power systems with many nonlinear loads. For such applications, a decoupled approach is more appropriate.

At the fundamental frequency, the conventional power flow algorithm (Section 7.3) is used to model the system. At higher frequencies, harmonic couplings are neglected (to simplify the procedure, to reduce computing time, and to limit memory storage requirements) and the distorted power system is modeled by the harmonic admittance matrix. The general model of a linear load consisting of a resistance in parallel with a reactance is utilized [7, 8], and nonlinear loads are modeled with decoupled harmonic current sources. The magnitudes and phase angles of harmonic current sources depend on the nature of the nonlinear loads and can be computed

**TABLE 7.3** Classification and Comparison of Harmonic Power Flow Algorithms

| Method | Modeling technique: For the system | | | Modeling technique: For nonlinear loads | | | Solution approach | | System condition | |
|---|---|---|---|---|---|---|---|---|---|---|
| | Time | Frequency | Hybrid | Time | Frequency | Hybrid | Coupled | Decoupled | Balanced | Unbalanced |
| Newton | | × | | | × | + | × | | × | |
| HPF[a] | | | | | | | | | | |
| Decoupled | | × | | | × | | | × | × | |
| HPF | | | | | | | | | | b |
| Fast | | × | | | × | | | × | × | |
| HPF | | | | | | | | | | × |
| Modified fast | | × | | | × | | × | × | × | |
| HPF | | | | | | | | | | |
| Fuzzy HPF | | × | | × | × | × | × | | × | |
| Probabilistic | | × | | × | × | × | × | | × | |
| HPF | | | | | | | | | | |
| Modular | × | × | × | × | × | × | × | | × | |
| HPF | | | | | | | | | | × |

[a]Section 7.4.
[b]The HPF algorithm may be modified to include this feature.

using analytical models or may be estimated based on measured nonsinusoidal current waveforms. This simple approach of nonlinear load modeling is very practical for most industrial loads.

The hth harmonic load admittance at bus $i$ ($y_i^{(h)}$), shunt capacitor admittance at bus $i$ ($y_{ci}^{(h)}$), and feeder admittance between buses $i$ and $i+1$ ($y_{i,i+1}^{(h)}$) are [7, 8, 16, 18, 19]

$$y_i^{(h)} = \frac{P_i}{|V_i^{(1)}|^2} - j\frac{Q_i}{h|V_i^{(1)}|^2}, \tag{7-125}$$

$$y_{ci}^{(h)} = h y_{ci}^{(1)}, \tag{7-126}$$

$$y_{i,i+1}^{(h)} = \frac{1}{R_{i,i+1} + jhX_{i,i+1}}, \tag{7-127}$$

where $P_i$ and $Q_i$ are the fundamental active and reactive load powers at bus $i$, $y_{ci}^{(1)}$ is the fundamental frequency admittance of the capacitor bank connected to bus $i$, and the superscript $h$ indicates harmonic orders.

Nonlinear loads are modeled as decoupled harmonic current sources that inject harmonic currents into the system. The fundamental and the hth harmonic currents of the nonlinear load installed at bus $m$ with fundamental real power $P_m$ and fundamental reactive power $Q_m$ are [8, 16, 19]

$$I_m^{(1)} = [P_m + jQ_m)/V_m^{(1)}]^*, \tag{7-128}$$

$$I_m^{(h)} = C(h) I_m^{(1)}, \tag{7-129}$$

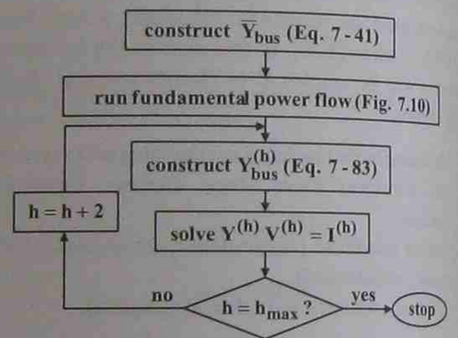



**FIGURE 7.17** Flowchart of the decoupled harmonic power flow (DHPF).

where $C(h)$ is the ratio of the hth harmonic current to its fundamental value. A conventional (fundamental) Newton–Raphson algorithm (Section 7.3) is used to solve the system at the fundamental frequency and harmonic voltages are calculated by solving the following decoupled load flow equation (derived from the node equations) [16, 17, 19]

$$Y^{(h)} V^{(h)} = I^{(h)}. \tag{7-130}$$

The flowchart of the decoupled harmonic power flow (DHPF) based on Eqs. 7-125 to 7-130 is shown in Fig. 7.17. This simple and fast approach for the calculation of harmonic voltages and currents provides acceptable solutions as compared with Newton-based HPF (Section 7.4), which considers harmonic couplings [5, 6].



### 7.5.2 Fast Harmonic Power Flow

This method employs the equivalent current injection transformation and the forward and backward sweep techniques to solve the harmonic load flow problem [17]. For bus $i$, the complex power $S_i$ is

$$S_i = (P_i + jQ_i),\ i = 1, \ldots, n, \tag{7-131}$$

where $n$ is the total number of buses. The equivalent current injection ($I_i^k$) at the kth iteration is

$$I_i^k = I_i^r(V_i^k) + jI_i^r(V_i^k) = \left(\frac{P_i + jQ_i}{V_i^k}\right)^*, \tag{7-132}$$

where $V_i^k$ is the voltage of bus $i$ at the kth iteration.

For fundamental load flow, the equivalent current injection needs to be iteratively transformed (e.g., Eq. 7-132 is used at the end of each iteration to compute the equivalent current injection ($I_i^k$) from the updated voltage ($V_i^k$), active ($P_i$), and reactive ($Q_i$) powers). However, this transformation is not required for harmonic currents since they have been obtained in a suitable form based on harmonic analysis (which represents nonlinear loads with harmonic current sources).

Figure 7.18 shows part of a lateral distribution system and the associated harmonic currents. The relationships between branch currents and harmonic currents are

$$B_{jk}^{(h)} = -I_k^{(h)}, \tag{7-133}$$

$$B_{jl}^{(h)} = -I^{(h)}, \tag{7-134}$$

$$B_{ij}^{(h)} = B_{jk}^{(h)} + B_{jl}^{(h)} - I_k^{(h)}, \tag{7-135}$$

where $B$ and $I$ are branch and injection (harmonic) currents, respectively.

It can be seen that the relationship between branch currents and harmonic (injection) currents of a radial feeder can be calculated by summing the injection currents from the receiving bus toward the sending bus of the feeder. The general form of the harmonic currents can be expressed as

$$B_{ij}^{(h)} = -I_k^{(h)} + \sum_j B_{jl}^{(h)}. \tag{7-136}$$

On the other hand, the relationship between branch currents and bus voltages can be shown to be

$$\begin{aligned} V_j^{(h)} &= V_i^{(h)} - B_{ij}^{(h)} Z_{ij}^{(h)} \\ V_k^{(h)} &= V_j^{(h)} - B_{jk}^{(h)} Z_{jk}^{(h)} \\ V_l^{(h)} &= V_j^{(h)} - B_{jl}^{(h)} Z_{jl}^{(h)}, \end{aligned} \tag{7-137}$$

where $Z^{(h)}$ is the equivalent impedance of the line section at the hth harmonic frequency.

It is evident for a radial distribution system that if branch currents have been calculated, then the bus voltages can be easily determined from

$$V_j^{(h)} = V_i^{(h)} - Z_{ij} B_{ij}^{(h)}. \tag{7-138}$$

The bus voltages can be obtained by calculating the voltage from the sending bus forward to the receiving bus of the feeder. Power system components are adjusted for each harmonic order.

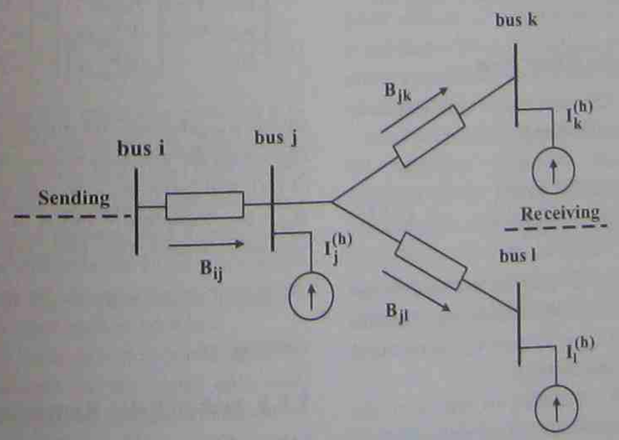



**FIGURE 7.18** Parts of a distribution system [17].

### 7.5.3 Modified Fast Decoupled Harmonic Power Flow

This method extends and generalizes the conventional fast decoupled (fundamental) power flow algorithm to accommodate harmonic sources [20]. The reduced and decoupled features of the fast decoupled algorithm is explored for the harmonic power flow application. A mathematical nonlinear model is integrated into an existing fast decoupled power flow program. This method allows separate modeling of nonlinear loads and subsequently integrating them in the main algorithm without substantially increasing computation time.

The hth harmonic bus injection current vector is defined as

$$I^{(h)} = Y^{(h)}V^{(h)}, \tag{7-139}$$

where $Y^{(h)}$ is the hth harmonic admittance matrix. The injected current at any bus $p$ is given by

$$I_p^{(h)} = \sum_{i=1}^{n} Y_{p,i}^{(h)} V_i^{(h)}. \tag{7-140}$$

This equation provides the change of voltage magnitude and phase angle for each harmonic as a result of the injected currents.

The problem is then solved by the Newton–Raphson method. The current injected by a nonlinear load is assumed to be constant throughout the iteration and is used to modify the solution of voltage amplitudes and angles without reinverting the Jacobian matrix. At the end of each iteration, the device parameters are adjusted to reflect the new voltage magnitudes and phase angles. The harmonic currents and injected power are then reevaluated and the process is repeated until convergence is achieved.

### 7.5.4 Fuzzy Harmonic Power Flow

All elements of Eq. 7-139 are complex valued. Therefore, it can be reformulated as [13]

$$\left[\psi^{(h)}\right]\begin{bmatrix} V_r^{(h)} \\ V_i^{(h)} \end{bmatrix} = \begin{bmatrix} I_r^{(h)} \\ I_i^{(h)} \end{bmatrix}, \tag{7-141}$$

where $V_r^{(h)}$, $V_i^{(h)}$, $I_r^{(h)}$, and $I_i^{(h)}$ are the real and imaginary parts of the hth harmonic voltage and current, respectively. $\psi^{(h)}$ is a $2n \times 2n$ matrix restructured from $Y^{(h)}$ and $n$ is the bus number.

Fuzzy set theory is employed to represent the injection harmonic currents. For an n bus distribution system the solution is obtained by solving a set of $4n \times 4n$ linear equations. The fuzzy solution for both harmonic magnitudes and phase angles can be individually expressed by two explicit linear equations. The solutions for any harmonic level can be easily obtained from these equations.

Harmonic sources are represented as (voltage-independent) current sources. Because harmonic penetration is a steady-state phenomenon, monitoring harmonics requires a long period of time for accurate measurements. It can be shown that the value of the harmonic currents at a bus is most likely near the center of a monitored range. Therefore, it is suitable to model the harmonic current source with a triangle fuzzy number, denoted by $\tilde{I}_h$. With a proper fuzzy model, the new fuzzy harmonic power flow equations can be expressed in the following form [13]:

$$\left[\psi^{(h)}\right]\begin{bmatrix} \tilde{V}_r^{(h)} \\ \tilde{V}_i^{(h)} \end{bmatrix} = \begin{bmatrix} \tilde{I}_r^{(h)} \\ \tilde{I}_i^{(h)} \end{bmatrix}, \tag{7-142}$$

Note that $\psi^{(h)}$ is a constant whereas the harmonic voltages $\tilde{V}_r^{(h)}$ and $\tilde{V}_i^{(h)}$ are fuzzy numbers.

An arbitrary fuzzy number can be represented by an ordered pair of functions $(u_{\min}(r), u_{\max}(r)), 0 \le r \le 1$, which meet the following conditions:

- $u_{\min}(r)$ is a bounded left continuous nondecreasing function over [0,1].
- $u_{\max}(r)$ is a bounded right continuous nonincreasing function over [0,1].
- $u_{\min}(r) \le u_{\max}(r)$, $0 \le r \le 1$.

The fuzzy harmonic power flow can then be expressed as follows [13]:

$$\begin{bmatrix} \psi_{11} & \psi_{12} \\ \psi_{21} & \psi_{22} \end{bmatrix}\begin{bmatrix} V_{r\min}^h(r) \\ V_{i\min}^h(r) \\ -V_{r\max}^h(r) \\ -V_{i\max}^h(r) \end{bmatrix} = \begin{bmatrix} I_{r\min}^h(r) \\ I_{i\min}^h(r) \\ -I_{r\max}^h(r) \\ -I_{i\max}^h(r) \end{bmatrix}, \tag{7-143}$$

where $\psi_{11}$ contains the positive entries of $[\psi]$, $\psi_{11}$ represents the absolute values of the negative entries of $[\psi]$, and $[\psi] = \psi_{11} - \psi_{12}$; moreover $\psi_{12} = \psi_{21}$ and $\psi_{11} = \psi_{22}$. Equation 7-143 is linear and can then be uniquely solved for $[V_{r\min}^{(h)}(r), V_{i\min}^{(h)}(r), -V_{r\max}^{(h)}(r), -V_{i\max}^{(h)}(r)]^t$ if and only if the matrix $\begin{bmatrix} \psi_{11} & \psi_{12} \\ \psi_{21} & \psi_{22} \end{bmatrix}$ is nonsingular.

### 7.5.5 Probabilistic Harmonic Power Flow

Unavoidable uncertainties in a power system affect the input data of the modeling for the evaluation of



voltage and current harmonics caused by nonlinear loads. These uncertainties are mainly due to time variations of linear load demands, network configurations, and operating modes of nonlinear loads. The variations have a random character and, therefore, are expressed using the probabilistic method. The models available for evaluating voltage distortion are

- Direct method, in which the probability functions of harmonic voltages are calculated for assigned probability functions of harmonic currents injected by nonlinear loads.
- Integrated method, in which the probability functions of the voltage and current harmonics are calculated together by properly taking into account the interactions between voltage distortions and harmonic currents.

The probabilistic method is employed for harmonic power flow analysis to describe the interactions between the supply voltage distortions and the injected harmonic currents. It transfers the deterministic approach, which is based on the solution of a nonlinear equation system, to the field of probability.

To reduce the computational effort and to overcome the convergence problem, this method linearizes the nonlinear equation describing the steady-state behavior around an expected value region. Then, the first-order approximations are used to directly establish the means and covariance matrix of the output probability density function, starting from knowledge of the means and covariance matrix of the input probability density functions.

The following vector is defined as an input parameter (the values of the vector are kept fixed and assigned as input data [21, 22]):

$$T_a = [T_1\ T_2\ T_3]^t, \tag{7-144}$$

where $T_1$ includes the active generator power at fundamental frequency (with the exception of the slack), $T_2$ includes the active and reactive linear load powers at fundamental frequency and the total active and apparent nonlinear load powers, and $T_3$ represents the generator voltage magnitudes. In all cases, some input parameters may be affected by uncertainties; hence, a probabilistic approach is adopted.

Every probabilistic formulation requires, first, the statistical characterization of the input data and, second, the evaluation of the statistical features of the output variables of interest. The statistical characterization of the input data consists of checking

*(i)* which components of vector $T_a$ have to be considered as random and which ones can be kept fixed, and

*(ii)* what are the statistical features to characterize the randomness of the variables identified in step (i).

The most realistic approach to solve the problem is to refer to past experience, looking at both available historical data collections and technical knowledge of the electrical power system under study. According to (i), the generator voltage magnitudes can be considered deterministic if the set points of the regulator are not deliberately changed. With regard to (ii), the random nature, which appears in $T_1$ and $T_2$, is applied. A probabilistic method can be used to evaluate the statistical features of the output variable and may be based on the linearization around an expected value region of the nonlinear equation. The change of active and reactive linear loads is assumed to be Gaussian (normally distributed).

A probabilistic steady-state analysis of a harmonic power flow can be performed by either iterative probabilistic methods (e.g., Monte Carlo) or by analytical approaches. Iterative probabilistic procedures require knowledge of probability density functions of the input variables; for every random input data, a value is generated according to its proper probability density function. According to the generated input values, the operating steady-state conditions of the harmonic power flow are evaluated by solving the nonlinear equations by means of an iterative numerical method. Once convergence has been achieved, the state of the power system is completely known and the values of all the variables of interest are stored. The procedure is repeated to achieve a good estimate of probability of the output variables according to the stated accuracy. Unfortunately, iterative probabilistic procedures require a high computational effort.

An analytical approach is employed to linearize the nonlinear equations describing steady-state behavior of the power system around an expected value region. As a result, it offers a faster solution than the iterative probabilistic method. To evaluate the statistical procedure, the harmonic power flow equation is expressed as [21, 22]

$$f(N) = T_b \tag{7-145}$$

where $N$ and $T_b$ are the output and input random vector variables, respectively. Let the vector $\mu(T_b)$ be

ST. GEORGE BOOKSTORE

the expected values of $T_b$. Using $\mu(T_b)$ as input data for the deterministic power flow calculation results in vector $N_o$ as solutions:

$$f(N_o) = \mu(T_b). \tag{7-146}$$

Linearizing the equation around the point $N_o$ results in

$$N \equiv N_o + J^{-1}\Delta T_b = N_o' + AT_b, \tag{7-147}$$

where

$$\Delta T_b : Tb - \mu(T_b), \tag{7-148}$$

$$N_o' : N_o - J^{-1}\mu(T_b). \tag{7-149}$$

$J$ is the Jacobian matrix. Once the statistical features of the random output vector $N$ are known, the statistics of other variables on which it depends can also be evaluated.

The use of a proper linearized approach allows a drastic reduction of computational effort because the computation required practically consists of the solution of only one deterministic harmonic power flow. Since the harmonic power flow equations are linearized around an expected value of the input vector, any movement away from this region produces an error. The errors can grow with the variance of the input random vector components, with the entity linked to the nonlinear behavior of the equation system.

### 7.5.6 Modular Harmonic Power Flow

The coupled harmonic power flow calculation (Section 7.4) is established by directly involving nonlinear loads as integral parts of the solution. This makes the calculation complicated. The procedure can be simplified by detaching nonlinear device models from the main program [9, 11, 14, 23]. As most nonlinear devices can be represented by harmonic sources, detaching their models is relatively simple, and due to the iterative nature of the solution, this representation does not limit the accuracy of the results.

In modular approaches, nonlinear loads are included within the harmonic power flow as black boxes. In a black box each node has two quantities: the nodal voltage and the injected current. One quantity is specified and used to calculate the other (unknown) quantity. The procedure involves the solution of the harmonic bus voltages and using them to compute harmonic current penetration, which is then used to obtain (updated) harmonic bus voltages.

The harmonic modeling of a nonlinear load can be obtained by either a direct or an iterative approach [11, 23]. The Newton method may be employed to achieve the solution. For the nonlinear buses, the mismatches are the difference between the calculated nodal values and the transferred values from the nonlinear device models. This formulation simplifies the calculation of the mismatch vector and Jacobian matrix.

The exact modeling of complex components (e.g., nonlinear loads) is carried out individually in the time domain for that particular component using the best-suited method. The calculations are performed in a modular fashion and separately for each component. The components are then assembled via a systemwide harmonic matrix that enables the bus voltages to be corrected so that the current mismatches $\Delta I$ at all nodes are iteratively forced to zero.

The modular harmonic power flow (MHPF) is performed iteratively. Each step consists of two stages:

(i) *Updating the periodic steady state of the individual components (black boxes) using voltage corrections from stage (ii).* The inputs to a component are the voltages at its terminals and the outputs are the terminal currents. This stage provides accurate outputs for the given inputs. The initial input voltages (at the first iteration) are usually obtained from the fundamental power flow algorithm.

(ii) *Calculation of voltage corrections for stage (i).* The currents obtained from stage (i) are combined for buses with adjacent components into the current mismatch $\Delta I$, which are expressed in the harmonic domain. These become injections into a systemwide incremental harmonic admittance matrix $Y_{bus}$, calculated in advance from such matrices for all individual components. The following equation is then solved for $\Delta V$ to be used in stage (i) to update all bus voltages:

$$\Delta I = Y_{bus}\Delta V. \tag{7-150}$$

The approach is modular in stage (i), but at stage (ii) the voltage correction $\Delta V$ is calculated globally for the entire system. The main procedures of the MHPF algorithm are

- A fundamental power flow algorithm is used to obtain initial voltages at all nodes.
- The incremental harmonic admittance matrix $Y_{bus}$ is identified. This is first done separately for each component (black box) and then the systemwide $Y_{bus}$ matrix is assembled.
- Currents and their mismatches $\Delta I$ are obtained for each node.
- $\Delta I$ and $Y$ are used to obtain $\Delta V$ (Eq. 7-150) and the nodal voltages are finally updated for the next iteration.

The modular approach facilitates the development of new component models and the formation of a wide range of system configurations. It is also appropriate for an unbalanced system with asymmetric loads. In practice some power quality problems relate to uncharacteristic harmonic frequencies resulting from nonlinear loads and/or system asymmetries and thus requiring three-phase harmonic simulation. The solutions of MHPF algorithms are reported to be accurate as compared with those generated by the conventional (nonmodular) HPF. The computing times depend of the required accuracy of the solution at harmonic frequencies and the maximum order of harmonics.



### 7.5.7 Application Example 7.19: Accuracy of Decoupled Harmonic Power Flow

Apply the coupled (Section 7.4) and decoupled (Section 7.5.1) harmonic power flow algorithm to the distorted 18-bus system of Fig. E7.18.1 and compare simulation results including the fundamental and rms (including harmonics) voltages, distortion factor, and $THD_v$. The nonlinear load (installed at bus 5) is a 3 MW, 5 MVAr six-pulse converter. Line and load parameters are provided in [29]. For the DHPF calculations, the converter may be modeled with harmonic current sources (Table E7.18.1).

## 7.6 SUMMARY

After an overview of the interconnected power system and its components, power system matrices are introduced, in particular the bus admittance matrix. Bus-building algorithms are explained, and the concepts of singularity and nonsingularity of matrices and their physical interpretation with respect to power systems are discussed. After a brief review of matrix solution techniques under the aspects of matrix sparsity, the fundamental power

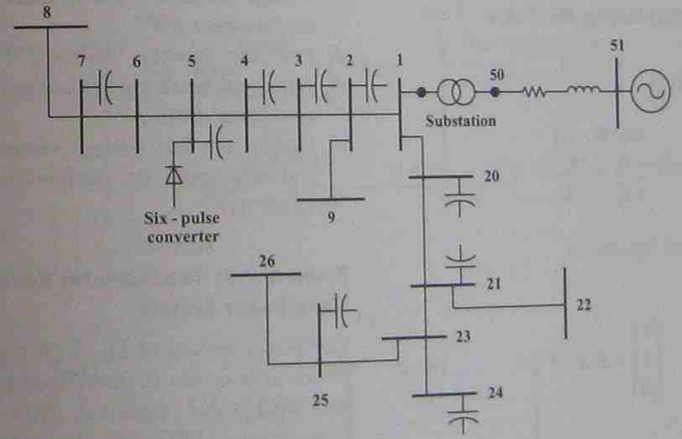



**FIGURE E7.18.1** The distorted IEEE 18-bus system used for simulation [29].

**TABLE E7.18.1** Magnitude of Harmonic Currents (as a Percentage of the Fundamental) Used to Model Six-Pulse Converters[a]

| Harmonic order | Magnitude (%) | Harmonic order | Magnitude (%) | Harmonic order | Magnitude (%) |
|---|---|---|---|---|---|
| 1 | 100 | 19 | 2.4 | 37 | 0.5 |
| 5 | 19.1 | 23 | 1.2 | 41 | 0.5 |
| 7 | 13.1 | 25 | 0.8 | 43 | 0.5 |
| 11 | 7.2 | 29 | 0.2 | 47 | 0.4 |
| 13 | 5.6 | 31 | 0.2 | 49 | 0.4 |
| 17 | 3.3 | 35 | 0.4 | | |

[a]All harmonic phase angles are assumed to be zero.

flow technique is used to explain the Newton–Raphson solution method. The harmonic power flow problem is firmly grounded on the fundamental power flow: additional circuit conditions are introduced for the harmonic power flow problem.

Numerous application examples detail for the fundamental power flow analysis the bus-building algorithm, matrix manipulations – such as multiplication and triangular factorization – formation of the Jacobian, definition of mismatch vector, and the recursive application of the Newton–Raphson algorithm. Similarly, the application examples cover the step-by-step approach for one iteration of the harmonic Newton-type solution method. The chapter concludes with a classification of existing power flow techniques.

## 7.7 PROBLEMS

### Problem 7.1: Determination of Admittance Matrices $\bar{Y}_{bus}$

a) Determine the bus admittance matrices $\bar{Y}_{bus}$ referenced to ground for Fig. P7.1a,b,c,d.
b) The system of Fig. P7.1d has no admittance connected from any one of the buses to ground. Show that its admittance matrix is singular.

### Problem 7.2: Establishing the Table of Factors

For the real matrix $\bar{A}$

$$\bar{A}=\begin{bmatrix}1 & 5 & 1\\ 5 & 2 & 0\\ 1 & 0 & 1\end{bmatrix}, \qquad \text{(P2-1)}$$

a) Find the table of factors.
b) Solve

$$\begin{bmatrix}1\\ 1\\ 0\end{bmatrix}=\bar{A}\cdot\bar{x}, \qquad \text{(P2-2)}$$

for the vector $\bar{x}$.

### Problem 7.3: Voltage Control Via Inductive Load (e.g., Reactors)

Apply the Newton–Raphson load flow analysis technique to the three-bus power system of Fig. P7.3, provided switch $S_1$ is closed and switch $S_2$ is open.

a) Find the fundamental bus admittance matrix in polar form.
b) Assume that bus 1 is the swing (slack) bus and buses 2 and 3 are PQ buses. Make an initial guess for the bus voltage vector $\bar{x}^{(0)}$ and evaluate the initial mismatch power $\Delta\bar{W}^{(0)}$.
c) Find the Jacobian $\bar{J}^{(0)}$ for this power system configuration and compute the bus voltage correction vector $\Delta\bar{x}^{(0)}$.
d) Update the bus voltage vector $\bar{x}^{(1)}=\bar{x}^{(0)}-\Delta\bar{x}^{(0)}$ and recompute the updated mismatch power vector $\Delta\bar{W}^{(1)}$.

### Problem 7.4: Voltage Control Via Capacitive Load (e.g., Capacitors)

Repeat Problem 7.3 for the condition when switch $S_1$ is open and switch $S_2$ is closed.

### Problem 7.5: Fundamental Power Flow Exploiting the Symmetry of a Power System

Apply to the two-bus system of Fig. P7.5 the Newton-Raphson load flow analysis technique.

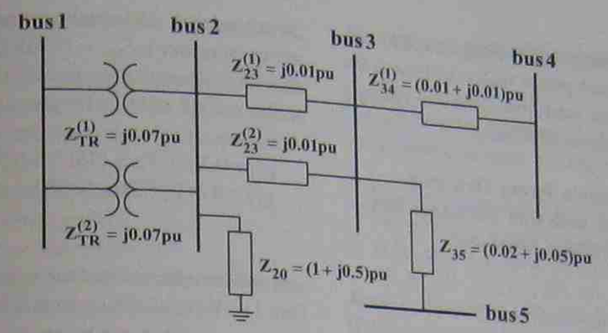
a) Simplify the two-bus system.
b) Find the fundamental bus admittance matrix in polar form.
c) Assume that bus 1 is the swing (slack) bus, and bus 2 is a PQ bus. Make an initial guess for the voltage vector $\bar{x}^{(0)}$ and evaluate the initial mismatch power $\Delta\bar{W}^{(0)}$.
d) Find the Jacobian matrix $\bar{J}^{(0)}$ for this power system configuration and compute the bus voltage correction vector $\Delta\bar{x}^{(0)}$.
e) Update the bus voltage vector $\bar{x}^{(1)}=\bar{x}^{(0)}-\Delta\bar{x}^{(0)}$ and recompute the updated mismatch power vector $\Delta\bar{W}^{(1)}$.

### Problem 7.6: Fundamental Power Flow in a Weak Power System

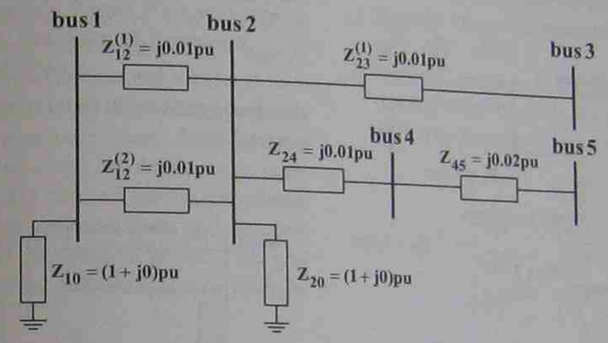
The power system of Fig. P7.6 represents a weak feeder as it occurs in distributed generation (DG) with wind-power plants and photovoltaic plants as power sources. All impedances are in pu and the base apparent power is $S_{base}=10$ MVA.

a) Compute the fundamental admittance matrix for this system.
b) Assuming bus 1 is the swing bus ($\delta_1=0$ and $|\tilde{V}_1|=1.0$ pu) then we can make an initial guess for bus voltage vector $\bar{x}^0=(\delta_2,\ |\tilde{V}_2|,\ \delta_3,\ |\tilde{V}_3|,\ \delta_4,\ |\tilde{V}_4|)^t=(0,\ 1,\ 0,\ 1,\ 0,\ 1)^t$. Note, the superscript 0 means initial guess. Compute the mismatch power vector for this initial condition.
c) Compute the Jacobian matrix.
d) Compute the inverse of the Jacobian matrix.

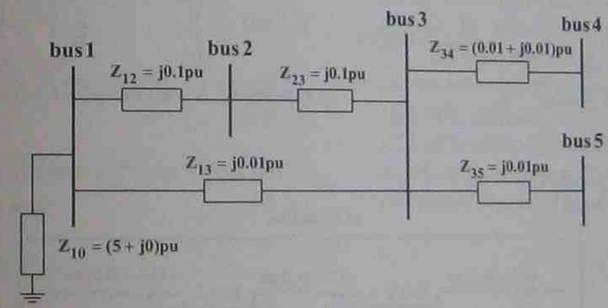




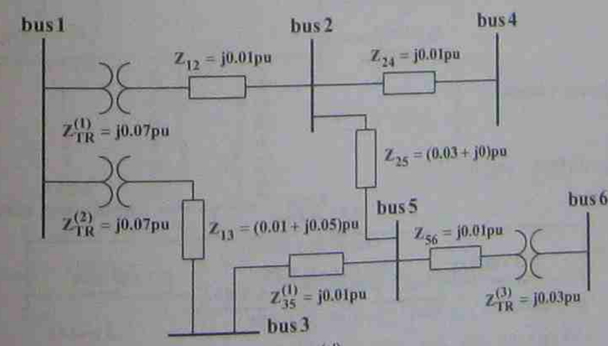

(a)




(b)




(c)




(d)

**FIGURE P7.1** (a) Five-bus system with two transformers and admittances to ground. (b) Five-bus system with admittances to ground. (c) Five-bus system with one admittance to ground. (d) Six-bus system with three transformers and no admittance to ground.

e) Compute the correction voltage vector $\Delta\bar{x}^0$, update the mismatch power vector, and check the convergence of the load flow algorithm (using a convergence tolerance of 0.0001).

### Problem 7.7: Harmonic Power Flow in a Weak Power System with One Nonlinear Bus and One Set of Harmonic Nonlinear Device Currents

The power system of Fig. P7.7 represents a weak feeder as it occurs in distributed generation (DG) with wind-power plants and photovoltaic plants as power sources. All impedances are in pu and the base apparent power is $S_{base} = 10$ MVA. The harmonic v–i characteristic of the nonlinear load at bus 4 (referred to the voltage at bus 4) is given as

$$g_{r,4}^{(5)} = 0.3(V_4^{(1)})^3\cos(3\delta_4^{(1)}) + 0.3(V_4^{(5)})^2\cos(3\delta_4^{(5)})$$
$$g_{i,4}^{(5)} = 0.3(V_4^{(1)})^3\sin(3\delta_4^{(1)}) + 0.3(V_4^{(5)})^2\sin(3\delta_4^{(5)}) \quad \text{(P7-1)}$$

It will be assumed that the voltage at the swing bus (bus 1) is $|\tilde{V}_1^{(1)}| = 1.00$ p.u. and $\delta_1^{(1)} = 0$ rad. The fundamental power flow can be based on Fig. P7.6. For the 5th harmonic the synchronous machine impedance $Z_1$ is replaced by the (subtransient) impedance $Z_2 = jX^{-} = j0.25$ p.u. at 60 Hz. In this case the subtransient reactance has been chosen to be that of a synchronous generator in order to approximate bus 1 as a weak bus.

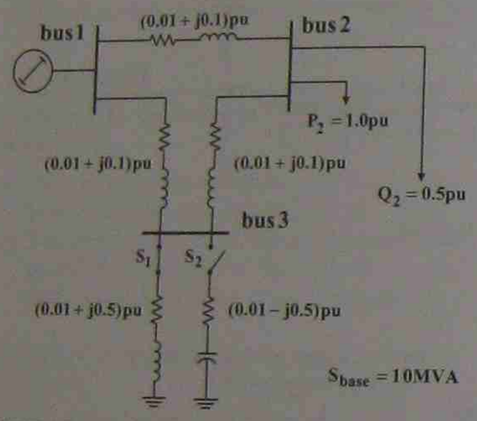



**FIGURE P7.3** Three-bus system.

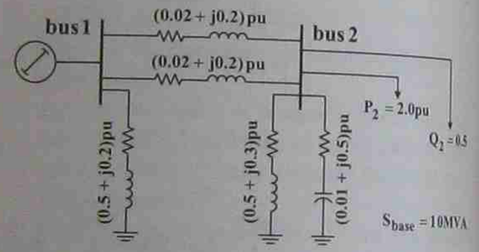



**FIGURE P7.5** Two-bus power system.

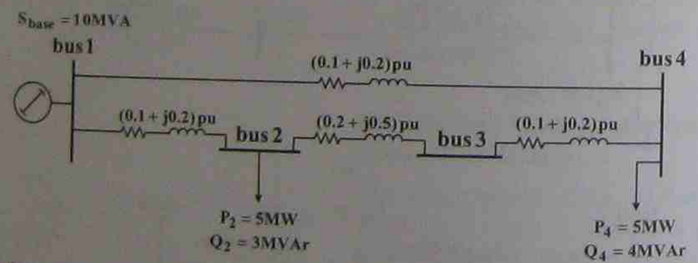



**FIGURE P7.6** Four-bus power system.

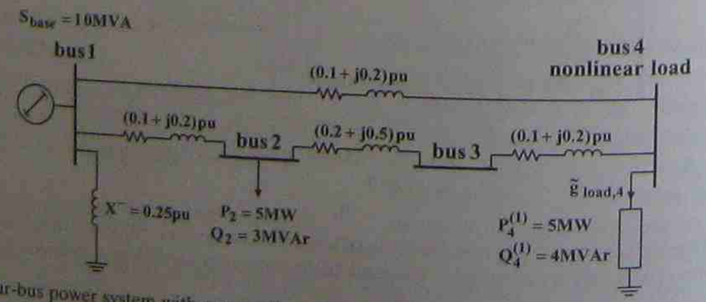



**FIGURE P7.7** Four-bus power system with one nonlinear bus and one set of harmonics.



a) Compute the fundamental and 5th harmonic admittance matrices.
b) Assume an initial value for the bus vector $\bar{U}^0$ and compute the fundamental and the 5th harmonic currents injected into the system by the nonlinear load.
c) Evaluate the mismatch vector.
d) Evaluate the Jacobian matrix.
e) Evaluate the correction vector $\Delta U^o$.
f) Update the mismatch vector and comment on the convergence of the harmonic load flow.

### Problem 7.8: Harmonic Power Flow with one Nonlinear Bus and Two Sets of Harmonic Nonlinear Device Currents

To the three-bus system of Fig. P7.8 apply the Newton–Raphson harmonic load flow analysis technique. Assume that bus 1 is the swing or slack bus, bus 2 is a linear PQ bus, and bus 3 is a nonlinear bus, where the fundamental real and reactive powers are specified. In addition, at bus 3 the real and imaginary harmonic nonlinear device currents are given as

$$g_{r,3}^{(5)} = |\tilde{V}_3^{(1)}|\cos(\delta_3^{(1)}) + |\tilde{V}_3^{(5)}|^2\cos(2\delta_3^{(5)}) + |\tilde{V}_3^{(7)}|\cos(\delta_3^{(7)}), \quad \text{(P8-1a)}$$

$$g_{i,3}^{(5)} = |\tilde{V}_3^{(1)}|\sin(\delta_3^{(1)}) + |\tilde{V}_3^{(5)}|^2\sin(2\delta_3^{(5)}) + |\tilde{V}_3^{(7)}|\sin(\delta_3^{(7)}), \quad \text{(P8-1b)}$$

$$g_{r,3}^{(7)} = |\tilde{V}_3^{(1)}|\cos(\delta_3^{(1)}) + |\tilde{V}_3^{(5)}|\cos(\delta_3^{(5)}) + |\tilde{V}_3^{(7)}|^2\cos(2\delta_3^{(7)}), \quad \text{(P8-2a)}$$

$$g_{i,3}^{(7)} = |\tilde{V}_3^{(1)}|\sin(\delta_3^{(1)}) + |\tilde{V}_3^{(5)}|\sin(\delta_3^{(5)}) + |\tilde{V}_3^{(7)}|^2\sin(2\delta_3^{(7)}). \quad \text{(P8-2b)}$$

The 5th and 7th nonlinear currents are referred to the harmonic voltages $\tilde{V}_3^{(5)}$ and $\tilde{V}_3^{(7)}$, respectively.

a) Find the fundamental and harmonic (5th and 7th) bus admittance matrices in polar form.
b) Make an initial guess for the bus vector $\bar{U}^0 = [\delta_2^{(1)}, v_2^{(1)}, \delta_3^{(1)}, v_3^{(1)}, \delta_1^{(7)}, v_1^{(5)}, \delta_2^{(5)}, v_2^{(5)}, \delta_3^{(5)}, v_3^{(5)}, \delta_1^{(7)}, v_1^{(7)}, \delta_2^{(7)}, v_2^{(7)}, \delta_3^{(7)}, v_3^{(7)}]^t$ and compute the nonlinear load device currents $G_{r,3}^{(1)}$, $G_{i,3}^{(1)}$, $G_{r,3}^{(5)}$, $G_{i,3}^{(5)}$, $G_{r,3}^{(7)}$ and $G_{i,3}^{(7)}$ which are referred to the swing bus.
c) Evaluate the initial mismatch vector $\Delta\bar{M}^0 = [\Delta\bar{W}, \Delta\bar{I}^{(5)}, \Delta\bar{I}^{(7)}, \Delta\bar{I}^{(1)})]^t$.
d) Find the Jacobian $\bar{J}^0$ for this power system configuration and compute the bus correction vector $\Delta\bar{U}^0$. The Jacobian $\bar{J}^0$ is of the form

$$\bar{J}^0 = \begin{bmatrix} \bar{J}^{(1)} & \bar{J}^{(5)} & \bar{J}^{(7)} \\ \overline{YG}^{(5,1)} & \overline{YG}^{(5,5)} & \overline{YG}^{(5,7)} \\ \overline{YG}^{(7,1)} & \overline{YG}^{(7,5)} & \overline{YG}^{(7,7)} \\ \overline{YG}^{(1,1)} & \overline{YG}^{(1,5)} & \overline{YG}^{(1,7)} \end{bmatrix}. \quad \text{(P8-3)}$$

In particular, this matrix (Eq. P8-3 or Eq. P8-4) has the following 16 unknowns: $\delta_2^{(1)}$, $V_2^{(1)}$, $\delta_3^{(1)}$, $V_3^{(1)}$, $\delta_1^{(5)}$, $V_1^{(5)}$, $\delta_2^{(5)}$, $V_2^{(5)}$, $\delta_3^{(5)}$, $V_3^{(5)}$, $\delta_1^{(7)}$, $V_1^{(7)}$, $\delta_2^{(7)}$, $V_2^{(7)}$, $\delta_3^{(7)}$, $V_3^{(7)}$, (see identification of columns of Eq. P8-4) and the following 16 equations: $\Delta P_2^{(1)}$, $\Delta Q_2^{(1)}$, $\Delta I_{r,1}^{(5)}$, $\Delta I_{i,1}^{(5)}$, $\Delta I_{r,2}^{(5)}$, $\Delta I_{i,2}^{(5)}$, $\Delta I_{r,3}^{(5)}$, $\Delta I_{i,3}^{(5)}$, $\Delta I_{r,1}^{(7)}$, $\Delta I_{i,1}^{(7)}$, $\Delta I_{r,2}^{(7)}$, $\Delta I_{i,2}^{(7)}$, $\Delta I_{r,3}^{(7)}$, $\Delta I_{i,3}^{(7)}$, $\Delta I_{r,3}^{(1)}$, $\Delta I_{i,3}^{(1)}$ (see identification of rows of Eq. P8-4). Note there are no $\bar{H}$ matrices (e.g., $\bar{H}^{(1)}$, $\bar{H}^{(5)}$ and $\bar{H}^{(7)}$) related to $\alpha_3$ and $\beta_3$. This reduces

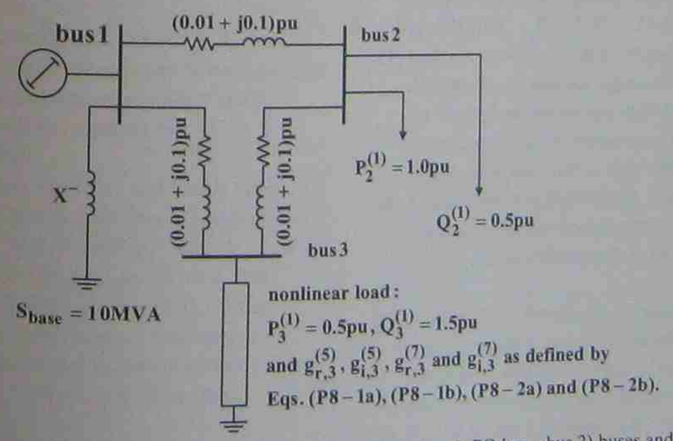



**FIGURE P7.8** Three-bus system consisting of two linear (swing bus = bus 1, PQ bus = bus 2) buses and one nonlinear bus (bus 3). The negative sequence impedance (= subtransient reactance at 60 Hz) of the swing bus is $Z_2 = jX^{-} = j0.10$ pu and there are two sets of harmonics.

ST. GEORGE POLICE

the equation system by two equations. In this case we can define the matrix $\bar{J}^0$ (Eq. P8-4).

e) Update the bus vector $\bar{U}^1 = (\bar{U}^0 - \Delta\bar{U}^0)$ and recompute the updated mismatch vector $\Delta\bar{M}^1$.

Hint: The top row – not part of the Jacobian – of Eq. P8-4 lists the variables:

$$[\delta_2^{(1)}\ v_2^{(1)}\ \delta_3^{(1)}\ v_3^{(1)}\ \delta_1^{(5)}\ v_1^{(5)}\ \delta_2^{(5)}\ v_2^{(5)}\ \delta_3^{(5)}\ v_3^{(5)}\ \delta_1^{(7)}\ v_1^{(7)}\ \delta_2^{(7)}\ v_2^{(7)}\ \delta_3^{(7)}\ v_3^{(7)}],$$

and the right-hand side column – not part of the Jacobian – lists the mismatch quantities which must be satisfied:

$$[\Delta P_2^{(1)}\ \Delta Q_2^{(1)}\ \Delta I_{r,1}^{(5)}\ \Delta I_{i,1}^{(5)}\ \Delta I_{r,2}^{(5)}\ \Delta I_{i,2}^{(5)}\ \Delta I_{r,3}^{(5)}\ \Delta I_{i,3}^{(5)}\ \Delta I_{r,1}^{(7)}\ \Delta I_{i,1}^{(7)}\ \Delta I_{r,2}^{(7)}\ \Delta I_{i,2}^{(7)}\ \Delta I_{r,3}^{(7)}\ \Delta I_{i,3}^{(7)}]^t.$$

These two identifications help in defining the partial derivatives of the Jacobian. For example,

$$J_{3,5}^0 = \frac{\partial(\Delta I_{r,1}^{(5)})}{\partial(\delta_1^{(5)})},\quad J_{3,10}^0 = \frac{\partial(\Delta I_{r,1}^{(5)})}{\partial(V_3^{(5)})},\quad J_{8,5}^0 = \frac{\partial(\Delta I_{i,3}^{(5)})}{\partial(\delta_1^{(5)})},$$

$$J_{8,10}^0 = \frac{\partial(\Delta I_{i,3}^{(5)})}{\partial(V_3^{(5)})},\quad J_{9,11}^0 = \frac{\partial(\Delta I_{r,1}^{(7)})}{\partial(\delta_1^{(7)})},\ \text{and}$$

$$J_{12,16}^0 = \frac{\partial(\Delta I_{i,2}^{(7)})}{\partial(V_3^{(7)})}.$$

$$\bar{J}^0 = \begin{array}{c|cccccccccccccccc|l}
 & \delta_2^{(1)}\downarrow & V_2^{(1)}\downarrow & \delta_3^{(1)}\downarrow & V_3^{(1)}\downarrow & \delta_1^{(5)}\downarrow & V_1^{(5)}\downarrow & \delta_2^{(5)}\downarrow & V_2^{(5)}\downarrow & \delta_3^{(5)}\downarrow & V_3^{(5)}\downarrow & \delta_1^{(7)}\downarrow & V_1^{(7)}\downarrow & \delta_2^{(7)}\downarrow & V_2^{(7)}\downarrow & \delta_3^{(7)}\downarrow & V_3^{(7)}\downarrow & \\
\hline
 & 19.8 & 1.98 & -9.9 & -0.99 & 0 & 0 & 0 & 0 & 0 & 0 & 0 & 0 & 0 & 0 & 0 & 0 & \leftarrow \Delta P_2^{(1)} \\
 & -1.98 & 19.8 & 0.99 & -9.9 & 0 & 0 & 0 & 0 & 0 & 0 & 0 & 0 & 0 & 0 & 0 & 0 & \leftarrow \Delta Q_2^{(1)} \\
 & 0 & 0 & 0 & 0 & J_{3,5}^0 & J_{3,6}^0 & J_{3,7}^0 & J_{3,8}^0 & J_{3,9}^0 & J_{3,10}^0 & 0 & 0 & 0 & 0 & 0 & 0 & \leftarrow \Delta I_{r,1}^{(5)} \\
 & 0 & 0 & 0 & 0 & J_{4,5}^0 & J_{4,6}^0 & J_{4,7}^0 & J_{4,8}^0 & J_{4,9}^0 & J_{4,10}^0 & 0 & 0 & 0 & 0 & 0 & 0 & \leftarrow \Delta I_{i,1}^{(5)} \\
 & 0 & 0 & 0 & 0 & J_{5,5}^0 & J_{5,6}^0 & J_{5,7}^0 & J_{5,8}^0 & J_{5,9}^0 & J_{5,10}^0 & 0 & 0 & 0 & 0 & 0 & 0 & \leftarrow \Delta I_{r,2}^{(5)} \\
 & 0 & 0 & 0 & 0 & J_{6,5}^0 & J_{6,6}^0 & J_{6,7}^0 & J_{6,8}^0 & J_{6,9}^0 & J_{6,10}^0 & 0 & 0 & 0 & 0 & 0 & 0 & \leftarrow \Delta I_{i,2}^{(5)} \\
 & 0 & 0 & 0 & 1 & J_{7,5}^0 & J_{7,6}^0 & J_{7,7}^0 & J_{7,8}^0 & J_{7,9}^0 & J_{7,10}^0 & 0 & 0 & 0 & 0 & 0 & 1 & \leftarrow \Delta I_{r,3}^{(5)} \\
 & 0 & 0 & 1 & 0 & J_{8,5}^0 & J_{8,6}^0 & J_{8,7}^0 & J_{8,8}^0 & J_{8,9}^0 & J_{8,10}^0 & 0 & 0 & 0 & 0 & 0.1 & 0 & \leftarrow \Delta I_{i,3}^{(5)} \\
 & 0 & 0 & 0 & 0 & 0 & 0 & 0 & 0 & 0 & 0 & J_{9,11}^0 & J_{9,12}^0 & J_{9,13}^0 & J_{9,14}^0 & J_{9,15}^0 & J_{9,16}^0 & \leftarrow \Delta I_{r,1}^{(7)} \\
 & 0 & 0 & 0 & 0 & 0 & 0 & 0 & 0 & 0 & 0 & J_{10,11}^0 & J_{10,12}^0 & J_{10,13}^0 & J_{10,14}^0 & J_{10,15}^0 & J_{10,16}^0 & \leftarrow \Delta I_{i,1}^{(7)} \\
 & 0 & 0 & 0 & 0 & 0 & 0 & 0 & 0 & 0 & 0 & J_{11,11}^0 & J_{11,12}^0 & J_{11,13}^0 & J_{11,14}^0 & J_{11,15}^0 & J_{11,16}^0 & \leftarrow \Delta I_{r,2}^{(7)} \\
 & 0 & 0 & 0 & 0 & 0 & 0 & 0 & 0 & 0 & 0 & J_{12,11}^0 & J_{12,12}^0 & J_{12,13}^0 & J_{12,14}^0 & J_{12,15}^0 & J_{12,16}^0 & \leftarrow \Delta I_{i,2}^{(7)} \\
 & 0 & 0 & 0 & 1 & 0 & 0 & 0 & 0 & 0 & 1 & J_{13,11}^0 & J_{13,12}^0 & J_{13,13}^0 & J_{13,14}^0 & J_{13,15}^0 & J_{13,16}^0 & \leftarrow \Delta I_{r,3}^{(7)} \\
 & 0 & 0 & 1 & 0 & 0 & 0 & 0 & 0 & 0.1 & 0 & J_{14,11}^0 & J_{14,12}^0 & J_{14,13}^0 & J_{14,14}^0 & J_{14,15}^0 & J_{14,16}^0 & \leftarrow \Delta I_{i,3}^{(7)} \\
 & -9.90 & -0.99 & 21.3 & 1.48 & 0 & 0 & 0 & 0 & 0 & 0 & 0 & 0 & 0 & 0 & 0 & 0 & \leftarrow \Delta I_{r,3}^{(1)} \\
 & -0.99 & 9.9 & -2.51 & -18.3 & 0 & 0 & 0 & 0 & 0 & 0 & 0 & 0 & 0 & 0 & 0 & 0 & \leftarrow \Delta I_{i,3}^{(1)}
\end{array} \quad \text{(P8-4)}$$



## 7.8 REFERENCES




1) Abolins, A.; Achenbach, H.; and Lambrecht, D.; "Design and performance of large four-pole turbogenerators with semiconductor excitation for nuclear power stations," *Cigre-Report*, 1972 Session, August 28–September, Paper No 11-04.

2) Fuchs, E.F.; "Numerical determination of synchronous, transient, and subtransient reactances of a synchronous machine," Ph.D. Thesis, University of Colorado, Boulder, 1970.

3) http://www.powerfrontiers.com/ngccplants.htm

4) http://en.wikipedia.org/wiki/Combined_cycle

5) Xia, D.; and Heydt, G.T.; "Harmonic power flow studies, part I – formulation and solution," *IEEE Transactions on Power Apparatus and System*, vol. 101, no. 6, pp. 1257–1265, 1982.

6) Xia, D.; and Heydt, G.T.; "Harmonic power flow studies, part II – implementation and practical application," *IEEE Transactions on Power Apparatus and System*, vol. 101, no. 6, pp. 1266–1270, 1982.

7) Baghzouz, Y.; and Ertem, S.; "Shunt capacitor sizing for radial distribution feeders with distorted substation voltage," *IEEE Transactions on Power Delivery*, vol. 5, no. 2, pp. 650–657, 1990.

8) Baghzouz, Y.; "Effects of nonlinear loads on optimal capacitor placement in radial feeders," *IEEE Transactions on Power Delivery*, vol. 6, no. 1, pp. 245–251, 1991.

9) Semlyen, A.; and Shlash, M.; "Principles of modular harmonic power flow methodology," *IEE Proceedings – Generation, Transmission and Distribution*, vol. 147, no. 1, pp. 1–6, 2000.

10) Arrillaga, J.; Watson, N.R.; and Bathurst, G.N.; "A multi-frequency power flow of general applicability," *IEEE Transactions on Power Delivery*, vol. 19, no. 1, pp. 342–349, 2004.

11) Bathurst, C.N.; Smith, B.C.; Watson, N.R.; and Arrillaga, J.; "A modular approach to the solution of the three-phase harmonic power-flow," *IEEE Transactions on Power Delivery*, vol. 15, no. 3, pp. 984–989, 2000.

12) Moreno Lopez de Saa, M.A.; and Usaola Garcia, J.; "Three-phase harmonic load flow in frequency and time domains," *IEE Proceedings – Electric Power Applications*, vol. 150, no. 3, pp. 295–300, 2003.

13) Hong, Y.-Y.; Lin, J.-S.; and Liu, C.-H.; "Fuzzy harmonic power flow analyses," presented at International Conference on Power System Technology, PowerCon 2000, vol. 1, 4–7 Dec. 2000, pp. 121–125.

14) Shlash, M.; and Semlyen, A.; "Efficiency issues of modular harmonic power flow," *IEE Proceedings – Generation, Transmission and Distribution*, vol. 148, no. 2, pp. 123–127, 2001.

15) Williams, S.M.; Brownfield, G.T.; and Duffus, J.W.; "Harmonic propagation on an electric distribution system: field measurements compared with computer simulation," *IEEE Transactions on Power Delivery*, vol. 8, no. 2, pp. 547–552, 1993.

16) Chin, H.-C.; "Optimal shunt capacitor allocation by fuzzy dynamic programming," *Electric Power Systems Research*, vol. 35, no. 2, pp. 133–139, 1995.

17) Teng, J.-H.; and Chang, C.-Y.; "A fast harmonic load flow method for industrial distribution systems," *International Conference on Power System Technology*, vol. 3, pp. 1149–1154, December 2000.

18) Masoum, M.A.S.; Jafarian, A.; Ladjevardi, M.; Fuchs, E.F.; and Grady, W.M.; "Fuzzy approach for optimal placement and sizing of capacitor banks in the presence of harmonics," *IEEE Transactions on Power Delivery*, vol. 19, no. 2, pp. 822–829, 2004.

19) Chung, T.S.; and Leung, H.C.; "A genetic algorithm approach in optimal capacitor selection with harmonic distortion considerations," *International Journal of Electrical Power & Energy Systems*, vol. 21, no. 8, pp. 561–569, 1999.

20) Elamin, I.M.; "Fast decoupled harmonic load flow method," *Conference Record of the 1990 IEEE Industry Applications Society Annual Meeting, 1990*, 7–12 Oct. 1990, pp. 1749–1756.

21) Carpinelli, G.; Esposito, T.; Varilone, P.; and Verde, P.; "First-order probabilistic harmonic power flow," *IEE Proceedings – Generation, Transmission and Distribution*, vol. 148, no. 6, pp. 541–548, 2001.

22) Esposito, T.; Carpinelli, G.; Varilone, P.; and Verde, P.; "Probabilistic harmonic power flow for percentile evaluation," *Canadian Conference on Electrical and Computer Engineering, 2001*, vol. 2, 13–16 May 2001, pp. 831–838.

23) Bathurst, G.N.; Smith, B.C.; Watson, N.R.; and Arillaga, J.; "A modular approach to the solution of the three-phase harmonic power-flow," *8th International Conference on Harmonics and Quality of Power, 1998*, vol. 2, 14–16 Oct. 1998, pp. 653–659.

24) Valcarel, M.; and Mayordomo, J.G.; "Harmonic power flow for unbalanced systems," *IEEE Transactions on Power Delivery*, vol. 8, no. 4, pp. 2052–2059, 1993.

25) Marinos, Z.A.; Pereira, J.L.R.; and Carneiro Jr., S.; "Fast harmonic power flow calculation using parallel processing," *IEE Proceedings – Generation, Transmission and Distribution*, vol. 141, no. 1, pp. 27–32, 1994.

26) Rios, M.S.; and Castaneda, P.R.; "Newton-Raphson probabilistic harmonic power flow through Monte Carlo simulation," *Symposium on Circuits and*


ST. GEORGE COLLEGE OF TEST

*Systems, Midwest, 1995*, vol. 2, 13–16 Aug. 1995, pp. 1297–1300.

27) Baghzouz, Y.; Burch, R.F.; Capasso, A.; Cavallini, A.; Emanuel, A.E.; Halpin, M.; Imece, A.; Ludbrook, A.; Montanari, G.; Olejniczak, K.J.; Ribeiro, P.; Rios-Marcuello, S.; Tang, L.; Thaliam, R.; and Verde, P.; "Time-varying harmonics. I. Characterizing measured data," *IEEE Transactions on Power Delivery*, vol. 13, no. 3, pp. 938–944, 1998.

28) Baghzouz, Y.; Burch, R.F.; Capasso, A.; Cavallini, A.; Emanuel, A.E.; Halpin, M.; Imece, A.; Ludbrook, A.; Montanari, G.; Olejniczak, K.J.; Ribeiro, P.; Rios-Marcuello, S.; Tang, L.; Thaliam, R.; and Verde, P.; "Time-varying harmonics. II. Harmonic summation and propagation," *IEEE Transactions on Power Delivery*, vol. 17, no. 1, pp. 279–285, 2002.

29) Grady, W.M.; Samotyj, M.J.; and Noyola, A.H.; "The application of network objective functions for actively minimizing the impact of voltage harmonics in power systems," *IEEE Transactions on Power Delivery*, vol. 7, no. 3, pp. 1379–1386, 1992.

ST. GEORGE POWER UK LTD

# 8 CHAPTER

# Impact of Poor Power Quality on Reliability, Relaying, and Security

New technical and legislative developments shape the electricity market, whereby the reliability of power systems and the profitability of the utility companies must be maintained. To achieve these objectives the evaluation of the power system and, in particular, the distribution system reliability is an important task. It enables utilities to predict the reliability level of an existing system after improvements have been achieved through restructuring and improved design and to select the most appropriate configuration among various available options.

This chapter addresses the impact of poor power quality on reliability, relaying, and security. Section 8.1 introduces reliability indices. Degradation of reliability and security due to poor power quality including the effects of harmonics and interharmonics on the operation of overcurrent and under-frequency relays, electromagnetic field (EMF) generation, corona in transmission lines, distributed generation, cogeneration, and frequency/voltage control are discussed in Section 8.2. Tools for detecting poor power quality and for improving reliability or security are treated in Sections 8.3 and 8.4, respectively. The remainder of this chapter is dedicated to techniques for improving and controlling the reliability of power systems including load shedding and load management (Section 8.5), energy-storage methods (Section 8.6), and matching the operation of intermittently operating renewable power plants with energy storage facilities (Section 8.7).

## 8.1 RELIABILITY INDICES

It is worth noting that the reliability indices as defined in the literature [1–9] are not absolute measures, but they provide relative information based on the comparison of alternative solutions. The set of reliability indices can be divided into four categories:

**Load-point indices:** average failure (fault) rate ($\lambda$), average outage time ($r$), annual outage time ($U$), repair time ($t_r$), and switching time ($t_s$).

**Customer-oriented system indices:** system average interruption frequency index (SAIFI), system average interruption duration index (SAIDI), customer average interruption duration index (CAIDI), and system average rms (variation) frequency index (SARFI, usually written as $SARFI_{x,v}$).

**Load-oriented system indices:** average service availability index (ASAI), average service unavailability index (ASUI), energy not supplied (ENS), and average energy not supplied (AENS).

**Economical evaluation of reliability:** composite customer damage function (CCDF), customer outage cost (COC), and system customer outage cost (SCOC).

In typical distribution systems, radial circuits are formed by a main feeder and some laterals as depicted in Fig. 8.1. The main feeder is supplied by a primary substation (PS or HV/MV) and connects various switching substations (SWSU), that do not include power transformers to which the laterals are connected to supply the secondary substations (SS)$_i$. This radial configuration is simple and economical, but provides the lowest reliability level because secondary substations have only one source of supply. In Fig. 8.1 (PDu)$_i$ and (PDd)$_i$ are upstream and downstream protection devices, respectively, and (LP)$_i$ are load points.

The open-loop configuration of Fig. 8.2 is formed by two main feeders supplied by the same primary substation (PS or HV/MV). Each feeder has eight switching substations that each supply one secondary substation (SS)$_i$. No laterals are present in this configuration, but each load point (LP)$_i$ is supplied through a connection line of short length. The two feeder ends are typically disconnected by NO (normally open) switches, thus forming an open loop. Under normal conditions the NO switches separate the two main feeders of the system, but in the event of a fault they can be closed in order to supply power to loads that have been disconnected from the primary substation. In Fig. 8.2 (NOSW)$_1$ and (NOSW)$_2$ are normally open switches for the two main feeders 1 and 2, respectively.


ISBN 978-0-12-369536-9
© Elsevier Inc. All rights reserved.

Ring configurations are similar to open-loop schemes but are not operated in a radial manner. The main feeder is supplied at both ends by one primary substation (PS or HV/MV), but it forms a ring without normally open switches. Appropriate protection schemes allow higher reliability than for radial or open-loop configurations because one fault of the main feeder does not cause power failure at any LP. The ring configuration is shown in Fig. 8.3 whereby the number of load points (LPs), their topology, and their relative positions are the same as for the open-loop scheme.

Flower configurations are formed by ring schemes—resembling flower petals—and are supplied by the same primary substation (PS or HV/MV). Normally, the number of rings ranges from two to four for each PS. The rings belonging to different flower petals can be connected to one another through NO switches, increasing the system reliability. Figure 8.4 illustrates two flower configurations supplying eight LPs each. Each PS is supposed to be placed at a load center. The number of LPs, their topology, and their relative positions are the same as in the cases previously considered.

The reliability evaluation of power systems is concerned besides traditional approaches [4] with the impact of automation on distribution reliability [2, 5, 7], the reliability worth for distribution planning [3], and the role of automation on the restoration of distribution systems [6]. Reliability test systems are addressed in [8] and a reliability assessment of traditional versus automated approaches is presented in [9].

### 8.1.1 Application Example 8.1: Calculation of Reliability Indices

In this example, July has been chosen because in Colorado there are short-circuit faults, demand overload, line switching, capacitor switching, and lightning strikes as indicated in Table E8.1.1. The total number of customers is $N_T = 40000$.

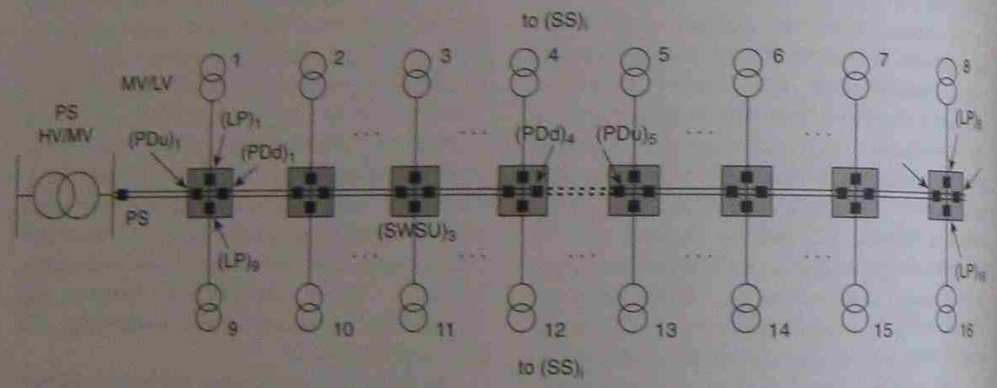



FIGURE 8.1 Radial configuration with possible locations for protection devices (PD) at each switching substation (SWSU) with load points (LP).

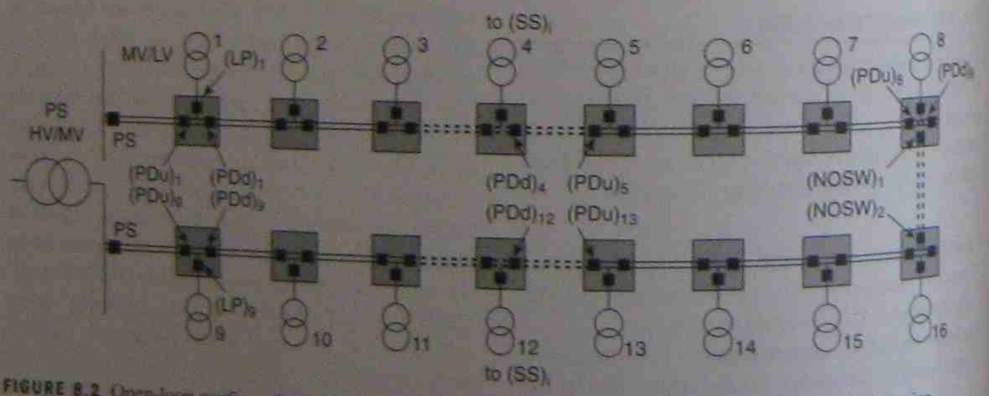



FIGURE 8.2 Open-loop configuration with possible locations for protection devices at each switching substation.



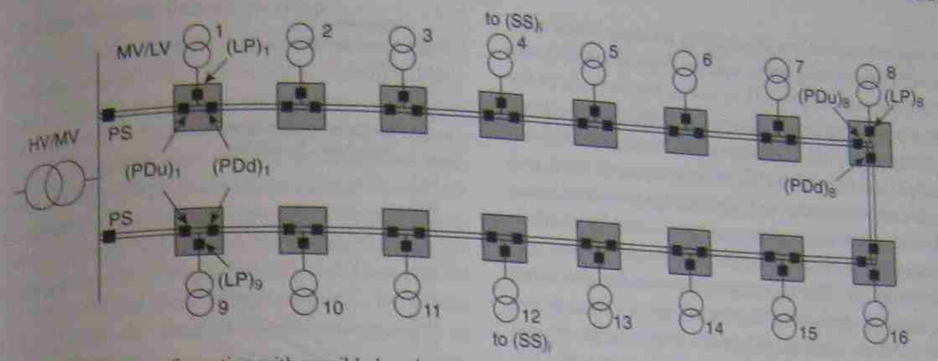



FIGURE 8.3 Ring configuration with possible locations for protection devices at each switching substation.

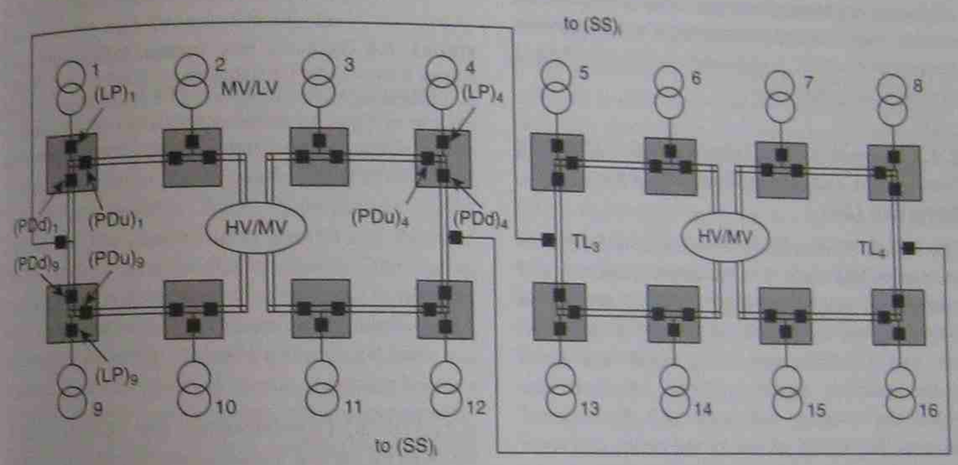



FIGURE 8.4 Flower configuration with possible locations for protection devices at each switching substation.

TABLE E8.1.1 Interruptions and Transients during July 2006

| Number of interruptions or transients | Interruption or transient duration | Voltage (% of rated value) | Total number of customers affected | Cause of interruption or transient |
|---|---|---|---|---|
| 4 | 4.5 h | 0 | 1,000 | Overload |
| 6 | 3 h | 0 | 1,500 | Repair |
| 25 | 1 min | 90 | 2,000 | Switching transients |
| 30 | 1 s | 130 | 3,000 | Capacitor switching |
| 50 | 0.1 s | 40 | 15,000 | Short-circuits |
| 55 | 0.1 s | 150 | 4,000 | Lightning |
| 70 | 0.01 s | 50 | 3,000 | Short-circuits |

## 8.2 DEGRADATION OF RELIABILITY AND SECURITY DUE TO POOR POWER QUALITY

### 8.2.1 Single-Time and Nonperiodic Events

The reliability and security of power systems is impaired by natural and man-made phenomena. Both types change in their severity as the power system protection develops over time. There are single-time, periodic, nonperiodic, and intermittent events. Although before the advent of interconnected systems lightning strikes [10], ice storms [11–18], ferroresonance [19], faults [20], and component failures were mainly a concern, the fact that interconnected systems are predominantly used gave rise to the influence of sunspot cycles [21] on long transmission lines built on igneous rock formations,

subsynchronous resonance [22] through series compensation of long lines, nuclear explosions [23], and terrorist attacks [24–27] as well as the increase of the ambient temperature above $T_{amb} = 40°C$ due to global warming [28, 29]. It is interesting to note that utilities install ice monitors [15] on transmission lines and make an attempt to melt ice through dielectric losses [16–18]. Ferroresonance can be avoided by employing gas ($SF_6$)-filled cables [30] for distribution systems above 20 kV. The effect of sunspot cycles and those of nuclear explosions can be mitigated through the use of three-limb transformers with a large air gap between the transformer iron core and the tank [31]. The increase of the ambient temperature will necessitate in a revision of existing design standards for electric machines and transformers, and an ambient temperature of 50°C is recommended for new designs of electrical components.

### 8.2.2 Harmonics and Interharmonics Affecting Overcurrent and Under-Frequency Relay Operation [32]

The effects of nonsinusoidal voltages and currents on the performance of static under-frequency and overcurrent relays are experimentally studied in [33]. Tests are conducted for harmonics as well as sub- and interharmonics. Most single- and three-phase induction motors generate interharmonics within the rotating flux wave and the terminal currents due to the choice of the stator and rotor slots and because of air-gap eccentricity (spatial harmonics).

**Under-Frequency Relays.** The increases in operating time due to voltage harmonics from 0 to 15% of the fundamental are shown in Fig. 8.5 for a frequency set point of 58.99 Hz at frequency rate of changes of 1 Hz/s and 2 Hz/s, at a delay time of $T_D = 0$ s. Tests indicate [33] that under-frequency relays are very sensitive to interharmonics of the voltage because of the occurrence of additional zero crossings within one voltage period and, therefore, interharmonics should be limited from this point of view to less than 0.5%.

**Overcurrent Relays.** A three-phase solid-state time and instantaneous over-current relay is self-contained and can have short time, long time, instantaneous, and ground protection on the options selected. The percentage deviations from the nominal (sinusoidal) rms current values operating the overcurrent relay at lower (e.g., –0.95%) or higher

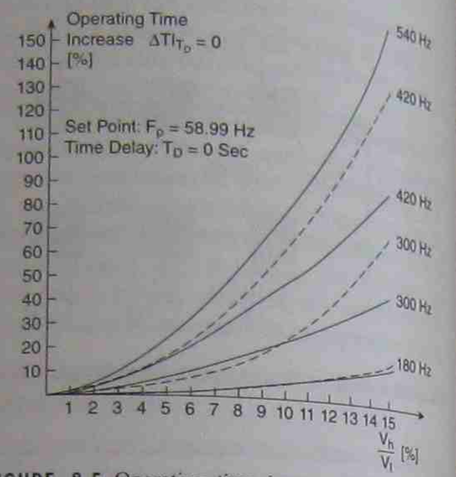



**FIGURE 8.5** Operating time increase $\Delta T|_{TD=0}$ due to voltage harmonics for the frequency set point $F_p = 58.99$ Hz. (—) Frequency rate of change of $\Delta f = 1$ Hz/s and an operating time of $T_{T1} = 60.5$ cycles or 1.008 s. (– – –) Frequency rate of change of $\Delta f = 2$ Hz/s and an operating time of $T_{T2} = 25$ cycles or 0.417 s.

(e.g., +1.43%) (nonsinusoidal) rms current values are listed for various harmonic amplitudes and phase shifts (e.g., min, max) in [33]. One notes that current harmonics cause the overcurrent device in the worst case to pick up at (100% ± 10%) of the nominal rms value based on a sinusoidal wave shape. Similar measurements reveal that the same overcurrent relay has changes at the time delay—for a given pickup rms current setting—up to 45% shorter and up to 26% longer than the nominal time delay with no harmonics. The long-time delay pickup current value is reduced for most harmonics by 20% and increased for certain harmonics by 7%. An electromechanical relay, subjected to similar tests as the solid-state relay, performed in a similar manner as the latter. With regard to the instantaneous pickup, rms current harmonics cause the overcurrent relay to pick up in the worst case at (100% + 10%) of the nominal rms value based on a sinusoidal wave shape. With regard to the time delay for given pickup rms current values, harmonics cause the hinged armature over-current relay to pick up in the worst case ($I_h/I_1 = 60\%$) at (100% + 43%) of the nominal rms value based on sinusoidal wave shape.



### 8.2.3 Power-Line Communication

Power-line carrier applications are described in [34–39]. They consist of the control of nonessential loads (load shedding) to mitigate undervoltage conditions and to prevent voltage collapse. High-frequency harmonics, interharmonics caused by solid-state converters, and voltage fluctuations caused by electric arc furnaces can cause interferences with power-line communication and control. Newer approaches for automatic meter reading [40–42] and load control are based on wireless communication. Reference [43] addresses the issue of optimal management of electrical loads.

### 8.2.4 Electromagnetic Field (EMF) Generation and Corona Effects in Transmission Lines

The minimization and mitigation of electromagnetic fields (EMFs) and corona effects, e.g., radio and television interference, coronal losses, audible noise, ozone production at or above 230/245 kV high-voltage transmission lines, is important. After addressing the generation of electric and magnetic fields, mechanisms leading to corona, the factors influencing the generation of corona, and its negative effects are explained. Solutions for the minimization of corona in newly designed transmission lines and reduction or mitigation of corona of existing lines are well known but not, however, always inexpensive. California's Public Utilities Commission initiated hearings in order to explore the possibilities of "no-cost/low-cost" EMF mitigation. A review of these ongoing hearings and their outcomes will be given. The difficulties associated with obtaining the right of way for new transmission lines lead to the upgrading of existing transmission lines with respect to higher voltages in order to increase transmission capacity. In the past, high-voltage lines with voltages of up to $V_{L-L} = 200$ kV were considered acceptable in terms of the generation of corona effects [35, 44–46]. However, the concern that electromagnetic fields may cause in addition to corona also detrimental health effects lead to renewed interest in reexamining the validity of the stated voltage limit with respect to their impact on the health of the general population. This section presents a brief summary of many publications.

#### 8.2.4.1 Generation of EMFs

**Electric Field Strength $\vec{E}$.** The electric field strength $\vec{E}$ of a single conductor having a per-unit length charge of $Q$ is

$$\vec{E} = \frac{1}{4\pi\varepsilon_o}\frac{Q}{r^2}\vec{r}, \tag{8-1}$$

where $\varepsilon_o$ and $\vec{r}$ are the permittivity of free space and the unit vector in radial direction of a cylindrical coordinate system, respectively. Note that $\vec{E}$ reduces inversely in a quadratic manner with the radial distance $r$. For a three-phase system the three electric field components $E_a$, $E_b$, and $E_c$ must be geometrically superimposed at the point of interest. $Q$ is proportional to the transmission line voltage $V$, that is, the absolute value of $\vec{E}$ is proportional to $V$.

#### 8.2.4.2 Application Example 8.2: Lateral Profile of Electric Field at Ground Level below a Three-Phase Transmission Line

If the calculation of the electric field at ground is repeated at different points in a section perpendicular to the transmission line, the lateral profile of the transmission-line electric field is obtained. Examples of calculated lateral profiles are presented in Fig. E8.2.1. Particularly important for the line design are the maximum (worst case) field and the field at the edge of the transmission corridor. The maximum field occurs within the transmission corridor, though for flat configurations it might occur slightly outside the outer phases.

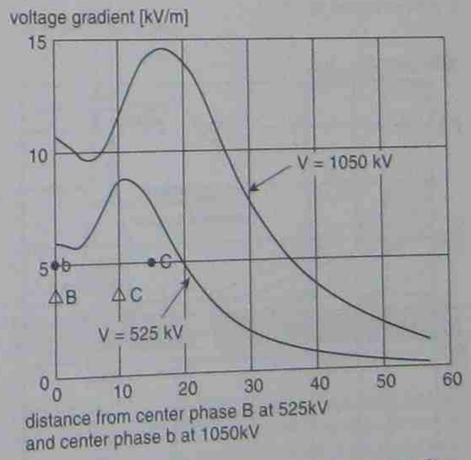



**FIGURE E8.2.1** Lateral profiles of electric field $|\vec{E}|$ at ground level. Line at $V_{L-L} = 525$ kV with 3 × 3.3 cm (bundle) conductors on $D = 30$ cm diameter, 45 cm spacing, spaced 10 m, and 10.6 m above ground, flat configuration (phases B and C). Line at $V_{L-L} = 1050$ kV with 8 × 3.3 cm (bundle) conductors on $D = 101$ cm diameter, spaced 18.3 m, and 18.3 m above ground, flat configuration (phases b and c).

Figure E8.2.2 shows universal curves using nondimensional quantities that may be used to calculate the maximum electric field at ground for a flat configuration. Results for other configurations are given in [47].

For a rated line-to-line voltage of $V_{L-L} = 525$ kV, a $3 \times 3.3$ cm conductor bundle with 45 cm spacing, phase-to-phase distance $S = 10$ m, the equivalent bundle diameter of $D = 0.3$ m, and height of the center of the bundle to ground $H = 10.6$ m the ratios $H/D = 10.6/0.3 = 35.3$, $S/H = 10/10.6 = 0.94$ result with Fig. E8.2.2 in $HE/V = 0.179$. The maximum (worst case) electric field at ground is then $|\vec{E}| = E = 0.179 \cdot 525\,\text{k}/10.6 = 8.8\,\text{kV/m} = 8.8\,\text{V/mm}$; this value is confirmed by Fig. E8.2.1. The presence of overhead ground wires has a negligible effect on the field at ground.

**Magnetic Field Strength $\vec{H}$.** The magnetic field strength $\vec{H}$ of a single conductor carrying a current $I$ is

$$\vec{H} = \frac{1}{2\pi} \cdot \frac{I}{r} \vec{\phi}, \tag{8-2}$$

where $\vec{\phi}$ is the azimuthal unit vector of a cylindrical coordinate system. Note that $\vec{H}$ decreases inversely with the radial distance $r$. For a three-phase system the three magnetic field components $H_a$, $H_b$, and $H_c$ must be geometrically superimposed at the point of interest. The absolute value of the magnetic field $\vec{H}$ is proportional to $I$ [48].

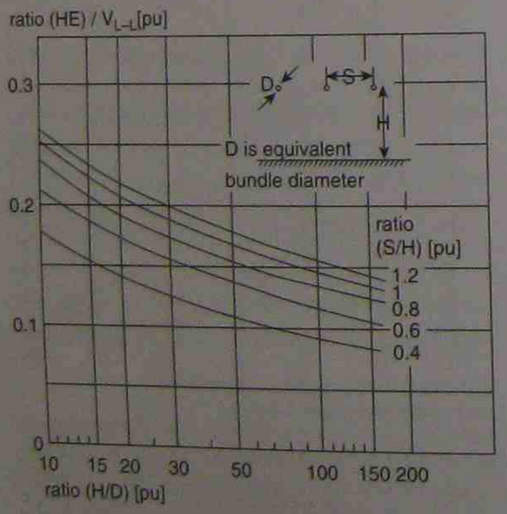



**FIGURE E8.2.2** Universal curves to calculate the maximum (worst case) electric field $|\vec{E}| = E$ at ground level for lines of flat configuration. H is the height to the center of the bundle.

### 8.2.4.3 Application Example 8.3: Lateral Profile of Magnetic Field at Ground Level under a Three-Phase Transmission Line

In most practical cases, the magnetic field in proximity to balanced three-phase lines may be calculated considering the currents in the conductors and in the ground wires and neglecting the earth currents. As a result one obtains a magnetic field ellipse with minor and major axes. The maximum (worst case) ground level magnetic field occurs at the center line of the transmission line and is $|\vec{H}_{\text{worst}}| = H_{\text{worst}} = 14$ A/m (see Fig. E8.3.1), which corresponds to a flux density $|\vec{B}_{\text{worst}}| = B_{\text{worst}} = 0.176\,\text{G} = 176\,\text{mG}$. For comparison, the earth magnetic field is about $B_{\text{earth}} = 0.5\,\text{G} = 500$ mG. It should be noted, however, that the earth field is not time-varying, whereas the transmission line field varies with 60 Hz frequency.

### 8.2.4.4 Mechanism of Corona

Electrical discharges are usually triggered by an electric field $|\vec{E}|$ accelerating free electrons through a gas. When these electrons acquire sufficient energy from an electric field, they may produce fresh ions by knocking electrons from atoms and molecules by collision. This process is called ionization by electron impact. The electrons multiply, as illustrated in Fig. 8.6, where secondary effects from the electrodes make the discharge self-sustaining. The initial electrons that start the ionizing process are often created by photoionization: a photon from some distant source imparts enough energy to an atom so that the atom breaks into an electron and a positively charged ion. During acceleration in the electric field, the electron collides with the atoms of nitrogen, oxygen, and other gases present. Most of these collisions are elastic collisions similar to the collision between two

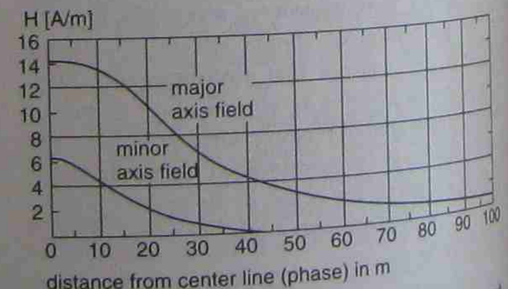
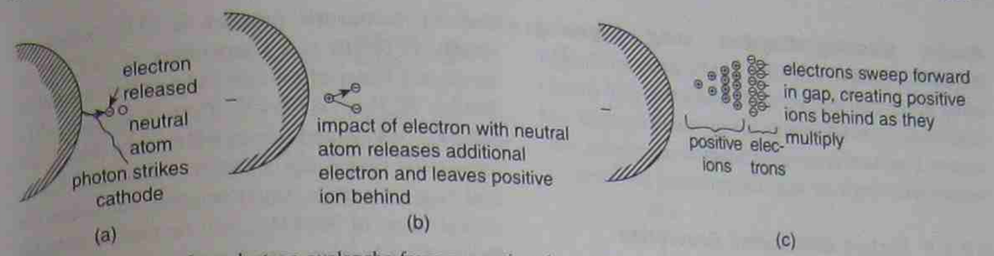



**FIGURE E8.3.1** Magnetic field strength $|\vec{H}| = H$ at ground level given as magnitudes of the major (real part of $|\vec{H}|$ phasor) and minor (imaginary part of $|\vec{H}|$ phasor) axes of the field ellipse. Conductor currents $i_a$, $i_b$, and $i_c$ have a magnitude of 2000 A each.






**FIGURES 8.6** Start of an electron avalanche from a negative electrode: (a) initiation, (b) formation of an electron pair, (c) multiplication of electron pairs or forming of avalanche.

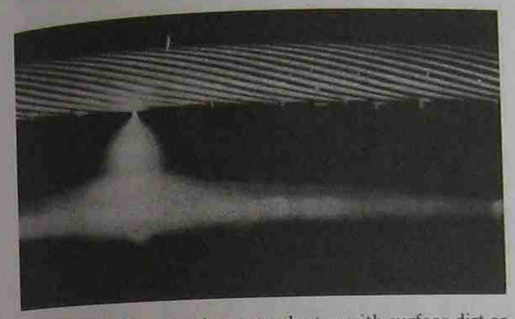


**FIGURE 8.7** Energized wet conductor with surface dirt or an insect generates plasma during discharge [47].

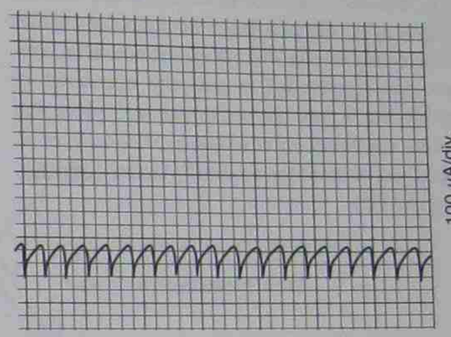



**FIGURE 8.8** Corona discharge at cathode resulting in 50 kHz electric noise signal [47].

billiard balls. The electron loses only a small part of its kinetic energy with each collision. Occasionally, an electron may strike an atom sufficiently hard so that excitation occurs, and the atom shifts to a higher energy state. The orbital states of one or more electrons changes, and the impacting electron loses part of its kinetic energy. Later, these excited atoms may revert to normal state, resulting in a radiation of the excess energy in the form of light (visible corona) and electromagnetic waves. An electron may also collide (recombine) with a positive ion, converting the ion to a neutral atom. Figure 8.7 shows the development of corona along an energized wet conductor, and Fig. 8.8 illustrates the frequency of corona discharge.

### 8.2.4.5 Factors Reducing the Effects of EMFs

**Active Shielding or Cancellation/Compensation of EMFs.** Active shielding is possible through compensation of electric and magnetic fields by suspending several transmission-line systems on the same towers (e.g., reverse-phased double circuit). This method is useful for newly designed transmission lines: it mitigates the generation of EMFs and reduces the amount of land used for transmission-line corridors.

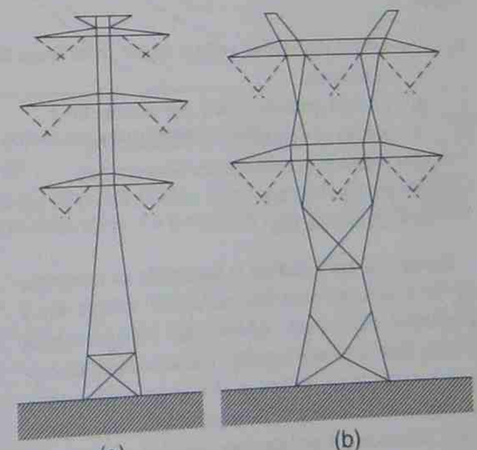



**FIGURE 8.9** Two transmission line configurations for line-to-line voltages of 345 kV, where the magnetic (as well as electric) fields are partially compensated (e.g., reverse-phased double circuit).

Figure 8.9 presents two configurations that are frequently used in practice. Within buildings and residences E. A. Leeper [49] explains how the EMFs can be compensated by active circuits.

**Passive Shielding/Mitigation using Bypassing Networks.** Passive shielding can be accomplished by using horizontal and vertical conducting grid (mesh) structures. Natural shields are provided by trees and houses. Conductive suits for linemen can protect individuals working in or near transmission corridors.

### 8.2.4.6 Factors Influencing Generation of Corona

At a given voltage, corona is determined by conductor diameter, line configuration, type of conductor (e.g., stranded), condition of its surface, and weather. Rain is by far the most important aspect of weather in increasing corona. The effect of atmospheric pressure and temperature is generally considered to modify the critical disruptive voltage (where the corona effects set in) of a conductor directly, or as the 2/3 exponent of the air density factor, $\delta$, which is given by [35]

$$\delta = \frac{17.9 \cdot (\text{barometric pressure in inches Hg})}{459 + {}^{\circ}\text{Fahrenheit}}. \tag{8-3}$$

The equation for the critical disruptive voltage is

$$V_{L\text{-}N_o} = g_o \cdot \delta^{2/3} \cdot r \cdot m \cdot \ln\left(\frac{D}{r}\right), \tag{8-4}$$

where

$V_{L\text{-}N_o}$ = critical disruptive voltage in kV from line to neutral,
$g_o$ = critical gradient in kV per centimeter,
$r$ = radius of conductor in centimeters,
$D$ = distance in centimeters between two conductors, and
$m$ = surface factor.

Corona in fair weather is negligible or moderate up to a voltage near the disruptive voltage for a particular conductor. Above this voltage corona effects increase very rapidly. The calculated disruptive voltage is an indicator of corona performance. A high value of critical disruptive voltage is not the only criterion of satisfactory corona performance. Consideration should also be given to the sensitivity of the conductor to foul weather.

### 8.2.4.7 Application Example 8.4: Onset of Corona in a Transmission Line

A $V_{\text{rated}} = 345\ \text{kV}_{L\text{-}L}$ transmission line with $g_o = 21.1$ kV/cm (e.g., see Fig. E8.4.1b), $r = 1.6$ cm, $D = 760$ cm, $m = 0.84$ where at an altitude of 6000 feet the barometric pressure is 23.98 inches Hg (mercury) results at a temperature of −30°F in an air density factor of $\delta = 1.00$ and a critical disruptive voltage of $V_{L\text{-}N_o} = 174$ kV. That is, $(V_{L\text{-}N_o} \cdot \sqrt{3})_L$ = 300 kV $V_{L\text{-}L} < V_{\text{rated}}$ and corona will exist on this 345 kV line—even under fair weather conditions. Under foul (e.g., dirt, rain, frost) weather conditions the critical value of 300 kV $V_{L\text{-}L}$ will be further reduced. Figure E8.4.1a gives the transmission line dimensions in meters for the $V_{L\text{-}L} = 362$ kV class. Figure E8.4.1b presents the conductor surface gradient $g_o$ for a 362 kV class of transmission lines. $N$ is the number of phase (sub) conductors. Similar plots are given in [47] for other classes of transmission lines, e.g., aluminum-cable steel reinforced (ACSR).

The power loss associated with corona can be represented by shunt conductance. Figure E8.4.2 presents the coronal loss during fair weather conditions for different types of transmission lines. Corona loss ranges from about 0 up to 35 kW per three-phase mile. For a 500 mile transmission line the latter loss per mile value amounts to 17.5 MW. At line-to-line voltages above 230 kV, it is preferable to use more than one conductor per phase, which is known as bundling of conductors. The bundle can consist of two, three, four, or more subconductors. Figure E8.4.3 illustrates a flat configuration consisting of three bundles with six subconductors each. Bundling increases the effective radius of the line's conductor per phase and reduces the electric field strength $\vec{E}$ near the conductors, which reduces corona power loss, audible noise, radio and television interference, and the generation of ozone ($O_3$) and nitrogen oxides ($NO_x$). Another important advantage of bundling is reduced transmission line reactance, therefore increasing transmission capacity. Table E8.4.1 illustrates bundle dimensions as a function of the number of subconductors.

### 8.2.4.8 Negative Effects of EMFs [50, 51] and Corona

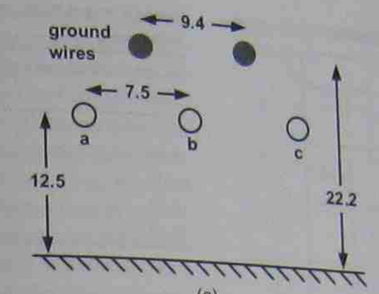
**Biological Effects of Electric Fields $\vec{E}$ on People and Animals.** To date, no specific biological effect of AC electric fields of the type and value applicable to transmission lines has been conclusively found and accepted by the scientific community. It is noteworthy to mention the rules established in the USSR (Union of Soviet Socialist Republics) for extrahigh voltage (EHV) substations and EHV transmission lines. For substations, limits for the duration of work in a day have been established as indicated in Table 8.1.

For transmission lines, considering the infrequent and nonsystematic exposure, higher values of the electric field strength $|\vec{E}|$ are accepted:

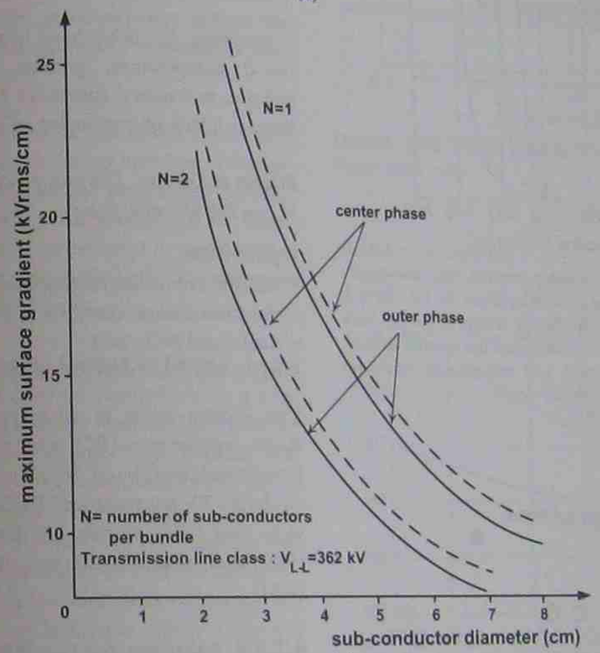
- 20 kV/m for difficult terrain,
- 15–20 kV/m for nonpopulated region, and
- 10–12 kV/m for road crossing.

**Suggested Biological Effects of Magnetic Fields $\vec{H}$ and $\vec{B}$ on People and Animals.** The value of the magnetic field strength $\vec{H}$ at ground level close to transmission lines is of the order of 5–14 A/m corresponding to magnetic field densities of $|\vec{B}|$ from 0.08 to 0.3 G. Note that 1 gauss is equivalent to $10^{-4}$ tesla or $10^{-4}$ Wb/m$^2$ or $10^{-4}$ Vs/m$^2$ in the meter-kilogram-second-ampere (MKSA) system of units.






(a)




(b)

**FIGURE E8.4.1** (a) Transmission line dimensions in meters for the $V_{L\text{-}L} = 362$ kV class. (b) Conductor surface gradient $g_o$ as a function of subconductor diameter, horizontal, $V_{L\text{-}L} = 362$ kV class, where N is the number of (sub) conductors within a bundle per phase.

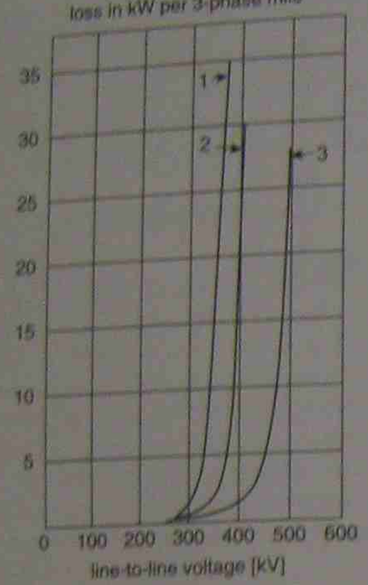



**FIGURE E8.4.2** Fair weather corona loss curves for smooth conductors at an air density factor $\delta = 1.0$. Curve 1: 1.4 inch hollow copper conductor (HH), $V_{L\text{-}L} = 287.5$ kV line; Curve 2: 1.1 inch HH conductor has smooth surface, $V_{L\text{-}L} = 230$ kV line; Curve 3: 1.65 inch smooth conductor has poor surface, $V_{L\text{-}L} = 230$ kV line.

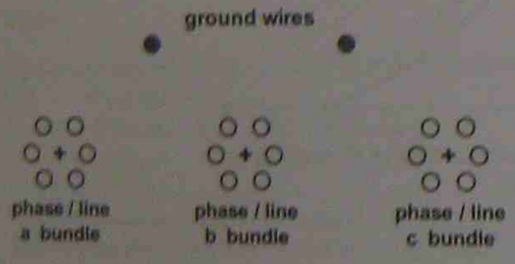



**FIGURE E8.4.3** Single-circuit horizontal (flat) line configuration.

**TABLE E8.4.1** Bundle Diameters as a Function of Number of Subconductors

| Conductors per phase | Bundle diameter (cm) |
|---|---|
| 2 | 45.7 |
| 3 | 52.8 |
| 4 | 64.6 |
| 6 | 91.4 |
| 8 | 101.6 |
| 12 | 127.0 |
| 16 | 152.4 |



**TABLE 8.1** USSR Rules for Duration of Work in Substations

| Electric field strength $\lvert\vec{E}\rvert$ (kV/m) | Permissible duration (minutes per day) |
|---|---|
| <5 | No restriction |
| 5–10 | 180 |
| 10–15 | 90 |
| 15–20 | 10 |
| 20–25 | 5 |

Magnetic AC fields have been reported to affect blood composition, growth, behavior, immune systems, and neural functions. However, at present, there is a lack of conclusive evidence.

**Effects of Corona.** Corona produces in the range of $V_{L\text{-}L} = 230$ kV and higher

- power loss,
- audible (acoustic) hissing sound in the vicinity of the transmission corridor,
- ozone and $NO_x$, and
- radio and television interference.

The audible noise is an environmental concern. Radio interference (RI) occurs in the AM (amplitude modulation) band. Rain and snow may produce moderate TV interference (TVI) in a low signal area. Note that voice signals are frequency modulated (FM), and video signals are amplitude modulated (AM).

### 8.2.4.9 Solutions for the Minimization of EMFs, Corona, and Other Environmental Concerns in Newly Designed Transmission Lines

Designing a transmission line with minimum environmental impact requires a study of five key factors:

1. impact of electric $\vec{E}$ and magnetic fields $\vec{H}$,
2. visual impact of the design,
3. generation of corona and its influence on radio and television interference,
4. air pollution via the generation of ozone and $NO_x$, and
5. impact of physical location.

A properly designed transmission line will have almost no perceptible negative environmental effects during fair weather, thus reducing disturbances, if they occur at all, to a small fraction of time.





**EMFs.** Although electric fields can be more readily reduced by shielding through structures with high conductivity (e.g., fences, trees), the reduction of magnetic fields is more difficult to achieve through shields with high permeability. Compensation or canceling of magnetic fields through the suspension of several transmission-line systems (e.g., reverse-phased double circuits) on the same tower as well as mounting the lines on higher towers near populated areas are frequently employed solutions. The employment of higher transmission-line voltages increases electric fields; however, they reduce the magnetic fields, which are more difficult to deal with.

**Visual Impact.** Reduction of the visual impact of a transmission line requires proper blending of the line with the countryside. Also the design and the location of supporting structures should not be objectionable to observers. Improvement in visual impact must be evaluated in conjunction with the economic penalty that the design incurs.

**Audible Noise, RI, and TVI Caused by Corona.** In the United States, there exist no regulations on a local or federal level that expressly limit the level of radio noise that a transmission line may produce. The Federal Communications Commission (FCC) places power transmission lines in the category of "incidental radiation device." As such, the FCC requires that the "device shall be operated so that the radio frequency energy that is emitted does not cause any emissions, radiation or induction which endangers the function of a radio navigation service or other safety services, or seriously degrades, obstructs or repeatedly interrupts a radio communication service" operating in accordance with FCC regulations. Figure 8.10 shows typical frequency spectra of corona-induced radio noise, and Figure 8.11 illustrates a typical lateral profile of radio noise. Figure 8.12 illustrates radio noise tolerability criteria caused by corona, one for fair weather and one for foul weather; in addition there exists a 120 Hz hum due to the changing energy content of the lines. Video signals are more affected than sound signals because they are amplitude modulated whereas the latter are frequency modulated. A reduction of the radio noise entails a reduction of corona effects (e.g., bundle conductors). Note that the number of decibels (dB) is defined by $\text{dB} = 20\log_{10}(v_{out}/v_{in})$.

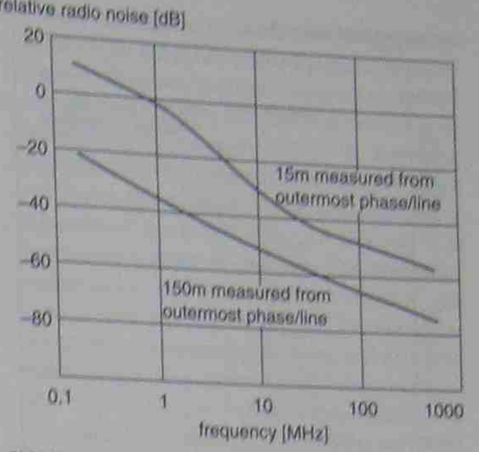



**FIGURE 8.10** Typical frequency spectra of corona-produced radio noise.

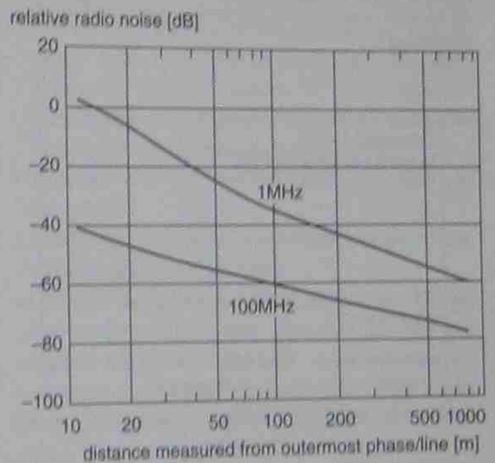



**FIGURE 8.11** Typical lateral profiles of radio noise.

**Ozone and $NO_x$ Generation.** Figure 8.13 shows an example of ozone recordings for a 1300 kV line with large corona loss of 650 kW/km. Although ozone is the primary gaseous corona product, nitrogen oxides ($NO_x$) may also be generated. The percentage of nitrogen oxide production is about one-sixth of that of ozone. The generation of ozone due to disassociation of oxygen in the corona region around the conductor is not of sufficient magnitude to be harmful. At ground level it has been found to be less than the daily natural variation. Conductor bundling is one method of reducing corona and its associated ozone generation.

**Impact of Physical Location of Transmission Lines.** The designer must also consider the environmental effects that the transmission line will have by

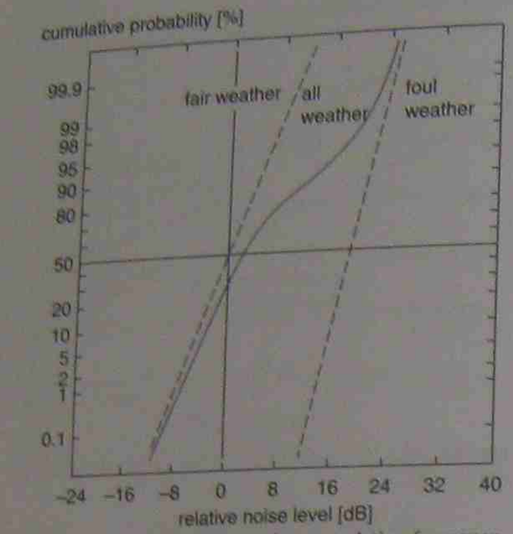



**FIGURE 8.12** Typical all-weather cumulative frequency distribution of radio noise, and approximation by Gaussian distribution.

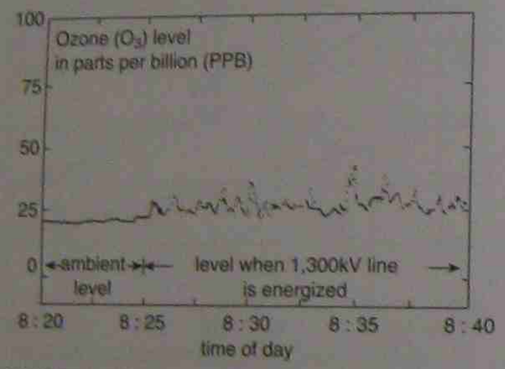



**FIGURE 8.13** Detection of ozone from a 1300 kV test line. Coronal loss is 650 kW/km and wind velocity is 1.6 m/s with sensors at line height. Ozone ($O_3$) is measured in parts per billion (ppb).

its presence on certain land. These include the effect on wildlife, use of park areas, access to property, future planning, land values, and existing electromagnetic signal sources (e.g., communication transmitters). This is accomplished by rating each land parcel and selecting a route with a minimum environmental impact.

#### 8.2.4.10 Economic Considerations

Corona loss of a well-designed transmission line should be below 1 kW per three-phase mile. This loss can be controlled by selecting proper configurations of bundle conductors (see Fig. E8.4.3 and Table E8.4.1). A bundle conductor is a conductor made up of two or more subconductors, and is used as one-phase conductor. Bundle conductors are not economical at or below 200 kV, but for rated voltages of 400 kV or more they are the best solution for overhead transmission lines. The increase in transmitting capacity justifies economically the use of two-conductor bundles on 220 kV lines.

The advantages of bundle conductors are higher disruptive voltage with conductors of reasonable dimensions, reduced surge impedance and consequent higher power capabilities, and less rapid increase of corona loss and RI with increased voltage. These advantages must be weighed against increased circuit cost and increased charging apparent power (kVA). Theoretically there is an optimum subconductor separation for bundle conductors that will give the minimum crest gradient on the surface of a subconductor and hence highest disruptive voltage.

#### 8.2.4.11 No-Cost/Low-Cost EMF Mitigation Hearings of PUC of California [52]

Electric fields $\vec{E}$ are created whenever power lines are energized with a voltage, whereas magnetic fields $\vec{H}$ measured in A/m (or $\vec{B}$ measured in milligauss) are created when current flows through the lines. Both electric and magnetic fields attenuate rapidly with distance from the source. Electric fields are effectively shielded by materials such as trees or buildings, whereas magnetic fields are not easily shielded by objects or materials. Therefore, concerns regarding potential power line EMF health effects arise primarily due to exposure to magnetic fields $\vec{H}$.

On January 15, 1991, the California Public Utilities Commission (CPUC) began an investigation to consider the Commission's potential role in mitigating health effects, if any, of EMFs created by

1. electric utility power lines, and
2. cellular radiotelephone facilities.

Due to the lack of scientific or medical conclusions about potential health effects from utility electric facilities and power lines, the CPUC adopted seven interim measures that help to address public concern on this subject.

- No-cost and low-cost steps to reduce EMF levels: When regulated utilities design new projects or upgrade existing facilities, approximately 4% of the project's budget may be used for reducing EMFs. The CPUC did not set specific reduction levels for EMFs. It was considered to be inappropriate to set a specific numerical standard until a scientific basis for doing so exists. No-cost measures are those steps taken in the design stage, including changes in standard practices, that will not increase the project cost but will reduce the magnetic flux density. Maximum (worst case) magnetic flux densities that could be permitted are ranging from 1 to 10 mG. Low-cost measures are those steps that will cost about 4% or less of the total project cost and will reduce the magnetic field flux density in an area (e.g., by a school, near residence) by approximately 15% or more at the edge of the right-of-way.
- New designs to reduce EMF levels: The CPUC initiated workshops to establish guidelines for new and rebuilt facilities. These guidelines incorporate alternative sites, increase the size of rights-of-way, place facilities underground, and use other suggested methods for reducing EMF levels at transmission, distribution, and substation facilities.
- Uniform residential and workplace EMF measurement methods are to be established.
- Promotion of education and research: The Department of Health Services (DHS) should manage such programs supported by public and utility funds.

CPUC-regulated utilities and municipal utilities may use ratepayer funds to pay their share of development costs for the following programs:

- EMF education,
- EMF research, and
- other research.

It has been many years since the CPUC devised the above-mentioned seven interim measures. During this time a significant body of scientific research has developed. In 2002 the DHS completed its comprehensive evaluation of existing scientific studies. Although there is still no consensus in the scientific community regarding health risks of EMF exposure, DHS reported troubling indications that EMF exposure may increase risk of certain diseases (e.g., childhood and to some extent adult leukemia, adult brain cancer, Lou Gehrig's disease) and other health problems.

#### 8.2.4.12 Summary and Conclusions

The results of the many papers and books published in the area of generation of EMFs and corona by transmission lines can be summarized as follows:

- Transmission lines with line-to-line voltages of up to 200 kV do not generate any significant amount of corona; however, such lines can generate significant amounts of EMFs. For transmission lines with line-to-line voltages above 200 kV the following conclusions can be drawn: Maximum (worst case) AC electric field strength $\vec{E}$ at ground level below transmission line is up to $|\vec{E}_{worst}| = 15$ V/mm at a line-to-line voltage of 1050 kV. The maximum occurs at the edge of transmission corridor. An electric field strength of $|\vec{E}_{acceptable}| = 5$ V/mm is acceptable. Maximum (worst case) AC magnetic field strength $\vec{H}$ at ground level below transmission line is $|\vec{H}_{worst}| = 14$ A/m corresponding to a maximum flux density $|\vec{B}_{worst}| = 0.176\,\text{G} = 176\,\text{mG}$ at a phase current of 2000 A. Note the DC earth field is about $B_{earth} = 0.5$ G. A flux density of $|\vec{B}_{acceptable}| = 3$ mG is acceptable.
- Corona depends on construction of transmission towers including type of conductors, e.g., hollow copper cable (e.g., HH) or aluminum cable steel reinforced (ACSR), surface of cable, type of bundle, fair or foul weather conditions, temperature, barometric pressure, and air density.
- Corona loss of 1 kW/three-phase mile is acceptable.
- Radio and television interference occurs within the 0.1 MHz to 1 GHz range.
- Audible noise ranges from 50 Hz to 120 Hz (power-frequency hum) to 10 kHz (hissing noise).
- Additional ozone ($O_3$) production is in the range of 15 ppb (parts per billion). The naturally occurring level is 25 ppb. That is, $O_3$ production by power lines is insignificant.
- Nitrogen oxide ($NO_x$) production is about one-sixth of the ozone generation. That is, $NO_x$ production by power lines is insignificant.
- Active compensation (e.g., through compensation of EMFs by arranging several transmission systems on one tower, by reducing, compensating, or canceling EMFs in houses through compensation circuits) is possible.
- Passive (e.g., horizontal or vertical mesh structures, conductive suits) and natural shielding (e.g., trees, houses) is possible.
- Overall control of EMFs and corona through transmission line (e.g., bundle conductors, reverse-phased double circuit) and tower construction (e.g., height) is feasible; it is, however, more expensive.
- For newly designed transmission lines all environmental concerns (e.g., limits for EMFs, RI, and

TVI) and technical constraints (corona loss of 1 kW/three-phase mile) can be satisfied.

- The mitigation of detrimental environmental, technical, or economic effects of existing transmission lines will be difficult to achieve at no or low cost as proposed by the Public Utilities Commission of California.
- The issue has surfaced that corona on transmission lines may create X-rays. A practical lower bound of X-rays is at least 2 keV. However, the electrical discharges of coronal activity on transmission lines can produce electron energies on the order of about 1–10 eV. This is sufficient for production of visible light but is orders of magnitude below electron energies necessary for the production of X-rays by transmission line corona [53]. That is, transmission lines do not generate X-rays.

### 8.2.5 Distributed-, Cogeneration, and Frequency/Voltage Control

Renewable energy sources such as solar and wind-power [54, 55] plants have an intermittent power output. Nevertheless it is desirable to operate them at maximum power output, for example, employment of peak-power tracker for photovoltaic plant [56]. With such peak-power and intermittent-power constraints it is impossible to operate a power system with distributed generation (DG) sources only because the drooping characteristics [57] which are responsible for load sharing require that at least one plant can deliver the additional power as requested by the utility customers, thus serving as base-load plant with spinning reserve capability. This is the reason why in Denmark [58] the control of the power system becomes more difficult as the renewable contribution approaches 30% of the total generation. This is so because the entire system exhibits properties of so-called weak systems with low short-circuit capabilities. As an alternative to a large power plant serving as a frequency leader—which can deliver sufficient additional power so that the frequency control will not be impaired—it is possible to strategically place storage peak-power plants based on pumped-hydro [59, 60] or compressed-air facilities [61, 62] that can provide peak power for several hours per day, for example, 22 h of continuous generation at 1600 MW.

Related to the availability of spinning reserve—which should be in the neighborhood of about 5–10% of the total installed power capacity—is the fast valving [63, 64] so that the time constants of the speed control circuit (e.g., governor) can be maintained within certain limits. In addition near-term [65, 66] and long-term [67, 68] load forecasts are important for the reliable operation of the power system with intermittently operating renewable energy sources. It is the task of control and dispatch centers to set the load reference points for each and every generation plant within an interconnected power system. From the following application examples one learns that renewable energy sources alone—operated at their maximum-power points [56]—cannot maintain frequency and voltage control. This is so because there must be a spinning reserve of power generation and sufficient facilities to control reactive power.

#### 8.2.5.1 Application Example 8.5: Frequency Control of an Interconnected Power System Broken Into Two Areas: The First One with a 300 MW Coal-Fired Plant and the Other One with a 5 MW Wind-Power Plant

Figure P4.12 of Chapter 4 shows the block diagram of two generating plants interconnected by a tie line (transmission line). Data for generation set #1 (steam turbine and generator) are as follows:

Frequency change ($\Delta\omega_1$) per change in generator output power ($\Delta P_1$) having the droop characteristic of $R_1 = \dfrac{\Delta\omega_1}{\Delta P_1}\text{ pu} = 0.01\text{ pu}$,

The load change ($\Delta P_{L1}$) per frequency change ($\Delta\omega_1$) resulting in $D_1 = \dfrac{\Delta P_{L1}}{\Delta\omega_1} = 0.8\text{ pu}$,

Step load change $\Delta P_{L1}(s) = \dfrac{\Delta P_{L1}}{s}\text{ pu} = \dfrac{0.2}{s}\text{ pu}$,

Angular momentum of steam turbine and generator set $M_1 = 4.5$,
Base apparent power $S_{base} = 500$ MVA,
Governor time constant $T_{G1} = 0.01$ s,
Valve changing (charging) time constant $T_{CH1} = 0.1$ s,
(Load reference set point)$_1 = 0.8$ pu.

Data for generation set #2 (wind turbine and generator) are as follows:

Frequency change ($\Delta\omega_2$) per change in generator output power ($\Delta P_2$) having the droop characteristic

$R_2 = \dfrac{\Delta\omega_2}{\Delta P_2}\text{ pu} = 0.02\text{ pu}$,



The load change ($\Delta P_{L2}$) per frequency change ($\Delta\omega_2$) resulting in $D_2 = \dfrac{\Delta P_{L2}}{\Delta\omega_2} = 1.0\text{ pu}$,

Step load change $\Delta P_{L2}(s) = \dfrac{\Delta P_{L2}}{s}\text{ pu} = \dfrac{-0.2}{s}\text{ pu}$,

Angular momentum of wind turbine and generator set $M_2 = 6$,
Base apparent power $S_{base} = 500$ MVA,
Governor time constant $T_{G2} = 0.02$ s,
Valve (blade control) changing (charging) time constant $T_{CH} = 0.75$ s,
(Load reference set point)$_2 = 0.8$ pu.

Data for tie line: $T = \dfrac{377}{X_{tie}}$ with $X_{tie} = 0.2\text{ pu}$.

a) List the ordinary differential equations and the algebraic equations of the block diagram of Fig. P4.12 of Chapter 4.
b) Use either Mathematica or MATLAB to establish transient and steady-state conditions by imposing a step function for load reference set point$(s)_1 = \dfrac{0.8}{s}\text{ pu}$, load reference set point$(s)_2 = \dfrac{0.8}{s}\text{ pu}$, and run the program with zero step load changes $\Delta P_{L1} = 0$, $\Delta P_{L2} = 0$ for 5 s. After 5 s impose the step load change $\Delta P_{L1}(s) = \dfrac{\Delta P_{L1}}{s}\text{ pu} = \dfrac{0.2}{s}\text{ pu}$, and after 7 s impose the step change $\Delta P_{L2}(s) = \dfrac{\Delta P_{L2}}{s}\text{ pu} = \dfrac{-0.2}{s}\text{ pu}$ for the droop characteristics $R_1 = 0.01$ pu and $R_2 = 0.02$ pu to find the transient and steady-state responses $\Delta\omega_1(t)$ and $\Delta\omega_2(t)$.
c) Use either Mathematica or MATLAB to establish transient and steady-state conditions by imposing a step function for load reference set point$(s)_1 = \dfrac{0.8}{s}\text{ pu}$, load reference set point$(s)_2 = \dfrac{0.8}{s}\text{ pu}$, and run the program with zero step load changes $\Delta P_{L1} = 0$, $\Delta P_{L2} = 0$ for 5 s. After 5 s impose step load change $\Delta P_{L1}(s) = \dfrac{\Delta P_{L1}}{s}\text{ pu} = \dfrac{0.1}{s}\text{ pu}$, and after 7 s impose the step load change $\Delta P_{L2}(s) = \dfrac{\Delta P_{L2}}{s}\text{ pu} = \dfrac{-0.1}{s}\text{ pu}$ for the droop characteristics $R_1 = 0.01$ pu (coal-fired plant) and $R_2 = 0.5$ pu (wind-power plant) to find the transient and steady-state responses $\Delta\omega_1(t)$ and $\Delta\omega_2(t)$.

#### 8.2.5.2 Application Example 8.6: Frequency Control of an Interconnected Power System Broken Into Two Areas: The First One with a 5 MW Wind-Power Plant and the Other One with a 5 MW Photovoltaic Plant

Figure P4.12 of Chapter 4 shows the block diagram of two generators interconnected by a tie line (transmission line).

Data for generation set #1 (wind turbine and generator) as follows:

Frequency change ($\Delta\omega_1$) per change in generator output power ($\Delta P_1$) having the droop characteristic $R_1 = \dfrac{\Delta\omega_1}{\Delta P_1}\text{ pu} = 0.5\text{ pu}$,

The load change ($\Delta P_{L1}$) per frequency change ($\Delta\omega_1$) yields $D_1 = \dfrac{\Delta P_{L1}}{\Delta\omega_1} = 0.8\text{ pu}$,

Step load change $\Delta P_{L1}(s) = \dfrac{\Delta P_{L1}}{s}\text{ pu} = \dfrac{0.1}{s}\text{ pu}$,

Angular momentum of wind turbine and generator set $M_1 = 4.5$,
Base apparent power $S_{base} = 50$ MVA,
Governor time constant $T_{G1} = 0.01$ s,
Valve (blade control) changing (charging) time constant $T_{CH1} = 0.1$ s,
(Load reference set point)$_1 = 0.8$ pu.

Data for generation set #2 (photovoltaic array and inverter):

Frequency change ($\Delta\omega_2$) per change in inverter output power ($\Delta P_2$) having the droop characteristic $R_2 = \dfrac{\Delta\omega_2}{\Delta P_2}\text{ pu} = 0.5\text{ pu}$,

The load change ($\Delta P_{L2}$) per frequency change ($\Delta\omega_2$) yields $D_2 = \dfrac{\Delta P_{L2}}{\Delta\omega_2} = 1.0\text{ pu}$,

Step load change $\Delta P_{L2}(s) = \dfrac{\Delta P_{L2}}{s}\text{ pu} = \dfrac{-0.1}{s}\text{ pu}$,

Equivalent angular momentum $M_2 = 6$,
Base apparent power $S_{base} = 50$ MVA,
Governor time constant $T_{G2} = 0.02$ s,
Equivalent valve changing (charging) time constant $T_{CH2} = 0.1$ s,
(Load reference set point)$_2 = 0.8$ pu.

Data for tie line: $T = \dfrac{377}{X_{tie}}$ with $X_{tie} = 0.2\text{ pu}$.

Use either Mathematica or MATLAB to establish transient and steady-state conditions by imposing a step function for load reference

set point$(s)_1 = \frac{0.8}{s}$ pu, load reference set point$(s)_2 = \frac{0.8}{s}$ pu and run the program with a zero step load changes $\Delta P_{L1} = 0$, $\Delta P_{L2} = 0$ for 5 s. After 5 s impose step load change $\Delta P_{L1}(s) = \frac{\Delta P_{L1}}{s}\text{pu} = \frac{0.1}{s}\text{pu}$, and after 7 s impose the step load change $\Delta P_{L2}(s) = \frac{\Delta P_{L2}}{s}\text{pu} = \frac{-0.1}{s}\text{pu}$ to find the transient and steady-state responses $\Delta\omega_1(t)$ and $\Delta\omega_2(t)$.

From Application Examples 8.5 and 8.6 one draws the following conclusions:

1. Renewable energy sources stemming from solar and wind are likely to be operated at their maximum output power. This requires that the slope $R$ of the drooping characteristic of a renewable power source is large as is depicted in Figs. 8.14 and 8.15. As a consequence of the large $R$, the change in output of the renewable source results in a large frequency change $\Delta\omega$.
2. Solar, wind, and tidal power sources are intermittent in nature and their output power cannot be controlled by the dispatch center of a utility system.
3. Due to issues 1 and 2 distributed generation (DG) based on solar and wind power is not possible unless either a base load plant (e.g., gas- or coal-fired plant) or a storage plant (e.g., pumped hydro, compressed air) is ready to deliver the additional power required. That is, the base load plant or the storage plant acts as a spinning reserve plant.
4. It has been discussed in Chapter 4 (Section 4.2.2.3) that an inverter requires a larger DC input voltage for capacitive/resistive load than for inductive/resistive operation. To utilize inverter components to their fullest unity power (about resistive operation) factor operation is preferred. This means a renewable power plant cannot be very effectively employed for reactive power or voltage control.
5. The governor time constant (e.g., $T_{G1}$, $T_{G2}$) and the valve changing (charging) time constant (e.g., $T_{CH1}$, $T_{CH2}$) must be as small as possible to guarantee stability. The latter time constant is fairly large for steam, hydro, and wind-power plants. This issue has been addressed in [63, 64].
6. In summary it is not possible to operate a power system solely based on renewable power plants because they do not easily lend themselves to frequency and voltage control.

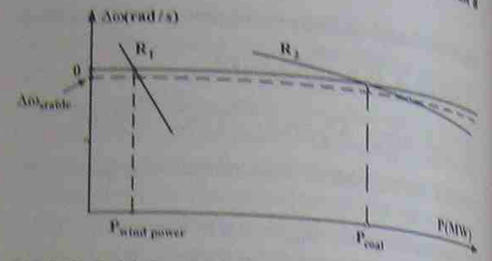



**FIGURE 8.14** Load sharing of a renewable plant (operated at maximum power with droop characteristic $R_1 = 0.5$ pu) with a coal-fired plant (operated at less than maximum power with droop characteristic $R_2 = 0.01$ pu) for a load increase of 10%, resulting in an acceptable change in angular frequency.

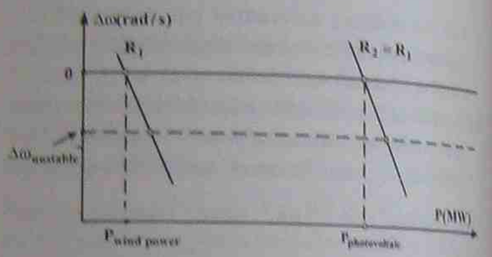



**FIGURE 8.15** Load sharing of a renewable solar plant (either photovoltaic or thermal) with a wind-power plant for a load increase of 10%. Both types of plants are operated at maximum power to maximize the renewable energy contribution within a power system both with droop characteristics of $R_1 = R_2 = 0.5$ pu, resulting in an inacceptably large change in angular frequency.

## 8.3 TOOLS FOR DETECTING POOR POWER QUALITY

### 8.3.1 Sensors

To be able to detect power quality problems one must rely on voltage and current sensors such as low-inductive voltage dividers for voltage pickup, and low-inductive shunts and Hall sensors for current pickup. Components representing the interface between sensors and measuring instruments are potential and current transformers as well as optocouplers. Voltmeters, amperemeters, oscillographs, spectrum analyzers, and network analyzers are indispensable. Special power quality tools and selection guides have been developed for detecting power quality for single- and three-phase systems, such as power quality clamp meters, power quality analyzers, voltage event recorder systems, three-phase power loggers, series three-phase power quality loggers, three-phase power quality recorders, AC



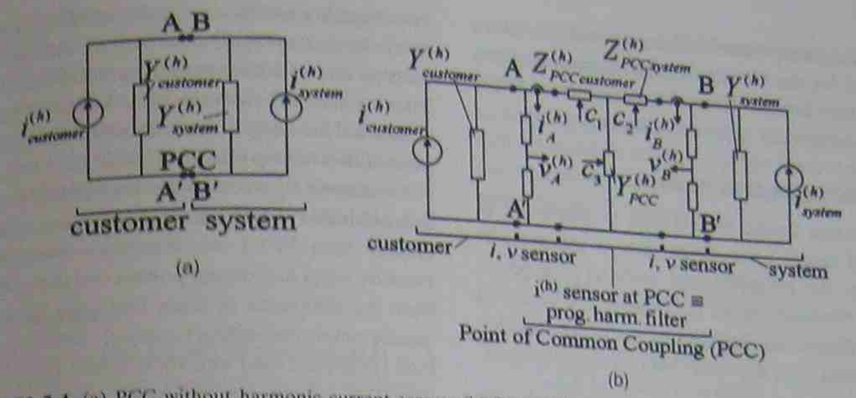



**FIGURE E8.7.1** (a) PCC without harmonic current sensor, (b) PCC with harmonic current sensor and programmable filter.

leakage current clamp meters, series three-phase power quality analyzers, high precision power analyzers, reliable power meters, multipoint power recorders, and other power quality-specific equipment. Some of them [69, 70] are useful to analyze steady-state phenomena, and some of them are transient overvoltage/under-voltage meters recording outage time, deviation from rated voltage values (e.g., sags, swells), or the number of outages within a given time period, and an instrument that distinguishes the direction of the harmonic power flow as is described in the following application example.

### 8.3.2 Application Example 8.7: Detection of Harmonic Power Flow Direction at Point of Common Coupling (PCC)

The discrimination between the contributions of the customer and the power system to generated harmonic currents at PCC is based on Fig. E8.7.1 and on references [70–84]. Figure E8.7.1a represents the equivalent circuit of one customer connected to the power system at PCC indicated by the terminals $A-A'$ and $B-B'$. To measure individual harmonic currents $i_A^{(h)}$, $i_B^{(h)}$ with respect to direction and amplitude a harmonic current sensing network (see Fig. E8.7.1b), which represents a programmable harmonic filter, is configured and connected by computer commands $c_1$, $c_2$, and $c_3$ for a fraction of a second during which measurements take place. For measuring the current $i_{\text{customer}}^{(h)}$ the impedance and admittance $Z_{\text{PCCcustomer}}^{(h)}$ and $Y_{\text{PCC}}^{(h)}$, respectively, will provide a short-circuit for $i_{\text{customer}}^{(h)}(t)$ during a fraction of a second, whereas the impedance $Z_{\text{PCCsystem}}^{(h)}$ is blocking $i_{\text{system}}^{(h)}(t)$. For measuring the current $i_{\text{system}}^{(h)}(t)$ the impedance and admittance $Z_{\text{PCCsystem}}^{(h)}$ and $Y_{\text{PCC}}^{(h)}$, respectively, will provide a short-circuit for $i_{\text{system}}^{(h)}(t)$ during a fraction of a second, whereas the impedance $Z_{\text{PCCcustomer}}^{(h)}$ is blocking $i_{\text{customer}}^{(h)}(t)$. The harmonic impedance and admittance consists of inductors and capacitors whose very small losses—to achieve a high $Q$ of the programmable filters—will be determined as described in [83]. Current and voltage sensors (e.g., Hall sensors [81] or low-inductive current shunts and voltage dividers [82] with optocouplers) will measure the direction of the harmonic power flow as detailed in [70–74].

The main advantages of this approach are

1. Nonintrusive measurements lasting a fraction of a second. Field tests can be executed in three steps, each step lasting less than 0.1 s. In the first step the harmonic current $i_{\text{customer}}^{(h)}(t)$ will be measured by configuring the programmable filter so that $Z_{\text{PCCcustomer}}^{(h)}$ and $Y_{\text{PCC}}^{(h)}$ represent a short-circuit for a harmonic customer current of hth order, while $Z_{\text{PCCsystem}}^{(h)}$ represents an open-circuit for the system harmonic current of hth order. In the second step $Z_{\text{PCCsystem}}^{(h)}$ and $Y_{\text{PCC}}^{(h)}$ represent a short-circuit for the system harmonic current of hth order, while $Z_{\text{PCCcustomer}}^{(h)}$ represents an open circuit for the system current of hth order. In the third step the total harmonic current will be measured when $Z_{\text{PCCcustomer}}^{(h)}$ and $Z_{\text{PCCsystem}}^{(h)}$ are bypassed and $Y_{\text{PCC}}^{(h)} = 0$ is an open circuit.
2. Real-time measurement while system operates under load.
3. No additional dissipation occurs.
4. Very small ohmic components of inductors and capacitors can be accurately determined [83], resulting in high $Q$ of programmable harmonic filters.
5. In most harmonic standards [76, 77] the harmonic current injection from the customer installation is limited. To enforce such limits by utilities these customer-injected harmonic currents at PCC $i_{\text{customer}}^{(h)}(t)$ must be reliably and

accurately measured. This approach provides a tool for the utilities to measure customer harmonic currents. This will increase the reliability and efficiency of power system operation.

### 8.3.3 Maximum Error Analysis

The accurate online or real-time measurement of losses of circuit components such as transformers improves the reliability and security of a power system. Normally circuit components are equipped with temperature sensors (e.g., thermocouples, thermistors). This approach has two disadvantages.

1. Circuit components must be equipped with sensors during their construction, and off-the-shelf components cannot be used.
2. Temperature sensors provide information about the temperature at their location and not necessarily the temperature at the hot spot of an energy conversion device, and any temperature alarm may come too late to prevent an outage due to a fault.

The advantages of the real-time monitoring of losses of components (e.g., transformers) are that loss increases can be sensed or recorded at the time when a fault develops. In addition, the measurement components or instruments can be exchanged, thus minimizing the outage time of the transformer supplying the power system. Such a monitoring of the losses must rely on small maximum errors of the monitoring equipment.

Maximum error analysis has been extensively used in the past [70–73, 85–87]. The online measurement of transformer losses under nonsinusoidal operation is discussed in detail in [87]. The real-time monitoring of iron-core and copper losses of single- and three-phase transformers is important, particularly for transformers feeding nonlinear loads. This section devises a new digital data-acquisition method for the separate online measurement of iron-core and copper losses of three-phase transformers under any full or partial load conditions. The accuracy requirements of the instruments employed (voltage and current sensors, volt and current meters) are addressed. The maximum errors are acceptably low if voltage and current sensors with 0.1 to 0.5% errors are used.

#### 8.3.3.1 Review of Existing Methods

The separate online monitoring of the iron-core and copper losses of single- and three-phase transformers is desirable because additional losses due to power quality problems (e.g., harmonics, DC excitation) can be readily detected before any significant damage due to additional temperature rises occurs. Those losses can accurately and economically be measured for single-phase transformers via computer-aided testing (CAT) [71, 88].

The known approaches for on-line loss measurement of high-efficiency transformers (e.g., efficiency greater than 97%) are inaccurate because they measure input and output powers and derive the loss from the difference of these two large values. The usually employed indirect method consisting of no-load (iron-core loss) and short-circuit (copper loss) tests [35] cannot be performed online while the transformer is partially or fully loaded. The same is valid for the loading back method [89].

Arri *et al.* presented an analog measurement circuit [90]. It is well known that there may occur zero-sequence currents on the Y-grounded side of a three-phase transformer, and these currents will produce corresponding losses in the transformer. The measuring circuit presented by Arri *et al.* cannot measure these zero-sequence components, and therefore the method is not suitable for transformers with grounding on any side (either primary or secondary). Moreover, Arri *et al.* rely on many instrument transformers (nine CTs and nine PTs) to convert the Δ connection to Y connection for a Y/Δ connected transformer: as a result the measuring accuracy is decreased. In [91] an analog measuring circuit with wattmeters is presented within a single-phase circuit.

This section presents a more accurate real-time method for digitally and separately measuring the steady-state iron-core and copper losses of three-phase transformers with various grounded connections while the transformers are operating at any load condition. This digital measuring circuit is based on voltage and current sensors (voltage dividers, shunts, PTs, CTs, or Hall devices), A/D converter, and personal computer. Using a computer-aided testing program (CATEA) [70] losses, efficiency, harmonics, derating, and wave shapes of all voltages and currents can be monitored within a fraction of a second.

The maximum measurement errors of the losses are acceptably small and vary in the range from 0.5 to 15%, mainly contingent on the accuracy of the voltage and current sensors used. Depending on the application, voltage dividers with optocouplers [73], current shunts with optocouplers, potential and current transformers (error < 0.1%), as well as Hall sensors [92] (error < 0.5%) can be employed.



When both voltage and current signals are obtained from Hall devices [92], the copper losses will include DC losses, if they exist. Provided voltage and current signals are generated by PT and CT sensors, the DC losses are not included in the copper losses, and must be measured by additional DC voltmeters and ammeters or sensors. In this case, the total loss consists of the iron-core, AC, and DC copper losses.

#### 8.3.3.2 Approach

It is well known that for any Y (ungrounded) or Δ connected three-phase windings, the two-wattmeter method is often used to measure the power based on the voltages and currents of any two phases. For a Y grounded three-phase winding, an additional wattmeter is necessary for the voltage and current of the third phase, or those of the zero sequence. Therefore, for a transformer without grounding on any side (primary or secondary), power loss is measured with eight signals (voltages and currents of two phases for each side). If the primary or/and the secondary are grounded, the power loss can be measured with ten or twelve signals. This section deals with ten- and twelve-channel measuring circuits. The eight-channel measuring circuits for Y/Y ungrounded or Δ/Δ and Δ–Y ungrounded three-phase transformers are discussed in [73].

A ten-channel CAT circuit applied to Δ–$Y_0$ ($Y_0$ means Y grounded) connected three-phase transformers is shown in Fig. 8.16. The flowchart for the ten-channel signals is shown in Fig. 8.17. The output power (at the $Y_0$ side) is

$$\begin{aligned} P_{out} &= \frac{1}{T}\int_0^T (v'_{an}i'_a + v'_{bn}i'_b + v'_{cn}i'_c)dt \\ &= \frac{1}{T}\int_0^T [v'_{an}i'_a + (v'_b - v'_{an} - v'_{cn})i'_b + v'_{cn}i'_c]dt \\ &= \frac{1}{T}\int_0^T [v'_{ac}i'_a - v'_{cn}i'_b + v'_n i'_n]dt \end{aligned} \tag{8-5}$$

where $i'_a = (i'_A - i'_a)$, $i'_b = (i'_B - i'_b)$, and $v'_n = (v'_{an} + v'_{bn} + v'_{cn})$. The transformer loss is

$$\begin{aligned} P_{in} - P_{out} &= \frac{1}{T}\int_0^T [(v_{AC}i_{AC} + v_{BC}i_{BC}) \\ &\quad -(v'_{ac}i'_a - v'_{cn}i'_b + v'_n i'_n)]dt \\ &= \frac{1}{T}\int_0^T [v_{AC}(i_{AC} - i'_a) + v_{BC}(i_{BC} - i'_b) + \\ &\quad (v_{AC} - v'_{cn})i'_a + (v_{BC} + v'_{cn})i'_b - v'_n i'_n]dt. \end{aligned} \tag{8-6}$$

The loss component $(-v'_n i'_n)$ in Eq. 8-6 is included in the copper loss, which can be proved below:

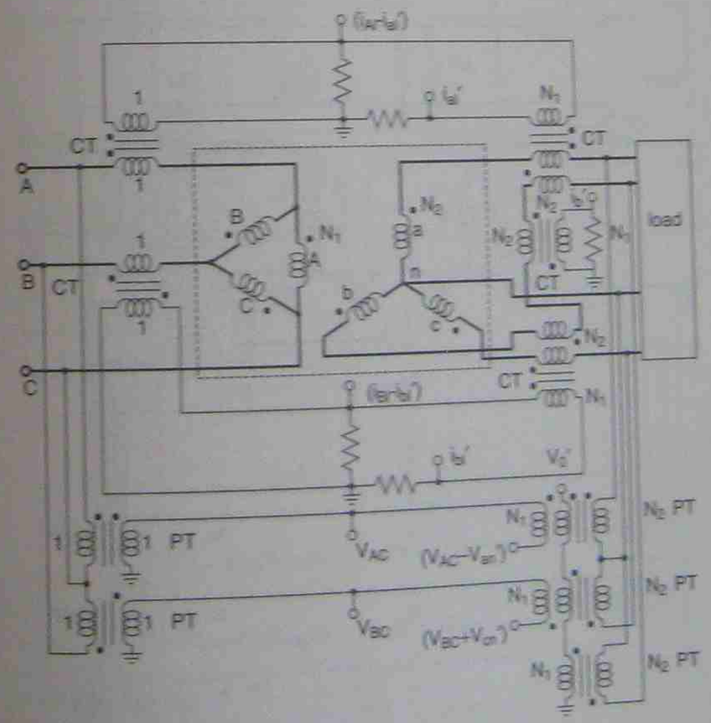



FIGURE 8.16 Ten-channel CAT circuit for accurate Δ–$Y_0$ three-phase transformer loss monitoring.

$$
\begin{aligned}
p_{ss} &= (v_{AC}-v'_{ac})i'_a + (v_{CB}-v_{ca}')i'_c + (v_{BA}-v'_{ab})i'_b \\
&= (v_{AC}-v'_{ac})i'_a + (-v_{BC}-v'_{ca})i'_c + \\
&\quad (v_{BC}-v_{AC}-v'_b+v'_{ca}+v'_{ab})i'_b \\
&= (v_{AC}-v'_{ac})(i'_a-i'_b)+(v_{BC}+v'_{ca})(i'_c-i'_b)-v'_n i'_b \\
&= (v_{AC}-v'_{ac})i'_a+(v_{BC}+v'_{ca})i'_c-v'_n i'_b
\end{aligned}
\tag{8-7}
$$

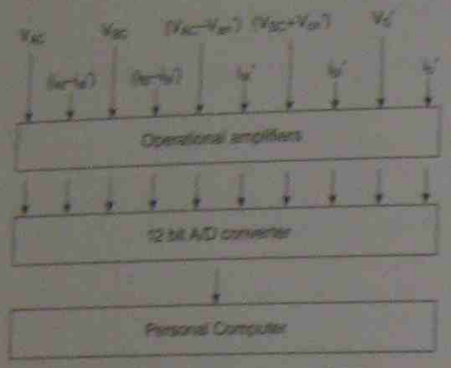



**FIGURE 8.17** Flowchart for ten-channel signals.

Note that the analog measuring circuit of [90] does not take into account zero-sequence components and, therefore, does not apply to general asymmetric operating conditions.

For $Y$–$Y_0$ connected three-phase transformers (see Fig. 8.18), the output power can be written as

$$
\begin{aligned}
P_{out} &= \frac{1}{T}\int_0^T (v'_{ac}i'_a + v'_{bc}i'_b + v'_{nc}i'_c)dt \\
&= \frac{1}{T}\int_0^T [v'_{ac}i'_a + v'_{bc}i'_b + v'_{nc}(i'_a - i'_a - i'_b)]dt \\
&= \frac{1}{T}\int_0^T [(v'_{ac}i'_a + v'_{bc}i'_b + v'_{nc}i'_a]dt
\end{aligned}
\tag{8-8}
$$

where $i'_a = (i'_a + i'_b + i'_c)$. The transformer loss can be formulated as

$$
\begin{aligned}
P_{ss} - P_{out} &= \frac{1}{T}\int_0^T [(v_{AC}i_A + v_{BC}i_B) - (v'_{ac}i'_a + v'_{bc}i'_b + v'_{nc}i'_a)]dt \\
&= \frac{1}{T}\int_0^T [v_{AC}(i_A - i'_a) + v_{BC}(i_B - i'_b) - v'_{nc}i'_a + \\
&\quad (v_{AC} - v'_{ac})i'_a + (v_{BC} - v'_{bc})i'_b]dt
\end{aligned}
\tag{8-9}
$$

where $(-v_{nc}'i_a')$ is included in the iron-core loss. This can be shown as follows:

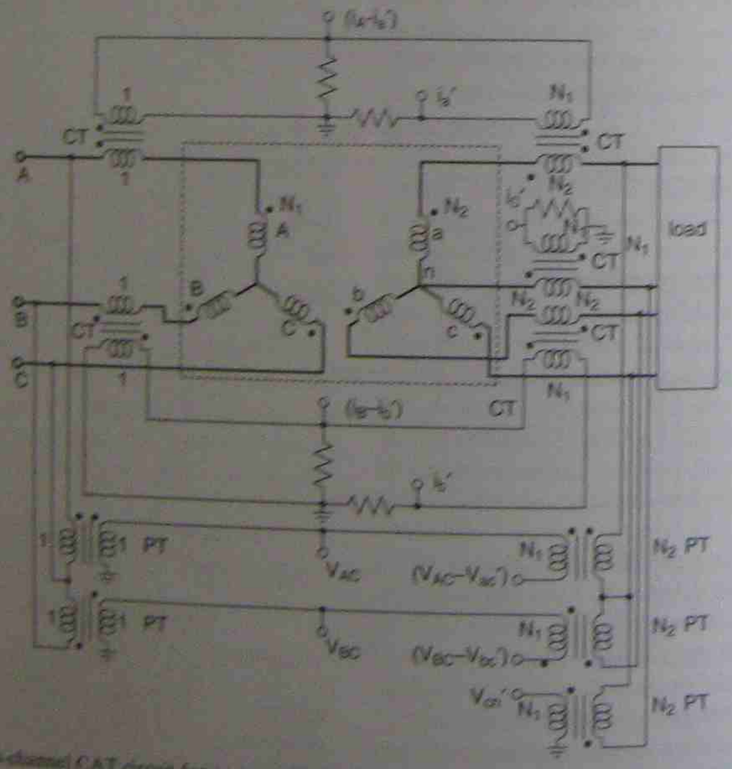



**FIGURE 8.18** Ten-channel CAT circuit for accurate $Y$–$Y_0$ three-phase transformer loss monitoring.



$$
\begin{aligned}
p_{ll} &= v_{ab}(i_a - i'_a) + v_{bn}(i_b - i'_b) + v_{cn}(i_c - i'_c) \\
&= v_{ab}(i_a - i'_a) + v_{bn}(i_b - i'_b) - \\
&\quad v_{cn}(i_a + i_b + i'_a - i'_a - i'_b) \\
&= (v_{ab} - v_{cn})(i_a - i'_a) + (v_{bn} - v_{cn})(i_b - i'_b) - v_{nn}'i'_n \\
&= v_{ab}i_a - i'_a) + v_{bn}(i_b - i'_b) - v_{nn}'i'_n
\end{aligned}
\tag{8-10}
$$

For $Y_0$–$Y_0$ connected transformers, a twelve-channel circuit is used as shown in Fig. 8.19. The loss of the transformer can be derived directly from

$$
\begin{aligned}
P_{ll} - P_{out} &= \frac{1}{T}\int_0^T [(v_{Aa}i_A + v_{Bn}i_B + v_{Cn}i_C) - \\
&\quad (v'_{ac}i'_a + v'_{bc}i'_b + v'_{nc}i'_c)]dt \\
&= \frac{1}{T}\int_0^T [v_{Aa}(i_A - i'_a) + v_{Bn}(i_B - i'_b) + v_{Cn}(i_C - i'_c) + \\
&\quad (v_{Aa} - v'_{ac})i'_a + (v_{Bn} - v'_{bc})i'_b + (v_{Cn} - v'_{nc})i'_c]dt.
\end{aligned}
\tag{8-11}
$$

The instantaneous expression $p_{ll}(t)$ in Eq. 8-10 includes two power components: the instantaneous iron-core loss and the instantaneous exciting reactive power. Similarly, $p_{cu}(t)$ in Eq. 8-7 includes the instantaneous copper loss and the instantaneous reactive power due to the leakage flux. At steady state, the average value of reactive power during one electric cycle is zero; therefore, the average values of $p_{ll}(t)$ and $p_{cu}(t)$ during one electric cycle reflect the steady-state iron-core and copper losses.

The instantaneous expressions of $p_{ll}(t)$ and $p_{cu}(t)$ of various three-phase transformer connections are listed in Table 8.2, where all current and voltage differences can be calibrated directly under either sinusoidal or nonsinusoidal conditions.

If the neutral line is disconnected, and $v_0'$ and $i_0'$ are not measured, Fig. 8.16 becomes the eight-channel loss-measuring circuit of $\Delta$–$Y$ connected three-phase transformers (Fig. 8.20), and the transformer loss is obtained from Eq. 8-6 with $v_0' = 0$ [73]. Similarly, if the neutral line is disconnected, and $i_0'$ and $v_{nn}'$ are not measured, Fig. 8.18 becomes the eight-channel loss-measuring circuit of $Y$–$Y$ connected three-phase transformers, and the transformer loss is obtained

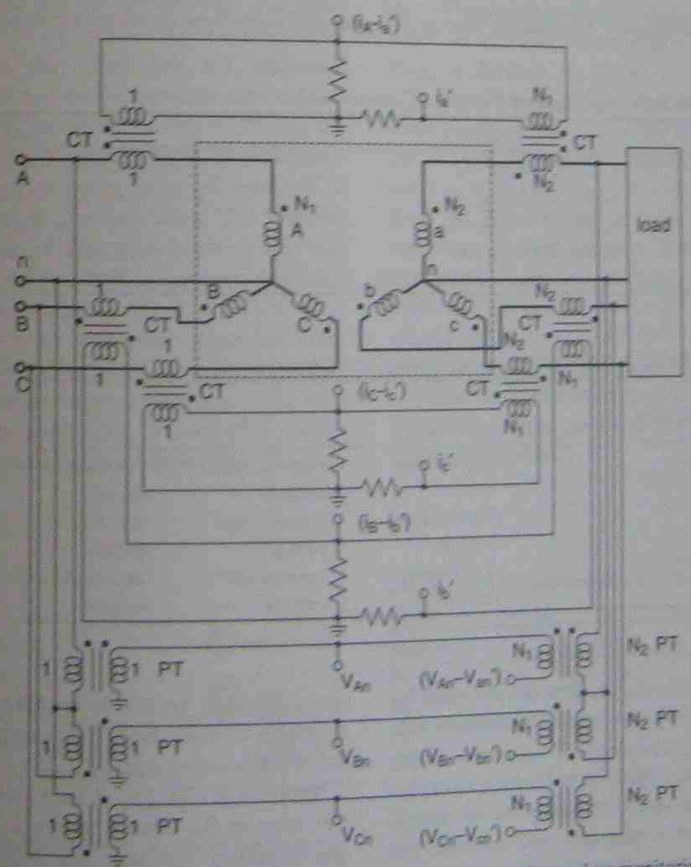



**FIGURE 8.19** Twelve-channel CAT circuit for accurate $Y_0$–$Y_0$ three-phase transformer loss monitoring.

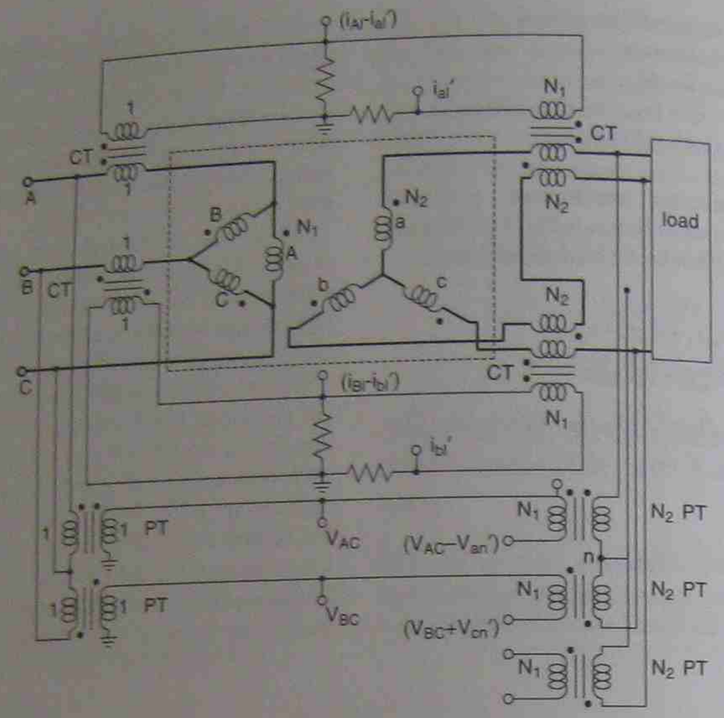



**FIGURE 8.20** Eight-channel CAT circuit for accurate Δ–*Y* connected three-phase transformer loss monitoring.

**TABLE 8.2** Iron-Core and Copper Losses of Three-Phase Transformers

| | $p_{fe}(t)$ | $p_{cu}(t)$ |
|---|---|---|
| *Y*–*Y* (or Δ–Δ) | $v_{AC}(i_A - i_a') + v_{BC}(i_B - i_b')$ | $(v_{AC} - v_{ac}')i_a' + (v_{BC} - v_{bc}')i_b'$ |
| Δ–*Y* | $v_{AC}(i_A - i_a') + v_{BC}(i_B - i_b')$ | $(v_{AC} - v_{an}')i_{a1}' + (v_{BC} + v_{cn}')i_{b1}'$ |
| Δ–$Y_0$ | $v_{AC}(i_A - i_a') + v_{BC}(i_B - i_b')$ | $(v_{AC} - v_{an}')i_{a1}' + (v_{BC} + v_{cn}')i_{b1}' - v_{gn}'i_g'$ |
| *Y*–$Y_0$ | $v_{AC}(i_A - i_a') + v_{BC}(i_B - i_b') - v_{cn}'i_c'$ | $(v_{AC} - v_{ac}')i_a' + (v_{BC} - v_{bc}')i_b'$ |
| $Y_0$–$Y_0$ | $v_{An}(i_A - i_a') + v_{Bn}(i_B - i_b') + v_{Cn}(i_C - i_c')$ | $(v_{An} - v_{an}')i_a' + (v_{Bn} - v_{bn}')i_b' + (v_{Cn} - v_{cn}')i_c'$ |

**TABLE 8.3** Valid Methods for Various Connections

| Primary \ Secondary | Δ | *Y* | $Y_0$ |
|---|---|---|---|
| Δ | Eight-channel method | Eight-channel method | Ten-channel method |
| Y | Eight-channel method | Eight-channel method | Ten-channel method |
| $Y_0$ | Ten-channel method | Ten-channel method | Twelve-channel method |

from Eq. 8-9 with $i_0' = 0$ [73]. The circuits valid for Δ–*Y*, Δ–$Y_0$, and *Y*–$Y_0$ connected transformers also apply for *Y*–Δ, $Y_0$–Δ, and $Y_0$–*Y* connected three-phase transformers, respectively. In these cases, the capital letters A, B, and C represent the secondary, and the lower case letters a, b, and c denote the primary. The corresponding iron-core and copper losses, listed in Table 8.2, are then negative. Table 8.3 shows valid methods for three-phase transformers of various connections.

Note that in Figs. 8.16, 8.18, 8.19, and 8.20, CT and PT ratios on the primary side are 1 : 1, whereas on the secondary side they are $N_2 : N_1$. In this way, secondary signals are referred to the primary. In



Fig. 8.20, only four CTs and five PTs are required for the loss measurement, comparing to the measurement circuit of [90] with nine CTs and nine PTs. Using fewer sensors means having higher measurement accuracy.

#### 8.3.3.3 Accuracy Requirements for Instruments

The efficiencies of high-power electrical apparatus such as single- and three-phase transformers in the kVA and MVA ranges are about 98% or higher. For a 25 kVA single-phase transformer [88] with an efficiency of 98.46% at rated operation, the total losses are $P_{Loss} = 390$ W, where the copper and iron-core losses are $P_{cu} = 325$ W and $P_{fe} = 65$ W, respectively [70]. The measurement errors of losses are derived for three different configurations: the conventional, new, and back-to-back approaches.

#### 8.3.3.4 Application Example 8.8: Conventional Approach $P_{Loss} = P_{in} - P_{out}$

Even if current and voltage sensors (e.g., CTs, PTs) as well as current and voltmeters with maximum error limits of 0.1% are employed, the conventional approach—where the losses are the difference between the input and output powers—always leads to relatively large maximum errors (>50%) in the loss measurements of highly efficient transformers.

The maximum error in the measured losses will be demonstrated for the 25 kVA, 240 V/7200 V single-phase transformer of Fig. E8.8.1, where the low-voltage winding is connected as primary, and rated currents are therefore $I_{2rat} = 3.472$ A, $I_{1rat} = 104.167$ A [72]. The instruments and their maximum error limits are listed in Table E8.8.1, where errors of all current and potential transformers (e.g., CTs, PTs) are referred to the meter sides. In Table E8.8.1, error limits for all ammeters and voltmeters are given based on the full-scale errors, and those for all current and voltage transformers are derived based on the measured values of voltages and currents (see Appendix A6.1).

The maximum error of losses at unity power factor is

$$\begin{aligned} P_{Loss} &= (240\,\text{V} \pm \varepsilon_{PT1} \pm \varepsilon_{V1})(5.20835\,\text{A} \pm \varepsilon_{CT1} \pm \varepsilon_{A1})20 - \\ &\quad 30(240\,\text{V} \pm \varepsilon_{PT2} \pm \varepsilon_{V2}) \\ &\quad (3.472\,\text{A} \pm \varepsilon_{CT2} + \varepsilon_{A2}) \\ &= 240.54\,\text{V}104.28\,\text{A} - 7183.8\,\text{V}3.4635\,\text{A} \\ &= 202.5\,\text{W}; \end{aligned}$$

therefore,

$$\frac{\Delta P_{Loss}}{P_{Loss}} = \frac{\pm 202.5}{390} \times 100\% = \pm 51.9\%.$$

#### 8.3.4 Application Example 8.9: New Approach $p_{cu} = i_2'(v_1 - v_2')$ and $p_{fe} = v_1(i_1 - i_2')$

The determination of the losses from voltage and current differences greatly reduces this maximum error. The copper and iron-core losses are measured based on $p_{cu} = i_2'(v_1 - v_2')$ and $p_{fe} = v_1(i_1 - i_2')$, respectively, as shown in Fig. E8.9.1.

The series voltage drop and exciting current at rated operation referred to the low-voltage side of the 25 kVA, 240 V/7200 V single-phase transformer are $(v_1 - v_2') = 4.86$ V and $(i_1 - i_2') = 0.71$ A, respectively [70, 72]. Note that in Table 2 of [70] one-half the losses of two identical 25 kVA single-phase transformers—connected back-to-back—are given while the voltage drop $(v_1 - v_2') = 9.72$ V and the current difference $(i_1 - i_2') = 1.41$ A pertain to the series connection of both single-phase transformers at linear load; the same applies to the nonlinear loads. The instruments and their full-scale errors are listed in Table E8.9.1.

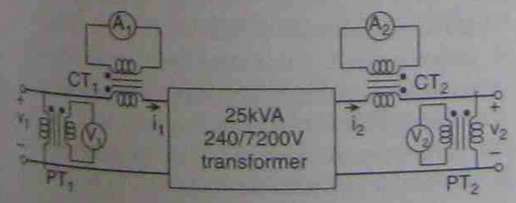



**FIGURE E8.8.1** Instrumentation for single-phase transformers employing conventional approach for loss measurement.

**TABLE E8.8.1** Instruments and Their Error Limits of Fig. E8.8.1

| Instrument | Rating | Error limits |
|---|---|---|
| $PT_1$ | 240 V/240 V | $\varepsilon_{PT1} = \pm 0.24$ V |
| $PT_2$ | 7200 V/240 V | $\varepsilon_{PT2} = \pm 0.24$ V |
| $CT_1$ | 100 A/5 A | $\varepsilon_{CT1} = \pm 5.2$ mA |
| $CT_2$ | 5 A/5 A | $\varepsilon_{CT2} = \pm 3.47$ mA |
| $V_1$ | 300 V | $\varepsilon_{V1} = \pm 0.3$ V |
| $V_2$ | 300 V | $\varepsilon_{V2} = \pm 0.3$ V |
| $A_1$ | 5 A | $\varepsilon_{A1} = \pm 5$ mA |
| $A_2$ | 5 A | $\varepsilon_{A2} = \pm 5$ mA |

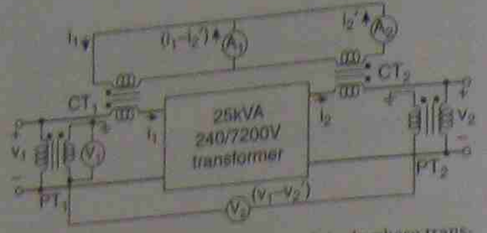



**FIGURE E8.9.1** Loss measurements of single-phase transformers from voltage and current differences.

**TABLE E8.9.1** Instruments and Their Error Limits of Fig. E8.9.1

| Instrument | Rating | Error limits |
|---|---|---|
| $PT_1$ | 240 V/240 V | $\varepsilon_{PT1} = \pm 0.24$ V |
| $PT_2$ | 7200 V/240 V | $\varepsilon_{PT2} = \pm 0.24$ V |
| $CT_1$ | 100 A/5 A | $\varepsilon_{CT1} = \pm 5.2$ mA |
| $CT_2$ | 5 A/5 A | $\varepsilon_{CT2} = \pm 3.47$ mA |
| $V_1$ | 300 V | $\varepsilon_{V1} = \pm 0.3$ V |
| $V_2$ | 10 V | $\varepsilon_{V2} = \pm 0.01$ V |
| $A_1$ | 100 mA | $\varepsilon_{A1} = \pm 0.1$ mA |
| $A_2$ | 5 A | $\varepsilon_{A2} = \pm 5$ mA |

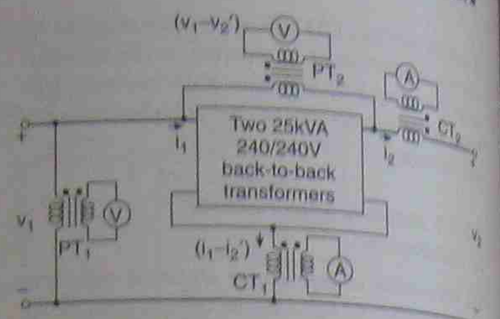



**FIGURE E8.10.1** Instrumentation for single-phase transformer employing back-to-back method of loss measurement.

**TABLE E8.10.1** Instruments and Their Error Limits of Fig. E8.10.1

| Instrument | Rating | Error limits |
|---|---|---|
| $PT_1$ | 240 V/240 V | $\varepsilon_{PT1} = \pm 0.24$ V |
| $PT_2$ | 12 V/12 V | $\varepsilon_{PT2} = \pm 9.7$ mV |
| $CT_1$ | 2 A/2 A | $\varepsilon_{CT1} = \pm 1.4$ mA |
| $CT_2$ | 100 A/5 A | $\varepsilon_{CT2} = \pm 5.2$ mA |
| $V_1$ | 300 V | $\varepsilon_{V1} = \pm 0.3$ V |
| $V_2$ | 10 V | $\varepsilon_{V2} = \pm 0.01$ V |
| $A_1$ | 2 A | $\varepsilon_{A1} = \pm 2$ mA |
| $A_2$ | 5 A | $\varepsilon_{A2} = \pm 5$ mA |

### 8.3.5 Application Example 8.10: Back-to-Back Approach of Two Transformers Simulated with CTs and PTs

If two transformers of the same type are available, the copper and iron-core losses can be measured via the back-to-back method. The testing circuit for this method is shown in Fig. E8.10.1. The series voltage drop and exciting current at rated operation referred to the low-voltage side of the two 25 kVA, 240 V/7200 V single-phase transformers are therefore 9.72 V and 1.41 A, respectively (see Table 2 of [70], where the data were measured via the back-to-back approach, and therefore the exciting currents and voltage drops are those of two transformers in series). The instruments and their full-scale errors are listed in Table E8.10.1.

### 8.3.6 Application Example 8.11: Three-Phase Transformer with DC Bias Current

As an application example, the losses of a 4.5 kVA three-phase transformer bank supplying power to resistive load under various DC bias conditions are measured. The measuring circuit for the $\Delta$–$Y_0$ connected three-phase transformer bank (see Appendix 6.2) is shown in Fig. 8.16. The transformer is operated at 75% of rated load with various balanced DC bias currents injected on the $Y_0$ side, and the DC copper, AC copper, and iron-core losses are measured separately. Such DC currents can be generated by either unbalanced rectifiers, geomagnetic storms [31, 80, 93, 94], or nuclear explosions. Measured iron-core and copper losses vary with the DC bias current and are listed in Table E8.11.1.

Table E8.11.1 demonstrates that the DC copper loss due to the DC bias current is negligibly small. However, the AC copper losses and the iron-core losses increase at rated input voltage (240 V) about 10% and 40%, respectively, due to a DC bias current of 100% of the magnetizing current magnitude ($I_m = 1.25$ A) within the $Y_0$ connected windings; thus the efficiency of the transformer decreases from

$$\frac{3340\,\text{W}}{3340\,\text{W} + 150.3\,\text{W}} = 95.71\%$$

to

$$\frac{3293\,\text{W}}{3293\,\text{W} + 188.7\,\text{W}} = 94.6\%.$$





**TABLE E8.11.1a** Measured Iron-Core and Copper Losses of 4.5 kVA $\Delta$–$Y_0$ Connected Transformer with DC Bias for a Rated Line-to-Line Input Voltage of 242 V

| DC bias current (A) | Iron-core losses (W) | AC copper losses (W) | DC copper losses (W) | Total losses (W) | Output power (W) |
|---|---|---|---|---|---|
| 0.00 | 72.2 | 78.1 | 0.0 | 150.3 | 3340 |
| 0.56 | 79.9 | 78.9 | 0.4 | 159.2 | 3327 |
| 0.74 | 83.1 | 79.1 | 0.7 | 162.9 | 3316 |
| 1.01 | 88.7 | 81.8 | 1.3 | 171.8 | 3306 |
| 1.25 | 101.7 | 85.2 | 1.9 | 188.7 | 3293 |

**TABLE E8.11.1b** Measured Iron-Core and Copper Losses of 4.5 kVA $\Delta$–$Y_0$ Connected Transformer with DC Bias for a Below-Rated Line-to-Line Input Voltage of 230 V

| DC bias current (A) | Iron-core losses (W) | AC copper losses (W) | DC copper losses (W) | Total losses (W) | Output power (W) |
|---|---|---|---|---|---|
| 0.00 | 62.9 | 67.9 | 0.0 | 130.8 | 2958 |
| 0.55 | 68.6 | 69.3 | 0.4 | 138.3 | 2950 |
| 0.76 | 72.0 | 72.1 | 0.7 | 144.8 | 2944 |
| 1.03 | 90.7 | 72.3 | 1.3 | 164.3 | 2940 |
| 1.24 | 95.1 | 76.2 | 1.9 | 173.2 | 2925 |

**TABLE E8.11.1c** Measured Iron-Core and Copper Losses of 4.5 kVA $\Delta$–$Y_0$ Connected Transformer with DC Bias for an Above-Rated Line-to-Line Input Voltage of 254 V

| DC bias current (A) | Iron-core losses (W) | AC copper losses (W) | DC copper losses (W) | Total losses (W) | Output power (W) |
|---|---|---|---|---|---|
| 0.00 | 82.5 | 87.0 | 0.0 | 169.5 | 3663 |
| 0.56 | 88.4 | 86.7 | 0.4 | 175.5 | 3657 |
| 0.74 | 93.9 | 87.4 | 0.7 | 182.0 | 3658 |
| 1.02 | 103.0 | 90.0 | 1.7 | 194.3 | 3654 |
| 1.25 | 109.8 | 93.5 | 1.9 | 205.3 | 3645 |

### 8.3.7 Discussion of Results and Conclusions

New approaches for the real-time monitoring of three-phase transformer power loss have been described and applied under nonsinusoidal operation. Accurate (maximum error of 0.5 to 15%), inexpensive ($3,000 for PC and A/D converter) computer-aided monitoring circuits have been devised and their applications demonstrated.

The digital version of the proposed measuring circuits has the following advantages as compared with the analog circuit of Arri *et al.* [90]:

a) Measuring circuits are suitable for three-phase transformers with various commonly used connections (any combination of $Y$ ungrounded, $Y$ grounded, and $\Delta$ connections). Because the iron-core and copper losses of grounded three-phase transformers can be correctly measured, the method is also applicable for loss monitoring of power transformers under DC bias that can be generated by either unbalanced rectifiers, geomagnetic storms [31, 80, 93, 94], or nuclear explosions.

b) Fewer current and voltage transformers are used (only four CTs and five PTs are required, as shown in Fig. 8.20, comparing to nine CTs and nine PTs used in [90]), and therefore, the measurement accuracy is higher.

c) The software [70] of this monitoring approach does not rely on the discrete Fourier transform (DFT) but on a more accurate transform, which is based on functional derivatives and can also be computed via the fast Fourier transform (FFT). With such online monitoring, the iron-core and copper losses can be sampled within a fraction of a second. Moreover, current and voltage wave shapes, harmonic components, total harmonic distortions, input, output, apparent powers, and the efficiency can be dynamically displayed and updated, and it is quite straightforward to measure the transformer derating under various nonsinusoidal operations [73]. The software is compatible with some commercially available data-acquisition tools [95, 96].

Online measurement of power transformer losses has the following practical applications: apparent power derating, loading guide, prefault recognition, predictive maintenance, and transformer aging and remaining life quantification. The method proposed in this section can be used as a powerful monitoring tool in these applications. The method is suitable for any kind of transformer regardless of size, rating, type, different magnetic circuit (core or shell, three or five limbs), cooling system, power system topology (nonsinusoidal and unbalanced), etc.

### 8.3.8 Uncertainty Analysis [102]

The standard ANSI/NCSL Z540-2-1997 (R2002) recommends that the maximum error analysis as used in Section 8.3.3 be replaced by the expression of uncertainty in measurement. The rationale is that the growing international cooperation and the National Conference of Standards Laboratories International (NCSLI) have recommended that standard. The standard ANSI/NCSL Z540-2-1997 (R2002) "is an adoption of the International Organization for Standardization (ISO) Guide to the Expression of Uncertainty in Measurement to promote consistent international methods in the expression of measurement uncertainty within U.S. standardization, calibration, laboratory accreditation, and metrology services." This standard serves the following purposes:

1. It makes the comparison of measurements more reliable than the maximum error method.
2. Even when all of the known or suspected components of error have been evaluated and appropriate corrections have been applied there still remains an uncertainty about the correctness of the stated result.
3. The evaluation and expression of uncertainty should be universal and the method should be applicable to all kinds of measurements.
4. The expression of uncertainty must be internally consistent and transferable.
5. The approach of this standard has been approved by the Bureau International des Poids et Mesures (BIPM).

It is for these reasons that the measurement errors in [74] have been expressed by the uncertainty as recommended by the standard.

### 8.3.9 SCADA and National Instrument LabVIEW Software [103]

Supervisory control and data acquisition (SCADA) plays an important role in distribution system components such as substations. There are many parts of a working SCADA system, which usually includes signal hardware (input and output), controllers, networks, human–machine interface (HMI), communications equipment, and software. The term SCADA refers to the entire central system, which monitors data from various sensors that are either in close proximity or off site. Remote terminal units (RTUs) consist of programmable logic controllers (PLCs). RTUs are designed for specific requirements but they permit human intervention; for example, in a factory, the RTU might control the setting of a conveyer belt, but the speed can be changed or overridden at any time by human intervention. Any changes or errors are usually automatically logged and/or displayed. Most often, a SCADA system will monitor and make slight changes to function optimally and they are closed-loop systems and monitor an entire system in real time. This requires

- data acquisitions including meter reading,
- checking the status of sensors, the data of which are transmitted at regular intervals depending on the system. Besides the data being used by the RTU, it is also displayed to a human who is able to interface with the system to override settings or make changes when necessary.

## 8.4 TOOLS FOR IMPROVING RELIABILITY AND SECURITY

SCADA equipment such as RTUs and PLCs are applications of telecommunications principles. Interdisciplinary telecommunications programs (ITPs) [104] combine state-of-the-art technology skills with the business, economic, and regulatory insights necessary to thrive in a world of increasingly ubiquitous communications networks. ITPs are served by faculties in economics, electrical engineering, computer science, law, business, telecommunications industry, and government. They address research in wireless, cyber-security, network protocols, telecom economics and strategy, current national policy debates, multimedia, and so forth. Key topics by ITPs are

- Security and reliability of utility systems addressing a range of security-related issues on physical and information security as well as vulnerability assessment and management. The major areas discussed include physical security and access control, asset protection, information systems analysis and protection, vulnerability, assessment, risk management, redundancy, review of existing security and reliability in power systems, new security guidelines, threat response plan, and contingency operation.
- Risk analysis and public safety review various kinds of risks ranging from floods, power outages, and shock to biological hazards. Various approaches to setting safety standards and minimizing risks are explored.
- Current, future, and basic technical concepts of telecommunications systems are studied. They include an in-depth look at basic telecom terminology and concepts, introductions to voice and data networks, signaling, modulation/multiplexing, frequency-band and propagation characteristics, spectral analysis of signals, modulation (amplitude modulation AM, frequency modulation FM, phase modulation PM, and pulse-code modulation PCM), digital coding, modulation multiplexing, detection, transmission systems, and switching systems with an introduction to different network configurations and traffic analysis.
- Data communications define data and computer communications terminology, standards, network models, routing and switching technologies, and communication and network protocols that apply to wide-area networks WANs, metropolitan-area networks MANs, community wireless networks CWNs, and local-area networks LANs. Studies therefore focus on asynchronous and synchronous wide-area networks such as frame relay and synchronous optical networks SONETs, the Internet, routers, selected Internet applications, and Ethernets.
- Applied network security examines the critical aspects of network security. A technical discussion of threats, vulnerabilities, detection, and prevention is presented. Issues addressed are cryptography, firewalls, network protocols, intrusion detection, security architecture, security policy, forensic investigation, privacy, and the law.
- The emerging technology of internet access via the distribution system is addressed [105].

The 2003 U.S.–Canada blackout is analyzed in [106] and recommendations are given for prevention of similar failures in the future. Reliability questions are addressed in [1, 107]. With the advent of distributed generation [108, 109], the control of power systems will become more complicated due to the limited short-circuit capability of renewable sources and their nonsinusoidal voltage and current wave shapes [110].



### 8.4.1 Fast Interrupting Switches and Fault-Current Limiters

Fast interrupting switches and fault-current limiters serve to maintain the stability of an interconnected system by isolating the faulty portion or by mitigating the effect of a fault on the healthy part of the power system. Fast interrupting switches are used to prevent ferroresonance due to the not quite simultaneous closing of the three phases, and to ease reclosing applications. In the first application the almost simultaneous switching of the three phases prevents the current flows through the capacitance of a cable, which is required for inducing ferroresonant currents (see Chapter 2), whereas in the latter the reclosing should occur within a few cycles as indicated in Chapter 4.

**Fast Interrupting Switches (FIS).** Fast interrupting switches [111] rely on sulfur hexafluoride ($SF_6$) as a quenching medium resulting in an increased interrupting capability of the circuit breaker. $SF_6$ is an inorganic compound; it is a colorless, odorless, nontoxic, and nonflammable gas. $SF_6$ has an extremely great influence on global warming and therefore its use should be minimized or entirely avoided. From an environmental point of view a circuit breaker is expected to use smaller amounts of $SF_6$ or to adopt as a quenching medium a gas that causes no greenhouse effect. Research is performed to substitute $SF_6$ by a greenhouse benign alternative quenching gas. The series connection of an FIS with a fault-current limiter either reduces the interrupting conditions or makes the substitution of $SF_6$ with a less effective quenching gas possible. For this reason it is important to investigate the dependence of the interrupting condition on the circuit parameters as will be done in the next section.

**Fault-Current Limiters (FCLs).** Fault-current limiters are installed in transmission and distribution systems to reduce the magnitude of the fault current and thereby mitigate the effect of the fault on the remaining healthy network. The fault-current limiter is a device having variable impedance, connected in series with a circuit breaker (CB) to limit the current under fault conditions. Several concepts for designing FCLs have been proposed: some are based on superconductors [112–114], power electronics components [115–118], polymer resistors [119], and control techniques based on conventional components [120]. FCLs not only limit the fault currents but can have the following additional functions:

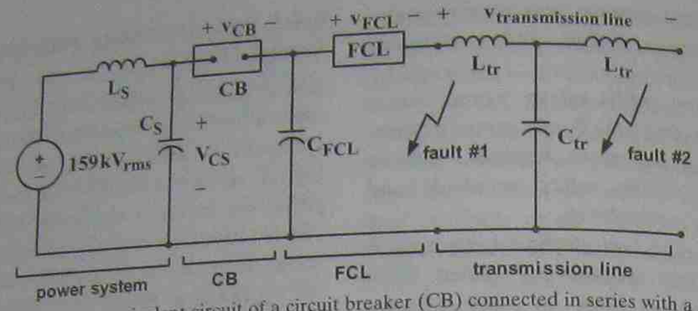



**FIGURE E8.12.1** Single-phase equivalent circuit of a circuit breaker (CB) connected in series with a fault-current limiter (FCL) with two three-phase to ground faults at different locations.

- reduction of voltage sags during short-circuits [121],
- improvement of power system stability [122, 123],
- reduction of the maximum occurring mechanical and electrical torques of a generator [124], and
- easement of the interrupting burden on circuit breakers by limiting the fault current to a desirable level.

Note that in the latter case the burden on the circuit breaker depends not only on the interrupting current but also on the transient recovery voltage (TRV) appearing across the contacts of a circuit breaker. It is conceivable that a limiting impedance of the FCL and a stray capacitance can result in a change of the TRV and may bring about a more severe interrupting duty than in the absence of an FLC. In the following section the influence of a resistive and an inductive FLC on the interrupting duty of a circuit breaker will be investigated for various fault locations. First, a fault occurring near an FCL must be addressed because it produces the maximum fault current that a circuit breaker must interrupt. In this case the TRV across the circuit breaker will be not as severe as compared with the case where the fault occurs a few kilometers from the terminals of the FCL. However, a fault a few kilometers from the FCL must also be taken into account because the rate of rise of the recovery voltage (rrrv) is higher in this case than for a fault occurring near the FCL.

### 8.4.2 Application Example 8.12: Insertion of a Fault Current Limiter (FCL) in the Power System

The system voltage and frequency of the transmission system are assumed to be $V_{L\text{-}L} = 275$ kV (or $V_{L\text{-}N} = 159$ kV) and 60 Hz, respectively. A symmetrical three-phase to ground short-circuit is assumed to occur at a distance $\ell$ of 0 to 8 km from the load-side terminals of the FCL. Figure E8.12.1 shows the corresponding single-phase equivalent circuit; on the supply-side the inductance $L_s = 6.69$ mH and the capacitor $C_s = 750$ nF are given. At a fault near the circuit breaker (CB)—in the absence of an FCL—the CB is assumed to interrupt 63 $kA_{rms}$ at a rate of rise of the recovery voltage (rrrv) of 2.3 kV/μs. In the absence of an FCL the current at a distance $\ell$ of 1 km, 4 km, and 8 km is 90%, 68%, and 51% of 63 $kA_{rms}$. $C_{FCL} = 1$ nF represents the stray capacitance to ground of the FCL, and the transmission line inductance $L_{tr}$ and capacitance $C_{tr}$ per unit length are 0.8 mH/km and 15 nF/km, respectively. The FCL is assumed to produce a limiting impedance $Z_{FCL}$ of either a resistive type or an inductive type as is illustrated in Fig. E8.12.2. The resistance $R_{FCL}$ is in the range of 1 to 9 Ω and the inductance $L_{FCL}$ in the range of 2.6 to 23.9 mH; that is, for 60 Hz the resistive ($R_{FCL}$) and reactive ($2\pi f \cdot L_{FCL}$) components are about the same. In the latter case the capacitance $C_{stray}$ (10 to 100 nF) represents a stray capacitance and is connected in parallel with $L_{FCL}$. The current interruption process of the circuit breaker can be assumed to be that of an ideal switch.

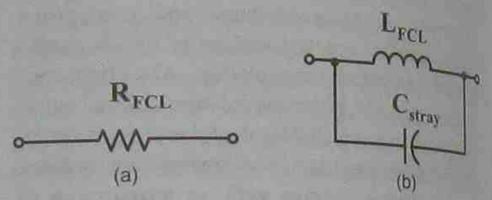



**FIGURE E8.12.2** Model for resistive (a) and inductive (b) fault current limiter.

ST. GEORGE COLLEGE LIBRARY



### 8.4.3 Intentional Islanding, Interconnected, Redundant, and Self-Healing Power Systems

The present interconnected power system evolved after 1940 and represents an efficient however complicated energy generation, distribution, and utilization network. It is reliable but also vulnerable to sabotage, economic issues, distributed generation, and regulations as well as a lack of appropriately trained or educated engineers. Power systems can be configured in multiple ways: at one extreme we have one large power source that delivers all the required power to multiple loads over transmission lines of varying lengths. At the other extreme there are individual sources that supply the needs for each and every load. In between we have multiple sources (e.g., distributed generation) and loads of varying size that are connected by many transmission lines to supply the loads. The fundamental issue is how to balance efficiency, reliability, and security. For relatively small systems a single source serving multiple loads that are distributed over relatively small distances has the advantages of being able to share capacity as the demand varies from load to load as a function of time and to take advantage of the efficiencies of size. A single source for either one single load or several loads is the easiest to control (e.g., isochronous control) and, in many respects, the most secure, as possible failure mechnisms are associated with one source only. By connecting given loads to multiple sources (e.g., with drooping frequency-load characteristics, see Problems 4.12 to 4.14 of Chapter 4) with multiple transmission lines we increase the reliability, as the failure of any one source or transmission line can be compensated for by picking up the load from other sources or over other transmission lines. However, as the number of lines and sources becomes large the control problem becomes too large to be managed centrally. This problem of distributed control for complicated power networks is closely related to the same problem in communications, biological, economic, political, and many other systems.

In the case of distributed generation with renewable energy sources (e.g., wind, solar) additional constraints enter the control approach where the renewable sources are operated at near 100% capacity by imposing droop characteristics with steep slopes. The intermittent operation of renewable sources requires that peak-power plants are able to take over when the renewable sources are unable to generate power. In order to minimize peak-power generation (e.g., spinning reserve) capacity it will be advisable to also rely on energy storage plants (e.g., hydro, compressed air, supercapacitors).

In the following we explore the requirements necessary so that power systems can organize themselves. The information that is required to operate a conventional stand-alone power plant with isochronous control is relatively well known. However, it is much less clear what information one needs to operate a network that is faced with new and changing requirements and constraints that are brought about by new security problems, environmental regulations, distributed generation, competition, etc. Questions to be addressed by the control and dispatch center of a power system include the following: capacity at which each transmission line and power plant is operating, fuel reserves, frequency and phase of the generators, weather forecast, scheduled and nonscheduled power exchanges, times to shed noncritical loads or pick up new loads, repair times for various kinds of damage and maintenance, hierarchy of controls, and design of the system so that if a terrorist has access to a port on the network the damage he can do is limited. How does the probability that this can happen increase with the number of ports/buses on the network? It is advisable to look at the design of other complex systems that organize themselves as possible models for our power system. Systems that can be considered as role models include the Internet, multistream multiprocessor computer systems for parallel computing, and biological systems.

The systems with the most closely related set of constraints to the problem of the allocation of generation capacity and the distribution of power for varying loads with the loss of a generator or a transmission line are communications networks. These networks have a large number of sources and sinks for information that may be connected by many transmission or communication lines. Strategies for the design of these networks that take into account the cutting of communication lines or the loss of nodes such as telephone switches have been developed [125]. Typical designs for reliability include dual rings and meshes. Considerable savings can be obtained as well as an increase in reliability by the use of meshes. In order for these networks to be effective under varying levels and patterns of use, each node needs information about the traffic flow and the state of adjacent nodes on the network. If the proper information on the bandwidth and traffic are updated on a continuing basis, then the nodes can be prepared to allocate the traffic around a given fault when it occurs. Thus a given node can know at

all times how it will reroute the traffic if a communication line is broken or an adjacent node is lost. This can be done without a central command system and in a sense provides a self-organizing system to correct for communication line outages or the loss of a node. Strategies used in communication theory can be effectively employed or modified to improve the reliability of power systems and their efficient operation.

Biological systems can serve as a role model for the design of power systems. Biological systems are highly adaptive and provide both repair and controls that allow them to deal with a large number of unexpected events. These systems use a hierarchy of control systems to coordinate a large number of processes. The brain typically controls the action of the body as a whole, but individual components such as the heart have local control systems that respond to demand for oxygen as communicated to it by signals from other sensory systems such as the baroreceptors. Thus there are functions that require a global response and there are others that are better dealt with locally. Additionally, different biological control systems respond with different time constants [126]. Similarly, power systems have parameters such as fuel reserves with relatively long time constants and other events such as transmission line short-circuits that need to be responded to in fractions of seconds or minutes.

Neural networks are useful ways to approach many complex pattern recognition and control problems that are at least philosophically modeled on biological systems, which use both feedback and feed-forward networks to generate adaptive responses to problems. One of the most common neural networks adjusts the connection weights, using a back propagation algorithm to adapt the network to recognize the desired pattern. This property can be used to develop a control system that has the best response to a wide variety of network problems. Feed-forward networks can be used to anticipate the power system behavior and to prevent problems such as a cascade of network overloads. Power system control and security problems can be formulated in such a way that neural networks can be used as portions of an effective control system. It is to be noted that we can now place computers in the feedback loop of a control system to perform much more complex functions than the classical control systems with a few passive elements.

The three power pools (Western, Eastern, and Texan) within the contiguous United States and their DC links operate quite effectively and reliably. This is so because there is distributed control within the transmission system and the distribution feeders; the integrity of the power pools – including the DC link between the three pools – is maintained through relaying and supervisory control. The everyday operation of power systems takes into account single power plant and single transmission line outages; contingency plans are readily available for the operators. The question arises: what must be done if major emergencies happen? We can identify four types of emergencies:

1. Failure of a major power system component (e.g., power plant, transmission line).
2. Simultaneous failure of more than one major component at different locations such as caused by terrorist attacks.
3. Outage of a power system within an entire region caused by a nuclear explosion or geomagnetically induced currents (GICs) [127].
4. Disruption of the sensing or communication network.

Although the first type of failure can be handled by the present expertise or equipment of power system operators by established contingency plans, the last three failure modes are not planned for because they do not commonly occur. Strategies and countermeasures must be devised so that the power system will be able to survive such major emergencies.

### 8.4.4 Definition of Problem

The problem at hand is multifaceted: it involves behavior, chemical, biological, economic, and engineering sciences. Although interdisciplinary in its nature, only topics involving electrical, telecommunications, and civil or architectural engineering will be addressed.

These sciences will be employed to discuss the following:

1. What can be done to prepare the power system prior to an emergency?
2. What should be done during the failure?
3. What will be done after the failure has occurred?
4. What strategies for efficiency improvements and maintaining regulatory constraints must be addressed?
5. What educational aspects must be highlighted at the undergraduate and graduate levels?

These queries will now be addressed in detail.



### 8.4.5 Solution Approach

There are several approaches for the control of the power networks. The first one draws on the techniques that have been used to control communications networks, that is, to provide each power source with the intelligence to keep track of its local environment and maintain the plans on how it would reroute power if a transmission line is cut or if an adjacent node is either dropped out of the network or has a sudden change in load. This leads to an examination of the power distribution networks to see how the network can be configured to increase its reliability, and this may well mean adding some new transmission lines that enable loads to be supplied from multiple sources. In addition it will require multiple communication links between critical loads and generating power plants. A result of this approach is to allow local nodes on the network to have a high degree of independence that lets them control themselves. This gives both the loads and the generators great flexibility. Writing the rules so that such a system is stable, economical, reliable, and secure is major.

A second approach uses biological systems as a model to develop a hierarchy of controls and information processing that will improve the overall efficiency and reliability of the system. The objective of this effort is the separation of the control problems so that the control of each function is handled by a network that functions as efficiently as possible. This means handling local problems locally and scaling up to larger regions only when it leads to improved system performance in terms of efficiency, reliability, and security. It also means finding a way to make the control system respond on the time scale needed to handle the problem; that is, there are multiple control systems that interface and transmit information between them. Biological systems are often extremely good at optimizing the distribution of controls and efficiency; they are a good starting point to look for ideas for solving related problems. For example, sharks and rays can detect electric fields as small as $10^{-7}$ V/m using a combination of antennas, gain, and parallel processing to detect fish and navigate with signals that at first glance are below the noise level. The way humans use past experience to anticipate future problems may well provide us with an approach to using neural networks as a part of the control system and preventing terrorist attacks.

**What Can Be Done to Prepare the Power System Prior to an Emergency?** This is the most important part for coping with emergencies where several power plants or transmission lines fail or where the power system of an entire region is affected. It is recommended to divide each of the three power pools into independently operating power regions (IOPRs), with distributed intelligence so that in the case of a major emergency – where short-circuits occur – fault-current limiters (FCLs) separate [121–124] within a fraction of a 60 Hz cycle the healthy grid from the faulty section. Each of the designated IOPRs must be able to operate independently and maintain frequency and voltage at about their nominal values either with isochronous or drooping frequency-load control. To achieve this, optimal reconfiguration of the power system must occur within milliseconds permitting intentional islanding operation. If necessary, optimal load shedding must take place but maintaining power to essential loads. To ease such an optimal reconfiguration, provisions must be made to relax usually strict requirements such as voltage and power quality constraints. The ability to communicate and to limit short-circuit currents within milliseconds will be an essential feature of this strategy. It is well known that nuclear explosions generate plasma that is similar to that of solar flares and therefore induce low frequency or quasi-DC currents within the high-voltage transmission system. To minimize the impact of nuclear explosions on the transmission system, three-limb, three-phase transformers with small zero-sequence impedances $Z_0$ will have to be used [31, 80, 94, 127] and DC current compensation networks [94] will have to be installed at key transformers connected to long transmission lines to enforce balanced DC and AC currents.

**What Should Be Done during the Failure?** In an emergency the fault current limiters sense overcurrents and limit these. Thereafter, reclosing switches connected in series with the FCLs will attempt to restore the connection within a few 60 Hz cycles. If the fault duration is longer than a few 60 Hz cycles then circuit breakers connected in series with the FCLs (see Fig. 8.21) will permanently open the faulty line until the source of the fault has been diagnosed. Reclosing switches are employed first because a great number of faults are temporary in their nature. This even applies to a nuclear explosion that lasts only a few seconds but generates plasma that exists for about 60 s. This plasma consists of charged particles that radiate electromagnetic waves and therefore induce low-frequency or quasi-DC currents in the long high-voltage transmission lines. If these quasi-DC currents are balanced within the three phases, the reactive power demand and its

ST. GEORGE POLLEGE OF LAW

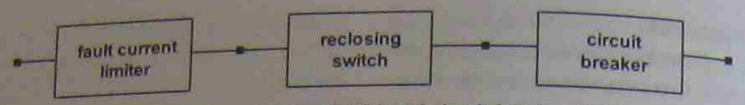



**FIGURE 8.21** Series connection of fault current limiter (FCL) and circuit breaker (CB) where reclosing switch (RCS) is in series to the FCL.

associated voltage drops are manageable if the zero-sequence impedance $Z_0$ of three-limb, three-phase transformers is small. For unbalanced DC currents the reactive power demand and its associated voltage drops are large. For this reason a temporary (seconds) interruption of transmission lines might be beneficial until the plasma has dispersed. This is analogous to a patient who will be rendered unconscious while the operation progresses. Instead of enforcing an interruption another possibility is to enforce a balance of the quasi-DC currents with DC current compensation networks [94].

**What Will Be Done after the Failure Has Occurred?** It is essential that the IOPRs can operate for a longer period of time (e.g., days) so that essential loads can be supplied. If there is a problem with maintaining frequency and voltage control then optimal load shedding will take place. The protocol for optimal load shedding must be defined before an emergency occurs. Relying on a central clock (e.g., National Institute of Standards and Technology, NIST), the paralleling of individual IOPRs can proceed to restore the integrity of each of the three power pools. An alternate strategy is to have a number of atomic clocks located throughout the networks that can provide both the frequency and phase information.

**What Strategies for Efficiency Improvements and Maintaining Regulatory Constraints Must Be Addressed?** Efficiency improvement and maintaining power quality and other regulatory constraints will be unimportant while the failure occurs. For all other times an algorithm developed operates the power system efficiently for given constraints. The development of such software combines harmonic load flow [78], power quality [32, 110, 128–130] constraints, capacitor switching, and optimization where efficiency and cost are components of the objective function [131–134].

**Reliability.** Most short-circuits in power systems occur because of insulation failure. The breakdown of the insulation depends on the voltage stress integrated over time. Although the time component cannot be influenced, the voltage stress across a dielectric can be reduced. With improved semiconductor technology and variable-frequency drives (VFDs) based on pulse-width modulation (PWM), the induction motor has become a viable alternative – as compared with DC motor drives – for many applications. The majority of these applications are usually under the 2 kV and the 1 MW range. Even with advancements in technology, the induction, synchronous, or permanent-magnet motors or generators experience failures of their windings due to large voltage stress when fed by PWM frequency current- or voltage-source converters. Repair work and fault analysis and research show that the majority of insulation failures occur near the last turn of the first coil prior to entering the second coil of the windings. Wave-propagation theory shows that forward- and backward-traveling waves superimpose so that the maximum voltage stress does not necessarily occur at the terminals of a winding but somewhere in between the two terminals. Because of the repetitive nature of PWM pulses the damping due to losses in the winding and iron core cannot be neglected. Work by Gupta [135–137] and many others [138–154] neglect the damping of the traveling waves; therefore it cannot predict the maximum voltage stress of the winding insulation. Figure E3.14.1 of Chapter 3 illustrates a part of a machine winding that can be modeled by inductances and capacitances – a model suitable for the traveling wave theory. This model neglecting losses has been used in [135]. By computing and measuring the maximum voltage stress as a function of PWM switching frequency and duty cycle, one finds that current-source inverters and lightning strikes generate the largest voltage stress because of their inherent current spikes resulting in a large L(di/dt).

**Demand-Side Management Programs.** In the upcoming years, utilities continue to face fundamental changes:

- Distributed generation
- Greater access by utilities and others to the transmission systems of other utilities
- Competition for retail customers from other power sources, self-generation or cogeneration, and from other utility suppliers
- Reduction in the cost of renewable resources
- Growing use of demand-side management (DSM) programs as capacity and energy resources
- Increased concern with the environmental consequences of electricity production
- Growing public opposition to construction of new power plants
- Uncertainty about future load growth, fossil-fuel prices and availability, and possible additional regulations

The traditional approach to utility planning with its narrow focus on utility-built power plants is no longer adequate. A new paradigm for utility resource planning has been promoted [155]. The new approach should account for the availability of DSM and renewable-energy technologies and the public concern with environmental qualities.

Demand-side management programs present modest but growing sources of energy and capacity resources. In 1993, DSM programs cut annual electricity sales by 1.5% and potential peak demand by 6.8% [156, 157]. DSM programs include a variety of technologies related to energy efficiency, load management, and fuel switching.

A survey of 2321 DSM programs conducted by 666 electric utilities in the United States indicated a wide range of technology alternatives, market implementation techniques, and incentive structures [158]. Of the total programs surveyed, 64% include residential customers, 50% commercial customers, 30% industrial customers, and 13% agricultural customers. Moreover, 56% of the programs emphasize peak-clipping goals and 54% feature energy-efficiency goals. Load-shifting, valley-filling, and load-growth objectives are also associated with reported DSM programs.

Load control programs are the most prevalent forms of demand-side management practiced by utilities interested in peak clipping. Three types of techniques are commonly used by utilities that would want to exercise control over customer loads:

- Direct control techniques by utilizing a communications system to remotely affect load operation. The communication technologies used include VHF radio, power liner carrier, ripple, FM-SCA radio, cable TV, and telephone.
- Local control techniques through the promotion and use of demand control equipment that operates according to local conditions. The technologies used in local control include temperature-activated cycling (mostly for the control of air conditioners), timer tripping (on pumps), and various mechanisms that employ timers, interlocks, and/or multiple function demand limiters.
- Distributed control techniques that merge both direct and local control concepts by using a communications system to interface with and/or activate a local control device.

In the EPRI survey [158], a total of 467 load control programs have been reported by 445 different U.S. utilities. The vast majority (440) of reported programs utilize direct control technologies. Only 19 programs employ local control technologies and 8 programs use distributed controls involving interfacing between direct and local control technologies.

A crucial part of any DSM program is electrical load monitoring. Most utilities rely on revenue meters at the point of electrical entrance service to individual buildings or group of buildings. Some DSM programs may require the installation of additional meters for individual electricity-consuming devices such as lighting systems, ventilation fans, or chillers. With these additional meters, controls of targeted equipment can be performed. To make implementation of DSM programs cost-effective, there is an increased interest in monitoring techniques that allow detection and separation of individual loads from measurements performed at a single point (such as the service entrance of a building) serving several electricity-consuming devices. Such techniques have been proposed and have been shown to work relatively well for residential buildings but have not been effective for commercial buildings with irregular and variable loads [159].

Electricity production, transmission, and distribution have substantial environmental costs. Utilities use different methods to assess these impacts [160]. The simplest approach ignores externalities and assumes that compliance with all government environmental regulations yields zero externalities. A more complicated approach consists of ranking and weighting the individual air, water, and terrestrial impacts of different resource options. Some utilities utilize approaches that require quantification (such as tons of either sulfur dioxide or carbon dioxide emitted per million BTU of coal) and monetization (dollars of environmental damage per ton of either carbon dioxide or sulfur dioxide) of the emissions associated with resource options. However, since the estimates of monetized environmental costs vary so much, many utilities are reluctant to use these approaches to assess the environmental externalities of resource options.



ST. GEORGE POLICE DEPT. LIBRARY

Distribution circuits with high reliability indices (e.g., flower configuration) and the use of self-healing system configurations are more expensive than the radial, open-loop, and ring configurations. At present the distribution system contains not much intelligence if one ignores SCADA. In the future the subtransmission and distribution system will have to be equipped with intelligent components as well so that the distributed generation can play a role even if central power stations go off-line because of faults.

### 8.4.6 Voltage Regulation, Ride-Through Capabilities of Load Components; CBEMA, ITIC Tolerance Curves, and SEMI F47 Standard

**Voltage Regulation $V_R$.** Faults (e.g., short-circuits), as discussed in Chapters 1 and 4, and environmental (e.g., lightning) events addressed in Chapter 1 cause the voltage to deviate from its rated wave shape (e.g., magnitude and waveform). The steady-state voltage deviation is measured by the voltage regulation [161]

$$V_R = \left(1 - \frac{V_{\text{rated}} - |V|}{V_{\text{rated}}}\right) \cdot 100\%,$$

where $V_R$ is the percent voltage regulation, which is 100% for $|V| = V_{\text{rated}}$. The voltages $|V|$ and $V_{\text{rated}}$ are the measured rms voltage and the rated (nominal) voltage, respectively. The voltage regulation is a measure for the strength of a bus, that is, the ability of the bus to supply current without changing its voltage amplitude. The short-circuit ratio ($SCR = I_{sc}/I_{\text{rated}}$) discussed in Chapter 1 is indicative of the strength of a power system. Renewable sources have a limited short-circuit current capability, and for this reason they lead to weak systems. Typical values of $SCR$ are in the range from 20 to 200 for residential and 1000 or more for industrial circuits. Whereas the voltage regulation characterizes steady-state voltage amplitudes, the voltage-tolerance (also called power-acceptability and equipment-immunity) curves measure the change in bus voltage during a few 60 Hz cycles.

**Voltage-Tolerance CBEMA and ITIC Curves.** The voltage-tolerance curves [162–165] are loci drawn in the bus voltage versus duration time semilogarithmic plane. The loci indicate the tolerance of a load to withstand either low or high voltages of short duration (few 60 Hz cycles). Figure 8.22 illustrates the voltage-tolerance curve established by the Computer Business Equipment Manufacturers Association (CBEMA), usually called the CBEMA curve. There are two loci: the overvoltage locus above the rated voltage value and the undervoltage locus below the rated voltage value. The linear vertical axis (ordinate) of Fig. 8.22 represents the percent change in bus voltage from its rated value. The semilogarithmic horizontal (abscissa) axis indicates the duration of the voltage disturbance either expressed in 60 Hz cycles or seconds. The steady-state value of the undervoltage locus approaches –13% below the rated voltage. Overvoltages of very short duration are tolerable if the voltage values are below the upper locus of the voltage-tolerance curve. The term "voltage tolerance region" in Fig. 8.22 identifies the permissible magnitudes for transient voltage events. Voltage events are due to lightning strikes, capacitor switching, and line switching due to faults.

In 1996 the CBEMA curve was replaced by the ITIC curve of Fig. 8.23 as recommended by the Information Technology Industry Council (ITIC).

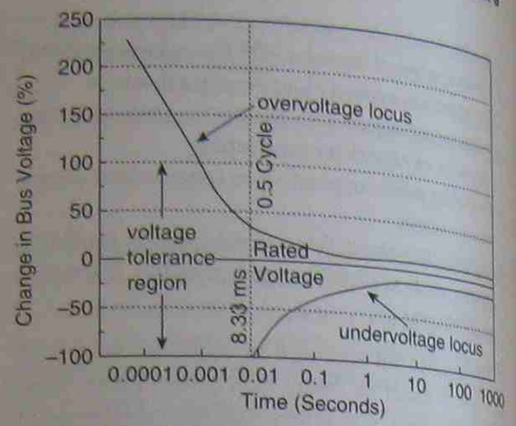



**FIGURE 8.22** CBEMA voltage-tolerance curve.

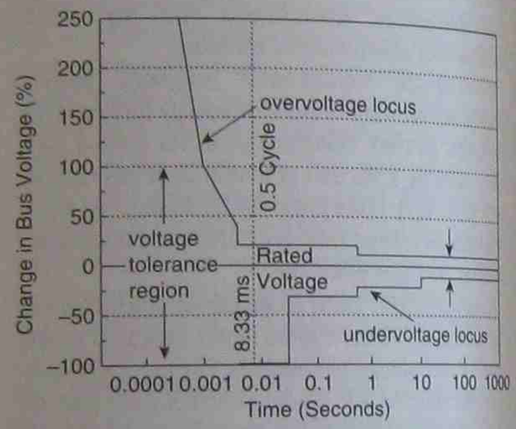



**FIGURE 8.23** ITIC voltage-tolerance curve.





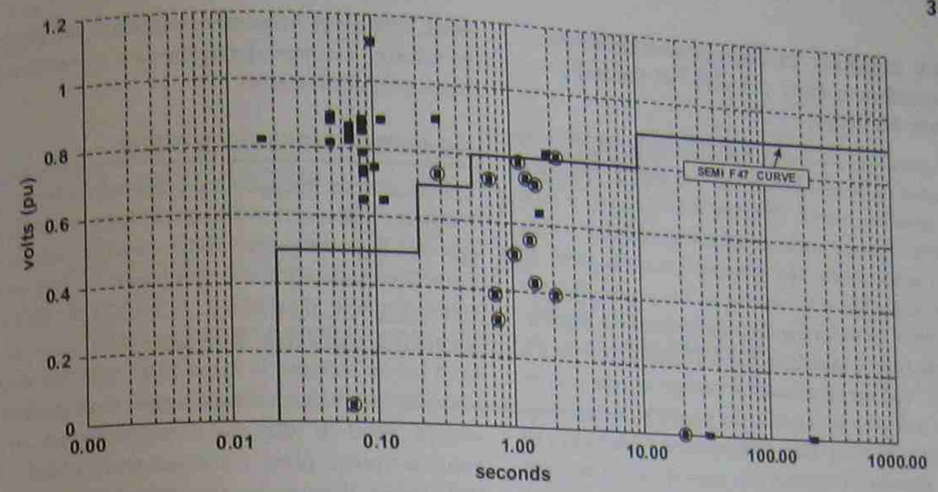



**FIGURE 8.24** Equipment ride-through standard SEMI F47 curve obtained from $V_{L\text{-}L} = 13.8$ kV voltage sags; during a time frame of 60 s 38 sags are obtained. The circled data points lead to plant outages. $V_{\text{base}} = 13.8$ kV.

**SEMI F47 Standard.** The manufacturing process for semiconductor equipment is very sensitive to voltage sags. For this reason the semiconductor industry joined forces and established criteria for permissible sags that will not affect the manufacturing process. Figure 8.24 shows measured voltage sags that have been characterized by their magnitudes and durations and are plotted along with the equipment ride-through standard for semiconductor manufacturing equipment [166–169]. The circled data in Figure 8.24 represent events that resulted in the process interruption of semiconductor manufacturing. In comparison to the CBEMA and ITIC curves, the SEMI F47 curve addresses low-voltage conditions only.

### 8.4.7 Application Example 8.13: Ride-Through Capability of Computers and Semiconductor Manufacturing Equipment

Determine for the data given in Table E8.1.1 the ride-through capability of

- computers, and
- semiconductor manufacturing equipment.

### 8.4.8 Backup, Emergency, or Standby Power Systems (Diesel-Generator Set, Batteries, Flywheels, Fuel Cells, and Supercapacitors)

Standard IEEE-446 [170] gives definitions related to emergency and standby power systems, general need guidelines, systems and hardware, maintenance, protection, grounding, and industry applications. An important variable – besides the voltage amplitude characterized by the voltage regulation $V_R$ – for the safe operation of a power system is the frequency regulation $\%R$. The frequency regulation [170] is defined by

$$\%R = \frac{(F_{nl} - F_{fl})}{F_{nl}} \cdot 100\%.$$

It represents the percentage change in frequency from steady-state no-load operation of an emergency or standby power system to steady-state full-load operation. The frequency regulation is a function of the prime mover (e.g., diesel engine) and the governing system.

Typical ratings of engine-driven generators are from 5 kW to 1 MW. The engine is mostly of the internal-combustion type – fueled with either diesel, gasoline, or natural gas. There are single- and multiple-engine generator set systems. Some of the emergency and standby power systems use steam or gas turbines. The latter ones are available beyond 3 MW. Simple inertia "ride-through" systems are available powered by induction motors or by batteries with DC machines as an interface between the DC and AC system. Parallel-supplied, parallel-redundant uninterruptible power supplies powered by diesel-driven generators are available up to a few megawatts, mostly used for critical computer loads. Battery-supplied systems with inverters are available as well. Combinations of rectifier/inverter (static), battery, and rotating uninterruptible power supplies provide emergency power within seconds.

ST. GEORGE SOLLEGE U

### 8.4.9 Automatic Disconnect of Distributed Generators in Case of Failure of Central Power Station(s)

The paradigm for controlling existing power systems is based on central power stations with an appropriate spinning reserve of about 5 to 10%. At a total installed power capacity of about 800 GW within the United States, the spinning reserve is about 40 to 80 GW. The load sharing of the power plants is governed by drooping characteristics as discussed in Application Examples 8.5 and 8.6 and Problems 8.5 to 8.7. The use of renewable energy sources such as solar and wind is based on the principle of maximum power extraction. Due to the intermittent nature of such renewable sources the central power stations cannot be dispensed with or they have to be replaced by storage devices in the hundreds of gigawatts range on a nationwide basis. In the present scenario, where at least 70% of the power is generated by coal, gas, and nuclear power plants, the frequency control and to some degree the voltage (reactive power) control is governed by central power stations. Distributed generation (DG) sources can augment or displace the power provided by central power stations, but they cannot increase their output powers on demand because they are operated at the maximum output power point. If now an important central power station (having a drooping characteristic with a small slope) – which controls the frequency – shuts down due to failure then renewable sources must be disconnected from the system because they can neither control the frequency (due to their drooping characteristics with large slopes) nor can they significantly control the voltage. This is one of the drawbacks of distributed generation unless storage (e.g., pumped-storage hydro or compressed-air) plants are available on a large scale. Application Examples 8.5 and 8.6 and Problems 8.5 to 8.7 address such control issues. The Danish experience with a relatively high penetration of DG indicates that the percentage of DG can assume values in the range of 30% before weak power system effects become dominant.

## 8.5 LOAD SHEDDING AND LOAD MANAGEMENT

Load shedding is an important method to maintain the partial operation of the power system. Some utilities make agreements with customers who do not necessarily require power at all times. In case of a shortage of electrical power due to failures or overloads due to air conditioning on a very hot day, customers will be removed from the load on a temporary basis. Utilities try to entice customers to this program by offering a lower electricity rate or other reimbursement mechanisms.

## 8.6 ENERGY-STORAGE METHODS

Energy storage methods have played an important role in the past and they will even play a more important role in future power system architectures when distributed generation contributes about 30% of the entire electricity production. As long as the DG contribution is well below 30% there will be not much need for an increase in large (e.g., gigawatt range) scale storage facilities. One example for a large-scale storage plant is the Raccoon Mountain hydro pumped-storage plant commissioned around 1978 [60]. Other than hydro-storage plants there are compressed-air storage [61, 62], flywheel [171], magnetic storage [172], and supercapacitor, battery, or fuel cell [173, 174] storage.

## 8.7 MATCHING THE OPERATION OF INTERMITTENT RENEWABLE POWER PLANTS WITH ENERGY STORAGE

The operation of renewable intermittent energy sources must be matched with energy storage facilities. This is so because the wind may blow when there is no power demand and the wind may not blow when there is demand. A similar scenario applies to photovoltaic plants. It is therefore recommended to design a wind farm of, say, 100 MW power capacity together with a hydro pumped-storage plant so that the latter can absorb 100 MW during a 3–day period; that is, the pumped-storage plant must be able to store water so that the electricity storage amounts to 7.2 GWh. Similar storage capacity can be provided by compressed-air facilities where the compressed air is stored in decommissioned mines [61].

### 8.7.1 Application Example 8.14: Design of a Hydro Pumped-Storage Facility Supplied by Energy from a Wind Farm

A pumped-storage hydro-power plant (Fig. E8.14.1) is to be designed with a rated power of 250 MW and a rated energy capacity of 1500 MWh per day. It consists of an upper and a lower reservoir with a water capacity $C_{H2O}$ each. In addition there must be an emergency reserve for 625 MWh. Water evaporation must be taken into account and is 10% per year for each reservoir, and the precipitation per year is 20 inches. The maximum and minimum elevation (water level) of the upper reservoir is 1000 ft and





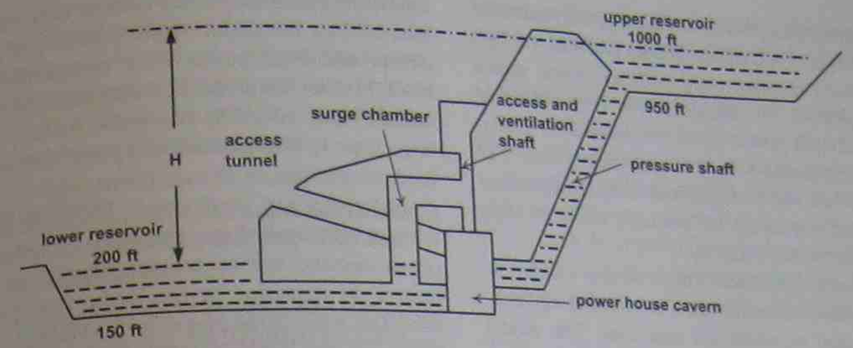



**FIGURE E8.14.1** Pumped-storage power plant for peak-power generation.

950 ft, respectively. The maximum and minimum elevations (water level) for the lower reservoir are 200 ft and 150 ft, respectively. The water turbine is of the Francis type and is coupled with a salient-pole synchronous machine with 24 poles, which can be used as a generator for generating electricity by releasing the water from the upper reservoir to the lower one, and as a motor for pumping the water from the lower reservoir to the upper one.

a) If the power efficiencies of the water turbine and the synchronous generator are $\eta_{\text{turbine}} = 0.8$ and $\eta_{\text{synchronous machine}} = 0.95$, respectively, compute the power required at the turbine input $P_{\text{turbine}}^{\text{required}}$.
b) Provided the head of the water is $H = 800$ ft, the frictional losses between water and pipe amount to 15%, and the water flow measured in cubic feet per second is $Q = 6000$ cfs, compute the mechanical power available in kW at the turbine input $P_{kW}$.
c) How does $P_{\text{turbine}}^{\text{required}}$ compare with $P_{kW}$?
d) Compute the specific speed $N_q$. Is the selection of the Francis turbine justified?
e) What other types of water turbines exist?
f) What is the amount of water the upper or lower reservoirs must hold to generate $E = (1500 \text{ MWh} + 625 \text{ MWh}) = 2125 \text{ MWh}$ per day during an 11.3 hour period?
g) Is the given precipitation per year sufficient to replace the evaporated water? If not, what is the required "rain-catch" area to replace the yearly water loss through evaporation?
h) The pumped-storage plant delivers the energy $E = (1500 \text{ MWh} + 625 \text{ MWh}) = 2125 \text{ MWh}$ per day for which customers pay \$0.20/kWh due to peak-power generation. What is the payback period of this pumped-storage plant if the construction price is \$2,000 per installed power of 1 kW, the cost for pumping is \$0.03/kWh, and the interest rate is 3%?
i) Design a wind farm that can supply the hydro pumped-storage plant with sufficient energy during off-peak power times.

### 8.7.2 Application Example 8.15: Peak-Power Tracker [56] for Photovoltaic Power Plants

Next to wind power, photovoltaic systems have become an accepted renewable source of energy. Sunshine (insolation, irradiation, solar radiation) is in some regions abundant and distributed throughout the earth. The main disadvantages of photovoltaic plants are high installation cost and low energy conversion efficiency, which are caused by the nonlinear and temperature-dependent v–i and p–i characteristics, and the shadowing effect due to clouds, dust, snow, and leaves. To alleviate some of these effects many maximum power point tracking techniques have been proposed, analyzed, and implemented. They can be categorized [56] as

1. Look-up table methods: Maximum-power operating points of solar plants at different insolation and temperature conditions are measured and stored in "look-up tables." Any peak-power tracking (PPT) process will be based on recorded information. The problem with this approach is the limited amount of stored information. The nonlinear nature of solar cells and their dependency on insolation and temperature levels as well as degradation (aging) effects make it impossible to record and store all possible system conditions.

2. Perturbation and observation (P&O) methods. Measured cell characteristics (current, voltage, power) are used along with an on-line search algorithm to compute the corresponding maximum-power point, regardless of insolation, temperature, or degradation levels. The problem with this approach is the measurement errors (especially for current), which strongly affect tracker accuracy.
3. Numerical methods. The nonlinear v–i characteristics of a solar panel is modeled using mathematical or numerical equations. The model must be valid under different insolation, temperature, and degradation conditions. Based on the modeled v–i characteristics, the corresponding maximum-power points are computed as a function of cell open-circuit voltages or cell short-circuit currents under different insolation and temperature conditions.

In [56] two simple and powerful maximum-power point tracking techniques (based on numerical methods) – known as voltage-based PPT and current-based PPT – are modeled, constructed, and compared. Relying on theoretical and experimental results, the advantages and shortcomings of each technique are given and their optimal applications are classified. Unfortunately, none of the existing maximum-power tracking methods can accommodate the partial covering of the solar cells [175] through shadowing effects, and bypass diodes are one means of mitigating these detrimental effects.

## 8.8 SUMMARY

The well-established reliability indices are reviewed, and their application to frequently occurring feeder configurations within a distribution system are addressed. An estimation of electric and magnetic fields generated by transmission lines and their associated corona effects are important from an environmental and from a power quality point of view, respectively. Distributed generation (DG) – where renewable sources are a significant (e.g., 20–30%) part of the generation mix – may lead to frequency and voltage control problems. This is so because renewable sources will be operated near their maximum power range and cannot deliver large transient currents during non-steady-state conditions; that is, renewable sources such as solar and wind-power plants contribute to the properties of a weak generation system. This in turn makes a power system that consists of only intermittently operating renewable plants inoperable because they are operated at their maximum output powers and cannot deliver additional power when demanded by the loads. In other words, the drooping characteristics of intermittently operating renewable sources have a large slope $R$, whereas base load plants such as coal-fired, natural-gas, or storage plants can have droop characteristics with small slopes. The droop characteristics with small slopes guarantee that additional power demand can be covered, through spinning reserve, as requested by the loads. This aspect is important when in the case of severe faults or terrorist attacks the interconnected power system must be separated into several independently operating power system regions where each and every part has its own frequency and voltage control resulting in intentional islanding operation. To maintain a stable operation of each independently operating power region, each one must have sufficient spinning reserve. The maximum error and uncertainty principles are introduced to estimate to total measurement error as applied to power system components. Reliable measurement errors are important for the decision making of dispatch and control centers. Fast switches and current limiters play an important role for the stable operation of a utility system because the faulty part of an interconnected system can be isolated before a domino effect sets in, which may bring down the entire system.

In systems with distributed generation – based on renewable intermittently operating energy sources – larger than 20–30%, storage plants become important to augment the spinning reserve. Storage plants can be put on line within a few (e.g., 6) minutes. This is not fast enough, however, to replace the output of wind-power plants, which may reduce as much as 60 MW per minute. Thus the concept of spinning reserve is important, where the delivery of electric energy can be increased within a few cycles. Peak-power tracking equipment such as batteries for small island photovoltaic plants and peak-power trackers for grid-connected photovoltaic plants are indispensable for maximizing the output power of intermittently operating renewable energy sources. In case of a blackout or brownout of a local power system, emergency power supplies must be employed; these can be based on the conventional diesel-generator or the fuel-cell type. The CBEMA or the newer ITIC curves will make sure that computer loads will not be affected during short outage periods because the power supplies of these components can provide sufficient energy and override a few cycles of voltage outage, reduction, increase, sags, or swells.



Lastly, various demand-side management (DSM) programs can play an important role in maintaining the reliability and security of a distribution system. These appear to be very effective with rate increases or decreases in managing peak-power conditions without requiring additional generation.

## 8.9 PROBLEMS

### Problem 8.1: Reliability, CBEMA, ITIC, and SEMI F47 Calculations

a) For interruptions listed in Table P8.1.1 calculate reliability indices (e.g., SAIDI, SAIFI, $\text{SARFI}_{\%V}$). The total number of customers is 490,000.
b) Determine whether for the interruptions of Table P8.1.1 computer (CBEMA and ITIC voltage-tolerance curves) and semiconductor manufacturing (SEMI F47 curve) equipment have a ride-through capability.

### Problem 8.2: $|\vec{E}|$ = E-field Calculation

For a $V_{L\text{-}L} = 362$ kV transmission line of flat configuration (Fig. E8.2.2) compute the $|\vec{E}|$ = E-field measured in V/mm for the transmission-line data: equivalent bundle diameter $D = 0.2$ m, phase-to-phase distance $S = 12$ m, and height of the center of the bundle to ground $H = 15$ m.

### Problem 8.3: Voltage Pick-up Through the $|\vec{H}|$ = H-field from a Transmission Line Via a Coil in the Ground

A utility requires a 60 V DC voltage source to transmit data to the control and dispatch center from a distant $V_{L\text{-}L} = 262$ kV transmission line operating at a phase rms current of $I_{\text{phase}} = 500$ A resulting at the ground level in the magnetic field strength of $H_{\text{ground}} = 1.4$ A/m or a maximum flux density of $B_{\text{ground_max}} = 17.6$ mG. To avoid any step-down transformer connection attached to the transmission line it was decided to put a single-phase coil into the ground and rectify the induced voltage supplying DC voltage to the transmitter's battery. The transmitter requires a battery current of $I_{\text{DC}} = 1$ A.

a) Sketch the transmission line and the location of the single-phase coil buried in the ground.
b) Assume that the rectangular single-phase coil has a length of $l = 10$ m, a width of $w = 3$ m, and a very small wire cross section. Determine the number of turns N required to obtain a rectified DC voltage of 60 V. You may assume that the magnetic field is tangential to the ground level.

### Problem 8.4: Maximum Surface Gradients $E_{\text{L-L_outer}}$, $E_{\text{L-L_center}}$ and Critical Disruptive Voltage $V_{\text{L-L_o}}$, Determine the Susceptibility of a Transmission Line to Corona [35]

a) For a transmission line with the line-to-line voltage $V_{L\text{-}L} = 362$ kV and the basic geometry of the three-phase transmission line (flat configuration) of Fig. E8.4.1a where the phase spacing is $S = 7.5$ m, the subconductor diameter $d = 3$ cm, the conductor height $H = 12.5$ m, the number of conductors per bundle $N = 2$, and the bundle diameter $D_{\text{bundle}} = 45.7$ cm, determine the maximum surface gradients $E_{\text{L-L_outer}}$ and $E_{\text{L-L_center}}$ measured in $\text{kV}_{\text{rms}}$/cm [47].
b) Determine the crititical disruptive voltage $V_{\text{L-L_o}}$ in kV for the maximum gradients found in part a, where the radius of a subconductor is $r = 1.5$ cm, the equivalent phase spacing (distance) for the three-phase system is $D_{\text{equi}} = 500$ cm, the surface factor $m = 0.84$, and the air density factor $\delta = 0.736$ [35].

### Problem 8.5: Frequency Variation Within an Interconnected Power System as a Result of Two Load Changes [57]

A block diagram of two interconnected areas of a power system (e.g., area #1 and area #2) is shown in Fig. P4.12 of Chapter 4. The two areas are connected

**TABLE P8.1.1** Electricity interruptions/transients

| Number of interruptions/ transients | Number of interruptions/ transients duration | Voltage in % of rated value | Total number of customers affected | Cause of interruption/ transient |
|---|---|---|---|---|
| 10 | 4.5 h | 0 | 1000 | overload |
| 15 | 3 h | 0 | 1500 | repair |
| 60 | 1 min | 90 | 500 | switching transients |
| 90 | 1 s | 130 | 500 | capacitor switching |
| 110 | 0.1 s | 40 | 15000 | short-circuits |
| 95 | 0.1 s | 150 | 4000 | lightning |
| 130 | 0.01 s | 50 | 3000 | short-circuits |

by a single transmission line. The power flow over the transmission line will appear as a positive load to one area and an equal but negative load to the other, or vice versa, depending on the direction of power flow.

a) For steady-state operation show that with $\Delta\omega_1 = \Delta\omega_2 = \Delta\omega$ the change in the angular velocity (which is proportional to the frequency f) is

$$\Delta\omega = \text{function of } (\Delta P_{L1}, \Delta P_{L2}, D_1, D_2, R_1, R_2) \quad \text{(P5-1)}$$

and

$$\Delta P_{tie} = \text{function of the same parameters as in Eq. P5-1.} \quad \text{(P5-2)}$$

b) Determine values for $\Delta\omega$ (Eq. P5-1), $\Delta P_{tie}$ (Eq. P5-2), and the new frequency $f_{new}$, where the nominal (rated) frequency is $f_{rated} = 60$ Hz, for the parameters $R_1 = 0.05$ pu, $R_2 = 0.1$ pu, $D_1 = 0.8$ pu, $D_2 = 1.0$ pu, $\Delta P_{L1} = 0.2$ pu, and $\Delta P_{L2} = -0.3$ pu.

c) For a base apparent power $S_{base} = 1000$ MVA compute the power flow across the transmission line.

d) How much is the load increase in area #1 ($\Delta P_{mech1}$) and area #2 ($\Delta P_{mech2}$) due to the two load steps?

e) How would you change $R_1$ and $R_2$ in case $R_1$ is a wind or solar power plant operating at its maximum power point (and cannot accept any significant load increase due to the two load steps) and $R_2$ is a coal-fired plant that can supply additional load?

### Problem 8.6: Load Sharing Control of Renewable and Coal-fired Plants

This problem is concerned with the frequency and load-sharing control of an interconnected power system broken into two areas: the first one with a 50 MW wind-power plant and the other one with a 600 MW coal-fired plant. Figure P4.12 of Chapter 4 shows the block diagram of two generators interconnected by a tie line (transmission line).

Data for generation set (steam turbine and generator) #1:

Frequency change ($\Delta\omega_1$) per change in generator output power ($\Delta P_1$) having the droop characteristic of $R_1 = \dfrac{\Delta\omega_1}{\Delta P_1}\text{pu} = 0.01\,\text{pu}$,

Load change ($\Delta P_{L1}$) per frequency change ($\Delta\omega_1$) yielding $D_1 = \dfrac{\Delta P_{L1}}{\Delta\omega_1} = 0.8\,\text{pu}$,

Step load change $\Delta P_{L1}(s) = \dfrac{\Delta P_{L1}}{s}\text{pu} = \dfrac{0.2}{s}\text{pu}$,

Angular momentum of steam turbine and generator set $M_1 = 4.5$,

Base apparent power $S_{base} = 500$ MVA,

Governor time constant $T_{G1} = 0.01$ s,

Valve changing (charging) time constant $T_{CH1} = 0.5$ s,

(Load reference set point)$_1 = 0.8$ pu.

Data for generation set (wind turbine and generator) #2:

Frequency change ($\Delta\omega_2$) per change in generator output power ($\Delta P_2$) having the droop characteristic of $R_2 = \dfrac{\Delta\omega_2}{\Delta P_2}\text{pu} = 0.5\,\text{pu}$,

Load change ($\Delta P_{L2}$) per frequency change ($\Delta\omega_2$) yielding $D_2 = \dfrac{\Delta P_{L2}}{\Delta\omega_2} = 1.0\,\text{pu}$,

Step load change $\Delta P_{L2}(S) = \dfrac{\Delta P_{L2}}{s}\text{pu} = \dfrac{-0.2}{s}\text{pu}$,

Angular momentum of wind turbine and generator set $M_2 = 6$,

Base apparent power $S_{base} = 500$ MVA,

Governor time constant $T_{G2} = 0.01$ s,

Valve (blade control) changing (charging) time constant $T_{CH2} = 0.7$ s,

(Load reference set point)$_2 = 0.8$ pu.

Data for tie line: $T = \dfrac{377}{X_{tie}}$ with $X_{tie} = 0.2$ pu.

a) List the ordinary differential equations and the algebraic equations of the block diagram of Figure P4.12 of Chapter 4.

b) Use either Mathematica or MATLAB to establish transient and steady-state conditions by imposing a step function for load reference set point $(s)_1 = \dfrac{0.8}{s}\text{pu}$, load reference set point $(s)_2 = \dfrac{0.8}{s}\text{pu}$, and run the program with no load changes $\Delta P_{L1} = 0, \Delta P_{L2} = 0$ for 5 s. After 5 s impose step load change $\Delta P_{L1}(s) = \dfrac{\Delta P_{L1}}{s}\text{pu} = \dfrac{0.2}{s}\text{pu}$, and after 7 s impose step load change $\Delta P_{L2}(s) = \dfrac{\Delta P_{L2}}{s}\text{pu} = \dfrac{-0.2}{s}\text{pu}$ to find the transient and steady-state responses $\Delta\omega_1(t)$ and $\Delta\omega_2(t)$.

c) Repeat part b for $R_1 = 0.01$ pu, $R_2 = 0.5$ pu, $T_{CH1} = 0.1$ s, and $T_{CH2} = 0.1$ s.

d) Repeat part b for $R_1 = 0.01$ pu, $R_2 = 0.01$ pu, $T_{CH1} = 0.1$ s, and $T_{CH2} = 0.1$ s.



### Problem 8.7: Load Sharing Control of Wind and Solar Power Plants

This problem addresses the frequency and load-sharing control of an interconnected power system broken into two areas, each having one 5 MW wind-power plant and one 5 MW photovoltaic plant. Figure P4.12 of Chapter 4 shows the block diagram of two generators interconnected by a tie line (transmission line).

Data for generation set (wind turbine and generator) #1:

Frequency change ($\Delta\omega_1$) per change in generator output power ($\Delta P_1$) having the droop characteristic of $R_1 = \dfrac{\Delta\omega_1}{\Delta P_1}\text{pu} = 0.5\,\text{pu}$

Load change ($\Delta P_{L1}$) per frequency change ($\Delta\omega_1$) yielding $D_1 = \dfrac{\Delta P_{L1}}{\Delta\omega_1} = 0.8\,\text{pu}$,

Step load change $\Delta P_{L1}(s) = \dfrac{\Delta P_{L1}}{s}\text{pu} = \dfrac{0.2}{s}\text{pu}$,

Angular momentum of wind turbine and generator set $M_1 = 4.5$,

Base apparent power $S_{base} = 5$ MVA,

Governor time constant $T_{G1} = 0.01$ s,

Valve (blade control) changing (charging) time constant $T_{CH1} = 0.1$ s,

(Load reference set point)$_1 = 0.8$ pu.

Data for generation set (photovoltaic array and inverter) #2:

Frequency change ($\Delta\omega_2$) per change in inverter output power ($\Delta P_2$) having the droop characteristic of $R_2 = \dfrac{\Delta\omega_2}{\Delta P_2}\text{pu} = 0.5\,\text{pu}$,

Load change ($\Delta P_{L2}$) per frequency change ($\Delta\omega_2$) $D_2 = \dfrac{\Delta P_{L2}}{\Delta\omega_2} = 1.0\,\text{pu}$,

Step load change $\Delta P_{L2}(s) = \dfrac{\Delta P_{L2}}{s}\text{pu} = \dfrac{-0.2}{s}\text{pu}$,

Equivalent angular momentum $M_2 = 6$,

Base apparent power $S_{base} = 5$ MVA,

Governor time constant $T_{G2} = 0.02$ s,

Equivalent valve changing (charging) time constant $T_{CH2} = 0.1$ s,

(Load reference set point)$_2 = 0.8$ pu.

Data for tie line: $T = \dfrac{377}{X_{tie}}$ with $X_{tie} = 0.2$ pu.

a) List the ordinary differential equations and the algebraic equations of the block diagram of Fig. P4.12 of Chapter 4.

b) Use either Mathematica or MATLAB to establish transient and steady-state conditions by imposing a step function for load reference set point $(s)_1 = \dfrac{0.8}{s}\text{pu}$, load reference set point $(s)_2 = \dfrac{0.8}{s}\text{pu}$, and run the program with no load changes $\Delta P_{L1} = 0, \Delta P_{L2} = 0$ for 5 s. After 5 s impose step load change $\Delta P_{L1}(s) = \dfrac{\Delta P_{L1}}{s}\text{pu} = \dfrac{0.2}{s}\text{pu}$, and after 7 s impose step load change $\Delta P_{L2}(s) = \dfrac{\Delta P_{L2}}{s}\text{pu} = \dfrac{-0.2}{s}\text{pu}$ to find the transient and steady-state responses $\Delta\omega_1(t)$ and $\Delta\omega_2(t)$.

c) Repeat part b for $R_1 = 0.1$ pu and $R_2 = 0.05$ pu.

### Problem 8.8: Calculation of Uncertainty of Losses $P_{Loss} = P_{In} - P_{out}$ Based on the Conventional Approach

Even if current and voltage sensors (e.g., CTs, PTs) as well as current meters and voltmeters with error limits of 0.1% are employed, the conventional approach – where the losses are the difference between the input and output powers – always leads to relatively large uncertainties (>15%) in the loss measurements of highly efficient transformers.

The uncertainty of power loss measurement will be demonstrated for the 25 kVA, 240 V/7200 V single-phase transformer of Fig. E8.8.1, where the low-voltage winding is connected as primary, and rated currents are therefore $I_{2rat} = 3.472$ A, $I_{1rat} = 104.167$ A [72]. The instruments and their error limits are listed in Table E8.8.1, where errors of all current and potential transformers (e.g., CTs, PTs) are referred to the meter sides. In Table E8.8.1, error limits for all ammeters and voltmeters are given based on the full-scale errors, and those for all current and voltage transformers are derived based on the measured values of voltages and currents (see Appendix A6.1).

Because the measurement error of an ammeter or a voltmeter is a random error, the uncertainty of the instrument is $\varepsilon/\sqrt{3}$, if the probability distribution of the true value within the error limits $\pm\varepsilon$ (as shown in Table E8.8.1) is assumed to be uniform. However, the measurement error of an instrument transformer is a systematic error, and therefore its uncertainty equals the error limit (see Appendix A6.1).

For the conventional approach, power loss is computed by

$$p_{loss} = v_1 i_1 - v_2 i_2,$$

ST. GEORGE COLLEGE OF LAW

where $v_1$ is measured by $PT_1$ and voltmeter $V_1$ (see Fig. E8.8.1). The type B variance of measured $v_1$ is $u_{v1}^2 = \varepsilon_{PT1}^2 + \varepsilon_{V1}^2/3 = 0.24^2 + 0.3^2/3^2$.

Similarly, the variances of measured $i_1$, $v_2$, and $i_2$ referred to the primary sides of the instrument transformers are, with $k_{CT1} = 100\text{ A}/5\text{ A} = 20$, $k_{PT2} = 7200\text{ V}/240\text{ V} = 30$,

$$u_{i1}^2 = k_{CT1}^2(\varepsilon_{CT1}^2 + \varepsilon_{A1}^2/3),$$
$$u_{v2}^2 = k_{PT2}^2(\varepsilon_{PT2}^2 + \varepsilon_{V2}^2/3),$$
$$u_{i2}^2 = \varepsilon_{CT2}^2 + \varepsilon_{A2}^2/3.$$

The variance of the measured power loss is

$$u_{loss}^2 = \left(\frac{\partial p_{loss}}{\partial v_1}\right)^2 u_{v1}^2 + \left(\frac{\partial p_{loss}}{\partial i_1}\right)^2 u_{i1}^2 + \left(\frac{\partial p_{loss}}{\partial v_2}\right)^2 u_{v2}^2 + \left(\frac{\partial p_{loss}}{\partial i_2}\right)^2 u_{i2}^2$$
$$= (i_1 u_{v1})^2 + (v_1 u_{i1})^2 + (i_2 u_{v2})^2 + (v_2 u_{i2})^2.$$

Answer: The uncertainty of power loss measurement is 61.4 W, resulting in the relative uncertainty of 15.7%.

### Problem 8.9: Calculation of Uncertainty of Losses Based on the New Approach

The determination of the losses from voltage and current differences greatly reduces the relative uncertainty of the power loss measurement. The copper and iron-core losses are measured based on $p_{cu} = i_2'(v_1 - v_2') = i_2' v_0$ and $p_{fe} = v_1(i_1 - i_2') = v_1 i_0$, respectively, as shown in Fig. E8.9.1.

The series voltage drop and exciting current at rated operation referred to the low voltage side of the 25 kVA, 240 V/7200 V single-phase transformer are $(v_1 - v_2') = 4.86$ V and $(i_1 - i_2') = 0.71$ A, respectively [70, 71]. The instruments and their error limits are listed in Table E8.9.1.

In Fig. E8.9.1, $v_1$ is measured by $PT_1$ and voltmeter $V_1$. Therefore, the relative uncertainty of the $v_1$ measurement is

$$\frac{u_{v1}}{v_1} = \frac{1}{v_1}\sqrt{\varepsilon_{PT1}^2 + \varepsilon_{V1}^2/3}.$$

Similarly, the relative uncertainties of the $(i_1 - i_2')$, $(v_1 - v_2')$, and $i_2$ measurements are, with $k_{CT1} = 100\text{ A}/5\text{ A} = 20$,

$$\frac{u_{i0}}{i_0} = \frac{k_{CT1}}{(i_1 - i_2')}\sqrt{\varepsilon_{CT1}^2 + \varepsilon_{CT2}^2 + \varepsilon_{A1}^2/3},$$

$$\frac{u_{v0}}{v_0} = \frac{1}{(v_1 - v_2')}\sqrt{\varepsilon_{PT1}^2 + \varepsilon_{PT2}^2 + \varepsilon_{V2}^2/3},$$

$$\frac{u_{i2}}{i_2} = \frac{1}{i_2}\sqrt{\varepsilon_{CT2}^2 + \varepsilon_{A2}^2/3}.$$

The relative uncertainty of iron-core loss measurement is

$$\frac{u_{Pfe}}{P_{fe}} = \sqrt{(u_{v1}/v_1)^2 + (u_{i0}/i_0)^2}.$$

The relative uncertainty of copper loss measurement is

$$\frac{u_{Pcu}}{P_{cu}} = \sqrt{(u_{v0}/v_0)^2 + (u_{i2}/i_2)^2}.$$

Answer: The uncertainty of power loss measurement is $u_{loss} = \sqrt{(0.176P_{fe})^2 + (0.071P_{cu})^2}$, and the relative uncertainty is (25.8/390)100% = 6.6%.

The uncertainty of power loss measurements can be reduced further by using three-winding current and potential transformers as shown in Fig. E8.9.2a,b for the measurement of exciting current and series voltage drop. The input and output currents pass though the primary and secondary windings of the current transformer, and the current in the tertiary winding represents the exciting current of the power transformer. Similarly, the input and output voltages are applied to the two primary windings of the potential transformers and the secondary winding measures the voltage drop of the power transformer. For this 25 kVA single-phase transformer, the turns ratio for both the *CT* and the *PT* is $N_{p1} : N_{p2} : N_t = 1 : 30 : 1$. The power loss uncertainty by using three-winding current and potential transformers can be reduced to as small a value as to that of the back-to-back method, which will be described next.

### Problem 8.10: Calculation of Uncertainty of Losses $P_{Loss} = P_{in} - P_{out}$ Based on Back-to-back Approach

If two transformers of the same type and manufacturing batch are available, the copper and iron-core losses can be measured via the back-to-back method. The testing circuit for this method is shown in Fig. E8.10.1. The series voltage drop $(v_1 - v_2')$ and exciting current $(i_1 - i_2')$ at rated operation referred to the low-voltage side of the two 25 kVA, 240 V/7200 V single-phase transformers are therefore 9.72 V and 1.41 A, respectively (see Table 2 of [70], where the data were measured via the back-to-back approach, and therefore the exciting current and series voltage drop are those of two transformers in series). The instruments and their error limits are listed in Table E8.10.1.



The relative uncertainties of $(i_1 - i_2')$, $v_1$, $(v_1 - v_2')$, and $i_2$ measurements are, for $k_{CT2} = 5\text{ A}/5\text{ A} = 1$,

$$\frac{u_{i0}}{i_0} = \frac{1}{(i_1 - i_2')}\sqrt{\varepsilon_{CT1}^2 + \varepsilon_{A1}^2/3},$$

$$\frac{u_{v1}}{v_1} = \frac{1}{v_1}\sqrt{\varepsilon_{PT1}^2 + \varepsilon_{V1}^2/3},$$

$$\frac{u_{v0}}{v_0} = \frac{1}{(v_1 - v_2')}\sqrt{\varepsilon_{PT2}^2 + \varepsilon_{V2}^2/3},$$

$$\frac{u_{i2}}{i_2} = \frac{k_{CT2}}{i_2}\sqrt{\varepsilon_{CT2}^2 + \varepsilon_{A2}^2/3}.$$

The relative uncertainty of iron-core loss measurement is

$$\frac{u_{Pfe}}{P_{fe}} = \sqrt{(u_{v1}/v_1)^2 + (u_{i0}/i_0)^2}.$$

The relative uncertainty of copper loss measurement is

$$\frac{u_{Pcu}}{P_{cu}} = \sqrt{(u_{v0}/v_0)^2 + (u_{i2}/i_2)^2}.$$

Answer: The uncertainty of power loss measurement is $u_{loss} = \sqrt{(0.00178P_{fe})^2 + (0.00163P_{cu})^2}$, and the relative uncertainty is (0.54/390)100% = 0.14%.

### Problem 8.11: Fault-current Limiter

a) Design a fault-current limiter (FCL) based on the inductive current limiter of Fig. E8.12.2b employing a current sensor (e.g., low-inductive shunt with optical separation of potentials via optocoupler, Hall sensor) and a semiconductor switch (e.g., thyristor, triac, MOSFET, IGBT).
b) Use the FCL designed in part a and analyze the single-phase circuit of Fig. E8.12.1 using PSpice for the parameters as given in Application Example 8.12 for a three-phase fault occurring at location #1 corresponding to a distance $\ell = 0$ km and a three-phase fault at location #2 at a distance of either $\ell = 1$ km, 4 km, or 8 km from the FCL connected in series with the circuit breaker (CB). In particular $L_{FCL} = 2.6$ mH, $C_{FCL} = 1$ nF, $C_{stray} = 100$ nF, $V_{L\text{-}N} = 159$ kV, $L_{\ell} = 0.8$ mH/km, and $C_{\ell} = 15$ nF/km.

### Problem 8.12: Batteries Used for Peak-power Tracking Connected to a Small Residential Photovoltaic Power Plant

Figure P8.12.1 shows the circuit diagram of a battery directly connected to a solar generator (array), and Fig. P8.12.2 depicts the 12 V lead–acid battery and solar power plant characteristics. The operating points (intersections of battery and solar panel characteristics) can be made rather close to the maximum power points of the solar power plant.

Note that a 12 V lead–acid battery has a rated voltage of $V_{BAT} = E_0 = 12.6$ V if fully charged and a voltage of $V_{BAT} = E_0 = 11.7$ V if almost empty, whereby the voltage drops across the electrochemical capacitance $C_B$ and the nonlinear capacitance $C_b = f(V_{BAT_over})$ of the battery are zero. A voltage of $V_{BAT} = V_{BAT_oc} + V_{BAT_over} = 14$ V if fully charged provided the voltage drops across the electrochemical capacitance $C_B$ and the nonlinear capacitance $C_b = f(V_{BAT_over})$ of battery are included.

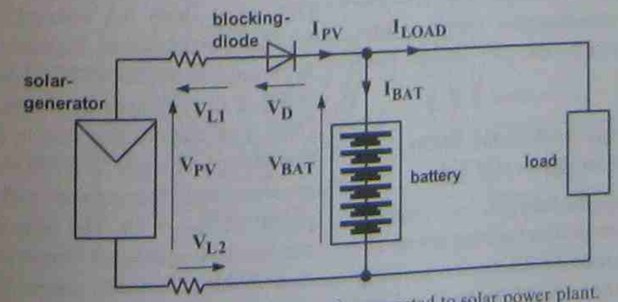



**FIGURE P8.12.1** Circuit diagram of lead–acid battery directly connected to solar power plant.

ST. GEORGE SOLLEGE OF TAFE

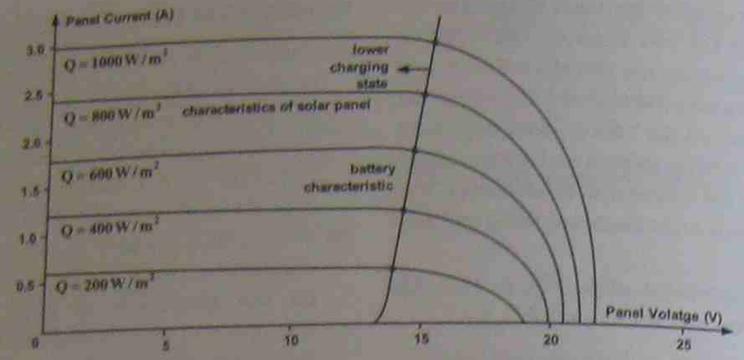



**FIGURE P8.12.2** Operating points of a lead–acid battery directly connected to a solar plant. Q is the insolation.

**TABLE P8.13.1** Interruptions or Transients during February 2006

| Number of interruptions or transients | Interruption or transient duration | Voltage (% of rated value) | Total number of customers affected | Cause of interruption or transient |
|---|---|---|---|---|
| 110 | 2 s | 90 | 2,000 | Switching transients |
| 60 | 1 s | 130 | 3,000 | Capacitor switching |
| 90 | 0.5 s | 40 | 15,000 | Short-circuits due to snow and ice |

Design a peak-power tracking system for a 360 V lead–acid battery and an appropriate photovoltaic system.

### Problem 8.13: Computer Tolerance Curves CBEMA, ITIC, and Semiconductor Manufacturing Ride-Through Standard SEMI F47

a) Determine whether the voltage sags or swells of Table P8.13.1 are within the CBEMA and ITIC voltage tolerance regions. That is, can the computing equipment ride-through and withstand the either low or high voltages of short duration? In this problem February has been chosen because there are line switching, capacitor switching, and snow and ice induced faults as is indicated in Table P8.13.1. The total number of customers is 40,000.

b) Determine whether the voltage sags of Table P8.13.1 lead to semiconductor plant outages according to the equipment ride-through standard SEMI F47.

### Problem 8.14: Emergency Standby Power Supply Based on Diesel-Generator Set

An emergency standby generating set for a commercial building is to be sized. The building has an air-conditioning unit (10 tons, SEER (seasonal energy efficiency ratio) = 14) and an air handler (consisting of two variable-speed drives for the indoor air circulation fan and the outdoor condenser), two high-efficiency refrigerator/freezers (18 cubic feet each), 100 lightbulbs, three fans, two microwave ovens, three drip coffee makers, one clothes washer (not including energy to heat hot water), one clothes dryer, one range (with oven), radio, TV and VCR, three computers, three printers, and one 3 hp motor for a water pump.

Find the wattage of the required emergency standby diesel-generator set, provided the typical wattage values of Table P8.14.1 are used.

### Problem 8.15: Emergency Power Supply Based on Fuel Cells

The transient performance of an inverter – feeding into three-phase power system – supplied by a fuel cell is investigated in this problem. Replace the DC source (with the voltage $V_Q = 390$ V) of Fig. E1.5.1 of Application Example 1.5 of Chapter 1 by the equivalent circuit of the fuel cell as described in Fig. 2 of the paper by Wang, Nehrir, and Shaw [176]. You may assume that in Fig. 2 of that paper the voltage changes $E = 390\text{ V} \pm 30\text{ V}$, where the superimposed rectangular voltage $\pm 30$ V has a period of $T_{\pm 30\text{ V}} = 1$ s. The remaining parameters of the fuel cell equivalent circuit can be extrapolated from Table III of the paper by Wang *et al.* for $E = 390$ V.



### Problem 8.16: Operation of Induction Generator with Injected Voltage in Wound-rotor Circuit as Used for State-of-the-art, Variable-speed Wind-power Plants [177]

Induction machines with wound-rotor circuits are used in wind-power plants as generators as shown in Fig. P8.16. To minimize the rating of the solid-state rectifier and the PWM inverter the three-phase stator winding is directly connected to the power system and the rectifier/inverter combination is supplying or extracting power into or from the rotor circuit of the induction generator. A $P_{out} = 5.7$ MW, $V_{L\text{-}L} = 4$ kV, $f = 60$ Hz, 8-pole Y-connected wound-rotor induction motor has these parameters: $R_s = 0.02\ \Omega$, $X_s = 0.3\ \Omega$, $R'_r = 0.05\ \Omega$, $X'_r = 0.4\ \Omega$, $X_m \to \infty$, and a stator-to-rotor turns ratio $a_{rs} = 10$. The rated slip of this machine when operation as a motor is $s_{rat} = 0.02$.

When the induction machine is operated as a motor, determine the following:

a) phase voltage $|\tilde{V}_{s_ph_rat}|$
b) synchronous mechanical speed $n_{ms_rat}$
c) synchronous angular velocity $\omega_{ms\text{-}rat}$
d) speed of the shaft $n_{m_rat}$

When the machine is operated as a generator with injected voltage $\tilde{V}_r = |\tilde{V}_r|\angle\Phi_r$ in the rotor circuit:

e) Derive a complex, second-order equation for the rotor voltage $\tilde{V}_r = |\tilde{V}_r|\angle\Phi_r$, provided the induction generator operates at $n_{m_new} = 600$ rpm, rated (negative) torque $T_{rat}$, and a leading power factor of $\cos(\varepsilon) = 0.8$, that is, the generator current $\tilde{I}'_r$ leads the generator phase voltage $\tilde{V}_{s_ph_rat} = |\tilde{V}_{s_ph_rat}|\angle 0°$ by $\varepsilon = 36.87°$. Solve this complex, second-order equation for $|\tilde{V}_r|$ and $\Phi_r$.

f) Determine the ratio of the mechanical gear provided the rated speed of the wind turbine is $n_{m_wind\ turbine} = 20$ rpm.

**TABLE P8.14.1** Typical Wattage of Appliances

| Appliance | Value (W) |
|---|---|
| Clothes dryer | 4800 |
| Clothes washer (not including energy to heat hot water) | 500 |
| Drip coffee maker | 1500 |
| Fan (ceiling) | 100–200 |
| Microwave oven | 1450 |
| Range (with conventional oven) | 3200 |
| Range (with self-cleaning oven) | 4000 |
| High efficiency refrigerator/freezer (18 cubic feet) | 300 |
| Radio | 60 |
| VCR (including operation of TV) | 100 |
| Lightbulbs | 30–200 |
| Computer | 200 |
| Printer | 100 |
| Compressor of air conditioning unit (8 tons, SEER = 14) | 6000 |
| Indoor air handler and outdoor condenser of air conditioning unit | 2000 |

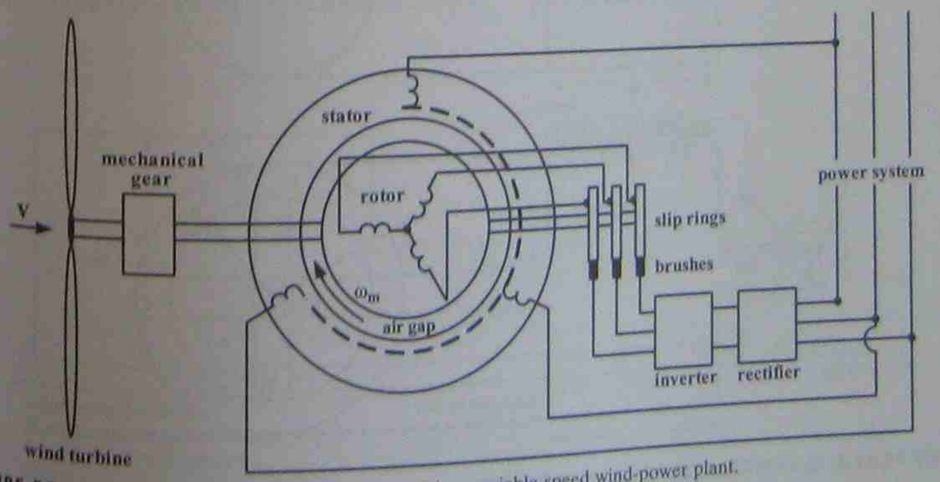



**FIGURE P8.16** Doubly fed induction generator used in a variable-speed wind-power plant.

### Problem 8.17: Design of a Flywheel Storage Power Plant

Design a flywheel storage system which can provide for about 6 minutes power of 100 MW, that is, energy of 10 MWh. The flywheel power plant consists (see Fig. P8.17.1) of a flywheel, mechanical gear, synchronous machine, inverter/rectifier set, and a step-up transformer. The individual components of this plant must be designed as follows:

a) Possible flywheel configurations. For the flywheels (made from steel) based on a spherical ($R_{1o} = 1.5$ m), cylindrical ($R_{1o} = 1.5$ m, $h = 0.9$ m), and wheel-type (with four spokes) configurations as shown in Fig. P8.17.2 ($h = 1.8$ m, $R_{1o} = 1.5$ m, $R_{1i} = 1.3$ m, $R_{2o} = 0.50$ m, $R_{2i} = 0.10$ m, $b = 0.2$ m), compute the ratio of inertia ($J$) to the weight ($W$) of the flywheel, that is, $J/W$. You may assume that the flywheel has magnetic bearings; see http://www.skf.com/portal/skf_rev/home.

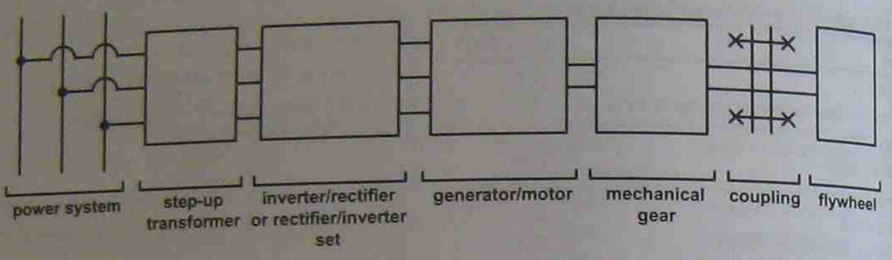



**FIGURE P8.17.1** Flywheel-power plant.

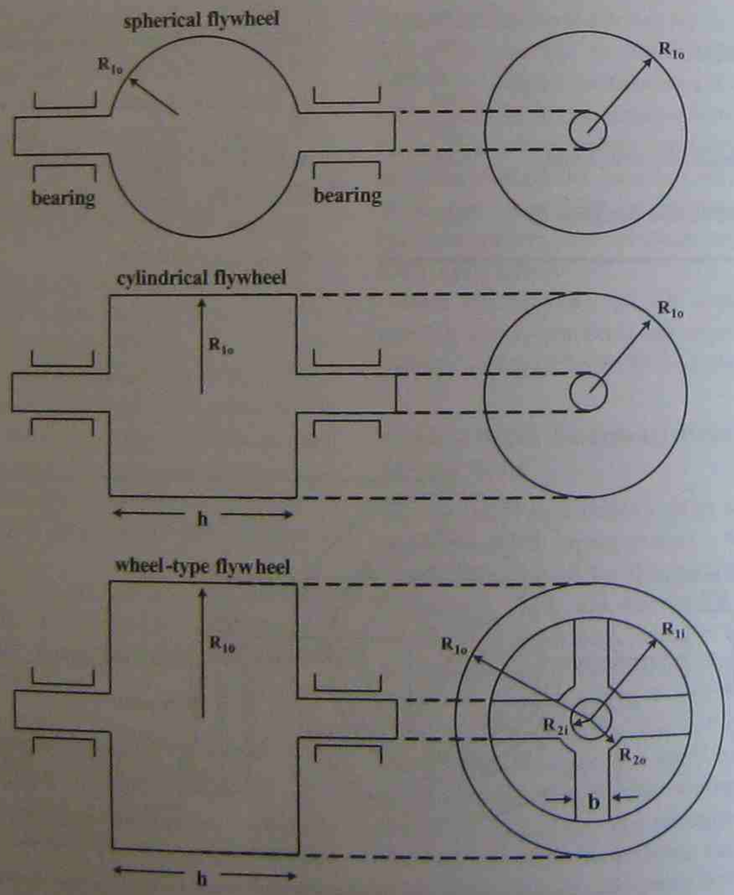



**FIGURE P8.17.2** Three flywheel configurations.



The axial moment of inertia of a rotating sphere is

$$J_{\text{sphere}} = \frac{8}{15} \cdot \pi \cdot \gamma \cdot R_{1o}^5 [\text{kgm}^2], \qquad \text{(P17-1)}$$

where the specific mass of iron is

$$\gamma_{\text{steel}} = 7.86 \text{ [kg/dm}^3\text{]}. \qquad \text{(P17-2)}$$

The axial moment of inertia of a rotating cylinder is

$$J_{\text{cylinder}} = \frac{1}{2} \cdot \pi \cdot \gamma \cdot h \cdot R_{1o}^4 [\text{kgm}^2]. \qquad \text{(P17-3)}$$

The axial moment of inertia of a rotating wheel-type configuration with 4 spokes is

$$J_{\text{wheel}} = \frac{1}{2} \cdot \pi \cdot \gamma \cdot h \cdot (R_{1o}^4 - R_{1i}^4) + \frac{4}{3} \cdot h \cdot b \cdot \gamma \cdot (R_{1i}^3 - R_{2o}^3) + \frac{1}{2} \cdot \pi \cdot \gamma \cdot h \cdot (R_{2o}^4 - R_{2i}^4) [\text{kgm}^2]. \qquad \text{(P17-4)}$$

b) For the given values $h = 1.8$ m, $R_{1o} = 1.5$ m, $R_{1i} = 1.3$ m, $R_{2o} = 0.50$ m, $R_{2i} = 0.10$ m, $b = 0.2$ m, calculate for the wheel-type configuration the stored energy $E_{\text{stored rated}}$ provided the flywheel rotates at $n_{\text{fly-wheel rated}} = 15{,}000$ rpm.

c) Would a homopolar machine [178–182] be more suitable for this application than a synchronous machine?

### Problem 8.18: Steady-state Characteristics of a DC Series Motor Powered by Solar Cells [183]

The performance of a DC series motor supplied by a solar cell array (Fig. P8.18) is to be analyzed. Load matching (solar array, DC series motor, and mechanical load) plays an important role. In this case there is no need for a peak-power tracker because the load matching provides inherent peak-power tracking at steady-state operation.

The solar array is governed by the relation

$$V_g = -0.9 I_g + \frac{1}{0.0422} \ln\left(1 + \frac{I_{phg} - I_g}{0.0081}\right), \qquad \text{(P18-1)}$$

where $V_g$ is the output voltage and $I_g$ is the output current of the solar array. The current $I_{phg}$ is the photon current, which is proportional to the insolation $Q$. The value $I_{phg} = 13.6$ A corresponds to 100% of insolation, that is, $Q = 1000$ W/m$^2$.

The series DC motor has the rated parameters $V_{\text{rat}} = 120$ V, $I_{\text{rat}} = 9.2$ A, $n_{\text{rat}} = 1500$ rpm, $R_a = 1.5\ \Omega$, $R_f = 0.7\ \Omega$, $M_{af} = 0.0675$ H and can be described by the relation

$$\omega = \frac{V_g - (T_m/M_{af})^{1/2} R}{M_{af} (T_m/M_{af})^{1/2}}, \qquad \text{(P18-2)}$$

where $R = R_a + R_f$ and $T_m = M_{af} I_a^2$.

The mechanical load (water pump) can be described by the relation

$$T_m = T_{m1} = A + B\omega + T_{L1} = 4.2 + 0.002387\omega, \qquad \text{(P18-3)}$$

where $A = 0.2$ Nm, $B = 0.0002387$ Nm/(rad/s), and $T_{L1} = 4.0$ Nm.

a) Plot the solar array characteristic $I_g$ versus $V_g$ for the three insolation levels of $Q = 100\%$, 80%, and 60% using Eq. P18-1 with $I_{phg}$ as parameter.

b) Based on Eqs. P18-2 and P18-3 plot the motor torque relation (Eq. P18-2) and the water pump torque relation (Eq. P18-3) in the angular velocity ($\omega$) versus torque ($T_m$) plane.

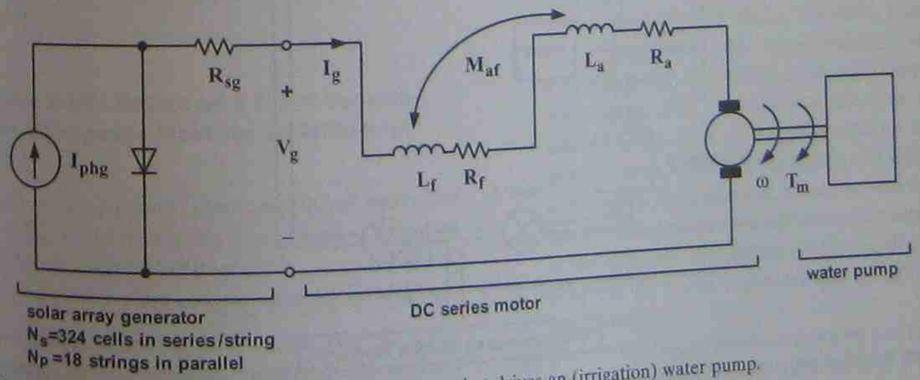



**FIGURE P8.18** Solar array powering a DC series motor that drives an (irrigation) water pump.

c) Using the relations $V_m = V_g = M_{af} I_a \omega + R I_a$ and $T_m = M_{af} I^2_a$, where $I_a = I_g$, plot the load line $T_{m1}$ in the $I_g$–$V_g$ plane. Does a good load matching exist?

d) Calculate the input power of the series DC motor $P_{in}$ from $V_{rat}$ and $I_{rat}$.

e) Calculate the power delivered to the pump by the solar array $P_{solar}$ at $Q = 100\%$, 80%, and 60% insolation.

f) How does $P_{solar}$ compare with $P_{in}$ for the three different insolation levels?

### Problem 8.19: Design of a Compressed-Air Storage Facility [61, 62]

Design a compressed-air energy storage (CAES) plant for $P_{rated} = 100$ MW, $V_{L\text{-}L} = 13800$ V, and $\cos \Phi = 1$ that can deliver rated power for 2 hours. The overall block diagram of such a plant is shown in Fig. P8.19. It consists of a compressor, cooler 1, booster compressor, cooler 2, booster-compressor three-phase 2-pole induction motor with a 1 : 2 mechanical gear ratio, underground air-storage reservoir, combustor fired either by natural gas, oil, or coal, a modified (without compressor) gas turbine, and a three-phase 2-pole synchronous generator/motor.

Design data are as follows:

Air inlet temperature of compressor: 50°F ≡ 283.16°K at ambient pressure 1 atm ≡ 14.696 psi ≡ 101.325 kPa(scal).

Output pressure of compressor: 11 atm ≡ 161 psi ≡ 1114.5 kPa.

Output temperature of cooler 2: 120°F ≡ 322.05°K at 1000 psi ≡ 6895 kPa.

Output temperature of combustor: 1500°F ≡ 1089°K at 650 psi ≡ 4482 kPa.

Output temperature of gas turbine: 700°F ≡ 644°K at ambient pressure 1 atm ≡ 14.696 psi ≡ 101.325 kPa.

Generation operation: 2 h at 100 MW.

Recharging (loading) operation: 8 h at 40 MW.

Capacity of air storage reservoir: $3.5 \cdot 10^6$ ft$^3$ ≡ $97.6 \cdot 10^3$ m$^3$ ≡ (46 m × 46 m × 46 m).

Start-up time: 6 minutes.

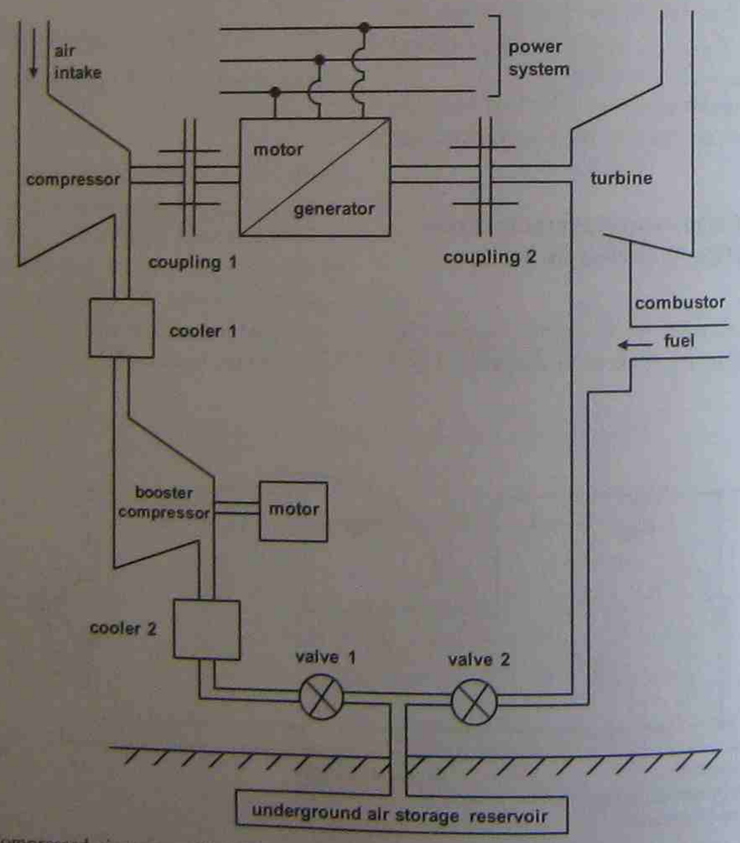



**FIGURE P8.19** Compressed-air storage (CAES) power plant.

ST. GEORGE POLYTECHNIC





Turbine and motor/generator speed: $n_{s\ mot/gen} = 3600$ rpm.

Compressor speed: $n_{s\ comp} = 7200$ rpm.

a) Calculate the Carnot efficiency of the gas turbine:

$$\eta_{carnot\ gas\ turbine} = \eta_{compressor_turbine} \cdot \eta_{combustor_turbine}.$$

b) Note that the compressor of a gas turbine has an efficiency of $\eta_{compressor_turbine} = 0.50$. In this case the compressor is not needed because pressurized air is available from the underground reservoir. The absence of a compressor increases the overall efficiency of the CAES. If "free," that is, low-cost wind power is available for charging the reservoir, this large-scale energy storage method is suitable for most geographic locations relying on either natural or man-made reservoirs. Provided the motor/generator set has an efficiency of $\eta_{mot/gen} = 0.9$, the two air compressors (charging the reservoir) including the two coolers require an input power of 40 MW, and the combustor input fuel must deliver 5500 BTU/kWh, calculate the overall efficiency of the CAES:

$$\eta_{overall} = \frac{P_{out_generator}}{P_{combustor} + P_{2_compressors+2_coolers}}.$$

c) The CAES plant delivers the energy $E = 200$ MWh per day for which customers pay \$0.30/kWh due to peak-power generation. What is the payback period of this CAES plant if the construction price is \$2,000 per installed power of 1 kW, the cost for pumping (recharging) is \$0.03/kWh, and the interest rate is \$3%?

***Hint:*** For the calculation of the Carnot efficiency of the gas turbine and of the compressors you may use software available on the Internet: http://hyperphysics.phy-astr.gsu.edu/hbase/thermo/adiab.html#c3.

### Problem 8.20: Design of a 5 MW Variable-speed Wind-power Plant for an Altitude of 1600 m

Design a wind-power plant supplying the rated power $P_{out} = 5$ MW into the three-phase distribution system at a line-to-line voltage of $V_{L\text{–}L\,system} = 12.47$ kV. The wind-power plant consists of the following:

- One (Y-grounded/Δ) three-phase, step-up transformer, $N_{inverter}$ parallel-connected three-phase PWM inverters with an input voltage of $V_{DC} = 1200$ V, where each inverter delivers an output AC current $I_{phase_inverter}$ at unity power factor $\cos \Phi = 1$ to the low-voltage winding of the transformer (e.g., the angle $\Phi$ between the line-to-neutral voltage of the inverter $V_{L\text{-}n_inverter}$ and the phase current of the inverter $I_{phase_inverter}$ is zero).
- $N_{rectifier}$ ($= N_{inverter}$) three-phase rectifiers, each one equipped with one self-commutated switch and 6 diodes operating at a duty cycle of $\delta = 0.5$. Note that each rectifier feeds one inverter.
- One synchronous generator.
- One mechanical gear.
- One wind turbine.

a) Sketch the block diagram of the entire wind-power plant. At rated operation, the efficiencies of (one) gear box, (one) generator, (one) rectifier, (one) inverter, and (one) transformer are $\eta = 0.95$, each. Note there are $N_{rectifier}$ parallel rectifiers and $N_{inverter}$ parallel inverters, and each rectifier feeds one inverter. At an operation of less than rated load the efficiencies will be smaller. The parallel configuration of inverters and rectifiers permits an efficiency increase, because at light and medium loads only a few inverters and rectifiers must be operated, and some can be disconnected.

b) Determine the output power of each component, e.g., transformer, inverters, rectifiers, generator, gear box, wind turbine, at rated operation.

c) Determine for a modulation index of $m = 0.8$ the inverter output line-to-neutral voltage $V_{L\text{-}n\ inverter}$ such that the inverter can deliver at unity power factor an approximately sinusoidal current to the transformer. $N_{inverter}$ commercially available three-phase PWM inverters are connected in parallel and one inverter has the output power rating $P_{inverter} = 500$ kW. What is the number of inverters required? Determine $I_{phase_inverter}$ of one inverter, the resulting output current of all $N_{inverter}$ inverters, that is, $\Sigma\ I_{phase_inverters}$ and the transformation ratio $a = (N_s/N_p)$ of the (Y-grounded/Δ) step-up transformer. For your calculations you may assume (one) ideal transformer and an ideal power system, where all resistances and leakage inductances are neglected. However, the resistances of the transformer are taken into account in the efficiency calculation of the transformer. Why do we use a Y-grounded/Δ transformer configuration?

d) Each of the $N_{inverter}$ inverters is fed by one three-phase rectifier with one self-commuted PWM-

ST. GEORGE'S COLLEGE OF TECHNOLOGY LIBRARY



operated switch (IGBT) and 6 diodes, and all $N_{rectifier}$ three-phase rectifiers are fed by (one) three-phase synchronous generator with $p = 8$ poles at $n_s = 900$ rpm, utilization factor $C = 3.5$ kWmin/m$^3$, $D_{rotor} = 1.0$ m. The input line-to-line voltage $V_{L\text{-}L\ rectifier} = 1.247$ kV of one three-phase rectifier results at a duty cycle of $\delta = 0.5$ in the DC output voltage (of one rectifier, including filter) $V_{DC} = 1200$ V. Determine the line-to-line output voltage $V_{L\text{-}L\ generator}$ of the nonsalient-pole (round-rotor) synchronous generator such that it matches the required input line-to-line voltage of the rectifier $V_{L\text{-}L\ rectifier}$; thus a transformer between synchronous generator and rectifier can be avoided. Find all pertinent parameters of the synchronous generator including its synchronous reactance $X_s$ in per unit and in ohms.

e) Design the mechanical gear between wind turbine and synchronous generator so that the wind turbine can operate at $n_{turbine} =$ 10 rpm.

f) Determine the geometric dimensions of the wind turbine – using the Lanchester-Betz equation – for the power efficiency coefficient $c_p = 0.4$ of the wind turbine, and the rated wind velocity of $v = 8$ m/s.

g) What are the advantages and disadvantages of this variable-speed wind-power plant design?



## 8.10 REFERENCES


1) Billinton, R.; and Allan, R.N.; *Reliability Evaluation of Power Systems*, Plenum Press, New York, 1996.
2) Pahwa, A.; Redmon, J.; and Clinard, K.; "Impact of automation on distribution reliability," *Proc. IEEE Power Engineering Society Summer Meeting*, Vancouver, Canada, 2001, Vol. 1, p. 736.
3) Goel, L.; and Billinton, R.; "Determination of reliability worth for distribution system planning," *IEEE Transactions on Power Delivery*, Vol. 9, Issue 3, 1994, pp. 1577–1583.
4) Goel, L.; "A comparison of distribution system reliability indices for different operating configurations," *Journal of Electric Machines and Power Systems*, 27, 1999, pp. 1029–1039.
5) Redmon, J.R.; "Traditional versus automated approaches to reliability," *Proceedings of the IEEE Power Engineering Society Summer Meeting*, Vancouver, Canada, 2001, Vol. 1, pp. 739–742.
6) Pahwa, A.; "Role of distribution automation in restoration of distribution systems after emergencies," *Proceedings of the IEEE Power Engineering Society Summer Meeting*, Vancouver, Canada, 2001, Vol. 1, pp. 737–738.
7) Rigler, D.M.; Hodgkins, W.R.; and Allan, R.N.; "Quantitative reliability analysis of distribution systems: automation," *Power Engineering Journal*, Vol. 13, Issue 4, 1999, pp. 201–204.
8) Allan, R.N.; Billinton, R.; Sjarief, I.; Goel, L.; and So, K.S.; "A reliability test system for educational purposes: basis distribution system data and results," *IEEE Transactions on Power Systems*, Vol. 6, Issue 2, 1991, pp. 813–820.
9) Conti, S; and Tina, G.; "Reliability assessment for distribution systems: automated vs. traditional configurations," *International Journal of Power and Energy Systems*, 2006, digital object identifier (DOI): 10.2316/Journal.203.2006.2.203-3407.
10) Kraft, L.A.; "Modeling lightning performance of transmission systems using PSpice," *IEEE Transactions on Power Systems*, Vol. 6, Issue 2, May 1991, pp. 543–549.
11) Jiang, X.; Shu, L.; Sima, W.; Xie, S.; Hu, J.; and Zhang, Z.; "Chinese transmission lines' icing characteristics and analysis of severe ice accidents," *International Journal of Offshore and Polar Engineering*, Vol. 14, No. 3, Sept. 2004 (ISSN 1053-5381).
12) Zhang, J.H.; and Hogg, B.W.; "Simulation of transmission line galloping using finite element method," *Proceedings of the IEE 2nd International Conference on Advances in Power System Control, Operation and Management*, Dec. 1993, Hong Kong, 5 pages.
13) Sullivan, C.R.; Petrenko, V.F.; McCurdy, J.D.; and Kozliouk, V.; "Breaking the ice [transmission line ice]," *IEEE Industry Applications Magazine*, Vol. 9, Issue 5, Sept.–Oct. 2003, pp. 49–54.
14) http://www.isope.org/publications/journals/ijope-14-3/ijope-14-3-p196-abst-JC-348-Jiang.pdf
15) http://tdworld.com/overhead_transmission/power_deutsche_bahn_installs/
16) McCurdy, J.D.; Sullivan, C.R.; and Petrenko, V.F.; "Using dielectric losses to de-ice power transmission lines with 100 kHz high-voltage excitation," *Conf. Rec. of IEEE Industry Applications Society Annual Meeting*, 2001, pp. 2515–2519.
17) Petrenko, V.F.; and Whitworth, R.W.; *Physics of Ice*, London: Oxford Univ. Press, 1999.
18) Petrenko, V.F.; and Sullivan, C.R.; *Methods and systems for removing ice from surfaces*, U.S. Patent Application PCT/US99/28330, 1999.
19) Kieny, C.; Le Roy, G.; and Sbai, A.; "Ferroresonance study using Galerkin method with pseudo-arclength continuation method," *IEEE Transactions on Power Delivery*, Vol. 4, Issue 1, Jan. 1989, pp. 1841–1847.
20) Grainger, J.J.; and Stevenson, Jr., W.D.; *Power System Analysis*, McGraw-Hill, 1994.
21) Boteler, D.H.; Shier, R.M.; Watanabe, T.; and Horita, R.E.; "Effects of geomagnetically induced currents in the BC Hydro 500 kV system," *IEEE Transactions on Power Delivery*, Vol. 4 Issue 1, Jan. 1989, pp. 818–823.
22) Agrawal, B.L.; and Farmer, R.G.; "Effective damping for SSR analysis of parallel turbine generators," *IEEE Transactions on Power Systems*, Vol. 3, Issue 4, Nov. 1988, pp. 1441–1448.
23) McConnell, B.W.; Barnes, P.R.; Tesche, T.M.; and Schafer, D.A.; "Impact of quasi-dc currents on three-phase distribution transformer installations," ORNL/Sub/89-SE912/1, *Report prepared by the Oak Ridge National Laboratory*, Oak Ridge, Tennessee 37831-6285, June 1992.
24) Amin, M.; "Security challenges for the electricity infrastructure," *Computer*, April 2002, Vol. 35, Issue 4, pp. 8–10, ISSN 0018-9162.
25) EPRI, *Electricity Infrastructure Security Assessment*, Vol. I–II, EPRI, Palo Alto, CA, Nov. and Dec. 2001.
26) Amin, M.; "EPRI/DOD Complex interactive networks/systems initiative: self-healing infrastructures," *Proc. 2nd DARPA-JFACC Symp.*

*Advances in Enterprise Control*, IEEE Computer Soc. Press, Los Alamitos, CA, 2000.

27) Silberman, S.; "The energy web," *Wired*, Vol. 9, No. 7, July 2001.

28) Jones, P.D.; "Recent warming in global temperature series," *Geophysical Research Letters*, Vol. 21, Issue 12, 15 June 1994.

29) Ellsaesser, H.W.; MacCracken, M.C.; Walton, J.J.; and Grotch, S.L.; "Global climatic trends as revealed by the recorded data," *Rev. Geophys. Space Phys.*, Vol. 24, Issue 4.

30) Koch, H.; and Hillers, T.; "Second-generation gas-insulated line," *Power Engineering Journal*, June 2002, pp. 111–116.

31) You, Y.; Fuchs, E.F.; Lin, D.; and Barnes, P.R.; "Reactive power demand of transformers with dc bias," *IEEE Industry Applications Society Magazine*, Vol. 2, No. 4, July/August 1996, pp. 45–52.

32) Fuchs, E.F.; "Are harmonic recommendations according to IEEE 519 and CEI/IEC 555 too restrictive?" *Proceedings of Annual Frontiers of Power Conference*, Oklahoma State University, Stillwater, Oklahoma, Oct. 28–29, 2002, pp. IV-1 to IV-18.

33) Fuller, J.F.; Fuchs, E.F.; and Roesler, D.J.; "Influence of harmonics on power system distribution protection," *IEEE Transactions on Power Delivery*, Vol. PWRD-3, No. 2, April 1988, pp. 546–554.

34) Dennhart, A.; *Grundzüge der Tonfrequenz-Rundsteuertechnik und ihre Anwendung*, Verlags- und Wirtschaftsgesellschaft der Elektrizitätswerke m.b.H. VWEW, 6000 Frankfurt (Main) 70-Stresemannalleee 23, 1971.

35) *Electrical Transmission and Distribution Reference Book*, Westinghouse Electric Corporation, East Pittsburgh, PA, 1964.

36) Xiao Hui; Zeng Xiangjun; Fan Shaosheng; Wu Xuebin; and Kuang Lang; "Medium-voltage power line carrier communication system," *Proceedings of the 2004 International Conference on Power SystemTechnology, PowerCon 2004*, Vol. 2, 21–24 Nov. 2004, pp. 1536–1539.

37) Franklin, G.A.; and Hsu, S.-M.; "Power line carrier interference caused by DC electric arc furnaces," *Proceedings of the IEEE Power Engineering Society General Meeting 2004*, Vol. 2, 13–17 July 2003

38) Arnborg, S.; Andersson, G.; Hill, D.J.; and Hiskens, I.A.; "On undervoltage load shedding in power systems," *International Journal of Electrical Power and Energy Systems*, Vol. 19, No. 2, February 1997, pp. 141–149(9).

39) Feng, Z.; Ajjarapu, V.; and Maratukulam, D.J.; "A practical minimum load shedding strategy to mitigate voltage collapse," *IEEE Transactions on Power Systems*, Vol. 13, No. 4, pp. 1285–1290, Nov. 1998.

40) Ando, N.; Takashima, M.; Doi, Y.; Sugitate, Y.; and Menda, N.; "Automatic meter reading system adopting automatic routing technology," *IEEE/PES Transmission and Distribution Conference and Exhibition 2002: Asia Pacific*, Vol. 3, 6–10 Oct. 2002, pp. 2305–2309.

41) Thumaty, S.; Pham, A.; and van Wyk, H.; "Development of a low-IF receiver and a fixed wireless utility network," *Microwave Symposium Digest, 2002 IEEE MTT-S International*, Vol. 2, 2-7 June 2002, pp. 935–938.

42) Chih-Hung Wu; Shun-Chien Chang; and Yu-Wei Huang; "Design of a wireless ARM-based automatic meter reading and control system," *IEEE Power Engineering Society General Meeting, 2004*, Vol. 1, 6–10 June 2004, pp. 957–962.

43) Gaul, A.J.; Handschin, E.; and Hoffmann, W.; "Evolutionary strategies applied for an optimal management of electrical loads," *Proceedings of the International Conference on Intelligent Systems Applications to Power Systems, 1996, ISAP '96*, 28 Jan.–2 Feb. 1996, pp. 368–372.

44) Marti, J.R.; Castellanos, F.; and Santiago, N.; "Wide-band corona circuit model for transient simulations," *IEEE Transactions on Power Systems*, Vol. 10, Issue 2, May 1995, pp. 1003–1013.

45) Podporkin, G.V.; and Sivaev, A.D.; "Lightning impulse corona characteristics of conductors and bundles," *IEEE Transactions on Power Delivery*, Vol. 12, Issue 4, Oct. 1997, pp. 1842–1847.

46) *EHV Transmission Line Reference Book*, Edison Electric Institute, 750 Third Ave., New York, NY, 1968.

47) *Transmission Line Reference Book*, Electric Research Institute, Palo Alto, CA, 1982.

48) Filippopoulos, G.; and Tsanakas, D.; "Analytical calculation of the magnetic field produced by electric power lines," *IEEE Transactions on Power Delivery*, Vol. 20, No. 2, April 2005, pp. 1474–1482.

49) Leeper, E.A.; *Silencing the Fields: A Practical Guide to Reducing AC Magnetic Fields*, Symmetry Books, Boulder, CO, 2001.

50) Barnes, F.S.; "Interaction of DC and ELF electric fields with biological materials and systems," *Handbook on Biological Effects of Electromagnetic Fields*, C. Polk and E. Postow, Eds., pp. 103–147, CRC Press, Boca Raton, FL.



51) Barnes, F.S.; "Typical electric and magnetic field exposures at power-line frequencies and their coupling to biological systems," Chapter 3 of *Electromagnetic Fields*, published by American Chemical Society, 1995, pp. 37–55.

52) Publications of the Public Utilities Commission of the State of California.

53) Silva, J.M.; Fleischmann, H.H.; and Shih, C.H.; "Transmission line corona and X-rays," *IEEE Transactions on Power Delivery*, Vol. 19, No. 3, July 2004, pp. 1472–1482.

54) Anaya-Lara, O.; Hughes, F.M.; Jenkins, N.; and Strbac, G.; "Contribution of DFIG-based wind farms to power system short-term frequency regulation," *IEE Proceedings – Generation, Transmission and Distribution*, Vol. 153, Issue 2, 16 March 2006, pp. 164–170.

55) Ekanayake, J.; and Jenkins, N.; "Comparison of the response of doubly fed and fixed-speed induction generator wind turbines to changes in network frequency," *IEEE Transactions on Energy Conversion*, Vol. 19, Issue 4, Dec. 2004, pp. 800–802.

56) Masoum, M.A.S.; Dehbonei, H.; and Fuchs, E.F.; "Theoretical and experimental analyses of photovoltaic systems with voltage- and current-based maximum power point tracking," *IEEE Trans. on Energy Conversion*, Vol. 17, No. 4, December 2002, pp. 514–522.

57) Wood, A.J.; and Wollenberg, B.F.; *Power Generation Operation and Control*, John Wiley & Sons, Inc., 1984.

58) Mandelbaum, R.; "Reap the wild wind [offshore wind farm]," *IEEE Spectrum*, Vol. 39, Issue 10, Oct. 2002, pp. 34–39.

59) 90 MW Pumpspeicherwerk Glems, Technische Werke der Stadt Stuttgart A.G., 1964.

60) http://www.tva.gov/sites/raccoonmt.htm

61) Mattick, W.; Haddenhorst, H.G.; Weber, O.; and Stys, Z.S., "Huntorf- the world's first 290 MW gas turbine air storage peaking plant," *Proceedings of the American Power Conference*, Vol. 37, 1975, pp. 322–330.

62) Vosburgh, K.G., "Compressed air energy storage," *J. Energy*, Vol. 2, No. 2, March–April 1978, pp. 106–112.

63) Park, R.H.; "Fast turbine valving," *IEEE Transactions on Power Apparatus and Systems*, Vol. PAS-92, Issue 3, May 1973, pp. 1065–1073.

64) Cushing, E.W.; Drechsler, G.E.; Killgoar, W.P.; Marshall, H.G.; and Stewart, H.R.; "Fast valving as an aid to power system transient stability and prompt resynchronization and rapid reload after full load rejection," *IEEE Transactions on Power Apparatus and Systems*, Vol. PAS-91, Issue 4, July 1972, pp. 1624–1636.

65) Hsiao-Dong Chiang; Cheng-Shan Wang; and Flueck, A.J.; "Look-ahead voltage and load margin contingency selection functions for large-scale power systems," *IEEE Transactions on Power Systems*, Vol. 12, Issue 1, Feb. 1997, pp. 173–180.

66) Sharif, S.S.; and Taylor, J.H.; "Real-time load forecasting by artificial neural networks," *Proceedings of the IEEE Power Engineering Society Summer Meeting 2000*, Vol. 1, 16–20 July 2000, pp. 496–501.

67) Kandil, M.S.; El-Debeiky, S.M.; and Hasanien, N.E.; "Long-term load forecasting for fast developing utility using a knowledge-based expert system," *IEEE Transactions on Power Systems*, Vol. 17, Issue 2, May 2002, pp.491–496.

68) Nagasaka, K.; and Al Mamun, M.; "Long-term peak demand prediction of 9 Japanese power utilities using radial basis function networks," *Proceedings of the IEEE Power Engineering Society General Meeting 2004*, Vol. 1, 6–10 June 2004, pp. 315–322.

69) Dranetz – Basic Measuring Instruments (BMI), 1000 New Durham Rd, Edison, NJ 08818.

70) Lin, D.; Fuchs, E.F.; and Doyle, M.; "Computer-aided testing program of electrical apparatus supplying nonlinear loads," *IEEE Transactions on Power Systems*, Vol. 12, No. 1, Feb. 1997, pp. 11–21.

71) Fuchs, E.F.; and Fei, R.; "A new computer-aided method for the efficiency measurement of low-loss transformers and inductors under non-sinusoidal operation," *IEEE Transactions on Power Delivery*, January 1996, Vol. PWRD-11, No. 1, pp. 292–304.

72) Fuchs, E.F.; Yildirim, D.; and Batan, T.; "Innovative procedure for measurement of losses of transformers supplying nonsinusoidal loads," *IEE Proceedings – Generation, Transmission and Distribution*, Vol. 146, No. 6, November 1999, IEE Proceedings online no. 19990684.

73) Fuchs, E.F.; Lin, D.; and Martynaitis, J.; "Measurement of three-phase transformer derating and reactive power demand under nonlinear loading conditions," *Transactions on Power Delivery*, Vol. 21, Issue 2, April 2006, pp. 665–672.

74) Lin, D.; and Fuchs, E.F.; "Real-time monitoring of iron-core and copper losses of three-phase transformers under (non)sinusoidal operation," *IEEE Transactions on Power Delivery*, Vol. 21, No. 3, July 2006, pp. 1333–1341.

75) Stensland, T.; Fuchs, E.F.; Grady, W.M.; and Doyle, M.; "Modeling of magnetizing and core-loss currents in single-phase transformers with voltage harmonics

ST. GEORGE'S COLLEGE OF HE. LIBRARY

for use in power flow," *IEEE Transactions on Power Delivery*, Vol. 12, No. 2, April 1997, pp. 768–774.

76) *IEEE Standard 519*, "IEEE recommended practices and requirements for harmonic control in electric power systems," *IEEE-519*, 1992.

77) IEC 61000-3-2 (2001–10): *Consolidated Edition*, "Electromagnetic compatibility – Part 3-2: limits for harmonic current emissions."

78) Heydt, G.T.; and Grady, W.M.; "User manual HARMFLOW, Version 3.1," *Electric Power Research Institute Publication, EL-4366-CMM*, Palo Alto, CA, 1985.

79) Fuchs, E.F.; Yildirim, D.; and Grady, W.M.; "Measurement of eddy-current loss coefficient $P_{EC\text{-}R}$, derating of single-phase transformers, and comparison with K-factor approach," *IEEE Transactions on Power Delivery*, Vol. 15, No. 1, January 2000, pp. 148–154, and Vol. 15, No. 4, October 2000, pp. 1331–1333 (discussions/closure) and p. 1357.

80) Fuchs, E.F.; and You, Y.; "Measurement of ($\lambda$-i) characteristics of asymmetric three-phase transformers and their applications," *IEEE Transactions on Power Delivery*, Vol. 17, No. 4, Oct. 2002, pp. 983–990.

81) *Current and Voltage Transducer Catalog*, Third Edition, LEM USA, Inc., 6643 West Mill Road, Milwaukee, WI 53218.

82) Rieman, S.; "An optically isolated data acquisition system," *Independent Study Report*, University of Colorado at Boulder, December 1997.

83) Yildirim, D.; and Fuchs, E.F.; "Computer-aided measurements of inductor losses at high-frequencies (0 to 6 kHz)," *Proceedings of the 14th Annual Applied Power Electronics Conference and Exposition*, March 14–18, 1999, Dallas, TX.

84) EMTP program, *Electric Power Research Institute*, Palo Alto, CA.

85) Stöckl, M.; *Elektrische Messtechnik*, Reihe 1, Band IV, B.G. Teubner Verlagsgesellschaft, Stuttgart, 2. Auflage, 1961.

86) Lin, D.; Batan, T.; Fuchs, E.F.; and Grady, W.M.; "Harmonic losses of single-phase induction motors under nonsinusoidal voltages," *IEEE Transactions on Energy Conversion*, Vol. 11, No. 2, June 1996, pp. 273–286.

87) Lin, D.; and Fuchs, E.F.; "On-line measurement of transformer losses under nonsinusoidal operation," *Proceedings of the IASTED International Conference on Power and Energy Systems (PES 2007)*, Clearwater, Florida, January 2007, pp. 239–247.

88) Fuchs, E.F.; Stensland, T.; Grady, W.M.; and Doyle, M.; "Measurement of harmonic losses of pole transformers and single-phase induction motors," *Proceedings of the IEEE-IAS Industry Applications Society Annual Meeting*, Denver, CO, October 2-7 1994, Paper No. EM-03-162, pp. 128–134.

89) American National Standards Institute, IEEE standard test code for liquid-immersed distribution, power, and regulating transformers and IEEE guide for short-circuit testing of distribution and power transformers, ANSI/IEEE C57.12.90-1987, Institute of Electrical and Electronics Engineers, Inc., New York, NY, 1988.

90) Arri, E.; Locci, N.; and Mocci, F.; "Measurement of transformer power losses and efficiency in real working conditions," *IEEE Transactions on Instrumentation and Measurement*, Vol. 40, No. 2, April 1991, 384–387.

91) Mocci, F.; "Un nuovo metodo per la determinazione della potenza assorbita dai doppi bipoli," *L'Energia Elettrica*, No. 7–8, 1989, 323–329.

92) Current and voltage transducer catalog, Third edition, LEM USA Inc., Milwaukee, WI 53218.

93) Fuchs, E.F.; "Transformers, liquid filled," Encyclopedia of Electrical and Electronics Engineering online, September 1, 2000, J. Webster ed., John Wiley & Sons, New York, NY 10158, paper No. 934C, 40 pages, http://www.interscience.wiley.com:38/eeee/32/6132/w.6132-toc.html

94) Fuchs, E.F.; You, Y.; and Lin, D.; "Development and validation of GIC transformer models," Final Report for Contract 19X-SK205V, Prepared for Martin Marietta Energy Systems, Inc., Oak Ridge, TN, June 1996.

95) *DAS-50, User's Guide*, Keithley MetraByte Corp., Taunton, MA 02780, Part # 24851.

96) *uCDAS-16G Manual*, Keithley MetraByte Corp., Taunton, MA 02780, Part # 24845.

97) *Requirements for Instrument Transformers* (IEEE Standard ANSI/IEEE C57.13- 1993).

98) *Instrument Transformers – Part 8: Electronic Current Transformers* (IEC 60044-8-2002-07).

99) *Messwandler für Elektrizitätszähler*, PTB-A-20.2, Physikalisch-Technische Bundesanstalt (PTB), Braunschweig.

100) *AEG-Hilfsbuch*, 9th Edition, Allgemeine Elektrizitäts-Gesellschaft, Grunewald, Berlin, 5/97-5/104, 1965.

101) Grady, W.M.; Fuchs, E.F.; Lin, D.; and Stensland, T.D.; "The potential effects of single-phase power electronic-based loads on power system distortion and losses, Volume 2: single-phase transformers and induction motors," *Technical Report* (Electric Power Research Institute, Palo Alto, CA, 1000655, 2003).

102) ANSI/NCSL Z540-2-1997(R2002), American National Standard for Calibration – U.S. Guide to the Expression of Uncertainty in Measurement, American National Standard Institute, Nov. 12, 2002.

103) Adamo, F.; Attivissimo, F.; Cavone, G.; and Giaquinto, N.; "SCADA/HMI systems in advanced educational courses," *IEEE Transactions on Instrumentation and Measurement*, Vol. 56, Issue 1, Feb. 2007, pp. 4–10.

104) Barnes, F.S.; Fuchs, E.F.; Tietjen, J.S.; Silverstein, J.; Ko, H-Y.; Lockabaugh, T.; Brown, T.X.; and Sicker, D.C.; "A proposal for an integrated utilities engineering management M.E. program," *Proceedings of the IASTED International Conference on Power and Energy Systems (EuroPES 2005)*, Paper # 468-153, Benalmadena, Spain, June 15–17, 2005.

105) Stahlkopf, K.; "Dream jobs 2004, engineer in paradise," *IEEE Spectrum*, February 2004, p. 32.

106) U.S.–Canada Power System Outage Task Force, *Final Report on the August 14, 2003 Blackout in the United States and Canada: Causes and Recommendations*, April 2004, 228 pages.

107) Fairley, P.; "The unruly power grid," *IEEE Spectrum*, Vol. 41, Issue 8, Aug. 2004, pp. 22–27.

108) Hassan, M.; and Klein, J.; "Distributed photovoltaic systems: utility interface issues and their present status," *Report DOE/ET-20356-3*, Jet Propulsion Laboratory, California Institute of Technology, Pasadena, CA, September 15, 1981.

109) Yildirim, D.; Fuchs, E.F.; and Batan, T.; "Test results of a 20 kW, direct drive, variable-speed windpower plant," *Proceedings of the International Conference on Electrical Machines*, Istanbul, Turkey, September 2–4, 1998, pp. 2039–2044.

110) Fuchs, E.F.; Roesler, D.J.; and Masoum, M.A.S.; "Are harmonic recommendations according to IEEE and IEC too restrictive?" *IEEE Transactions on Power Delivery*," Vol. 19, No. 4, October 2004, pp. 1775–1786.

111) Ragaller, K.; *Current Interruption in High-Voltage Networks*, Plenum Press, New York, 1978.

112) Cha, Y.S.; Yang, Z.; Turner, R.; and Poeppel, B.; "Analysis of a passive superconducting fault current limiter," *IEEE Transactions on Applied Superconductivity*, Vol. 8, No. 1, March 1998, pp. 20–25.

113) Matsumura, T.; Uchii, T.; and Yokomizu, Y.; "Development of flux-lock-type fault current limiter with high $T_c$ superconducting element," *IEEE Transactions on Applied Superconductivity*, Vol. 7, No. 2, June 1997, pp. 1001–1004.

114) Hara, T.; Okuma, T.; Yamamoto, T.; Ito, D.; Takaki, K.; and Tsurunaga, K.; "Development of a new 6.6 kV/1000 A class superconducting fault current limiter for electric power systems," *IEEE Transactions on Power Delivery*, Vol. 8, No. 1, January 1993, pp. 182–191.

115) Ueda, T.; Morita, M.; Arita, H.; Kida, J.; Kurosawa, Y.; and Yamagiwa, T.; "Solid-state current limiter for power distribution system," *IEEE Transactions on Power Delivery*, Vol. 8, No. 4, October 1993, pp. 1796–1801.

116) Smith, R.K.; Slade, P.G.; Sarkozi, M.; Stacey, E.J.; Bonk, J.J.; and Mehta, H.; "Solid state distribution current limiter and circuit breaker: application requirements and control strategies," *IEEE Transactions on Power Delivery*, Vol. 8, No. 3, July 1993, pp. 1155–1164.

117) King, E.F.; Chikhani, A.Y.; Hackam, R.; and Salama, M.M.A.; "A microprocessor-controlled variable impedance adaptive fault current limiter," *IEEE Transactions on Power Delivery*, Vol. 5, No. 4, November 1990, pp. 1830–1838.

118) Sugimoto, S.; Kida, J.; Fukui, C.; and Yamagiwa, T.; "Principle and characteristics of a fault current limiter with series compensation," *IEEE Transactions on Power Delivery*, Vol. 11, No. 2, April 1996, pp. 842–847.

119) Skindhoj, J.; Glatz-Reichenbach, J.; and Strümpler, R.; "Repetitive current limiter based on polymer PTC resistor," *IEEE Transactions on Power Delivery*, Vol. 13, No. 2, April 1998, pp. 489–494.

120) Engelman, N.; Schreurs, E.; and Drugge, B.; "Field test results for a multi-shot 12.47 kV fault current limiter," *IEEE Transactions on Power Delivery*, Vol. 6, No. 3, July 1991, pp. 1081–1086.

121) Tosato, F.; and Quania, S.; "Reducing voltage sags through fault current limitation," *IEEE Transactions on Power Delivery*, Vol. 16, No. 1, January 2001, pp. 12–17.

122) Lee, S.; Lee, C.; Ko, T.K.; and Hyun, O.; "Stability analysis of a power system with fault current limiter installed," *IEEE Transactions on Applied Superconductivity*, Vol. 11, No. 1, March 2001, pp. 2098–2101.

123) Sjöström, M.; Cherkaoui, R.; and Dutoit, B.; "Enhancement of power system transient using superconducting fault current limiters," *IEEE Transactions on Applied Superconductivity*, Vol. 9, No. 2, June 1999, pp. 1328–1330.

124) Iioka, D.; Shimizu, H.; Yokomizu, Y.; and Kano, I.; "The effect of resistive and inductive fault current

limiter on shaft torsional torque of synchronous generator installed in consumer systems," *Proceedings of the IASTED International Conference, Power and Energy Systems*, November 19–22, 2001, Tampa, FL, pp. 329–333.

125) Grover, W.; Lecture notes, 2000.

126) Guyton, A.; *Textbook of Medical Physiology*, Eighth Edition, W.B. Saunders Co., 1991.

127) Fuchs, E.F.; You, Y.; and Roesler, D.J.; "Modeling, simulation and their validation of three-phase transformers with three legs under DC bias," *IEEE Transactions on Power Delivery*, Vol. 14, No. 2, April 1999, pp. 443–449.

128) *Military standards* MIL 454, MIL 461C, MIL 1275A, MILB 5087, MIL 220A, and MIL 810E.

129) Hughes, D.; *Grounding for the Control of EMI*, DWCI Virginia, 1983.

130) Vance, E.F.; "Electromagnetic interference control," *IEEE Transactions on EMC*, Vol. 22, EMC-11, pp. 319–328, Nov. 1980.

131) Masoum, M.A.S.; Ladjevardi, M.; Fuchs, E.F.; and Grady, W.M.; "Optimal placement and sizing of fixed and switched capacitor banks under nonsinusoidal operating conditions," *Proceedings of the Summer Power Meeting 2002*, Chicago, July 21–25, 2002, pp. 807–813.

132) Masoum, M.A.S.; Ladejvardi, M.; Fuchs, E.F.; and Grady, W.M.; "Application of local variations and maximum sensitivities selection for optimal placement of shunt capacitor banks under nonsinusoidal operating conditions," *International Journal of Electrical Power and Energy Systems*, Elsevier Science Ltd., Vol. 26, Issue 10, December 2004, pp. 761–769.

133) Masoum, M.A.S.; Jafarian, A.; Ladjevardi, M.; Fuchs, E.F.; and Grady, W.M.; "Fuzzy approach for optimal placement and sizing of capacitor banks in the presence of harmonics," *IEEE Transactions on Power Delivery*, Vol. 19, No. 2, April 2004, pp. 822–829.

134) Masoum, M.A.S.; Ladjevardi, M.; Jafarian, A.; and Fuchs, E.F.; "Optimal placement, replacement and sizing of capacitor banks in distorted distribution networks by genetic algorithms," *IEEE Transactions on Power Delivery*, Vol. 19, No. 4, October 2004, pp. 1794–1801.

135) Gupta, B.K.; et al.; "Turn insulation capability of large AC motors, part 1 – surge monitoring," *IEEE Transactions on Energy Conversion*, Vol. EC-2, No. 4, December 1987, pp. 658–665.

136) Gupta, B.K.; et al.; "Turn insulation capability of large ac motors, part 2 – surge strength," *IEEE Transactions on Energy Conversion*, Vol. EC-2, No. 4, December 1987, pp. 666–673.

137) Gupta, B.K.; et al.; "Turn insulation capability of large AC motors, part 3 – insulation coordination," *IEEE Transactions on Energy Conversion*, Vol. EC-2, No. 4, December 1987, pp. 674–679.

138) Dick, E.P.; et al.; "Practical calculation of switching surges at motor terminals," *IEEE Transactions on Energy Conversion*, Vol. 3, No. 4, December 1988, pp. 864–872.

139) Narang, A.; et al.; "Measurement and analysis of surge distribution in motor windings," *IEEE Transactions on Energy Conversion*, Vol. 4, No. 1, March 1989, pp. 126–134.

140) Acosta, J.; and Cornick, K.J.; "Field investigations into the factors governing the severity of pre-striking transients," *IEEE Transactions on Energy Conversion*, Vol. EC-2, No. 4, December 1987, pp. 638–645.

141) Guardado, J.L.; and Cornick, K.J.; "The effects of coil parameters on the distribution of steep-fronted surges in machine windings," *IEEE Transactions on Energy Conversion*, Vol. 7, No. 3, September 1992, pp. 552–556.

142) Guardado, J.L.; and Cornick, K.J.; "A computer model for calculating steep-fronted surge distribution in machine windings," *IEEE Transactions on Energy Conversion*, Vol. 4, No. 1, March 1989, pp. 95–101.

143) Oyegoke, B.S.; "Voltage distribution in the stator winding of an induction motor following a voltage surge," *Electrical Engineering 82 (2000)*, Springer-Verlag, 2000, pp. 199–205.

144) Oyegoke, B.S.; "A comparative analysis of methods for calculating the transient voltage distribution within the stator winding of an electric machine subjected to steep-fronted surge," *Electrical Engineering 82 (2000)*, pp. 173–182.

145) Oyegoke, B.S.; "Indirect boundary integral equation method as applied for wave propagation in the stator winding of an electric machine," *IEE Proc. Sci. Meas. Technol.*, 1997, 144, No. 5, pp. 223–227.

146) Oyegoke, B.S.; "Effect of the overhang capacitance on the fast-rising surge distribution in winding of a large motor," *IEE Proc. Sci. Meas. Technol.*, 1999, 146, No. 6, November 1999, pp. 299–303.

147) Oyegoke, B.S.; "A comparative analysis of methods for calculating the transient voltage distribution within the stator winding of an electric machine subjected to steep-fronted surge," *IEE 1997 Conference Publication No. 444*.

148) Kaufhold, M.; et al.; "Electrical stress and failure mechanism of the winding insulation in PWM-inverter-fed low-voltage induction motors," *IEEE Transactions on Industrial Electronics*, Vol. 47, No. 3, April 2000, pp. 396–402.



149) Agrawal, A. K.; et al.; "Application of modal analysis to the transient response of multi-conductor transmission lines with branches," *IEEE Transactions on Electromagnetic Compatibility*, Vol. EMC-21, No. 3, August 1979, pp. 256–262.

150) Wang, J.; McInerny, S.; and Haskew, T.; "Insulation fault detection in a PWM-controlled induction motor experimental design and preliminary results," *Proceedings of the 9th International Conference on Harmonics and Quality of Power*, Vol. 2, 1–4 Oct. 2000, pp. 487–492.

151) Bonnet, A.H.; "Analysis of the impact of pulse-width modulated inverter voltage waveforms on ac induction motors," *IEEE Transactions on Industry Applications*, Vol. 32, No. 2, March/April 1996, pp. 386–392.

152) Penrose, H.W.; "Electric motor repair for low voltage induction motors in PWM inverter duty environments," *Proceedings of Electrical Insulation and Electrical Manufacturing and Coil Winding Conference (Cat. No. 97CH36075)*, pp. 841–848.

153) EPRI Project RP2307.

154) Guide for testing turn-to-turn insulation on form-wound stator coils for AC rotating electric machines – for trial use, *IEEE Standard 522*.

155) Hirst, E.; "A good integrated resource plan: guidelines for electric utilities and regulators," ORNL/CON-354, Oak Ridge National Laboratory, Oak Ridge, TN.

156) Eto, J.; Vine, E.; Shown, L.; Sonnenblick, R.; and Payne, C.; "The cost and performance of utility commercial lighting programs," LBL-34967, Lawrence Berkley National Laboratory, Berkeley, CA, 1994.

157) Hadley, S.; and Hirst, E.; "Utility DSM programs from 1989 through 1998: continuation or crossroad," ORNL/CON-405, Oak Ridge National Laboratory, Oak Ridge, TN, 1995.

158) ERPI, "1992 Survey of utility demand-side management programs," prepared by Plexus Research Inc. and Scientific Communications Inc., Palo Alto, CA, 1993.

159) Eco Northwest; "Environmental externalities and electric utility regulation," Report prepared for National Association of Regulatory Utility Commissioners, Washington DC, 1993.

160) Leeb, S.B.; Shaw, S.; and Kirtley, J.L.; 1995, "Transient event detection in spectral envelope estimates for non-intrusive load monitoring," *IEEE Transactions on Power Delivery*, Vol. 10, No. 3, pp. 1200–1210.

161) Heydt, G.T.; Ayyanar, R.; and Thallam, R.; "Power acceptability," *IEEE Power Engineering Review*, September 2001, pp. 12–15.

162) Collins Jr., E.R.; and Morgan, R.L.; "Three phase sag generator for testing industrial equipment," *IEEE Transactions on Power Delivery*, Vol. 11, Jan. 1996, pp. 526–532.

163) Key, T.; "Predicting behavior of induction motors during service faults and interruptions," *IEEE Ind. Applicat. Mag.*, Vol. 1, No. 1, Jan./Feb. 1995, p. 7.

164) Waggoner, R.; "Understanding the CBEMA curve," *Elect. Construction and Maintenance*, Vol. 90, No. 10, Oct. 1991, pp. 55–57.

165) Turner, A.E.; and Collins, E.R.; "The performance of AC contactors during voltage sags," *Proc. IEEE Int. Conf. Harmonics and Quality of Power*, Las Vegas, NV, Oct. 1996, pp. 589–595.

166) McGranaghan, M.; and Roettger, W.; "Economic evaluation of power quality," *IEEE Power Engineering Review*, February 2002, pp. 8–12.

167) *IEEE Recommended Practice for Monitoring Electric Power Quality*, IEEE Standard 1159, 1995.

168) *Specification for Semiconductor Processing Equipment Voltage Sag Immunity*, SEMI F47-0200.

169) *IEEE Recommended Practice for Evaluating Electric Power System Compatibility with Electronic Process Equipment*, IEEE Standard 1346, 1998.

170) IEEE Std. 446-1980, IEEE Recommended Practice for Emergency and Standby Power Systems for Industrial and Commercial Applications (orange book), John Wiley & Sons, Inc.

171) http://www.upei.ca/~physics/p261/projects/flywheel1/flywheel1.htm

172) http://www.doc.ic.ac.uk/~matti/ise2grp/energystorage_report/node8.html

173) http://www.mpoweruk.com/supercaps.htm

174) http://electricitystorage.org/technologies_applications.htm

175) Masoum, M.S.; Dehbonei, H.; and Fuchs, E.F.; Closure of "Theoretical and experimental analyses of photovoltaic systems with voltage- and current-based maximum power tracking," *IEEE Transactions on Energy Conversion*, Vol. 19, No. 3, September 2004, pp. 652–653.

176) Wang, C.; Nehrir, M.H.; and Shaw, S.R.; "Dynamic models and model validation for PEM fuel cells using electrical circuits," *IEEE Transactions on Energy Conversion*, Vol. 20, No. 2, June 2005, pp. 442–451.

177) Dubey, G.K.; *Power Semiconductor Controlled Drives*, Prentice Hall, Englewood Cliffs, NJ, 1989.

178) Schenk, K.F.; Fuchs, E.F.; and Trutt, F.C.; "Load analysis of nonlinear homopolar inductor alternators," *IEEE Transactions on Power Apparatus and Systems*, March/April 1973, Vol. PAS-92, No. 2, pp. 442–448.

ST. GEORGE POLYTECHNIC LIBRARY

179) Siegl, M.; Fuchs, E.F.; and Erdelyi, E.A.; "Medium frequency homopolar inductor alternators with amortisseur bars connected to rectifiers, part 1: saturated position-dependent reactances," Proceedings of the Midwest Power Symposium, Cincinnati, Ohio, October 1973.

180) Siegl, M.; Fuchs, E.F.; and Erdelyi, E.A.; "Medium frequency homopolar inductor alternators with amortisseur bars connected to rectifiers, part 2: the effect of reduced subtransient reactance on rectifier operation," *Proceedings of the Midwest Power Symposium*, Cincinnati, Ohio, October 1973.

181) Fuchs, E.F.; and Frank, U.V.; "High-speed motors with reduced windage and eddy current losses, part I: mechanical design," *ETZ Archiv*, Vol. 5, January 1983, H.1, pp. 17–23.

182) Fuchs, E.F.; and Frank, U.V.; "High-speed motors with reduced windage and eddy current losses, part II: magnetic design," *ETZ Archiv*, Vol. 5, February 1983, H.2, pp. 55–62.

183) Appelbaum, J.; "Starting and steady-state characteristics of dc motors powered by solar cell generators," *IEEE Transactions on Energy Conversion*, Vol. EC-1, No. 1, March 1986, pp. 17–25.

## 8.11 ADDITIONAL BIBLIOGRAPHY

184) Hart, G.W.; "Non-intrusive appliance load monitoring," *Proceedings of IEEE, 80*, (12), 1992, pp. 1870–1891.

ST. GEORGE POLYTECHNIC COLLEGE OF LANE



185) Krarti, M.; Kreider, J.; Cohen, D.; and Curtiss, P.; "Estimation of energy savings for building retrofits using neural networks," *ASME Transactions Journal of Solar Energy Engineering*, Vol. 120, No. 3. 1998.

186) Krarti, M.; *Energy Audit for Building Systems: An Engineering Approach*, CRC Press, Boca Raton, FL, 2000.

187) Fuchs, E.F.; and Fuchs, H.A.; "Distributed generation and frequency/load control of power systems," *Proceedings of the 40th Annual Frontiers of Power Conference*, Oklahoma State University, Stillwater, Oklahoma, October 29–30, 2007, pp. II-1 to II-9.

188) Fuchs, E.F.; and Fuchs, F.S.; "Intentional islanding - maintaining power systems operation during major emergencies," *Proceedings of the 10th IASTED International Conference on Power and Energy Systems (PES 2008)*, Baltimore, Maryland, April 16–18, 2008.

189) Fuchs, E.F.; and Fuchs, H.A.; "Power quality of electric machines and power systems," *Proceedings of the 8th IASTED International Conference on Power and Energy Systems (EuroPES 2008)*, Corfu, Greece 2008, June 16–18, 2008.

# 9
CHAPTER

# The Roles of Filters in Power Systems

The implementation of harmonic filters has become an essential element of electric power networks. With the advancements in technology and significant improvements of power electronic devices, utilities are continually pressured to provide high-quality and reliable energy. Power electronic devices such as computers, printers, fax machines, fluorescent lighting, and most other office equipment generate harmonics. These types of devices are commonly classified as nonlinear loads. These loads (e.g., rectifiers, inverters) create harmonics by drawing current in short pulses rather than in a sinusoidal manner.

Harmonic currents and the associated harmonic powers must be supplied from the utility system. The major issues associated with the supply of harmonics to nonlinear loads are severe overheating: increased operating temperatures of generators and transformers degrade the insulation material of their windings. If this heating were continued to the point at which the insulation fails, a flashover would occur. This would partially or permanently damage the device and result in loss of generation or transmission that could cause blackouts. Impacts of harmonics on the insulation of transformers and electrical machines are discussed in Chapter 6.

One solution to this problem is to install a harmonic filter for each nonlinear load connected to the power system. There are different types of harmonic filters including passive, active, and hybrid configurations [1–8]. The installation of active filters proves indispensable for solving power quality problems in distribution networks such as the compensation of harmonic current and voltage, reactive power, voltage sags, voltage flicker, and negative-phase sequence currents. Ultimately, this would ensure a system with increased reliability and better power quality.

Filters can only compensate harmonic currents and/or harmonic voltages at the installed bus and do not consider the power quality of other buses. On the other hand, as the number of nonlinear loads increases, more harmonic filters are required. New generations of active filters are unified power quality conditioners (UPQCs) and active power line conditioners (APLCs). The UPQCs are discussed in Chapter 11.

This chapter begins with a discussion of the different types of nonlinear loads. Section 9.2 presents a broad classification of filters as they are employed in supply systems, and thereafter the subclassification of filters according to their topology. The next three sections focus on different types of filter topologies including passive, active, and hybrid configurations. Block diagrams of active filters are reviewed in Section 9.6. Detailed discussion and classification of control methods for active and hybrid filters are presented in Section 9.7. The chapter ends with general comments and conclusions.

## 9.1 TYPES OF NONLINEAR LOADS

There are three main types of nonlinear loads in power systems: current-source loads, voltage-source loads, and their combinations.

The first category of nonlinear loads includes the current-source (current-fed or current-stiff) loads. Traditionally, most nonlinear loads have been represented as current sources because their current waveforms on the AC side are distorted. Examples of this category include the phase-controlled thyristor rectifier with a filter inductance on the DC side of the rectifier resulting in DC currents (Fig. 9.1); thyristor rectifiers convert an AC voltage source to a DC current source supplying current-source inverters (CSIs) and high-voltage DC (HVDC) systems, and diode rectifiers with sufficient filter inductance supply DC loads. In general, highly inductive loads are served by silicon-controlled rectifiers (SCRs) converting AC power to DC power. Of course, the inverse operation – where an inverter supplies AC power from a DC power source – results in similar current distortions (e.g., harmonics) on the AC side of the inverter. The transfer characteristics and resulting harmonic currents of current-source nonlinear loads are less dependent on the circuit parameters of the AC side than those on the DC side. Accordingly, passive shunt, active shunt, or hybrid (e.g., a combination of active shunt in series


ISBN 978-0-12-369536-9
© Elsevier Inc. All rights reserved.

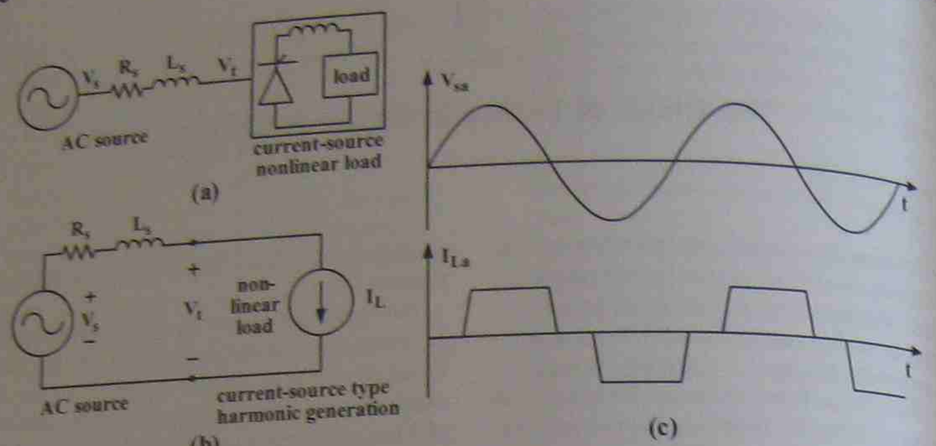



**FIGURE 9.1** Typical current-source nonlinear load: (a) thyristor rectifier for DC drives, (b) per-phase equivalent circuit of thyristor rectifier, (c) typical phase-voltage and line-current waveforms of thyristor rectifier.

with passive shunt) filters for harmonic compensation are commonly applied on the AC side of the converters serving nonlinear loads. The principle of the passive shunt filter is to provide a low-impedance shunt branch for the harmonic currents caused by the nonlinear load. These passive filters have been applied in Chapter 1. The principle of the active shunt filter is to inject into the power system harmonic currents with the same amplitudes and opposite phases of the harmonic currents due to nonlinear loads, thus eliminating harmonic current flowing into the AC source.

The second category of nonlinear loads comprises voltage-source (or voltage-fed or voltage-stiff) loads, such as diode rectifiers with a capacitive filter at the DC link feeding variable-frequency voltage-source inverter (VSI)-based AC motor drives, power supplies with front-end diode rectifier and capacitive filters installed in computers and other household appliances, battery chargers, etc. These voltage-stiff loads draw discontinuous and nonsinusoidal currents resulting in very high $THD_i$, low power factor, and distortions of the AC terminal voltage at the point of common coupling (PCC) defined in Chapter 1. These loads generate harmonic voltage sources, rather than harmonic current sources (Fig. 9.2). Their harmonic amplitudes are greatly affected by the AC side impedance and source voltage imbalance, whereas their rectified voltages are less dependent on the impedance of the AC system. Therefore, diode rectifiers behave like a voltage source, rather than a current source. Accordingly, passive series, active series, or hybrid (e.g., a combination of active series with passive series) filters are relied on to compensate distortions due to nonlinear loads. Current-source and voltage-source nonlinear loads exhibit dual relations to one another with respect to circuits and properties, and can be effectively compensated by parallel and series filters discussed in Chapter 1, respectively [1].

The third category of nonlinear loads is characterized by the combination of current- and voltage-source loads. They are neither of the current-source nor of the voltage-source type and may contain loads of both kinds. For example, adjustable-speed drives behave as several types of nonlinear loads; variable-frequency VSI-fed AC motors perform as voltage-stiff loads, whereas CSI-fed AC motor drives act as current-stiff loads. For these loads a hybrid topology consisting of active series with passive shunt filter elements is appropriate, provided that the power supply is ideal and adjustable reactive power compensation is not required.

The assessment of harmonic injection of nonlinear loads may not be easy and depends on the following [4]:

- type and topology of nonlinear loads producing harmonics. A voltage-source converter with diode front end may inject an entirely different harmonic spectrum as compared with a current-source converter. Switching power supplies, pulse-width-modulation (PWM) drives, cycloconverters, and arc furnaces have their own specific harmonic spectra;
- interaction of nonlinear loads with the AC system impedance; and



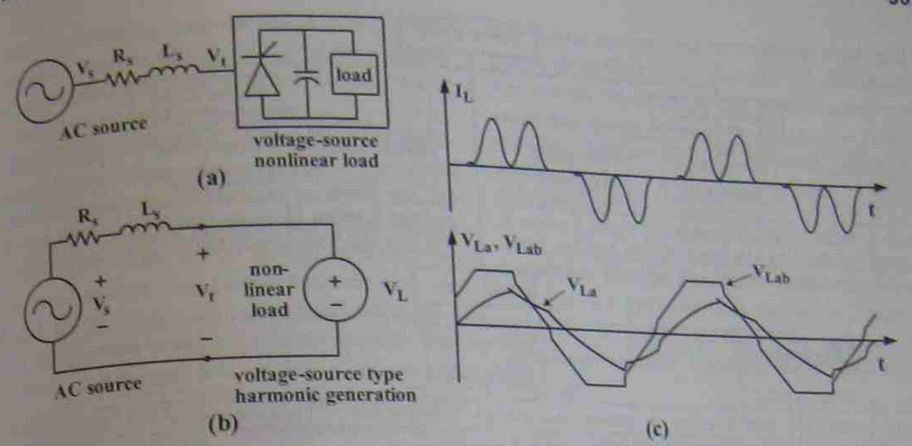



**FIGURE 9.2** Typical voltage-source nonlinear load: (a) diode rectifier for AC drives, electronic equipment, etc., (b) per-phase equivalent circuit of diode rectifier, (c) typical line-current and phase and line-to-line voltage waveforms of thyristor rectifier.

- the harmonic spectra may vary as a function of the nonlinear load. For example, the input AC waveform to a current-source converter and its ripple content depends on the firing angle $\alpha$ and the length of the commutation interval – due to the commutating inductance – as pointed out in Chapter 1. In addition, a small amount of noncharacteristic harmonics may be generated. Therefore, worst-case scenarios should be considered for the analyses of these load types.

## 9.2 CLASSIFICATION OF FILTERS EMPLOYED IN POWER SYSTEMS

During the past few decades the number and types of nonlinear loads have tremendously increased. This has motivated the utilities and consumers of electric power to implement different harmonic filters. Filters are capable of compensating harmonics of nonlinear loads through current-based compensation. They can also improve the quality of the AC supply, for example, compensating voltage harmonics, sags, swells, notches, spikes, flickers, and imbalances through voltage-based techniques. Filters are usually installed near or close to the points of distortion, for example, across nonlinear loads, to ensure that harmonic currents do not interact with the power system. They are designed to provide a bypass for the harmonic currents, to block them from entering the power system, or to compensate them by locally supplying harmonic currents and/or harmonic voltages. Filters can be designed to trap harmonic currents and shunt them to ground through the use of capacitors, coils, and resistors. Due to the lower impedance of a filter element (at a certain frequency) in comparison to the impedance of the AC source, harmonic currents will circulate between the load and the filter and do not affect the entire system; this is called series resonance as defined in Chapter 1. A filter may contain several of these filter elements, each designed to compensate a particular harmonic frequency or an array of frequencies. Filters are often the most common solution approaches that are used to mitigate harmonics in power systems. Unlike other solutions, filters offer a simple and inexpensive alternative with high benefits.

Classifications of filters may be performed based on various criteria, including the following:

- number and type of elements (e.g., one, two, or more passive and/or active filters),
- topology (e.g., shunt-connected, series-connected, or a combination of the two),
- supply system (e.g., single-phase, three-phase three-wire, and three-phase four-wire),
- type of nonlinear load such as current-source and/or voltage-source loads,
- power rating (e.g., low, medium, and high power),
- compensated variable (e.g., harmonic current, harmonic voltage, reactive power, and phase balancing, as well as multiple compensation),

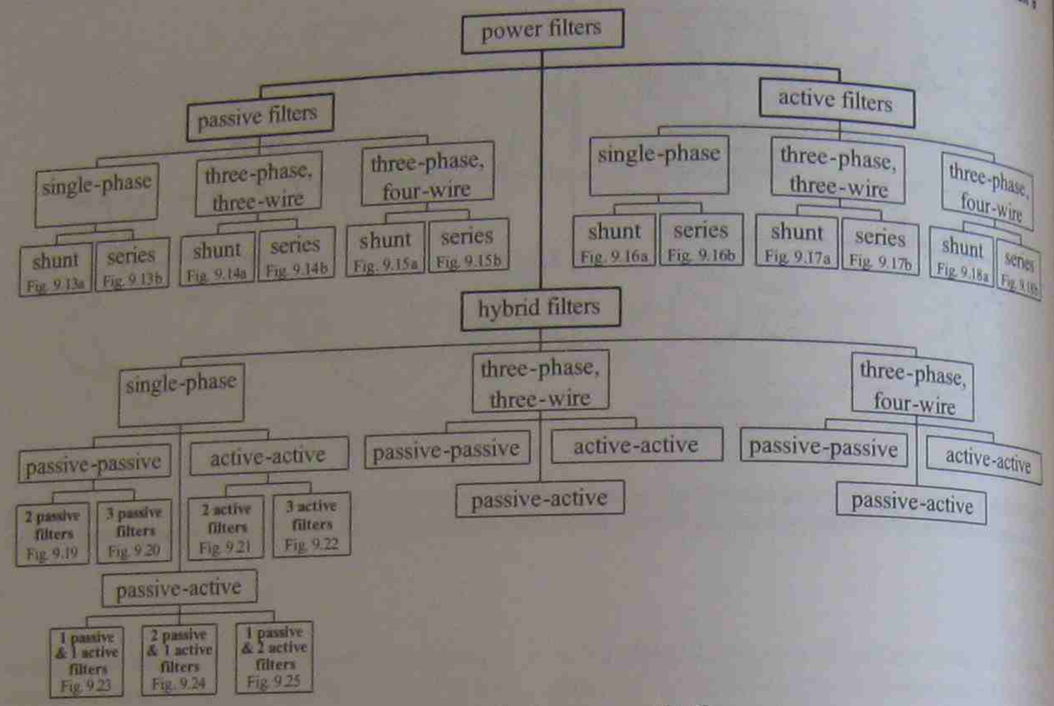



**FIGURE 9.3** Classification of filters used for power quality improvement [1–5].

- converter type (e.g., VSI and/or CSI to realize active elements of filter),
- control technique (e.g., open loop, constant capacitor voltage, constant inductor current, linear voltage control, or optimal control), and
- reference estimation technique (e.g., time and/or frequency current/voltage reference estimation).

Various topologies such as passive filter (PF), active filter (AF), and hybrid filter (HF) in shunt, series, and shunt/series for single-phase, three-phase three-wire, and three-phase four-wire systems have been installed using current-source inverters and voltage-source inverters for implementation of the control of active filters. Figure 9.3 shows the classification of filters as used in power systems based on the supply system with the topology as a subclassification [1–5]. Further classification is made on the basis of the numbers and types of elements employed in different topologies. According to Fig. 9.3, there are 156 valid configurations of passive, active, and hybrid filters. Each class of filters offers its own unique solution to improve the quality of electric power. The choice of filter depends on the nature of the power quality problem, the required level and speed of compensation, as well as the economic cost associated with its implementation.

## 9.3 PASSIVE FILTERS AS USED IN POWER SYSTEMS

If a nonlinear load is locally causing significant harmonic distortion, passive filters may be installed to prevent the harmonic currents from being injected into the system. Passive filters are inexpensive compared with most other mitigating devices. They are composed of only passive elements (inductances, capacitances, and resistances) tuned to the harmonic frequencies of the currents or voltages that must be attenuated. Passive filters have better performances when they are placed close to the harmonic-producing nonlinear loads. They create a sharp parallel resonance at a frequency below the notch (tuned) frequency as introduced in Chapter 1. The resonant frequency of the power system must be carefully placed far from any significant harmonic distortion caused by the nonlinear load. For this reason, passive filters should be tuned slightly lower than the harmonic to be attenuated. This will provide a margin of safety in case there is some change in the system parameters. Otherwise, variations in either filter capacitance and/or filter inductance (e.g., with temperature or failure) might shift resonance conditions such that harmonics cause problems in the power system. In practice, passive filters are added



to the system starting with the lowest order of harmonics that must be filtered; for example, installing a seventh-harmonic filter usually requires that a fifth-harmonic filter also be included.

There are various types of passive filters for single-phase and three-phase power systems in shunt and series configurations. Shunt passive filters are the most common type of filters in use. They provide low-impedance paths for the flow of harmonic currents. A shunt-connected passive filter carries only a fraction of the total load current and will have a lower rating than a series-connected passive filter that must carry the full load current. Consequently, shunt filters are desirable due to their low cost and fine capability to supply reactive power at fundamental frequency. It is possible to use more than one passive filter in either shunt and/or series configuration. These topologies are classified as passive–passive single- and three-phase hybrid filters (Fig. 9.3) and will be discussed in Section 9.5. The structure chosen for implementation depends on the type of the dominant harmonic source (voltage source, current source) and the required compensation function (e.g., harmonic current or voltage, reactive power).

### 9.3.1 Filter Transfer Function

Transfer functions are extensively used for filter design and system modeling. Figure 9.4a shows the single-phase presentation of a balanced three-phase distribution system with a nonlinear load and a passive shunt filter installed at the PCC. At harmonic frequencies, the system can be approximated by the equivalent circuit of Fig. 9.4b. Three main types of transfer functions can be defined: impedance, current-divider, and voltage-divider transfer functions.

**Impedance Transfer Functions.** Impedance transfer functions are the most basic blocks for design and modeling of power systems. Two types of filter impedance transfer functions have been defined (Fig. 9.4):

- ***Filter impedance transfer function*** is the impedance frequency response of the filter expressed in the s domain as

$$H_f(s) = Z_f(s) = \frac{V_f(s)}{I_f(s)}, \qquad (9\text{-}1a)$$

where $Z_f(s)$, $V_f(s)$, and $I_f(s)$ are the filter impedance, complex voltage, and current, respectively, and $s = j\omega$ is the Laplace operator.

- ***Filter system impedance transfer function*** is defined after the filter is designed and connected to the network. It is the impedance frequency response of the system (with the filter installed) expressed in the s domain:

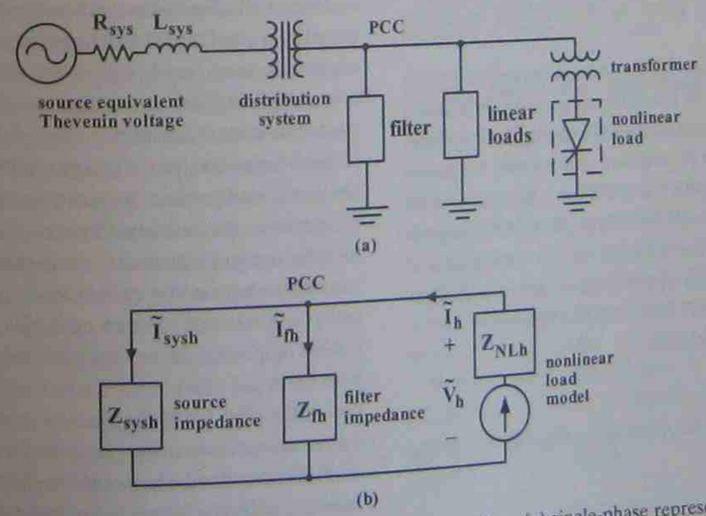



**FIGURE 9.4** Distribution system with nonlinear load and passive shunt filter; (a) single-phase representation, (b) equivalent circuit for harmonic (of order h) filter installation, see Chapter 1.

$$H_{fsys}(s) = Z_{fsys}(s) = \frac{V_{sys}(s)}{I_f(s) + I_{sys}(s)} = \frac{1}{\frac{1}{Z_f(s)} + \frac{1}{Z_{sys}(s)}}, \quad (9\text{-}1b)$$

where $Z_{fsys}(s)$ is the impedance of the system after the connection of the filter and $V_{sys}(s)$ and $I_{sys}(s)$ are the system complex voltage and current, respectively.

**Current-Divider Transfer Functions.** Two types of current-divider transfer functions are derived for a filter (Fig. 9.4):

- $H_{cds}(s)$ is the ratio of system (sys) harmonic current to the injected harmonic nonlinear (NL) current:

$$H_{cds}(s) = \frac{I_{sys}(s)}{I_{NL}(s)} = \frac{Z_f(s)}{Z_f(s) + Z_{sys}(s)} = \rho_{sys}(s). \quad (9\text{-}2a)$$

- $H_{cdf}(s)$ is the ratio of filter (f) harmonic current to injected harmonic nonlinear current:

$$H_{cdf}(s) = \frac{I_f(s)}{I_{NL}(s)} = \frac{Z_{sys}(s)}{Z_f(s) + Z_{sys}(s)} = \rho_f(s). \quad (9\text{-}2b)$$

In Eqs. 9-2, $\rho_{sys}(s)$ and $\rho_f(s)$ are complex quantities that determine the distribution of the harmonic currents in the filter and the system and have been introduced in Chapter 1. A properly designed filter will have $\rho_f(s)$ close to unity, typically 0.995, and $\rho_{sys}(s)$ about 0.045 with the corresponding angles of about 2.6° and 81°, respectively. It is desirable that $\rho_{sys}(s) = \rho_{sys}(j\omega)$ be small at the various occurring harmonics.

According to Eqs. 9-2 the system impedance plays an important role in the filtering process. Without a filter, all harmonic currents pass through the system. For a large system impedance and a given harmonic frequency, the bypass via the filter is perfect and all current harmonics will flow through the filter impedance. Conversely, for a system of low impedance at a given harmonic frequency most current of harmonic frequency will flow into the system.

It is easy to show that

$$H_{cdf}(s) = \frac{Z_{sys}(s)}{Z_f(s)} H_{cds}(s) = \frac{1}{Z_f(s)} H_{fsys}(s), \quad (9\text{-}3a)$$

$$H_{cds}(s) = \frac{1}{Z_{sys}(s)} H_{fsys}(s). \quad (9\text{-}3b)$$

When designing a filter the impedance transfer functions (Eqs. 9-1) can be used to evaluate the overall system performance. After the filter is installed, computed and measured current-divider ratios (Eqs. 9–2) can be plotted to evaluate filter performance and determine whether harmonic current distortion limits comply with the IEEE-519 Standard [11], as discussed in Chapter 1 (Application Examples 1.8 and 1.9).

**Voltage-Divider Transfer Functions.** Similar transfer functions can be developed for systems with loads that are sensitive to harmonic voltages. Filters are used to provide frequency detuning or voltage distortion control. These transfer functions are based on a voltage division between an equivalent harmonic voltage source – representing nonlinear loads – and harmonic sensitive loads. Applications of these transfer functions are concerned with the voltage distortion amplification of shunt power factor capacitors due to parallel and series resonances.

### 9.3.2 Common Types of Passive Filters for Power Quality Improvement

The configuration of a filter depends on the frequency spectrum and nature of the distortion. Figure 9.5 depicts common types of passive filters.

The first-order damped and undamped high-pass filter (Fig. 9.5a with and without the resistor, respectively) is used to attenuate high-frequency current harmonics that cause telephone interference, reduce voltage notching caused by commutation of SCRs, and provide partial displacement power factor correction of the fundamental load current. The single-tuned low-pass (also called band-pass or second-order series resonant band-pass) filter (Fig. 9.5b) is most commonly applied for mitigation of a single dominant low-order harmonic. Fig. 9.5c represents a second-order damped high-pass filter. Most nonlinear loads and devices generate more than one harmonic, however, and one filter is not usually adequate to effectively compensate, mitigate, or reduce all harmonics within the power system. There are different approaches to overcome this problem.

One approach is to use two single-tuned filters with identical characteristics to form a double band-pass filter (Fig. 9.5d). In practice, there is more than one dominant low-order harmonic and combinations of three or more single-tuned filters are applied. Starting with the lowest harmonic order (e.g., 5th), each filter is tuned to one harmonic frequency. This approach is not practical when the number of dominant low-order harmonics is large and/or higher order harmonics are present.



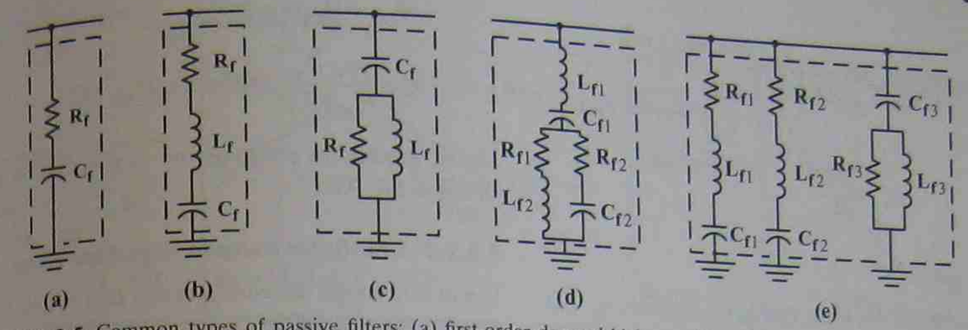



**FIGURE 9.5** Common types of passive filters; (a) first-order damped high-pass filter, (b) second-order series resonant band-pass filter, (c) second-order damped high-pass filter, (d) fourth-order double band-pass filter, (e) composite filter consisting of two band-pass filters and one high-pass filter.

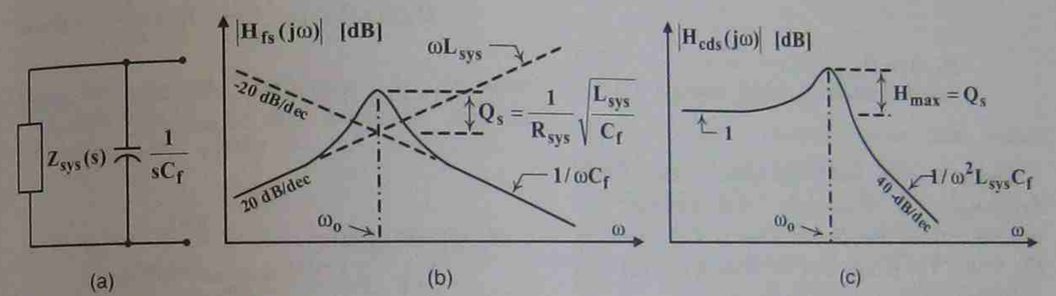



**FIGURE 9.6** First-order high-pass filter; (a) equivalent circuit, (b) filter system impedance transfer function, (c) current-divider transfer function.

Another approach is to use a first-order high-pass filter (consisting of a resistor connected in series with a capacitor) or a second-order high-pass filter (consisting of a series capacitor and a parallel combination of inductor and resistor; Fig. 9.5c) and set the resonant frequency below the lowest order dominant harmonic frequency. However, the $Z - \omega$ plot of a second-order high-pass filter shows that the minimum impedance of this filter (e.g., in the pass-band region) is higher than that of a single-tuned band-pass filter. Therefore, the high-pass filter allows a percentage of all harmonics above its notch frequency to pass through and will result in large fundamental filter rating and high resistive losses. This filter is commonly applied for higher frequencies and notch reduction.

The third and most implemented approach is to install a composite filter consisting of two or more branches of band-pass filters tuned at low-order harmonic frequencies and a parallel branch of high-pass filter tuned at higher frequencies (called a passive filter element; Figs. 9.5e, 9.11, and 9.12). This configuration is suitable for most residential, domestic, and industrial nonlinear loads such as arc furnaces. In addition, there are other configurations of higher order filters (e.g., third-order damped filter) for transmission systems.

This section derives the equations and general relations of basic filter types.

#### 9.3.2.1 First-Order, High-Pass Filter

A first-order, high-pass filter consists of a shunt capacitor (Fig. 9.6a) and can be used to attenuate high-frequency harmonic current components causing telephone interference, to reduce voltage notching (e.g., caused by rectifier commutation), and to improve the displacement (fundamental) load power factor. Such filters are amply described in currently available circuit textbooks [12, 13].

If the system impedance is purely inductive ($Z_{sys}(s) = sL_{sys}$), filter impedance and filter system impedance transfer functions can be derived using Eqs. 9-1:

$$H_f(s) = Z_f(s) = \frac{V_f(s)}{I_f(s)} = \frac{1}{sC_f}, \quad (9\text{-}4a)$$

$$H_{fsys}(s)=Z_{fsys}(s)=\frac{V_{sys}(s)}{I_f(s)+I_{sys}(s)}=\frac{1}{\frac{1}{Z_f(s)}+\frac{1}{Z_{sys}(s)}}$$

$$=\frac{1}{sC_f+\frac{1}{sL_{sys}}}. \qquad (9\text{-}4b)$$

The order of this filter, that is, the highest exponent of the characteristic (denominator) polynomial of $H_f(s)$, is one.

The current-divider transfer function, Eq. 9-2a, can be derived as

$$H_{cds}(s)=H_{cds}(j\omega)=\frac{\frac{1}{j\omega C_f}}{j\omega L_{sys}+\frac{1}{j\omega C_f}}. \qquad (9\text{-}5)$$

Simple algebra yields analytical (closed-form) expressions for asymptotes, local maxima, and minima of these transfer functions as is illustrated in Fig. 9.6b,c. The procedures for plotting $H_{cds}(j\omega)$ on a logarithm paper as shown in Fig. 9.6c are

- For low frequencies
  $(\omega << 1/\sqrt{L_{sys}C_f} \Rightarrow |1/j\omega C_f| >> |j\omega L_{sys}|)$:

$$H_{cds}(j\omega)\approx\frac{\frac{1}{j\omega C_f}}{\frac{1}{j\omega C_f}}=1.$$

Therefore, the roll-off of the low-frequency components is one or 0 dB per decade.

- For high frequencies
  $(\omega >> 1/\sqrt{L_{sys}C_f} \Rightarrow |1/j\omega C_f| << |j\omega L_{sys}|)$:

$$H_{cds}(j\omega)\approx\frac{\frac{1}{j\omega C_f}}{j\omega L_{sys}}=\frac{-1}{\omega^2 L_{sys}C_f}.$$

Therefore, the roll-off of the high frequency components is $1/\omega^2$ or –40 dB per decade.

If system resistance is included $(Z_{sys}(s)=R_{sys}+sL_{sys})$, the maximum can be found as

$$H_{cds}(s=j\omega)|_{\omega=\frac{1}{\sqrt{L_{sys}C_f}}}=-j\frac{1}{R_{sys}}\sqrt{\frac{L_{sys}}{C_f}}$$

and

$$H_{max}=|H_{cds}(s=j\omega)|_{\omega=\frac{1}{\sqrt{L_{sys}C_f}}} \quad \text{with}$$

$$Q=\frac{1}{R_{sys}}\sqrt{\frac{L_{sys}}{C_f}}, \text{ therefore, } H_{max}=Q.$$

Similar procedures are relied on to plot $H_{fs}(j\omega)$ as shown in Fig. 9.6b.

### 9.3.2.2 First-Order Damped High-Pass Filter

Figure 9.7a shows the configuration of a first-order damped high-pass filter. A series connected resistance ($R_f$) is included to provide a damping characteristic.

Filter transfer functions are

$$H_f(s)=Z_f(s)=\frac{V_f(s)}{I_f(s)}=R_f+\frac{1}{sC_f}. \qquad (9\text{-}6a)$$

$$H_{fsys}(s)=Z_{fsys}(s)=\frac{1}{\frac{1}{R_f+1/sC_f}+\frac{1}{sL_{sys}}}, \qquad (9\text{-}6b)$$

$$H_{cds}(s)=H_{cds}(j\omega)=\frac{R_f+\frac{1}{j\omega C_f}}{R_f+\frac{1}{j\omega C_f}+j\omega L_{sys}}. \qquad (9\text{-}6c)$$

As discussed in the previous section, $H_{cds}(s)$ can be determined analytically (Fig. 9.7c):

- For low frequencies
  $(\omega << 1/\sqrt{L_{sys}C_f} \Rightarrow |1/j\omega C_f| >> |j\omega L_{sys}|)$:

$$H_{cds}(j\omega)\approx\frac{\frac{1}{j\omega C_f}}{\frac{1}{j\omega C_f}}=1.$$

- For moderate high frequencies
  $(1/\sqrt{L_{sys}C_f} < \omega < 1/R_fC_f \Rightarrow |1/j\omega C_f| << |j\omega L_{sys}|)$:

$$H_{cds}(j\omega)\approx\frac{\frac{1}{j\omega C_f}}{j\omega L_{sys}}=\frac{-1}{\omega^2 L_{sys}C_f}$$

$\Rightarrow$ roll-off is $1/\omega^2$ or – 40 dB per decade.

- For high frequencies ($\omega >> 1/R_fC_f \Rightarrow R_f \gg |1/j\omega C_f|$ and $|j\omega L_{sys}| >> |R_f + 1/j\omega C_f|$):

$$H_{cds}(j\omega)=\frac{R_f+\frac{1}{j\omega C_f}}{j\omega L_{sys}+\left(R_f+\frac{1}{j\omega C_f}\right)}\approx\frac{R_f}{j\omega L_{sys}}$$

$\Rightarrow$ roll-off is $1/\omega$ or – 20 dB per decade.





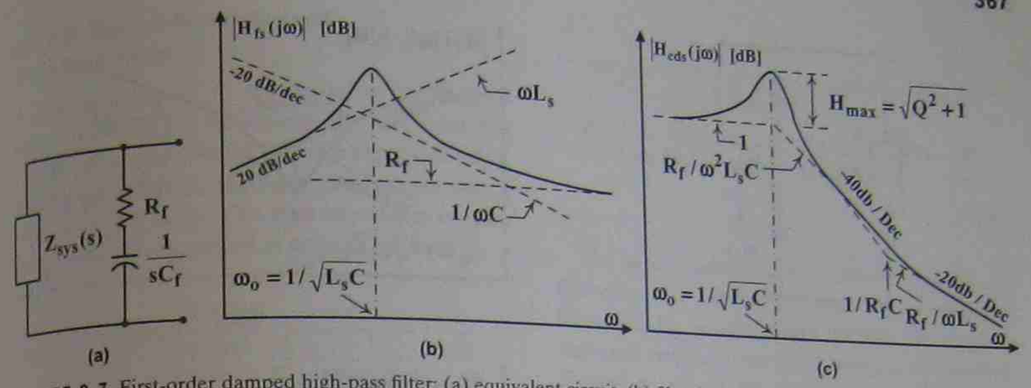



**FIGURE 9.7** First-order damped high-pass filter; (a) equivalent circuit, (b) filter impedance transfer function, (c) current-divider transfer function.

- If the system resistance is included $(Z_{sys}(s)=R_{sys}+sL_{sys})$, the maximum can be found as

$$H_{cds}(s=j\omega)|_{\omega=\frac{1}{\sqrt{L_{sys}C_f}}}=1-j\frac{1}{R_{sys}}\sqrt{\frac{L_{sys}}{C_f}}$$

and

$$H_{max}=|H_{cds}(s=j\omega)|_{\omega=\frac{1}{\sqrt{L_{sys}C_f}}}=\sqrt{Q^2+1}\approx Q$$

with $Q=\frac{1}{R_{sys}}\sqrt{\frac{L_{sys}}{C_f}}$.

Similar procedures are employed to plot $H_{fs}(j\omega)$ as illustrated in Fig. 9.7b. Comparison of Figs. 9.6 and 9.7 indicates the following:

- the damping resistance significantly limits the high-frequency performance (e.g., roll-off of high-frequency components is only $1/\omega$ or –20 dB per decade). Therefore, the damped filter is less desirable for telephone interference reduction applications; and
- for parallel resonant conditions (e.g., cancellation of $L_{sys}$ by $C_f$), if the resonant frequency falls on or near a critical harmonic frequency, a high-pass damping resistance ($R_f$) can be used to control and reduce the amplification. However, this will increase the fundamental frequency power loss and reduces the effectiveness of the high-pass attenuation above the frequency $1/(R_fC_f)$.

### 9.3.2.3 Second-Order Band-Pass Filter

The second-order band-pass filter (also called single-tuned or series-resonant filter) is a series combination of capacitor ($C_f$), inductor ($L_f$), and a small damping resistor ($R_f$), as depicted in Fig. 9.8a. The damping resistance is usually due to the internal resistance of either the inductor and/or capacitor. This filter is tuned to attenuate one single low-order harmonic. Typically, combinations of band-pass filters are used because the power system contains a number of dominant low-order harmonics.

Assuming a pure inductive system ($Z_{sys}(s)=sL_{sys}$), filter transfer functions can be derived using Eqs. 9-1a and 9-2a:

$$H_f(s)=Z_f(s)=\frac{V_f(s)}{I_f(s)}=R_f+sL_f+\frac{1}{sC_f}$$

$$=\frac{A}{s}\left[1+\frac{1}{Q}\left(\frac{s}{\omega_0}\right)+\left(\frac{s}{\omega_0}\right)^2\right]. \qquad (9\text{-}7)$$

$$H_{cds}(s)=H_{cds}(j\omega)=\frac{R_f+j\omega L_f+\frac{1}{j\omega C_f}}{R_f+j\omega L_f+\frac{1}{j\omega C_f}+j\omega L_{sys}}. \qquad (9\text{-}8)$$

where A is the gain. The filter quality factor (Q) and the series-resonant frequency ($\omega_0$) are

$$Q=\frac{1}{R_f}\sqrt{\frac{L_f}{C_f}}. \qquad (9\text{-}9a)$$

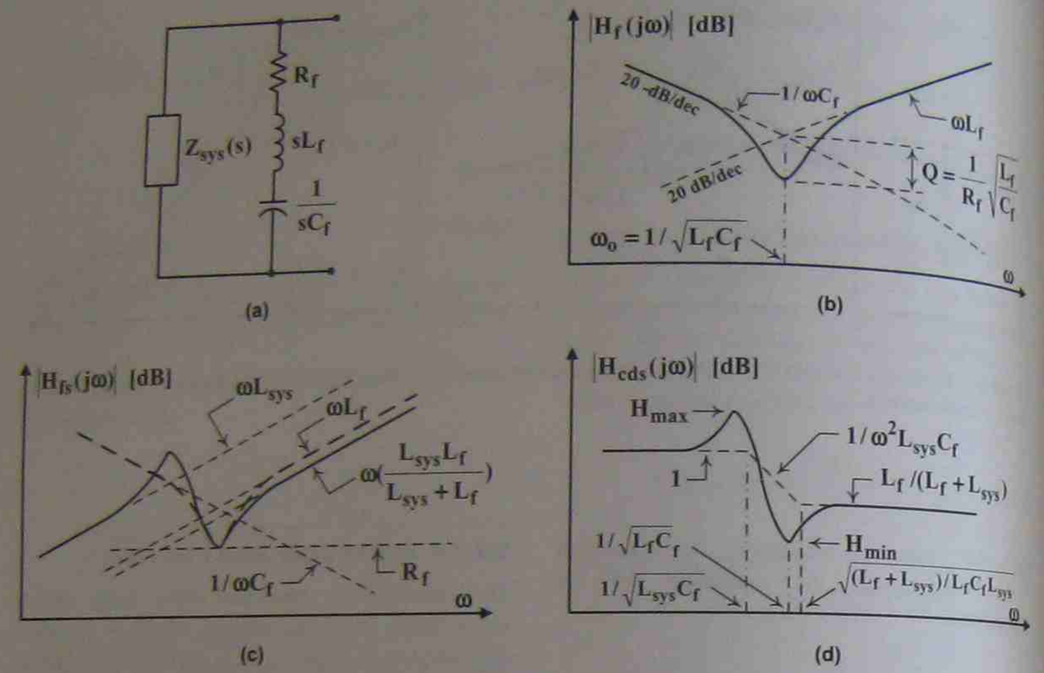



**FIGURE 9.8** Second-order band-pass filter; (a) equivalent circuit, (b) filter impedance transfer function, (c) filter system impedance transfer function with $L_{sys} > L_f$, (d) current-divider transfer function with $L_{sys} > L_f$.

$$\omega_0 = \frac{1}{\sqrt{L_f C_f}}. \tag{9-9b}$$

For high-voltage applications, the filter current has a low rms magnitude and does not require large current carrying conductors; therefore, air-core inductors are regularly used and the filter quality factor is relatively large (e.g., $50 < Q < 150$). For low-voltage applications, gapped iron-core inductors and conductors with a large cross section are employed (e.g., $10 < Q < 50$).

The filter impedance transfer function ($H_f(j\omega)$) is presented graphically as shown in Fig. 9.8b. It is evaluated at low and high frequencies to determine its asymptotes:

- At low frequencies ($\omega \ll \omega_0 \Rightarrow |1/j\omega C_f| \gg |R + j\omega L_{sys}|$), the filter is dominantly capacitive and provides reactive power to the system. Therefore, $H_f(s) \approx 1/j\omega C_f$ and the roll-off of the low frequency components is –20 dB per decade.
- At high frequencies ($\omega \gg \omega_0 \Rightarrow |j\omega L_{sys}| \gg |R + 1/j\omega C_f|$), the filter is dominantly inductive and consumes reactive power with little influence on high-frequency distortions. Therefore, $H_f(s) \approx j\omega L_f$ and the roll-off of the high frequency components is 20 dB per decade.
- At the resonant frequency ($\omega = \omega_0$), the filter is entirely resistive, that is, $H_f(s) = R_f$ More attenuation is provided with lower filter resistances; however, there are practical limits to the value of $R_f$.

Similar procedures are applied to plot $H_{fs}(j\omega)$ and $H_{cds}(j\omega)$ as illustrated in Fig. 9.8c,d, respectively. Note that the minima of the transfer functions ($H_{min}$) are very close to the series resonant frequency; however, due to the interaction between the capacitive reactance and the filter inductive reactance, $H_{min}$ does not occur at the parallel resonant frequency formed by filter capacitance and system inductance. The derivatives of the transfer functions are usually evaluated numerically to determine frequencies where maxima occur.

The second-order band-pass (series resonant) filters are very popular and have many applications in power system design including transmission (e.g., connected in parallel at the AC terminals of HVDC converters), distribution (e.g., for detuning power factor capacitor banks to avoid parallel resonant frequencies), and utilization (e.g., across terminals of nonlinear loads).



### 9.3.2.4 Second-Order Damped Band-Pass Filter

A popular topology of the second-order damped filter is shown in Fig. 9.9a where a bypass resistance ($R_{bp}$) is included across the inductor to provide attenuation for harmonic frequency components over a wide frequency range. The filter impedance transfer function can be expressed in normalized form

$$H_f(s) = Z_f(s) = \frac{V_f(s)}{I_f(s)} = \frac{1}{\frac{1}{R_{bp}} + \frac{1}{R_f + sL_f}} + \frac{1}{sC_f}$$
$$= \frac{A}{s\left(1 + \frac{s}{\omega_p}\right)}\left[1 + \frac{1}{Q_{bp}}\left(\frac{s}{\omega_0}\right) + \left(\frac{s}{\omega_0}\right)^2\right], \tag{9-10a}$$

where the gain A, the series resonant angular frequency $\omega_0$, the quality factor $Q_{bp}$, and the pole frequency [13] for typical cases (whereby $R_f \ll R_{bp}$) are

$$A = \frac{1}{C_f},\quad \omega_0 = \sqrt{\frac{R_f + R_{bp}}{R_{bp}L_f C_f}} \approx \frac{1}{\sqrt{L_f C_f}},$$
$$Q_{bp} = \frac{R_f + R_{bp}}{\omega_0(R_{bp}L_f C_f + L_f)},\quad \omega_p = \frac{R_f + R_{bp}}{L_f} \approx \frac{R_{bp}}{L_f}. \tag{9-10b}$$

The series resistance $R_f$ is determined by the desired quality factor of the second-order band-pass filter and $R_{bp}$ is selected to achieve the required high-pass response and series resonant attenuation. Typical values of the bypass quality factor are $0.5 < Q_{bp} < 2.0$. However, there is a trade-off between larger values (e.g., more series resonant attenuation and less high-pass response) and smaller values (e.g., less series resonant attenuation and greater high-pass response) of the quality factor.

### 9.3.2.5 Composite Filter

Higher order filters are constructed by increasing the number of storage elements (e.g., capacitors, induc-

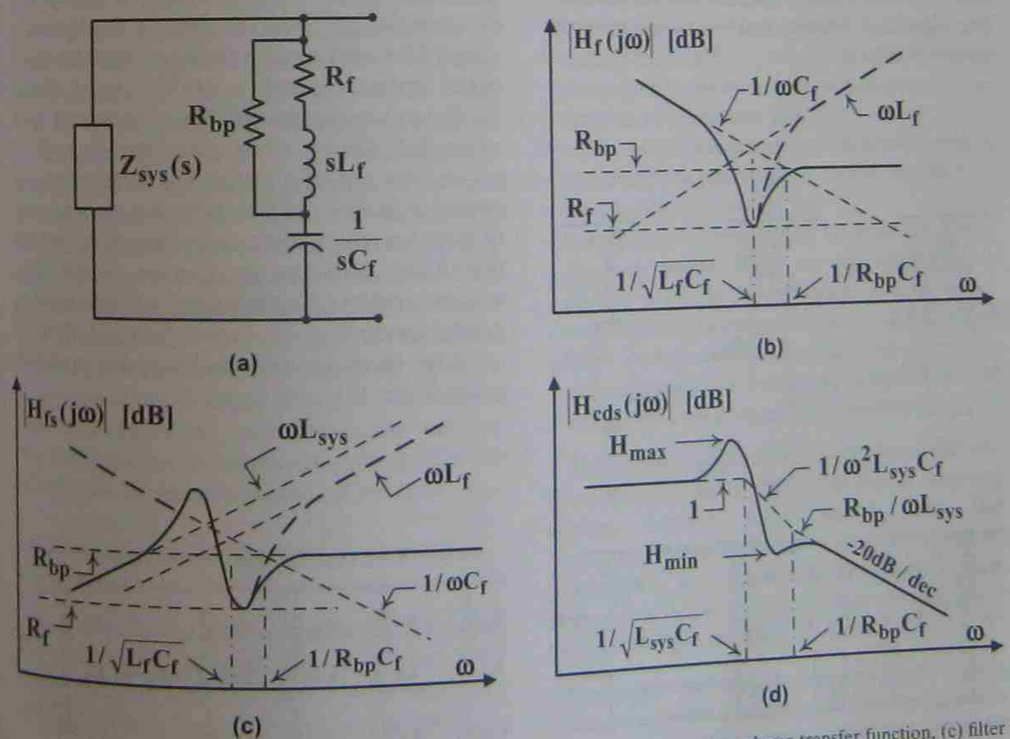



**FIGURE 9.9** Second-order damped band-pass filter; (a) equivalent circuit, (b) filter impedance transfer function, (c) filter system impedance transfer function, (d) current-divider transfer function.

tors). However, their application in power systems is limited due to economic and reliability factors.

A third-order filter may be constructed by adding a series capacitance $C_{f2}$ to the inductor bypass resistance (Fig. 9.10a) to limit $I_{bp}$ and reduce the corresponding fundamental frequency losses or by including $C_{f2}$ in series with $L_f$ (Fig. 9.10b) and sizing it to form a series resonant branch at the fundamental frequency to reduce $I_{bp}$ and to increase filter efficiency. If a second inductor $L_{f2}$ is added to the circuit of Fig. 9.10a, a fourth-order double band-pass filter will be obtained, as shown in Fig. 9.10c.

A common type of an nth-order composite filter for power quality improvement is shown in Fig. 9.11. Several band-pass filters are connected in parallel and individually tuned to selected harmonic frequencies to provide compensation over a wide frequency range. The last branch is a high-pass filter attenuating high-order harmonics, which usually are a result of fast switching actions. Composite filters are only applied when even-order harmonics are small since a parallel resonance will occur between any two adjacent band-pass filter branches and cause amplification of the distortion in that frequency range. For example, composite filter systems with shunt branches tuned at the 5th and 7th harmonics will have a resonant frequency about at the 6th harmonic. The impedance transfer function of the nth-order composite filter is

$$H_f(s) = Z_f(s) = \frac{V_f(s)}{I_f(s)} = \frac{1}{\frac{1}{Z_f^{(5)}} + \frac{1}{Z_f^{(7)}} + \frac{1}{Z_f^{(11)}} + \ldots + \frac{1}{Z_f^{(n)}}} \quad (9\text{-}11)$$

It is time-consuming to derive the transfer functions of multiple-order filters in terms of factorized expressions of poles and zeros [13]. Therefore, numerical approaches are typically applied to plot the transfer function, and an iterative design procedure is used to optimize a filter configuration.

### 9.3.3 Classification of Passive Power Filters

Passive filters cause harmonic currents to flow at their resonant frequency. Due to this resonance, the harmonic currents are attenuated in the power system through the LC filter circuits tuned to the harmonic orders that require filtering. In practice, a single passive filter is not adequate since there is more than one harmonic to be attenuated; therefore, a shunt or series passive composite filter unit (Fig. 9.12) is used. Passive filter units are generally designed to remove a few low-order harmonics, for example, the 5th, 7th, and 11th. Normally passive filter units employ three (or more for high-power applications such as HVDC) tuned filters, the first two being for the lowest dominant harmonics followed by a high-pass filter. In a shunt passive filter unit, two lossless LC components are connected in series to sink harmonic currents and all three (or more) filters are connected in parallel (Fig. 9.12a). However, in a series passive filter unit, two lossless LC components are connected in parallel for creating a harmonic dam and all three (or more) filters are connected in series, as shown in Fig. 9.12b.

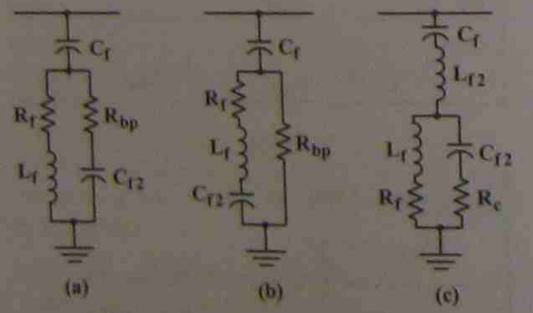



**FIGURE 9.10** Higher order filters; (a) and (b) third-order filters, (c) fourth-order filter.

**FIGURE 9.11** Nth-order composite filter.



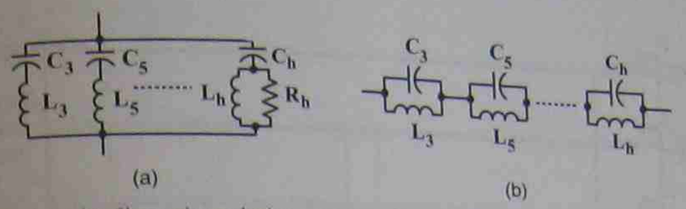



**FIGURE 9.12** Typical passive filter unit employing a number of tuned filter units, the first $(h-1)$ units are tuned to the lowest dominant harmonic frequencies followed by a high-pass element; (a) shunt passive filter block, (b) series passive filter block.

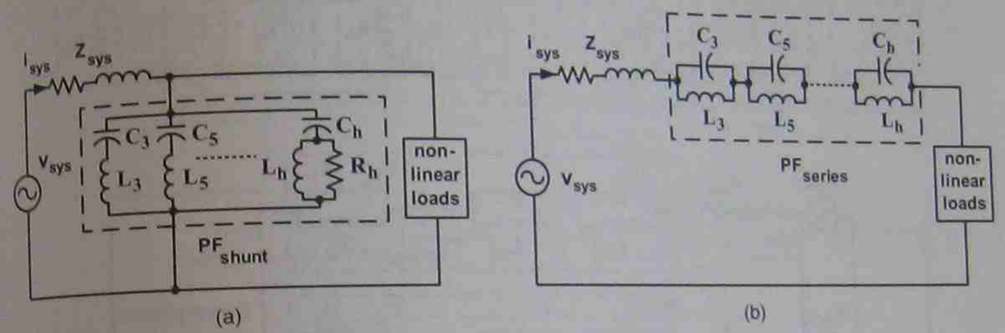



**FIGURE 9.13** Single-phase passive filter; (a) shunt configuration, (b) series configuration.

The inductors should have high quality factors to reduce system losses and must not saturate in the entire current operating region. Capacitor values are decided by the required reactive power of the system, and then inductor values are calculated by tuning them for the particular harmonic frequencies. Resistor values are calculated by the corresponding quality factors based on the desired sharpness of the characteristics. Similarly, the resistance of the high-pass filter is computed based on the sharpness or attenuation of the higher order harmonics on the one hand, and reducing the losses on the other hand to achieve an optimum value for the quality factor. Passive filter units with shunt and series configurations are extensively used in single-phase (Fig. 9.13), three-phase three-wire (Fig. 9.14), and three-phase four-wire (Fig. 9.15) systems to improve the quality of power and mitigate harmonic currents and voltages.

### 9.3.4 Potentials and Limitations of Passive Power Filters

Design, construction, and implementation of passive filters are straightforward and easier than their counterparts, for example, synchronous condensers and active filters. They have many advantages:

- they are robust, economical, and relatively inexpensive;
- they can be implemented in large sizes of MVArs and require low maintenance;
- they can provide a fast response time (e.g., one cycle or less with SVC), which is essential for some power quality problems such as flickering voltage dips due to arc-furnace loads;
- unlike rotating machines (e.g., synchronous motors or condensers) passive filters do not contribute to the short-circuit currents; and
- in addition to power quality improvement, well-designed passive filters can be configured to provide power factor correction, reactive power compensation, or voltage support (e.g., on critical buses in case of a source outage) and reduce the starting impact and associated voltage drops due to large loads (e.g., large induction motors).

These advantages have resulted in broad applications of passive filters in different sectors of power systems. However, power engineers have also encountered some limitations and shortcomings of passive filters, which have called for alternative solutions such as active and hybrid filter systems. Some limitations of passive filters are as follows:

- fixed compensation or harmonic mitigation, large size, and possible resonance with the supply system impedance at fundamental and/or other harmonic frequencies;

ST. GEORGE SOUTH LANE

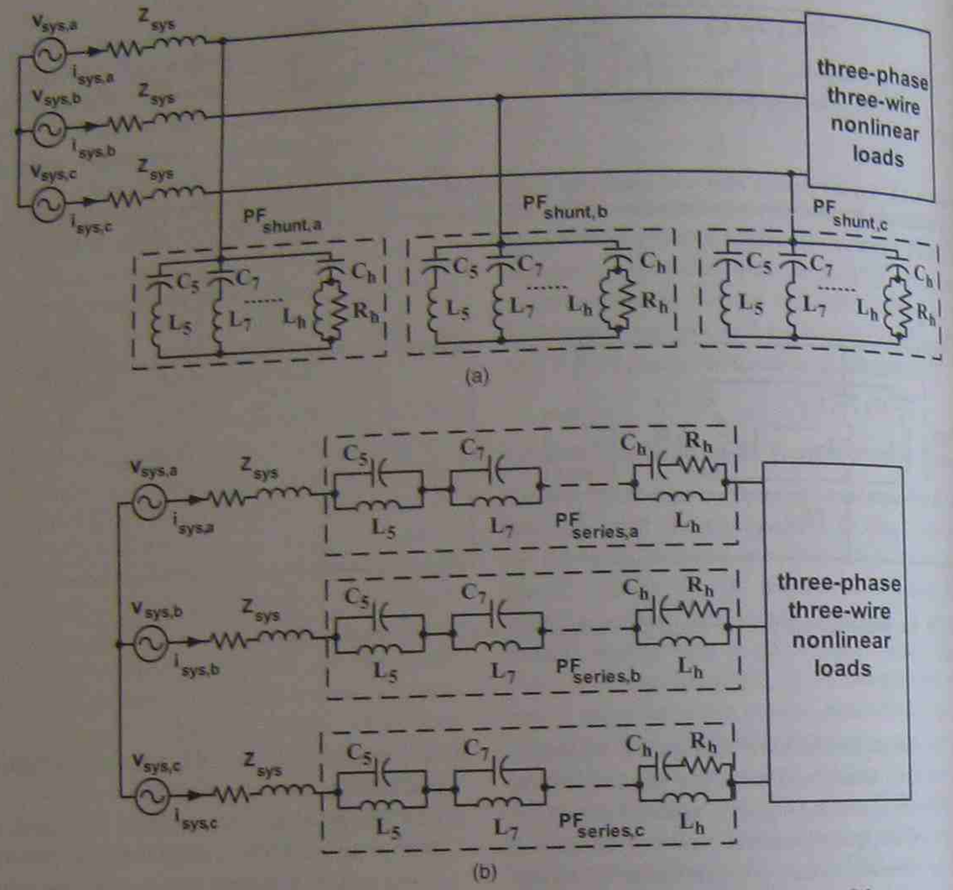



**FIGURE 9.14** Three-phase three-wire passive filter; (a) shunt configuration, (b) series configuration [4].

- compensation is limited to a few orders of harmonics;
- once installed, the tuned frequency and/or filter size cannot be changed easily;
- unsatisfactory performance (e.g., detuning) may occur due to variations of filter parameters (caused by aging, deterioration, and temperature effects) and nonlinear load characteristics;
- change in system operating conditions (e.g., inclusion of capacitors and/or other filters) has large influence on filter designs. Therefore, to be effective, filter impedance should be less than system impedance, which can become a problem for strong or stiff systems [2];
- resonance between system and filter (e.g., shifted resonance frequency) for single- and double-tuned filters can cause an amplification of characteristics and noncharacteristic harmonic currents. Therefore, the designer has a limited choice in selecting tuned frequencies and ensuring adequate bandwidth between shifted frequencies and integer (even and odd) harmonics [2];
- special protective and monitoring devices might be required to control switching surges, although filter reactors will reduce the magnitude of the switching inrush current magnitude and its associated high frequency; and
- stepless control (of reactive power, power factor correction, and voltage support) is not possible since the filter can either be switched on or switched off only.



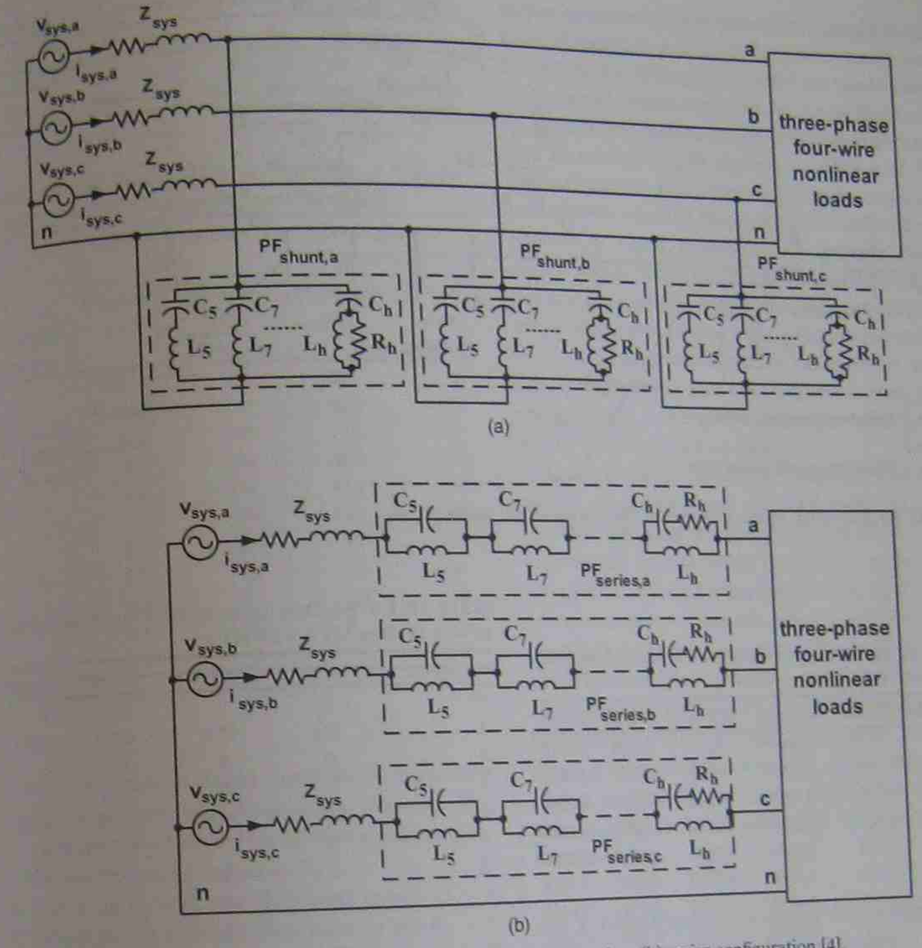



**FIGURE 9.15** Three-phase four-wire passive filter; (a) shunt configuration, (b) series configuration [4].

### 9.3.5 Application Example 9.1: Hybrid Passive Filter Design to Improve the Power Quality of the IEEE 30-Bus Distribution System Serving Adjustable-Speed Drives

Consider the IEEE 23 kV, 30-bus distribution system [9, 10] shown in Fig. E9.1.1. System transmission-line data, bus data, and capacitor data are provided in Tables E9.1.1 to E9.1.3, respectively. To investigate the impact of large AC drive systems on the power quality of the distribution system, a PWM adjustable-speed drive (675 kW, 439 kVAr) and a variable-frequency drive (350 kW, 175 kVAr) are connected to buses 15 and 18, respectively. Table E9.1.4 depicts the spectra of the current harmonics injected by typical AC drives into the system. Use harmonic current sources to model the two nonlinear loads and utilize the decoupled harmonic power flow algorithm (Chapter 7, Section 7.5.1) to simulate the system. Determine the total harmonic voltage distortion ($THD_v$) of the system and at the individual buses before and after the installation of the hybrid passive filter banks listed below. Plot the voltage and current waveforms at bus 15 before and after filtering.

a) Two filter banks are placed at the terminals of nonlinear loads (buses 15 and 18). Each bank consists of a number of shunt-connected series

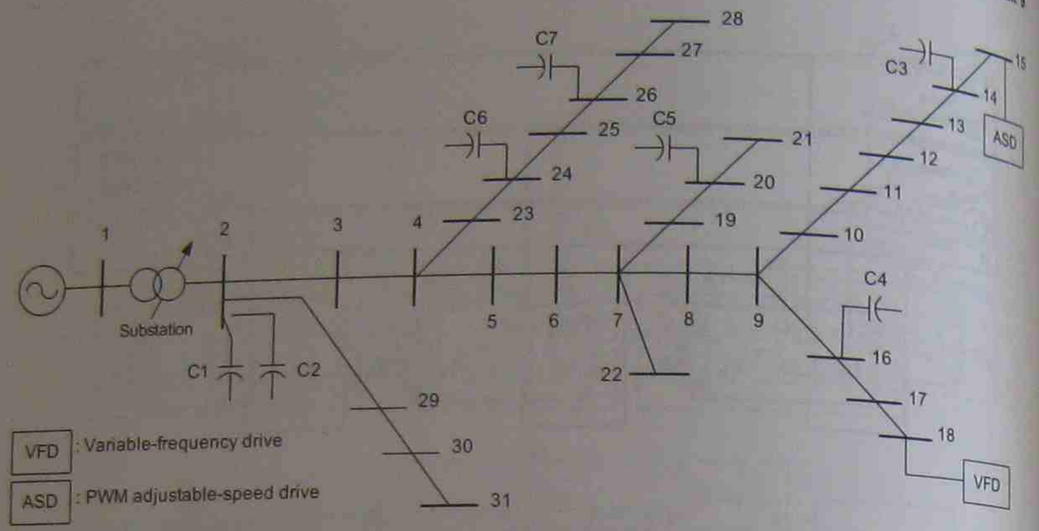



**FIGURE E9.1.1** IEEE 30-bus system with two nonlinear AC drives [9, 10].

**TABLE E9.1.1** Line Data for the IEEE 30-Bus System (Base kV = 23 kV, Base MVA = 100 MVA)

| From bus | To bus | R (ohm) | X (ohm) | R (pu) | X (pu) |
|---|---|---|---|---|---|
| 1 | 2 | 0.0021 | 0.0365 | 0.0004 | 0.0069 |
| 2 | 3 | 0.2788 | 0.0148 | 0.0527 | 0.0028 |
| 3 | 4 | 0.4438 | 0.4391 | 0.0839 | 0.0830 |
| 4 | 5 | 0.8639 | 0.7512 | 0.1633 | 0.1420 |
| 5 | 6 | 0.8639 | 0.7512 | 0.1633 | 0.1420 |
| 6 | 7 | 1.3738 | 0.7739 | 0.2597 | 0.1463 |
| 7 | 8 | 1.3738 | 0.7739 | 0.2597 | 0.1463 |
| 8 | 9 | 1.3738 | 0.7739 | 0.2597 | 0.1463 |
| 9 | 10 | 1.3738 | 0.7739 | 0.2597 | 0.1463 |
| 10 | 11 | 1.3738 | 0.7739 | 0.2597 | 0.1463 |
| 11 | 12 | 1.3738 | 0.7739 | 0.2597 | 0.1463 |
| 12 | 13 | 1.3738 | 0.7739 | 0.2597 | 0.1463 |
| 13 | 14 | 1.3738 | 0.7739 | 0.2597 | 0.1463 |
| 14 | 15 | 1.3738 | 0.7739 | 0.2597 | 0.1463 |
| 9 | 16 | 0.8639 | 0.7512 | 0.1633 | 0.1420 |
| 16 | 17 | 1.3738 | 0.7739 | 0.2597 | 0.1463 |
| 17 | 18 | 1.3738 | 0.7739 | 0.2597 | 0.1463 |
| 7 | 19 | 0.8639 | 0.7512 | 0.1633 | 0.1420 |
| 19 | 20 | 0.8639 | 0.7512 | 0.1633 | 0.1420 |
| 20 | 21 | 1.3738 | 0.7739 | 0.2597 | 0.1463 |
| 7 | 22 | 0.8639 | 0.7512 | 0.1633 | 0.1420 |
| 4 | 23 | 0.4438 | 0.4391 | 0.0839 | 0.0830 |
| 23 | 24 | 0.4438 | 0.4391 | 0.0839 | 0.0830 |
| 24 | 25 | 0.8639 | 0.7512 | 0.1633 | 0.1420 |
| 25 | 26 | 0.8639 | 0.7512 | 0.1633 | 0.1420 |
| 26 | 27 | 0.8639 | 0.7512 | 0.1633 | 0.1420 |
| 27 | 28 | 1.3738 | 0.7739 | 0.2597 | 0.1463 |
| 2 | 29 | 0.2788 | 0.0148 | 0.0527 | 0.0028 |
| 29 | 30 | 0.2788 | 0.0148 | 0.0527 | 0.0028 |
| 30 | 31 | 1.3738 | 0.7739 | 0.2597 | 0.1463 |

**TABLE E9.1.2** Bus Data for the IEEE 30-Bus System (Base kV = 23 kV, Base MVA = 100 MVA)

| Bus number | P (kW) | Q (kVAr) | P (pu) | Q (pu) |
|---|---|---|---|---|
| 1[a] | 0 | 0 | 0 | 0 |
| 2 | 52.2 | 17.2 | 0.522 | 0.172 |
| 3 | 0 | 0 | 0 | 0 |
| 4 | 0 | 0 | 0 | 0 |
| 5 | 93.8 | 30.8 | 0.938 | 0.308 |
| 6 | 0 | 0 | 0 | 0 |
| 7 | 0 | 0 | 0 | 0 |
| 8 | 0 | 0 | 0 | 0 |
| 9 | 0 | 0 | 0 | 0 |
| 10 | 18.9 | 6.2 | 0.189 | 0.062 |
| 11 | 0 | 0 | 0 | 0 |
| 12 | 33.6 | 11 | 0.336 | 0.11 |
| 13 | 65.8 | 21.6 | 0.658 | 0.216 |
| 14 | 78.4 | 25.8 | 0.784 | 0.258 |
| 15 | 73 | 24 | 0.73 | 0.24 |
| 16 | 47.8 | 15.7 | 0.478 | 0.157 |
| 17 | 55 | 18.1 | 0.55 | 0.181 |
| 18 | 47.8 | 15.7 | 0.478 | 0.157 |
| 19 | 43.2 | 14.2 | 0.432 | 0.142 |
| 20 | 67.3 | 22.1 | 0.673 | 0.221 |
| 21 | 49.6 | 16.3 | 0.496 | 0.163 |
| 22 | 20.7 | 6.8 | 0.207 | 0.068 |
| 23 | 52.2 | 17.2 | 0.522 | 0.172 |
| 24 | 192 | 63.1 | 1.92 | 0.631 |
| 25 | 0 | 0 | 0 | 0 |
| 26 | 111.7 | 36.7 | 1.117 | 0.367 |
| 27 | 55 | 18.1 | 0.55 | 0.181 |
| 28 | 79.3 | 26.1 | 0.793 | 0.261 |
| 29 | 88.3 | 29 | 0.883 | 0.29 |
| 30 | 0 | 0 | 0 | 0 |
| 31 | 88.4 | 29 | 0.884 | 0.29 |

[a]Swing bus.

ST. GEORGE COLLEGE OF LAW



**TABLE E9.1.3** Capacitor Data for the IEEE 30-Bus System

| Capacitor | C1 | C2 | C3 | C4 | C5 | C6 | C7 |
|---|---|---|---|---|---|---|---|
| Bus location | 2 | 2 | 14 | 16 | 20 | 24 | 26 |
| kVAr | 900 | 600 | 600 | 600 | 300 | 900 | 900 |

**TABLE E9.1.4** Typical Harmonic Spectrum of Variable-Frequency and PWM Adjustable-Speed Drives [14]

| | Variable-frequency drive | | PWM adjustable-speed drive | |
|---|---|---|---|---|
| Harmonic order h | Magnitude (%) | Phase angle (degree) | Magnitude (%) | Phase angle (degree) |
| 1 | 100 | 0 | 100 | 0 |
| 5 | 23.52 | 111 | 82.8 | −135 |
| 7 | 6.08 | 109 | 77.5 | 69 |
| 11 | 4.57 | −158 | 46.3 | −62 |
| 13 | 4.2 | −178 | 41.2 | 139 |
| 17 | 1.8 | −94 | 14.2 | 9 |
| 19 | 1.37 | −92 | 9.7 | −155 |
| 23 | 0.75 | −70 | 1.5 | −158 |
| 25 | 0.56 | −70 | 2.5 | 98 |
| 29 | 0.49 | −20 | 0 | 0 |
| 31 | 0.54 | 7 | 0 | 0 |

resonance passive filters tuned at the respective dominant harmonic frequencies. Assume $R_f$ = 100 Ω and $L_f$ = 100 $mH$ for all filters and compute the corresponding values of $C_f$.

b) Repeat part a with one filter bank at bus 15.

c) Repeat part b with one filter bank at bus 9.

d) Compare the results of parts a to c and make comments regarding the impact of numbers and locations of filters on the power quality of the system.

## 9.4 ACTIVE FILTERS

Active filters (AFs) are feasible alternatives to passive filters (PFs). For applications where the system configuration and/or the harmonic spectra of nonlinear loads (e.g., orders, magnitudes, and phase angles) change, active elements may be used instead of the passive components to provide dynamic compensation.

An active filter is implemented when the order numbers of harmonic currents are varying. This may be due to the nature of nonlinear loads injecting time-dependent harmonic spectra (e.g., variable-speed drives) or may be caused by a change in the system configuration. The structure of an active filter may be that of series or parallel architectures. The proper structure for implementation depends on the types of harmonic sources in the power system and the effects that different filter solutions would cause to the overall system performance. Active filters rely on active power conditioning to compensate undesirable harmonic currents replacing a portion of the distorted current wave stemming from the nonlinear load. This is achieved by producing harmonic components of equal amplitude but opposite phase angles, which cancel the injected harmonic components of the nonlinear loads. The main advantage of active filters over passive ones is their fine response to changing loads and harmonic variations. In addition, a single active filter can compensate more than one harmonic, and improve or mitigate other power quality problems such as flicker.

Active filters are expensive compared with their passive counterparts and are not feasible for small facilities. The main drawback of active filters is that their rating is sometimes very close to the load (up to 80% in some typical applications), and thus it becomes a costly option for power quality improvement in a number of situations. Moreover, a single active filter might not provide a complete solution in many practical applications due to the presence of both voltage and current quality problems. For such cases, a more complicated filter design consisting of two or three passive and/or active filters (called a hybrid filter) is recommended as discussed in Section 9.5.

### 9.4.1 Classification of Active Power Filters Based on Topology and Supply System

Active filters have become a mature technology for harmonic and reactive power compensation of single- and three-phase electric AC power networks with high penetration of nonlinear loads. This section classifies active filters based on the supply system taking into consideration their (shunt or/and series) topology. Therefore, there are six types of shunt and series connected active filters for single-phase two-wire, three-phase three-wire, and three-phase four-wire AC networks, as shown in Figs. 9.16, 9.17, and 9.18, respectively. Composite filters consisting of two or more active filters are realized as hybrid filters and are discussed in Section 9.5.

### 9.4.2 Classification of Active Power Filters Based on Power Rating

Active filters can also be classified according to their power rating and speed of response required for their application in a compensated system [5]:

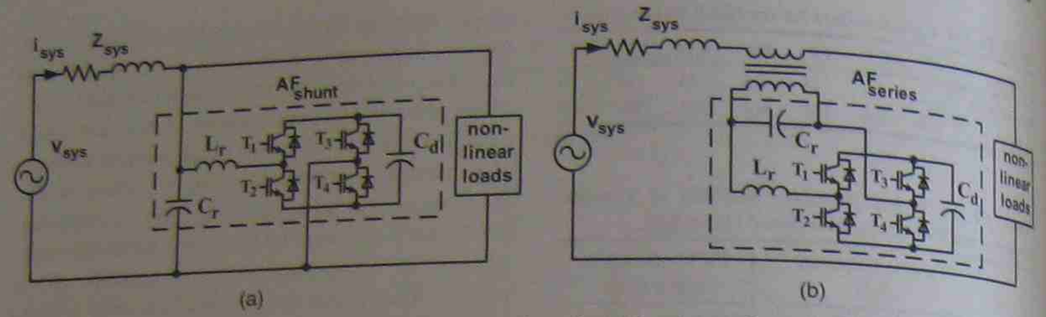



**FIGURE 9.16** Single-phase active filter (AF); (a) shunt configuration, (b) series configuration [4].

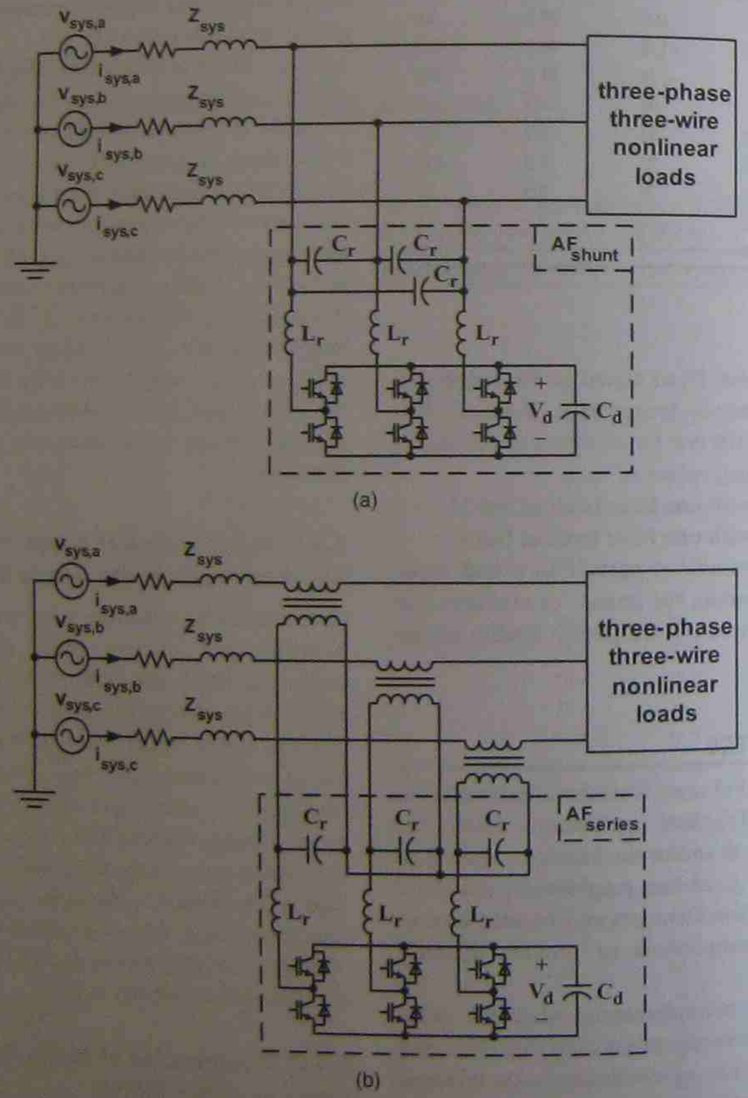



**FIGURE 9.17** Three-phase three-wire active filter; (a) shunt configuration, (b) series configuration.



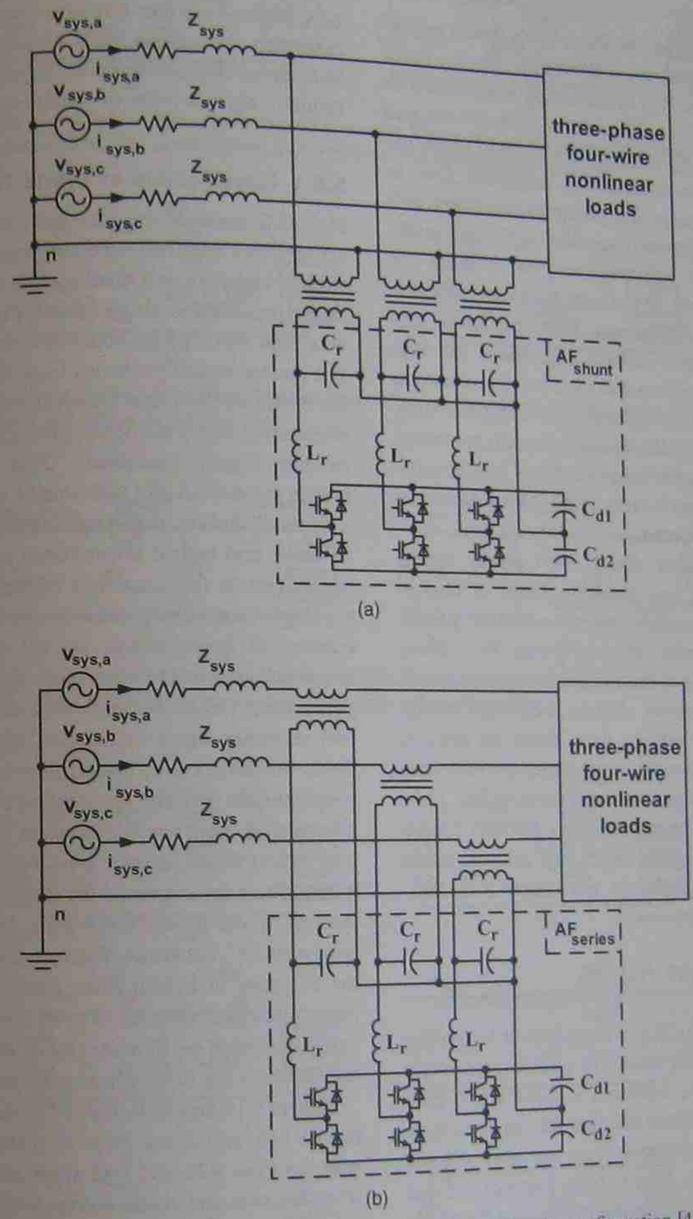



**FIGURE 9.18** Three-phase four-wire active filter; (a) shunt configuration, (b) series configuration [4].

- ***Low-power active filters*** (with power ratings below 100 kVA and response times of about 10 $\mu$s to 10 ms) are mainly used in residential areas, small to medium-sized factories, electric drives, commercial buildings, and hospitals. These applications require sophisticated dynamic filtering techniques and include single-phase and three-phase systems.
- Single-phase active filters are mainly available for low power ratings, and hence can be operated at relatively high frequencies leading to improved performance and lower prices. They have many retrofit applications such as commercial and educational buildings with many computer loads.
- For balanced three-phase low power applications a three-phase filter can be used. However, for unbalanced load currents or unsymmetrical supply voltages, especially in three-phase four-wire distribution systems, three single-phase filters or a hybrid filter are usually required.

- ***Medium-power active filters*** (with power ratings of about 100 kVA to 10 MVA and response times of about 100 ms to 1 s) are mainly associated with medium- to high-voltage distribution systems and high-power, high-voltage drive systems, where the effect of phase imbalance is negligible. Due to economic concerns and problems associated with high-voltage systems (isolation, series or parallel connections of switches, etc.), these filters are usually designed to perform harmonic cancellation, and reactive-power compensation is not included in their control algorithms. At high voltage, other approaches of reactive power compensation such as capacitive or inductive static compensators, synchronous condensers, controlled LC filters, tuneable harmonic filters, line-commutated thyristor converters, and VAr compensators should be considered.
- ***High-power active filters*** (with power ratings above 10 MVA and response times of tens of seconds) are mainly associated with power-transmission grids, ultrahigh-power DC drives, and HVDC. Due to the availability of high switching-frequency power devices with high-voltage and high-power ratings, these filters are not cost effective. It is possible to use series–parallel combinations of low-power switches; however, there are many implementation issues and cost considerations. Fortunately, there are not too many power quality problems associated with high-voltage power systems.

## 9.5 HYBRID POWER FILTERS

A major drawback of active filters is their high rating (e.g., up to 80% of the nonlinear load in some practical applications). In addition, a single active filter cannot offer a complete solution for the simultaneous compensation of both voltage and current power quality disturbances. Due to higher ratings and cost considerations, the acceptability of active filters has been limited in practical applications. In response to these factors, different structures of hybrid filters have evolved as a cost-effective solution for the compensation of nonlinear loads. Hybrid filters are found to be more effective in providing complete compensation of various types of nonlinear loads.

### 9.5.1 Classification of Hybrid Filters

Hybrid filters combine a number of passive and/or active filters and their structure may be of series or parallel topology or a combination of the two. They can be installed in single-phase, three-phase three-wire, and three-phase four-wire distorted systems. The passive circuit performs basic filtering action at the dominant harmonic frequencies (e.g., 5th or 7th) whereas the active elements, through precise control, mitigate higher harmonics. This will effectively reduce the overall size and cost of active filtering.

In the literature, there are different classifications of active and hybrid filters based on power rating, supply system (e.g., number of wires and phases), topology (e.g., shunt and/or series connection), number of (passive and active) elements, speed of response, power circuit configuration, system parameter(s) to be compensated, control approach, and reference-signal estimation technique. In this book, classification of hybrid filters is based on the supply system with the topology as a further subclassification. If there are a maximum of three (passive and active) filters in each phase, then 156 types of hybrid filters are expected for single-phase two-wire systems, three-phase three-wire, and three-phase four-wire AC networks. Figures 9.19 to 9.25 show the 52 types of hybrid filter topologies for single-phase two-wire systems. These topologies can be easily extended to illustate the other 104 types of hybrid filters for three-phase systems.

Figures 9.19 and 9.20 depict hybrid filters consisting of two and three passive filters, respectively, whereas Figs. 9.21 and 9.22 show similar configurations for two and three active filters. There are 8 topologies of hybrid filters consisting of one passive and one active filter as shown in Fig. 9.23. There are many possible combinations if three filters are

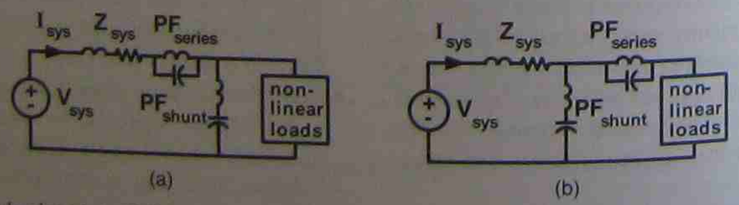



**FIGURE 9.19** Single-phase hybrid filter (including two passive filters) as a combination of (a) passive-series and passive-shunt filters, (b) passive-shunt and passive-series filters [4].

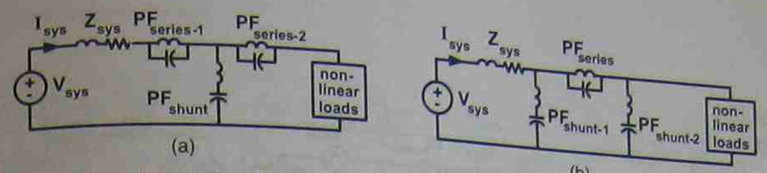



**FIGURE 9.20** Single-phase hybrid filter (including three passive filters) as a combination of (a) passive-series, passive-series, and passive-shunt filters, (b) passive-shunt, passive-series, and passive-shunt filters [4].

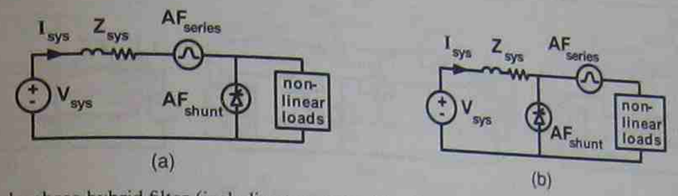



**FIGURE 9.21** Single-phase hybrid filter (including two active filters) as a combination of (a) active-series and active-shunt filters, (b) active-shunt and active-series filters [4].

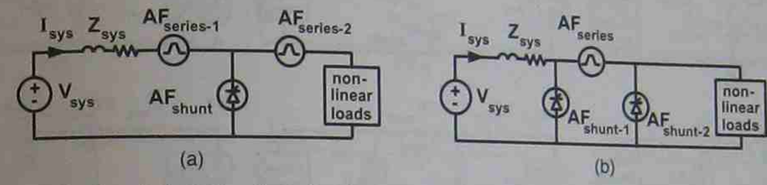



**FIGURE 9.22** Single-phase hybrid filter (including three active filters) as a combination of (a) active-series, active-series, and active-shunt filters, (b) active-shunt, active-series, and active-shunt filters [4].

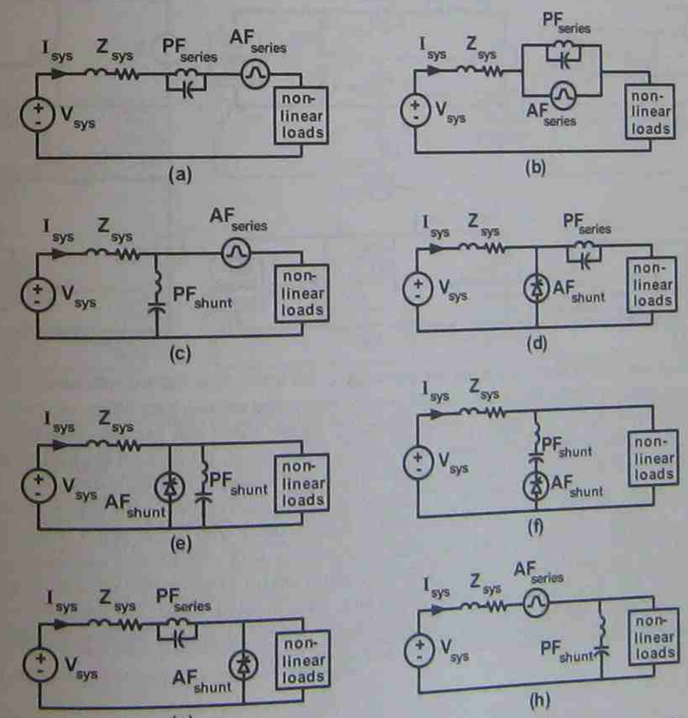



**FIGURE 9.23** Single-phase hybrid filter (including one passive and one active filter) as a combination of (a) series-connected passive-series and active-series filters, (b) parallel-connected passive-series and active-series filters, (c) passive-shunt and active-series filters, (d) active-shunt and passive-series filters, (e) active-shunt and passive-shunt filters, (f) series-connected passive-shunt and active-shunt filters, (g) passive-series and active-shunt filters, (h) active-series and passive-shunt filters [4].

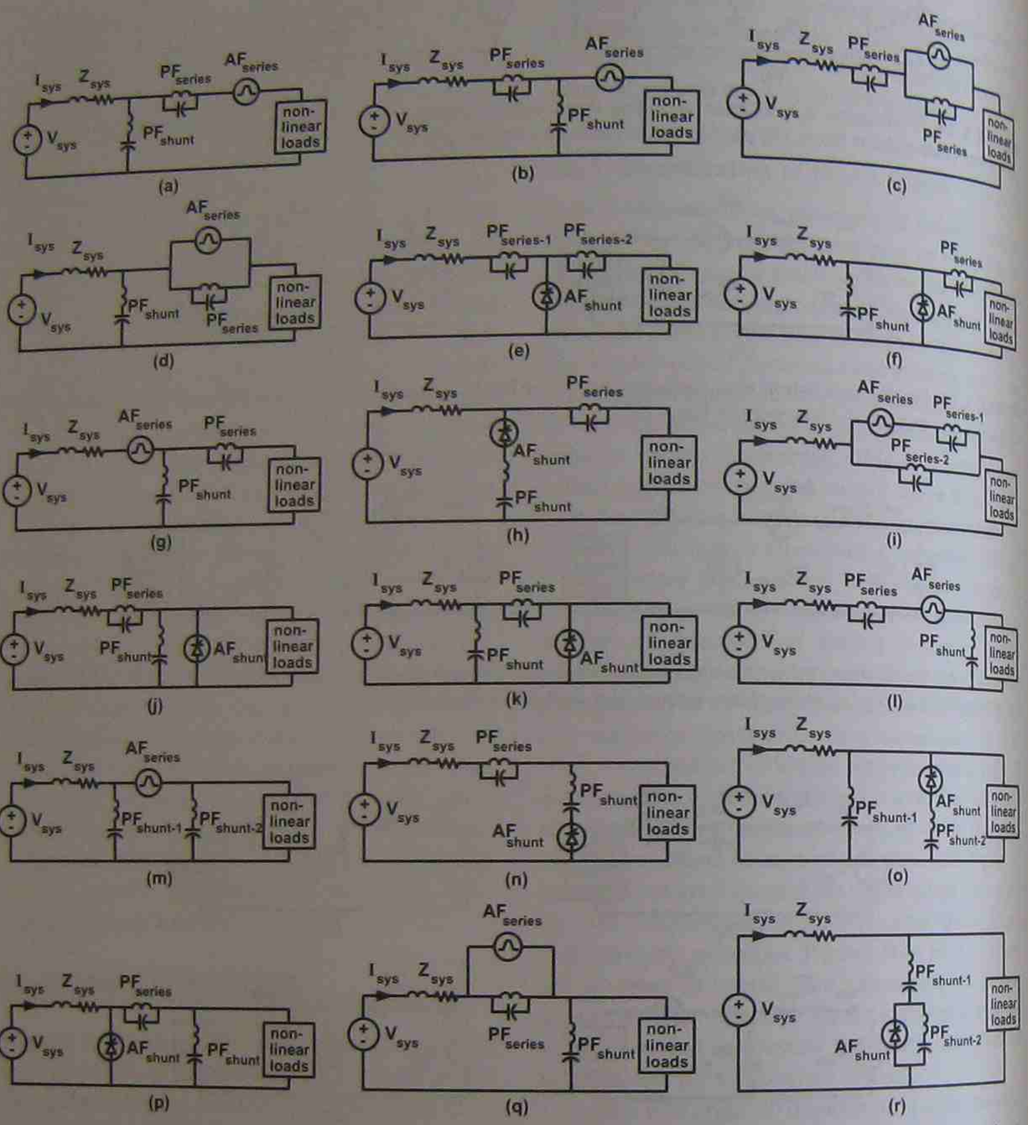



**FIGURE 9.24** Single-phase hybrid filter (including two passive and one active filter) as a combination of (a) passive-shunt, passive–series, and active-series filters, (b) passive-series, passive shunt, and active-series filters, (c) passive-series in series with parallel-connected active-series and passive-series filters, (d) passive-shunt and parallel-connected active-series and passive-series filters, (e) passive-series, active-shunt, and passive-series filters, (f) parallel-connected passive-shunt with active-shunt and passive-series filters, (g) active-series, passive-shunt, and passive-series filters, (h) series-connected passive-shunt with active-series and passive-series filters, (i) series-connected passive-series with active-series in parallel with passive-series filters, (j) passive-series and parallel-connected passive-shunt with active-shunt filters, (k) passive-shunt, passive-series, and active-shunt filters, (l) series-connected passive-series with active-series and passive-shunt filters, (m) passive-shunt, active-series, and passive-shunt filters, (n) passive-series and series-connected passive-shunt with active-shunt filters, (o) passive-shunt and series-connected active-series with passive-shunt filters, (p) combination of active-shunt, passive-series, and passive-shunt filters, (q) parallel-connected active-series with passive-series and passive-shunt filters, (r) passive-shunt and parallel-connected passive-shunt with active-series filters [4].



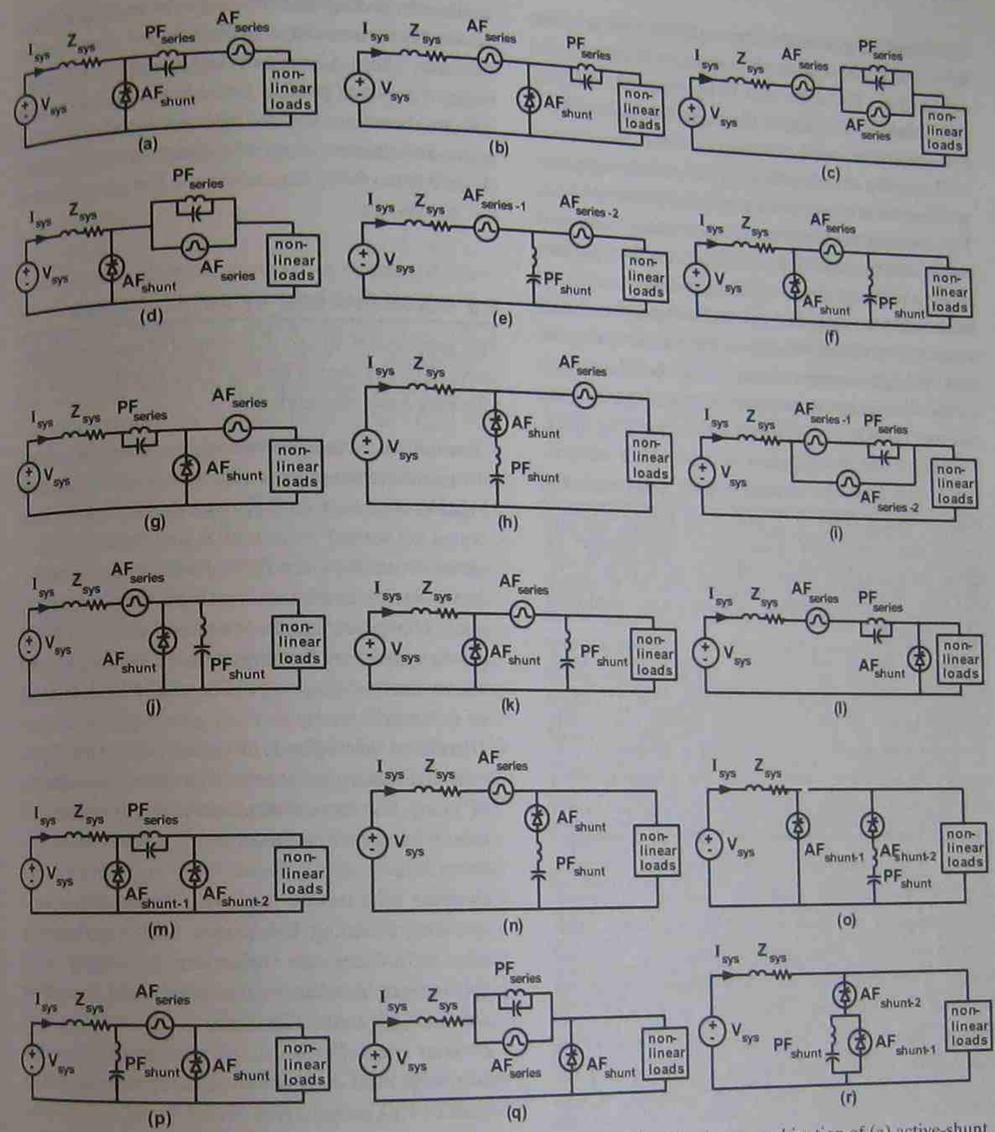



**FIGURE 9.25** Single-phase hybrid filter (including one passive and two active filters) as a combination of (a) active-shunt, passive-series, and active-series filters, (b) active-series, active-shunt, and passive-series filters, (c) active-series, parallel-connected passive-series with active-series filters, (d) active-shunt, parallel-connected passive–series with active-series filters, (e) active-series, passive-shunt, and active-series filters, (f) active-shunt, passive-shunt, and active-series filters, (g) passive-series, active-shunt, and active-series filters, (h) series-connected active-shunt with passive-shunt and actives-series filters, (i) active-series in parallel with passive-series and active-series filters, (j) active-series, active-shunt and passive-shunt filters, (k) active-shunt, active-series, and passive-shunt filters, (l) active-series, passive-series, and active-shunt filters, (m) active-shunt, passive-series, and active-shunt filters, (n) active-series, series-connected active-shunt, and passive-shunt filters, (o) active-shunt, series-connected active-shunt, and passive-shunt filters, (p) passive-shunt, active-series, and active-shunt filters, (q) parallel-connected passive-series with active-series and active-shunt filters, (r) active-shunt in series with parallel-connected active-shunt and passive-shunt filters [4].

ST. GEORGE POLLEGE OF LAW

combined. Figure 9.24 illustrates the 18 possible hybrid filters consisting of two passive filters and one active filter. There are also 18 possible hybrid filters consisting of one passive filter and two active filters as represented in Fig. 9.25.

The rating of active filters is reduced through augmenting them by passive filters to form hybrid filters. This reduces the overall cost and in many cases provides better compensation than when either passive or active filters alone are employed. However, a more efficient approach is to combine shunt and series active filters, which can provide both current and voltage compensation. This (active–active) hybrid filter is known as a unified power quality conditioner (UPQC) or universal active filter (Fig. 9.21). Therefore, the development in hybrid filter technology began from the arrangement of (two or three) passive filters (Figs. 9.19 and 9.20) and progressed to the more effective combination of a number of shunt and/or series active filters (Figs. 9.21 to 9.25), yielding a cost-effective solution and complete compensation.

Hybrid filters are usually considered a cost-effective option for power quality improvement, compensation of the poor power quality effects due to nonlinear loads, or to provide a sinusoidal AC supply to sensitive loads. There are a large number of low-power nonlinear loads in a single-phase power system, such as ovens, air conditioners, fluorescent lamps, TVs, computers, power supplies, printers, copiers, and battery chargers. Low-cost harmonic compensation of these residential nonlinear loads can be achieved using passive filters (Figs. 9.19 and 9.20). Compensation of single-phase high-power traction systems are effectively performed with hybrid filters (Figs. 9.21 and 9.22). Three-phase three-wire power systems are supplying a large number of nonlinear loads with moderate power levels – such as adjustable-speed drives – up to large power levels associated with HVDC transmission systems. These loads can be compensated using either a group of passive filters (e.g., a passive filter unit as shown in Fig. 9.13a) or a combination of active and passive filters of different configurations (Figs. 9.23 to 9.25) depending on the properties of the AC system.

## 9.6 BLOCK DIAGRAM OF ACTIVE FILTERS

The generalized block diagram of shunt-connected active filters is shown in Fig. 9.26. It consists of the following basic elements [6]:

- ***Sensors and transformers*** (not shown) are used to measure waveforms and inject compensation signals. Nonsinusoidal voltage and current waveforms are sensed via potential transformers (PTs), current transformers (CTs), Hall-effect sensors, and isolation amplifiers (e.g., optocouplers). Connection transformers in shunt and series with the power system are employed to inject the compensation current ($I_{APF}$, see Fig. 9.26) and voltage ($V_{APF}$), respectively.
- ***Distortion identifier*** is a signal-processing function that takes the measured distorted waveform, $d(t)$ (e.g., line current or phase voltage) and generates a reference waveform, $r(t)$, to reduce the distortion.
- ***Inverter*** is a power converter (with the corresponding coupling inductance and transformer) that reproduces the reference waveform with appropriate amplitude for shunt ($I_{APF}$) and/or series ($V_{APF}$) active filtering.
- ***Inverter controller*** is usually a pulse-width modulator with local current control loop to ensure $I_{APF}$ (and/or $V_{APF}$) tracks $r(t)$.

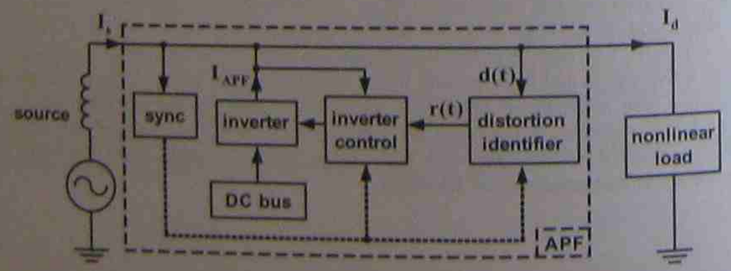



**FIGURE 9.26** Control diagram of shunt-connected active power filters (APFs) [6]. For series-connected active filters, the inverter injects the series voltage $V_{APF}$ via a series-connected transformer. For hybrid filters, two inverters are used for the simultaneous injection of $I_{APF}$ and $V_{APF}$.



- ***Synchronizer*** is a signal-processing block (based on phase-lock-loop techniques) to ensure compensation waveforms ($I_{APF}$ and/or $V_{APF}$) are correctly synchronized with the power system voltage. Certain control methods do not require this block.
- ***DC bus*** is an energy storage device that supplies the fluctuating instantaneous power demand of the inverter.

The control diagram of the series-connected active filter is identical to that given in Fig. 9.26; however, the inverter injects the series voltage $V_{APF}$ via a series-connected transformer. For the implementation of hybrid filters, the control diagram of Fig. 9.26 can be expanded to include both shunt ($I_{APF}$) and series ($V_{APF}$) compensation. Detailed implementation and control of a hybrid filter with active shunt and series converters (UPQC) is presented in Chapter 11.

The inverter block represents either a voltage-source inverter (VSI) or a current-source inverter (CSI). The VSI configuration includes an AC inductor $L_f$ along with optional small AC capacitor $C_f$ to form a ripple filter (for eliminating the switching ripple and improving the voltage profile) and a self-supporting DC bus with capacitor $C_d$. The CSI arrangement uses inductive energy storage at the DC link with current control and the shunt AC capacitors form a filter element. However, VSI structures have more advantages (lower losses, smaller size, less noise, etc.) and are usually preferred. Depending on the supply system, the inverter may be a single-phase two-arm bridge, a three-phase three-arm bridge and a three-phase four-arm bridge, or a mid point or three single-phase (e.g., for a four-wire system) bridge.

The inverter can be connected directly in series with the power system in single phase (to reduce the cost) or through connection transformers (usually with a higher number of turns on the inverter side) to act as a high active impedance blocking harmonic current and representing a low impedance for the fundamental current. In the same manner, the inverter may be connected in shunt either directly to the power system or through step-down transformers to act as an adjustable sink for harmonic currents.

The solid-state switching device is a MOSFET (metal oxide semiconductor field-effect transistor) for low power ratings, an IGBT (insulated-gate bipolar transistor) for medium power ratings, and a GTO (gate turn-off) thyristor for very high power ratings. These switching devices are manufactured in modular form (with gating, protection, and interfacing elements) to reduce the overall size, cost, and weight.

An essential component of the active filter is the control unit, which consists of a microprocessor. The voltage and current signals are sensed using potential transformers (PTs), current transformers (CTs), Hall-effect sensors, and isolation amplifiers. The control approach (Section 9.7) is implemented online by the microprocessor after receiving input signals through analog-to-digital (A/D) converter channels, phase-lock loop (PLL), and synchronized interrupt signals. All control tasks are carried out concurrently in specially designed processors at a very low cost.

## 9.7 CONTROL OF FILTERS

The initial stage for any filtering process is the selection of the filter configuration. Depending on the nature of the distortion and system structure, as well as the required precision and speed of the compensation, an appropriate filter configuration (e.g., shunt, series, passive, active, or hybrid, as presented in Sections 9.2 to 9.5) is selected. Implementation of passive filters is relatively straightforward, as discussed in Section 9.3. This section presents a classification of control approaches for active and hybrid power filters and identifies their performance strengths.

The control configuration of Fig. 9.26 is open loop because load current $I_d$ (not supply current $I_s$) is measured, load distortion is identified, and a correction signal is fed-forward to compensate the distortion in the supply current. The open-loop approach has some limitations including inadequate correction (due to errors in calculations and/or inaccuracy in current injection), unstable compensation (e.g., injected current perturbs load and/or source currents such that the distortion is changed), and processing delay (e.g., slow transient response). In contrast, the closed-loop control approach (e.g., measuring the supply current $I_s$) identifies remaining distortion and updates the injected compensation signal.

The choice of control strategy strongly depends on the required compensation response. Active and hybrid filters have the capability to correct a wide range of power quality problems:

- ***Harmonic distortion*** is taken as a core function of all filter designs. Shunt and series filters are capable of compensating current and voltage distortion, respectively, whereas hybrid filters (with shunt and series components) can correct both current and voltage waveform distortions.

ST. GEORGE POLYTECHNIC COLLEGE OF LAW

- ***Reactive power control*** at fundamental frequency is often included in the performance of active filters. It is possible to include harmonic reactive power control with more sophisticated control strategies.
- ***Correction of negative- and zero-sequence components*** at fundamental frequency due to imbalance and neutral current may be compensated with three-wire and four-wire three-phase hybrid active filters, respectively.
- ***Flicker*** (e.g., low irregular modulation of power flow) can also be compensated with active filters.
- ***Voltage sag and voltage swell*** are usually considered to be compensated by a dynamic voltage restorer (DVR); however, sophisticated hybrid active filters such as the UPQC (Fig. 9.21 and Chapter 11) can perform these types of compensations as well.

It is possible to consider and include all various types of power quality problems by adding the corresponding control functions to the basic active filter converter circuit; however, power rating and cost factors will become important and will raise challenging issues, especially in high-power applications.

There are three stages for the implementation of active (or hybrid) power filters (Fig. 9.26) [8]:

- ***Stage One: Measurement of Distorted Waveform d(t).*** For implementation and monitoring of the control algorithm, as well as recording various performance indices (e.g., either/both voltage or/and current THDs, power factor, active and reactive power), instantaneous distorted voltage and/or current waveforms need to be measured. This is done using voltage transformers (PTs), current transformers (CTs), or Hall-effect sensors including isolation amplifiers. Measured waveforms are filtered to avoid associated noise problems.
- ***Stage Two: Derivation of Reference Signal r(t).*** Measured distorted waveforms (consisting of fundamental component and distortion) are used to derive the reference signal (e.g., distortion components) for the inverter. This is done by the distortion identifier block. There are three main control approaches for the separation of the reference signal from the measured waveform, as discussed in Sections 9.7.1 to 9.7.3. The selected control method affects the rating and performance of the filter.
- ***Stage Three: Generation of Compensation Signal $I_{Arc}$ for $V_{And}$.*** The inverter reproduces the reference waveform with appropriate amplitude for both/either shunt ($I_{Arc}$) and/or series ($V_{Arc}$) active filtering. These compensation signals are injected into the system to perform the required compensation task. The inverter control block uses reference-following techniques (discussed in Section 9.7.5) to generate the gating signals for the solid-state switches of the inverter.

Shunt active filters are often placed in low-voltage distribution networks, where there is usually a considerable amount of voltage distortion due to the propagation of current harmonics injected by nonlinear loads. Nonsinusoidal voltages at the terminals of an active filter will deteriorate its performance and require additional control functions.

Control objectives of filters are classified based on the supply current components to be compensated and by the response required to correct the distorted system voltage. An important question for the selection of filter control is, what is the most desirable response (of the combined filter and load) to the distortion of the supply voltage? Considering this question, there are three main control categories of compensation (Stage Two, as discussed in Section 9.7.1):

- ***Waveform compensation*** is based on achieving a sinusoidal supply current. The combination of filter and load is resistive at fundamental frequency and behaves like an open circuit for harmonic frequencies.
- ***Instantaneous power compensation*** relies on drawing a constant instantaneous three-phase power from the supply. In response to supply harmonic voltages, significant harmonic currents are drawn that result in nonsinusoidal current flow. The combination of filter and load generates a complicated and nonlinear response to the distorted excitation that cannot be described in terms of impedance.
- ***Impedance synthesis*** responds to voltage distortion with a resistive characteristic and draws harmonic currents in phase with the harmonic voltage excitation. The combination of filter and load draws power at all harmonic frequencies of the supply voltage and can be made to closely approximate a passive system.

There are a variety of reference-following techniques (Stage Three) that can be implemented to generate the compensation signal $I_{Arc}$, including hysteresis-band, PWM, deadbeat, sliding, and fuzzy control, etc. A number of these control approaches are discussed in Section 9.7.5.



### 9.7.1 Derivation of Reference Signal using Waveform Compensation

The objective of waveform compensation is to achieve a sinusoidal supply current. There are many signal-processing techniques that can be used to decompose the distorted waveform into its fundamental (to be retained) and harmonic (to be cancelled) components. This is essentially a filtering task; however, in addition to the analytical approaches, there are also pattern-learning techniques that may be implemented.

#### 9.7.1.1 Waveform Compensation using Time-Domain Filtering

Distortion identification is a filtering task that can be performed by time-domain techniques or by Fourier-based frequency decomposition. The nonideal properties of real filters such as attenuation (e.g., preserving the identified components and heavily attenuating other components with a narrow bandwidth), phase distortion (e.g., preserving the phase of the identified components), and time response (e.g., considering the time-varying nature of the distortion signal and enforcing rapid filter response without large overshoot) must be recognized. The performance considerations of time-domain filters are linked, for example, smoothness of the magnitude response has to be traded off versus the phase response, and a well-damped transient response is in conflict with a narrow transition region. There are two general approaches to identify the distortion components in the time domain (Fig. 9.27a):

- ***Direct distortion identification*** applies a high-pass filter to the distorted signal $d(t)$ to determine the reference $r(t)$. Therefore, the identification process is subject to the transient response of the filter.
- ***Indirect distortion identification*** uses the filter to determine the fundamental component $f(t)$ and

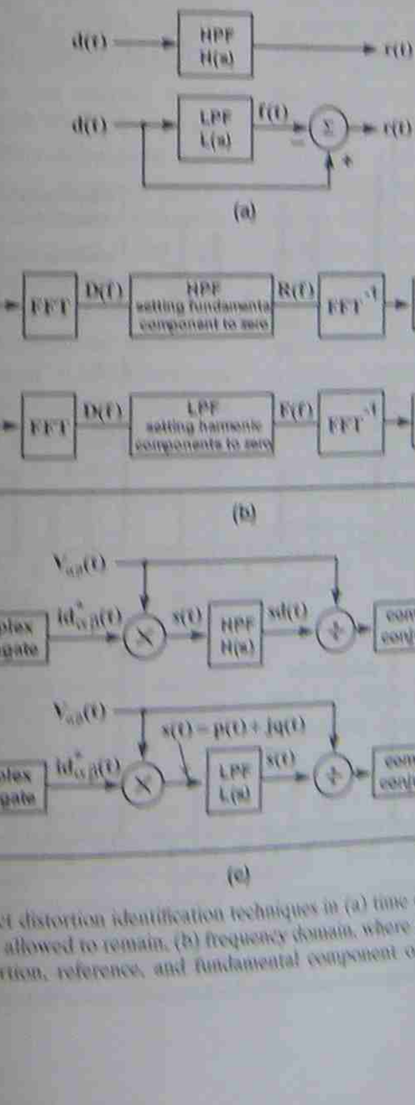



**FIGURE 9.27** Direct and indirect distortion identification techniques in (a) time domain, where $f(t)$ is the identified fundamental frequency signal that is allowed to remain, (b) frequency domain, where $D(f)$, $R(f)$, and $F(f)$ are the frequency-domain representations of distortion, reference, and fundamental component of the distorted signal, respectively [6], (c) instantaneous power domain.

subtracts it from the distorted signal $d(t)$ to form the reference $r(t)$.

Due to the inherent time lag of actual filters, the distortion term of the direct method will be out of date and the distortion cancellation will be in error. The disadvantage of the indirect method is the out-of-date fundamental term that requires additional exchange of real power through the inverter, resulting in DC-bus voltage disturbance and increased rating of the inverter. Most active filters use indirect distortion identification to achieve the best distortion cancellation during transients. Direct methods are preferred in applications where specific ranges of harmonics are to be compensated or where different groups of harmonics are to be treated differently.

To facilitate the separation of fundamental and harmonic components of the signal, active filter control algorithms rely on transformation techniques to transfer the signal from the conventional three-phase (abc) reference frame to an orthogonal two-phase representation. This will reduce the burden of intensive computations. Two well-known transformations, the stationary $\alpha\beta0$ reference and the rotating $dq0$ reference (also called Park transformation) frames, are widely employed (see Fig. 9.27). The spectra of a nonlinear load current (supplied by undistorted sinusoidal supply voltage) in abc, $\alpha\beta0$, and $dq0$ reference frames are shown in Fig. 9.28a,b,c, respectively. Analysis of these graphs indicates:

- The nonlinear load is assumed to be three-wire, three-phase and unbalanced that injects harmonics of the order $(6k \pm 1)$, where $k$ is any positive integer. This is clearly demonstrated by the frequency spectrum in the (abc) phase domain (Fig. 9.28a). Note that there is no distinction between harmonic components of the same order with different phase rotation.
- Both $\alpha\beta0$ and $dq0$ decompositions (Fig. 9.28b,c, respectively) transfer the zero-sequence component into a separate component set. Harmonic components with the same order and opposite phase rotation (e.g., $-h$ and $h$) are separated because positive and negative sets are shifted to orders $(h-1)$ and $-(h-1)$, respectively.

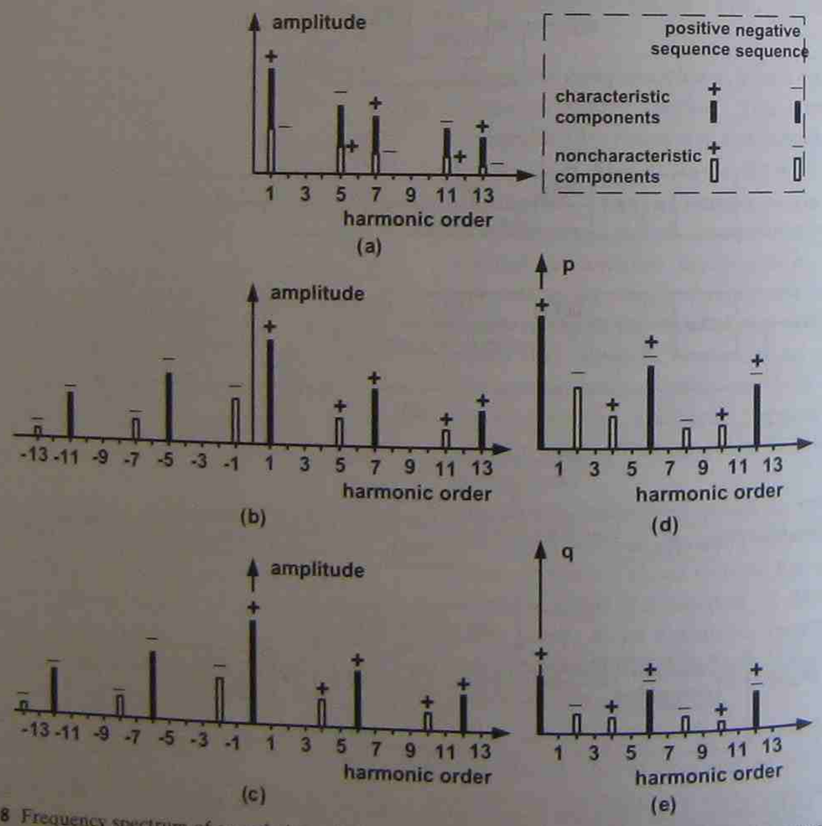



**FIGURE 9.28** Frequency spectrum of an unbalanced, three-wire three-phase nonlinear load (injecting current harmonics of order $h = (6k \pm 1)$: (a) current in phase domain, (b) current in $\alpha\beta0$ domain, (c) current in $dq0$ domain, (d) active power (p) in instantaneous power domain, (e) reactive power (q) in instantaneous power domain [6].

ST. GEORGE COLLEGE OF LAW



- The $\alpha\beta0$ transformation (Fig. 9.28b) has no effect on the frequency spectra and does not separate sequence sets. The sequence can be determined from whether either the "$\alpha$" or the "$\beta$" component leads. The negative harmonic term of order –1 indicates the imbalance of the fundamental. Balanced nonlinear loads produce characteristic harmonics of order $-5, +7, -11, +13, \ldots, 6k+1$. Unbalanced nonlinear loads generate in addition noncharacteristic harmonic components of order $+5, -7, +11, -13, \ldots, 6k-1$.
- With the rotating $dq0$ transformation (Fig. 9.28c) all frequency components are shifted downward by one harmonic order. The positive-sequence fundamental becomes a DC term and the negative-sequence fundamental becomes a double-frequency term (order –2). The characteristic and noncharacteristic distortions are of orders 6k and $(6k-2)$, respectively.
- There is no difference between filtering in the abc or $\alpha\beta0$ domains, but the $dq0$ domain is a better alternative because it offers frequency separation of fundamental, positive, and negative sequences, which makes the filtering task simpler. In the abc domain the fundamental may be separated using a low-pass filter that cuts off between orders 1 and 5 (or 1 and 3 if there is zero-sequence/four-wire harmonic distortion). In the $dq0$ domain, the filter cutoff should be between 0 and 6 for balanced conditions. For unbalanced conditions, a cutoff between 0 and 2 will allow the negative-sequence (unbalanced) fundamental to be corrected and a cutoff between 2 and 4 will not cancel the unbalanced fundamental but will cancel harmonic distortion. Zero-sequence distortion is conveniently placed in a separate component set that may be cancelled or retained as required.

#### 9.7.1.2 Waveform Compensation Using Frequency-Domain Filtering

Filtering in the frequency domain requires discrete or fast Fourier transform (DFT or FFT) on a section of the signal that contains at least one cycle of the lowest frequency of interest and that has been sampled at over twice the highest harmonic frequency as prescribed by the Nyquist theorem. The advantage of filtering in the frequency domain is that completely abrupt cutoffs (with no transition band, low-pass band ripple, and phase distortion) can be obtained. The main disadvantage is that the filtering process is not very suitable for real-time filters and sufficient time is required for sampling the signal and performing the transformation. In addition, the signals must be steady state and periodic because FFT implicitly assumes periodicity of the sampled waveform. If the FFT window is properly synchronized to the fundamental signal then the phase and magnitudes of the components can be accurately determined. If the sampling window does not cover an integer number of fundamental cycles, accuracy will be degraded (spectral leakage).

Distortion identification may also be performed with a direct or indirect approach using frequency-domain filtering (Fig. 9.27b). FFT is performed to transfer the distorted signal $d(t)$ to the frequency domain $D(f)$. In the direct method, the fundamental component is set to zero to form a cancellation reference. The filter may also cancel the reactive component if only the real (in-phase) component of the signals are set to zero. In the indirect method, all harmonic terms are set to zero; the fundamental is subtracted from the instantaneous signal to generate the reference signal. The filter may also cancel the reactive component if the imaginary (quadrature) fundamental component is set to zero. The final step is the application of the inverse FFT to generate $r(t)$.

A problem with frequency-domain filtering is that during transient conditions, the periodicity of the distortion is lost and the cancellation is not accurate. There is also time delay in filtering that can affect the distortion identification performance. For most applications, one complete cycle of data is stored in a buffer, processed during the next cycle, and de-buffered for use as a cancellation reference in the following cycle, that is, the cancellation reference is two cycles out of date. For applications requiring fast compensation, shorter update rates are possible by performing a FFT every half-cycle using one half-cycle of fresh data plus data from the previous half-cycle. This will reduce the filtering delay to one cycle.

#### 9.7.1.3 Other Methods for Waveform Compensation

There are other waveform compensation schemes that attempt to overcome the disadvantages of time-domain techniques (e.g., compromises or imperfections in filter design) and the inherent time delay of frequency-domain approaches, such as heterodyne methods and neural networks.

The heterodyne methods of waveform compensation involve multiplying the distorted signal by a

sinusoid [6]. If the sinusoid is of fundamental frequency then the fundamental frequency component of the distorted signal will be transformed to DC and double-frequency terms. The DC term can be separated with a low-pass filter. If the heterodyning sinusoid is in phase with the voltage, the fundamental active current is identified; otherwise, the fundamental reactive current can be identified using a quadrature sinusoid. As with the time-domain approaches, a low-order filter provides poor separation of the DC and double-frequency terms and a sharp (high-order) filter will have a long step response. Heterodyne methods of waveform compensation are popular in single-phase systems where $\alpha\beta0$ and $dq0$ transformations are not applicable.

Separation of a signal into the fundamental and distorted components can also be performed by using neural networks [6]. Both direct and indirect principles can be implemented. Neural networks can be used as harmonic identifiers to estimate the Fourier coefficients of the distorted signal. They can be trained to learn the characteristics of the load current (or that of the local grid system) to produce the cancellation reference. They may also be employed to provide fast-frequency decomposition to identify the fundamental component (e.g., for indirect algorithms) or low-order harmonics for a range of load current amplitudes.

### 9.7.2 Derivation of Compensated Signals Using Instantaneous Power Compensation

Another approach to control active filters is to cancel the fluctuating component of instantaneous power and perhaps compensate the fundamental component of the reactive power. A common approach is to start with the definitions of instantaneous active and reactive powers and express them in terms of average and alternating (fluctuating) components. This can be performed in either the abc, $\alpha\beta0$, or $dq0$ domain:

- In the $\alpha\beta0$ domain:

$$\begin{bmatrix} v_0 \\ v_\alpha \\ v_\beta \end{bmatrix} = \sqrt{\frac{2}{3}} \begin{bmatrix} 1/\sqrt{2} & 1/\sqrt{2} & 1/\sqrt{2} \\ 1 & -1/2 & -1/2 \\ 0 & \sqrt{3/2} & -\sqrt{3/2} \end{bmatrix} \begin{bmatrix} v_a \\ v_b \\ v_c \end{bmatrix}. \quad (9\text{-}12)$$

Without the zero-sequence component, the instantaneous power can be written as

$$\begin{aligned} s(t) &= p(t) + jq(t) \\ &= v_{\alpha\beta}\, i^*_{\alpha\beta} = (v_\alpha + jv_\beta)(i_\alpha - ji_\beta) \\ &= (v_\alpha i_\alpha + v_\beta i_\beta) + j(v_\beta i_\alpha - v_\alpha i_\beta), \end{aligned} \quad (9\text{-}13a)$$

where the superscript * denotes the complex conjugate. Therefore,

$$\begin{bmatrix} p \\ q \end{bmatrix} = \begin{bmatrix} (v_\alpha i_\alpha + v_\beta i_\beta) \\ (v_\beta i_\alpha - v_\alpha i_\beta) \end{bmatrix} = \begin{bmatrix} v_\alpha & v_\beta \\ v_\beta & -v_\alpha \end{bmatrix} \begin{bmatrix} i_\alpha \\ i_\beta \end{bmatrix}. \quad (9\text{-}13b)$$

- In the $dq0$ domain:

$$\begin{bmatrix} v_d \\ v_q \\ v_0 \end{bmatrix} = \sqrt{\frac{2}{3}} \begin{bmatrix} \cos\theta_d & \cos(\theta_d - 2\pi/3) & \cos(\theta_d + 2\pi/3) \\ -\sin\theta_d & -\sin(\theta_d - 2\pi/3) & -\sin(\theta_d + 2\pi/3) \\ 1/\sqrt{2} & 1/\sqrt{2} & 1/\sqrt{2} \end{bmatrix} \begin{bmatrix} v_a \\ v_b \\ v_c \end{bmatrix}. \quad (9\text{-}14)$$

In this equation $\theta_d = \omega_d + \varphi$, where $\omega_d$ is the angular velocity of voltages and $\varphi$ is the initial voltage angle. With no zero-sequence components:

$$\begin{aligned} s(t) &= p(t) + jq(t) \\ &= v_{dq}\, i^*_{dq} = (v_d + jv_q)(i_d - ji_q) \\ &= (v_d i_d + v_q i_q) + j(v_q i_d - v_d i_q). \end{aligned} \quad (9\text{-}15)$$

In four-wire systems there is the additional term of zero-sequence instantaneous (real or reactive [6]) power; with Eqs. 9-13 and 9-15 the instantaneous power may be written as

$$\begin{aligned} p(t) &= \bar{p} + \tilde{p}(t) \\ q(t) &= \bar{q} + \tilde{q}. \end{aligned} \quad (9\text{-}16)$$

Figure 9.28a,d,e shows the spectra of current, active, and reactive powers for the case of a sinusoidal supply voltage, which is harmonically distorted and generates unbalanced currents. Characteristic harmonics of order $h = 6k + 1$ (e.g., $-11, -5, 7, 13, \ldots$, where negative orders represent negative-sequence harmonics) produce power terms of order $6|k|$, whereas noncharacteristic harmonics of order $h = 6k - 1$ (e.g., $-13, -7, 5, 11, \ldots$) yield power terms of order $6|k| \pm 2$.

The inverse transform (e.g., conversion from power domain to the phase domain) is

$$i^*_{\alpha\beta} = i_\alpha - ji_\beta = \frac{s}{v_{\alpha\beta}} = \frac{(pv_\alpha + qv_\beta) + j(qv_\alpha - pv_\beta)}{v_\alpha^2 + v_\beta^2} \quad (9\text{-}17)$$

or

$$\begin{bmatrix} i_\alpha \\ i_\beta \end{bmatrix} = \frac{1}{v_\alpha^2 + v_\beta^2} \begin{bmatrix} v_\alpha & v_\beta \\ v_\beta & -v_\alpha \end{bmatrix} \begin{bmatrix} p \\ q \end{bmatrix}. \quad (9\text{-}18)$$



Figure 9.27c depicts direct and indirect distortion identification approaches based on the instantaneous power domain as given by Eq. 9-18. The concept is analogous to that of the frequency domain and similar comments apply.

Equation 9-18 assumes sinusoidal supply voltages and distorted currents. However, active filter control relying on the instantaneous power method causes harmonic currents to flow when the supply voltage is either distorted or unbalanced (see Application Examples 9.3 and 9.4). The following comments apply to the instantaneous power decomposition:

- Since p and q terms are readily available (e.g., by setting the $q$-term to zero in the indirect method and not removing it by filtering in the direct method), it is easy to include the compensation of fundamental reactive power in the active filter control algorithm and perform optimal power follow.
- Fundamental-frequency negative-sequence current appears as a second harmonic in the instantaneous power domain and may be easily filtered.
- The instantaneous power method applied in the $\alpha\beta0$ domain has low processing burden because it does not require rotational transformation and explicit synchronization.
- The inverse transformation of Eq. 9-18 assumes sinusoidal supply voltages with current distortions. If both the supply voltage and the load current are distorted, active filter (with instantaneous power compensation) will result in harmonic current flow through the supply (Eq. 9-22). A similar scenario occurs when the supply contains negative-sequence voltages introducing imbalance in the currents and harmonic distortion [6]. Efforts such as modifying the inverse transformation and altering the definition of p and q have been made to overcome this problem.
- This section has focused on the control of shunt active filters. Similar discussions apply to the control of series active filters for which dual equations can be generated.

#### 9.7.2.1 *Application Example 9.2: Instantaneous Power for Sinusoidal Supply Voltages and Distorted Load Currents*

Assuming a sinusoidal supply voltage and a distorted load current (with fundamental and a single harmonic component of order h), find the equations for instantaneous power as well as average and fluctuating, pulsating, or oscillating real and reactive powers.

***Solution:***

$$\begin{aligned} p(t) &= V_1 I_1 + V_1 I_h \cos[(1-h)\omega t] \\ &\Rightarrow \begin{cases} \bar{p} = V_1 I_1 \\ \tilde{p} = V_1 I_h \cos[(1-h)\omega t] \end{cases} \\ q(t) &= -V_1 I_h \sin[(1-h)\omega t] \Rightarrow \begin{cases} \bar{q} = 0 \\ \tilde{q} = -V_1 I_h \sin[(1-h)\omega t] \end{cases} \end{aligned} \quad (9\text{-}19)$$

#### 9.7.2.2 *Application Example 9.3: Instantaneous Power Consumed by a Resistive Load Subjected to Distorted Supply Voltages*

A three-phase distorted voltage waveform consisting of the fundamental and one harmonic component of order $h$ is connected across the terminals of a balanced three-phase resistor bank in ungrounded $Y$ configuration. Compute the components of voltages and currents in the $\alpha\beta0$ domain and determine the average and the fluctuating active power consumed by the load.

***Solution:***

The load is balanced and has no zero-sequence terms due to the ungrounded Y. The $\alpha$ and $\beta$ components are

$$\begin{aligned} v_\alpha &= V^{(1)}\cos(\omega t) + V^{(h)}\cos(h\omega t) \\ v_\beta &= V^{(1)}\sin(\omega t) + V^{(h)}\sin(h\omega t) \\ &\Rightarrow \begin{aligned} i_\alpha &= \frac{V^{(1)}}{R}\cos(\omega t) + \frac{V^{(h)}}{R}\cos(h\omega t) \\ i_\beta &= \frac{V^{(1)}}{R}\sin(\omega t) + \frac{V^{(h)}}{R}\sin(h\omega t) \end{aligned} \end{aligned} \quad (9\text{-}20)$$

Applying Eqs. 9–13 and 9–16:

$$\begin{aligned} p(t) &= (v_\alpha i_\alpha + v_\beta i_\beta) = \bar{p} + \tilde{p}(t) \\ &\Rightarrow \begin{cases} \bar{p} = \dfrac{(V^{(1)})^2}{R} + \dfrac{(V^{(h)})^2}{R} \\ \tilde{p}(t) = 2\dfrac{V^{(1)}V^{(h)}}{R}\cos[(1-h)\omega t] \end{cases} \end{aligned} \quad (9\text{-}21)$$

Note that an oscillatory power with the difference frequency (e.g., $(1-h)f_1$) is generated. Based on these equations, a nonsinusoidal current must be drawn from a distorted supply voltage to maintain a constant instantaneous power. Similarly, a nonsinusoidal current is required to draw constant instanta-

ST. GEORGE COLLEGE OF

neous power from an unbalanced supply voltage (containing a fundamental-frequency negative-sequence component). Therefore, both/either distorted and/or unbalanced supply voltages will force the active filter (with instantaneous power based controller) to inject harmonic currents.

#### 9.7.2.3 Application Example 9.4: Supply Current Distortion Caused by Active Filters with Instantaneous Power-Based Controllers

An active filter with an instantaneous power controller is applied to the system of Application Example 9.3. Compute $\alpha$ and $\beta$ components of the supply current after the filter has been installed and the nonsinusoidal load current (through the resistive load) has been compensated.

***Solution:***
Relying on Eqs. 9-18 and 9-21, the supply current corresponding to constant power is

$$\begin{aligned} i_\alpha &= \frac{pv_\alpha}{v_\alpha^2+v_\beta^2} \\ &= \frac{p[V^{(1)}\cos(\omega t)+V^{(h)}\cos(h\omega t)]}{(V^{(1)})^2+2V^{(1)}V^{(h)}\cos[(1-h)\omega t]+(V^{(h)})^2} \\ i_\beta &= \frac{-pv_\beta}{v_\alpha^2+v_\beta^2} \\ &= \frac{p[V^{(1)}\sin(\omega t)+V^{(h)}\sin(h\omega t)]}{(V^{(1)})^2+2V^{(1)}V^{(h)}\cos[(1-h)\omega t]+(V^{(h)})^2}. \end{aligned} \tag{9-22}$$

Note the presence of different harmonics in the numerators and denominators which are not of the same order as that of the voltage excitation (e.g., order $h$). Therefore, a single voltage harmonic distortion gives rise to an infinite series of current harmonics when the active filter controller is based on instantaneous power compensation.

### 9.7.3 Derivation of Compensating Signals Using Impedance Synthesis

Impedance synthesis is based on the idea of modifying the inverse transform of the instantaneous power (Eq. 9-17) to prevent injection of higher frequency current harmonics. If Eq. 9-17 is modified using the root-mean-square (rms) value of the current, that is, replace $v_\alpha^2+v_\beta^2$ with $(v_\alpha)_{rms}+(v_\beta)_{rms}$, the denominator will not be time varying and a modulation of the current is avoided. There are two impedance synthesis approaches where the voltage and current are related by a chosen value of the impedance: impedance-based blocking and impedance-based compensation.

#### 9.7.3.1 Impedance-Based Blocking

Impedance-based blocking control presents resistive characteristics at all frequencies. A filter arrangement with a number of shunt and series (passive and/or active) branches is used to block or enable a signal path. An inverter acting as an impedance relating voltage to current by a simple transfer function can form one branch of the filter. This normally takes the form of a hybrid filter consisting of active and passive elements, although combinations of active units – without passive elements – are also possible.

There are many forms of hybrid filters (Section 9.5) that can be used for impedance-based blocking. For example, a hybrid combination consisting of a series active filter and a shunt passive filter can be used to perform impedance synthesis. The role of the series branch is to block harmonic currents by representing a high impedance. The instantaneous power theory can be utilized to separate the distortion terms of the current. The active filter then injects a voltage proportional to this current to synthesize a moderately high impedance. In practice, the filter employed to separate the oscillatory terms in the instantaneous power may not be perfect and might influence the impedance presented by the overall active filter [6].

#### 9.7.3.2 Impedance-Based Compensation

A difficulty faced in designing the control of active filters for general purposes (e.g., correcting a group of nonlinear loads) is that the system dynamics are unknown. Furthermore, the compensation current – in response to the detected distortion – might activate one of the system resonances or perturb the voltage and cause instability [6].

One solution is to use a shunt device that draws a current proportional to the voltage. This is done by utilizing a dissipative active filter that absorbs energy at harmonic frequencies; thus voltage harmonics are detected and damped. This is a passive controller because it presents a resistive characteristic. Therefore, the operation of the active filter is stable regardless of the system structure.



### 9.7.4 DC Bus Energy Balance

The DC buses of inverters in active power filter systems are not DC links but energy storage devices. If a voltage-source inverter is used, the link contains a capacitor; otherwise an inductor acts as the DC link for the current-source inverter.

In practice, the link voltage will not usually remain constant due to various effects:

- real power exchange between the active filter and the AC grid,
- converter (conduction and switching) losses,
- undesirable real power components in the compensation reference signal due to magnitude and phase errors of the distortion identifier or because of time delays in responding to a transient condition,
- the error between the identified correction current and the actual output current of the inverter that may lead to some power exchange, and
- distortion in the grid voltage that might cause some real power exchange.

To overcome these deficiencies, converter power losses are compensated by drawing a balancing power into the DC bus from the AC grid. This may be performed through a DC-bus voltage regulator (Fig. 9.29) as follows:

- The voltage error signal is generated based on a reference DC voltage;
- The error is passed through a controller;
- A PI compensator operates on the voltage error. It should have a low crossover frequency to avoid interaction with the compensation system;
- Controller output is taken as a demand for fundamental active current and is added to the compensation reference;
- The control algorithm can be implemented in any convenient domain (e.g., abc, $\alpha\beta 0$, or $dq0$ domain); and
- The bandwidth of the controller must be carefully selected: if it is too high (comparable with the fundamental frequency), the injected balancing current will contain components at harmonic frequencies that will add distortion to the system; if it is too low, the DC-link voltage may deviate from its nominal value.

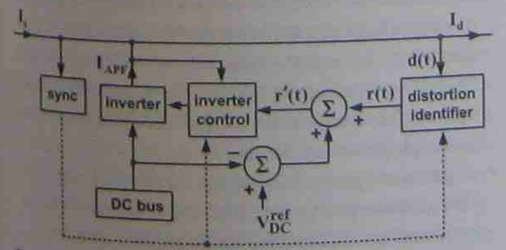



**FIGURE 9.29** A simple DC-bus voltage regulator [6].

### 9.7.5 Generation of Compensation Signal Using Reference-Following Techniques

The identified reference signal (with one of the techniques discussed in Sections 9.7.1 to 9.7.3) must be generated or reproduced by the inverter (Fig. 9.26) and injected into the system to eliminate the power quality problem. Generation of the compensation signal that accurately follows the identified reference may be difficult because of the following:

- the high rate of change and the wide bandwidth of the reference signal,
- the errors in the generated reference caused by the *di/dt* limit of a voltage-source inverter,
- the voltage imposed on the inverter (e.g., difference between the available DC-bus voltage and the instantaneous voltage of the AC system),
- the impact of increasing the DC-bus voltage – to improve the reference following – on the ratings of the inverter, and
- the effect of the processing delay on the formation of the reference waveform.

Three approaches to force the inverter output current to follow a reference signal are widely implemented: PWM current regulation, hysteresis regulation, and deadbeat or predictive control.

***PWM Current Regulation.*** The current error, for example, the difference between identified (reference) and generated signals, is acted on by a PI controller and its output is passed through a PWM or space-voltage vector modulation to define the voltage to be produced by the inverter. The controller may be of the open- or closed-loop type and can be implemented in any convenient (abc, $\alpha\beta 0$, or $dq0$) domain.

***Hysteresis Regulation.*** The main idea is to force the compensation signal to follow the reference signal within a given hysteresis band error (e.g., $i_{compensation} = i_{reference} \pm \Delta i_{hysteresis}/2$). The implementation of this controller is easy as it requires an op-amp operating in the hysteresis mode. Hysteresis regulation is unconditionally stable, does not require detailed plant data, and can achieve high rates of change in the controlled variable. Unfor-

tunately, there are several drawbacks such as the unpredictable switching frequency and the broad-band switching noise injected by the nonconstant switching frequency. Consequently, different approaches have been considered to maintain constant (or near constant) switching frequency and to synchronize the switching of all three phases.

***Deadbeat or Predictive Control.*** Deadbeat or predictive control is attractive for following rapidly changing reference signals of active filters because it selects a voltage command for the inverter that will force the generated current to reach a target value by the end of the next sample period [6]. However, it requires knowledge of the system to accurately model the rate of change of current ($di/dt$) and to properly select the voltage command. The interface inductance of the inverter is a key parameter and the opposing AC system voltage must be measured or estimated. Deadbeat controllers may be applied when there is some parameter uncertainty (e.g., the coupling inductor). Adaptive filters can be employed to predict the current reference, and the deadbeat controller can use the predicted current at the end of the sample period as the target current [6].

### 9.7.6 Application Example 9.5: Hybrid of Passive and Active Power Filters for Harmonic Mitigation of Six-Pulse and Twelve-Pulse Rectifier Loads [16]

This example demonstrates the application of hybrid filters to compensate harmonics of a nonlinear load consisting of two six-pulse rectifiers. The two rectifiers are connected to the secondary of a ($Y/\Delta$, $Y$) transformer. The simultaneous operation of the two six-pulse rectifiers represents a twelve-pulse rectifier load. Two arrangements of hybrid filters are considered:

***Hybrid Filter #1*** is composed of a shunt-hybrid filter in parallel with a passive filter as shown in Fig. E9.5.1. The passive filter consists of a set of tuned branches. The hybrid power filter is a series combination of an active filter with a small rating (converter) and a passive branch. Due to the use of a parallel passive filter, the converter rating is decreased and the performance and resonance problems of the passive filter are expected to improve.

***Hybrid Filter #2*** is composed of a shunt-hybrid filter in parallel with two passive filters tuned at the 5th and 7th harmonics as shown in Fig. E9.5.2. The hybrid filter consists of an active filter with a small rating in series with two passive branches and is tuned at the dominant 11th and 13th harmonics.

a) Plot the load current waveforms and calculate *THD*, with twelve-pulse and six-pulse rectifier configurations.
b) Derive the equations for power system and passive and hybrid filter currents.
c) With a six-pulse rectifier load, plot the waveforms of the power system, load, passive filter, and hybrid filter branch currents before and after the installation of hybrid filters #1 and #2.
d) Plot the power system current under resonant conditions before and after the addition of hybrid filter #2.
e) Compare the performances of hybrid filters #1 and #2.

## 9.8. SUMMARY

With the increase of harmonic currents and voltages in present-day power systems, the installation of passive, active, and hybrid filters gains in importance. In the future, recommended practices such as IEEE-519 [11] will result in further increased use of filters within the distribution system. There are a great variety of filter configurations (Figs. 9.3 and 9.13 to 9.25). Classification of filters can be based on different criteria such as supply type, filter connection, number of filter elements, power rating, compensation type, speed of response, and control technique. In this chapter the classification of power filters is performed based on the type of supply (Fig. 9.3) and the control method (Section 9.7). Proper selection of filter configurations depends primarily on the properties of nonlinear loads, type of supply, and system rating:

- Passive filter blocks (Fig. 9.12 and 9.13) and a combination of passive filters (Figs. 9.19 and 9.20) are the most qualified candidates for single-phase systems – with high penetration of nonlinear loads – and low-power applications.
- Hybrid filters (Figs. 9.21 and 9.22) are considered as a cost-effective option for power quality improvement, compensation of the poor power quality effects of nonlinear loads, or to provide a sinusoidal AC supply to sensitive loads, especially for high-power applications. They are also good options for compensation of single-phase systems and high-power applications.
- A group of passive filters (Fig. 9.13a) or a combination of active and passive filters in different configurations (Figs. 9.23 to 9.25) should be used for the compensation of three-phase three-wire power systems that have a great amount of current or



voltage harmonics due to a large number of small- and moderate-rating nonlinear loads, as well as feeding terminals of HVDC transmission systems.

Selection of the control approach (Sections 9.7.1 to 9.7.3 and 9.7.5) greatly depends on the choice of the control objective, for example, the required waveform of the supply current after compensation. The selection of the domain (e.g., time or frequency) and the reference frame (e.g., $dq0$ or $\alpha\beta0$) will affect the computational burden required to implement appropriate filters. All active filters perform harmonic mitigation. However, depending on the selected control strategies, additional forms of compensation (e.g., fundamental reactive power, negative-sequence, zero-sequence, phase balancing, sag, swell, and flicker) can be accommodated within the apparent power rating of an active filter. There exist three different definitions for the control objective:

***First Definition:*** Supply currents (after filtering) should contain only fundamental frequency components. This is the main task of active filter controllers using waveform compensation (Section 9.7.1).

***Second Definition:*** Supply currents (after filtering) should be such that the instantaneous active power is constant while the instantaneous reactive power is zero. This is performed by active filter controllers that use instantaneous power compensation (Section 9.7.2).

***Third Definition:*** Supply currents (after filtering) should be entirely active. This is the main function of active filter controllers using impedance-based compensation (Section 9.7.3).

If the supply voltage is not distorted (with nearly sinusoidal waveform), the following remarks should be considered for the selection of the control method:

- The three aforementioned objective definitions are equivalent and the choice of the control method should be based on the ease of their implementation and their instrumentation requirements.
- Given the harmonic limits provided by relevant guidelines, recommended practices, or standards such as IEEE-519 [11], waveform compensation (first definition) is the most important approach. The techniques for this approach separate the fundamental from the harmonic components. Time-domain filters have the advantage of continuity during transient conditions, whereas frequency-domain filters have a better selectivity under steady-state conditions. The synchronous $dq0$ reference frame can ease the filter implementation of three-phase systems at the expense of longer processing time.
- The instantaneous power methods (second definition) are beneficial in three-phase systems due to their ease of filter design without the need for $dq0$ transformation.
- The active current approaches (third definition) are relatively easy to implement because they require only the identification of the (average) real power. These approaches are implicit in controllers that use the energy balance at the DC bus to identify the desired current.

Further complications regarding the selection of the control method for active filters arise if the supply voltage (before filtering) is distorted. This is the case for most practical power quality problems, for example, when active filters are operating on weak feeders of the distribution network. If the supply voltage is distorted, the following guidelines should also be considered for the selection of the control method:

- Distorted supply voltage may increase the apparent power rating of the active power filter.
- Waveform compensation approaches only draw fundamental current and do not generate extra distortion; however, they will not provide damping of the existing distortion.
- Instantaneous active power methods respond to harmonic supply voltages by introducing additional harmonic currents at other frequencies (Eq. 9-22). In particular, a negative-sequence fundamental voltage will cause these controllers to inject harmonic currents.
- Controllers with impedance-based compensation – resulting in active supply current – represent resistive characteristics at all frequencies, and therefore convert nonlinear loads into linear loads. They inherently provide damping and reduce the propagation of harmonic voltages. However, the design of active filters will have to be coordinated with existing approaches for the damping of network resonances.

Active filters can be designed to perform phase balancing if the exchange of instantaneous power between phases is within their ratings.

- All three control approaches (waveform compensation, instantaneous power compensation, and impedance synthesis) can enforce phase balanc-

ST. GEORGE COLLEGE OF LAW

ST. GEORGE POLYTECHNIC LIBRARY



ing. Waveform compensation and impedance synthesis (active current) methods can be implemented on a phase-by-phase basis to avoid rebalancing.

- Instantaneous power methods (in their original form) have an unacceptable response under unbalanced operating conditions, and will inject additional harmonic currents at different frequencies. Modifications (e.g., redefining the inverse transformation) are necessary to control harmonic generation.
- Waveform compensation methods result in balanced currents despite unbalanced voltages.
- Impedance synthesis methods present balanced impedances to unbalanced voltages. As a result, they draw the least current from the smallest phase voltage. In contrast, the constant instantaneous power approaches draw the greatest current from the smallest phase voltage.



## 9.9 REFERENCES


1) Peng, F.Z.; "Harmonic sources and filtering approaches," *IEEE Industrial Application Magazine*, Vol. 7, pp. 18–25, 2001.
2) Das, J.C.; "Passive filters – potentialities and limitations," *IEEE Transactions on Power Industry Applications*, Vol. 40, no. 1, pp. 232–241, 2004.
3) Akagi, H.; "Active harmonic filters," *Proceedings of the IEEE*, Vol. 93, no. 12, pp. 2128–2141, 2005.
4) Singh, B.; Verma, V.; Chandra, A.; and Al-Hadded, K.; "Hybrid filters for power quality improvement," *IEE Proceedings – Generation, Transmission and Distribution*, Vol. 152, no. 3, pp. 365–378, 2005.
5) El-Habrouk, M.; Darwish, M.K.; and Mehta, P.; "Active power filters: a review," *IEE Proceedings – Electric Power Application*, Vol. 147, no. 5, pp. 403–413, 2000.
6) Green, T.C.; Marks, J.H.; "Control techniques for active power filters," *IEE Proceedings – Electric Power Application*, Vol. 152, no. 2, pp. 369–381, 2005.
7) Phipps, J.K.; "A transfer function approach to harmonic filter design," *IEEE Industrial Application Magazine*, pp. 68–82, 1997.
8) Singh, B.; Al-Haddad, K.; and Chandra, A.; "A review of active filters for power quality improvement," *IEEE Transactions on Industrial Electronics*, Vol. 46, no. 5, pp. 960–971, 1999.
9) Grainger, J.J.; and Civanlar, S.; "Volt/VAr control on distribution systems with lateral branches using shunt capacitors and voltage regulators. Part III: the numerical result," *IEEE Transactions on Power Apparatus and Systems*, Vol. 104, no. 11, pp. 3291–3297, 1985.
10) Hu, Z.; Wang, X.; Chen, H.; and Taylor, G.A.; "Volt/VAr control in distribution systems using a time-interval based approach," *IEE Proceedings – Generation, Transmission and Distribution*, Vol. 150, no. 5, pp. 548–554, 2003.
11) *IEEE Recommended Practice and Requirements for Harmonic Control in Electric Power Systems*, IEEE Standard 519, 1992.
12) Nilsson, J.W.; *Electric Circuits*, Addison-Wesley Publishing Company, Reading, Massachusetts, 1983.
13) Thomas, R.E.; and Rosa, A. J.; *The Analysis and Design of Linear Circuits*, 4th Edition, John Wiley & Sons, Inc., 2004.
14) Masoum, M.A.S.; Ulinuha, A.; Islam S.; and Tan, K.; "Hybrid passive filter design for distribution systems with adjustable speed drives," *The Seventh International Conference on Power Electronics and Drive Systems (PEDS-2007)*, November 27–30, 2007, Bangkok, Thailand.
15) Jou, H.L.; Wu, J.C.; and Wu, K.D.; "Parallel operation of passive power filter and hybrid power filter for harmonic suppression," *IEE Proc. on Generation, Transmission and Distribution*, Vol. 148, Issue 1, pp. 8–14, Jan 2001.
16) Gholamrezaei, M.; Masoum, M.A.S.; and Kalantar, M.; "Parallel combination of passive and hybrid power filters for harmonic mitigation," *18th International Power System Conference*, Vol. 1, pp. 7–15, PSC 2003.

ST. GEORGE'S COLLEGE OF LAW

# 10
CHAPTER

# Optimal Placement and Sizing of Shunt Capacitor Banks in the Presence of Harmonics

At the distribution level about 13% of the total generated power consists of losses due to active and reactive current components. Research over the past several decades has shown that proper placement of shunt-capacitor banks can reduce the losses caused by reactive currents [1–34]. In addition to the reduction of energy and peak-power losses, effective capacitor installation can also release additional reactive power capacity within the distribution system and can improve the system voltage profile. Studies [35–46] indicate that the proper placement of shunt capacitors in the presence of voltage and current harmonics can also improve power quality and reduce the total voltage harmonic distortion ($THD_v$) of distribution systems. Thus, the problem of capacitor allocation involves the determination of the optimal locations, sizes, and number of capacitors to be installed within a distribution system such that maximum benefits are achieved, while all operational constraints (e.g., voltage profile, $THD_v$, and total number of capacitor banks at each bus and the entire system) are satisfied at different loading levels. There are a great many papers describing capacitor placement algorithms: the Capacitor Subcommittee of the IEEE Transmission and Distribution Committee has published 10 bibliographies on power capacitors from 1950 to 1980 [33]. Moreover, the VAr Management Working Group of the IEEE System Control Subcommittee has published another bibliography on reactive power and voltage control [34]. The total publication count listed in these bibliographies is over 400, and many of the papers are specific to the problem of optimal capacitor allocation [1–46]. Recent efforts mainly focus on the capacitor placement under nonsinusoidal operating conditions.

In power systems, the predominantly inductive nature of loads and distribution feeders as well as transformers and lines accounts for significant power losses due to lagging currents. The introduction of strategically sized and placed shunt capacitors within the distribution system helps to reduce the losses created by an inductive system, thus increasing the system capacity, reducing system losses, and improving the voltage profile. Due to the fact that there are many constraints and variables present, the process for calculating the placement and sizing of shunt capacitors involves the evaluation of an optimization function. Often this function will not only address technical aspects of a problem, but will evaluate its cost as well. Therefore, it becomes necessary to design an approach that will optimize the solution at minimal cost.

Analyses of this chapter are restricted to the application of shunt capacitor banks for reactive power compensation of distribution systems under sinusoidal as well as nonsinusoidal operating conditions. The capacitor placement problem of a distribution system consists of determining the optimal locations, sizes, and types of capacitor banks in order to achieve maximum annual benefits within the permissible region of constraints (e.g., bus voltage deviation, total harmonic distortion, number of capacitor banks at each bus and the entire system). Various techniques and algorithms have been proposed and implemented for solving this problem under normal sinusoidal conditions and in the presence of voltage and current harmonics. All such methods have their own advantages, disadvantages, and limitations as stated by their assumptions.

The goal of this chapter is to show the progression of research in optimal capacitor placement for sinusoidal operating conditions and to introduce a number of algorithms for solving this problem in the presence of harmonics. Section 10.1 presents the concept of reactive power compensation based on capacitors. Section 10.2 addresses common types of shunt capacitor banks as used in power systems. A survey of various optimization algorithms for the placement and sizing of shunt capacitor banks under sinusoidal operating conditions is presented in Section 10.3. The last part of the chapter includes analysis and comparison of various solution approaches for the optimal placement and sizing of fixed capacitor banks in the presence of voltage and current harmonics.

*Power Quality in Power Systems and Electrical Machines*
ISBN 978-0-12-369536-9



© Elsevier Inc.
All rights reserved.

## 10.1 REACTIVE POWER COMPENSATION

Reactive power compensation is an important issue in electric power systems involving operational, economic, and quality of service aspects. Consumer loads (residential, commercial, industrial, service sector, etc.) impose active and reactive power demands. Active power is converted into useful energy, such as light, heat, and rotary motion. Reactive power must be compensated to guarantee an efficient delivery of active power to loads.

Capacitor banks are widely employed in distribution systems for reactive power compensation in order to achieve power and energy loss reduction, system capacity release, and acceptable voltage profiles. The extent of these benefits depends on the location, size, type, and number of shunt capacitors (sources of reactive power) and also on their control settings. Hence an optimal solution for placement and sizing of shunt capacitors in a distribution system is a very important aspect of power system analysis.

### 10.1.1 Benefits of Reactive Power Compensation

Shunt capacitors applied at the receiving end of a power system feeder supplying a load at lagging power factor have several benefits, which may be the reason for their extensive applications. This section highlights some advantages of reactive power compensation.

**Improved Voltage Profile.** Highly utilized feeders with high reactive power demands have poor voltage profiles and experience large voltage variations when loading levels change significantly. In a power system, it is desirable to regulate bus voltages within a narrow range (e.g., +5%, –8% of their nominal values) and to have a balanced load on all three phases (eliminating negative- and zero-sequence currents with undesirable consequences such as equipment heating and torque pulsations in generators and turbines). However, loads of the power system fluctuate and can result in voltage deviations beyond their acceptable limits. In view of the fact that the internal impedance of the AC system is mainly inductive, it is the reactive power change of the load that has the most adverse effect on voltage regulation.

Traditionally, line voltage drop is compensated with distributed capacitors along a feeder, and by switching them according to the reactive power demand a rather constant voltage profile is achieved. Furthermore, by keeping the power factor close to unity along the section in question, the number of expensive voltage regulators can be minimized.

Impacts of active and reactive current variations on the terminal load voltage ($V_t$) are demonstrated in Fig. 10.1. An increase of $\Delta Q$ in the lagging VAr drawn by the load (indicated by quantities with primes in Fig. 10.1b) causes the reactive current component to increase to $(I_q + \Delta I_q)$ while the active current component $I_p$ is assumed to be unchanged. This will result in a terminal voltage drop of $\Delta V_t$ and decreases the real power. Figure 10.1c shows the phasor diagram where the active current component increases to $(I_p + \Delta I_p)$ with $\Delta I_p = \Delta I_q$ (of Fig. 10.1b) while $I_q$ is assumed to be unchanged. Comparison of phasor diagrams indicates that variations in reactive power (Fig. 10.1b) have more impact on voltage regulation as compared with active power variations (Fig. 10.1c).

**Reduced Power System Losses.** Correcting the power factor can substantially reduce network losses in between the point in the network where the correction is performed and the source of generation. This can result in an annual gross return of as much as 15% on the capacitor investment [48]. To maximize benefits, power factor correction should be implemented as close to the customer load as possible. However, due to economies of scale, installation of capacitors at the low-voltage (LV) level is very costly when compared with high-voltage (HV) options.

In most industrial plant power distribution systems, the $I^2R$ losses vary from 2.5 to 7.5% of the load kWh. This depends on the hours of full-load and no-load plant operation, wire size, and length of the main and branch feeder circuits. Capacitors are effective in reducing only that portion of the losses that is due to the reactive current. Losses are proportional to the current squared, and since current is reduced in direct proportion to power factor improvement, the losses are inversely proportional to the square of the power factor. Hence, as the power factor is increased with the addition of capacitor banks to the system, the amount of the losses is reduced. The connected capacitor banks have losses, but they are relatively small. Losses account for approximately one-third of one percent of the reactive power rating [48].

**Released Power System Capacity.** When capacitors are placed in a power system, they deliver reactive power and furnish magnetizing current for motors, transformers, and other electromagnetic devices. This increases the power factor and it means that for a lower current (or apparent power) level a higher real power utilization occurs. Therefore, capacitor banks can be used to reduce overloading or permit additional load to be added to the existing system. Release of system capacity by power factor improvement due to capacitors is becoming extremely important because of the associated economic and system benefits.

Reactive power compensation improves network utilization; that is, capacity is released and it allows more customers to be connected to what could have been a highly utilized feeder, without going to the costly extreme of adding an additional feeder.

**Increased Plant Ratings.** Another undesirable effect of a network with poor power factor is a possible reduction in plant ratings. This is often noticeable when transformer ratings are limited by overvoltage available from tapping. Correcting power factor to unity at the zone substation will maximize the real-power rating of transformers by providing access to thermal emergency ratings.

**Capital Deferment.** As ratings are based on apparent power rather than active power, reduced apparent power utilization reduces operating risks and can therefore defer expenditure related to the network expansion. This deferment can be applied from the distribution feeder, back to the zone substation, subtransmission, terminal station, transmission network, and generation.



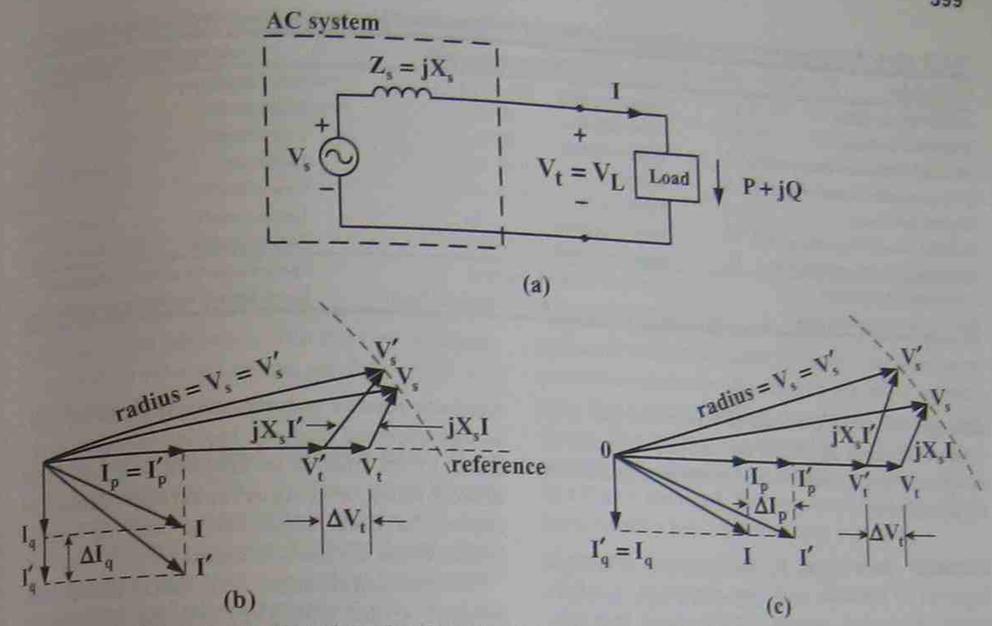



**FIGURE 10.1** Effect of active ($I_p$) and reactive ($I_q$) current on terminal voltage $V_t$: (a) Thevenin's equivalent circuit of the AC system with a purely inductive internal impedance, (b) change in $I_q$, (c) change in $I_p$ [47].

## 10.2 DRAWBACKS OF REACTIVE POWER COMPENSATION

Although capacitor banks can undoubtedly provide many benefits to a power system, there are several situations where they can cause deterioration of the power system. They may result in power quality problems, and in damage of connected equipment. In some situations, capacitor banks themselves may also become victims of unfortunate circumstances. Optimal placement and sizing of shunt capacitor banks as discussed in Sections 10.3 and 10.4 will prevent most of these problems. This section highlights some drawbacks of reactive power compensation.

**Resonance.** Resonance is the condition where the capacitive and inductive reactances of a system cancel each other, thus leaving the resistive elements in the system as the only form of impedance. The frequency at which this offsetting effect takes place is called the resonant frequency of the system. Resonance conditions will cause unacceptable high currents and overvoltages to occur with the potential to

TABLE 10.1 Advantages and Disadvantages of Distributed (Pole-Mounted) Capacitors over Zone Substation Installations

| Component | Distributed capacitors | Zone substation capacitors |
|---|---|---|
| Initial capital outlay | Less expensive | More expensive |
| Reduction in losses | More effective | Less effective |
| Network-utilization improvement | More effective | Less effective |
| Voltage-profile improvement | Effective | Ineffective |
| Capital deferment | More effective | Less effective |
| Remote monitoring and control | More expensive | Less expensive |
| Maintenance and setting review | More expensive | Less expensive |
| Accommodation/space | Overhead network required | Space required at zone substation |
| Failure of a capacitor unit | Small impact on apparent power load | Large impact on apparent power load |

damage not only the installed capacitor but also other equipment operating on the system. In case of resonance large power losses could be experienced by the system.

**Harmonic Resonance.** If the resonant frequency happens to coincide with one generated by a harmonic source (e.g., nearby nonlinear load) then voltages and currents will increase disproportionately, causing damage to capacitors and other electrical equipment. Harmonic resonance may cause capacitor failure due to harmonic overvoltages and overcurrents.

**Magnification of Capacitor-Switching Transients.** Capacitor-switching transients typically occur when a large capacitor on the high-voltage side of the power system (usually at the utility side) is energized. This results in magnification of transients at low-voltage capacitors. The magnified transient at a low-voltage remote end can reach up to 400% of its rated values.

**Overvoltages.** The voltages of a power system are often maintained within a specified upper and lower limit of the rated value. Capacitors, especially switched types, can cause overvoltage problems by increasing the voltage beyond its maximum desired value. This causes complications in the power system and can damage and deteriorate the system.

## 10.2 COMMON TYPES OF DISTRIBUTION SHUNT CAPACITOR BANKS

There are many reasons and benefits for utilizing distribution capacitors; reactive power compensation remains one of the most effective solutions for permitting growth in a network. It has long been popular to have reactive compensation based at zone substations. However, there has been a growing trend to distribute reactive compensation (e.g., along high-voltage overhead feeders). Moving capacitor banks closer to the load is an effective way to reduce network losses, defer costly capital expenditure, and improve network utilization as well as voltage profiles of the distribution network.

Pole-mounted capacitor banks can be of either the switched or fixed type. They have the ability to be distributed along overhead feeders with ease and as such are a very popular choice for reactive compensation. Fixed capacitors are usually sized for minimum base-load conditions, whereas switched units are designed for loads above the minimum. Switched capacitor banks provide the capability and the flexibility to control the reactive power along the feeder as the load changes. Table 10.1 shows some of the different advantages of distributed versus zone substation capacitors.

There are several control strategies available for switched capacitors, the number of which is mainly constrained by the needs and the complexity of the capacitor bank. Some of the more well used and documented techniques are

- Voltage control: Capacitor switching relies on a known upper and lower voltage limit set by the utility. The bank is switched in and switched out at those voltage limits.
- Time control: It does not require any measured values, as capacitor switching is solely based on time. This approach is often used with well-known, time-dependent load conditions.
- Reactive-power control: Capacitor switching is performed when the measured reactive power flow of the line exceeds a preset level.

### 10.2.1 Open-Rack Shunt Capacitor Bank

The open-rack shunt capacitor bank [49] is one of the most common types of capacitor banks used by utilities. It is available with internally fused, externally fused, or fuseless capacitor units (Table 10.2). The major advantage with this type of capacitor bank is its compact design, small footprint, and ease of maintenance.



TABLE 10.2 Typical Ratings and Locations of Distribution Shunt Capacitor Banks [49]

| Type of shunt capacitor bank | | Maximum power (MVAr) | Maximum voltage (V)] | Location |
|---|---|---|---|---|
| Open-rack | Internally fused | Up to 600 | Up to 700 | Outdoor |
| | Externally fused | 1.2–600 | 2.4–765 | Outdoor |
| | Fuseless | 1.2–600 | 35–765 | Outdoor |
| Pole-mounted | | 150–3600 | 2.4–36 | |
| Modular | | Up to 100 | 5–138 | |
| Enclosed fixed | | 15 | 24 | |
| Enclosed switched | | 1000 kVAr/step | 24 | |

**Internally Fused Open-Rack Capacitor Bank.** These banks have internal fuses for the current-limiting action; one fuse is connected in series with each element within the capacitor. They are designed and coordinated to isolate internal faults at the capacitor-element level and allow continued operation of the remaining elements of that capacitor unit. A very small part of the capacitor is being disconnected (self-healing), and therefore the capacitor bank remains in service. The designs are customized per customer specifications and generally include racks, capacitors, insulators, switches, imbalance protection scheme, and current-limiting reactors. An internally fused open-rack capacitor bank provides the following main advantages:

- cost-effective,
- utilizes large kVAr size units,
- few live parts are exposed,
- well-known technology (over 50 years of experience), and
- decreased installation and maintenance time and cost with proven reliability in the field.

**Externally Fused Open-Rack Capacitor Bank.** These open-rack capacitor banks [49] are typically used at substations and utilize an external fuse (current limiting) as a means of unit protection. The designs are customized per customer specifications and generally include racks, capacitors, insulators, fuses, elevation structures, switches, imbalance protection scheme, and current-limiting reactors. An externally fused open-rack capacitor bank provides the following main advantages:

- visual indication of blown fuses,
- utilizes small kVAr size units, and
- well-known technology (over 70 years of experience).

**Fuseless Open-Rack Capacitor Bank.** These types of open-rack substation banks [49] utilize an imbalance protection scheme as the primary means of protection. There are no internal or external fuses in this design. The "string" configuration provides a very reliable and cost-effective design for banks rated 35 kV and above. A fuseless open-rack capacitor bank provides the following main advantages:

- cost-effective and compact size,
- utilizes large kVAr size units,
- few live parts are exposed,
- reduced installation and maintenance time as well as reduced cost, and
- proven reliability in the field.

### 10.2.2 Pole-Mounted Capacitor Bank

Pole-mounted capacitor banks [49] provide an economical way to apply capacitors to a distribution feeder. The aim is to provide voltage support, lower system losses, release system capacity, and eliminate power-factor penalties. They are normally factory prewired and assembled, ready for installation. Table 10.2 outlines some of the typical ratings of pole-mounted capacitor banks.

Pole-mounted capacitor banks are typically supplied with the following set of options:

- aluminum or galvanized steel rack,
- oil or vacuum switches,
- junction box,
- switching controller,
- wildlife guards,
- insulated conductor,
- control power transformer,
- distribution class arresters,
- fused cutout, and
- current-limiting reactors.

### 10.2.3 Modular Capacitor Bank

The modular capacitor bank [49] is preengineered with a power circuit breaker, protection, and control panel, all factory mounted and tested on a

ST. GEORGE POLLEGE OF LAW E

**TABLE 10.1** Advantages and Disadvantages of Distributed (Pole-Mounted) Capacitors over Zone Substation Installations

| Component | Distributed capacitors | Zone substation capacitors |
|---|---|---|
| Initial capital outlay | Less expensive | More expensive |
| Reduction in losses | More effective | Less effective |
| Network-utilization improvement | More effective | Less effective |
| Voltage-profile improvement | Effective | Ineffective |
| Capital deferment | More effective | Less effective |
| Remote monitoring and control | More expensive | Less expensive |
| Maintenance and setting review | More expensive | Less expensive |
| Accommodation/space | Overhead network required | Space required at zone substation |
| Failure of a capacitor unit | Small impact on apparent power load | Large impact on apparent power load |

damage not only the installed capacitor but also other equipment operating on the system. In case of resonance large power losses could be experienced by the system.

**Harmonic Resonance.** If the resonant frequency happens to coincide with one generated by a harmonic source (e.g., nearby nonlinear load) then voltages and currents will increase disproportionately, causing damage to capacitors and other electrical equipment. Harmonic resonance may cause capacitor failure due to harmonic overvoltages and overcurrents.

**Magnification of Capacitor-Switching Transients.** Capacitor-switching transients typically occur when a large capacitor on the high-voltage side of the power system (usually at the utility side) is energized. This results in magnification of transients at low-voltage capacitors. The magnified transient at a low-voltage remote end can reach up to 400% of its rated values.

**Overvoltages.** The voltages of a power system are often maintained within a specified upper and lower limit of the rated value. Capacitors, especially switched types, can cause overvoltage problems by increasing the voltage beyond its maximum desired value. This causes complications in the power system and can damage and deteriorate the system.

## 10.2 COMMON TYPES OF DISTRIBUTION SHUNT CAPACITOR BANKS

There are many reasons and benefits for utilizing distribution capacitors; reactive power compensation remains one of the most effective solutions for permitting growth in a network. It has long been popular to have reactive compensation based at zone substations. However, there has been a growing trend to distribute reactive compensation (e.g., along high-voltage overhead feeders). Moving capacitor banks closer to the load is an effective way to reduce network losses, defer costly capital expenditure, and improve network utilization as well as voltage profiles of the distribution network.

Pole-mounted capacitor banks can be of either the switched or fixed type. They have the ability to be distributed along overhead feeders with ease and as such are a very popular choice for reactive compensation. Fixed capacitors are usually sized for minimum base-load conditions, whereas switched units are designed for loads above the minimum. Switched capacitor banks provide the capability and the flexibility to control the reactive power along the feeder as the load changes. Table 10.1 shows some of the different advantages of distributed versus zone substation capacitors.

There are several control strategies available for switched capacitors, the number of which is mainly constrained by the needs and the complexity of the capacitor bank. Some of the more well used and documented techniques are

- Voltage control: Capacitor switching relies on a known upper and lower voltage limit set by the utility. The bank is switched in and switched out at those voltage limits.
- Time control: It does not require any measured values, as capacitor switching is solely based on time. This approach is often used with well-known, time-dependent load conditions.
- Reactive-power control: Capacitor switching is performed when the measured reactive power flow of the line exceeds a preset level.

### 10.2.1 Open-Rack Shunt Capacitor Bank

The open-rack shunt capacitor bank [49] is one of the most common types of capacitor banks used by utilities. It is available with internally fused, externally fused, or fuseless capacitor units (Table 10.2). The major advantage with this type of capacitor bank is its compact design, small footprint, and ease of maintenance.



**TABLE 10.2** Typical Ratings and Locations of Distribution Shunt Capacitor Banks [49]

| Type of shunt capacitor bank | Maximum power (MVAr) | Maximum voltage (V)] | Location |
|---|---|---|---|
| Open-rack | | | |
| Internally fused | Up to 600 | Up to 700 | Outdoor |
| Externally fused | 1.2–600 | 2.4–765 | Outdoor |
| Fuseless | 1.2–600 | 35–765 | Outdoor |
| Pole-mounted | 150–3600 | 2.4–36 | |
| Modular | Up to 100 | 5–138 | |
| Enclosed fixed | 15 | 24 | |
| Enclosed switched | 1000 kVAr/step | 24 | |

**Internally Fused Open-Rack Capacitor Bank.** These banks have internal fuses for the current-limiting action; one fuse is connected in series with each element within the capacitor. They are designed and coordinated to isolate internal faults at the capacitor-element level and allow continued operation of the remaining elements of that capacitor unit. A very small part of the capacitor is being disconnected (self-healing), and therefore the capacitor bank remains in service. The designs are customized per customer specifications and generally include racks, capacitors, insulators, switches, imbalance protection scheme, and current-limiting reactors. An internally fused open-rack capacitor bank provides the following main advantages:

- cost-effective,
- utilizes large kVAr size units,
- few live parts are exposed,
- well-known technology (over 50 years of experience), and
- decreased installation and maintenance time and cost with proven reliability in the field.

**Externally Fused Open-Rack Capacitor Bank.** These open-rack capacitor banks [49] are typically used at substations and utilize an external fuse (current limiting) as a means of unit protection. The designs are customized per customer specifications and generally include racks, capacitors, insulators, fuses, elevation structures, switches, imbalance protection scheme, and current-limiting reactors. An externally fused open-rack capacitor bank provides the following main advantages:

- visual indication of blown fuses,
- utilizes small kVAr size units, and
- well-known technology (over 70 years of experience).

**Fuseless Open-Rack Capacitor Bank.** These types of open-rack substation banks [49] utilize an imbalance protection scheme as the primary means of protection. There are no internal or external fuses in this design. The "string" configuration provides a very reliable and cost-effective design for banks rated 35 kV and above. A fuseless open-rack capacitor bank provides the following main advantages:

- cost-effective and compact size,
- utilizes large kVAr size units,
- few live parts are exposed,
- reduced installation and maintenance time as well as reduced cost, and
- proven reliability in the field.

### 10.2.2 Pole-Mounted Capacitor Bank

Pole-mounted capacitor banks [49] provide an economical way to apply capacitors to a distribution feeder. The aim is to provide voltage support, lower system losses, release system capacity, and eliminate power-factor penalties. They are normally factory prewired and assembled, ready for installation. Table 10.2 outlines some of the typical ratings of pole-mounted capacitor banks.

Pole-mounted capacitor banks are typically supplied with the following set of options:

- aluminum or galvanized steel rack,
- oil or vacuum switches,
- junction box,
- switching controller,
- wildlife guards,
- insulated conductor,
- control power transformer,
- distribution class arresters,
- fused cutout, and
- current-limiting reactors.

### 10.2.3 Modular Capacitor Bank

The modular capacitor bank [49] is preengineered with a power circuit breaker, protection, and control panel, all factory mounted and tested on a

ST. GEORGE POLLEGE OF LAW

steel structure. A modular capacitor bank requires minimal field installation and commissioning work. Table 10.2 outlines some of the typical power and voltage ratings of a modular capacitor bank.

A modular capacitor bank provides the following main advantages:

- many standardized configurations with flexibility to fit customer needs,
- factory tested and assembled, reducing environmental project delays and enhancing quality,
- available as a stand-alone unit or integrated into preexisting substation,
- easily relocatable, and
- future expandability with lower costs than traditional banks.

### 10.2.4 Enclosed Fixed Capacitor Bank

The enclosed fixed bank [49] is a fully insulated and fixed reactive compensation system. Its compact design and its full insulation makes the enclosed fixed bank easy to place and it requires no fencing or extra protection. Table 10.2 outlines some of the typical power and voltage ratings of an enclosed fixed capacitor bank.

### 10.2.5 Enclosed Switched Capacitor Bank

The enclosed switched bank [49] is a reactive compensation system with modular, multistage switched capacitor steps that will automatically compensate the network to maintain a preset power-factor level. Table 10.2 outlines some of the typical power and voltage ratings of an enclosed switched capacitor bank.

The enclosed switched bank is available with the following options:

- inrush or detuning reactor,
- cooling or heating,
- imbalance protection,
- stainless steel,
- user defined step sizes,
- switched or fixed,
- indoor or outdoor, and
- automatic or manual.

## 10.3 CLASSIFICATION OF CAPACITOR ALLOCATION TECHNIQUES FOR SINUSOIDAL OPERATING CONDITIONS

The problem of capacitor allocation for loss reduction in electric distribution systems has been extensively researched and many documents have been published [1]. Solution techniques for the capacitor allocation problem can be classified into following categories:

- analytical methods,
- numerical programming (including dynamic programming (DP), local variations (LV), mixed integer programming, and integer quadratic programming),
- heuristic approaches,
- artificial intelligence-based algorithms (including expert systems, simulated annealing, artificial neural networks, fuzzy set theory, and genetic algorithms),
- graph search algorithm,
- particle swarm algorithm,
- tabu search algorithm, and
- sequential quadratic programming.

This section introduces each method and presents their merits and shortcomings.

### 10.3.1 Analytical Methods

All early works on optimal capacitor allocation under sinusoidal operating conditions with linear loads used analytical methods. These algorithms were devised when computing resources were unavailable or expensive. These methods mainly rely on analytical approaches and calculus to determine the maximum of a capacitor savings function. The savings function has often been given by

$$S = K_E\Delta E + K_P\Delta P - K_C C, \qquad (10\text{-}1)$$

where $K_E\Delta E$ and $K_P\Delta P$ are the economic energy and peak-power loss reductions due to capacitor placement, respectively, and $K_C C$ is the capacitor installation cost.

Initial techniques (by Neagle and Samson [2], Cook [3], Schmill [4], Chang [5], and Bae [6]) achieved simple closed-form solutions to maximize some form of the cost function (Eq. 10-1) based on unrealistic assumptions such as constant feeder conductor sizes and uniform current loading. This early work established the famous ***two-thirds rule*** that advocates for maximum loss reduction, a capacitor rated at two-thirds of the peak-reactive load, and installed at a position two-thirds of the distance along the total feeder length. Despite these unrealistic assumptions on which the two-thirds rule relies, some utilities today still implement their capacitor placement program based on this rule and some capacitor manufacturers list this rule in their application guides.



Later techniques (Grainger [7] and Salama [8]) achieve more accurate results by formulating equivalent normalized feeders with sections of different conductor sizes and nonuniformly distributed loads, as well as the inclusion of switching capacitors and load variations.

**Drawbacks of Analytical Methods.** One drawback of all analytical methods is the assumption of continuous variables. The calculated capacitor sizes may not match the available standard sizes and the optimized placements may not coincide with the physical node locations in the distribution system. The results would need to be rounded up or down to the nearest practical value and may result in an overvoltage situation or a loss saving less than the calculated one.

Therefore, the earlier works provide a rough rule of thumb for capacitor placement on feeders with evenly distributed loads. More sophisticated analytical methods are suitable for distribution systems of considerable sizes, but they require more distribution system information and more time to implement.

### 10.3.2 Numerical Programming Methods

Various numerical programming methods were devised to solve the capacitor allocation problem as computing power became more readily available and computer memory less expensive. These are iterative optimization techniques used to maximize (or minimize) an objective function of decision variables. The values of the decision variables must also satisfy a set of constraints. For optimal capacitor allocation, the saving represents the objective function, and operational restrictions (e.g., locations, sizes, and numbers of capacitors, bus voltages, and currents) are the decision variables that must all satisfy operational constraints. Numerical programming methods allow the use of more elaborate cost functions for the optimal capacitor placement problem and the objective functions can consider all voltage and line loading constraints, discrete sizes of capacitors, and physical locations of nodes. Using numerical programming methods, the capacitor allocation problem can be formulated as follows:

$$\begin{aligned} &\text{maximize} \quad S = K_L\Delta L - K_C C \\ &\text{subject to } \Delta V \le \Delta V_{\max} \end{aligned}, \qquad (10\text{-}2)$$

where $K_L\Delta L$ is the cost saving, which may include energy and peak-power loss reductions and released capacity, $K_C C$ is the installation costs of the capacitors, and $\Delta V$ is the change in voltage due to capacitor installation, which must not exceed a maximum of $\Delta V_{\max}$.

The first applications of dynamic programming (DP) to the capacitor placement problem (by Duran [9] and Fawzi *et al.* [10]) were simple algorithms considering only the energy-loss reduction, released apparent power, and the discrete nature of capacitor sizes. Later works include applications of local variations (by Ponnavaikko and Rao [11]), mixed integer programming and integer quadratic programming (by Baran and Wu [12]) to account for the effects of load growth, switched capacitors for varying load, and regulators in a distribution system.

**Drawbacks of Numerical Programming Methods.** The level of sophistication and the complexity of the numerical programming models increase in chronological order of their publication time. This progression concurs with the advancement in computing capability. At the present time, computing is relatively inexpensive and many general numerical optimization packages are available to implement any of the above algorithms. Some of the numerical programming methods have the advantage of considering feeder node locations and capacitor sizes as discrete variables, which is an advantage over analytical methods. However, the data preparation and interface development for numerical techniques may require more time than for analytical methods. The main drawback of all numerical programming approaches is the possibility of arriving at a local optimal solution. Therefore, one must determine the convexity of the capacitor placement problem to determine whether the result yielded by a numerical programming technique is either a local or global extreme.

### 10.3.3 Heuristic Methods

Heuristics are rules of thumb that are developed through intuition, experience, and judgment. They produce fast and practical strategies that reduce the exhaustive search space and can lead to a solution that is near optimal with a good level of confidence. In applying heuristic search strategies to the optimum placement and sizing of capacitors in a distribution system, often a small number of nodes, named sensitive nodes, are selected for installing capacitors that optimize the net savings while achieving a large overall loss reduction. This is to decrease the exhaustive search space, while keeping the end result (objective function) at an optimal or near optimal value. Heuristic approaches, due to the

ST. GEORGE COLLEGE OF LAW

reduced computational time compared to other techniques, can be suitable for large distribution systems and also in on-line implementation.

Abdel-Salam *et al.* [13] proposed a heuristic technique to determine the sensitive nodes in sections of the distribution system that have the greatest effect on loss reduction and then maximized the power-loss reduction from capacitor compensation. Chis *et al.* [14] improved on the work of [13] by determining the sensitive nodes that have the greatest impact on loss reduction for the entire distribution system and the effect of load variations.

**Drawbacks of Heuristic Methods.** Heuristic methods are intuitive, easier to understand, and simpler to implement than other optimization techniques such as analytical and numerical programming approaches. However, the results produced by heuristic algorithms are not guaranteed to be optimal. Other disadvantages associated with the use of a heuristic search algorithm are as follows:

- The criterion of selecting the nodes with the highest impact on the losses in a feeder section is not totally representative for the state of the power losses of the whole system and may result in inaccurate results;
- Compensation is based on loss reduction in the system rather than net dollar savings;
- It requires a large number of power flow runs;
- It only considers fixed capacitors; and
- It does not have the flexibility to control the balance between the global and local exploration of the search space, and its results may not be globally optimal.

### 10.3.4 Artificial Intelligence–Based (AI-Based) Methods

The popularity of artificial intelligence (AI) has led many researchers to investigate its applications in power system engineering and electrical machines. In particular, genetic algorithms (GAs), simulated annealing (SA), expert systems (ESs), artificial neural networks (ANNs), and fuzzy set theory (FST) have been proposed and implemented for optimal placement and sizing of shunt capacitor banks.

All of the above AI methods can be implemented using commercially available AI development shells or be hardcoded using any programming language with relative ease.

**Drawbacks of AI-Based Methods.** The user may encounter convergence problems with GAs, SA, and ANNs methods. For on-line applications, ANNs can only be used for a particular load pattern. ANNs would need to be retrained for every different set of load curves that are characteristic of the distribution system. However, the use of ESs is better suited for on-line and dynamic applications.

#### 10.3.4.1 Genetic Algorithms

The progressive introduction of genetic algorithms (GAs) as powerful tools allows complicated, multinodal, discrete optimization problems to be solved. Genetic algorithms use biological evolution to develop a series of search space points toward an optimal solution. Similar to the natural evolution of life, GAs tend to evolve a group of initial poorly generated solutions to a set of acceptable solutions through successive generations. This approach involves coding of the parameter set rather than working with the parameters themselves. GAs operate by selecting a population of the coded parameters with the highest fitness levels (e.g., parameters yielding the best results) and performing a combination of mating, crossover, and mutation operations on them to generate a better set of coded parameters.

Most traditional optimization methods move from one point in the decision hyperspace to another using some deterministic rule. The problem with this is that the solution is likely to get trapped at a local optimum. Genetic algorithms start with a diverse set (population) of potential solutions (hyperspace vectors). This allows for the exploration of many optima in parallel, lowering the probability of getting trapped at a local optimum. Genetic algorithms are simple to implement and are capable of locating the global optimal solution.

Boone and Chiang [15] devised a method based on GAs to determine optimal capacitor sizes and locations. The sizes and locations of capacitors are encoded into binary strings, and crossover is performed to generate a new population. However, their problem formulation only considered the costs of the capacitors and the reduction of peak-power losses. Sundhararajan and Pahwa [16] performed a similar work with the exception of including energy losses and implementing an elitist strategy whereby the coded strings chosen for the next generation do not undergo mutation or crossover procedures. Miu *et al.* [17] revisited the GA formulation to include additional features of capacitor replacement and control for unbalanced distribution systems.

There are five components that are required to implement a genetic algorithm: representation, initialization, evaluation function, genetic operators, and genetic parameters.



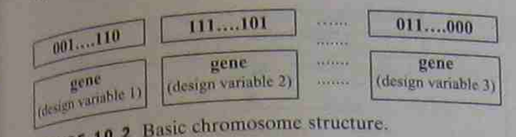



**FIGURE 10.2** Basic chromosome structure.

**Genetic Representation.** Genetic algorithms are derived from a study of biological systems. In biological systems evolution takes place on organic components used to encode the structure of living beings. These organic components are known as chromosomes. A living being is only a decoded structure of the chromosomes. Natural selection is the link between chromosomes and the performance of their decoded structures. In genetic algorithms the design variables or features that characterize an individual are represented in an ordered list called a string. Each design variable corresponds to a gene and the string of genes corresponds to a chromosome. A group of chromosomes is called a population. The number of chromosomes in a population is usually selected to be between 30 and 300. Each chromosome is a string of binary codes (genes) and may contain substrings. The merit of a string is judged by the fitness function, which is derived from the objective function and is used in successive genetic operations. During each iterative procedure (referred to as generation), a new set of strings with improved performance is generated using three GA operators (namely, reproduction, crossover, and mutation).

**Structure of Chromosomes.** Figure 10.2 shows an example illustrating the basic structure of a chromosome. Bit strings consisting of 0's and 1's have been found to be most effective in representing a wide variety of information in the problem domain involving function optimization. Many other representation schemes such as ordered lists, embedded lists, and variable-element lists have been developed for specific industrial applications of genetic algorithms.

**Initialization.** Genetic algorithms operate with a set of strings instead of a single string. This set of strings is known as a population and is put through the process of evolution to produce new individual strings. To begin with, the initial population could be seeded with heuristically chosen strings or at random. In either case, the initial population should contain a wide variety of structures to ensure the complete problem space is covered.

**Evaluation (Fitness) Function.** The evaluation function is a procedure to determine the fitness of each chromosome in the population and is very much application orientated. Since genetic algorithms proceed in the direction of evolving the fittest chromosomes, and the fitness value is the only information available to the algorithm, the performance is highly sensitive to the fitness values. In the case of optimization routines, the fitness is the value of the objective function to be optimized. Genetic algorithms are basically unconstrained search procedures in the given problem domain. Any constraints associated with the problem can be incorporated into the objective function as penalty functions.

**Genetic Operators.** Genetic operators are the stochastic transition rules applied to each chromosome during each generation procedure to generate a new improved population from an old one. A genetic algorithm usually consists of reproduction, crossover, and mutation operators.

- *Reproduction* is a probabilistic process for selecting two parent strings from the population of strings on the basis of roulette-wheel mechanism, using their fitness values. This process is accomplished by calculating the fitness function for each chromosome in the population and normalizing their values. A roulette wheel is constructed where each section of the wheel represents a certain chromosome and its relative fitness value. This ensures that the expected number of times a string is selected is proportional to its fitness relative to the rest of the population. Therefore, strings with higher fitness values have a higher probability of contributing offspring and are simply copied on into the next generation.
- *Crossover* is the process of selecting a random position in the string and swapping the characters either left or right of this point with another similarly partitioned string. This random position is called the crossover point. For example, if two parent strings are $x_1 = 1010:11$ and $x_2 = 1001:00$ and the crossover point has been selected as shown by the colon, then if swapping is implemented to the right of this point, the resulting offspring structures would be $y_1 = 1010:00$ and $y_2 = 1001:11$ (e.g., the two digits "11" to the right of the colon in $x_1$ are swapped with the two digits "00" to the right of the colon in $x_2$). The probability of

ST. GEORGE POLLEGE OF LAW

crossover occurring for two parent chromosomes is usually set to a large value in range of 0.7 to 1.0.

- *Mutation* is the process of random modification of a string position by changing "0" to "1" or vice versa, with a small probability. It prevents complete loss of genetic material through reproduction and crossover by ensuring that the probability of searching any region in the problem space is never zero. The probability of mutation is usually assumed to be small (e.g., between 0.01 and 0.1).

**Genetic Parameters.** Genetic parameters are the entities that help to regulate and improve the performance of a genetic algorithm. Some of the parameters that can characterize the genetic space are as follows:

- *Population size* affects the efficiency and performance of the genetic algorithm. A smaller population would not cover the entire problem space, resulting in poor performance. A larger population would cover more space and prevent premature convergence to local solutions; however, it requires more evaluations per generation and may slow down the convergence rate.
- *Crossover rate* affects the rate at which the process of crossover is applied. In each new population, the number of strings that undergo the process of crossover can be depicted by a chosen probability (crossover rate). A higher crossover rate introduces new strings more quickly into the population; however, if the rate is too high, high-performance strings are eliminated faster than selection can produce improvements. A low crossover rate may cause stagnations due to the lower exploration rate, and convergence problems may occur.
- *Mutation rate* is the probability with which each bit position of each string in the new population undergoes a random change after the selection process. A low mutation rate helps to prevent any bit position from getting stuck to a single value, whereas a high mutation rate can result in essentially random search.

**Convergence Criterion.** The iterations (regenerations) of genetic algorithms are continued until all generated chromosomes become equal or the maximum number of iterations is achieved. Due to the randomness of the GA method, the solution tends to differ for each run, even with the same initial population. For this reason, it is suggested to perform multiple runs and select the "most acceptable" solution (e.g., with most benefits, within the permissible region of constraints).

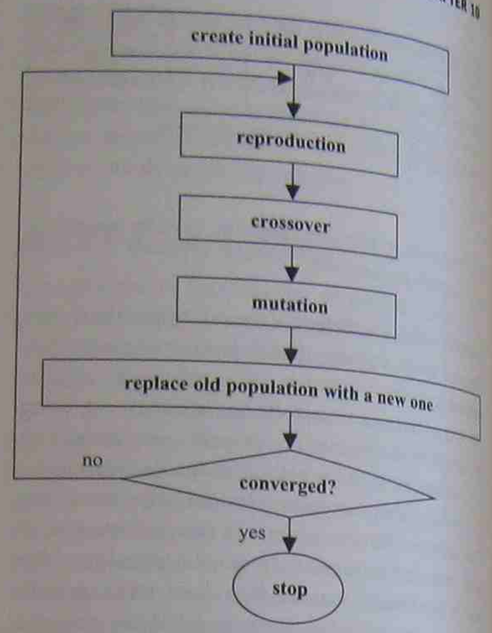



**FIGURE 10.3** Simplified flowchart of a typical genetic algorithm structure.

**Flowchart of Genetic Algorithm for Capacitor Placement and Sizing.** Figure 10.3 shows a simplified flowchart of an iterative genetic algorithm for optimal placement and sizing of capacitor banks in distribution system under sinusoidal operating conditions. An initial population is randomly selected, genetic operators are applied, and the old population is replaced with the new generation. This process is repeated until the algorithm has converged.

**Drawbacks of Genetic Algorithms.** There are disadvantages associated with the use of a genetic algorithm:

- It does not have flexibility to control the balance between global and local exploration of search space;
- It requires relatively large computational time and effort; and
- Convergence problems may occur, which may be overcome by solving the problem a number of times with different initial populations and selecting the best solution.

ST. GEORGE'S UNIVERSITY LIBRARY



**TABLE 10.3** Yearly Costs of Fixed Capacitors [37, 45]

| $Q_c$ (kVAr) | 150 | 300 | 450 | 600 | 750 | 900 |
|---|---|---|---|---|---|---|
| $K_{cfp}$ ($/kVAr) | 0.500 | 0.350 | 0.253 | 0.220 | 0.276 | 0.183 |
| $Q_c$ (kVAr) | 1050 | 1200 | 1350 | 1500 | 1650 | 1800 |
| $K_{cfp}$ ($/kVAr) | 0.228 | 0.170 | 0.207 | 0.201 | 0.193 | 0.187 |
| $Q_c$ (kVAr) | 1950 | 2100 | 2250 | 2400 | 2550 | 2700 |
| $K_{cfp}$ ($/kVAr) | 0.211 | 0.176 | 0.197 | 0.170 | 0.189 | 0.187 |
| $Q_c$ (kVAr) | 2850 | 3000 | 3150 | 3300 | 3450 | 3600 |
| $K_{cfp}$ ($/kVAr) | 0.183 | 0.180 | 0.195 | 0.174 | 0.188 | 0.170 |

### 10.3.4.2 Expert Systems

Expert systems (ESs) or knowledge-based systems consist of a collection of rules, facts (knowledge), and an inference engine to perform logical reasoning. The ES concept has been proposed and implemented for many power system problems that require decision-making, empirical judgments, or heuristics such as fault diagnosis, planning, scheduling, and reactive power control.

Salama and colleagues [18] developed an ES containing technical literature expertise (TLE) and human expertise (HE) for reactive power control of a distribution system. The TLE includes the capacitor allocation method based on [8] for maximum savings from the reduction of peak-power and energy losses. The HE component of the knowledge base contains information to guide the user to perform reactive power control for the planning, operation, and expansion stages of distribution systems. Application of ESs for the capacitor placement problem is yet to be explored and requires more attention.

### 10.3.4.3 Simulated Annealing

Simulated annealing (SA) is an iterative optimization algorithm that is based on the annealing of solids. When a material is annealed, it is heated to a high temperature and slowly cooled according to a cooling schedule to reach a desired state. At the highest temperature, particles of the material are arranged in a random formation. As the material is cooled, the particles become organized into a lattice-like structure, which is a minimum energy state. For the capacitor allocation problem, a total cost function is formulated instead of a savings function. Analogous to reaching a minimum energy state of the annealing of solids, Ananthapadmanabha *et al.* [19] used SA to minimize a total cost function given by

$$T_{\text{loss}} = K_P P_{\text{loss}} + K_E E_{\text{loss}} + K_C C, \qquad (10\text{-}3)$$

where $C$ is the size of capacitor, $K_P P_{\text{loss}}$ is the cost of peak-power losses, $K_E E_{\text{loss}}$ is the cost of energy losses, and $K_C C$ is the capacitor installation costs. Also, $K_C = K_{cfp}$ (see Table 10.3) is the cost of kVAr.

### 10.3.4.4 Artificial Neural Networks

Application of artificial neural networks (ANNs) in power engineering is gaining interest. An ANN is the connection of artificial neurons that simulates the nervous system of a human brain. The potential advantage of the ANN is its ability to handle the nonlinear mapping of an input–output space. The difficulty in designing an ANN is to generate the training patterns. To overcome this problem, a reinforcement learning process is usually proposed. An ANN typically consists of three types of layers: an input layer, one or more hidden layers, and an output layer. The ANN accepts given input data and minimizes the difference between known output data and generated output information. The relationships between inputs and outputs are embedded as parameters in the hidden layer. Correct output patterns can be generated by the ANN provided that there are enough hidden layers and nodes to encode the input–output pattern, and enough known data to train the ANN. Once an ANN is trained, it can provide very fast results for any given set of inputs.

Santoso and Tan [20] used ANNs for the optimal control of switched capacitors. In their work, two neural networks are designed and trained. One network predicts the load profile from a set of previous load values obtained from direct measurement at various buses. A second network determines the optimal capacitor tap positions based on the load profile as predicted by the first network. The first network is trained with a set of prerecorded load profiles and the second network is trained to maximize the energy loss reduction for a given load condition. To reduce the complexity of training, the distribution system is partitioned into many smaller subsystems.

**Drawbacks of Artificial Neural Networks.** ANNs may not be suitable for a large distribution system since many smaller subsystems are required and the training time becomes excessive. However, once networks are trained, iterative calculations are no longer required and a fast solution for a given set of inputs can be provided. Gu and Rizy [21] followed the method of [20] and included an additional functionality of regulator control.

### 10.3.4.5 Fuzzy Set Theory

The concept of fuzzy set theory (FST) was introduced by Zadeh [22] in 1965 as a formal tool for dealing with uncertainty and soft modeling. A fuzzy variable is modeled by a membership function, which assigns a degree of membership to a set. Usually, this degree of membership varies from zero to one.

Chin [23] used FST for the capacitor allocation problem. Three membership functions (for power loss, bus voltage deviation, and harmonic distortion) are defined. A fuzzy decision variable (e.g., the intersection of the three membership functions for each node in the distribution system) is calculated to determine the most appropriate buses for capacitor placement. However, no mathematical optimization procedure is provided for capacitor sizing. Ng *et al.* [24–25] applied FST to the capacitor placement problem by using fuzzy approximate reasoning. Voltage and power loss indices of the distribution system buses are modeled by membership functions, and a fuzzy expert system (FES) containing a set of heuristic rules performs the inferencing to determine a capacitor placement suitability index of each node. Capacitors are placed at the nodes with the highest suitability.

**Fuzzy Logic and Fuzzy Inference System.** Fuzzy logic in terms of fuzzy sets is about mapping an input space to an output space. The main operation to achieve this end is through the use of if–then statements called rules. These rules are used to refer to variables and the adjectives that describe those variables. This is the main theory behind the operation of a fuzzy inference system. For the system to interpret these rules, they must first be defined in terms of the data they will control and the adjectives that will be used. A good example of this is a system defining how hot the water is coming out of a hot water system. We need to define the range of the expected water temperatures, as well as what is meant by the word "hot."

**Fuzzy Sets.** A fuzzy set is a set without a crisp, clearly defined boundary. It can contain elements with partial, full, or no membership. This differs quite dramatically from the notion of a classical set, which is defined by the inclusion or exclusion of certain elements.

Fuzzy logic is based on the fact that the truth of any statement becomes a matter of degree. The true power of using fuzzy logic is not that it is an extremely complex tool which can give a direct answer, rather that it can model human perception, language, and thinking, thus being able to use linguistic descriptors to answer a problem that would normally need or expect a yes–no answer with a not-quite-yes–no answer. This is done by expanding the familiar Boolean logic of 1 for yes and 0 for no. This means that if absolute truth is defined by 1 and that absolute falsehood is defined by 0, fuzzy logic will permit alternative logical answers between the range of [0 1] such as 0.35 or 0.6521 and by doing so be able to recreate such linguistic descriptors in relation to an element's relationship to a set as medium, high, low, very low, very high, and so on. Now with the possibility of a range of logical answers a more descriptive set can be created. A plot mapping an input space to an output space is considered to be a membership function.

**Membership Function.** A membership function is a curve that defines how each point in the input space is mapped to a membership value (or degree of membership) between 0 and 1. The main requirement for a membership function is that it varies between 1 and 0. The shape of membership functions are created from such requirements as simplicity, convenience, speed, and efficiency.

A fuzzy set is an extension of a classical set. If $X$ is the universe of discourse and its elements are denoted by $x$, then a fuzzy set $A$ in $X$ is defined as a set of ordered pairs

$$A = \{x, \mu_A(x) | xX\},$$

where $\mu_A(x)$ (called the membership function of $x$ in $A$) maps each element of $X$ to a membership value between 0 and 1.

Many types of membership functions have been proposed and implemented. They can be created from scratch or even tailored or trained to conform to a set of data. There are many types of membership functions such as triangular, trapezoidal, symmetric Gaussian (defines a $f(x;\sigma,c) = \exp(-(x-c)^2/2\sigma^2))$ and sigmoidal. The possibility of creating membership functions based on already existing mathematical formulas and functions is endless, such as membership functions created from the difference and/or product of two sigmoidal functions.



**TABLE 10.4** Comparison of Boolean and Fuzzy Logic Operations in Terms of Two Sets A and B

| Boolean operation | Fuzzy logic operation |
|---|---|
| A AND B | min(A,B) |
| A OR B | max(A,B) |
| NOT A | 1 – A |

**Fuzzy Logic Operators.** The logical operations associated with fuzzy logic can be described as a superset of standard Boolean logic. The operations in Boolean known as AND, OR, and NOT can all be repeated in fuzzy logic. Shown in Table 10.4 are these three integral Boolean operations with their related logical operations in fuzzy.

**Fuzzy If–Then Rules.** If–then rules are used to define the relationships between variables based on defined logic and membership functions. An if–then rule is created in the form

If $x$ is $A$ then $y$ is $B$.

$A$ and $B$ are linguistic values defined by fuzzy sets on the ranges (universes of discourse) $X$ and $Y$, respectively. The if-part of the rule is called the antecedent (or premise), whereas the then-part of the rule ($y$ is $B$) is called the consequent (or conclusion).

Interpreting if-then rules is a three-part process:

- Fuzzify inputs: Resolve all fuzzy statements in the antecedent to a degree of membership between 0 and 1. If there is only one part to the antecedent, this is the degree of support for the rule.
- Apply fuzzy operator to multiple part antecedents: If there are multiple parts to the antecedent, apply fuzzy logic operators and resolve the antecedent to a single number between 0 and 1. This is the degree of support for the rule.
- Apply implication method: Use the degree of support for the entire rule to shape the output fuzzy set. The consequent of a fuzzy rule assigns an entire fuzzy set to the output. This fuzzy set is represented by a membership function that is chosen to indicate the qualities of the consequent. If the antecedent is only partially true (i.e., is assigned a value less than 1), then the output fuzzy set is truncated according to the implication method.

**Implication.** Implication is the method used to create a final consequent function or set. The if–then rule is often not sufficient enough and more rules may be necessary to create a satisfying result. Consider an extension to this rule shown below,

If $x$ is $A$ OR $y$ is $B$ then $z$ is $C$.

This *expanded if–then* statement now has two rules involved that are controlled by the logical operation OR. Implication becomes the means by which the consequent is created from this rule, which is the "$z$ is $C$" part.

Two main methods of implication are often used. These are entitled minimum (similar to the AND operation previously discussed) and the product methods. The minimum method will truncate the output fuzzy set, and the product method will scale the output fuzzy set deriving an aggregated output from a set of triggered rules.

**Fuzzy Inference.** The Mamdani implication methods [50] are usually used for inferencing. Two implication methods are relied on to determine the aggregated output from a set of triggered rules:

- *The Mamdani max–min implication method* of truncating the consequent membership function of each discarded rule (at the minimum membership value of all the antecedents) and determining the final aggregated membership function.
- *The Mamdani max–prod implication method* of scaling the consequent membership function of each discarded rule (to the minimum membership value of all the antecedents) and determining the final aggregated membership function.

**Defuzzification.** Defuzzification is the process of obtaining a single number from the output of the aggregated fuzzy set. It is used to transfer fuzzy inference results into a crisp output. In other words, defuzzification is realized by a decision-making algorithm that selects the best crisp value based on a fuzzy set. There are several forms of defuzzification including center of gravity (COG), mean of maximum (MOM), and center average methods. The COG method returns the value of the center of area under the curve and the MOM approach can be regarded as the point where balance is obtained on a curve.

ST. GEORGE POLICE DE LAKE

ST. GEORGE'S COLLEGE OF J.A.H.



**Fuzzy Expert System for Capacitor Placement and Sizing.** A fuzzy expert system based on approximate reasoning is defined and relied on to determine suitable candidate buses in a distribution system for capacitor placement. Voltages and power loss reduction indices of distribution system buses are modeled by fuzzy membership functions. A fuzzy expert system (FES) containing a set of heuristic rules is then employed to determine the capacitor placement suitability of each bus in the distribution system. Capacitors are then placed on the nodes with the highest suitability using the following steps:

- A load flow program calculates the power-loss reduction (PLR) of the system with respect to each bus when the reactive load current at that bus is compensated. The PLRs are then linearly normalized into a [0, 1] range with the highest loss reduction being 1 and the lowest being 0.
- The PLR indices along with the per-unit nodal voltages (before PLR compensation) are the two inputs that are used by the fuzzy expert system. The FES then determines the most suitable node for capacitor installation by fuzzy inferencing.
- A savings function relating to the annual cost of the capacitor (determined by size) and the savings achieved from the power-loss reduction is maximized to determine the optimal sizing of capacitor bank to be placed at that node.
- The above process will be repeated, finding another node for capacitor placement, until no more financial savings can be realized (Fig. 10.4).

**Drawbacks of Fuzzy Set Theory.** The fuzzy optimization approach is very simple and naturally fast as compared to other optimization methods. However, for some problems the procedure might get trapped in a local optimal point and fail to converge to the global (or near global) optimal solution.

### 10.3.5 Graph Search Algorithm

In a graph search algorithm a graph is commonly defined by a set of nodes connected by ares. Each node corresponds to a possible combination of capacitor sizes and locations for a given number of capacitors to be placed within the system. A separate graph is used for each possible number of capacitors to be placed at a certain location. This makes it possible to search the nodes of a graph in an attempt to determine the optimal solution. Beginning with some minimum number of capacitors to be placed (user-defined parameter), a search is performed to locate

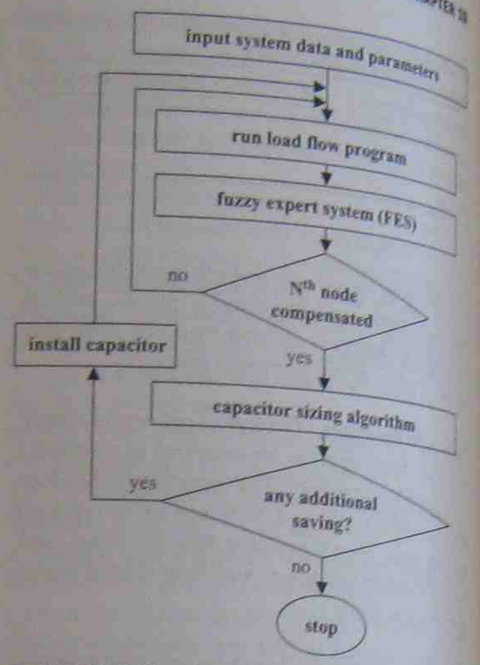



**FIGURE 10.4** Flowchart of an iterative fuzzy algorithm for optimal placement and sizing of capacitor banks in distribution system under sinusoidal operating conditions.

the node in the graph that produces maximum savings. The mathematical simplicity of this method makes it possible to include many features (e.g., capacitor location constraints) in the algorithm that would be rather difficult with other solution methods. Carlisle [26] developed graph search algorithms for the capacitor placement and sizing problem.

**Drawbacks of Graph Search Algorithm.** Many assumptions and constraints are required to obtain an optimal solution. This is not always possible for the operating conditions of actual distribution systems. Therefore, solutions based on graph search algorithms may not be very accurate.

### 10.3.6 Particle Swarm Algorithm

Similar to an evolutionary algorithm, the particle swarm optimization (PSO) technique conducts searches using a population of particles, corresponding to individuals. PSO systems combine two models:

- A social-only model suggesting that individuals ignore their own experience and adjust their behavior according to the successful beliefs of the individual in their neighborhood.



- A cognition-only model treating individuals as isolated beings.

A particle (representing a candidate solution to the optimal reactive power problem) changes its position in a multidimensional search space using these models. PSO uses payoff (performance index or objective function) information to guide the search in the problem space and can easily deal with nondifferentiable objective functions. Additionally, this property relieves PSO of many assumptions and approximations that are often required by traditional optimization models. Mantawy [27] proposed a particle swarm optimization algorithm for reactive power optimization problem.

**Drawbacks of Particle Swarm Algorithm.** The performance of particle swarm optimization is not competitive with respect to some problems. In addition, representation of the weights is difficult and the genetic operators have to be carefully selected or developed.

### 10.3.7 Tabu Search Algorithm

The tabu search strategy is a metaheuristic search method superimposed on another heuristic approach and is employed for solving combinatorial optimization problems. It has been applied for various problems and its capability to obtain high-quality solutions with reasonable computing times has been demonstrated. The approach is to avoid entrainment in cycles by penalizing moves that take the solution to points in the solution space previously visited (hence "tabu"). This ensures new regions of solution space will be investigated with the goal of avoiding local minima and ultimately capturing the optimal solution. The tabu search method is built on a descent mechanism of a search process that biases the search toward points with a lower objective function, while special features are added to avoid being trapped at a local minimum. To avoid retracing previous steps, recent moves (iterations) are recorded in one or more tabu lists (memories). The basic differences between various implementations of the tabu method are the size, variability, and adaptability of the tabu memory to a particular problem domain. Yang *et al.* [28], Mori [29], and Chang [30] applied the tabu search algorithm to the capacitor placement problem in radial distribution systems.

**Drawbacks of Tabu Search Algorithm.** The main disadvantage of tabu approach is its low solution speed. In addition, it uses certain control parameters that may be system dependent and difficult to determine.

### 10.3.8 Sequential Quadratic Programming

Sequential quadratic programming is a generalized Newton method for constrained optimization. This algorithm replaces the objective function with quadratic approximation and constraint functions with linear approximations to solve a quadratic programming problem at each iteration.

Abril [31] presents an application of the sequential quadratic programming algorithm to find the optimal sizing of shunt capacitors and/or passive filters for maximizing the net present value resulting from energy-loss reduction while taking investment cost into account and complying with set standards. The approach considers fixed and switched reactive power (VAr) compensators by considering a characteristic load variation curve for each linear and nonlinear load.

**Drawbacks of Sequential Quadratic Programming.** Large numbers of computations are involved in sequential quadratic programming. Many mathematical assumptions have to be made in order to simplify the problem; otherwise it is very difficult to calculate the variables.

### 10.3.9 Application Example 10.1: Fuzzy Capacitor Placement in an 11 kV, 34-Bus Distribution System with Lateral Branches under Sinusoidal Operating Conditions

Application of the fuzzy set theory for the capacitor allocation problem will be demonstrated for the 34-bus, three-phase, 11 kV radial distribution system of Fig. E10.1.1. The line and load data of this system are given in Tables E10.1.1 and E10.1.2, respectively [32]. One load level with fixed (not switched) capacitors under balanced operating conditions is assumed. The cost of fixed capacitor banks are listed in Table 10.3 where the size of the capacitor ($Q_c$ in kVAr) as a function of the yearly cost ($F_{cost}$ in \$/kVAr) is given by $K_{cp}$ (e.g., $F_{cost} = K_{cp}Q_c$).

### 10.3.10 Application Example 10.2: Genetically Optimized Placement of Capacitor Banks in an 11 kV, 34-Bus Distribution System with Lateral Branches under Sinusoidal Operating Conditions

Solve Application Example 10.1 using a genetic algorithm.

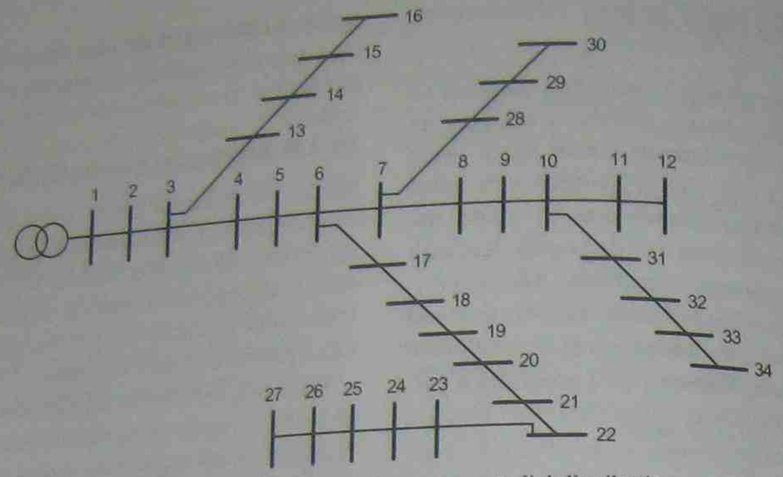



**FIGURE E10.1.1** Single-line diagram of the 11 kV, 34-bus, three-phase, radial distribution system [32].

**TABLE E10.1.1** Bus Data [32] of the 11 kV, 34-Bus, Three-Phase, Radial Distribution System (Fig. E10.1.1)

| | Load | | Generator | | | | Injected |
|---|---|---|---|---|---|---|---|
| Bus number | MW | MVAr | MW | MVAr | Qmin | Qmax | MVAr |
| 1 | 0.0000 | 0.0000 | 0 | 0 | 0 | 0 | 0 |
| 2 | 0.2300 | 0.1425 | 0 | 0 | 0 | 0 | 0 |
| 3 | 0.0000 | 0.0000 | 0 | 0 | 0 | 0 | 0 |
| 4 | 0.2300 | 0.1425 | 0 | 0 | 0 | 0 | 0 |
| 5 | 0.2300 | 0.1425 | 0 | 0 | 0 | 0 | 0 |
| 6 | 0.0000 | 0.0000 | 0 | 0 | 0 | 0 | 0 |
| 7 | 0.0000 | 0.0000 | 0 | 0 | 0 | 0 | 0 |
| 8 | 0.2300 | 0.1425 | 0 | 0 | 0 | 0 | 0 |
| 9 | 0.2300 | 0.1425 | 0 | 0 | 0 | 0 | 0 |
| 10 | 0.0000 | 0.0000 | 0 | 0 | 0 | 0 | 0 |
| 11 | 0.2300 | 0.1425 | 0 | 0 | 0 | 0 | 0 |
| 12 | 0.1370 | 0.0840 | 0 | 0 | 0 | 0 | 0 |
| 13 | 0.0720 | 0.0450 | 0 | 0 | 0 | 0 | 0 |
| 14 | 0.0720 | 0.0450 | 0 | 0 | 0 | 0 | 0 |
| 15 | 0.0720 | 0.0450 | 0 | 0 | 0 | 0 | 0 |
| 16 | 0.0135 | 0.0075 | 0 | 0 | 0 | 0 | 0 |
| 17 | 0.2300 | 0.1425 | 0 | 0 | 0 | 0 | 0 |
| 18 | 0.2300 | 0.1425 | 0 | 0 | 0 | 0 | 0 |
| 19 | 0.2300 | 0.1425 | 0 | 0 | 0 | 0 | 0 |
| 20 | 0.2300 | 0.1425 | 0 | 0 | 0 | 0 | 0 |
| 21 | 0.2300 | 0.1425 | 0 | 0 | 0 | 0 | 0 |
| 22 | 0.2300 | 0.1425 | 0 | 0 | 0 | 0 | 0 |
| 23 | 0.2300 | 0.1425 | 0 | 0 | 0 | 0 | 0 |
| 24 | 0.2300 | 0.1425 | 0 | 0 | 0 | 0 | 0 |
| 25 | 0.2300 | 0.1425 | 0 | 0 | 0 | 0 | 0 |
| 26 | 0.2300 | 0.1425 | 0 | 0 | 0 | 0 | 0 |
| 27 | 0.1370 | 0.0850 | 0 | 0 | 0 | 0 | 0 |
| 28 | 0.0750 | 0.0480 | 0 | 0 | 0 | 0 | 0 |
| 29 | 0.0750 | 0.0480 | 0 | 0 | 0 | 0 | 0 |
| 30 | 0.0750 | 0.0480 | 0 | 0 | 0 | 0 | 0 |
| 31 | 0.0570 | 0.0345 | 0 | 0 | 0 | 0 | 0 |
| 32 | 0.0570 | 0.0345 | 0 | 0 | 0 | 0 | 0 |
| 33 | 0.0570 | 0.0345 | 0 | 0 | 0 | 0 | 0 |
| 34 | 0.0570 | 0.0345 | 0 | 0 | 0 | 0 | 0 |



**TABLE E10.1.2** Line Data [32] of the 11 kV, 34-Bus, 3-Phase, Radial Distribution System (Fig. E10.1.1)

| Line | | | | |
|---|---|---|---|---|
| From bus | To bus | $R_{line}$ (pu) | $X_{line}$ (pu) | Tap setting |
| 1 | 2 | 0.0967 | 0.0397 | 1 |
| 2 | 3 | 0.0886 | 0.0364 | 1 |
| 3 | 4 | 0.1359 | 0.0377 | 1 |
| 4 | 5 | 0.1236 | 0.0343 | 1 |
| 5 | 6 | 0.1236 | 0.0343 | 1 |
| 6 | 7 | 0.2598 | 0.0446 | 1 |
| 7 | 8 | 0.1732 | 0.0298 | 1 |
| 8 | 9 | 0.2598 | 0.0446 | 1 |
| 9 | 10 | 0.1732 | 0.0298 | 1 |
| 10 | 11 | 0.1083 | 0.0186 | 1 |
| 11 | 12 | 0.0866 | 0.1488 | 1 |
| 3 | 13 | 0.1299 | 0.0223 | 1 |
| 13 | 14 | 0.1732 | 0.0298 | 1 |
| 14 | 15 | 0.0866 | 0.1488 | 1 |
| 15 | 16 | 0.0433 | 0.0074 | 1 |
| 6 | 17 | 0.1483 | 0.0412 | 1 |
| 17 | 18 | 0.1359 | 0.0377 | 1 |
| 18 | 19 | 0.1718 | 0.0391 | 1 |
| 19 | 20 | 0.1562 | 0.0355 | 1 |
| 20 | 21 | 0.1562 | 0.0355 | 1 |
| 21 | 22 | 0.2165 | 0.0372 | 1 |
| 22 | 23 | 0.2165 | 0.0372 | 1 |
| 23 | 24 | 0.2598 | 0.0446 | 1 |
| 24 | 25 | 0.1732 | 0.0298 | 1 |
| 25 | 26 | 0.1083 | 0.0186 | 1 |
| 26 | 27 | 0.0866 | 0.1488 | 1 |
| 7 | 28 | 0.1299 | 0.0223 | 1 |
| 28 | 29 | 0.1299 | 0.0223 | 1 |
| 29 | 30 | 0.1299 | 0.0223 | 1 |
| 10 | 31 | 0.1299 | 0.0223 | 1 |
| 31 | 32 | 0.1732 | 0.0298 | 1 |
| 32 | 33 | 0.1299 | 0.0223 | 1 |
| 33 | 34 | 0.0866 | 0.1488 | 1 |

## 10.4 OPTIMAL PLACEMENT AND SIZING OF SHUNT CAPACITOR BANKS IN THE PRESENCE OF HARMONICS

The problem of shunt capacitor allocation in distribution networks for reactive power compensation, voltage regulation, power factor correction, and power or energy loss reduction is discussed in the previous section. Optimal capacitor bank placement is a well-researched subject. However, limited attention is given to this problem in the presence of voltage and current harmonics.

With the increasing application of nonlinear loads and (power electronic and electromagnetic) devices causing voltage and current harmonics in distribution networks, special attention should be given to placement and sizing of capacitors in such systems with nonsinusoidal voltages and currents. If (shunt) capacitor banks are not properly sized and placed in such a power system, they may cause various operational and power quality problems:

- amplification and propagation of current and voltage harmonics,
- deterioration of power quality to unacceptable levels,
- increased losses at fundamental and harmonic frequencies,
- extensive reactive power demand and overvoltages at fundamental and harmonic frequencies,
- decreased capacities of distribution lines and transformers,
- poor power-factor conditions, and
- harmonic parallel resonances.

The problem of optimal capacitor placement and sizing under nonsinusoidal operating conditions is a newly researched area with limited publications that requires more attention. Early works by Baghzouz [35, 36], Gou [37], Hsu *et al.* [39], Wu [40], and Chin [43] capture local optimal points and ignore harmonic couplings. This will result in inaccurate solutions. More recent documents by Masoum *et al.* [41, 42, 44–46] achieve accurate (near) global optimal solutions by incorporating artificial intelligence–based (AI-based) techniques and relying on a harmonic power flow that takes into account harmonic couplings caused by nonlinear loads. Document [38] addresses the problem under unbalanced three-phase conditions.

Proposed solution techniques for the capacitor allocation problem in the presence of harmonics can be classified into following categories:

- exhaustive search [35],
- local variations [36],
- mixed integer-nonlinear programming [37, 38],
- heuristic methods [39],
- maximum sensitivities selection [40–42],
- fuzzy set theory [43, 44],
- genetic algorithms [45], and
- genetic algorithm with fuzzy logic (approximate reasoning) [46].

Most of these techniques are fast, but they suffer from the inability to escape local optimal solutions. Simulated annealing (SA), tabu search (TS), and genetic algorithms (GAs) are three near global optimization techniques that have demonstrated fine capabilities for capacitor placement, but the computational burden is heavy. This section introduces some of these methods and presents their merits and shortcomings.

### 10.4.1 Reformulation of the Capacitor Allocation Problem to Account for Harmonics

#### 10.4.1.1 System Model at Fundamental and Harmonic Frequencies

A harmonic load flow algorithm is required to model the distribution system with nonlinear loads at fundamental and harmonic frequencies. This book relies on the Newton-based harmonic load flow formulation and notations of Chapter 7 (Section 7.4). System solution is achieved by forcing total (fundamental and harmonic) mismatch active and reactive powers as well as mismatch active and reactive fundamental and harmonic currents to zero.

Define bus 1 to be the swing bus, buses 2 through $m-1$ to be the linear ($PQ$ and $PV$) buses, and buses m through n as nonlinear buses ($n$ = total number of buses). We assume that nonlinear load models – representing the coupling between harmonic voltages and currents – are given either in the frequency domain (e.g., $\tilde{V}^{(h)}$ and $\tilde{I}^{(h)}$ characteristics) or in the time domain (e.g., $v(t)$ and $i(t)$ characteristics). These models are available for many nonlinear loads and systems such as power electronic devices, nonlinear transformers, discharge lighting, and EHV and HVDC networks [44]. In the above formulation of harmonic power flow, we assume that the capacitors are shunt capacitor banks with variable reactances, and capacitor placement is possible for MC number of buses (candidate buses). We also use the proposed formulation of [35] in the harmonic power flow for the admittance of linear loads at harmonic frequencies:

$$y_i^{(h)} = \frac{P_i^{(1)} - jQ_i^{(1)}/h}{\left|V_i^{(1)}\right|^2} \quad \text{for } i = 2, \ldots, m-1. \tag{10-4}$$

#### 10.4.1.2 Constraints

Voltage constraints will be taken into account by specifying upper (e.g., $V^{\max} = 1.1$ pu) and lower (e.g., $V^{\min} = 0.9$ pu) bounds of rms voltage ($n$ = total number of buses, $i$ = bus number, $h$ = harmonic order):

$$V^{\min} \le \sqrt{\sum_h \left(V_i^{(h)}\right)} \le V^{\max} \quad \text{for } i = 1, \ldots, n. \tag{10-5}$$

The distortion of voltage is considered by defining

Bounds for Eq. 10-6 are specified by the IEEE-519 standard [51]. Let $u^{\max}$ denote the maximum number of capacitor units allowed at each bus. The number of capacitors on bus $i$ is limited by

$$u = u_{fi} \le u^{\max} \quad \text{for} \quad i \in MC, \tag{10-7}$$

where $u_{fi}$ denotes the number of fixed capacitor banks at bus $i$ and $MC$ is the set of possible buses for capacitor placement.

#### 10.4.1.3 Objective Function (Cost Index)

The objective function (*cost*) selected for capacitor placement in the presence of harmonics is [35–37, 44–46]

$$\begin{aligned} \min F &= F_{\text{loss}} + F_{\text{cap.}} + F_{\text{capacity}} \\ &= K_E T P_{\text{loss}}(V^{(1)}, \ldots, V^{(L)}, C) + \sum_{i \in MC} K_{cfp} C_i \\ &\quad + K_A P_{\text{loss}}(V^{(1)}, \ldots, V^{(L)}, C), \end{aligned} \tag{10-6}$$

where

$F_{\text{loss}}$ = energy loss cost,

$F_{\text{cap.}}$ = cost of fixed capacitors,

$F_{\text{capacity}}$ = cost corresponding to losses (e.g., used capacity of the system),

$P_{\text{loss}}$ = total system losses,

$V^{(h)}$ = bus voltage vector at harmonic $h$,

$L$ = highest order of harmonics considered,

$C$ = size of connected capacitors,

$T$ = duration of load (hours/year),

$MC$ = set of possible shunt capacitor buses,

$K_{cfp}$ = cost per unit of fixed capacitance (Table 10.3 [37, 45]),

$K_E$ = cost per MWh (e.g., $K_E = 50$ \$/MWh [40, 45]), and

$K_A$ = saving per MW for reduction in losses (e.g., $K_A = 120{,}000$ \$/MW [40]).

be computed using harmonic



where $V_i^{(h)}$ and $\theta_i^{(h)}$ are magnitude and phase of the hth harmonic voltage at bus $i$ and $y_{ij}^{(h)}$ and $\delta_{ij}^{(h)}$ are magnitude and phase of hth harmonic line admittance between buses $i$ and $j$, respectively.

### 10.4.2 Application of Maximum Sensitivities Selection (MSS) for the Capacitor Allocation Problem

This section outlines the application of maximum sensitivities selection (MSS) in conjunction with a Newton-based harmonic load flow program to generate the local solution of the capacitor placement and sizing problem in the presence of voltage and current harmonics. If the initial condition is near the global point, the MSS algorithm will generate a near global solution. Otherwise, the MSS algorithm has a high chance of getting stuck at a local point. This section introduces the application of MSS for the capacitor allocation problem as proposed by [41].

#### 10.4.2.1 Sensitivity Functions for MSS

Sensitivities of the objective function (Eq. 10-8) to capacitance values at compensation buses can be computed using partial derivatives:

$$\begin{aligned} \frac{\partial P_{\text{loss},k}}{\partial Q} &= \sum_{h=1}^{L} W_h \frac{\partial P_{\text{loss},k}^{(h)}}{\partial Q^{(h)}}, \\ \frac{dF_{\text{cost}}}{dQ_p} &= \frac{F_{\text{cost}}^{(p+1)} - F_{\text{cost}}^{(p)}}{Q_{(p+1)} - Q_p} \end{aligned} \tag{10-10}$$

where $W_h = 1/h$ is the weight function at harmonic $h$, and $P_{\text{loss},k}^{(h)}$ are the total system losses at harmonic $h$ for load level $k$ and $F_{\cos t}^{(p+1)}$ is the cost corresponding to capacitor of size $Q_{(p+1)}$. Subscript $p$ indicates the discrete step sizes of capacitor cost as listed in Table 10.3 (e.g., $Q_1 = 150$ kVAr, $Q_2 = 300$ kVAr, . . .). Note the application of linear interpolation in Eq. 10-10 due to the discrete nature of the capacitor cost (Table 10.3).

The partial derivatives of $P_{\text{loss},k}^{(h)}$ are computed as follows:

$$\begin{bmatrix} \frac{\partial P_{\text{loss},k}^{(h)}}{\partial P^{(h)}} \\ \frac{\partial P_{\text{loss},k}^{(h)}}{\partial Q^{(h)}} \\ \frac{\partial P_{\text{loss},k}^{(h)}}{\partial I_r^{(h)}} \\ \frac{\partial P_{\text{loss},k}^{(h)}}{\partial I_i^{(h)}} \end{bmatrix} = \begin{bmatrix} \frac{\partial P^{(h)}}{\partial \theta^{(h)}} & \frac{\partial Q^{(h)}}{\partial \theta^{(h)}} & \frac{\partial I_r^{(h)}}{\partial \theta^{(h)}} & \frac{\partial I_i^{(h)}}{\partial \theta^{(h)}} \\ \frac{\partial P^{(h)}}{\partial V^{(h)}} & \frac{\partial Q^{(h)}}{\partial V^{(h)}} & \frac{\partial I_r^{(h)}}{\partial V^{(h)}} & \frac{\partial I_i^{(h)}}{\partial V^{(h)}} \\ \frac{\partial P^{(h)}}{\partial \theta^{(h)}} & \frac{\partial Q^{(h)}}{\partial \theta^{(h)}} & \frac{\partial I_r^{(h)}}{\partial \theta^{(h)}} & \frac{\partial I_i^{(h)}}{\partial \theta^{(h)}} \\ \frac{\partial P^{(h)}}{\partial V^{(h)}} & \frac{\partial Q^{(h)}}{\partial V^{(h)}} & \frac{\partial I_r^{(h)}}{\partial V^{(h)}} & \frac{\partial I_i^{(h)}}{\partial V^{(h)}} \end{bmatrix}^{-1} \begin{bmatrix} \frac{\partial P_{\text{loss},k}^{(h)}}{\partial \theta^{(h)}} \\ \frac{\partial P_{\text{loss},k}^{(h)}}{\partial V^{(h)}} \\ \frac{\partial P_{\text{loss},k}^{(h)}}{\partial \theta^{(h)}} \\ \frac{\partial P_{\text{loss},k}^{(h)}}{\partial V^{(h)}} \end{bmatrix}, \end{bmatrix}$$

where all right-hand side matrix entries are easily computed using the outputs of the harmonic power flow, as outlined in Chapter 7 (Section 7.4). The subscripts $r$ and $i$ denote real and imaginary components, respectively.

#### 10.4.2.2 The MSS Algorithm

The shunt capacitor placement and sizing problem in the presence of linear and nonlinear loads is an optimization problem with discrete variables (e.g., discrete values of capacitors). This problem is solved using the harmonic power flow algorithm and the maximum sensitivities selection (MSS) method as follows (Fig. 10.5):

**Step 1:** Input system parameters (e.g., line and load specifications, system topology, and number of load levels). Select the first load level (e.g., $k = 1$) and set initial capacitance values at all possible compensation nodes to zero. For other load levels ($k \ge 2$), use the capacitor values, computed for the preceding load levels, as the initial capacitor values of the compensation buses.

**Step 2:** Calculate harmonic power flow at load level $k$ and compute the objective function (Eq. 10-8).

**Step 3:** Calculate sensitivities of the objective function with respect to capacitances at compensation buses (Eqs. 10-10 to 10-11).

**Step 4:** Select $SC$ candidate buses with maximum sensitivities.

**Step 5 (temporary change of system topology):** Add one unit of capacitor to one of the candidate buses. Calculate harmonic power flow and the related objective function. Remove the newly added capacitor unit from the corresponding candidate bus.

**Step 6:** Repeat Step 5 for all candidate buses.

**Step 7 (change of system topology):** Among all candidate buses, select the one with the minimum objective function value and place one unit of capacitor at this bus. Record the corresponding system topology, $F$, $THD_v$, and $V_{\text{rms}}$.

**Step 8 (check convergence):** If the reactive power of the total capacitance of shunt capacitors does not exceed the sum of reactive loads, the algorithm has not converged; go to Step 3.

**Step 9:** According to the calculated information (objective functions, $THD_v$, and $V_{\text{rms}}$ values), select the topology with the minimum objective function that satisfies the problem constraints (Eqs. 10-5 to 10-7). This is the optimal solution at topology does not exist,

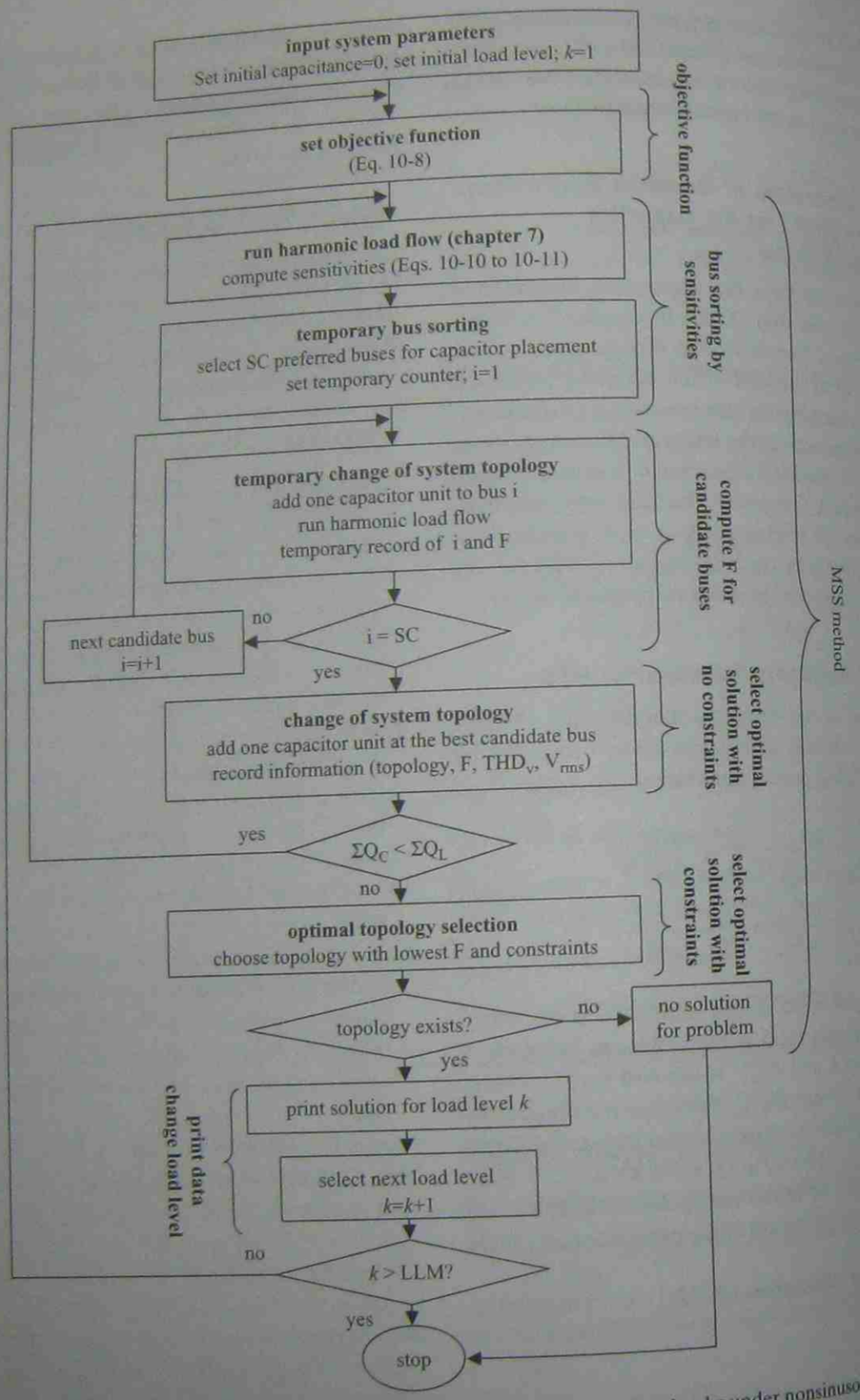



**FIGURE 10.5** Iterative algorithm for optimal placement and sizing of shunt capacitor banks under nonsinusoidal operating conditions using harmonic power flow and MSS method. SC refers to the preferred (candidate) buses for capacitor placement.



**Step 10:** Print the solution for this load level. If the final load level is not reached, select the next load level and go to Step 2.
**Step 11:** Stop.

#### 10.4.2.3 Convergence of the MSS Algorithm

The burden of calculation in the MSS algorithm is much less than those of the analysis and dynamic programming (DP) methods. Assuming $N_c$ number of capacitor units and $K_c$ number of compensation buses, the average number of power flow calculations in DP algorithm is $K_c(K_c+1)(N_c+1)$. Total number of power flow calculations of the MSS algorithm is $N_cK_c$, which is much less than that of the DP method, especially when $N_c$ is large.

### 10.4.3 Application of Local Variation (LV) for the Capacitor Allocation Problem

The shunt capacitor placement and sizing problem in the presence of linear and nonlinear loads is solved using the harmonic power flow algorithm (Chapter 7, Section 7.4) and the local variations (LV) method [36]. The solution procedure as proposed by [42] is as follows (Fig. 10.6):

**Step 1:** Input system parameters (e.g., line and load specifications, system topology, and number of load levels). Select the first load level (e.g., $k=1$).
**Step 2:** Select SC buses as optimal (or preferred) locations for capacitor bank placements. If such locations are not available, select all buses. Set iteration, capacitor location, and step interval numbers ($i=1$, $j=1$, $L_j=1$). Set initial value for the optimal objective function ($F^*=0$).
**Step 3:** Start with a random combination of capacitor sizes $Q^c=\{Q_1^c, Q_2^c, \ldots, Q_{SC}^c\}$.
**Step 4:** Set the objective function (Eq. 10-8).
**Step 5:** Perform harmonic power flow to compute fundamental and harmonic bus voltages.
**Step 6:** If power quality constraints (Eqs. 10-5 and 10-6) are satisfied go to Step 7, else:
**Step 6a:** If $i=1$, go to Step 3 and repeat Steps 3–5 until a feasible combination is found.
**Step 6b:** If $i\neq 1$ go to Step 8.
**Step 7:** Compute objective function (Eq. 10-8). If $i=1$, increase $i$, save the objective function value ($F^*=F$) and capacitor locations $Q^C=\{Q_1^c, Q_2^c, \ldots, Q_{SC}^c\}$. Else, compare $F$ with $F^*$.
**Step 7a:** If $F\geq F^*$, go to Step 8.
**Step 7b:** Else, set $F^*\geq F$ and $Q^C=\{Q_1^c, Q_2^c, \ldots, Q_{SC}^c\}$.
**Step 8:** Change capacitor size at capacitor location $j$ in small steps from $Q_o$ to $LQ_o$ while keeping the capacitance of other capacitor locations unchanged. Repeat Steps 5–7 for each step change ($Q_j=L_jQ_o$, $L_j=1, \ldots, L$).
**Step 9:** Select a combination of capacitor sizes that corresponds to the lowest objective function ($Q^c=Q^{C*}$). This will be the starting point of Step 10.
**Step 10:** Repeat Steps 8 and 9 for each capacitor location (e.g., $j\in MC$).
**Step 11:** If solution has not converged (e.g., $F^*$ is changing in two subsequent iterations), set $i=i+1$, $j=1$ and repeat Steps 8–10.
**Step 12:** This is the optimal solution at load level $k$. If the final load level is reached, go to Step 14.
**Step 13:** Select the next load level ($k=k+1$), put $Q^c$ as system parameters and go to Step 2.
**Step 14:** Print the solution and stop.

### 10.4.4 A Hybrid MSS-LV Algorithm for the Capacitor Allocation Problem

Reference [42] presents a hybrid algorithm based on a combination of maximum sensitivities selection (to direct solution toward the permissible region by selecting candidate buses) and local variations (to improve accuracy). MSS is used as a fast technique to obtain the proper initial conditions for the LV method. Therefore, this algorithm takes advantage of MSS speed and LV accuracy. Unlike the LV scheme, however, its solution does not strongly depend on the initial conditions and is not limited to a local optimum. Therefore, solution accuracy is improved at the expense of more computing time.

If the initial conditions generated by the MSS method do not satisfy the power quality constraints (e.g., MSS algorithm fails to locate a solution), the proposed algorithm will apply these constraints in the second iteration of the LV algorithm.

### 10.4.5 Application Example 10.3: Optimal Placement and Sizing of Capacitor Banks in the Distorted 18-Bus IEEE Distribution System by MSS and MSS-LV Methods

The MSS and MSS-LV algorithms are applied to the 23 kV, 18-bus, distorted IEEE distribution system (Fig. E10.3.1). Specifications of this system are given in reference [42]. Simulation results are shown in Table E10.3.1 and Fig. E10.3.2 for the following three operating conditions:

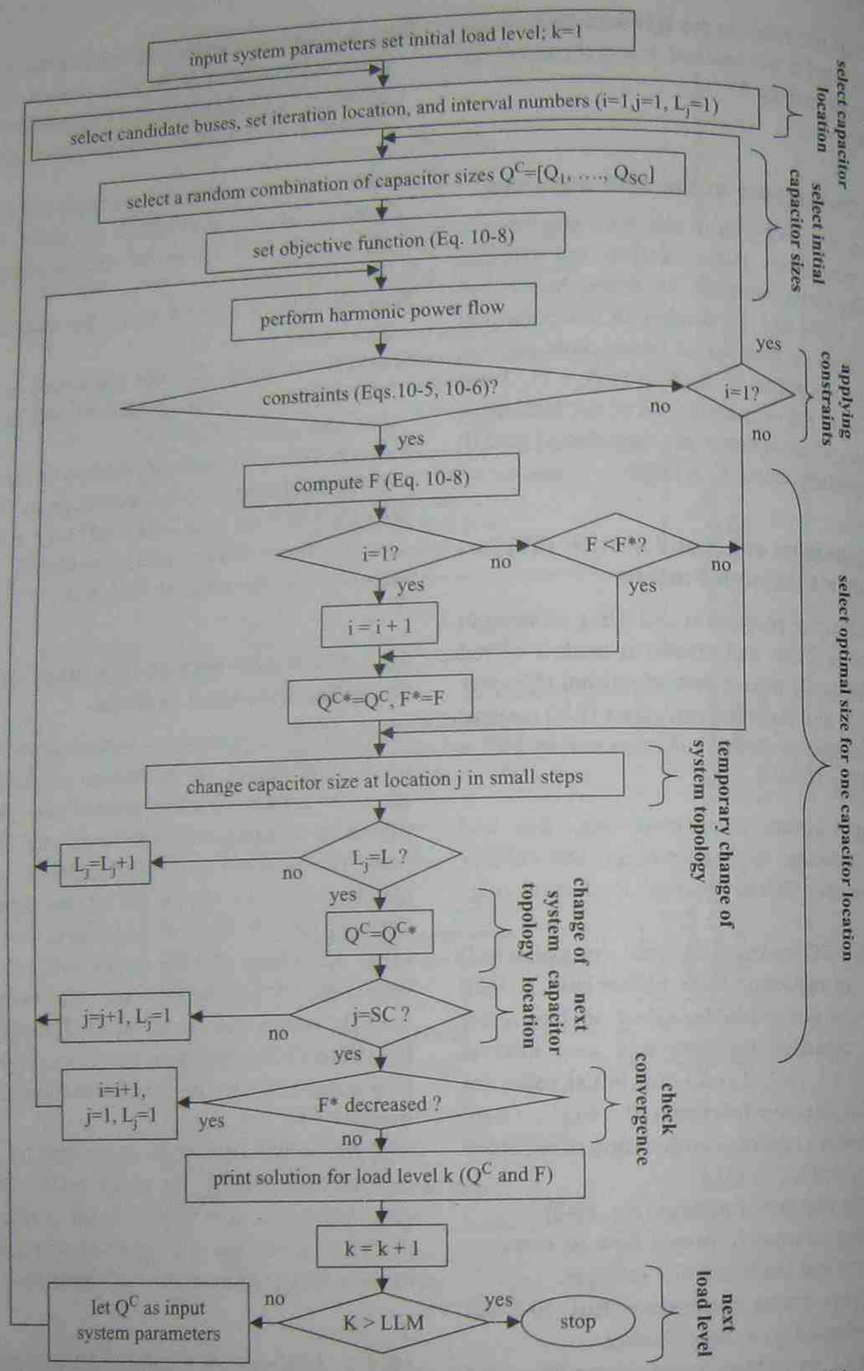



**FIGURE 10.6** Iterative algorithm for optimal placement and sizing of capacitor banks under nonsinusoidal operating conditions using harmonic power flow and the local variations (LV) method.



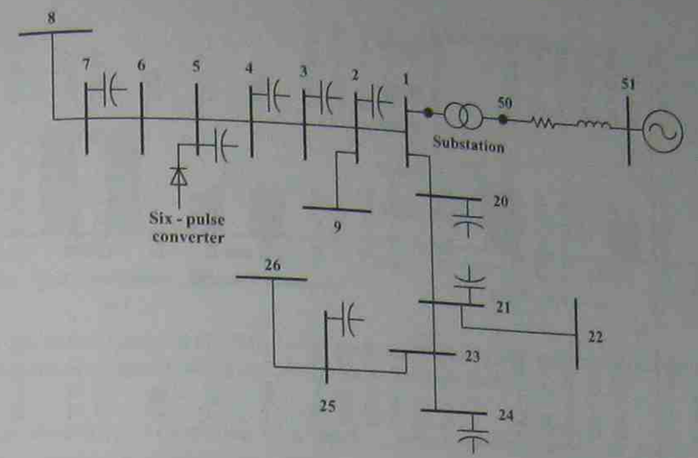



**FIGURE E10.3.1** Single-line diagram of the 18-bus IEEE distorted system.

**Case 1: High Harmonic Distortion.** The nonlinear load in Fig. E10.3.1 is a six-pulse rectifier with active and reactive powers of 0.3 pu (3 MW) and 0.226 pu (2.26 MVAr), respectively. Results based on harmonic power flow show for this system a maximum voltage $THD_v$ of 8.48%. The MSS and MSS-LV algorithms are applied to this system for optimal placement and sizing of capacitor banks.

Results of the MSS method show a yearly benefit of \$20360 (last row of Table E10.3.1) and different locations and sizes of capacitor banks before (column 2 of Table E10.3.1) and after (column 3 of Table E10.3.1) optimization. The maximum voltage $THD_v$ is only reduced to 6.37% (row 19 of Table E10.3.1 and Fig. E10.3.2). Therefore, considerable yearly benefit is achieved but power quality constraints are not satisfied.

By applying the MSS-LV algorithm, we can decrease the level of voltage $THD_v$ to 4.72% (row 19 of Table E10.3.1). As expected (due to power quality improvement), yearly benefit is slightly decreased (to \$18162). If in highly harmonic distorted systems the MSS-LV algorithm does not satisfy power quality constraints, the application of passive filters and active filters (Chapter 9) before capacitor placement is recommended.

**Case 2: Medium Harmonic Distortion.** The size of the nonlinear load is reduced such that its active and reactive powers are 0.12 pu and 0.166 pu, respectively. After optimal placement and sizing of capacitor banks by the MSS method, voltage $THD_v$ decreases from 5.18 to 5.00% and a yearly benefit of \$11650 is achieved. Applying the hybrid MSS-LV algorithm causes minor changes (e.g., eliminating one capacitor unit). Therefore, the performances of the two algorithms are similar for this case. This means that the output of MSS algorithm is near the system global solution.

**Case 3: Low Harmonic Distortion.** The size of the nonlinear load is further decreased such that its active and reactive powers are 0.02 pu and 0.046 pu, respectively. After optimal placement and sizing of capacitor banks by the MSS method, voltage $THD_v$ increases from 2.1 to 2.95% (which is lower than the desired limit of 3%), total capacitance of capacitor banks decreases from 1.005 to 0.63 pu, and a yearly benefit of \$12608 results. By applying the MSS-LV algorithm, considerable benefit is achieved (\$44787), while voltage $THD_v$ is at 2.87%.

### 10.4.6 Fuzzy Approach for the Optimal Placement and Sizing of Capacitor Banks in the Presence of Harmonics

All mathematical optimization methods require that the objective function be (pseudo-) convex and the constraints be (quasi-) convex. Only if convexity exists is there one optimal solution within the feasible or permissible multidimensional region. Experience teaches that the above-mentioned conditions of convexity are not necessarily met. The method of the steepest decent or ascent may lead to a conditional optimum of which several may exist due to the violation of convexity of the objective and constraint functions.

To avoid a trajectory leading to a conditional but not necessarily best conditional optimum, fuzzification of the objective and constraint functions has been introduced [44]. This process makes it possible

ST. GEORGE COLLEGE OF LAW



**TABLE E10.3.1** Simulation Results for the 18-Bus, Distorted IEEE Distribution System (Fig. E10.3.1) at Different Distortion Levels with per Unit VA = 10 MVA, per Unit V = 23 kV, and Swing Bus Voltage = 1.05 pu*

| | Case 1 (high distortion) | | | Case 2 (medium distortion) | | | Case 3 (low distortion) | | |
|---|---|---|---|---|---|---|---|---|---|
| | Before optimization | MSS optimization | MSS-LV optimization | Before optimization | MSS optimization | MSS-LV optimization | Before optimization | MSS optimization | MSS-LV optimization |
| Capacitor bank locations and sizes (kVAr) | Q2 = 0.105<br>Q3 = 0.060<br>Q4 = 0.060<br>Q5 = 0.180<br>Q7 = 0.060<br>Q20 = 0.06<br>Q21 = 0.12<br>Q24 = 0.15<br>Q25 = 0.09<br>Q50 = 0.12 | Q2 = 0.030<br>Q3 = 0.090<br>Q4 = 0.180<br>Q5 = 0.240<br>Q7 = 0.120<br>Q20 = 0.09<br>Q21 = 0.12<br>Q25 = 0.03 | Q2 = 0.120<br>Q3 = 0.060<br>Q4 = 0.180<br>Q5 = 0.240<br>Q7 = 0.120<br>Q20 = 0.09<br>Q21 = 0.12 | Q2 = 0.105<br>Q3 = 0.060<br>Q4 = 0.060<br>Q5 = 0.180<br>Q7 = 0.060<br>Q20 = 0.06<br>Q21 = 0.12<br>Q24 = 0.15<br>Q25 = 0.09<br>Q50 = 0.12 | Q1 = 0.090<br>Q2 = 0.120<br>Q3 = 0.060<br>Q4 = 0.060<br>Q5 = 0.180<br>Q7 = 0.060<br>Q8 = 0.060<br>Q9 = 0.030<br>Q20 = 0.06<br>Q21 = 0.12<br>Q24 = 0.15<br>Q50 = 0.03 | Q1 = 0.090<br>Q2 = 0.120<br>Q3 = 0.060<br>Q4 = 0.060<br>Q5 = 0.180<br>Q7 = 0.060<br>Q8 = 0.060<br>Q9 = 0.030<br>Q20 = 0.06<br>Q21 = 0.12<br>Q24 = 0.15 | Q2 = 0.105<br>Q3 = 0.060<br>Q4 = 0.060<br>Q5 = 0.180<br>Q7 = 0.060<br>Q20 = 0.06<br>Q21 = 0.12<br>Q24 = 0.15<br>Q25 = 0.09<br>Q50 = 0.12 | Q2 = 0.090<br>Q4 = 0.060<br>Q5 = 0.180<br>Q7 = 0.060<br>Q20 = 0.03<br>Q24 = 0.18<br>Q25 = 0.03 | Q2 = 0.090<br>Q3 = 0.120<br>Q4 = 0.030<br>Q5 = 0.180<br>Q7 = 0.060<br>Q20 = 0.09<br>Q24 = 0.06<br>Q25 = 0.09<br>Q50 = 0.09 |
| Total capacitor (pu) | Qt = 1.005 | Qt = 0.900 | Qt = 0.930 | Qt = 1.005 | Qt = 1.020 | Qt = 0.990 | Qt = 1.005 | Qt = 0.630 | Qt = 0.810 |
| Minimum voltage (pu) | 1.029 | 1.016 | 1.013 | 1.044 | 1.048 | 1.043 | 1.050 | 1.020 | 1.065 |
| Maximum voltage (pu) | 1.055 | 1.056 | 1.059 | 1.062 | 1.074 | 1.071 | 1.073 | 1.050 | 1.05 |
| Maximum $THD_v$ (%) | **8.48** | **6.37** | **4.72** | **5.18** | **5.00** | **5.00** | **2.10** | **2.95** | **2.87** |
| Losses (kW) | 282.93 | 246.43 | 250.37 | 213.69 | 192.81 | 192.84 | 189.91 | 167.32 | 109.64 |
| Capacitor cost ($) | 2432.70 | 2204.7 | 2206.8 | 2432.70 | 2535.3 | 2430.3 | 2432.70 | 1754.70 | 1830.6 |
| Total cost ($/year) | 157872.98 | 137512.00 | 139710.47 | 119237.90 | 107587.47 | 107604.72 | 105969.20 | 93361.15 | 61181.74 |
| Benefits ($/year) | | **20360** | **18162.51** | | **11650.43** | **11633.18** | | **12608** | **44787.46** |

*All capacitors were removed before the optimization process.




**FIGURE E10.3.2** Simulated results of Fig. E10.3.1: (a) maximum voltage $THD_v$ before and after optimal capacitor placement, (b) yearly benefit after optimal sizing and placement of capacitor banks.



that the solution trajectory – consisting of a band which is broad – avoids a conditional optimum, which exists due to the pseudo- or quasi-convex objective and constraint functions.

#### 10.4.6.1 Sensitivity of Objective Function and $THD_v$

Sensitivities of constraints and objective function are used to limit the number of calculations while a fuzzy combination of constraints and objective function is constructed to guarantee the monotonous convergence of the solution.

**Sensitivity of Objective Function.** Sensitivities of objective function (Eq. 10-8) to capacitance values at compensation buses can be computed using Eqs. 10-10 and 10-11.

**Sensitivity of $THD_v$.** Sensitivities of $THD_v$ (Eq. 10-6) to capacitance values at compensation buses is computed using the partial derivatives

$$S_{THDv,i} = \frac{\partial THD_{v,i}}{\partial Q} = \sum_{h=1}^{L} W_h \frac{\partial THD_{v,i}}{\partial Q^{(h)}}, \qquad (10\text{-}12)$$

where $W_h = 1/h$ is the proposed weighting function for harmonic order h. The partial derivatives of $THD_{vi}$ are computed as follows:

$$\begin{bmatrix} \frac{\partial THD_{v,i}}{\partial P^{(h)}} \\ \frac{\partial THD_{v,i}}{\partial Q^{(h)}} \end{bmatrix} = \begin{bmatrix} \frac{\partial P^{(h)}}{\partial \theta^{(h)}} & \frac{\partial Q^{(h)}}{\partial \theta^{(h)}} & \frac{\partial I_r^{(h)}}{\partial \theta^{(h)}} & \frac{\partial I_i^{(h)}}{\partial \theta^{(h)}} \\ \frac{\partial P^{(h)}}{\partial V^{(h)}} & \frac{\partial Q^{(h)}}{\partial V^{(h)}} & \frac{\partial I_r^{(h)}}{\partial V^{(h)}} & \frac{\partial I_i^{(h)}}{\partial V^{(h)}} \end{bmatrix}^{-1} \begin{bmatrix} \frac{\partial THD_{v,i}}{\partial \theta^{(h)}} \\ \frac{\partial THD_{v,i}}{\partial V^{(h)}} \end{bmatrix}, \qquad (10\text{-}13)$$

where all right-hand-side matrix entries are easily computed using results from the application of a harmonic power flow program.

#### 10.4.6.2 Fuzzy Implementation

Fuzzy set theory (FST) is relied on to determine the candidate buses and to select the most suitable bus for capacitor placement.

**Fuzzification of Sensitivities.** For the sensitivities of objective function (Eqs. 10-10 and 10-11) and constraints (Eqs. 10-12 and 10-13) with respect to the reactive power injection at each bus, the exponential fuzzifier functions $\mu_F^{sensitivity}$, $\mu_{THDv}^{sensitivity}$, $\mu_{-I}^{sensitivity}$ are employed. Figure 10.7a shows the fuzzifier for the sensitivity of $THD_{v,i}$. $S_{THD}^{max}$ is a large number, that is, buses with higher sensitivities have higher values of membership.

**Fuzzification of Objective Function and Constraints.** For the objective function (Eq. 10-8) a membership function ($\mu_o$) is defined as depicted in Fig. 10.7b. $F_o$ is the initial value of objective function and $F_i$ is the value of objective function after compensating the total reactive (inductive) loads at every bus of the distribution system. High objective values are given a low membership value, whereas low objective values are assigned a high membership function value.

For voltage constraints, it is suitable to use a membership function ($\mu_v$) with trapezoidal form, as shown in Fig. 10.7c. $V^{min}$ and $V^{max}$ correspond to Eq. 10-5 such that buses with voltages values between the two limit values $V_{min}$ and $V_{max}$ have full membership. $V_o$ and $V_o^*$ correspond to initial values of the bus effective voltage. Therefore, a bus with high rms voltage deviation (Eq. 10-5) is given a low value and a bus with low rms voltage deviation is given a high value.

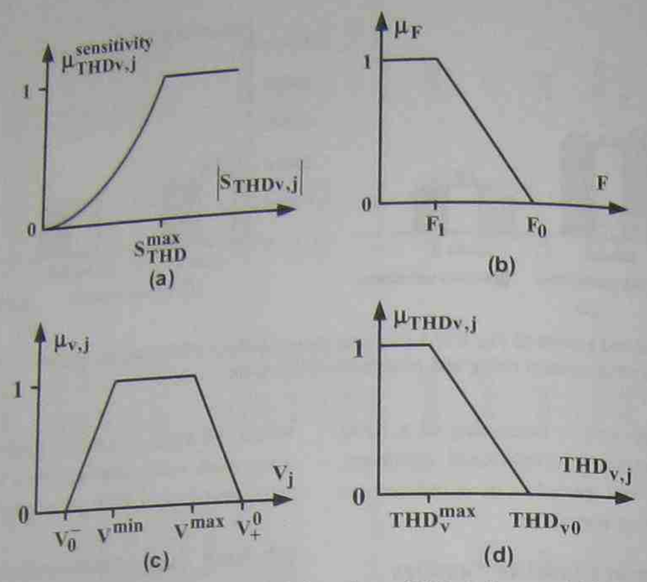



**FIGURE 10.7** Membership functions for (a) sensitivity of the voltage $THD_v$ (other sensitivity membership functions are similar), (b) objective function, (c) rms voltage, (d) voltage $THD_{v,j}$ at bus $j$.

For $THD_{v,j}$ a membership function ($\mu_{THD\,\theta,j}$) is defined as illustrated in Fig. 10.7d. $THD_v^{max}$ and $THD_{VO}$ are the limit and the initial value of $THD_{v,j}$ corresponding to Eq. 10-6, respectively. Buses are given a high value (e.g., $\mu_{THDJ,j} = 1$) unless their $THD_v$ are higher than the IEEE-519 limits.

**Fuzzy Combination of Membership Functions.** The algebraic product of the membership functions is used such as the t-norm for $THD_{v,j}$:

$$\mu_{THDv} = t_1(\mu_{THDv,1} \cdot \mu_{THDv,2} \cdots \mu_{THDv,n}) = \prod_{j=1}^{n} \mu_{THDv,j}. \quad (10\text{-}14)$$

The same formulations apply to t-norms of the bus voltages, sensitivity of $THD_{v,j}$ and sensitivity of voltage constraints, the combination of objective function and constraints, as well as their sensitivities to reactive power injection:

$$\mu_{total}^{sensitivity} = t_2(\mu_{THDv}^{sensitivity}, \mu_V^{sensitivity}, \mu_F^{sensitivity}), \quad (10\text{-}15a)$$

$$\mu_{total} = t_3(\mu_{THDv}, \mu_V, \mu_F). \quad (10\text{-}15b)$$

**Alpha-Cut Process.** In order to direct the algorithm toward the permissible region bordered by constraints, the $\alpha$-cut process is used at each iteration. To do this, the values of $\alpha$ for F, $THD_v$, and $V$ are set to their corresponding membership values in the previous iteration (e.g., $\alpha_F^{\ell+1} = \alpha_F^{\ell}$, where $\ell$ is the iteration number).

**Analysis.** The initial starting point of Eq. 10-8 (e.g., the initial compensation buses) does not usually reside inside the permissible solution region. Therefore, some type of criteria (based on simultaneous improvements of F, $THD_v$, and $V$ in consecutive iterations) is required to direct the solution toward the permissible region and to select the most appropriate buses for capacitor placement. The section uses the fuzzy set theory to measure individual improvements, generate a single criterion to direct the solution, and guarantee the monotonous convergence of the solution at each iteration. Other approaches with similar characteristics (e.g., analytical hierarchy process) could also be used.

Note that the locations of candidate buses as indicated by the sensitivities of $F$, $THD_v$, and $V$ are usually different. A single criterion – a fuzzy combination – is employed to determine the optimal locations of candidate buses. The exponential sensitivity functions of Fig. 10.7a are solely used for ranking of candidate buses. Other methods could be employed for this ranking (e.g., weighted average, statistical methods). The selected method will not have any



impact on the capacitor placement algorithm. However, the selected trapezoidal membership functions of Fig. 10.7b–d for $F$, $V$, and $THD_v$ have major impacts on the solution process (e.g., improving or deteriorating convergence).

The inclusion of sensitivity functions and fuzzification of objective and power quality constraints will automatically eliminate all solutions generating extreme values of voltages and/or currents and prevents fundamental and harmonic parallel resonances.

### 10.4.6.3 Solution Methodology

The shunt capacitor placement and sizing problem in the presence of linear and nonlinear loads is an optimization problem with discrete variables (e.g., discrete values of capacitors). This problem is solved using the harmonic power flow algorithm and the fuzzy set theory (Fig. 10.8) as follows:

**Step 1:** Input system parameters (e.g., line and load specifications and system topology). Initial capacitor values of all possible compensation buses are set to zero.

**Step 2:** Calculate harmonic power flow.

**Step 3:** Evaluate the objective function (Eq. 10-8), sensitivities of objective function, constraints, and their fuzzy combination (Eq. 10-15a) in order to determine the list of candidate buses.

**Step 4:** Sort candidate buses (CB) and from among them select several buses with maximum sensitivities and total number of installed capacitor banks less than $u^{max}$.

**Step 5:** Apply $\alpha$-cut process and compute the membership functions for the objective function

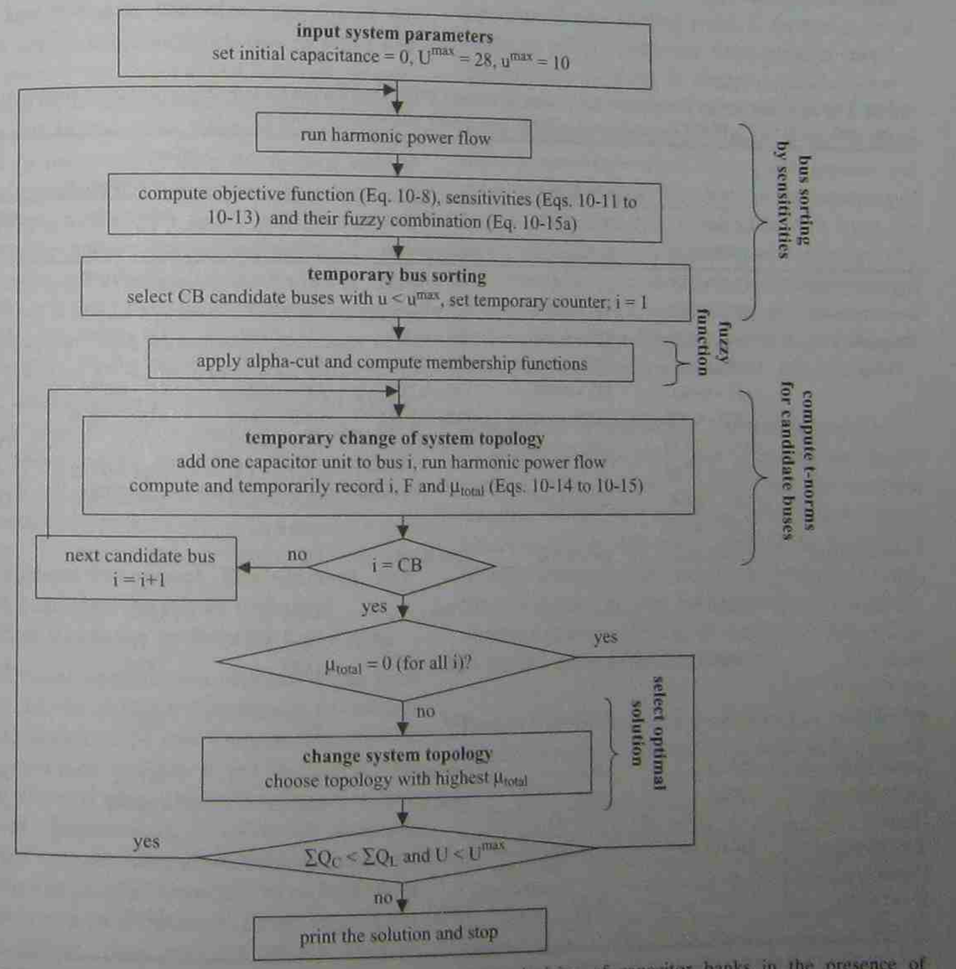



**FIGURE 10.8** Iterative fuzzy algorithm for optimal placement and sizing of capacitor banks in the presence of harmonics.

ST. GEORGE COLLEGE OF LAW

and constraints with respect to the present topology.

**Step 6:** Add one unit of capacitor to one of the candidate buses. Calculate harmonic power flow and record the values of related membership functions. Remove the newly added capacitor unit from the corresponding candidate bus.

**Step 7:** Repeat Step 6 for all other candidate buses.

**Step 8:** If all total membership functions are zero, go to Step 11.

**Step 9:** Among all candidate buses, select the one with maximum value of total membership function and place one unit of capacitor at this bus.

**Step 10:** If the reactive power of the total capacitance of shunt capacitors does not exceed the sum of reactive loads and the total number of installed capacitor banks are less than $U^{max}$, go to Step 2.

**Step 11:** Print the solution and stop.

### 10.4.7 Application Example 10.4: Optimal Placement and Sizing of Capacitor Banks in the Distorted 18-Bus IEEE Distribution System by Fuzzy Expert System

The fuzzy and MSS algorithms for capacitor placement and sizing are applied to the 23 kV, 18-bus distorted IEEE distribution system (Fig. E10.3.1). Simulation results are compared in Table E10.4.1 for the following operating conditions.

**Case 1: High Harmonic Distortion.** The nonlinear load in Fig. E10.3.1 is a six-pulse rectifier with active and reactive powers of 0.3 pu (3 MW) and 0.226 pu (2.26 MVAr), respectively. Results of harmonic power flow indicate a maximum voltage $THD_v$ of 8.48% for this system (column 2 of Table E10.4.1).

**TABLE E10.4.1** Simulation Results for the 18-Bus, Distorted IEEE Distribution System (Fig. E10.3.1) at Different Distortion Levels with per Unit S = 10 MVA, per Unit V = 23 kV, and Swing Bus Voltage = 1.05 pu[a]

| | Case 1 (high distortion) | | | Case 2 (low distortion) | | |
|---|---|---|---|---|---|---|
| | Before optimization | After MSS optimization | After fuzzy optimization | Before optimization | After MSS optimization | After fuzzy optimization |
| Capacitor bank locations and sizes (pu) | Q2 = 0.105<br>Q3 = 0.060<br>Q4 = 0.060<br>Q5 = 0.180<br>Q7 = 0.060<br>Q20 = 0.060<br>Q21 = 0.120<br>Q24 = 0.150<br>Q25 = 0.090<br>Q50 = 0.120 | Q2 = 0.030<br>Q3 = 0.090<br>Q4 = 0.180<br>Q5 = 0.240<br>Q7 = 0.120<br>Q20 = 0.090<br>Q21 = 0.120<br>Q25 = 0.030 | Q2 = 0.015<br>Q3 = 0.030<br>Q4 = 0.060<br>Q5 = 0.240<br>Q7 = 0.210<br>Q20 = 0.090<br>Q21 = 0.120 | Q2 = 0.105<br>Q3 = 0.060<br>Q4 = 0.060<br>Q5 = 0.180<br>Q7 = 0.060<br>Q20 = 0.060<br>Q21 = 0.120<br>Q24 = 0.150<br>Q25 = 0.090<br>Q50 = 0.120 | Q2 = 0.090<br>Q4 = 0.060<br>Q5 = 0.180<br>Q7 = 0.060<br>Q20 = 0.030<br>Q24 = 0.180<br>Q25 = 0.030 | Q3 = 0.255<br>Q4 = 0.030<br>Q5 = 0.060<br>Q7 = 0.030<br>Q20 = 0.165<br>Q21 = 0.015<br>Q24 = 0.075<br>Q25 = 0.045 |
| Total capacitor (pu) | Qt = 1.005 | Qt = 0.900 | Qt = 0.765 | Qt = 1.005 | Qt = 0.630 | Qt = 0.675 |
| Minimum voltage (pu) | 1.029 | 1.016 | 0.998 | 1.050 | 1.020 | 1.021 |
| Maximum voltage (pu) | 1.055 | 1.056 | 1.050 | 1.073 | 1.050 | 1.054 |
| Max. THD, (%) | 8.48 | 6.37 | 4.89 | 2.10 | 2.95 | 2.63 |
| Losses (kW) | 282.93 | 246.43 | 257.46 | 189.91 | 167.32 | 160.48 |
| Capacitor cost ($/year) | 1978.2 | 1692 | 1458.30 | 1978.20 | 1311.90 | 1538.25 |
| Total cost ($/year) | 159853.14 | 139199.94 | 145120.98 | 107947.98 | 94676.46 | 91086.09 |
| Benefits ($/year) | | 20653 | 14732 | | 13271 | 16861 |

[a]All capacitors were removed before the optimization process.



Application of the MSS method to Fig. E10.3.1 shows that optimal capacitor placement results in considerable yearly benefit (e.g., $20653 per year) but it does not limit $THD_v$ to the desired level of 5% (column 3 of Table E10.4.1). This is expected from the MSS method dealing with rich harmonic configurations, where capacitor placement is not the primary solution for harmonic mitigation.

The fuzzy algorithm of Fig. E10.3.1 is also applied to this system for optimal placement and sizing of capacitor banks. Results show a yearly benefit of $14732 per year (last row of Table E10.4.1) and different locations and sizes of capacitor banks before (column 2 of Table E10.4.1) and after (column 4 of Table E10.4.1) the fuzzy optimization. In addition, maximum voltage $THD_v$ is reduced to 4.89% (row 16 of Table E10.4.1) and total capacitance is decreased by 24%.

**Case 2: Low Harmonic Distortion.** The size of the nonlinear load is decreased such that its active and reactive powers are 0.02 pu and 0.046 pu, respectively. After optimal placement and sizing of capacitor banks with MSS method, $THD_v$ increases from 2.1 to 2.95% (which is lower than the desired limit of 5%), total capacitance of capacitor banks is decreased from 1.005 pu to 0.630 pu and a yearly benefit of $13271 is achieved (column 6 of Table E10.4.1).

Application of the fuzzy algorithm results in $THD_v$ increase from 2.1 to 2.63% (which is in the permitted region) and also total capacitance decreases from 1.005 to 0.675 pu (column 7 of Table E10.4.1). In addition, annual savings are increased to $16861 (e.g., 27% greater savings than that of the MSS method). These results demonstrate the fine capability of the fuzzy method for capacitor placement in the presence of harmonics.

### 10.4.8 Optimal Placement, Replacement, and Sizing of Capacitor Banks in Distorted Distribution Networks by Genetic Algorithms

Most traditional optimization methods move from one point in the decision hyperspace to another using some deterministic rule. The problem with this is that the solution is likely to get stuck at a local optimum. Genetic algorithms (GAs) start with a diverse set (population) of potential solutions (hyperspace vectors). This allows for exploration of many optima in parallel, lowering the probability of getting stuck at a local optimum. Even though GAs are probabilistic, they are not strictly random searches. The stochastic operators used on the population direct the search toward regions of the hyperspace that are likely to have higher fitness values.

This section presents a genetic method to formulate the capacitor placement and sizing problem in the presence of voltage and current harmonics, taking into account fixed capacitors with a limited number of capacitor banks at each bus and the entire feeder [45]. Operational and power quality constraints include bounds for rms voltage, $THD_v$, and the number and size of installed capacitors.

#### 10.4.8.1 Genetic Algorithm

Genetic algorithms use the principles of natural evolution and population genetics to search and arrive at a near global solution. The required design variables are encoded into a binary string as a set of genes corresponding to chromosomes in biological systems. Unlike traditional optimization techniques that require one starting point, GAs use a set of points as initial conditions. Each point is called a chromosome. A group of chromosomes is called a population. The number of chromosomes in a population is usually selected to be from 30 to 300. Each chromosome is a string of binary codes (genes) and may contain substrings. The merit of a string is judged by the fitness function, which is derived from the objective function and is used in successive genetic operations. During each iterative procedure (referred to as a generation), a new set of strings with improved performance is generated relying on three GA operators (i.e., reproduction, crossover, and mutation).

**Structure of Chromosomes.** Different types of chromosomes for GAs have been proposed and implemented. This section employs the chromosome structure of Fig. 10.9 consisting of MC substrings of binary numbers, where MC denotes the number of possible compensation (candidate) buses for capacitor placement in the entire feeder. The binary numbers indicate the size of the installed capacitor at the bus under consideration.

**Fitness Functions.** The inverse algebraic product of penalty functions (Fig. 10.10) is used as the fitness

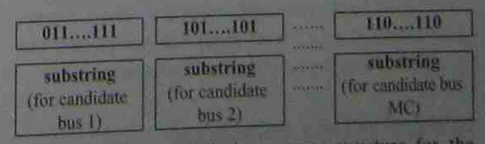



**FIGURE 10.9** A typical chromosome structure for the genetic algorithm.

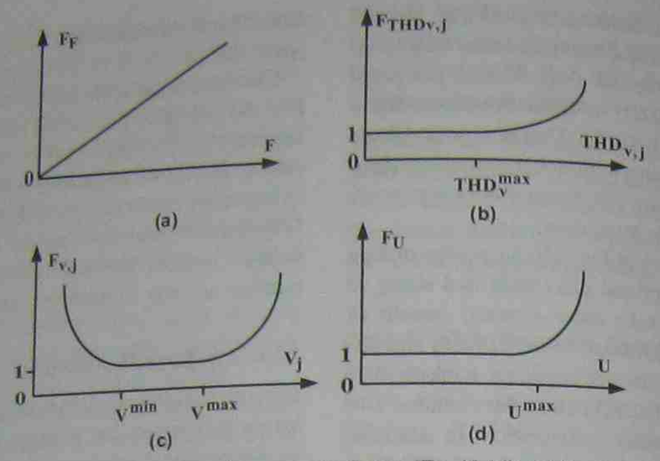



**FIGURE 10.10** Penalty functions of the GA used to compute fitness (Eq. 10-16): (a) for the objective function, (b) for $THD_{v,j}$, (c) for $v,j$, (d) for total number of capacitors of the entire feeder (U).

function combining objective and constraint functions:

$$F_{fitness} = 1/(F_F \cdot F_{THDv} \cdot F_V \cdot F_U)$$
$$F_{THDv} = \prod_{i=1}^{n} F_{THDv,i} \qquad (10\text{-}16)$$
$$F_v = \prod_{i=1}^{n} F_{v,i}$$

where penalty functions $F_F$, $F_{THDv,j}$, $F_{v,j}$, and $F_U$ are shown in Fig. 10.10.

**Genetic Operators.** Three genetic operators including reproduction (based on the roulette-wheel mechanism), crossover (with crossover probability of 0.6 to 1.0), and mutation (with mutation probability of 0.01 to 0.1) are established.

**Convergence Criterion.** The iterations (regenerations) of the genetic algorithm are continued until all generated chromosomes become equal or the maximum number of iterations ($N^{max} = 40$) is reached. Due to the randomness of the GA method, the solution tends to differ for each run, even with the same initial population. For this reason, it is suggested to perform multiple runs and select the "most acceptable" solution (e.g., with most benefits, within the permissible region bounded by constraints).

### 10.4.8.2 Solution Methodology

The shunt capacitor placement and sizing problem in the presence of linear and nonlinear loads is solved based on the genetic algorithm of Fig. 10.11 as follows:

**Step 1:** Input system parameters (e.g., system topology, line and load specifications). Input the initial population with $N_{ch}$ chromosomes.
**Step 2:** Set initial counter and parameter values (e.g., $N_{ch} = N_{ii} = N_R = 1$ and $F_{MIN}$ = a high number).
**Step 3 (Fitness Process):**
**Step 3a:** Run harmonic power flow for $N_{ch}$ chromosomes and save results.
**Step 3b:** Compute proposed penalty functions (Fig. 10.10) employing data generated by harmonic power flow program. Compute fitness functions (Eq. 10-16) for chromosome $N_{ch}$. Set $N_{ch} = N_{ch} + 1$.
**Step 3c:** If $N_{ch} \le N_{chrom}$ go to Step 3a.
**Step 4 (Reproduction Process):**
**Step 4a:** Define total fitness as the sum of all fitness values for all chromosomes.
**Step 4b:** Select a percentage of "roulette wheel" for each chromosome that is equal to the ratio of its fitness value to the total fitness value.
**Step 4c:** Improve generation by rolling the roulette wheel $N_{ch}$ times. Select a new combination of chromosomes.
**Step 5 (Crossover Process):**
**Step 5a:** Select a random number ($R_1$) for mating two parent chromosomes.
**Step 5b:** If $R_1$ is between 0.6 and 1.0 then combine the two parents, generate two offspring, and go to Step 5d.
**Step 5c:** Else, transfer the chromosome with no crossover.



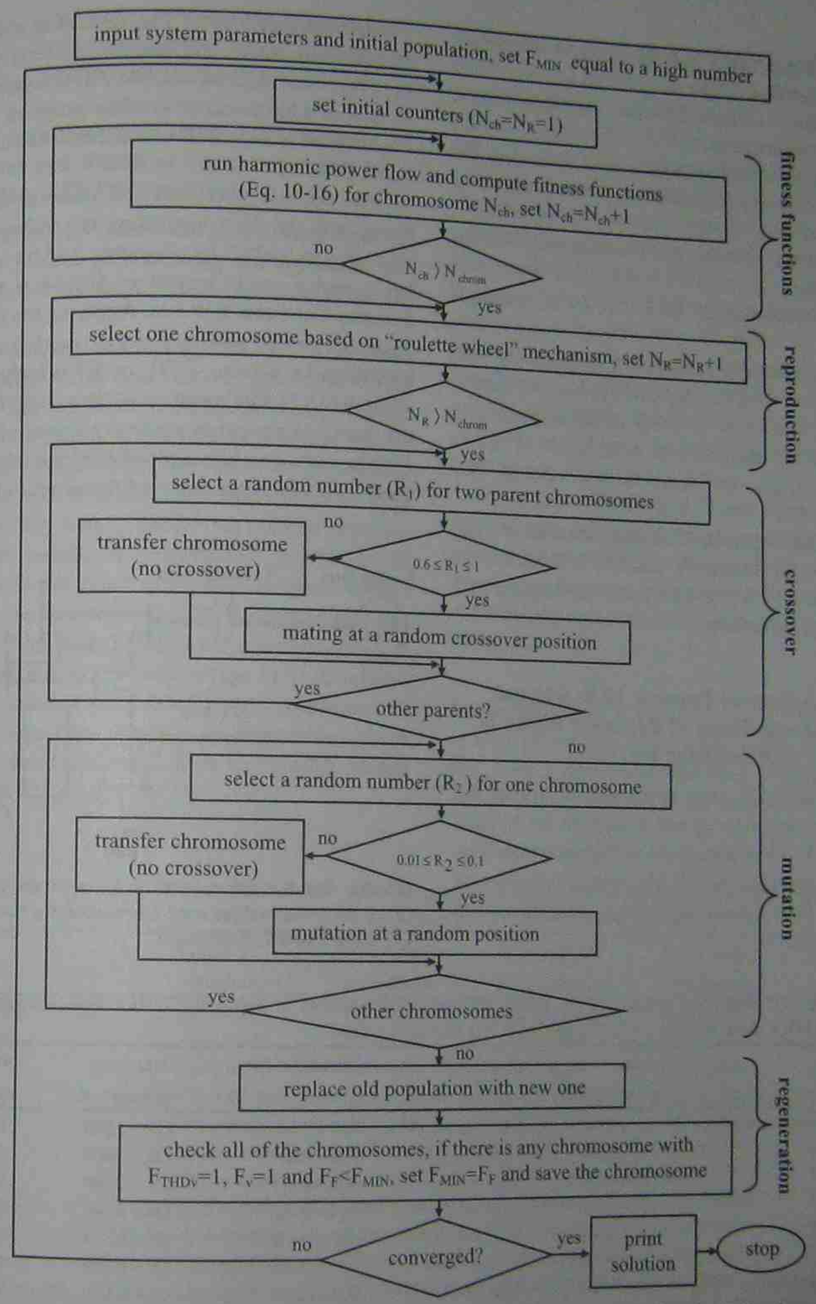



**FIGURE 10.11** Iterative genetic algorithm for optimal placement and sizing of capacitor banks in the presence of harmonics.

ST. GEORGE'S COLLEGE OF LAW

**Step 5d:** Repeat steps 5a to 5c for all chromosomes.

**Step 6 (Mutation Process):**

**Step 6a:** Select a random number ($R_2$) for mutation of one chromosome.

**Step 6b:** If $R_2$ is between 0.01 and 0.1 then apply the mutation process at a random position and go to Step 6d.

**Step 6c:** Else, transfer the chromosome with no mutation.

**Step 6d:** Repeat steps 6a to 6c for all chromosomes.

**Step 7 (Updating Populations):** Replace the old population with the improved population generated by Steps 2 to 6. Check all chromosomes; if there is any chromosome with $F_{THD_v} = 1$, $F_v = 1$, and $F_F < F_{MIN}$, set $F_{MIN} = F_F$ and save it. Set $N_{it} = N_{it} + 1$.

**Step 8 (Convergence):** If all chromosomes are the same or the maximum number of iterations is reached ($N_{it} = N^{max}$), then print the solution and stop, else go to Step 2.

### 10.4.9 Application Example 10.5: Optimal Placement and Sizing of Capacitor Banks in the 6-Bus IEEE Distorted System

The MSS, MSS-LV, fuzzy, and genetic algorithms for optimal capacitor sizing and placement are applied to the 69 kV, 6-bus, distorted distribution system (Fig. E10.5.1). Specifications of this system are given in reference [42]. Simulation results are compared in Table E10.5.1.

The nonlinear load in Fig. E10.5.1 is a six-pulse rectifier with active and reactive powers of 0.2 pu (2 MW) and 0.25 pu (2.5 MVAr), respectively. Results of a harmonic power flow program indicate a maximum voltage $THD_v$ of 5.270% (column 2 of Table E10.5.1).

After optimal placement and sizing of capacitor banks with the MSS algorithm, the voltage $THD_v$ decreases to 5.007% by allocating 0.15 pu capacitor banks and a yearly benefit of $35968 is achieved (column 3 of Table E10.5.1). Applying the MSS-LV algorithm to the system yields a yearly benefit of $40098 and a voltage $THD_v$ of 4.970 (column 4 of Table E10.5.1). Optimization of the system based on the fuzzy set algorithm generates voltage $THD_v$ of 4.990% and a yearly benefit of $33758 (column 5 of Table E10.5.1). Application of the genetic algorithm

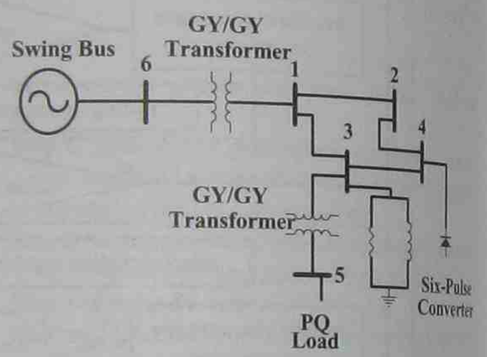



**FIGURE E10.5.1** Single-line diagram of the 6-bus [43] IEEE distorted system used for simulation and analysis. GY is a grounded transformer.

**TABLE E10.5.1** Simulation Results for the 6-Bus, Distorted IEEE System of Fig. E10.5.1 with Base Apparent Power S = VA = 10 MVA, Base Voltage V = 69 kV, and Swing Bus Voltage = 1.00 pu[a]

| | Before optimization | After MSS optimization | After MSS-LV optimization | After fuzzy optimization | After GA optimization |
|---|---|---|---|---|---|
| Capacitor bank locations and sizes (pu) | Q1 = 0.000 | Q1 = 0.000 | Q1 = 0.405 | Q1 = 0.000 | Q1 = 0.120 |
| | Q2 = 0.000 | Q2 = 0.000 | Q2 = 0.000 | Q2 = 0.000 | Q2 = 0.000 |
| | Q3 = 0.000 | Q3 = 0.000 | Q3 = 0.315 | Q3 = 0.000 | Q3 = 0.45 |
| | Q4 = 0.000 | Q4 = 0.000 | Q4 = 0.000 | Q4 = 0.000 | Q4 = 0.00 |
| | Q5 = 0.000 | Q5 = 0.150 | Q5 = 0.150 | Q5 = 0.135 | Q5 = 0.405 |
| | Q6 = 0.000 | Q6 = 0.000 | Q6 = 0.000 | Q6 = 0.000 | Q6 = 0.000 |
| Total capacitor (pu) | Qt = 0.000 | Qt = 0.150 | Qt = 0.870 | Qt = 0.135 | Qt = 0.495 |
| Minimum voltage (pu) | 0.935 | 0.965 | 1.000 | 0.962 | 0.990 |
| Maximum voltage (pu) | 1.005 | 1.013 | 1.070 | 1.012 | 1.044 |
| Maximum THD$_v$ (%) | 5.270 | 5.007 | 4.970 | 4.990 | 4.943 |
| Losses (kW) | 360 | 295 | 285.2 | 299 | 276.7 |
| Capacitor cost ($/year) | 0.00 | 301.50 | 1640.7 | 279.45 | 725.85 |
| Total cost ($/year) | 200880.0 | 164911.5 | 160782.0 | 167121.45 | 155103.85 |
| Computing time (sec)[b] | – | 6 | 115 | 10 | 639 |
| Benefits ($/year) | | 35968.5 | 40098.0 | 33758.55 | 45778.15 |

[a]All capacitors were removed before the optimization process.
[b]Using a Pentium III (550 MHz) personal computer.



(with $N_{ch} = 100$) results in about the same voltage $THD_v$ (e.g., 4.943%), and the annual savings are increased to $45778 (column 6 of Table E10.5.1).

### 10.4.10 Application Example 10.6: Optimal Placement and Sizing of Capacitor Banks in the 18-Bus IEEE Distorted System

The MSS, MSS-LV, fuzzy, and genetic algorithms for capacitor placement and sizing are applied to the 23 kV, 18-bus distorted IEEE distribution system (Fig. E10.3.1).

The nonlinear load in Fig. E10.3.1 is a six-pulse rectifier with active and reactive powers of 0.3 pu (3 MW) and 0.226 pu (2.26 MVAr), respectively. Results of a harmonic power flow program show a maximum voltage $THD_v$ of 8.486% for this system (column 2 of Table E10.6.1). Application of MSS method to Fig. E10.3.1 shows that optimal capacitor placement results in considerable yearly benefit (e.g., $20653 per year), but it does not limit voltage $THD_v$ to the desired level of 5% (column 3 of Table E10.6.1). Applying the MSS-LV algorithm yields a yearly benefit of $17939 and voltage $THD_v$ is reduced to 4.72% (column 4 of Table E10.6.1). Application of the fuzzy algorithm results in an acceptable voltage $THD_v$ level and benefits (4.899% and $14732, column 5 of Table E10.6.1).

The genetic algorithm (GA) of Fig. 10.11 is also applied to this system for optimal placement and sizing of capacitor banks ($N_{ch} = 250$). Results reveal a yearly benefit of $18949 per year (last row of Table E10.6.1); maximum voltage $THD_v$ is limited to 4.880% (column 6 of Table E10.6.1), and the total allocated capacitance is decreased by 16%.

Greater power quality control mitigation is achieved with the GA at the expense of lower benefits compared with the MSS solution. The GA yields greater yearly benefits while the power quality conditions are the same than those of the MSS-LV solution. Compared with the fuzzy solution, the same power quality conditions result (rows 12–15 of Table E10.6.1), but greater benefits (e.g., 28% greater savings) are achieved with GA.

The results of Tables E10.5.1 and E10.6.1 indicate that the genetic algorithm captures more advantageous solutions than the MSS, MSS-LV, and fuzzy algorithms. This is expected because the genetic algorithm has the capability of computing the near global solution.

**Computing Time.** Unfortunately, the application of GAs often looks like a never-ending process. In fact, only a compromise between population size, mutation rate, and so on can lead to an adequate

**TABLE E10.6.1** Simulation Results of MSS, MSS-LV, Fuzzy, and Genetic Algorithms for the 18-Bus, Distorted IEEE Distribution System (Fig. E10.3.1) with per Unit VA = 10 MVA, per Unit V = 23 kV, and Swing Bus Voltage = 1.05 pu[a]

| | Before optimization | After MSS optimization | After MSS-LV optimization | After fuzzy optimization | After GA optimization |
|---|---|---|---|---|---|
| Capacitor bank locations and sizes (pu) | Q2 = 0.105 | Q2 = 0.030 | Q2 = 0.120 | Q2 = 0.015 | Q2 = 0.030 |
| | Q3 = 0.060 | Q3 = 0.090 | Q3 = 0.060 | Q3 = 0.030 | Q3 = 0.000 |
| | Q4 = 0.060 | Q4 = 0.180 | Q4 = 0.180 | Q4 = 0.060 | Q4 = 0.165 |
| | Q5 = 0.180 | Q5 = 0.240 | Q5 = 0.240 | Q5 = 0.240 | Q5 = 0.330 |
| | Q7 = 0.060 | Q7 = 0.120 | Q7 = 0.120 | Q7 = 0.210 | Q7 = 0.105 |
| | Q20 = 0.060 | Q20 = 0.090 | Q20 = 0.090 | Q20 = 0.090 | Q20 = 0.060 |
| | Q21 = 0.120 | Q21 = 0.120 | Q21 = 0.120 | Q21 = 0.120 | Q21 = 0.090 |
| | Q24 = 0.150 | Q24 = 0.000 | Q24 = 0.000 | Q24 = 0.000 | Q24 = 0.015 |
| | Q25 = 0.090 | Q25 = 0.030 | Q25 = 0.000 | Q25 = 0.000 | Q25 = 0.015 |
| | Q50 = 0.120 | Q50 = 0.000 | Q50 = 0.000 | Q50 = 0.000 | Q50 = 0.030 |
| Total capacitor (pu) | Qt = 1.005 | Qt = 0.900 | Qt = 0.930 | Qt = 0.765 | Qt = 0.840 |
| Minimum voltage (pu) | 1.029 | 1.016 | 1.013 | 0.998 | 1.003 |
| Maximum voltage (pu) | 1.055 | 1.056 | 1.059 | 1.050 | 1.050 |
| Maximum THD$_v$ (%) | 8.486 | 6.370 | 4.720 | 4.899 | 4.883 |
| Losses (kW) | 282.93 | 246.43 | 250.37 | 257.46 | 249.31 |
| Capacitor cost ($/year) | 1978.20 | 1692.00 | 2206.80 | 1458.30 | 1788.75 |
| Total cost ($/year) | 159853.14 | 139199.94 | 141913.26 | 145120.98 | 140903.73 |
| Computing time (sec)[b] | – | 96 | 141 | 48 | 2780 |
| Benefits ($/year) | | 20653.6 | 17939.88 | 14732.16 | 18949.41 |

[a]All capacitors were removed before the optimization process.
[b]Using a Pentium III (550 MHz) personal computer.

ST. GEORGE'S COLLEGE OF LAW

algorithm that finds good solutions in a relatively short time. However, capacitor bank placement is usually considered a planning problem and its computing time is not of great concern. The computational burden associated with the genetic algorithm is included and compared with those of the MSS, MSS-LV, and fuzzy methods as shown in row 15 of Table E10.5.1 and row 19 of Table E10.6.1. As expected, the computing times of the genetic algorithm are much longer.

### 10.4.11 Genetically Optimized Fuzzy Placement and Sizing of Capacitor Banks in Distorted Distribution Networks

This section presents a genetic algorithm in conjunction with fuzzy logic (GA-FL) to formulate the capacitor placement and sizing problem in the presence of voltage and current harmonics, taking into account fixed capacitors with a limited number of capacitor banks at each bus [46]. Operational and power quality constraints include bounds for rms voltage, $THD_v$, and the number as well as the size of installed capacitors. In this hybrid global optimization method, fuzzy approximate reasoning is introduced to determine the suitability (fitness function) of each GA chromosome for capacitor placement. This will improve the evolution process of the GA, lowering the probability of getting stuck at local optima. Fuzzy logic has shown good results for capacitor bank allocation when combined with genetic algorithms under sinusoidal operating conditions [1].

#### 10.4.11.1 Solution Method

Suitability of THD, and voltage are defined for each chromosome based on fuzzy approximate reasoning. These variables are used with a cost index to determine the suitability (fitness function) of each GA chromosome for capacitor placement.

Fuzzy set theory (FST) contains a set of rules that are developed from qualitative descriptions. When suitability of $THD_v$, voltage, and cost of the distribution system are studied, an engineer can choose the most appropriate locations and sizes of shunt capacitor banks. These rules are defined to determine the suitability of each chromosome ($S_{chrom}$) and may be executed employing fuzzy inferencing. $S_{chrom}$ serves as the fitness function in the GA to further improve the evolution process, reducing the probability of converging to a local optimum.

**Structure of Chromosomes.** The chromosome structure of Fig. 10.9 is used.

**Fuzzy Fitness (Suitability) Functions.** The suitability level of each chromosome ($S_{chrom}$) is computed by defining fuzzy membership functions for suitability of total harmonic distortion ($\mu_{S_{THD}}$), voltage ($\mu_{S_V}$), and cost ($\mu_{cost}$). A fuzzy expert system (FES) uses the number of buses with high $THD_v$ and voltage values and the average of the $THD_v$ and voltage deviation (at these buses) to determine the suitability of $THD_v$ and voltage.

A concern for the development of fuzzy expert systems is the assignment of appropriate membership functions, which could be performed based on intuition, rank ordering, or probabilistic methods. However, the choice of membership degree in the interval [0, 1] does not matter, as it is the order of magnitude that is important [1].

***Suitability of $THD_v$ ($S_{THD}$).*** For a given chromosome, define the average unacceptable value of $THD_v$ as

$$THD_{avg}^{high} = \Sigma_{j=1}^{N_{THD}} THD/N_{THD_v} \quad (10\text{-}17)$$

where $N_{THD}$ is the number of buses with high total voltage harmonic distortions (e.g., $THD_v > THD_v^{max}$). The following steps are performed to compute $S_{THD}$:

- Fuzzification of $THD_{avg}^{high}$ and $N_{THD}$ (based on membership functions of Fig. 10.12a and 10.12b, respectively) to compute the corresponding membership values ($\mu_{THD}$ and $\mu_{N_{THD}}$).
- Fuzzy inferencing and defuzzification based on the decision matrix of Table 10.5, the membership function of Fig. 10.13, *Mamdani max-prod* implication, and center average methods [50]:

$$S_{THD} = \Sigma \bar{y} \mu_{N_{THD}} \mu_{THD} / \Sigma \mu_{N_{THD}} \mu_{THD}. \quad (10\text{-}18)$$

**Suitability of Voltage ($S_V$).** For a given chromosome, define the average unacceptable value of voltage deviation as

$$\Delta V_{avg} = \frac{\sum_{j=1}^{N_{\Delta|V|}} \Delta V_j}{N_{\Delta|V|}}, \quad \begin{cases} \Delta V_j = |V| - V^{max} \text{ (if } |V| > V^{max}) \\ \Delta V_j = V^{min} - |V| \text{ (if } |V| < V^{min}) \end{cases} \quad (10\text{-}19)$$

where $N_{\Delta|V|}$ is the number of buses with unacceptable (high) values of voltage, $V^{max} = 1.1$ pu and $V^{min} = 0.9$ pu are upper and lower bounds of rms voltage, respectively. The following steps are performed to compute $S_V$:

- Fuzzification of $\Delta V_{ave}$ and $N_{\Delta|V|}$ (based on membership functions of Fig. 10.14a and 10.14b, respectively) to compute the corresponding membership values ($\mu_{\Delta|V|}$ and $N_{N_{\Delta|V|}}$).
- Fuzzy inferencing and defuzzification (using the decision matrix of Table 10.5, Fig. 10.13, and Eq. 10-18) to determine the suitability of voltage ($S_V$).

***Cost Index (cost).*** Compute the cost for all chromosomes (Eq. 10-8) and linearly normalize them into [0, 1] range with the largest cost having a value of one and the smallest one having a value of zero.

***Fitness (Suitability) of a Chromosome ($S_{chrom}$).*** Suitability level for a given chromosome is computed from $S_{THD}$, $S_V$, and cost using the following steps:

- Fuzzification of $S_{THD}$, $S_V$, and cost (based on Fig. 10.13) to compute the corresponding membership values ($\mu_{S_{THD}}$, $\mu_{S_V}$, and $\mu_{cost}$).
- Fuzzy inferencing and defuzzification (using the decision matrix of Table 10.6, Fig. 10.14b, and Eq. 10-18) to determine the suitability of the chromosome ($S_{chrom}$).

**Genetic Operators.** Three genetic operators including reproduction (based on the "roulette-wheel" mechanism), crossover (with crossover probability of 0.6 to 1.0), and mutation (with mutation probability of 0.01 to 0.1) are used.



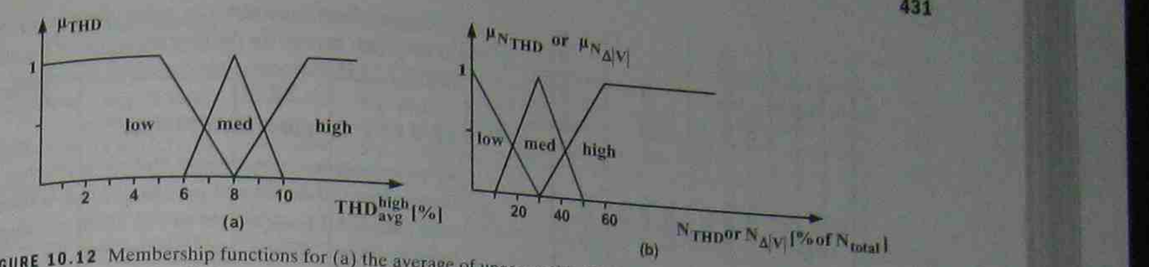



**FIGURE 10.12** Membership functions for (a) the average of unacceptable (high) $THD_v$ values (Eq. 10-17), (b) number of buses with unacceptable $THD_v$ or voltage, where "avg" means average.

**TABLE 10.5** Decision Matrix for Determining Suitability of $THD_v$ (and V)

| | | $THD_v$ (or $\Delta\|V\|$) | | |
|---|---|---|---|---|
| AND | | Low | Medium | High |
| $N_{THD}$ (or $N_{\Delta\|V\|}$) | Low | ***High*** | ***Medium*** | ***Medium*** |
| | Medium | ***Medium*** | ***Low*** | ***Low*** |
| | High | ***Medium*** | ***Low*** | ***Low*** |

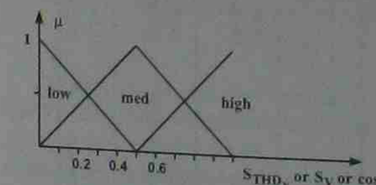



**FIGURE 10.13** Membership functions for suitability of $THD_v$, $V$, and "cost."

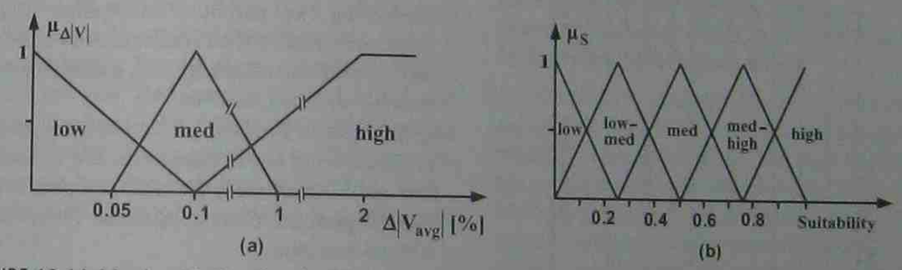



**FIGURE 10.14** Membership functions for (a) voltage deviation, (b) suitability of a chromosome ($S_{chrom}$).

ST. GEORGE COLLEGE OF LAW

**TABLE 10.6** Decision Matrix for Determining Suitability of a Chromosome ($S_{chrom}$)

| $S_{THD}$ | | | | | | | | | |
|---|---|---|---|---|---|---|---|---|---|
| | | Low | | | Medium | | | High | |
| $S_V$ | Low | "cost" | | | | | | | |
| | | Low | Medium | High | Low | Medium | High | Low | Medium | High |
| | | **Low–medium** | **Low** | **Low** | **Medium** | **Low–medium** | **Low** | **Medium** | **Medium** | **Low** |
| | Medium | "cost" | | | "cost" | | | "cost" | | |
| | | Low | Medium | High | Low | Medium | High | Low | Medium | High |
| | | **Medium** | **Low–medium** | **Low** | **Medium** | **Medium** | **Low** | **Medium** | **Medium** | **Low** |
| | High | "cost" | | | "cost" | | | "cost" | | |
| | | Low | Medium | High | Low | Medium | High | Low | Medium | High |
| | | **Medium** | **Low–medium** | **Low** | **High** | **High** | **Low** | **High** | **High** | **Low** |

ST. GEORGE COLLEGE OF LAW



Figure 10.15 illustrates the block diagram of the fuzzy expert system for the determination of the suitability of a chromosome for capacitor placement.

#### 10.4.11.2 Solution Methodology

The shunt capacitor placement and sizing problem in the presence of linear and nonlinear loads is solved using the GA-FL algorithm of Fig. 10.16 as follows:

**Step 1:** Input system parameters and the initial population.

**Step 2: Fuzzy Fitness or Suitability.** Perform the following steps for all chromosomes (Fig. 10.15):

**Step 2a:** Run the Newton-based harmonic power flow program.

**Step 2b:** Compute suitability of $THD_v$ and voltage (Fig. 10.13, Table 10.5, and Eq. 10-18).

**Step 2c:** Compute cost index.

**Step 2d:** Compute suitability, $S_{chrom}$ (Fig. 10.14b, Table 10.6, and Eq. 10-18).

**Step 3: Reproduction Process.** Select a new combination of chromosomes by rolling the roulette wheel.

**Step 4: Crossover Process.** Select a random number for mating two parent chromosomes. If it is between 0.6 and 1.0 then combine the two parents and generate two offspring. Else, transfer the chromosome with no crossover.

**Step 5: Mutation Process.** Select a random number for mutation of one chromosome. If it is between 0.01 and 0.1 then apply the mutation process at a random position. Else, transfer the chromosome with no mutation.

**Step 6: Updating Populations.** Replace the old population with the improved population generated by Steps 2 to 5. Check all chromosomes and save the one with minimum cost, satisfying all constraints.

**Step 7: Convergence.** If all chromosomes are the same or the maximum number of iterations is achieved ($N_{max} = 40$), then print the solution and stop, else go to Step 2.

### 10.4.12 Application Example 10.7: Genetically Optimized Fuzzy Placement and Sizing of Capacitor Banks in the 18-Bus IEEE Distorted System

The hybrid GA-FL method (Fig. 10.16) and the capacitor placement techniques of prior sections (MSS, MSS-LV, fuzzy, and genetic) are applied to the 23 kV, 18-bus distorted IEEE distribution system (Fig. E10.3.1). The six-pulse rectifier (with P = 0.3 pu = 3 MW and Q = 0.226 pu = 2.26 MVAr)



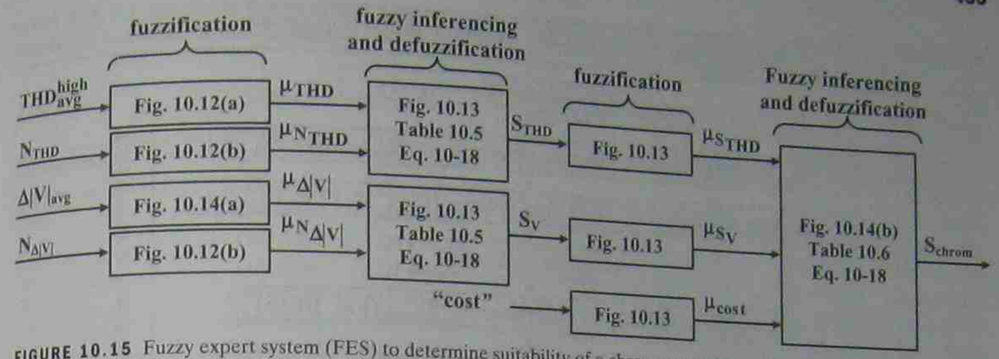



**FIGURE 10.15** Fuzzy expert system (FES) to determine suitability of a chromosome ($S_{chrom}$) for capacitor placement from total harmonic distortion ($THD_v$), voltage deviation ($\Delta|V|_{avg}$), "cost," number of buses with unacceptable $THD_v$ ($N_{THD}$) and unacceptable $|V|$ ($N_{\Delta|V|}$) [46].

causes a maximum voltage $THD_v$ of 8.486% (column 2 of Table E10.7.1).

Simulation results for the MSS, MSS-LV, fuzzy, and genetic algorithms are listed in columns 3 to 6 of Table E10.7.1, respectively. Among these algorithms, the GA approach results in a near global solution with the best yearly benefit of $18949 per year (column 6 of Table E10.7.1).

The GA-FL approach of Fig. 10.16 is also applied to this system for optimal placement and sizing of capacitor banks. Results show a yearly benefit of $19550 per year (last row of Table E10.7.1) and maximum voltage $THD_v$ is limited to 4.982% (column 7 of Table E10.7.1). Compared to the GA approach, total yearly benefit is increased by $600 (e.g., 3.2%), and the total allocated capacitance is decreased by 0.015 pu.

**Analysis and Convergence Criterion of the GA-FL Algorithm.** The iterations of the GA-FL algorithm are continued until all generated chromosomes become equal or the maximum number of iterations is reached.

At each iteration, a fuzzy expert system (Fig. 10.15) is used to compute the fitness function of each chromosome and to select the parent population. As a result, new generations have more variety of chromosomes and higher probability of capturing the global solution. As demonstrated in Fig. E10.7.1, the relatively narrow search band of the conventional GA does not allow a large variation of chromosomes between iterations and the solution (e.g., benefits) is trapped at a near global point after the 14th iteration. However, the larger search space of the GA-FL approach (allowing large variations of benefits in consecutive iterations) has resulted in a better near global solution at the 35th iteration.

The inclusion of objective function and power quality constraints will automatically eliminate all solutions generating extreme values for voltages and/or currents and prevents fundamental and harmonic parallel resonances.

### 10.4.13 Application Example 10.8: Genetically Optimized Fuzzy Placement and Sizing of Capacitor Banks in the 123-Bus IEEE System with 20 Nonlinear Loads

The GA (Fig. 10.11) and GA-FL (Fig. 10.16) methods are applied to the 4.16 kV, 123-bus IEEE radial distribution network of Fig. E10.8.1. Specifications of this system are given in reference [51]. To introduce harmonic distortion, 20 nonlinear loads (Table E10.8.1) with different harmonic spectra (Table E10.8.2) are included. These loads are modeled as harmonic current sources. The coupling between harmonics is not considered and the decoupled harmonic power flow algorithm of Chapter 7 (Section 7.5.1) is used.

The high penetration of these nonlinear loads causes a maximum $THD_v$ of 8.03% (column 2, Table E10.8.3). The results of the GA-FL algorithm show a 5.5% increase in total annual benefit compared with those generated by the GA method (last row of Table E10.8.3), whereas the maximum $THD_v$ is significantly limited to 2.76%.

**Analysis and Convergence Criterion.** The generations (iterations) of the GA-FL algorithm are continued until all chromosomes of the population become equal or the maximum number of generations is achieved. The initial conditions for Eq. 10-8 (e.g., the initial capacitor values) do not usually reside inside the permissible solution region. In this section, a GA-FL approach is used to minimize the objective

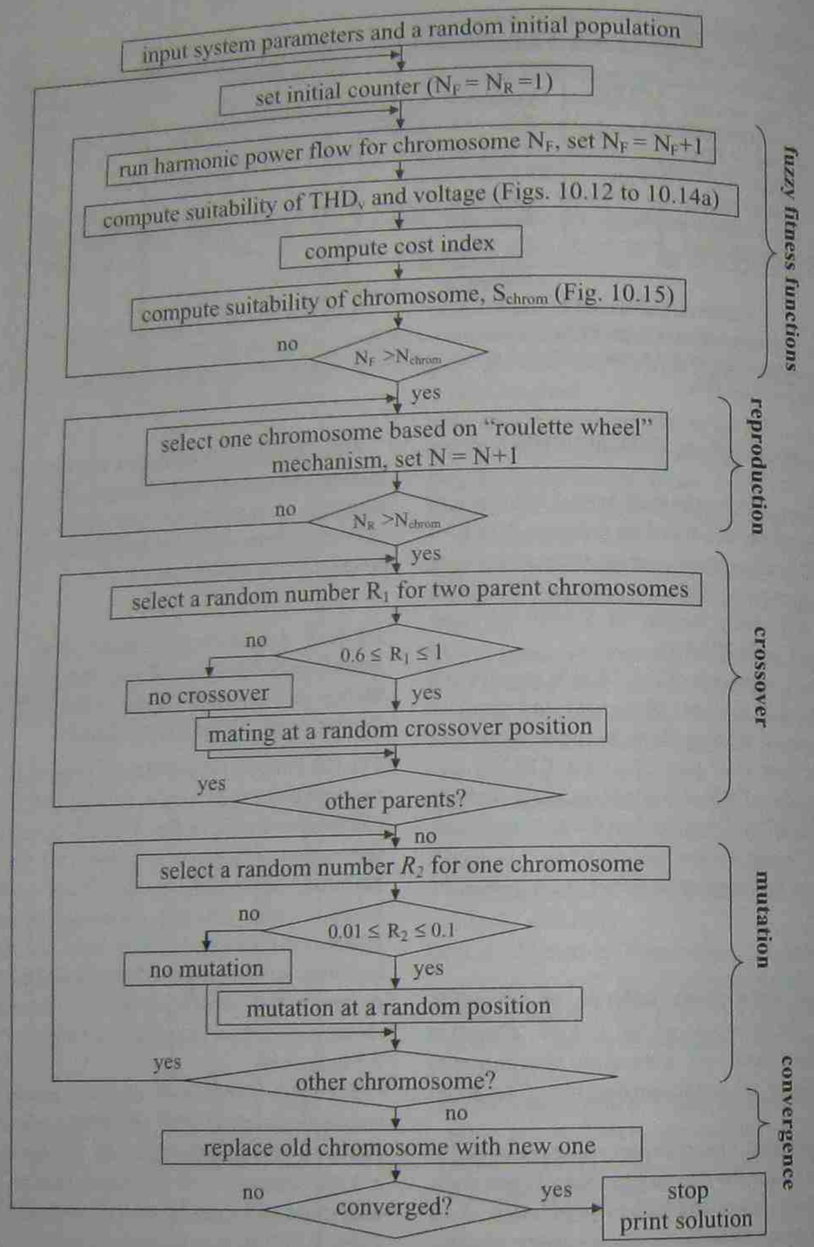



**FIGURE 10.16** Iterative GA-FL method for optimal placement and sizing of capacitor banks in the presence of harmonics.



**TABLE E10.7.1** Simulation Results of MSS, MSS-LV, Fuzzy, Genetic and GA-FL Algorithms for the 18-Bus, Distorted IEEE Distribution System of Fig. E10.3.1 with per Unit VA = 10 MVA, per Unit V = 23 kV, and Swing Bus Voltage = 1.05 pu[a]

| | | Local optimization | | | (Near) global optimization | |
|---|---|---|---|---|---|---|
| | Before optimization | After MSS optimization | After MSS-LV optimization | After fuzzy optimization | After GA optimization | After GA-FL optimization |
| Capacitor bank locations and sizes (pu) | Q2 = 0.105<br>Q3 = 0.060<br>Q4 = 0.060<br>Q5 = 0.180<br>Q7 = 0.060<br>Q20 = 0.060<br>Q21 = 0.120<br>Q24 = 0.150<br>Q25 = 0.090<br>Q50 = 0.120 | Q2 = 0.030<br>Q3 = 0.090<br>Q4 = 0.180<br>Q5 = 0.240<br>Q7 = 0.120<br>Q20 = 0.090<br>Q21 = 0.120<br>Q24 = 0.000<br>Q25 = 0.030<br>Q50 = 0.000 | Q2 = 0.120<br>Q3 = 0.060<br>Q4 = 0.180<br>Q5 = 0.240<br>Q7 = 0.120<br>Q20 = 0.090<br>Q21 = 0.120<br>Q24 = 0.000<br>Q25 = 0.000<br>Q50 = 0.000 | Q2 = 0.015<br>Q3 = 0.030<br>Q4 = 0.060<br>Q5 = 0.240<br>Q7 = 0.210<br>Q20 = 0.090<br>Q21 = 0.120<br>Q24 = 0.000<br>Q25 = 0.000<br>Q50 = 0.000 | Q2 = 0.030<br>Q3 = 0.000<br>Q4 = 0.165<br>Q5 = 0.330<br>Q7 = 0.105<br>Q20 = 0.060<br>Q21 = 0.090<br>Q24 = 0.015<br>Q25 = 0.015<br>Q50 = 0.030 | Q2 = 0.030<br>Q3 = 0.000<br>Q4 = 0.195<br>Q5 = 0.300<br>Q7 = 0.105<br>Q20 = 0.090<br>Q21 = 0.075<br>Q24 = 0.015<br>Q25 = 0.015<br>Q50 = 0.000 |
| Total capacitor (pu) | Qt = 1.005 | Qt = 0.900 | Qt = 0.930 | Qt = 0.765 | Qt = 0.840 | Qt = 0.825 |
| Minimum voltage (pu) | 1.029 | 1.016 | 1.013 | 0.998 | 1.003 | 1.005 |
| Maximum voltage (pu) | 1.055 | 1.056 | 1.059 | 1.050 | 1.050 | 1.050 |
| Maximum THD, (%) | 8.486 | 6.370 | 4.720 | 4.899 | 4.883 | 4.982 |
| Losses (kW) | 282.93 | 246.43 | 250.37 | 257.46 | 249.31 | 248.18 |
| Capacitor cost ($/year) | 1978.20 | 1692.00 | 2206.80 | 1458.30 | 1788.75 | 1817.55 |
| Total cost ($/year) | 159853.14 | 139199.94 | 141913.26 | 145120.98 | 140903.73 | 140302.8 |
| Benefits ($/year) | | 20653.6 | 17939.88 | 14732.16 | 18949.41 | 19550.34 |

[a]All capacitors were removed before the optimization process.

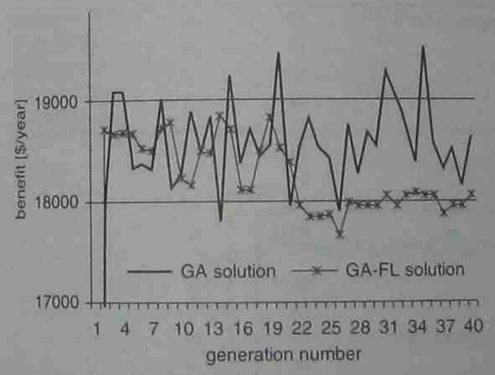



**FIGURE E10.7.1** Comparison of the solution progress for the GA-FL and the GA methods (Table E10.7.1) for the 18-bus, distorted IEEE distribution system (Fig. E10.3.1) using the same initial population.

function while directing the constraints toward the permissible region.

To select the parent population at each generation, a fuzzy expert system (Fig. 10.15) is used to compute the fitness function of each chromosome considering the uncertainty of decision making based on the objective function and constraints. As a result, new generations have a higher probability of capturing the global solution.

As demonstrated in Fig. E10.8.2, the relatively narrow search band of the conventional GA does not allow a large variation of chromosomes between generations, and thus it is more difficult to escape from local optima. For the 18-bus and 123-bus systems, the solution is trapped at a near global point after the 14th and 22nd iterations, respectively. In the GA-FL approach, there is more variety in the generated parent population as the chromosome evaluation is based on fuzzy logic. The larger search space (allowing large variations of benefits in consecutive iterations) has resulted in a better near global solution at the 35th and 29th iterations for the 18-bus and 123-bus systems, respectively.

The inclusion of objective function and power quality constraints will automatically eliminate all solutions that generate extreme values for voltages and/or currents and prevents fundamental and harmonic parallel resonances.

## 10.5 SUMMARY

Related to reactive power compensation is the placement and sizing of capacitor banks so that the transmission efficiency can be increased at minimum cost. First filter designs are addressed for sinusoidal conditions. Various optimization methods are described such as analytical methods, numerical programming,

ST. GEORGE COLLEGE OF LAW

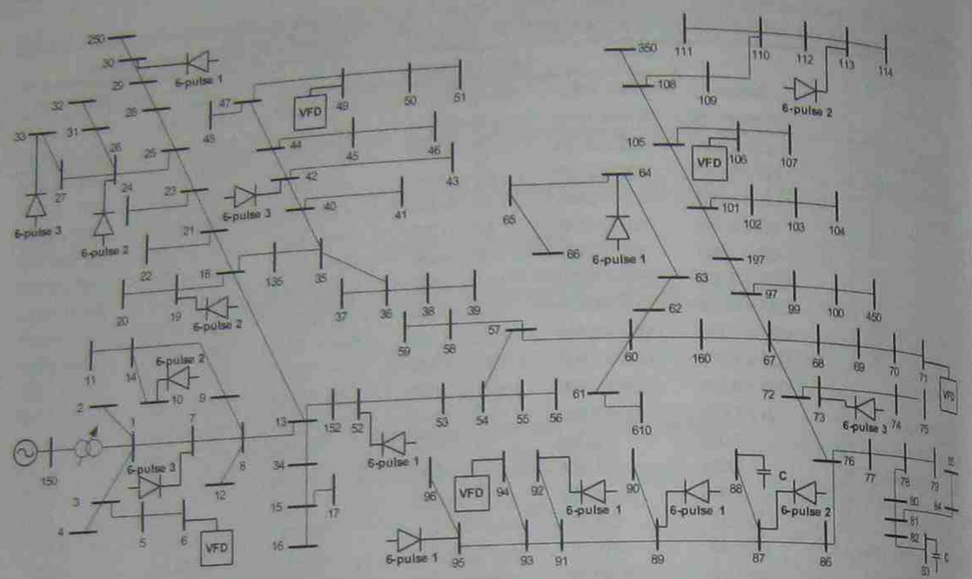



**FIGURE E10.8.1** The IEEE 123-bus distribution system [51] with 20 nonlinear loads.

**TABLE E10.8.1** Nonlinear Load Data for the IEEE 123-Bus System (Fig. E10.8.1)

| Nonlinear bus | Nonlinear load type (Table E10.8.2) | kW | kVAr |
|---|---|---|---|
| 6 | Six-pulse variable-frequency drive | 15 | 10 |
| 7 | Six-pulse 3 | 15 | 10 |
| 10 | Six-pulse 2 | 24 | 3 |
| 19 | Six-pulse 2 | 24 | 3 |
| 26 | Six-pulse 2 | 15 | 10 |
| 30 | Six-pulse 1 | 24 | 3 |
| 33 | Six-pulse 3 | 24 | 3 |
| 42 | Six-pulse 3 | 15 | 10 |
| 49 | Six-pulse variable-frequency drive | 60 | 45 |
| 52 | Six-pulse 1 | 24 | 3 |
| 64 | Six-pulse 1 | 24 | 3 |
| 71 | Six-pulse variable-frequency drive | 15 | 10 |
| 73 | Six-pulse 3 | 24 | 3 |
| 87 | Six-pulse 2 | 60 | 45 |
| 89 | Six-pulse 1 | 24 | 3 |
| 92 | Six-pulse 1 | 24 | 3 |
| 94 | Six-pulse variable-frequency drive | 15 | 10 |
| 95 | Six-pulse 1 | 24 | 3 |
| 106 | Six-pulse variable-frequency drive | 15 | 10 |
| 113 | Six-pulse 2 | 24 | 3 |

**TABLE E10.8.2** Harmonic Spectra of Nonlinear Loads for the IEEE 123-Bus System (Fig. E10.8.1)

| | Nonlinear load | | | | | | | |
|---|---|---|---|---|---|---|---|---|
| | Six-pulse 1 | | Six-pulse 2 | | Six-pulse 3 | | Six-pulse VFD | |
| Order | Magnitude (%) | Phase (deg) | Magnitude (%) | Phase (deg) | Magnitude (%) | Phase (deg) | Magnitude (%) | Phase (deg) |
| 1 | 100 | 0 | 100 | 0 | 100 | 0 | 100 | 0 |
| 5 | 20 | 0 | 19.1 | 0 | 20 | 0 | 23.52 | 111 |
| 7 | 14.3 | 0 | 13.1 | 0 | 14.3 | 0 | 6.08 | 109 |
| 11 | 9.1 | 0 | 7.2 | 0 | 9.1 | 0 | 4.57 | −158 |
| 13 | 7.7 | 0 | 5.6 | 0 | 0 | 0 | 4.2 | −178 |
| 17 | 5.9 | 0 | 3.3 | 0 | 0 | 0 | 1.8 | −94 |
| 19 | 5.3 | 0 | 2.4 | 0 | 0 | 0 | 1.37 | −92 |
| 23 | 4.3 | 0 | 1.2 | 0 | 0 | 0 | 0.75 | −70 |
| 25 | 4 | 0 | 0.8 | 0 | 0 | 0 | 0.56 | −70 |
| 29 | 3.4 | 0 | 0.2 | 0 | 0 | 0 | 0.49 | −20 |
| 31 | 3.2 | 0 | 0.2 | 0 | 0 | 0 | 0.54 | 7 |
| 35 | 2.8 | 0 | 0.4 | 0 | 0 | 0 | 0 | 0 |
| 37 | 2.7 | 0 | 0.5 | 0 | 0 | 0 | 0 | 0 |

**TABLE E10.8.3** Simulation Results of GA (Fig. 10.11) and GA-FL (Fig. 10.16) Algorithms for the 123-Bus, Distorted IEEE Distribution System (Fig. E10.8.1) Using Decoupled Harmonic Power Flow (Chapter 7, Section 7.5.1)

| | Before optimization | GA optimization | GA-FL optimization |
|---|---|---|---|
| Capacitor bank locations and sizes (pu) | Q83 = 200<br>Q88 = 50 | Q26 = 150<br>Q42 = 300<br>Q72 = 150<br>Q76 = 300 | Q42 = 300<br>Q52 = 300<br>Q72 = 300<br>Q105 = 150 |
| Total capacitor (kW) | Qt = 350 | Qt = 900 | Qt = 1050 |
| Minimum voltage (pu) | 0.874 | 0.904 | 0.915 |
| Maximum voltage (pu) | 0.980 | 0.980 | 0.980 |
| Maximum THD, (%) | 8.0319 | 3.1018 | 2.7603 |
| Losses (kW) | 94.96 | 82.021 | 81.28 |
| Capacitor cost ($/year) | 125 | 360 | 390 |
| Total cost ($/year) | 53114.5 | 46127.72 | 45744.24 |
| Benefits ($/year) | | 6986.8 | 7370.3 |

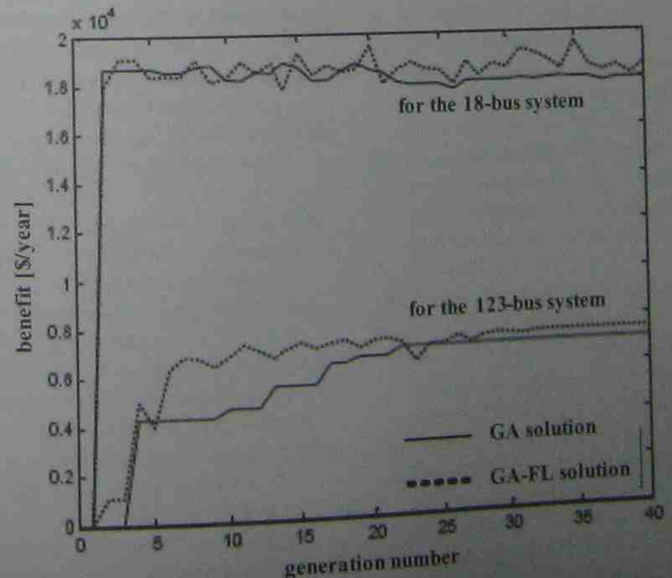



**FIGURE E10.8.2** Solution progress of the GA-FL and the GA methods for the 18-bus (Fig. E10.3.1) and 123-bus (Fig. E10.8.1) distorted IEEE distribution systems (Table E10.8.3).

ST. GEORGE'S COLLEGE OF

heuristic approaches, and artificial intelligence (AI-based) methods. The latter ones comprise genetic algorithms, expert systems, simulated annealing, artificial neural networks, and fuzzy set theory. Furthermore, graph search, particle swarm, tabu search, and sequential quadratic programming algorithms are explained. Thereafter, the optimal placement and sizing of capacitor banks is studied under the influence of harmonics relying on some of the same optimization methods as used for sinusoidal conditions. Thus, the nonsinusoidal case is an extension of the sinusoidal approach. It is recommended that the reader first applies some of the optimization procedures to the sinusoidal case and then progresses to nonsinusoidal conditions.

Eight application examples highlight the advantages and disadvantages of the various optimization methods under given constraints (e.g., $THD_v$, $V_{rms}$) and objective functions (e.g., cost). Unfortunately, there is not one single method that incorporates all the advantages and no disadvantages. It appears that the more advanced methods such as fuzzy set theory, genetic algorithms, artificial neural networks, and particle swarm methods are more able to identify the global optimum than the straightforward search methods where the gradient (e.g., steepest decent) is employed guiding the optimization process. This is so because the more advanced methods proceed not along a single trajectory but search for the global optimum within a certain region in a simultaneous manner.

ST. GEORGE'S COLLEGE OF LAW





## 10.6 REFERENCES


1) Ng, H.N.; Salama, M.M.A.; and Chikhani, A.Y.; "Classification of capacitor allocation techniques," *IEEE Transactions on Power Delivery*, Vol. 15, No. 1, pp. 387–392, January 2000.
2) Neagle, N.M.; and Samson, D.R.; "Loss reduction from capacitors installed on primary feeders," *AIEE Transactions*, Vol. 75, pp. 950–959, Oct. 1956.
3) Cook, R.F.; "Optimizing the application of shunt capacitors for reactive-voltampere control and loss reduction," *AIEE Transactions*, Vol. 80, pp. 430–444, Aug. 1961.
4) Schmill, J.V.; "Optimum size and location of shunt capacitors on distribution feeders," *IEEE Transactions on Power Apparatus and Systems*, Vol. 84, No. 9, pp. 825–832, Sept. 1965.
5) Chang, N.E.; "Locating shunt capacitors on primary feeder for voltage control and loss reduction," *IEEE Transactions on Power Apparatus and Systems*, Vol. 88, No. 10, pp. 1574–1577, Oct. 1969.
6) Bae, Y.G.; "Analytical method of capacitor allocation on distribution primary feeders," *IEEE Transactions on Power Apparatus and Systems*, Vol. 97, No. 11, pp. 1232–1238, July/Aug. 1978.
7) Lee, S.H.; and Grainger, J.J.; "Optimum placement of fixed and switched capacitors on primary distribution feeders," *IEEE Transactions on Power Apparatus and Systems*, Vol. 100, No. 1, pp. 345–352, Jan. 1981.
8) Salama, M.M.A.; Chikhani, A.Y.; and Hackam, R.; "Control of reactive power in distribution systems with an end-load and fixed load conditions," *IEEE Transactions on Power Apparatus and Systems*, Vol. 104, No. 10, pp. 2779–2788, Oct. 1985.
9) Duran, H.; "Optimum number, location, and size of shunt capacitors in radial distribution feeders, a dynamic programming approach," *IEEE Transactions on Power Apparatus and Systems*, Vol. 87, No. 9, pp. 1769–1774, Sept. 1968.
10) Fawzi, T.H.; El-Sobki, S.M.; and Abdel-Halim, M.A.; "New approach for the application of shunt capacitors to the primary distribution feeders," *IEEE Transactions on Power Apparatus and Systems*, Vol. 102, No. 1, pp. 10–13, Jan. 1983.
11) Ponnavaikko, M.; and Prakasa Rao, K.S.; "Optimal choice of fixed and switched shunt capacitors on radial distributors by the method of local variations," *IEEE Transactions on Power Apparatus and Systems*, Vol. 102, No. 6, pp. 1607–1615, June 1983.
12) Baran, M.E.; and Wu, F.F.; "Optimal sizing of capacitors placed on a radial distribution system," *IEEE Transactions on Power Delivery*, Vol. 4, No. 1, pp. 735–743, Jan. 1989.
13) Abdel-Salam, T.S.; Chikhani, A.Y.; and Hackam, R.; "A new technique for loss reduction using compensating capacitors applied to distribution systems with varying load condition," *IEEE Transactions on Power Delivery*, Vol. 9, No. 2, pp. 819–827, Apr. 1994.
14) Chis, M.; Salama, M.M.A.; and Jayaram, S.; "Capacitor placement in distribution systems using heuristic search strategies," *IEE Proceedings on Generation, Transmission and Distribution*, Vol. 144, No. 2, pp. 225–230, May 1997.
15) Boone, G.; and Chiang, H.D.; "Optimal capacitor placement in distribution systems by genetic algorithm," *Electrical Power and Energy Systems*, Vol. 15, No. 3, pp. 155–162, 1993.
16) Sundhararajan, S.; and Pahwa, A.; "Optimal selection of capacitors for radial distribution systems using a genetic algorithm," *IEEE Transactions on Power Systems*, Vol. 9, No. 3, pp. 1499–1507, Aug. 1994.
17) Miu, K.N.; Chiang, H.D.; and Darling, G.; "Capacitor placement, replacement and control in large-scale distribution systems by a GA-based two-stage algorithm," *IEEE Transactions on Power Systems*, Vol. 12, No. 3, pp. 1160–1166, Aug. 1997.
18) Laframboise, J.R.P.R.; Ferland, G.; Chikhani, A.Y.; and Salama, M.M.A.; "An expert system for reactive power control of a distribution system, part 2: system implementation," *IEEE Transactions on Power Systems*, Vol. 10, No. 3, pp. 1433–1441, Aug. 1995.
19) Ananthapadmanabha, T.; Kulkarni, A.D.; Gopala Rao, A.S.; and Rao, K.R.; "Knowledge-based expert system for optimal reactive power control in distribution system," *Electrical Power and Energy Systems*, Vol. 18, No. 1, pp. 27–31, 1996.
20) Santoso, N.I.; and Tan, O.T.; "Neural-net based real-time control of capacitors installed on distribution systems," *IEEE Transactions on Power Delivery*, Vol. 5, No. 1, pp. 266–272, Jan. 1990.
21) Gu, Z.; and Rizy, D.T.; "Neural networks for combined control of capacitor banks and voltage regulators in distribution systems," *IEEE Transactions on Power Delivery*, Vol. 11, No. 4, pp. 1921–1928, Oct. 1996.
22) Zadeh, L.A.; "Fuzzy sets," *Information and Control*, Vol. 8, pp. 338–353, 1965.
23) Chin, H.C.; "Optimal shunt capacitor allocation by fuzzy dynamic programming," *Electric Power Systems Research*, Vol. 35, pp. 133–139, 1995.
24) Ng, H.N.; Salama, M.M.A.; and Chikhani, A.Y.; "Capacitor allocation by approximate reasoning: fuzzy capacitor placement," *IEEE Transactions on Power Delivery*, Vol. 15, Issue 1, Jan. 2000, pp. 393–398
25) Ng, H.N.; and Salama, M.M.A.; "Fuzzy optimal capacitor sizing and placement," *Proceedings of*

*Canadian Conference on Electrical and Computer Engineering*, Vol. 2, pp. 680–683, 1995.

26) Carlisle, J.C.; and El-Keib, A.A.; "A graph search algorithm for optimal placement of fixed and switched capacitors on radial distribution systems," *IEEE Transactions on Power Delivery*, Vol. 15, No. 1, pp. 423–428, January 2000.

27) Mantawy, A.H.; and Al-Ghamdi, M.S.; "A new reactive power optimization algorithm," *IEEE Conference*, Bologna, Italy, June 2003.

28) Yang, H.T.; Huang, Y.C.; and Huang, C.L.; "Solution to capacitor placement in a radial distribution system using tabu search method," *Proceedings of International Conference on Energy Management and Power Delivery*, EMPD 95, Vol. 1, pp. 388–393, 1995.

29) Mori, H.; and Ogita, Y.; "Parallel tabu search for capacitor placement in radial distribution systems," *Proceedings of the IEEE Power Engineering Society Winter Meeting 2000*, Vol. 4, 23–27 Jan. 2000, pp. 2334–2339.

30) Chang, C.S.; and Lern, L.P.; "Application of tabu search strategy in solving non-differentiable savings function for the calculation of optimum savings due to shunt capacitor installation in a radial distribution system," *Proceedings of the Power Engineering Society Winter Meeting 2000*, Vol. 4, 23–27 Jan. 2000 pp. 2323–2328.

31) Abril, I.P.; and Quintero, J.A.G.; "VAR compensation by sequential quadratic programming," *IEEE Transactions on Power Systems*, Vol. 18, No. 1, pp. 36–41, February 2003.

32) Ng, H.N.; Salama, M.M.A.; and Chikhani, A.Y.; "Capacitor allocation by approximate reasoning: fuzzy capacitor placement," *IEEE Transactions on Power Delivery*, Vol. 15, No. 1, pp. 393–398, January 2000.

33) Capacitor Subcommittee of the IEEE Transmission and Distribution Committee, "Bibliography on power capacitors 1975–1980," *IEEE Transactions on Power Apparatus and Systems*, Vol. 102, No. 7, pp. 2331–2334, July 1983.

34) IEEE VAR Management Working Group of the IEEE System Control Subcommittee, "Bibliography on reactive power and voltage control," *IEEE Transactions on Power Systems*, Vol. 2, No. 2, pp. 361–370, May 1997.

35) Baghzouz, Y.; "Effects of nonlinear loads on optimal capacitor placement in radial feeders," *IEEE Transactions on Power Delivery*, Vol. PD-6, No. 1, pp. 245–251, January 1991.

36) Baghzouz, Y.; and Ertem, S.; "Shunt capacitor sizing for radial distribution feeders with distorted substation voltage," *IEEE Transactions on Power Delivery*, Vol. PD-5, No. 2, pp. 650–657, 1990.

37) Gou, B.; and Abur, A.; "Optimal capacitor placement for improving power quality," *Proceedings of the IEEE Power Engineering Society Summer Meeting 1999*, Vol. 1, 18–22 July 1999, pp. 488–492.

38) Carpinelli, G.; Varilone, P.; Vito, V.D.; and Abur, A.; "Capacitor placement in three-phase distribution systems with nonlinear and unbalanced loads," *IEE Proceedings on Generation, Transmission and Distribution*, Vol. 152, No. 1, pp. 47–51, 2005.

39) Hsu, C.T.; Yan, Y.H.; Chen, C.S.; and Her, S.L.; "Optimal reactive power planning for distribution systems with nonlinear loads," *IEEE Region 10 International Conference on Computer, Communication, Control and Power Engineering TENCON '93*, pp. 330–333, 1993.

40) Wu, Z.Q.; and Lo, K.L.; "Optimal choice of fixed and switched capacitors in radial distributions with distorted substation voltage," *IEE Proceedings on Generation, Transmission and Distribution*, Vol. 142, No. 1, pp. 24–28, January 1995.

41) Masoum, M.A.S.; Ladjevardi, M.; Fuchs, E.F.; and Grady, W.M.; "Optimal sizing and placement of fixed and switched capacitor banks under non-sinusoidal operating conditions," *Proceedings of the IEEE Summer Power Meeting 2002*, pp. 807–813, July 2002.

42) Masoum, M.A.S.; Ladjevardi, M.; Fuchs, E.F.; and Grady, W.M.; "Application of local variations and maximum sensitivities selections for optimal placement of shunt capacitor banks under nonsinusoidal operating conditions," *34th Annual North American Power Symposium*, pp. 507–515, NAPS-2002.

43) Chin, H.C.; "Optimal shunt capacitor allocation by fuzzy dynamic programming," *Electric Power Systems Research*, Vol. 35, pp. 133–139, 1995.

44) Masoum, M.A.S.; Jafarian, A.; Ladjevardi, M.; Fuchs, E.F.; and Grady, W.M.; "Fuzzy approach for optimal placement and sizing of capacitor banks in the presence of harmonics," *IEEE Transactions on Power Delivery*, Vol. 19, No. 2, April 2004.

45) Masoum, M.A.S.; Ladjevardi, M.; Jafarian, M.; and Fuchs, E.F.; "Optimal placement, replacement and sizing of capacitor banks in distorted distribution networks by genetic algorithms," *IEEE Transactions on Power Delivery*, Vol. 19, No. 4, October 2004.

46) Ladjevardi, M.; and Masoum, M.A.S.; "Genetically optimized fuzzy placement and sizing of capacitor banks in distorted distribution networks," *IEEE Transactions on Power Delivery*, Accepted for Publication, Paper Number TPWRD-00741-2005.R1.

47) Mohan, N.; Undeland, T.M.; and Robbins, W.P.; *Power Electronics, Converters, Applications and Design*, John Wiley & Sons, USA, 2003.

48) Saric, A.T.; Calovic, M.S.; and Djukanovic, M.B.; "Fuzzy optimization of capacitors in distribution systems," *IEE Proceedings on Generation, Transmission and Distribution*, Vol. 144, No. 5, pp. 415–422, September 1997.

49) http://www.abb.com, Retrieved: Feb. 2005.

50) Mamdani, E.H.; and Asilian, S.; "An experiment in linguistic synthesis with a fuzzy logic controller," *International Journal of Man–Machine Studies*, Vol. 7, pp. 1–13, 1975.

51) IEEE recommended practices and requirements for harmonic control in electric power systems, *IEEE Standard 519-1992*, New York, NY, 1993.



ST. GEORGE COLLEGE OF T.A.F.E.

ST. GEORGE COLLEGE OF LAW

# 11
CHAPTER

# Unified Power Quality Conditioner (UPQC)

One of the main responsibilities of a utility system is to supply electric power in the form of sinusoidal voltages and currents with appropriate magnitudes and frequency for the customers at the points of common coupling (PCC). Design and analysis of system equipment and user apparatus are based on sinusoidal current and voltage waveforms with nominal or rated magnitudes and frequency. Although the generated voltages of synchronous machines in power plants are nearly sinusoidal, some undesired and/or unpredictable conditions – such as lightning and short-circuit faults – and nonlinear loads cause steady-state and/or transient voltage and current disturbances. For example, electric arc furnaces cause voltage fluctuations, power electronic converters generate current harmonics and distort voltage waveforms, and short-circuit faults result in voltage sags and swells. On the other hand, most customer loads such as computers, microcontrollers, programmable logic controllers (PLCs), and hospital equipment are sensitive and unprotected to power quality disturbances and their proper operation depends on the quality of the voltage that is delivered to them.

To optimize the performance and stability of power systems and to overcome power quality problems, many techniques and devices have been proposed and implemented. Conventional devices used for voltage regulation, power factor correction, and power quality improvement include shunt or series power capacitors, phase shifters, and passive or active filters (Chapter 9). Advanced technical solutions are flexible AC transmission system (FACTS) devices [1, 2] to improve voltage regulation, as well as steady-state and instantaneous active and reactive power control at fundamental frequency. Other approaches are based on custom power devices [3, 4] that offer a variety of options including series and shunt active (P) and reactive (Q) power compensation to improve power quality, voltage regulation, as well as steady-state and dynamic performances at fundamental and harmonic frequencies.

The concept of hybrid active filtering with shunt and series branches was introduced by Akagi and colleagues [5–7]. The most complete configuration of hybrid filters is the unified power quality conditioner (UPQC), which is also known as the universal active filter [8–13]. UPQC is a multifunction power conditioner that can be used to compensate various voltage disturbances of the power supply, to correct voltage fluctuation, and to prevent the harmonic load current from entering the power system. It is a custom power device designed to mitigate the disturbances that affect the performance of sensitive and/or critical loads. UPQC has shunt and series compensation capabilities for (voltage and current) harmonics, reactive power, voltage disturbances (including sags, swells, flicker, etc.), and power-flow control. Normally, a UPQC consists of two voltage-source converters with a common DC link designed in single-phase, three-phase three-wire, or three-phase four-wire configurations. One converter is connected in series through a transformer between the source and the critical load at the PCC and operates as a voltage-source inverter (VSI). The other converter is connected in shunt at the PCC through a transformer and operates as a current-source inverter (CSI). The active series converter compensates for voltage supply disturbances (e.g., including harmonics, imbalances, negative and zero-sequence components, sags, swells, and flickers), performs harmonic isolation, and damps harmonic oscillations. The active shunt converter compensates for load current waveform distortions (e.g., caused by harmonics, imbalances, and neutral current) and reactive power, and performs the DC link voltage regulation.

UPQC is specifically designed to protect the critical load at the point of installation connected to distorted distribution systems by correcting any of the following shortcomings:

- harmonic distortions (of source voltage and load current) at the utility–consumer PCC,
- voltage disturbances (sags, swells, flickers, imbalances, and instability),
- voltage regulation,
- reactive power flow at fundamental and harmonic frequencies,


ISBN 978-0-12-369536-9
© Elsevier Inc.
All rights reserved.

- neutral and negative-sequence currents, and
- harmonic isolation (e.g., between a subtransmission and a distribution system).

Therefore, UPQC has the capability of improving power quality at the point of installation of power distribution systems. This includes compensation of voltage-based disturbances across the sensitive load (such as voltage harmonics, voltage imbalances, voltage flickers, sags, and swells) and current-based distortions of the system (such as current harmonics, reactive power, and neutral current). However, UPQC is not capable of improving the power quality of the entire system.

This chapter starts with a section about compensation devices. Section 11.2 introduces the UQPC including its structure and operation. Section 11.3 discusses the control system of the UPQC. The following two sections provide detailed analyses and discussions of two main approaches for implementing UPQC control systems including the Park ($dq0$) transformation and the instantaneous real and reactive power approach. Section 11.6 explores UPQC performance through six application examples.

## 11.1 COMPENSATION DEVICES AT FUNDAMENTAL AND HARMONIC FREQUENCIES

Over the past several decades the transmission and distribution of electric power has become extremely complicated and subject to very tight operational and power quality specifications: the loads are increasing, power transfer grows, and the power system becomes increasingly more difficult to operate and less secure with respect to major disturbances and outages. The full potential of transmission interconnections may not be utilized due to

- large power flow with inadequate control pooling,
- excessive reactive power in various part of the power system, and
- large dynamic power swings between different parts of the system.

The main problems with interconnected transmission lines are

- at no-load or light-load condition the voltage increases at receiving ends resulting in reduced stability,
- at loaded conditions the voltage drop increases resulting in the decrease of transmittable power,
- voltage collapse and voltage instability,
- power and power angle variation due to small disturbances, and
- transient instability due to sudden and severe power variations or oscillations.

As the length of a line increases these problems become more pronounced. The ultimate solution is the instantaneous control of the bus voltage (V), the active power (P), the reactive power (Q), and the total harmonic voltage distortion ($THD_v$).

### 11.1.1 Conventional Compensation Devices

The conventional approaches for voltage regulation and power compensation at fundamental frequency are relatively simple and inexpensive. They include

- shunt compensators (capacitors, reactors),
- series compensators (series capacitors), and
- phase shifters.

These devices are mechanically controlled at low speed and there are wear-and-tear problems resulting in greater operating margins and redundancies. If conventional compensation devices are employed, the system is not fully controlled and optimized from a dynamic and steady-state point of view.

Conventional devices used for power quality improvement are passive and active power filters, as discussed in Chapter 9. Passive filters are simple and inexpensive. However, they have fixed (tuned) frequencies and will not perform properly under changing system configurations and/or variable (nonlinear) load conditions. Active filters eliminate harmonics at the point of installation without considering the power quality status of the entire system. In addition, they do not solve the stability problem, and are not generally capable of optimizing the performance (e.g., voltage regulation, reactive power compensation) of power systems.

### 11.1.2 Flexible AC Transmission Systems (FACTS)

In order to meet stringent specifications and the established contractual obligations set out in supply agreements, various technologies have been used. Among the newly developed technical solutions are FACTS, which were introduced by GyuGyi [1, 2]. They offer a variety of options including series and shunt compensation of power at fundamental frequency to achieve instantaneous and individual or simultaneous control of V, P, and Q. FACTS devices are designed to improve the reliability and the quality of power transmission. However, they do not consider the quality of power that is delivered to



customers. This section briefly introduces different types of FACTS controllers [2].

**Shunt FACTS Controllers.** Three types of shunt FACTS controllers are employed to inject compensation current into the system. An injected current in phase quadrature with the phase voltage results in Q control; other phase relations provide simultaneous control of P and Q.

- ***Variable impedance shunt FACTS controllers*** are also called static VAr generators (SVGs) or static VAr compensators (SVCs). They are thyristor-controlled reactors and/or thyristor-switched capacitors and consist of the following types:
  - Thyristor-controlled reactors (TCRs) and thyristor-switched reactors (TSRs),
  - Thyristor-switched capacitor (TSC),
  - Fixed capacitor, thyristor-controlled reactor (FC-TCR), and
  - Thyristor-switched capacitor, thyristor-controlled reactor (TSC-TCR).
- ***Switching converter SVG shunt FACTS controllers*** are switching converter based controllable synchronous voltage sources and consist of the following type:
  - Static synchronous compensator (STATCOM).
- ***Hybrid SVG and switching converter shunt FACTS controllers*** are switching type SVGs with fixed (or controllable) capacitors and/or reactors. They include:
  - STATCOM with fixed capacitors (STATCOM & FC),
  - STATCOM with fixed reactors (STATCOM & FR), and
  - STATCOM with TSC and TCR units (STATCOM & TSC-TCR).

**Series FACTS Controllers.** There are two basic types of series compensation:

- ***Variable impedance series FACTS controllers*** use thyristor-switches to provide series variable reactive impedances. They include:
  - Gate turn-off (GTO) thyristor-controlled series capacitor (GCSC),
  - Thyristor-switched series capacitor (TSSC), and
  - Thyristor-controlled series capacitor (TCSC).
- ***Switching converter series FACTS controllers*** use switching converters to provide variable series voltage sources. They include
  - Static synchronous series compensator (SSSC).

**Combined Shunt–Series FACTS Controllers.** These controllers may consist of a number of shunt, a number of series, or a combination of shunt and series FACTS devices. Three popular combined shunt–series FACTS controllers are

- Unified power flow controller (UPFC) has one converter in series and the other in shunt with the transmission line,
- Interline power flow controller (IPFC) has both converters in series with usually a different line, and
- Back-to-back STATCOM has both converters in shunt, each connected to a different power system.

**FACTS Controllers with Storage.** Any of the converter-based FACTS devices can generally accommodate storage such as capacitors, batteries, and superconducting coils. These controllers are more effective for controlling system dynamics due to their ability to dynamically provide/extract real power P to/from a system.

**Development of FACTS Controllers.** The first generation of FACTS (e.g., SVC, TSSC, TCSC, thyristor controlled phase shifters, etc) use thyristor controlled switches as control devices. The second generation (e.g., STATCOM, SSSC, UPFC, IPFC, etc) are converter-based devices and use switching static converters as fast controllable voltage and current sources.

The application of FACTS devices is increasing as their advantages become more evident to power system engineers and researchers. FACTS controllers are primarily designed to operate at fundamental power frequency under sinusoidal conditions and do not necessarily improve the quality of electric power. In fact, most FACTS controllers use switching devices that inject current and voltage harmonics into power systems. Corrective approaches (e.g., sinusoidal PWM techniques) have been proposed to minimize their limitations.

### 11.1.3 Custom Power Devices

The introduction of power electronic loads has raised much concern about power quality problems caused by harmonics, distortions, interruptions, and surges. Equipment such as large industrial drives (e.g., cycloconverters) generate significantly high voltage and current (inter-, sub-) harmonics and create extensive voltage fluctuation. This is more evident in power systems that make use of long transmission lines with limited reactive capacities.

ST. GEORGE'S COLLEGE OF LAW

The application of harmonic filters and SVCs to radial transmission systems can offer partial solution to high THD levels and voltage fluctuations. Yet, the lack of dynamic capabilities of these devices limits them to bulk correction. In addition, they might be effective in one application but fail to correct other power quality issues.

The concept of custom power was introduced by Hingorani [3] as the solution to V, P, and Q compensation and power quality problems at the expense of high cost and network complexity. As FACTS controllers improve the reliability and quality of power transmission – by simultaneously enhancing both power transfer capacity and stability – custom power devices enhance the quality and reliability of power delivered to the customer. With a custom power device, a customer (e.g., a sensitive load) will be able to receive a prespecified quality of electric power with a combination of specifications including but not limited to

- magnitude and duration of over- and under-voltages with specified limits,
- low harmonic distortion in the supply, load voltages, and currents,
- small phase imbalance,
- low flicker in the supply voltage,
- control of power interruptions, and
- control of supply voltage frequency within specified limits.

Custom power devices are classified based on their power electronic controllers, which can be either of the network-reconfiguration type or of the compensation type. The network-reconfiguration devices – also called switchgear – include the solid-state and/or static versions of current limiting, current breaking, and current transferring components. The compensation-type custom power devices either compensate a load (e.g., correct its power factor, imbalance) or improve the quality of the supply voltage (e.g., eliminate its harmonics). They are either connected in shunt or in series or a combination of both. Custom power devices are classified as follows [4]:

- **Network-reconfiguration custom power devices** include
  - Solid-state current limiter (SSCL),
  - Solid-state breaker (SSB), and
  - Solid-state transfer switch (SSTS).
- **Compensation-custom power devices** include
  - Distribution STATCOM (DSTATCOM),
  - Dynamic voltage restorer/regulator (DVR), and
  - Unified power quality conditioner (UPQC).

Custom power devices are designed to improve the quality of power at their point of installation of the power distribution systems. They are not primarily designed to improve the power quality of the entire system.

### 11.1.4 Active Power Line Conditioner (APLC)

The APLC is a converter-based compensation device designed to improve the power quality of the entire distribution system by injecting corrective harmonic currents at selected (sensitive) buses. It is usually necessary to use more than one APLC unit to improve the power quality of the entire distribution system. Therefore, APLC units can be considered as a group of shunt active filters; their placement, sizing, and compensation levels (e.g., orders, magnitudes, and phases of injected current harmonics) are optimally designed to improve the power quality of the entire distribution system. The number of required APLC units depends on the severity of distortion, the nature of the distribution system, and types of nonlinear loads, as well as the required quality of electric power (e.g., as specified by IEEE-519). At present, the design of APLCs does not consider transient distortions and stability issues.

### 11.1.5 Remark Regarding Compensation Devices

In the absence of saturation and nonlinearity, power system voltage and current waveforms are sinusoidal and FACTS controllers are employed to solve the associated steady-state, transient, and stability problems. Custom power devices are designed to improve the steady-state and transient problems of distorted distribution systems at the point of installation. Power filters and APLCs mitigate power quality problems at a given location and throughout the power system, respectively. However, at present, none of them are designed to simultaneously consider stability and power quality issues. This is highly related to the fact that in conventional centralized power systems, power quality problems are limited to the low- and medium-voltage distribution systems, whereas stability issues are mainly occurring in high-voltage transmission systems. With the introduction of distributed generation (DG) and the fast growing rate of renewable energy sources in today's power system, there will be an overlap between stability and power quality issues. More attention and further research is required to analyze and examine stability issues in decentralized distorted networks, as well as isolated and DG power systems.





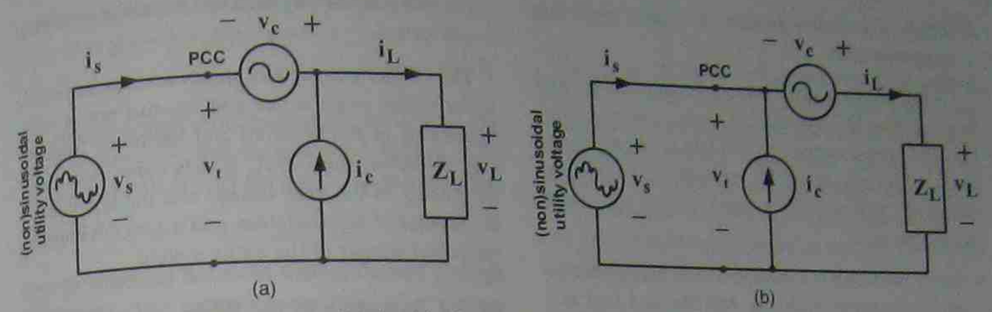



FIGURE 11.1 Ideal UPQC structure; (a) the right-shunt UPQC, (b) the left-shunt UPQC [4].

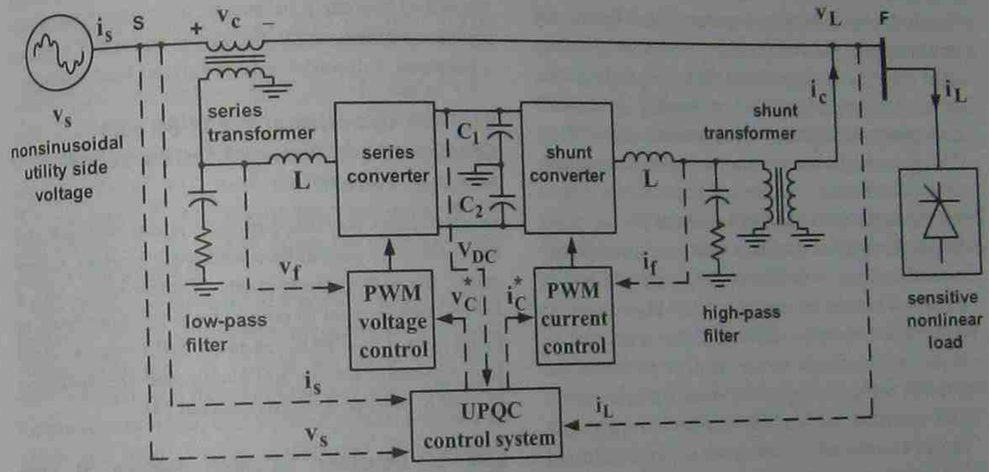



FIGURE 11.2 Detailed configuration of the right-shunt UPQC.

## 11.2 UNIFIED POWER QUALITY CONDITIONER (UPQC)

Unified power quality conditioners are viable compensation devices that are used to ensure that delivered power meets all required standards and specifications at the point of installation. The ideal UPQC can be represented as the combination of a voltage-source converter (injecting series voltage $v_c$), a current-source converter (injecting shunt current $i_c$), and a common DC link (connected to a DC capacitor). There are two possible ways of connecting the unit to the terminal voltage ($v_t$) at PCC:

- Right-shunt UPQC (Fig. 11.1a), where the shunt compensator ($i_c$) is placed at the right side of the series compensator ($v_c$).
- Left-shunt UPQC (Fig. 11.1b), where the shunt compensator ($i_c$) is placed at the left side of $v_c$.

These two structures have similar features; however, the overall characteristics of the right-shunt UPQC are superior (e.g., operation at zero power injection/absorption mode, achieving unity power factor at load terminals, and full reactive power compensation). In this chapter, a right-shunt UPQC configuration is assumed and analyzed. References [4] and [9] present detailed analysis of the left-shunt structure.

### 11.2.1 UPQC Structure

The detailed structure of the right-shunt UPQC is shown in Fig. 11.2. Assuming a three-phase, four-wire configuration with an unbalanced and distorted system voltage ($v_s$) and nonsinusoidal load current ($i_L$), the UPQC shall perform the following functions:

- convert the feeder (system) current $i_s$ to balanced sinusoids through the shunt compensator,
- convert the load voltage $v_L$ to balanced sinusoids through the series compensator,
- ensure zero real power injection (and/or absorption) by the compensators, and

- supply reactive power to the load (Q compensation).

UPQC employs two converters that are connected to a common DC link with an energy storage capacitor. The main components of a UPQC are series and shunt power converters, DC capacitors, low-pass and high-pass passive filters, and series and shunt transformers:

- ***Series converter*** is a voltage-source converter connected in series with the AC line and acts as a voltage source to mitigate voltage distortions. It eliminates supply voltage flickers or imbalance from the load terminal voltage and forces the shunt branch to absorb current harmonics generated by the nonlinear load. Control of the series converter output voltage is usually performed using sinusoidal pulse-width modulation (SPWM). The gate pulses are generated by the comparison of a fundamental voltage reference signal with a high-frequency triangular waveform.
- ***Shunt converter*** is a voltage-source converter connected in shunt with the same AC line and acts as a current source to cancel current distortions, to compensate reactive current of the load, and to improve the power factor. It also performs the DC-link voltage regulation, resulting in a significant reduction of the DC capacitor rating. The output current of the shunt converter is adjusted (e.g., using a dynamic hysteresis band) by controlling the status of semiconductor switches such that output current follows the reference signal and remains in a predetermined hysteresis band.
- ***Midpoint-to-ground DC capacitor bank*** is divided into two groups, which are connected in series. The neutrals of the secondary transformers are directly connected to the DC link midpoint. As the connection of both three-phase transformers is $Y/Y_0$, the zero-sequence voltage appears in the primary winding of the series-connected transformer in order to compensate for the zero-sequence voltage of the supply system. No zero-sequence current flows in the primary side of both transformers. It ensures the system current to be balanced even when the voltage disturbance occurs.
- ***Low-pass filter*** is used to attenuate high-frequency components at the output of the series converter that are generated by high-frequency switching.
- ***High-pass filter*** is installed at the output of shunt converter to absorb current switching ripples.
- ***Series and shunt transformers*** are implemented to inject the compensation voltages and currents, and for the purpose of electrical isolation of UPQC converters.

The UPQC is capable of steady-state and dynamic series and/or shunt active and reactive power compensations at fundamental and harmonic frequencies. However, the UPQC is only concerned about the quality of the load voltage and the line current at the point of its installation, and it does not improve the power quality of the entire system.

### 11.2.2 Operation of the UPQC

The shunt converter forces the feeder (system) current to become a balanced (harmonic-free) sinusoidal waveform, while the series converter ensures a balanced, sinusoidal, and regulated load voltage.

#### 11.2.2.1 Operation of the UPQC with Unbalanced and Distorted System Voltage and Load Current

In most cases the three-phase system voltages and load currents are unbalanced and contain higher order frequency components (harmonics), and a UPQC unit is used to compensate for both types of distortions. The UPQC takes the following two steps to compensate for the imbalance and the distortion of system voltage and line current [4].

**Step 1: Obtaining Balanced Voltage at Load Terminals.** The imbalance or distortion of a three-phase system may consist of positive, negative, and zero-sequence fundamental and harmonic components. The system (utility) voltage at point $S$ (Fig. 11.2) can be expressed as

$$v_S(t) = v_{S+}(t) + v_{S-}(t) + v_{S0}(t) + \sum v_{Sh}(t), \quad (11\text{-}1)$$

where subscripts +, −, and 0 refer to the positive-, negative-, and zero-sequence fundamental components, respectively; $v_{s+}(t) = V_{s+}\sin(\omega t + \phi_+)$, $v_{s-}(t) = V_{s-}\sin(\omega t + \phi_-)$, and $v_{s0}(t) = V_{s0}\sin(\omega t + \phi_0)$ are positive-, negative-, and zero-sequence fundamental frequency components of the system voltage; $\sum V_{sh}(t) = \sum V_{sh}\sin(h\omega t + \delta_h)$ represents the harmonics in the voltage, $h$ is harmonic order; and $\phi_+$, $\phi_-$, $\phi_0$, and $\phi_h$ are the corresponding voltage phase angles.

Usually, the voltage at the load at PCC is expected to be sinusoidal with a fixed amplitude $V_L$:

$$v_L(t) = V_L\sin(\omega t + \phi_+). \quad (11\text{-}2)$$

Hence the series converter will need to compensate for the following components of voltage:



$$v_c(t) = v_L(t) - v_S(t) = (V_L - V_{s+})\sin(\omega t + \phi_+) - v_{s-}(t) - v_{s0}(t) - \sum v_{sh}(t). \quad (11\text{-}3)$$

The control system should automatically control the series converter so that its generated voltage at its output terminals is $v_c(t)$ (in Fig. 11.2) and matched with Eq. 11-3.

**Step 2: Obtaining Balanced System Current Through the Feeder.** The distorted nonlinear load current (Fig. 11.2) can be expressed as

$$i_L(t) = i_{L+}(t) + i_{L-}(t) + i_{L0}(t) + \sum i_{Lh}(t), \quad (11\text{-}4)$$

where $i_{L+}(t) = I_{L+}\sin(\omega t + \delta_+)$, $i_{L-}(t) = I_{L-}\sin(\omega t + \delta_-)$, and $i_{L0}(t) = I_{L0}\sin(\omega t + \delta_0)$ are the fundamental frequency positive-, negative- and zero-sequence components of the load current and $\sum i_{Lh}(t) = \sum I_{Lh}\sin(h\omega t + \delta_h)$ represents the harmonics of the load current. $\delta_+$, $\delta_-$, $\delta_0$, and $\delta_h$ are the corresponding current phase angles.

The shunt converter is supposed to provide compensation of the load harmonic currents to reduce voltage distortion. It should act as a controlled current source and its output current must consist of harmonic, negative-, and zero-sequence currents to cancel the load current distortions. It is usually desired to have a certain phase angle (displacement power factor angle), $\theta_L$, between the positive sequences of voltage and current at the load terminals:

$$\theta_L = (\delta_+ - \phi_+) \Rightarrow \delta_+ = (\phi_+ + \theta_L). \quad (11\text{-}5)$$

Substituting Eq. 11-5 into Eq. 11-4 and simplifying yields

$$i_L(t) = I_{L+}\sin(\omega t + \phi_+)\cos\theta_L + [I_{L+}\cos(\omega t + \phi_+)\sin\theta_L + i_{L-}(t) + i_{L0}(t) + \sum i_{Lh}(t)]. \quad (11\text{-}6)$$

It is clear that the output current of the shunt converter should be controlled and must assume a wave shape as specified by the 2nd, 3rd, 4th, and 5th terms of Eq. 11-6. That is,

$$i_c(t) = I_{L+}\cos(\omega t + \phi_+)\sin\theta_L + i_{L-}(t) + i_{L0}(t) + \sum i_{Lh}(t). \quad (11\text{-}7)$$

This will ensure that the system (feeder) current has a sinusoidal waveform:

$$i_s(t) = i_L(t) - i_c(t) = (I_{L+}\cos\theta_L)\sin(\omega t + \phi_+). \quad (11\text{-}8)$$

Equations 11-3 and 11-7 demonstrate the principles of an ideal UPQC. If these equations are dynamically implemented by the UPQC controller, terminal load voltage and system current will be sinusoidal. In addition, system voltage and current will be in phase if $\theta_L = 0$ (e.g., unity power factor), and neither positive nor negative reactive power will be supplied by the source.

#### 11.2.2.2 Operation of UPQC with Unbalanced System Voltages and Load Currents

Assuming that the system voltages and load currents are unbalanced but not distorted (harmonic-free), one can generate UPQC equations as shown below. The UPQC takes the following four steps to compensate the imbalance of the system voltages and line currents [4].

**Step 1: Obtaining Balanced Voltages at Load Terminals.** From the structure of the ideal right-hand UPQC (Fig. 11.2) follows

$$v_L(t) = v_s(t) + v_c(t). \quad (11\text{-}9)$$

To obtain balanced voltages at the load terminals, $v_c(t)$ must cancel the imbalance of the system voltages; therefore,

$$V_{s0} = -V_{s0},\ V_{c-} = -V_{s-}, \quad (11\text{-}10)$$

which implies that $V_L$ is of positive sequence. Note that the positive-sequence magnitude of the load voltage ($V_L$) should be set to the desired regulated voltage, whereas its phase angle depends on the load displacement power factor.

One defines an injected positive-sequence voltage ($|V_{c+}|$) such that the series compensator does not require any positive-sequence (real) power. Because $i_s$ flows through the series compensator, $v_{c+}$ must have a phase difference of 90° with $i_{s+}$. This implies

$$V_{L+} = V_{s+} + V_{c+}(a + jb), \quad (11\text{-}11)$$

where $(a + jb)$ is the unit vector that is perpendicular to $I_{s+}$. Assuming $V_{L+} = V_L\angle 0°$, Eq. 11-11 results in the following second-order equation:

$$|V_{c+}|^2 - 2a|V_L||V_{c+}| + |V_L|^2 - |V_{s+}|^2 = 0. \quad (11\text{-}12)$$

If the desired regulated voltage level $V_L$ is achievable, this quadratic equation will have two real

ST. GEORGE COLLEGE OF LAW

solutions for $|V_{c+}|$. The minimum solution should be selected because it will result in less cost (e.g., smaller rating) of the UPQC.

**Step 2: Obtaining Balanced System Currents Through the Feeder.** From the structure of the ideal right-hand UPQC (Fig. 11.2) one gets

$$i_L(t) = i_s(t) + i_c(t). \tag{11-13}$$

To obtain balanced system currents, the injected current $i_c(t)$ must become zero and one gets for the sequence components of the load current

$$I_{c0} = I_{L0},\ I_{c+} = 0,\ I_{c-} = I_{L-} \tag{11-14}$$

This will ensure a positive-sequence current (equal to the positive-sequence load current) only passing through the system.

**Step 3: Ensuring Zero Real Power Injection/Absorption by the Compensators.** Equations 11-9 to 11-14 guarantee that imbalances in both the system voltages and the load currents are cancelled by the UPQC. Moreover,

- The series compensator (converter) will consume zero average (real) power because its voltage and current are in quadrature (e.g., $\tilde{V}_{c+}$ is in quadrature with $\tilde{I}_{s+}$).
- The shunt compensator (converter) will also inject zero average (real) power since its positive-sequence injected current is zero ($I_{c+} = 0$) and the load voltage is of positive sequence only.

Therefore, the UPQC does neither inject nor absorb real power.

**Step 4: Reactive Power Injection by the Compensators.** The UPQC can supply part of the load reactive power through its shunt compensator (converter). To do this Eq. 11-14 has to be modified while keeping in mind that the zero and negative-sequence components of the load current must also be canceled by the shunt converter. The new conditions for the injected shunt currents are now

$$I_{c0} = I_{L0},\ I_{c+} \neq 0,\ I_{c-} = I_{L-}. \tag{11-15}$$

We can divide the average component of the load reactive power between the shunt converter, the series converter, and the system. Due to the fact that the average values of the active and the reactive powers of the shunt converter depend only on the positive-sequence current and its real power consumption (or absorption) must be zero, one gets

$$|V_{L+}|\,|I_{c+}|\cos\theta = 0 \Rightarrow \theta = \pm 90^\circ \quad \text{because } (|V_{L+}| \neq 0 \text{ and } |I_{c+}| \neq 0), \tag{11-16a}$$

$$|V_{L+}|\,|I_{c+}|\sin\theta = \beta(Q_{L\text{-}avg}), \tag{11-16b}$$

where $\theta$ is the angle between $V_{L+}$ and $I_{c+}$, scalar $\beta$ indicates how much reactive power must be supplied by the shunt converter, and $Q_{L\text{-}avg}$ is the average of the load reactive power.

For inductive loads (e.g., negative $Q_{L\text{-}avg}$), compensator (converter) current $I_{c+}$ must lag $V_L$ by 90° (to satisfy Eq. 11-16a) and one can write

$$|I_{c+}| = \beta\frac{|Q_{L\text{-}avg}|}{|V_L|}. \tag{11-17}$$

The cancellation of the supply and load current imbalances using an UPQC is addressed in [4, pp. 383–385] and the reactive power compensation with a UPQC is discussed in [4, pp. 386–388].

## 11.3 THE UPQC CONTROL SYSTEM

It is possible to distinguish between disturbances related to the quality of the system (supply) voltage and those related to the quality of the load current. The UPQC corrects both problems at the point of installation (e.g., at the terminals of a sensitive or critical load). It combines a shunt active filter together with a series active filter in a back-to-back configuration to simultaneously improve the power quality of the supply current through the power system and the load voltage at PCC. The main functions of the UPQC are summarized in Table 11.1.

The main components of a UPQC are the series and shunt converters representing active filters, high

**TABLE 11.1** Main Functions of UPQC Controller

| Series converter | Shunt converter |
|---|---|
| • Compensation of voltage harmonics (including negative- and zero-sequence components at fundamental frequency) | • Compensation of current harmonics (including negative- and zero-sequence components at fundamental frequency) |
| • Mitigation of harmonic currents through the power line (harmonic isolation) | • Compensation of the reactive power at the load |
| • Improving system stability (damping) | • Regulation of the DC capacitor voltage |
| • Controlling active and reactive powers | • Regulation of the load voltage |



and low-pass passive filters, DC capacitors, and series and shunt transformers, as shown in Fig. 11.2. The shunt converter is a STATCOM that injects nonsinusoidal corrective current to improve the power quality, regulate load voltage, and control the load power factor. It also compensates for the load reactive power demand, corrects supply current harmonics, and regulates the DC-link voltage. The series converter represents a dynamic voltage regulator (DVR) that introduces corrective harmonic voltages to ensure sinusoidal supply current and constant voltage conditions under steady-state and transient operating conditions (e.g., during voltage sags and swells).

The power electronic converters are frequently voltage-source inverters (VSIs) with semiconductor switches. The output current of the shunt converter is adjusted using an appropriate control scheme (e.g., dynamic hysteresis band). The states of semiconductor switches are controlled so that the output current tracks the reference signal and remains in a predetermined hysteresis band. The installed passive high-pass filter – at the output of shunt converter – absorbs the current switching ripples.

Control of the series converter output voltage is performed using PWM techniques. The gate pulses are generated by the comparison of a fundamental-voltage reference signal with a high-frequency triangular waveform. The low-pass filter attenuates high-frequency components at the output of the series converter, generated by high-frequency switching.

For the compensation of the zero-sequence components, the split-capacitor scheme is usually used on the DC side of converters and the capacitor's midpoint is connected to the neutral. In order to inject the generated voltages and currents, and for the purpose of electrical isolation of UPQC converters, series and shunt transformers may also be included in the UPQC configuration.

### 11.3.1 Pattern of Reference Signals

Provided unbalanced and distorted source voltages and nonlinear load currents exist, then – based on Eqs. 11-1 to 11-17 – the output voltage of the series converter ($v_c(t)$, Fig. 11.2) and the output current of shunt converter ($i_c(t)$, Fig. 11.2) must obey the following equations:

$$\begin{cases} v_c(t) = (V_L - V_{s+})\sin(\omega t + \phi_+) - v_{s-}(t) - v_{s0}(t) - \sum v_{sh}(t) \\ i_c(t) = I_{L+}\cos(\omega t + \delta_+)\sin\theta_L + i_{L-}(t) + i_{L0}(t) + \sum i_{Lh}(t), \end{cases} \tag{11-18}$$

so that the current drawn from the source and the voltage appearing across the load will be sinusoidal.

Generation, tracking, and observation of these reference signals are performed by the UPQC control system. There are two main classes of UPQC control: the first one is based on the Park transformation [15], and the second one on the instantaneous real and imaginary power theory [9, 13, 14]. These will be introduced in the following sections. There are other control techniques for active and hybrid (e.g., UPQC) filters as discussed in Section 9.7 of Chapter 9.

## 11.4 UPQC CONTROL USING THE PARK (*DQ*0) TRANSFORMATION

It is clear that the UPQC should first separate the fundamental positive-sequence component from other components (e.g., derivation of reference signal using either waveform compensation, instantaneous power compensation, or impedance synthesis, as discussed in Sections 9.7.1 to 9.7.3, respectively), and then control the outputs of series and shunt converters according to Eq. 11-18 (e.g., generation of compensation signal using reference-following techniques as discussed in Section 9.7.5). The conventional approach to perform the first task for the UPQC relies on the synchronous *dq*0 reference frame.

### 11.4.1 General Theory of the Park (*dq*0) Transformation

In the study of power systems, mathematical transformations are often used to decouple variables, to facilitate the solution of time-varying equations, and to refer variables to a common reference frame. A widely used transformation is the Park (*dq*0) transformation [15]. It is can be applied to any arbitrary (sinusoidal or distorted) three-phase, time-dependent signals.

The Park (*dq*0) transformation is defined as

$$\begin{bmatrix} x_d \\ x_q \\ x_0 \end{bmatrix} = \sqrt{\frac{2}{3}}\begin{bmatrix} \cos\theta_d & \cos(\theta_d - 2\pi/3) & \cos(\theta_d + 2\pi/3) \\ -\sin\theta_d & -\sin(\theta_d - 2\pi/3) & -\sin(\theta_d + 2\pi/3) \\ 1/\sqrt{2} & 1/\sqrt{2} & 1/\sqrt{2} \end{bmatrix} \begin{bmatrix} x_a \\ x_b \\ x_c \end{bmatrix}. \tag{11-19}$$

In this equation, $\theta_d = \omega_d + \varphi$, where $\omega_d$ is the angular velocity of signals to be transformed and $\varphi$ is the initial angle.

As discussed in Chapter 9 (Section 9.7), the main advantage of the $dq0$ transformation is that the fundamental (positive-sequence) component of wave-form will be transferred to a constant DC term under steady-state conditions. In addition, a harmonic component with frequency $\omega_h$ will appear as a sinusoidal signal with frequency of $\omega_h - \omega_d$ in the $dq0$ domain.

### 11.4.2 Control of Series Converter Based on the $dq0$ Transformation

The system (supply) voltage may contain negative- and zero-sequence components as well as harmonic distortions that need to be eliminated by the series compensator. The control of the series compensator based on the $dq0$ transformation is shown in Fig. 11.3.

The system voltages are first detected and then transformed into the synchronous $dq0$ reference frame. If the system voltages are unbalanced and contain harmonics, then the Park transformation (Eq. 11-19) results in

$$\begin{bmatrix} v_d \\ v_q \\ v_0 \end{bmatrix} = \sqrt{\frac{2}{3}} \begin{bmatrix} \cos\theta_d & \cos(\theta_d - 2\pi/3) & \cos(\theta_d + 2\pi/3) \\ -\sin\theta_d & -\sin(\theta_d - 2\pi/3) & -\sin(\theta_d + 2\pi/3) \\ 1/\sqrt{2} & 1/\sqrt{2} & 1/\sqrt{2} \end{bmatrix} \begin{bmatrix} v_a \\ v_b \\ v_c \end{bmatrix}$$
$$= \sqrt{\frac{3}{2}} \left\{ \begin{bmatrix} V_{sp}\cos\phi_p \\ V_{sp}\sin\phi_p \\ 0 \end{bmatrix} + \begin{bmatrix} V_{sn}\cos(2\omega t + \phi_n) \\ -V_{sn}\sin(2\omega t + \phi_n) \\ 0 \end{bmatrix} + \begin{bmatrix} 0 \\ 0 \\ V_{s0}\cos(2\omega t + \phi_0) \end{bmatrix} + \begin{bmatrix} \sum V_{sh}\cos[(h-1)(2\omega t + \phi_h)] \\ \sum V_{sh}\sin[(h-1)(2\omega t + \phi_h)] \\ 0 \end{bmatrix} \right\}$$
$$= \begin{bmatrix} V_{dp} \\ V_{qp} \\ 0 \end{bmatrix} + \begin{bmatrix} V_{dn} \\ V_{qn} \\ 0 \end{bmatrix} + \begin{bmatrix} 0 \\ 0 \\ V_{00} \end{bmatrix} + \begin{bmatrix} V_{dh} \\ V_{qh} \\ 0 \end{bmatrix} \tag{11-20}$$

where $\phi_p$ is the phase difference between the positive-sequence component and the reference voltage. Based on Eq. 11-20, the fundamental positive-sequence component of the voltage is represented by DC terms (e.g., $V_{sp}\cos\phi_p$ and $V_{sp}\sin\phi_p$) in the $dq0$ reference frame.

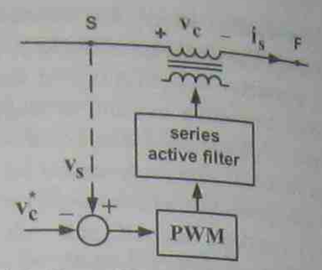



**FIGURE 11.3** Control block of the UPQC series compensator using Park (dq0) transformation [15].

The load bus voltage should be maintained sinusoidal with constant amplitude even if the source voltage is distorted. Therefore, the expected load voltage in the $dq0$ domain will only consist of one value:

$$V_{dq0}^{\text{expected}} = \begin{bmatrix} V_{dF} \\ V_{qF} \\ V_{0F} \end{bmatrix} = [T_{dq0}(\theta_d)] V_{abc}^{\text{expected}} = \begin{bmatrix} V_m \\ 0 \\ 0 \end{bmatrix}, \tag{11-21}$$

where

$$V_{abc}^{\text{expected}} = \begin{bmatrix} V_S\cos(\omega t) \\ V_S\cos(\omega t + 120) \\ V_S\cos(\omega t - 120) \end{bmatrix}$$

are sinusoids and the compensation reference voltage is

$$V_{\text{hdq0}}^{\text{ref}} = V_{dq0}^{\text{expected}} - V_{\text{sdq0}}, \tag{11-22}$$

where $V_{\text{sdq0}}$ is the distorted source voltage in the $dq0$ frame (Eq. 11-20). Therefore, $V_{dp}$ of Eq. 11-20 should be maintained at $V_m$ and all other terms must be eliminated by the compensation voltage.

The compensation reference voltage of Eq. 11-22 is then inversely transformed into the abc reference frame. Comparing the compensation reference voltage with a triangular wave, the output voltage of the series converter can be obtained by a PWM voltage control unit.

### 11.4.3 Control of Shunt Converter Relying on the $dq0$ Transformation

Similar transformation as employed for voltages can be applied to current waveforms as well:





$$\begin{bmatrix} i_d \\ i_q \\ i_0 \end{bmatrix} = \sqrt{\frac{2}{3}} \begin{bmatrix} \cos\theta_d & \cos(\theta_d - 2\pi/3) & \cos(\theta_d + 2\pi/3) \\ -\sin\theta_d & -\sin(\theta_d - 2\pi/3) & -\sin(\theta_d + 2\pi/3) \\ 1/\sqrt{2} & 1/\sqrt{2} & 1/\sqrt{2} \end{bmatrix} \begin{bmatrix} i_a \\ i_b \\ i_c \end{bmatrix}$$
$$= \sqrt{\frac{3}{2}} \left\{ \begin{bmatrix} I_{LP}\cos\theta_p \\ I_{Lsp}\sin\theta_p \\ 0 \end{bmatrix} + \begin{bmatrix} I_{Ln}\cos(2\omega t + \theta_n) \\ -I_{Ln}\sin(2\omega t + \theta_n) \\ 0 \end{bmatrix} + \begin{bmatrix} \sum I_{Lh}\cos[(h-1)(2\omega t + \theta_h)] \\ \sum I_{Lh}\sin[(h-1)(2\omega t + \theta_h)] \\ 0 \end{bmatrix} \right\}. \tag{11-23}$$

Unlike the voltage waveforms, which are maintained at their rated values, the load currents will change with the load characteristics at the PCC and it will not be possible to have a fixed expected reference current value. To solve this problem, different techniques are proposed and implemented to extract the fundamental positive-sequence component (which becomes a DC term in the $dq0$ reference frame) and the corresponding harmonic components, as discussed in Sections 9.7.1 to 9.7.3.

Therefore, the expected current in the $dq0$ reference frame has only one value

$$i_{dq0}^{\text{expected}} = \begin{bmatrix} I_{Lp}\cos\theta_p \\ 0 \\ 0 \end{bmatrix}. \tag{11-24}$$

The compensation reference current is

$$i_{\text{hdq0}}^{\text{ref}} = i_{dq0}^{\text{expected}} - i_{\text{sdq0}}, \tag{11-25}$$

where $i_{\text{sdq0}}$ is the distorted load current in the $dq0$ frame (Eq. 11-23).

The shunt converter operates as a controlled current source and different techniques (e.g., hysteresis, predictive, and suboscillation control) are employed to ensure that its output current follows the corresponding reference signal $i_{\text{hdq0}}^{\text{ref}}$.

### 11.4.4 Control of DC Link Voltage using the $dq0$ Transformation

In the UPQC configuration, the DC link voltage is usually divided into two capacitor units $C_1$ and $C_2$ connected in series. The voltages of these capacitors are such that $V_{C1} = V_{C2}$ under balanced operation. Normally, the DC link voltage is maintained at a desired/nominal level for all operating conditions.

## 11.5 UPQC CONTROL BASED ON THE INSTANTANEOUS REAL AND IMAGINARY POWER THEORY

In this section, the UPQC control technique is based on the $\alpha\beta0$ transformation and the instantaneous active and reactive power theory is introduced [9, 13, 14].

### 11.5.1 Theory of Instantaneous Real and Imaginary Power

The $\alpha\beta0$ transformation applied to abc three-phase voltages in a four-wire system is

$$\begin{bmatrix} v_0 \\ v_\alpha \\ v_\beta \end{bmatrix} = \sqrt{\frac{2}{3}} \begin{bmatrix} 1/\sqrt{2} & 1/\sqrt{2} & 1/\sqrt{2} \\ 1 & -1/2 & -1/2 \\ 0 & \sqrt{3/2} & -\sqrt{3/2} \end{bmatrix} \begin{bmatrix} v_a \\ v_b \\ v_c \end{bmatrix}. \tag{11-26}$$

The inverse $\alpha\beta0$ transformation is

$$\begin{bmatrix} v_a \\ v_b \\ v_c \end{bmatrix} = \sqrt{\frac{2}{3}} \begin{bmatrix} 1/\sqrt{2} & 1 & 0 \\ 1/\sqrt{2} & -1/2 & \sqrt{3/2} \\ 1/\sqrt{2} & -1/2 & -\sqrt{3/2} \end{bmatrix} \begin{bmatrix} v_0 \\ v_\alpha \\ v_\beta \end{bmatrix}. \tag{11-27}$$

Identical relations hold for the currents.

The instantaneous three-phase active power is given by [14]

$$\begin{aligned} p_{\text{three-phase}}(t) &= v_a i_a + v_b i_b + v_c i_c = p_a(t) + p_b(t) + p_c(t) \\ &= v_\alpha i_\alpha + v_\beta i_\beta + v_0 i_0 = p_\alpha(t) + p_\beta(t) + p_0(t) \\ &= p(t) + p_0(t), \end{aligned} \tag{11-28}$$

where $p(t) = p_\alpha(t) + p_\beta(t) = v_\alpha i_\alpha + v_\beta i_\beta$ corresponds to the instantaneous three-phase real power and $p_0(t) = v_0 i_0$ is the instantaneous zero-sequence power. Note the separation of the zero-sequence component in the $\alpha\beta0$ system.

The instantaneous three-phase reactive power is defined as

$$\begin{aligned} q_{\text{three-phase}}(t) &= q_\alpha(t) + q_\beta(t) = v_a i_\beta - v_\beta i_\alpha \\ &= -[(v_a - v_b)i_c + (v_b - v_c)i_a + (v_c - v_a)i_b]/\sqrt{3}. \end{aligned} \tag{11-29}$$

Therefore, the instantaneous real, reactive, and zero-sequence powers are calculated from

$$\begin{bmatrix} p_0 \\ p \\ q \end{bmatrix} = \begin{bmatrix} v_0 & 0 & 0 \\ 0 & v_\alpha & v_\beta \\ 0 & -v_\beta & v_\alpha \end{bmatrix} \begin{bmatrix} i_0 \\ i_\alpha \\ i_\beta \end{bmatrix}. \tag{11-30}$$

ST. GEORGE COLLEGE OF LAW

Here, $p$ and $q$ (in the $\alpha\beta 0$ space) are not expressed in the conventional watts and VArs.

From Eq. 11-30, the $\alpha$ and $\beta$ components of currents may be calculated as

$$\begin{bmatrix} i_\alpha \\ i_\beta \end{bmatrix} = \frac{1}{\Delta}\begin{bmatrix} v_\alpha & -v_\beta \\ v_\beta & v_\alpha \end{bmatrix}\begin{bmatrix} p \\ q \end{bmatrix} \quad \text{with} \quad \Delta = v_\alpha^2 + v_\beta^2. \tag{11-31}$$

These are divided into two types of currents

$$\begin{bmatrix} i_\alpha \\ i_\beta \end{bmatrix} = \frac{1}{\Delta}\left\{\begin{bmatrix} v_\alpha & -v_\beta \\ v_\beta & v_\alpha \end{bmatrix}\begin{bmatrix} p \\ 0 \end{bmatrix} + \begin{bmatrix} v_\alpha & -v_\beta \\ v_\beta & v_\alpha \end{bmatrix}\begin{bmatrix} 0 \\ q \end{bmatrix}\right\} = \begin{bmatrix} i_{\alpha p} \\ i_{\beta p} \end{bmatrix} + \begin{bmatrix} i_{\alpha q} \\ i_{\beta q} \end{bmatrix}. \tag{11-32}$$

where

$i_{\alpha p} = v_\alpha p/\Delta$ is the $\alpha$-axis instantaneous active current,

$i_{\alpha p} = -v_\alpha q/\Delta$ is the $\alpha$-axis instantaneous reactive current,

$i_{\beta p} = v_\beta p/\Delta$ is the $\beta$-axis instantaneous active current, and

$i_{\beta q} = v_\beta q/\Delta$ is the $\beta$-axis instantaneous reactive current.

Now, the power components of the phases $\alpha$ and $\beta$ can be separated as

$$\begin{bmatrix} p_\alpha \\ p_\beta \end{bmatrix} = \begin{bmatrix} v_\alpha i_\alpha \\ v_\beta i_\beta \end{bmatrix} = \begin{bmatrix} v_\alpha i_{\alpha p} \\ v_\beta i_{\beta p} \end{bmatrix} + \begin{bmatrix} v_\alpha i_{\alpha q} \\ v_\beta i_{\beta q} \end{bmatrix} = \begin{bmatrix} p_{\alpha p} \\ p_{\beta p} \end{bmatrix} + \begin{bmatrix} p_{\alpha q} \\ p_{\beta q} \end{bmatrix}, \tag{11-33}$$

where

$$p_{\alpha p} = v_\alpha i_{\alpha p} = v_\alpha^2 p/\Delta,$$
$$p_{\alpha p} = v_\alpha i_{\alpha p} = -v_\alpha v_\beta q/\Delta,$$
$$p_{\beta p} = v_\beta i_{\beta p} = v_\beta^2 p/\Delta,$$
$$p_{\beta q} = v_\beta i_{\alpha q} = v_\alpha v_\beta q/\Delta,$$

because $p_{\alpha q} + p_{\beta q} = 0$, and thus $p_{\text{three-phase}} = p_\alpha + p_\beta + p_o = p_{\alpha p} + p_{\beta p} + p_0$.

All these instantaneous quantities are valid under steady-state, transient, and nonsinusoidal conditions of voltage and/or current waveforms. Furthermore,

- The conventional concept of reactive power corresponds to the peak value of $p(t)$ that has a zero average value. However, the new concept of instantaneous reactive power in the $\alpha\beta 0$ space corresponds to the parts of $p(t)$ that are dependent on the instantaneous imaginary power $q$, which independently exist in each phase but vanish when added (e.g., $p_{\alpha q} + p_{\beta q} = 0$). If these powers ($p_{\alpha q}$ and $p_{\beta q}$) are transformed back to the original abc system, they add up to zero.
- The instantaneous real power ($p$) represents the net energy per second being transferred from source to load and vice versa at any time. It depends only on the voltages and currents in phases $\alpha$ and $\beta$. It does not have any zero-sequence power components.
- The imaginary power ($q$) does not contribute to the total instantaneous flow of energy. It relates to a block of energy exchanged between the phases. For example, consider a balanced three-phase capacitor bank connected to a balanced three-phase voltage source. The energy stored in each capacitor changes with time $W(t) = Cv^2(t)/2$. However, $v_a^2(t) + v_b^2(t) + v_c^2(t)$ is constant. Therefore,

$$\begin{cases} p_{\text{three-phase}} = p + p_0 = 0 \\ q = \bar{q} = -3V_+ I_+ \sin(\phi_+ - \delta_+) \\ \quad = 3V_+ I_+ = -Q_{\text{three-phase}}. \end{cases}$$



### 11.5.1.1 Application Example 11.1: The $\alpha\beta 0$ Transformation for Three-Phase Sinusoidal System Supplying a Linear Load

Assume sinusoidal system voltages and sinusoidal load currents [14]:

$$\begin{cases} v_{as}(t) = \sqrt{2}V_S \sin\omega t \\ v_{bs}(t) = \sqrt{2}V_S \sin(\omega t + 120), \\ v_{CS}(t) = \sqrt{2}V_S \sin(\omega t - 120) \end{cases} \tag{E11.1-1a}$$

$$\begin{cases} i_{aL}(t) = \sqrt{2}I_L \sin(\omega t - \phi) \\ i_{bL}(t) = \sqrt{2}I_L \sin(\omega t + 120 - \phi). \\ i_{cL}(t) = \sqrt{2}I_L \sin(\omega t - 120 - \phi) \end{cases} \tag{E11.1-1b}$$

Then

$$\begin{cases} v_\alpha = \sqrt{3}V_S \sin\omega t \\ v_\beta = \sqrt{3}V_S \cos\omega t \\ v_0 = 0 \end{cases} \quad \text{and} \quad \begin{cases} i_\alpha = \sqrt{3}I_L \sin(\omega t - \phi) \\ i_\beta = \sqrt{3}I_L \cos(\omega t - \phi) \\ i_0 = 0 \end{cases} \tag{E11.1-2}$$

Therefore, from Eq. 11-30

$$p = v_\alpha i_\alpha + v_\beta i_\beta = 3V_s I_L \cos\phi = P_{3\text{-phase}} \tag{E11.1-3}$$
$$q = v_\alpha i_\beta - v_\beta i_\alpha = 3V_s I_L \sin\phi = Q_{3\text{-phase}}$$





Equation E11.1-3 is equivalent to the traditional active and reactive power concept.

### 11.5.1.2 Application Example 11.2: The $\alpha\beta 0$ Transformation for Three-Phase Sinusoidal System Supplying a Nonlinear Load

Assume sinusoidal system voltages (Eq. E11.1-1a) and nonsinusoidal load currents [14]:

$$\begin{cases} i_{aL}(t) = \sum_{h=1}^{\infty} \sqrt{2}I_{hL} \sin(h\omega t - \phi_h) \\ i_{bL}(t) = \sum_{h=1}^{\infty} \sqrt{2}I_{hL} \sin[h(\omega t + 120) - \phi_h] \\ i_{cL}(t) = \sum_{h=1}^{\infty} \sqrt{2}I_{hL} \sin[h(\omega t - 120) - \phi_h]. \end{cases} \tag{E11.2-1}$$

Then

$$\begin{cases} i_\alpha = \sum_{h=1}^{\infty} \frac{2}{\sqrt{3}} I_{hL} \sin(h\omega t - \phi_h)[1 - \cos(h120)] \\ i_\beta = \sum_{h=1}^{\infty} 2hI_L \cos(h\omega t - \phi_h)\sin(h120) \\ i_0 = \frac{1}{\sqrt{3}}(i_a + i_b + i_c) = \sum_{h=1}^{\infty} \sqrt{6}I_{3hL} \sin(3h\omega t - \phi_{3h}). \end{cases} \tag{E11.2-2}$$

It is interesting to note that only the triplen harmonics (e.g., $h = 3k$) are present in $i_0$. The power components are

$$\begin{cases} p(t) = v_\alpha i_\alpha + v_\beta i_\beta = \bar{p} + \tilde{p} \\ \quad = 3V_S I_{1L} \cos\phi_1 - 3V_S I_{2L} \cos(3\omega t - \phi_2) + \\ \quad 3V_S I_{4L} \cos(3\omega t + \phi_4) - 3V_S I_{5L} \cos(6\omega t - \phi_5) \\ \quad + 3V_S I_{7L} \cos(6\omega t + \phi_7) - \cdots \\ q(t) = v_\alpha i_\beta - v_\beta i_\alpha = \bar{q} + \tilde{q} \\ \quad = 3V_S I_{1L} \sin\phi_1 - 3V_S I_{2L} \sin(3\omega t - \phi_2) + \\ \quad 3V_S I_{4L} \sin(3\omega t + \phi_4) - 3V_S I_{5L} \sin(6\omega t - \phi_5) \\ \quad + 3V_S I_{7L} \sin(6\omega t + \phi_7) - \cdots \\ p_0 = v_0 i_0 \end{cases} \tag{E11.2-3}$$

where the bar (–) and the tilde (~) correspond to the average value and the alternating components, respectively. In this example, the following relationships exist between the conventional and the instantaneous power theories:

- The average values of power ($\bar{p} = P_{\text{there-phas}}$ and $\bar{q} = Q_{\text{there-phas}}$) correspond to the conventional active and reactive powers, respectively.
- The alternating components of the real power ($\tilde{p}$) represent the energy per second that is being transferred from source to load or vice versa at any time. This is the energy being stored (or released) at the three-phase (abc) or two-phase ($\alpha\beta$) load or source.
- The alternating (fluctuating) component of the imaginary power ($\tilde{q}$) is responsible for the harmonic reactive power (due to the nonlinear nature of the load) in each phase but will vanish when added.
- The instantaneous energy transferred does not depend on the imaginary power ($q = \bar{q} + \tilde{q}$), although reactive currents exist in each phase and flow in the conductor.
- The power H including harmonics can be expressed as $H = \sqrt{\bar{P}^2 + \bar{Q}_2}$ where $\bar{P}$ and $\bar{Q}$ are the root-mean-square values of $\bar{p}$ and $\bar{q}$, respectively.

### 11.5.1.3 Application Example 11.3: The $\alpha\beta 0$ Transformation for Unbalanced Three-Phase, Four-Wire System Supplying a Linear Load

Unbalanced three-phase system voltages may be expressed in terms of their symmetrical components using [14]

$$\begin{bmatrix} V_0 \\ V_+ \\ V_- \end{bmatrix} = \frac{1}{3}\begin{bmatrix} 1 & 1 & 1 \\ 1 & \alpha & \alpha^2 \\ 1 & \alpha^2 & \alpha \end{bmatrix}\begin{bmatrix} V_a \\ V_b \\ V_c \end{bmatrix}$$
$$\begin{bmatrix} V_a \\ V_b \\ V_c \end{bmatrix} = \frac{1}{3}\begin{bmatrix} 1 & 1 & 1 \\ 1 & \alpha^2 & \alpha \\ 1 & \alpha & \alpha^2 \end{bmatrix}\begin{bmatrix} V_0 \\ V_+ \\ V_- \end{bmatrix}, \tag{E11.3-1}$$

where $\alpha = e^{j2\pi/3}$ and subscripts +, –, and 0 correspond to the positive-, negative-, and zero-sequence components, respectively. Applying these relations to the unbalanced system voltages, we have

$$\begin{cases} v_a = \sqrt{2}V_{s0} \sin(\omega t + \phi_0) + \sqrt{2}V_{s+} \sin(\omega t + \phi_+) + \\ \quad \sqrt{2}V_{s-} \sin(\omega t + \phi_-) \\ v_b = \sqrt{2}V_{s0} \sin(\omega t + \phi_0) + \sqrt{2}V_{s+} \sin(\omega t - 120^\circ + \phi_+) + \\ \quad \sqrt{2}V_{s-} \sin(\omega t + 120^\circ + \phi_-) \\ v_c = \sqrt{2}V_{s0} \sin(\omega t + \phi_0) + \sqrt{2}V_{s+} \sin(\omega t + 120^\circ + \phi_+) + \\ \quad \sqrt{2}V_{s-} \sin(\omega t - 120^\circ + \phi_-) \end{cases} \tag{E11.3-2}$$

Expressing these instantaneous voltages in terms of the $\alpha\beta 0$-coordinate system yields

$$\begin{cases} v_\alpha = \sqrt{3}V_{s+} \sin(\omega t + \phi_+) + \sqrt{3}V_{s-} \sin(\omega t + \phi_-) \\ v_\beta = -\sqrt{3}V_{s+} \sin(\omega t + \phi_+) + \sqrt{3}V_{s-} \sin(\omega t + \phi_-). \\ v_0 = \sqrt{6}V_{s0} \sin(\omega t + \phi_0) \end{cases} \tag{E11.3-3}$$

Similarly, the load currents may be expresses in terms of their instantaneous $\alpha\beta 0$ components

$$\begin{cases} i_\alpha = \sqrt{3}I_{L+}\sin(\omega t+\delta_+)+\sqrt{3}I_{L-}\sin(\omega t+\delta_-) \\ i_\beta = -\sqrt{3}I_{L+}\sin(\omega t+\delta_+)+\sqrt{3}I_{L-}\sin(\omega t+\delta_-). \\ i_0 = \sqrt{6}I_{L0}\sin(\omega t+\delta_0) \end{cases} \quad \text{(E11.3-4)}$$

For this case, the instantaneous active, reactive, and zero-sequence powers are

$$\begin{cases} p(t)=\bar{p}+\tilde{p} \\ q(t)=\bar{q}+\tilde{q} \\ p_0(t)=\bar{p}_0+\tilde{p}_0 \end{cases} \quad \text{(E11.3-5)}$$

where

- instantaneous average real power is

$$\bar{p}=3V_+I_{L+}\cos(\phi_+-\delta_+)+3V_-I_{L-}\cos(\phi_--\delta_-) \quad \text{(E11.3-6a)}$$

- instantaneous average imaginary power is

$$\bar{q}=-3V_+I_{L+}\sin(\phi_+-\delta_+)+3V_-I_{L-}\sin(\phi_--\delta_-) \quad \text{(E11.3-6b)}$$

- instantaneous alternating real power is

$$\tilde{p}=-3V_+I_{L-}\cos(2\omega t+\phi_++\delta_-)-3V_-I_{L+}\cos(2\omega t+\phi_-+\delta_+) \quad \text{(E11.3-6c)}$$

- instantaneous alternating imaginary power is

$$\tilde{q}=3V_+I_{L-}\sin(2\omega t+\phi_++\delta_-)-3V_-I_{L+}\cos(2\omega t+\phi_-+\delta_+) \quad \text{(E11.3-6d)}$$

- instantaneous average zero-sequence power is

$$\bar{p}_0=3V_0I_{L0}\cos(\phi_0-\delta_0) \quad \text{(E11.3-6e)}$$



- instantaneous alternating zero-sequence power is

$$\tilde{p}_0=-3V_0I_{L0}\cos(2\omega t+\phi_0+\delta_0) \quad \text{(E11.3-6f)}$$

### 11.5.2 UPQC Control System Based on Instantaneous Real and Imaginary Powers

Operation of the UPQC isolates the utility voltage from current quality problems of the load and, at the same time, isolates load from voltage quality problems of the utility. The most important subject in the UPQC control is the generation of reference compensating currents of the shunt converter (e.g., signal $i_C^* \equiv [i_{ca}^*, i_{cb}^*, i_{cc}^*]$ Fig. 11.2) and the reference compensation voltages of the series converter (e.g., signal $v_C^* \equiv [v_{ca}^*, v_{cb}^*, v_{cc}^*]$ Fig. 11.2). PWM control blocks will use these references to generate corresponding switching signals of the shunt and series converters.

In this section, the concept of instantaneous real and imaginary power will be relied on to generate reference signals $i_C^*$ and $v_C^*$. The three-phase voltage and current signals are transformed from the abc reference frame to the $\alpha\beta 0$ frame (Eq. 11-26) and the instantaneous real, imaginary, and zero-sequence powers are calculated (Eq. 11-30). The decomposition of voltage and current harmonic components into symmetrical components shows that the average of real ($\bar{p}$) and imaginary ($\bar{q}$) powers consists of interacting components of voltage and current that have the same frequency and sequence order (Eq. E11.3-6). Therefore, with the calculation of instantaneous powers and the derivation of their oscillation parts (e.g., $\tilde{p}$ and $\tilde{q}$), the voltage and current reference signals can be obtained and applied to the PWM controls of power electronic converters (Fig. 11.2). Before analyzing the control systems of the shunt and series converters, the circuits of the phase-lock loop (PLL) and the positive-sequence voltage detector (PSVD) will be introduced.

#### 11.5.2.1 Phase-Lock Loop (PLL) Circuit

The phase-lock loop (PLL) circuit (Fig. 11.4) is one of the components of the positive-sequence voltage

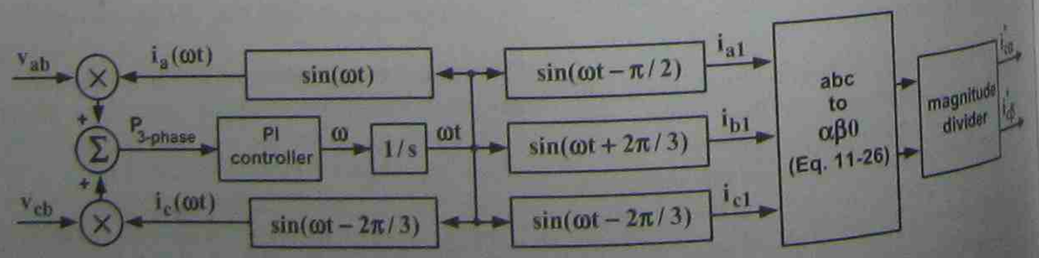



**FIGURE 11.4** Synchronizing circuit of the phase-lock loop (PLL) [9].





detector (Fig. 11.5). It detects the fundamental angular frequency ($\omega_1$) and generates synchronous sinusoidal signals that correspond to positive-sequence auxiliary currents under sinusoidal as well as highly distorted and unbalanced system voltages. The inputs of the PLL are $v_{ab}=v_a-v_b$ and $v_{cb}=(v_c-v_b)$.

Operation of PLL is based on the instantaneous active three-phase power theory ($p_{\text{three-phase}}=\bar{p}+\tilde{p}=v_{ab}i_a+v_{cb}i_c$):

- The current feedback signals $i_a(\omega t)=\sin(\omega t)$ and $i_c(\omega t)=\sin(\omega t-2\pi/3)$ are generated by sine generator circuits through integration of $\omega$ at the output of a PI-controller. These currents are 120 degrees out of phase and represent a feedback from a positive-sequence component at angular frequency $\omega$.
- The PLL circuit can reach a stable point of operation only if the input of the PI-controller has a zero average value ($\bar{p}=0$) with minimized low-frequency oscillations (e.g., small $\tilde{p}$). Because $i_a(\omega t)$ and $i_c(\omega t)$ contain only positive-sequence components and have unity magnitudes, the components of power (Eqs. E11.3-6a and E11.3-6c) simplify to

$$\begin{aligned} \bar{p}&=3V_+(1)\cos(\phi_+-\delta_+)=0 \\ \tilde{p}&=-3V_-I_+\cos(2\omega t+\delta_+)\approx 0 \end{aligned} \quad \text{(11-34)}$$

where $\phi_+$ and $\delta_+$ are the initial phase angles of the fundamental positive-sequence voltage and current $i_a(\omega t)$, respectively. According to these equations $\phi_+-\delta_+=\pi/2$. This means that the auxiliary currents $i_a(\omega t)=\sin(\omega t)$ and $i_c(\omega t)=\sin(\omega t-2\pi/3)$ become orthogonal to the fundamental positive-sequence component of the measured voltages $v_a$ and $v_c$, respectively. Therefore, $i_{a1}(\omega t)=\sin(\omega t-\pi/2)$ is in phase with the fundamental positive-sequence component of $v_a$. Similar relations hold for currents $i_{b1}$ and $i_{c1}$.

- Finally, signals $i_{a1}$, $i_{b1}$, and $i_{c1}$ are transformed to $i'_\alpha$ and $i'_\beta$ (with unity magnitudes) to the $\alpha\beta 0$ domain by using an $\alpha\beta 0$ block and magnitude divider blocks (which divide each signal by its magnitude).

#### 11.5.2.2 Positive-Sequence Voltage Detector (PSVD)

The positive-sequence voltage detector (PSVD) circuit (Fig. 11.5) is one of the components of the shunt converter controller (Fig. 11.6). It extracts the

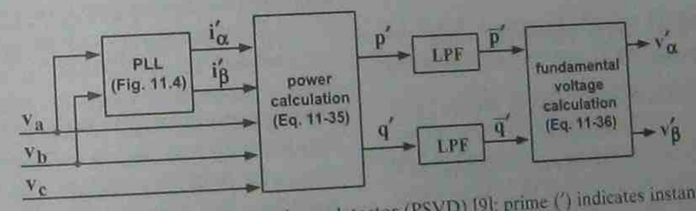



**FIGURE 11.5** Circuit of the positive-sequence voltage detector (PSVD) [9]; prime (′) indicates instantaneous voltages in the $\alpha\beta 0$ reference frame.

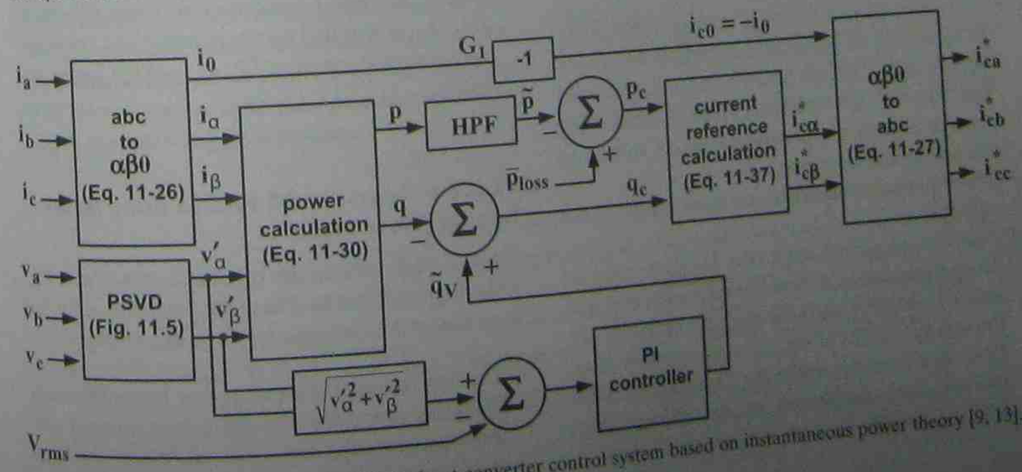



**FIGURE 11.6** Block diagram of the UPQC shunt converter control system based on instantaneous power theory [9, 13].

instantaneous $\alpha$ and $\beta$ values ($v'_\alpha$ and $v'_\beta$) of the fundamental positive-sequence components of the three-phase voltages $v_a$, $v_b$, and $v_c$ (Fig. 11.5).

The operation of the positive-sequence voltage detector is as follows:

- A phase-lock loop (PLL) circuit (Fig. 11.4) produces $i'_\alpha = \sin(\omega_1 t)$ and $i'_\beta = \cos(\omega_1 t)$ that correspond to an auxiliary fundamental positive-sequence current transformed into the $\alpha\beta 0$ reference frame.
- Because $i'_\alpha$ and $i'_\beta$ contain only the positive-sequence component, the average values of real power and imaginary powers comprise only the fundamental positive-sequence components of the voltages, and Eq. E11.3-6 simplifies to

$$\begin{aligned} \bar{p} &= 3V_+ I'_+ \cos(\phi_+ - \delta_+) \\ \bar{q} &= -3V_+ I'_+ \sin(\phi_+ - \delta_+) \end{aligned} \tag{11-35}$$

- The average values of instantaneous powers $\bar{p}'$ and $\bar{q}'$ are extracted using low-pass filters (LPFs). Consequently, the instantaneous values of the positive-sequence voltage can be calculated as

$$\begin{bmatrix} v'_\alpha \\ v'_\beta \end{bmatrix} = \frac{1}{i'^2_\alpha + i'^2_\beta} \begin{bmatrix} i'_\alpha & i'_\beta \\ i'_\beta & -i'_\alpha \end{bmatrix} \begin{bmatrix} \bar{p}' \\ \bar{q}' \end{bmatrix}. \tag{11-36}$$

#### 11.5.2.3 Control of Shunt Converter using Instantaneous Power Theory

Inputs of the shunt converter control system (Fig. 11.6) are three-phase load voltages ($v_a$, $v_b$, $v_c$) and the currents ($i_a$, $i_b$, $i_c$) and its outputs are the compensating reference currents $i^*_{ca}$, $i^*_{cb}$, and $i^*_{cc}$ (e.g., signal $i^*_C$ in Fig. 11.2).

The shunt controller operates as follows:

- A positive-sequence voltage detector (PSVD, Fig. 11.5) is used to generate the instantaneous voltages $v'_\alpha$ and $v'_\beta$. Primes indicate instantaneous voltages in the $\alpha\beta 0$ reference frame, which only corresponds to the positive-sequence voltage in the abc reference frame.
- Three-phase load currents are transformed to the $\alpha\beta 0$ space.
- A power calculation block (Eq. 11-30) is relied on for the generation of the instantaneous real and reactive powers. Due to the presence of the PSVD, the average values of the calculated powers (Eqs. E11.3-6a,b) contain only the fundamental positive-sequence component of the voltage (e.g., $\bar{p} = 3V_+ I_{L+} \cos(\phi_+ - \delta_+)$).
- The shunt converter is supposed to supply the oscillating instantaneous power $\tilde{p}$ and the instantaneous reactive power $q$ to the load while the load receives $\bar{p}$ from the source. Therefore, a high-pass passive filter is used to extract $\tilde{p}$ from the total power ($p = \bar{p} + \tilde{p}$). The oscillating part of the real power ($\tilde{p}$) consists of harmonic and negative-sequence components of the load current. Furthermore, the UPQC must also compensate for losses $\bar{p}_{loss}$ that will neutralize DC voltage variations caused by the series converter. Therefore, the amount of necessary instantaneous real power compensation is $p_c = -\tilde{p} + \bar{p}_{loss}$.
- In addition, the shunt converter will also compensate some reactive power ($\bar{q}_v$) required for the voltage regulation of the series converter. Therefore the amount of necessary instantaneous reactive power is $q_c = -q + \bar{q}_v = -(\bar{q} + \tilde{q}) + \bar{q}_v$. The imaginary power $\bar{q}_v$ is used for regulating the magnitude of the voltage ($|v|$), which is changed by the compensation voltage $v_C$ of the series converter. As shown in Fig. 11.6, the rms voltage value ($v_{rms}$) can be controlled to match $\bar{q}_v$ with the desired value $\sqrt{v'^2_\alpha + v'^2_\beta}$ through a PI controller.
- A current reference calculation block is employed to generate the reference compensation current in the $\alpha\beta 0$ reference frame:

$$\begin{bmatrix} i^*_{c\alpha} \\ i^*_{c\beta} \end{bmatrix} = \frac{1}{v'^2_\alpha + v'^2_\beta} \begin{bmatrix} v'_\alpha & v'_\beta \\ v'_\beta & v'_\alpha \end{bmatrix} \begin{bmatrix} -\tilde{p} + \bar{p}_{loss} \\ -q + \bar{q}_V \end{bmatrix}. \tag{11-37}$$

- To compensate for zero-sequence power, the zero-sequence current that is generated by the shunt converter must be equal to that of the load but negative. The sign is inverted by a gain block ($G_1$).
- Finally, the $\alpha\beta 0$ transformation block (based on Eq. 11-27) is relied on to generate the reference compensation currents ($i^*_{ca}$, $i^*_{cb}$, and $i^*_{cc}$) in the abc space.

#### 11.5.2.4 Control of DC Voltage using Instantaneous Power Theory

Figure 11.7 illustrates the block diagram of the DC voltage control system. There are two reasons for the variation of the DC capacitor average voltages.

- The first reason is the real power losses of power electronic converters and the power injected into the network by the series branch. When a voltage sag or voltage swell appears, the series branch of



the UPQC injects a fundamental component voltage into the network. The required (observed) real power to be injected is generated by the converter via the DC link, causing variation of the DC-link average voltage.
- Another factor that causes a variation of the average DC capacitor voltages is the zero-sequence component of the current, which is injected by the shunt converter into the system. These currents have no effect on the DC-link voltage but make the two capacitor voltages asymmetric.

The DC voltage controller performs the following two functions (Fig. 11.7):

- Regulating the DC-link average voltage by adding two capacitor voltages, comparing the sum with the reference DC voltage ($V_{ref}$), and applying the average voltage error to a PI controller. The output of this controller ($\bar{p}_{loss}$) is used by the shunt converter control system to absorb this power from the network and regulate the DC-link voltage. Note that the deviation of voltages is filtered by a low-pass passive filter and the PI controller matches the desired $\bar{p}_{loss}$ that neutralizes the DC bus voltage variations. The low-pass filter makes the voltage regulator insensitive to fundamental frequency voltage variations, which appear when the shunt active filter compensates the fundamental zero-sequence current of the load.
- The correction of the difference between two capacitor average voltages is performed by calculating the difference voltage signal, passing it through a low-pass filter, applying it to a limiter, and adding it (e.g., signal $\varepsilon$ in Fig. 11.7) with the upper and the lower hysteresis band limits. This process absorbs a zero-sequence current by the shunt converter and corrects the difference of the capacitor average voltages. Similarly, another low-pass filter is applied to filter the signal $V_{C2} - V_{C1}$. The filtered voltage difference produces $\varepsilon$ according to the following limit function:

$$\begin{cases} \varepsilon = -1 & \Leftrightarrow \Delta V < -0.05V_{ref} \\ \varepsilon = \dfrac{\Delta V}{0.05V_{ref}} & \Leftrightarrow -0.05V_{ref} \le \Delta V \le 0.05V_{ref}, \\ \varepsilon = 1 & \Leftrightarrow \Delta V \ge 0.05V_{ref} \end{cases} \tag{11-38}$$

where $V_{ref}$ is the DC bus voltage reference.

- Signal $\varepsilon$ and the reference compensation currents ($i^*_C \equiv [i^*_{ca}, i^*_{cb}, i^*_{cc}]$, Fig. 11.6) are employed to generate gating signals for the shunt converter switches (Fig. 11.2). For example, $\varepsilon$ can act as a dynamic offset level that is added to the hysteresis-band limits in the PWM current control of Fig. 11.2:

$$\begin{cases} \text{upper hysteresis band limit} = i^*_C + \Delta(1+\varepsilon) \\ \text{lower hysteresis band limit} = i^*_C - \Delta(1-\varepsilon) \end{cases} \tag{11-39}$$

where $i^*_C \equiv [i^*_{ca}, i^*_{cb}, i^*_{cc}]$ are the instantaneous current references (computed by the shunt converter control system) and $\Delta$ is a fixed semi-bandwidth of the hysteresis control. Therefore, signal $\varepsilon$ shifts the hysteresis band to change the switching times of the shunt converter such that

$$\begin{cases} \varepsilon > 0 & \text{increases } V_{C1} \text{ and decreases } V_{C2} \\ \varepsilon < 0 & \text{increases } V_{C2} \text{ and decreases } V_{C1} \end{cases}.$$

#### 11.5.2.5 Control of Series Converter using Instantaneous Power Theory

Inputs of the series converter control system (Fig. 11.8) are the three-phase supply voltages ($v_{sa}$, $v_{sb}$, $v_{sc}$), load voltages ($v_a$, $v_b$, $v_c$), and the line currents ($i_a$, $i_b$, $i_c$). Its outputs are the reference-compensating voltages $v^*_{ca}$, $v^*_{cb}$, and $v^*_{cc}$ (e.g., signal $v^*_C$ in Fig. 11.2). The compensating voltages consist of two components:

- One is the voltage-conditioning component $v'_s - v_s$ (e.g., the difference between the supply voltage $v_s \equiv [v_{sa}, v_{sb}, v_{sc}]$ and its fundamental positive-sequence component $v'_s \equiv [v'_{sa}, v'_{sb}, v'_{sc}]$) that com-

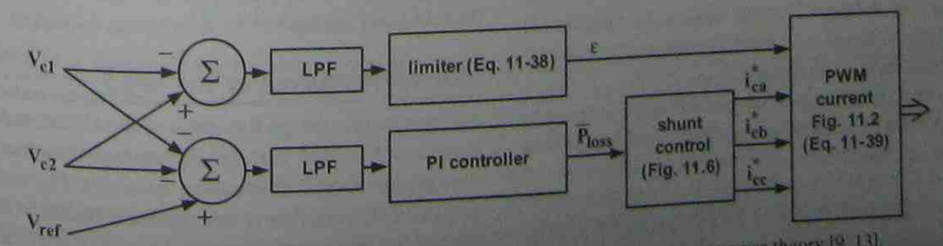



FIGURE 11.7 Block diagram of the DC voltage control system based on instantaneous power theory [9, 13].

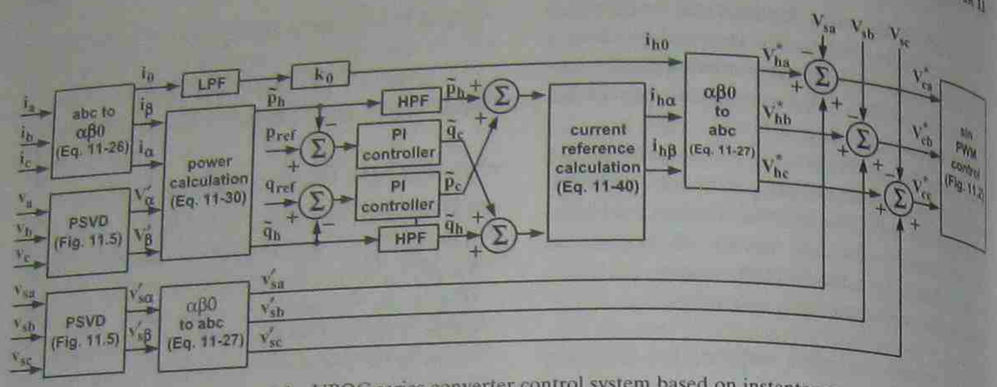



**FIGURE 11.8** Block diagram of the UPQC series converter control system based on instantaneous power theory [9].

pensates harmonics, fundamental negative-, and zero-sequence components of voltage, and regulates the fundamental component magnitude.

- The other voltage component ($v_h \equiv [v_{ha}, v_{hb}, v_{hc}]$) performs harmonic isolation and zero-sequence current damping, as well as damping of harmonic oscillations caused by the series resonance due to the series inductances and the shunt capacitor banks. $v_h$ can also compensate for the oscillating instantaneous active and reactive powers ($\tilde{p}_h$ and $\tilde{q}_h$).

The series controller operates as follows (Fig. 11.8):

- PSVD, $\alpha\beta0$, and power calculation blocks are relied on to compute oscillating instantaneous powers $\tilde{p}_h$ and $\tilde{q}_h$. This procedure is similar to the shunt converter control system.
- $\tilde{p}_h$ and $\tilde{q}_h$ are compared with their reference values ($p_{ref}$ and $q_{ref}$) to generate the desired compensation powers. The reference active power ($p_{ref}$) forces the converter to inject a fundamental voltage component orthogonal to the load voltage. This will cause change in the power angle $\delta$ (phase angle displacement between the voltages at both ends of transmission line) and mostly affects the active power flow. The reference reactive power ($q_{ref}$) will cause a compensation voltage in phase with the load voltage. This will change the magnitudes of the voltages and strongly affects the reactive power flow of the system.
- A current reference calculation block is used to generate the reference compensation currents in the $\alpha\beta0$ space:

$$\begin{bmatrix} i_{h\alpha} \\ i_{c\beta} \end{bmatrix} = \frac{1}{v_\alpha'^2 + v_\beta'^2} \begin{bmatrix} v_\alpha' & -v_\beta' \\ v_\beta' & v_\alpha' \end{bmatrix} \begin{bmatrix} \tilde{p}_h + \tilde{p}_C \\ \tilde{q}_h + \tilde{q}_C \end{bmatrix}. \quad (11\text{-}40)$$

- Signal $i_{h0}$, which provides harmonic isolation and damping for zero-sequence currents flowing through the series converter, is separated from the signal $i_0$ by a low-pass filter.
- The $\alpha\beta0$ transformation block is employed to generate the reference compensation voltages for harmonic isolation and harmonic oscillation damping ($v_h \equiv [v_{ha}, v_{hb}, v_{hc}]$). These voltages are added with $v_s' \equiv [v_{sa}', v_{sb}', v_{sc}']$ and subtracted from the supply voltages $v_s \equiv [v_{sa}, v_{sb}, v_{sc}]$ to form the reference compensation voltage for the series converter:

$$\begin{cases} v_{ca}^* = v_{ha} + (v_{sa}' - v_{sa}) \\ v_{cb}^* = v_{hb} + (v_{sb}' - v_{sb}). \\ v_{cc}^* = v_{hc} + (v_{sc}' - v_{sc}) \end{cases} \quad (11\text{-}41)$$

- The reference compensation voltages and a sinusoidal PWM control approach are relied on to produce the gating signals of the series converter (Fig. 11.2).

The UPQC series control system (Fig. 11.8) may be simplified by eliminating the reference compensation currents as shown in Fig. 11.9. Voltage regulation is controlled by $V_{ref}$. The converter is designed to behave like a resistor at harmonic frequencies to perform damping of harmonic oscillations. To do this, harmonic components of the line current are detected and multiplied by a damping coefficient.

## 11.6 PERFORMANCE OF THE UPQC

To demonstrate the performance of the UPQC in the presence of several current and voltage disturbance sources, the model distribution system of Fig. 11.10 consisting of seven (linear and nonlinear) buses is considered. System specifications are listed in Table 11.2.

The loads of this network (Fig. 11.10) are



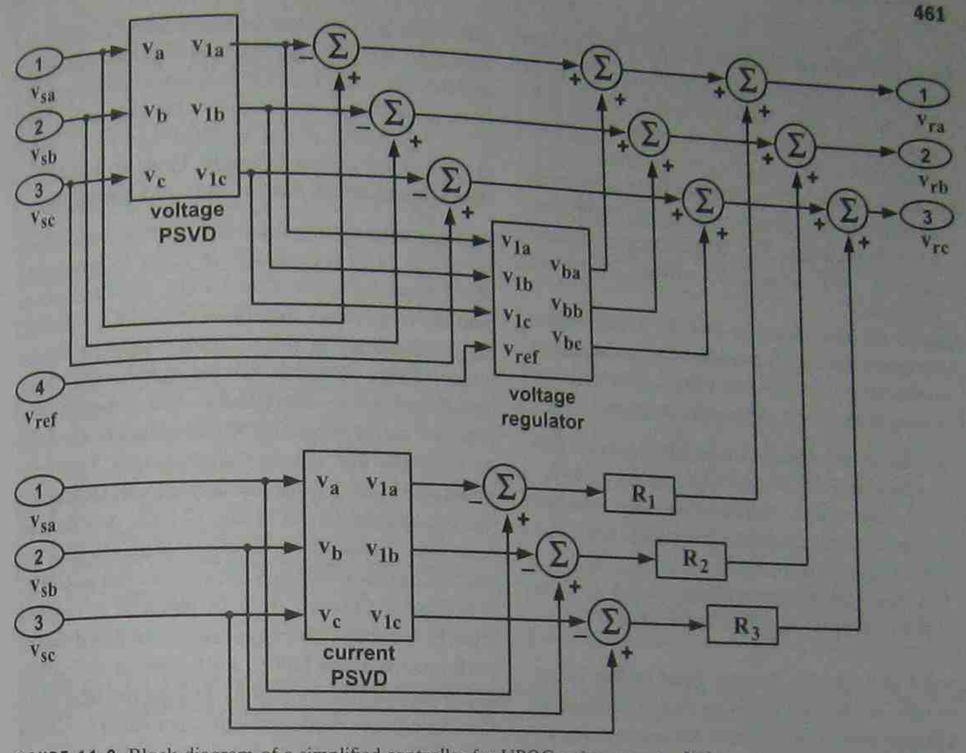



**FIGURE 11.9** Block diagram of a simplified controller for UPQC series converter [13].

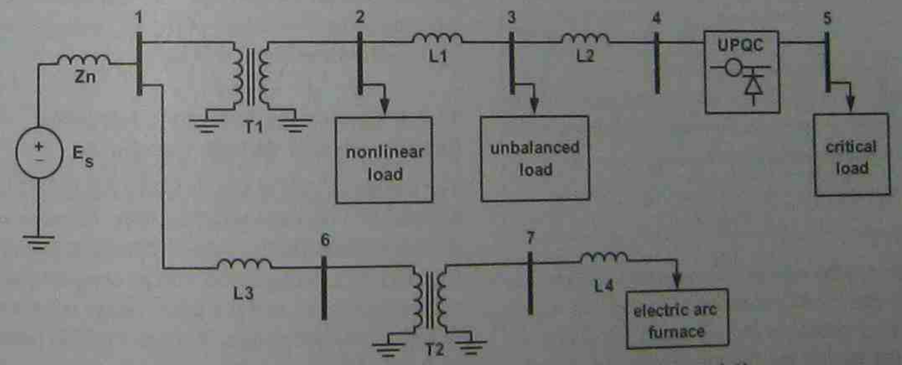



**FIGURE 11.10** Model distribution network used to analyze the performance of the UPQC [13].

**TABLE 11.2** Specifications of the Model Distribution System (Fig. 11.10)

| | |
|---|---|
| Medium voltage network | $V_L$ = 20 kV, $Z_s$ = (25 + j2.5) Ω, $R_s$ = 10 Ω |
| Distribution transformer ($T_1$) | S = 2 MVA, V: 20 kV/400 V, Z = (0.002 + j0.1) pu |
| Arc furnace transformer ($T_2$) | S = 5 MVA, V: 20 kV/700 V, Z = (0.01 + j0.1) pu |
| Nonlinear load | Thyristor-controlled rectifier, α = 0°, $I_{DC}$ = 400 A |
| Unbalanced linear load | $Z_a$ = (0.08 + j0.06) Ω, $Z_b$ = (1.0 + j0.7) Ω, $Z_c$ = (0.14 + j0.12) Ω |
| Transmission lines | $Z_{L1}$ = (0.01 + j0.003) Ω, $Z_{L2}$ = (0.03 + j0.006) Ω, $Z_{L3}$ = (0.1 + j0.3) Ω, $Z_{L4}$ = (0.01 + j0.08) Ω |

SL GEORGE POLLEGE OF LAW

***Load 1 (Nonlinear Load at Bus 2):*** a three-phase thyristor-controlled rectifier providing 700 A of DC current. This nonlinear load produces harmonic currents and causes network voltage distortion.

***Load 2 (Unbalanced Load at Bus 3):*** an unbalanced three-phase linear load consists of three different linear impedances. This load draws unbalanced currents and causes a voltage imbalance condition.

***Load 3 (Critical Load at Bus 5):*** a three-phase nonlinear load that is considered to be the critical load to be protected by the UPQC. This load consists of three power electronic converters:

- A three-phase thyristor-controlled rectifier with a firing angle of 30° and a DC current of 10 A.
- A single-phase thyristor-controlled rectifier placed in phase A, with a firing angle of 45° and a DC current of 10 A.
- A single-phase uncontrolled (diode) rectifier placed in phase B, with a DC current of 5 A.

***Load 4 (Electric Arc Furnace Load at Bus 7):*** an electric arc furnace produces voltage fluctuation (flicker). Due to its nonlinear volt-ampere characteristic, this load acts like a time-varying nonlinear resistor. This nonlinearity is considered for the positive half-cycle as follows [16]:

$$v_{arc} = v_t + c/(i_{arc} + d), \tag{11-42}$$

where $v_{arc}$ and $i_{arc}$ are the voltage and current of the arc furnace, $c$ and $d$ are constant coefficients, and $v_t$ is the threshold voltage:

$$v_t = v_e + kL. \tag{11-43}$$

Here $v_e$ is the voltage drop across the furnace electrodes and $kL$ corresponds to the variable voltage drop proportional to the arc length ($L$). There are different models for the arc length time variation [13]. In Fig. 11.10, the sinusoidal time variation law is used and arc length is considered as a sinusoidal function of time with a fixed frequency:

$$L = L_1 + L_2 \sin \omega t. \tag{11-44}$$

Since human eyes are most sensitive to flickers with a frequency of about 8–10 Hz, the frequency is assumed to be $f = 10$ Hz.

Simulation of the model distribution network and UPQC (with the control systems of Figs. 11.6, 11.7, and 11.9) is performed using the MATLAB/Simulink software package. The specifications of UPQC are listed in Table 11.3. UPQC performance is examined in the following six application examples [13].

### 11.6.1 Application Example 11.4: Dynamic Behavior of UPQC for Current Compensation

In this example, only the critical load at bus 5 (load 3) of Fig. 11.10 is activated. In order to investigate the dynamic behavior of the UPQC, the single-phase and the three-phase controlled rectifiers are operating continuously in the network, while the single-phase diode rectifier is connected and then disconnected at $t = 0.06$ s and $t = 0.12$ s, respectively. The gate pulses of the UPQC converter are activated at $t = 0.04$ s. The results including load 3 current, shunt converter current, line current, and DC capacitor voltages are shown in Fig. E11.4.1. As expected sinusoidal balanced currents are achieved and the neutral current is reduced to zero, as soon as UPQC is activated. Current $THD_i$ of phase A is reduced from 19.2 to 0.6%. This figure shows the fine dynamic performance of the UPQC for nonlinear and unbalanced load current variations. During the time when the single-phase diode rectifier is activated ($t = 0.06$ s to $t = 0.12$ s), the UPQC distributes its load demand between the three phases and, as a result, the line currents increase. Compensation of the oscillatory parts of real power and the zero-sequence current has caused some variation of the DC capacitor voltages, as shown in Fig. E11.4.1d.

### 11.6.2 Application Example 11.5: UPQC Compensation of Voltage Harmonics

The nonlinear load at bus 2 (load 1) of Fig. 11.10 is connected to the network. Therefore, harmonic currents are injected and voltage distortion is generated (Fig. E11.5.1). As expected, UPQC compensates for voltage harmonics and the load voltage is corrected to a sinusoidal waveform. Voltage THD, is reduced from 9.1 to 0.1%.

**TABLE 11.3** Specifications of the UPQC Components in Fig. 11.10

| | |
|---|---|
| Shunt transformer | S = 4.6 kVA, V: 230/100 V, Z = (0.01 + j0.05) pu |
| Series transformer | S = 2 kVA, V: 95/190 V, Z = (0.01 + j0.05) pu |
| DC capacitors | C = 2000 μF, V = 300 V |
| Low-pass filter | L = 2 mH, C = 5 μF, R = 4 Ω |
| High-pass filter | C = 15 μF, R = 5 Ω |
| Commutation inductance | L = 3 mH |

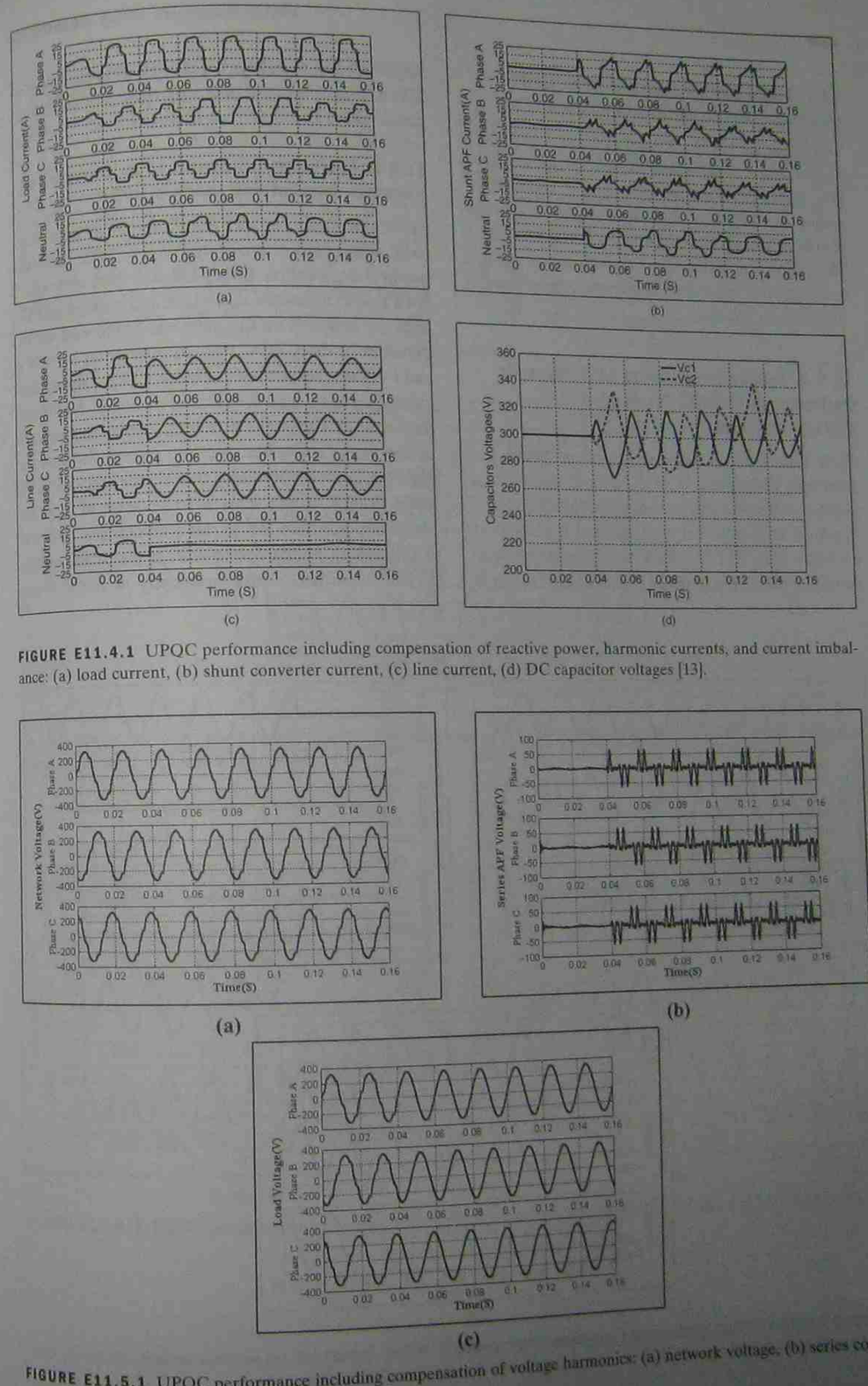



**FIGURE E11.4.1** UPQC performance including compensation of reactive power, harmonic currents, and current imbalance: (a) load current, (b) shunt converter current, (c) line current, (d) DC capacitor voltages [13].




**FIGURE E11.5.1** UPQC performance including compensation of voltage harmonics: (a) network voltage, (b) series converter voltage, (c) load voltage [13].

### 11.6.3 Application Example 11.6: UPQC Compensation of Voltage Imbalance

The linear load at bus 3 (load 2) of Fig. 11.10 is connected to the network and causes voltage imbalance (Fig. E11.6.1). Operation of the UPQC and compensation of negative- and zero-sequence currents results in the balanced voltage conditions at bus 4. The ratios of negative- and zero-sequence voltages to the positive-sequence voltage are reduced from 24 and 8.4% to about 0.

### 11.6.4 Application Example 11.7: Dynamic Performance of UPQC for Sudden Voltage Variation

With loads 2 and 3 connected (e.g., imbalance and harmonic distortion) in Fig. 11.10, a single-phase short-circuit with a fault resistance of 45 Ω is imposed at phase B of bus 6 at $t = 0.06$ s and is cleared at $t = 0.12$ s. (Fig. E11.7.1). Such an asymmetrical fault causes a voltage sag in phase *B* and voltage swells in phases *A* and *C*. However, the fast response of the UPQC (e.g., a delay of only 1 ms) does not allow any disturbances in the voltage of bus 5.

### 11.6.5 Application Example 11.8: Damping of Harmonic Oscillations Using a UPQC

In this example, a 1 kVAr three-phase capacitor bank is installed at bus 5 of Fig. 11.10 for reactive power compensation. Loads 1, 2, and 3 are activated. As a result, harmonic distortion and voltage imbalance are imposed on the network. Shunt and series branches of the UPQC start to operate at $t = 0.04$ s and $t = 0.08$ s, respectively. Figure E11.8.1 shows the voltage of bus 5 and the current of line 2. Although the harmonic components of load 3 are compensated by the shunt converter, the line current includes a high-frequency component before the operation of series branch occurs. This is so because of a series resonance between the series inductances and the shunt capacitor bank due to voltage distortion at bus 2. This condition occurs frequently in distribution

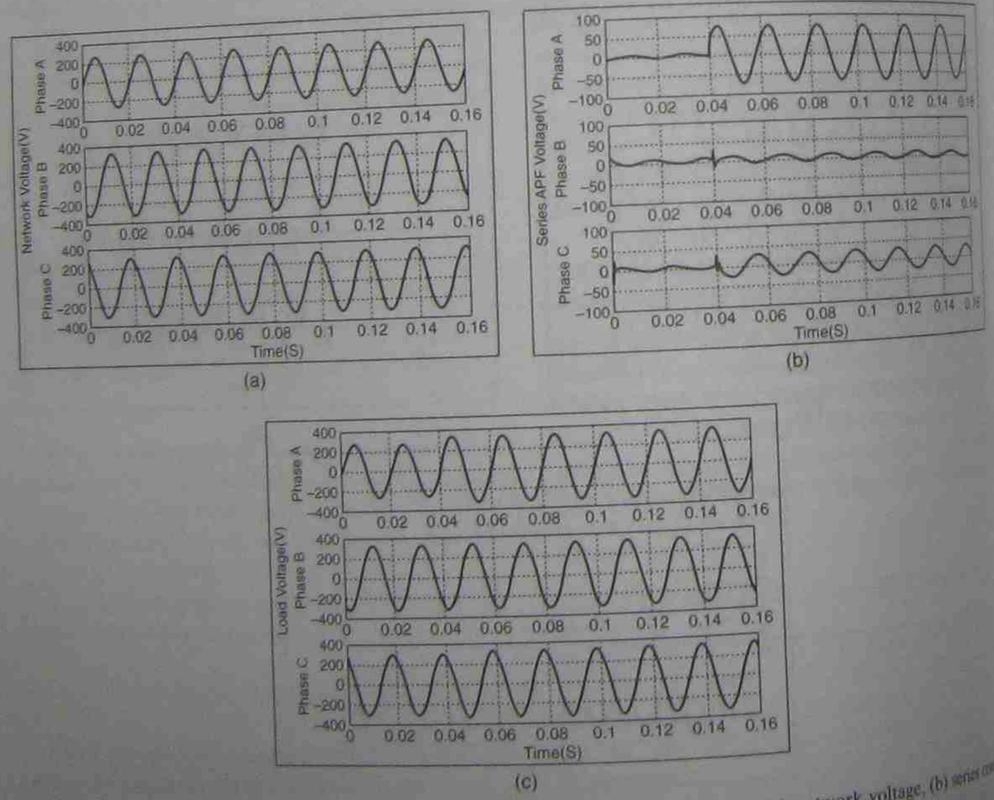



**FIGURE E11.6.1** UPQC performance including compensation of voltage imbalance: (a) network voltage, (b) series converter voltage, (c) load voltage [13].





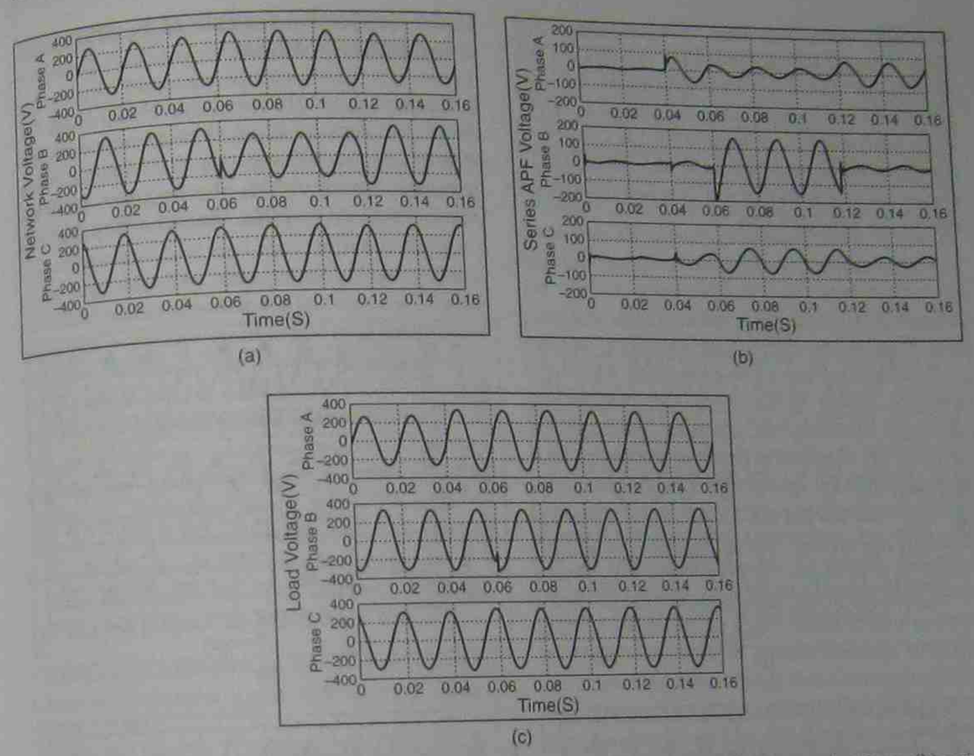



**FIGURE E11.7.1** UPQC performance including compensation of voltage sag and swell: (a) network voltage, (b) series converter voltage, (c) load voltage [13].

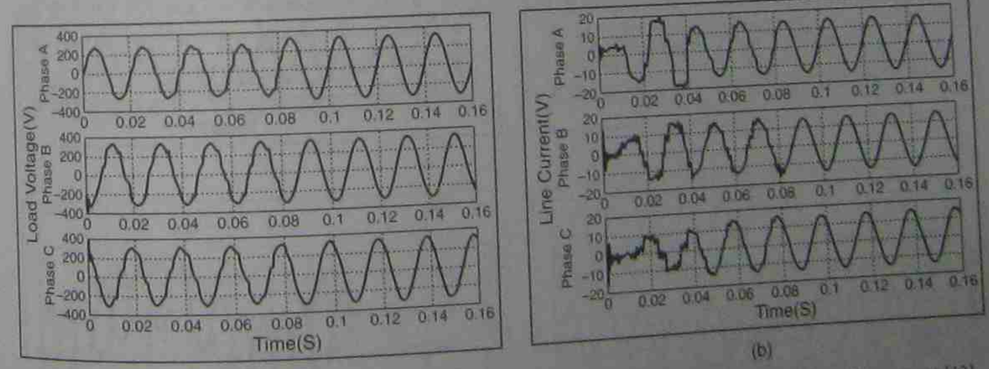



**FIGURE E11.8.1** UPQC performance including damping of harmonic resonance: (a) load voltage, (b) line current [13].

networks where significant harmonic distortion exists. Because the capacitor bank currents are not recorded by shunt branch current sensors, no compensation is performed. After the operation of the series converter has occurred at $t = 0.08$ s, resonant currents are damped significantly because the series branch acts like a resistor and increases the impedance of the resonance path.

### 11.6.6 Application Example 11.9: UPQC Compensation of Flicker

In the presence of all three loads of Fig. 11.10, the electric arc furnace (load 4) is connected to the network and causes fluctuation of the voltage with a magnitude change of 20% at a frequency of 10 Hz (Fig. E11.9.1). At $t = 0.04$ s, the series branch of the

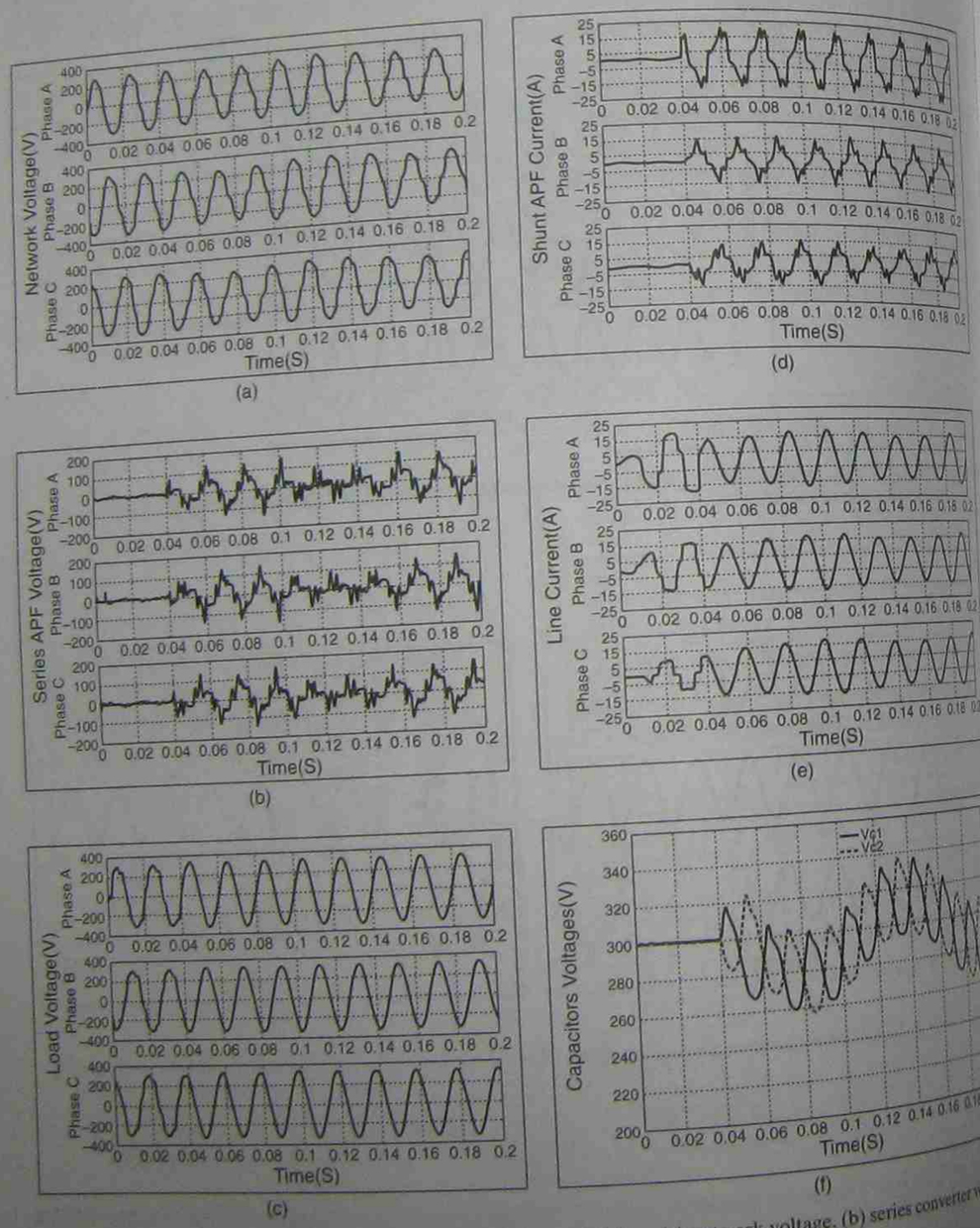



**FIGURE E11.9.1** UPQC performance including compensation of flicker: (a) network voltage, (b) series converter voltage, (c) load voltage, (d) shunt converter current, (e) line current, (f) DC capacitor voltages [13].



UPQC starts to operate, injecting voltage harmonics of high order (to correct voltage harmonic distortion) and low order (to compensate for voltage fluctuation) into the network. As a result, the voltage of bus 5 is restored to a sinusoid. Figure E11.9.1d,e,f illustrates shunt converter current, line 2 current, and DC capacitor voltages, respectively. By compensating harmonics, and negative- and zero-sequence components of the nonlinear load currents, balanced three-phase sinusoidal line currents are achieved. Some small fluctuations appear in the line currents because the UPQC requires a variable power to compensate voltage fluctuations. This power is provided by the DC capacitors and, as a result, the DC-link voltage includes low-frequency oscillations (Fig. E11.9.1f). This slow variation is sensed by the DC voltage control system, and for its compensation the UPQC absorbs an oscillatory power from the network. Therefore, both the shunt branch current and the line current will have low frequency variations.

Other application examples discussed in [4, pp. 117–129] and [3, pp. 129–130] include

- operation of solid-state current limiters (SSCLs),
- load compensation (with stiff source) using a STATCOM,
- load compensation (with nonstiff source) using a STATCOM,
- voltage regulation using a STATCOM, and
- protecting sensitive loads using a DVR.

## 11.7 SUMMARY

The unified power quality conditioner (UPQC) is an advanced hybrid filter that consists of a series active power filter for compensation of voltage disturbances and a shunt active power filter for eliminating current distortions. This custom power device is mainly employed to protect a critical nonlinear load by improving the quality of voltage across it, and to improve the waveform of the supply current. Different control approaches may be implemented to simultaneously perform these tasks. This chapter introduces two commonly relied on UPQC control approaches based on the $dq0$ transformation and the instantaneous real and reactive powers. Detailed UPQC block diagrams are provided for these approaches and application examples are used to demonstrate their effectiveness. Different control approaches for hybrid filters (which are part of UPQCs) are also presented in Chapter 9. Using an appropriate control algorithm, a UPQC can improve the utility current and protect the critical load at the point of installation in distorted distribution systems by taking a number of actions including reducing harmonic distortions, voltage disturbance compensation, voltage regulation, reactive (harmonic) power flow, harmonic isolation, and neutral and negative-sequence current compensations.

## 11.8 REFERENCES


1) GyuGyi, L.; "A unified flow control concept for flexible AC transmission systems," *Proc. Inst. Elect. Eng.*, Vol. 139, Part C, No. 4, pp. 323–331, 1992.
2) Hingorani, N.G.; and GyuGyi, L.; *Understanding FACTS – Concepts and Technology of Flexible Transmission Systems*, IEEE Press, 2000.
3) Hingorani, N.G.; "Introducing custom power," *IEEE Spectrum*, Vol. 32, No. 6, pp. 41–48, June 1995.
4) Ghosh, A.; and Ledwich, G.; *Power Quality Enhancement Using Custom Power Devices*, Kluwer Academic Publishers, Boston, 2002.
5) Peng, F.Z.; Akagi, H.; and Nabae, A.; "A new approach to harmonic compensation in power system – a combined system of shunt passive and series active filters," *IEEE Transactions on Industry Applications*, Vol. 26, No. 6, pp. 983–990, 1990.
6) Akagi, H.; "New trends in active filters for power conditioning," *IEEE Transactions on Industry Applications*, Vol. 32, No. 6, pp. 1312–1322, 1996.
7) Fujita, H.; and Akagi, H.; "The unified power quality conditioner: the integration of series and shunt–active power filters," *IEEE Transactions on Power Electronics*, Vol. 13, No. 2, pp. 315–322, March 1998.
8) Kamran, F.; and Habetler, T.G.; "Combined deadbeat control of a series-parallel converter combination used as universal power filter," *Proceedings of the IEEE Power Electronic Specialist Conference (PESC)*, pp. 196–201, 1995, *IEEE Transactions on Power Electronics*, Vol. 13, No. 1, pp. 160–168, Jan. 1998.
9) Aredes, M.; Heumann, K.; and Watanabe, E.H.; "An universal active power line conditioner," *IEEE Transactions on Power Delivery*, Vol. 13, No. 2, pp. 545–551, April 1998.
10) Tolbert, L.M.; and Peng, F.Z.; "A multilevel converter-based universal power conditioner," *IEEE Transactions on Industrial Applications*, Vol. 36, No. 6, pp. 596–603, March/April 2000.
11) Graovac, D.; Katic, V.; and Rufer, A.; "Power quality compensation using universal power quality conditioning system," *IEEE Power Engineering Review*, pp. 58–60, Dec. 2000.
12) Ghosh, A.; and Ledwich, G.; "A unified power quality conditioner (UPQC) for simultaneous voltage and current compensation," *Electric Power Systems Research*, Vol. 59, pp. 55–63, 2001.
13) Mosavi, S.A.; and Masoum, M.A.S.; "Mitigation of temporary and sustained power quality disturbances by UPQC," *International Journal of Engineering*, Iran, Vol. 15, No. 3, pp. 109–120, 2004.
14) Watanabe, E.H.; Stephan, R.M.; and Aredes, M.; "New concepts of instantaneous active and reactive powers in electrical systems with generic loads," *IEEE Transactions on Power Delivery*, Vol. 8, No. 2, pp. 697–703, April 1993.
15) Vilathgamuwa, M.; Zhang, Y.H.; and Choi, S.S.; "Modeling, analysis and control of unified power quality conditioner," *Proceedings of the 8th International Conference on Harmonics and Quality of Power*, Vol. 2, pp. 1035–1040, 14–16 Oct, 1998.
16) Montanari, G.C.; Loggini, M.; Cavallini, A.; Pitti L.; and Zaninelli, D.; "Arc furnace model for the study of flicker compensation in electrical networks," *IEEE Transactions on Power Delivery*, Vol. 9, pp. 2026–2036, 1994.


ST. GEORGE POLLEGE OF LAW

# 1
APPENDIX

# Sampling Techniques

There are two sampling techniques:

- series (sequential) sampling with interpolation, and
- parallel sampling with holding network [79, Chapter 2].

**Series Sampling with Interpolation.** The derating measurements as described in Section 2.8 are based on sequential sampling utilizing the soft- and hardware specified by the UCDAS-16G Manual of the Keithley Corporation [80, Chapter 2]. The software program is written in Quick BASIC language. Sampling programs for two and five channels have been used [81, Chapter 2]. Some of the frequently asked questions concerning sequential sampling are addressed as follows.

### 1.1 WHAT CRITERION IS USED TO SELECT THE SAMPLING RATE (SEE LINE 500 OF TWO-CHANNEL PROGRAM [81, CHAPTER 2])?

The A/D converter UCDAS-16G has a maximum throughput (sampling) rate of 70 kHz in the direct memory access (DMA) mode, where the gain is 1.0.

**In the Two-Channel Program [81, Chapter 2]**

select $D\%(0) = 4$
$D\%(1) = 58$

from this follows the SAMPLE RATE
$= 10{,}000{,}000/[D\%(0) \cdot D\%(1)]$
$= 10{,}000{,}000/[4 \cdot 58] = 43.1 \text{ kHz} \approx 43 \text{ kHz}$

**In the Five-Channel Program [81, Chapter 2]**

select $D\%(0) = 5$
$D\%(1) = 37$

from this follows the SAMPLE RATE
$= 10{,}000{,}000/[D\%(0) \cdot D\%(1)]$
$= 10{,}000{,}000/[5 \cdot 37] \approx 54 \text{ kHz}$

### 1.2 WHAT CRITERION IS USED TO SELECT THE TOTAL NUMBER OF CONVERSIONS (LINE 850 OF THE TWO-CHANNEL PROGRAM [81, CHAPTER 2])?

**In the Two-Channel Program.** One period $T = 16.66$ ms of fundamental frequency ($f = 60$ Hz) signal is approximated by 360 equidistant intervals or $360 + 1 = 361$ points as indicated in Fig. A1.1. For two channels and sequential sampling $361 \cdot 2 = 722$ sample points are required. Due to interpolation procedure #1 at the end of the sampled period (discussed later), one chooses a somewhat larger number $722 + 11 = 733$.

**In the Five-Channel Program.** One period $T = 16.66$ ms of fundamental frequency ($f = 60$ Hz) signal is approximated by 180 equidistant intervals or $180 + 1 = 181$ points as explained in Fig. A1.2. For five channels and sequential sampling $181 \cdot 5 = 905$ sample points are required. Due to interpolation one chooses a somewhat larger number $905 + 9 = 914$.

### 1.3 WHY ARE THE TWO-CHANNEL PROGRAM DIMENSION AND THE ARRAY FOR THE CHANNEL NUMBER NOT USED FOR THE FIVE-CHANNEL PROGRAM [81, CHAPTER 2]?

There are two ways to store the data:

- For the two-channel program, the array $DT\%(N)$ comprises the sampled points of both (2) channels (e.g., in an interleaved manner). Therefore, $CH\%(N)$ is needed to separate the sample points for each channel, and $DT\%(N)$ results in $DA(N + 10)$ (increased due to interpolation).
- For the five-channel program, the array $DA(368)$ contains the sample points of channel #1, $DB(368)$ contains the sample points of channel #2, etc. That is, the sampled data are separated for each channel and no channel number $CH\%(N)$ is required.



© Elsevier Inc.
All rights reserved.

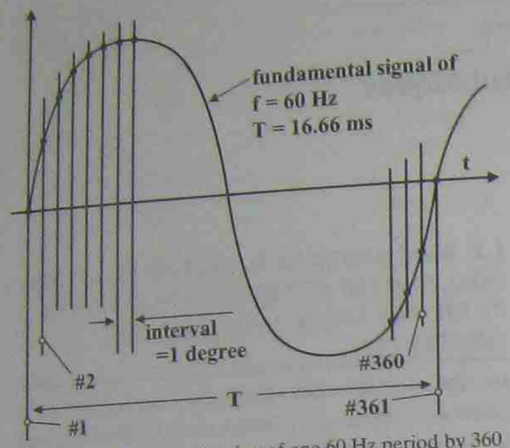



**FIGURE A1.1** Approximation of one 60 Hz period by 360 equidistant intervals.

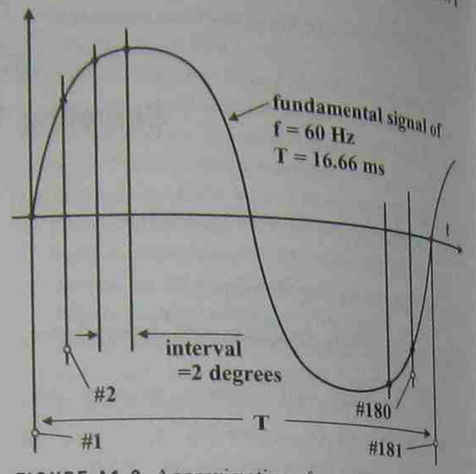



**FIGURE A1.2** Approximation of one 60 Hz period by 180 equidistant intervals.

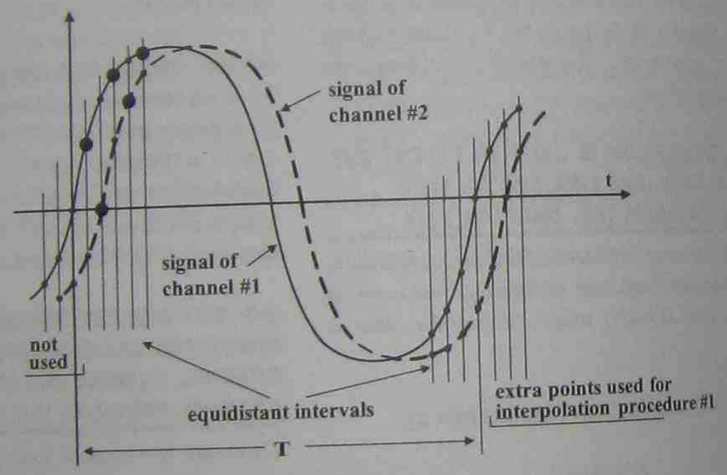



**FIGURE A1.3** Sampling of two signals in two-channel configuration.

### 1.4 WHAT IS THE CRITERION FOR SELECTING THE MULTIPLYING FACTOR IN STEP 9 (0.0048 82812 ≈ 0.004883) FOR THE TWO- AND FIVE-CHANNEL CONFIGURATIONS?

The UCDAS-16G is a 12 bit converter, that is, ±10 V is divided into $2^{12} = 4096$ steps. For a voltage peak-to-peak value of 10 V − (−10 V) = 20 V one step corresponds to 20 V/4096 = 0.004882812 V ≈ 0.004883 V.

### 1.5 WHY IS IN STEP 9 OF THE TWO-CHANNEL PROGRAM (LINE 1254) THE ARRAY DA(N + 10) OR DA(733), AND IN THE FIVE-CHANNEL PROGRAM (LINE 1233) THE ARRAY IS DA(368)?

For the two-channel program the sampled data of both channels are stored in *DA*(733) as indicated in Fig. A1.3.

For the five-channel program the sampled data are stored separately for each channel, that is, for channel #1 in *DA*, for channel #2 in *DB*, etc. explained in Fig. A1.4.

For *I* = 0 (line 1235):

```
DA(0) = DT%(0+5) * 0.004883
DB(0) = DT%(0+6) * 0.004883
          .          .
          .          .
          .          .
DE(0) = DT%(0+9) * 0.004883
```

For I = 2 (line 1235):

```
DA(2) = DT%(5+5) * 0.004883
DB(2) = DT%(5+6) * 0.004883
          .          .
          .          .
          .          .
DE(2) = DT%(5+9) * 0.004883
```



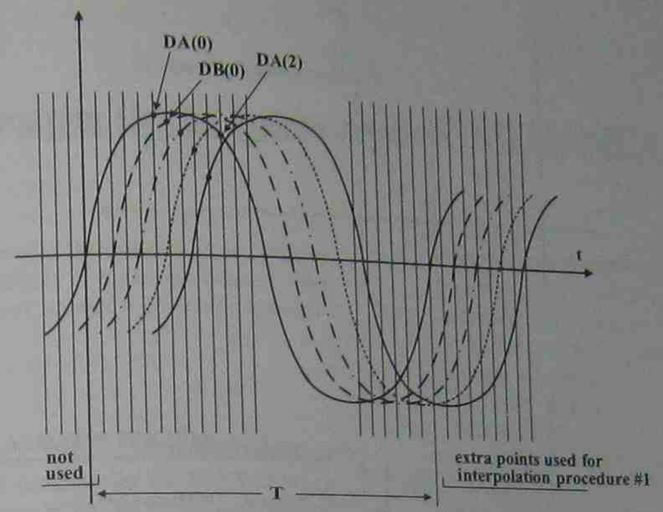



**FIGURE A1.4** Sampling of five signals in five-channel configuration.

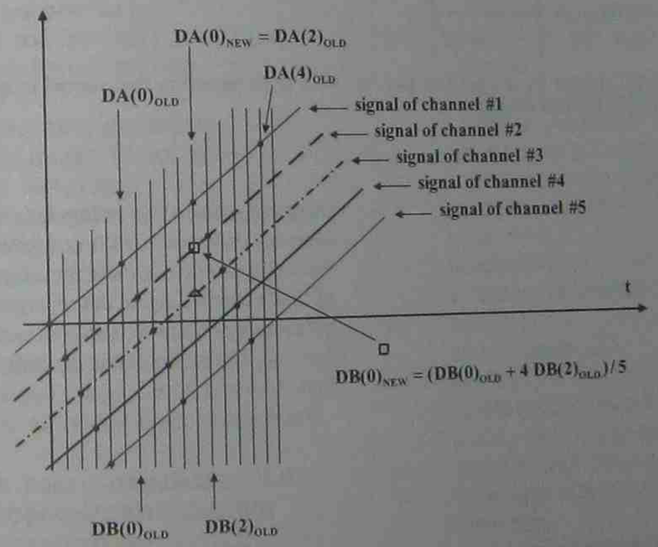



**FIGURE A1.5** Interpolation for five-channel configuration.

ST. GEORGE COLLEGE LIBRARY

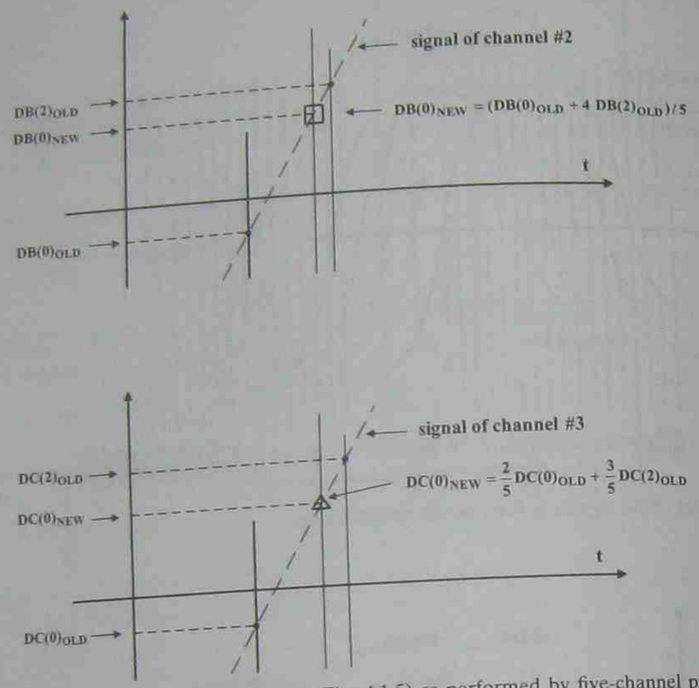



**FIGURE A1.6** Detailed example for interpolation (see Fig. A1.5) as performed by five-channel program: (a) signal for second channel, (b) signal for third channel.

For I = 4:

```
DA(4)  = DT%(10+5)  · 0.004883
DB(4)  = DT%(10+6)  · 0.004883
           .          .
           .          .
           .          .

DE(4)  = DT%(10+9)  · 0.004883
           .          .
           .          .
           .          .
```

One concludes that although there are only 181 sampled points for each channel of the five-channel program, the Fourier program [81, Chapter 2] requires $181 \cdot 2 = 362$ or $362 + 6 = 368$ dimensions for array $DA$, that is, $DA(368)$. The points between sampled points are obtained by interpolation procedure #2. Lines 1241 to 1247 of the five-channel program perform this interpolation. The sequential sampling does not provide at a given instant of time values for all five channels; therefore, at each instant of time a channel signal datum is generated by interpolation procedure #2 for each and every sampled function. The interpolation procedure is explained in Figs. A1.5 and A1.6.

For $J = 0$:

$$DA(0)_{NEW} = DA(2)_{OLD} \quad \text{and} \quad DB(0)_{NEW} = \{DB(0)_{OLD} + DB(2)_{OLD} \cdot 4\}/5, \text{ and}$$

$$DB(0)_{NEW} = \frac{DB(0)_{OLD}}{5} + DB(2)_{OLD} \cdot \frac{4}{5},$$

where (1/5) is the weighting function for $DB(0)_{OLD}$ and (4/5) is the weighting function for $DB(2)_{OLD}$.

Statements (line 1248 to line 1257) restore the data because FORTRAN cannot handle $DA(0)$, that is, $DA(0)$ becomes $DA(1)$, etc.

# 2
APPENDIX

## Program List for Fourier Analysis [81, Chapter 2]

This appendix contains the program list to compute the Fourier coefficient of a periodic nonsinusoidal function. An output example is given for a rectangular wave.

### A2.1 FOURIER ANALYSIS PROGRAM LIST

Following is the program list (in FORTRAN) to compute the Fourier terms (DC offset, even and odd harmonics) of a periodic nonsinusoidal function:

```
C       PROGRAM ANAFOR
C       test, square wave
        COMMON NW,DEG(361),RAD(361),
          XV(361),YVALUE(361)
        COMMON
        NPTS,NPS,INT,INC,NH,GA,
          PI,WW,OM,NC,RF,ER,EL
        COMMON ERR,ITMAX
        DIMENSION Y(30,365),SCALE(30),
          YMAX(30),X(365)
        DIMENSION
        CURVT(100),
          CURVC(100),CURVS(100),CURVP(100)
        DIMENSION AMP(30,100),
            ANG(30,100)
C       READ DATA FROM DATA FILE.
C
        OPEN(5,FILE='INDUCTOR.
          DAT',STATUS='OLD',
          ACCESS='SEQUENTIAL')
C       REWIND 5
C*******************
        NSETS=1
        NPTS=42
C***************
        SCALE(1)=1.0
C       CLOSE(UNIT=5)
C       OPEN(3,FILE='FODA.DAT',
          STATUS='OLD',
          ACCESS='SEQUENTIAL')
C       REWIND 3
C       DO 5 J=1,NSETS
C 5     READ(3,132)
          (Y(J,I),I=1,NPTS+4)
 132    FORMAT(E11.4,2X,E11.4,2X,
          E11.4,2X,E11.4,2X,E11.4)
C       Input of data
        Do 1320 J=1,20
 1320   Y(1,J)=1.0
        Do 1321 J=21,41
 1321   Y(1,J)=-1.0
        Y(1,42)=1.0
C       ECHO THE DATA ON THE SCREEN.
        DO 10 J=1,NSETS
 10     WRITE(0,1000)
          J,SCALE(J),(Y(J,I),I=1,NPTS)
 1000   FORMAT(//' SET NO.',I4,' SCALE
          FACTOR:'
        *,F16.10/ 'Y-COORDINATES
          BEFORE SCALING:'(/5E11.4))
C       SUBTRACT D.C. COMPONENT AND
          MULTIPLY THE SCALE FACTORS
        DO 30 J=1,NSETS
        YMAX(J)=0.
        DC=0.0
        DO 37 K=1,NPTS-1
 37     DC=DC+Y(J,K)
        DC=DC/(NPTS-1)
        WRITE(0,*) 'DC=', DC
        DO 20 I=1,NPTS
        Y(J,I)=SCALE(J)*(Y(J,I)-DC)
 20     IF (ABS(Y(J,I)) .GT. YMAX(J))
          YMAX(J)=ABS(Y(J,I))
 30     CONTINUE
C       WRITE THE SCALED DATA
        DO 40 J=1,NSETS
 40     WRITE(0,1010)
          J,YMAX(J),(Y(J,I),I=1,NPTS)
 1010   FORMAT(// ,SET NO.',I4,' PEAK
          ABSOLUTE VALUE:',
        *F16.10/' Y-COORDINATES AFTER
          SCALING:'(/5E11.4))
        DO 50 I=1,NPTS
 50     X(I)=FLOAT(I-1)
        NSPACE=NPTS-1
        DEGMULT = 360.0/NSPACE
```


ISBN 978-0-12-369536-9
© Elsevier Inc. All rights reserved.

```
      DO 19 J=1,NPTS
      X(J) = X(J)*DEGMULT
   19 IF (J.EQ.NPTS) X(J) =
        X(J)+0.001
      OPEN(10,FILE='FODA01.
     C  DAT',STATUS='OLD')
      WRITE (0,*) 'THE NUMBER OF
        KNOWN POINT (NPTS) IS
        ',NPTS
      WRITE (0,*) 'THE NUMBER OF
        DATA SETS (NSETS) IS'
        ,NSETS
      WRITE (0,*) 'THE KNOWN POINTS
        OF X AND F(X) ARE : '
     C  THIS PART IS BASED ON THE
        ALGORITHMS IN PAGE 119
     C  OF VANDERGRAFT.
      OM = 314.1592654
      GA = 0.017453292
      PI=3.141593
      INTF=42
      INT=42
      INC=5
      NW=1
      NH=29
      RADIN = PI/20.5
      DEGIN = 180./20.5
      T1 = -RADIN
      T2 = -DEGIN
      DO 22 I=1,INT
      T1 = T1+RADIN
      RAD(I) = T1
      T2 = T2+DEGIN
      DEG(I) = T2
   22 CONTINUE
      Write(0,*) (RAD(I), I=1,NPTS)
      Write(0,*) (DEG(I), I=1,NPTS)
      DO 1 J=1,NH+1
      CURVC(J) =0.0
      CURVS(J) =0.0
      CURVT(J) =0.0
      CURVP(J) =0.0
    1 CONTINUE
      DO 17 I=1,361
      XV(I)=FLOAT(I)-1.0
   17 CONTINUE
      DO 12 J=1,NSETS
      NC=J
      DO 13 I=1,361
      YVALUE(I) = Y(J,I)
   13 CONTINUE
      YMAX(J)=0.0
      DO 137 I=1,361
      IF(YVALUE(I) .GE. YMAX(J))
        YMAX(J)=YVALUE(I)
  137 CONTINUE
      WRITE(0,*)'J=',J
      WRITE(0,*)'YMAX(J)=',YMAX(J)
      WRITE(0,1013)
        J,YMAX(J),(YVALUE(I),I=1,NPTS)
 1013 FORMAT(// 'SET NO.',I4,' PEAK
        ABSOLUTE VALUE:',
     *F16.10/' Y-COORDINATES AFTER
        SCALING:'(/5E11.4))
      CALL HARM
        (YVALUE,CURVC,CURVS,CURVT,CURVP)
      DO 133 I=1,NH
  133 AMP(J,I)=CURVT(I)
      DO 144 I=1,NH
  144 ANG(J,I)=CURVP(I)
      DO 14 K=1,NH
      CURVP(K) = CURVP(K)/GA
   14 CONTINUE
      WRITE(0,*)
        '********MAIN*************'
      WRITE(0,*) 'CURVT(',NH,J,')=:'
      WRITE(0,100)(CURVT(K),K=1,NH)
      WRITE(0,*) 'THE COSINE BASED
        PHASOR ANGLES ARE:'
      WRITE(0,100)(-CURVT(K)-90.,
        K=1,NH)
      WRITE(0,*)'THE MAGNITUDE OF
        THE HARMONICS AS A',
     *'PERCENTAGE OF THE
        FUNDAMENTAL:'
      IF (CURVT(1) .EQ.0.00000) THEN
      WRITE(0,100) (0.0, K=1,NH)
      ELSE
      WRITE(0,100)(100.*CURVT(K)/
        CURVT(1),K=1,NH)
      END IF
   12 CONTINUE
  100 FORMAT (6(1X,1PE11.4))
      ENDFILE(10)
      REWIND 10
      CLOSE(10)
      THDI=0.0
      Do 1111 K=2,NH
 1111 THDI=THDI+(CURVT(K))*(CURVT(K))
      THDIFINAL=(SQRT(THDI))/
        CURVT(1)
      WRITE(0,*) THDIFINAL
      RMSIWITHOUT=0
      Do 1112 K=1,NH
 1112 RMSIWITHOUT=RMSIWITHOUT
        +(CURVT(K))*(CURVT(K))
```



```
      RMSIWITHOUTF=(SQRT
        (RMSIWITHOUT))/10.
      WRITE(0,*) RMSIWITHOUTF
      RMSIWITH=(DC)*(DC)
      Do 1113 K=1,NH
 1113 RMSIWITH=RMSIWITH+(CURVT(K))*
        (CURVT(K))
      RMSIWITHF=(SQRT(RMSIWITH))/10.
      WRITE(0,*) RMSIWITHF
      STOP
      END
      SUBROUTINE HARM (VALUE,COMPC,
        COMPS,COMPT,COMPP)
      COMMON NW,DEG(361),RAD(361),
        XV(361),YVALUE(361)
      COMMON NPTS,NPS,INT,INC,NH,GA,
        PI,WW,OM,NC,RF,ER,EL
      COMMON ERR,ITMAX
      DIMENSION VALUE(361),
        COMPC(100),COMPS(100),
        COMPT(100)
      DIMENSION COMPP(100),
        VALUEC(361)
      CHECK=1.0
      WRITE(0,1013) (VALUE(I),
        I=1,NPTS)
 1013 FORMAT(// ' Y-COORDINATES
        AFTER SCALING:'(/5E11.4))
      P=SQRT(0.6)
      A1=5./9.
      A2=8./9.
      FK1=0.5*P*(1.+P)
      FK2=(1.+P)*(1.-P)
      FK3=0.5*P*(P-1.)
      DO 44 J=1,NH
      DL1=0.0
      DL2=0.0
      H=FLOAT(J)
      DO 33 I=1,INT-2,2
      T1=H*(RAD(I))
      T2=H*(RAD(I+1))
      T3=H*(RAD(I+2))
      X1=FK1*T1+FK2*T2+FK3*T3
      X2=T2
      X3=FK3*T1+FK2*T2+FK1*T3
      C1=VALUE(I)
      C2=VALUE(I+1)
      C3=VALUE(I+2)
      C4=FK1*C1+FK2*C2+FK3*C3
      C6=FK3*C1+FK2*C2+FK1*C3
      D1=C4*COS(X1)
      D2=C2*COS(X2)
      D3=C6*COS(X3)
      D4=C4*SIN(X1)
      D5=C2*SIN(X2)
      D6=C6*SIN(X3)
      DL1=DL1+A1*(D1+D3)+A2*D2
      DL2=DL2+A1*(D4+D6)+A2*D5
   33 CONTINUE
      COMPC(J)=DL1*2./41.
      COMPS(J)=DL2*2./41.
      COMPT(J)=SQRT(COMPC(J)**2
        +COMPS(J)**2)
      If (COMPS(J).EQ.0.00000) THEN
      COMPP(J)=0.0
      ELSE

        COMPP(J)=-ATAN(COMPC(J)/COMPS(J))
      END IF
      IF (COMPS(J) .LT. 0.0)
        COMPP(J)= COMPP(J)+PI
   44 CONTINUE
      WRITE(0,*)
        '*******SUBROUTINE*********'
      WRITE(0,*) 'COMPT(',NH,J,')=:'
      WRITE(0,100)(COMPT(K),K=1,NH)
      WRITE(0,*) 'THE COSINE BASED
        PHASOR ANGLES ARE:'
      WRITE(0,100)(-COMPT(K)-90.,
        K=1,NH)
      WRITE(0,*)'THE MAGNITUDE OF
        THE HARMONICS AS A',
     *'PERCENTAGE OF THE
        FUNDAMENTAL:'
  100 FORMAT (6(1X,1PE11.4))
      NWW=1*NW
      IF ((CHECK.EQ.1) .AND. (NC
        .EQ. NWW)) THEN
      EMDIF = 0
      DO 51 I=1,INT
      VALUEC(I)=0.
      DO 52 J=1,NH,1
      H=FLOAT(J)
      VALUEC(I)=VALUEC(I)
        +COMPC(J)*COS(H*RAD(I))+
     *COMPS(J)*SIN(H*RAD(I))
   52 CONTINUE
      DIF=ABS(VALUE(I)-VALUEC(I))
      IF (DIF.GT.EMDIF) THEN
      EMDIF=DIF
      DIFN=FLOAT(I)
      ENDIF
   51 CONTINUE
      WRITE(0,*)
        '***CHECKING FOURIER
        ANALYSIS*'
```

ST. GEORGE COLLEGE OF LA...

```
      WRITE(0,*)
      WRITE(0,*) 'VALUE(361) AT
        NC=',NC
      WRITE(0,1001) (VALUE(I),
        I=1,42)
      WRITE(0,1001) (VALUEC(I),
        I=1,42)
1001  FORMAT (10(1X,1PE11.4))
      WRITE(0,*) 'THE MAXIMUM
        DIFFERENCE IS :',EMDIF,'AT
        I=', DIFN
      ENDIF
      RETURN
      END
```

## A2.2 OUTPUT OF THE FOURIER ANALYSIS PROGRAM

The output of the Fourier program for a square wave is as follows:

```
 SET NO.    1 SCALE FACTOR:
  1.0000000000
Y-COORDINATES BEFORE SCALING:

 0.1000E+01 0.1000E+01 0.1000E+01
 0.1000E+01 0.1000E+01

 0.1000E+01 0.1000E+01 0.1000E+01
 0.1000E+01 0.1000E+01

 0.1000E+01 0.1000E+01 0.1000E+01
 0.1000E+01 0.1000E+01

 0.1000E+01 0.1000E+01 0.1000E+01
 0.1000E+01 0.1000E+01

-0.1000E+01-0.1000E+01-0.1000E
  +01-0.1000E+01-0.1000E+01

-0.1000E+01-0.1000E+01-0.1000E
  +01-0.1000E+01-0.1000E+01

-0.1000E+01-0.1000E+01-0.1000E
  +01-0.1000E+01-0.1000E+01

-0.1000E+01-0.1000E+01-0.1000E
  +01-0.1000E+01-0.1000E+01

-0.1000E+01 0.1000E+01
 DC=    -2.43902E-02

SET NO.    1 PEAK ABSOLUTE VALUE:
  1.0243902206
 Y-COORDINATES AFTER SCALING:

 0.1024E+01 0.1024E+01 0.1024E+01
 0.1024E+01 0.1024E+01
```



```
 0.1024E+01 0.1024E+01 0.1024E+01
 0.1024E+01 0.1024E+01

 0.1024E+01 0.1024E+01 0.1024E+01
 0.1024E+01 0.1024E+01

0.1024E+01 0.1024E+01 0.1024E+01
 0.1024E+01 0.1024E+01

-0.9756E+00-0.9756E+00-0.9756E
  +00-0.9756E+00-0.9756E+00

-0.9756E+00-0.9756E+00-0.9756E
  +00-0.9756E+00-0.9756E+00

-0.9756E+00-0.9756E+00-0.9756E
  +00-0.9756E+00-0.9756E+00

-0.9756E+00-0.9756E+00-0.9756E
  +00-0.9756E+00-0.9756E+00

-0.9756E+00 0.1024E+01

 THE NUMBER OF KNOWN POINT (NPTS)
  IS      42
 THE NUMBER OF DATA SETS (NSETS)
  IS   1
 THE KNOWN POINTS OF X AND F(X) ARE :
    0.     0.153248     0.306497
  0.459745     0.612994     0.766242
  0.919491      1.07$
       1.22599      1.37924      1.53248
  1.68573      1.83898      1.99223
  2.14548
       2.29873      2.45198      2.60522
  2.75847      2.91172      3.06497
  3.21822
       3.37147      3.52472      3.67796
  3.83121      3.98446      4.13771
  4.29096
       4.44421      4.59745      4.75070
  4.90395      5.05720      5.21045
  5.36370
       5.51694      5.67019      5.82344
  5.97669      6.12994      6.28319
    0.      8.78049      17.5610
  26.3415      35.1220      43.9024
  52.6829      61.4$
       70.2439      79.0244      87.8049
  96.5854      105.366      114.146
  122.927
       131.707      140.488      149.269
  158.049      166.829      175.610
  184.390
       193.171      201.951      210.732
  219.512      228.293      237.073
  245.854
```





```
       254.634      263.415      272.195
  280.976      289.756      298.537
  307.317
       316.098      324.878      333.659
  342.439      351.220      360.000
 J=   1
 YMAX(J)=       1.02439

 SET NO.    1 PEAK ABSOLUTE VALUE:
  1.0243902206
 Y-COORDINATES AFTER SCALING:

 0.1024E+01 0.1024E+01 0.1024E+01
 0.1024E+01 0.1024E+01

 0.1024E+01 0.1024E+01 0.1024E+01
 0.1024E+01 0.1024E+01

 0.1024E+01 0.1024E+01 0.1024E+01
 0.1024E+01 0.1024E+01

 0.1024E+01 0.1024E+01 0.1024E+01
 0.1024E+01 0.1024E+01

-0.9756E+00-0.9756E+00-0.9756E
  +00-0.9756E+00-0.9756E+00

-0.9756E+00-0.9756E+00-0.9756E
  +00-0.9756E+00-0.9756E+00

-0.9756E+00-0.9756E+00-0.9756E
  +00-0.9756E+00-0.9756E+00

-0.9756E+00-0.9756E+00-0.9756E
  +00-0.9756E+00-0.9756E+00

-0.9756E+00 0.1024E+01

 Y-COORDINATES AFTER SCALING:

 0.1024E+01 0.1024E+01 0.1024E+01
 0.1024E+01 0.1024E+01

 0.1024E+01 0.1024E+01 0.1024E+01
 0.1024E+01 0.1024E+01

 0.1024E+01 0.1024E+01 0.1024E+01
 0.1024E+01 0.1024E+01

 0.1024E+01 0.1024E+01 0.1024E+01
 0.1024E+01 0.1024E+01

-0.9756E+00-0.9756E+00-0.9756E
  +00-0.9756E+00-0.9756E+00

-0.9756E+00-0.9756E+00-0.9756E
  +00-0.9756E+00-0.9756E+00

-0.9756E+00-0.9756E+00-0.9756E
  +00-0.9756E+00-0.9756E+00

-0.9756E+00-0.9756E+00-0.9756E
  +00-0.9756E+00-0.9756E+00

-0.9756E+00 0.1024E+01
 ************SUBROUTINE**********
 COMPT(   29   30)=:
  1.2717E+00   3.4488E-02   4.1969E-01
  3.6450E-02   2.4608E-01   3.8742E-02
  1.6870E-01   4.0489E-02   1.2299E-01
  4.1067E-02   9.1722E-02   4.0183E-02
  6.8664E-02   3.7860E-02   5.1330E-02
  3.4436E-02   3.8801E-02   3.0685E-02
  3.1712E-02   3.8456E-02   3.7949E-02
  2.5107E-02   2.4685E-02   2.1601E-02
  2.5122E-02   2.0924E-02   2.7380E-02
  2.2261E-02   3.0684E-02
 THE COSINE BASED PHASOR ANGLES ARE:
 -9.1272E+01 -9.0034E+01 -9.0420E+01
 -9.0036E+01 -9.0246E+01 -9.0039E+01
 -9.0169E+01 -9.0040E+01 -9.0123E+01
 -9.0041E+01 -9.0092E+01 -9.0040E+01
 -9.0069E+01 -9.0038E+01 -9.0051E+01
 -9.0034E+01 -9.0039E+01 -9.0031E+01
 -9.0032E+01 -9.0038E+01 -9.0038E+01
 -9.0025E+01 -9.0025E+01 -9.0022E+01
 -9.0025E+01 -9.0021E+01 -9.0027E+01
 -9.0022E+01 -9.0031E+01
 THE MAGNITUDE OF THE HARMONICS AS
  APERCENTAGE OF THE FUNDAMENTAL:
 *** CHECKING FOURIER ANALYSIS*

VALUE(361) AT NC=   1
  1.0244E+00   1.0244E+00   1.0244E+00
  1.0244E+00   1.0244E+00   1.0244E+00
  1.024$
  1.0244E+00   1.0244E+00   1.0244E+00
  1.0244E+00   1.0244E+00   1.0244E+00
  1.024$
 -9.7561E-01 -9.7561E-01 -9.7561E-01
 -9.7561E-01 -9.7561E-01 -9.7561E-01
 -9.756$
 -9.7561E-01 -9.7561E-01 -9.7561E-01
 -9.7561E-01 -9.7561E-01 -9.7561E-01
 -9.756$
 -9.7561E-01   1.0244E+00
  5.0335E-01   1.1156E+00   9.8548E-01
  1.0407E+00   9.6388E-01   1.0831E+00
  9.720$
  9.5716E-01   1.0451E+00   9.9427E-01
  1.0748E+00   9.3542E-01   1.0637E+00
  1.022$
 -8.8539E-01 -9.6836E-01 -9.0364E-01
 -1.0717E+00 -9.4528E-01 -9.9542E-01
 -9.457$
```

ST. GEORGE SCHOOL OF LAW

```
-9.5329E-01 -1.0331E+00 -9.2584E-01
-1.0258E+00 -9.5068E-01 -1.0254E+00
-9.310$
-5.0985E-01  5.0335E-01
THE MAXIMUM DIFFERENCE IS :
 0.521040AT I=     1.00000
**********MAIN******************

CURVT(  29   1)=:
 1.2717E+00  3.4488E-02  4.1969E-01
3.6450E-02  2.4608E-01  3.8742E-02
 1.6870E-01  4.0489E-02  1.2299E-01
4.1067E-02  9.1722E-02  4.0183E-02
 6.8664E-02  3.7860E-02  5.1330E-02
3.4436E-02  3.8801E-02  3.0685E-02
 3.1712E-02  3.8456E-02  3.7949E-02
2.5107E-02  2.4685E-02  2.1601E-02
 2.5122E-02  2.0924E-02  2.7380E-02
 2.2261E-02  3.0684E-02
THE COSINE BASED PHASOR ANGLES ARE:
-9.1272E+01 -9.0034E+01 -9.0420E+01
 -9.0036E+01 -9.0246E+01 -9.0039E+01
-9.0169E+01 -9.0040E+01 -9.0123E+01
```



```
 -9.0041E+01 -9.0092E+01 -9.0040E+01
-9.0069E+01 -9.0038E+01 -9.0051E+01
 -9.0034E+01 -9.0039E+01 -9.0031E+01
-9.0032E+01 -9.0038E+01 -9.0038E+01
 -9.0025E+01 -9.0025E+01 -9.0022E+01
-9.0025E+01 -9.0021E+01 -9.0027E+01
 -9.0022E+01 -9.0031E+01
THE MAGNITUDE OF THE HARMONICS AS
 APERCENTAGE OF THE FUNDAMENTAL:
 1.0000E+02   2.7118E+00   3.3001E+01
2.8661E+00   1.9350E+01   3.0463E+00
 1.3265E+01 3.1837E+00 9.6712E+00
3.2292E+00 7.2123E+00 3.1597E+00
 5.3992E+00  2.9770E+00 4.0362E+00
2.7078E+00 3.0510E+00 2.4128E+00
 2.4936E+00  3.0239E+00 2.9840E+00
1.9742E+00 1.9410E+00 1.6985E+00
 1.9754E+00 1.6453E+00 2.1530E+00
1.7504E+00 2.4127E+00
    0.444086
    0.139151
    0.139172
```

ST. GEORGE COLLEGE OF LAW

3
APPENDIX

# Program List for Propagation of a Surge through a Distribution Feeder with an Insulator Flashover (Application Example 2.9)

```
lightning performance of a
 transmission line
*lightning current source
i1 1 0 exp(0 15.4k 0 1.0u 2.0111u
 5u)
*span#1
t1 1 0 3 0 z0=300 f=60 NL=100u
*insulator #1
d1 13 3 DMOD
L1 13 53 20u
vs1 23 53 dc 0
w1 23 33 vs1 wmod1
rvs1 33 43 20
vd1 0 43 3700k
rft1 23 0 20
*span#2
t2 3 0 5 0 z0=300 f=60 NL=200u
*insulator #2
d2 15 5 dmod
L2 15 55 20u
vs2 25 55 dc 0
w2 25 35 vs2 wmod1
rvs2 35 45 20
vd2 0 45 3700k
rft2 25 0 20
*span#3
t3 5 0 7 0 z0=300 f=60 NL=200u
*z
RL3 7 0 300
*span#4
t4 1 0 9 0 z0=300 f=60 NL=500u
*z
RL4 9 0 300
.model dmod d(is=1e-14)
.model wmod1 iswitch(ron=1 roff=1E6
 ion=1 ioff=1.01`)
.tran 0.1u 20u 0 0.05u
.options ITL4=200 ITL5=0
 LIMPTS=100000 RELTOL=0.001
.probe
*.print tran v(3) v(5) i(vs1) i(vs2)
.end
```


ISBN 978-0-12-369536-9
© Elsevier Inc.
All rights reserved.

ST. GEORGE COLLEGE OF

4

APPENDIX

# Program List for Lightning Arrester Operation (Application Example 2.10)

```
lightning performance of a
 transmission line, lightning
 arrester operation
*lightning current source
i1 1 0 exp(0 7.44k 0 1.0u 2.011u 5u)
*span#1
t1 1 0 3 0 z0=300 f=60 NL=100u
*insulator #1
d1 13 3 DMOD
L1 13 53 20u
vs1 23 53 dc 0
w1 23 33 vs1 wmod1
rvs1 33 43 20
vd1 0 43 3700k
rft1 23 0 20
*span#2
t2 3 0 5 0 z0=300 f=60 NL=200u
*insulator #2
d2 15 5 dmod
L2 15 55 20u
vs2 25 55 dc 0
w2 25 35 vs2 wmod1
rvs2 35 45 20
vd2 0 45 600k
rft2 25 0 20
*span#3
t3 5 0 7 0 z0=300 f=60 NL=200u
*z
RL3 7 0 300
*span#4
t4 1 0 9 0 z0=300 f=60 NL=500u
*z
RL4 9 0 300
.model dmod d(is=1e-14)
.model wmod1 iswitch(ron=1 roff=1E6
 ion=1 ioff=1.01)
.tran 0.1u 20u 0 0.05u
.options ITL4=25 ITL5=0 LIMPTS=100000
 RELTOL=0.001
.probe
*.print tran v(3) v(5) i(vs1) i(vs2)
.end
```


ISBN 978-0-12-369536-8
© Elsevier Inc.
All rights reserved.

ST. GEORGE SCHOOL OF NURSE

5
APPENDIX

# Equipment for Tests

## A5.1 THE 9 kVA THREE-PHASE TRANSFORMER BANK

A *Y–Y* connected three-phase transformer bank with 416/416 V of rated line-to-line voltages consists of three single-phase transformers. The type numbers of the three single-phase transformers are J7065, J7610, and J7065 (bank #1), and the nameplate data are

| | |
|---|---|
| Powerformer | Dry-type transformer |
| CAT. NO.: 211-101 | 3 kVA, single-phase, 60 Hz |
| High voltage: 240/480 V | Low voltage: 120/240 V |

## A5.2 THE 4.5 kVA THREE-PHASE TRANSFORMER BANK #1

Single-phase transformers with the nameplate data listed in Section A5.1 are used in transformer bank #1 and are connected in such a way that the rated line-to-line voltages are 240/240 V. Only the two high-voltage windings of each single-phase transformer are employed as primary and secondary, and the rated apparent power of the three-phase transformer bank is therefore 4.5 kVA.

## A5.3 THE 4.5 kVA THREE-PHASE TRANSFORMER BANK #2

Single-phase transformers with the nameplate data listed in Section A5.1 having the type numbers J7605, J7606, and J7605 are used in transformer bank #2, and are connected in such a way that the rated line-to-line voltages are 240/240 V. Only the two high-voltage windings of each single-phase transformer are employed as primary and secondary, and the rated apparent power of the three-phase transformer bank is therefore 4.5 kVA.

## A5.4 THE 15 kVA THREE-PHASE TRANSFORMER BANK

The 15 kVA, 240/240, Δ–Δ connected bank consists of three 5 kVA transformers. The original rated apparent power of the single-phase units is 10 kVA. The two high-voltage windings are used as primary and secondary, and the rated power of the bank is therefore 15 kVA. The nameplate data are

| | |
|---|---|
| Westinghouse | Type: EP transformer |
| Frame NO.: 179 | 10 kVA, single-phase, 60 Hz |
| High voltage: 240/480 V | Low voltage: 120/240 V |

## A5.5 THREE-PHASE DIODE BRIDGE

$I_{max} = 100$ A, $V_{max} = 1200$ V.

## A5.6 HALF-CONTROLLED THREE-PHASE SIX-STEP INVERTER

General Electric AC adjustable frequency drive:

Model NO.: 6VGAW2007C1

| Input: | Output: |
|---|---|
| Volts: 230 | HP: 7.5 |
| Hertz: 50/60 | kVA: 8.8 |
| Amps.: 22 | Volts: variable |
| Phase 3 | Hertz: 6–60 |
| | Amps. AC: variable |
| | Phase 3 |

## A5.7 CONTROLLED THREE-PHASE RESONANT RECTIFIER [12, CHAPTER 2]

University of Colorado:

ID NO.: 5484

| Input: | Output: |
|---|---|
| Volts: 340–600 AC | 20 kW |
| Hertz: 12–60 | Volts: 380 DC |
| Amps.: 45 | Amps.: 60 DC |
| Phase 3 | |

## A5.8 CONTROLLED THREE-PHASE PWM INVERTER [12, CHAPTER 2]

University of Colorado:

ID NO.: 5485

| Input: | Output: |
|---|---|
| Volts: 360 DC | 20 kW |
| Amps.: 70 DC | Volts: 240 AC |
| | Amps.: 80 AC |
| | Power factor: 0.7 (lead, generator notation) to 1.0 pu |
| | Hertz: 50/60 |


ISBN 978-0-12-369536-9
© Elsevier Inc.
All rights reserved.

# 6
APPENDIX

# Measurement Error of Powers

## A6.1 MEASUREMENT ERROR OF POWERS

Assume the input power of a load with power factor (lagging') between 0.6 and 1.0 is measured with a $CT$, an ammeter, a $PT$, and a voltmeter, as shown in Fig. A6.1. The ammeter and the voltmeter have an error of $\varepsilon_A$ and $\varepsilon_V$, respectively. The $CT$ has a ratio correction factor $RCF_{CT}$ and a phase angle shift $\gamma$ measured in minutes. The $PT$ has a ratio correction factor $RCF_{PT}$ and a phase angle shift $\beta$ measured in minutes [97–100, Chapter 8].

The input power is expressed as

$$P = V\,I\cos\Omega.$$

The measurement error of the input power is given by

$$\frac{\Delta P}{P} = \frac{\Delta V}{V} + \frac{\Delta I}{I} - \frac{\sin\varphi\cdot\Delta\varphi}{\cos\varphi},$$

$$= \left(RCF_{PT} - 1 + \frac{\varepsilon_V}{V}\right) + \left(RCF_{CT} - 1 + \frac{\varepsilon_A}{I}\right) - \frac{\sin\varphi}{\cos\varphi}\frac{\pi(\beta-\gamma)}{180\times 60}.$$

For power factors ranging from 0.6 to 1.0 (lagging, based on consumer notation), the worst case in power measurement error is when $\cos\varphi = 0.6$, therefore,

$$\frac{\Delta P}{P} \approx \left(RCF_{PT} - 1 + \frac{\varepsilon_V}{V}\right) + \left(RCF_{CT} - 1 + \frac{\varepsilon_A}{I}\right) - \frac{(\beta-\gamma)}{2600},$$

$$= \left(TCF_{PT} - 1 + \frac{\varepsilon_V}{V}\right) + \left(TCF_{CT} - 1 + \frac{\varepsilon_A}{I}\right)$$
$$= \left(\frac{\varepsilon_{PT} + \varepsilon_V}{V}\right) + \left(\frac{\varepsilon_{CT} + \varepsilon_A}{I}\right),$$

where

$$TCF_{CT} = RCF_{CT} + \gamma/2600,$$

$$TCF_{PT} = RCF_{PT} - \beta/2600,$$

$$\varepsilon_{CT} = (TCF_{CT} - 1)\cdot I,$$

$$\varepsilon_{PT} = (TCF_{PT} - 1)\cdot V.$$

According to American National Standard [97, Chapter 8], transformer correction factors $TCF_{CT}$ and $TCF_{PT}$ ($\varepsilon_{CT}$ and $\varepsilon_{PT}$) can directly be obtained based on the accuracy class from the device nameplates. Normally, the maximum absolute errors for ammeters and voltmeters are based on the full-scale errors. For instrument transformers, the maximum absolute errors ($\varepsilon_{CT}$ and $\varepsilon_{PT}$) are proportional to the actually measured values of currents and voltages, as derived above.

Note that the maximum errors of an instrument transformer derived above are systematic errors that can be reduced by ratio and angle corrections. If the measured results are not corrected, the overall uncertainty of measurement is derived from the systematic uncertainty and random uncertainty:

$$u = \sqrt{u_s^2 + u_r^2}.$$

The random uncertainty is normally much smaller than the systematic uncertainty and can be ignored; therefore,

$$u = u_s = \varepsilon_{CT} \text{ or } \varepsilon_{PT}.$$

## A6.2 NAMEPLATE DATA OF MEASURED TRANSFORMERS

**3 kVA single-phase transformers**

| | |
|---|---|
| Powerformer | Dry-type transformer |
| CAT. NO.: 211-101 | 3 kVA, single-phase, 60 Hz |
| High voltage: 240/480 V | Low voltage: 120/240 V |

**4.5 kVA three-phase transformer bank.** Three single-phase transformers with the nameplate data just listed for the 3 kVA single-phase transformers having the type numbers J7065, J7610, and J7065 are used in the three-phase transformer bank and are connected in $\Delta$–$Y_0$ with rated phase voltages of


ISBN 978-0-12-369536-9
© Elsevier Inc.
All rights reserved.

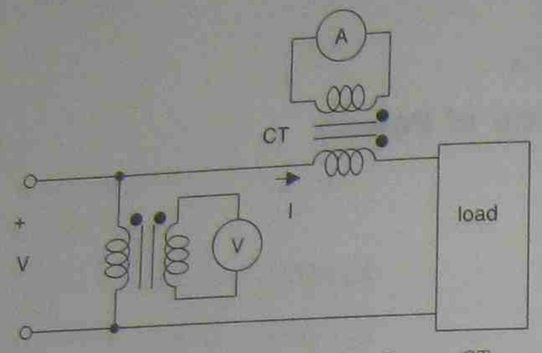



**FIGURE A6.1** Power measurement based on a *CT*, an ammeter, a *PT*, and a voltmeter.

240/240 V. Only the two high-voltage windings of each single-phase transformer are employed as primary and secondary, and the rated apparent power of the three-phase transformer bank is therefore 4.5 kVA.

**25 kVA single-phase transformer [101, Chapter 8]**

| | |
|---|---|
| ABB | MFG Date: July 93 |
| Serial #: 93A312106 | 25 kVA, 60 Hz |
| High voltage: 7200 V | Low voltage: 120/240 V |

ST. GEORGE COLLEGE LIBRARY

# 7
APPENDIX

# Solutions to Examples from Chapters

## CHAPTER 1 SOLUTIONS

### 1.4.18 Application Example 1.1: Calculation of Input/Output Currents and Voltages of a Three-Phase Thyristor Rectifier: Solution (see also Figure E1.1.3)

```
*thyristor rectifier
Va 1 2 SIN(0V  339.41V 60 Hz 0 0)
Vb 2 3 SIN(0V  339.41V 60 Hz 5.556m
 0)
Vc 3 3a SIN(0V 339.41V 60 Hz 11.111m
 0)
R3 3a 1 0.01
Rarb 14 0 .01
*5 deg delay = .231
*50 deg delay = 2.31
*150 deg delay = 6.94
*Vfet1 sp1 A1 pulse(0 15 .231m   1u
 1u 9m 16.667ms)
*Vfet2 sp2 A2 pulse(0 15 3.01m   1u
 1u 9m 16.667ms)
*Vfet3 sp3 A3 pulse(0 15 5.79m   1u
 1u 9m 16.667ms)
*Vfet4 sp4 A4 pulse(0 15 8.56m  1u
 1u 9m 16.667ms)
*Vfet5 sp5 A5 pulse(0 15 11.32m  1u
 1u 9m 16.667ms)
*Vfet6 sp6 A6 pulse(0 15 14.12m  1u
 1u 9m 16.667ms)
Vfet1 sp1 A1 pulse(0 15 2.31m   1u
 1u 9m 16.667ms)
Vfet2 sp2 A2 pulse(0 15 5.089m   1u
 1u 9m 16.667ms)
Vfet3 sp3 A3 pulse(0 15 7.869m   1u
 1u 9m 16.667ms)
Vfet4 sp4 A4 pulse(0 15 10.639m  1u
 1u 9m 16.667ms)
Vfet5 sp5 A5 pulse(0 15 13.399m  1u
 1u 9m 16.667ms)
Vfet6 sp6 A6 pulse(0 15 16.199m  1u
 1u 9m 16.667ms)
*Vfet1 sp1 A1 pulse(0 15 6.94m   1u
 1u 9m 16.667ms)
*Vfet2 sp2 A2 pulse(0 15 9.72m   1u
 1u 9m 16.667ms)
*Vfet3 sp3 A3 pulse(0 15 12.50m  1u
 1u 9m 16.667ms)
*Vfet4 sp4 A4 pulse(0 15 15.27m  1u
 1u 9m 16.667ms)
*Vfet5 sp5 A5 pulse(0 15 18.04m  1u
 1u 9m 16.667ms)
*Vfet6 sp6 A6 pulse(0 15 20.83m  1u
 1u 9m 16.667ms)
RAB 7 8 10Meg
M1 7  sp1 A1 A1 SMM
M2 14 sp2 A2 A2 SMM
M3 8  sp3 A3 A3 SMM
M4 14 sp4 A4 A4 SMM
M5 9  sp5 A5 A5 SMM
M6 14 sp6 A6 A6 SMM
La 1  4 300uH
Ra 4  7 0.05
Lb 2  5 300uH
Rb 5  8 0.05
Lc 3  6 300uH
Rc 6  9 0.05
d1 A1 13 D1N4001
d2 A2 12 D1N4001
L2 12  9 5nH
d3 A3 13 D1N4001
d4 A4 10 D1N4001
L4 10  7 5nH
d5 A5 13 D1N4001
d6 A6 11 D1N4001
L6 11  8 5nH
Lf 13 15 5mH
Cf 15 14 500u
R1 15 14 10
.model D1N4001 D(IS=1E-12)
.model SMM nmos(level=3 gamma=0
 delta=0 eta=0 theta=0
+ kappa=0 vmax=0 xj=0 tox=100n
 uo=600 phi=0.6 rs=42.69M kp=20.87u
+ l=2u w=2.9 vto=3.487 rd=0.19
 cbd=200n pb=0.8 mj=0.5 cgso=3.5n
+ cgdo=100p rg=1.2 is=10f)
```



© Elsevier Inc.
All rights reserved

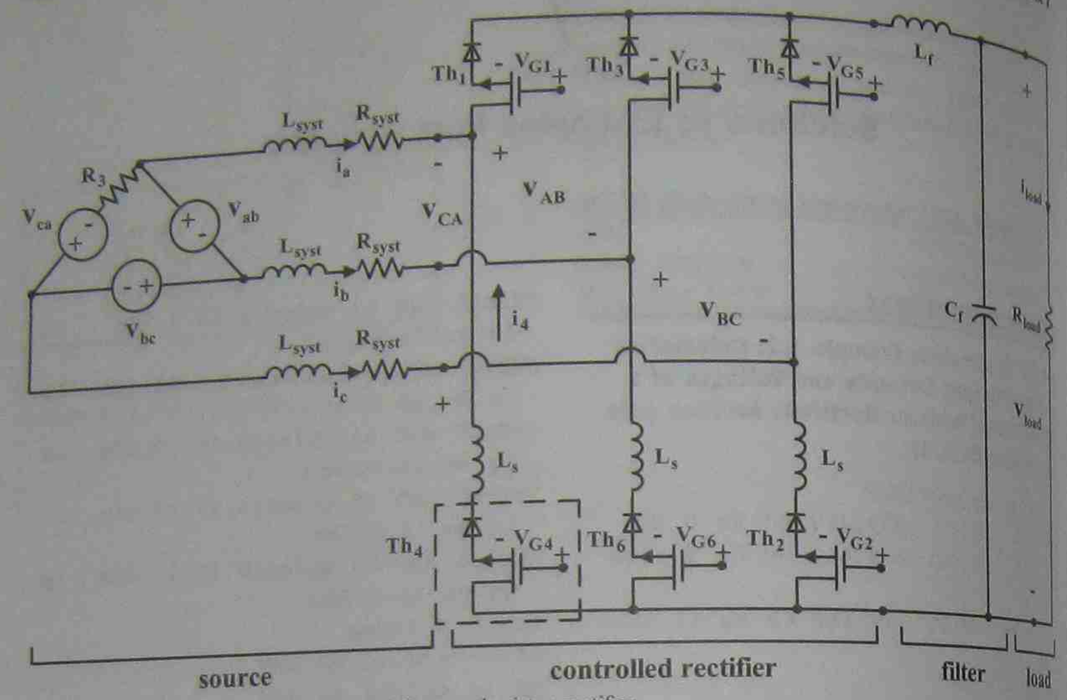



**FIGURE E1.1.1** Controlled three-phase, full-wave thyristor rectifier.

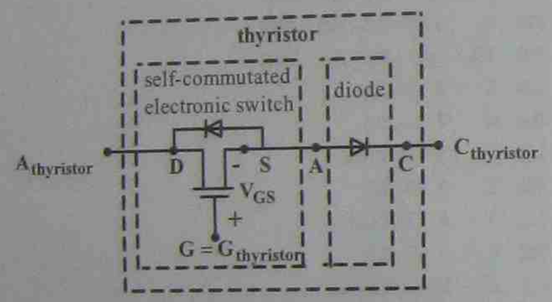



**FIGURE E1.1.2** Model for thyristor consisting of self-commuted switch and diode.

```
.tran .01u 60m 30m uic
.options abstol=1m chgtol=1m
 reltol=10m vntol=10m gmin=1m
.four 60 I(ra) V(RAB)
.probe
.end
```

### 1.4.19 Application Example 1.2: Calculation of Input/Output Currents and Voltages of a Three-Phase Rectifier with One Self-Commutated Electronic Switch: Solution (see also Figure E1.2.2)

```
*rectifier with one self-commutated
 switch
Va 1 2 SIN(0V 339.41V 60 Hz 0 0)
Vb 2 3 SIN(0V 339.41V 60 Hz 5.56m 0)
Vc 3 3a SIN(0V 339.41V 60 Hz 11.1m
 0)
R3 3a 1 0.1
Rarb 14 0 .1
RAB 7 8 10Meg
Vfet sp 15 pulse(0 15 0 1u 1u 833u
 1.67m)
M1 13 sp 15 15 SMM
La 1  4 10mH
Ra 4  7 0.05
Lb 2  5 10mH
Rb 5  8 0.05
Lc 3  6 10mH
Rc 6  9 0.05
d1 7 13 D1N4001
d2 14 12 D1N4001
L2 12 9 5nH
d3 8 13 D1N4001
d4 14 10 D1N4001
L4 10 7 5nH
d5 9 13 D1N4001
d6 14 11 D1N4001
L6 11 8 5nH
Df  14 15 D1N4001
Lf 15 16 5mH
Cf 16  14 500u
R1 16 14 10
```



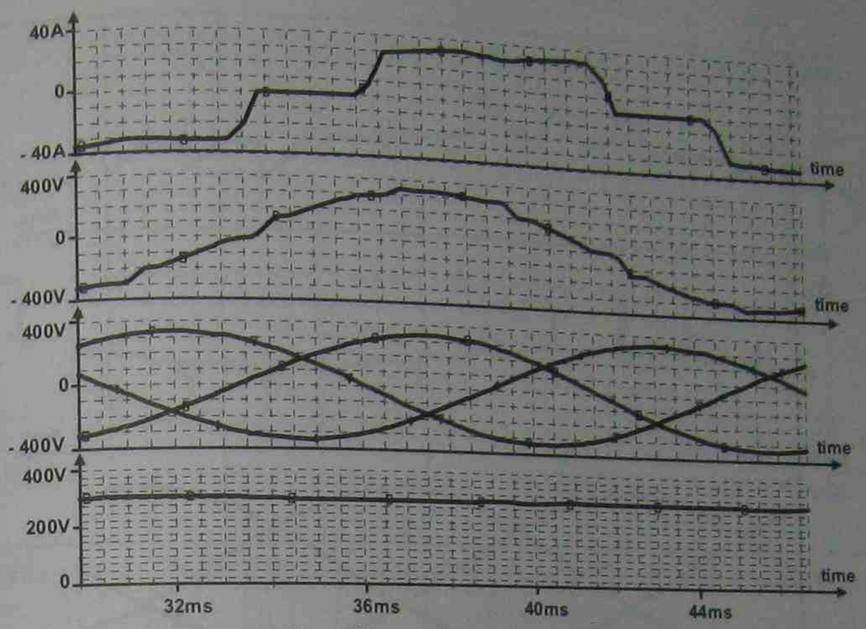



**FIGURE E1.1.3** Plots of input current $i_a$ (top), line-to-line voltage $v_{AB}$ (second from top), line-to-line voltages $v_{ab}$, $v_{bc}$, $v_{ca}$, and output voltage $v_{load}$ for a firing angle of $\alpha = 50°$.

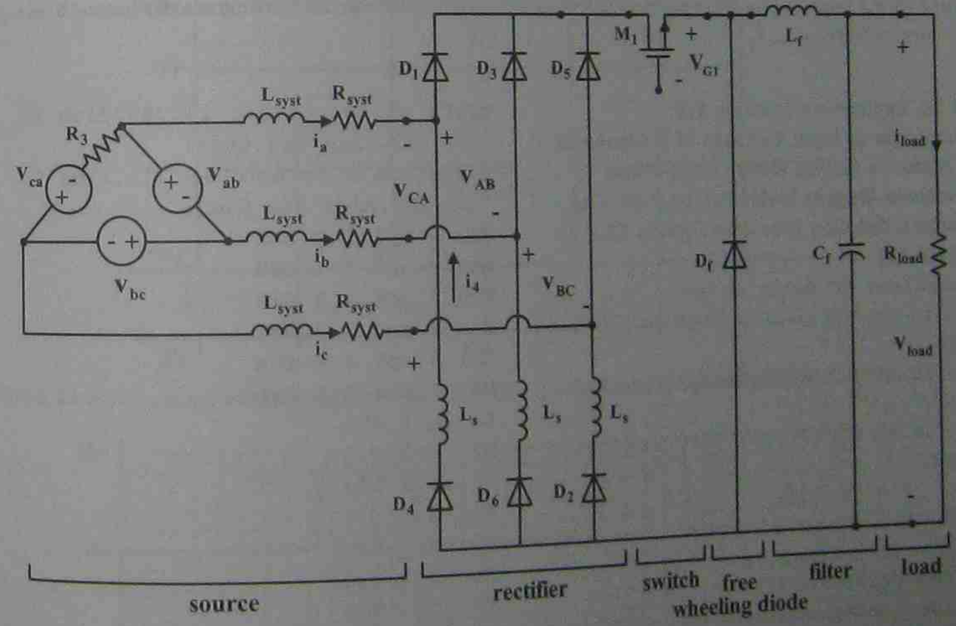



**FIGURE E1.2.1** Three-phase, full-wave rectifier with one self-commutated switch.

```
.model D1N4001 D(IS=1E-12)
.model SMM nmos(level=3 gamma=0
 delta=0 eta=0 theta=0
+ kappa=0 vmax=0 xj=0 tox=100n
 uo=600 phi=0.6 rs=42.69M kp=20.87u
+ l=2u w=2.9 vto=3.487 rd=0.19
 cbd=200n pb=0.8 mj=0.5 cgso=3.5n
+ cgdo=100p rg=1.2 is=10f)
.tran .010u 60m 30m uic
.options abstol=1m chgtol=1m
 reltol=10m vntol=10m gmin=1m
.four 60 I(ra) V(RAB)
.probe
.end
```

ST. GEORGE POLYTECHNIC LANE

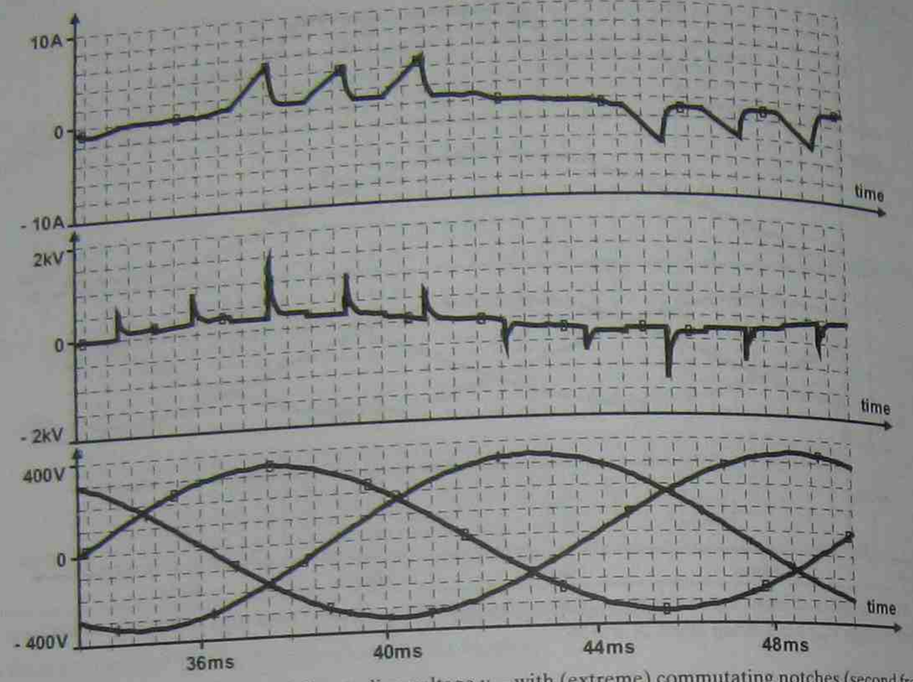



**FIGURE E1.2.2** Input line current $i_a$ (top), line-to-line voltage $v_{AB}$ with (extreme) commutating notches (second from top), line-to-line voltages $v_{ab}$, $v_{bc}$, $v_{ca}$.

### 1.4.20 Application Example 1.3: Calculation of Input Currents of a Brushless DC Motor in Full-on Mode (Three-Phase Permanent-Magnet Motor Fed by a Six-Step Inverter): Solution (see also Figures E1.3.3a to E1.3.3d)

```
*brushless DC motor drive
Va   1a st SIN(0 160V 1500 Hz   0 0
  60)
Vb   3a st SIN(0 160V 1500 Hz   0 0
  180)
Vc   5a st SIN(0 160V 1500 Hz   0 0
  300)
Vdc1   7 0 DC 150V
Vdc2   8 0 DC -150
Rshunt st 0 10Meg
*5 deg delay = .231
*50 deg delay = 2.31
*150 deg delay = 6.94
Vfet1 sp1 2 pulse(0 15 0
  1u 1u 222.22us 666.66us)
Vfet2 sp2 6 pulse(0 15 222.22us 1u
  1u 222.22us 666.66us)
Vfet3 sp3 4 pulse(0 15 444.44us 1u
  1u 222.22us 666.66us)
Vfet4 sp4 8 pulse(0 15 333.33us 1u
  1u 222.22us 666.66us)
Vfet5 sp5 8 pulse(0 15 555.51us 1u
  1u 222.22us 666.66us)
Vfet6 sp6 8 pulse(0 15 111.11us 1u
  1u 222.22us 666.66us)
Mau 7 sp1 2 2 SMM
Mbu 7 sp2 6 6 SMM
Mcu 7 sp3 4 4 SMM
Mal 2 sp4 8 8 SMM
Mbl 6 sp5 8 8 SMM
Mcl 4 sp6 8 8 SMM
L1 1a 1 50u
R1   1 2 0.5
L3 3a 3 50u
R3   3 4 0.5
L5 5a 5 50u
R5   5 6 0.5
C1 7 0 100u
C2 0 8 100u
Dau 2 7 D1N4001
Dbu 6 7 D1N4001
Dal 8 2 D1N4001
Dbl 8 6 D1N4001
Dcu 4 7 D1N4001
Dcl 8 4 D1N4001
.model D1N4001 D(IS=1E-12)
.model SMM nmos(level=3 gamma=0
  delta=0 eta=0 theta=0
```



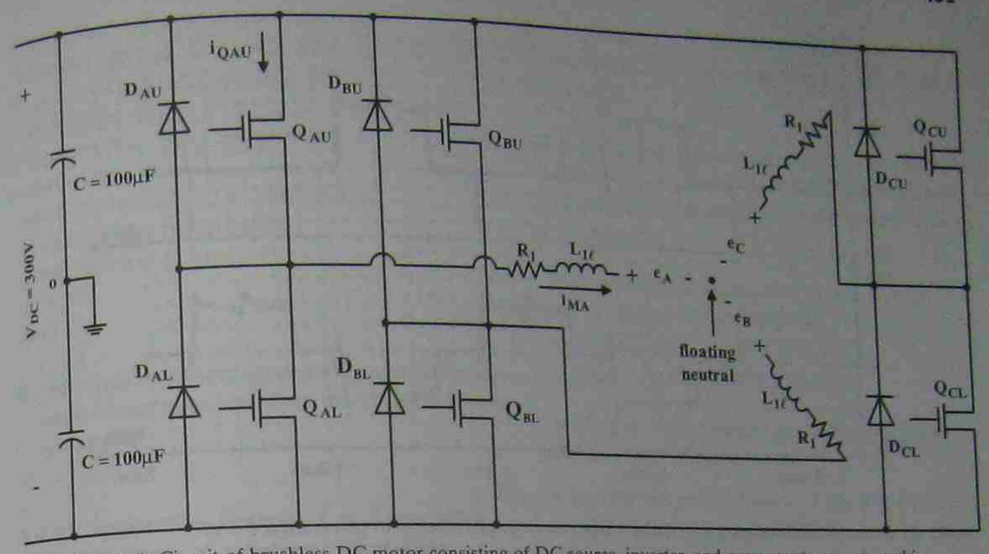



**FIGURE E1.3.1** Circuit of brushless DC motor consisting of DC source, inverter, and permanent-magnet machine.

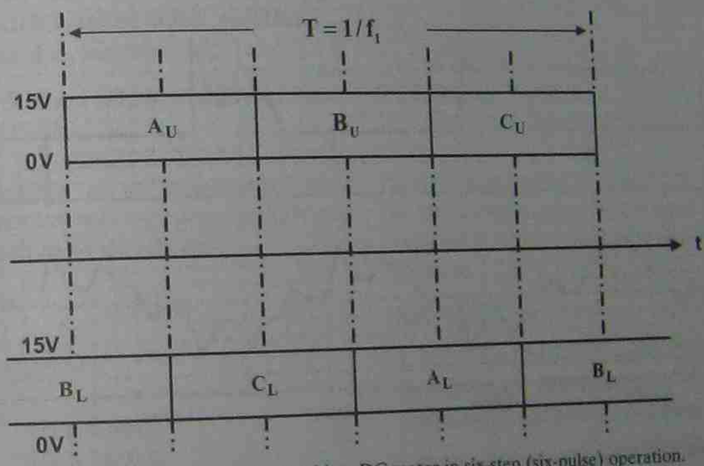



**FIGURE E1.3.2** Sequence of gating signals for brushless DC motor in six-step (six-pulse) operation.

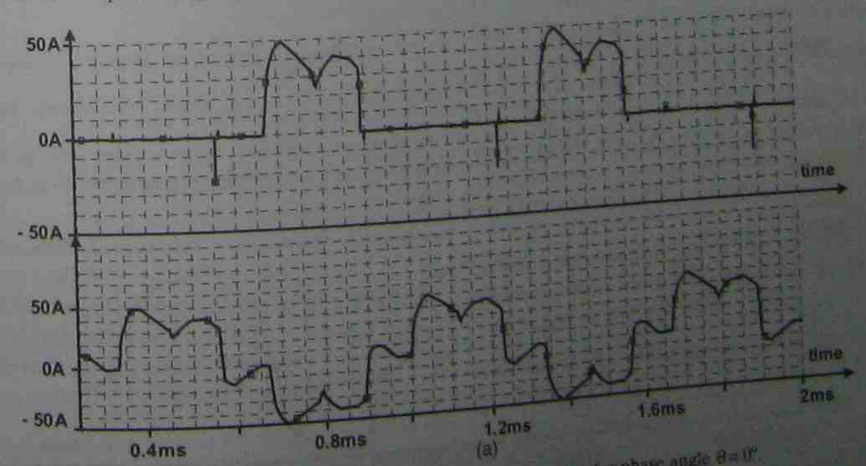



**FIGURE E1.3.3a** MOSFET (upper graph) and motor (lower graph) current for phase angle $\theta = 0°$.

ST. GEORGE COLLEGE OF LAW

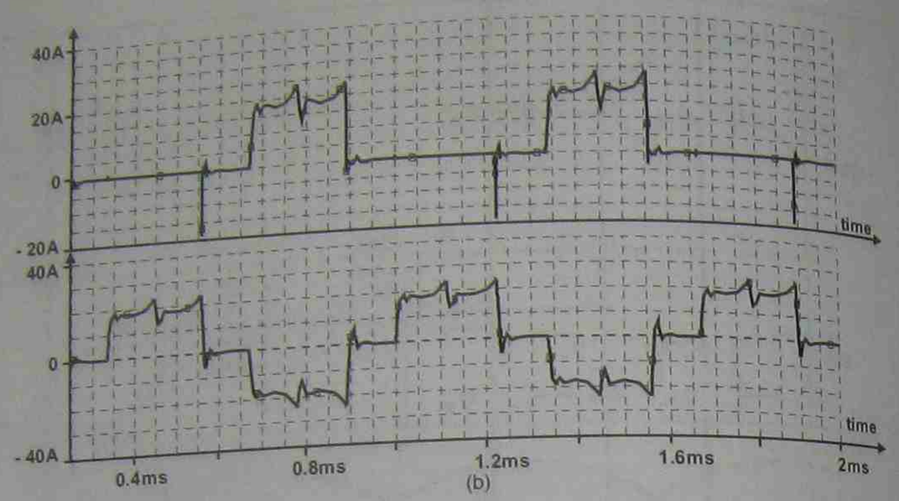



**FIGURE E1.3.3b** MOSFET (upper graph) and motor (lower graph) current for phase angle $\theta = 30°$.

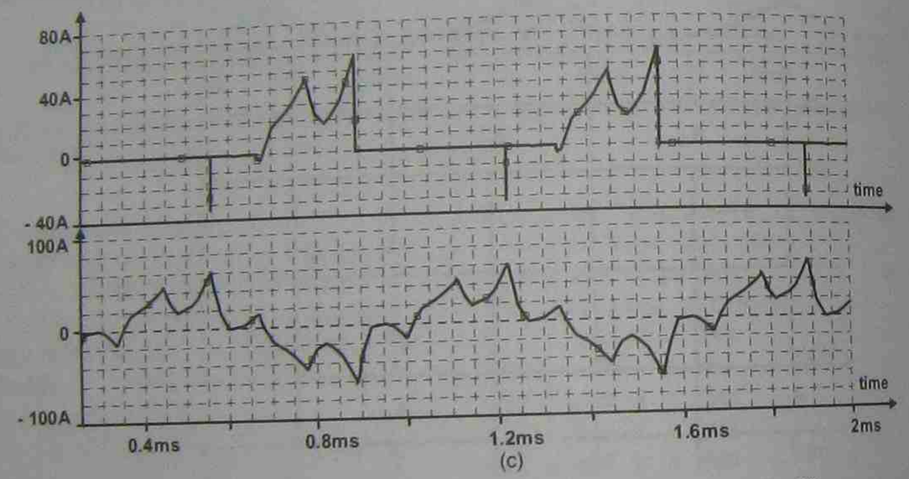



**FIGURE E1.3.3c** MOSFET (upper graph) and motor (lower graph) current for phase angle $\theta = 60°$.

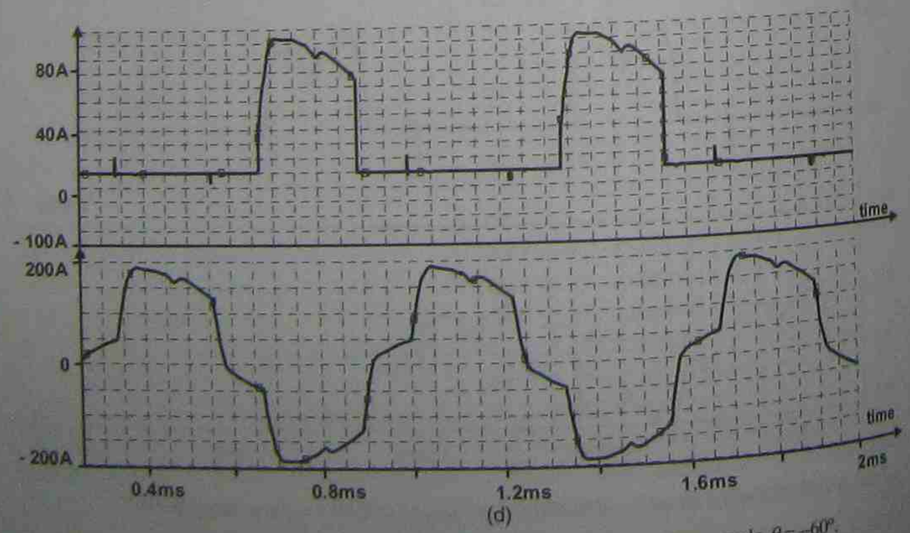



**FIGURE E1.3.3d** MOSFET (upper graph) and motor (lower graph) current for phase angle $\theta = -60°$.

ST. GEORGE POLYTECHNIC LIBRARY



```
+ kappa=0 vmax=0 xj=0 tox=100n
 uo=600 phi=0.6 rs=42.69m kp=20.87u
+ l=2u w=2.9 vto=3.487 rd=0.19
 cbd=200n pb=0.8 mj=0.5 cgso=3.5n
+ cgdo=100p rg=1.2 is=10f)
.tran .05u 2m uic
.options abstol=1m chgtol=1m
 reltol=10m vntol=10m
.four 1500 I(L1)
.probe
.end
```

b) The reversed phase sequence will result in nonperiodic waveshapes, and thus this solution is not meaningful.

### 1.4.21 Application Example 1.4: Calculation of the Efficiency of a Polymer Electrolyte Membrane (PEM) Fuel Cell Used as an Energy Source in a Variable-Speed Drive: Solution

a) The power efficiency is defined by

$\eta_{power}$ = (rated electrical output power)/(hydrogen input power) = $P_{out}/P_{in}$.

*Method #1.* The PEM fuel cell generates 0.87 liters or 0.87 kg of water per hour by converting hydrogen and oxygen according to the relation

$$2H_2 + O_2 = 2H_2O.$$

The atomic weights are

$$1H \triangleq 1.0080,$$
$$1O \triangleq 16.0000,$$
$$1H_2O \triangleq 18.0160,$$

The required mass of hydrogen to generate 0.87 liters of water per hour is $\frac{2}{18.0160}0.87$ kg = 0.09658 kg. The energy input per hour in form of hydrogen is (0.09658 kg)(28 kWh/kg) = 2704.26 Wh.

Output (electrical) power of PEM fuel cell $P_{out} = 1200$ W.
Input (hydrogen) power (or energy per hour) of PEM fuel cell $P_{in} = 2704.26$ W.
Power (energy per hour) efficiency $\eta_{power} = P_{out}/P_{in} = 0.4437$ pu = 44.4%.

*Method #2.* Hydrogen input power of PEM fuel cell is

$P_{in}$ = (mass density of hydrogen) (hydrogen consumption during one hour) (energy density of hydrogen).

With (hydrogen consumption during one hour) = 18.5 SLPM·60 minutes/hour = (18.5)(60) liters/hour = 1110 liters/hour, one obtains the input power in form of hydrogen:

$P_{in}$ = (0.0899·10$^{-3}$ kg/liter) (1110 liters/hour) (28·10$^{+3}$ W/kg) = 2794 W.
Power (energy per hour) efficiency $\eta_{power} = P_{out}/P_{in} = 0.4295$ pu = 43%.

*Conclusion.* Both methods generate about the same efficiency for a PEM fuel cell.

b) The specific power density of this PEM fuel cell expressed in W/kg is defined as

$$\frac{P_{out}}{\text{mass}} = 1200\,\text{W}/13\,\text{kg} = 92.3\,\text{W/kg}.$$

c) The specific power density of a PEM fuel cell is 92.3 W/kg as compared with that of a lead-acid battery of about 150 W/kg [66 in Chapter 1].

### 1.4.22 Application Example 1.5: Calculation of the Currents of a Wind-Power Plant PWM Inverter Feeding Power into the Power System: Solution

See Fig. E1.5.3

#### 1.8.3.1 Application Example 1.6: Interharmonic Reduction by Dedicated Transformer: Solution

Computations are shown in Figs. E1.6.5 and E1.6.6 for the above three cases. As illustrated, for $V_{load1} = V_{load2}$ the 1128th interharmonic amplitude is $V_{1128} = \frac{(122.64 - 120)}{120}(100\%) = 2.2\%$, whereas for $V_{load3}$ this interharmonic is only 0.006%. This demonstrates the effectiveness of a dedicated line or transformer, other than an isolation transformer with a turns ratio 1 : 1.

#### 1.8.6.1 Application Example 1.7: Hand Calculation of Harmonics Produced by Twelve-Pulse Converters: Solution

**Calculating Current Harmonics at PCC #1.**
At PCC #1:

- $S_{pk} = \frac{|\bar{V}||\bar{I}|}{3} = \frac{50\,\text{MVA}}{3} = 16.67\,\text{MVA}$

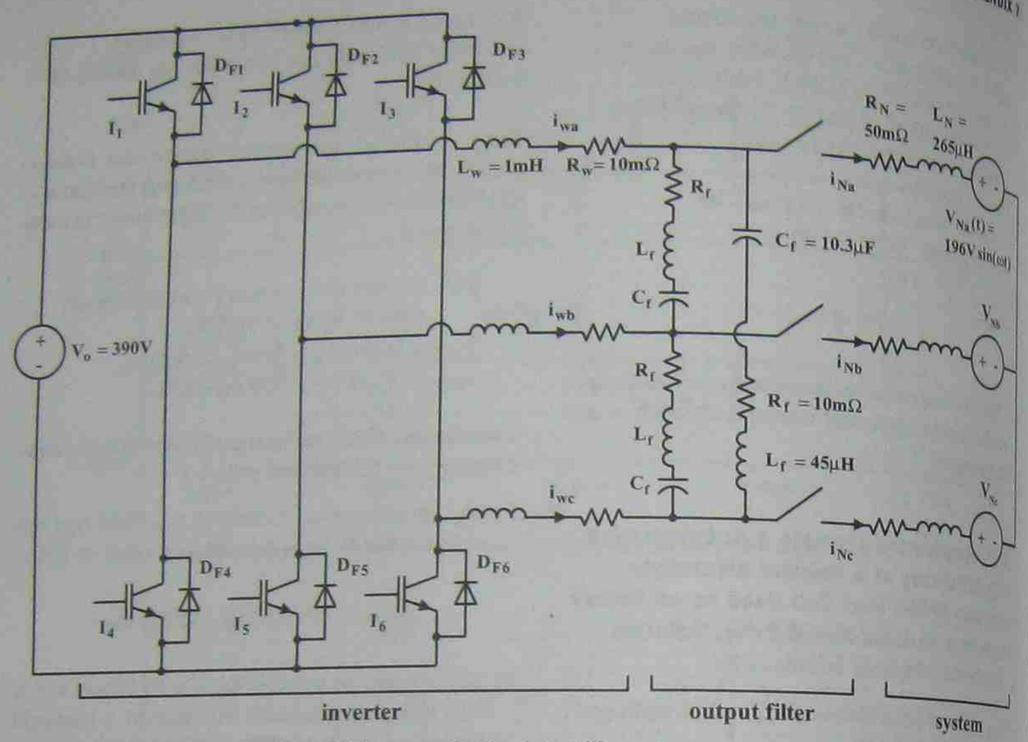



**FIGURE E1.5.1** Current-controlled PWM inverter feeding into utility system.

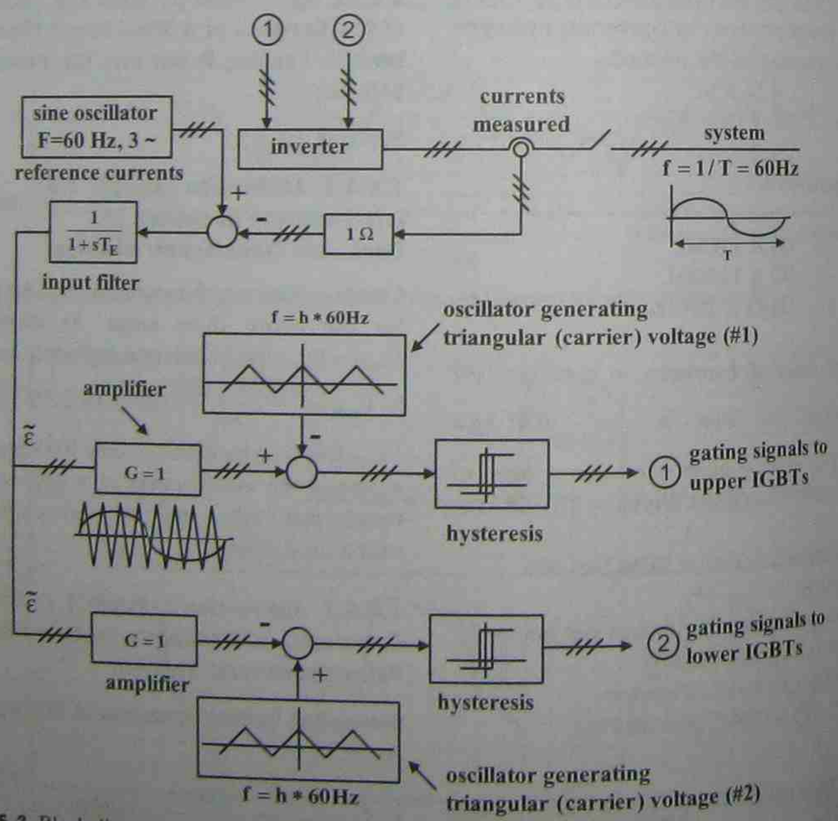



**FIGURE E1.5.2** Block diagram of control circuit for current-controlled PWM inverter.



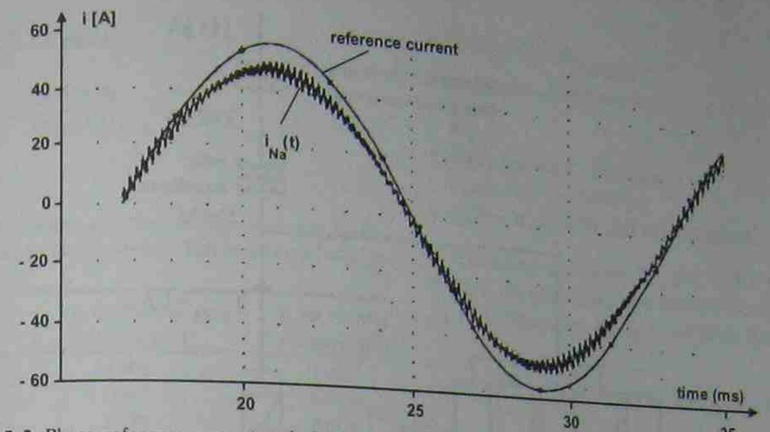



**FIGURE E1.5.3** Phase reference current and phase current $i_{Na}(t)$ delivered by inverter to power system at about unity power factor.

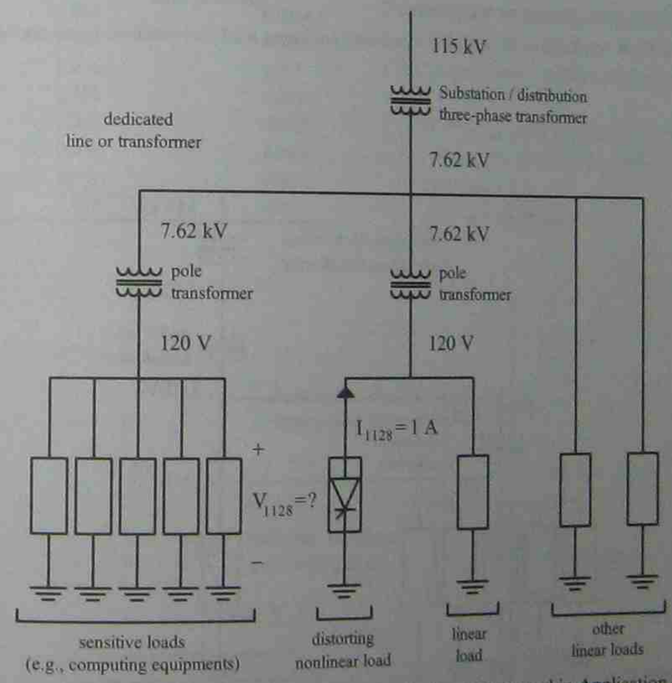



**FIGURE E1.6.1** Overall (per phase) one-line diagram of the distribution system used in Application Example 1.6.

ST. GEORGE COLLEGE OF LAW

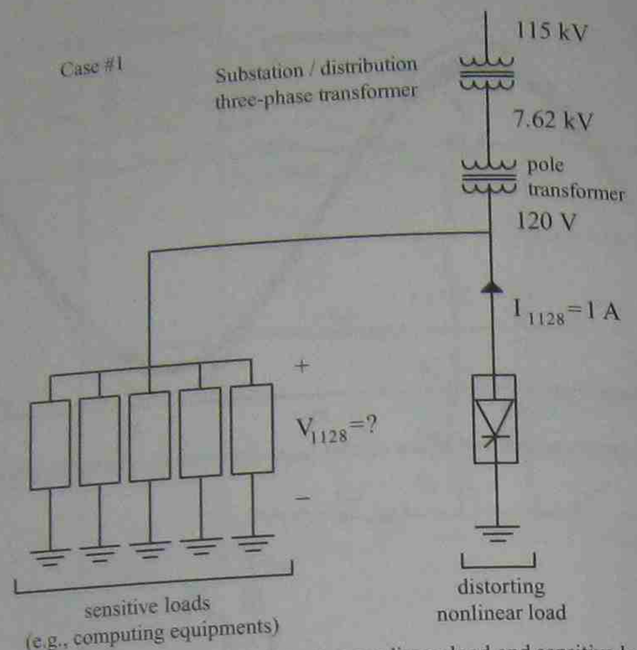



**FIGURE E1.6.2** Case #1 of Application Example 1.6: distorting nonlinear load and sensitive loads are fed from same pole transformer.




**FIGURE E1.6.3** Case #2 of Application Example 1.6: use of an isolation transformer with a turns ratio 1 : 1 between distorting (nonlinear) load and sensitive loads.

ST. GEORGE COLLEGE OF LIBRARY



- $V_{ph} = \frac{115\text{kV}}{\sqrt{3}} = 66.4\text{kV}$
- $I_{ph} = \frac{S_{ph}}{V_{ph}} = \frac{50\text{MVA}}{3(66.4\text{kV})}$

**TABLE E1.7.1** Harmonic Current ($I_h$) Generated by Six-Pulse and Twelve-Pulse Converters [64] Based on $X_t^* = 0.12$ pu and $\alpha = 30°$

| Harmonic order ($h$) | $I_h$ for 6-pulse converter (pu) | $I_h$ for 12-pulse converter (pu) |
|---|---|---|
| 1 | 1.000 | 1.000 |
| **1** | 0.192 | **0.0192** |
| **5** | 0.132 | **0.0132** |
| **7** | 0.073 | 0.073 |
| 11 | 0.057 | 0.057 |
| 13 | 0.035 | **0.0035** |
| **17** | 0.027 | **0.0027** |
| **19** | 0.020 | 0.020 |
| 23 | 0.016 | 0.016 |
| 25 | 0.014 | **0.0014** |
| **29** | 0.012 | **0.0012** |
| **31** | 0.011 | 0.011 |
| 35 | 0.010 | 0.010 |
| 37 | 0.009 | **0.0009** |
| **41** | 0.008 | **0.0008** |
| **43** | 0.008 | 0.008 |
| 47 | 0.007 | 0.007 |
| 49 | | |

- $I_L = I_{ph} = 251$ A.
- At a short-circuit ratio of $R_{SC} = \frac{I_{SC}}{I_L} = 40$ (at PCC #1)
- The system's impedance is $Z_{sys}$ (10 MVA base) = 0.5% = 0.005 pu.
- $I_{SC}^{PCC\#1} = R_{SC} I_L = 40\ (251\text{ A}) = 10000$ A.

According to Table 1.7, for PCCs from 69 to 138 kV, the current harmonic limits should be divided by two. Therefore, for $I_{SC}/I_L = (20 \text{ to } 50)$:

$$I_{hlimit} = \frac{7.0}{2} = 3.5\% \quad \text{for } 5 \le h < 11;$$

$$I_{hlimit} = \frac{3.5}{2} \cong 1.8\% \quad \text{for } 11 \le h < 17;$$

$$I_{hlimit} = \frac{2.5}{2} \cong 1.3\% \quad \text{for } 17 \le h < 23.$$

The actually occurring harmonic currents are for $I_{spc} = (251/2)$ A = 125.5 A for 12-pulse converter (SPC means static power converter):

$I_5^{actual} = I_{spc}\ (0.0192) = 125.5(0.0192) = 2.41$ A
$I_7^{actual} = 125.5(0.0132) = 1.65$ A
$I_{11}^{actual} = 9.15$ A
$I_{13}^{actual} = 7.15$ A

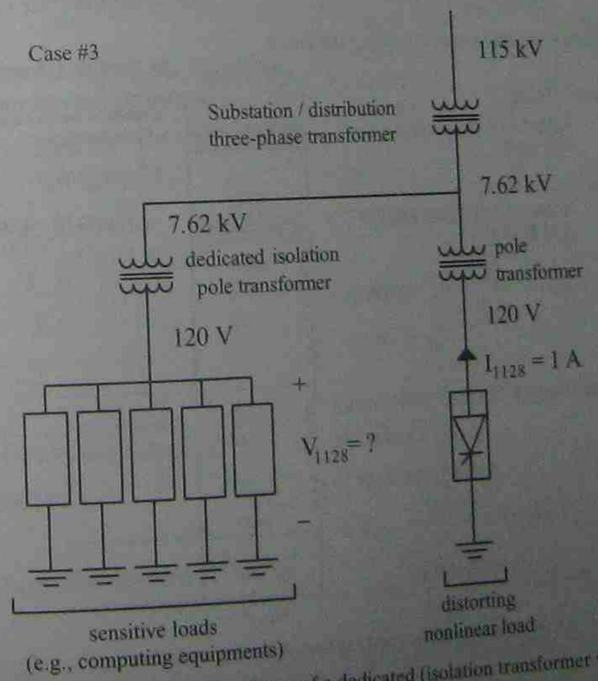
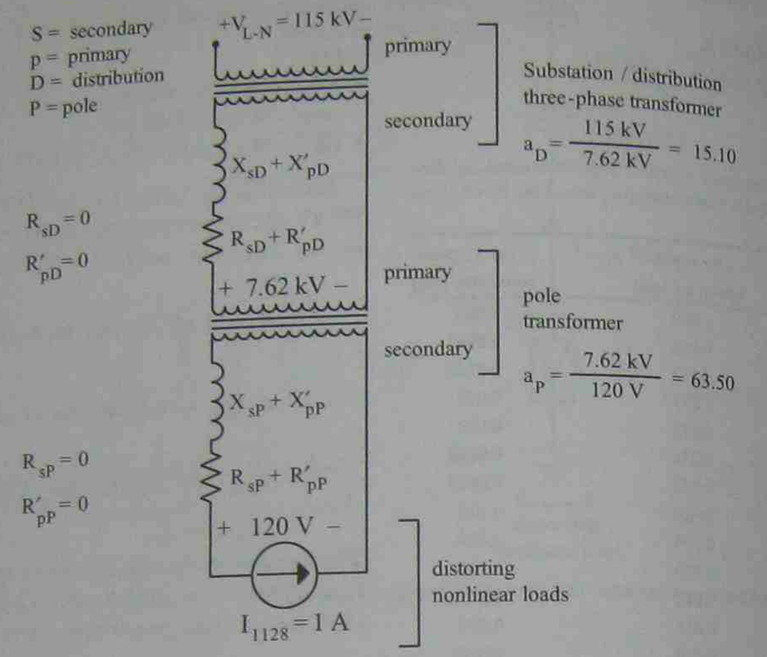



**FIGURE E1.6.4** Case #3 of Application Example 1.6: use of a dedicated (isolation transformer with turns ratio 7620 : 120) pole transformer between distorting nonlinear load and sensitive loads.

Analysis of dedicated isolated transformer




$X_{sD} = X'_{pD} = 0.7\Omega$ referred to secondary of distributed transformer

$X_{sP} = X'_{pP} = 0.07\Omega$ referred to secondary of pole transformer

**FIGURE E1.6.5** Equivalent circuit of distribution and pole transformers.

Analysis of dedicated isolated transformer) continued (:

$V_{load1} = V_{load2} =$
$= 120V + 1A\,(0.1404\Omega)(18.8) =$
$= 122.64\ V$

$V_{load\,3} =$
$= 120V + 1A(0.0004\Omega)(18.8) =$
$= 120.0075\ V$

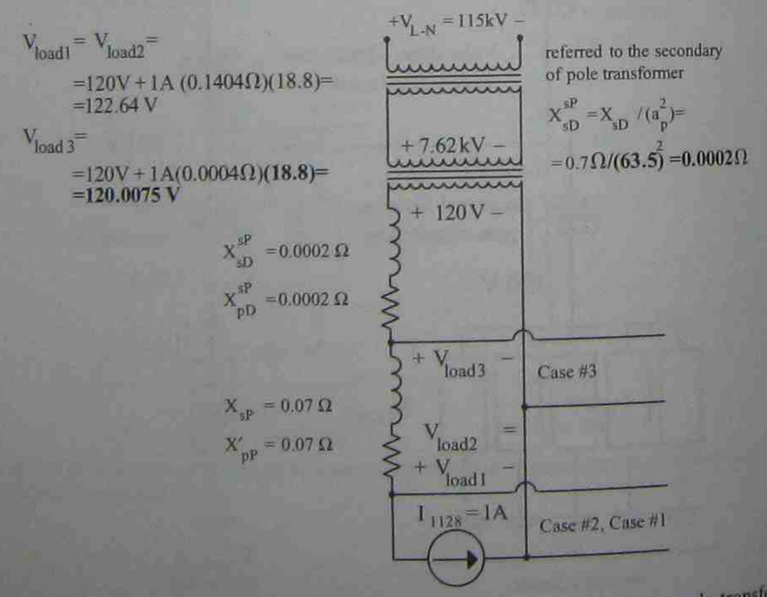



**FIGURE E1.6.6** Equivalent circuit referring all lumped reactances to the secondary of the pole transformer.

ST. GEORGE COLLEGE OF LAW





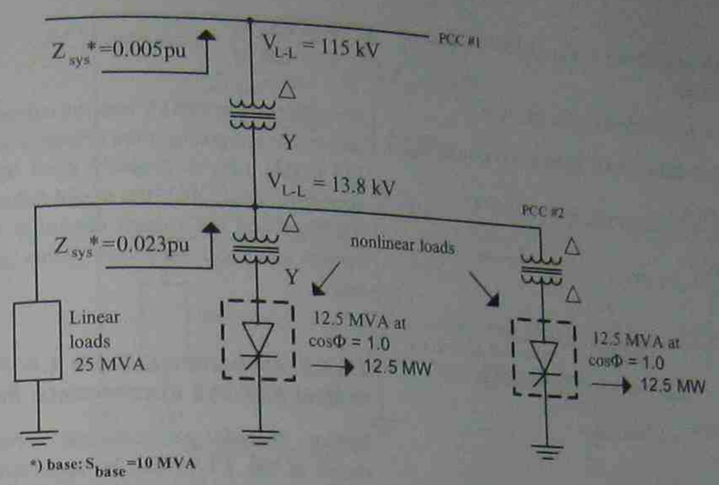



**FIGURE E1.7.1** One-line diagram of a large industrial plant fed from transmission voltage [64 in Chapter 1].

with $I_L = 251$ A

$$I_5^{\text{actual}\%} = \frac{I_5^{\text{actual}}}{I_L} 100\%$$

$I_5^{\text{actual}\%} = 0.96\%$
$I_7^{\text{actual}\%} = 0.66\%$
} allowed limits are 3.5%

$I_{11}^{\text{actual}\%} = 3.65\%$
$I_{13}^{\text{actual}\%} = 2.85\%$
} allowed limits are 1.8%

As can be seen, $I_{11}^{\text{actual}}$ and $I_{13}^{\text{actual}}$ are too large!

**Calculating Voltage Harmonics at PCC #1.** Calculation of short-circuit (apparent) power $S_{SC}$:

- $I_{SC} = I_L \cdot R_{SC} = 251(40) = 10040$ A
- $\frac{I_{SC}}{I_L} = R_{SC}$
- $S_{SC} = 3 \cdot V_{ph} \cdot I_{SC} = 3\left(\frac{115\text{kV}}{\sqrt{3}}\right)(10.04\text{kA})$
  $= 2000\,\text{MVA}$

Checking:

$$S_{SC} = MVA_{SC} = \frac{S_{\text{base}}[\text{MVA}]}{Z_{\text{syst}}[\text{in per unit at base MVA}]}$$
$$= \frac{10\,\text{MVA}}{0.005\ \text{pu}} = 2{,}000\,\text{MVA}.$$

Calculation of voltage harmonics (at PCC #1) for the current harmonics:

- $V_h = \frac{I_h}{I_{\text{base}}}(h) \cdot Z_{sys} \cdot 100\%$
- $S_{\text{base}} = 10$ MVA (all three phases)
- $I_{\text{base}} = \frac{S_{\text{basephase}}}{V_{\text{phase}}}$
- $I_{\text{base}} = \frac{10\text{MVA}/3}{115\text{kV}/\sqrt{3}} = 50.2\,\text{A}$

Harmonic (actually occurring) voltages:

$$V_5 = \frac{2.41}{50.2}(5)(0.005)(100\%)$$
$V_5 = 0.120\%$
$$V_7 = \frac{1.65}{50.2}(7)(0.005)(100\%)$$
$V_7 = 0.115\%$
$V_{11} = 1.0\%$
$V_{13} = 0.93\%$
} allowed limit is 1.5% for individual harmonic voltage (Table 1.8).

Also:

- $\text{THD}_V^{\text{limit}} \le 2.5\%$
- $THD_V^{\text{actual}} = \frac{\sqrt{\sum_{h=5,7,\ldots} V_h^2}}{V_{\text{phase}}}(100\%) = 1.64\%$

**Calculating Current Harmonics at PCC #2.** At PCC #2:

- $S_{ph} = 16.67$ MVA
- $V_{ph} = \frac{13.8\text{kV}}{\sqrt{3}} = 7.968\text{kV}$
- $I_{ph} = \frac{16.67\text{MVA}}{7.968\text{kV}} = 2092\,\text{A}$
- At a short-circuit ratio of $R_{SC} = \frac{I_{SC}}{I_L} = 8.7$ (at PCC #2)

- The system's impedance is $Z_{sys}$ (10 MVA base) = 2.3% = 0.023 pu,
- $I_{SC}^{PCC\#2} = R_{SC} \times I_L = 8.7(2092\text{ A}) = 18.2\text{ kA}$.

Calculation of short-circuit (apparent) power $S_{SC}$:

- $S_{phase} = \dfrac{50\text{MVA}}{3} = 16.67\text{MVA}$
- $V_{phase} = \dfrac{13.8\text{kV}}{\sqrt{3}} = 7.97\text{kV}$
- $I_{phaseL} = \dfrac{50\text{MVA}}{3} \times \dfrac{\sqrt{3}}{13.8\text{kV}} = 2.092\text{kA}$
- $I_{SCphase} = R_{SC} \times I_{phaseL} = 8.7(2.092) = 18.2\text{ kA}$
- $I_{SPCphase} = \dfrac{I_{phaseL}}{2} = 1.046\text{kA}$
- $R_{SC} = \dfrac{I_{SCphase}}{I_{phaseL}} = \dfrac{18.2}{2.092} = 8.7$
- $Z_{sys} = 2.3\% = 0.023$ pu.

Actually occurring harmonic currents at PCC #2 for 12-pulse converter:

$$I_5^{actual} = 1046(0.0192) = 20.08\text{ A}$$
$$I_7^{actual} = 1046(0.0132) = 13.81\text{ A}$$
$$I_{11}^{actual} = 1046(0.073) = 76.35\text{ A}$$
$$I_{13}^{actual} = 1046(0.057) = 59.62\text{ A}$$

in percent

$$I_5^{actual\%} = \frac{I_5^{actual}}{I_{phaseL}}(100\%)$$

$$I_5^{actual\%} = \frac{20.08}{2092}(100\%) = 0.96\%$$

$$I_7^{actual\%} = 0.66\%$$

$$\left.\begin{aligned} I_{11}^{actual\%} &= 3.65\% \\ I_{13}^{actual\%} &= 2.85\% \end{aligned}\right\} \text{above limits (see analysis for PCC \#1)}$$

**Calculating Voltage Harmonics at PCC #2.**

$$V_h = \frac{I_h}{I_{base}}(h) \cdot Z_{sys} \cdot 100\%.$$

where

$$I_{base} = \frac{10\text{MVA}/3}{13.8\text{kV}/\sqrt{3}}$$

$$I_{base} = 418.4\text{ A}$$

$$\left.\begin{aligned} V_5 &= \frac{20.08}{418.4}(5)(0.023)100\% \\ V_5 &= 0.552\% \\ V_7 &= \frac{13.81}{418.4}(7)(0.023)100\% \\ V_7 &= 0.531\% \end{aligned}\right\} \text{below limit of 3\%.}$$

$$\left.\begin{aligned} V_{11} &= 4.61\% \\ V_{13} &= 4.26\% \end{aligned}\right\} \text{above limit of 3\%.}$$

Note that on the 13.8 kV bus, the current and voltage distortions are greater than recommended by IEEE-519 (Table 1.8). A properly sized harmonic filter applied on the 13.8 kV bus would reduce the current distortion and the voltage distortion to within the current limits and the voltage limits on the 13.8 kV bus.

### 1.8.6.2 Application Example 1.8: Filter Design to Meet IEEE-519 Requirements: Solution

**System Analysis.** At harmonic frequencies, the circuit of Fig. E1.8.1 can be approximated by the equivalent circuit shown by Fig. E1.8.2. This circuit should be analyzed at each frequency of interest by calculating series and parallel resonances.

For series resonance $\tilde{I}_{fh}$ is large whereas for parallel resonance $\tilde{I}_{fh}$ and $\tilde{I}_{sysh}$ are large. The major impedance elements in the circuit respond differently as frequency changes. The impedance of the transmission line $Z_{lineh}$ is a complex relationship between the inductive and capacitive reactances. Using the fundamental frequency resistance R and inductance of the transmission line, however, gives acceptable results. For most industrial systems $Z_{th}$ and $Z_{lineh}$ can be approximated by the short-circuit impedance if low-frequency phenomena are considered.

**The Impedance versus Frequency Characteristic of a Transformer.** The impedance versus frequency characteristic of a transformer depends on its design, size, voltage, etc. Its load loss, $I^2R$, will constitute 75 to 85% of the total transformer loss and about 75% of this is not frequency dependent (skin effect). The remainder varies with the square of the frequency. The no-load loss (core loss) constitutes between 15 and 25% of the total loss and, depending on flux density, the loss varies as $f^{3/2}$ to $f^3$. From this with the reactance increasing directly with frequency (inductance L is assumed to be constant), it can be seen that the harmonic $(X_h/R_h)$ ratios will be less than the fundamental $(h = 1)$ frequency $(X_1/R_1)$ ratio, that is,

$$\left(\frac{X_h}{R_h}\right) < \left(\frac{X_1}{R_1}\right).$$

If the fundamental frequency ratio $(X_1/R_1)$ is used there will be less damping of the high-frequency current than in actuality.





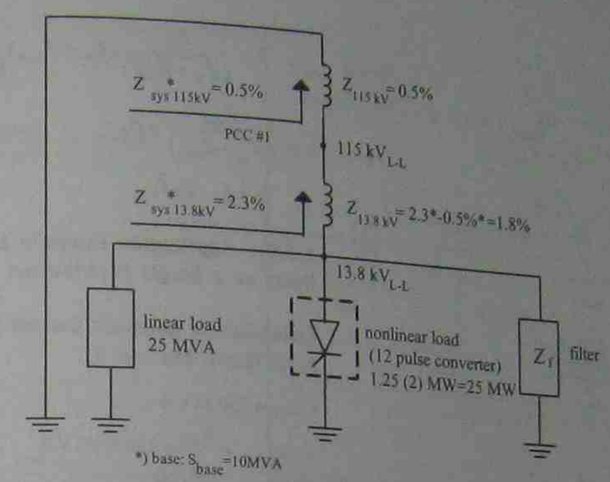



**FIGURE E1.8.1** One-line diagram of a large industrial plant fed from transmission voltage (Fig. E1.7.1) with a passive filter placed at PCC #2.

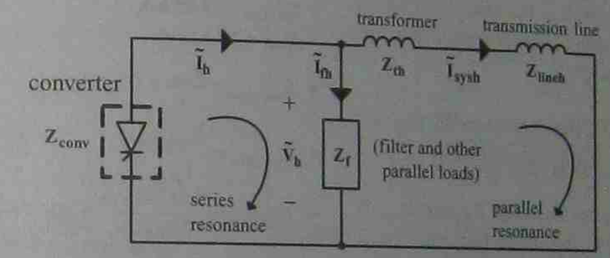



**FIGURE E1.8.2** Equivalent circuit of Fig. E1.8.1 at harmonic frequencies.

**Adjacent Capacitor Banks.** If there are large capacitor banks or filters connected to the utility system, it is necessary to consider their effect.

**Converter as a Harmonic Generator.** The converter is usually considered to be a generator of harmonic currents $i_h$, and is considered to be a constant-current source. Thus $Z_{conv}$ is very large and can be ignored. If the converter is a constant-voltage source $Z_{conv}$ should be included.

**Circuit Analysis.** Using Ohm's and Kirchhoff's laws (Fig. E1.8.2):

$$Z_{sysh} = Z_{th} + Z_{lineh}$$
$$\tilde{I}_h = \tilde{I}_{sysh} + \tilde{I}_{fh}$$
$$\tilde{I}_{fh} Z_{fh} = \tilde{I}_{sysh} Z_{sysh},$$

or

$$\tilde{I}_{fh} = \tilde{I}_{sysh}\left(\frac{Z_{sysh}}{Z_{fh}}\right)$$
$$\tilde{I}_{sysh} = \tilde{I}_h - \tilde{I}_{fh}$$

$$\tilde{I}_{sysh} = \tilde{I}_h - \tilde{I}_{sysh}\left(\frac{Z_{sysh}}{Z_{fh}}\right),$$

or

$$\tilde{I}_{sysh}\left(1 + \frac{Z_{sysh}}{Z_{fh}}\right) = \tilde{I}_{fh}$$
$$\tilde{I}_{sysh}\left(\frac{Z_{fh} + Z_{sysh}}{Z_{fh}}\right) = \tilde{I}_h,$$

or

$$\tilde{I}_{sysh} = \left(\frac{Z_{fh}}{Z_{fh} + Z_{sysh}}\right)\tilde{I}_h.$$

Correspondingly,

$$\tilde{I}_{fh} = \left(\frac{Z_{sysh}}{Z_{fh} + Z_{sysh}}\right)\tilde{I}_h.$$

ST. GEORGE SCHOOL OF LAW

Define

$$\rho_{sysh} = \frac{Z_{fh}}{Z_{fh} + Z_{sysh}},$$

$$\rho_{fh} = \frac{Z_{sysh}}{Z_{fh} + Z_{sysh}}.$$

Then

$$\tilde{I}_{sysh} = \rho_{sysh}\tilde{I}_h,$$
$$\tilde{I}_{fh} = \rho_{fh}\tilde{I}_h.$$

Because of

$$\tilde{I}_h = \tilde{I}_{sysh} + \tilde{I}_{fh}$$
$$\rho_{sysh} + \rho_{fh} = 1.$$

Note that $\rho_{sysh}$ and $\rho_{fh}$ are complex quantities. It is desirable that $\rho_{sysh}$ be small at the various occurring harmonics. Typical values for a series tuned filter are (at the tuned frequency $hf_1$)

$\rho_{sysh} = 0.045 \angle -80.6°$, (for series tuned filters)
$\rho_{fh} = 0.994 \angle +2.6°$, (for series tuned filters).

Parallel resonances occur between $Z_{fh}$ and $Z_{sysh}$ if $\rho_{sysh}$ and $\rho_{fh}$ are large at the tuned frequency ($hf_1$). Typical values are

$$\rho_{sysh} = 16.67 \angle -92.9°,$$
$$\rho_{fh} = 16.75 \angle +83.6°.$$

The approximate 180° phase difference emphasizes why a parallel resonance cannot be tolerated at a frequency near a harmonic current generated by the converter: a current of the resonance frequency will excite the circuit and a 16.67 pu current will oscillate between the two energy storage units, the system impedance $Z_{sysh}$ and that of the filter capacitors $Z_{fh}$.

A plot of $\rho_{sysh}$ versus $h$ is a useful display of filter performance. Frequently a plot of $\log(\rho_{sysh})$ is more convenient. The harmonic voltage $\tilde{V}_h$ is

$$\tilde{V}_h = Z_{sysh}\tilde{I}_{sysh} = Z_{fh}\tilde{I}_{fh}$$
$$\tilde{V}_h = \rho_{sysh}(Z_{fh} + Z_{sysh})\tilde{I}_{fh}$$
$$\tilde{V}_h = \rho_{sysh}(Z_{fh} + Z_{sysh})\rho_{fh}\tilde{I}_h$$

$$\tilde{V}_h = \rho_{sysh}(Z_{fh} + Z_{sysh})\frac{Z_{sysh}}{(Z_{fh} + Z_{sysh})}\tilde{I}_h$$

$$\tilde{V}_h = \rho_{sysh} \cdot Z_{sysh} \cdot \tilde{I}_h,$$

or

$$\tilde{V}_h = \frac{Z_{fh}}{(Z_{fh} + Z_{sysh})}(Z_{fh} + Z_{sysh})\frac{Z_{sysh}}{(Z_{fh} + Z_{sysh})}\tilde{I}_h$$

$$\frac{Z_{sysh}}{(Z_{fh} + Z_{sysh})} = \rho_{fh}$$

$$\tilde{V}_h = \rho_{fh} \cdot Z_{fh}\tilde{I}_h.$$

### 1.8.6.3 Application Example 1.9: Several Users on a Single Distribution Feeder

**Calculation of Harmonic Current for User #1 (Case A, No Filter).** For user #1:

- $S_{SC} = 350$ MVA
- $S_{SCphase} = \frac{S_{SC}}{3} = 116.68\text{MVA}$
- $S_{SCphase} = I_{SCphase}V_{phase}$
- $I_{SCphase} = \frac{S_{SCphase}}{V_{phase}} = \frac{116.67\text{MVA}}{7.959\text{kV}}$
- $I_{SCphase} = 14.65$ kA
- $S_{load} = 2.5$ MVA
- $S_{loadphase} = \frac{S_{load}}{3} = 0.833\text{MVA}$
- $I_{loadphase} = \frac{S_{loadphase}}{V_{phase}}$
- $I_{loadphase} = \frac{0.833\text{MVA}}{7.959\text{kV}} = 104.7\text{A}.$

For this user, there is a 25% static power converter (SPC) load:

- $I_{loadSPC} = \frac{104.7\text{A}}{4} = 26.2\text{A}$
- $R_{SC} = \frac{I_{SCphase}}{I_{loadphase}} = \frac{14.65\text{kA}}{104.7\text{A}} = 140.$

Therefore, harmonic currents for the six-pulse static power converter of user #1 are

- $I_{5[A]} = 26.2(0.192) = 5.03\text{A} \rightarrow$
  $I_{5[\%]} = \frac{I_{5[A]}}{I_{loadphase}}(100\%) = \frac{5.03\text{A}}{104.7\text{A}}(100\%) = 4.8\%$
- $I_{7[A]} = 26.2(0.132) = 3.46\text{A} \rightarrow$
  $I_{7[\%]} = \frac{I_{7[A]}}{I_{loadphase}}(100\%) = \frac{3.46}{104.7} = 3.3\%$
- $I_{11[A]} = 1.91$ A $\rightarrow I_{11[\%]} = 1.82\%$
- $I_{13[A]} = 1.49$ A $\rightarrow I_{13[\%]} = 1.42\%$

**Calculation of Harmonic Current for User #2 (Case A, No Filter).** For user #2:

- $S_{SC} = 300$ MVA
- $S_{SCphase} = \frac{S_{SC}}{3} = 100\text{MVA}$





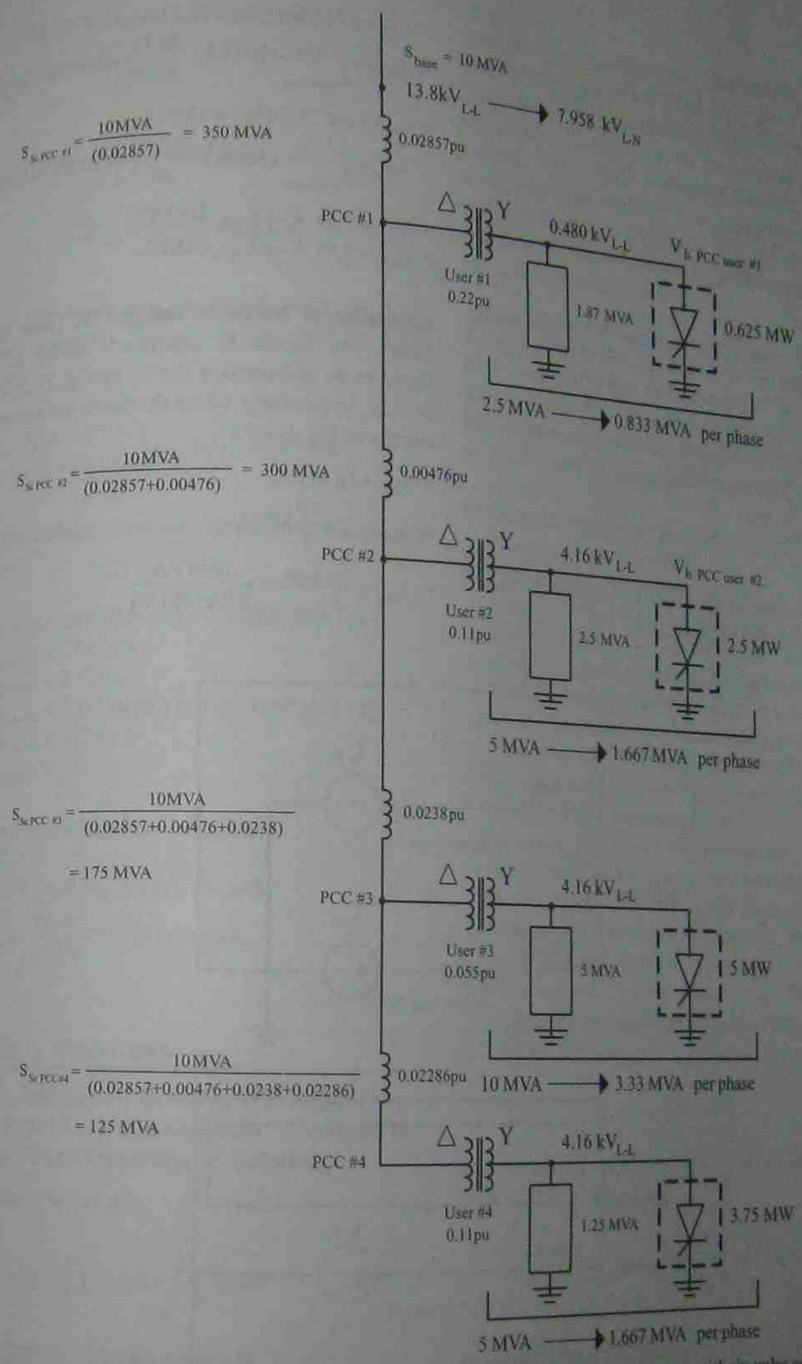



**FIGURE E1.9.1** Overall one-line diagram of the distribution system feeder containing four users with six-pulse converters [64].

- $V_{phase} = 7.9585\,kV$
- $I_{SCphase} = \dfrac{S_{SCphase}}{V_{phase}} = \dfrac{100MVA}{7.9585kV} = 12.56kA$
- $S_{load} = 5\,MVA$
- $S_{loadphase} = 1.667\,MVA$
- $I_{loadphase} = \dfrac{S_{loadphase}}{V_{phase}}$
- $I_{loadphase} = 209.5\,A.$

The 50% static power converter (SPC) load of this user yields:

- $I_{loadSPC} = 104.73\,A$
- $R_{SC} = \dfrac{I_{SCphase}}{I_{loadphase}} = \dfrac{12560\,A}{209.5\,A} = 59.95$
- $R_{SC} = 60.$

Therefore, harmonic currents for the six-pulse static power converter of user #2 are

- $I_{5[A]} = 104.73(0.192) = 20.11A \rightarrow I_{5[\%]} = \dfrac{I_{5[A]}}{I_{loadphase}}(100\%) = \dfrac{20.11A}{209.5A}(100\%) = 9.6\%,$
- $I_{7[A]} = 104.73(0.132) = 13.82A \rightarrow I_{7[\%]} = \dfrac{I_{7[A]}}{I_{loadphase}}(100\%) = \dfrac{13.82A}{209.5A}(100\%) = 6.6\%,$
- $I_{11[A]} = 7.64\,A \rightarrow I_{11[\%]} = 3.65\%$
- $I_{13[A]} = 5.96\,A \rightarrow I_{13[\%]} = 2.9\%$

**Calculation of Harmonic Voltages $V_h$ (Case A, No Filter).** The harmonic equivalent circuit of Fig. E1.9.1 in pu and ohms is shown by Fig. E1.9.2a and E1.9.2b, respectively. Using the harmonic equivalent circuits of Fig. E.1.9.2:

- $S_{base} = 10\,MVA$
- $S_{basephase} = \dfrac{10}{3}MVA$
- $I_{base} = \dfrac{S_{basephase}}{V_{phase}} = \dfrac{10MVA}{3(7.9585kV)}$

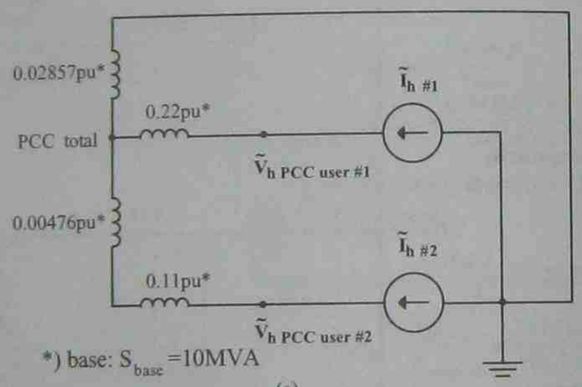



**FIGURE E1.9.2** Harmonic equivalent circuit of Fig. E1.9.1 with impedances expressed in (a) pu without harmonic order h, (b) ohms.



- $I_{base} = 418.83\,A$
- $Z_{base} = \dfrac{V_{phase}}{I_{base}} = \dfrac{V_{base}}{I_{base}}$

Note that $V_{base} = V_{phase}$; therefore,

$$Z_{base} = \frac{7.9585}{418.83} = 19\Omega.$$

Voltage harmonics are computed using the total harmonic currents. For example, for the fifth harmonic:

$$\left.\begin{aligned} I_{5\#1} &= 5.03\,A \\ I_{5\#2} &= 20.11\,A \end{aligned}\right\} I_{5\#1} + I_{5\#2} = 25.14\,A.$$

The fifth voltage harmonic amplitudes for users 1 and 2 are

- $V_{5PCCuser\#1} = 4.18(5)(5.03) + 0.5428(5)(25.14)$
  $V_{5PCCuser\#1} = 173.38\,V$
  $V_{5PCCuser\#1} = 2.18\%,$
- $V_{5PCCuser\#2} = 2.18(5)(20.11) + 0.5428(5)(25.14)$
  $V_{5PCCuser\#2} = 287.46\,V$
  $V_{5PCCuser\#2} = 3.61\%.$

The total fifth harmonic voltage is

$$V_{5PCCtot} = 0.5428(5)(25.14) = 68.26\,V$$
$$V_{5PCCtot} = \frac{68.26}{7.96kV}(100\%) = 0.86\%.$$

## CHAPTER 2 SOLUTIONS

### 2.2.4.3 *Application Example 2.3: Application of the Direct-Loss Measurement Technique to a Single-Phase Transformer: Solution*

Transformer losses are

$$P_{loss} = P_1 - P_2 = \frac{1}{T}\int_0^T v_1 i_1 dt - \frac{1}{T}\int_0^T v_2' i_2' dt. \qquad \text{(E2.3-1)}$$

Rearrangement of terms results in

$$P_{loss} = \frac{1}{T}\int_0^T i_1(v_1 - v_2')dt + \frac{1}{T}\int_0^T v_2'(i_1 - i_2')dt, \qquad \text{(E2.3-2)}$$

$$P_{series} = \frac{1}{T}\int_0^T i_1(v_1 - v_2')dt, \qquad \text{(E2.3-3)}$$

$$P_{shunt} = \frac{1}{T}\int_0^T v_2'(i_1 - i_2')dt. \qquad \text{(E2.3-4)}$$

Note that $P_{loss}$ consists of the sum (not the difference) of two components where $(v_1 - v_2')$ and $(i_1 - i_2')$ can be accurately measured and calibrated. Thus the difference of $P_{in}$ and $P_{out}$ is not computed as for the indirect, conventional method of Section 2.2.4.1. This method can be applied to polyphase systems as discussed in [8, 9, in Chapter 2]. The two available sampling methods – series and parallel sampling – are addressed in Appendix 1.

### 2.3.3.1 *Application Example 2.4: Sensitivity of K- and $F_{HL}$-Factors and Derating of 25 kVA Single-Phase Pole Transformer with Respect to the Number and Order of Harmonics: Solution*

a) The Fourier analysis program is listed in Appendix A2.1.
b) Output of the Fourier program for a square wave is listed in Appendix A2.2.
c) Taking into account the Nyquist criterion one can compute based on 42 sampled points per period the harmonics up to the 27th order. These harmonics are listed in Table E2.4.1 and the resulting Fourier approximation is shown in Fig. E2.4.1.
d) Taking into account the harmonics up to the 27th order (Table E2.4.2) one obtains for the K-factor: $K_{27} = 9.86$, and for the $F_{HL}$-factor: $F_{HL27} = 8.22$. Thereby it is assumed that the 25 kVA single-phase pole transformer [11] is loaded only by nonlinear loads having square wave currents. Using these factors and knowing the $P_{EC\text{-}R}$, one can compute the derating of a transformer. The $P_{EC\text{-}R}$ can be obtained from the manufacturer or it can be measured [11, in Chapter 2]. For $P_{EC\text{-}R} = 0.0186$ pu one obtains using the K-factor, Eq. 2-25 the derating:

$$I_{max27K\text{-}factor}(pu) = 0.94,$$

and the derating based on the $F_{HL}$-factor, with Eqs. 2-24 and Eq. 2-26:

$$I_{max27FHL\text{-}factor}(pu) = \sqrt{\frac{(1 + P_{EC\text{-}R})}{1 + F_{HL}P_{EC\text{-}R}}} = 0.94.$$

**Conclusion.** The calculation of the derating of transformers with the K- and $F_{HL}$-factors leads to the same result provided the same number and order of harmonics are considered.

To show that the K- and $F_{HL}$-factors and, therefore the derating calculation, critically depend on the number and order of harmonics (used in their calculation), in the following the number of harmonics is

**TABLE E2.4.1** Spectrum of Square Wave

| $I_{DC}$ (pu) | $I_1$ (pu) | $I_2$ (pu) | $I_3$ (pu) | $I_4$ (pu) | $I_5$ (pu) | $I_6$ (pu) |
|---|---|---|---|---|---|---|
| 0 | 1.27 | 0.04 | 0.42 | 0.04 | 0.25 | 0.04 |
| $I_7$ (pu) | $I_8$ (pu) | $I_9$ (A) | $I_{10}$ (pu) | $I_{11}$ (pu) | $I_{12}$ (pu) | $I_{13}$ (pu) |
| 0.17 | 0.04 | 0.12 | 0.04 | 0.09 | 0.04 | 0.07 |
| $I_{14}$ (pu) | $I_{15}$ (pu) | $I_{16}$ (pu) | $I_{17}$ (pu) | $I_{18}$ (pu) | $I_{19}$ (pu) | $I_{20}$ (pu) |
| 0.04 | 0.05 | 0.03 | 0.04 | 0.03 | 0.03 | 0.04 |
| $I_{21}$ (pu) | $I_{22}$ (pu) | $I_{23}$ (pu) | $I_{24}$ (pu) | $I_{25}$ (pu) | $I_{26}$ (pu) | $I_{27}$ (pu) |
| 0.04 | 0.03 | 0.03 | 0.02 | 0.03 | 0.02 | 0.03 |

reduced from 27 to 13. Thus one obtains $K_{13}=6.01$ and $F_{HL13}=5.08$, resulting in

$$I_{max13}\ (\text{pu}) = 0.97.$$

**Conclusion**

$K_{27} > K_{13}$ and $F_{HL27} > F_{HL13}$, therefore $I_{max13}$ (pu) > $I_{max27}$ (pu).

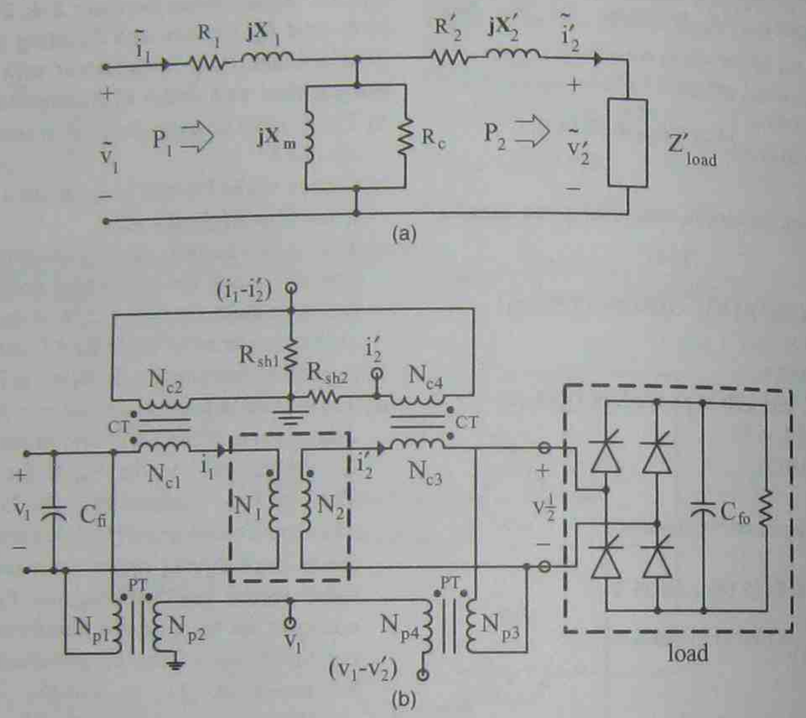



**FIGURE E2.3.1** Application of direct-loss measurement technique to a single-phase transformer; (a) equivalent circuit (b) measuring circuit.

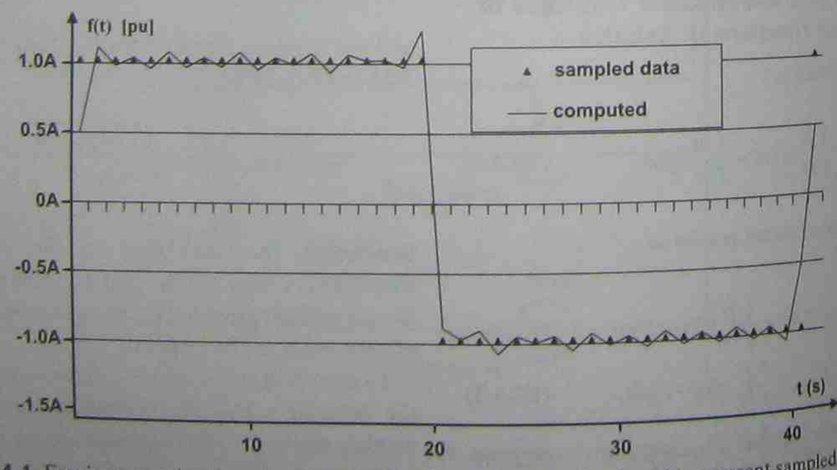



**FIGURE E2.4.1** Fourier approximation of rectangular function. Note: the triangles (▲) represent sampled values and the continuously drawn function represents the Fourier approximation.



**TABLE E2.4.2** Parameters for the Calculation of the K- and $F_{HL}$-Factors (Note the Values for the $I_h$ (pu) Are Truncated)

| $h$ | $I_h$ (pu) | $I_h^2$ | $h^2 I_h^2$ |
|---|---|---|---|
| 1 | 1.0 | 1.0 | 1.0 |
| 2 | 0.03 | 0.001 | 0.004 |
| 3 | 0.33 | 0.109 | 0.984 |
| 4 | 0.03 | 0.001 | 0.016 |
| 5 | 0.20 | 0.040 | 0.969 |
| 6 | 0.03 | 0.001 | 0.036 |
| 7 | 0.13 | 0.018 | 0.878 |
| 8 | 0.03 | 0.001 | 0.063 |
| 9 | 0.09 | 0.009 | 0.723 |
| 10 | 0.03 | 0.001 | 0.099 |
| 11 | 0.07 | 0.005 | 0.608 |
| 12 | 0.03 | 0.001 | 0.143 |
| 13 | 0.06 | 0.003 | 0.513 |
| 14 | 0.03 | 0.001 | 0.194 |
| 15 | 0.04 | 0.002 | 0.349 |
| 16 | 0.02 | 0.0006 | 0.143 |
| 17 | 0.03 | 0.001 | 0.287 |
| 18 | 0.02 | 0.0006 | 0.181 |
| 19 | 0.02 | 0.0006 | 0.201 |
| 20 | 0.03 | 0.001 | 0.397 |
| 21 | 0.03 | 0.001 | 0.438 |
| 22 | 0.02 | 0.0006 | 0.270 |
| 23 | 0.02 | 0.0006 | 0.295 |
| 24 | 0.02 | 0.0002 | 0.143 |
| 25 | 0.02 | 0.0006 | 0.348 |
| 26 | 0.02 | 0.0002 | 0.168 |
| 27 | 0.02 | 0.0006 | 0.407 |
| | Σ | **1.2006** | **9.860** |

### 2.3.3.2 Application Example 2.5: K- and $F_{HL}$-Factors and Their Application to Derating of 25 kVA Single-Phase Pole Transformer Loaded by Variable-Speed Drives: Solution

Taking into account the harmonics up to the 27th order (Tables E2.5.1 and E2.5.2) one obtains for the K-factor: $K_{27}=50.52$, and for the $F_{HL}$-factor: $F_{HL27}=19.42$. Using these factors and knowing the value of $P_{EC\text{-}R}$ one can compute the derating of a transformer. The $P_{EC\text{-}R}$ can be obtained from the manufacturer or it can be measured [11]. For $P_{EC\text{-}R}=0.0186$ pu one obtains the derating using the K-factor, Eq. 2-25:

$$I_{max27K\text{-}factor}(\text{pu}) = 0.87,$$

and the derating based on the $F_{HL}$-factor, with Eq. 2-24 and Eq. 2-26:

$$I_{max27FHL\text{-}factor}(\text{pu}) = \sqrt{\frac{(1+P_{EC-R})}{1+F_{HL}P_{EC-R}}} = 0.87.$$

Note that the influence of the DC component of the current has been disregarded. As is shown in [9], this

**TABLE E2.5.1** Current Spectrum of the Air Handler of a Variable-Speed Drive with (Medium or) 50% of Rated Output Power

| $I_{DC}$ (A) | $I_1$ (A) | $I_2$ (A) | $I_3$ (A) | $I_4$ (A) | $I_5$ (A) | $I_6$ (A) |
|---|---|---|---|---|---|---|
| −0.82 | 10.24 | 0.66 | 8.41 | 1.44 | 7.27 | 1.29 |
| $I_7$ (A) | $I_8$ (A) | $I_9$ (A) | $I_{10}$ (A) | $I_{11}$ (A) | $I_{12}$ (A) | $I_{13}$ (A) |
| 4.90 | 0.97 | 3.02 | 0.64 | 1.28 | 0.48 | 0.57 |
| $I_{14}$ (A) | $I_{15}$ (A) | $I_{16}$ (A) | $I_{17}$ (A) | $I_{18}$ (A) | $I_{19}$ (A) | $I_{20}$ (A) |
| 0.53 | 0.73 | 0.57 | 0.62 | 0.31 | 0.32 | 0.14 |
| $I_{21}$ (A) | $I_{22}$ (A) | $I_{23}$ (A) | $I_{24}$ (A) | $I_{25}$ (A) | $I_{26}$ (A) | $I_{27}$ (A) |
| 0.18 | 0.29 | 0.23 | 0.39 | 0.34 | 0.39 | 0.28 |

**TABLE E2.5.2** Parameters for the Calculation of the K- and $F_{HL}$-Factors (Note the Values for the $I_h$ (pu) Are Rounded)

| $h$ | $I_h$ (pu) | $I_h^2$ | $h^2 I_h^2$ |
|---|---|---|---|
| 1 | 1.024 | 1.0486 | 1.0486 |
| 2 | 0.066 | 0.0044 | 0.0176 |
| 3 | 0.841 | 0.7073 | 6.3657 |
| 4 | 0.144 | 0.0207 | 0.3312 |
| 5 | 0.727 | 0.5285 | 13.2125 |
| 6 | 0.129 | 0.01664 | 0.5990 |
| 7 | 0.490 | 0.2401 | 11.7649 |
| 8 | 0.097 | 0.0094 | 0.6016 |
| 9 | 0.302 | 0.0910 | 7.3710 |
| 10 | 0.064 | 0.0041 | 0.4100 |
| 11 | 0.128 | 0.0164 | 1.9844 |
| 12 | 0.048 | 0.0023 | 0.3312 |
| 13 | 0.057 | 0.0033 | 0.5577 |
| 14 | 0.053 | 0.00281 | 0.5508 |
| 15 | 0.073 | 0.0053 | 1.1925 |
| 16 | 0.057 | 0.0033 | 0.8448 |
| 17 | 0.062 | 0.0038 | 1.0982 |
| 18 | 0.031 | 0.0010 | 0.3240 |
| 19 | 0.032 | 0.0010 | 0.3610 |
| 20 | 0.014 | 0.0002 | 0.0800 |
| 21 | 0.018 | 0.0003 | 0.1323 |
| 22 | 0.029 | 0.0008 | 0.3872 |
| 23 | 0.023 | 0.0005 | 0.2645 |
| 24 | 0.039 | 0.0015 | 0.8640 |
| 25 | 0.034 | 0.0012 | 0.7500 |
| 26 | 0.039 | 0.0015 | 1.0140 |
| 27 | 0.028 | 0.0007 | 0.5103 |
| | Σ | **2.7271** | **52.9690** |

DC component contributes to additional AC losses and an additional temperature rise further increasing the derating.

Measured current wave shape of the air handler operating at variable speed with (medium or) 50% of rated output power with a DC component of $I_{DC}=-0.82$ A is shown in Fig. E2.5.1. The corresponding Fourier approximation (based on the Fourier coefficients of Table E2.5.1) without the DC offset is compared with measured current waveform in Fig. E2.5.2. In Table E2.5.2 the fundamental

ST. GEORGE COLLEGE OF LAW

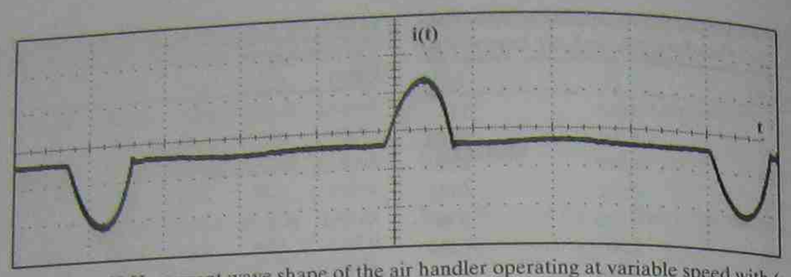



**FIGURE E2.5.1** Measured 60 Hz current wave shape of the air handler operating at variable speed with (medium or) 50% of rated output power.

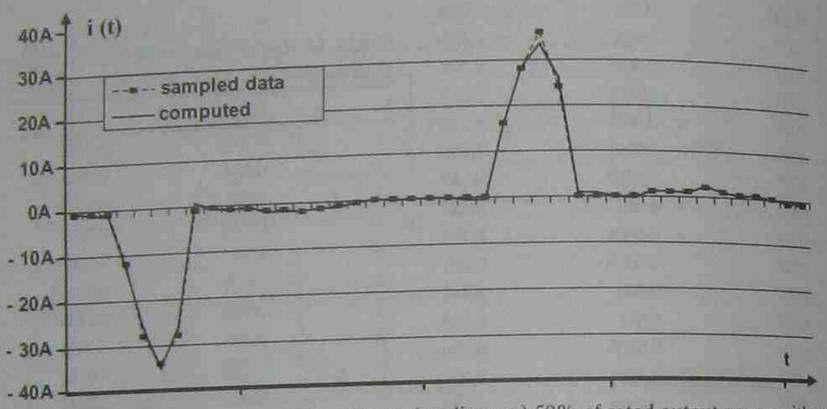



**FIGURE E2.5.2** Fourier analysis of current of air handler at (medium or) 50% of rated output power without DC component of $I_{DC} = -0.82$ A (see Fig. E2.5.1). The rectangles (■) represent measured (sampled) values and the continuous line is the Fourier approximation based on the Fourier coefficients of Table E2.5.2. All ordinate values must be divided by 10 to obtain pu values.

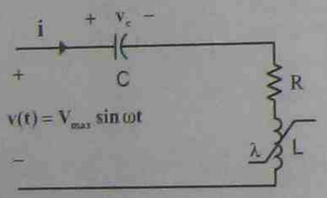



**FIGURE E2.7.1** Ferroresonant nonlinear circuit.

current is not normalized to 1.00 pu; this does not affect the calculation of the K- and $F_{HL}$-factors.

### 2.5.3.1 Application Example 2.7: Calculation of Ferroresonant Currents within Transformers: Solution

a) To show that the equations are true use the circuit of Fig. E2.7.1:
$i(t) = a\lambda^3$, $v(t) = V_{max}\sin(\omega t)$
By inspection of the circuit of Figure E2.7.1:

$$V_{max}\sin(\omega t) = v_c + aR\lambda^3 + \frac{d\lambda}{dt}$$

$$i_c(t) = i(t) = a\lambda^3 = C\frac{dv_c}{dt}, \text{ so } \frac{dv_c}{dt} = \frac{a\lambda^3}{C}$$

Taking the derivative of the circuit equation:

$$\omega V_{max}\cos(\omega t) = \frac{a\lambda^3}{C} + 3aR\lambda^2\frac{d\lambda}{dt} + \frac{d^2\lambda}{dt^2}$$

For $k = 3aR$, $b = \omega V_{max}$, and $C = a$,

$$\frac{d^2\lambda}{dt^2} + k\lambda^2\frac{d\lambda}{dt} + \lambda^3 = b\cos(\omega t)$$

b) To compute numerical values of $\lambda$, $d\lambda/dt$, and $i$ as a function of time for $0 < t < 0.5$ s ($f = 60$ Hz, $R = 0.1\ \Omega$, $C = a = 100\ \mu$F, $1000\sqrt{2}\ \text{V} < V_{max} < 20{,}000\sqrt{2}$ V, all initial conditions = 0) use the following MATLAB codes:

```
%    Matlab code
%
%    getting started
clear all;
close all;
nfig = 0;
%
%    define integration variables and
initial conditions
to = 0;     tf = 0.5;          % time in
seconds
xo = 0;     vo = 0;            % initial
conditions
zo = [xo vo]';                 % initial
conditions in vector form

%Vmax =
[1000*sqrt(2):100:20000*sqrt(2)];
%Vmax = 20000*sqrt(2);
%b = 2*pi*60*Vmax;
%w = 2*pi*60;
%k = 3*100e-6*0.1;

%    Evaluate z numerically
[t,z] = ode23('Hw5eqnfile',[to
tf],zo);
%x = dsolve('D2x+k*x^2*Dx+x^3=b*cos(w
*t)', 'x(0)=0');
%y = rk2('D2y+k*y^2*Dy+y^3=
b*cos(w*t)', [0 0.5], [0 0 0])
%dxdt = [x(2);
b*cos(w*t)-Dx(2)-k*x(1)^2*x(2)-x(1)^3];
%
%    Evaluate x(t) analytically
%       te = linspace(to,tf,200);
%       xe = 0.7737*exp(-3*te).
*cos(2*te-1.1903) - 0.3095*cos(5*te-0.3805);
%
%    Plot profiles
      nfig = nfig+1;
      figure(nfig)
      plot(t,z(:,1)),grid
      xlabel('Time
(s)'),ylabel('Inductor Flux Linkage')
      nfig = nfig+1;
      figure(nfig)
      plot(t,z(:,2)),grid
      xlabel('Time
(s)'),ylabel('Voltage')
      nfig = nfig+1;
      figure(nfig)
      plot(t,100e-6*z(:,1).^3),grid
      xlabel('Time
(s)'),ylabel('Current')
%    Plot dx/dt versus x(t)
      nfig = nfig+1;
      figure(nfig)

plot(z(:,2),z(:,1),zo(1),zo(2),'rx'),grid

xlabel('Voltage'),ylabel('Inductor
Flux Linkage')
%    Plot dx/dt versus i(t)
      nfig = nfig+1;
      figure(nfig)
plot(100e-6*z(:,1).^3,z(:,2),zo(1),zo(2),'rx'),grid

xlabel('Current'),ylabel('Voltage')
```

c) Plots of $\lambda$ versus $d\lambda/dt$ for the values as given in part *b* are shown in Figs. E2.7.2 and E2.7.3.
d) Plots of $\lambda$ and $d\lambda/dt$ as a function of time for the values given in part *b* are shown in Figs. E2.7.4 through E2.7.7.
e) Plots of $i$ as a function of time for the values as given in part *b* are shown in Figs. E2.7.8 and E2.7.9.
f) Plots of voltage versus $d\lambda \neq dt$ $i$ for the values as given in part *b* are shown in Figs. E2.7.10 and E2.7.11.

### 2.6.1 Application Example 2.8: Calculation of Magnetic Field Strength $\bar{H}$

Magnetic field strength $\bar{H}$ of a wire carrying 100 A at a distance of $R = 1\ m$ (Fig. E2.8.1) is

$$|\bar{H}| = \frac{I}{2\pi R} = \frac{100\,\text{A}}{2\pi\,1\text{m}} = 15.92\,\text{A/m}$$

or

$$|\bar{B}| = \mu_0|\bar{H}| = 20\mu\text{T}.$$

### 2.7.1.2 Application Example 2.9: Propagation of a Surge through a Distribution Feeder with an Insulator Flashover: Solution

a) The normalized length of a distance traveled by a wave (e.g., span) NL is a function of the frequency $f$, the span length $l$, and the speed of light $c = 2.99792 \cdot 10^8$ m/s [58]: $NL = \frac{l}{c}f$ or the length of a span is $l = c\frac{NL}{f}$. The time to travel the distance $NL \cdot \lambda$, where $\lambda$ is the wavelength, is $TD = \frac{NL}{f} = \frac{l}{c} = NL \cdot \lambda$.

Length of span #1: $l_1 = 2500$ m, length of span #2: $l_2 = 500$ m, length of span #3: $l_3 = 1000$ m, length of span #4: $l_4 = 1000$ m.

b) The PSpice program is listed in Appendix 3. One obtains the results of Figs. E2.9.2 and E2.9.3.

ST. GEORGE POLICE DEPT. LANE

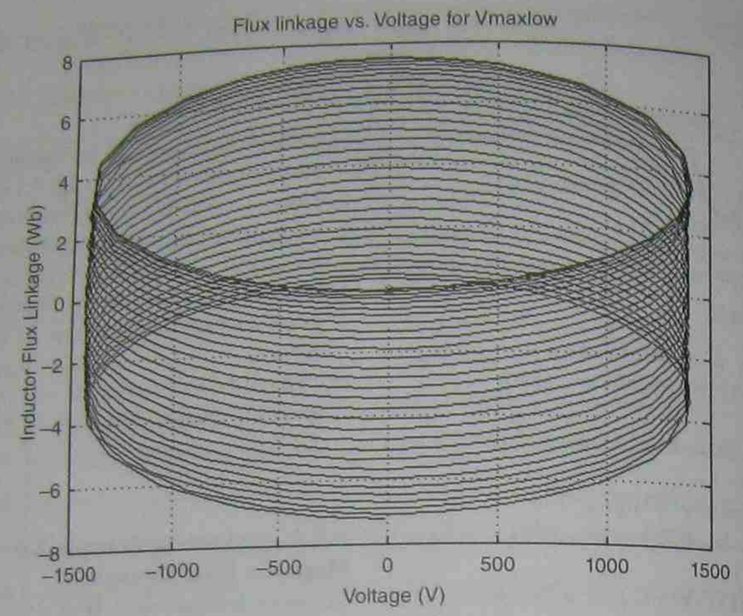



**FIGURE E2.7.2** Inductor flux linkage versus voltage at $V_{max_low} = \sqrt{2} \cdot 1000$ V.

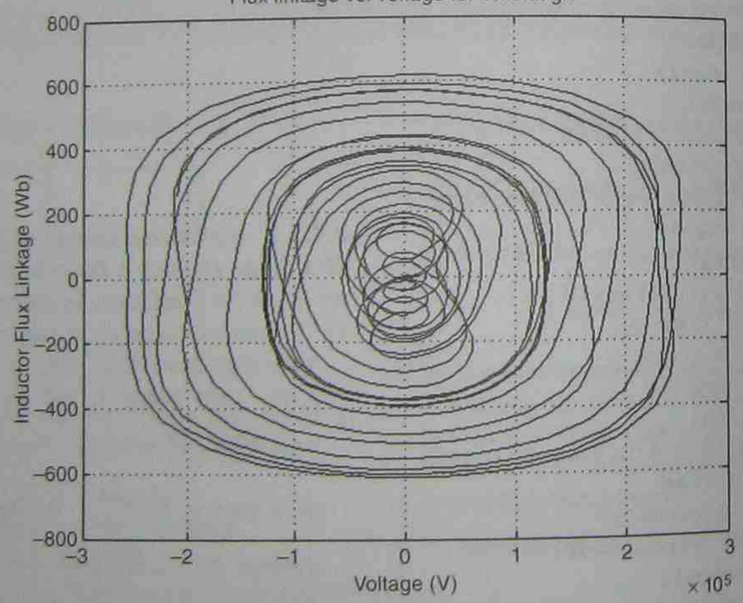



**FIGURE E2.7.3** Inductor flux linkage versus voltage at $V_{max_high} = \sqrt{2} \cdot 20000$ V.



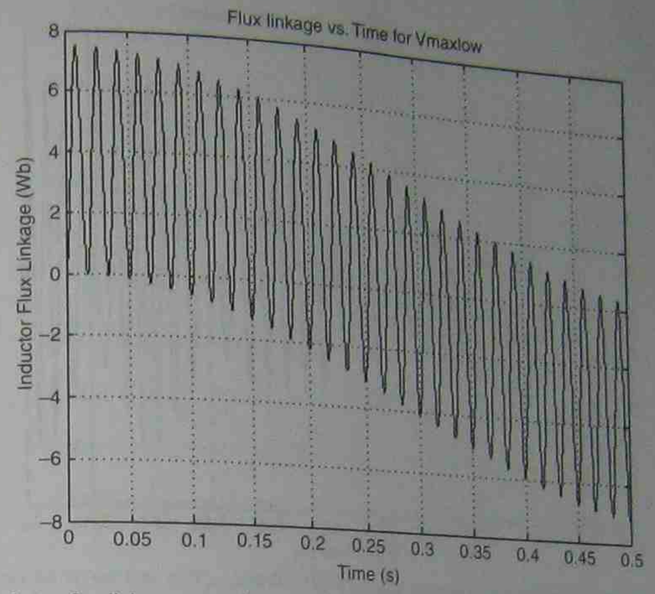



**FIGURE E2.7.4** Inductor flux linkage versus time at $V_{max_low} = \sqrt{2} \cdot 1000$ V.

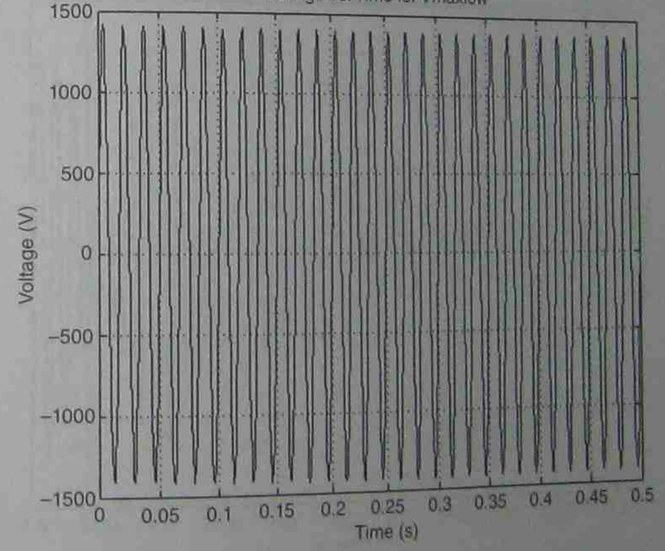



**FIGURE E2.7.5** Voltage versus time at $V_{max_low} = \sqrt{2} \cdot 1000$ V.

ST. GEORGE POLLEGE OF LAW

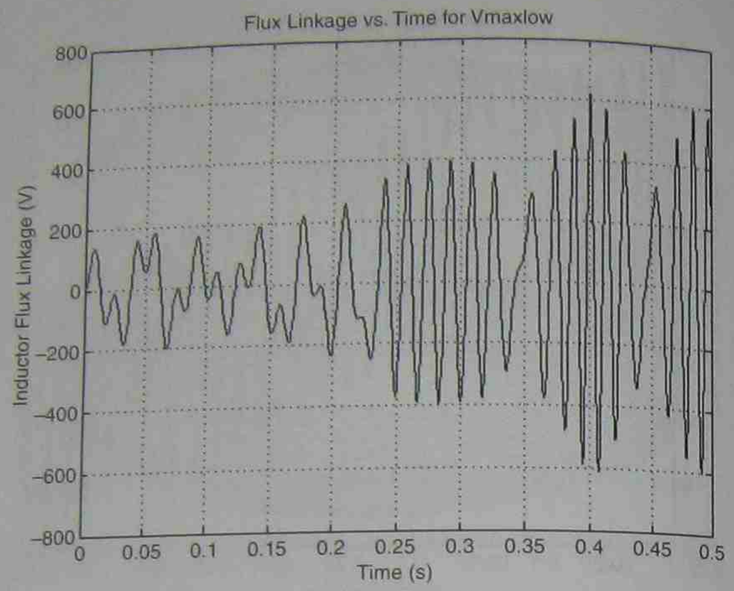



**FIGURE E2.7.6** Inductor flux linkage versus time at $V_{max_high} = \sqrt{2} \cdot 20000$ V.

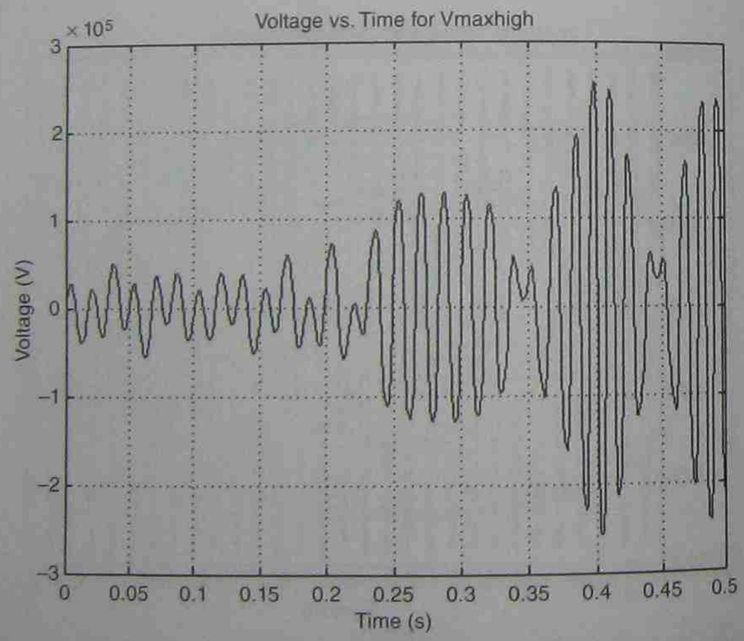



**FIGURE E2.7.7** Voltage versus time at $V_{max_high} = \sqrt{2} \cdot 20000$ V.



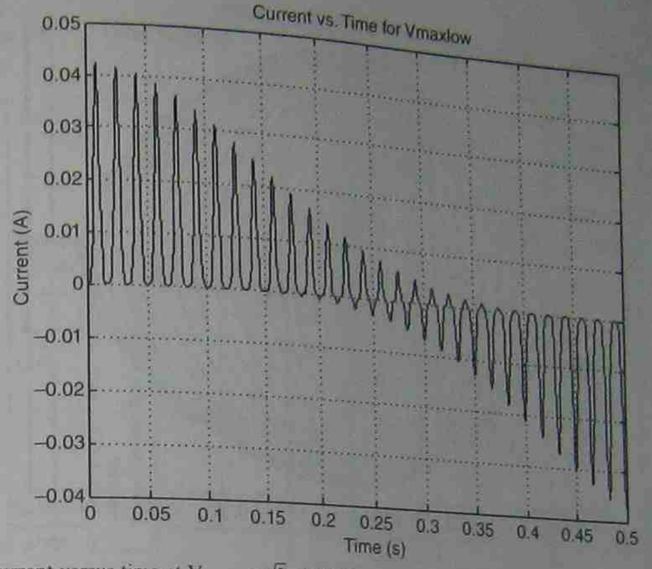



**FIGURE E2.7.8** Current versus time at $V_{max_low} = \sqrt{2} \cdot 1000$ V.

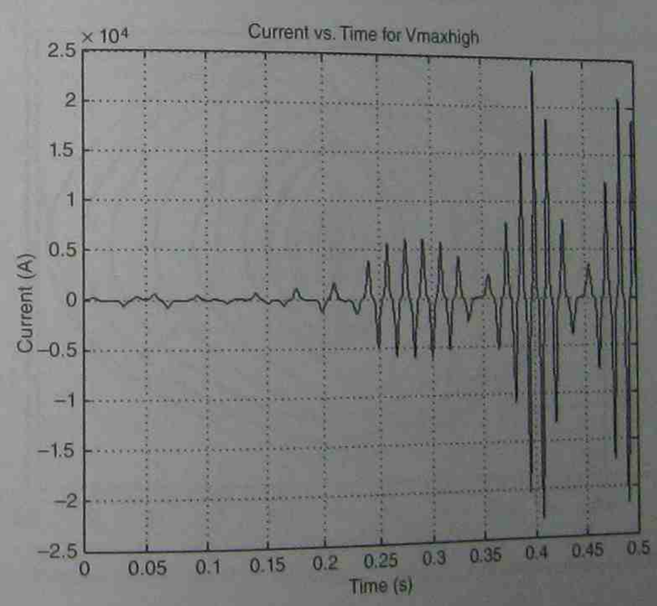



**FIGURE E2.7.9** Current versus time at $V_{max_high} = \sqrt{2} \cdot 20000$ V.

ST. GEORGE COLLEGE OF LAW

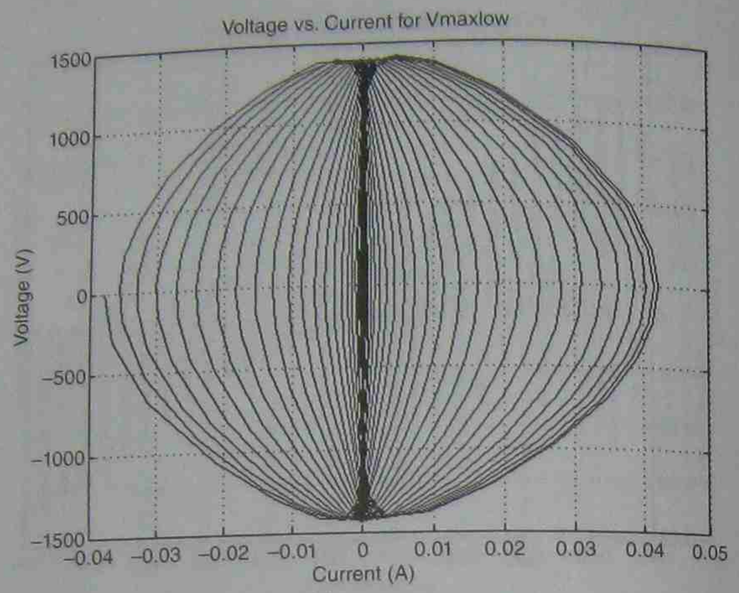



**FIGURE E2.7.10** Voltage versus current at $V_{max_low} = \sqrt{2} \cdot 1000$ V.

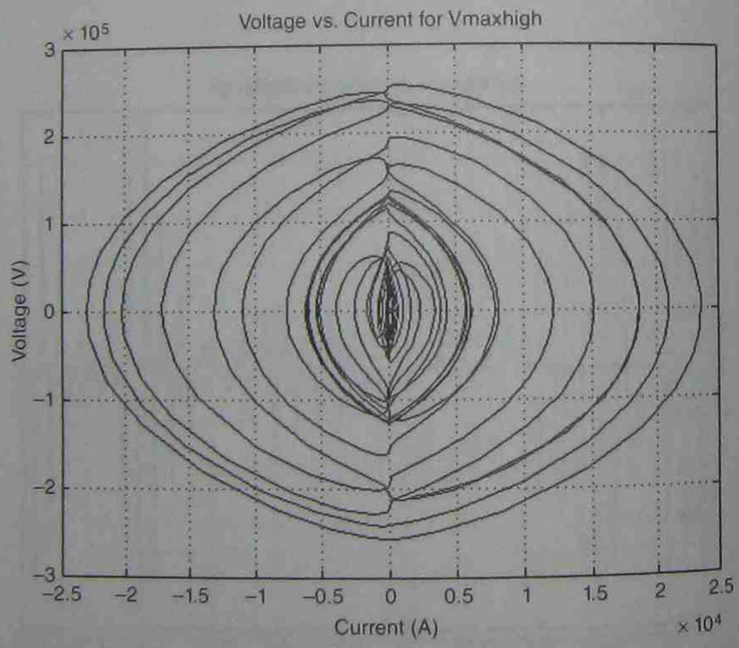



**FIGURE E2.7.11** Voltage versus current at $V_{max_high} = \sqrt{2} \cdot 20000$ V.

ST. GEORGE COLLEGE OF



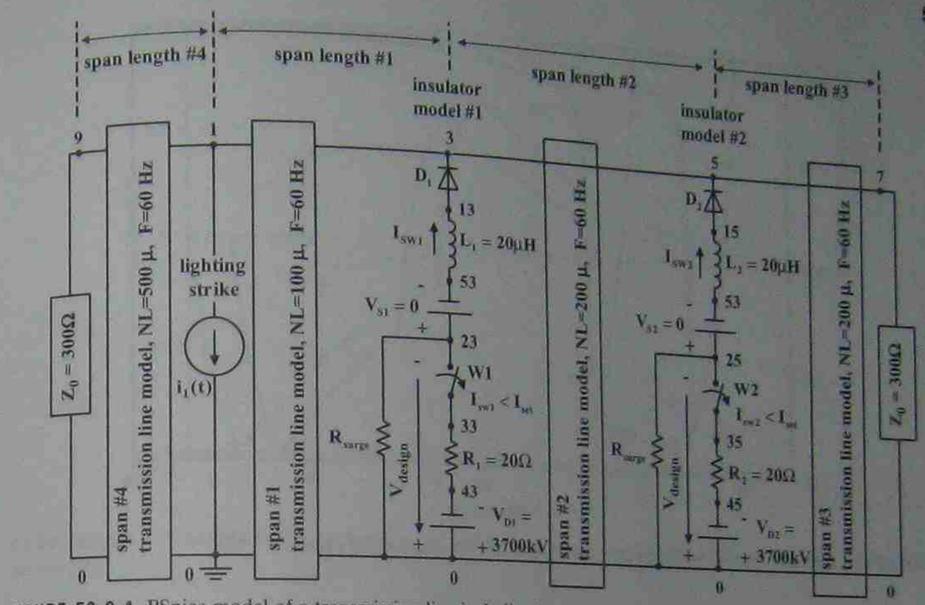



**FIGURE E2.9.1** PSpice model of a transmission line including insulators.

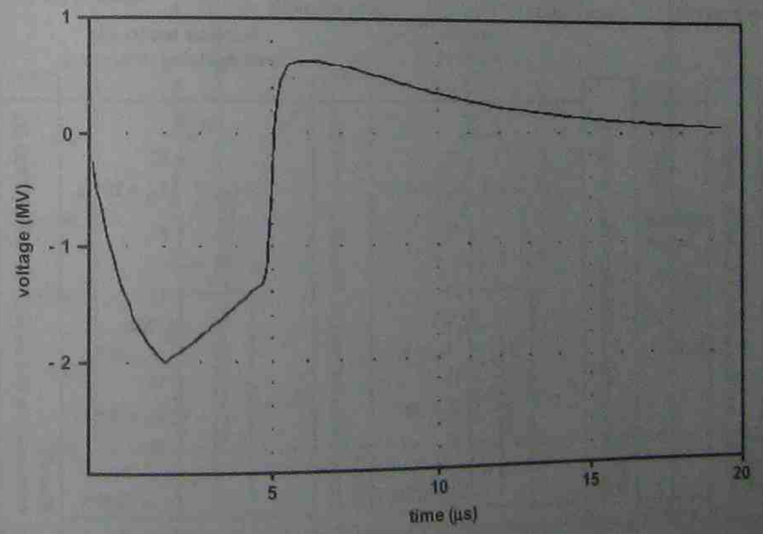



**FIGURE E2.9.2** Transmission line voltage at the point of strike V(1).

### 2.7.1.3 *Application Example 2.10: Lightning Arrester Operation: Solution*

a) Calculations are performed using PSpice, and the plots of the transmission line voltage (in MV) as a function of time (in $\mu$s) at the point of strike, at the insulator, and at the lightning arrester are shown in Figs. E2.10.2 and E2.10.3. The PSpice program is listed in Appendix 4.

b) One obtains the results of Figs. E2.10.4 and E2.10.5.

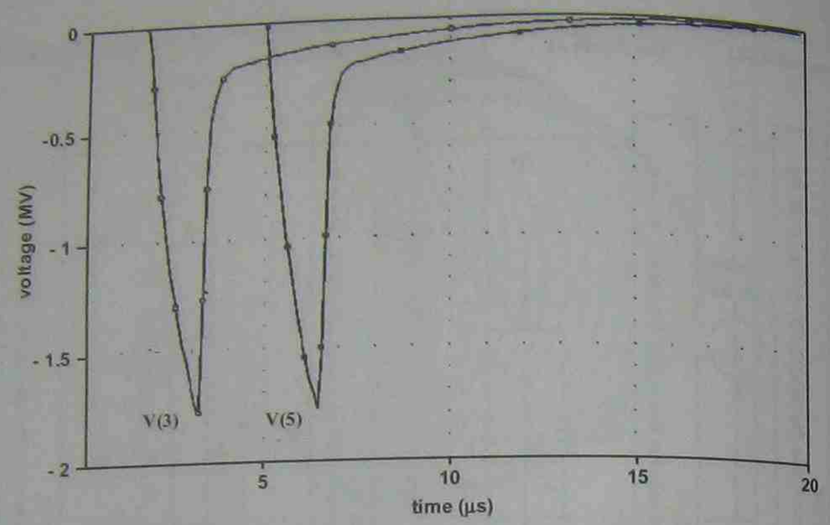



**FIGURE E2.9.3** Transmission line voltage at the first insulator V(3), and second insulator V(5).

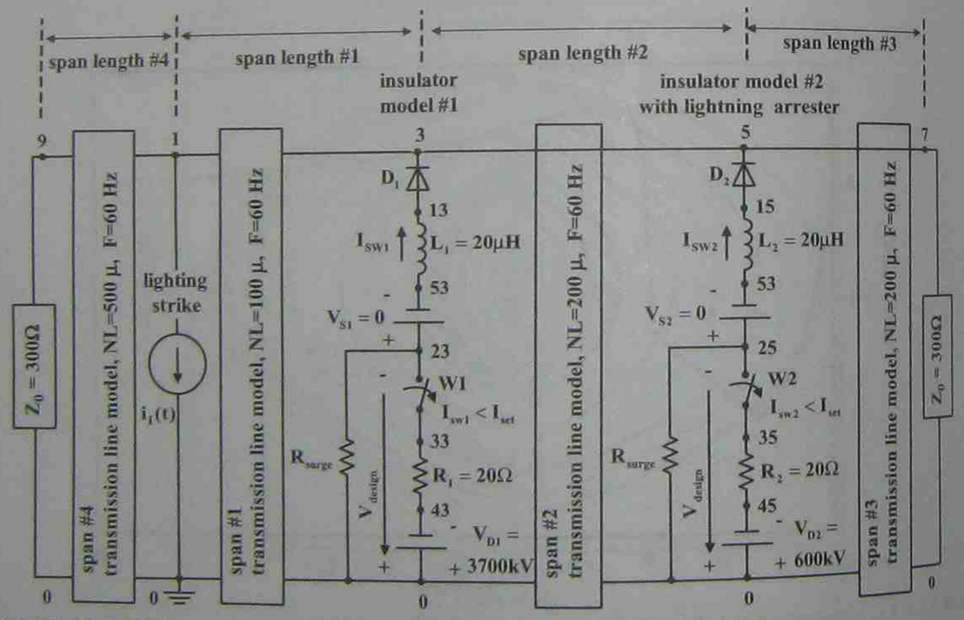



**FIGURE E2.10.1** PSpice model of a transmission line including insulator and lightning arrester.



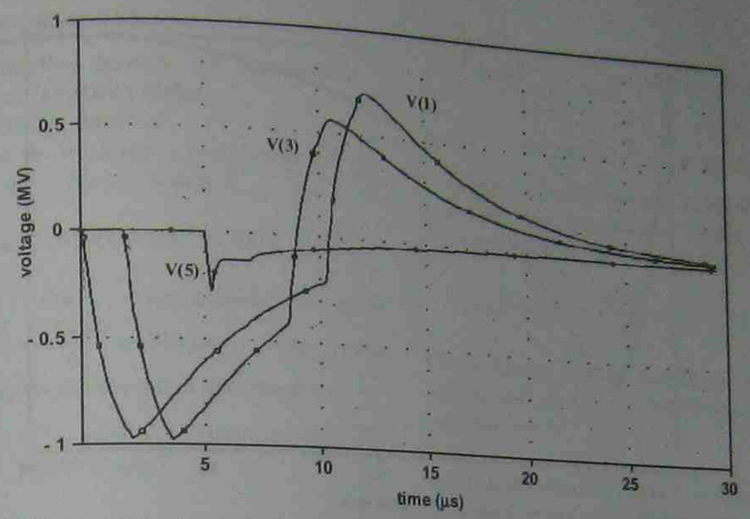



**FIGURE E2.10.2** Transmission line voltage at the point of strike V(1), at the first insulator V(3), and at the lightning arrester V(5).

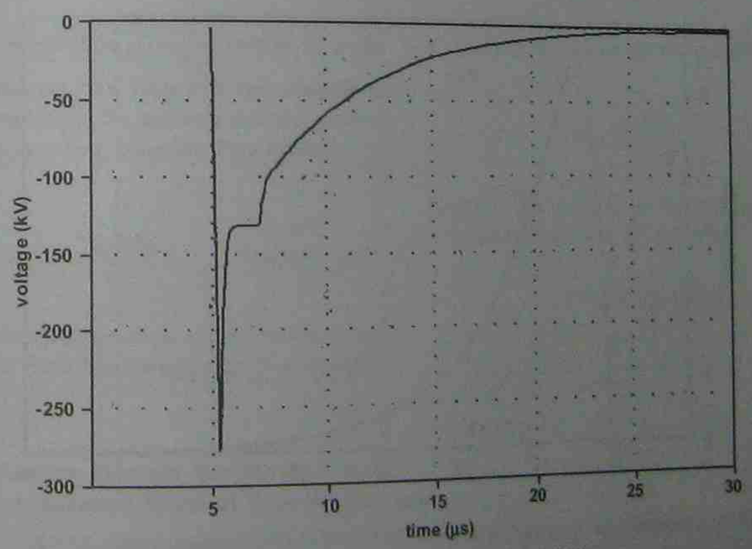



**FIGURE E2.10.3** Transmission line voltage at the lighning arrester (magnified) V(5).

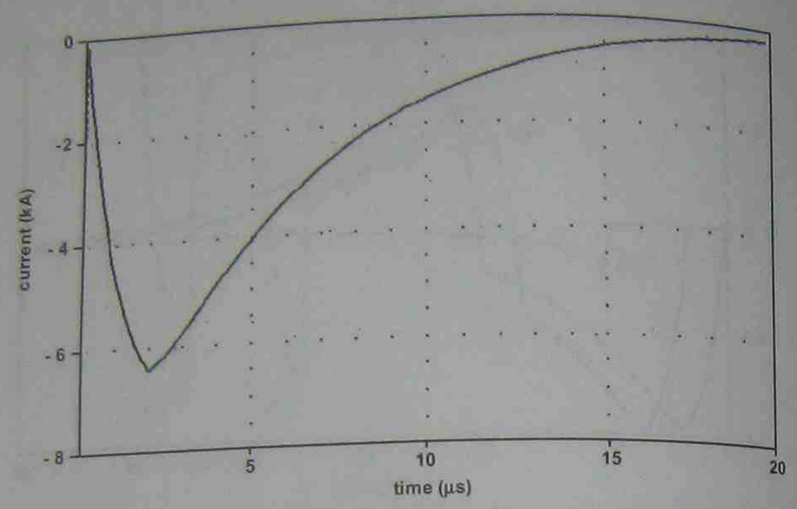



**FIGURE E2.10.4** Transmission line current at the point of strike I($i_1(t)$).

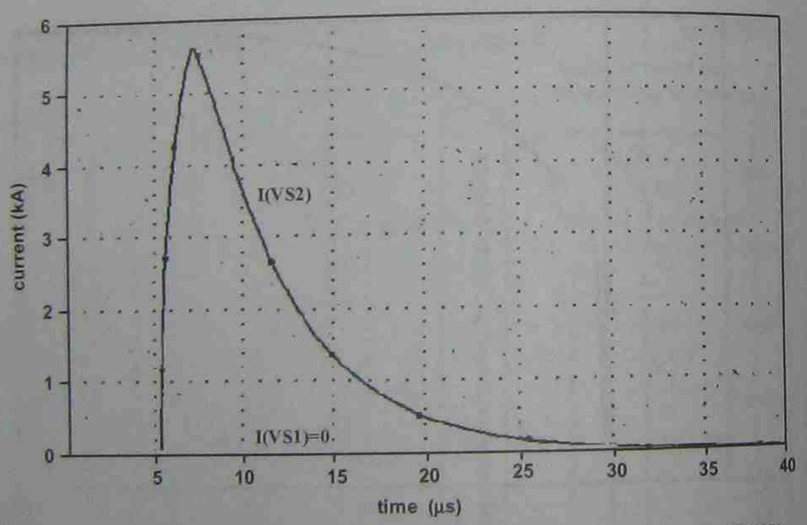



**FIGURE E2.10.5** Transmission line current at the insulator I(VS1) = 0 and the lightning arrester I(VS2).

ST. GEORGE COLLEGE OF LAW



## CHAPTER 3 SOLUTIONS

### 3.1.1 Application Example 3.1: Steady-State Operation of Induction Motor at Undervoltage: Solution

a) Based on the small-slip approximation $s \propto \frac{1}{V^2}$, the new slip at the low voltage is

$$s_{low} = 0.03(480/430)^2 = 0.0374.$$

b) With the synchronous speed $n_s = \frac{120f}{p} = \frac{120(60)}{6} = 1200\,\text{rpm}$ rpm one calculates the shaft speed at low voltage as

$$n_{m_low} = (1 - s_{low})n_s = (1 - 0.0374)(1200) = 1155.14\ \text{rpm}.$$

c) The output power at low voltage is $P_{out} = \omega_m \cdot T_m$. For constant mechanical torque one gets

$$P_{out_low} = \frac{(1-0.0374)}{(1-0.03)}(100\,\text{hp}) = 99.23\,\text{hp}.$$

d) Due to the relation $T = \frac{P_g}{\omega_{s1}}$ (where $P_g$ is the air-gap power), the torque is proportional to $P_g$, and therefore, for constant torque operation the air-gap power is constant. Thus the rotor loss is

$$P_{cur_low} = s_{low} P_g = \frac{0.0374}{0.03} P_{cur_rat} = 1.247\, P_{cur_rat}.$$

One concludes that a decrease of the terminal voltage increases the rotor loss (temperature) of an induction motor.

### 3.1.2 Application Example 3.2: Steady-State Operation of Induction Motor at Overvoltage: Solution

a) Based on the small-slip approximation $s \propto \frac{1}{V^2}$, the new slip at the low voltage is

$$s_{high} = 0.03(480/510)^2 = 0.02657.$$

b) With the synchronous speed $n_s = \frac{120f}{p} = \frac{120(60)}{6} = 1200\,\text{rpm}$ rpm one calculates the shaft speed at low voltage as $n_{m_high} = (1 - s_{high})n = (1 - 0.02657)(1200) = 1168.11$ rpm.

c) The output power at low voltage is $P_{out} = \omega_m \cdot T_m$. For constant mechanical torque one gets

$$P_{out_high} = \frac{(1-0.02657)}{(1-0.03)}(100\,\text{hp}) = 100.35\,\text{hp}.$$

d) Due to the relation $T = \frac{P_g}{\omega_{s1}}$, where $P_g$ is the air-gap power, the torque is proportional to $P_g$, and therefore, for constant torque operation the air-gap power is constant. Thus the rotor loss is

$$P_{our_high} = s_{high} P_g = \frac{0.02657}{0.03} P_{our_rat} = 0.886\, P_{our_rat}.$$

One concludes that an increase of the terminal voltage decreases the rotor loss (temperature) of an induction motor.

### 3.1.3 Application Example 3.3: Steady-State Operation of Induction Motor at Undervoltage and Under-Frequency: Solution

The small-slip approximation results in the torque equation

$$T = \frac{q_1 \cdot V_s^2 \cdot s}{\omega_{s1} \cdot R_r'}.$$

a) Applying the relation to rated conditions (1) one gets

$$T^{(1)} = \frac{q_1 \cdot V_s^{2(1)} \cdot s^{(1)}}{\omega_{s1}^{(1)} \cdot R_r'}.$$

Applying the relation to low-voltage and low-frequency conditions (2) one gets

$$T^{(2)} = \frac{q_1 \cdot V_s^{2(2)} \cdot s^{(2)}}{\omega_{s1}^{(2)} \cdot R_r'},$$

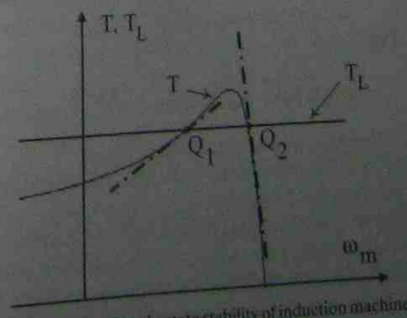



**FIGURE E3.4.1** Steady-state stability of induction machine with constant load torque.

With $T^{(1)} = T^{(2)}$ and the relations

$$\omega_{s1}^{(1)} = \frac{2\pi f^{(1)}}{p/2} \quad \text{and} \quad \omega_{s1}^{(2)} = \frac{2\pi f^{(2)}}{p/2}$$

one obtains

$$s^{(2)} = s^{(1)} \frac{(V_s^{(1)})^2}{(V_s^{(2)})^2} \frac{f^{(2)}}{f^{(1)}} = 0.0367.$$

b) The synchronous speed $n_s^{(2)}$ at $f^{(2)} = 59$ Hz is $n_s^{(2)} = \frac{120(59)}{6} = 1180$ rpm, or the corresponding shaft speed $n_m^{(2)} = n_s^{(2)}(1 - s^{(2)}) = 1137$ rpm.

c) The torque-output power relations are

$$T^{(1)} = \frac{P_{out}^{(1)}}{\omega_m^{(1)}} \quad \text{and} \quad T^{(2)} = \frac{P_{out}^{(2)}}{\omega_m^{(2)}}.$$

With $T^{(1)} = T^{(2)}$ one gets

$$\frac{P_{out}^{(1)}}{\omega_m^{(1)}} = \frac{P_{out}^{(2)}}{\omega_m^{(2)}} \quad \text{or} \quad \frac{P_{out}^{(1)}}{\omega_{s1}^{(1)}(1-s^{(1)})} = \frac{P_{out}^{(2)}}{\omega_{s1}^{(2)}(1-s^{(2)})} \quad \text{or}$$

$$\frac{P_{out}^{(1)}}{\frac{120f^{(1)}}{p}(1-s^{(1)})} = \frac{P_{out}^{(2)}}{\frac{120f^{(2)}}{p}(1-s^{(2)})}.$$

For the reduced output power it follows

$$P_{out}^{(2)} = \frac{(1-s^{(2)})}{(1-s^{(1)})} \frac{f^{(2)}}{f^{(1)}} P_{out}^{(1)} = 97.65\text{hp}.$$

d) The copper losses of the rotor are $P_{cur} = q_1 (I_r')^2 R_r'$ and the output power is $P_{out} = q_1 (I_r')^2 R_r' \frac{(1-s)}{s}$.

The application of the relations to the two conditions (1) and (2) yields

$$P_{out}^{(1)} = q_1 (I_r'^{(1)})^2 R_r' \frac{(1-s^{(1)})}{s^{(1)}} \quad \text{and}$$

$$P_{out}^{(2)} = q_1 (I_r'^{(2)})^2 R_r' \frac{(1-s^{(2)})}{s^{(2)}} \quad \text{or}$$

$$\frac{(I_r'^{(2)})^2}{(I_r'^{(1)})^2} = \frac{P_{out}^{(2)}}{P_{out}^{(1)}} \frac{s^{(2)}}{s^{(1)}} \frac{(1-s^{(1)})}{(1-s^{(2)})} = 1.20.$$

The rotor loss increase becomes now

$$\frac{P_{cur}^{(2)}}{P_{cur}^{(1)}} = \frac{(I_r'^{(2)})^2}{(I_r'^{(1)})^2} = 1.20.$$

One concludes that the simultaneous reduction of voltage and frequency increases the rotor losses (temperature) in a similar manner as discussed in Application Example 3.1. It is advisable not to lower the power system voltage beyond the levels as specified in standards.

### 3.3.1 Application Example 3.4: Unstable and Stable Steady-State Operation of Induction Machines: Solution

The stability conditions at the two points where the two curves intersect are

$$\mathbf{Q_1}: \left.\begin{aligned} &\frac{\Delta T_L}{\Delta \omega_m} = 0 \\ &\frac{\Delta T}{\Delta \omega_m} > \text{positive}. \end{aligned}\right\} 0 < \text{positive} \gg\gg\gg \textbf{unstable.}$$

$$\mathbf{Q_2}: \left.\begin{aligned} &\frac{\Delta T_L}{\Delta \omega_m} = 0 \\ &\frac{\Delta T}{\Delta \omega_m} = \text{negative}. \end{aligned}\right\} 0 > \text{negative} \gg\gg\gg \textbf{stable,}$$

Therefore, operation at $Q_1$ is unstable and will result in rapid speed reduction. This will stop the operation of the induction machine, while operating point $Q_2$ is stable.

### 3.3.2 Application Example 3.5: Stable Steady-State Operation of Induction Machines: Solution

The stability conditions at the point where the two curves intersect is

$$\mathbf{Q_1}: \left.\begin{aligned} &\frac{\Delta T_L}{\Delta \omega_m} = \text{positive} \\ &\frac{\Delta T}{\Delta \omega_m} = \text{negative} \end{aligned}\right\} \gg\gg\gg \textbf{stable.}$$

Therefore, an induction machine connected to a mechanical load with parabolic torque-speed characteristics as shown in Fig. E3.5.1 will not experience any steady-state stability problems.

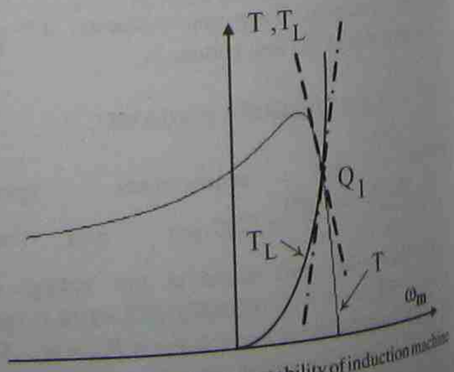



**FIGURE E3.5.1** Steady-state stability of induction machine with nonlinear load torque.





**TABLE E3.6.1** Main-Phase (m) Input Impedance at Single-Phase No-Load Operation as a Function of Input Voltage for R333MC

| $V_m$ (V) | $R_m$ (Ω) | $X_m$ (Ω) | $Z_m$ (Ω) | $L_m$ (mH) |
|---|---|---|---|---|
| 250.3 | 9.65 | 46.6 | 47.6 | 126 |
| **229.9** | **11.2** | **56.9** | **58.0** | **154** |
| 210.3 | 13.2 | 67.8 | 69.1 | 183 |
| 189.8 | 15.1 | 77.3 | 78.7 | 209 |
| 170.6 | 17.0 | 82.4 | 84.1 | 223 |
| 149.5 | 18.6 | 85.4 | 87.4 | 232 |
| 129.8 | 20.5 | 86.3 | 88.7 | 235 |
| 109.2 | 22.6 | 86.7 | 89.5 | 238 |
| 89.9 | 22.5 | 87.8 | 90.6 | 240 |
| 69.4 | 26.3 | 87.0 | 90.9 | 241 |

**TABLE E3.6.2** Auxiliary-Phase (a) Input Impedance at Single-Phase No-Load Operation as a Function of Input Voltage for R333MC

| $V_a$ (V) | $R_a$ (Ω) | $X_a$ (Ω) | $Z_a$ (Ω) | $L_a$ (mH) |
|---|---|---|---|---|
| **298.88** | **30.6** | **94.7** | **99.5** | **264** |
| 279.9 | 33.6 | 106.0 | 111.2 | 295 |
| 259.3 | 36.8 | 117.9 | 123.5 | 328 |
| 239.8 | 39.1 | 126.2 | 132.1 | 351 |
| 219.4 | 41.1 | 132.5 | 138.7 | 368 |
| 199.0 | 43.8 | 135.6 | 142.5 | 378 |
| 179.3 | 45.6 | 137.4 | 144.7 | 384 |
| 160.0 | 46.7 | 138.6 | 146.3 | 388 |
| 139.1 | 49.9 | 139.0 | 147.6 | 392 |
| 120.8 | 50.3 | 140.2 | 148.9 | 395 |
| 100.1 | 54.3 | 139.3 | 149.5 | 397 |

### 3.7.2 Application Example 3.6: Measurement of Harmonics within Yoke (Back Iron) and Tooth Flux Densities of Single-Phase Induction Machines

#### 3.7.2.1 *Data of Motor R333MC: Solution*

**Stator Parameters**

- 60 Hz AC main-phase resistance: 4.53 Ω,
- main-phase leakage reactance: 5.02 Ω,
- auxiliary-phase resistance: 17.77 Ω,
- auxiliary-phase leakage reactance: 6.70 Ω,
- turns ratio between auxiliary- and main-phase windings: 1.34, and
- angle enclosed by the axes of auxiliary- and main-phase windings: 90.8°.

**Rotor Parameters**

- DC resistance: 4.687 Ω,
- 60 Hz AC resistance: 4.703 Ω,
- 120 Hz AC resistance: 4.751 Ω,
- linear leakage reactance: 5.635 Ω,
- skin-effect coefficient: $k_r = 0.0572$, and
- nonlinear rotor leakage $(\lambda - i)$ characteristic (referred to stator) is shown in Fig. E3.6.1.

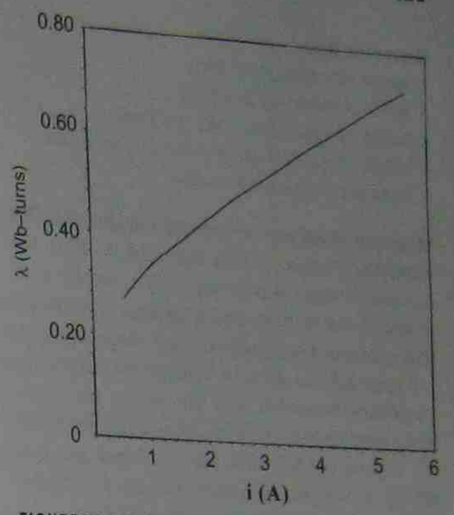



**FIGURE E3.6.1** Nonlinear rotor leakage $(\lambda - i)$ characteristic of R333MC.

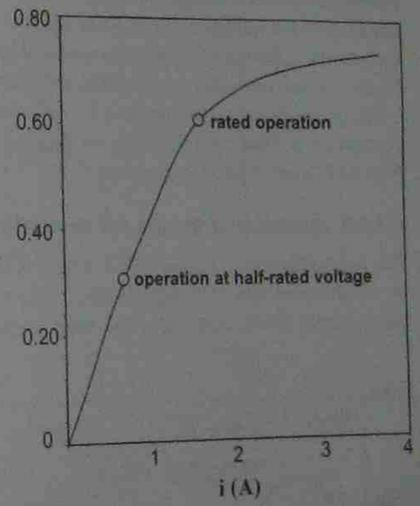



**FIGURE E3.6.2** Nonlinear magnetizing $(\lambda - i)$ characteristic of R333MC.

**Magnetizing Parameters**

- unsaturated magnetizing reactance: 166.1 Ω,
- resistance corresponding to iron-core loss: 580 Ω, and
- nonlinear magnetizing $(\lambda - i)$ characteristic is depicted in Fig. E3.6.2.

**No-Load Input Impedance.** The main- and auxiliary-phase input impedances are measured and recorded in Tables E3.6.1 and E3.6.2, respectively, at single-phase no-load operation as a function of the rms value of the input voltage. Note that in Table E3.6.1 the parameters $Z_m$ and $L_m$ are referred to the main-phase $(m)$ winding, whereas in Table E3.6.2 $Z_a$ and $L_a$ are referred to the auxiliary-phase $(a)$ winding.

ST. GEORGE POLLEGE OF LAW, E

**Geometric Data**

- length of iron core: 80 mm,
- width of stator tooth: 3.5 mm,
- height of main-phase yoke: 14.85 mm,
- height of auxiliary-phase yoke: 11.5 mm, and
- iron-core stacking factor: 0.95.

**Measured Waveforms of Induced Voltages and Flux Densities.** Figures E3.6.3a and E3.6.3b show the induced voltage waveforms within search coils wound on the teeth located at the axes of the main-phase and auxiliary-phase windings, respectively.

Figures E3.6.4a and E3.6.4b depict the flux density waveforms associated with the axis of the main-phase winding of all three machines as listed in Table 3.3. Figures E3.6.4c and E3.6.4d depict the flux density waveforms associated with the axis of the auxiliary-phase winding for all three machines.

Figures E3.6.5a, E3.6.5b, E3.6.5c, and E3.6.5d show that the flux densities are approximately a linear function of the input voltage. In Figs. E3.6.6a and E3.6.6b comparison of the flux densities in the teeth and yoke (back iron) are presented for the methods discussed in the prior subsections of Section 3.7. The no-load currents of R333MC and 80664346 are depicted in Figs. E3.6.7a and E3.6.7b, respectively.

### 3.7.2.2 Discussion of Results and Conclusions

The permanent-split capacitor (PSC) motors of the air conditioners 80664346 and R333MC have the same output power and about the same overall dimensions (length and outer diameter). However, their stator and rotor windings are different. Measurements indicate that the 80664346 motor [36] generates a nearly sinusoidal flux density in the stator teeth (Fig. E3.6.4a), whereas that of the R333MC motor exhibits nonsinusoidal waveform although its $(B_{mt})_{max}$ is smaller. In addition, the no-load current of the 80664346 (Fig. E3.6.7b) is about half that of R333MC (Fig. E3.6.7a), although the latter's maximum flux density in stator teeth and back iron (yoke) is less (Figs. E3.6.4a and E3.6.4c). This indicates that the proper designs of the stator and rotor windings are important for the waveform of the stator tooth flux density and its associated iron-core loss, and for the efficiency optimization of PSC motors.

The yoke flux densities (Figs. E3.6.4b and E3.6.4d) are mostly sinusoidal for all machines tested [36 in Chapter 3]. Although 80664346 has a larger flux density than R333MC, the no-load losses of 80664346 are smaller as can be seen from their stator, rotor, and magnetizing parameters. References [30], [37], and Appendix of [38] address how time-dependent waveforms of the magnetizing current depend on the spatial distribution/pitch of a winding. Figures E3.6.5a through E3.6.5d show that in these three PSC motors saturation in stator teeth and yokes is small as compared to transformers, and therefore the principle of superposition with respect to flux densities and losses can be applied. Figures E3.6.6a and E3.6.6b demonstrate that both the computer sampling and the oscilloscope methods lead to similar results with respect to maximum flux densities. One concludes that although a single-phase motor (e.g., 80664346) has relatively large flux densities in stator yoke and teeth the no-load current can be relatively small, although it is quite nonsinusoidal. One of the reasons for this is that the power factor at no load is relatively large. The best design of a PSC motor is thus not necessarily based on sinusoidal current wave shapes. Further work should investigate the following:

- the losses generated by alternating flux densities as they occur in the stator teeth, and rotating flux densities as they occur in the stator yoke, and
- the interrelation between time and space harmonics and their effects on loss generation.

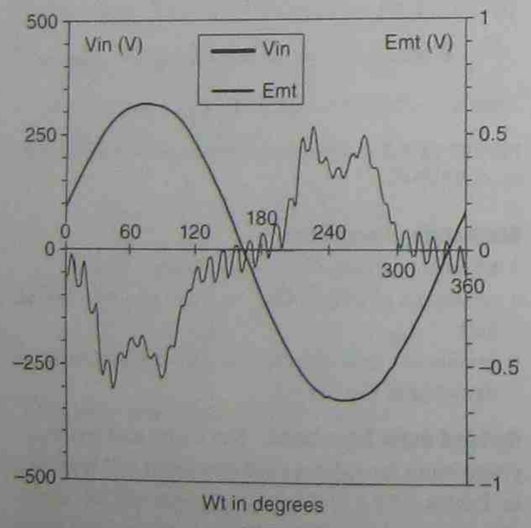



**FIGURE E3.6.3a** Waveforms of input ($V_{in}$, left-hand side ordinate) and main-phase winding tooth induced voltages ($e_{mt} \equiv E_{mt}$, right-hand side ordinate) of R333MC.

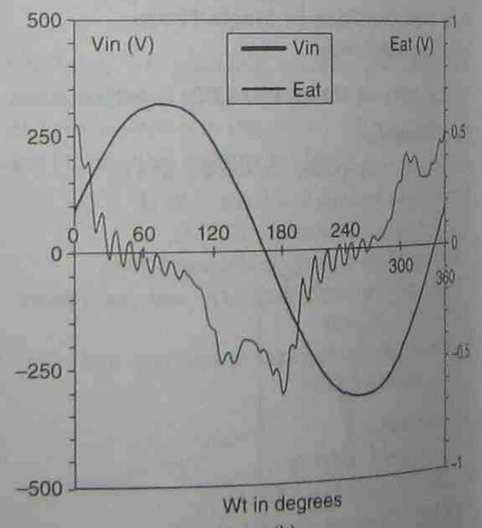



**FIGURE E3.6.3b** Waveforms of input ($V_{in}$, left-hand side ordinate) and auxiliary-phase winding tooth induced voltages ($e_{at} \equiv E_{at}$, right-hand side ordinate) of R333MC.



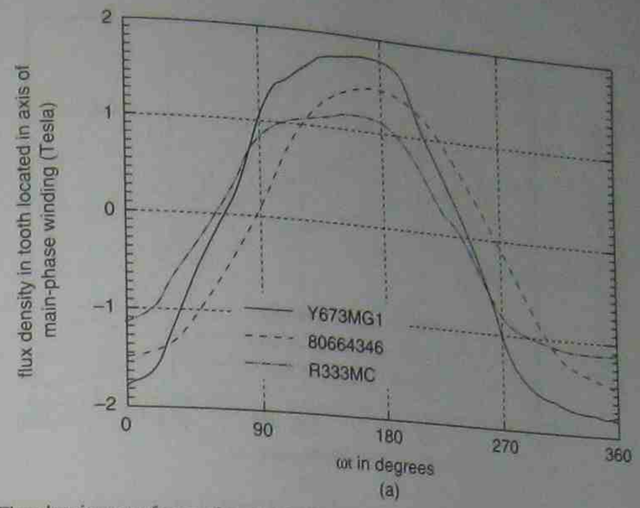



**FIGURE E3.6.4a** Flux density waveforms of tooth ($B_{mt}$) located in axis of main-phase winding at rated voltage of R333MC, 80664346, and Y673MG1.

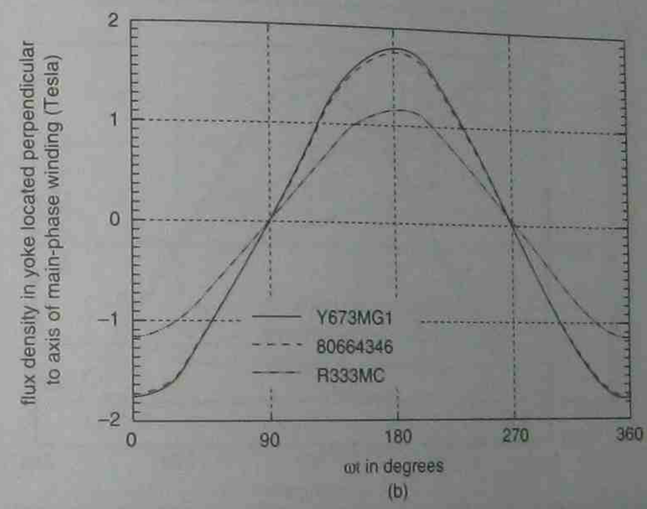



**FIGURE E3.6.4b** Flux density waveforms of yoke ($B_{my}$) associated with main-phase winding at rated voltage of R333MC, 80664346, and Y673MG1.

### 3.8.3 Application Example 3.7: Computation of Forward-Rotating Subharmonic Torque in a Voltage-Source-Fed Induction Motor: Solution

Parameters of Eqs. 3-47 to 3-54 are listed as a function of the fundamental ($h = 1$) and

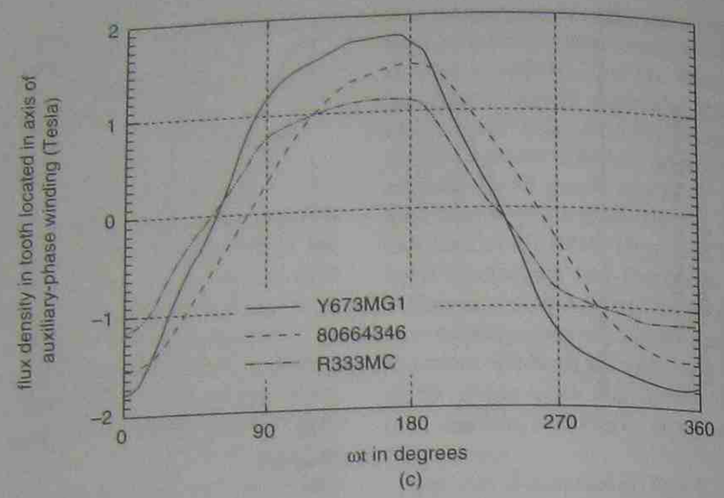



**FIGURE E3.6.4c** Flux density waveforms of tooth ($B_{at}$) located in axis of auxiliary-phase winding at rated voltage of R333MC, 80664346, and Y673MG1.

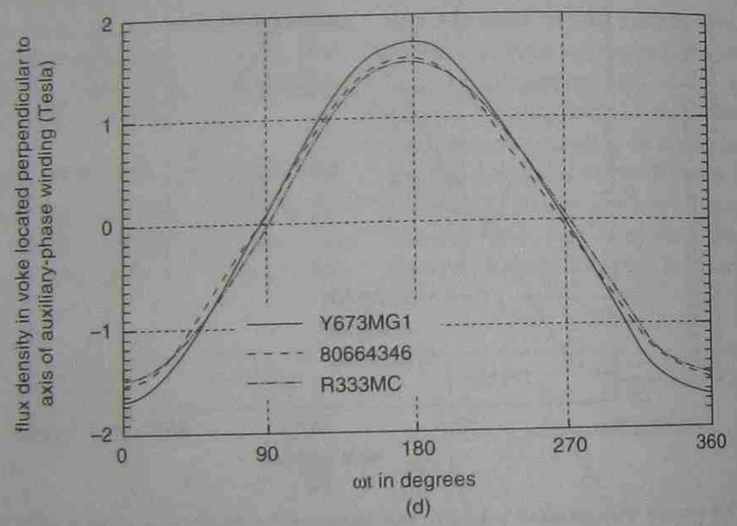



**FIGURE E3.6.4d** Flux density waveforms of yoke ($B_{ay}$) associated with auxiliary-phase winding at rated voltage of R333MC, 80664346, and Y673MG1.

subharmonic $h = 0.1$ in Table E3.7.1. Fundamental torque values $T_{e1}$ are listed in Table E3.7.2 as a function of the fundamental slip $s_1$.

The plot of the positively rotating fundamental torque characteristic $T_{e1} = f(s_1)$ is shown in Fig. E3.7.1 and the positively rotating torque $Te_{0.1} = f(s_{0.1})$ is depicted in Fig. E3.7.2, where the 6 Hz voltage component has an amplitude of 5%, that is, $V_{6Hz} = 0.05 \cdot V_{60Hz} = 0.05(240\ \text{V}) = 12\ \text{V}$.

Subharmonic torque values $T_{e0.1}$ are listed in Table E3.7.3 as a function of the subharmonic slip $s_{0.1}$.

Using Eqs. 3-4d and 3-25 one can compute the fundamental torque $T_{e1}$ and the subharmonic torque $T_{e0.1}$ as a function of the fundamental slip $s_1$ (Table E3.7.4). For example a subharmonic ($h = 0.1$) slip of $s_{0.1} = 1$ corresponds to a fundamental slip of (see Eqs. 3-31b, 3-32, and Table E3.7.3)



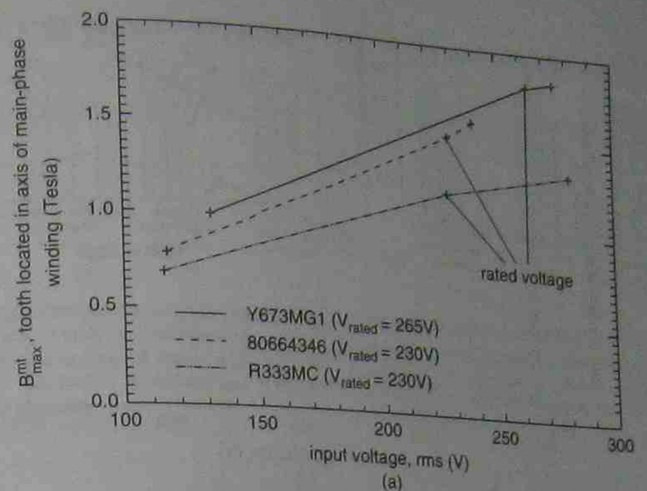



**FIGURE E3.6.5a** Maximum flux density in tooth located in axis of main-phase winding as a function of input voltage of R333MC, 80664346, and Y673MG1.

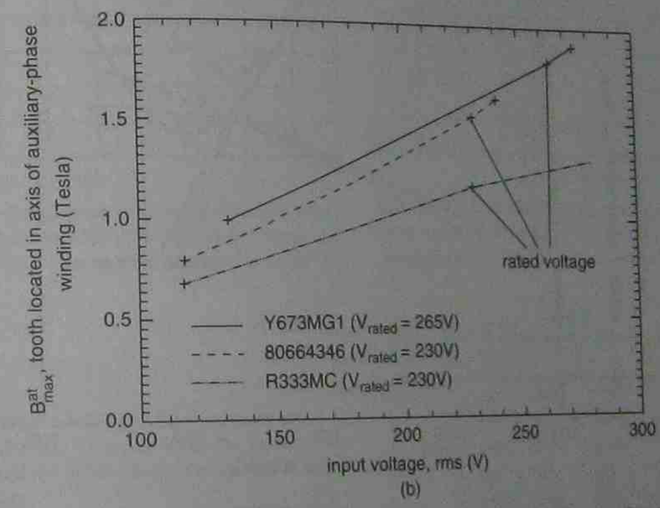



**FIGURE E3.6.5b** Maximum flux density in tooth located in axis of auxiliary-phase winding as a function of input voltage of R333MC, 80664346, and Y673MG1.

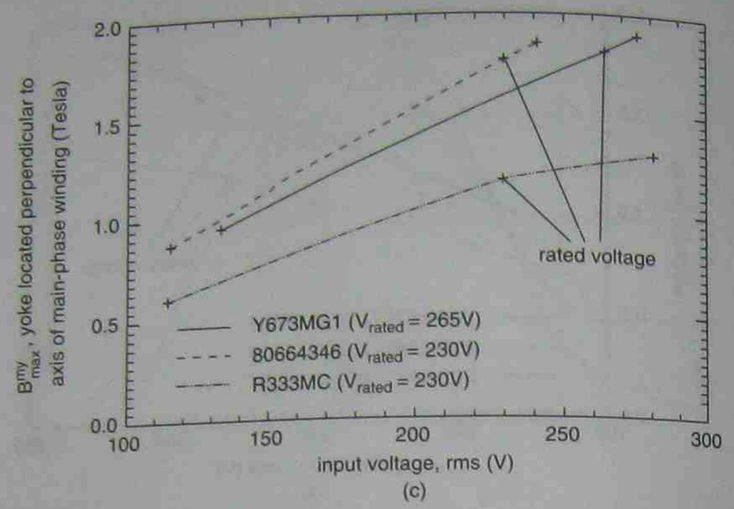
$$s_1 = (0.1)(s_{0.1}) + 0.9 = 1.0. \qquad \text{(E3.7-2)}$$

The plot of fundamental and subharmonic torque values ($T_{e1} + T_{e0.1}$) as a function of fundamental slip ($s_1$) is shown in Fig. E3.7.3.

### 3.8.4 Application Example 3.8: Rationale for Limiting Harmonic Torques in an Induction Machine: Solution

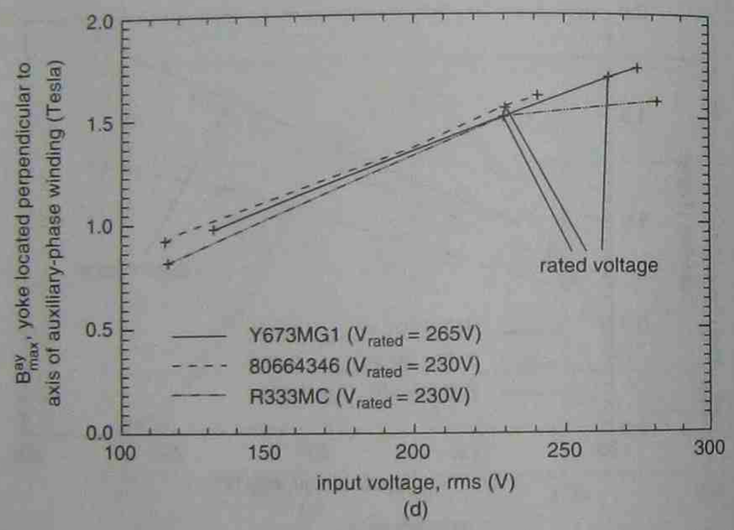
For subharmonic slip $s_{0.1} = 1.0$ one obtains with Eq. E3.7-2 the fundamental slip $s_1 = 1.0$. Correspondingly for subharmonic slip $s_{0.1} = 0.82$ one obtains $s_1 = 0.982$, and for subharmonic slip $s_{0.1} = -0.82$ one obtains $s_1 = 0.818$ (see Table E3.7.3).

One notes that the subharmonic torque at 6 Hz ($h = 0.1$) is relatively large in the generator region ($T_{e0.1} = -4.61$ Nm). If the worst case is considered as defined by Eq. 3-52 the corresponding low-frequency harmonic torque is even larger. This is the reason why the low-frequency harmonic voltages should be limited to less than a few percent (e.g., 2%) of rated voltage.




(c)

**FIGURE E3.6.5c** Maximum flux density in yoke located in axis of main-phase winding as a function of input voltage of R333MC, 80664346, and Y673MG1.




(d)

**FIGURE E3.6.5d** Maximum flux density in yoke located in axis of auxiliary-phase winding as a function of input voltage of R333MC, 80664346, and Y673MG1.

### 3.8.5 Application Example 3.9: Computation of Forward-Rotating Subharmonic Torque in Current-Source-Fed Induction Motor: Solution

The parameters of Eqs. 3-53 and 3-54 and the corresponding fundamental and subharmonic torques are listed in Table E3.9.1 through E3.9.3 as a function of the fundamental $h = 1$ and the subharmonic $h = 0.1$.

One notes that the low-frequency harmonic torques at 6 Hz and 5% harmonic current amplitudes are very small (about 0.0063 Nm).

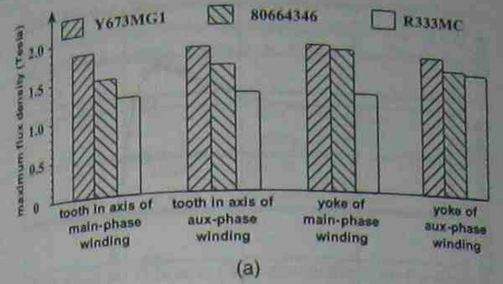
### 3.9.1 Application Example 3.10: Computation of Rotating MMF with Time and Space Harmonics: Solution

a) For $A_1 = 1$ pu, $A_H = 0.05$ pu, $I_{s1} = 1$ pu, $I_{mh} = 0.05$ pu, $H = 5$, and $h = 5$ one obtains the rotating mmf as

$$F_{total} = 1.5\cos(\theta - \omega_1 t) + 0.075\cos(\theta - 5\omega_1 t) + 0.075\cos(5\theta + \omega_1 t) + 0.00375\cos(5\theta - 5\omega_1 t)$$

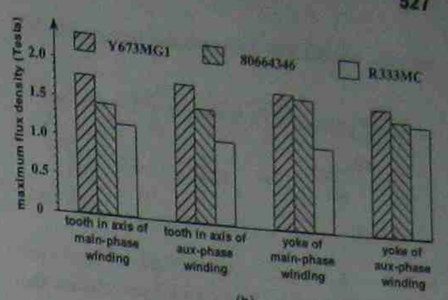
ST. GEORGE COLLEGE OF LAW





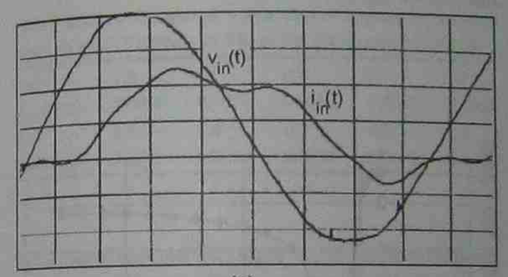

(a)

**FIGURE E3.6.6a** Comparison of maximum flux densities in teeth located in axis of main- and auxiliary-phase windings, and yokes located in axis of main- and auxiliary-phase windings for Y673MG1, 80664346, and R333MC (computer-sampling method).



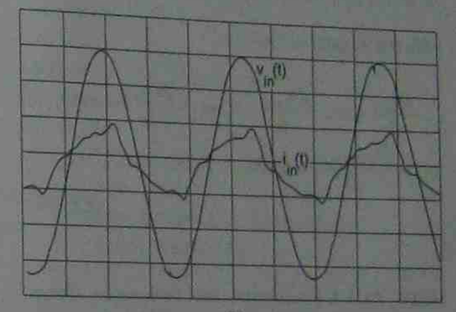

(b)

**FIGURE E3.6.6b** Comparison of maximum flux densities in teeth located in axis of main- and auxiliary-phase windings, and yokes located in axis of main- and auxiliary-phase windings for Y673MG1, 80664346, and R333MC (oscilloscope method).




(a)

**FIGURE E3.6.7a** Oscillogram of total input current waveform of R333MC, 2 A/div for current $i_{in}(t)$ and input AC voltage $v_{in}(t)$ with 100 V/div at minimum load at $f = 60$ Hz.




(b)

**FIGURE E3.6.7b** Oscillogram of total input current waveform of 80664346, 1 A/div for current $i_{in}(t)$ and input AC voltage $v_{in}(t)$ of 230.5 $V_{rms}$ at minimum load at $f = 60$ Hz.

**TABLE E3.7.1** Maximum Torques for Fundamental (h = 1) and Subharmonic (h = 0.1) Voltages, Where the Fundamental Voltage is 100% and the Subharmonic Voltage Is 5% of the Fundamental Voltage

| $h$ | $V_{shTH}$ (V) | $\pm S_{hmax}$ (–) | $\omega_{rsh}$ (rad/s) | $T^{mot}_{eh\,max}$ (Nm) | $T^{gen}_{eh\,max}$ (Nm) |
|---|---|---|---|---|---|
| 1 | 223.34 | 0.312 | 188.49 | 17.98 | –39.89 |
| 0.1 | 9.62 | 0.820 | 18.849 | 0.696 | –4.61 |

**TABLE E3.7.2** Fundamental Torque $T_{e1}$ as a Function of Fundamental Slip $s_1$

| $S_1$ (–) | 2.0 | 1.0 | 0.9 | 0.8 | 0.7 |
|---|---|---|---|---|---|
| $T_{e1}$ (Nm) | 6.78 | 11.61 | 12.44 | 13.37 | 14.40 |
| $S_1$ (–) | 0.6 | 0.5 | 0.4 | 0.3 | 0.2 |
| $T_{e1}$ (Nm) | 15.5 | 16.63 | 17.59 | 17.97 | 16.76 |
| $S_1$ (–) | 0.1 | 0.0344 | 0 | –0.1 | –0.2 |
| $T_{e1}$ (Nm) | 11.8 | 4.99 | 0 | –18.46 | –34.32 |

**TABLE E3.7.3** Subharmonic Torque $T_{e0.1}$ as a Function of Subharmonic Slip $s_{0.1}$

| $S_{0.1}$ (–) | 1.0 | 0.9 | 0.82 | 0.8 | 0.7 | 0.6 |
|---|---|---|---|---|---|---|
| $S_1$ (–) | 1.0 | 0.99 | 0.982 | 0.98 | 0.97 | 0.96 |
| $T_{e0.1}$ (Nm) | 0.687 | 0.693 | 0.696 | 0.695 | 0.69 | 0.676 |
| $S_{0.1}$ (–) | 0.5 | 0.4 | 0.3 | 0.2 | 0.1 | 0 |
| $S_1$ (–) | 0.95 | 0.94 | 0.93 | 0.92 | 0.91 | 0.9 |
| $T_{e0.1}$ (Nm) | 0.648 | 0.602 | 0.528 | 0.415 | 0.247 | 0 |
| $S_{0.1}$ (–) | –0.1 | –0.2 | –0.3 | –0.4 | –0.5 | –0.6 |
| $S_1$ (–) | 0.89 | 0.88 | 0.87 | 0.86 | 0.85 | 0.84 |
| $T_{e0.1}$ (Nm) | –0.353 | –0.842 | –1.488 | –2.28 | –3.12 | –3.88 |
| $S_{0.1}$ (–) | –0.7 | –0.8 | –0.82 | –0.9 | –1 | –1.1 |
| $S_1$ (–) | 0.83 | 0.82 | 0.818 | 0.81 | 0.8 | 0.79 |
| $T_{e0.1}$ (Nm) | –4.40 | –4.60 | –4.61 | –4.53 | –4.29 | –3.95 |
| $S_{0.1}$ (–) | –1.2 | –1.3 | –1.4 | –1.5 | –1.6 | –1.7 |
| $S_1$ (–) | 0.78 | 0.77 | 0.76 | 0.75 | 0.74 | 0.73 |
| $T_{e0.1}$ (Nm) | –3.60 | –3.26 | –2.96 | –2.68 | –2.45 | –2.24 |
| $S_{0.1}$ (–) | –2.0 | –3.0 | –4.0 | –5.0 | –6.0 | –7.0 |
| $S_1$ (–) | 0.70 | 0.60 | 0.50 | 0.40 | 0.30 | 0.20 |
| $T_{e0.1}$ (Nm) | –1.76 | –0.98 | –0.67 | –0.51 | –0.40 | –0.34 |
| $S_{0.1}$ (–) | –8.0 | –9.0 | –10.0 | –11.0 | –12.0 | –13.0 |
| $S_1$ (–) | 0.1 | 0 | –0.1 | –0.20 | –0.30 | –0.40 |
| $T_{e0.1}$ (Nm) | –0.29 | –0.25 | –0.22 | –0.20 | –0.18 | –0.17 |

with the angular velocities

$$\frac{d\theta_{h=1}}{dt}=\omega_1,\quad \frac{d\theta_{h=5}}{dt}=5\omega_1,\quad \frac{d\theta_{H=5}}{dt}=-\omega_1/5,$$
$$\frac{d\theta_{H=5,h=5}}{dt}=\omega_1,$$

(E3.10-1)

b) For $A_1=1$ pu, $A_H=0.05$ pu, $I_{m1}=1$ pu, $I_{mh}=0.05$ pu, $H=13$, and $h=0.5$ one obtains the rotating mmf as

$$F_{\text{total}}=1.5\cos(\theta-\omega_1 t)+0.075\cos(\theta-0.5\omega_1 t)$$
$$+0.075\cos(13\theta-\omega_1 t)$$
$$+0.0035\cos(13\theta-0.5\omega_1 t)$$

with the angular velocities

$$\frac{d\theta_{h=1}}{dt}=\omega_1,\quad \frac{d\theta_{h=0.5}}{dt}=0.5\omega_1,\quad \frac{d\theta_{H=13}}{dt}=\omega_1/13,$$
$$\frac{d\theta_{H=13,h=0.5}}{dt}=\omega_1/26.$$

(E3.10-2)

**TABLE E3.7.4** Fundamental and Subharmonic Torque ($T_{e1}+T_{e0.1}$) as a Function of Fundamental Slip $s_1$

| | | | | | | |
|---|---|---|---|---|---|---|
| $S_1$ (–) | 1.0 | 0.99 | 0.982 | 0.98 | 0.97 | 0.96 |
| $T_{e1}$ (Nm) | 11.61 | 11.69 | 11.75 | 11.77 | 11.85 | 11.93 |
| $T_{e1}+T_{e0.1}$ (Nm) | 12.30 | 12.38 | 12.45 | 12.46 | 12.54 | 12.60 |
| $S_1$ (–) | 0.95 | 0.94 | 0.93 | 0.92 | 0.91 | 0.9 |
| $T_{e1}$ (Nm) | 12.01 | 12.10 | 12.18 | 12.27 | 12.35 | 12.44 |
| $T_{e1}+T_{e0.1}$ (Nm) | 12.66 | 12.70 | 12.71 | 12.68 | 12.60 | 12.44 |
| $S_1$ (–) | 0.89 | 0.88 | 0.87 | 0.86 | 0.85 | 0.83 |
| $T_{e1}$ (Nm) | 12.53 | 12.62 | 12.71 | 12.80 | 12.89 | 13.08 |
| $T_{e1}+T_{e0.1}$ (Nm) | 12.18 | 11.78 | 11.22 | 10.52 | 9.77 | 8.68 |
| $S_1$ (–) | 0.82 | 0.818 | 0.81 | 0.8 | 0.79 | 0.78 |
| $T_{e1}$ (Nm) | 13.18 | 13.19 | 13.27 | 13.37 | 13.47 | 13.57 |
| $T_{e1}+T_{e0.1}$ (Nm) | 8.58 | 8.58 | 8.74 | 9.08 | 9.52 | 9.97 |
| $S_1$ (–) | 0.77 | 0.76 | 0.75 | 0.74 | 0.73 | 0.70 |
| $T_{e1}$ (Nm) | 13.67 | 13.77 | 13.87 | 13.97 | 14.08 | 14.40 |
| $T_{e1}+T_{e0.1}$ (Nm) | 10.41 | 10.81 | 11.19 | 11.52 | 11.84 | 12.64 |
| $S_1$ (–) | 0.60 | 0.50 | 0.40 | 0.30 | 0.20 | 0.10 |
| $T_{e1}$ (Nm) | 15.50 | 16.63 | 17.59 | 17.97 | 16.76 | 11.80 |
| $T_{e1}+T_{e0.1}$ (Nm) | 14.52 | 15.96 | 17.08 | 17.57 | 16.42 | 11.51 |
| $S_1$ (–) | 0 | –0.10 | –0.20 | –0.30 | –0.40 | — |
| $T_{e1}$ (Nm) | 0 | –18.46 | –34.32 | –39.84 | –38.01 | — |
| $T_{e1}+T_{e0.1}$ (Nm) | –0.25 | –18.68 | –34.52 | –40.02 | –38.19 | — |

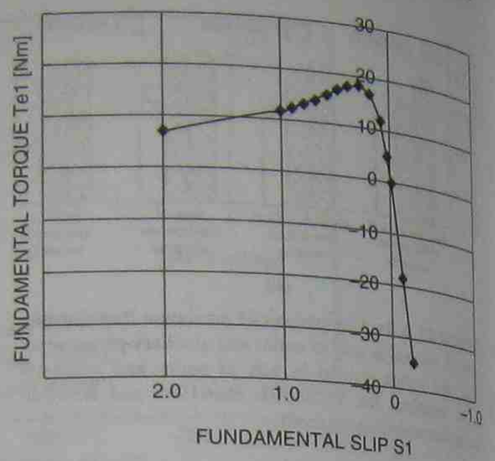



**FIGURE E3.7.1** Fundamental torque $T_{e1}$ as a function of fundamental slip $s_1$.

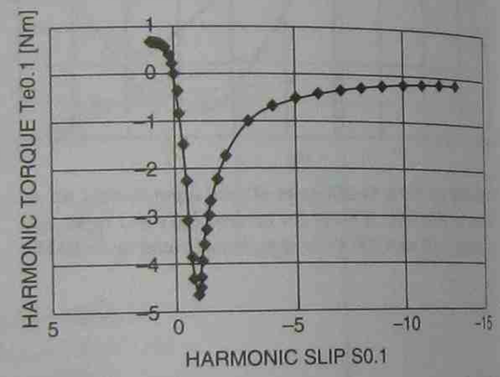



**FIGURE E3.7.2** Subharmonic torque $T_{e0.1}$ as a function of subharmonic slip $s_{0.1}$.

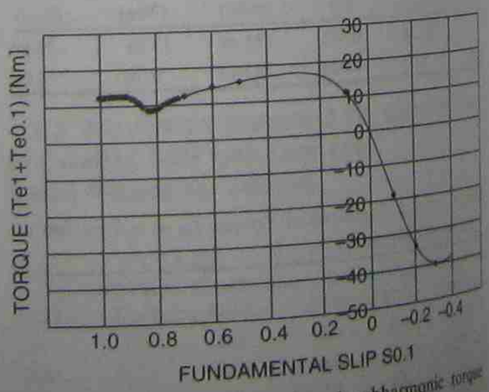



**FIGURE E3.7.3** Fundamental and subharmonic torque ($T_{e1}+T_{e0.1}$) as a function of fundamental slip $s_1$.





**TABLE E3.9.1** Maximum Torques for Fundamental and Subharmonic Currents, Where the Fundamental Current is 1.73 A and the Subharmonic Current is 5% of the Fundamental Current

| $h$ | $\lvert\tilde{V}_{sh}\rvert$ (V)] | $\pm S_{h\max}$ (–) | $\omega_{msh}$ (rad/s) | $T_{eh\max}^{mot}$ (Nm) | $T_{eh\max}^{gen}$ (Nm) |
|---|---|---|---|---|---|
| 1 | 190.3 | 0.044 | 188.49 | 2.53 | –2.35 |
| 0.1 | 0.952 | 0.439 | 18.849 | 0.0063 | –0.0063 |

**TABLE E3.9.2** Torque as a Function of Slip $s_i$ for Fundamental ($h=1$) Currents

| | | | | | |
|---|---|---|---|---|---|
| $S_1$ (–) | 1.0 | 0.9 | 0.8 | 0.7 | 0.6 |
| $T_{e1}$(Nm) | 0.221 | 0.246 | 0.276 | 0.316 | 0.368 |
| $S_1$ (–) | 0.5 | 0.4 | 0.3 | 0.2 | 0.1 |
| $T_{e1}$(Nm) | 0.440 | 0.548 | 0.724 | 1.058 | 1.860 |

**TABLE E3.9.3** Torque as a Function of Slip $s_{0.1}$ for Subharmonic ($h=0.1$) Currents of 5% of the Fundamental Current

| | | | | | |
|---|---|---|---|---|---|
| $S_{0.1}$ (–) | 1.0 | 0.9 | 0.8 | 0.7 | 0.6 |
| $T_{e0.1}$ (Nm) | 0.0047 | 0.0050 | 0.0053 | 0.0057 | 0.0060 |
| $S_{0.1}$ (–) | 0.5 | 0.4 | 0.3 | 0.2 | 0.1 |
| $T_{e0.1}$ (Nm) | 0.0063 | 0.0063 | 0.0059 | 0.0048 | 0.0027 |

### 3.9.2 Application Example 3.11: Computation of Rotating MMF with Even Space Harmonics: Solution

$$F_{\text{total}}=1.5\cos(\theta-\omega_1 t)+0.075\cos(\theta-0.1\omega_1 t)$$

with the angular velocities

$$\frac{d\theta_{h=1}}{dt}=\omega_1,\quad \frac{d\theta_{h=0.1}}{dt}=0.1\omega_1.\quad \text{(E3.11-1)}$$

### 3.9.3 Application Example 3.12: Computation of Rotating MMF with Noninteger Space Harmonics: Solution

$$F_{\text{total}}=1.5\cos(\theta-\omega_1 t)+0.75\cos(\theta-0.1\omega_1 t)$$
$$+0.025\{\cos(13.5\theta-\omega_1 t)$$
$$+\cos(13.5\theta-60^\circ-\omega_1 t)$$
$$+\cos(13.5\theta+60^\circ-\omega_1 t)\}$$
$$+0.025\{\cos(13.5\theta+\omega_1 t)$$
$$+\cos(13.5\theta+60^\circ+\omega_1 t)$$
$$+\cos(13.5\theta-60^\circ+\omega_1 t)\}$$
$$+0.00125\{\cos(13.5\theta-0.1\omega_1 t)$$
$$+\cos(13.5\theta-60^\circ-0.1\omega_1 t)$$
$$+\cos(13.5\theta-60^\circ-0.1\omega_1 t)\}$$
$$+0.00125\{\cos(13.5\theta-0.1\omega_1 t)$$
$$+\cos(13.5\theta+60^\circ+0.1\omega_1 t)$$
$$+\cos(13.5\theta-60^\circ+0.1\omega_1 t)\},$$

with the angular velocities

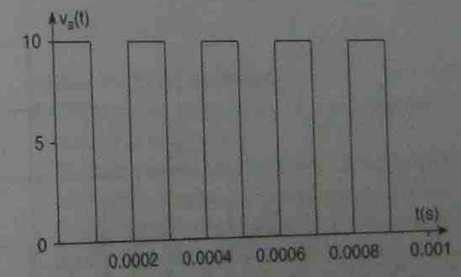
$$\frac{d\theta_{h=1}}{dt}=\omega_1,\quad \frac{d\theta_{h=0.1}}{dt}=0.1\omega_1,\quad \frac{d\theta_{H=13.5}}{dt}=\pm\omega_1/13.5,$$
$$\frac{d\theta_{H=13.5,h=0.1}}{dt}=\pm\omega_1/13.5.$$

(E3.12-1)

### 3.11.1 Application Example 3.13: Calculation of Winding Stress Due to PMW Voltage-Source Inverters: Solution #1 (based on Mathematica)

a) Solution based on simplified equivalent circuit is as follows.

```
Hval=10;
Lval=0;
period=200*^-6;
duty=.5;
Vs[t_]:=If[Mod[t,period]<duty*period,Hval,Lval];
      Plot[Vs[t],{t,0,.001},
      PlotRange→All,AxesLabel→
      {"t","Vs(t)"}]
```




```
R1=25*^-6;R2=25*^-6;R3=25*^-
6;R4=25*^-6;R5=25*^-6;R6=25*^-6;
R7=25*^-6;R8=25*^-6;
L1=1*^-3;L3=1*^-3;L5=1*^-3;L7=1*^-3;
L2=10*^-3;L4=10*^-3;L6=10*^-3;L8=10*^-3;
L15=5*^-6;L37=5*^-6;
L26=10*^-6;L48=10*^-6;
C1=.7*^-12;C3=.7*^-12;C5=.7*^-12;C7=.7*^-12;
C2=7*^-12;C4=7*^-12;C6=7*^-12;C8=7*^-12;
C15=.35*^-12;C37=.35*^-12;
C26=3.5*^-12;C48=3.5*^-12;
G1=1/5000;G3=1/5000;G5=1/5000;G7=1/5000;
G2=1/500;G4=1/500;G6=1/500;G8=1/500;
   Z=1*^-6;
```

ST. GEORGE COLLEGE OF LAW

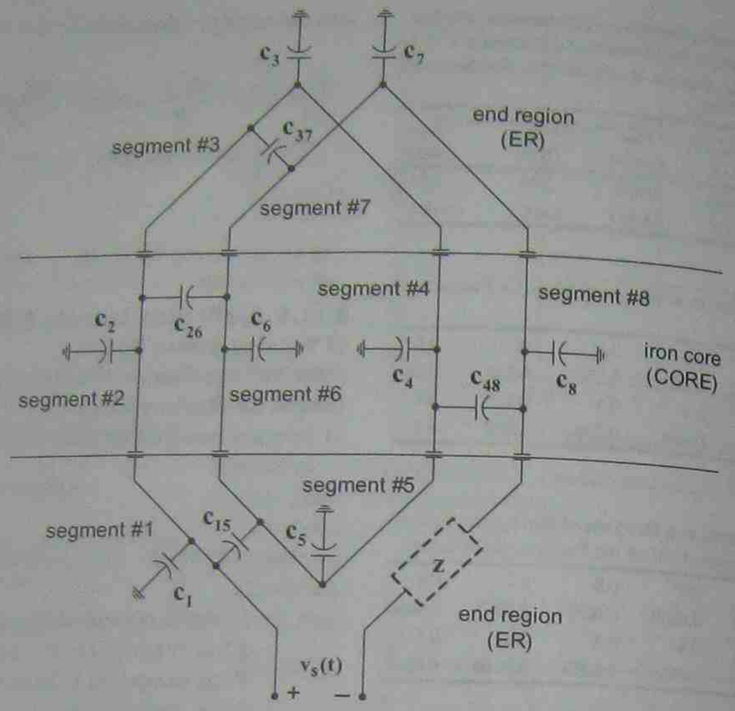



**FIGURE E3.13.1** Winding consisting of two turns, and each turn consists of four segments.

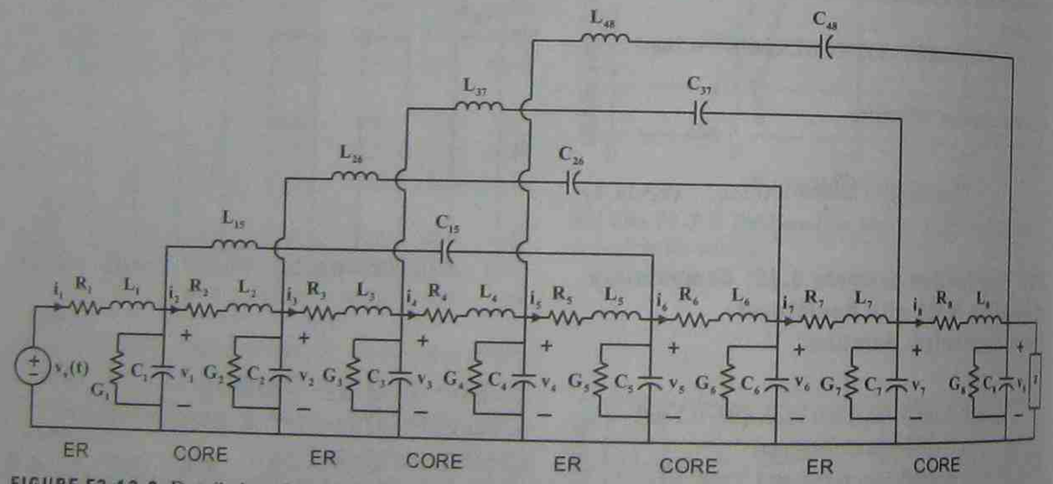



**FIGURE E3.13.2** Detailed equivalent circuit of Fig. E3.13.1.

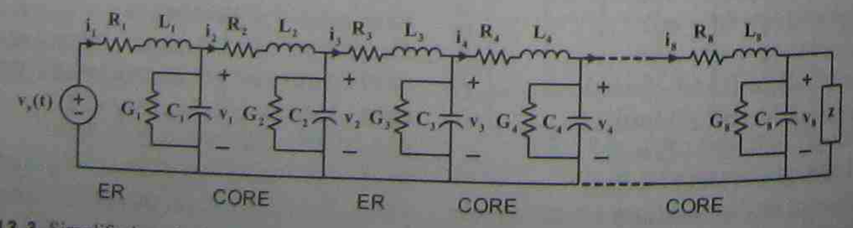



**FIGURE E3.13.3** Simplified equivalent circuit of Fig. E3.13.1.

ST. GEORGE COLLEGE OF LAW



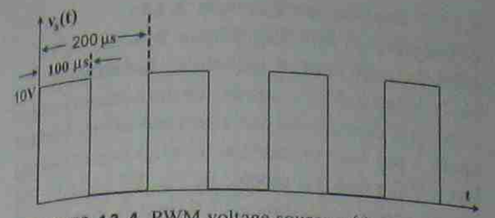



**FIGURE E3.13.4** PWM voltage source $v_s(t)$.

```
I1d=I1'[t]==-R1/L1*I1[t]-V1[t]/L1+Vs[t]/L1;
ic1=I1[0]==0;
V1d=V1'[t]==
I1[t]/C1-G1/C1*V1[t]-I2[t]/C1;
ic2=V1[0]==0;
I2d=I2'[t]==-R2/L2*I2[t]-V2[t]/L2+V1[t]/L2;
ic3=I2[0]==0;
V2d=V2'[t]==I2[t]/C2-G2/C2*V2[t]-I3[t]/C2;
ic4=V2[0]==0;
I3d=I3'[t]==-R3/L3*I3[t]-V3[t]/L3+V2[t]/L3;
ic5=I3[0]==0;
V3d=V3'[t]==I3[t]/C3-G3/C3*V3[t]-I4[t]/C3;
ic6=V3[0]==0;
I4d=I4'[t]==-R4/L4*I4[t]-V4[t]/L4+V3[t]/L4;
ic7=I4[0]==0;
V4d=V4'[t]==I4[t]/C4-G4/C4*V4[t]-I5[t]/C4;
ic8=V4[0]==0;
I5d=I5'[t]==-R5/L5*I5[t]-V5[t]/L5+V4[t]/L5;
ic9=I5[0]==0;
V5d=V5'[t]==I5[t]/C5-G5/C5*V5[t]-I6[t]/C5;
ic10=V5[0]==0;
I6d=I6'[t]==-R6/L6*I6[t]-V6[t]/L6+V5[t]/L6;
ic11=I6[0]==0;
V6d=V6'[t]==I6[t]/C6-G6/C6*V6[t]-I7[t]/C6;
ic12=V6[0]==0;
I7d=I7'[t]==-R7/L7*I7[t]-V7[t]/L7+V6[t]/L7;
ic13=I7[0]==0;
V7d=V7'[t]==I7[t]/C7-G7/C7*V7[t]-I8[t]/C7;
ic14=V7[0]==0;
I8d=I8'[t]==-R8/L8*I8[t]-V8[t]/L8+V7[t]/L8;
ic15=I8[0]==0;
V8d=V8'[t]==I8[t]/C8-V8[t]*(1/(Z*C8)+G8/C8);
                ic16=V8[0]==0;
                sol1=NDSolve[{I1d,V1d,I
                2d,V2d,I3d,V3d,I4d,V4d,
                I5d,V5d,I6d,V6d,I7d,V7d
                ,I8d,V8d,ic1,ic2,ic3,
                ic4,ic5,ic6,ic7,ic8,
                ic9,ic10,ic11,ic12,
                ic13,ic14,ic15,ic16},
                {I1[t],V1[t],I2[t],
                V2[t],I3[t],V3[t],
                I4[t],V4[t],I5[t],
                V5[t],I6[t],V6[t],
                I7[t],V7[t],I8[t],
                V8[t]},{t,0,.0021},
                MaxSteps→100000]
Plot[Vs[t]-Evaluate[V1[t]/.sol1],{t,0,
.002},AxesLabel→{"Time", "Vs - V1"}]
Plot[Evaluate[V1[t]/.sol1] -
Evaluate[V5[t]/.sol1],{t,0,.002},Axes
Label→{"Time", "V1 - V5"}]
Plot[Evaluate[V2[t]/.sol1] -
Evaluate[V6[t]/.sol1],{t,0,.002},Axes
Label→{"Time", "V2 - V6"}]
Plot[Evaluate[V3[t]/.sol1] -
Evaluate[V7[t]/.sol1],{t,0,.002},Axes
Label→{"Time", "V3 - V7"}]
      Plot[Evaluate[V4[t]/.sol1] -
      Evaluate[V8[t]/.sol1],{t,0,
      .002},AxesLabel→{"Time",
      "V4 - V8"}]
```

b) The detailed equivalent circuit (Fig. E3.13.2) generates about the same result as the simplified equivalent circuit (Fig. E3.13.3) and the results are therefore not given.

**Solution #2 (Based on MATLAB)**

a) Graphs shown below apply to a short-circuited load, for example, $Z = 0$.

b) The state variable equations from above are still valid for the detailed equivalent circuit. The following four equations need to be added (assuming that the initial current through all the branches is zero):

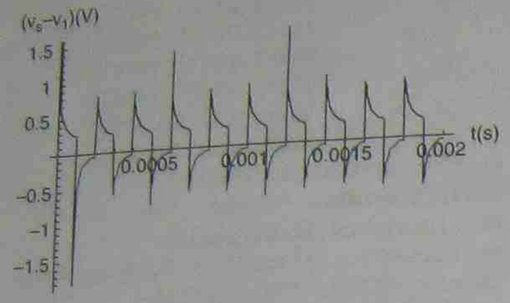
$$\frac{di_{15}}{dt} = \frac{v_1}{L_{15}} - \frac{i_{15}}{L_{15}C_{15}} - \frac{v_5}{L_{15}}, \quad \text{(E3.13-9)}$$

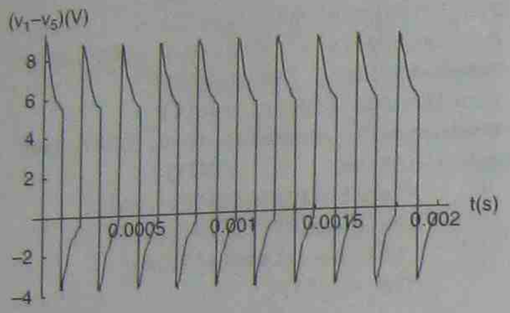
$$\frac{di_{26}}{dt} = \frac{v_2}{L_{26}} - \frac{i_{26}}{L_{26}C_{26}} - \frac{v_6}{L_{26}}, \quad \text{(E3.13-10)}$$

$$\frac{di_{37}}{dt} = \frac{v_3}{L_{37}} - \frac{i_{37}}{L_{37}C_{37}} - \frac{v_7}{L_{37}}, \quad \text{(E3.13-11)}$$

$$\frac{di_{48}}{dt} = \frac{v_4}{L_{48}} - \frac{i_{48}}{L_{48}C_{48}} - \frac{v_8}{L_{48}}. \quad \text{(E3.13-12)}$$

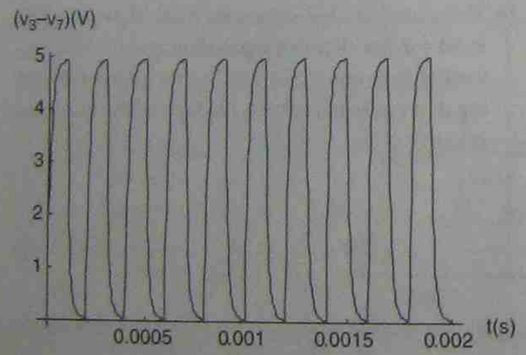
For an open-circuited winding (e.g., $Z = 1\ M\Omega$) the results are about the same as above.

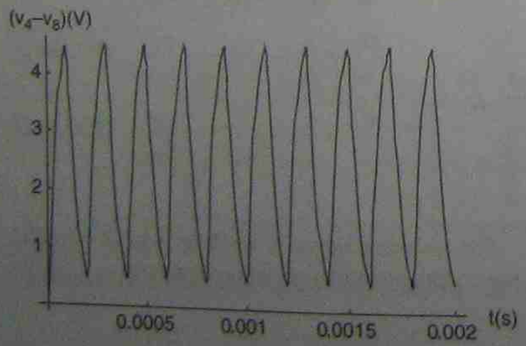






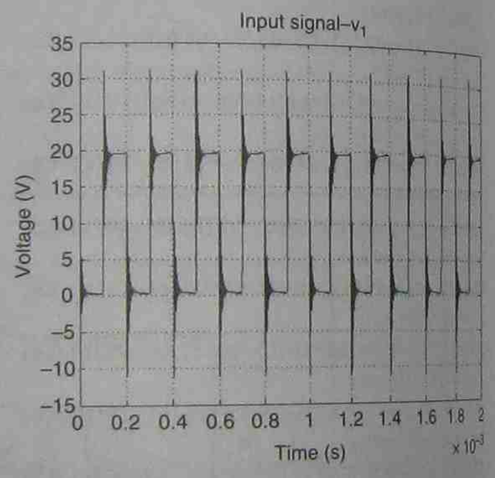


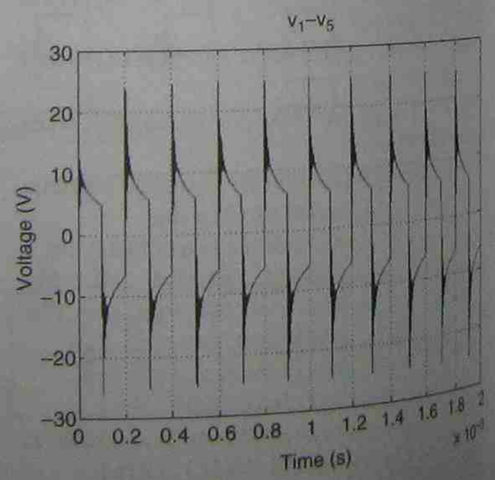




### 3.11.2 Application Example 3.14: Calculation of Winding Stress Due to PWM Current-Source Inverters: Solution

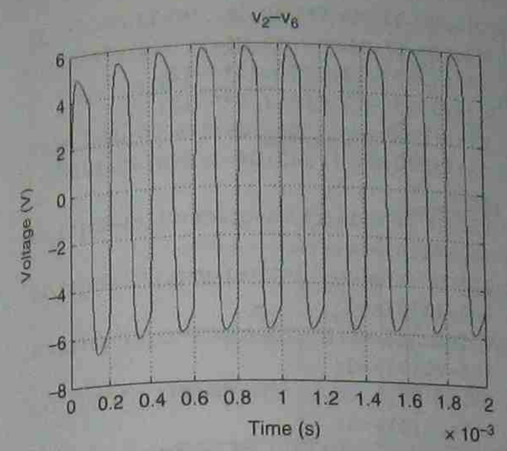
To demonstrate the sensitivity of the induced voltage stress as a function of the rise time of the current ripple, a rise time of less that 5 $\mu$s has been assumed first and the result is plotted in Fig. E3.14.5a,b. The voltage across capacitance C15 (that is, the voltage between the first turn and the second turn at the end region (ER)) is very large.

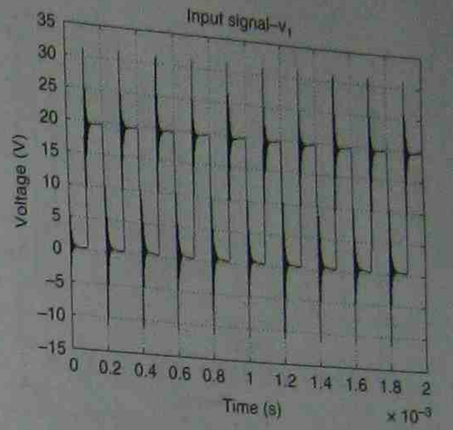
Figure E3.14.6 illustrates the voltage stress ($v_1 - v_5$) for the load $Z = 1\ \text{M}\Omega$ at a rise time of 5 $\mu$s. That is the considered winding is open-circuited.

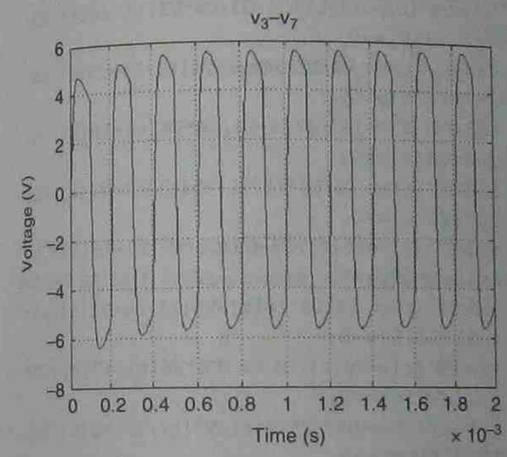


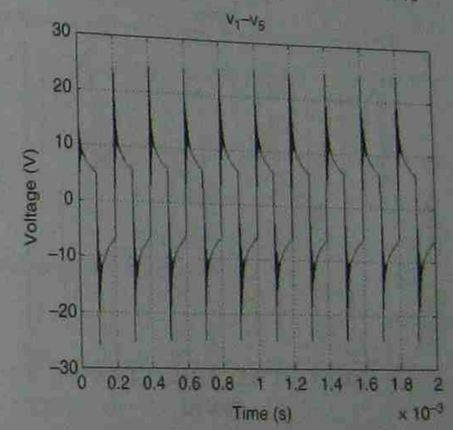



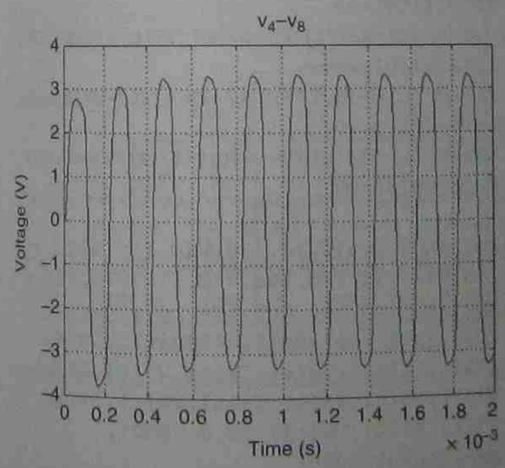


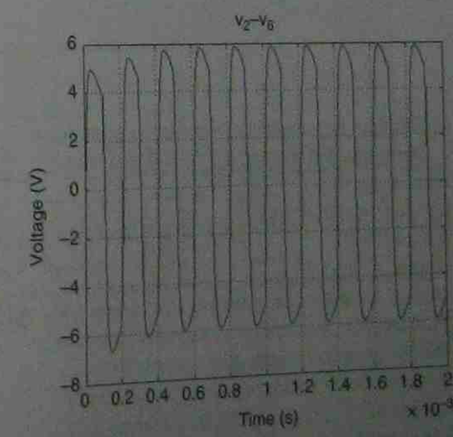



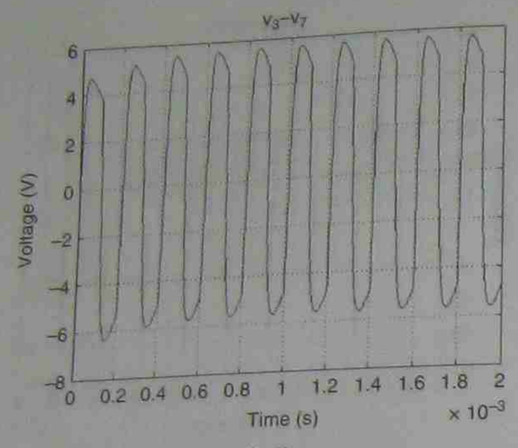



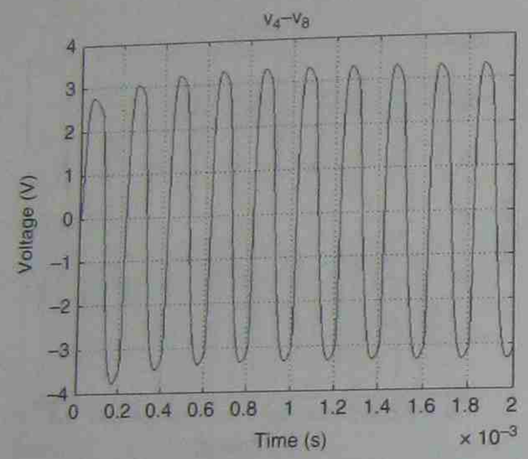






a) Solution for simplified equivalent circuit for a short-circuited winding $Z = 1\ \mu\Omega$ is as follows.

```
amp = 5;
period = 200*^-6;
duty=0.5;
trise = 5*^-6;
Is[t_]:=If[Mod[t,period]>duty*period,
0,If[Mod[t,period]<trise,amp/(trise)
*Mod[t,period],amp-amp/(period*
duty-trise)*(Mod[t,period]-trise)]]
Plot[Is[t],{t,0,.001},PlotRange→All,
AxesLabel→{"t","Is(t)"}]
R1=25*^-6;R2=25*^-6;R3=25*^-6;
R4=25*^-6;R5=25*^-6;R6=25*^-6;R7=25*^-6;R8=25*^-6;
L1=1*^-3;L3=1*^-3;L5=1*^-3;L7=1*^-3;
L2=10*^-3;L4=10*^-3;L6=10*^-3;L8=10*^-3;
L15=5*^-6;L37=5*^-6;
L26=10*^-6;L48=10*^-6;
C1=.7*^-12;C3=.7*^-12;C5=.7*^-12;C7=.7*^-12;
C2=7*^-12;C4=7*^-12;C6=7*^-12;C8=7*^-12;
C15=.35*^-12;C37=.35*^-12;
C26=3.5*^-12;C48=3.5*^-12;
G1=1/5000;G3=1/5000;G5=1/5000;G7=1/5000;
G2=1/500;G4=1/500;G6=1/500;G8=1/500;
Z=1*^-6;
V1d=V1'[t]==Is[t]/C1-G1/C1*V1[t]-I2[t]/C1;
ic2=V1[0]==0;
I2d=I2'[t]==-R2/L2*I2[t]-V2[t]/L2+V1[t]/L2;
ic3=I2[0]==0;
V2d=V2'[t]==I2[t]/C2-G2/C2*V2[t]-I3[t]/C2;
ic4=V2[0]==0;
I3d=I3'[t]==-R3/L3*I3[t]-V3[t]/L3+V2[t]/L3;
ic5=I3[0]==0;
V3d=V3'[t]==I3[t]/C3-G3/C3*V3[t]-I4[t]/C3;
ic6=V3[0]==0;
I4d=I4'[t]==-R4/L4*I4[t]-V4[t]/L4+V3[t]/L4;
ic7=I4[0]==0;
V4d=V4'[t]==I4[t]/C4-G4/C4*V4[t]-I5[t]/C4;
ic8=V4[0]==0;
I5d=I5'[t]==-R5/L5*I5[t]-V5[t]/L5+V4[t]/L5;
ic9=I5[0]==0;
V5d=V5'[t]==I5[t]/C5-G5/C5*V5[t]-I6[t]/C5;
ic10=V5[0]==0;
I6d=I6'[t]==-R6/L6*I6[t]-V6[t]/L6+V5[t]/L6;
ic11=I6[0]==0;
V6d=V6'[t]==I6[t]/C6-G6/C6*V6[t]-I7[t]/C6;
ic12=V6[0]==0;
I7d=I7'[t]==-R7/L7*I7[t]-V7[t]/L7+V6[t]/L7;
ic13=I7[0]==0;
V7d=V7'[t]==I7[t]/C7-G7/C7*V7[t]-I8[t]/C7;
ic14=V7[0]==0;
I8d=I8'[t]==-R8/L8*I8[t]-V8[t]/L8+V7[t]/L8;
ic15=I8[0]==0;
V8d=V8'[t]==I8[t]/C8-V8[t]*(1/(Z*C8)+G8/C8);
ic16=V8[0]==0;

sol1=NDSolve[{V1d,I2d,V2d,I3d,V3d,
I4d,V4d,I5d,V5d,I6d,V6d,I7d,V7d,I8d,
V8d,ic2,ic3,ic4,ic5,ic6,ic7,ic8,ic9,
ic10,ic11,ic12,ic13,ic14,ic15,ic16},
{V1[t],I2[t],V2[t],I3[t],V3[t],I4[t],
V4[t],I5[t],V5[t],I6[t],V6[t],I7[t],
V7[t],I8[t],V8[t]},{t,0,.002},
MaxSteps→100000]

Plot[Evaluate[V1[t]/.sol1] -
Evaluate[V5[t]/.sol1],{t,0,.002},Axes
Label→{"Time", "V1 - V5"}]
Plot[Evaluate[V2[t]/.sol1] -
Evaluate[V6[t]/.sol1],{t,0,.002},Axes
Label→{"Time", "V2 - V6"}]
```



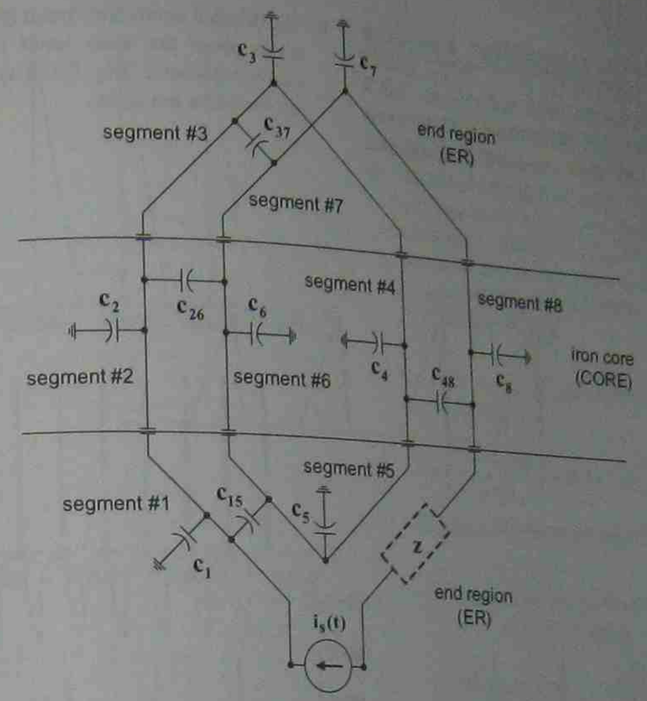



**FIGURE E3.14.1** Winding consisting of two turns, and each turn consists of four segments.

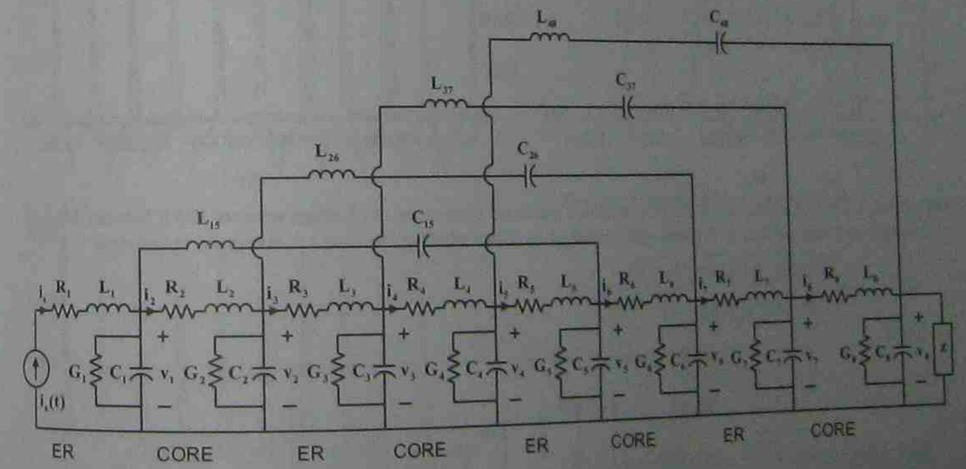



**FIGURE E3.14.2** Detailed equivalent circuit of Fig. E3.14.1.

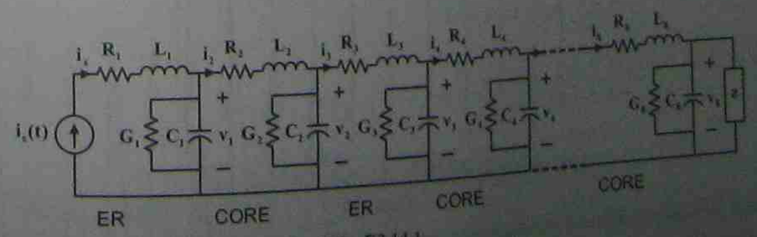



**FIGURE E3.14.3** Simplified equivalent circuit of Fig. E3.14.1.

```
Plot[Evaluate[V3[t]/.sol1] -
Evaluate[V7[t]/.sol1],{t,0,.002},Axes
Label→{"Time", "V3 - V7"}]
Plot[Evaluate[V4[t]/.sol1] -
Evaluate[V8[t]/.sol1],{t,0,.002},Axes
Label→{"Time", "V4 - V8"}]
```

b) The detailed equivalent circuit (Fig. E3.14.2) generates about the same result as the simplified equivalent circuit (Fig. E3.14.3) and the results are therefore not given.

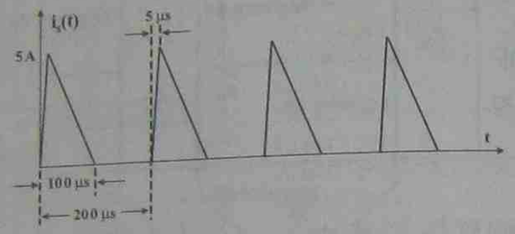



**FIGURE E3.14.4** PWM current source $i_s(t)$.

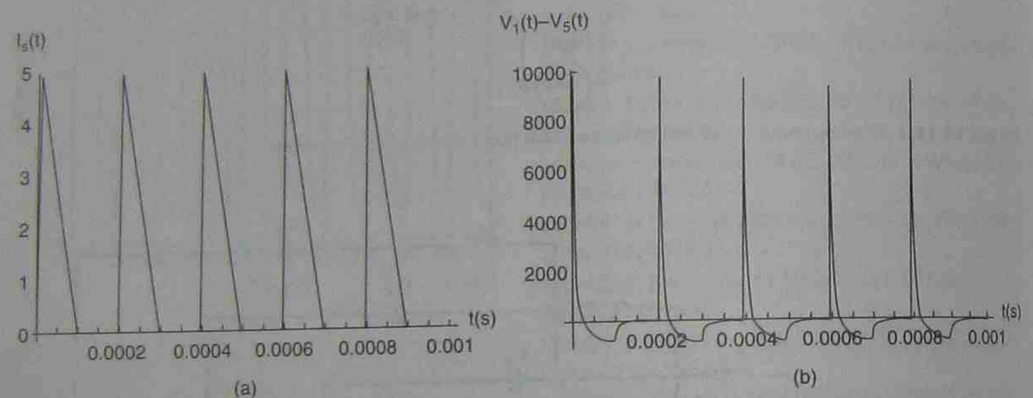



**FIGURE E3.14.5** (a) Current ripple of 5 A of induction motor fed by inverter. (b) Voltage stress of 10 kV between segment #1 (voltage $v_1(t)$) and segment #5 (voltage $v_5(t)$) of induction motor winding; the time t is measured in seconds.

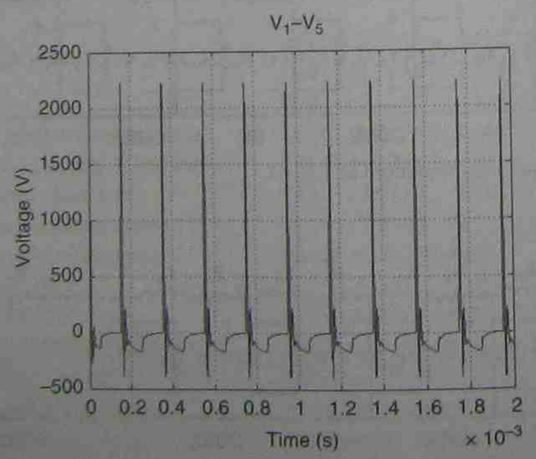
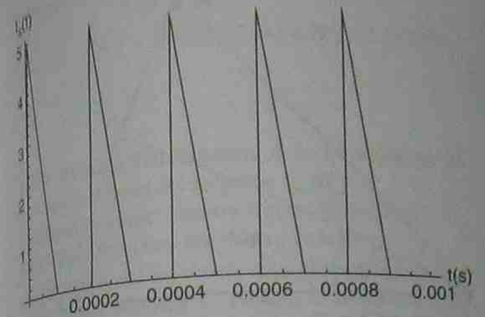
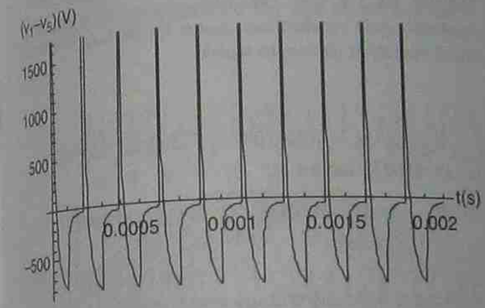
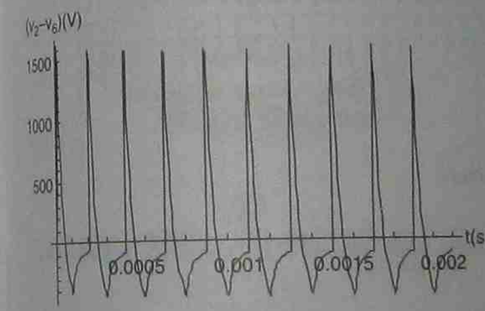


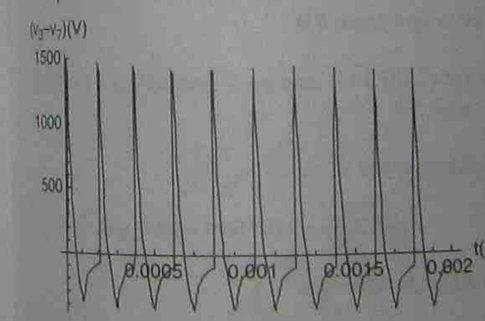

**FIGURE E3.14.6** Voltage $(v_1 - v_5)$ for $Z = 1$ MΩ at a rise time of 5 µs.

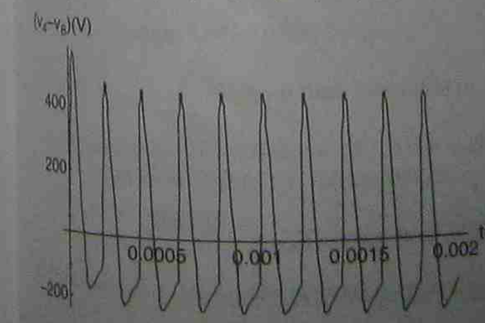





## CHAPTER 4 SOLUTIONS

### 4.2.3 Application Example 4.1: Steady-State Analysis of a Nonsalient-Pole (Round-Rotor) Synchronous Machine: Solution

a) The per-phase equivalent circuit of a nonsalient-pole synchronous machine based on generator notation is shown in Fig. 4.15a. The parameters of the machine are in ohms: $R_a = 0.05 \cdot Z_{base} = (0.05)(17.14\ \Omega) = 0.857\ \Omega$, $X_s = 2 \cdot Z_{base} = 2(17.14\ \Omega) = 34.28\ \Omega$.

b) $S_{rated} = 3 \cdot V_{a_rated} \cdot I_{a_rated} = 3(24\text{ kV})(1.4\text{ kA})$
$= 100.8$ MVA. (E4.1-1)

c) $P_{rated} = S_{rated} \cdot \cos\varphi = 80.64$ MW. (E4.1-2)

d) The phasor diagram is given in Fig. E4.1.1.

$\varphi = \cos^{-1}(0.8) = 0.6435$ rad
or 36.87° lagging (E4.1-3)

$|\tilde{V}_{a\text{-rated}}| = 1$ pu $= 24$kV $= 3$ inches

$|\tilde{I}_{a\text{-rated}}| = 1$ pu $= 1.4$ kA $= 2.5$ inches

$|\tilde{I}_{a\text{-rated}}| \cdot R_a = 1.4\text{kA}(0.05)(17.141\ \Omega)$
$= 1199.8$ V $= 0.15$ inches

$|\tilde{I}_{a\text{-rated}}| \cdot X_s = 1.4\text{ kA}(2)(17.141\ \Omega)$
$= 47992$ V $= 6$ inches.

e) For the induced voltage one obtains

$$E_a = \sqrt{\frac{(|\tilde{V}_a| + |\tilde{V}_R|\cos\varphi + |\tilde{V}_X|\sin\varphi)^2}{+(|\tilde{V}_X|\cos\varphi - |\tilde{V}_R|\sin\varphi)^2}} = 2.735\text{pu} \quad \text{(E4.1-4)}$$

where

$|\tilde{V}_a| = 1$ pu, $|\tilde{V}_X| = 2$ pu, $|\tilde{V}_R| = 0.05$ pu, $\sin\varphi = 0.6$, and $\cos\varphi = 0.8$.

The torque angle $\delta$ is

$\delta = \cos^{-1}\{(|\tilde{V}_a| + |\tilde{V}_R|\cos\varphi + |\tilde{V}_X|\sin\varphi)/E_a\}$
$= 0.611$rad or 35°.

f) Rated speed is

$n_s = 120f/p = 120(60)/4 = 1800$ rpm. (E4.1-5)

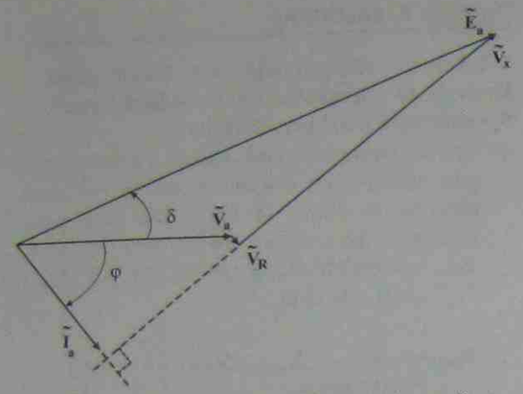



**FIGURE E4.1.1** Per-phase phasor diagram of nonsalient-pole (round-rotor) synchronous motor for lagging (overexcited) operation (drawn to-scale).

g) Angular velocity is

$$\omega_S = 2\,\pi n_S/60 = 188.7 \text{ rad/s.} \qquad \text{(E4.1-6)}$$

h) Approximate shaft power is

$$P_{shaft} \approx 3(E_a \cdot V_a \cdot \sin\delta)/X_S = 3[(2.735)(24\text{k})(24\text{k}) \sin(0.611 \text{ rad})]/[(2)(17.14)] = 79.1 \text{ MW.} \qquad \text{(E4.1-7)}$$

i) The shaft torque $T_{shaft}$ is

$$T_{shaft} = P_{shaft}/\omega_S = 419.14 \text{ kNm.} \qquad \text{(E4.1-8)}$$

j) The total ohmic loss of the motor is

$$P_{loss} = 3 \cdot R_a|\tilde{I}_a|^2 = 3(0.05)(17.14)(1.4\text{k})^2 = 5.04 \text{ MW.} \qquad \text{(E4.1-9)}$$

k) Repeat the above analysis for underexcited (leading current based on generator reference system) displacement power factor $\cos\varphi = 0.8$ leading and $|\tilde{I}_a| = 0.5$ pu.

a) see Fig. 4.15a

b) $S_{rated} = 3 \cdot V_{a_rated} \cdot I_{a_rated} = 3(24\text{kV})(0.7\text{kA}) = 50.4$ MVA.

c) $P_{rated} = S_{rated} \cdot \cos\varphi = 40.32$ MW.

d) The phasor diagram is given in Fig. E4.1.2.

$\varphi = \cos^{-1}(0.8) = 0.6435$ rad or 36.87° leading (underexcited)

$|\tilde{V}_{a\text{-rated}}| = 1$ pu = 24kV = 3 inches

$|\tilde{I}_{a\text{-rated}}| = 0.5$ pu = 700kA = 1.25 inches

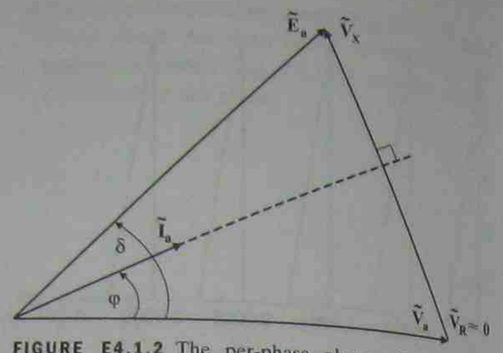



**FIGURE E4.1.2** The per-phase phasor diagram of a nonsalient-pole synchronous motor for leading (underexcited) operation (drawn to-scale).

$|\tilde{I}_{a\text{-rated}}| \cdot R_a = 700\text{A}(0.05)(17.141\ \Omega) = 599.9$ V = 0.075 inches

$|\tilde{I}_{a\text{-rated}}| \cdot X_S = 700\text{A}(2)(17.14\ \Omega) = 23.996$kV = 3 inches

e) For the induced voltage one obtains

$$E_a = \sqrt{(|\tilde{V}_a| + |\tilde{V}_R|\cos\varphi - |\tilde{V}_X|\sin\varphi)^2 + (|\tilde{V}_X|\cos\varphi + |\tilde{V}_R|\sin\varphi)^2} = 0.917 \text{ pu or } 22.004 \text{ kV,}$$

where

$|\tilde{V}_a| = 1$ pu, $|\tilde{V}_X| = 1$ pu, $|\tilde{V}_R| = 0.025$ pu, $\sin\varphi = 0.6$, $\cos\varphi = 0.8$.

The torque angle $\delta$ is

$$\delta = \cos^{-1}\{(|\tilde{V}_a| + |\tilde{V}_R\cos\varphi - |\tilde{V}_X|\sin\varphi)|/E_a\} = 1.095 \text{ rad or } 62.74°.$$

f) Rated speed is

$$n_S = 120\text{f/p} = 120 \cdot 60/4 = 1800 \text{ rpm.}$$

g) Angular velocity is

$$\omega_S = 2\pi n_S/60 = 188.7 \text{ rad/s.}$$

h) Approximate shaft power is

$$P_{shaft} \approx 3(E_a \cdot V_a \cdot \sin\delta)/X_S = 3[(0.917)(24\text{k})(24\text{k}) \sin(1.095 \text{ rad})]/[(2)(17.14)] = 41.09 \text{ MW.}$$

i) The shaft torque $T_{shaft}$ is

$$T_{shaft} = P_{shaft}/\omega_S = 217.75 \text{ kNm.}$$



j) The total ohmic loss of the motor is

$$P_{loss} = 3 \cdot R_a|\tilde{I}_a|^2 = 3(0.05)(17.14)(0.7\text{k})^2 = 1.26 \text{ MW.}$$

### 4.2.4 Application Example 4.2: Calculation of the Synchronous Reactance $X_S$ of a Cylindrical-Rotor (Round-Rotor, Nonsalient-Pole) Synchronous Machine: Solution

a) Calculation of the distribution (breadth) factor of the stator winding $k_{st\ b} = k_{st\ d}$ is as follows. The breadth factor is defined for one phase belt as

$$k_{stb} = \frac{\text{geometric sum } \sum_{i=1}^{k} F_i}{\text{algebraic sum } \sum_{i=1}^{k} F_i} \qquad \text{(E4-2.1)}$$

It is convenient to evaluate Eq. E4.2-1 graphically, as shown in Fig. E4.2.4. Note that one slot pitch corresponds to $360°/48 = 7.5°$. Thus, one gets from Fig. E4.2.4

$$k_{stb} = 0.96. \qquad \text{(E4-2.2)}$$

b) Calculation of the pitch factor of the stator winding $k_{Sp1}$ is as follows. One stator turn spans

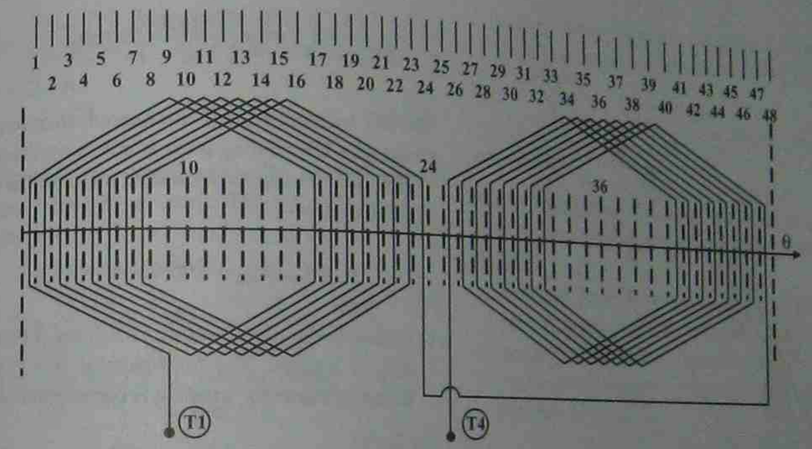



**FIGURE E4.2.1** Stator winding of two-pole, three-phase synchronous machine.

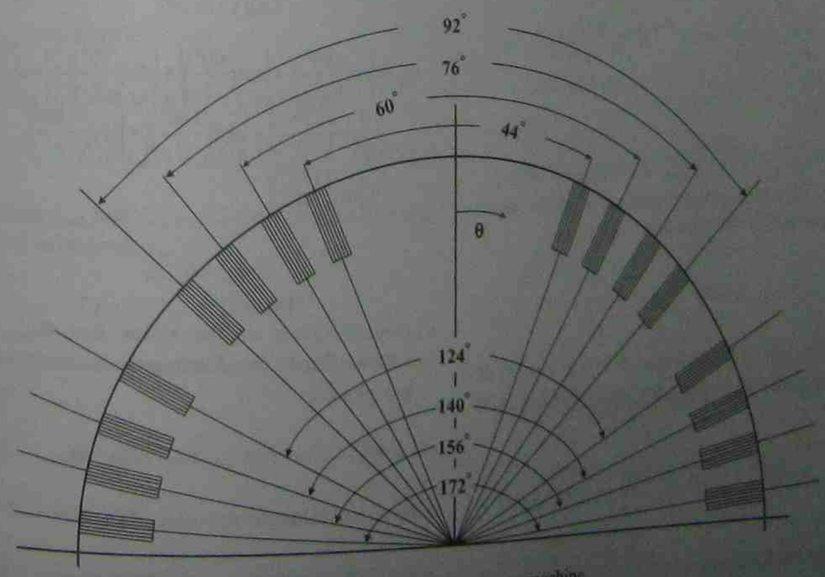



**FIGURE E4.2.2** Rotor winding of two-pole, three-phase synchronous machine.

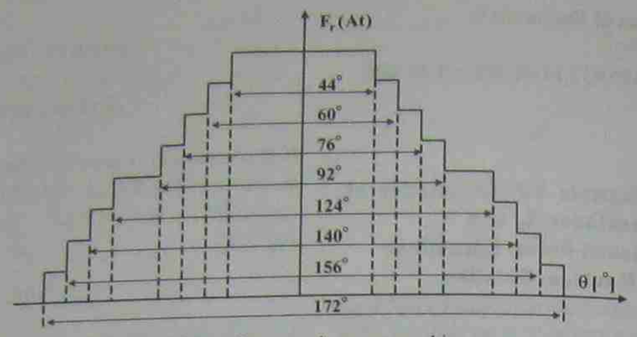



**FIGURE E4.2.3** Rotor mmf $F_r$ of two-pole, three-phase synchronous machine.

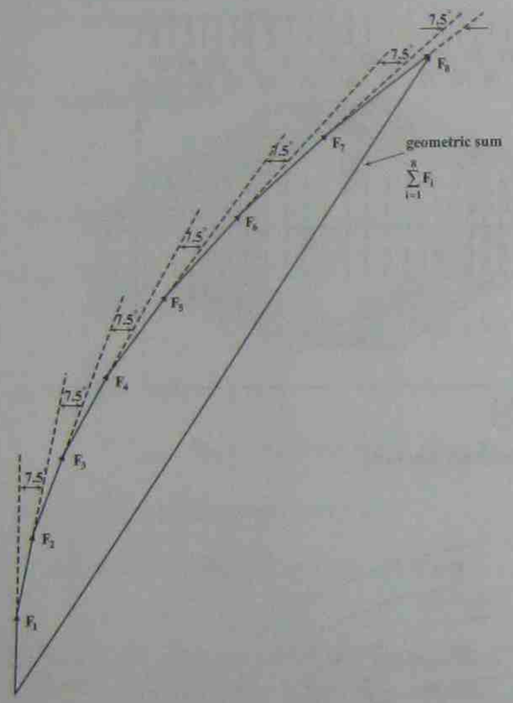



**FIGURE E4.2.4** Graphical determination of the stator breadth or distribution factor $k_{stp1}$.

16 slots out of 24 slots, that is, it has a pitch of (2/3); therefore, one obtains for the fundamental $n = 1$

$$k_{stp1} = \left|\sin\left(\frac{n\beta}{2}\right)\right| = \left|\sin\left(\frac{(1)(120)}{2}\right)\right| = 0.866 \quad \text{(E4-2.3)}$$

or for the 5th harmonic $n = 5$

$$k_{stp5} = \left|\sin\left(\frac{(5)(120)}{2}\right)\right| = 0.866.$$

The 5th harmonic is not attenuated; therefore, the choice of a 2/3 winding pitch is not recommended.

The total fundamental winding factor of the stator winding is now

$$k_{st} = k_{stb} \cdot k_{stp1} = 0.96(0.866) = 0.831.$$

c) Calculate the pitch factor of the rotor (r) winding $k_{rp}$ as follows. The fundamental ($n = 1$) pitch-factor of the rotor winding is correspondingly

$$k_{rp} = \frac{\left|\sum_{i=1}^{8} \sin\left(\frac{n\beta_i}{2}\right)\right|}{8} \quad \text{(E4-2.4)}$$

$$k_{rp} = \left|\sin\left(\frac{44°}{2}\right)\right| + \left|\sin\left(\frac{60°}{2}\right)\right| + \left|\sin\left(\frac{76°}{2}\right)\right| + \left|\sin\left(\frac{92°}{2}\right)\right| + \left|\sin\left(\frac{124°}{2}\right)\right| + \left|\sin\left(\frac{140°}{2}\right)\right| + \left|\sin\left(\frac{156°}{2}\right)\right| + \left|\sin\left(\frac{172°}{2}\right)\right|$$

$$k_{rp} = 0.751.$$

d) Determination of the stator flux $\Phi_{Stmax}$ is as follows. The induced voltage in the stator winding per phase is

$$E_{ph} = 4.44 \cdot f \cdot N_{stph} \cdot k_{stb} \cdot K_{stp1} \cdot \Phi_{stmax} \quad \text{(E4-2.5)}$$

or one obtains for the stator flux

$$\Phi_{st\,max} = \frac{E_{L-L}}{\sqrt{3} \cdot 4.44 \cdot f \cdot N_{stph} \cdot k_{stb} \cdot k_{stp1}} \quad \text{(E4-2.6)}$$



with $E_{L-L} = V_{L-L} = 13{,}800$ V at no load, one gets the flux for no-load condition:

$$\Phi_{st\,max}^{no\text{-}load} = \frac{13800}{\sqrt{3}(4.44)(60)(16)(0.96)(0.866)} = 2.25 \frac{\text{Wb}}{\text{pole}}. \quad \text{(E4-2.7)}$$

e) Compute the area (area$_p$) of one pole:

$$\text{area}_p = \frac{\Phi_{st\,max}^{no\text{-}load}}{B_{max}} = 2.25\,\text{m}^2. \quad \text{(E4-2.8)}$$

f) Compute the field (f) current $I_{fo}$ required at no load:

$$I_{fo} = \frac{B_{st\,max} \cdot p \cdot g \cdot \pi}{4 \cdot \mu_0 \cdot k_{rp} \cdot N_{riot}} = \frac{1(2)(0.0127)(\pi)}{4(4\pi \times 10^{-7})(0.751)(288)} = 73.4\,\text{A}. \quad \text{(E4-2.9)}$$

g) Determine the synchronous (S) reactance (per phase value) $X_S$ in ohms. The self-inductance of phase a is

$$L_{aa} = \frac{\lambda_{aa}}{i_a} = \frac{N_{st} \cdot \phi_{st\,max}}{i_a} = \frac{N_{st} \cdot B_{st\,max} \cdot \text{area}_p}{i_a} = \frac{\mu_0 \cdot 4 \cdot k_{stb} \cdot k_{stp1} \cdot (\text{Nstph})^2 \cdot \text{area}_p}{p \cdot g \cdot \pi} \quad \text{(E4-2.10)}$$

$$L_{aa} = \frac{4\pi \times 10^{-7}(4)(0.96)(0.866)(16)^2(2.25)}{2(0.0127)(\pi)} = 30.16\,\text{mH}.$$

According to Concordia [7 in Chapter 4]

$$L_d = L_{aa} + L_{ab} + 1.5L_{aa2}. \quad \text{(E4-2.11)}$$

Neglecting $L_{aa2}$ and $L_{aa} \approx L_{ab}$ one gets for the synchronous inductance $L_d$

$$L_d \approx 2 \cdot L_{aa} = 60.33\ \text{mH}$$

The synchronous reactance of the round-rotor machine is

$$X_S = \omega L_d = \omega L_S = 22.74\,\Omega. \quad \text{(E4-2.12)}$$

The base voltage is

$$V_{base} = \frac{V_{L-L}}{\sqrt{3}} = V_{phase} = 7{,}967\,\text{V}. \quad \text{(E4-2.13)}$$

The base apparent power is per phase

$$S_{base} = S_{phase} = \frac{S_{sat}}{3} = 5.33\,\text{MVA} \quad \text{(E4-2.14)}$$

and the base current is

$$I_{base} = I_{phase} = \frac{S_{base}}{V_{base}} = 669\,\text{A}. \quad \text{(E4-2.15)}$$

h) Find the base impedance $Z_{base}$ expressed in ohms. The base impedance becomes

$$Z_{base} = \frac{V_{base}}{I_{base}} = 11.9\,\Omega. \quad \text{(E4-2.16)}$$

i) Express the synchronous reactance $X_S$ in per unit (pu). The per-unit synchronous reactance is now

$$X_S^{pu} = \frac{X_S}{Z_{base}} = \frac{22.74}{11.9} = 1.91\,\text{pu}. \quad \text{(E4-2.17)}$$

### 4.2.5 Application Example 4.3: dq0 Modeling of a Salient-Pole Synchronous Machine: Solution

a) Balanced Three-Phase Short-Circuit. If the terminals of a synchronous generator are short circuited at rated no-load excitation one obtains the balanced short-circuit currents in per unit [31 in Chapter 4]:

$$i_a(\varphi) = \frac{1}{X_d}\cos(\varphi+\alpha) + \frac{(X_d - X_d')}{X_d X_d'} e^{-\varphi/T_d'} \cos(\varphi+\alpha) - \frac{1}{2}\left(\frac{1}{X_d'} + \frac{1}{X_q}\right) e^{-\varphi/T_a} \cos\alpha - \frac{1}{2}\left(\frac{1}{X_d'} + \frac{1}{X_q}\right) e^{-\varphi/T_a} \cos(2\varphi+\alpha) \quad \text{(E4.3-1)}$$

$$i_b(\varphi) = \frac{1}{X_d}\cos(\varphi+\alpha-120°) + \frac{(X_d - X_d')}{X_d X_d'} e^{-\varphi/T_d'} \cos(\varphi+\alpha-120°) + \frac{1}{4}\left(\frac{1}{X_d'} + \frac{1}{X_q}\right) e^{-\varphi/T_a} \cos\alpha + \frac{1}{2}\left(\frac{1}{X_d'} - \frac{1}{X_q}\right) e^{-\varphi/T_a} \cos(2\varphi+\alpha+\delta) \quad \text{(E4.3-2)}$$

$$i_c(\varphi) = \frac{1}{X_d}\cos(\varphi+\alpha+120°) + \frac{(X_d - X_d')}{X_d X_d'} e^{-\varphi/T_d'} \cos(\varphi+\alpha+120°) + \frac{1}{4}\left(\frac{1}{X_d'} + \frac{1}{X_q}\right) e^{-\varphi/T_a} \cos\alpha + \frac{1}{2}\left(\frac{1}{X_d'} - \frac{1}{X_q}\right) e^{-\varphi/T_a} \cos(2\varphi+\alpha-\delta). \quad \text{(E4.3-3)}$$

where $\tan\delta = \sqrt{3}$, $\varphi = \omega t$.

The field current is

$$i_f(\varphi) = 1 + \frac{(X_d - X'_d)}{X'_d}\left(e^{-\varphi/T'_{do}} - \cos\varphi e^{-\varphi/T_a}\right) \quad \text{(E4.3-4)}$$

and the torque is

$$T_{3-phase} = \frac{(X'_d - X_q)}{2X'_d X_q}\cdot\sin(2\varphi) + \frac{1}{X'_d}\sin\varphi. \quad \text{(E4.3-5)}$$

The maximum torque occurs at the angle $\varphi_{max}$ which can be obtained from

$$\cos\varphi_{max} = \frac{1}{4}\left(\frac{X_q}{(X_q - X'_d)} \pm \sqrt{\left(\frac{X_q}{(X'_d - X_q)}\right)^2 + 8}\right). \quad \text{(E4.3-6)}$$

Figure E4.3.1 illustrates the torque of Eqs. E4.3-5 and E4.3-6.

b) Line-to-Line Short-Circuit. The short-circuit of the two terminals b and c of a synchronous generator results in the line-to-line short-circuit current [31 in Chapter 4]

$$i_b = \frac{\sqrt{3}(\cos\varphi - \cos\varphi_o)}{(X_q + X'_d) - (X_q - X'_d)\cos 2\varphi} \quad \text{(E4.3-7)}$$

or for $\varphi_o = 0$

$$i_b = \frac{\sqrt{3}(\cos\varphi - 1)}{(X_q + X'_d) - (X_q - X'_d)\cos 2\varphi} \quad \text{(E4.3-8)}$$

and the torque is

$$T_{L-L} = -\frac{2}{\sqrt{3}}(\sin\varphi)i_b + \frac{2}{3}\sin 2\varphi(X'_d - X_q)i_b^2 \quad \text{(E4.3-9)}$$

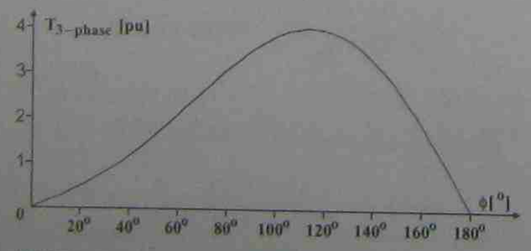



**FIGURE E4.3.1** First half-cycle of torque described by Eqs. E4.3-5 and E4.3-6 (for the parameters $X'_d = 0.2909$ pu and $X_q = 0.8$ pu).

or

$$T_{L-L} = \frac{-2\sin(\cos\varphi - 1)}{[(X_q + X'_d) - (X_q - X'_d)\cos 2\varphi]} + \frac{2\sin 2\varphi(X'_d - X_q)(\cos\varphi - 1)^2}{[(X_q + X'_d) - (X_q - X'_d)\cos 2\varphi]^2}. \quad \text{(E4.3-10)}$$

Figure E4.3.2 illustrates the torques of Eqs. E4.3-5, E4.3-6 and E4.3-10.

The open-circuit voltage induced in phase a in case of a short-circuit of line b with line c is

$$e_a = -\cos\varphi - b\left(\frac{[-\sin\varphi\sin 2\varphi + (\cos\varphi - \cos\varphi_o)2\cos 2\varphi]}{[a - b\cos 2\varphi]} - \frac{(\cos\varphi - \cos\varphi_o)(\sin 2\varphi)^2 2b}{[a - b\cos 2\varphi]^2}\right), \quad \text{(E4.3-11)}$$

where

$$a = (X_q + X'_d) \text{ and } b = (X_q - X'_d). \quad \text{(E4.3-12a,b)}$$

The maximum value of $e_a$ occurs for $\varphi_o = 0$

Figure E4.3.3 illustrates the induced voltage $e_a$ of Eqs. E4.3-11 and E4.3-12a,b.

c) Line-to-Neutral Short-Circuit. The current when phase a of a synchronous machine at no load is short-circuited is for $\theta = 90° + \varphi$ [31 in Chapter 4]

$$i_a = \frac{3(\cos\theta - \cos\theta_o)}{(X_q - X'_d)} \times \frac{1}{\frac{(X'_d + X_q + X_o)}{(X_q - X'_d)} - \cos 2\theta} \quad \text{(E4.3-13)}$$

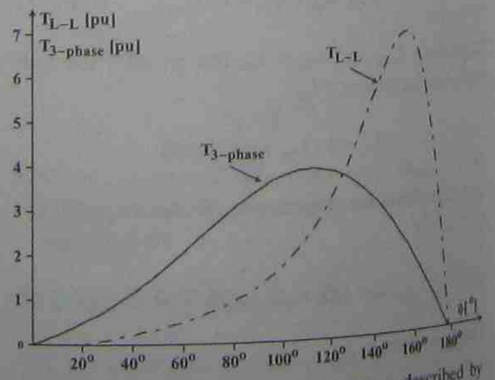



**FIGURE E4.3.2** First half-cycle of torque described by Eqs. E4.3-5, E4.3-6, and E4.3-10 (for the parameters $X'_d = 0.2909$ pu and $X_q = 0.8$ pu).



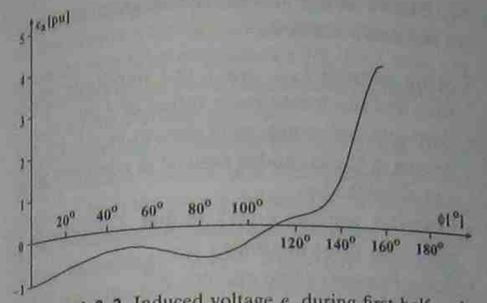



**FIGURE E4.3.3** Induced voltage $e_a$ during first half-cycle at an initial condition $\varphi_o = 0$ described by Eqs. E4.3-11 and E4.3-12a,b (for the parameters $X'_d = 0.2909$ pu and $X_q = 0.8$ pu).

or in terms of an infinite series

$$i_a = \frac{3(\cos\theta - \cos\theta_o)}{(X_q - X'_d)} \cdot \frac{2a}{1-a^2}(1 + 2a\cos 2\theta + 2a^2\cos 4\theta + \ldots), \quad \text{(E4.3-14)}$$

where

$$a = \frac{\sqrt{X_q + \frac{X_o}{2}} - \sqrt{X'_d + \frac{X_o}{2}}}{\sqrt{X_q + \frac{X_o}{2}} + \sqrt{X'_d + \frac{X_o}{2}}}. \quad \text{(E4.3-15)}$$

Note that $i_a$ must be initially zero, that is, $\varphi = \varphi_o = 0$ or $\theta_o = 90°$.

The fundamental component becomes now

$$i_{a1} = \frac{3\cos\theta}{X'_d + \sqrt{X_q + \frac{X_o}{2}}\cdot\sqrt{X'_d + \frac{X_o}{2}} + \frac{X_o}{2}} \quad \text{(E4.3-16)}$$

or in terms of symmetrical components

$$i_{a1} = \frac{3\cos\theta}{X'_d + X_2 + X_o}. \quad \text{(E4.3-17)}$$

d) Out-of-Phase Synchronization. When synchronizing a generator (either machine or inverter) with the power system the following conditions must be met:

- Phase sequence must be the same;
- The phase angle between the two voltage systems must be sufficiently small; and
- The slip must be small.

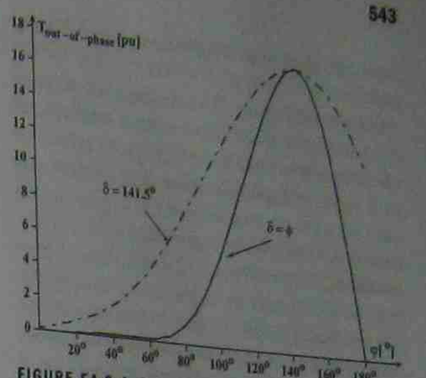



**FIGURE E4.3.4** Out-of-phase synchronizing torque when $\delta = 141.5°$ (worst case) and when $\varphi = \delta$ in Eq. E4.3-18 (for the parameters $X'_d = 0.2909$ pu and $X_q = 0.80$ pu).

Synchronizing out of phase is an important issue because it generates the highest torques and forces (in particular within the end winding of a machine) when paralleled with the power system [31 in Chapter 4]. The torque during out-of-phase synchronization is as a function of time $\varphi = \omega t$ and the angle $\delta$ between the power system's voltage and that of the synchronous machine voltage at the time of paralleling:

$$T_{out\text{-}of\text{-}phase} = \frac{1}{X_q}[\sin\delta(1-\cos\varphi) + (1-\cos\delta)\sin\varphi] \left\{1 + \frac{(X_q - X'_d)}{X'_d}[(1-\cos\delta)(1-\cos\varphi) - \sin\delta\sin\varphi]\right\}. \quad \text{(E4.3-18)}$$

Note this expression is symmetrical in $\delta$ and $\varphi$, that is, $\delta$ and $\varphi$ can be interchanged without altering the relation. Introducing $\delta = \varphi$ in Eq. E4.3-18, one obtains for the torque

$$T_{out\text{-}of\text{-}phase} = \frac{2\sin\delta(1-\cos\delta)}{X'_d} - \sin\delta\left[\frac{X_q - X'_d}{X_q X'_d}\right][2 + 2\cos\delta - 8(\cos\delta)^2 + 4(\cos\delta)^3]. \quad \text{(E4.3-19)}$$

The corresponding field current is

$$i_f(\varphi) = \frac{X_d - X'_d}{X'_d}[1 - \cos\delta + (\cos\delta - 1)\cos\varphi - \sin\delta\sin\varphi] + 1. \quad \text{(E4.3-20)}$$

Figure E4.3.4 illustrates the very large torque if the generator is out-of-phase synchronized with the

worst case angle of $\delta = 141.5°$ and when $\varphi = \delta$ in Eq. E4.3-18.

Experimental results [32–34] during out-of-phase synchronization show that for small synchronous machines below 100 kVA a voltage difference of $\Delta V \leq \pm 10\%$, a phase angle difference of $\Delta\delta \leq \pm 5°$, and a slip of $s \leq 1\%$ can be permitted. For large machines these conditions must be more stringent; that is, the voltage difference $\Delta V \leq \pm 1\%$, the phase angle difference $\Delta\delta \leq \pm 0.5°$, and the slip $s \leq 0.1\%$. During the past first analog [32–34 in Chapter 4] and then digital paralleling devices have been employed to connect synchronous generators to the grid. Although these devices are very reliable, once in a while a faulty paralleling occurs.

Figure E4.3.5 depicts the various parameters when out-of-phase synchronization occurs with an angle of $\delta = 255°$ – which is not the worst-case condition (see Fig. E4.3.4). In this analysis subtransient reactances are taken into account.

- Stator currents $i_a$, $i_b$, and $i_c$ are amplitude modulated and reach maximum values of 4 pu;
- Zero-sequence component current ($i_o = i_a + i_b + i_c$) flowing in the grounded neutral is relatively small and about 0.5 pu;
- Electrical generator ($G$) torque $T_G$ assumes a maximum value of about 4 pu;
- Rotor (torque) angle exceeds 90°;
- Real $P_G$ and reactive $Q_G$ power oscillations occur;
- Slip s reaches values of more than 3 pu; and
- Mechanical torque $T_M$ between generator and turbine is below 1 pu.

Not shown in this graph are the extremely large winding forces in the end region of the stator winding,

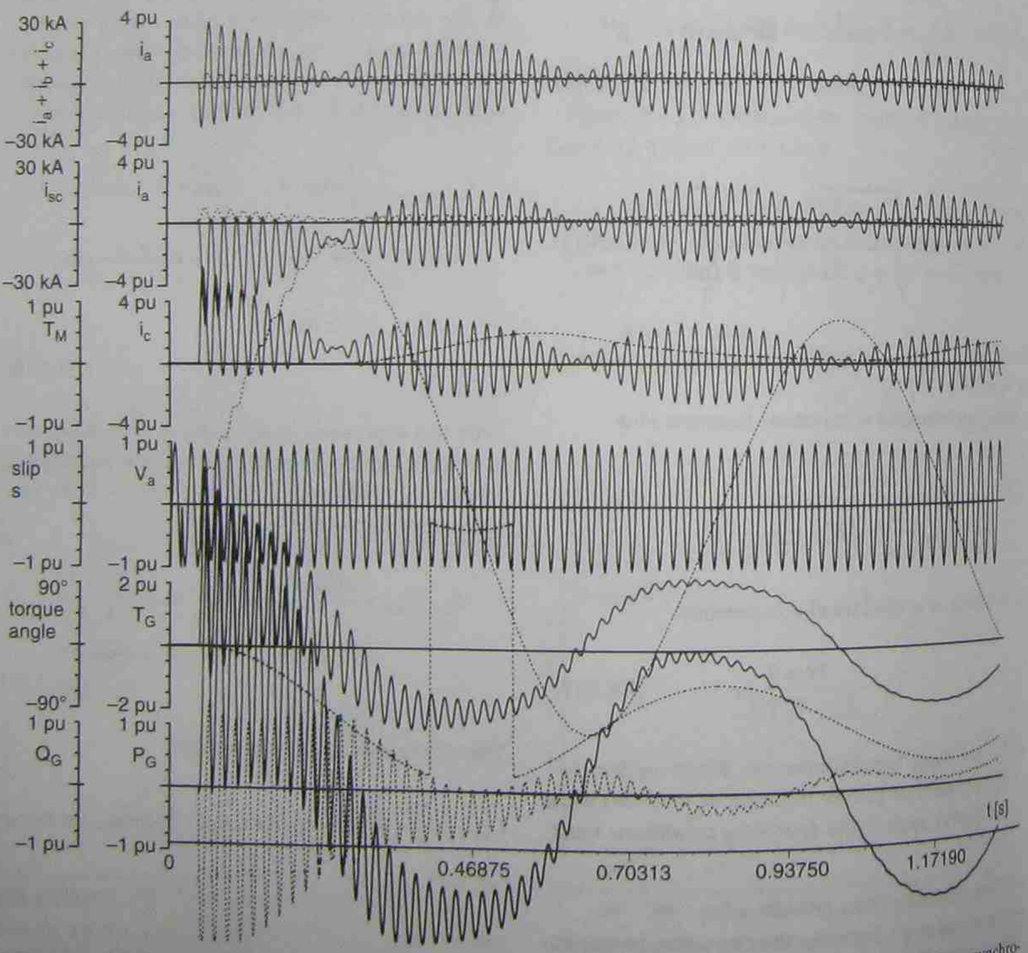


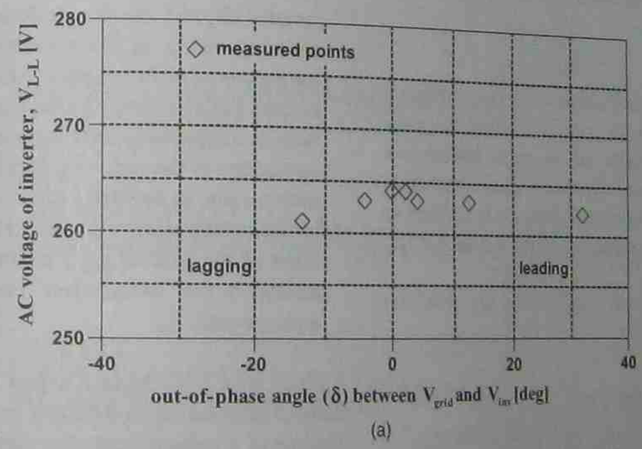

**FIGURE E4.3.5** Various parameters for out-of-phase synchronization of a turbogenerator when the out-of-phase synchronizing angle is $\delta = 255°$.



and the excessive heating of the amortisseur bars and the solid-rotor pole face. The latter issue will be addressed in a later example. In Fig. E4.3.5 the left scale pertains to the dotted signals and the right scale belongs to the full-line signals.

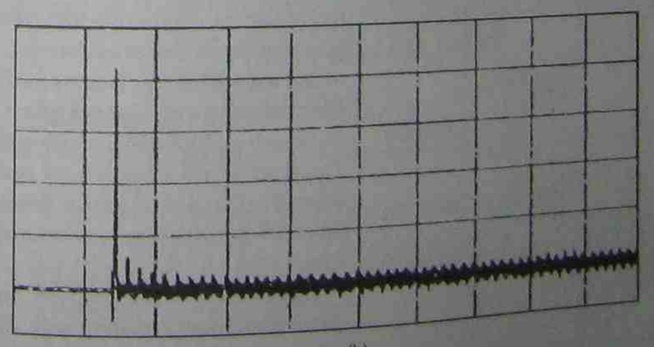
Figure E4.3.6a illustrates the conditions under which a 30 kVA inverter of a wind-power plant was paralleled with the power system [29, 30 in Chapter 4]. The switching frequency and therefore the fundamental (nominally 60 Hz) frequency was phase-locked with the power system's frequency and thus the slip is by definition $s = 0$. However, the voltage differences and the phase differences must be within certain limits. Experiments showed it was advisable to choose the inverter rms value of the line-to-line voltage always somewhat larger (e.g., $V_{\text{L-Linverter}} = 260\ V_{\text{rms}}$) than that of the power system's line-to-line voltage (e.g., $V_{\text{L-Lpower system}} = 240\ V_{\text{rms}}$). Figure E4.3.6b depicts the transient current flowing from inverter to power system when inverter is paralleled at an inverter voltage of $V_{\text{L-Linverter}} = 260\ V_{\text{rms}}$ at an out-of-phase voltage angel of $\delta = 24°$, where the inverter voltage leads that of the power system. As can be seen, the transient current is more than 200 A.

Figure E4.3.7 illustrates the stator flux distribution when a large synchronous generator is paralleled out-of-phase [21 in Chapter 4]: the stator flux leaves the iron core (stator back iron) and currents are induced in the key bars of the iron-core suspension as well as in the aluminum bars within the dovetails of the iron core. The flux density within the space between the iron core and the frame is 17 mT at a terminal voltage of 1.23 pu. This flux density is sufficient to heat up the solid iron key bars and melt the aluminum bars within the dovetails of the iron core.




(a)

**FIGURE E4.3.6a** Voltage rms values $V_{L\text{-}L}$ and out-of-phase voltage angles $\delta$ (°) when 30 kVA inverter is out-of-phase synchronized with power system.



(b)

**FIGURE E4.3.6b** Measured transient current (0.1 s/div, 50 A/div) during the time of paralleling the 30 kVA inverter with the power system at $V_{L\text{-}L\ \text{power system}} = 240\ V_{\text{rms}}$ and out-of-phase synchronizing angle is $\delta = 24°$ (inverter voltage leads the power system voltage).

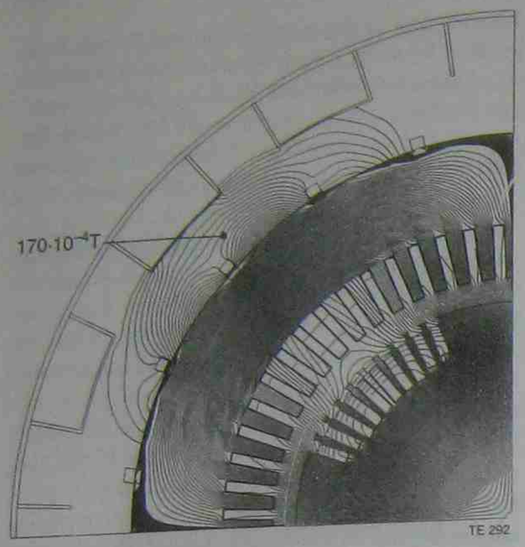



**FIGURE E4.3.7** Flux distribution when a large generator is out-of-phase synchronized with power system [21 in Chapter 4].

e) Synchronizing and Damping Torques. When a synchronous generator is paralleled with the power system one obtains for the angle perturbation $\Delta\sin\omega t$ from the steady-state angle $\delta_0$ the synchronizing $T_S$ and damping $T_D$ torques in addition to the steady-state torque $T_o$ [31 in Chapter 4]:

$$T = T_0 + T_S(\Delta\sin\omega t) + T_D(\omega\cdot\Delta\cos\omega t), \quad \text{(E4.3-21)}$$

where

$$T_0 = \frac{V_{l\text{-}n}\cdot V_{l\text{-}n0}}{X_d}\sin\delta_0 + V_{l\text{-}n}^2\left[\frac{X_d - X_q}{2X_qX_d}\right]\sin 2\delta_0, \quad \text{(E4.3-22)}$$

$$T_S = \frac{V_{l\text{-}n}\cdot V_{l\text{-}n0}}{X_d}\cos\delta_0 + V_{l\text{-}n}^2\left(\frac{1}{X_q} - \frac{1}{X_d}\right)\cos 2\delta_0 + V_{l\text{-}n}^2\frac{(X_d - X_d')}{X_dX_d'}\cdot\frac{(\omega T_d')^2}{1+(\omega T_d')^2}(\sin\delta_0)^2, \quad \text{(E4-3.23)}$$

$$T_D = V_{l\text{-}n}^2(\sin\delta_0)^2\left[\frac{(X_d - X_d')}{X_dX_d'}\right]\frac{T_d'}{1+(\omega T_d')^2}, \quad \text{(E4-3.24)}$$

where $T_{d0}' = \dfrac{X_F}{R_F} = \dfrac{X_d}{X_d'} = T_d'$.

f) Torques during Reclosing. In order to minimize power quality problems after short-circuits have occurred, it is common practice to reclose the switches that have been opened due to the short-circuit. Short-circuits can be interrupted within four to six 60 Hz cycles. In the hope that the short-circuit has been cleared, the utilities reclose the previously opened switches after nine to fifteen 60 Hz cycles have elapsed. If the short-circuit still persists, then the fault will be cleared again after additional four to six 60 Hz cycles. At the most three to five reclosing operations are performed. The timing of the reclosing is important: if the timing is unfavorable the mechanical torques of the turbine stages become excessive, but under favorable conditions these mechanical torques can be minimized. Only an accurate dynamic calculation can approximately predetermine the most favorable reclosing times. Transient electromagnetic and shaft torques of synchronous generators can become as high as 5–6 during reclosing [35–39 in Chapter 4]. The magnitudes of the torques depend on the reclosing time. If the reclosing occurs at a time when the electrical torque due to reclosing adds to the transient shaft torque, the resulting mechanical shaft becomes large as compared to the case where the electrical torque due to the reclosing opposes the transient shaft torque; in the latter case the resulting shaft torque will be relatively small. This amplification effect of the mechanical transient torque has its analogy in the "swing effect" one encounters on a playground.

Joyce *et al.* [35, 36 in Chapter 4] have recommended introducing a measure for the theoretical lifetime of a turbine shaft: the occurrence of many high torsional torques reduces the lifetime of a shaft more quickly than the occurrence of low torsional torques. Figure E4.3.8 illustrates a common connection of a power plant to the high-voltage system. One generator feeds two transformers, which are connected to high-voltage feeders each. This is to minimize the outage of a power plant due to external faults such as short-circuits within the power system. The short-circuit is caused by making the impedances $Z_{Fa}$, $Z_{Fb}$, and $Z_{Fc}$ zero. Breaker #2 interrupts the short-circuit and recloses after a preprogrammed time.

Figures E4.3.9a and E4.3.9b depict the various parameters when reclosing with different reclosing times but with the same short-circuit duration (104 ms) occurs. In these graphs the left scale pertains to the dotted signals and the right scale belongs to the full-line signals.





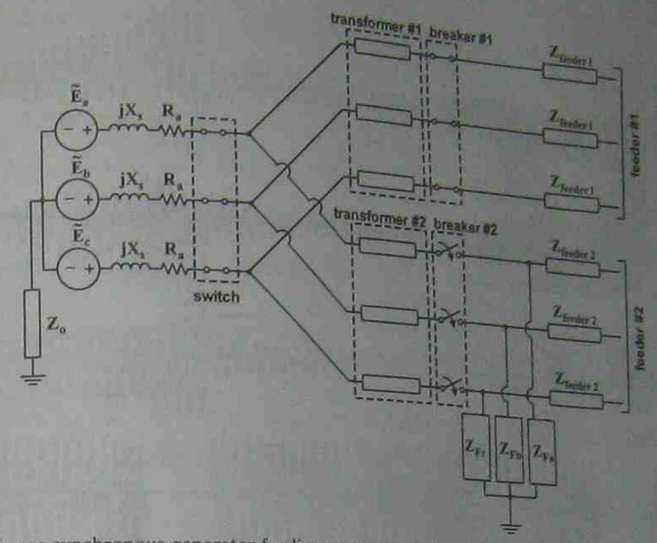



**FIGURE E4.3.8** Large synchronous generator feeding two transmission lines via two transformers.

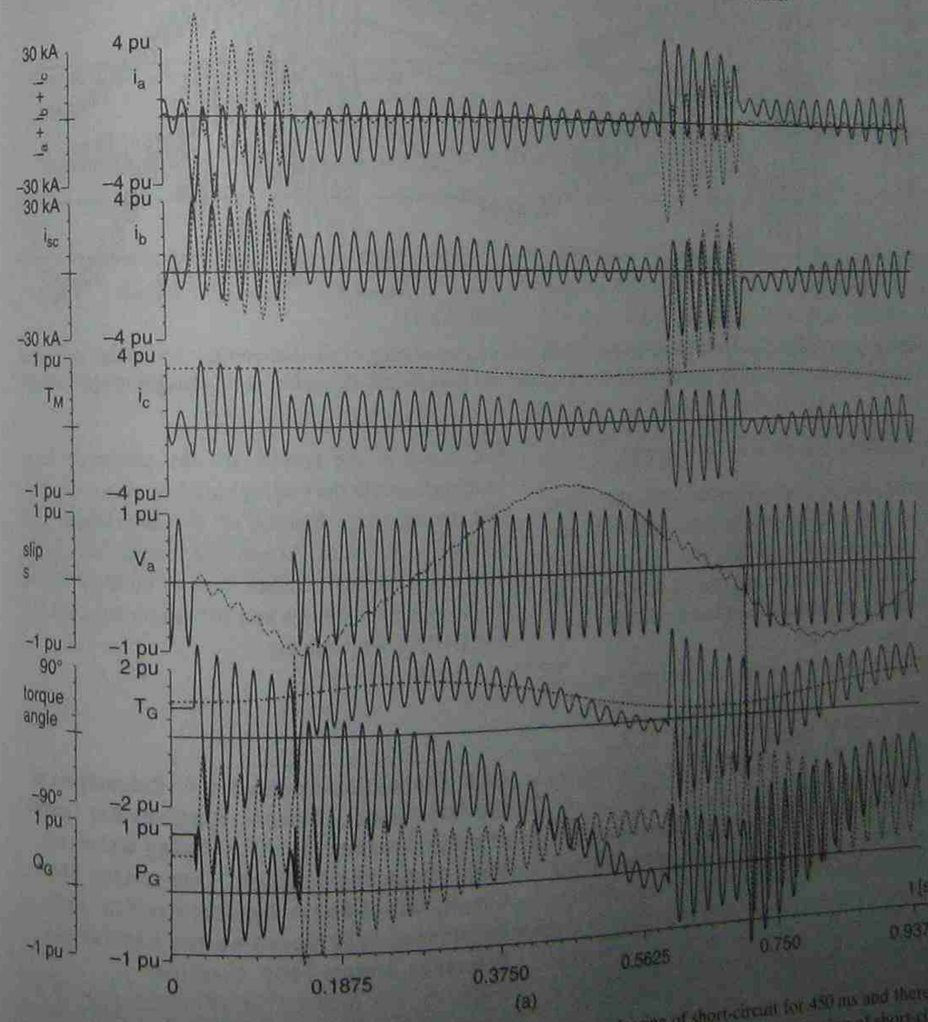
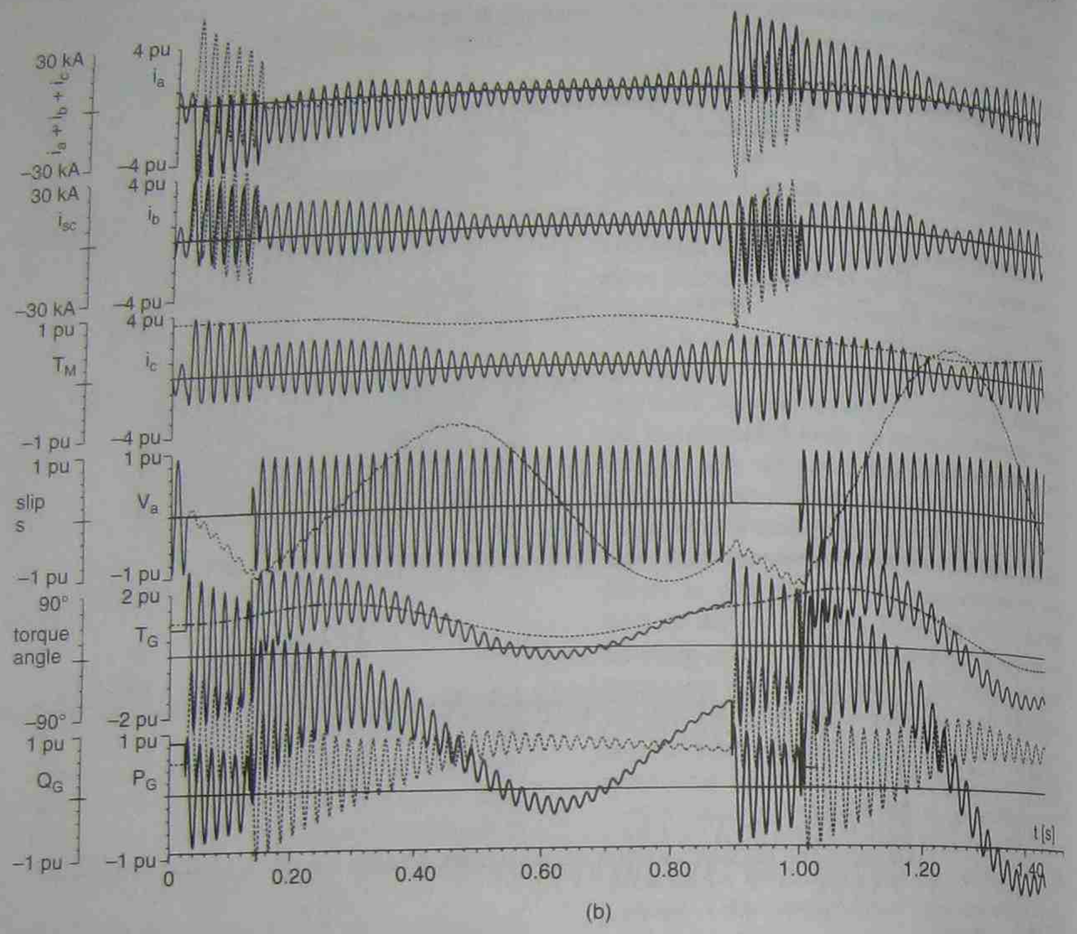



**FIGURE E4.3.9a** Three-phase short-circuit lasting 104 ms followed by clearing of short-circuit for 480 ms and thereafter followed by reclosing whereby the short-circuit has not cleared and lasts 104 ms, thereafter again clearing of short-circuit.




(b)

**FIGURE E4.3.9b** Three-phase short-circuit lasting 104 ms followed by clearing of short-circuit for 745 ms and thereafter followed by reclosing whereby the short-circuit has not cleared and lasts 104 ms, thereafter again clearing of short-circuit.

Summarizing one can state the following:

- During the three-phase short-circuit the stator currents $i_a$, $i_b$, and $i_c$ are amplitude modulated and exceed maximum values of 4 pu;
- Zero-sequence component current ($i_o = i_a + i_b + i_c$) flowing in the grounded neutral is relatively large and exceeds 4 pu;
- Electrical torque $T_G$ assumes a maximum value of about 3 pu;
- Rotor (torque) angle is below 90°;
- Very large (about 2 pu) real $P_G$ and reactive $Q_G$ power swings occur;
- Maximum slip reaches values of more than 1 pu;
- Mechanical torque $T_M$ between generator and turbine is below 1 pu, but it has an alternating component causing mechanical stress; and
- In both cases the stability of the synchronous generators is maintained due to the torque angle $\delta$ being less than 90°.

Not shown is the graphs are the extremely large winding forces in the end region of the stator winding, and the excessive heating of the amortisseur bars residing on the rotor. As can be expected, the electrical and mechanical stresses depend on the reclosing times, which are 450 ms and 745 ms for Figs. E4.3.9a and E4.3.9b, respectively.

### 4.2.6 Application Example 4.4: Calculation of the Amortisseur (Damper Winding) Bar Losses of a Synchronous Machine during Balanced Three-Phase Short-Circuit, Line-to-Line Short-Circuit, Out-of-Phase Synchronization, and Unbalanced Load Based on the Natural abc Reference System [40]: Solution

Following the notation of [7 in Chapter 4] one obtains the voltage equations:



$$e_a = p\Psi_a - r \cdot i_a \quad \text{(E4.4-25a)}$$

$$e_b = p\Psi_b - r \cdot i_b \quad \text{(E4.4-25b)}$$

$$e_c = p\Psi_c - r \cdot i_c \quad \text{(E4.4-25c)}$$

$$e_{fd} = p\Psi_{fd} + r_{fd} \cdot i_{fd} \quad \text{(E4.4-25d)}$$

$$0 = p\Psi_{kd} - r_{kd} \cdot i_{kd} + v_{kd} \quad \text{(E4.4-25e)}$$

$$0 = p\Psi_{kq} - r_{kq} \cdot i_{kq} + v_{kq} \quad \text{(E4.4-25f)}$$

for $k = 1, 2, 3, \ldots, 8$ damper windings in d- or q-axes.

The flux linkage equations are

$$\Psi_a = -L_{aa}i_a - L_{ab}i_b - L_{ac}i_c + L_{afd}i_{fd} + L_{akd}i_{kd} + L_{akq}i_{kq} \quad \text{(E4.4-26a)}$$

$$\Psi_b = -L_{ba}i_a - L_{bb}i_b - L_{bc}i_c + L_{bfd}i_{fd} + L_{bkd}i_{kd} + L_{bkq}i_{kq} \quad \text{(E4.4-26b)}$$

$$\Psi_c = -L_{ca}i_a - L_{cb}i_b - L_{cc}i_c + L_{cfd}i_{fd} + L_{ckd}i_{kd} + L_{ckq}i_{kq} \quad \text{(E4.4-26c)}$$

$$\Psi_{fd} = -L_{fda}i_a - L_{fdb}i_b - L_{fdc}i_c + L_{fdfd}i_{fd} + L_{fdkd}i_{kd} \quad \text{(E4.4-26d)}$$

$$\Psi_{kd} = -L_{kda}i_a - L_{kdb}i_b - L_{kdc}i_c + L_{kdfd}i_{fd} + L_{kd1d}i_{1d} + L_{kd2d}i_{2d} + \ldots + L_{kdld}i_{ld} \quad \text{(E4.4-26e)}$$

$$\Psi_{kq} = -L_{kqa}i_a - L_{kqb}i_b - L_{kqc}i_c + L_{kk1q}i_{1q} + L_{kq2q}i_{2q} + \ldots + L_{kqlq}i_{lq} \quad \text{(E4.4-26f)}$$

for $k = 1, 2, \ldots, 8$ and $l = 1, 2, \ldots, 8$.

Following the notation of Fig. E4.4.2, the self-inductance of the kth damper winding is

$$L_{kd}^R = 2 \cdot l_R \cdot A_{Rkd}/I_{kd} \quad \text{(E4.4-27)}$$

and the leakage inductance with respect to stator winding is

$$L_{kdl}^R = 2 \cdot l_R \cdot (A_{Rkd} - A_{Skd})/I_{kd} \quad \text{(E4.4-28)}$$

or referred to the stator reference frame, where $m_1$ and $m_2$ are the number of stator and rotor phases, respectively:

$$L_{kd} = m_1(2 \cdot l_R \cdot A_{Rkd}/I_{kd})M_{ikd}^2/m_2 \quad \text{(E4.4-29)}$$

$$L_{kdl} = m_1[2 \cdot l_R \cdot (A_{Rkd} - A_{Skd})/I_{kd}]M_{ikd}^2/m_2. \quad \text{(E4.4-30)}$$

The mutual inductances between the kth and the *l*th d-axis windings are

$$L_{kdld} = m_1 \cdot L_{kdld}^{fd} \cdot M_{kdld}^2 \cdot M_{ild}^2/m_2) \quad \text{(E4.4-31a)}$$

$$L_{ldkd} = m_1 \cdot L_{ldkd}^{fd} \cdot M_{ldkd}^2 \cdot M_{ikd}^2/m_2. \quad \text{(E4.4-31b)}$$

Correspondingly the ohmic resistance is

$$r_{kd} = m_1 \cdot R_{kd} \cdot M_{ikd}^2/m_2. \quad \text{(E4.4-32)}$$

The same procedure applies to the q-axis parameters, as indicated in Fig. E4.4.3. In these equations $l_R$ is the rotor length. $M_{kda}$, $M_{kdld}$, $M_{ldq}$, and $M_{ldkd}$ are transformation ratios. The calculation of the stator inductances (Fig. E4.4.4) is performed in the same manner as for the rotor inductances.

If Eqs. E4.4-26 to E4.4-32 are introduced in Eq. E4.4-25 one obtains

$$[L] \cdot \left[\frac{di}{dt}\right] = [V]. \quad \text{(E4.4-33)}$$

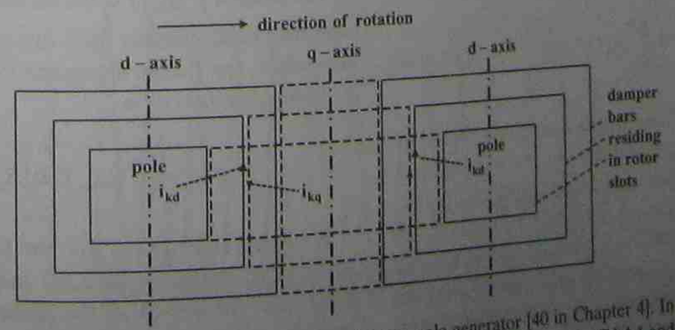



**FIGURE E4.4.1** Decomposition of amortisseur winding of a two-pole generator [40 in Chapter 4]. In this graph only six damper windings are shown: three in the d-axis and three in the q-axis. Figures E4.4.2 to E4.4.4 and E4.4.11 to E4.4.13 provide details about the location of the 16 damper bars within the rotor slots.

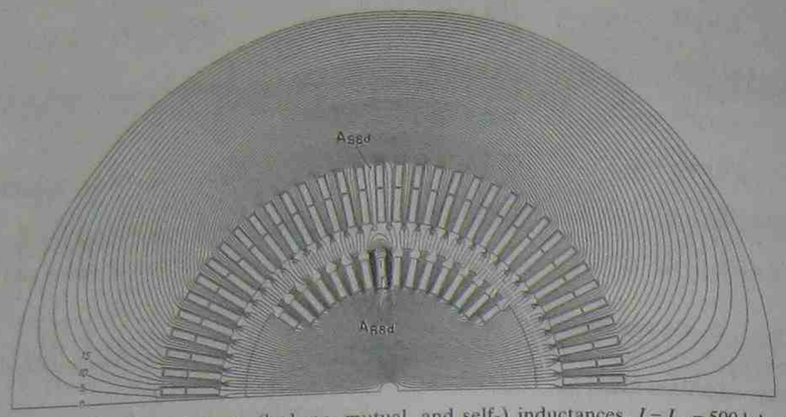



**FIGURE E4.4.2** Calculation of d-axis rotor (leakage, mutual, and self-) inductances, $I = I_{kd} = 500$ kA, where $k = 8$. All vector potentials must be multiplied by $10^{-2}$ Wb/m [40 in Chapter 4].

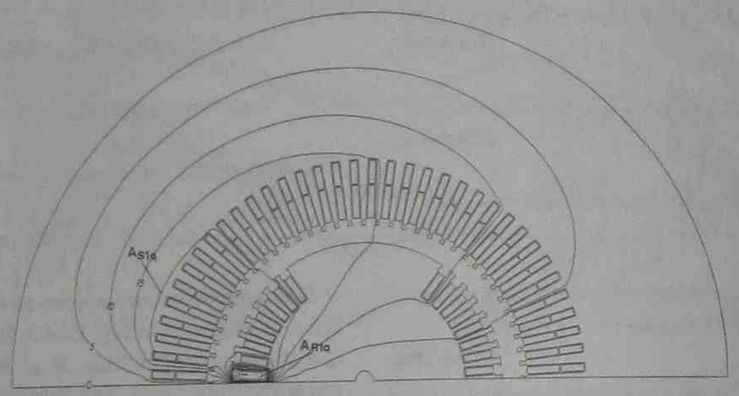



**FIGURE E4.4.3** Calculation of q-axis rotor (leakage, mutual, and self-) inductances, $I = I_{kq} = 500$ kA, where $k = 1$. All vector potentials must be multiplied by $10^{-2}$ Wb/m [40 in Chapter 4].

where $[L]$ is an inductance matrix with time-varying coefficients, $\left[\frac{di}{dt}\right]$ is the derivative of the solution vector $[i]$ and $[V]$ represents the forcing sources. Using Gaussian elimination one gets

$$\left[\frac{di}{dt}\right] = [L]^{-1} \cdot [V]. \qquad \text{(E4.4-34)}$$

Subsequently a Runge-Kutta integration procedure of the fourth order provides the first starting steps for the Adams-Moulton method, which is a predictor-corrector integration procedure, and one obtains the solution vector $[i]$. A line-to-line short-circuit including the (generator) transformer leakage impedance is performed. The line-to-neutral voltages in per unit (referred to the rated voltage of the generator) are shown in Fig. E4.4.5. The stator currents are depicted in Fig. E4.4.6, and field and damper bar currents are shown in Figs. E4.4.7 and E4.4.8a,b. The resulting electrical and mechanical torques are depicted in Figs. E4.4.9 and E4.4.10.

The integral $\int_1^{t_2} (i_{k\,\mathrm{bar}})^2 dt$ is a measure for the energy absorbed by the damper bar k due to the current $i_{k\,\mathrm{bar}}$. Therefore, the energy dissipated in the damper bar $k$ during time $(t_2 - t_1)$ is

$$E_{k\,\mathrm{bar}} = \left\{\int_1^{t_2} (i_{k\,\mathrm{bar}})^2 dt\right\} R_{k\,\mathrm{bar}}. \qquad \text{(E4.4-35)}$$

It is well known that the bar (e.g., #16) of the amortisseur (see Fig. E4.4.11) located before the rotor pole as viewed in the direction of rotation incurs greater loss than the bar (e.g., #1) of the amortisseur located behind the rotor pole as viewed in the direction of rotation. Figure E4.4.12 shows the

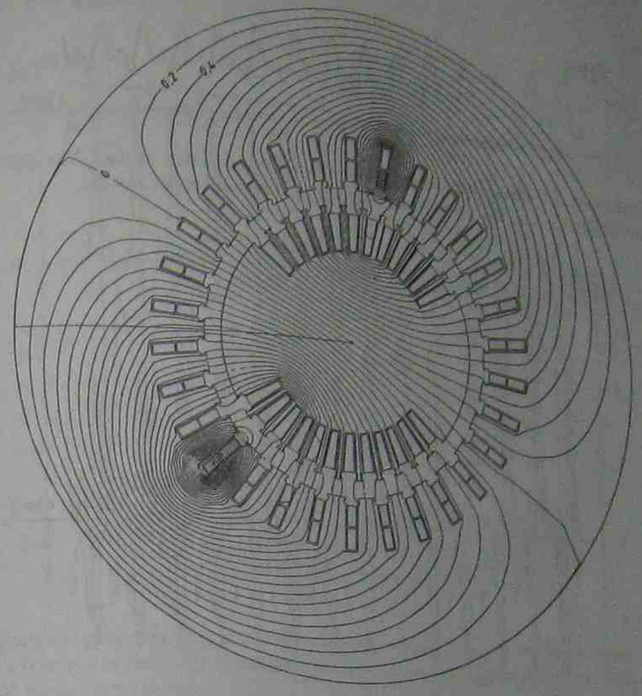



**FIGURE E4.4.4** Calculation of stator (leakage, mutual, and self-) inductances. One stator winding turn is excited with the current $I = 50$ A; all vector potentials must be multiplied by $10^{-2}$ Wb/m [40 in Chapter 4].

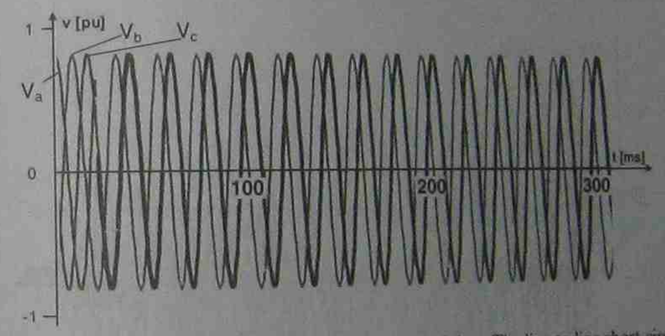



**FIGURE E4.4.5** Line-to-neutral voltages $v_a$, $v_b$, and $v_c$ as a function of time. The line-to-line short-circuit occurs at 25 ms at no load and $v_c = v_a$. The voltages are referred to rated line-to-neutral voltage.

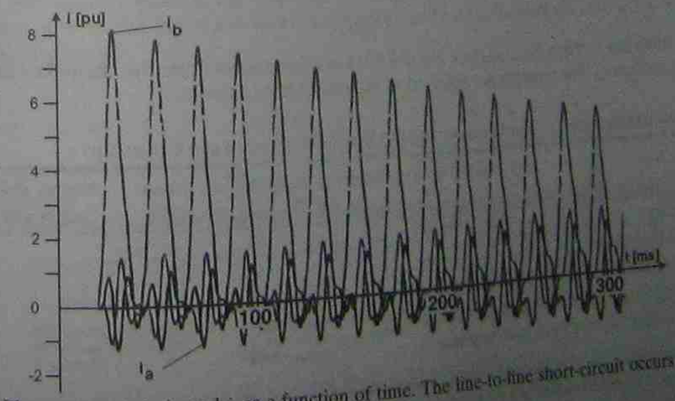



**FIGURE E4.4.6** Phase currents $i_a$, $i_b$, and $i_c$ as a function of time. The line-to-line short-circuit occurs at 25 ms at no load and $v_c = v_a$. The currents are referred to the rated stator current.

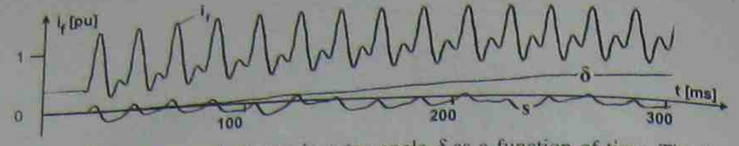
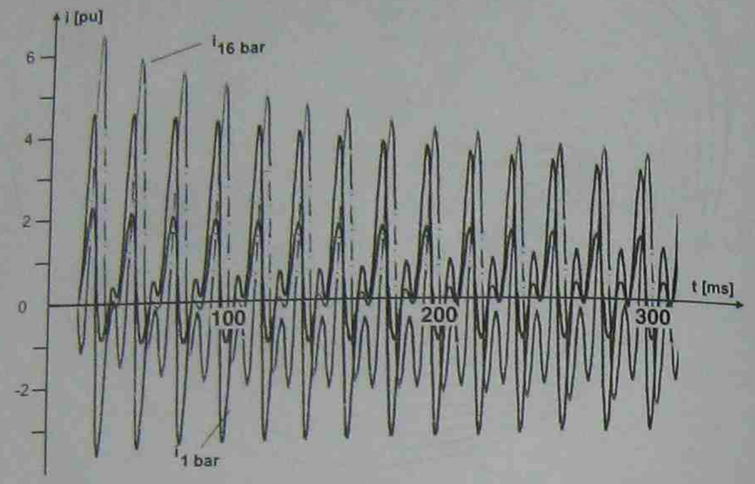
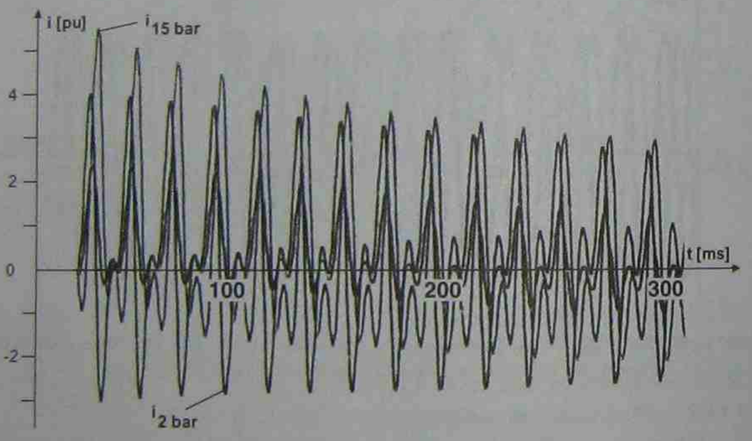



**FIGURE E4.4.7** Field currents $i_f$, slip s, and change in rotor angle $\delta$ as a function of time. The line-to-line short-circuit occurs at 25 ms at no load and $v_c = v_a$. The field current is referred to the rated stator current.




(a)

**FIGURE E4.4.8a** Rotor bar currents $i_{1bar}$, $i_{16bar}$ (see Fig. E4.4.11) as a function of time. The line to-line short-circuit occurs at 25 ms at no load and $v_c = v_a$. The currents are referred to the rated stator current.




(b)

**FIGURE E4.4.8b** Rotor bar currents $i_{2bar}$, $i_{15bar}$ (see Fig. E4.4.11) as a function of time. The line-to-line short-circuit occurs at 25 ms at no load and $v_c = v_a$. The currents are referred to the rated stator current.

**TABLE E4.4.1** Dissipated Energies in Amortisseur #1 and #16 Bars for Different Fault Conditions

| Fault condition | Energy dissipated in per unit[a] in bar #1 during first 1.25 s | Energy dissipated in per unit[a] in bar #16 during first 1.25 s |
|---|---|---|
| Line-to-line short-circuit | 0.95 | 1.05 |
| Balanced three-phase short-circuit | 0.92 | 1.12 |
| Out-of-phase synchronization with a 120° leading rotor angle | 2.36 | 2.43 |
| Out-of-phase synchronization with a 120° lagging rotor angle | 1.25 | 1.57 |
| Unbalanced stator currents resulting in an inverse stator current of $\|\bar{I}_2\| = 8.7\%$. | 0.049 | 0.053 |

[a]Energy dissipated in a bar is referred to the heat energy required to melt one bar if there is no cooling.

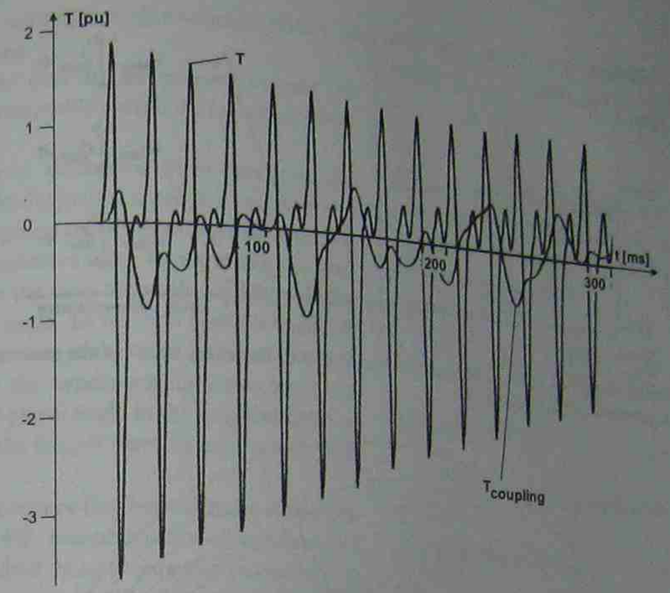



**FIGURE E4.4.9** Electrical generator torque T and mechanical torque $T_{coupling}$ at coupling between generator and steam turbine stage #1 as a function of time. The line-to-line short-circuit occurs at 25 ms at no load and $v_c = v_a$. The torques are referred to the rated torque of generator.

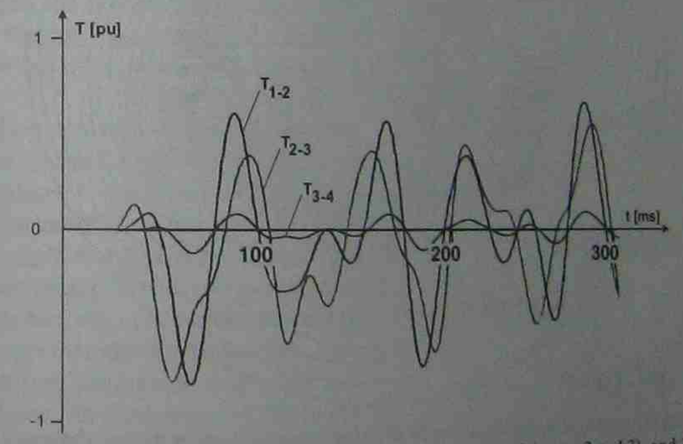



**FIGURE E4.4.10** Mechanical torques at the couplings 1–2 (stages 1 and 2), 2–3 (stages 2 and 3), and 3–4 (generator and exciter) as a function of time. The line-to-line short-circuit occurs at 25 ms at no load and $v_c = v_a$. The torques are referred to the rated torque of generator.

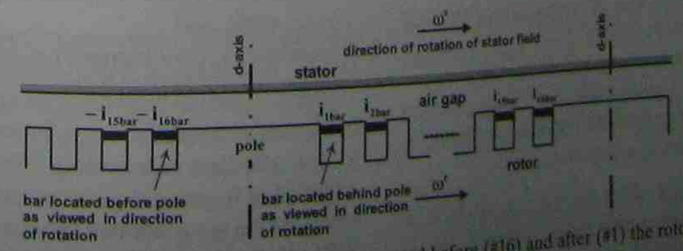



**FIGURE E4.4.11** Definition of the bars of the amortisseur located before (#16) and after (#1) the rotor pole as viewed in direction of rotation.

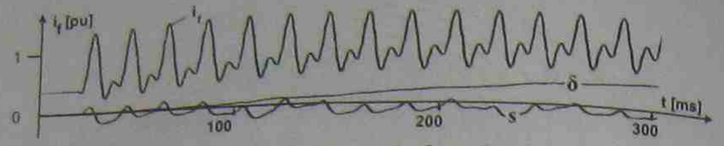
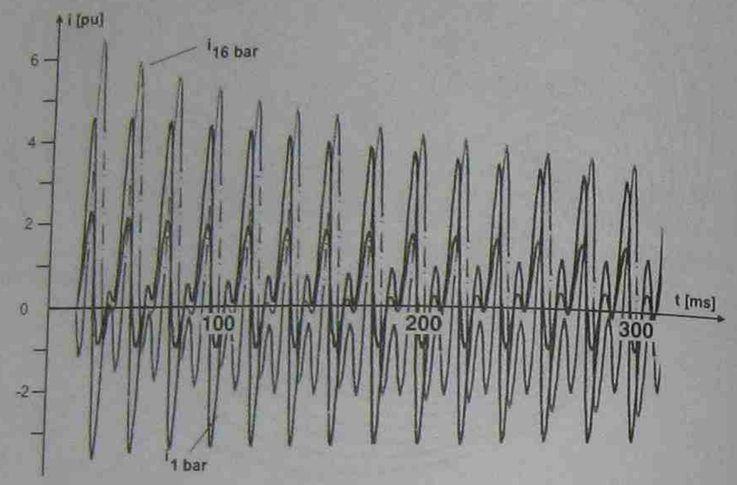
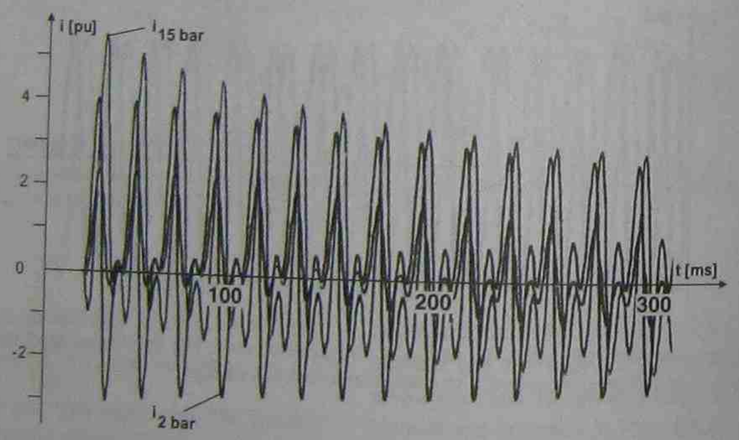



**FIGURE E4.4.7** Field currents $i_f$, slip $s$, and change in rotor angle $\delta$ as a function of time. The line-to-line short-circuit occurs at 25 ms at no load and $v_c = v_a$. The field current is referred to the rated stator current.




(a)

**FIGURE E4.4.8a** Rotor bar currents $i_{1bar}$, $i_{16bar}$ (see Fig. E4.4.11) as a function of time. The line to-line short-circuit occurs at 25 ms at no load and $v_c = v_a$. The currents are referred to the rated stator current.




(b)

**FIGURE E4.4.8b** Rotor bar currents $i_{2bar}$, $i_{15bar}$ (see Fig. E4.4.11) as a function of time. The line-to-line short-circuit occurs at 25 ms at no load and $v_c = v_a$. The currents are referred to the rated stator current.

**TABLE E4.4.1** Dissipated Energies in Amortisseur #1 and #16 Bars for Different Fault Conditions

| Fault condition | Energy dissipated in per unit[a] in bar #1 during first 1.25 s | Energy dissipated in per unit[a] in bar #16 during first 1.25 s |
|---|---|---|
| Line-to-line short-circuit | 0.95 | 1.05 |
| Balanced three-phase short-circuit | 0.92 | 1.12 |
| Out-of-phase synchronization with a 120° leading rotor angle | 2.36 | 2.43 |
| Out-of-phase synchronization with a 120° lagging rotor angle | 1.25 | 1.57 |
| Unbalanced stator currents resulting in an inverse stator current of $\|\bar{I}_2\| = 8.7\%$. | 0.049 | 0.053 |

[a]Energy dissipated in a bar is referred to the heat energy required to melt one bar if there is no cooling.

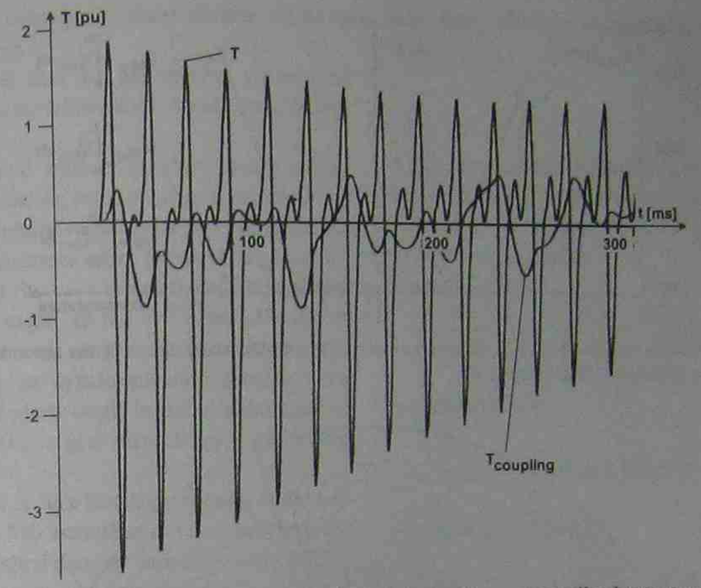



**FIGURE E4.4.9** Electrical generator torque T and mechanical torque $T_{coupling}$ at coupling between generator and steam turbine stage #1 as a function of time. The line-to-line short-circuit occurs at 25 ms at no load and $v_c = v_a$. The torques are referred to the rated torque of generator.

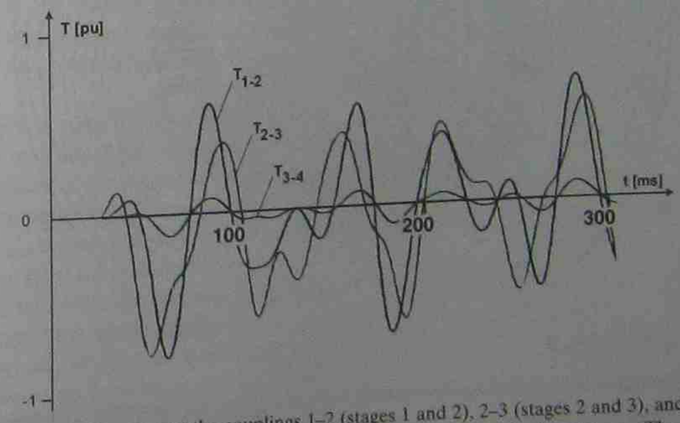



**FIGURE E4.4.10** Mechanical torques at the couplings 1–2 (stages 1 and 2), 2–3 (stages 2 and 3), and 3–4 (generator and exciter) as a function of time. The line-to-line short-circuit occurs at 25 ms at no load and $v_c = v_a$. The torques are referred to the rated torque of generator.

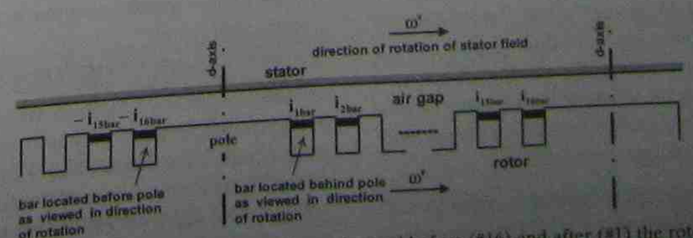



**FIGURE E4.4.11** Definition of the bars of the amortisseur located before (#16) and after (#1) the rotor pole as viewed in direction of rotation.

ST. GEORGE COLLEGE OF LAW

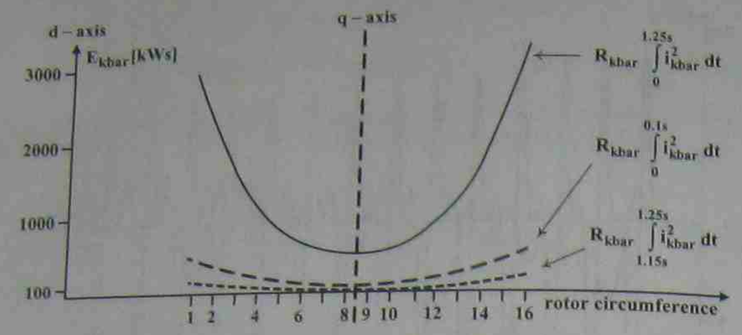



**FIGURE E4.4.12** Energy dissipated in the k damper bars during line-to-line short-circuit at the secondary terminals of a transformer fed by a generator [40 in Chapter 4].

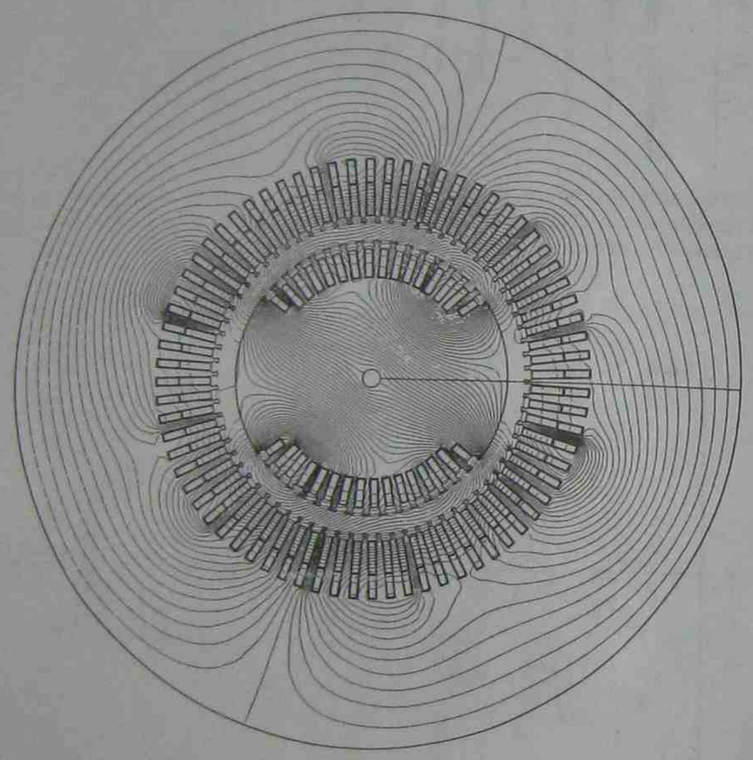


**FIGURE E4.4.13** Subtransient field during the first cycle of a synchronous generator during a balanced three-phase short circuit.

values $E_{kbar}$ for a sudden line-to-line short-circuit at the terminals including transformer impedance for various time intervals $(t_2 - t_1)$. Figure E4.4.13 depicts the subtransient field of a generator during the first cycle of a three-phase short-circuit.

Table E4.4.1 summarizes the dissipated energies in the 1st and 16th amortisseur bars during various fault conditions of a generator including the (generator) transformer leakage impedance:

1) line-to-line short-circuit,
2) balanced three-phase short-circuit,
3) out-of-phase synchronization with a 120° leading rotor angle,
4) out-of-phase synchronization with a 120° lagging rotor angle, and
5) unbalanced stator currents resulting in an inverse stator current of $|\bar{I}_2| = 8.7\%$.

**Discussion of Results**

- Most transients decay within 1 to 2 s.
- The 2nd harmonic in the stator currents of Fig. E4.4.6 are confirmed by measurements.
- The thermal stress of the amortisseur bars due to a balanced short-circuit can be tolerated, provided there are no subsequent short-circuits within a brief time frame.
- An imbalance due to an inverse current of $|\bar{I}_2| = 8.7\%$ is acceptable—even during steady-state operation.
- There is a great difference when synchronizing with either a leading rotor angle or a lagging rotor angle. Out-of-phase synchronization with a leading rotor angle generates more losses within the generator than in the case of synchronization with a lagging rotor angle. In the first case the machine acts as a generator and in the latter it acts as a motor during the synchronization process. Note that an out-of-phase angle in the neighborhood of 140° leads to the largest currents and torques (see Fig. E4.3.4).
- To mitigate or reduce the thermal stress of damper bars #1 and #16 manufacturers of synchronous generators embed damper bars also on the surface of the rotor poles. In this manner the thermal stress of all amortisseur bars will be made more equal.
- Not neglecting saturation and the generation of eddy currents within the solid rotor poles will in addition mitigate the thermal stress of the entire amortisseur because the inductive coupling between stator and rotor damper windings will be reduced.
- A similar analysis applies to the induced currents of an induction machine. Under normal operation the currents induced in the rotor bars of an induction machine are uniform and have the same rated magnitude $I_{bar_rated}$ in each and every bar. However, if a bar is broken (that is, no current can flow) then the neighboring bars will have currents that can be significantly larger than the rated magnitude. Such an unequal current distribution may result in a thermal imbalance. As a consequence due to this imbalance and the very small air gap of induction machines, the rotor may become eccentric and rub against the stator core, and this may lead to failure of the induction machine. See Chapter 3 for more details.

The abc-reference frame employed in this example has been subsequently used in references [41–43]. The above results are confirmed in these references. However, the out-of-phase synchronizing angle of 180° as used in [43] does not yield the largest currents, losses, and torques (see Fig. E4.3.4). These references teach that the large losses in the damper bars next to the poles (e.g., bar #1 and bar #16) can be reduced by the deployment of amortisseur bars, which are embedded within the pole faces.



### 4.2.9 Application Example 4.7: Design of a Low-Speed 20 kW Permanent-Magnet Generator for a Wind-Power Plant: Solution

a) Synchronous speed

$$n_s = \frac{120f}{p} \quad \text{or} \quad f = \frac{n_s p}{120} = \frac{60(12)}{120} = 6\text{Hz}. \qquad \text{(E4.7-1)}$$

b) Ampere's law

$$H_m l_m + H_g l_g = 0. \qquad \text{(E4.7-2)}$$

c) Continuity of flux

$$\Phi = B_m A_m = B_g A_g. \qquad \text{(E4.7-3)}$$

d) Constituent relation

$$B_g = \mu_0 H_g. \qquad \text{(E4.7-4)}$$

From Eq. E4.7-2

$$H_m l_m = -H_g l_g. \qquad \text{(E4.7-5)}$$

With Eq. E4.7-4

$$H_m l_m = -B_g l_g / \mu_0. \qquad \text{(E4.7-6)}$$

and with Eq. E4.7-3

$$B_g = B_m \left(\frac{A_m}{A_g}\right). \qquad \text{(E4.7-7)}$$

the load-line equation becomes

$$H_m = -\left(\frac{A_m}{A_g}\right)\left(\frac{l_g}{l_m}\right)\frac{B_m}{\mu_0}. \qquad \text{(E4.7-8)}$$

Introducing the given numerical values into load-line equation gives

$$H_m = -91.7\,B_m \left[\frac{kA}{m}\right]. \qquad \text{(E4.7-9)}$$

This equation is plotted in Fig. E4.7.4. Note that the magnet material is not operated in the point of the maximum energy product.

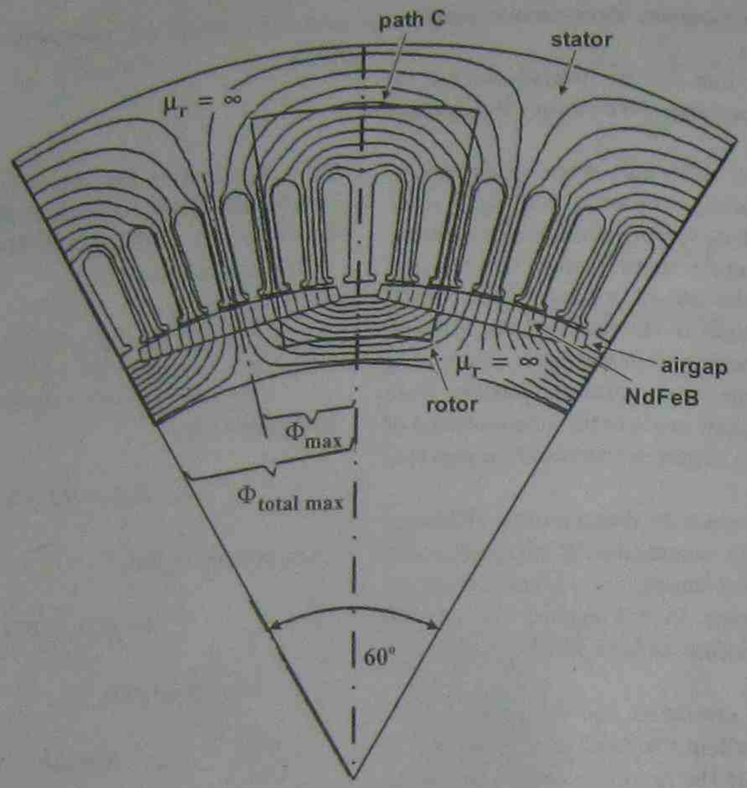



**FIGURE E4.7.1** Cross section of one period (two pole pitches) of permanent-magnet machine with no-load field.

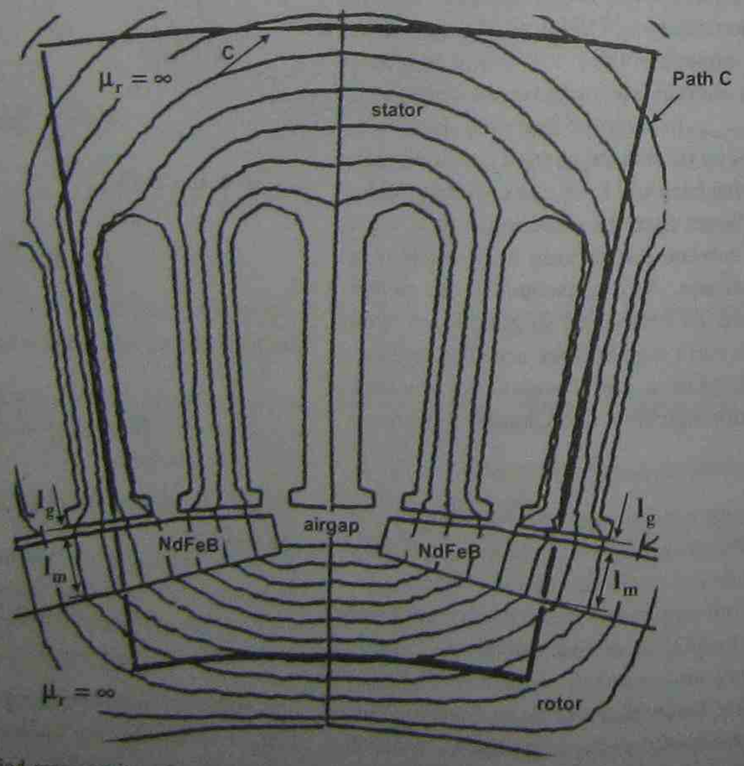



**FIGURE E4.7.2** Magnified cross section of area enclosed by path C of a pole pitch of permanent-magnet machine (see Fig. E4.7.1).



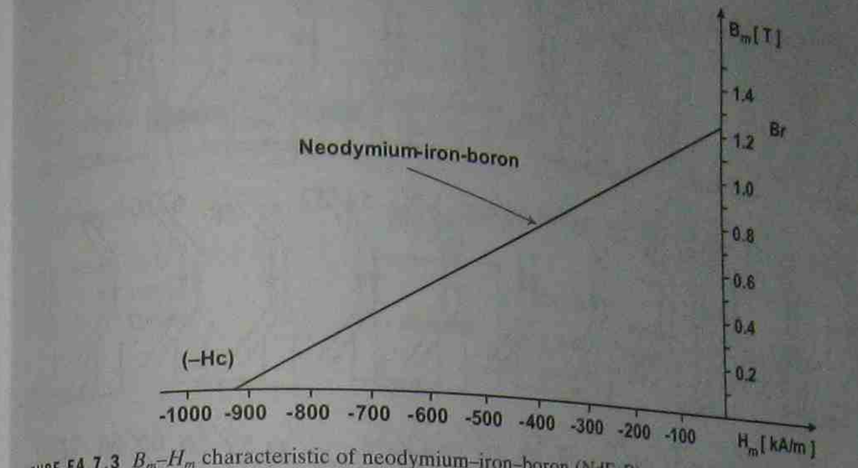



**FIGURE E4.7.3** $B_m$–$H_m$ characteristic of neodymium–iron–boron (NdFeB) permanent-magnet material.

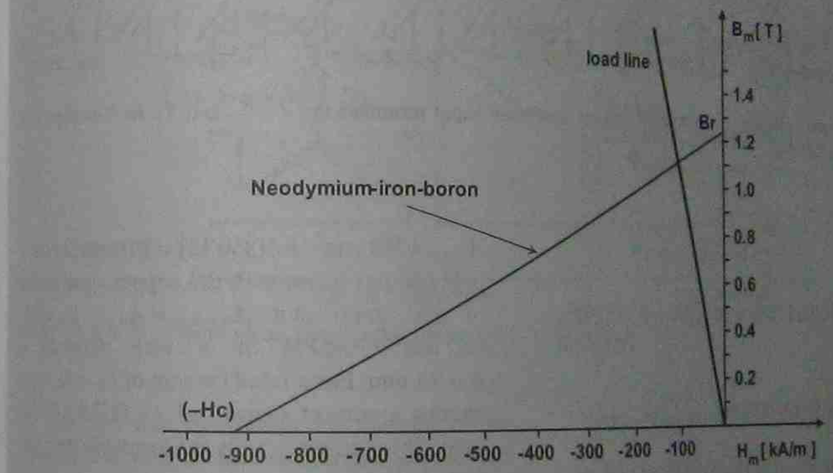



**FIGURE E4.7.4** Magnet (NdFeB) characteristic and load line.

e) Recoil permeability of NdFeB (slope of the permanent-magnet characteristic)

$$\mu_R = \frac{(y_2 - y_1)}{(x_2 - x_1)} = \frac{(B_r - 0)}{(0 - (-H_c))} = \frac{1.25}{950(10^3)} \quad \text{(E4.7-10)}$$
$$= 1.316 \times 10^{-6}\ \text{(H/m)}$$

or

$$\mu_R = 1.047\ \mu_0. \quad \text{(E4.7-11)}$$

f) Induced voltage

$$\Phi_{max} = B_m A_m \quad \text{(E4.7-12)}$$

$$\Phi_{totalmax} = 2\Phi_{max} = 2B_m A_m \quad \text{(E4.7-13)}$$

The flux is defined as

$$\Phi(t) = \Phi_{totalmax} \cos \omega t. \quad \text{(E4.7-14)}$$

Therefore, the induced voltage is

$$E_{max} = N(d\Phi/dt) = \omega N_{ph} k_w k_s \Phi_{totalmax}. \quad \text{(E4.7-15)}$$

From load line and magnet characteristic one obtains the operating point:

$$B_m = 1.1\ \text{T}, \quad \text{(E4.7-16a)}$$

$$H_m = -100\text{k A/m}. \quad \text{(E4.7-16b)}$$

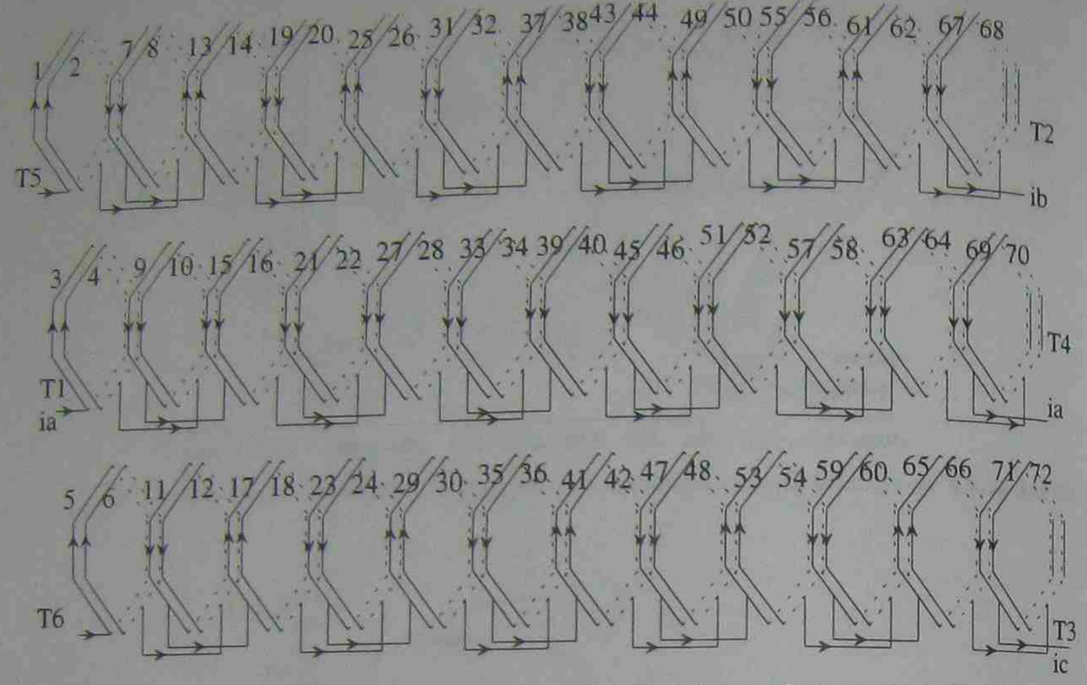



**FIGURE E4.7.5** Stator winding of permanent-magnet generator. Input terminals are $T_1$, $T_2$, and $T_3$. In Y-configuration connect $T_4$, $T_5$, and $T_6$.

Therefore,

$$\Phi = \Phi_{\text{totalmax}} = (2)(1.1)(11668 \times 10^{-6})\text{Wb} = 0.0257 \text{ Wb}, \quad \text{(E4.7-17)}$$

and the induced voltage is now

$$e(t) = (360)\ (0.0257)\ (2\pi)\ (6)\ (0.8)\ (0.94) \sin \omega t = E_{\max} \sin \omega t, \quad \text{(E4.7-18a)}$$

or

$$E_{\max} = 262.3 \text{ V}, \quad \text{(E4.7-18b)}$$

$$E_{rms} = E_{\max}/\sqrt{2} = 185.48 \text{ V}, \quad \text{(E4.7-18c)}$$

and the line-to-line terminal voltage is approximately

$$V_{L\text{-}L} = \sqrt{3}\ V_{L\text{-}N} = \sqrt{3}(1.05)E_{rms} = 337.3 \text{ V}. \quad \text{(E4.7-19)}$$

g) Determination of wire diameter of the stator winding. Figure E4.7.5 depicts the stator winding housed in 72 slots. It is a full-pitch, double-layer winding. Using a copper-fill factor of $k_{cu} = 0.62$ one obtains for a stator slot cross section of $A_{st_slot} = 368 \text{ mm}^2$ and $(360/12) = 30$ turns per stator pole and per phase with the copper cross section of one stator slot $A_{st_slot_cu} = A_{st_slot} \cdot k_{cu} = 368 \cdot 0.62 \text{ mm}^2 = 30\pi D^2/4$ or a wire diameter of $D = 3.1$ mm. For a rated current of $I_{rat} = 31$ A one obtains a current density of $J = 31/7.6 = 4.07 \text{ A/mm}^2$. This current density is acceptable for a ventilated machine.

### 4.2.10 Application Example 4.8: Design of a 10 kW Wind-Power Plant Based on a Synchronous Machine: Solution

a) $P_{\text{out_transformer}} = 10$ kW, $P_{\text{out_inverter}} = 10.53$ kW, $P_{\text{out_rectifier}} = 11.08$ kW, $P_{\text{out_generator}} = 11.67$ kW, $P_{\text{out_gear}} = 12.28$ kW, $P_{\text{out_wind turbine}} = 12.92$ kW. (E4.8-1)

b) $$\left(\frac{N_Y}{N_\Delta}\right) = \frac{1}{89.9}. \quad \text{(E4.8-2)}$$

c) Note $\tilde{V}_{L\text{-}L\ \text{system}} = \tilde{V}_{L\text{-}L\Delta}$ and $\tilde{V}_{L\text{-}L\ \text{inverter}} = \tilde{V}_{L\text{-}LY}$; therefore,

$$\tilde{V}_{L\text{-}L\Delta} = \tilde{V}_{L\text{-}LY} \angle +30°. \quad \text{(E4.8-3)}$$

d) $$\tilde{I}_{L\ \text{system}} = \tilde{I}_{L\ \text{inverter}} \angle +30°. \quad \text{(E4.8-4)}$$



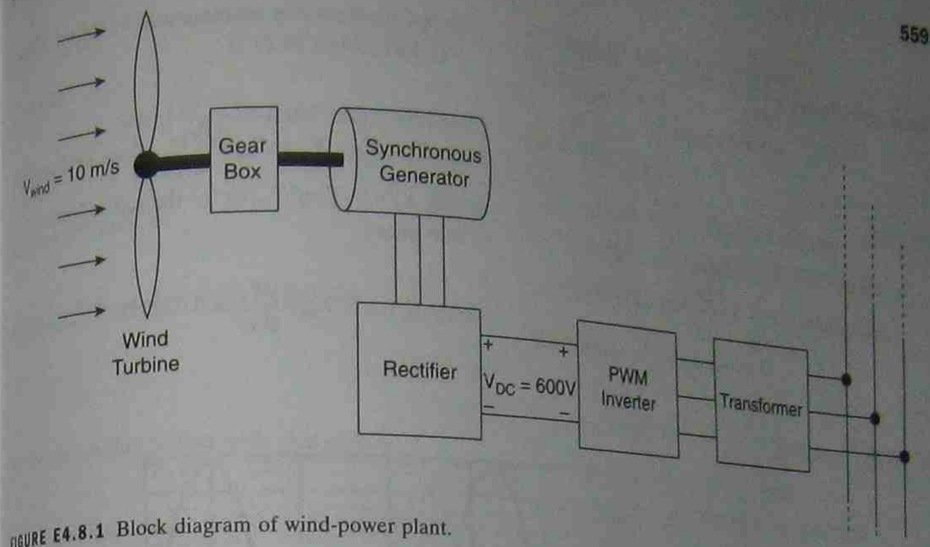



**FIGURE E4.8.1** Block diagram of wind-power plant.

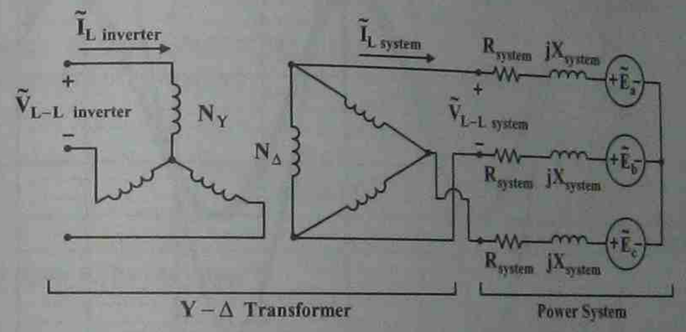



**FIGURE E4.8.2** Y–Δ three-phase transformer connected to power system.

One concludes that the line-to-line voltages of the secondary Δ as well as the line currents fed into the power system are shifted by +30 degrees.

d) The computer program for the inverter is given in Chapter 1, resulting in an inverter output current of $I_{\text{out_inverter}} = 25.33$ A and an inverter input current of $I_{\text{in_inverter}} = 18.47$ A. The inverter output phase voltage and output line current are shown in Fig. E4.8.3.

f) Computer program for rectifier is given in Chapter 1 resulting in a rectifier output current of $I_{\text{out_rectifier}} = 18.47$ A and an rectifier input current of $I_{\text{in_rectifier}} = 14.04$ A. The output voltage of the rectifier is depicted in Fig. E4.8.4.

i) Design of synchronous generator

Stator frequency $$f = \frac{n_s \cdot p}{120} = \frac{(3600)(2)}{120} = 60 \text{ Hz}, \quad \text{(E4.8-5)}$$

phase voltage $V_{L\text{-}N} = 480 \text{ V}/1.732 = 277.14 \text{ V}$, (E4.8-6a)

base voltage $V_{base} = V_{L\text{-}N} = 277.14$ V, (E4.8-6b)

base (rated) current $$I_{base} = \frac{P_{out_generator}}{3 \cdot V_{L\text{-}N}} = \frac{11670}{3(277.14)} = 14.04 \text{ A}, \quad \text{(E4.8-7)}$$

base impedance $$Z_{base} = \frac{V_{base}}{I_{base}} = \frac{277.14 \text{ V}}{14.04 \text{ A}} = 19.74 \Omega, \quad \text{(E4.8-8)}$$

generator loss $$P_{loss} = P_{in_generator} - P_{out_generator} = (12280 - 11670) \text{ W} = 610 \text{ W}, \quad \text{(E4.8-9)}$$

stator resistance $$R_s = \frac{P_{loss}}{3 \cdot I_{base}^2} = 1.03 \Omega, \quad \text{(E4.8-10)}$$

ideal core length $l_i = \dfrac{P_{out_generator}}{D_{rotor}^2 \cdot C \cdot n_s} = \dfrac{11670}{(0.2^2)(1.3)(3600)} = 0.0623\,\text{m},$ (E4.8-11)

actual iron core length (with interlamination insulation) $l_{act} = \dfrac{l_i}{k_{fe}} = \dfrac{0.0623}{0.95}\,\text{m} = 0.0656\,\text{m},$ (E4.8-12)

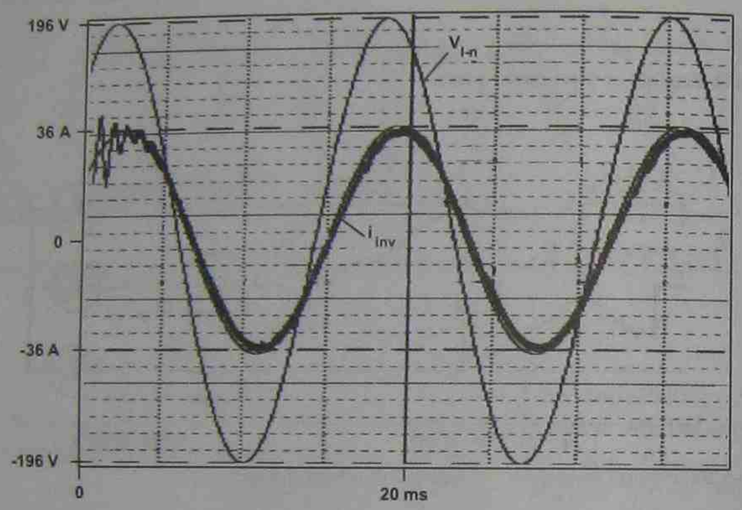



**FIGURE E4.8.3** Inverter output phase voltage and line current.

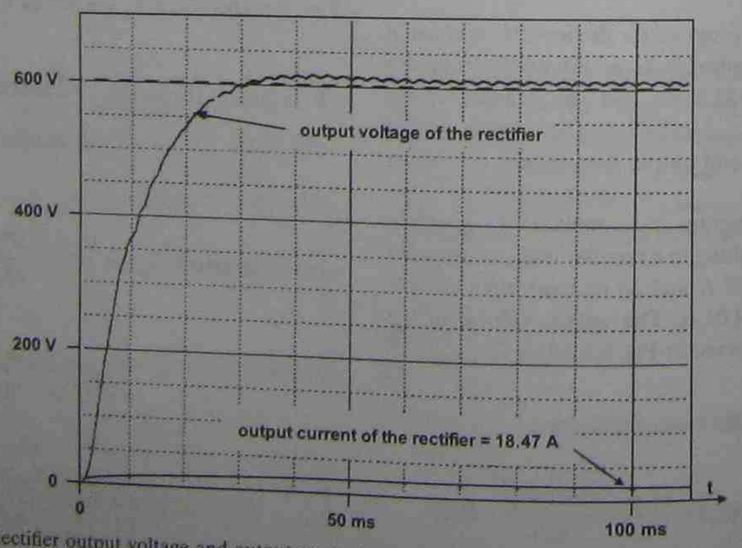



**FIGURE E4.8.4** Rectifier output voltage and output current.

stator synchronous reactance $X_S = X_S[\text{pu}] \cdot Z_{base} = (1.5)(19.74) = 29.61\ \Omega,$ (E4.8-13)

with $X_d = X_S = X_{aa} + X_{ab} + \dfrac{3}{2}X_{aa2}$ one gets approximately $X_S = 2 \cdot (2\pi f) L_{aa}$ or for the self-inductance $L_{aa}$ of one phase

$$L_{aa} = \frac{X_S}{4\pi f} = 0.0393\,\text{H} \qquad \text{(E4.8-14)}$$



and the leakage inductance of one stator (s) phase

$$L_{sl} = 0.1\left(\frac{29.61}{2\pi 60}\right) = 0.0079\,\text{H}. \qquad \text{(E4.8-15)}$$

The area per pole is

$$\text{area}_p = \frac{2\pi \cdot D_{rotor}}{2} \cdot \frac{l_i}{2} = \frac{2\pi(0.2)(0.0623)}{4} = 0.0196\,\text{m}^2 \qquad \text{(E4.8-16)}$$

the maximum flux linked with one pole is

$$\Phi_{s_max} = B_{max} \cdot \text{area}_p = 0.7(0.0196) = 0.0137\text{Wb}. \qquad \text{(E4.8-17)}$$

The induced voltage in one phase of the stator winding becomes (generator operation)

$$E_{ph} = 1.05 \cdot V_{L-N} = 4.44 \cdot f \cdot N_s \cdot k_s \cdot \Phi_{s_max} = 291.0\ \text{V} \qquad \text{(E4.8-18)}$$

or the number of stator turns per phase is

$$N_s = \frac{E_{ph}}{4.44 \cdot f \cdot k_s \cdot \Phi_{s_max}} = \frac{291}{4.44(60)(0.8)(0.0137)} = 100\,\text{turns}. \qquad \text{(E4.8-19)}$$

The one-sided air-gap length can be obtained from

$$L_{aa} = \frac{\lambda_{aa}}{i_a} = \frac{N_s \cdot \Phi_{s_max}}{i_{max}}, \qquad \text{(E4.8-20)}$$

where

$$\Phi_{s_max} = \frac{\mu_o \cdot \dfrac{4}{\pi} \cdot k_s \cdot N_s \cdot i_{max} \cdot \text{area}_p}{p \cdot g}. \qquad \text{(E4.8-21)}$$

Therefore,

$$L_{aa} = \frac{\mu_o \cdot \dfrac{4}{\pi} \cdot k_s \cdot N_s^2 \cdot \text{area}_p}{p \cdot g}$$

or solved for the air-gap length

$$g = \frac{\mu_o \dfrac{4}{\pi} \cdot k_s \cdot N_s^2 \cdot \text{area}_p}{p \cdot L_{aa}} = \frac{(4\pi \times 10^{-7})\left(\dfrac{4}{\pi}\right)(0.8)(10000)(0.0196)}{2(0.0393)} = 0.0032\,\text{m} = 3.2\,\text{mm}. \qquad \text{(E4.8-22)}$$

The torque of the generator is

$$(-T) = \frac{P_{out_generator}}{\omega_r} = \frac{11670}{377} = 30.94\,\text{Nm}. \qquad \text{(E4.8-23)}$$

For a torque angle of $\delta = 30°$ one gets with

$$T = -\frac{p \cdot \pi \cdot D_{rotor} \cdot l_{act} \cdot B_{max} \cdot F_r}{4} \cdot \sin\delta, \qquad \text{(E4.8-24)}$$

or the rotor mmf

$$F_r = \frac{(-T) \cdot 4}{p \cdot \pi \cdot D_{rotor} \cdot l_{act} \cdot B_{max} \cdot \sin\delta} = \frac{(30.94)(4)}{(2)(\pi)(0.2)(0.0656)(0.7)(0.5)} = 4289.6\,\text{At}. \qquad \text{(E4.8-25)}$$

The ampere turns for the rotor are $F_r = \dfrac{4}{\pi} \cdot k_r \cdot \dfrac{N_{r(tot)}}{p} \cdot I_r$

or solved for the ampere turns

$$N_{r(tot)} \cdot I_r = \frac{F_r \cdot p \cdot \pi}{4 \cdot k_r} = \frac{(4289.6)(2)(\pi)}{(4)(0.8)} = 8422.4\,\text{At}. \qquad \text{(E4.8-26)}$$

Selecting 16 rotor slots with 20 turns each, one obtains the field (rotor) current:

$$I_r = 8422.4\ \text{Aturns}/(16 \cdot 20\text{turns}) = 26.3\ \text{A}. \qquad \text{(E4.8-27)}$$

h) Gear ratio. The gear ratio is

$$\text{gear ratio} = \frac{n_{generator}}{n_{wind\ turbine}} = \frac{3600}{30} = 120. \qquad \text{(E4.8-28)}$$

i) Radius of (three) wind turbine blades. The limiting efficiency for wind turbines is according to Lanchester–Betz [45 in Chapter 4] $\eta_{Lanchester} = (16/27) = 0.59$. The wind turbine design depends on the density of the air and the ambient tempera-

**TABLE E4.8.1** Air Density as a Function of Altitude

| | | | | | | | | |
|---|---|---|---|---|---|---|---|---|
| Altitude (m) | –500 | 0 | 500 | 1000 | 1500 | 2000 | 2500 | 3000 |
| Air (mass) density ρ (kg/m³) | 1.2854 | 1.2255 | 1.1677 | 1.112 | 1.0583 | 1.0067 | 0.957 | 0.9092 |
| Altitude (m) | 3500 | 4000 | 4500 | | | | | |
| Air (mass) density ρ (kg/m³) | 0.8623 | 0.8191 | 0.7768 | | | | | |

ture. Table E4.8.1 provides the air density as a function of altitude.

The wind turbine has to provide a rated output power of $P_{\text{out_wind turbine}} = 12.92\,\text{kW}$ at a rated wind velocity of $v = 10$ m/s. The efficiency (coefficient of performance) is $c_p = 0.3$, where $c_p$ is the ratio between the power delivered by the rotor of the wind turbine to the power in the wind with velocity v striking the area A swept by the rotor.

According to [45 in Chapter 4] the output power of the wind turbine is

$$P_{\text{wind_turbine}} = \frac{1}{2} \cdot c_p \cdot v^3 \cdot A \cdot \rho. \qquad \text{(E4.8-29)}$$

The area swept by the rotor is

$$A = \frac{2 \cdot P_{\text{wind-turbine}}}{c_p \cdot v^3 \cdot \rho} = \frac{2(12920)}{0.3(1000)(1.05)} = 82\,\text{m}^2, \qquad \text{(E4.8-30)}$$

or the rotor blade radius is

$$R_{\text{blade}} = \sqrt{\frac{A}{\pi}} = \sqrt{\frac{82}{\pi}} = 5.1\,\text{m}. \qquad \text{(E4.8-31)}$$

The height of the tower can be assumed to be about 2 times the blade radius, that is, $H_{\text{tower}} = 10$ m.

## CHAPTER 5 SOLUTIONS

### 5.1.2.1 Application Example 5.1: Computation of Displacement Power Factor (DPF) and Total Power Factor (TPF): Solution

a) PSpice code

```
*Computation of DPF and TPF
Van 2p 1p SIN(0V 489.3V 60Hz 0 0 0)
Vbn 3p 1p SIN(0V 489.3V 60Hz 0 0
-120)
Vcn 4p 1p SIN(0V 489.3V 60Hz 0 0
-240)
Rgnd 1p 0 1u
Rsysa 2p 5p 0.05
Rsysb 3p 6p 0.05
Rsysc 4p 7p 0.05
Lsysa 5p 1 265u
Lsysb 6p 2 265u
Lsysc 7p 3 265u
D1a 5 1 D1N4001
D1b 5 6 D1N4001
M1 1 7 5 5 SMM
R1 6 23 1u
V1 7 5 PULSE(0 2.7778ms 0 0
10.4167ms 16.66667ms)
D2a 8 24 D1N4001
D2b 8 9 D1N4001
M2 24 10 8 8 SMM
R2 9 3 1u
V2 10 8 PULSE(0 5.5556ms 0 0
10.4167ms 16.66667ms)
D3a 11 2 D1N4001
D3b 11 12 D1N4001
M3 2 13 11 11 SMM
R3 12 23 1u
V3 13 11 PULSE(0 8.3333ms 0 0
10.4167ms 16.66667ms)
D4a 14 24 D1N4001
D4b 14 15 D1N4001
M4 24 16 14 14 SMM
R4 15 1 1u
V4 16 14 PULSE(0 11.1111ms 0 0
10.4167ms 16.66667ms)
D5a 17 3 D1N4001
D5b 17 18 D1N4001
M5 3 19 17 17 SMM
R5 18 23 1u
V5 19 17 PULSE(0 13.8888ms 0 0
10.4167ms 16.66667ms)
D6a 20 24 D1N4001
D6b 20 21 D1N4001
M6 24 22 20 20 SMM
R5 21 2 1u
V6 22 20 PULSE(0 0ms 0 0 10.4167ms
16.66667ms)
Cf 23 24 500u
Rload 23 24 10
```



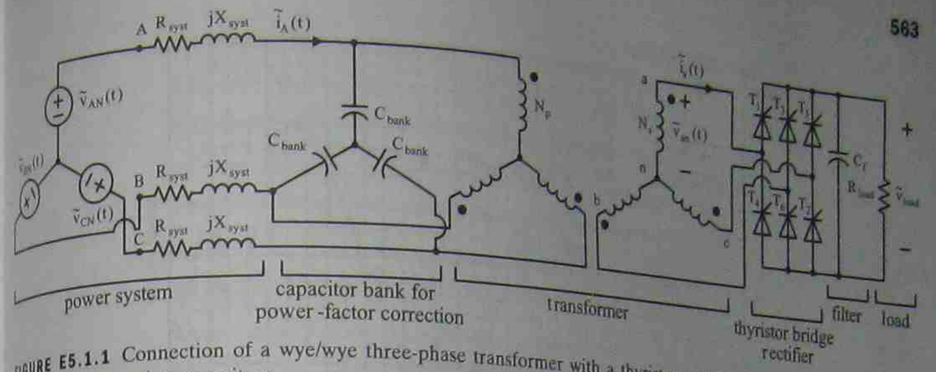



**FIGURE E5.1.1** Connection of a wye/wye three-phase transformer with a thyristor rectifier, filter, load, and a bank of power-factor correction capacitors.

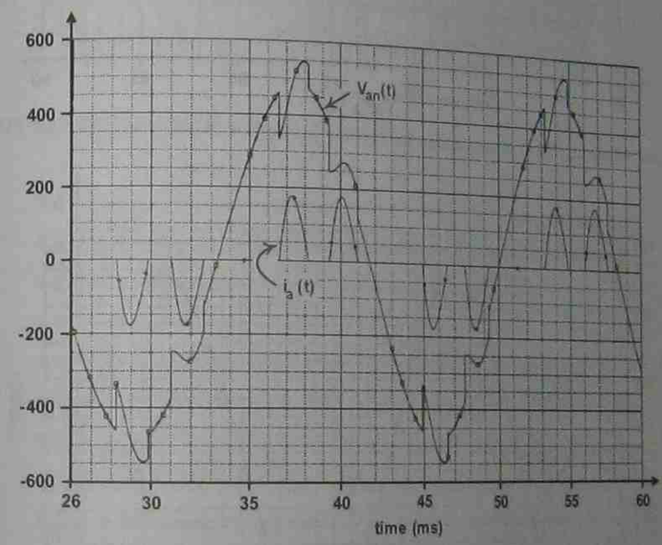



**FIGURE E5.1.2** Phase voltage $v_{an}(t)$ and phase current for $i_a(t)$ for $\alpha = 10°$.

```
Rgnd2 24 0 1Meg
.model SMM NMOS(Level=3 Gamma=0
Delta=0 Eta=0 Theta=0 Kappa=0 Vmax=0
Xj=0
+ Tox=100n Uo=600 Phi=0.6 Rs=42.69m
Kp=20.87u L=2u W=2.9 Vto=3.487
+ Rd=0.19 Cbd=200n Pb=0.8 Mj=0.5
Cgso=3.5n Cgdo=100p Rg=1.2 Is=10f)
.model D1N4001 D(Is=1e-12)
.options list node opts
.options abstol=0.01 chgtol=0.01
reltol=0.1 vntol=100m trtol=20
.options itl1=500 itl2=500 itl4=100
itl5=0
.tran 0.1u 60ms 26ms 1u UIC
.four 60Hz V(1) I(Lsysa)
.probe
.end
```

b) to d) Figures E5.1.2 to E5.1.4 show the line to neutral (phase) voltage $v_{an}(t)$ and the phase current $i_a(t)$ for $\alpha = 10°$, 40°, and 80°, respectively. Table E5.1.1 lists the Fourier coefficients (magnitude and phase angles) for the phase voltage $v_{an}(t)$ and phase current $i_a(t)$ as a function of $\alpha$.

e) Table E5.1.2 gives a summary of the DPF and TPF and their ratio (TPF/DPF) as a function of the firing angle $\alpha$. Fig. E5.1.5 shows the DPF and TPF as a function of $\alpha$, and Fig. E5.1.6 illustrates the ratio (TPF/DPF). Figure E5.1.5 shows that the displacement power factor (DPF) as a function of the firing angle $\alpha$ obeys the relation $\cos\varphi = 0.955 \cos\alpha$ [14, in Chapter 5]. Figure E5.1.6 illustrates the ratio (TPF/DPF) as a function of the firing angle $\alpha$.

f) By introducing the capacitor bank into the above PSpice program and performing a series of runs for capacitor bank capacitance values $C_{bank}$ from 400 to 10 μF one finds that for $C_{bank} = 115\,\mu\text{F}$ a DPF value of 0.9178 lagging is obtained. Figure E5.1.7 illustrates the voltage $v_{an}(t)$ and $i_a(t)$ for this

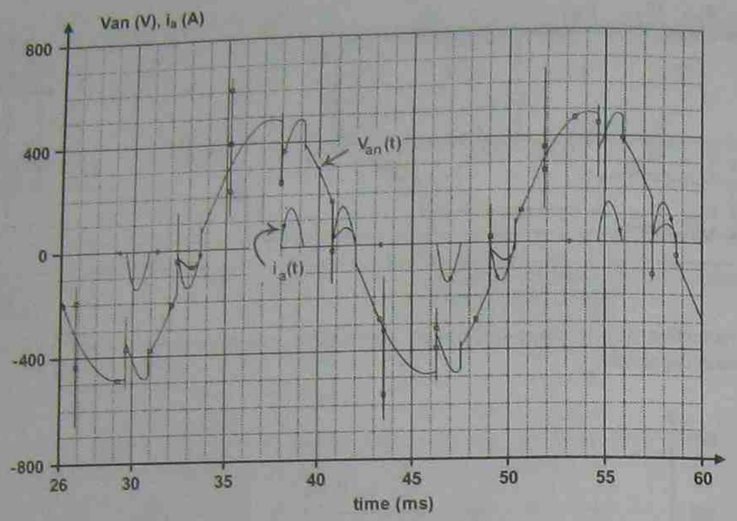



**FIGURE E5.1.3** Phase voltage $v_{an}(t)$ and phase current for $i_a(t)$ for $\alpha = 40°$.

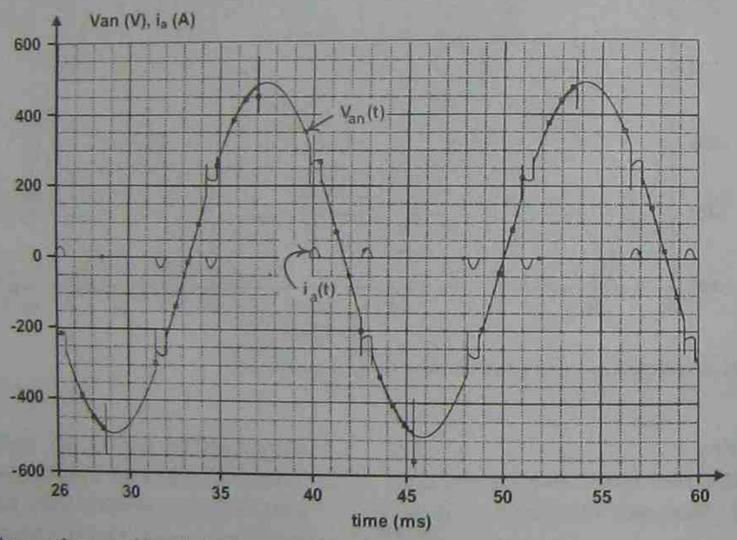



**FIGURE E5.1.4** Phase voltage $v_{an}(t)$ and phase current for $i_a(t)$ for $\alpha = 80°$.

**TABLE E5.1.1** Fourier Components of $v_{an}(t)$ and $i_a(t)$ for the Firing Angles $\alpha = 10°, 40°$, and $80°$

| $\alpha = 10°$ | $v_{anh}$(V) | $\angle v_{anh}$(°) | $i_{ah}$(A) | $\angle i_{ah}$(°) |
|---|---|---|---|---|
| $h = 1$ | 482.5 | −144.6 | 75.9 | −170.5 |
| $h = 5$ | 30.52 | −47.91 | 60.76 | 47.8 |
| $h = 7$ | 33.62 | −153.5 | 47.93 | −112.4 |
| $\alpha = 40°$ | $v_{anh}$(V) | $\angle v_{anh}$(°) | $i_{ah}$(A) | $\angle i_{ah}$(°) |
| $h = 1$ | 483.8 | −144.1 | 49.86 | 163.1 |
| $h = 5$ | 21.92 | 179.9 | 43.64 | −84.45 |
| $h = 7$ | 26.63 | −32.15 | 37.98 | 61.99 |
| $\alpha = 80°$ | $v_{anh}$(V) | $\angle v_{anh}$(°) | $i_{ah}$(A) | $\angle i_{ah}$(°) |
| $h = 1$ | 488.8 | −144 | 4.666 | 129.8 |
| $h = 5$ | 2.274 | 12.87 | 4.537 | 109.0 |
| $h = 7$ | 3.097 | 94.55 | 4.403 | −171.4 |

**TABLE E5.1.2** Displacement Power Factor (DPF), Total Power Factor (TPF) and Their Ratio TPF/DPF

| $\alpha$(°) | DPF (pu) | TPF (pu) | TPF/DPF (pu) |
|---|---|---|---|
| 0 | 0.9537 | 0.6831 | 0.7162 |
| 10 | 0.8996 | 0.6214 | 0.6908 |
| 20 | 0.8211 | 0.5518 | 0.6720 |
| 30 | 0.7230 | 0.4749 | 0.6569 |
| 40 | 0.6046 | 0.3892 | 0.6437 |
| 50 | 0.4726 | 0.2982 | 0.6311 |
| 60 | 0.3338 | 0.2064 | 0.6183 |
| 70 | 0.1942 | 0.1173 | 0.6038 |
| 80 | 0.0663 | 0.0388 | 0.5857 |



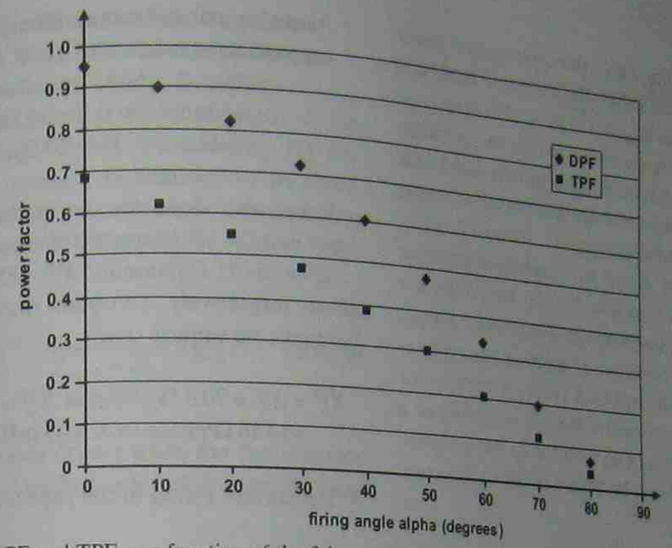



**FIGURE E5.1.5** DPF and TPF as a function of the firing angle $\alpha$.

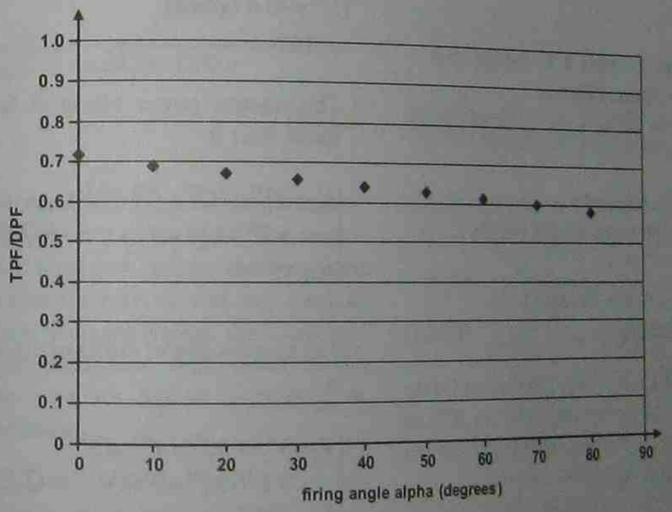



**FIGURE E5.1.6** Ratio (TPF/DPF) as a function of the firing angle $\alpha$.

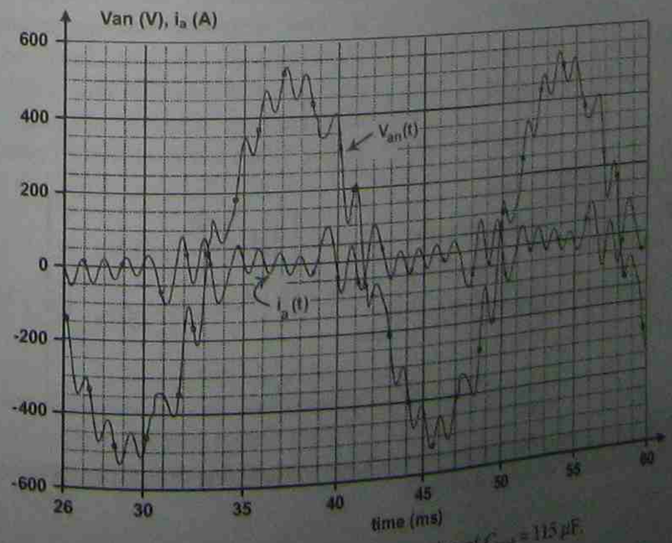



**FIGURE E5.1.7** Voltage $v_{an}(t)$ and current $i_a(t)$ for a capacitance value of $C_{sub} = 115\,\mu F$.

case. These wave shapes demonstrate that a resonance condition exists: the capacitor bank with the capacitance $C_{bank} = 115\ \mu F$ is able to increase the DPF but is unable to reduce the harmonic components of voltages and currents, indeed the harmonic components are increased due to the resonance condition.

g) As mentioned above the displacement power factor can be increased but the harmonics are increased due to resonance. The solution to this power factor correction problem is the replacement of the capacitor bank (with the capacitance value $C_{bank}$) by a passive filter $Z_f$ consisting of a series connection of an inductor $L_f$ and a capacitor $C_f$, which can be tuned to an appropriate frequency.

### 5.3.1 Application Example 5.2: Design of a Tuned Harmonic Filter: Solution

The following steps will be followed to design the filter:

- Calculation of the required reactive power $Q_{required}$ for improving DPF to the desired value:

$$Q_{required} = P(\tan\cos^{-1} 0.42 - \tan\cos^{-1} 0.97) = 1180.38\ \text{kVAr/phase}. \quad \text{(E5.2-1)}$$

- According to IEEE-519 [8], THD, should drop from 30.47% to 4.0%. We employ about 30% of the required $Q_{required}$ for filtering (tuned) and the remaining for (untuned) DPFC:

$$Q_{filter} = 0.30(1180.38) \approx 354\ \text{kVar}. \quad \text{(E5.2-2)}$$

- Assuming star-connected (filter) capacitor banks one obtains

$$\text{capacitor/phase} = C = 1/(2\pi \cdot f \cdot X_C^{(1)}) = 1/(2\pi \cdot 50 \cdot 354 \cdot 1000) \approx 9\ \mu\text{F/phase}.$$

From this follows for the fundamental (1) reactance and the 5th harmonic (5) reactance $X_C^{(1)} = 354.11\ \Omega$/phase and $X_C^{(5)} = 354.11/5 = 69.16\ \Omega$/phase, respectively. To obtain resonance at the 5th harmonic we require

$$X_L^{(5)} = X_C^{(5)} = 70.8\ \Omega/\text{phase} \Rightarrow X_L^{(1)} = 70.8/5 = 14.16\ \Omega/\text{phase} \Rightarrow L = 45\ \text{mH}. \quad \text{(E5.2-3)}$$

- The current rating of the capacitor at $f = 50$ Hz is

$$\begin{cases} I_C^{(1)} = V^{(1)}/X_C^{(1)} = 6.35\text{k}/354.11 \approx 19\ \text{A} \\ I_C^{(5)} \approx 40\ \text{A (given)} \end{cases} \Rightarrow I_{rms} \approx 44\ \text{A}. \quad \text{(E5.2-4)}$$

- The reactive power rating of the reactor of the tuned filter is

$$\begin{cases} V_L = V_L^{(1)} + V_L^{(5)} = I^{(1)} \cdot X_L^{(1)} \\ \quad + I^{(5)} \cdot X_L^{(5)} \approx 3.1\text{kV} \\ I_{rms} = 44\ \text{A} \end{cases} \Rightarrow Q_{\text{rating}}^{\text{reactor}} = 137\ \text{kVAr}. \quad \text{(E5.2-5)}$$

- The reactive power rating of the selected capacitor is

$$\begin{cases} V_C = V_C^{(1)} + V_C^{(5)} = I^{(1)} \cdot X_C^{(1)} \\ \quad + I^{(5)} \cdot X_C^{(5)} \approx 9.5\text{kV} \\ I_{rms} = 44\ \text{A} \end{cases} \Rightarrow Q_{\text{rating}}^{\text{capacitor}} = 418\ \text{kVAr} \quad \text{(E5.2-6)}$$

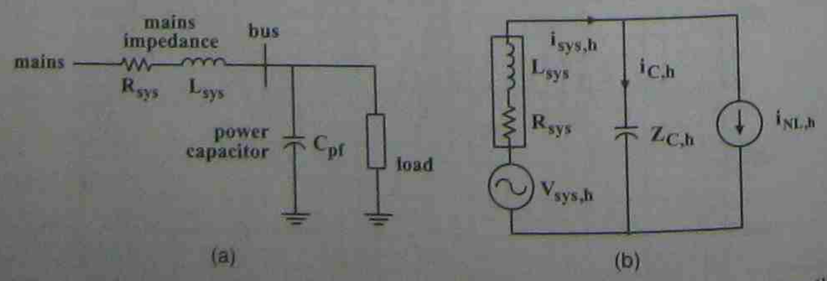



**FIGURE E5.3.1** A simplified industrial power system with capacitor and nonlinear load; (a) configuration, (b) the harmonic equivalent circuit [2 in Chapter 5] with $Z_{sys,h} = R_{sys} + jhL_{sys}$.





### 5.4.3 Application Example 5.3: Harmonic Resonance in a Distorted Industrial Power System with Nonlinear Loads: Solution

i) To observe the effect of the nonlinear load, the harmonic voltage source (representing the distorted utility voltage) is assumed to be short-circuited. The harmonic current injected into the capacitor due to the nonlinear load is

$$\tilde{I}_{C,h}^{\text{due}\,NL} = \frac{Z_{sys,h}}{Z_{sys,h} + Z_{C,h}} \tilde{I}_{NL,h}. \quad \text{(E5.3-3)}$$

A parallel resonance occurs when the denominator approaches zero. The frequency of the parallel resonance is

$$f_{\text{parallel}} = \frac{1}{2\pi\sqrt{L_{sys}C}} = \frac{1}{2\pi\sqrt{0.1m \cdot 1300\,\mu}} \approx 420\ \text{Hz}. \quad \text{(E5.3-4)}$$

This condition will result in a large harmonic current being injected into the capacitor bank. The magnitude of the injected harmonic current can be several times the rated capacitor current, and may result in extensive harmonic voltages across the capacitor. Therefore, parallel resonance may result in the destruction of the capacitor due to overvoltage or over-current conditions.

ii) To investigate the effect of the distorted utility voltage on the capacitor, the harmonic current source (approximating the nonlinear load) is assumed to be ideal, that is, its impedance approaches infinity and behaves like an open circuit. The harmonic current injected into the capacitor due to the distorted utility source is

$$\tilde{I}_{C,h}^{\text{due}\,sys} = \frac{1}{Z_{sys,h} + Z_{C,h}} \tilde{V}_{sys,h}. \quad \text{(E5.3-5)}$$

A series resonance occurs when the denominator approaches zero. Therefore, for this system the frequencies of the series and parallel resonances are identical:

$$f_{\text{series}} = f_{\text{parallel}} = \frac{1}{2\pi\sqrt{L_{sys}C}} \approx 420\ \text{Hz}. \quad \text{(E5.3-6)}$$

The harmonic current injection into the power capacitor will be increased if the utility voltage contains harmonic components near resonance frequencies.

iii) The total harmonic current injected into the power capacitor is

$$\tilde{I}_{C,h} = \tilde{I}_{C,h}^{\text{due}\,NL} + \tilde{I}_{C,h}^{\text{due}\,sys} = \frac{Z_{sys,h}}{Z_{sys,h} + Z_{C,h}} \tilde{I}_{NL,h} + \frac{1}{Z_{sys,h} + Z_{C,h}} \tilde{V}_{sys,h}. \quad \text{(E5.3-7)}$$

Therefore, the 5th harmonic component of the injected current into the capacitor is

$$\begin{aligned}
\tilde{I}_{C,5} &= \tilde{I}_{C,5}^{\text{due}\,NL} + \tilde{I}_{C,5}^{\text{due}\,sys} \\
\tilde{I}_{C,5}^{\text{due}\,NL} &= \frac{Z_{sys,5}}{Z_{sys,5} + Z_{C,5}} \tilde{I}_{NL,5} \\
&= \frac{[0.06 + j5(2\pi \cdot 60 \cdot 0.11 \cdot 10^{-3})]\tilde{I}_{NL,5}}{[0.06 + j5(2\pi \cdot 60 \cdot 0.11 \cdot 10^{-3})] + [j/5(2\pi \cdot 60 \cdot 1300 \cdot 10^{-6})]} \\
&= \frac{0.06 + j0.2074}{0.06 + j0.2074 - j0.408} \tilde{I}_{NL,5} \\
&= \frac{0.06 + j0.2074}{0.06 - j0.2} \tilde{I}_{NL,5} = \frac{0.2159\angle 73.87^\circ}{0.2\angle -73.3^\circ} \tilde{I}_{NL,5} \\
&= (1.08\angle 147.17^\circ)\tilde{I}_{NL,5} \\
&= 1.08\angle 147.17^\circ)(\sqrt{2}(0.3)\angle 0^\circ) \\
&= \sqrt{2}(0.324)\angle 147.17^\circ\ \text{A} \\
\tilde{I}_{C,5}^{\text{due}\,sys} &= \frac{1}{Z_{sys,5} + Z_{C,5}} \tilde{V}_{sys,5} = \frac{1}{0.2\angle -73.3^\circ} \tilde{V}_{sys,5} \\
&= (5\angle 73.3^\circ)\tilde{V}_{sys,5} = (5\angle 73.3^\circ)(\sqrt{2}(3)\angle 0^\circ) \\
&= \sqrt{2}(15)\angle 73.3^\circ\ \text{A} \\
\Rightarrow\Rightarrow \tilde{I}_{C,5} &= \tilde{I}_{C,5}^{\text{due}\,NL} + \tilde{I}_{C,5}^{\text{due}\,sys} \\
&= (\sqrt{2}(0.324)\angle 147.17^\circ) + (\sqrt{2}(15)\angle 73.3^\circ \\
&= \sqrt{2}(4.04 + j14.54) = \sqrt{2}(15.1)\angle 74.47^\circ\ \text{A}.
\end{aligned} \quad \text{(E5.3-8)}$$

The 7th harmonic component of the injected current into the power capacitor is

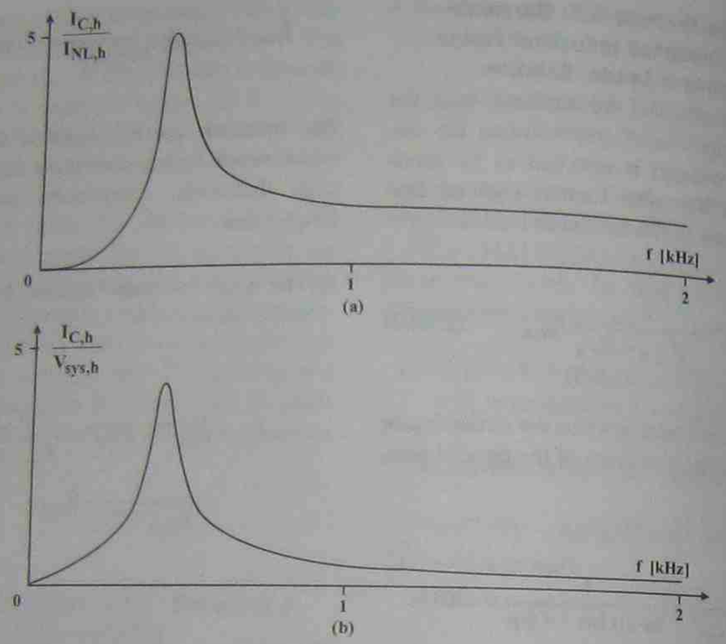



**FIGURE E5.3.2** Frequency response of capacitor current (a) divided by the nonlinear load harmonic current, (b) divided by the utility harmonic voltage [2 in Chapter 5].

$$\tilde{I}_{C,7} = \tilde{I}_{C,7}^{\text{due NL}} + \tilde{I}_{C,7}^{\text{due sys}}$$

$$\tilde{I}_{C,7}^{\text{due NL}} = \frac{Z_{sys,7}}{Z_{sys,7} + Z_{C,7}} \tilde{I}_{NL,7}$$

$$= \frac{[0.06 + j7(2\pi \cdot 60 \cdot 0.11 \cdot 10^{-3})]\tilde{I}_{NL,7}}{0.06 + j7(2\pi \cdot 60 \cdot 0.11 \cdot 10^{-3}) + j7(2\pi \cdot 60 \cdot 1300 \cdot 10^{-6})}$$

$$= \frac{0.06 + j7 \cdot 0.04147}{0.06 + j7 \cdot 0.04141 - j2.040/7} \tilde{I}_{NL,7}$$

$$= \frac{0.06 + j0.29029}{0.06 - j0.0011} \tilde{I}_{NL,7} = \frac{0.2964\angle 78.32^\circ}{0.06\angle -1.05^\circ} \tilde{I}_{NL,7}$$

$$= (4.964\angle 79.37^\circ)\tilde{I}_{NL,7}$$

$$= (4.964\angle 79.37^\circ)(\sqrt{2}(0.2)\angle 0^\circ)$$

$$= \sqrt{2}(0.993)\angle 79.37^\circ \text{ A}$$

$$\tilde{I}_{C,7}^{\text{due sys}} = \frac{1}{Z_{sys,7} + Z_{C,7}} \tilde{V}_{sys,7} = \frac{1}{0.06\angle -1.05^\circ} \tilde{V}_{sys,7}$$

$$= (16.7\angle 1.05^\circ)\tilde{V}_{sys,7}$$

$$= (16.7\angle 1.05^\circ)(\sqrt{2}(2)\angle 0^\circ)$$

$$= \sqrt{2}(33.4)\angle 1.05^\circ \text{ A}$$

$$\Rightarrow\Rightarrow \tilde{I}_{C,7} = \tilde{I}_{C,7}^{\text{due NL}} + \tilde{I}_{C,7}^{\text{due sys}}$$

$$= (\sqrt{2}(0.993)\angle 79.37^\circ) + (\sqrt{2}(33.4)\angle 1.05^\circ)$$

$$= \sqrt{2}(33.58 + 1.59)$$

$$= \sqrt{2}(33.62)\angle 2.7^\circ \text{ A}. \qquad \text{(E5.3-9)}$$

**iv)** As expected, the 7th harmonic current of the nonlinear load and the distorted utility voltage are magnified (it is a relatively weak system, $R_{sys} = 0.06\ \Omega$ and $X_{sys} = 2\pi(60)(0.11 \times 10^{-3}) = 0.042\ \Omega$) due to the parallel and series and resonances at $f = 420$ Hz.

**v)** The frequency responses of the capacitor current divided by the load harmonic current and divided by the utility harmonic voltage are shown in Fig. E5.3.2.

### 5.4.4 Application Example 5.4: Parallel Resonance Caused by Capacitors: Solution

The equivalent circuit (neglecting resistances) is shown in Fig E5.4.1b. The resonance frequency is with $S_{sc} = MVA_{sc}$ and $Q_{cap} = MVAr_{cap}$

$$h = \sqrt{\frac{MVA_{SC}}{MVAr_{cap}}} = \sqrt{\frac{72.6}{0.6}} = 11. \qquad \text{(E5.4-2)}$$

This is a characteristic frequency of the six-pulse nonlinear load. Figure E5.4.1c shows a plot of the equivalent system impedance magnitude as seen from bus 1. This plot is known as a frequency scan.



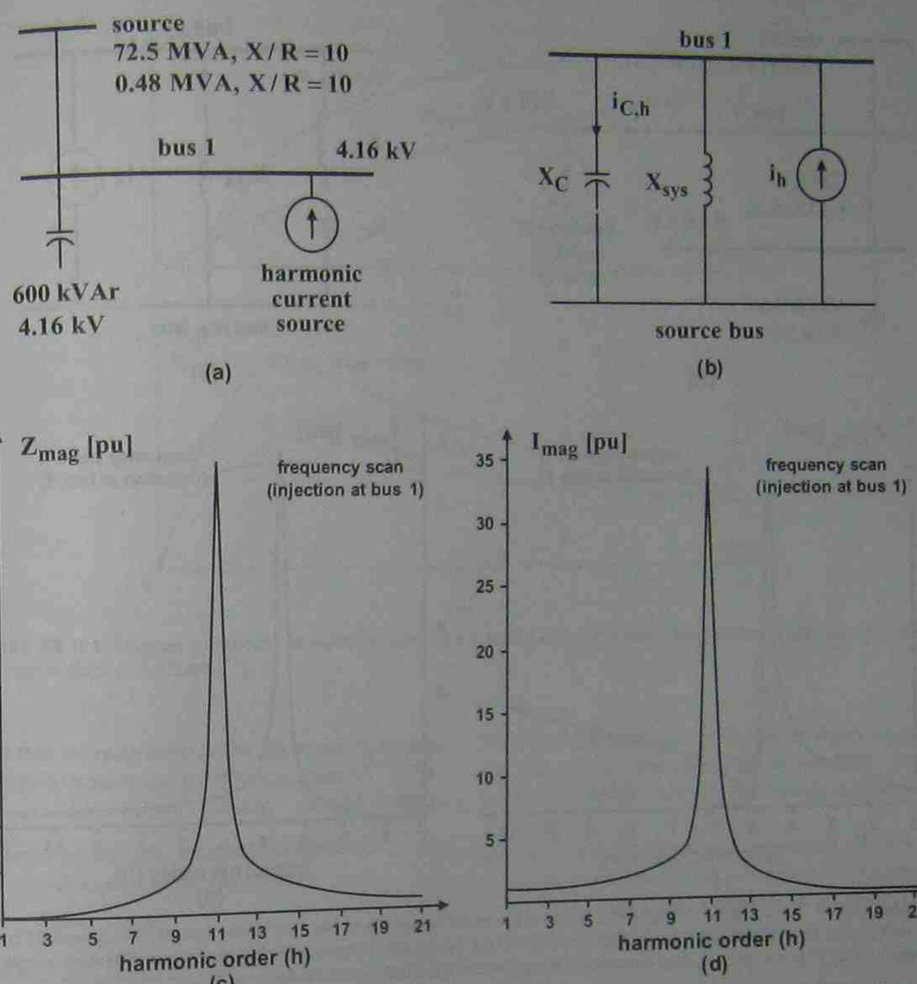



**FIGURE E5.4.1** (a) Example of single-line diagram for parallel resonance at bus 1, (b) equivalent circuit for parallel resonance, (c) frequency scan of bus 1 equivalent impedance, (d) current amplification of bus 1 parallel resonant circuit [7 in Chapter 5]. The harmonic-current source is a six-pulse converter.

A plot of the current amplification is given in Fig. E5.4.1d. Note that 1 A of the 11th harmonic current injection by the nonlinear load (into the system) will result in about 33 A of harmonic current flowing into the source and the capacitor.

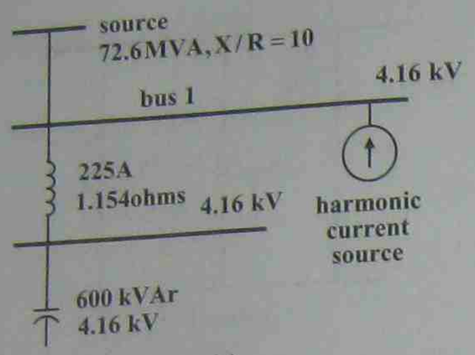
### 5.4.5 Application Example 5.5: Series Resonance Caused by Capacitors: Solution

The series resonance frequency is

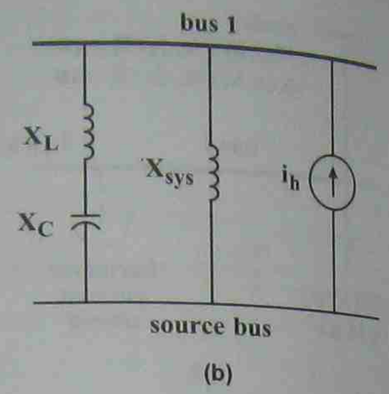
$$h = \sqrt{\frac{X_C}{X_L}} = \sqrt{\frac{X_C/h^2}{X_L}} \sqrt{\frac{28.843}{1.154}} = 5. \qquad \text{(E5.5-1)}$$

This circuit produces a low-frequency path for the 5th harmonic current. A plot of the magnitude of the system impedance – as seen from bus 1 – is shown in Fig. E5.5.1c. The value of $Z = j0.049pu$ at $h = 5$ and the phase angle (crossing the zero axis at $h = 5$) are not shown. A plot of the current amplification through the series-resonant circuit is given in Fig. E5.5.1d, pertaining to the tuned point, $h = 5$, and $I_{pu} = 0.99$. The current amplification should be near unity at the tuned frequency. Note that this circuit also has a parallel resonance at $h = 4.6$, where the amplification factor (AF) is $I_{pu} = 5.9$. This is the frequency at which the series-resonant circuit has a capacitive reactance equal in magnitude to the inductive reactance of the source.

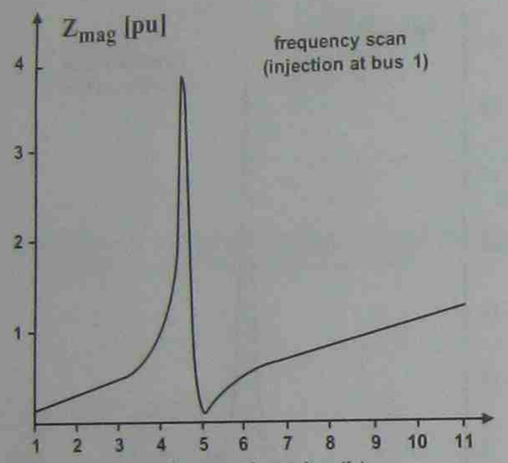
SJ. GEORGE POLYTECHNIC Mr. LARIE



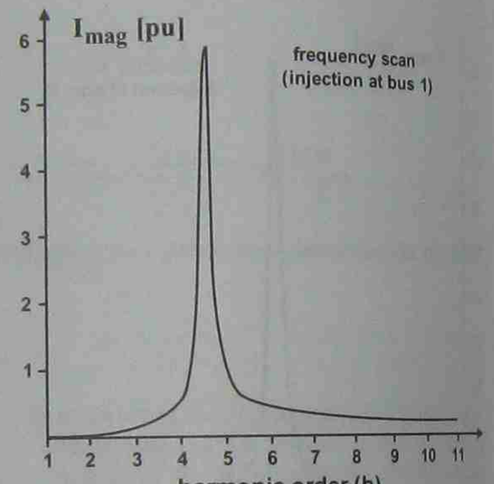

(a)




(b)




(c)




(d)

**FIGURE E5.5.1** (a) Example of single-line diagram for series resonance at bus 1 of power system, (b) equivalent circuit for series resonance-tuned filter, (c) frequency scan of bus 1 equivalent impedance, (d) current amplification across the tuning reactor [7 in Chapter 5]. The harmonic-current source is a six-pulse converter.

### 5.4.6 Application Example 5.6: Protecting Capacitors by Virtual Harmonic Resistors: Solution

**i)** The virtual resistor is only activated at harmonic frequencies; therefore, the 5th harmonic component of the injected current in the capacitor is

$$\tilde{I}_{C,5} = \tilde{I}_{C,5}^{\text{due NL}} + \tilde{I}_{C,5}^{\text{due sys}}$$

$$\tilde{I}_{C,5}^{\text{due NL}} = \frac{Z_{sys,5}}{Z_{sys,5} + Z_{C,5} + R_{vir}} \tilde{I}_{NL,5}$$

$$= \frac{0.06 + j0.2074}{0.06 + j0.2074 - j0.408 + 0.5} \tilde{I}_{NL,5}$$

$$= \frac{0.06 + j0.2074}{0.56 - j0.2} \tilde{I}_{NL,5} = \frac{0.2159\angle 73.87^\circ}{0.595\angle -19.65^\circ} \tilde{I}_{NL,5}$$

$$= (0.363\angle 93.52^\circ)\tilde{I}_{NL,5}$$

$$= (0.363\angle 93.52^\circ)(\sqrt{2}(0.3)\angle 0^\circ)$$

$$= \sqrt{2}(0.109)\angle 93.52^\circ \text{ A}$$

$$\tilde{I}_{C,5}^{\text{due sys}} = \frac{1}{Z_{sys,5} + Z_{C,5} + R_{vir}} \tilde{V}_{sys,5}$$

$$= \frac{1}{0.595\angle -19.65^\circ} \tilde{V}_{sys,5} = (1.68\angle 19.65^\circ)\tilde{V}_{sys,5}$$

$$= (1.68\angle 19.65^\circ)(\sqrt{2}(3)\angle 0^\circ)$$

$$= \sqrt{2}(5.4)\angle 19.65^\circ \text{ A}$$

$$\Rightarrow\Rightarrow \tilde{I}_{C,5} = \tilde{I}_{C,5}^{\text{due NL}} + \tilde{I}_{C,5}^{\text{due sys}}$$

$$= (\sqrt{2}(0.109)\angle 93.52^\circ) + (\sqrt{2}(5.4)\angle 19.65^\circ)$$

$$= \sqrt{2}(5.09 + j1.93) = \sqrt{2}(5.44)\angle 20.77^\circ \text{ A.} \quad \text{(E5.6-1)}$$



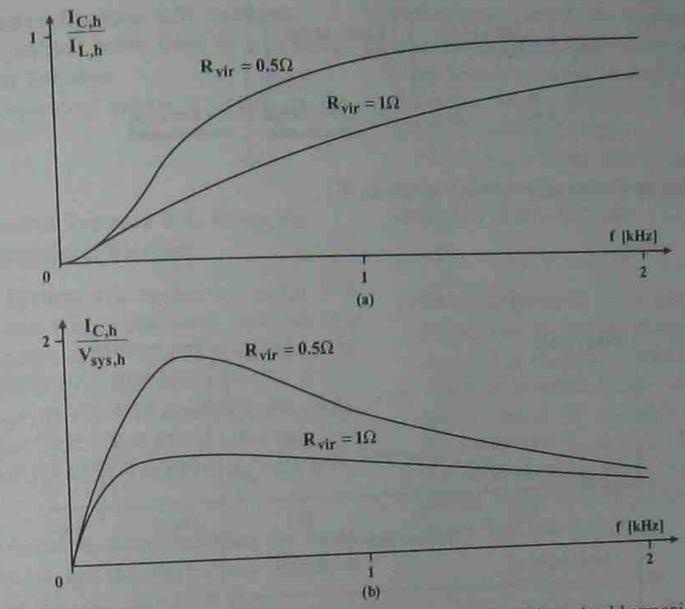



**FIGURE E5.6.1** Frequency response of capacitor bank as a function of (a) nonlinear load harmonic current, (b) utility harmonic voltage [2 in Chapter 5].

Note that the magnitude of the 5th harmonic capacitor current is decreased by 64% (e.g., from $\sqrt{2}\cdot 15.1$A, without the virtual resistor, to $\sqrt{2}\cdot 5.44$A).

**ii)** Similarly, the 7th harmonic component of the injected current in the capacitor is

$$\tilde{I}_{C,7} = \tilde{I}_{C,7}^{\text{due NL}} + \tilde{I}_{C,7}^{\text{due sys}}$$

$$\tilde{I}_{C,7}^{\text{due NL}} = \frac{Z_{sys,7}}{Z_{sys,7} + Z_{C,7} + R_{vir}} \tilde{I}_{NL,7}$$

$$= \frac{0.06 + j0.29029}{0.06 - j0.0011 + 0.5} \tilde{I}_{NL,7}$$

$$= \frac{0.2964\angle 78.32^\circ}{0.56\angle -0.11^\circ} \tilde{I}_{NL,7}$$

$$= (0.53\angle 78.43^\circ)\tilde{I}_{NL,7}$$

$$= (0.53\angle 78.43^\circ)(\sqrt{2}(0.2)\angle 0^\circ)$$

$$= \sqrt{2}(0.106)\angle 78.43^\circ \text{ A}$$

$$\tilde{I}_{C,7}^{\text{due sys}} = \frac{1}{Z_{sys,7} + Z_{C,7} + R_{vir}} \tilde{V}_{sys,7}$$

$$= \frac{1}{0.56\angle -0.11^\circ} \tilde{V}_{sys,5} = (1.79\angle 0.11^\circ)\tilde{V}_{sys,7}$$

$$= (1.79\angle 0.11^\circ)(\sqrt{2}(2)\angle 0^\circ)$$

$$= \sqrt{2}(3.58)\angle 0.11^\circ \text{ A}$$

$$\Rightarrow\Rightarrow \tilde{I}_{C,7} = \tilde{I}_{C,7}^{\text{due NL}} + \tilde{I}_{C,7}^{\text{due sys}}$$

$$= (\sqrt{2}(0.106)\angle 78.43^\circ) + (\sqrt{2}(3.58)\angle 0.11^\circ)$$

$$= \sqrt{2}(3.60 + 0.11) = \sqrt{2}(3.60)\angle 1.75^\circ \text{ A.} \quad \text{(E5.6-2)}$$

Note that the magnitude of the 7th harmonic capacitor current is decreased by about 90% (e.g., from $\sqrt{2}\cdot 33.62$A, without the virtual resistor, to $\sqrt{2}\cdot 3.60$A).

**iii)** The improved frequency responses of power capacitor current for virtual harmonic resistors of $R_{vir} = 0.5\ \Omega$ and $1\ \Omega$ as a function of load harmonic current and utility harmonic voltage are shown in Fig. E5.6.1.

### 5.5.1 Application Example 5.7: Frequency and Capacitance Scanning [9]: Solution

The frequency scan can be done by calculating and inverting the admittance matrix of the network. Magnitude and phase angle plots of the driving-point impedance at bus 3 (Fig. E5.7.2a) indicate a resonance at the 71th harmonic, where the magnitude rises to about 1729 Ω. This is also evident from the zero crossing of the phase plot.

A capacitance scan is performed in a similar manner by computing the driving-point impedance at bus 3 for different capacitance values of the capacitor. The result is shown in Fig. E5.7.2b for several values of h. Note that resonances at the 5th and the 7th harmonics occur for a capacitance in the range of 0.1/a, F. These resonances should be avoided in the presence of six-pulse rectifiers.

ST. GEORGE COLLEGE OF

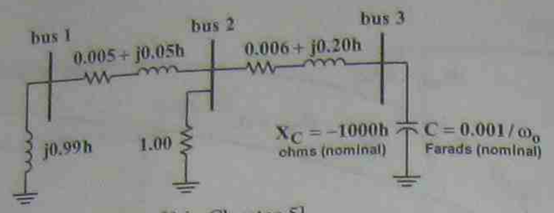
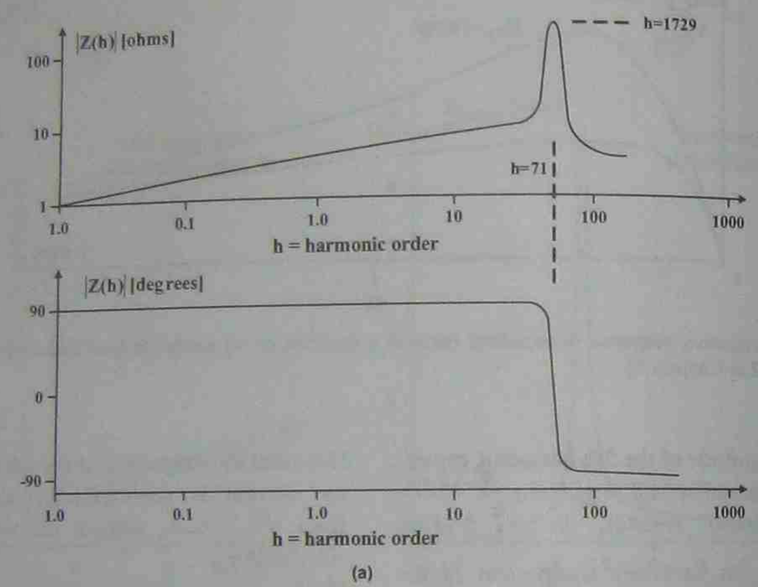
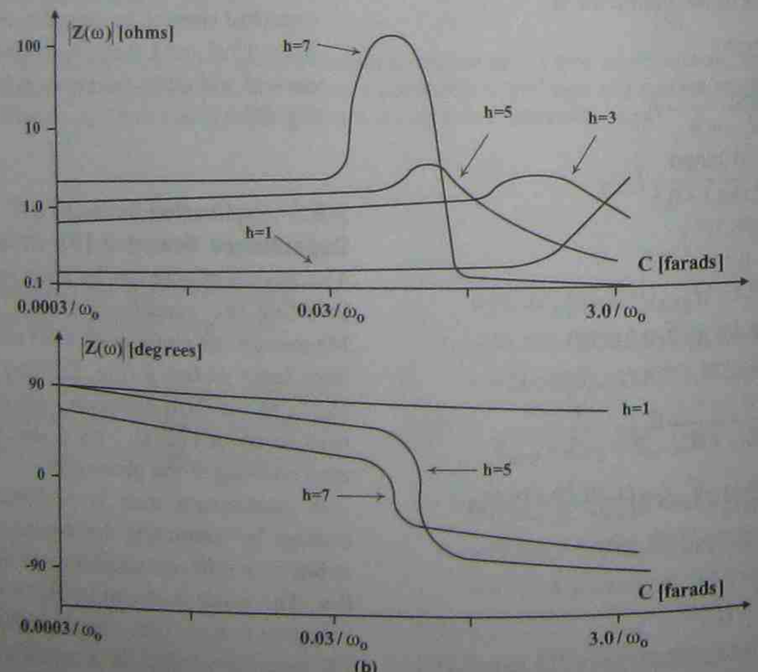



**FIGURE E5.7.1** The three-bus example system [9 in Chapter 5].




(a)




(b)

**FIGURE E5.7.2** Simulation results for the three bus system of Fig. E5.7.1; (a) frequency scan as seen at bus 3, (b) capacitance scan for impedance at bus 3 [9].



### 5.6.5 Application Example 5.8: Harmonic Limits for Capacitors when Used in a Three-Phase System: Solution

The feasible operating region is shown in Fig. E5.8.1.

### 5.7.1 Application Example 5.9: Harmonic Losses of Capacitors: Solution

***Single-Phase System.*** The application of Eq. 5-19 for $h = 1$ yields the fundamental loss for the single-phase system at $R_{s1} = 0.01\ \Omega$, $P_1 = (100 \times 10^{-6})^2 (0.01)[(377)(1)]^2(460)^2 = 3005$ mW.

For $h = h_{max} = 19$, Eq. 5-19 results for the single-phase system and $R_{s1} = 0.01\ \Omega$ in the loss $P_{19} = (100 \times 10^{-6})^2(0.01)[(377)(19)]^2(4.6)^2 = 109$ mW.

a) The total harmonic losses including the fundamental loss is for the single-phase system at $R_{sh} = 0.01\ \Omega$, $P_{total_single\text{-}phase} = 3.608$ W.
b) The total harmonic losses including the fundamental loss is for the single-phase system at $R_{sh} = 0.01(h)\ \Omega$, $P_{total_single\text{-}phase} = 10.035$ W.
c) The total harmonic losses including the fundamental loss is for the single-phase system at $R_{sh} = 0.01(h^2)\ \Omega$, $P_{total_single\text{-}phase} = 107.62$ W.

Fundamental and harmonic losses for the single-phase system are listed in columns 3–5 of Table E5.9.1.

***Three-Phase System.*** The application of Eq. 5-19 for $h = 1$ yields the fundamental loss for the three-phase system provided the capacitor bank is in Δ-connection at $R_{s1} = 0.01\ \Omega$, $P_1 = (100 \times 10^{-6})^2(0.01)[(377)(1)]^2(460)^2 = 3005$ mW.

For $h = h_{max} = 19$ Eq. 5-19 results for the three-phase system at $R_{s1} = 0.01\ \Omega$, $P_{19} = (100 \times 10^{-6})^2(0.01)[(377)(19)]^2(2.3)^2 = 21.7$ mW.

a) The total harmonic losses including the fundamental loss is for the three-phase system at $R_{sh} = 0.01\ \Omega$, $P_{total_three\text{-}phase} = 3.636$ W.
b) The total harmonic losses including the fundamental loss is for the three-phase system at $R_{sh} = 0.01(h)\ \Omega$, $P_{total_three\text{-}phase} = 8.571$ W.
c) The total harmonic losses including the fundamental loss is for the three-phase system at $R_{sh} = 0.01(h^2)\ \Omega$, $P_{total_three\text{-}phase} = 62.54$ W.

Fundamental and harmonic losses for the single-phase system are listed in columns 7-9 of Table E5.9.1.

**Conclusion.** The results of this application example stress that the harmonic losses of capacitors are indeed one of the reasons why the higher order harmonic voltage amplitudes must be limited as recommended in Table E5.9.1.

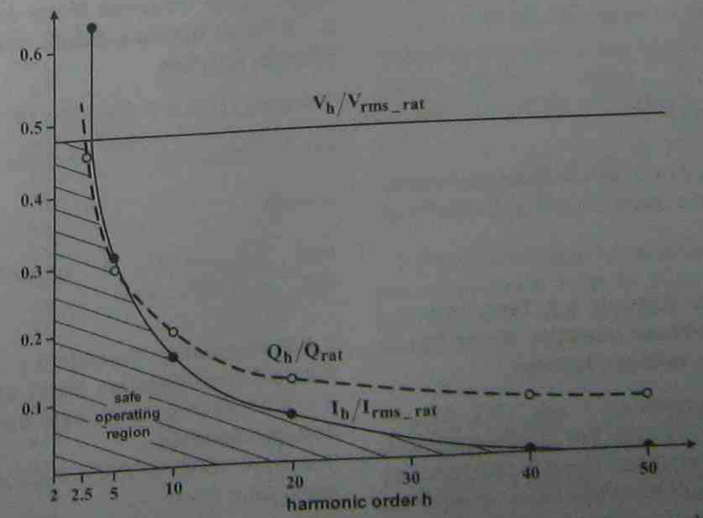



**FIGURE E5.8.1** Feasible operating region of capacitors with voltage, current, and reactive power harmonics (only one harmonic is present at any time).

**TABLE E5.9.1** Possible Voltage Spectra and Associated Capacitor Losses

| $h$ | $\left(\frac{V_h}{V_{60Hz}}\right)_{1\Phi}$ (%) | $P_h$ for part $a$ (mW) | $P_h$ for part $b$ (mW) | $P_h$ for part $c$ (mW) | $\left(\frac{V_h}{V_{60Hz}}\right)_{3\Phi}$ (%) | $P_h$ for part $a$ (mW) | $P_h$ for part $b$ (mW) | $P_h$ for part $c$ (mW) |
|---|---|---|---|---|---|---|---|---|
| 1 | 100 | 3005 | 3005 | 3005 | 100 | 3005 | 3005 | 3005 |
| 2 | 0.5 | 0.3 | 0.6 | 1.2 | 0.5 | 0.3 | 0.6 | 1.2 |
| 3 | 4.0 | 40 | 120 | 360 | 2.0[a] | 10.8 | 32.4 | 97.2 |
| 4 | 0.3 | 0.4 | 1.6 | 6.4 | 0.5 | 1.2 | 4.8 | 19.2 |
| 5 | 3.0 | 67.7 | 339 | 1695 | 5.0 | 188 | 940 | 4700 |
| 6 | 0.2 | 0.43 | 2.6 | 15.6 | 0.2 | 0.43 | 2.6 | 15.6 |
| 7 | 2.0 | 58.9 | 412 | 2880 | 3.5 | 181 | 1267 | 8869 |
| 8 | 0.2 | 0.77 | 6.16 | 49.3 | 0.2 | 0.77 | 6.16 | 49.3 |
| 9 | 1.0 | 24.4 | 220 | 1980 | 0.3 | 2.19 | 19.71 | 177.4 |
| 10 | 0.1 | 0.3 | 3 | 30 | 0.1 | 0.3 | 3 | 30 |
| 11 | 1.5 | 81.9 | 900 | 9900 | 1.5 | 81.9 | 900 | 9900 |
| 12 | 0.1 | 0.433 | 5.2 | 62.4 | 0.1 | 0.433 | 5.2 | 62.4 |
| 13 | 1.5 | 114 | 1480 | 19240 | 1.0 | 114 | 1482 | 19270 |
| 14 | 0.1 | 0.59 | 8.26 | 115.6 | 0.05 | 0.15 | 2.58 | 28.81 |
| 15 | 0.5 | 16.9 | 254 | 3810 | 0.1 | 0.68 | 10.2 | 153.0 |
| 16 | 0.05 | 0.192 | 3.07 | 49.1 | 0.05 | 0.192 | 3.07 | 49.1 |
| 17 | 1.0 | 87 | 1480 | 25140 | 0.5 | 22 | 374 | 6358 |
| 18 | 0.05 | 0.244 | 4.4 | 79.2 | 0.01 | 0.0097 | 0.175 | 3.143 |
| 19 | 1.0 | 109 | 2070 | 39200 | 0.5 | 27.1 | 513 | 9750 |
| | All higher voltage harmonics < 0.5% | | | | | | | |

[a]Under certain conditions (e.g., DC bias of transformers as discussed in Chapter 2, and the harmonic generation of synchronous generators as outlined in Chapter 4) triplen harmonics are not of the zero-sequence type and can therefore exist in a three-phase system.

## CHAPTER 6 SOLUTIONS

### 6.5.1 Application Example 6.1: Temperature Rise of a Single-Phase Transformer Due to Single Harmonic Voltage: Solution

The rated temperature rise is $\Delta T_{rated} = T_{rated} - T_{amb} = T_{rise\ rat} = 60°C$. For the harmonic with order $h = 3$ and amplitude $V_3 = 0.10\ \text{pu} \equiv 10\%$, one obtains (through linear extrapolation) the weighted-harmonic factor by replacing $\frac{V_{ph}}{V_{p1}}$ by 10:

$$\sum_{h=3} \frac{1}{(3)^{0.9}}(10)^{1.75} = 20.98,$$

resulting with Fig. 6.14 in the additional temperature increase due to the 3rd harmonic $\Delta T_{h=3} = 3.3\%$ or $\Delta T_{h=3} = 1.98°C$.

### 6.5.2 Application Example 6.2: Temperature Rise of a Single-Phase Induction Motor Due to Single Harmonic Voltage: Solution

The rated temperature rise is $\Delta T_{rated} = T_{rated} - T_{amb} = T_{rise\ rat} = 60°C$. For the harmonic with order $h = 3$ and amplitude $V_3 = 0.10\ \text{pu} \equiv 10\%$ one obtains the weighted-harmonic factor by replacing $\frac{V_{ph}}{V_{p1}}$ by 10:

$$\sum_{h=3} \frac{1}{(3)^{0.85}}(10)^{1.40} = 9.88,$$

resulting with Fig. 6.14 in the additional temperature increase due to the 3rd harmonic $\Delta T_{h=3} = 11\%$ or $\Delta T_{h=3} = 6.6°C$.

### 6.8.1 Application Example 6.3: Aging of a Single-Phase Induction Motor with $E = 0.74$ eV Due to a Single Harmonic Voltage: Solution

The slope $(E/K)$ is $E/K = 8.58 \times 10^3$°Kelvin. Thus one obtains from $t_l = 40e^{-8.58\times10^3 \frac{\Delta T_h}{373(373+\Delta T_h)}}$,

$t_1 = 40\ e$

with $\Delta T_{h=3} = 6.6°C$, a reduced lifetime of $t_1|_{\Delta T_{h=3}=6.6°C} = 26.81$ years.

### 6.8.2 Application Example 6.4: Aging of a Single-Phase Induction Motor with $E = 0.51$ eV Due to a Single Harmonic Voltage: Solution

The slope $(E/K)$ is $E/K = 5.91 \times 10^3$ °Kelvin. Thus one obtains from

$$t_1 = 40e^{-5.91\times10^3 \frac{\Delta T_h}{373(373+\Delta T_h)}},$$



with $\Delta T_h = 6.6°C$, a reduced lifetime of $t_1|_{\Delta T_{h=3}=6.6°C} = 30.37$ years.

From Application Examples 6.3 and 6.4 one concludes that lower values of the activation energy E result in lower decreases in lifetime.

### 6.10.1 Application Example 6.5: Estimation of Lifetime Reduction for Given Single-Phase and Three-Phase Voltage Spectra with High-Harmonic Penetration with $E = 1.1$ eV: Solution

Calculation of weighted harmonic factor for single-phase spectrum of Table E6.5.1 based on the values for $k_{avg} = 0.85$ and $l_{avg} = 1.4$ for single-phase induction motors:

$$\frac{1}{2^{0.85}}(2.5)^{1.4} = 2.000, \frac{1}{3^{0.85}}(5.71)^{1.4} = 4.506,$$
$$\frac{1}{4^{0.85}}(1.6)^{1.4} = 0.594, \ldots, \frac{1}{17^{0.85}}(0.23)^{1.4} = 0.0115,$$
$$\frac{1}{18^{0.85}}(0.22)^{1.4} = 0.0103, \frac{1}{19^{0.85}}(1.03)^{1.4} = 0.0853.$$

Summing all contributions results in the weighted harmonic-voltage factor for single-phase induction motors:

$$\sum_{h=2}^{h\max} \frac{1}{h^k}\left(\frac{V_{ph}}{V_{p1}}\right)^l \approx 8.5.$$

Calculation of weighted harmonic factor for three-phase spectrum of Table E6.5.1 using the values for $k_{avg} = 0.95$ and $l_{avg} = 1.6$ for three-phase induction motors:

$$\frac{1}{2^{0.95}}(0.5)^{1.6} = 0.1707, \frac{1}{3^{0.95}}(1.0)^{1.6} = 0.3522,$$
$$\frac{1}{4^{0.95}}(0.5)^{1.6} = 0.0884, \ldots, \frac{1}{17^{0.95}}(1.5)^{1.6} = 0.1297,$$
$$\frac{1}{18^{0.95}}(0.01)^{1.6} = 0.00004, \frac{1}{19^{0.95}}(1.0)^{1.6} = 0.0609.$$

Summing all contributions results in the weighted harmonic-voltage factor for three-phase induction motors:

$$\sum_{h=2}^{h\max} \frac{1}{h^k}\left(\frac{V_{ph}}{V_{p1}}\right)^l \approx 8.6.$$

Calculation of weighted harmonic factor for single-phase spectrum of Table E6.5.1 based on the values for $k_{avg} = 0.90$ and $l_{avg} = 1.75$ for single-phase transformers:

$$\frac{1}{2^{0.9}}(2.5)^{1.75} = 2.664, \frac{1}{3^{0.9}}(5.71)^{1.75} = 7.847,$$
$$\frac{1}{4^{0.9}}(1.6)^{1.75} = 0.6536, \ldots, \frac{1}{17^{0.9}}(0.23)^{1.75} = 0.00597,$$
$$\frac{1}{18^{0.9}}(0.22)^{1.75} = 0.00524, \frac{1}{19^{0.9}}(1.03)^{1.75} = 0.744.$$

Summing all contributions results in the weighted harmonic-voltage factor for single-phase transformers

$$\sum_{h=2}^{h\max} \frac{1}{h^k}\left(\frac{V_{ph}}{V_{p1}}\right)^l \approx 12.3.$$

Calculation of weighted harmonic factor for three-phase spectrum of Table E6.5.1 based on the values for $k_{avg} = 0.90$ and $l_{avg} = 1.75$ for three-phase transformers:

$$\frac{1}{2^{0.9}}(0.5)^{1.75} = 0.1593, \frac{1}{3^{0.9}}(1)^{1.75} = 0.37203,$$
$$\frac{1}{4^{0.9}}(0.5)^{1.75} = 0.0854, \ldots, \frac{1}{17^{0.9}}(1.5)^{1.75} = 0.15876,$$
$$\frac{1}{18^{0.9}}(0.01)^{1.75} = 0.0000234, \frac{1}{19^{0.9}}(1)^{1.75} = 0.07065.$$

**TABLE E6.5.1** Possible Voltage Spectra with High-Harmonic Penetration

| $h$ | $\left(\frac{V_h}{V_{60Hz}}\right)_{1\Phi}$ (%) | $\left(\frac{V_h}{V_{60Hz}}\right)_{3\Phi}$ (%) |
|---|---|---|
| 1 | 100 | 100 |
| 2 | 2.5 | 0.5 |
| 3 | 5.71 | 1.0 |
| 4 | 1.6 | 0.5 |
| 5 | 1.25 | 7.0 |
| 6 | 0.88 | 0.2 |
| 7 | 1.25 | 5.0 |
| 8 | 0.62 | 0.2 |
| 9 | 0.96 | 0.3 |
| 10 | 0.66 | 0.1 |
| 11 | 0.30 | 2.5 |
| 12 | 0.18 | 0.1 |
| 13 | 0.57 | 2.0 |
| 14 | 0.10 | 0.05 |
| 15 | 0.10 | 0.1 |
| 16 | 0.13 | 0.05 |
| 17 | 0.23 | 1.5 |
| 18 | 0.22 | 0.01 |
| 19 | 1.03 | 1.0 |
| | All higher harmonics < 0.2% | |

ST. GEORGE COLLEGE OF JAPAN

Summing all above contributions results in the weighted harmonic-voltage factor for three-phase transformers:

$$\sum_{h=2}^{h\max}\frac{1}{h^k}\left(\frac{V_{ph}}{V_{p1}}\right)^l \approx 11.8.$$

Calculation of weighted harmonic factor for single-phase spectrum of Table E6.5.1 based on the values for $k_{avg}=1.0$ and $l_{avg}=2.0$ for universal motors:

$$\frac{1}{2}(2.5)^2=3.125,\ \frac{1}{3}(5.71)^2=10.868,\ \frac{1}{4}(1.6)^2=0.640,$$
$$\ldots,\ \frac{1}{17}(0.23)^2=0.00311,\ \frac{1}{18}(0.22)^2=0.0027,$$
$$\frac{1}{19}(1.03)^2=0.0558.$$

Summing all contributions results in the weighted harmonic-voltage factor for universal motors:

$$\sum_{h=2}^{h\max}\frac{1}{h^k}\left(\frac{V_{ph}}{V_{p1}}\right)^l \approx 15.6.$$

Based on Fig. 6.14, $T_2=85°C$, $T_{amb}=23°C$, $E=1.1$ eV, and rated lifetime of $t_2=40$ years the above harmonic factors result in the additional temperature rises and lifetime reductions of Table E6.5.2.

### 6.10.2 Application Example 6.6: Estimation of Lifetime Reduction for Given Single-Phase and Three-Phase Voltage Spectra with Moderate-Harmonic Penetration with $E = 1.1$ eV: Solution

Calculation of weighted harmonic factor for single-phase spectrum of Table E6.6.1 based on the values for $k_{avg}=0.85$ and $l_{avg}=1.4$ for single-phase induction motors:

$$\frac{1}{2^{0.85}}(0.5)^{1.4}=0.2103,\ \frac{1}{3^{0.85}}(3)^{1.4}=1.8297,$$
$$\frac{1}{4^{0.85}}(0.3)^{1.4}=0.05703,\ldots,\ \frac{1}{17^{0.85}}(0.5)^{1.4}=0.0341,$$
$$\frac{1}{18^{0.85}}(0.05)^{1.4}=0.0013,\ \frac{1}{19^{0.85}}(0.4)^{1.4}=0.0227.$$

Summing all contributions results in the weighted harmonic-voltage factor for single-phase induction motors:

$$\sum_{h=2}^{h\max}\frac{1}{h^k}\left(\frac{V_{ph}}{V_{p1}}\right)^l \approx 3.4.$$

Calculation of weighted harmonic factor for three-phase spectrum of Table E6.6.1 using the values for $k_{avg}=0.95$ and $l_{avg}=1.6$ for three-phase induction motors:

$$\frac{1}{2^{0.95}}(0.5)^{1.6}=0.1707,\ \frac{1}{3^{0.95}}(0.5)^{1.6}=0.1162,$$
$$\frac{1}{4^{0.95}}(0.5)^{1.6}=0.0884,\ldots,\ \frac{1}{17^{0.95}}(0.3)^{1.6}=0.00986,$$
$$\frac{1}{18^{0.95}}(0.01)^{1.6}=0.00004,\ \frac{1}{19^{0.95}}(0.2)^{1.6}=0.00464.$$

Summing all contributions results in the weighted harmonic-voltage factor for three-phase induction motors:

$$\sum_{h=2}^{h\max}\frac{1}{h^k}\left(\frac{V_{ph}}{V_{p1}}\right)^l \approx 2.6.$$

Calculation of weighted harmonic factor for single-phase spectrum of Table E6.6.1 based on the values for $k_{avg}=0.90$ and $l_{avg}=1.75$ for single-phase transformers:

$$\frac{1}{2^{0.90}}(0.5)^{1.75}=0.1593,\ \frac{1}{3^{0.90}}(3)^{1.75}=2.544,$$
$$\frac{1}{4^{0.90}}(0.3)^{1.75}=0.0349,\ldots,\ \frac{1}{17^{0.90}}(0.5)^{1.75}=0.0232,$$
$$\frac{1}{18^{0.90}}(0.05)^{1.75}=0.000392,\ \frac{1}{19^{0.90}}(0.4)^{1.75}=0.01421.$$

Summing all contributions results in the weighted harmonic-voltage factor for single-phase transformers:

**TABLE E6.5.2** Additional Temperature Rise and Associated Lifetime Reduction of Induction Motors, Transformers, and Universal Motors Due to the Harmonic Spectra of Table E6.5.1

| | | Three-phase induction motors | Single-phase transformers | Three-phase transformers | Universal motors |
|---|---|---|---|---|---|
| $\Delta T_h$ (%) | 9.2 | 4.5 | 1.9 | 1.8 | 24 |
| $\Delta T_h$ (°C) | 5.7 | 2.8 | 1.2 | 1.1 | 15 |
| Lifetime reduction (%) | 43 | 24 | 11 | 10 | 14 |



$$\sum_{h=2}^{h\max}\frac{1}{h^k}\left(\frac{V_{ph}}{V_{p1}}\right)^l = 4.1.$$

Calculation of weighted harmonic factor for three-phase spectrum of Table E6.6.1 based on the values for $k_{avg}=0.90$ and $l_{avg}=1.75$ for three-phase transformers:

$$\frac{1}{2^{0.90}}(0.5)^{1.75}=0.1593,\ \frac{1}{3^{0.90}}(0.5)^{1.75}=0.1106,$$
$$\frac{1}{4^{0.90}}(0.5)^{1.75}=0.0854,\ldots,\ \frac{1}{17^{0.90}}(0.3)^{1.75}=0.00949,$$
$$\frac{1}{18^{0.90}}(0.01)^{1.75}=0.0000234,\ \frac{1}{19^{0.90}}(0.2)^{1.75}=0.00423.$$

Summing all contributions results in the weighted harmonic-voltage factor for three-phase transformers:

$$\sum_{h=2}^{h\max}\frac{1}{h^k}\left(\frac{V_{ph}}{V_{p1}}\right)^l \approx 3.1.$$

**TABLE E6.6.1** Possible Voltage Spectra with Moderate-Harmonic Penetration

| $h$ | $\left(\frac{V_h}{V_{60\text{Hz}}}\right)_{1\Phi}$ (%) | $\left(\frac{V_h}{V_{60\text{Hz}}}\right)_{3\Phi}$ (%) |
|---|---|---|
| 1 | 100 | 100 |
| 2 | 0.5 | 0.5 |
| 3 | 3.0 | 0.5 |
| 4 | 0.3 | 0.5 |
| 5 | 2.0 | 3.0 |
| 6 | 0.2 | 0.2 |
| 7 | 1.0 | 2.5 |
| 8 | 0.2 | 0.2 |
| 9 | 0.75 | 0.3 |
| 10 | 0.1 | 0.1 |
| 11 | 1.0 | 1.0 |
| 12 | 0.1 | 0.1 |
| 13 | 0.9 | 0.85 |
| 14 | 0.1 | 0.05 |
| 15 | 0.3 | 0.1 |
| 16 | 0.05 | 0.05 |
| 17 | 0.5 | 0.3 |
| 18 | 0.05 | 0.01 |
| 19 | 0.4 | 0.2 |
| All higher harmonics < 0.2% | | |

Calculation of weighted harmonic factor for single-phase spectrum of Table E6.6.1 based on the values for $k_{avg}=1.0$ and $l_{avg}=2.0$ for universal motors:

$$\frac{1}{2}(0.5)^2=0.125,\ \frac{1}{3}(3)^2=3.0,\ \frac{1}{4}(0.3)^2=0.0225,\ldots,$$
$$\frac{1}{17}(0.5)^2=0.0147,\ \frac{1}{18}(0.05)^2=0.000139,$$
$$\frac{1}{19}(0.4)^2=0.00842.$$

Summing all contributions results in the weighted harmonic-voltage factor for universal motors:

$$\sum_{h=2}^{h\max}\frac{1}{h^k}\left(\frac{V_{ph}}{V_{p1}}\right)^l \approx 4.4.$$

Based on Fig. 6.14 the above harmonic factors, $T_2=85°C$, $T_{amb}=23°C$, $E=1.1$ eV, and rated lifetime of $t_2=40$ years result in the additional temperature rises and lifetime reductions of Table E6.6.2.

### 6.13.1 Application Example 6.7: Temperature Increase of Rotating Machine with a Step Load: Solution

With Eq. 6-39 one obtains

$$0.95\cdot\theta_f=\theta_f-(\theta_f-\theta_{amb})e^{\left(\frac{-t_{95\%}}{\tau_\theta}\right)}$$
$$=0.95\cdot120=120-(120-40)e^{\left(\frac{-t_{95\%}}{\tau_\theta}\right)}$$

or

$$t_{95\%}=2.59\cdot\tau_\theta=7.77\text{ h}.$$

### 6.14.6 Application Example 6.8: Steady State with Superimposed Periodic Intermittent Operation with Irregular Load Steps: Solution

The induction motor is operated at 60 Hz (natural torque-speed characteristic) [46 in Chapter 6].

a)

$n_S=1800$ rpm, $\Omega_{mi}=188.49$ rad/s, $\omega_m=180.1$ lrad/s, $s_{rat}=0.044$, $|\bar{I}_s(t)|=49.82$A, $|\bar{I}'_r(t)|=47.66$ A, $|\bar{E}|=221.75$ V, and $T_{rat}=164.31$ Nm (E6.8-1)

**TABLE E6.6.2** Additional Temperature Rise and Associated Lifetime Reduction of Induction Motors, Transformers, and Universal Motors Due to the Harmonic Spectra of Table E.6.6.1

| | Single-phase induction motors | Three-phase induction motors | Single-phase transformers | Three-phase transformers | Universal motors |
|---|---|---|---|---|---|
| $\Delta T_h$ (%) | 3.7 | 1.3 | 0.6 | 0.4 | 0.7 |
| $\Delta T_h$ (°C) | 2.3 | 0.81 | 0.37 | 0.25 | 0.43 |
| Lifetime reduction (%) | 20 | 7.7 | 3.6 | 2.5 | 4.2 |

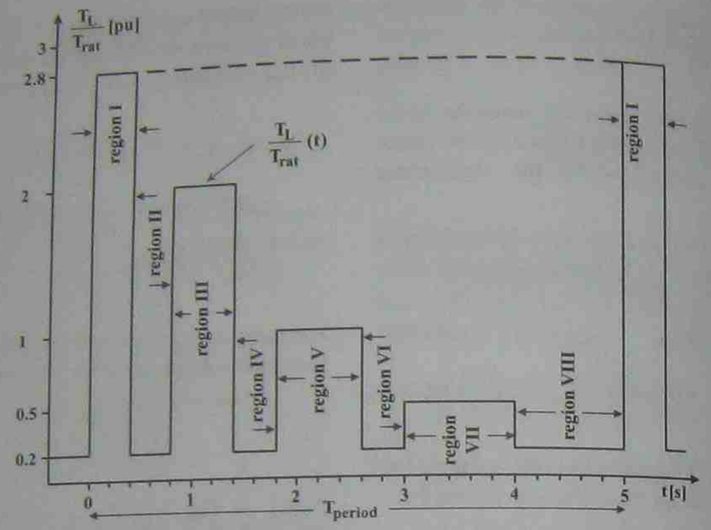



**FIGURE E6.8.1** Steady-state/intermittent load cycle.

b) Due to constant flux control, the $\Omega_m$–$T$ or the $s$–$T$ characteristic consists of a family of parallel lines as indicated in Fig. E6.8.2.

The maximum torque $T_{max}$ and the slip $s_m$ where the maximum torque occurs are [46]

$$T_{max} = 391.32 \text{ Nm}, \; s_m = 0.20. \qquad \text{(E6.8-2)}$$

From the relation (see Fig. E6.8.2)

$$\frac{T_{rat}}{T_{max_fict}} = \frac{s_{rat}}{1} \qquad \text{(E6.8-3)}$$

one obtains for the maximum fictitious torque

$$T_{max_fict} = T_{rat}/s_{rat} = 3734.3 \text{ Nm}. \qquad \text{(E6.8-4)}$$

c) Equation of motion (or fundamental torque equation) is

$$T - T_L - J\frac{d\omega_m}{dt} = 0, \qquad \text{(E6.8-5)}$$

where $T_L$ and $T$ are the load and the motor torques, respectively. $J$ is the total axial moment of inertia $J = J_m + J_{load}$. Dividing this equation by $T_{max_fict}$ one gets

$$\frac{T}{T_{max_fict}} - \frac{T_L}{T_{max_fict}} - \frac{J}{T_{max_fict}}\cdot\frac{d\omega_m}{dt} = 0 \qquad \text{(E6.8-6)}$$

or with $\frac{T}{T_{max_fict}} = s$ follows

$$s - \frac{T_L}{T_{max_fict}} - \frac{J}{T_{max_fict}}\cdot\frac{d\omega_m}{dt} = 0. \qquad \text{(E6.8-7)}$$

with $\omega_m = \omega_{ms}(1 - s)$ the differential equation becomes

$$\tau_m\frac{ds}{dt} + s = \frac{T_L}{T_{max_fict}}, \qquad \text{(E6.8-8)}$$

where

$$\tau_m = (J \cdot \omega_{ms})/T_{max_fict} = (5 \cdot 188.49)/3734.3 = 0.252 \text{ s} \qquad \text{(E6.8-9)}$$

is the mechanical time constant.

The general solution of this differential equation is

$$s(t) = \text{const}\cdot e^{\left(-\frac{t}{\tau_m}\right)} + \frac{T_L}{T_{max_fict}}. \qquad \text{(E6.8-10)}$$

For the initial condition where at t = 0 one assigns $s = s(0)$

$$s(t) = \left(s(0) - \frac{T_L(t)}{T_{max_fict}}\right)\cdot e^{\left(-\frac{t}{\tau_m}\right)} + \frac{T_L(t)}{T_{max_fict}}. \qquad \text{(E6.8-11)}$$

d) Application of s(t) to eight different regions of Fig. E6.8.1.



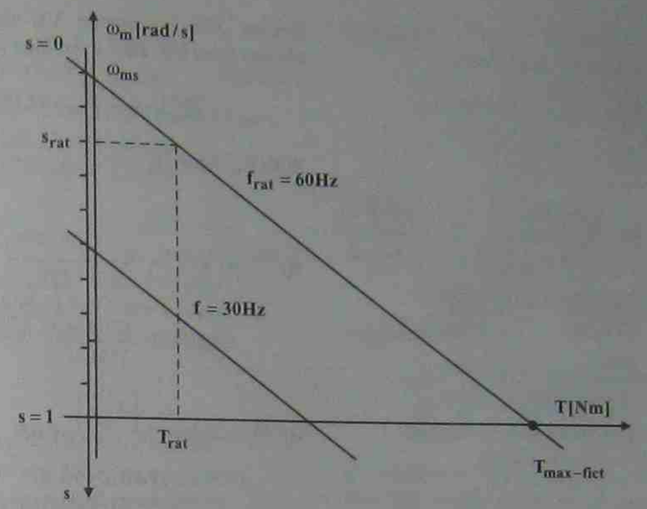



**FIGURE E6.8.2** $\Omega_m$–$T$ or $s$–$T$ characteristics for $f_{rat} = 60$ Hz (natural characteristic) and for $f = 30$ Hz.

***Region I.*** It is assumed that the motor at time $t = 0$ s (at the start of the load cycle) has the steady-state slip of $s(0)$. This slip is obtained from

$$\frac{T(0)}{T_{rat}} = \frac{s(0)}{s_{rat}} \qquad \text{(E6.8-12)}$$

and

$$T(0) = 0.2 \cdot T_{rat} = 32.86 \text{ Nm},$$
$$s(0) = 32.86 \cdot 0.044/(164.31) = 0.0088.$$

Therefore, the slip at the start of region *I* is

$$s(t^{(I)} = 0) = 0.0088.$$

It is best to introduce for each region a new coordinate system for the time axis. Thus for region *I* $0 \le t^{(I)} \le 0.4$ s one obtains from Fig. E6.8.1 the load torque

$$T_L^{(I)} = 2.8 \times T_{rat} = 460.07 \text{ Nm}.$$

With Eq. E6.8-11

$$s(t^{(I)}) = \left(s(t^{(I)} = 0) - \frac{T_L^{(I)}(t^{(I)})}{T_{max_fict}}\right)\cdot e^{\left(-\frac{t^{(I)}}{\tau_m}\right)} + \frac{T_L^{(I)}(t^{(I)})}{T_{max_fict}}$$
$$= \left(0.0088 - \frac{460.07}{3734.3}\right)e^{\left(-\frac{t^{(I)}}{\tau_m}\right)} + \frac{460.07}{3734.3}$$

$$s(t^{(I)}) = -0.1144e^{\left(-\frac{t^{(I)}}{\tau_m}\right)} + 0.1232$$

$s(t^{(I)} = 0.4 \text{ s}) = 0.0998 = s(t^{(II)} = 0)$ and
$s(t^{(I)} = 0.2 \text{ s}) = 0.07147.$

***Region II.*** For region II $(0 \le t^{(II)} \le 0.4$ s) one obtains from Fig. E6.8.1 the load torque

$$T_L^{(II)} = 0.2 \cdot T_{rat} = 32.86 \text{ Nm}.$$

With Eq. E6.8-11

$$s(t^{(II)}) = \left(s(t^{(II)} = 0) - \frac{T_L^{(II)}(t^{(II)})}{T_{max_fict}}\right)\cdot e^{\left(-\frac{t^{(II)}}{\tau_m}\right)} + \frac{T_L^{(II)}(t^{(II)})}{T_{max_fict}}$$
$$= \left(0.0998 - \frac{32.86}{3734.3}\right)e^{\left(-\frac{t^{(II)}}{\tau_m}\right)} + \frac{32.86}{3734.3}$$

$$s(t^{(II)}) = 0.091e^{\left(-\frac{t^{(II)}}{\tau_m}\right)} + 0.0088$$

$s(t^{(II)} = 0.4 \text{ s}) = 0.0274 = s(t^{(III)} = 0)$ and
$s(t^{(II)} = 0.2 \text{ s}) = 0.04994.$

***Region III.*** For region III $(0 \le t^{(III)} \le 0.6$ s) one obtains from Fig. E6.8.1 the load torque

$$T_L^{(II)} = 2 \cdot T_{rat} = 328.62 \text{ Nm}.$$

With Eq. E6.8-11

$$s(t^{(III)}) = \left(s(t^{(III)} = 0) - \frac{T_L^{(III)}(t^{(III)})}{T_{max_fict}}\right)\cdot e^{\left(-\frac{t^{(III)}}{\tau_m}\right)} + \frac{T_L^{(III)}(t^{(III)})}{T_{max_fict}}$$
$$= \left(0.0274 - \frac{328.62}{3734.3}\right)e^{\left(-\frac{t^{(III)}}{\tau_m}\right)} + \frac{328.62}{3734.3}$$

$$s(t^{(III)}) = -0.0606e^{\left(-\frac{t^{(III)}}{\tau_m}\right)} + 0.088$$

$s(t^{(III)} = 0.6 \text{ s}) = 0.0824 = s(t^{(IV)} = 0)$ and
$s(t^{(III)} = 0.3 \text{ s}) = 0.06957.$

ST. GEORGE POLYTECHNIC

***Region IV.*** For region IV ($0 \le t^{(IV)} \le 0.4$ s) one obtains from Fig. E6.8.1 the load torque

$$T_L^{(IV)} = 0.2 \cdot T_{rat} = 32.86 \text{ Nm}.$$

With Eq. E6.8-11

$$s(t^{(IV)}) = \left(s(t^{(IV)}=0) - \frac{T_L^{(IV)}(t^{(IV)})}{T_{max_fict}}\right) \cdot e^{\left(-\frac{t^{(IV)}}{\tau_m}\right)} + \frac{T_L^{(IV)}(t^{(IV)})}{T_{max_fict}}$$

$$= \left(0.0824 - \frac{32.86}{3734.3}\right) e^{\left(-\frac{t^{(IV)}}{\tau_m}\right)} + \frac{32.86}{3734.3},$$

$$s(t^{(IV)}) = 0.0736 e^{\left(-\frac{t^{(IV)}}{\tau_m}\right)} + 0.0088.$$

$s(t^{(IV)} = 0.4 \text{ s}) = 0.02385 = s(t^{(V)} = 0)$ and
$s(t^{(IV)} = 0.2 \text{ s}) = 0.04208.$

***Region V.*** For region V ($0 \le t^{(V)} \le 0.8$ s) one obtains from Fig. E6.8.1 the load torque

$$T_L^{(V)} = T_{rat} = 164.3 \text{ Nm}.$$

With Eq. E6.8-11

$$s(t^{(V)}) = \left(s(t^{(V)}=0) - \frac{T_L^{(V)}(t^{(V)})}{T_{max_fict}}\right) \cdot e^{\left(-\frac{t^{(V)}}{\tau_m}\right)} + \frac{T_L^{(V)}(t^{(V)})}{T_{max_fict}}$$

$$= \left(0.02385 - \frac{164.31}{3734.3}\right) e^{\left(-\frac{t^{(V)}}{\tau_m}\right)} + \frac{164.31}{3734.3}$$

$$s(t^{(V)}) = -0.0202 e^{\left(-\frac{t^{(V)}}{\tau_m}\right)} + 0.044$$

$s(t^{(V)} = 0.8 \text{ s}) = 0.0432 = s(t^{(VI)} = 0)$ and
$s(t^{(V)} = 0.4 \text{ s}) = 0.03987.$

***Region VI.*** For region VI ($0 \le t^{(VI)} \le 0.4$ s) one obtains from Fig. E6.8.1 the load torque

$$T_L^{(IV)} = 0.2 \cdot T_{rat} = 32.86 \text{ Nm}.$$

With Eq. E6.8-11

$$s(t^{(VI)}) = \left(s(t^{(VI)}=0) - \frac{T_L^{(VI)}(t^{(VI)})}{T_{max_fict}}\right) \cdot e^{\left(-\frac{t^{(VI)}}{\tau_m}\right)} + \frac{T_L^{(VI)}(t^{(VI)})}{T_{max_fict}}$$

$$= \left(0.0432 - \frac{32.86}{3734.3}\right) e^{\left(-\frac{t^{(VI)}}{\tau_m}\right)} + \frac{32.86}{3734.3}$$

$$s(t^{(VI)}) = 0.0344 e^{\left(-\frac{t^{(VI)}}{\tau_m}\right)} + 0.0088$$

$s(t^{(VI)} = 0.4 \text{ s}) = 0.01583 = s(t^{(VII)} = 0)$ and
$s(t^{(VI)} = 0.2 \text{ s}) = 0.0244.$

***Region VII.*** For region VII ($0 \le t^{(VII)} \le 1$ s) one obtains from Fig. E6.8.1 the load torque

$$T_L^{(VII)} = 0.5 \cdot T_{rat} = 82.155 \text{ Nm}.$$

With Eq. E6.8-11

$$s(t^{(VII)}) = \left(s(t^{(VII)}=0) - \frac{T_L^{(VII)}(t^{(VII)})}{T_{max_fict}}\right) \cdot e^{\left(-\frac{t^{(VII)}}{\tau_m}\right)} + \frac{T_L^{(VII)}(t^{(VII)})}{T_{max_fict}}$$

$$= \left(0.01583 - \frac{82.155}{3734.3}\right) e^{\left(-\frac{t^{(VII)}}{\tau_m}\right)} + \frac{82.155}{3734.3}$$

$$s(t^{(VII)}) = -0.00617 e^{\left(-\frac{t^{(VII)}}{\tau_m}\right)} + 0.022$$

$s(t^{(VII)} = 1 \text{ s}) = 0.0219 = s(t^{(VIII)} = 0)$ and
$s(t^{(VII)} = 0.5 \text{ s}) = 0.02115.$

***Region VIII.*** For region VIII ($0 \le t^{(VIII)} \le 1$ s) one obtains from Fig. E6.8.1 the load torque

$$T_L^{(IV)} = 0.2 \cdot T_{rat} = 32.86 \text{ Nm}.$$

With Eq. E6.8-11

$$s(t^{(VIII)}) = \left(s(t^{(VIII)}=0) - \frac{T_L^{(VIII)}(t^{(VIII)})}{T_{max_fict}}\right) \cdot e^{\left(-\frac{t^{(VIII)}}{\tau_m}\right)}$$

$$+ \frac{T_L^{(VIII)}(t^{(VIII)})}{T_{max_fict}} = \left(0.0219 - \frac{32.86}{3734.3}\right) e^{\left(-\frac{t^{(VIII)}}{\tau_m}\right)}$$

$$+ \frac{32.86}{3734.3}$$

$$s(t^{(VIII)}) = 0.0131 e^{\left(-\frac{t^{(VIII)}}{\tau_m}\right)} + 0.0088$$

$s(t^{(VIII)} = 1 \text{ s}) = 0.0090 \approx s(t^{(I)} = 0) = 0.0088$. That is, the periodicity of the slip s(t) is about satisfied.
$s(t^{(VIII)} = 0.5 \text{ s}) = 0.0106.$
The plot of $s(t)$ is given in Fig. E6.8.3.

e) Calculation of the torque $T(t)$ and its plot from $t = 0$ to $t = 5$ s. From

$$\frac{T}{T_{max_fict}} = \frac{s}{1}$$

follows

$$T = s \cdot T_{max_fict}. \qquad \text{(E6.8-13)}$$



***Region I***

$$T(t^{(I)}) = s(t^{(I)}) \cdot T_{max_fict} \qquad \text{(E6.8-14)}$$

$T(t^{(I)} = 0) = 0.0088 \cdot 3734.3\ 32.86 \text{ Nm} \equiv 0.2\ pu^*,$
$T(t^{(I)} = 0.2 \text{ s}) = 266.9 \text{ Nm} \equiv 1.62\ pu,$
$T(t^{(I)} = 0.4 \text{ s}) = 372.7 \text{ Nm} \equiv 2.27\ pu.$

***Region II***

$T(t^{(II)} = 0 \text{ s}) = 372.7 \text{ Nm} \equiv 2.27\ pu,$
$T(t^{(II)} = 0.2 \text{ s}) = 186.5 \text{ Nm} \equiv 1.14\ pu,$
$T(t^{(II)} = 0.4 \text{ s}) = 102.3 \text{ Nm} \equiv 0.62\ pu.$

***Region III***

$T(t^{(III)} = 0 \text{ s}) = 102.3 \text{ Nm} \equiv 0.62\ pu,$
$T(t^{(III)} = 0.3 \text{ s}) = 259.8 \text{ Nm} \equiv 1.58\ pu,$
$T(t^{(III)} = 0.6 \text{ s}) = 307.7 \text{ Nm} \equiv 1.87\ pu.$

***Region IV***

$T(t^{(IV)} = 0 \text{ s}) = 307.7 \text{ Nm} \equiv 1.87\ pu,$
$T(t^{(IV)} = 0.2 \text{ s}) = 157.1 \text{ Nm} \equiv 0.96\ pu,$
$T(t^{(IV)} = 0.4 \text{ s}) = 89.1 \text{ Nm} \equiv 0.54\ pu.$

***Region V***

$T(t^{(V)} = 0 \text{ s}) = 89.1 \text{ Nm} \equiv 0.54,$
$T(t^{(V)} = 0.4 \text{ s}) = 148.9 \text{ Nm} \equiv 0.91\ pu,$
$T(t^{(V)} = 0.8 \text{ s}) = 161.3 \text{ Nm} \equiv 0.98\ pu.$

***Region VI***

$T(t^{(VI)} = 0 \text{ s}) = 161.3 \text{ Nm} \equiv 0.982\ pu,$
$T(t^{(VI)} = 0.2 \text{ s}) = 9.91 \text{ Nm} \equiv 0.55\ pu,$
$T(t^{(VI)} = 0.4 \text{ s}) = 59.1 \text{ Nm} \equiv 0.36\ pu.$

***Region VII***

$T(t^{(VII)} = 0 \text{ s}) = 59.1 \text{ Nm} \equiv 0.36\ pu,$
$T(t^{(VII)} = 0.5 \text{ s}) = 79 \text{ Nm} \equiv 0.48\ pu,$
$T(t^{(VII)} = 1 \text{ s}) = 81.8 \text{ Nm} \equiv 0.50\ pu.$

***Region VIII***

$T(t^{(VIII)} = 0 \text{ s}) = 81.8 \text{ Nm} \equiv 0.50\ pu,$
$T(t^{(VIII)} = 0.5 \text{ s}) = 39.6 \text{ Nm} \equiv 0.24\ pu,$
$T(t^{(VIII)} = 1 \text{ s}) = 33.6 \text{ Nm} \equiv 0.024\ pu.$

(*) referred to rated torque $T_{rat} = 164.31$ Nm. Note that the motor torque is at any time less than $T_{max} = 391.32$ Nm. The motor torque $T(t)$ is proportional to the slip s(t) and is depicted in Fig. E6.8.4.

f) Point-wise calculation of the stator current $|\tilde{I}_s(t)|$ for the eight different regions. For the calculation of the stator current $|\tilde{I}_s(t)|$ the equivalent circuit of Fig. E6.8.5 is employed.

For $s(t^{(I)} = 0) = 0.0088$ one gets

$$\frac{R_r'}{s} = \frac{0.2}{0.0088} = 22.73\Omega.$$

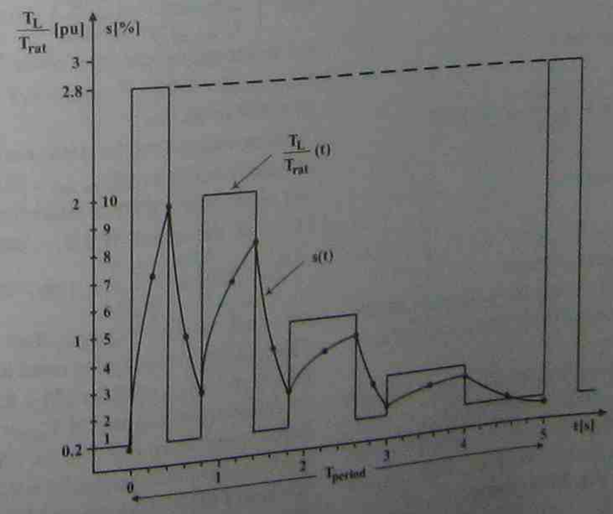



**FIGURE E6.8.3** Slip $s(t)$.

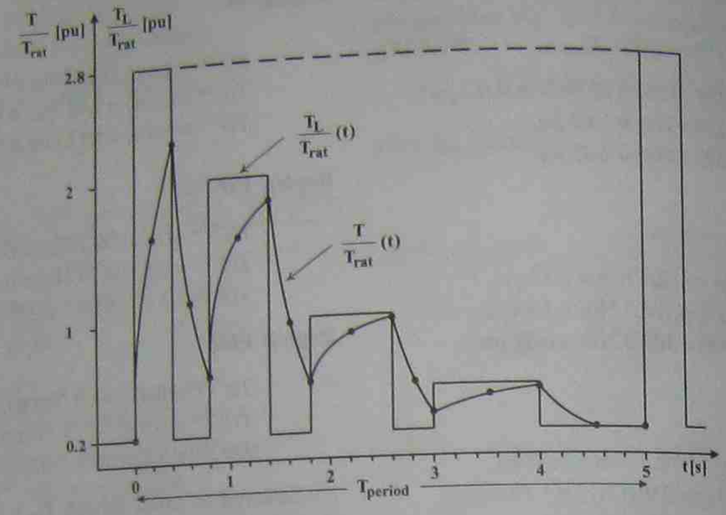



**FIGURE E6.8.4** Motor torque $T(t)$.

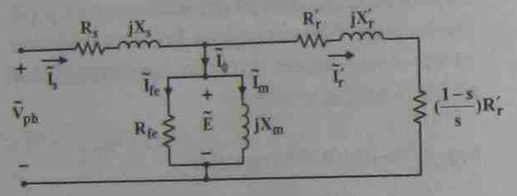



**FIGURE E6.8.5** Equivalent circuit of induction motor.

With $\tilde{E} = 221.75\ V\angle 0°$ the rotor current becomes

$$\tilde{I}'_r = \frac{\tilde{E}}{\left(\frac{R'_r}{s} + jX'_r\right)} = \frac{221.75\text{V}\angle 0°}{(22.73 + j)} = (9.737 - j0.428)\,A.$$

The magnetizing current is

$$\tilde{I}_m = \frac{\tilde{E}}{jX_m} = \frac{221.75\angle °}{j30\Omega} = -j7.392\,A$$

and the stator current

$$\tilde{I}_s = \tilde{I}_m + \tilde{I}'_r = (9.737 - j7.82)\Omega$$

where $\tilde{E}$ is the reference phasor.

Table E6.8.1 summarizes the point-wise calculation of the rms values of $|\tilde{I}_s(t)|$ over a load cycle.

g) Figure E6.8.6 shows the plot of $|\tilde{I}_s(t)|$ as a function of time and Fig. E6.8.7 depicts $|\tilde{I}_s(t)|^2$.

h) The rms current value of the stator current $I_{s_rms_actual}$ for the load cycle of Fig. E6.8.1 can be calculated from Fig. E6.8.7 using

$$I_{s_rms_actual} = \sqrt{\frac{1}{T}\int_{t}^{t+T} |\tilde{I}_s(t)|^2 dt}.$$

The evaluation of this integral can be done mathematically or graphically. The graphic evaluation leads to $I_{s_rms_actual} = 47.7A$.

i) Comparison of rated $I_{s_rms_rat}$ and actual current $I_{s_rms_actual}$. Is the motor over- or underdesigned?

The losses of an induction motor are about proportional to the square of the stator current $I_{s_rms}$. The ratio $\left(\frac{I_{s_rms_actual}}{I_{s_rms_rat}}\right)^2 = \left(\frac{47.4}{49.82}\right)^2 = 0.91$ indicates that the motor rating can be reduced by 9%, that is, $P_{out_reduced} = 0.91 \cdot P_{out_rat} = 0.91 \cdot 29.594\,\text{kW} = 26.93\,\text{kW}$ or 36.1 hp.

Let us assume that the stator current is larger than the rated current, say, $I_{s_rms_high} = 52A$; then the motor will experience a lifetime reduction – if the service factor of the motor is 1.0 – based on the ratio $\left(\frac{I_{s_rms_high}}{I_{s_rms_rat}}\right)^2 = \left(\frac{52}{49.82}\right)^2 = 1.09$, that is, the losses are about $\Delta P_{loss} = 9\%$ larger than the rated losses. This leads for a steady-state rated temperature of the hottest spot of $T_2 = 85°C \equiv 273 + 85 = 358\,°\text{Kelvin}$ at an ambient temperature of $T_{amb} = 40°C$ to an additional temperature rise of $\Delta T = 9\%$ or $\Delta T = 4.05°C$. With an activation energy of $E = 0.74\,\text{eV}$ and a rated lifetime of 40 years the reduced lifetime of the three-phase induction motor is with $\Delta T = 4.05°C$

ST. GEORGE POLYTECHNIC UNIVERSITY



**TABLE E6.8.1** Point-Wise Calculation of the rms Values of $|\tilde{I}_s(t)|$ Measured in Amperes

| Region I | $\lvert\tilde{I}_s\rvert$ | Region II | $\lvert\tilde{I}_s\rvert$ | Region III | $\lvert\tilde{I}_s\rvert$ |
|---|---|---|---|---|---|
| $s(t^{(I)} = 0) = 0.0088$ | 12.49 | $s(t^{(II)} = 0) = 0.0998$ | 102.69 | $s(t^{(III)} = 0) = 0.0274$ | 31.95 |
| $s(t^{(I)} = 0.2\ s) = 0.07147$ | 77.44 | $s(t^{(II)} = 0.2\ s) = 0.04994$ | 56.04 | $s(t^{(III)} = 0.3\ s) = 0.06957$ | 75.56 |
| $s(s^{(I)} = 0.4\ s) = 0.0998$ | 102.69 | $s(t^{(II)} = 0.4\ s) = 0.0274$ | 31.95 | $s(t^{(III)} = 0.6\ s) = 0.0824$ | 101.74 |
| **Region IV** | $\lvert\tilde{I}_s\rvert$ | **Region V** | $\lvert\tilde{I}_s\rvert$ | **Region VI** | $\lvert\tilde{I}_s\rvert$ |
| $s(t^{(IV)} = 0) = 0.082$ | 101.74 | $s(t^{(V)} = 0) = 0.02385$ | 28.11 | $s(t^{(VI)}) = 0) = 0.0432$ | 48.92 |
| $s(t^{(IV)} = 0.2\ s) = 0.04208$ | 47.76 | $s(t^{(V)} = 0.4\ s) = 0.03987$ | 45.38 | $s(t^{(VI)} = 0.2\ s) = 0.0244$ | 28.706 |
| $s(t^{(IV)} = 0.4\ s) = 0.02385$ | 28.11 | $s(t^{(V)} = 0.8\ s) = 0.0432$ | 48.92 | $s(t^{(VI)} = 0.4\ s) = 0.01583$ | 19.53 |
| **Region VII** | $\lvert\tilde{I}_s\rvert$ | **Region VIII** | $\lvert\tilde{I}_s\rvert$ | | |
| $s(t^{(VII)} = 0) = 0.01583$ | 19.53 | $s(t^{(VIII)} = 0) = 0.0219$ | 26 | | |
| $s(t^{(VIII)} = 0.5\ s) = 0.02115$ | 25.19 | $s(t^{(VIII)} = 0.5\ s) = 0.0106$ | 14.2 | | |
| $s(t^{(VII)} = 1\ s) = 0.0219$ | 26 | $s(t^{(VIII)} = 1\ s) = 0.009$ | 12.68 | | |

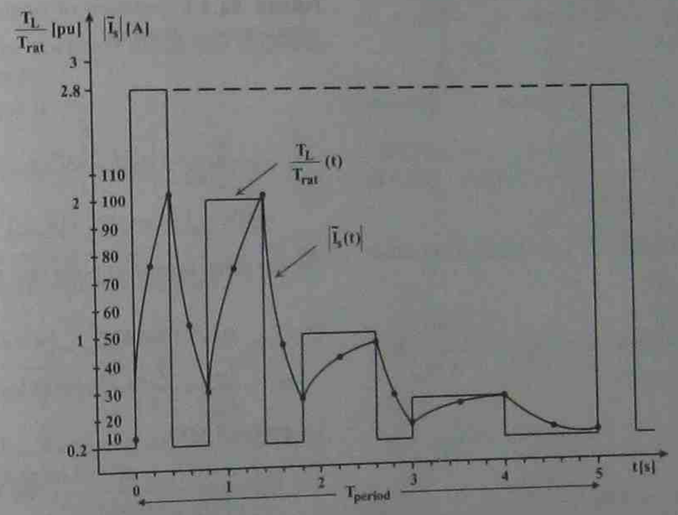



**FIGURE E6.8.6** $|\tilde{I}_s(t)|$.

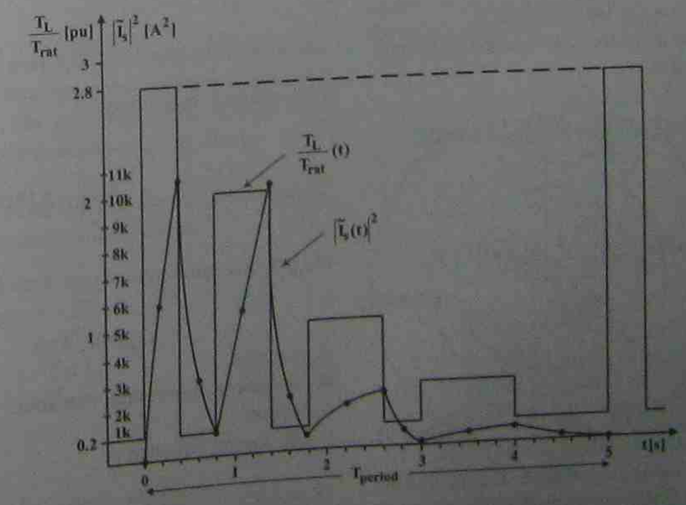



**FIGURE E6.8.7** $|\tilde{I}_s(t)|^2$.

$$t_1 = 40e^{\frac{-8.58\times10^3\left(\frac{\Delta T}{358(358+\Delta T)}\right)}{}} = 30.6\,\text{years}.$$

Most induction motors are designed with a service factor of 1.1–1.15, that is, the motor can be overloaded by 10 to 15 %. If this motor were designed with a service factor of 1.10 then no lifetime reduction would occur for a stator current of $I_{s_rms_high} = 52\text{A}$.

### 6.14.8 Application Example 6.9: Reduction of Harmonic Torques of a Piston-Compressor Drive with Synchronous Motor as Prime Mover: Solution

a) $n_{ms} = (120 \cdot \text{f})/p = 257.14\,\text{rpm}$, $\omega_{ms} = (2\pi \cdot n_{ms})/60 = 26.927\,\text{rad/s}$,

$$T_{rat} = \frac{P_{rat}}{\omega_{ms}} = 278.53\,\text{kNm}, \qquad \text{(E6.9-5)}$$

$$|\tilde{I}_{a_rat}| = \frac{P_{rat}}{\sqrt{3}\cdot V_{L-L\,rat}\cos\phi_{rat}\eta_{rat}} = 827.6\,\text{A}. \qquad \text{(E6.9-6)}$$

The average load torque $T_{Lavg} = 265.53\,\text{kNm}$ leads with

$$T_{Lavg} = \frac{3|\tilde{E}_a||\tilde{V}_{a_rat}|}{X_s\omega_{ms}}\sin\delta \quad \text{and} \quad T_{max} = \frac{3|\tilde{E}_a||\tilde{V}_{a_rat}|}{X_s\omega_{ms}}$$

to the ratio

$$\frac{T_{Lavg}}{T_{max}} = \sin\delta \quad \text{or} \quad \delta = \sin^{-1}\left(\frac{T_{Lavg}}{2.3\cdot T_{rat}}\right) \qquad \text{(E6.9-7)}$$
$$= 0.427\,\text{rad or } 24.48°.$$

Figure E6.9.1 defines the torque angle $\delta$.

From the phasor diagram (overexcited, consumer notation) one obtains

$$|\tilde{E}_a|^2 = (|\tilde{V}_{a_rat}| + |\tilde{I}_a|X_s\sin\phi)^2 + (|\tilde{I}_a|X_s\cos\phi)^2$$

or

$$|\tilde{E}_a|^2 = |\tilde{V}_{a_rat}|^2 + 2|V_{a_rat}||I_a|X_s\sin\phi + (|\tilde{I}_a|X_s)^2 \qquad \text{(E6.9-8)}$$

and with

$$P = \frac{3|\tilde{E}_a||\tilde{V}_{a_rat}|\sin\delta}{X_s} \qquad \text{(E6.9-9)}$$

follows the second-order equation for $X_S$



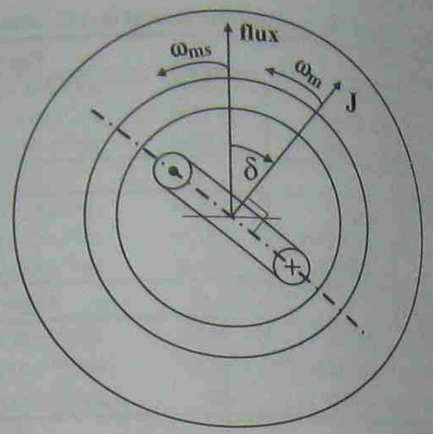



**FIGURE E6.9.1** Definition of torque angle $\delta$ without induction motor damping.

$$\left[\left(\frac{P}{3|\tilde{V}_{a_rat}|\sin\delta}\right)^2 - |\tilde{I}_a|^2\right]X_s^2 - (2|\tilde{V}_{a_rat}||\tilde{I}_a|\sin\phi)X_s - |\tilde{V}_{a\text{-}rat}|^2 = 0. \qquad \text{(E6.9-10)}$$

For the given operating point one gets

$$P = T_{Lavg}\cdot\omega_s = 7.14\,\text{MW}, |\tilde{V}_{a_rat}| = 3.464\,\text{kV},$$
$$\sin\delta = \frac{T_{lavg}}{T_{max}} = \frac{T_{Lavg}}{2,3\cdot T_{rat}} = 0.4145.\ \cos\Phi = 0.9,$$
$$\sin\Phi = 0.4359,$$
$$|\tilde{I}_a| = \frac{T_{Lavg}\cdot\omega_s}{3\cdot|\tilde{V}_{a_rat}|\cdot\cos\phi\cdot\eta_{rat}} = 789\,\text{A}, \qquad \text{(E6.9-11)}$$

and therefore

$$X_S = 3.07\,\Omega. \qquad \text{(E6.9-12)}$$

With the base impedance of

$$Z_{base} = \frac{|\tilde{V}_{a_rat}|}{|\tilde{I}_{a_rat}|} = 4.18\Omega \qquad \text{(E6.9-13)}$$

the per-unit synchronous reactance is

$$X_{s_pu} = 0.74\,\text{pu} \qquad \text{(E6.9-14)}$$

b) Nonlinear differential equation for the motor torque.

The torque equation is

$$T - T_L - J\frac{d\omega_m}{dt} = 0, \qquad \text{(E6.9-15)}$$





where

$$T = T_{max}\cdot\sin\delta, \delta = \frac{p}{2}\alpha, T_L = T_{Lavg} + T_{L1}, \alpha = \omega_{ms}t - \omega_m t,$$
$$\frac{d\alpha}{dt} = \omega_{ms} - \omega_m, \frac{d\delta}{dt} = \frac{p}{2}\cdot\frac{d\alpha}{dt}, \frac{d\delta}{dt} = \frac{p}{2}(\omega_{ms} - \omega_m),$$
$$\omega_m = \omega_{ms} - \frac{1}{p/2}\cdot\frac{d\delta}{dt}, \frac{d\omega_m}{dt} = -\frac{1}{p/2}\frac{d^2\delta}{dt^2}.$$

(E6.9-16)

The nonlinear differential equation becomes

$$T_{max}\sin\delta - T_{Lavg} - T_{L1} + \frac{J}{p/2}\frac{d^2\delta}{dt^2} = 0. \qquad \text{(E6.9-17)}$$

Linearization of the nonlinear differential equation is based on Fig. E6.9.2.

The motor torque is

$$T = T_{max}\sin(\delta_0 + \delta_1) = T_{max}\sin\delta_0 + T_{max}\delta_1\cos\delta_0 \qquad \text{(E6.9-18)}$$

or with the synchronizing torque $S = T_{max}\cos\delta_0$, the linearized differential equation becomes

$$\delta_1 + \frac{J}{(p/2)S}\frac{d^2\delta_1}{dt^2} = \frac{T_{L1}}{S}. \qquad \text{(E6.9-19)}$$

The eigen-angular frequency of the undamped machine can be defined by

$$\omega_{eigen} = \sqrt{\frac{(p/2)S}{J}}. \qquad \text{(E6.9-20)}$$

c) Repetition of part b, but not neglecting damping provided by induction motor action as is indicated in Fig. E6.9.3. The small-slip approximation of an induction motor is depicted in Fig. E6.9.4.

From Fig. E6.9.4 one obtains for the motor torque developed by induction-motor action

$$T_{induction} = \frac{T_{rat}\cdot s}{s_{rat}}, s = 1 - \frac{n_m}{n_{ms}} = 1 - \frac{\omega_m}{\omega_{ms}},$$
$$T_{induction} = \frac{T_{rat}}{s_{rat}}\left(1 - \frac{\omega_m}{\omega_{ms}}\right), \qquad \text{(E6.9-21a)}$$

or

$$T_{induction} = \frac{T_{rat}}{S_{rat}}\frac{1}{(p/2)\cdot\omega_{ms}}\cdot\frac{d\delta}{dt}. \qquad \text{(E6.9-21b)}$$

With the power system's frequency $\omega_s = 2\pi f$ and $\omega_s = (p/2\omega_{ms})$ one obtains the total motor torque

$$T = T_{max}\sin\delta + \frac{T_{rat}}{s_{rat}}\cdot\frac{1}{\omega_s}\cdot\frac{d\delta}{dt} \qquad \text{(E6.9-21c)}$$

or the nonlinear differential equation including the damping due to induction-motor action

$$\frac{J}{p/2}\frac{d^2\delta}{dt^2} + \frac{T_{rat}}{s_{rat}\cdot\omega_s}\frac{d\delta}{dt} + T_{max}\sin\delta = T_{Lavg} + T_{L1}. \qquad \text{(E6.9-22)}$$

Linearization leads to the differential equation

$$\frac{J}{p/2}\frac{d^2\delta_1}{dt^2} + D\frac{d\delta_1}{dt} + S\delta_1 = T_{L1}, \qquad \text{(E6.9-23)}$$

where the damping factor is

$$D = \frac{T_{rat}}{s_{rat}\cdot\omega_s}. \qquad \text{(E6.9-24)}$$

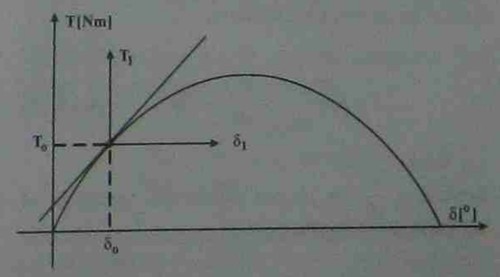



**FIGURE E6.9.2** Linearization of sine function for a given operating point $\delta = \delta_0 + \delta_1$, where $\delta_1 \ll \delta_0$.

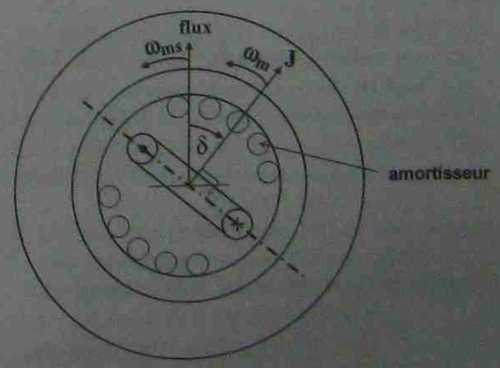



**FIGURE E6.9.3** Definition of torque angle $\delta$ with induction motor damping.

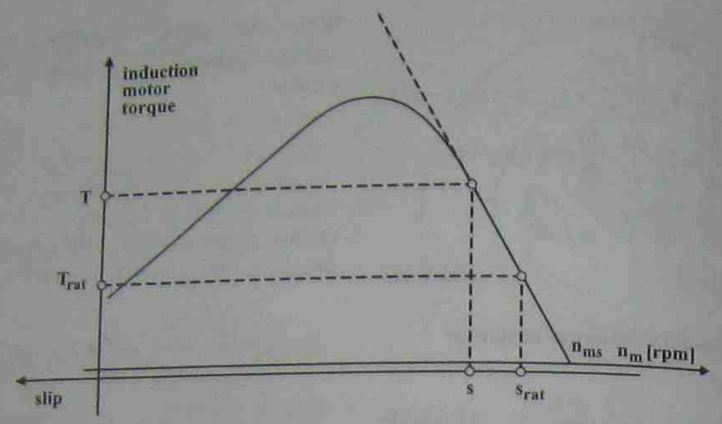



**FIGURE E6.9.4** Small-slip approximation of induction motor characteristic.

d) Solution of the linearized differential equations of part b – without damping – and determining (by introducing phasors indicated by "–") the axial moment of inertia J required so that the first harmonic motor torque will be reduced to ±4% of the average torque (Eq. E6.9-2).

Neglecting damping one obtains for the kth harmonic the differential equation

$$\delta_1 + \frac{1}{\omega_{eigen}^2}\frac{d^2\delta_1}{dt^2} = \frac{T_{Lk}}{S}. \qquad \text{(E6.9-25)}$$

Replacing $\frac{d}{dt}$ by $j\omega_k$ for sine/cosine variations of harmonic torques one gets

$$\tilde{\delta}_1 + \frac{1}{\omega_{eigen}^2}(j\omega_k)^2\tilde{\delta}_1^2 = \frac{\tilde{T}_{Lk}}{S}. \qquad \text{(E6.9-26)}$$

With

$$\hat{T}_k = T_{max}\cos\delta_0,\ \tilde{\delta}_1 = S\cdot\tilde{\delta}_1 \qquad \text{(E6.9-27)}$$

follows

$$\frac{\hat{T}_k}{\hat{T}_{Lk}} = \frac{1}{\left(1-\frac{\omega_k^2}{\omega_{eigen}^2}\right)}, \qquad \text{(E6.9-28)}$$

or magnitudes only where "^" indicates amplitude

$$\frac{|\tilde{T}_k|}{|\tilde{T}_{Lk}|} = \frac{\hat{T}_k}{\hat{T}_{Lk}} = \frac{1}{\left[1-\left(\frac{\omega_k}{\omega_{eigen}}\right)^2\right]}, \qquad \text{(E6.9-29)}$$

where $\tan(\varepsilon) = 0$ for $\omega_k < \omega_{eigen}$ and $\tan(\varepsilon) = -180°$ for $\omega_k > \omega_{eigen}$.

For the first harmonic torque one can write

$$T_{L1} = 31.04\ \text{kNm}\sin(\omega_{ms} - \pi),\ \hat{T}_1 = \pm 0.04 T_{rat} = \pm 0.04 T_{Leq} \qquad \text{(E6.9-30)}$$

$$\frac{\hat{T}_1}{\hat{T}_{L1}} = \frac{1}{\left(1-\frac{\omega_1^2}{\omega_{eigen}^2}\right)}. \qquad \text{(E6.9-31)}$$

The required inertia becomes for the worst case (– sign):

$$J = \frac{S(p/2)}{\omega_1^2}\left(1-\frac{\hat{T}_{L1}}{\hat{T}_1}\right) = \frac{2.3\cdot T_{rat}\cdot\cos\delta_0\cdot(p/2)^3}{\omega^2}$$
$$\left(1-\frac{\hat{T}_{L1}}{\hat{T}_1}\right) = 11.256\cdot 10^3\left(1-\frac{31.04}{\pm 0.04\cdot 265.53}\right)$$
$$= 44\cdot 10^3\ \text{kgm}^2. \qquad \text{(E6.9-32)}$$

Solution of the linearized differential equations of part c – with damping – and determining (by introducing phasors) the axial moment of inertia J required so that the first harmonic motor torque will be reduced to ±4% of the average torque (Eq. E6.9-2).

Not neglecting damping one obtains for the kth harmonic the differential equation

$$\frac{J}{p/2}\frac{d^2\delta_1}{dt^2} + D\frac{d\delta_1}{dt} + S\delta_1 = T_{Lk} \qquad \text{(E6.9-33)}$$



or for sine/cosine variations of harmonic load torques

$$(j\omega_k)^2\frac{J}{(p/2)}\cdot\tilde{\delta}_1 + j\omega_k D\tilde{\delta}_1 + S\tilde{\delta}_1 = \tilde{T}_{Lk} \qquad \text{(E6.9-34)}$$

with

$$S\tilde{\delta}_1 = \tilde{T}_k \qquad \text{(E6.9-35)}$$

$$\frac{\tilde{T}_k}{\tilde{T}_{Lk}} = \frac{1}{(j\omega_k)^2\cdot\frac{J}{(p/2)\cdot S} + j\omega_k\frac{D}{S} + 1} \qquad \text{(E6.9-36)}$$

or the magnitudes only

$$\frac{|\tilde{T}_k|}{|\tilde{T}_{Lk}|} = \frac{\hat{T}_k}{\hat{T}_{Lk}} = \frac{1}{\sqrt{\left(1-\omega_k^2\frac{J}{(p/2)\cdot S}\right)^2 + \left(\omega_k\frac{D}{S}\right)^2}} \qquad \text{(E6.9-37)}$$

with

$$\tan(\varepsilon) = \frac{\omega_k\frac{D}{S}}{1-\omega_k^2\frac{J}{(p/2)\cdot S}}. \qquad \text{(E6.9-38)}$$

The inertia is now

$$J = \frac{(p/2)\cdot S}{\omega_k^2}\left[1 \mp \sqrt{\left(\frac{\hat{T}_{Lk}}{\hat{T}_k}\right)^2 - \left(\omega_k\cdot\frac{D}{S}\right)^2}\right] \qquad \text{(E6.9-39)}$$

with

$$\omega_k = \omega_{ms} = \frac{\omega_s}{(p/2)},\ \hat{T}_{Lk} = \hat{T}_{L1} = 31.04\,\text{kNm},$$
$$\hat{T}_k = \hat{T}_1 = 0.04\cdot 265.53\,\text{kNm} = 10.62\,\text{kNm},$$

one obtains with D and S defined above

$$J = 43.66\cdot 10^3\ \text{kgm}^2 \approx 44\cdot 10^3\ \text{kgm}^2, \qquad \text{(E6.9-40)}$$

***Conclusion.*** Damping does not significantly influence the calculation of the required axial moment of inertia!

e) Comparison of the eigen frequency $f_{eigen}$ with the pulsation frequencies occurring at the eccentric shaft.

The angular eigen (resonance) frequency of the undamped oscillation is

$$\omega_{eigen} = \sqrt{\frac{S(p/2)}{J}} = 13.62\ \text{rad/s}$$

or the eigen frequency is

$$f_{eigen} = \frac{\omega_{eigen}}{2\pi} = 2.17\frac{1}{s}.$$

The first harmonic pulsation (given by the load) frequency of the eccentric shaft is

$$\omega_1 = \omega_{ms} = \frac{\omega_s}{(p/2)} = \frac{2\pi 60}{14} = 26.93\frac{1}{s}. \qquad \text{(E6.9-41)}$$

The ratio between first harmonic pulsation frequency and resonance frequency is

$$\frac{\omega_1}{\omega_{eigen}} = \frac{f_1}{f_{eigen}} = 1.98 \approx 2.0. \qquad \text{(E6.9-42)}$$

The fourth harmonic pulsation (given by the load) frequency of the eccentric shaft is

$$\omega_4 = 4\cdot\omega_{ms} = 4\cdot\omega_1. \qquad \text{(E6.9-43)}$$

The ratio between fourth harmonic pulsation frequency and resonance frequency is

$$\frac{\omega_4}{\omega_{eigen}} = \frac{f_4}{f_{eigen}} = 4\cdot 1.98 \approx 8.0. \qquad \text{(E6.9-44)}$$

Note that from a dynamic performance point of view it is desirable if

$$\frac{\omega_k}{\omega_{eigen}} \geq 3-4. \qquad \text{(E6.9-45)}$$

As can be seen the ratio $\omega_1/\omega_{eigen} = 1.98 \approx 2.0$ does not satisfy this condition and therefore the calculated axial moment of inertia of $44\cdot 10^3\ \text{kgm}^2$ is not large enough. It is recommended to select a desirable axial moment of inertia of $J_{desirable}$ that is larger than $44\times 10^3\ \text{kgm}^2$ and results in $\omega_1/\omega_{eigen} \approx 3.0$.

f) List the total motor torque T(t) as a function of time (neglecting damping) for one revolution of the eccentric shaft and compare it with the load torque $T_L(t)$. Why are they different?

The total motor torque is now

$$\tilde{T} = \tilde{T}_{avg} + \tilde{T} + \tilde{T} \qquad \text{(E6.9-46)}$$

where

$$\bar{T}_{avg} = 265.53\,\text{kNm} \qquad \text{(E6.9-47)}$$

and the motor torque for the kth harmonic is

$$\bar{T}_k = \frac{\bar{T}_{Lk}}{1-\left(\frac{\omega_k^2}{\omega_{eigen}^2}\right)}. \qquad \text{(E6.9-48)}$$

For the first harmonic load torque one obtains

$$\begin{aligned} T_{L1}(t) &= 31.04\,\text{kNm}\,\sin(\omega_{ms}t - \pi) \\ &= -31.04\,\text{kNm}\,\sin(\omega_{ms}t) \end{aligned} \qquad \text{(E6.9-49)}$$

and the first harmonic motor torque becomes

$$T_1(t) = \frac{-31.04\,\text{kNm}}{1-\left(\frac{\omega_1^2}{\omega_{eigen}^2}\right)}\sin\omega_{ms}t = 10.35\,\text{kNm}\,\sin(\omega_{ms}t). \qquad \text{(E6.9-50)}$$

For the fourth harmonic motor torque one gets

$$\begin{aligned} T_4(t) &= \frac{50.65\,\text{kNm}}{1-\left(\frac{\omega_1^2}{\omega_{eigen}^2}\right)}\sin\left(\omega_{ms}t - \frac{\pi}{6}\right) \qquad \text{(E6.9-51)} \\ &= -0.804\,\text{kNm}\,\sin\left(\omega_{ms}t - \frac{\pi}{6}\right). \end{aligned}$$

***Conclusions.*** The total load torque is

$$\begin{aligned} T_L(t) = {} & 265.53\,\text{kNm} + 31.04\,\text{kNm}\,\sin(\omega_{ms}t - \pi) + \\ & 50.6\,\text{kNm}\,\sin(4\omega_{ms} - \pi/6) \end{aligned} \qquad \text{(E6.9-52)}$$

and the total motor torque becomes

$$\begin{aligned} T(t) = {} & 265.53\,\text{kNm} + 10.35\,\text{kNm}\,\sin(\omega_{ms}t) \\ & - 0.804\,\text{kNm}\,\sin\left(\omega_{ms}t - \frac{\pi}{6}\right). \end{aligned} \qquad \text{(E6.9-53)}$$

The difference in the harmonic torques is provided by the flywheel with inertia of $J = 44 \cdot 10^3\ \text{kgm}^2$.

### 6.14.10 Application Example 6.10: Temperature-Rise Equations for a Totally Enclosed Fan-Cooled 100 hp Motor: Solution

From Fig. E6.10.1 one notes that the stator ohmic loss generates a temperature drop across the slot insulation ($\Delta T_i$). The temperature drop across the stator back iron or yoke ($\Delta T_{y1}$) is produced by the sum of the stator and rotor ohmic losses, stator teeth

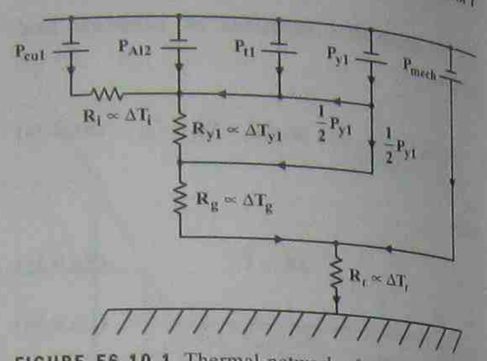



**FIGURE E6.10.1** Thermal network of a totally enclosed fan-cooled induction motor

loss, and half of the stator back iron loss. The calculation of $\Delta T_{y1}$ is based on half of the stator back iron loss because this loss is assumed to be generated uniformly throughout the stator back iron; therefore, the stator back iron loss generated radially through the stator back iron varies from zero to $P_{y1}$ from the inner to the outer surfaces of the stator back iron, respectively. The temperature drop across the small air gap between stator back iron and the frame ($\Delta T_\delta$) is produced by the sum of the ohmic and the iron-core losses of the motor. Finally, the total losses cause a temperature drop from the motor frame to the moving air ($\Delta T_f$).

The temperature difference between the stator winding and the iron core (across the stator winding insulation) is

$$\Delta T_i = P_{cu1}\frac{\beta_i}{\lambda_i \cdot S_i}, \qquad \text{(E6.10-2)}$$

where

$\beta_i$ is the thickness of stator slot insulation
$\lambda_i$ is the thermal conductivity (W/m°C) of stator slot insulation
$S_i$ is the total surface area of (all) stator slots

The temperature drop across the stator back iron can be expressed as

$$\Delta T_{y1} = \left(P_{cu1} + \frac{1}{2}P_{y1} + P_{fl} + P_{sp1} + P_{Al2} + P_{sp2}\right)\frac{h_{y1}}{\lambda_c \cdot S_{y1}}, \qquad \text{(E6.10-3a)}$$

where

$h_{y1}$ is the radial height of stator back iron

$\lambda_c$ is the thermal conductivity (W/m°C) of the stator laminations





$S_{y1}$ is the cross-sectional area of the stator core at the radial middle of the back iron

$P_{sp1}$ is the surface and pulsation loss caused by stator teeth (note that these losses are very small and have been neglected in Fig. E6.10.1)

$P_{sp2}$ is the surface and pulsation loss caused by rotor teeth (note that these losses are very small and have been neglected in Fig. E6.10.1)

The temperature difference across the small air gap between the stator back iron and the frame can be expressed as

$$\Delta T_\delta = \left(P_{cu1} + P_{y1} + P_{fl} + P_{sp1} + P_{Al2} + P_{sp2}\right)\frac{\beta_\delta}{\lambda_\delta \cdot S_\delta}, \qquad \text{(E6.10-3b)}$$

where

$\beta_\delta$ is the air gap length between stator back iron and frame

$\lambda_\delta$ is the thermal conductivity (W/m°C) of the airgap

$S_\delta$ is the outside surface of stator core

$P_{sp1}$ is the surface and pulsation loss caused by stator teeth (note that these losses are very small and have been neglected in Fig. E6.10.1)

$P_{sp2}$ is the surface and pulsation loss caused by rotor teeth (note that these losses are very small and have been neglected in Fig. E6.10.1)

The heat of the motor is dissipated to the air at ambient temperature through the end bells of the motor frame to the stationary air, and through the cylindrical frame surface containing the cooling ribs (which increase the frame surface) to the moving air. The temperature difference between the outer surface of the frame and the ambient temperature is

$$\Delta T_f = \frac{\sum P}{\alpha_o S_o + \alpha_v S_v} \qquad \text{(E6.10-4)}$$

where

$\Sigma P$ represents total losses of the motor

$\alpha_o$ is the surface thermal coefficient (W/m²°C) for dissipating the heat from the surface of the frame to the stationary air (near end bells)

$\alpha_v$ is the surface thermal coefficient (W/m²°C) for dissipating the heat from the surface of the frame to the moving air (near cylindrical frame)

$S_o$ is the surface area in contact with stationary air

$S_v$ is the surface area in contact with moving air

The relation between $\alpha_o$ and $\alpha_v$ is given by

$$\alpha_v = \alpha_o(1 + k_v\sqrt{v}) \qquad \text{(E6.10-5)}$$

where

$k_v$ is a coefficient, and $v$ is the air velocity (m/s)

### 6.14.11 Application Example 6.11: Temperature-Rise Equations for a Drip-Proof 5 hp Motor: Solution

From the thermal network of Fig. E6.11.1 one obtains for the temperature drop across the stator winding insulation

$$\Delta T_i = P_{em}\frac{\beta_i}{\lambda_i \cdot S_i}, \qquad \text{(E6.11-1)}$$

and the temperature drop across the stator back iron is

$$\Delta T_{y1} = \left(P_{em} + \frac{1}{2}P_{y1} + P_{fl} + P_{sp1} + P_b + P_{sp2}\right)\frac{h_{y1}}{\lambda_c \cdot S_{y1}}, \qquad \text{(E6.11-2)}$$

where $P_b$ are the ohmic losses in the rotor bars.

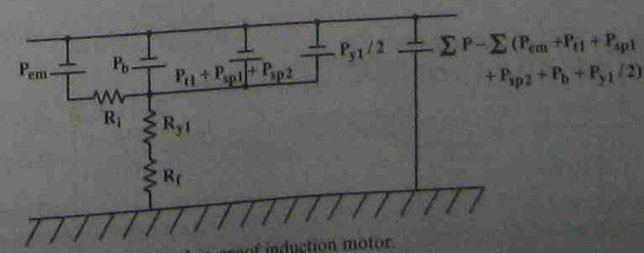



**FIGURE E6.11.1** Thermal network of a drip-proof induction motor.

Finally, the temperature drop from the motor frame to the ambient temperature is

$$\Delta T_f = \frac{\left(P_{em} + P_h + P_{f1} + P_{sp1} + P_{sp2} + \frac{1}{2}P_{y1}\right)}{\alpha_o \pi (D + 2h_1 + 2h_{y1} + 2h_f)(L + L_e)} \quad \text{(E6.11-3)}$$

where

$h_t$ is the radial height of stator tooth

$h_f$ is the radial thickness of stator frame

$h_{y1}$ is the radial height of stator back iron

$L$ is the embedded (cylindrical) length of stator winding

$L_e$ is the length of the two stator end windings

The temperature rise of the stator winding is therefore

$$\Delta T = \Delta T_i + \Delta T_{y1} + \Delta T_f. \quad \text{(E6.11-4)}$$

## CHAPTER 7 SOLUTIONS

### 7.2.3.1 Application Example 7.7: Jacobian Matrices: Solution

Given

$$\begin{bmatrix} 1 & 0 \\ l_{21} & 1 \end{bmatrix}\begin{bmatrix} u_{11} & u_{12} \\ 0 & u_{22} \end{bmatrix} = \begin{bmatrix} J_{11} & J_{12} \\ J_{21} & J_{22} \end{bmatrix}. \quad \text{(E7.7-1)}$$

Find $u_{11}$, $u_{12}$, $u_{22}$ and $l_{21}$.

$$\begin{aligned} J_{11} &= u_{11} && \text{or} \quad u_{11} = J_{11} \\ J_{12} &= u_{12} && \text{or} \quad u_{12} = J_{12} \\ J_{21} &= l_{21}u_{11} && \text{or} \quad l_{21} = J_{21}/u_{11} \\ J_{22} &= l_{21}u_{12} + u_{22} && \text{or} \quad u_{22} = J_{22} - l_{21}u_{12} \end{aligned}$$

In general:

$$\begin{aligned} u_{11} &= J_{11} \\ u_{12} &= J_{12} \\ &\cdots\cdots \\ u_{1c} &= J_{1c} \\ &\cdots\cdots \\ u_{1n} &= J_{1n} \end{aligned}$$

Since the first row of the table of factors is row 1 of $\bar{U}$, the first row of the table of factors is simply row 1 of $\bar{J}$.

In row 2 of $\bar{J}$:

$$\begin{aligned} l_{21}u_{11} &= J_{21} \\ l_{21}u_{12} + u_{22} &= J_{22} \\ l_{21}u_{13} + u_{23} &= J_{23} \\ &\cdots\cdots \end{aligned}$$



These equations yield $l_{21}$, $u_{22}$, $u_{23}$, $u_{24}$, ...

$$\begin{aligned} l_{21} &= J_{21}/u_{11} \\ u_{22} &= J_{22} - l_{21}u_{12} \\ u_{23} &= J_{23} - l_{21}u_{13} \\ &\cdots\cdots \end{aligned}$$

Thus in the expansion of row 2 of $\bar{J}$, one $l$ and $(n-1)$ $u$'s are formed. The generalization for the expansion of row r of $\bar{J}$ is straightforward:

$$l_{rc} = \frac{J_{rc} - \sum_{q=1}^{c-1} l_{rq}u_{qc}}{u_{cc}}, \quad \text{for } c = 1, 2, \ldots, (r-1) \quad \text{(E7.7-2)}$$

$$u_{rc} = J_{rc} - \sum_{q=1}^{r-1} l_{rq}u_{qc}, \quad \text{for } c = r, r+1, \ldots, n. \quad \text{(E7.7-3)}$$

The rules for the formation of the table of factors *in situ* are as follows:

1) Row 1 of $\bar{J}$ is not modified.
2) Row 2 of $\bar{J}$ is modified to yield one $l$ and $(n-1)$ $u$'s. These entries are found using the above two equations for $l_{rc}$ and $u_{rc}$. For these equations, when the summation upper index is zero, there are no terms in the sum (e.g., ignore the summation term). When the upper and lower indices of summation are the same, there is a single term in the sum.
3) Rule 2 is repeated for each row and $\bar{J}$ is replaced by the table of factors. In row r, there will be $(r-1)$ $l$-terms calculated and $(n-r+1)$ $u$-terms. The above equations for $l_{rc}$ and $u_{rc}$ are used.

### 7.3.5 Application Example 7.8: Computation of Fundamental Admittance Matrix: Solution

For this example $y_{14} = -\tilde{y}_{14}$, where $\tilde{y}_{14}$ is the admittance between bus 1 and bus 4 and $y_{14}$ is an entry of the bus admittance matrix $Y_{bus}$. Note the minus sign.

$$y_{14} = -\tilde{y}_{14} = \frac{-1}{0.01 + j0.02} = \frac{-1}{0.02236\angle 1.1071\text{rad}}$$
$$= \frac{1\angle \pm 3.1415\text{rad}}{0.02236\angle 1.1071\text{rad}} = 44.72\text{pu}\angle 2.034\text{rad}$$

$$y_{12} = -\tilde{y}_{12} = \frac{-1}{0.01 + j0.01} = \frac{-1}{0.01414\angle 0.7854}$$
$$= \frac{1\angle \pm 3.1415\text{rad}}{0.01414\angle 0.7854} = 70.72\text{pu}\angle 2.356\text{rad}$$

$$y_{11} = -\{y_{14} + y_{12}\} = -\{44.72\cos(2.034) + 70.72\cos(2.356) + j[44.72\sin(2.034) + 70.72\sin(2.356)]\} = -\{-19.98 - 49.997 + j[40.008 + 50.02]\} = (69.98 - j90.03) = 114.03\text{pu}\angle -0.910\text{rad}$$





$y_{13} = -\tilde{y}_{13} = 0$ (because there is no direct line between buses 1 and 3)

$$y_{23} = -\tilde{y}_{23} = \frac{-1}{0.02 + j0.08} = \frac{1\angle \pm 3.1415\text{rad}}{0.082462\angle 1.3258\text{rad}}$$
$$= 12.127\text{pu}\angle 1.816\text{rad}$$

$$y_{34} = -\tilde{y}_{34} = \frac{-1}{0.01 + j0.02} = \frac{1\angle \pm 3.1415\text{rad}}{0.02236\angle 1.1071\text{rad}}$$
$$= 44.72\text{pu}\angle 2.034\text{rad}$$

$$y_{22} = -(y_{12} + y_{23}) = -\{70.72\cos(2.356) + 12.127\cos(1.816) + j(70.72\sin(2.356) + 12.127\sin(1.816))\} = -\{-49.997 - 2.994 + j(50.102 + 11.764)\} = -\{-52.941 + j61.862\} = 81.42\text{pu}\angle -0.863\text{rad}$$

$$y_{33} = -(y_{23} + y_{34}) = -\{12.127\cos(1.816) + 44.72\cos(2.034) + j[12.127\sin(1.8161) + 44.72\sin(2.034)]\} = -\{-2.944 - 19.982 + j(11.764 + 40.008)\} = -\{-22.93 + j51.772\} = 56.62\text{pu}\angle -1.154$$

$$y_{44} = -(y_{14} + y_{34}) = -\{44.72\cos(2.034) + 44.72\cos(2.034) + j(44.72\sin(2.034) + 44.72\sin(2.034))\} = -\{-19.982 - 19.982 + j(40.008 + 40.008)\} = \{-39.964 + j80.016\} = 89.44\text{pu}\angle -1.1076\text{rad}.$$

The bus admittance matrix is now

$$\bar{Y}_{bus} = \begin{bmatrix} 114.03\text{pu}\angle -0.910\text{rad} & 70.72\text{pu}\angle 2.356\text{rad} & 0 & 44.72\text{pu}\angle 2.034\text{rad} \\ 70.72\text{pu}\angle 2.356\text{rad} & 81.42\text{pu}\angle -0.863\text{rad} & 12.127\text{pu}\angle 1.816\text{rad} & 0 \\ 0 & 12.127\text{pu}\angle 1.816\text{rad} & 56.62\text{pu}\angle -1.154\text{rad} & 44.72\text{pu}\angle 2.034\text{rad} \\ 44.72\text{pu}\angle 2.034\text{rad} & 0 & 44.72\text{pu}\angle 2.034\text{rad} & 89.44\text{pu}\angle -1.1076\text{rad} \end{bmatrix}.$$

Note that $\bar{Y}_{bus}$ is singular; that is, $\bar{Y}_{bus}^{-1}$ cannot be found, because there is no admittance connected to the ground bus. This is unimportant for the Newton-Raphson approach because for forming of the Jacobian the entries of $\bar{Y}_{bus}$ are used and $\bar{Y}_{bus}$ is not inverted.

### 7.3.6 Application Example 7.9: Evaluation of Fundamental Mismatch Vector: Solution

$$\Delta\bar{W}^0 = (P_2 + F_{r,2}, Q_2 + F_{i,2}, P_3 + F_{r,3}, Q_3 + F_{i,3}, P_4 + F_{r,4}, Q_4 + F_{i,4})^t$$

$$\Delta P_2 = P_2 + F_{r,2} = P_2 + \sum_{j=1}^{4} y_{2j}V_jV_2\cos(-\theta_{2j} - \delta_j + \delta_2)$$
$$= P_2 + y_{21}V_1V_2\cos(-\theta_{21} - \delta_1 + \delta_2) + y_{22}V_2V_2\cos(-\theta_{22} - \delta_2 + \delta_2) + y_{23}V_3V_2\cos(-\theta_{23} - \delta_3 + \delta_2) + y_{24}V_4V_2\cos(-\theta_{24} - \delta_4 + \delta_2)$$

$$\Delta P_2 = P_2 + F_{r,2} = 0.10 + \{70.72 \cdot 1 \cdot 1 \cdot \cos(-2.356 - 0 + 0) + 81.42 \cdot 1 \cdot 1 \cdot \cos(0.863 - 0 + 0) + 12.127 \cdot 1 \cdot 1 \cdot \cos(-1.816 - 0 + 0) + 0\} = 0.10 - 49.996 + 52.936 - 2.942 = 0.0978$$

$$\Delta Q_2 = Q_2 + F_{i,2} = Q_2 + \sum_{j=1}^{4} y_{2j}V_jV_2\sin(-\theta_{2j} - \delta_j + \delta_2)$$
$$= Q_2 + y_{21}V_1V_2\sin(-\theta_{21} - \delta_1 + \delta_2) + y_{22}V_2V_2\sin(-\theta_{22} - \delta_2 + \delta_2) + y_{23}V_3V_2\sin(-\theta_{23} - \delta_3 + \delta_2) + y_{24}V_4V_2\sin(-\theta_{24} - \delta_4 + \delta_2)$$

$$\Delta Q_2 = Q_2 + F_{i,2} = 0.10 + \{70.72 \cdot 1 \cdot 1 \cdot \sin(-2.356 - 0 + 0) + 81.42 \cdot 1 \cdot 1 \cdot \sin(0.863 - 0 + 0) + 12.127 \cdot 1 \cdot 1 \cdot \sin(-1.816 - 0 + 0) + 0\} = 0.10 - 50.016 + 61.86 - 11.57 = 0.374$$

$$\Delta P_3 = P_3 + F_{r,3} = P_3 + y_{31}V_1V_3\cos(-\theta_{31} - \delta_1 + \delta_3) + y_{32}V_2V_3\cos(-\theta_{32} - \delta_2 + \delta_3) + y_{33}V_3V_3\cos(-\theta_{33} - \delta_3 + \delta_3) + y_{34}V_4V_3\cos(-\theta_{34} - \delta_4 + \delta_3)$$

$$\Delta P_3 = P_3 + F_{r,3} = 0.0 + 0.0 + \{12.127 \cdot 1 \cdot 1 \cdot \cos(-1.816 - 0 + 0) + 56.62 \cdot 1 \cdot 1 \cdot \cos(1.154 - 0 + 0) + 44.72 \cdot 1 \cdot 1 \cdot \cos(-2.034 - 0 + 0)\} = 0.0 + 0.0 - 2.944 + 22.92 - 19.98 = -0.0056$$

$$\Delta Q_3 = Q_3 + F_{i,3} = Q_3 + y_{31}V_1V_3\sin(-\theta_{31} - \delta_1 + \delta_3) + y_{32}V_2V_3\sin(-\theta_{32} - \delta_2 + \delta_3) + y_{33}V_3V_3\sin(-\theta_{33} - \delta_3 + \delta_3) + y_{34}V_4V_3\sin(-\theta_{34} - \delta_4 + \delta_3)$$

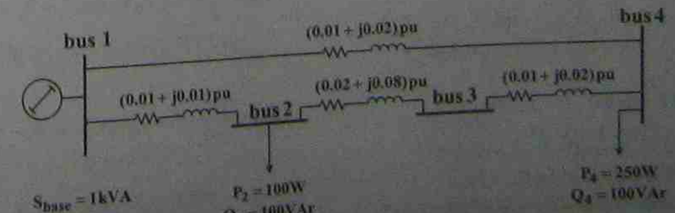



**FIGURE E7.8.1** Four-bus power systems with per unit (pu) line impedances.

$$\Delta Q_3 = Q_3 + F_{i,3} = 0.0 + 0.0 + \{12.127 \cdot 1 \cdot 1 \cdot \sin(-1.816 - 0 + 0) + 56.62 \cdot 1 \cdot 1 \cdot \sin(1.154 - 0 + 0) + 44.72 \cdot 1 \cdot 1 \cdot \sin(-2.034 - 0 + 0)\} = 0.0 + 0.0 - 11.764 + 51.77 - 40.008 = -0.00166$$

$$\Delta P_4 = P_4 + F_{r,4} = P_4 + y_{41}V_1V_4\cos(-\theta_{41} - \delta_1 + \delta_4) + y_{42}V_2V_4\cos(-\theta_{42} - \delta_2 + \delta_4) + y_{43}V_3V_4\cos(-\theta_{43} - \delta_3 + \delta_4) + y_{44}V_4V_4\cos(-\theta_{44} - \delta_4 + \delta_4)$$

$$\Delta P_4 = P_4 + F_{r,4} = 0.25 + \{44.72 \cdot 1 \cdot 1 \cdot \cos(-2.034 - 0 + 0) + 0 + 44.72 \cdot 1 \cdot 1 \cdot \cos(-2.034 - 0 + 0) + 89.44 \cdot 1 \cdot 1 \cdot \cos(1.1076 - 0 + 0)\} = 0.25 - 19.98 + 0 - 19.98 + 39.96 = 0.2527$$

$$\Delta Q_4 = Q_4 + F_{i,4} = Q_4 + y_{41}V_1V_4\sin(-\theta_{41} - \delta_1 + \delta_4) + y_{42}V_2V_4\sin(-\theta_{42} - \delta_2 + \delta_4) + y_{43}V_3V_4\sin(-\theta_{43} - \delta_3 + \delta_4) + y_{44}V_4V_4\sin(-\theta_{44} - \delta_4 + \delta_4)$$

$$\Delta Q_4 = Q_4 + F_{i,4} = 0.1 + \{44.72 \cdot 1 \cdot 1 \cdot \sin(-2.034 - 0 + 0) + 0 + 44.72 \cdot 1 \cdot 1 \cdot \sin(-2.034 - 0 + 0) + 89.44 \cdot 1 \cdot 1 \cdot \sin(1.1076 - 0 + 0) + 0\} = 0.1 - 40.0076 + 0 - 40.0076 + 80.016 = 0.1004.$$

The mismatch power vector is now

$$\Delta\overline{W}^0 = (0.0978,\ 0.374,\ -0.0056,\ -0.00166,\ 0.2527,\ 0.1004)^t.$$

### 7.3.7 Application Example 7.10: Evaluation of Fundamental Jacobian Matrix: Solution

$$J_{11} = \frac{\partial \Delta P_2}{\partial \delta_2} = -\sum_{\substack{j=1 \\ \neq 2}}^{4} y_{2j}V_2V_j\sin(\delta_2 - \delta_j - \theta_{2j})$$
$$= -y_{21}V_2V_1\sin(\delta_2 - \delta_1 - \theta_{21}) - y_{23}V_2V_3\sin(\delta_2 - \delta_3 - \theta_{23}) - y_{24}V_2V_4\sin(\delta_2 - \delta_4 - \theta_{24})$$

$$J_{11} = \frac{\partial \Delta P_2}{\partial \delta_2} = -70.72 \cdot 1 \cdot 1 \cdot \sin(0 - 0 - 2.356) - 12.127 \cdot 1 \cdot 1 \cdot \sin(0 - 0 - 1.816) - 0 = 61.68$$

$$J_{12} = \frac{\partial \Delta P_2}{\partial V_2} = \sum_{\substack{j=1 \\ \neq 2}}^{4} y_{2j}V_j\cos(\delta_2 - \delta_j - \theta_{2j}) + 2y_{22}V_2\cos(-\theta_{22})$$
$$= y_{21}V_1\cos(\delta_2 - \delta_1 - \theta_{21}) + y_{23}V_3\cos(\delta_2 - \delta_3 - \theta_{23}) + y_{24}V_4\cos(\delta_2 - \delta_4 - \theta_{24}) + 2V_2y_{22}\cos(-\theta_{22})$$

$$J_{12} = \frac{\partial \Delta P_2}{\partial V_2} = 70.72 \cdot 1 \cdot \cos(0 - 0 - 2.356) + 12.127 \cdot 1 \cdot \cos(0 - 0 - 1.816) + 0 + 2 \cdot 1 \cdot 81.42\cos(0.863) = -49.996 - 2.944 + 0 + 105.872 = 52.932$$



$$J_{13} = \frac{\partial \Delta P_2}{\partial \delta_3} = y_{23}V_1V_3\sin(\delta_2 - \delta_3 - \theta_{23}) = 12.127 \cdot 1 \cdot 1 \cdot \sin(0 - 0 - 1.816) = -11.764$$

$$J_{14} = \frac{\partial \Delta P_2}{\partial V_3} = y_{23}V_2\cos(\delta_2 - \delta_3 - \theta_{23}) = 12.127 \cdot 1 \cdot \cos(0 - 0 - 1.816) = -2.944$$

$$J_{15} = \frac{\partial \Delta P_2}{\partial \delta_4} = y_{24}V_1V_5\sin(\delta_2 - \delta_5 - \theta_{25}) = 0$$

$$J_{16} = \frac{\partial \Delta P_2}{\partial V_4} = y_{24}V_2\cos(\delta_2 - \delta_4 - \theta_{24}) = 0$$

$$J_{21} = \frac{\partial \Delta Q_2}{\partial \delta_2} = \sum_{\substack{j=1 \\ \neq 2}}^{4} y_{2j}V_2V_j\cos(\delta_2 - \delta_j - \theta_{2j})$$
$$= y_{21}V_2V_1\cos(\delta_2 - \delta_1 - \theta_{21}) + y_{23}V_2V_3\cos(\delta_2 - \delta_3 - \theta_{23}) + y_{24}V_2V_4\cos(\delta_2 - \delta_4 - \theta_{24})$$

$$J_{21} = \frac{\partial \Delta Q_2}{\partial \delta_2} = 70.72 \cdot 1 \cdot 1 \cdot \cos(0 - 0 - 2.3560) + 12.127 \cdot 1 \cdot 1 \cdot \cos(0 - 0 - 1.816) + 0 = -49.996 - 2.944 + 0 = -52.94$$

$$J_{22} = \frac{\partial \Delta Q_2}{\partial V_2} = \sum_{\substack{j=1 \\ \neq 2}}^{4} y_{2j}V_j\sin(\delta_2 - \delta_j - \theta_{2j}) + 2V_2y_{22}\sin(-\theta_{22})$$
$$= y_{21}V_1\sin(\delta_2 - \delta_1 - \theta_{21}) + y_{23}V_3\sin(\delta_2 - \delta_3 - \theta_{23}) + y_{24}V_4\sin(\delta_2 - \delta_4 - \theta_{24}) + 2V_2y_{22}\sin(-\theta_{22})$$

$$J_{22} = \frac{\partial \Delta Q_2}{\partial V_2} = 70.72 \cdot 1 \cdot \sin(0 - 0 - 2.356) + 12.127 \cdot 1 \cdot \sin(0 - 0 - 1.816) + 0 + 2 \cdot 1 \cdot 81.42\sin(0.863) = -50.016 - 11.764 + 0 + 123.725 = 61.945$$

$$J_{23} = \frac{\partial \Delta Q_2}{\partial \delta_3} = -y_{23}V_2V_3\cos(\delta_2 - \delta_3 - \theta_{23}) = -12.127 \cdot 1 \cdot 1 \cdot \cos(0 - 0 - 1.816) = 2.944$$

$$J_{24} = \frac{\partial \Delta Q_2}{\partial V_3} = y_{23}V_2\sin(\delta_2 - \delta_3 - \theta_{23}) = 12.127 \cdot 1 \cdot \sin(0 - 0 - 1.816) = -11.764$$

$$J_{25} = \frac{\partial \Delta Q_2}{\partial \delta_4} = -y_{24}V_2V_4\cos(\delta_2 - \delta_4 - \theta_{24}) = 0$$

$$J_{26} = \frac{\partial \Delta Q_2}{\partial V_4} = y_{24}V_2\sin(\delta_2 - \delta_4 - \theta_{24}) = 0$$





$$J_{31} = \frac{\partial \Delta P_3}{\partial \delta_2} = y_{32}V_3V_2\sin(\delta_3 - \delta_2 - \theta_{32}) = 12.127 \cdot 1 \cdot 1 \cdot \sin(0 - 0 - 1.816) = -11.764$$

$$J_{32} = \frac{\partial \Delta P_3}{\partial V_2} = y_{32}V_3\cos(\delta_3 - \delta_2 - \theta_{32}) = 12.127 \cdot 1 \cdot \cos(0 - 0 - 1.816) = -2.944$$

$$J_{33} = \frac{\partial \Delta P_3}{\partial \delta_3} = -\sum_{\substack{j=1 \\ \neq 3}}^{4} y_{3j}V_3V_j\sin(\delta_3 - \delta_j - \theta_{3j})$$

$$J_{33} = \frac{\partial \Delta P_3}{\partial \delta_3} = -y_{31}V_3V_1\sin(\delta_3 - \delta_1 - \theta_{31}) - y_{32}V_3V_2\sin(\delta_3 - \delta_2 - \theta_{32}) - y_{34}V_3V_4\sin(\delta_3 - \delta_4 - \theta_{34}) = 0 - 12.127 \cdot 1 \cdot 1 \cdot \sin(0 - 0 - 1.816) - 44.72 \cdot 1 \cdot 1 \cdot \sin(0 - 0 - 2.034) = 51.772$$

$$J_{34} = \frac{\partial \Delta P_3}{\partial V_3} = \sum_{\substack{j=1 \\ \neq 3}}^{4} y_{3j}V_j\cos(\delta_3 - \delta_j - \theta_{3j}) + 2V_3y_{33}\cos(-\theta_{33})$$
$$= y_{31}V_1\cos(\delta_3 - \delta_1 - \theta_{31}) + y_{32}V_2\cos(\delta_3 - \delta_2 - \theta_{32}) + y_{34}V_4\cos(\delta_3 - \delta_4 - \theta_{34}) + 2V_3y_{33}\cos(-\theta_{33})$$

$$= 0 + 12.127 \cdot 1 \cdot \cos(0 - 0 - 1.816) + 44.72 \cdot 1 \cdot \cos(0 - 0 - 2.034) + 2 \cdot 1 \cdot 56.62\cos(1.154) = 0 - 2.944 - 19.982 + 45.843 = 22.917$$

$$J_{35} = \frac{\partial \Delta P_3}{\partial \delta_4} = y_{34}V_3V_4\sin(\delta_3 - \delta_4 - \theta_{34}) = 44.72 \cdot 1 \cdot 1 \cdot \sin(0 - 0 - 2.034) = -40.0076$$

$$J_{36} = \frac{\partial \Delta P_3}{\partial V_4} = y_{34}V_3V_4\cos(\delta_3 - \delta_4 - \theta_{34}) = 44.72 \cdot 1 \cdot 1 \cdot \cos(0 - 0 - 2.034) = -19.98$$

$$J_{41} = \frac{\partial \Delta Q_3}{\partial \delta_2} = -y_{32}V_3V_2\cos(\delta_3 - \delta_2 - \theta_{32}) = -12.127 \cdot 1 \cdot 1 \cdot \cos(0 - 0 - 1.816) = 2.944$$

$$J_{42} = \frac{\partial \Delta Q_3}{\partial V_2} = y_{32}V_3\sin(\delta_3 - \delta_2 - \theta_{32}) = 12.127 \cdot 1 \cdot \sin(0 - 0 - 1.816) = -11.764$$

$$J_{43} = \frac{\partial \Delta Q_3}{\partial \delta_3} = \sum_{\substack{j=1 \\ \neq 3}}^{4} y_{3j}V_3V_j\cos(\delta_3 - \delta_j - \theta_{3j})$$

$$J_{43} = \frac{\partial \Delta Q_3}{\partial \delta_3} = y_{31}V_3V_1\cos(\delta_3 - \delta_1 - \theta_{31}) + y_{32}V_3V_2\cos(\delta_3 - \delta_2 - \theta_{32}) + y_{34}V_3V_4\cos(\delta_3 - \delta_4 - \theta_{34})$$

$$J_{43} = \frac{\partial \Delta Q_3}{\partial \delta_3} = 0 + 12.127 \cdot 1 \cdot 1 \cdot \cos(0 - 0 - 1.816) + 44.72 \cdot 1 \cdot 1 \cdot \cos(0 - 0 - 2.034) = -2.944 - 19.982 = -22.926$$

$$J_{44} = \frac{\partial \Delta Q_3}{\partial V_3} = \sum_{\substack{j=1 \\ \neq 3}}^{4} y_{3j}V_j\sin(\delta_3 - \delta_j - \theta_{3j}) + 2V_3y_{33}\sin(-\theta_{33})$$
$$= y_{31}V_1\sin(\delta_3 - \delta_1 - \theta_{31}) + y_{32}V_2\sin(\delta_3 - \delta_2 - \theta_{32}) + y_{34}V_4\sin(\delta_3 - \delta_4 - \theta_{34}) + 2V_3y_{33}\sin(-\theta_{33})$$

$$J_{44} = \frac{\partial \Delta Q_3}{\partial V_3} = 0 + 12.127 \cdot 1 \cdot \sin(0 - 0 - 1.816) + 44.72 \cdot 1 \cdot \sin(0 - 0 - 2.034) + 2 \cdot 1 \cdot 56.62\sin(1.154) = -11.764 - 40.0076 + 103.546 = 51.773$$

$$J_{45} = \frac{\partial \Delta Q_3}{\partial \delta_4} = -y_{34}V_3V_4\cos(\delta_3 - \delta_4 - \theta_{34}) = -44.72 \cdot 1 \cdot 1 \cdot \cos(0 - 0 - 2.034) = 19.982$$

$$J_{46} = \frac{\partial \Delta Q_3}{\partial V_4} = y_{34}V_3\sin(\delta_3 - \delta_4 - \theta_{34}) = 44.72 \cdot 1 \cdot \sin(0 - 0 - 2.034) = -40.0076$$

$$J_{51} = \frac{\partial \Delta P_4}{\partial \delta_2} = y_{42}V_4V_2\sin(\delta_4 - \delta_2 - \theta_{42}) = 0$$

$$J_{52} = \frac{\partial \Delta P_4}{\partial V_2} = y_{42}V_4\cos(\delta_4 - \delta_2 - \theta_{42}) = 0$$

$$J_{53} = \frac{\partial \Delta P_4}{\partial \delta_3} = y_{43}V_4V_3\sin(\delta_4 - \delta_2 - \theta_{43}) = 44.72 \cdot 1 \cdot 1 \cdot \sin(0 - 0 - 2.034) = -40.0076$$

$$J_{54} = \frac{\partial \Delta P_4}{\partial V_3} = y_{43}V_4\cos(\delta_4 - \delta_2 - \theta_{43}) = 44.72 \cdot 1 \cdot \cos(0 - 0 - 2.034) = -19.982$$

$$J_{55} = \frac{\partial \Delta P_4}{\partial \delta_4} = -\sum_{\substack{j=1 \\ \neq 4}}^{4} y_{4j}V_4V_j\sin(\delta_4 - \delta_j - \theta_{4j})$$
$$= -y_{41}V_4V_1\sin(\delta_4 - \delta_1 - \theta_{41}) - y_{42}V_4V_2\sin(\delta_4 - \delta_2 - \theta_{42}) - y_{43}V_4V_3\sin(\delta_4 - \delta_3 - \theta_{43})$$

$$J_{55} = \frac{\partial \Delta P_4}{\partial \delta_4} = -44.72 \cdot 1 \cdot 1 \cdot \sin(0 - 0 - 2.034) - 0 - 44.72 \cdot 1 \cdot 1 \cdot \sin(0 - 0 - 2.034) = 40.0076 - 0 + 40.0076 = 80.015$$

$$J_{56}=\frac{\partial\Delta P_4}{\partial V_4}=-\sum_{\substack{j=1\\ \neq 4}}^{4} y_{4j}V_j\cos(\delta_4-\delta_j-\theta_{4j})$$
$$+2V_4y_{44}\cos(-\theta_{44})$$

$$J_{56}=\frac{\partial\Delta P_4}{\partial V_4}=y_{41}V_1\cos(\delta_4-\delta_1-\theta_{41})$$
$$+y_{42}V_2\cos(\delta_4-\delta_2-\theta_{42})$$
$$+y_{43}V_3\cos(\delta_4-\delta_3-\theta_{43})$$
$$+2V_4y_{44}\cos(-\theta_{44})$$

$$J_{56}=\frac{\partial\Delta P_4}{\partial V_4}=44.72\cdot1\cdot\cos(0-0-2.034)+0$$
$$+44.72\cdot1\cdot\cos(0-0-2.034)$$
$$+2\cdot1\cdot89.44\cos(1.1076)$$

$$J_{56}=\frac{\partial\Delta P_4}{\partial V_4}=-19.982-19.982+79.925=39.961$$

$$J_{61}=\frac{\partial\Delta Q_4}{\partial\delta_2}=-y_{42}V_4V_2\cos(\delta_4-\delta_2-\theta_{42})=0$$

$$J_{62}=\frac{\partial\Delta Q_4}{\partial V_2}=y_{42}V_4\sin(\delta_4-\delta_2-\theta_{42})=0$$

$$J_{63}=\frac{\partial\Delta Q_4}{\partial\delta_3}=-y_{43}V_4V_3\cos(\delta_4-\delta_3-\theta_{43})$$
$$=-44.72\cdot1\cdot1\cdot\cos(0-0-2.034)=19.982$$

$$J_{64}=\frac{\partial\Delta Q_4}{\partial V_3}=y_{43}V_4\sin(\delta_4-\delta_3-\theta_{43})$$
$$=44.72\cdot1\cdot\sin(0-0-2.034)=-40.0076$$

$$J_{65}=\frac{\partial\Delta Q_4}{\partial\delta_4}=\sum_{\substack{j=1\\ \neq 4}}^{4} y_{4j}V_4V_j\cos(\delta_4-\delta_j-\theta_{4j})$$

$$J_{65}=\frac{\partial\Delta Q_4}{\partial\delta_4}=y_{41}V_4V_1\cos(\delta_4-\delta_1-\theta_{41})$$
$$+y_{42}V_4V_2\cos(\delta_4-\delta_2-\theta_{42})$$
$$+y_{43}V_4V_3\cos(\delta_4-\delta_3-\theta_{43})$$

$$J_{65}=\frac{\partial\Delta Q_4}{\partial\delta_4}=44.72\cdot1\cdot1\cdot\cos(0-0-2.034)+0$$
$$+44.72\cdot1\cdot1\cdot\cos(0-0-2.034)$$
$$=-19.982-19.982=-39.963$$

$$J_{66}=\frac{\partial\Delta Q_4}{\partial V_4}=\sum_{\substack{j=1\\ \neq 4}}^{4} y_{4j}V_j\sin(\delta_4-\delta_j-\theta_{4j})$$
$$+2V_4y_{44}\sin(-\theta_{44})$$

$$J_{66}=\frac{\partial\Delta Q_4}{\partial V_4}=y_{41}V_1\sin(\delta_4-\delta_1-\theta_{41})$$
$$+y_{42}V_2\sin(\delta_4-\delta_2-\theta_{42})+y_{43}V_3\sin(\delta_4-\delta_3-\theta_{43})$$
$$+2V_4y_{44}\sin(-\theta_{44})$$

$$J_{66}=\frac{\partial\Delta Q_4}{\partial V_4}=44.72\cdot1\cdot\sin(0-0-2.034)$$
$$+0+44.72\cdot1\cdot\sin(0-0-2.034)$$
$$+2\cdot1\cdot89.44\sin(1.1076)$$

$$J_{66}=\frac{\partial\Delta Q_4}{\partial V_4}=-40.0076-40.0076+160.031=80.$$

The Jacobian matrix is

$$\bar{J}=\begin{bmatrix}J_{11}&J_{12}&J_{13}&J_{14}&J_{15}&J_{16}\\J_{21}&J_{22}&J_{23}&J_{24}&J_{25}&J_{26}\\J_{31}&J_{32}&J_{33}&J_{34}&J_{35}&J_{36}\\J_{41}&J_{42}&J_{43}&J_{44}&J_{45}&J_{46}\\J_{51}&J_{52}&J_{53}&J_{54}&J_{55}&J_{56}\\J_{61}&J_{62}&J_{63}&J_{64}&J_{65}&J_{66}\end{bmatrix}$$

$$\bar{J}^0=\begin{bmatrix}61.68&52.932&-11.764&-2.944&0&0\\-52.94&61.945&2.944&-11.764&0&0\\-11.764&-2.944&51.772&22.917&-40.0076&-19.98\\2.944&-11.764&-22.926&51.773&19.982&-40.0076\\0&0&-40.0076&-19.982&80.015&39.961\\0&0&19.982&-40.0076&-39.963&80\end{bmatrix}.$$

### 7.3.8 Application Example 7.11: Calculation of the Inverse of Jacobian Matrix: Solution

Calculation of the inverse of $\bar{J}^0$, that is. $(\bar{J}^0)^{-1}$.

$$(\bar{J}^0)^{-1}=\frac{\text{Adj}(\bar{J}^0)}{\det(\bar{J}^0)},$$

where $\text{Adj}(\bar{J}^0)$ is the adjoint of matrix $\bar{J}^0$ and $\det(\bar{J}^0)=|\bar{J}^0|$ is the determinant of $\bar{J}^0$.

The adjoint of $\bar{J}^0$ is obtained by first taking the transpose of $\bar{J}^0$, that is, $(\bar{J}^0)^t$, and then replacing each element in the transpose with its cofactor.

$$[(\bar{J}^0)^t]_{ij}=[\bar{J}^0]_{ji}.$$

The transpose of $\bar{J}^0$ is



$$(\bar{J}^0)^t=\begin{bmatrix}J_{11}&J_{21}&J_{31}&J_{41}&J_{51}&J_{61}\\J_{12}&J_{22}&J_{32}&J_{42}&J_{52}&J_{62}\\J_{13}&J_{23}&J_{33}&J_{43}&J_{53}&J_{63}\\J_{14}&J_{24}&J_{34}&J_{44}&J_{54}&J_{64}\\J_{15}&J_{25}&J_{35}&J_{45}&J_{55}&J_{65}\\J_{16}&J_{26}&J_{36}&J_{46}&J_{56}&J_{66}\end{bmatrix}$$

$$(\bar{J}^0)^t=\begin{bmatrix}61.68&-52.94&-11.764&2.944&0&0\\52.932&61.945&-2.944&-11.764&0&0\\-11.764&2.944&51.772&-22.926&-40.0076&-19.982\\-2.944&-11.764&22.917&51.773&-19.982&-40.0076\\0&0&-40.0076&19.982&80.015&-39.963\\0&0&-19.98&-40.0076&39.961&80\end{bmatrix}$$

$$Adj(\bar{J}^0)=\begin{bmatrix}+\text{Adj}(\bar{J}^0)_{11}-\text{Adj}(\bar{J}^0)_{12}+\text{Adj}(\bar{J}^0)_{13}-\text{Adj}(\bar{J}^0)_{14}+\text{Adj}(\bar{J}^0)_{15}-\text{Adj}(\bar{J}^0)_{16}\\-\text{Adj}(\bar{J}^0)_{21}+\text{Adj}(\bar{J}^0)_{22}-\text{Adj}(\bar{J}^0)_{23}+\text{Adj}(\bar{J}^0)_{24}-\text{Adj}(\bar{J}^0)_{25}+\text{Adj}(\bar{J}^0)_{26}\\+\text{Adj}(\bar{J}^0)_{31}-\text{Adj}(\bar{J}^0)_{32}+\text{Adj}(\bar{J}^0)_{33}-\text{Adj}(\bar{J}^0)_{34}+\text{Adj}(\bar{J}^0)_{35}-\text{Adj}(\bar{J}^0)_{36}\\-\text{Adj}(\bar{J}^0)_{41}+\text{Adj}(\bar{J}^0)_{42}-\text{Adj}(\bar{J}^0)_{43}+\text{Adj}(\bar{J}^0)_{44}-\text{Adj}(\bar{J}^0)_{45}+\text{Adj}(\bar{J}^0)_{46}\\+\text{Adj}(\bar{J}^0)_{51}-\text{Adj}(\bar{J}^0)_{52}+\text{Adj}(\bar{J}^0)_{53}-\text{Adj}(\bar{J}^0)_{54}+\text{Adj}(\bar{J}^0)_{55}-\text{Adj}(\bar{J}^0)_{56}\\-\text{Adj}(\bar{J}^0)_{61}+\text{Adj}(\bar{J}^0)_{62}-\text{Adj}(\bar{J}^0)_{63}+\text{Adj}(\bar{J}^0)_{64}-\text{Adj}(\bar{J}^0)65+\text{Adj}(\bar{J}^0)_{66}\end{bmatrix}$$

or

$$\text{Adj}(\bar{J}^0)=\begin{bmatrix}+\begin{vmatrix}J_{22}J_{32}J_{42}J_{52}J_{62}\\J_{23}J_{33}J_{43}J_{53}J_{63}\\J_{24}J_{34}J_{44}J_{54}J_{64}\\J_{25}J_{35}J_{45}J_{55}J_{65}\\J_{26}J_{36}J_{46}J_{56}J_{66}\end{vmatrix}-\begin{vmatrix}J_{12}J_{32}J_{42}J_{52}J_{62}\\J_{13}J_{33}J_{43}J_{53}J_{63}\\J_{14}J_{34}J_{44}J_{54}J_{64}\\J_{15}J_{35}J_{45}J_{55}J_{65}\\J_{16}J_{36}J_{46}J_{56}J_{66}\end{vmatrix}+\begin{vmatrix}J_{12}J_{22}J_{42}J_{52}J_{62}\\J_{13}J_{23}J_{43}J_{53}J_{63}\\J_{14}J_{24}J_{44}J_{54}J_{64}\\J_{15}J_{25}J_{45}J_{55}J_{65}\\J_{16}J_{26}J_{46}J_{56}J_{66}\end{vmatrix}-\begin{vmatrix}J_{12}J_{22}J_{32}J_{52}J_{62}\\J_{13}J_{23}J_{33}J_{53}J_{63}\\J_{14}J_{24}J_{34}J_{54}J_{64}\\J_{15}J_{25}J_{35}J_{55}J_{65}\\J_{16}J_{26}J_{36}J_{56}J_{66}\end{vmatrix}+\begin{vmatrix}J_{12}J_{22}J_{32}J_{42}J_{62}\\J_{13}J_{23}J_{33}J_{43}J_{63}\\J_{14}J_{24}J_{34}J_{44}J_{64}\\J_{15}J_{25}J_{35}J_{45}J_{65}\\J_{16}J_{26}J_{36}J_{46}J_{66}\end{vmatrix}-\begin{vmatrix}J_{12}J_{22}J_{32}J_{42}J_{52}\\J_{13}J_{23}J_{33}J_{43}J_{53}\\J_{14}J_{24}J_{34}J_{44}J_{54}\\J_{15}J_{25}J_{35}J_{45}J_{55}\\J_{16}J_{26}J_{36}J_{46}J_{56}\end{vmatrix}\\-\begin{vmatrix}J_{21}J_{31}J_{41}J_{51}J_{61}\\J_{23}J_{33}J_{43}J_{53}J_{63}\\J_{24}J_{34}J_{44}J_{54}J_{64}\\J_{25}J_{35}J_{45}J_{55}J_{65}\\J_{26}J_{36}J_{46}J_{56}J_{66}\end{vmatrix}+\begin{vmatrix}J_{11}J_{31}J_{41}J_{51}J_{61}\\J_{13}J_{33}J_{43}J_{53}J_{63}\\J_{14}J_{34}J_{44}J_{54}J_{64}\\J_{15}J_{35}J_{45}J_{55}J_{65}\\J_{16}J_{36}J_{46}J_{56}J_{66}\end{vmatrix}-\begin{vmatrix}J_{11}J_{21}J_{41}J_{51}J_{61}\\J_{13}J_{23}J_{43}J_{53}J_{63}\\J_{14}J_{24}J_{44}J_{54}J_{64}\\J_{15}J_{25}J_{45}J_{55}J_{65}\\J_{16}J_{26}J_{46}J_{56}J_{66}\end{vmatrix}+\begin{vmatrix}J_{11}J_{21}J_{31}J_{51}J_{61}\\J_{13}J_{23}J_{33}J_{53}J_{63}\\J_{14}J_{24}J_{34}J_{54}J_{64}\\J_{15}J_{25}J_{35}J_{55}J_{65}\\J_{16}J_{26}J_{36}J_{56}J_{66}\end{vmatrix}-\begin{vmatrix}J_{11}J_{21}J_{31}J_{41}J_{61}\\J_{13}J_{23}J_{33}J_{43}J_{63}\\J_{14}J_{24}J_{34}J_{44}J_{64}\\J_{15}J_{25}J_{35}J_{45}J_{65}\\J_{16}J_{26}J_{36}J_{46}J_{66}\end{vmatrix}+\begin{vmatrix}J_{11}J_{21}J_{31}J_{41}J_{51}\\J_{13}J_{23}J_{33}J_{43}J_{53}\\J_{14}J_{24}J_{34}J_{44}J_{54}\\J_{15}J_{25}J_{35}J_{45}J_{55}\\J_{16}J_{26}J_{36}J_{46}J_{56}\end{vmatrix}\\+\begin{vmatrix}J_{21}J_{31}J_{41}J_{51}J_{61}\\J_{22}J_{32}J_{42}J_{52}J_{62}\\J_{24}J_{34}J_{44}J_{54}J_{64}\\J_{25}J_{35}J_{45}J_{55}J_{65}\\J_{26}J_{36}J_{46}J_{56}J_{66}\end{vmatrix}-\text{Adj}(\bar{J}^0)_{32}+\text{Adj}(\bar{J}^0)_{33}-\text{Adj}(\bar{J}^0)_{34}+\text{Adj}(\bar{J}^0)_{35}-\text{Adj}(\bar{J}^0)_{36}\\-\begin{vmatrix}J_{21}J_{31}J_{41}J_{51}J_{61}\\J_{22}J_{32}J_{42}J_{52}J_{62}\\J_{23}J_{33}J_{43}J_{53}J_{63}\\J_{25}J_{35}J_{45}J_{55}J_{65}\\J_{26}J_{36}J_{46}J_{56}J_{66}\end{vmatrix}+\text{Adj}(\bar{J}^0)_{42}-\text{Adj}(\bar{J}^0)_{43}+\text{Adj}(\bar{J}^0)_{44}-\text{Adj}(\bar{J}^0)_{45}+\text{Ad}(\bar{J}^0)j_{46}\\+\begin{vmatrix}J_{21}J_{31}J_{41}J_{51}J_{61}\\J_{22}J_{32}J_{42}J_{52}J_{62}\\J_{23}J_{33}J_{43}J_{53}J_{63}\\J_{24}J_{34}J_{44}J_{54}J_{64}\\J_{26}J_{36}J_{46}J_{56}J_{66}\end{vmatrix}-\text{Adj}(\bar{J}^0)_{52}+\text{Adj}(\bar{J}^0)_{53}-\text{Ad}(\bar{J}^0)j_{54}+\text{Adj}(\bar{J}^0)_{55}-\text{Adj}(\bar{J}^0)_{56}\\-\begin{vmatrix}J_{21}J_{31}J_{41}J_{51}J_{61}\\J_{22}J_{32}J_{42}J_{52}J_{62}\\J_{23}J_{33}J_{43}J_{53}J_{63}\\J_{24}J_{34}J_{44}J_{54}J_{64}\\J_{25}J_{35}J_{45}J_{55}J_{65}\end{vmatrix}+\text{Adj}(\bar{J}^0)_{62}-\text{Adj}(\bar{J}^0)_{63}+\text{Ad}(\bar{J}^0)j_{64}-\text{Adj}(\bar{J}^0)_{65}+\text{Ad}(\bar{J}^0)j_{66}\end{bmatrix}$$

As an example, the calculation of the first entry of the adjonint $\text{Adj}(\bar{J}^0)_{11}$ will be outlined:

$$\text{Adj}(\bar{J}^0)_{11}=\begin{bmatrix} J_{22} & J_{32} & J_{42} & J_{52} & J_{62} \\ J_{23} & J_{33} & J_{43} & J_{53} & J_{63} \\ J_{24} & J_{34} & J_{44} & J_{54} & J_{64} \\ J_{25} & J_{35} & J_{45} & J_{55} & J_{65} \\ J_{26} & J_{36} & J_{46} & J_{56} & J_{66} \end{bmatrix}=\begin{bmatrix} 61.945 & -2.944 & -11.764 & 0 & 0 \\ 2.944 & 51.772 & -22.926 & -40.0076 & 19.982 \\ -11.764 & 22.917 & 51.773 & -19.982 & -40.0076 \\ 0 & -40.0076 & 19.982 & 80.015 & -39.963 \\ 0 & -19.98 & -40.0076 & 39.961 & 80.0 \end{bmatrix}$$

$$\text{Adj}(\bar{J}^0)_{11}=61.945\begin{bmatrix} 51.772 & -22.926 & -40.0076 & 19.982 \\ 22.917 & 51.772 & -19.982 & -40.0076 \\ -40.0076 & 19.982 & 80.015 & -39.963 \\ -19.98 & -40.0076 & 39.961 & 80 \end{bmatrix}$$
$$+2.944\begin{bmatrix} 2.944 & -22.917 & -40.0076 & 19.98 \\ -11.764 & 51.773 & -19.982 & -40.0076 \\ 0 & 19.982 & 80.015 & -39.963 \\ 0 & -40.0076 & 39.961 & 80 \end{bmatrix}$$
$$-11.764\begin{bmatrix} 2.944 & 51.772 & -40.0076 & 19.98 \\ -11.764 & 22.917 & -19.982 & -40.0076 \\ 0 & -40.0076 & 80.015 & -39.963 \\ 0 & -19.982 & 39.961 & 80 \end{bmatrix}.$$

The determinant is

$$\det(\bar{J})=J_{11}\begin{bmatrix} J_{22}J_{23}J_{24}J_{25}J_{26} \\ J_{32}J_{33}J_{34}J_{35}J_{36} \\ J_{42}J_{43}J_{44}J_{45}J_{46} \\ J_{52}J_{53}J_{54}J_{55}J_{56} \\ J_{62}J_{63}J_{64}J_{65}J_{66} \end{bmatrix}-J_{12}\begin{bmatrix} J_{21}J_{23}J_{24}J_{25}J_{26} \\ J_{31}J_{33}J_{34}J_{35}J_{36} \\ J_{41}J_{43}J_{44}J_{45}J_{46} \\ J_{51}J_{53}J_{54}J_{55}J_{56} \\ J_{61}J_{63}J_{64}J_{65}J_{66} \end{bmatrix}$$
$$+J_{13}\begin{bmatrix} J_{21}J_{22}J_{24}J_{25}J_{26} \\ J_{31}J_{32}J_{34}J_{35}J_{36} \\ J_{41}J_{43}J_{44}J_{45}J_{46} \\ J_{51}J_{52}J_{54}J_{55}J_{56} \\ J_{61}J_{62}J_{64}J_{65}J_{66} \end{bmatrix}-J_{14}\begin{bmatrix} J_{21}J_{22}J_{23}J_{25}J_{26} \\ J_{31}J_{32}J_{33}J_{35}J_{36} \\ J_{41}J_{42}J_{43}J_{45}J_{46} \\ J_{51}J_{52}J_{53}J_{55}J_{56} \\ J_{61}J_{62}J_{63}J_{65}J_{66} \end{bmatrix}$$
$$+J_{15}\begin{bmatrix} J_{21}J_{22}J_{23}J_{24}J_{26} \\ J_{31}J_{32}J_{33}J_{34}J_{36} \\ J_{41}J_{42}J_{43}J_{44}J_{46} \\ J_{51}J_{52}J_{53}J_{54}J_{56} \\ J_{61}J_{62}J_{63}J_{64}J_{66} \end{bmatrix}-J_{16}\begin{bmatrix} J_{21}J_{22}J_{23}J_{24}J_{25} \\ J_{31}J_{32}J_{33}J_{34}J_{35} \\ J_{41}J_{42}J_{43}J_{44}J_{45} \\ J_{51}J_{52}J_{53}J_{54}J_{55} \\ J_{61}J_{62}J_{63}J_{64}J_{65} \end{bmatrix}.$$

The $(\bar{J}_{11}^0)^{-1}$ entry is now

$$(J_{11}^0)^{-1}=\frac{\text{Adj}(\bar{J}^0)}{\det(\bar{J}^0)}$$

### 7.3.9 Application Example 7.12: Inversion of a 3 × 3 Matrix: Solution

Transpose of $\bar{A}$ is

$$\bar{A}^t=\begin{bmatrix} 1 & 2 & 3 \\ 3 & -4 & 1 \\ -1 & 2 & 1 \end{bmatrix}.$$

The cofactors of $A^t$ are

$$A_{11}^t=(-1)^{(1+1)}\begin{vmatrix} -4 & 1 \\ 2 & 1 \end{vmatrix}=(-4-2)=-6,$$

$$A_{12}^t=(-1)^{(1+2)}\begin{vmatrix} 3 & 1 \\ -1 & 1 \end{vmatrix}=-(3+1)=-4,$$

$$A_{13}^t=(-1)^{(1+3)}\begin{vmatrix} 3 & -4 \\ -1 & 2 \end{vmatrix}=(6-4)=2,$$

$$A_{21}^t=(-1)^{(2+1)}\begin{vmatrix} 2 & 3 \\ 2 & 1 \end{vmatrix}=(-2+6)=4,$$



$$A_{22}^t=(-1)^{(2+2)}\begin{vmatrix} 1 & 3 \\ -1 & 1 \end{vmatrix}=(1+3)=4,$$

$$A_{23}^t=(-1)^{(2+3)}\begin{vmatrix} 1 & 2 \\ -1 & 2 \end{vmatrix}=-(2+2)=-4,$$

$$A_{31}^t=(-1)^{(3+1)}\begin{vmatrix} 2 & 3 \\ -4 & 1 \end{vmatrix}=(2+24)=14,$$

$$A_{32}^t=(-1)^{(3+2)}\begin{vmatrix} 1 & 3 \\ 3 & 1 \end{vmatrix}=-(1-9)=8,$$

$$A_{33}^t=(-1)^{(3+3)}\begin{vmatrix} 1 & 2 \\ 3 & -4 \end{vmatrix}=(-4-6)=-10.$$

The determinant is

$$|\bar{A}|=1\cdot\begin{vmatrix} -4 & 2 \\ 1 & 1 \end{vmatrix}-3\cdot\begin{vmatrix} 2 & 2 \\ 3 & 1 \end{vmatrix}-1\cdot\begin{vmatrix} 2 & -4 \\ 3 & 1 \end{vmatrix}$$
$$=-4-2-6+18-2-12=-26+18=-8.$$

The inverse of $\bar{A}$ is now

$$(\bar{A})^{-1}=\frac{\text{Adj}(\bar{A})}{|\bar{A}|}=-\frac{1}{8}\begin{bmatrix} -6 & -4 & 2 \\ 4 & 4 & -4 \\ 14 & 8 & -10 \end{bmatrix}.$$

### 7.3.10 Application Example 7.13: Computation of the Correction Voltage Vector: Solution

Based on the results of Application Examples 7.9 to 7.11, the correction voltage vector $\Delta\bar{x}^0$ can be computed from

$$\Delta\bar{x}^0=(\bar{J}^0)^{-1}\Delta\bar{W}(\bar{x}^0)=(2.68\text{E}-4,\ 2.39\text{E}-3,\ 2.79\text{E}-3,\ 3.57\text{E}-3,\ 3.39\text{E}-3,\ 4.03\text{E}-3)^t.$$

The updated mismatch power vector is

$$\Delta\bar{W}^1=(1.41\text{E}-4,\ 3.01\text{E}-4,\ -9.63\text{E}-6,\ 7.62\text{E}-5,\ 1.20\text{E}-3,\ 5.96\text{E}-4)^t.$$

Since the components of $\Delta\bar{W}^1$ are larger than the specified convergence tolerance (e.g., 0.0001), the Newton–Raphson solution has not converged. However, it will converge in two iterations:

Fundamental power flow iteration summary (Fig. E7.8.1):

| | Absolute real power mismatch | | | Absolute reactive power mismatch | | |
|---|---|---|---|---|---|---|
| Iteration | Average (%) | Worst (%) | Worst bus | Average (%) | Worst (%) | Worst bus |
| 0 | 11.67 | 25 | 4 | 6.67 | 10.00 | 4 |
| 1 | 0.05 | 0.12 | 4 | 0.03 | 0.06 | 4 |
| 2 | 0.00 | 0.00 | 4 | 0.00 | 0.00 | 4 |

Fundamental power flow output solution (Fig. E7.8.1):

| | Bus voltage | | Bus generation (G) and load (L) powers | | | | | Line power* | |
|---|---|---|---|---|---|---|---|---|---|
| From bus | \|V\| (%) | δ (°) | $P_G$ (%) | $Q_G$ (%) | $P_L$ (%) | $Q_L$ (%) | To bus | $P_{line}$ (%) | $Q_{line}$ (%) |
| 1 | 100.0 | 0.00 | 35.09 | 20.15 | 0.00 | 0.00 | 2 | 13.35 | 10.69 |
| | | | | | | | 4 | 21.73 | 9.47 |
| 2 | 99.76 | −0.02 | 0.00 | 0.00 | 10.00 | 10.00 | 1 | −13.32 | −10.66 |
| | | | | | | | 3 | 3.32 | 0.66 |
| 3 | 99.64 | −0.16 | 0.00 | 0.00 | 0.00 | 0.00 | 2 | −3.32 | −0.65 |
| | | | | | | | 4 | 3.32 | 0.65 |
| 4 | 99.59 | −0.20 | 0.00 | 0.00 | 25.00 | 10.00 | 3 | −3.32 | −0.65 |
| | | | | | | | 1 | −21.68 | −9.35 |

*Active and reactive powers in the line between "from bus" and "to bus."

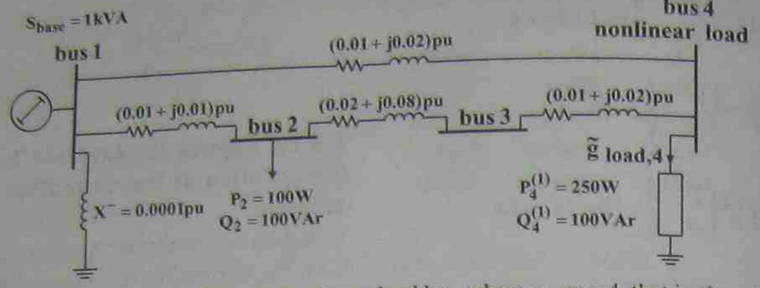



**FIGURE E7.14.1** Four-bus power system with one nonlinear load bus, where $n = m = 4$, that is, there is one nonlinear bus (bus 4), 2 linear buses (buses 2 and 3) and the swing bus (bus 1).

### 7.4.7 Application Example 7.14: Computation of Harmonic Admittance Matrix: Solution

The fundamental bus admittance matrix ($X^-$ does not exist for fundamental quantities) is computed in Application Example 7.8. The 5th harmonic bus admittance matrix takes into account $X^-$ and its entries are calculated as follows:

$$y_{11}^{(5)} = \frac{1}{0.01 + j(0.02 \cdot 5)} + \frac{1}{0.01 + j(0.01 \cdot 5)} + \frac{1}{j(0.0001 \cdot 5)}$$
$$= 2029.137\text{pu}\angle -1.5684\text{rad}$$

$$y_{12}^{(5)} = \frac{-1}{0.01 + j(0.01 \cdot 5)} = 19.612\text{pu}\angle 1.7681\text{rad}$$

$$y_{13}^{(5)} = 0$$

$$y_{14}^{(5)} = \frac{-1}{0.01 + j(0.02 \cdot 5)} = 9.9503\text{pu}\angle 1.6704\text{rad}$$

$$y_{21}^{(5)} = y_{12}^{(5)}$$

$$y_{22}^{(5)} = \frac{1}{0.01 + j(0.01 \cdot 5)} + \frac{1}{0.02 + j(0.08 \cdot 5)}$$
$$= 22.084\text{pu}\angle -1.3900\text{rad}$$

$$y_{23}^{(5)} = \frac{-1}{0.02 + j(0.08 \cdot 5)} = 2.4969\text{pu}\angle 1.62066\text{rad}$$

$$y_{24}^{(5)} = 0$$

$$y_{31}^{(5)} = y_{13}^{(5)}$$

$$y_{32}^{(5)} = y_{23}^{(5)}$$

$$y_{33}^{(5)} = \frac{1}{0.02 + j(0.08 \cdot 5)} + \frac{1}{0.01 + j(0.02 \cdot 5)}$$
$$= 12.445\text{pu}\angle -1.4811\text{rad}$$

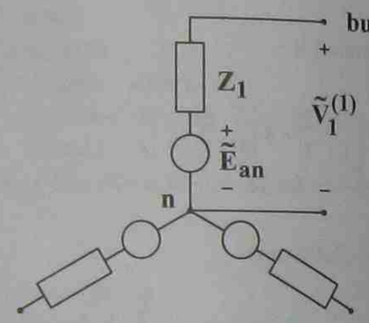



**FIGURE E7.14.2** Representation of swing bus (bus 1) for fundamental (h = 1) frequency.

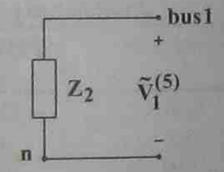



**FIGURE E7.14.3** Equivalent circuit of swing bus for the 5th harmonic (h = 5).

$$y_{34}^{(5)} = \frac{-1}{0.01 + j(0.02 \cdot 5)} = 9.9504\text{pu}\angle 1.6704\text{rad}$$

$$y_{41}^{(5)} = y_{14}^{(5)}$$

$$y_{42}^{(5)} = y_{24}^{(5)}$$

$$y_{43}^{(5)} = y_{34}^{(5)}$$

$$y_{44}^{(5)} = \frac{1}{0.01 + j(0.02 \cdot 5)} + \frac{1}{0.01 + j(0.02 \cdot 5)}$$
$$= 19.901\text{pu}\angle -1.4711\text{rad}.$$

Therefore,



$$\bar{Y}_{bus}^{(5)} = \begin{bmatrix} 2029.137\text{pu}\angle -1.5684\text{rad} & 19.61\text{pu}\angle 1.7681\text{rad} & 0 & 9.9503\text{pu}\angle 1.6704\text{rad} \\ 19.61\text{pu}\angle 1.7681\text{rad} & 22.0847\text{pu}\angle -1.3900\text{rad} & 2.4969\text{pu}\angle 1.62066\text{rad} & 0 \\ 0 & 2.4969\text{pu}\angle 1.62066\text{rad} & 12.445\text{pu}\angle -1.4811\text{rad} & 9.9504\text{pu}\angle 1.6704\text{rad} \\ 9.9503\text{pu}\angle 1.6704\text{rad} & 0 & 9.9504\text{pu}\angle 1.6704\text{rad} & 19.901\text{pu}\angle -1.4711\text{rad} \end{bmatrix}.$$

Note that: $-y_{ij}\angle\theta_{ij} = y_{ij}\angle(\theta_{ij} + \pi)$.

### 7.4.8 Application Example 7.15: Computation of Nonlinear Load Harmonic Currents: Solution

The Initial Step of Harmonic Load Flow is as follows:

The real and imaginary nonlinear device currents $G_{r,4}^{(1)}$ and $G_{i,4}^{(1)}$ – referred to the swing bus – may be computed as follows, where the following powers are referred to the nonlinear bus 4:

$$\begin{cases} P_4^{(1)} = V_4^{(1)} I_4^{(1)} \cos(\delta_4^{(1)} - \gamma_4^{(1)}) \\ Q_4^{(1)} = V_4^{(1)} I_4^{(1)} \sin(\delta_4^{(1)} - \gamma_4^{(1)}) \end{cases}$$

$I_4^{(1)}$ and $\gamma_4^{(1)} = \delta_4^{(1)} - \tan^{-1}(Q_4^{(1)}/P_4^{(1)})$ are the magnitude and phase angle of the fundamental nonlinear device current, respectively. The diagram of Fig. E7.15.1 demonstrates the phasor relationships.

The real part of the fundamental of the nonlinear device current at bus 4 (referred to the swing bus) is

$$G_{r,4}^{(1)} = I_4^{(1)} \cos\gamma_4^{(1)}$$

where

$$I_4^{(1)} = \frac{P_4^{(1)}}{V_4^{(1)} \cos(\delta_4^{(1)} - \gamma_4^{(1)})}.$$

Thus

$$G_{r,4}^{(1)} = \frac{P_4^{(1)} \cos\gamma_4^{(1)}}{V_4^{(1)} \cos(\delta_4^{(1)} - \gamma_4^{(1)})}.$$

Correspondingly one obtains for the imaginary part of the fundamental of the nonlinear device current at bus 4 (referred to the swing bus):

$$G_{i,4}^{(1)} = \frac{P_4^{(1)} \sin\gamma_4^{(1)}}{V_4^{(1)} \cos(\delta_4^{(1)} - \gamma_4^{(1)})}.$$

The real and imaginary harmonic (5th) nonlinear device currents are given as (referred to bus 4)

$$\begin{cases} g_{r,4}^{(5)} = 0.3(V_4^{(1)})^3 \cos(3\delta_4^{(1)}) + 0.3(V_4^{(5)})^2 \cos(3\delta_4^{(5)}) \\ g_{i,4}^{(5)} = 0.3(V_4^{(1)})^3 \sin(3\delta_4^{(1)}) + 0.3(V_4^{(5)})^2 \sin(3\delta_4^{(5)}) \end{cases}$$

where $\delta_4^{(5)}$ is the angle between $\tilde{V}_4^{(5)}$ and $\tilde{V}_1^{(1)}$, the swing bus voltage, $I_4^{(5)}$ is the fifth harmonic current magnitude

$$I_4^{(5)} = \sqrt{(g_{r,4}^{(5)})^2 + (g_{i,4}^{(5)})^2}$$

and $\gamma_4^{(5)}$ is the phase angle of $\tilde{I}_4^{(5)}$ with respect to the swing bus voltage $\tilde{V}_1^{(1)}$.

Assuming bus 1 to be the swing bus ($\delta_1^{(1)} = 0$ radians, $|\tilde{V}_1^{(1)}| = 1.00$ pu), the solution procedure is as follows.

***Step #1 of Harmonic Load Flow.*** Using the solution vector $\bar{x}$ of the fundamental power flow analysis (see Application Example 7.13) and assuming harmonic voltage magnitudes and phase angles of 0.1 pu and 0 radians, respectively, the bus vector $\bar{U}^0$ will be

$$\bar{U}^0 = (\delta_2^{(1)}, V_2^{(1)}, \delta_3^{(1)}, V_3^{(1)}, \delta_4^{(1)}, V_4^{(1)}, \delta_1^{(5)}, V_1^{(5)}, \delta_2^{(5)}, V_2^{(5)}, \delta_3^{(5)}, V_3^{(5)}, \delta_4^{(5)}, V_4^{(5)}, \alpha_4, \beta_4)^t$$

$$\bar{U}^0 = (-2.671 \cdot 10^{-4}, 0.9976, -2.810 \cdot 10^{-3}, 0.9964, -3.414 \cdot 10^{-3}, 0.9960, 0, 0.1, 0, 0.1, 0, 0.1, 0, 0.1, 0, 0)^t$$

Note that the nonlinear device variables ($\alpha_4$ and $\beta_4$) are assumed to be zero because there are no device variables defined in this example for the nonlinear load at bus 4.

***Step #2 of Harmonic Load Flow.*** Use $\bar{U}^0$ to compute the nonlinear device currents. With $P_4^{(1)} = 250$ W corresponding to 0.25 pu, $Q_4^{(1)} = 100$VAr corresponding to 0.100 pu, $V_4^{(1)} = 0.9960$ pu, and $\delta_4^{(1)} = -3.414 \cdot 10^{-3}$ radians, one gets

$$\varepsilon_4^{(1)} = \tan^{-1}\left(\frac{Q_4^{(1)}}{P_4^{(1)}}\right) = \tan^{-1}\left(\frac{0.1}{0.25}\right) = 0.3805\text{rad}$$

$$\gamma_4^{(1)} = \delta_4^{(1)} - \varepsilon_4^{(1)} = (-0.003414 - 0.3805) = -0.38391\,\text{rad}$$

$$G_{r,4}^{(1)} = \frac{P_4^{(1)} \cos(\gamma_4^{(1)})}{V_4^{(1)} \cos(\delta_4^{(1)} - \gamma_4^{(1)})}$$
$$= \frac{0.25 \cdot \cos(-0.38391)}{0.9960 \cdot \cos(-0.003414 - 0.38391)} = 0.2514\text{pu}$$

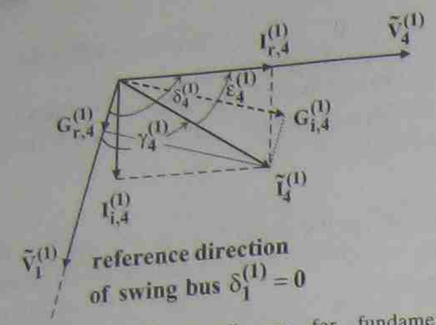



**FIGURE E7.15.1** Phasor diagram for fundamental quantities, where $\varepsilon_4^{(1)} = \tan^{-1}\left(Q_4^{(1)}/P_4^{(1)}\right) = (\delta_4^{(1)} - \gamma_4^{(1)})$ or $\delta_4^{(1)} = \varepsilon_4^{(1)} + \gamma_4^{(1)}$.

$$G_{i,4}^{(1)} = \frac{P_4^{(1)}\sin(\gamma_4^{(1)})}{V_4^{(1)}\cos(\delta_4^{(1)} - \gamma_4^{(1)})} = \frac{0.25\cdot\sin(-0.38391)}{0.9960\cdot\cos(-0.003414 - 0.38391)} = -0.1015\text{pu}.$$

The fundamental magnitude of the nonlinear current is

$$I_4^{(1)} = \sqrt{(G_{r,4}^{(1)})^2 + (G_{i,4}^{(1)})^2} = \sqrt{(0.2514)^2 + (-0.1015)^2} = 0.2711\text{pu} \quad \text{with} \quad \gamma_4^{(1)} = -0.38391\text{rad}.$$

The fifth harmonic current components of the nonlinear load current at bus 4 are (referred to bus 4)

$$\begin{cases} g_{r,4}^{(5)} = 0.3(V_4^{(1)})^3\cos(3\delta_4^{(1)}) + 0.3(V_4^{(5)})^2\cos(3\delta_4^{(5)}) \\ g_{i,4}^{(5)} = 0.3(V_4^{(1)})^3\sin(3\delta_4^{(1)}) + 0.3(V_4^{(5)})^2\sin(3\delta_4^{(5)}) \end{cases}$$

With $V_4^{(1)} = 0.9960\text{pu}$, $\delta_4^{(1)} = -0.003414\text{rad}$, $V_4^{(5)} = 0.1\text{pu}$, $\delta_4^{(5)} = 0\text{rad}$, one obtains

$$\begin{cases} g_{r,4}^{(5)} = 0.3(0.9960)^3\cos(-3\cdot 0.003414) \\ \qquad +0.3(0.1)^2\cos(3\cdot 0) = 0.2994\text{pu} \\ g_{i,4}^{(5)} = 0.3(0.9960)^3\sin(-3\cdot 0.003414) \\ \qquad +0.3(0.1)^2\sin(3\cdot 0) = -0.003036\text{pu} \end{cases}$$

$$I_4^{(5)} = \sqrt{(g_{r,4}^{(5)})^2 + (g_{i,4}^{(5)})^2} = \sqrt{(0.2994)^2 + (-0.003036)^2} = 0.2994\text{pu}$$

$$\varepsilon_4^{(5)} = \tan^{-1}\left(\frac{|g_{i,4}^{(5)}|}{|g_{r,4}^{(5)}|}\right) = 0.01014\text{rad}.$$

Therefore, the fifth harmonic currents at bus 4 referred to the swing bus are $G_{r,4}^{(5)} = I_4^{(5)}\cos\gamma_4^{(5)}$ and $G_{i,4}^{(5)} = I_4^{(5)}\sin\gamma_4^{(5)}$.

The phasor diagram for the 5th harmonic is shown in Fig. E7.15.2, where the angles are



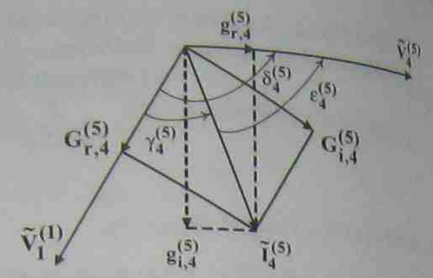



**FIGURE E7.15.2** Phasor diagram for 5th harmonic.

$$\delta_4^{(5)} = \varepsilon_4^{(5)} + \gamma_4^{(5)}$$

or

$$\gamma_4^{(5)} = \delta_4^{(5)} - \varepsilon_4^{(5)} = 0 - \varepsilon_4^{(5)} = -0.01014\text{rad}$$

resulting in $G_{r,4}^{(5)} = 0.2994\text{pu}$ and $G_{i,4}^{(5)} = -0.003036\text{pu}$.

These nonlinear currents referred to the swing bus are about the same as those referred to bus 4 because the angle $\gamma_4^{(5)}$ is very small for this first iteration.

Note that

$$\begin{cases} P_4^{(1)} = I_4^{(1)}V_4^{(1)}\cos(\delta_4^{(1)} - \gamma_4^{(1)}) \\ \qquad = 0.2711\cdot 0.9960\cdot\cos(-0.003414 + 0.38391) \\ \qquad = 0.250\text{pu} \\ Q_4^{(1)} = I_4^{(1)}V_4^{(1)}\sin(\delta_4^{(1)} - \gamma_4^{(1)}) \\ \qquad = 0.2711\cdot 0.9960\cdot\sin(-0.003414 + 0.38391) \\ \qquad = 0.100\text{pu} \end{cases}$$

are as expected. Correspondingly,

$$\begin{cases} P_4^{(5)} = I_4^{(5)}V_4^{(5)}\cos(\delta_4^{(5)} - \gamma_4^{(5)}) \\ \qquad = 0.2994\cdot 0.1\cdot\cos(0 + 0.01014) = 0.02994\text{pu} \\ Q_4^{(5)} = I_4^{(5)}V_4^{(5)}\sin(\delta_4^{(5)} - \gamma_4^{(5)}) \\ \qquad = 0.2994\cdot 0.1\cdot\sin(0 + 0.01014) = 0.000304\text{pu}. \end{cases}$$

Therefore, the total injected real and reactive powers at the nonlinear bus 4 are

$$\begin{cases} P_4^t = P_4^{(1)} + P_4^{(5)} = 0.250\text{pu} + 0.02994\text{pu} \\ \qquad = 0.27994\text{pu} \\ Q_4^t = Q_4^{(1)} + Q_4^{(5)} = 0.100\text{pu} + 0.000304\text{pu} \\ \qquad = 0.100304\text{pu}. \end{cases}$$

### 7.4.9 Application Example 7.16: Evaluation of Harmonic Mismatch Vector: Solution

***Step #3 of Harmonic Load Flow.*** Evaluation of the mismatch vector





$$\Delta\bar{M}^0 = (\Delta\bar{W}, \Delta\bar{I}^{(5)}, \Delta\bar{I}^{(1)})^t = (P_2^{(1)} + F_{r,2}^{(1)}, Q_2^{(1)} + F_{i,2}^{(1)}, P_3^{(1)} + F_{r,3}^{(1)}, Q_3^{(1)} + F_{i,3}^{(1)}, P_4^t + F_{r,4}^{(1)} + F_{r,4}^{(5)}, Q_4^t + F_{i,4}^{(1)} + F_{i,4}^{(5)}, I_{r,1}^{(5)}, I_{i,1}^{(5)}, I_{r,2}^{(5)}, I_{i,2}^{(5)}, I_{r,3}^{(5)}, I_{i,3}^{(5)}, I_{r,4}^{(5)} + G_{r,4}^{(5)}, I_{i,4}^{(5)} + G_{i,4}^{(5)}, I_{r,4}^{(1)} + G_{r,4}^{(1)}, I_{i,4}^{(1)} + G_{i,4}^{(1)}).$$

To compute these mismatches use equations Eqs. 7-80 and 7-81

$$\Delta P_i = P_i + F_{r,i} = P_i + \sum_{j=1}^{n} y_{ij}|\tilde{V}_i||\tilde{V}_i|\cos(-\theta_{ij} - \delta_j + \delta_i)$$

$$\Delta Q_i = Q_i + F_{i,i} = Q_i + \sum_{j=1}^{n} y_{ij}|\tilde{V}_j||\tilde{V}_i|\sin(-\theta_{ij} - \delta_j + \delta_i)$$

and Eqs. 7-119a,b

$$\Delta I_{r,i}^{(h)} = I_{r,i}^{(h)} + G_{r,i}^{(h)} = \sum_{j=1}^{n} y_{ij}^{(h)}|\tilde{V}_j^{(h)}|\cos(\theta_{ij}^{(h)} + \delta_j^{(h)}) + G_{r,i}^{(h)}$$

$$\Delta I_{i,i}^{(h)} = I_{i,i}^{(h)} + G_{i,i}^{(h)} = \sum_{j=1}^{n} y_{ij}^{(h)}|\tilde{V}_j^{(h)}|\sin(\theta_{ij}^{(h)} + \delta_j^{(h)}) + G_{i,i}^{(h)}.$$

Hence,

$$\Delta P_2^{(1)} = P_2^{(1)} + F_{r,2}^{(1)} = P_2 + y_{21}V_1V_2\cos(-\theta_{21} - \delta_1 + \delta_2) + y_{22}V_2V_2\cos(-\theta_{22} - \delta_2 + \delta_2) + y_{23}V_3V_2\cos(-\theta_{23} - \delta_3 + \delta_2) + y_{24}V_4V_2\cos(-\theta_{24} - \delta_4 + \delta_2) = -0.0170\text{pu}$$

$$\Delta Q_2^{(1)} = Q_2^{(1)} + F_{i,2}^{(1)} = Q_2 + y_{21}V_1V_2\sin(-\theta_{21} - \delta_1 + \delta_2) + y_{22}V_2V_2\sin(-\theta_{22} - \delta_2 + \delta_2) + y_{23}V_3V_2\sin(-\theta_{23} - \delta_3 + \delta_2) + y_{24}V_4V_2\sin(-\theta_{24} - \delta_4 + \delta_2) = 0.083\text{pu}$$

$$\Delta P_3^{(1)} = P_3^{(1)} + F_{r,3}^{(1)} = P_3 + y_{31}V_1V_3\cos(-\theta_{31} - \delta_1 + \delta_3) + y_{32}V_2V_3\cos(-\theta_{32} - \delta_2 + \delta_3) + y_{33}V_3V_3\cos(-\theta_{33} - \delta_3 + \delta_3) + y_{34}V_4V_3\cos(-\theta_{34} - \delta_4 + \delta_3) = -0.00325\text{pu}$$

$$\Delta Q_3^{(1)} = Q_3^{(1)} + F_{i,3}^{(1)} = Q_3 + y_{31}V_1V_3\sin(-\theta_{31} - \delta_1 + \delta_3) + y_{32}V_2V_3\sin(-\theta_{32} - \delta_2 + \delta_3) + y_{33}V_3V_3\sin(\theta_{33} - \delta_3 + \delta_3) + y_{34}V_4V_3\sin(-\theta_{34} - \delta_4 + \delta_3) = 0.00192\text{pu}$$

$$\begin{aligned}\Delta P_4^t &= P_4^t + F_{r,4}^{(1)} + F_{r,4}^{(5)} = P_4^t \\ &+ \sum_{j=1}^{4} y_{4j}V_j^{(1)}V_4^{(1)}\cos(-\theta_{4j} - \delta_j^{(1)} + \delta_4^{(1)}) \\ &+ \sum_{j=1}^{4} y_{4j}^{(5)}V_j^{(5)}V_4^{(5)}\cos(-\theta_{4j}^{(5)} - \delta_j^{(5)} + \delta_4^{(5)}) = P_4^t \\ &+ y_{41}V_1^{(1)}V_4^{(1)}\cos(-\theta_{41} - \delta_1^{(1)} + \delta_4^{(1)}) \\ &+ y_{43}V_3^{(1)}V_4^{(1)}\cos(-\theta_{43} - \delta_3^{(1)} + \delta_4^{(1)}) \\ &+ y_{44}V_4^{(1)}V_4^{(1)}\cos(-\theta_{44} - \delta_4^{(1)} + \delta_4^{(1)}) \\ &+ y_{41}^{(5)}V_1^{(5)}V_4^{(5)}\cos(-\theta_{41}^{(5)} - \delta_1^{(5)} + \delta_4^{(5)}) \\ &+ y_{43}^{(5)}V_3^{(5)}V_4^{(5)}\cos(-\theta_{43}^{(5)} - \delta_3^{(5)} + \delta_4^{(5)}) \\ &+ y_{44}^{(5)}V_4^{(5)}V_4^{(5)}\cos(-\theta_{44}^{(5)} - \delta_4^{(5)} + \delta_4^{(5)}) = 0.037\text{pu}\end{aligned}$$

$$\begin{aligned}\Delta Q_4^t &= Q_4^t + F_{i,4}^{(1)} + F_{i,4}^{(5)} = \\ &Q_4^t + \sum_{j=1}^{4} y_{4j}V_j^{(1)}V_4^{(1)}\sin(-\theta_{4j} - \delta_j^{(1)} + \delta_4^{(1)}) \\ &+ \sum_{j=1}^{4} y_{4j}^{(5)}V_j^{(5)}V_4^{(5)}\sin(-\theta_{4j}^{(5)} - \delta_j^{(5)} + \delta_4^{(5)}) = \\ &Q_4^t + y_{41}V_1^{(1)}V_4^{(1)}\sin(-\theta_{41} - \delta_1^{(1)} + \delta_4^{(1)}) \\ &+ y_{43}V_3^{(1)}V_4^{(1)}\sin(-\theta_{43} - \delta_3^{(1)} + \delta_4^{(1)}) \\ &+ y_{44}V_4^{(1)}V_4^{(1)}\sin(-\theta_{44} - \delta_4^{(1)} + \delta_4^{(1)}) \\ &+ y_{41}^{(5)}V_1^{(5)}V_4^{(5)}\sin(-\theta_{41}^{(5)} - \delta_1^{(5)} + \delta_4^{(5)}) \\ &+ y_{43}^{(5)}V_3^{(5)}V_4^{(5)}\sin(-\theta_{43}^{(5)} - \delta_3^{(5)} + \delta_4^{(5)}) \\ &+ y_{44}^{(5)}V_4^{(5)}V_4^{(5)}\sin(-\theta_{44}^{(5)} - \delta_4^{(5)} + \delta_4^{(5)}) = -0.188\text{pu}\end{aligned}$$

$$\begin{aligned}I_{r,1}^{(5)} &= \sum_{j=1}^{4} y_{1j}^{(5)}|\tilde{V}_j^{(5)}|\cos(\theta_{1j}^{(5)} + \delta_j^{(5)}) \\ &= y_{11}^{(5)}|\tilde{V}_1^{(5)}|\cos(\theta_{11}^{(5)} + \delta_1^{(5)}) \\ &+ y_{12}^{(5)}|\tilde{V}_2^{(5)}|\cos(\theta_{12}^{(5)} + \delta_2^{(5)}) \\ &+ y_{13}^{(5)}|\tilde{V}_3^{(5)}|\cos(\theta_{13}^{(5)} + \delta_3^{(5)}) \\ &+ y_{14}^{(5)}|\tilde{V}_4^{(5)}|\cos(\theta_{14}^{(5)} + \delta_4^{(5)}) = 0.201\text{pu}\end{aligned}$$

$$\begin{aligned}I_{i,1}^{(5)} &= \sum_{j=1}^{4} y_{1j}^{(5)}|\tilde{V}_j^{(5)}|\sin(\theta_{1j}^{(5)} + \delta_j^{(5)}) \\ &= y_{11}^{(5)}|\tilde{V}_1^{(5)}|\sin(\theta_{11}^{(5)} + \delta_1^{(5)}) \\ &+ y_{12}^{(5)}|\tilde{V}_2^{(5)}|\sin(\theta_{12}^{(5)} + \delta_2^{(5)}) \\ &+ y_{13}^{(5)}|\tilde{V}_3^{(5)}|\sin(\theta_{13}^{(5)} + \delta_3^{(5)}) \\ &+ y_{14}^{(5)}|\tilde{V}_4^{(5)}|\sin(\theta_{14}^{(5)} + \delta_4^{(5)}) = -201.98\text{pu}\end{aligned}$$

$$\begin{aligned}I_{r,2}^{(5)} &= \sum_{j=1}^{4} y_{2j}^{(5)}|\tilde{V}_j^{(5)}|\cos(\theta_{2j}^{(5)} + \delta_j^{(5)}) \\ &= y_{21}^{(5)}|\tilde{V}_1^{(5)}|\cos(\theta_{21}^{(5)} + \delta_1^{(5)}) \\ &+ y_{22}^{(5)}|\tilde{V}_2^{(5)}|\cos(\theta_{22}^{(5)} + \delta_2^{(5)}) \\ &+ y_{23}^{(5)}|\tilde{V}_3^{(5)}|\cos(\theta_{23}^{(5)} + \delta_3^{(5)}) \\ &+ y_{24}^{(5)}|\tilde{V}_4^{(5)}|\cos(\theta_{24}^{(5)} + \delta_4^{(5)}) = 0.000255\text{pu}\end{aligned}$$

$$\begin{aligned}I_{i,2}^{(5)} &= \sum_{j=1}^{4} y_{2j}^{(5)}|\tilde{V}_j^{(5)}|\sin(\theta_{2j}^{(5)} + \delta_j^{(5)}) \\ &= y_{21}^{(5)}|\tilde{V}_1^{(5)}|\sin(\theta_{21}^{(5)} + \delta_1^{(5)}) \\ &+ y_{22}^{(5)}|\tilde{V}_2^{(5)}|\sin(\theta_{22}^{(5)} + \delta_2^{(5)}) + y_{23}^{(5)}|\tilde{V}_3^{(5)}|\sin(\theta_{23}^{(5)} + \delta_3^{(5)}) \\ &+ y_{24}^{(5)}|\tilde{V}_4^{(5)}|\sin(\theta_{24}^{(5)} + \delta_4^{(5)}) = -0.000620\text{pu}\end{aligned}$$

$$\begin{aligned}I_{r,3}^{(5)} &= \sum_{j=1}^{4} y_{3j}^{(5)}|\tilde{V}_j^{(5)}|\cos(\theta_{3j}^{(5)} + \delta_j^{(5)}) \\ &= y_{31}^{(5)}|\tilde{V}_1^{(5)}|\cos(\theta_{31}^{(5)} + \delta_1^{(5)}) \\ &+ y_{32}^{(5)}|\tilde{V}_2^{(5)}|\cos(\theta_{32}^{(5)} + \delta_2^{(5)}) \\ &+ y_{33}^{(5)}|\tilde{V}_3^{(5)}|\cos(\theta_{33}^{(5)} + \delta_3^{(5)}) \\ &+ y_{34}^{(5)}|\tilde{V}_4^{(5)}|\cos(\theta_{34}^{(5)} + \delta_4^{(5)}) = 0.000104\text{ pu}\end{aligned}$$

$$I_{i,3}^{(5)} = \sum_{j=1}^{4} y_{3j}^{(5)} |\tilde{V}_j^{(5)}| \sin(\theta_{3j}^{(5)} + \delta_j^{(5)})$$
$$= y_{31}^{(5)} |\tilde{V}_1^{(5)}| \sin(\theta_{31}^{(5)} + \delta_1^{(5)}) + y_{32}^{(5)} |\tilde{V}_2^{(5)}| \sin(\theta_{32}^{(5)} + \delta_2^{(5)}) + y_{33}^{(5)} |\tilde{V}_3^{(5)}| \sin(\theta_{33}^{(5)} + \delta_3^{(5)}) + y_{34}^{(5)} |\tilde{V}_4^{(5)}| \sin(\theta_{34}^{(5)} + \delta_4^{(5)}) = 0.0000082\text{pu}$$

$$I_{r,4}^{(5)} + G_{r,4}^{(5)} = \sum_{j=1}^{4} y_{4j}^{(5)} |\tilde{V}_j^{(5)}| \cos(\theta_{4j}^{(5)} + \delta_j^{(5)}) + G_{r,4}^{(5)}$$
$$= y_{41}^{(5)} |\tilde{V}_1^{(5)}| \cos(\theta_{41}^{(5)} + \delta_1^{(5)}) + y_{43}^{(5)} |\tilde{V}_3^{(5)}| \cos(\theta_{43}^{(5)} + \delta_3^{(5)}) + y_{44}^{(5)} |\tilde{V}_4^{(5)}| \cos(\theta_{44}^{(5)} + \delta_4^{(5)}) + G_{r,4}^{(5)} = 0.2996\text{pu}$$

$$I_{i,4}^{(5)} + G_{i,4}^{(5)} = \sum_{j=1}^{4} y_{4j}^{(5)} |\tilde{V}_j^{(5)}| \sin(\theta_{4j}^{(5)} + \delta_j^{(5)}) + G_{i,4}^{(5)}$$
$$= y_{41}^{(5)} |\tilde{V}_1^{(5)}| \sin(\theta_{41}^{(5)} + \delta_1^{(5)}) + y_{43}^{(5)} |\tilde{V}_3^{(5)}| \sin(\theta_{43}^{(5)} + \delta_3^{(5)}) + y_{44}^{(5)} |\tilde{V}_4^{(5)}| \sin(\theta_{44}^{(5)} + \delta_4^{(5)}) + G_{i,4}^{(5)} = -0.00325\text{pu}$$

$$I_{r,4}^{(1)} + G_{r,4}^{(1)} = \sum_{j=1}^{4} y_{4j}^{(1)} |\tilde{V}_j^{(1)}| \cos(\theta_{4j}^{(1)} + \delta_j^{(1)}) + G_{r,4}^{(1)}$$
$$= y_{41} |\tilde{V}_1^{(1)}| \cos(\theta_{41}^{(1)} + \delta_1^{(1)}) + y_{43} |\tilde{V}_3^{(1)}| \cos(\theta_{43}^{(1)} + \delta_3^{(1)}) + y_{44} |\tilde{V}_4^{(1)}| \cos(\theta_{44}^{(1)} + \delta_4^{(1)}) + G_{r,4}^{(1)} = 0.0027\text{pu}$$

$$I_{i,4}^{(1)} + G_{i,4}^{(1)} = \sum_{j=1}^{4} y_{4j}^{(5)} |\tilde{V}_j^{(1)}| \sin(\theta_{4j}^{(1)} + \delta_j^{(1)}) + G_{i,4}^{(1)}$$
$$= y_{41} |\tilde{V}_1^{(1)}| \sin(\theta_{41}^{(1)} + \delta_1^{(1)}) + y_{43} |\tilde{V}_3^{(1)}| \sin(\theta_{43}^{(1)} + \delta_3^{(1)}) + y_{44} |\tilde{V}_4^{(1)}| \sin(\theta_{44}^{(1)} + \delta_4^{(1)}) + G_{i,4}^{(1)} = -0.0054\text{pu}.$$



The mismatch vector $\Delta\bar{M}^0$ is now

$$\Delta\bar{M}^0 = (\Delta\bar{W}, \Delta\bar{I}^{(5)}, \Delta\bar{I}^{(1)})^t = (P_2^{(1)} + F_{r,2}^{(1)}, Q_2^{(1)} + F_{i,2}^{(1)}, P_3^{(1)} + F_{r,3}^{(1)}, Q_3^{(1)} + F_{i,3}^{(1)}, P_4^s + F_{r,4}^{(1)} + F_{r,4}^{(5)}, Q_4^s + F_{i,4}^{(1)} + F_{i,4}^{(5)}, I_{r,1}^{(5)}, I_{i,1}^{(5)}, I_{r,2}^{(5)}, I_{i,2}^{(5)}, I_{r,3}^{(5)}, I_{i,3}^{(5)}, I_{r,4}^{(5)} + G_{r,4}^{(5)}, I_{i,4}^{(5)} + G_{i,4}^{(5)}, I_{r,4}^{(1)} + G_{r,4}^{(1)}, I_{i,4}^{(1)} + G_{i,4}^{(1)})^t$$

or

$$\Delta\bar{M}^0 = (-0.0170, 0.083, -0.00325, 0.00192, 0.037, -0.188, 0.201, -201.98, 0.000255, -0.000620, 0.000104, 0.0000082, 0.2996, -0.00325, 0.0027, -0.0054).$$

Note that for a mismatch residual of 0.0001 pu the solution has not converged yet.

### 7.4.10 Application Example 7.17: Evaluation of Fundamental and Harmonic Jacobian Submatrices: Solution

***Step #4 of Harmonic Load Flow.*** The matrix equation shown below makes it easy to identify the entries of the Jacobian matrix:





$$\bar{J}^0 = \begin{array}{c} \begin{matrix} \delta_2^{(1)} & V_2^{(1)} & \delta_3^{(1)} & V_3^{(1)} & \delta_4^{(1)} & V_4^{(1)} & \delta_1^{(5)} & V_1^{(5)} & V_2^{(5)} & V_2^{(5)} & \delta_3^{(5)} & V_3^{(5)} & \delta_4^{(5)} & V_4^{(5)} & \alpha & \beta \\ \downarrow & \downarrow & \downarrow & \downarrow & \downarrow & \downarrow & \downarrow & \downarrow & \downarrow & \downarrow & \downarrow & \downarrow & \downarrow & \downarrow & \downarrow & \downarrow \end{matrix} \\ \left|\begin{matrix} J_{1,1}^0 & J_{1,2}^0 & J_{1,3}^0 & J_{1,4}^0 & J_{1,5}^0 & J_{1,6}^0 & J_{1,7}^0 & J_{1,8}^0 & J_{1,9}^0 & J_{1,10}^0 & J_{1,11}^0 & J_{1,12}^0 & J_{1,13}^0 & J_{1,14}^0 & J_{1,15}^0 & J_{1,16}^0 \\ J_{2,1}^0 & J_{2,2}^0 & J_{2,3}^0 & J_{2,4}^0 & J_{2,5}^0 & J_{2,6}^0 & J_{2,7}^0 & J_{2,8}^0 & J_{2,9}^0 & J_{2,10}^0 & J_{2,11}^0 & J_{2,12}^0 & J_{2,13}^0 & J_{2,14}^0 & J_{2,15}^0 & J_{2,16}^0 \\ J_{3,1}^0 & J_{3,2}^0 & J_{3,3}^0 & J_{3,4}^0 & J_{3,5}^0 & J_{3,6}^0 & J_{3,7}^0 & J_{3,8}^0 & J_{3,9}^0 & J_{3,10}^0 & J_{3,11}^0 & J_{3,12}^0 & J_{3,13}^0 & J_{3,14}^0 & J_{3,15}^0 & J_{3,16}^0 \\ J_{4,1}^0 & J_{4,2}^0 & J_{4,3}^0 & J_{4,4}^0 & J_{4,5}^0 & J_{4,6}^0 & J_{4,7}^0 & J_{4,8}^0 & J_{4,9}^0 & J_{4,10}^0 & J_{4,11}^0 & J_{4,12}^0 & J_{4,13}^0 & J_{4,14}^0 & J_{4,15}^0 & J_{4,16}^0 \\ J_{5,1}^0 & J_{5,2}^0 & J_{5,3}^0 & J_{5,4}^0 & J_{5,5}^0 & J_{5,6}^0 & J_{5,7}^0 & J_{5,8}^0 & J_{5,9}^0 & J_{5,10}^0 & J_{5,11}^0 & J_{5,12}^0 & J_{5,13}^0 & J_{5,14}^0 & J_{5,15}^0 & J_{5,16}^0 \\ J_{6,1}^0 & J_{6,2}^0 & J_{6,3}^0 & J_{6,4}^0 & J_{6,5}^0 & J_{6,6}^0 & J_{6,7}^0 & J_{6,8}^0 & J_{6,9}^0 & J_{6,10}^0 & J_{6,11}^0 & J_{6,12}^0 & J_{6,13}^0 & J_{6,14}^0 & J_{6,15}^0 & J_{6,16}^0 \\ J_{7,1}^0 & J_{7,2}^0 & J_{7,3}^0 & J_{7,4}^0 & J_{7,5}^0 & J_{7,6}^0 & J_{7,7}^0 & J_{7,8}^0 & J_{7,9}^0 & J_{7,10}^0 & J_{7,11}^0 & J_{7,12}^0 & J_{7,13}^0 & J_{7,14}^0 & J_{7,15}^0 & J_{7,16}^0 \\ J_{8,1}^0 & J_{8,2}^0 & J_{8,3}^0 & J_{8,4}^0 & J_{8,5}^0 & J_{8,6}^0 & J_{8,7}^0 & J_{8,8}^0 & J_{8,9}^0 & J_{8,10}^0 & J_{8,11}^0 & J_{8,12}^0 & J_{8,13}^0 & J_{8,14}^0 & J_{8,15}^0 & J_{8,16}^0 \\ J_{9,1}^0 & J_{9,2}^0 & J_{9,3}^0 & J_{9,4}^0 & J_{9,5}^0 & J_{9,6}^0 & J_{9,7}^0 & J_{9,8}^0 & J_{9,9}^0 & J_{9,10}^0 & J_{9,11}^0 & J_{9,12}^0 & J_{9,13}^0 & J_{9,14}^0 & J_{9,15}^0 & J_{9,16}^0 \\ J_{10,1}^0 & J_{10,2}^0 & J_{10,3}^0 & J_{10,4}^0 & J_{10,5}^0 & J_{10,6}^0 & J_{10,7}^0 & J_{10,8}^0 & J_{10,9}^0 & J_{10,10}^0 & J_{10,11}^0 & J_{10,12}^0 & J_{10,13}^0 & J_{10,14}^0 & J_{10,15}^0 & J_{10,16}^0 \\ J_{11,1}^0 & J_{11,2}^0 & J_{11,3}^0 & J_{11,4}^0 & J_{11,5}^0 & J_{11,6}^0 & J_{11,7}^0 & J_{11,8}^0 & J_{11,9}^0 & J_{11,10}^0 & J_{11,11}^0 & J_{11,12}^0 & J_{11,13}^0 & J_{11,14}^0 & J_{11,15}^0 & J_{11,16}^0 \\ J_{12,1}^0 & J_{12,2}^0 & J_{12,3}^0 & J_{12,4}^0 & J_{12,5}^0 & J_{12,6}^0 & J_{12,7}^0 & J_{12,8}^0 & J_{12,9}^0 & J_{12,10}^0 & J_{12,11}^0 & J_{12,12}^0 & J_{12,13}^0 & J_{12,14}^0 & J_{12,15}^0 & J_{12,16}^0 \\ J_{13,1}^0 & J_{13,2}^0 & J_{13,3}^0 & J_{13,4}^0 & J_{13,5}^0 & J_{13,6}^0 & J_{13,7}^0 & J_{13,8}^0 & J_{13,9}^0 & J_{13,10}^0 & J_{13,11}^0 & J_{13,12}^0 & J_{13,13}^0 & J_{13,14}^0 & J_{13,15}^0 & J_{13,16}^0 \\ J_{14,1}^0 & J_{14,2}^0 & J_{14,3}^0 & J_{14,4}^0 & J_{14,5}^0 & J_{14,6}^0 & J_{14,7}^0 & J_{14,8}^0 & J_{14,9}^0 & J_{14,10}^0 & J_{14,11}^0 & J_{14,12}^0 & J_{14,13}^0 & J_{14,14}^0 & J_{14,15}^0 & J_{14,16}^0 \\ J_{15,1}^0 & J_{15,2}^0 & J_{15,3}^0 & J_{15,4}^0 & J_{15,5}^0 & J_{15,6}^0 & J_{15,7}^0 & J_{15,8}^0 & J_{15,9}^0 & J_{15,10}^0 & J_{15,11}^0 & J_{15,12}^0 & J_{15,13}^0 & J_{15,14}^0 & J_{15,15}^0 & J_{15,16}^0 \\ J_{16,1}^0 & J_{16,2}^0 & J_{16,3}^0 & J_{16,4}^0 & J_{16,5}^0 & J_{16,6}^0 & J_{16,7}^0 & J_{16,8}^0 & J_{16,9}^0 & J_{16,10}^0 & J_{16,11}^0 & J_{16,12}^0 & J_{16,13}^0 & J_{16,14}^0 & J_{16,15}^0 & J_{16,16}^0 \end{matrix}\right| \begin{matrix} \leftarrow \Delta P_2^{(1)} \\ \leftarrow \Delta Q_2^{(1)} \\ \leftarrow \Delta P_3^{(1)} \\ \leftarrow \Delta Q_3^{(1)} \\ \leftarrow \Delta P_4^s \\ \leftarrow \Delta Q_4^s \\ \leftarrow \Delta I_{r,1}^{(5)} \\ \leftarrow \Delta I_{i,1}^{(5)} \\ \leftarrow \Delta I_{r,2}^{(5)} \\ \leftarrow \Delta I_{i,2}^{(5)} \\ \leftarrow \Delta I_{r,3}^{(5)} \\ \leftarrow \Delta I_{i,3}^{(5)} \\ \leftarrow \Delta I_{r,4}^{(5)} \\ \leftarrow \Delta I_{i,4}^{(5)} \\ \leftarrow \Delta I_{r,4}^{(1)} \\ \leftarrow \Delta I_{i,4}^{(1)} \end{matrix} \end{array}$$

The top row, which is not part of the Jacobian, lists the variables:

$$\delta_2^{(1)}\ V_2^{(1)}\ \delta_3^{(1)}\ V_3^{(1)}\ \delta_4^{(1)}\ V_4^{(1)}\ \delta_1^{(5)}\ V_1^{(5)}\ \delta_2^{(5)}\ V_2^{(5)}\ \delta_3^{(5)}\ V_3^{(5)}\ \delta_4^{(5)}\ V_4^{(5)}\ \alpha\ \beta$$

and the right-hand side column, which is not part of the Jacobian, lists the mismatch quantities that must be satisfied:

$$[\Delta P_2^{(1)}\ \Delta Q_2^{(1)}\ \Delta P_3^{(1)} \Delta Q_3^{(1)}\ \Delta P_4^s\ \Delta Q_4^s\ I_{r,1}^{(5)}\ \Delta I_{i,1}^{(5)}\ \Delta I_{r,2}^{(5)}\ \Delta I_{i,2}^{(5)}\ \Delta I_{r,3}^{(5)}\ \Delta I_{i,3}^{(5)}\ \Delta I_{r,4}^{(5)}\ \Delta I_{r,4}^{(1)}\ \Delta I_{i,4}^{(1)}]^t.$$

These two identifications help in defining the partial derivatives of the Jacobian. For example,

$$J_{3,5}^0 = \frac{\partial(\Delta P_3^{(1)})}{\partial(\delta_4^{(1)})},\quad J_{3,10}^0 = \frac{\partial(\Delta P_3^{(1)})}{\partial(V_2^{(5)})},$$

$$J_{8,5}^0 = \frac{\partial(\Delta I_{i,1}^{(5)})}{\partial(\delta_4^{(1)})},\quad J_{8,10}^0 = \frac{\partial(\Delta I_{i,1}^{(5)})}{\partial(V_2^{(5)})},$$

$$J_{9,11}^0 = \frac{\partial(\Delta I_{r,2}^{(5)})}{\partial(\delta_3^{(5)})},\ \text{and}\ J_{12,16}^0 = \frac{\partial(\Delta I_{i,3}^{(5)})}{\partial(\beta)}.$$

In the solution below submatrices are defined, which is an alternative way of defining the Jacobian entries.

***Step #4 of Harmonic Load Flow.*** Evaluate the Jacobian matrix $\bar{J}$ and compute $\Delta\bar{U}^0$. The Jacobian matrix has the following form ($\bar{0}_{mxn}$ denotes an $n$ by $m$ zero submatrix with zero entries):

$$\bar{J} = \begin{vmatrix} \bar{J}^{(1)} & \bar{J}^{(5)} & \bar{0}_{6,2} \\ & & \bar{0}_{6,2} \\ \bar{G}^{(5,1)} & \bar{Y}^{(5,5)} + \bar{G}^{(5,5)} & \bar{H}^{(5)} \\ \bar{Y}^{(1,1)} + \bar{G}^{(1,1)} & \bar{G}^{(1,5)} & \bar{H}^{(1)} \end{vmatrix}.$$

The Jacobian submatrix for the fundamental is

$$\bar{J}^{(1)} = \begin{vmatrix} 61.68 & 52.932 & -11.764 & -2.944 & 0 & 0 \\ -52.94 & 61.945 & 2.944 & -11.764 & 0 & 0 \\ -11.764 & -2.944 & 51.772 & 22.917 & -40.0076 & -19.98 \\ 2.944 & -11.764 & -22.926 & 51.773 & 19.982 & -40.0076 \\ 0 & 0 & -40.0076 & -19.982 & 80.015 & 39.961 \\ 0 & 0 & 19.982 & -40.0076 & -39.963 & 80 \end{vmatrix}.$$

ST. GEORGE BOOKSTORE UC LAKE

The Jacobian submatrix for the 5th harmonic is

$$\bar{J}^{(5)} = \left| \begin{matrix} & & & \bar{0}_{4\times 8} & & & & \\ -0.099 & -0.099 & 0 & 0 & -0.099 & -0.09 & 0.198 & 0.198 \\ 0.010 & -0.099 & 0 & 0 & 0.010 & -0.99 & -0.020 & 1.98 \end{matrix} \right|.$$

Also

$$\bar{Y}^{(1,1)} = \begin{vmatrix} 0 & 0 & -39.889 & -19.89 & 79.81 & 39.73 \\ 0 & 0 & -19.81 & 40.06 & 39.56 & -80.14 \end{vmatrix}$$

$$\bar{Y}^{(5,5)} = \begin{vmatrix} 202.91 & 4.84 & -1.92 & -3.85 & 0 & 0 & -0.99 & -0.99 \\ 0.48 & -2029.1 & -0.39 & 19.23 & 0 & 0 & -0.10 & 9.90 \\ -1.92 & -3.846 & 2.17 & 3.97 & -0.25 & -0.13 & 0 & 0 \\ -0.39 & 19.23 & 0.40 & -21.73 & -0.01 & 2.45 & 0 & 0 \\ 0 & 0 & -0.25 & -0.13 & 1.24 & 1.12 & -0.99 & -0.99 \\ 0 & 0 & -0.01 & 2.49 & 0.11 & -12.40 & -0.10 & 9.90 \\ -0.99 & -0.99 & 0 & 0 & -0.99 & -0.99 & 1.98 & 1.98 \\ -0.01 & 9.90 & 0 & 0 & -0.01 & 9.90 & 0.20 & -19.80 \end{vmatrix}.$$

In this example, $\bar{H}^{(1)}$ and $\bar{H}^{(5)}$ are zero submatrices since there are no nonlinear device variables defined for the system of Fig. E7.14.1. However, setting $\bar{H}^{(1)}$ and $\bar{H}^{(5)}$ to zero introduces two columns of zeros in the Jacobian matrix, which makes it singular. In order to avoid this situation, $\bar{H}^{(1)}$ and $\bar{H}^{(5)}$ are set to random matrices. Note that the solution does not depend on the values of these submatrices.

In order to compute $\bar{G}^{(1,1)}$ and $\bar{G}^{(1,5)}$, we need to differentiate $G_{r,4}^{(1)}$ and $G_{i,4}^{(1)}$ as follows:

$$\frac{\partial G_{r,4}^{(1)}}{\partial \delta_4^{(1)}} = -\frac{P_4^{(1)} \sin\gamma_4^{(1)}}{V_4^{(1)} \cos(\delta_4^{(1)} - \gamma_4^{(1)})} = 0.1016$$

$$\frac{\partial G_{r,4}^{(1)}}{\partial V_4^{(1)}} = -\frac{P_4^{(1)} \cos\gamma_4^{(1)}}{(V_4^{(1)})^2 \cos(\delta_4^{(1)} - \gamma_4^{(1)})} = -0.252$$

$$\frac{\partial G_{i,4}^{(1)}}{\partial \delta_4^{(1)}} = -\frac{P_4^{(1)} \cos\gamma_4^{(1)}}{V_4^{(1)} \cos(\delta_4^{(1)} - \gamma_4^{(1)})} = -0.250$$

$$\frac{\partial G_{i,4}^{(1)}}{\partial V_4^{(1)}} = -\frac{P_4^{(1)} \sin\gamma_4^{(1)}}{(V_4^{(1)})^2 \cos(\delta_4^{(1)} - \gamma_4^{(1)})} = -0.102.$$

The partial derivatives of $G_{r,4}^{(1)}$ and $G_{i,4}^{(1)}$ with respect to $V_4^{(5)}$ and $\delta_4^{(5)}$ are zero. Therefore, $\bar{G}^{(1,5)}$ is a $2\times 8$ submatrix of zeros and

$$\bar{G}^{(1,5)} = \left| \begin{matrix} & & 0.102 & -0.252 \\ \bar{0}_{2\times 6} & & & \\ & & 0.250 & 0.102 \end{matrix} \right|.$$

In order to compute $\bar{G}^{(5,1)}$ and $\bar{G}^{(5,5)}$, we need to differentiate $G_{r,4}^{(5)}$ and $G_{i,4}^{(5)}$ as follows:

$$\frac{\partial G_{r,4}^{(5)}}{\partial \delta_4^{(1)}} = -0.9(V_4^{(1)})^3 \sin(3\delta_4^{(1)}) = 0.00896$$

$$\frac{\partial G_{r,4}^{(5)}}{\partial V_4^{(1)}} = 0.9(V_4^{(1)})^2 \cos(3\delta_4^{(1)}) = 0.893$$

$$\frac{\partial G_{i,4}^{(5)}}{\partial \delta_4^{(1)}} = 0.9(V_4^{(1)})^3 \cos(3\delta_4^{(1)}) = 0.8894$$

$$\frac{\partial G_{i,4}^{(5)}}{\partial V_4^{(1)}} = 0.9(V_4^{(1)})^2 \sin(3\delta_4^{(1)}) = -0.009.$$

Also

$$\frac{\partial G_{r,4}^{(5)}}{\partial \delta_4^{(5)}} = -0.9(V_4^{(5)})^2 \sin(3\delta_4^{(5)}) = 0.00$$

$$\frac{\partial G_{r,4}^{(5)}}{\partial V_4^{(5)}} = 0.6V_4^{(5)} \cos(3\delta_4^{(5)}) = 0.06$$

$$\frac{\partial G_{i,4}^{(5)}}{\partial \delta_4^{(5)}} = 0.9(V_4^{(5)})^2 \cos(3\delta_4^{(5)}) = 0.006$$

$$\frac{\partial G_{i,4}^{(5)}}{\partial V_4^{(5)}} = 0.6V_4^{(5)} \sin(3\delta_4^{(5)}) = 0.00.$$



Therefore,

$$\bar{G}^{(5,1)} = \left| \begin{matrix} & & \bar{0}_{6\times 8} & & \\ \bar{0}_{2\times 6} & & & 0.00896 & 0.893 \\ & & & 0.8894 & -0.009 \end{matrix} \right|,$$

$$\bar{G}^{(5,5)} = \left| \begin{matrix} & & \bar{0}_{6\times 8} & & \\ \bar{0}_{2\times 6} & & & 0 & 0.06 \\ & & & 0.006 & 0 \end{matrix} \right|.$$

The Jacobian matrix is

$$\left| \begin{matrix} -61.57 & 52.71 & -11.70 & -2.90 & 0 & 0 & 0 & 0 & 0 & 0 & 0 & 0 & 0 & 0 & 0 & 0 \\ -52.79 & 61.52 & 2.89 & -11.74 & 0 & 0 & 0 & 0 & 0 & 0 & 0 & 0 & 0 & 0 & 0 & 0 \\ -11.69 & -2.96 & 51.37 & 22.86 & -39.71 & -19.90 & 0 & 0 & 0 & 0 & 0 & 0 & 0 & 0 & 0 & 0 \\ 2.95 & -11.72 & -22.77 & 51.58 & 19.82 & -39.87 & 0 & 0 & 0 & 0 & 0 & 0 & 0 & 0 & 0 & 0 \\ 0 & 0 & -39.66 & -19.94 & 79.45 & 39.59 & -0.099 & -0.099 & 0 & 0 & -0.099 & -0.099 & 0.198 & 0.198 & 0 & 0 \\ 0 & 0 & 19.86 & -39.83 & -39.93 & 79.58 & 0.010 & -0.99 & 0 & 0 & 0.010 & -0.99 & -0.020 & 1.98 & 0 & 0 \\ 0 & 0 & 0 & 0 & 0 & 0 & 202.9 & 4.84 & -1.92 & -3.85 & 0 & 0 & -0.99 & -0.99 & 0 & 0 \\ 0 & 0 & 0 & 0 & 0 & 0 & 0.48 & -2029 & -0.39 & 19.23 & 0 & 0 & -0.10 & 9.90 & 0 & 0 \\ 0 & 0 & 0 & 0 & 0 & 0 & -1.92 & -3.846 & 2.17 & 3.97 & -0.25 & -0.13 & 0 & 0 & 0 & 0 \\ 0 & 0 & 0 & 0 & 0 & 0 & -0.39 & 19.23 & 0.40 & -21.73 & -0.01 & 2.45 & 0 & 0 & 0 & 0 \\ 0 & 0 & 0 & 0 & 0 & 0 & 0 & 0 & -0.25 & -0.13 & 1.24 & 1.12 & -0.99 & -0.99 & 0 & 0 \\ 0 & 0 & 0 & 0 & 0 & 0 & 0 & 0 & -0.01 & 2.49 & 0.11 & -12.40 & -0.10 & 9.90 & 0 & 0 \\ 0 & 0 & 0 & 0 & 0.009 & 0.893 & -0.99 & -0.99 & 0 & 0 & -0.99 & -0.99 & 1.98 & 2.04 & 0 & 0 \\ 0 & 0 & 0 & 0 & 0.889 & -0.009 & -0.01 & 9.90 & 0 & 0 & -0.01 & 9.90 & 0.201 & -19.80 & 0 & 0 \\ 0 & 0 & -39.89 & -19.89 & 79.91 & 39.48 & 0 & 0 & 0 & 0 & 0 & 0 & 0 & 0 & 1 & 2 \\ 0 & 0 & -19.81 & 40.06 & 39.81 & -80.04 & 0 & 0 & 0 & 0 & 0 & 0 & 0 & 0 & 3 & 4 \end{matrix} \right|.$$

### 7.4.11 Application Example 7.18: Computation of the Correction Bus Vector and Convergence of Harmonic Power Flow: Solution

***Step #5 of Harmonic Load Flow.*** Evaluate $\Delta\bar{U}^0$ and update $\Delta\bar{U}^0$.

The correction bus vector $\Delta\bar{U}^0$ is computed as follows:

$$\Delta\bar{U}^0 = (\bar{J}^0)^{-1} \begin{bmatrix} 3.43472\,E-6 \\ -1.33365\,E-6 \\ -7.62939\,E-6 \\ -3.81470\,E-6 \\ 2.99421\,E-2 \\ 2.97265\,E-4 \\ 4.217029\,E-6 \\ -200.0 \\ -4.09782\,E-8 \\ 2.384186\,E-7 \\ -1.93715\,E-7 \\ -5.960464\,E-8 \\ 0.29935 \\ -3.03515\,E-3 \\ -1.78814\,E-7 \\ 8.86619\,E-7 \end{bmatrix} = \begin{bmatrix} 1.20815\,E-6 \\ -8.59742\,E-7 \\ 9.552948\,E-6 \\ 1.54111\,E-6 \\ 1.184274\,E-5 \\ 2.3572\,E-6 \\ 1.46588\,E-3 \\ 0.10000228 \\ 2.38763\,E-2 \\ 0.1005407 \\ 0.2042002 \\ 0.1021379 \\ 0.249194 \\ 0.1027635 \\ -- \\ -- \end{bmatrix}.$$

The updated bus vector is

$$\bar{U}^1 = \bar{U}^0 - \Delta\bar{U}^0 = (-2.68332E-4,\ 0.99759,\ -2.80029E-3,\ 0.99640,\ -3.4257E-3,\ 0.99594,\ -1.465844E-3,\ -2.28E-6,\ -2.38763E-2,\ -5.407E-4,\ -0.2042,\ -2.138E-3,\ -0.24919,\ -2.7635E-3,\ 0,\ 0)'.$$

Note that all harmonic voltage magnitudes are negative. To prevent negative magnitudes, the corresponding phase angles are shifted by $\pi$ radians; therefore,

$$\bar{U}^1 = (-2.68332E-4,\ 0.99759,\ -2.80029E-3,\ 0.99640,\ -3.4257E-3,\ 0.99594,\ 3.14013,\ 2.28E-6,\ 3.11772,\ 5.407E-4,\ 2.93738,\ 2.138E-3,\ 2.89239,\ 2.7635E-3,\ 0,\ 0)'.$$

The new (updated) nonlinear device currents are $G_{r,4}^{(1)} = 0.256629$, $G_{i,4}^{(1)} = -0.1011142$, $G_{r,4}^{(5)} = 0.2965726$ and $G_{i,4}^{(5)} = -2.59613E-3$. The new (updated) mismatch vector is

$$\Delta\bar{W}^1 = (5.342E-6,\ -3.800E-7,\ 5.722E-6,\ 3.815E-6,\ -1.403E-3,\ 4.332E-4,\ -2.269E-3,\ -3.300E-2,\ -2.677E-3,\ 6.475E-3,\ -1.021E-3,\ -2.105E-3,\ 0.3023,\ 3.015E-2,\ -6.264E-4,\ -1.473E-4)'.$$

This mismatch vector is not small enough and the solution has not converged. However, the iterative procedure will converge in eight iterations. The final solution is (all magnitudes are in percentage of the base values and all angles are in degrees):

Fundamental power flow output solution (Fig. E7.14.1):

| | Bus voltage | | Bus generation (G) and load (L) powers | | | | | Line power[a] | |
|---|---|---|---|---|---|---|---|---|---|
| | $\lvert V\rvert$ | $\delta$ | $P_G$ | $Q_G$ | $P_L$ | $Q_L$ | | $P_{line}$ | $Q_{line}$ |
| From Bus | (%) | (°) | (%) | (%) | (%) | (%) | To Bus | (%) | (%) |
| 1 | 100.0 | 0.00 | 35.16 | 20.90 | 0.00 | 0.00 | 2 | 13.35 | 10.81 |
| | | | | | | | 4 | 21.81 | 10.09 |
| 2 | 99.76 | −0.01 | 0.00 | 0.00 | 10.00 | 10.00 | 1 | −13.33 | −10.78 |
| | | | | | | | 3 | 3.32 | 0.78 |
| 3 | 99.64 | −0.16 | 0.00 | 0.00 | 0.00 | 0.00 | 2 | −3.32 | −0.77 |
| | | | | | | | 4 | 3.32 | 0.77 |
| 4 | 99.58 | −0.19 | 0.00 | 0.00 | 25.00 | 10.00 | 3 | −3.32 | −0.77 |
| | | | | | | | 1 | −21.75 | −9.98 |

[a]Fundamental active and reactive powers in the line between "from bus" and "to bus."

Harmonic power flow output solution for harmonic number 5, frequency = 300 Hz (Fig. E7.14.1):

| | Bus voltage | | | Line power[a] | | Line current[a] | |
|---|---|---|---|---|---|---|---|
| | $\lvert V\rvert$ | $\delta$ | | $P_{line}$ | $Q_{line}$ | Magnitude | Angle |
| From bus | (%) | (°) | To bus | (%) | (%) | (%) | (°) |
| 1 | 0.0148 | −90.57 | 2 | 0.000015 | −0.000675 | 4.563896 | −1.88 |
| | | | 4 | −0.000015 | −0.003707 | 25.042787 | −0.33 |
| | | | Neutral shunt | 0.000000 | 0.004382 | 29.605302 | 179.43 |
| 2 | 0.2472 | −102.44 | 1 | 0.002067 | 0.011090 | 4.563896 | 178.12 |
| | | | 3 | −0.002067 | −0.011090 | 4.563895 | −1.88 |
| 3 | 2.0731 | −95.66 | 2 | 0.006233 | 0.094407 | 4.563895 | 178.12 |
| | | | 4 | −0.006233 | −0.094406 | 4.563865 | −1.88 |
| 4 | 2.5315 | −96.01 | 3 | 0.008315 | 0.115235 | 4.563865 | 178.12 |
| | | | 1 | 0.062730 | 0.630848 | 25.042787 | 179.67 |
| | | | Neutral nonlinear | −0.071046 | −0.746085 | 29.605308 | −0.57 |

[a]Harmonic power/current in the line between "from bus" and "to bus."



Total current/power:

| | | Line current | | | | Line power | | | |
|---|---|---|---|---|---|---|---|---|---|
| | | Fundamental value | rms value | Peak value | $THD_i$ (%) | $P$ (%) | $Q$ (%) | $D$ (%) | $S$ (%) |
| From bus | To bus | (%) | (%) | (%) | | | | | |
| 1 | 2 | 17.18 | 17.78 | 19.26 | 0.9665 | 13.35 | 10.81 | 4.57 | 17.78 |
| 1 | 4 | 24.03 | 34.71 | 46.94 | 0.6923 | 21.81 | 10.09 | 25.04 | 34.71 |
| 2 | 1 | 17.18 | 17.78 | 19.26 | 0.9665 | −13.32 | −10.77 | 4.59 | 17.73 |
| 2 | 3 | 3.42 | 5.70 | 7.90 | 0.6000 | 3.32 | 0.77 | 4.56 | 5.69 |
| 3 | 2 | 3.42 | 5.70 | 7.90 | 0.6000 | −3.32 | −0.68 | 4.57 | 5.69 |
| 3 | 4 | 3.42 | 5.71 | 7.90 | 0.6000 | 3.32 | 0.68 | 4.57 | 5.69 |
| 4 | 3 | 3.42 | 5.71 | 7.90 | 0.6000 | −3.31 | −0.65 | 4.57 | 5.69 |
| 4 | 1 | 24.03 | 34.71 | 46.94 | 0.6923 | −21.69 | −9.35 | 25.25 | 34.57 |
| 4 | Neutral nonlinear | 27.04 | 40.09 | 54.76 | 0.6744 | 24.93 | 9.25 | 29.80 | 39.94 |

Bus voltage summary:

| Bus number | Fundamental value (%) | rms value (%) | Peak value (%) | $THD_v$ (%) |
|---|---|---|---|---|
| 1 | 100.00 | 100.00 | 100.00 | 1.0000 |
| 2 | 99.76 | 99.76 | 99.71 | 1.0000 |
| 3 | 99.63 | 99.65 | 99.97 | 0.9998 |
| 4 | 99.58 | 99.61 | 100.11 | 0.9997 |

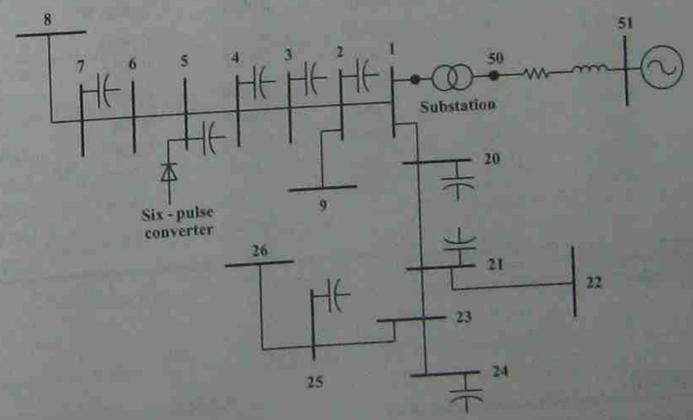



**FIGURE E7.18.1** The distorted IEEE 18-bus system used for simulation [29 in Chapter 7].

### 7.5.7 Application Example 7.19: Accuracy of Decoupled Harmonic Power Flow (DHPF): Solution

The Newton-based HPF (e.g., using an accurate converter model that includes harmonic couplings [5, 6 in Chapter 7]) and the DHPF (modeling the converter with harmonic current sources of Table E7.18.1) are applied to the 18 bus system. Simulation results are compared in Table E7.18.2. Small levels of the maximum and average deviations (last two rows of Table E7.18.2) show the acceptable accuracy of the decoupled approach.

ST. GEORGE POLYTECHNIC

**TABLE E7.18.1** Magnitude of Harmonic Currents (as a Percentage of the Fundamental) Used to Model Six-Pulse Converters[a]

| Harmonic order | Magnitude (%) | Harmonic order | Magnitude (%) | Harmonic order | Magnitude (%) |
|---|---|---|---|---|---|
| 1 | 100 | 19 | 2.4 | 37 | 0.5 |
| 5 | 19.1 | 23 | 1.2 | 41 | 0.5 |
| 7 | 13.1 | 25 | 0.8 | 43 | 0.5 |
| 11 | 7.2 | 29 | 0.2 | 47 | 0.4 |
| 13 | 5.6 | 31 | 0.2 | 49 | 0.4 |
| 17 | 3.3 | 35 | 0.4 | | |

[a]All harmonic phase angles are assumed to be zero.

**TABLE E7.18.2** Comparison of Simulation Results for the 18 Bus System (Fig. E7.18.1) using Coupled (Section 7.4) and Decoupled (Section 7.5.1) Harmonic Power Flow

| | Fundamental voltage (pu) | | rms voltage (pu) | | Distortion factor D (%) | | THD of voltage (%) | |
|---|---|---|---|---|---|---|---|---|
| Bus | Decoupled HPF | Coupled HPF | Decoupled HPF | Coupled HPF | Decoupled HPF | Coupled HPF | Decoupled HPF | Coupled HPF |
| 1 | 1.0545 | 1.0545 | 1.0549 | 1.0548 | 0.996 | 0.9997 | 2.7159 | 2.3828 |
| 2 | 1.0511 | 1.0510 | 1.0516 | 1.0516 | 0.9995 | 0.9995 | 3.1353 | 3.1942 |
| 3 | 1.0456 | 1.0455 | 1.0463 | 1.0465 | 0.9993 | 0.9991 | 3.6591 | 4.2593 |
| 4 | 1.0425 | 1.0424 | 1.0433 | 1.0436 | 0.9992 | 0.9989 | 3.9386 | 4.7737 |
| 5 | 1.0359 | 1.0358 | 1.0370 | 1.0377 | 0.9988 | 0.9981 | 4.8692 | 6.1886 |
| 6 | 1.0348 | 1.0347 | 1.0360 | 1.0367 | 0.9988 | 0.9981 | 4.8692 | 6.1886 |
| 7 | 1.0326 | 1.0325 | 1.0339 | 1.0347 | 0.9987 | 0.9979 | 5.1238 | 6.5404 |
| 8 | 1.0268 | 1.0267 | 1.0281 | 1.0289 | 0.9987 | 0.9978 | 5.1528 | 6.5775 |
| 9 | 1.0496 | 1.0496 | 1.0501 | 1.0501 | 0.9995 | 0.9995 | 3.1397 | 3.1965 |
| 20 | 1.0505 | 1.0504 | 1.0509 | 1.0509 | 0.9996 | 0.9996 | 2.9329 | 2.9248 |
| 21 | 1.0496 | 1.0495 | 1.0505 | 1.0506 | 0.9991 | 0.9990 | 4.1782 | 4.4609 |
| 22 | 1.0479 | 1.0479 | 1.0488 | 1.0489 | 0.9991 | 0.9990 | 4.1847 | 4.4682 |
| 23 | 1.0451 | 1.0451 | 1.0474 | 1.0477 | 0.9978 | 0.9974 | 6.6676 | 7.1620 |
| 24 | 1.0485 | 1.0485 | 1.0519 | 1.0523 | 0.9968 | 0.9964 | 7.9886 | 8.4865 |
| 25 | 1.0419 | 1.0418 | 1.0449 | 1.0452 | 0.9971 | 0.9967 | 7.6002 | 8.1187 |
| 26 | 1.0415 | 1.0414 | 1.0445 | 1.0449 | 0.9971 | 0.9967 | 7.6029 | 8.1220 |
| 50 | 1.0501 | 1.0501 | 1.0501 | 1.0501 | 1.0000 | 1.0000 | 0.2482 | 0.1217 |
| 51 | 1.0500 | 1.0500 | 1.0500 | 1.0500 | 1.0000 | 1.0000 | 0.2482 | 0.0035 |
| MD[a] | 0.0097 | – | 0.778 | – | 0.0009 | – | 1.42473 | - |
| AD[b] | 0.0059 | – | 0.0278 | – | 0.003 | – | 0.57242 | - |

[a]Maximum deviation with respect to the coupled HPF (%).
[b]Average deviation with respect to the couple HPF (%).

## CHAPTER 8 SOLUTIONS

### 8.1.1 Application Example 8.1: Calculation of Reliability Indices: Solution

The reliability indices are

SAIDI = (sum of the number of customer interruption durations)/(total number of affected customers) = 0.003 h/customer, where interruptions with 0 V are taken into account,

SAIFI = (sum of the number of customer interruptions)/(total number of affected customers) = 0.004 interruptions/customer, where interruptions with 0 V are taken into account,

$$\text{SARFI}_{\%V} = \Sigma N_i / N_T = 67.5\%,$$

where $\text{SARFI}_{\%V}$ is the number of specified short-duration rms variations per system customer (60 s aggregation). The notation "%V" refers to the bus voltage percent deviation that is counted as an event. $\text{SARFI}_{\%V} = \Sigma N_i / N_T$, where %V is the rms voltage threshold to define an event, $N_i$ is the number of customers that see the event, and $N_T$ is the total number of customers in the study. In this case %V = ±10%. For the SARFI index, the voltage threshold allows assessment of compatibility for voltage-sensitive devices. Typical annual value for SARFI is about 15% for a 70% voltage (%V) event.



**TABLE P8.1.1** Electricity interruptions/transients

| Number of interruptions/ transients | Number of interruptions/ transients duration | voltage in % of rated value | total number of customers affected | cause of interruption/ transient |
|---|---|---|---|---|
| 10 | 4.5 h | 0 | 1000 | overload |
| 15 | 3 h | 0 | 1500 | repair |
| 60 | 1 min | 90 | 500 | switching transients |
| 90 | 1 s | 130 | 500 | capacitor switching |
| 110 | 0.1 s | 40 | 15000 | short-circuits |
| 95 | 0.1 s | 150 | 4000 | lightning |
| 130 | 0.01 s | 50 | 3000 | short-circuits |

### 8.2.5.1 Application Example 8.5: Frequency Control of an Interconnected Power System Broken into Two Areas: The First One with a 300 MW Coal-Fired Plant and the Other One with a 5 MW Wind-Power Plant: Solution

a) List of ordinary differential equations

$$\varepsilon_{11} = \text{loadref}_1(s) - \frac{\Delta\omega_1}{R_1} \quad \text{(E8.5-1)}$$

$$\Delta P_{\text{valve1}} + T_{G1}\frac{d(\Delta P_{\text{valve1}})}{dt} = \varepsilon_{11} \quad \text{(E8.5-2)}$$

$$\Delta P_{\text{mech1}} + T_{CH1}\frac{d(\Delta P_{\text{mech1}})}{dt} = \Delta P_{\text{valve1}} \quad \text{(E8.5-3)}$$

$$\varepsilon_{21} = \Delta P_{\text{mech1}} - \Delta P_{L1} - \Delta P_{\text{tie}} \quad \text{(E8.5-4)}$$

$$\Delta\omega_1 D_1 + M_1\frac{d(\Delta\omega_1)}{dt} = \varepsilon_{21} \quad \text{(E8.5-5)}$$

$$\frac{\Delta P_{\text{tie}}}{\varepsilon_3} = T/s \quad \text{(E8.5-6)}$$

$$s\Delta P_{\text{tie}} = T\varepsilon_3 \quad \text{(E8.5-7)}$$

$$\frac{1}{T}\frac{d(\Delta P_{\text{tie}})}{dt} = T\varepsilon_3 \quad \text{(E8.5-8)}$$

$$\varepsilon_{12} = \text{loadref}_2(s) - \frac{\Delta\omega_2}{R_2} \quad \text{(E8.5-9)}$$

$$\Delta P_{\text{valve2}} + T_{G2}\frac{d(\Delta P_{\text{valve2}})}{dt} = \varepsilon_{12} \quad \text{(E8.5-10)}$$

$$\Delta P_{\text{mech2}} + T_{CH2}\frac{d(\Delta P_{\text{mech2}})}{dt} = \Delta P_{\text{valve2}} \quad \text{(E8.5-11)}$$

$$\varepsilon_{22} = \Delta P_{\text{mech2}} - \Delta P_{L2} + \Delta P_{\text{tie}} \quad \text{(E8.5-12)}$$

$$\Delta\omega_2 D_2 + M_2\frac{d(\Delta\omega_2)}{dt} = \varepsilon_{22}. \quad \text{(E8.5-13)}$$

There are 11 independent equations and 11 unknowns. The latter are $\varepsilon_{11}$, $\Delta P_{\text{valve1}}$, $\Delta P_{\text{mech1}}$, $\varepsilon_{21}$, $\Delta P_{\text{tie}}$, $\Delta\omega_1$, $\varepsilon_{12}$, $\Delta P_{\text{valve2}}$, $\Delta P_{\text{mech2}}$, $\varepsilon_{22}$, $\Delta\omega_2$.

b)

*Mathematica Program*

```
Remove[Dw1, R1, Loadref1, E11,
DPvalve1, DPmech1, DP11, E12, Tg1,
Tch1, M1, D1, Dw2, R2, Loadref2,
E22, DPvalve2, DPmech2, DP12, E21,
Tch2, M2, D2, Sbase, eq1, eq2, eq3,
ic1, ic2, ic3, DPtie, E3, Tie, Xtie,
ic4, ic5, ic6, ic7];
Sbase=500000000;
M1=4.5;
Tg1=0.01;
Tch1=0.5;
R1=0.01; D1=0.8; M2=6;
Tg2=0.02;
Tch2=0.75;
R2=0.02;
D2=1;
Xtie=0.2;
Tie=377/Xtie;
Loadref1[t_]:=If[t<0,0,0.8];
Loadref2[t_]:=If[t<0,0,0.8];
DP11[t_]:=If[t<5,0,0.2];
DP12[t_]:=If[t<5,0,-0.2];
ic1=Dw1[0]= =0;
ic2=DPmech1[0]= =0;
ic3=DPvalve1[0]= =0;
ic5=Dw2[0]= =0;
ic6=DPmech2[0]= =0;
ic7=DPvalve2[0]= =0;
ic4=DPtie[0]= =0;
E11[t_]:=Loadref1[t]-(Dw1[t]/R1);
E12[t_]:=DPmech1[t]-(DP11[t]-DPtie[t]);
E3[t_]:=Dw1[t]-Dw2[t];
E22[t_]:=Loadref2[t]-(Dw2[t]/R2);
E21[t_]:=DPmech2[t]-(DP12[t]-DPtie[t]);
eq1=Dw1'[t]=
=(1/M1)*(E12[t]-D1*Dw1[t]);
eq2=DPmech1'[t]=
=(1/Tch1)*(DPvalve1[t]-DPmech1[t]);
```

```
eq3=DPvalve1'[t]=
=(1/Tg1)*(E11[t]-DPvalve1[t]);
eq5=Dw2'[t]=
=(1/M2)*(E21[t]-D2*Dw2[t]);
eq6=DPmech2'[t]= =(1/Tch2)*(DPvalve2
[t]-DPmech2[t]);
eq7=
DPvalve2'[t]=
=(1/Tg2)*(E22[t]-DPvalve2[t]);
eq4=DPtie'[t]= =Tie*E3[t];
sol=NDSolve[{eq1,eq2,eq3,
eq4,eq5,eq6,eq7,ic1,ic2,ic3,ic4,ic5,ic6,ic7},Dw1[t],
DPmech1[t],DPvalve1[t],DPtie[t],
Dw2[t],DPmech2[t], Dpvalve2[t]},
{t,0,100},MaxSteps->
1000000];
Plot[Dw1[t]/sol,{t,0,100}, PlotRange-
>All, AxesLabel->{,,t","Dw1(t)"}];
Plot[Dw2[t]/sol,{t,0,100}, PlotRange-
>All, AxesLabel->{,,t","Dw2(t)"}];
```

b) The angular frequency deviations $\Delta\omega_1(t)$ and $\Delta\omega_2(t)$ based on Mathematica for droop characteristics with $R_1 = 0.01$ pu, $R_2 = 0.02$ pu are shown in Figs. E8.5.1 and E8.5.2. Note that there is instability, and both plots result in the same frequency response.

c) The angular frequency deviations $\Delta\omega_1(t)$ and $\Delta\omega_2(t)$ based on Mathematica for droop characteristics with $R_1 = 0.01$, $R_2 = 0.5$ are shown in Figs. E8.5.3 and E8.5.4. Note that there is stability, and both plots result in the same frequency response.

***MATLAB Program***

```
%defining the input
Sbase=500e6;
M1=4.5;
Tg1=0.01;
Tch1=0.5;
R1=0.01;
D1=0.8;
M2=6;
Tg2=0.02;
Tch2=0.75;
R2=0.02;
D2=1;
Xtie=0.2;
Tie=377/Xtie;
%time span
T1=0:0.001:20;
T=T1.';
%solving system of equations
opts=odeset('AbsTol',1e-11,'RelTol',1e-7;
[t0,x0]=ode45)@F2,T,[0;0;0;0;0;0;0],o
pts,M1,Tg1,Tch1,R1,D1,M2,Tg2,Tch2,R2,
D2,Tie);
%plot results
figure;
Plot(t0,x0(:;4));
Grid on, zoom on;
Title(,Transient response of \Delta\
omega1(t) vs t'));
xlabel('t');
```

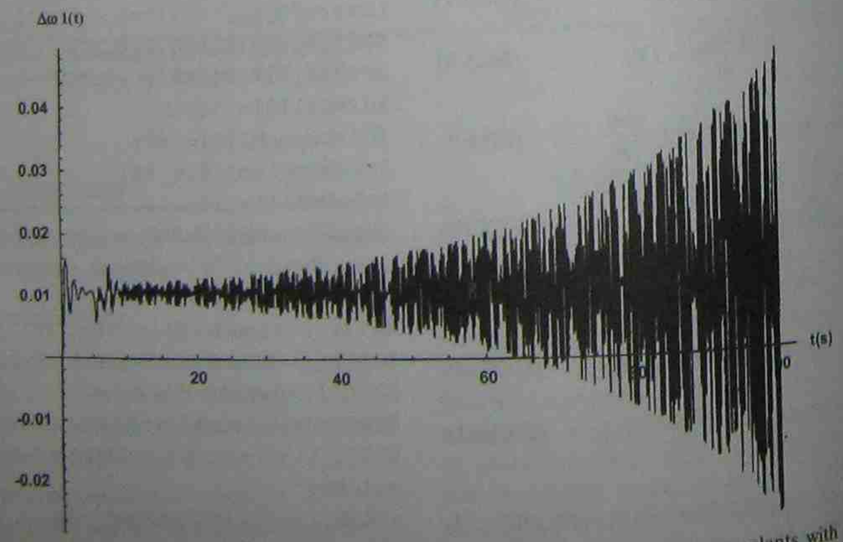



**FIGURE E8.5.1** Angular frequency deviation $\Delta\omega_1(t)$ indicating the instability of two power plants with similar droop characteristics.





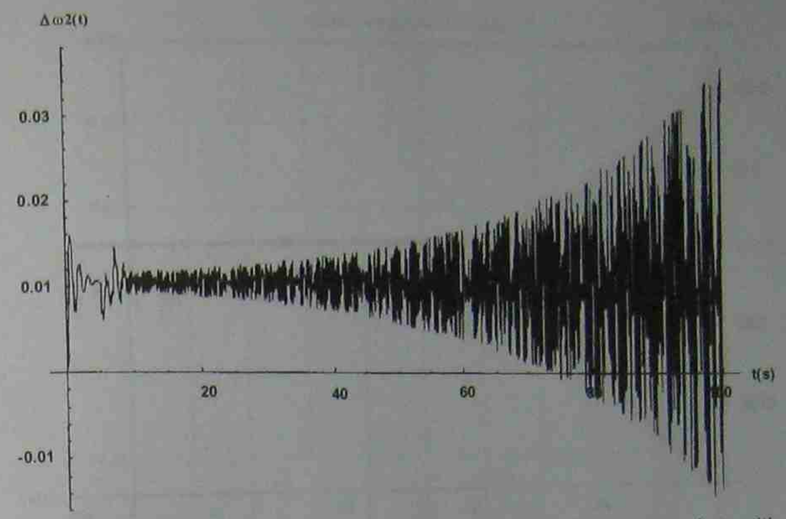



**FIGURE E8.5.2** Angular frequency deviation $\Delta\omega_2(t)$ indicating the instability of two power plants with similar droop characteristics.

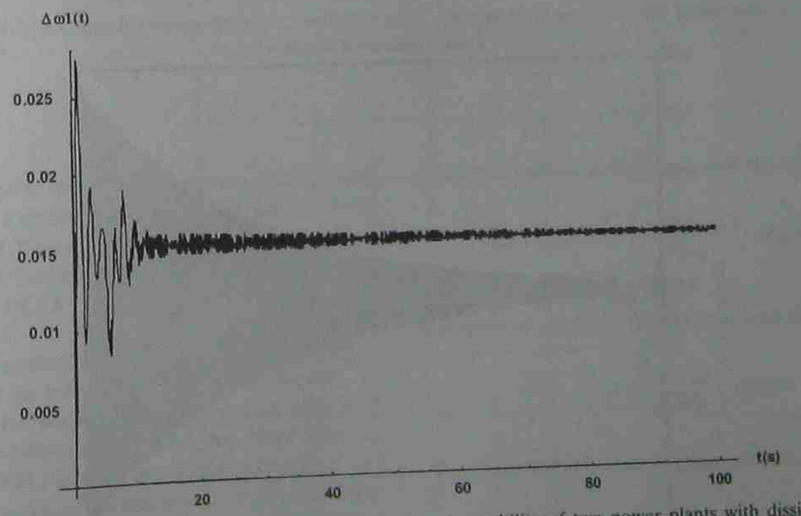



**FIGURE E8.5.3** Angular frequency deviation $\Delta\omega_1(t)$ indicating the stability of two power plants with dissimilar droop characteristics.

```
ylabel('\Delta\omega1(t)');
figure;
Plot(t0,x0(:;1));
Grid on, zoom on;
Title(,Transient response of \Delta\
omega2(t) vs t'));
xlabel('t');
ylabel('\Delta\omega2(t)');
where the function F2 is:
function xprime=F2(t,x,M1,Tg1,Tch1,
R1,D1,M2,Tg2,Tch2,R2,D2,Tie);
if t<5;
DPl1=0;
elseDPl1=0.2;
end
if t<7;
DPl2=0;
elseDPl2=-0.2;
end
if t<0;
load1=0;
else load1=0.8;
end
if t<0;
```

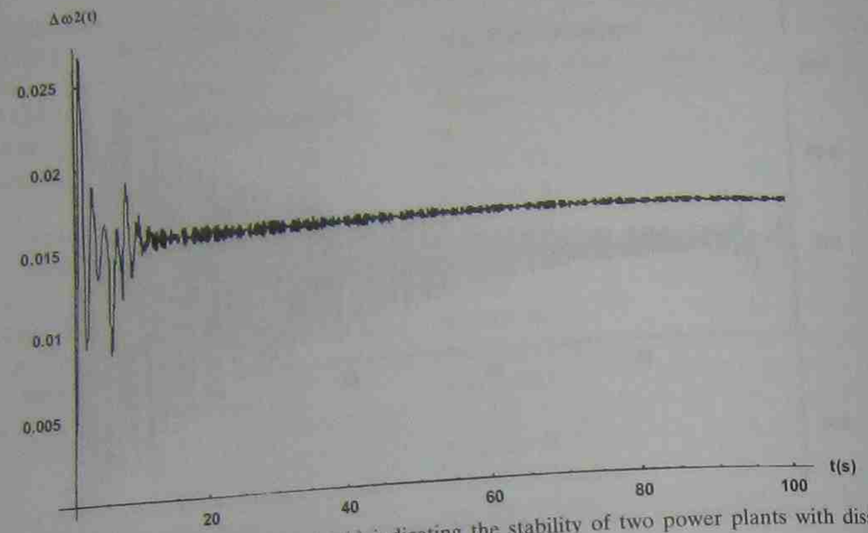



**FIGURE E8.5.4** Angular frequency deviation $\Delta\omega_2(t)$ indicating the stability of two power plants with dissimilar droop characteristics.

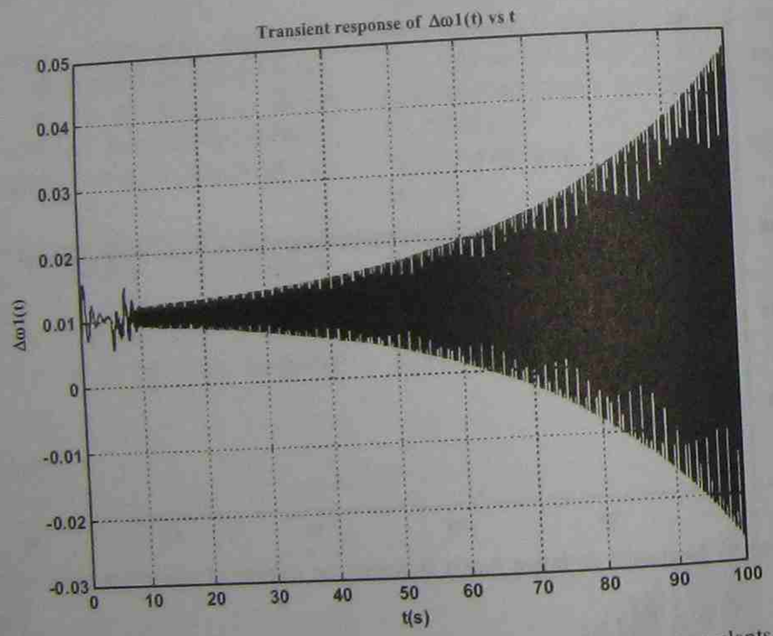



**FIGURE E8.5.5** Angular frequency deviation $\Delta\omega_1(t)$ indicating the instability of two power plants with similar droop characteristics.

```
load2=0;
else load2=0.8;
end
xprime=zeros(7,1);
xprime(1)=(1/M1)*(x(2)-DP11-x(7)-(D1*x(1)));
xprime(2)=(1/Tch1)*(x(3)-x(2);
xprime(3)=(1/Tg1)*(load1-(x(1))*(1/R1)-x(3)));
xprime(4)=(1/M2)*(x(5)-DP12-x(7)-(D2*x(4)));
xprime(5)=(1/Tch2)*(x(6)-x(5);
xprime(6)=(1/Tg2)*(load2-(x(4))*(1/R2)-x(6)));
xprime(7)=(Tie)*(x(12)-x(4));
```

The angular frequency deviations $\Delta\omega_1(t)$ and $\Delta\omega_2(t)$ based on MATLAB for droop characteristics with $R_1 = 0.01$ pu, $R_2 = 0.02$ pu are shown in Figs. E8.5.5 and E8.5.6 confirming the results of Figs. E8.5.1 and E8.5.2.



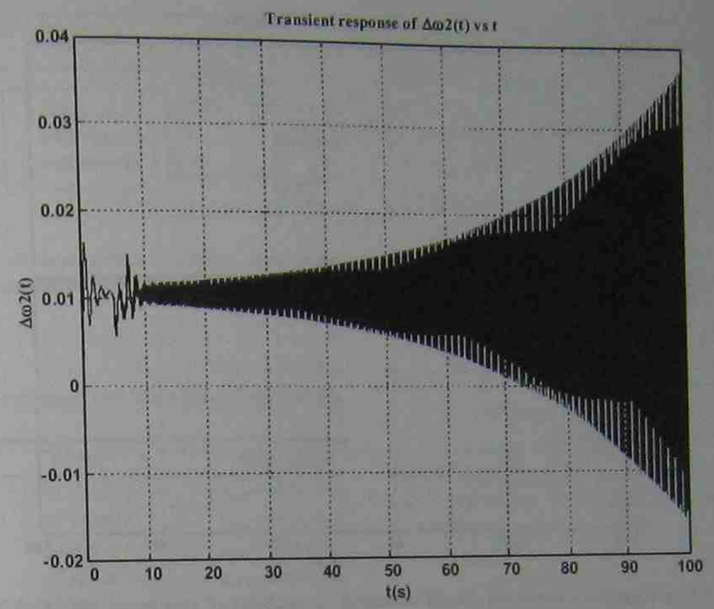



**FIGURE E8.5.6** Angular frequency deviation $\Delta\omega_2(t)$ indicating the instability of two power plants with similar droop characteristics.

The angular frequency deviations $\Delta\omega_1(t)$ and $\Delta\omega_2(t)$ based on MATLAB for droop characteristics with $R_1 = 0.01$ pu, $R_2 = 0.5$ pu are shown in Figs. E8.5.7 and E8.5.8 confirming the results of Figs. E8.5.3 and E8.5.4.

#### 8.2.5.2 Application Example 8.6: Frequency Control of an Interconnected Power System Broken into Two Areas: The First One with a 5 MW Wind-Power Plant and the Other One with a 5 MW Photovoltaic Plant: Solution

The angular frequency deviations $\Delta\omega_1(t)$ and $\Delta\omega_2(t)$ for droop characteristics with $R_1 = 0.5$ pu, $R_2 = 0.5$ pu are much larger than those in Application Example 8.5, that is, there is poor frequency control. See Problems 8.5 through 8.7.

#### 8.3.4 Application Example 8.9: New Approach $p_{cu} = i_2'(v_1 - v_2')$ and $p_{fe} = v_1(i_1 - i_2')$: Solution

The exciting current is measured with the error of (taking into account the maximum error limits of the instruments)

$$\frac{\Delta(i_1 - i_2')}{(i_1 - i_2')} = \frac{\varepsilon_{CT1} + \varepsilon_{CT2} + \varepsilon_{A1}}{(i_1 - i_2')/20} = \frac{(\pm 5.2 \pm 3.47 \pm 0.1)\text{mA}}{35.5\text{mA}} = \pm 0.247.$$

The input voltage is measured with the error of

$$\frac{\Delta v_1}{v_1} = \frac{\varepsilon_{PT1} + \varepsilon_{V1}}{v_1} = \frac{\pm 0.24 \pm 0.3}{240} = \pm 0.0023$$

and the iron-core loss is measured with the error of

$$\frac{\Delta P_{fe}}{P_{fe}} = \frac{\Delta v_1}{v_1} + \frac{\Delta(i_1 - i_2')}{(i_1 - i_2')} = \pm 0.249.$$

The series voltage drop is measured with the error of

$$\frac{\Delta(v_1 - v_2')}{(v_1 - v_2')} = \frac{\varepsilon_{PT1} + \varepsilon_{PT2} + \varepsilon_{V2}}{(v_1 - v_2')} = \frac{\pm 0.24 \pm 0.24 \pm 0.01}{4.86} = \pm 0.1008.$$

The output current is measured with the error of

$$\frac{\Delta i_2}{i_2} = \frac{\varepsilon_{CT2} + \varepsilon_{A2}}{i_2} = \frac{\pm 0.00347 \pm 0.005}{3.472} = \pm 0.00244$$

and the copper loss is measured with the error of

$$\frac{\Delta P_{cu}}{P_{cu}} = \frac{\Delta i_2}{i_2} + \frac{\Delta(v_1 - v_2')}{(v_1 - v_2')} = \pm 0.1032.$$

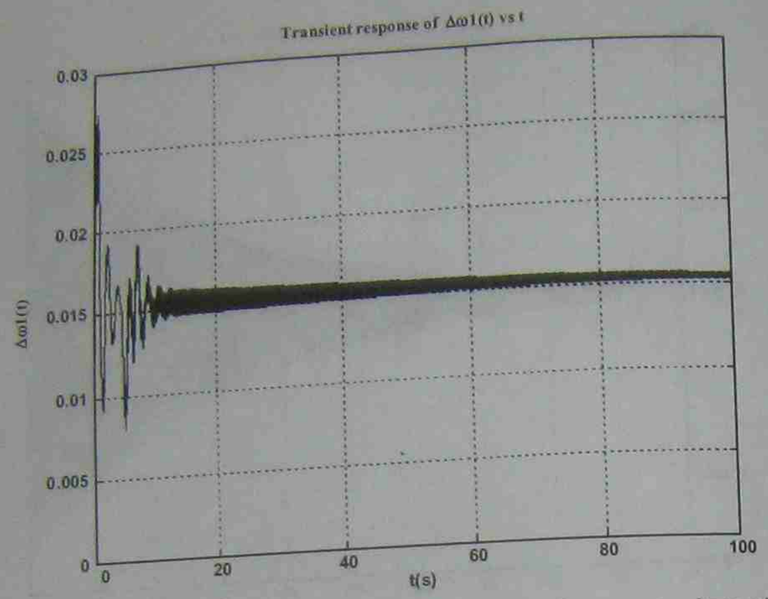



**FIGURE E8.5.7** Angular frequency deviation $\Delta\omega_1(t)$ indicating the stability of two power plants with dissimilar droop characteristics.

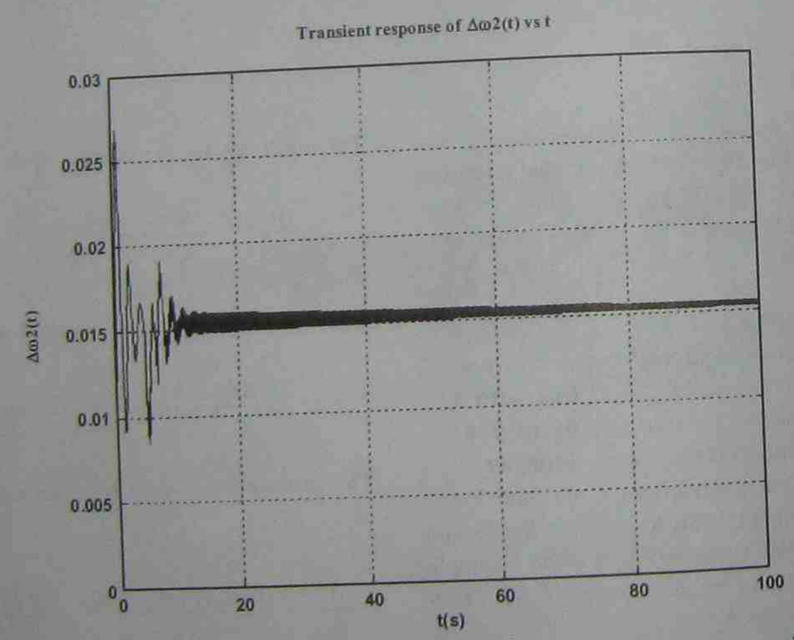



**FIGURE E8.5.8** Angular frequency deviation $\Delta\omega_2(t)$ indicating the stability of two power plants with dissimilar droop characteristics.

Therefore, the total loss is measured with the error of

$$\frac{\Delta P_{Loss}}{P_{Loss}} = \frac{\Delta P_{Cu} + \Delta P_{Fe}}{P_{Loss}} = \frac{\pm 0.1032 \times 325 \pm 0.249 \times 65}{390} = \pm 0.128 = \pm 12.8\%.$$

This maximum error can be reduced further by using three-winding current and potential transformers as shown in Fig. E8.9.2a,b for the measurement of exciting currents and voltage drops. The input and output currents pass though the primary and secondary windings of the current transformer, and the current in the tertiary winding represents the exciting current of the power transformer. Similarly, the input and output voltages are applied to the two primary windings of the potential transformers, and the secondary winding measures the voltage drop of



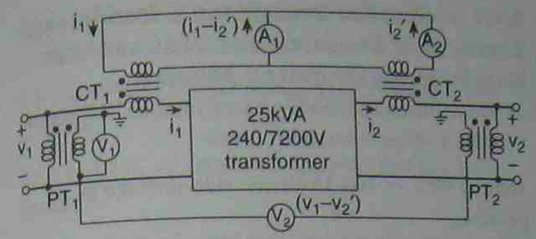



**FIGURE E8.9.1** Loss measurements of single-phase transformers from voltage and current differences.

**TABLE E8.9.1** Instruments and Their Error Limits of Fig. E8.9.1

| Instrument | Rating | Error limits |
|---|---|---|
| $PT_1$ | 240 V/240 V | $\varepsilon_{PT1} = \pm 0.24$ V |
| $PT_2$ | 7200 V/240 V | $\varepsilon_{PT2} = \pm 0.24$ V |
| $CT_1$ | 100 A/5 A | $\varepsilon_{CT1} = \pm 5.2$ mA |
| $CT_2$ | 5 A/5 A | $\varepsilon_{CT2} = \pm 3.47$ mA |
| $V_1$ | 300 V | $\varepsilon_{V1} = \pm 0.3$ V |
| $V_2$ | 10 V | $\varepsilon_{V2} = \pm 0.01$ V |
| $A_1$ | 100 mA | $\varepsilon_{A1} = \pm 0.1$ mA |
| $A_2$ | 5 A | $\varepsilon_{A2} = \pm 5$ mA |

the power transformer. For this 25 kVA single-phase transformer, the turns ratio for both the CT and the PT is $N_{p1}:N_{p2}:N_s = 1:30:1$. The maximum error by using three-winding current and potential transformers can be reduced to as small a value as to that of the back-to-back method, which will be described below.

### 8.3.5 Application Example 8.10: Back-to-Back Approach of Two Transformers Simulated with CTs and PTs: Solution

The exciting current is measured with the error of

$$\frac{\Delta(i_1 - i_2')}{(i_1 - i_2')} = \frac{\varepsilon_{CT1} + \varepsilon_{A1}}{(i_1 - i_2')} = \frac{\pm 0.0014 \pm 0.002}{1.41} = \pm 0.0024.$$

The input voltage is measured with the error of

$$\frac{\Delta v_1}{v_1} = \frac{\varepsilon_{PT1} + \varepsilon_{V1}}{v_1} = \frac{\pm 0.24 \pm 0.3}{240} = \pm 0.0023$$

and the iron-core loss is measured with the error of

$$\frac{\Delta P_{fe}}{P_{fe}} = \frac{\Delta v_1}{v_1} + \frac{\Delta(i_1 - i_2')}{(i_1 - i_2')} = \pm 0.0047.$$

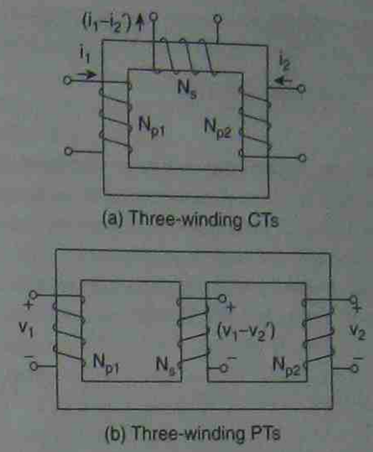



**FIGURE E8.9.2** (a) Three-winding current and (b) potential transformers as applied to new method of loss measurement.

**TABLE E8.10.1** Instruments and Their Error Limits of Fig. E8.10.1

| Instrument | Rating | Error limits |
|---|---|---|
| $PT_1$ | 240 V/240 V | $\varepsilon_{PT1} = \pm 0.24$ V |
| $PT_2$ | 12 V/12 V | $\varepsilon_{PT2} = \pm 9.7$ mV |
| $CT_1$ | 2 A/2 A | $\varepsilon_{CT1} = \pm 1.4$ mA |
| $CT_2$ | 100 A/5 A | $\varepsilon_{CT2} = \pm 5.2$ mA |
| $V_1$ | 300 V | $\varepsilon_{V1} = \pm 0.3$ V |
| $V_2$ | 10 V | $\varepsilon_{V2} = \pm 0.01$ V |
| $A_1$ | 2 A | $\varepsilon_{A1} = \pm 2$ mA |
| $A_2$ | 5 A | $\varepsilon_{A2} = \pm 5$ mA |

The series voltage drop is measured with the error of

$$\frac{\Delta(v_1 - v_2')}{(v_1 - v_2')} = \frac{\varepsilon_{PT2} + \varepsilon_{V2}}{(v_1 - v_2')} = \frac{\pm 0.0097 \pm 0.01}{9.72} = \pm 0.002.$$

The output current is measured with the error of

$$\frac{\Delta i_2}{i_2} = \frac{\pm \varepsilon_{CT2} \pm \varepsilon_{A2}}{i_2/20} = \frac{\pm 0.0052 \pm 0.005}{5.2} = \pm 0.002$$

and the copper loss is measured with the error of

$$\frac{\Delta P_{cu}}{P_{cu}} = \frac{\Delta i_2}{i_2} + \frac{\Delta(v_1 - v_2')}{(v_1 - v_2')} = \pm 0.004.$$

The total loss is measured with the error of

$$\frac{\Delta P_{Loss}}{P_{Loss}} = \frac{\Delta P_{cu} + \Delta P_{Fe}}{P_{Loss}} = \frac{\pm 0.004 \times 650 \pm 0.0047 \times 130}{780}$$
$$= \pm 0.0041 = \pm 0.41\%.$$

This error analysis shows that the maximum errors of the measurement approach of this section range from 0.5 to 15% mainly depending on the accuracy of the voltage and current sensors (e.g., PTs, CTs). The back-to-back method generates extremely small maximum errors because voltage and current differences are directly measured by one PT and one CT, respectively. In Fig. E8.9.1, the errors of voltage and current differences are large because they are measured by two PTs and two CTs. If three-winding PT and CT (see Fig. E8.9.2a,b) are employed to measure the voltage and current differences, the maximum errors will be as small as those of the back-to-back method – even though instruments with maximum errors of 0.5% are used the maximum errors in loss measurements will not exceed 2.5%. Hall sensors with maximum errors of 0.5% [92 in Chapter 8] are suitable for low-efficient transformers only.

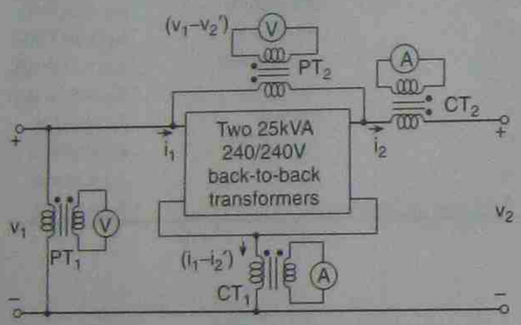



**FIGURE E8.10.1** Instrumentation for single-phase transformer employing back-to-back method of loss measurement.

### 8.4.7 Application Example 8.13: Ride-Through Capability of Computers and Semiconductor Manufacturing Equipment: Solution

a) Ride-through capability based on the CBEMA or ITIC voltage-tolerance curves:

1min at 90% of rated voltage: ride-through is possible,

1 s at 130% of rated voltage: ride-through is not possible,

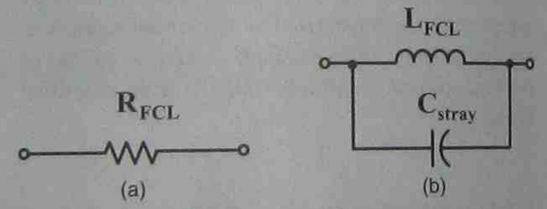
0.1 s at 40% of rated voltage: ride-through is not possible,

0.1 s at 150% of rated voltage: ride-through is not possible,

0.01 s at 50% of rated voltage: ride-through is possible.

b) Ride-through capability based on SEMI F47 standard:

1 min at 90% of rated voltage: ride-through is possible (borderline),




**FIGURES E8.12.2** Model for resistive (a) and inductive (b) fault current limiter.

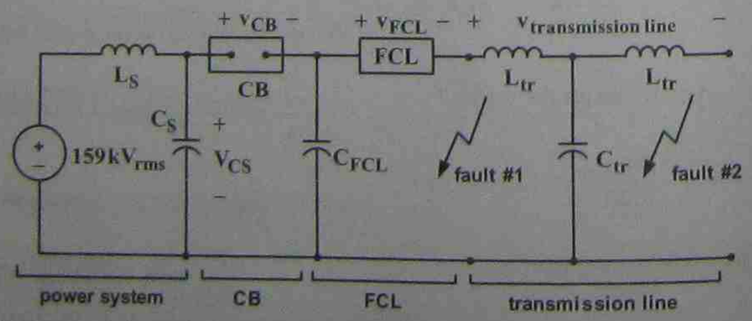



**FIGURE E8.12.1** Single-phase equivalent circuit of a circuit breaker (CB) connected in series with a fault-current limiter (FCL) with two three-phase to ground faults at different locations.





1 s at 130% of rated voltage: ride-through is possible,

0.1 s at 40% of rated voltage: ride-through is not possible,

0.1 s at 150% of rated voltage: ride-through is possible,

0.01 s at 50% of rated voltage: ride-through is possible.

## CHAPTER 9 SOLUTIONS

### 9.3.5 Application Example 9.1: Hybrid Passive Filter Design to Improve the Power Quality of the IEEE 30-Bus Distribution System Serving Adjustable-Speed Drives: Solution [14 in Chapter 9]

***a) Case A. Harmonic Compensation with Two Hybrid Passive Filter Banks at Buses 15 and 18.*** Harmonic analysis before the installation of passive filters indicates a very high distortion of both voltage and current waveforms (Fig. E9.1.3 and Table E9.1.5) due to the two AC drives with relatively high power ratings. According to the IEEE-519 standard [11 in Chapter 9], the individual harmonic current injections at bus 15 (for 5th, 7th, 11th, 13th, 17th, and 19th harmonics) and bus 18 (for 5th, 7th, and 11th harmonics) are higher than the allowable level of 4%, and thus the electric utility has the right to disconnect (reject) these nonlinear loads. In addition, propagation of the injected harmonic currents has resulted in unacceptable voltage THD, levels (e.g., larger than 5%) at buses 12 to 15. Buses 11 and 16 to 18 are also experiencing relatively high THD, of more than 4% (Fig. E9.1.6).

The common procedure is to require the owners of nonlinear loads (at buses 15 and 18) to install passive filter banks at the terminals of the AC drives. Figure E9.1.3 and Table E9.1.5 list the simulation results after the installation of the following two filter banks (Fig. E9.1.2), tuned at the dominant frequencies:

- ***Filter Bank 1:*** Passive filter (Fig. E9.1.2) consisting of five shunt branches tuned to the 5th, 7th, 11th, 13th, and 17th harmonic frequencies and installed at bus 15 with (Eq. 9-9b with $f_1 = 50$ Hz)

$$R_f = 100\,\Omega,\ L_f^{(h)} = 100\,\text{mH (for all branches)},$$
$$\omega_n^{(h)} = 2\pi hf = 1/\sqrt{L_f^{(h)} C_f^{(h)}} \Rightarrow C_f^{(5)} \Rightarrow 4.053\,\mu\text{F},$$
$$C_f^{(7)} = 2.068\,\mu\text{F}, C_f^{(11)} = 0.837\,\mu\text{F}, C_f^{(13)} = 0.680\,\mu\text{F},$$
$$C_f^{(17)} = 0.351\,\mu\text{F}.$$

- ***Filter Bank 2:*** Passive filters (Fig. E9.1.2) with only two shunt branches tuned to the 5th and 7th harmonic frequencies and installed at bus 18 with (Eq. 9-9b with $f_1 = 50$ Hz)

$$R_f = 100\,\Omega,\ L_f^{(h)} = 100\,\text{mH (at all branches)},$$
$$\omega_n^{(h)} = 2\pi hf = 1/\sqrt{L_f^{(h)} C_f^{(h)}} \Rightarrow C_f^{(5)} \Rightarrow 4.053\,\mu\text{F},$$
$$C_f^{(7)} = 2.068\,\mu\text{F}.$$

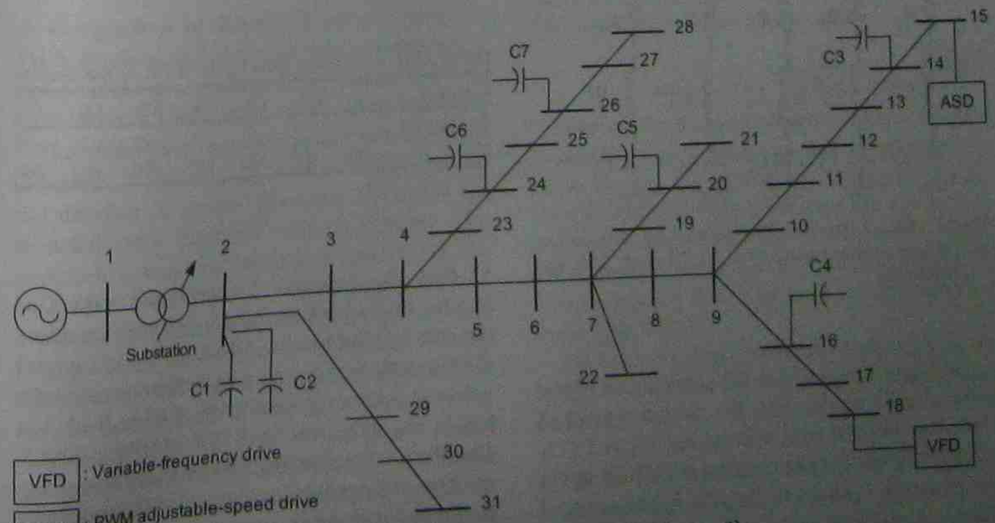



**FIGURE E9.1.1** IEEE 30-bus system with two nonlinear AC drives [9, 10 in Chapter 9].

**TABLE E9.1.1** Line Data for the IEEE 30-Bus System (Base kV = 23 kV, Base MVA = 100 MVA)

| From bus | To bus | R (ohm) | X (ohm) | R (pu) | X (pu) |
|---|---|---|---|---|---|
| 1 | 2 | 0.0021 | 0.0365 | 0.0004 | 0.0069 |
| 2 | 3 | 0.2788 | 0.0148 | 0.0527 | 0.0028 |
| 3 | 4 | 0.4438 | 0.4391 | 0.0839 | 0.0830 |
| 4 | 5 | 0.8639 | 0.7512 | 0.1633 | 0.1420 |
| 5 | 6 | 0.8639 | 0.7512 | 0.1633 | 0.1420 |
| 6 | 7 | 1.3738 | 0.7739 | 0.2597 | 0.1463 |
| 7 | 8 | 1.3738 | 0.7739 | 0.2597 | 0.1463 |
| 8 | 9 | 1.3738 | 0.7739 | 0.2597 | 0.1463 |
| 9 | 10 | 1.3738 | 0.7739 | 0.2597 | 0.1463 |
| 10 | 11 | 1.3738 | 0.7739 | 0.2597 | 0.1463 |
| 11 | 12 | 1.3738 | 0.7739 | 0.2597 | 0.1463 |
| 12 | 13 | 1.3738 | 0.7739 | 0.2597 | 0.1463 |
| 13 | 14 | 1.3738 | 0.7739 | 0.2597 | 0.1463 |
| 14 | 15 | 1.3738 | 0.7739 | 0.2597 | 0.1463 |
| 9 | 16 | 0.8639 | 0.7512 | 0.1633 | 0.1420 |
| 16 | 17 | 1.3738 | 0.7739 | 0.2597 | 0.1463 |
| 17 | 18 | 1.3738 | 0.7739 | 0.2597 | 0.1463 |
| 7 | 19 | 0.8639 | 0.7512 | 0.1633 | 0.1420 |
| 19 | 20 | 0.8639 | 0.7512 | 0.1633 | 0.1420 |
| 20 | 21 | 1.3738 | 0.7739 | 0.2597 | 0.1463 |
| 7 | 22 | 0.8639 | 0.7512 | 0.1633 | 0.1420 |
| 4 | 23 | 0.4438 | 0.4391 | 0.0839 | 0.0830 |
| 23 | 24 | 0.4438 | 0.4391 | 0.0839 | 0.0830 |
| 24 | 25 | 0.8639 | 0.7512 | 0.1633 | 0.1420 |
| 25 | 26 | 0.8639 | 0.7512 | 0.1633 | 0.1420 |
| 26 | 27 | 0.8639 | 0.7512 | 0.1633 | 0.1420 |
| 27 | 28 | 1.3738 | 0.7739 | 0.2597 | 0.1463 |
| 2 | 29 | 0.2788 | 0.0148 | 0.0527 | 0.0028 |
| 29 | 30 | 0.2788 | 0.0148 | 0.0527 | 0.0028 |
| 30 | 31 | 1.3738 | 0.7739 | 0.2597 | 0.1463 |

**TABLE E9.1.2** Bus Data for the IEEE 30-Bus System (Base kV = 23 kV, Base MVA = 100 MVA)

| Bus number | P (kW) | Q (kVAr) | P (pu) | Q (pu) |
|---|---|---|---|---|
| 1[a] | 0 | 0 | 0 | 0 |
| 2 | 52.2 | 17.2 | 0.522 | 0.172 |
| 3 | 0 | 0 | 0 | 0 |
| 4 | 0 | 0 | 0 | 0 |
| 5 | 93.8 | 30.8 | 0.938 | 0.308 |
| 6 | 0 | 0 | 0 | 0 |
| 7 | 0 | 0 | 0 | 0 |
| 8 | 0 | 0 | 0 | 0 |
| 9 | 0 | 0 | 0 | 0 |
| 10 | 18.9 | 6.2 | 0.189 | 0.062 |
| 11 | 0 | 0 | 0 | 0 |
| 12 | 33.6 | 11 | 0.336 | 0.11 |
| 13 | 65.8 | 21.6 | 0.658 | 0.216 |
| 14 | 78.4 | 25.8 | 0.784 | 0.258 |
| 15 | 73 | 24 | 0.73 | 0.24 |
| 16 | 47.8 | 15.7 | 0.478 | 0.157 |
| 17 | 55 | 18.1 | 0.55 | 0.181 |
| 18 | 47.8 | 15.7 | 0.478 | 0.157 |
| 19 | 43.2 | 14.2 | 0.432 | 0.142 |
| 20 | 67.3 | 22.1 | 0.673 | 0.221 |
| 21 | 49.6 | 16.3 | 0.496 | 0.163 |
| 22 | 20.7 | 6.8 | 0.207 | 0.068 |
| 23 | 52.2 | 17.2 | 0.522 | 0.172 |
| 24 | 192 | 63.1 | 1.92 | 0.631 |
| 25 | 0 | 0 | 0 | 0 |
| 26 | 111.7 | 36.7 | 1.117 | 0.367 |
| 27 | 55 | 18.1 | 0.55 | 0.181 |
| 28 | 79.3 | 26.1 | 0.793 | 0.261 |
| 29 | 88.3 | 29 | 0.883 | 0.29 |
| 30 | 0 | 0 | 0 | 0 |
| 31 | 88.4 | 29 | 0.884 | 0.29 |

[a]Swing bus.

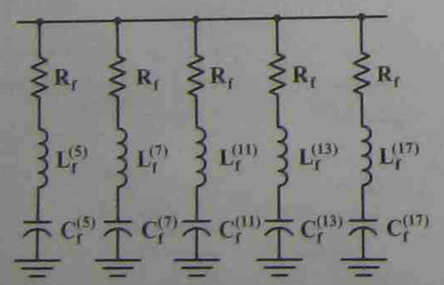



**FIGURE E9.1.2** Passive filter employing five series-resonance filter branches tuned at 5th, 7th, 11th, 13th, and 17th harmonics.

According to Table E9.1.5 the performance of the above filters is satisfactory: the maximum level of $THD_v$ has dropped from 6.51 (at bus 15) to 2.17% (at bus 18) while the average system $THD_v$ is within the permissible limits of the IEEE-519 standard [11].

**TABLE E9.1.3** Capacitor Data for the IEEE 30-Bus System

| Capacitor | C1 | C2 | C3 | C4 | C5 | C6 | C7 |
|---|---|---|---|---|---|---|---|
| Bus location | 2 | 2 | 14 | 16 | 20 | 24 | 26 |
| kVAr | 900 | 600 | 600 | 600 | 300 | 900 | 900 |

***b) Case B. Harmonic Compensation with One Passive Filter Bank at Bus 15.*** This case examines the possibility of meeting IEEE-519 [11 in Chapter 9] limits with only one filter bank. Simulation results before and after the installation of Filter Bank 1 at bus 15 are shown in Fig. E9.1.4 and Table E9.1.5. Therefore, by performing harmonic load flow analysis, it may be possible to eliminate unnecessary filter banks, and therefore reduce the overall cost of harmonic compensation.



**TABLE E9.1.4** Typical Harmonic Spectrum of Variable-Frequency and PWM Adjustable-Speed Drives [14]

| Harmonic order h | Variable-frequency drive: Magnitude (%) | Variable-frequency drive: Phase angle (degree) | PWM adjustable-speed drive: Magnitude (%) | PWM adjustable-speed drive: Phase angle (degree) |
|---|---|---|---|---|
| 1 | 100 | 0 | 100 | 0 |
| 5 | 23.52 | 111 | 82.8 | –135 |
| 7 | 6.08 | 109 | 77.5 | 69 |
| 11 | 4.57 | –158 | 46.3 | –62 |
| 13 | 4.2 | –178 | 41.2 | 139 |
| 17 | 1.8 | –94 | 14.2 | 9 |
| 19 | 1.37 | –92 | 9.7 | –155 |
| 23 | 0.75 | –70 | 1.5 | –158 |
| 25 | 0.56 | –70 | 2.5 | 98 |
| 29 | 0.49 | –20 | 0 | 0 |
| 31 | 0.54 | 7 | 0 | 0 |

***c) Case C. Harmonic Compensation with One Passive Filter Bank at Bus 9.*** To show the impact of filter location on the overall power quality of the distribution system, Filter Bank 1 is installed between the two drive systems at bus 9. The resulting voltage and current waveforms are depicted in Fig. E9.1.5 and the corresponding $THD_v$ levels are listed in Table E9.1.5. It is clear that improper placement of filters will not only deteriorate their performances, but might also favor harmonic propagation and cause additional power quality problems in other sectors of the system (e.g., in buses 10–15 and 16–18 for Case C).

***d) Comparison of Results.*** A comparison of the $THD_v$ levels as well as the rms voltage values before and after the placement of filters (Cases A, B, and C) is listed in Table E9.1.5 and shown in Fig. 9.1.6.

The decoupled harmonic power flow algorithm (Chapter 7, Section 7.5.1) is used to simulate the distribution system. Nonlinear AC drives are modeled with harmonic current sources. This approach is very practical and convenient for the analysis of large distorted industrial systems with inadequate information about the nonlinear loads (e.g., parameters and ratings of AC drives). Simulation results of this application example indicate that the common approach of placing filter banks at the terminals of each AC drive system is not always the most economical solution. It might be possible to limit the overall system distortion, as well as the individual bus $THD_v$ levels, with fewer filters. To do this, system conditions before and after compensation need to be carefully studied, which requires fast algorithms, as presented in this example.

### 9.7.6 Application Example 9.5: Hybrid of Passive and Active Power Filters for Harmonic Mitigation of Six-Pulse and Twelve-Pulse Rectifier Loads [16 in Chapter 9]: Solution [16]

a) Load-Current Waveforms without Filtering

Figure E9.5.3 illustrates simulated power system current waveforms for a twelve-pulse rectifier load, indicating a $THD_i$ of 9.36%. Provided one of the rectifiers (Fig. E9.5.2) is out of service (e.g., six-pulse rectifier configuration), the power system current $THD_i$ increases to 26.28%.

b) Current Equations with Hybrid Filter #2

The converter of hybrid filter #2 operates at harmonic frequencies like a resistor in series with the power system impedance. Therefore, the effective harmonic impedance of the power system is increased and the resonance of the passive power filter is suppressed. In addition, the filter performance is improved by imposing a voltage harmonic waveform at its terminals with the following amplitude:

$$v_{a1}(t) = K_1\, i_{sh}(t), \qquad \text{(E9.5-1)}$$

where $i_{sh}(t)$ is the harmonic content of the power system current, and $K_1$ is the converter gain. The power converter consumes fundamental power. This power is stored in the DC capacitor to regulate its voltage and compensate the inverter losses [15, 16 in Chapter 9]. Therefore, DC capacitor voltage regulation is performed without any external power supply. The output voltage can be written as

$$v_a(t) = v_{a1}(t) + v_{a2}(t). \qquad \text{(E9.5-2)}$$

Hybrid filter #2 is controlled using the synchronous reference frame (e.g., dq0 transformation), which changes the conventional three abc rotating phasors into direct (d), quadrature (q), and zero (0) sequence components. The fundamental components are transformed into a DC term and harmonic components are shifted by $\omega_1$ in the dq0 reference frame (Eq. 9-14).

The block diagram of the control scheme is shown in Fig. E9.5.4 where the control block is divided into two parts:

- The performance improvement block mitigates the resonance problem of the passive power filter and the overall performance of the filtering system.

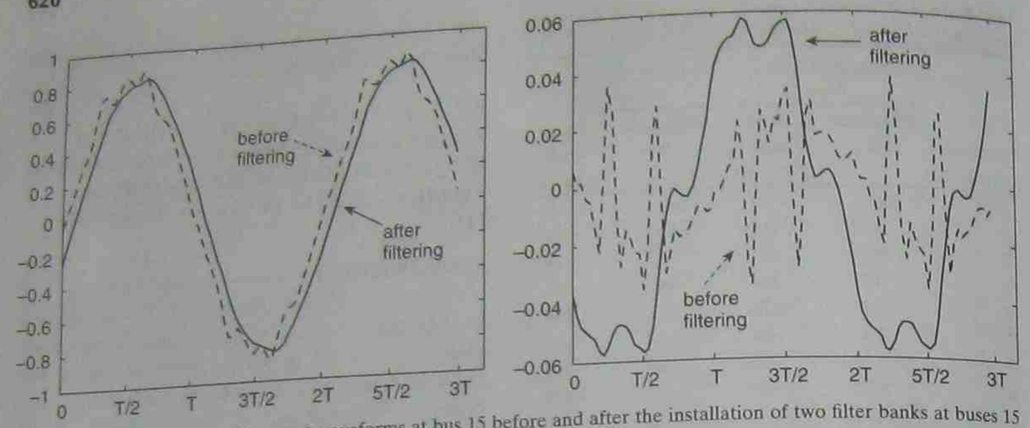



**FIGURE E9.1.3** Voltage and current waveforms at bus 15 before and after the installation of two filter banks at buses 15 and 18 (Case A).

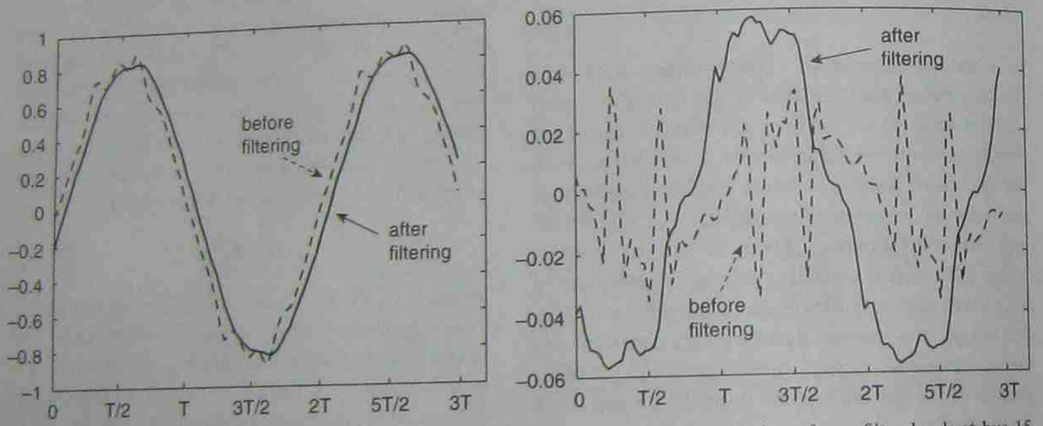



**FIGURE E9.1.4** Voltage and current waveforms at bus 15 before and after the installation of one filter bank at bus 15 (Case B).

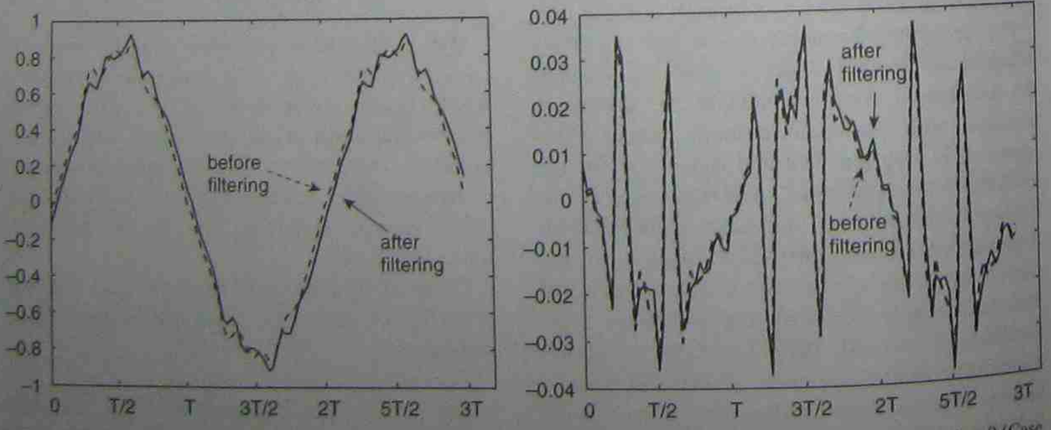



**FIGURE E9.1.5** Voltage and current waveforms at bus 15 before and after the installation of one filter bank at bus 9 (Case C).



**TABLE E9.1.5** Summary of Simulation Results for the IEEE 30-Bus System before and after the Installation of Filter(s)

| | Before filtering | | After filtering (Case A) | |
|---|---|---|---|---|
| | Minimum | Maximum | Minimum | Maximum |
| rms voltage | 0.8382 pu at bus 15 | 1.0003 pu at bus 1 | 0.8295 pu at bus 15 | 1.0003 pu at bus 2 |
| $THD_v$ | 1.8492% at bus 5 | 6.5089% at bus 15 | 1.0548% at bus 11 | 2.1691% at bus 18 |
| System $THD_v$ | 3.1820% | | 1.4818% | |
| | After filtering (Case B) | | After filtering (Case C) | |
| | Minimum | Maximum | Minimum | Maximum |
| rms voltage | 0.8337 pu at bus 5 | 1.0001 pu at bus 2 | 0.8469 pu at bus 15 | 1.0002 pu at bus 2 |
| $THD_v$ | 1.2520% at bus 22 | 1.8629% at bus 18 | 1.0938% at bus 6 | 5.8453% at bus 15 |
| System $THD_v$ | 1.4950% | | 1.8707% | |

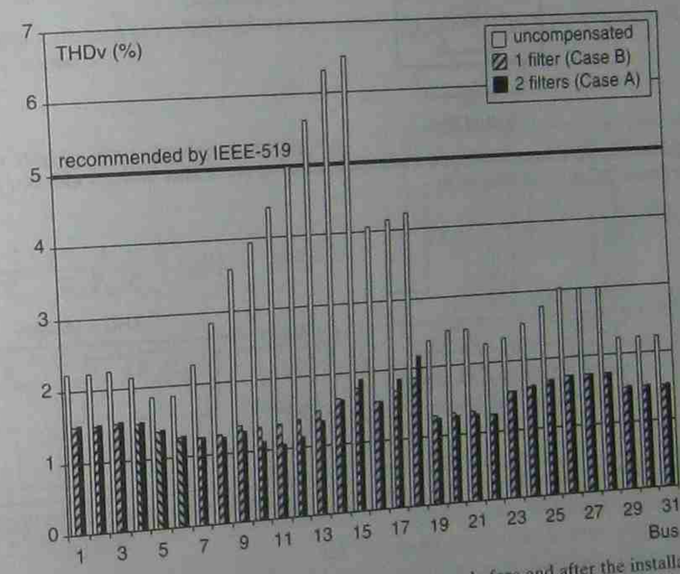



**FIGURE E9.1.6** Comparison of $THD_v$ levels of the IEEE 30-bus system before and after the installation of one (Case B) and two (Case A) filter banks [14 in Chapter 9].

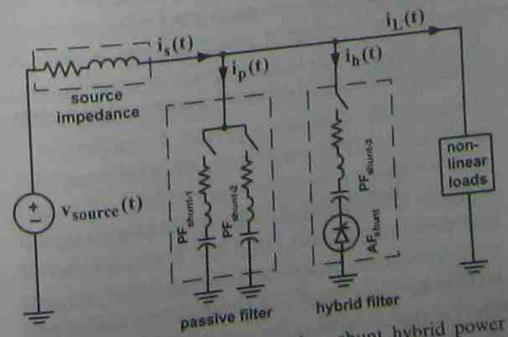



**FIGURE E9.5.1** Hybrid filter #1, a shunt hybrid power filter (series combination of a small rating active filter and a tuned passive branch) in parallel with tuned passive filters [15 in Chapter 9].

It contains high-pass filters in the dq0 frame to filter the fundamental component of the power system current. The output is passed through an amplifier and $v_{a1}(t)$ is obtained.

- The DC voltage regulator block maintains the DC bus voltage at a constant level and reduces possible voltage fluctuations due to the harmonic real power injection (for filter performance improvement) and the power loss of the converter.

A low-pass filter with a cutoff at line frequency is also employed to extract the fundamental component of the DC-link voltage. The DC capacitor voltage is compared with its reference value, and the output of the comparator serves as input to the PI

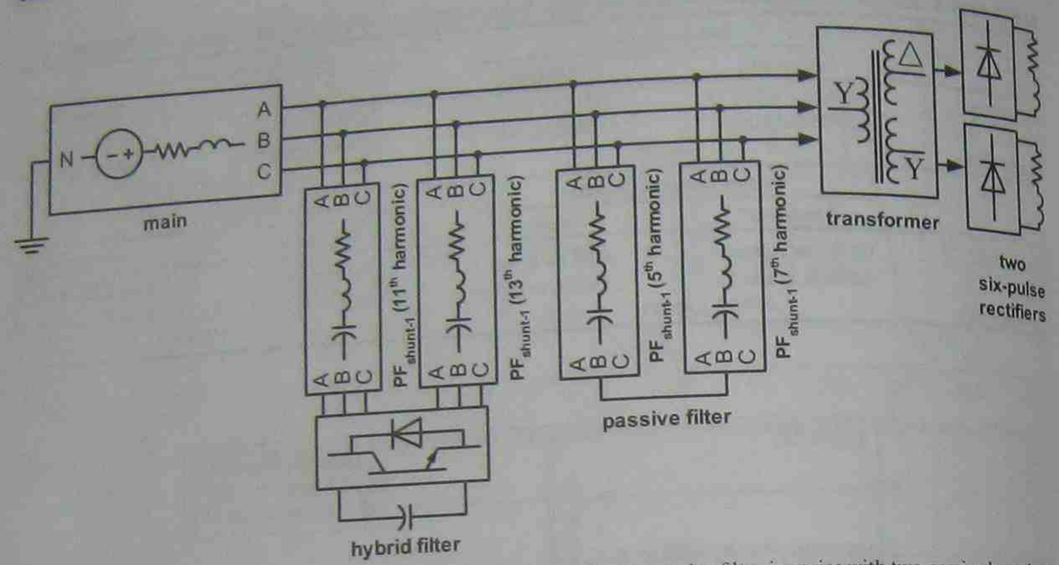
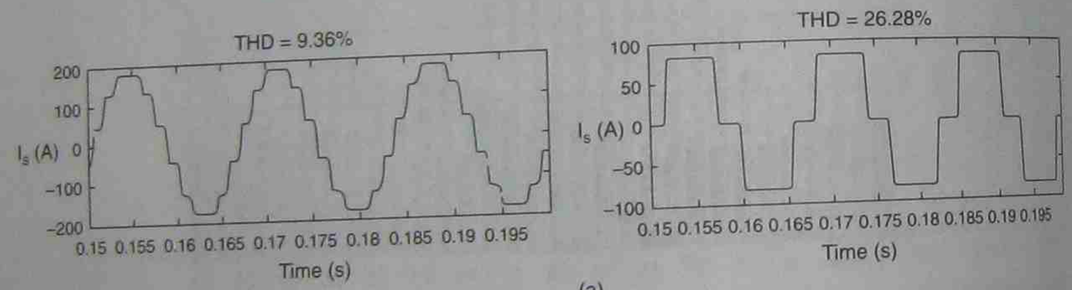



**FIGURE E9.5.2** Hybrid filter #2, a shunt hybrid power filter (a small rating active filter in series with two passive branches) in parallel with two passive filters [16 in Chapter 9].




(a)

| Load configuration | Twelve-pulse rectifier ($THD_i$=9.32%) | | | | Six-pulse rectifier ($THD_i$=26.28%) | | | |
|---|---|---|---|---|---|---|---|---|
| Harmonic order | 5th | 7th | 11th | 13th | 5th | 7th | 11th | 13th |
| Harmonic magnitude [% of fundamental] | 0.00 | 0.00 | 7.39 | 5.78 | 19.70 | 13.17 | 8.30 | 6.75 |

(b)

**FIGURE E9.5.3** Load characteristics for a twelve-pulse rectifier and a six-pulse rectifier: (a) simulated power system current waveforms, (b) harmonic spectra.

controller. Owing to the use of the PI controller, the DC voltage will be maintained at its desired reference value at steady-state conditions. Finally, the desired voltage $v_a(t)$ (e.g., the summation of $v_{a1}(t)$ and $v_{a2}(t)$) serves as input to the PWM generator to produce the switching gate signals of the converter/inverter. With this arrangement, the converter will generate the desired output voltage.

Figure E9.5.5 illustrates the single-phase equivalent circuit of hybrid filter #2. The converter is modeled by the controllable voltage source $v_{ah}(t)$, and the nonlinear load (e.g., twelve- or six-pulse rectifier) is represented as the current source $i_{Lh}(t)$. $Z_{ph}$, $Z_{sh}$, and $Z_{hh}$ are the source, passive branch, and hybrid branch impedances, respectively. Harmonic currents of power system, passive filter, and hybrid



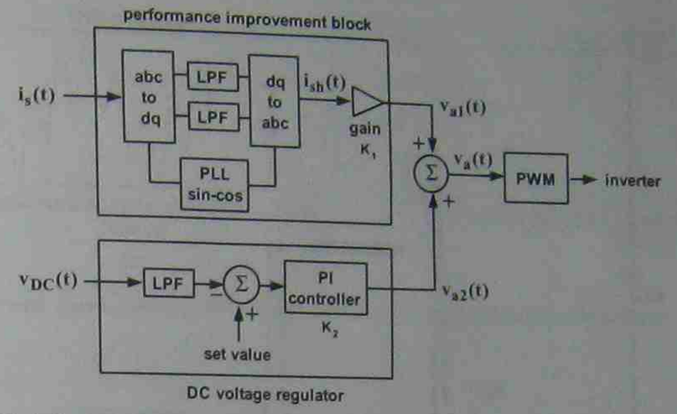



**FIGURE E9.5.4** Block diagram of the controller for hybrid filter #2. Details of the phase-lock-loop (PLL) block are provided in Fig. 11.4 (Chapter 11).

filter are determined by the following equations [14 in Chapter 9]:

$$i_{sh}(t) = \frac{1}{Z_{sh}}\left(\frac{1}{Z_{eq}} + \frac{1}{Z_{sh}Z_{hh}/K_1}\right)^{-1} i_{Lh}(t), \qquad \text{(E9.5-3)}$$

$$Z_{eq} = \frac{Z_{ph}Z_{hh}Z_{sh}}{Z_{ph}Z_{hh} + Z_{sh}Z_{hh} + Z_{sh}Z_{ph}}, \qquad \text{(E9.5-4)}$$

and

$$i_{ph}(t) = \frac{1}{Z_{ph}}\left(\frac{1}{Z_{eq}} + \frac{1}{Z_{sh}Z_{hh}/K_1}\right)^{-1} i_{Lh}(t), \qquad \text{(E9.5-5)}$$

$$i_{hh}(t) = \frac{1}{Z_{hh}}\left(\frac{1}{Z_{hh}} + \frac{1}{Z_{sh}Z_{hh}/K_1}\right)^{-1} i_{Lh}(t). \qquad \text{(E9.5-6)}$$

The power system impedance $Z_{sh}$ is usually inductive. Therefore, to avoid parallel resonance and to damp undesired resonant magnitudes, $Z_{hh}$ should be capacitive and the tuned frequency of the hybrid power filter must be larger than the tuned frequency of the passive filter.

In addition, $K_1$ acts as a resistor to damp parallel resonance between power system and passive filters. Figure E9.5.6 shows filtering characteristics for three selected cases (e.g., $K_1 = 0$, $K_1 = 1$, and $K_1 = 2$). It is found [14] that if $K_1 \neq 0$, the filtering characteristics are improved for all harmonic frequencies and no parallel resonance is encountered (Figs. E9.5.7 through E9.5.10).

c) Current Waveforms with Hybrid Filters #1 and #2

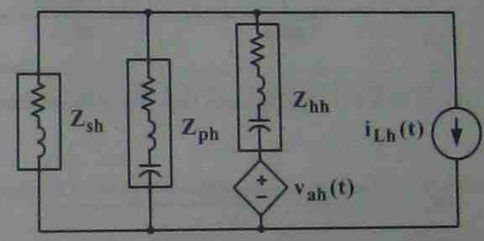



**FIGURE E9.5.5** Single-phase equivalent circuit of hybrid filter #2 at harmonic order h.

Hybrid filter #2 consists of a power converter in series with two passive filter branches, tuned at the dominant low-order harmonics (11th, 13th). Although a twelve-pulse rectifier does not produce significant 5th and 7th harmonic currents, a filter tuned at 11th and 13th harmonics cannot completely compensate the distortions of the power system current, because of series and parallel resonances between the line impedance and the passive filter branches that are likely to occur close to the 5th and 7th harmonic frequencies. For this reason, 5th and 7th LC tuned filters are installed to suppress 5th and 7th harmonic frequencies, respectively. In addition, this configuration will have more satisfactory results under the worst operating condition, that is, when only one rectifier is connected to the power system.

Simulated current waveforms for the worst case when only one six-pulse rectifier is activated and the passive branches of the hybrid power filter are tuned at the 5th and 7th harmonics (Table E9.5.1) are shown in Fig. E9.5.7. The rms and THD, values of

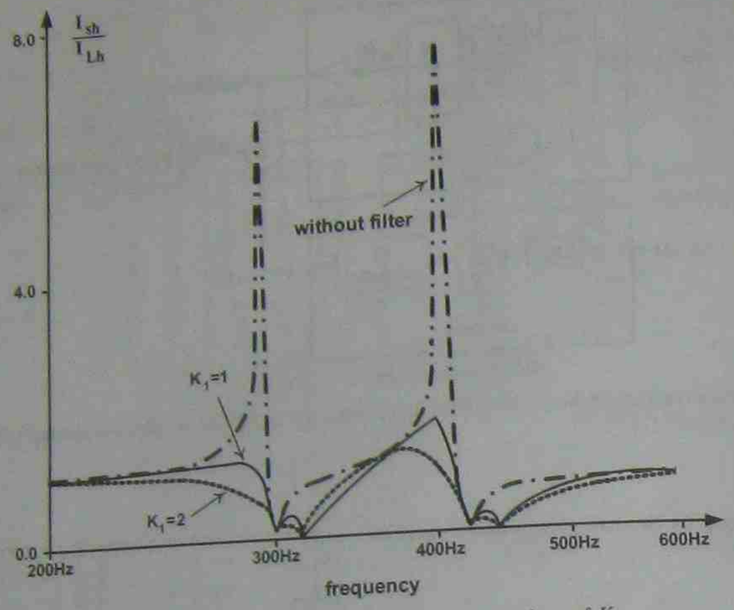



**FIGURE E9.5.6** System frequency responses of hybrid filter #2 for different values of $K_1$.

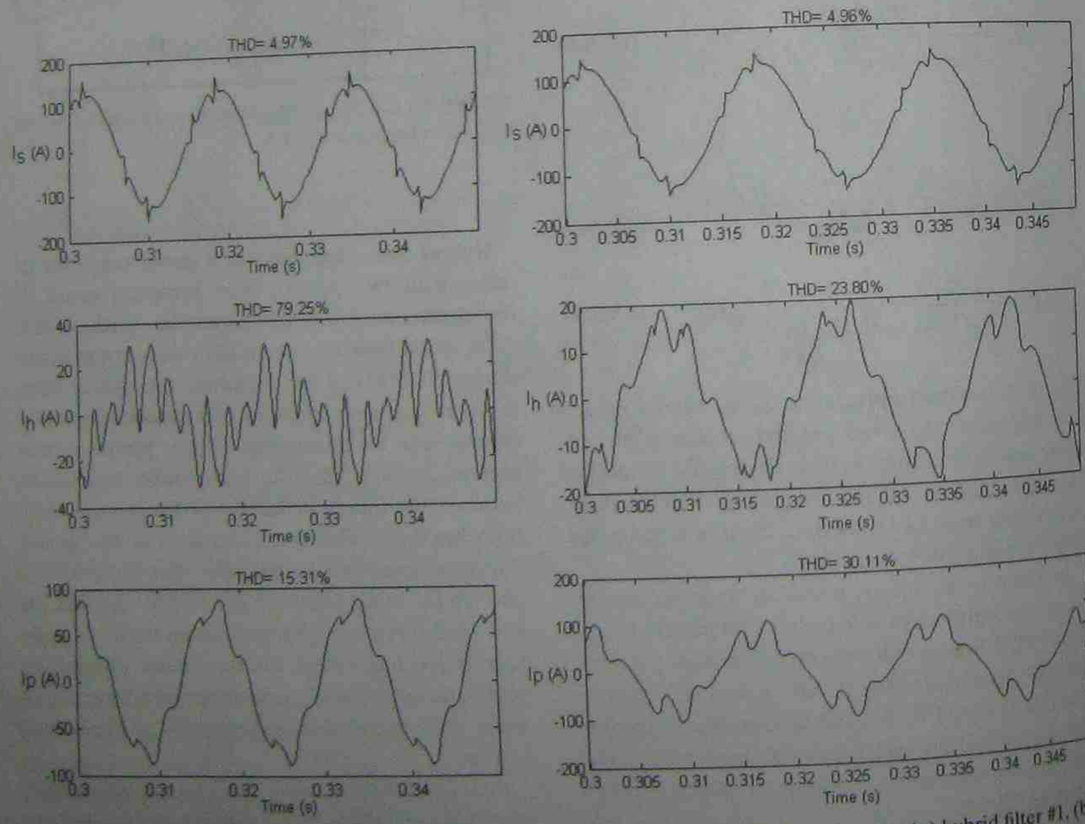



**FIGURE E9.5.7** Simulation results including power system, hybrid and passive filter currents using (a) hybrid filter #1, (b) hybrid filter #2.



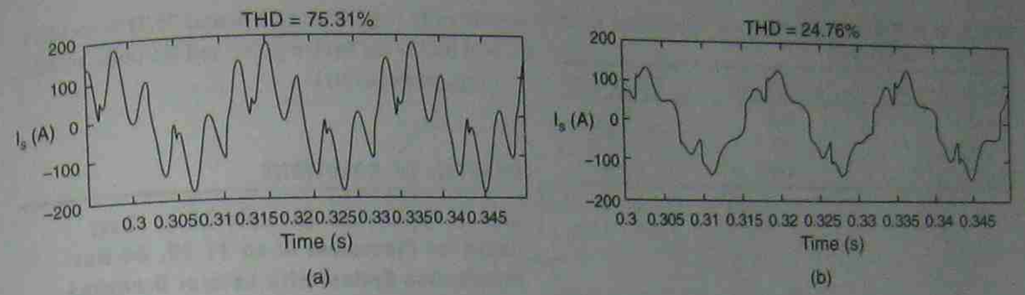



**FIGURE E9.5.8** Power system current under resonant condition (a) with no filter, (b) with hybrid filter #2 installed.

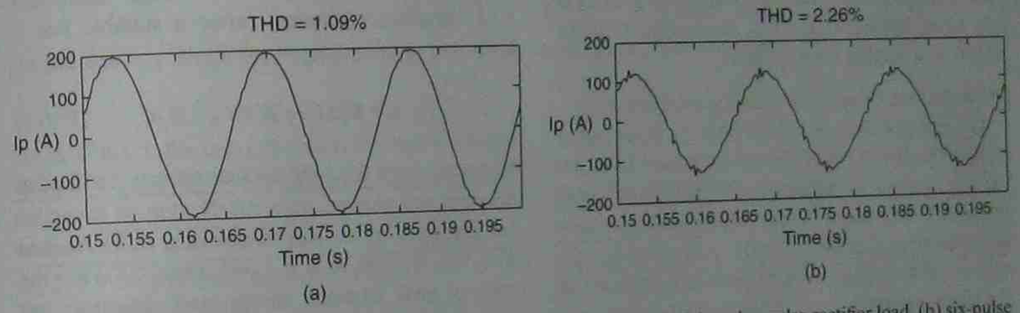



**FIGURE E9.5.9** Power system current waveform with hybrid filter #2 installed: (a) twelve-pulse rectifier load, (b) six-pulse rectifier load.

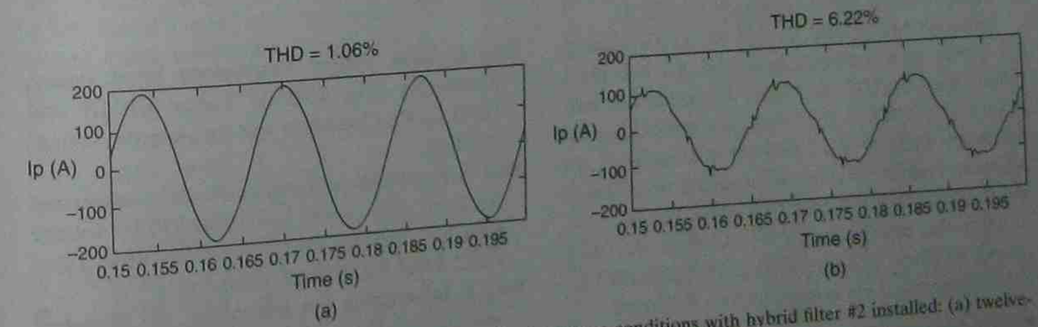



**FIGURE E9.5.10** Power system current waveform under resonance conditions with hybrid filter #2 installed: (a) twelve-pulse rectifier load, (b) six-pulse rectifier load.

**TABLE E9.5.1** Selected Parameters for Hybrid Filter #2 ($C_{DC\text{-}link}$ = 2500 μF, $V_{DC}$ = 80 V)

| | Power system | Passive filter | | Hybrid filter | |
|---|---|---|---|---|---|
| | | 5th | 7th | 5th | 7th |
| L (mH) | 0.05 | 1.13 | 0.575 | 5.1 | 2.6 |
| C (μF) | - | 250 | 250 | 50 | 50 |
| R (Ω) | 0.003 | 0.01 | 0.01 | 0.02 | 0.02 |

**TABLE E9.5.2** RMS and THD, Values of Currents for Hybrid Filters #1 and #2

| | | RMS (A) | THD, (%) | | | RMS (A) | THD, (%) |
|---|---|---|---|---|---|---|---|
| Hybrid filter #1 | $i_s$ | 91.36 | 4.97 | Hybrid filter #2 | $i_s$ | 90.19 | 4.96 |
| | $i_h$ | 17.74 | 79.25 | | $i_h$ | 21.12 | 23.80 |
| | $i_p$ | 55.20 | 15.31 | | $i_p$ | 55.65 | 30.11 |

**TABLE E9.5.3** Selected Parameters of Hybrid Filter #2 for Resonant Compensation

| Filter parameter | 11th harmonic | 13th harmonic |
|---|---|---|
| L (mH) | 1.85 | 1.34 |
| C (μF) | 30 | 30 |
| R (Ω) | 0.02 | 0.02 |

these currents are compared in Table E9.5.2. The power system current for both hybrid filters are about the same. However, the magnitude of the hybrid filter current and the corresponding $THD_i$ is less when hybrid filter #2 is implemented, which results in a smaller inverter rating.

d) Resonance Conditions with Hybrid Filter #2

The performance of hybrid filter #2 is simulated and analyzed in the presence of resonance. To do so, the inductance and capacitance of the passive power filter (that were tuned for the 5th harmonic) are now modified (e.g., 125 μF, 2.2 mH) to produce a resonant condition. Figure E9.5.8 depicts waveforms of the power system current before and after the installation of hybrid filter #2 with the passive branches tuned at 5th and 7th harmonic frequencies, respectively. Note that the value of current $THD_i$ is decreased from 75.31 to 24.76%.

e) Comparison of Hybrid Filters #1 and #2

Although with hybrid filter #1 the $THD_i$ value of the power system current is limited, the individual magnitudes of 11th and 13th harmonic currents (e.g., 3.6%, 3.11%, respectively) are higher than the harmonic limits of IEEE-519 [11 in Chapter 9]. In addition, system $THD_i$ under resonant condition is much higher than the above-mentioned limits.

After the installation of hybrid filter #2 (with proper selection of filter parameters, Table E9.5.3), system power quality is considerably improved:

- With both six-pulse rectifiers activated, the $THD_i$ of the power system current is reduced from 9.36 (Fig. E9.5.3) to 1.09% (Fig. E9.5.9a).
- Under the worst operating conditions (e.g., with one six-pulse rectifier in service), the $THD_i$ of the power system current is reduced from 26.28 (Fig. E9.5.3) to 2.26% (Fig. E9.5.9b).
- Individual magnitudes of the 11th and 13th harmonic currents are within the allowable limits of IEEE-519 [11 in Chapter 9].
- Under resonant condition, the $THD_i$ of the power system currents (Fig. E9.5.10) are improved significantly (e.g., from 6.38% and 75.31% to 1.06% and 6.22% for twelve-pulse and six-pulse rectifier loads, respectively).

## CHAPTER 10 SOLUTIONS

### 10.3.9 Application Example 10.1: Fuzzy Capacitor Placement in an 11 kV, 34-Bus Distribution System with Lateral Branches under Sinusoidal Operating Conditions: Solution

The following savings function is used to maximize the economic savings associated with capacitor placement (after a suitable bus is found):

$$S = K_P \Delta L_P + K_E \Delta L_E - K_C C \qquad \text{(E10-1)}$$

where $\Delta L_P$ and $\Delta L_E$ are the loss reductions in peak demand and energy, respectively, due to capacitor installation. $C$ is the size of capacitor in kVAr, and $K_P = 120$, $K_E = 50$, $K_C = K_{cfp}$ (see Table 10.3) are the costs of peak demand, energy, and capacitors per kW, kWh, and kVAr, respectively. The savings function is based on annual savings and thus the cost of energy per hour is multiplied with the hours in a year, namely, 8760 hours.

The fuzzy algorithm consists of the following steps (Fig. 10.14):

**Step 1. Input System Parameters:** Input system parameters (Fig. E10.1.1, Tables E10.1.1 and E10.1.2). Run load flow and compute the savings function.

**Step 2. Fuzzification:** Fuzzy rules and membership functions (for power loss index (PLI), voltage (pu), and capacitor suitability) are shown in Table E10.1.3 and Fig. E10.1.2, respectively.

**Step 3. Inferencing:** For inferencing, the *Mamdani max-prod method* [50 in Chapter 10] is used to determine the capacitor suitability membership function $\mu_S(i)$. Therefore, the capacitor placement suitability membership function for bus $i$ becomes:

$$\mu_S = \max[\mu_P(i) \cdot \mu_V(i)], \qquad \text{(E10-2)}$$

where, $\mu_P(i)$ and $\mu_V(i)$ are the membership functions of the power loss index and voltage level of bus $i$, respectively.

**Step 4. Defuzzification:** For defuzzification, the *center of gravity* (*COG*) method is used. There-





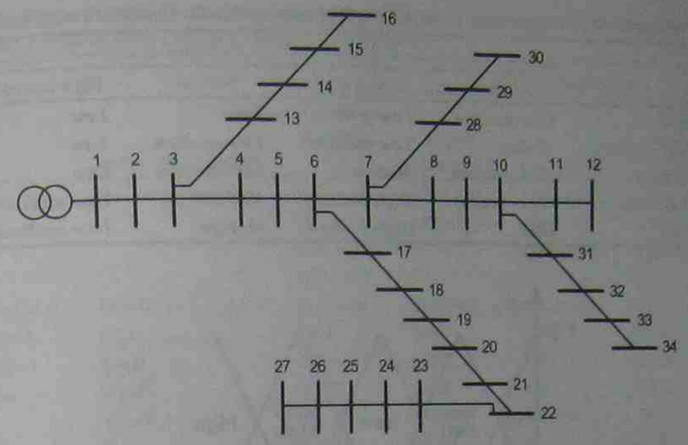



**FIGURE E10.1.1** Single-line diagram of the 11 kV, 34-bus, 3-phase, radial distribution system [32].

**TABLE E10.1.1** Bus Data [32] of the 11 kV, 34-Bus, 3-Phase, Radial Distribution System (Fig. E10.1.1)

| Bus number | Load | | Generator | | | | Injected MVAr |
|---|---|---|---|---|---|---|---|
| | MW | MVAr | MW | MVAr | $Q_{min}$ | $Q_{max}$ | |
| 1 | 0.0000 | 0.0000 | 0 | 0 | 0 | 0 | 0 |
| 2 | 0.2300 | 0.1425 | 0 | 0 | 0 | 0 | 0 |
| 3 | 0.0000 | 0.0000 | 0 | 0 | 0 | 0 | 0 |
| 4 | 0.2300 | 0.1425 | 0 | 0 | 0 | 0 | 0 |
| 5 | 0.2300 | 0.1425 | 0 | 0 | 0 | 0 | 0 |
| 6 | 0.0000 | 0.0000 | 0 | 0 | 0 | 0 | 0 |
| 7 | 0.0000 | 0.0000 | 0 | 0 | 0 | 0 | 0 |
| 8 | 0.2300 | 0.1425 | 0 | 0 | 0 | 0 | 0 |
| 9 | 0.2300 | 0.1425 | 0 | 0 | 0 | 0 | 0 |
| 10 | 0.0000 | 0.0000 | 0 | 0 | 0 | 0 | 0 |
| 11 | 0.2300 | 0.1425 | 0 | 0 | 0 | 0 | 0 |
| 12 | 0.1370 | 0.0840 | 0 | 0 | 0 | 0 | 0 |
| 13 | 0.0720 | 0.0450 | 0 | 0 | 0 | 0 | 0 |
| 14 | 0.0720 | 0.0450 | 0 | 0 | 0 | 0 | 0 |
| 15 | 0.0720 | 0.0450 | 0 | 0 | 0 | 0 | 0 |
| 16 | 0.0135 | 0.0075 | 0 | 0 | 0 | 0 | 0 |
| 17 | 0.2300 | 0.1425 | 0 | 0 | 0 | 0 | 0 |
| 18 | 0.2300 | 0.1425 | 0 | 0 | 0 | 0 | 0 |
| 19 | 0.2300 | 0.1425 | 0 | 0 | 0 | 0 | 0 |
| 20 | 0.2300 | 0.1425 | 0 | 0 | 0 | 0 | 0 |
| 21 | 0.2300 | 0.1425 | 0 | 0 | 0 | 0 | 0 |
| 22 | 0.2300 | 0.1425 | 0 | 0 | 0 | 0 | 0 |
| 23 | 0.2300 | 0.1425 | 0 | 0 | 0 | 0 | 0 |
| 24 | 0.2300 | 0.1425 | 0 | 0 | 0 | 0 | 0 |
| 25 | 0.2300 | 0.1425 | 0 | 0 | 0 | 0 | 0 |
| 26 | 0.2300 | 0.1425 | 0 | 0 | 0 | 0 | 0 |
| 27 | 0.1370 | 0.0850 | 0 | 0 | 0 | 0 | 0 |
| 28 | 0.0750 | 0.0480 | 0 | 0 | 0 | 0 | 0 |
| 29 | 0.0750 | 0.0480 | 0 | 0 | 0 | 0 | 0 |
| 30 | 0.0750 | 0.0480 | 0 | 0 | 0 | 0 | 0 |
| 31 | 0.0570 | 0.0345 | 0 | 0 | 0 | 0 | 0 |
| 32 | 0.0570 | 0.0345 | 0 | 0 | 0 | 0 | 0 |
| 33 | 0.0570 | 0.0345 | 0 | 0 | 0 | 0 | 0 |
| 34 | 0.0570 | 0.0345 | 0 | 0 | 0 | 0 | 0 |

**TABLE E10.1.2** Line Data [32] of the 11 kV, 34-Bus, 3-Phase, Radial Distribution System (Fig. E10.1.1)

| Line | | | | |
|---|---|---|---|---|
| From bus | To bus | $R_{line}$ (pu) | $X_{line}$ (pu) | Tap setting |
| 1 | 2 | 0.0967 | 0.0397 | 1 |
| 2 | 3 | 0.0886 | 0.0364 | 1 |
| 3 | 4 | 0.1359 | 0.0377 | 1 |
| 4 | 5 | 0.1236 | 0.0343 | 1 |
| 5 | 6 | 0.1236 | 0.0343 | 1 |
| 6 | 7 | 0.2598 | 0.0446 | 1 |
| 7 | 8 | 0.1732 | 0.0298 | 1 |
| 8 | 9 | 0.2598 | 0.0446 | 1 |
| 9 | 10 | 0.1732 | 0.0298 | 1 |
| 10 | 11 | 0.1083 | 0.0186 | 1 |
| 11 | 12 | 0.0866 | 0.1488 | 1 |
| 12 | 13 | 0.1299 | 0.0223 | 1 |
| 13 | 14 | 0.1732 | 0.0298 | 1 |
| 14 | 15 | 0.0866 | 0.1488 | 1 |
| 15 | 16 | 0.0433 | 0.0074 | 1 |
| 16 | 17 | 0.1483 | 0.0412 | 1 |
| 17 | 18 | 0.1359 | 0.0377 | 1 |
| 18 | 19 | 0.1718 | 0.0391 | 1 |
| 19 | 20 | 0.1562 | 0.0355 | 1 |
| 20 | 21 | 0.1562 | 0.0355 | 1 |
| 21 | 22 | 0.2165 | 0.0372 | 1 |
| 22 | 23 | 0.2165 | 0.0372 | 1 |
| 23 | 24 | 0.2598 | 0.0446 | 1 |
| 24 | 25 | 0.1732 | 0.0298 | 1 |
| 25 | 26 | 0.1083 | 0.0186 | 1 |
| 26 | 27 | 0.0866 | 0.1488 | 1 |
| 27 | 28 | 0.1299 | 0.0223 | 1 |
| 28 | 29 | 0.1299 | 0.0223 | 1 |
| 29 | 30 | 0.1299 | 0.0223 | 1 |
| 30 | 31 | 0.1299 | 0.0223 | 1 |
| 31 | 32 | 0.1732 | 0.0298 | 1 |
| 32 | 33 | 0.1299 | 0.0223 | 1 |
| 33 | 34 | 0.0866 | 0.1488 | 1 |

**TABLE E10.1.3** Decision Matrix for Application Example 10.1, Determining Suitable Capacitor Locations

| | | Voltage | | | | |
|---|---|---|---|---|---|---|
| AND | | Low | Low-normal | Normal | High-normal | High |
| Power loss index (PLI) | Low | *Low–medium* | *Low–medium* | *Low* | *Low* | *Low* |
| | Low–medium | *Medium* | *Low–medium* | *Low–medium* | *Low* | *Low* |
| | Medium | *High–medium* | *Medium* | *Low–medium* | *Low* | *Low* |
| | High–medium | *High–medium* | *High–medium* | *Medium* | *Low–medium* | *Low* |
| | High | *High* | *High–medium* | *Medium* | *Low–medium* | *Low–medium* |

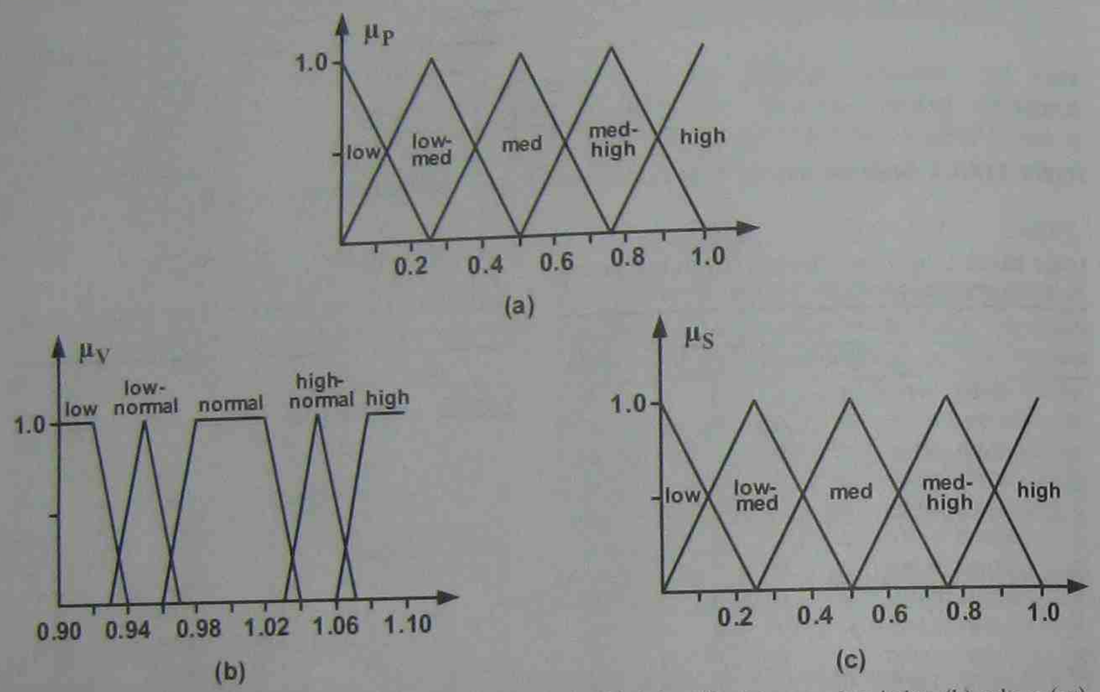



**FIGURE E10.1.2** Membership functions of Application Example 10.1 defined for (a) power loss index, (b) voltage (pu), and (c) capacitor suitability.

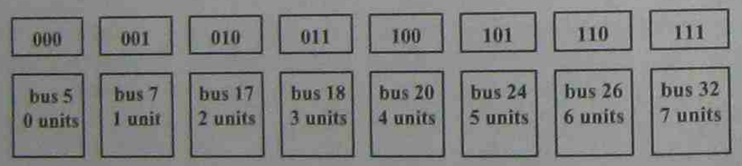



**FIGURE E10.2.1** Selected chromosome structure for Application Example 10.2.

**TABLE E10.2.1** Binary Representation of Capacitor Bank Sizes for Application Example 10.2

| Binary representation | Number of 250 kVAr units | Capacitor bank size (kVAr) |
|---|---|---|
| 000 | 0 | 0 |
| 001 | 1 | 250 |
| 010 | 2 | 500 |
| 011 | 3 | 750 |
| 100 | 4 | 1000 |
| 101 | 5 | 1250 |
| 110 | 6 | 1500 |
| 111 | 7 | 1750 |

fore, the final capacitor placement suitability index is determined by the following formula:

$$S = \frac{\int \mu_S(z) \cdot z dz}{\int \mu_S(z) \cdot dz}, \qquad \text{(E10-3)}$$

where $S$ is the suitability index and $\mu_S(z)$ is the capacitor placement suitability membership function.

**Step 5. Final Solution:** The final solution of the fuzzy placement and sizing of capacitor banks for the distribution system of Fig. E10.1.1 is shown in Table E10.2.2.



**TABLE E10.2.2** Simulation Results for Placement and Sizing of Capacitor Banks in the 34-Bus System (Fig. E10.1.1) under Sinusoidal Operating Conditions using Different Optimization Methods[a]

| | | After optimization | | | | |
|---|---|---|---|---|---|---|
| | Before optimization | Heuristic algorithm [1] | Expert systems [1] | Fuzzy [32] | Fuzzy (Section 10.3.10) | Genetic (Section 10.3.11) |
| Capacitor bank locations and sizes (kVAr) | No compensation | Q12 = 400<br>Q20 = 70<br>Q21 = 250<br>Q26 = 700 | Q5 = 750<br>Q22 = 900 | Q7 = 450<br>Q17 = 750<br>Q24 = 1500 | Q11 = 750<br>Q18 = 450<br>Q24 = 1350 | Q17 = 250<br>Q20 = 500<br>Q24 = 1000<br>Q32 = 500 |
| Total capacitance (kVAr) | $Q_t = 0$ | $Q_t = 1420$ | $Q_t = 1650$ | $Q_t = 2700$ | $Q_t = 2550$ | $Q_t = 2250$ |
| Minimum voltage (pu) | 0.942 | 0.948 | 0.947 | 0.951 | 0.951 | 0.950 |
| Maximum voltage (pu) | 1.000 | 1.000 | 1.000 | 1.000 | 1.000 | 1.000 |
| Average voltage (pu) | 0.966 | 0.969 | 0.968 | 0.971 | 0.971 | 0.971 |
| Total losses (kW) | 221.68 | 169.136 | 173.579 | 168.990 | 164.158 | 162.034 |
| Power loss reduction (kW) | 0 | 52.544 | 48.101 | 52.69 | 57.52 | 59.646 |
| Capacitor cost ($/year) | 0 | 710.00 | 825.00 | 1350.00 | 1275.00 | 1125.00 |
| Total cost ($/year) | 84859.10 | 65455.26 | 67271.04 | 66039.37 | 64114.68 | 63151.61 |
| Benefits ($/year) | | 19403.84 | 17588.06 | 18819.73 | 20744.42 | 21707.49 |

[a]All capacitors were removed before the optimization process.

### 10.3.10 Application Example 10.2: Genetically Optimized Placement of Capacitor Banks in an 11 kV, 34-Bus Distribution System with Lateral Branches under Sinusoidal Operating Conditions: Solution

The selected chromosome structure consists of N substrings (genes) of binary numbers (Fig. E10.2.1). N denotes the number of possible compensation (candidate) buses for shunt capacitor placement within the entire feeder. The binary numbers indicate the size of the installed capacitors at the bus under consideration. Candidate locations for capacitor placement are assumed to be buses 5, 7, 17, 18, 20, 24, 26, and 32. The 3-bit binary numbers (Fig. E10.2.1) indicate the size of the installed capacitor in terms of units. Only 250 kVAr banks are assumed to be available (Table E10.2.1).

The selected fitness function (incorporating energy and power losses in the system as well as the cost of the installed capacitor banks) is

$$\text{fitness} = K_e \sum_{i=1}^{n} T_i P_i + K_p P_O + \frac{K_c}{L} K_c \sum_{j=1}^{M} C_j, \qquad \text{(E10-4)}$$

where $K_e = 0.03\$/\text{kWh}$, $K_p = 120\$/\text{kW/year}$, and $K_c = 5\$/\text{kVAr}$ are constants for energy, peak power, and capacitor costs, respectively. $P_i$ is the power loss at load level $i$ with a time duration $T_i$. $P_o$ represents the peak power loss of the system. $C_j$ represents the size of the capacitor units to be installed at each of the M = 8 candidate buses. The constant denoted by $L$ (= 10 years) represents the life of the capacitor. Therefore, a chromosome that consists of a large number of capacitor banks and a high energy and power loss will result in an undesirable high fitness value.

The genetic algorithm consists of the following steps (Fig. 10.3):

**Step 1. Input System Parameters:** Input system parameters (Fig. E10.1.1, Tables E10.1.1 and E10.1.2) and an initial random population with $N_{chrom}$ chromosomes.

**Step 2. Fitness Process:**
Step 2A: Run load flow algorithm for chromosome $N_{ch}$, save value of total active power loss and the computed fitness function (FF).
Step 2B: Calculate 1/FF for chromosome $N_{ch}$.
Step 2C: If $N_{ch} \le N_{chrom}$ go to Step 2A.

**Step 3. Reproduction Process:**
Step 3A: Define total fitness as a sum of values obtained in Step 2B for all chromosomes.
Step 3B: Select a percentage of the "roulette wheel" for each chromosome that is equal to the ratio of its fitness value to the total fitness value.
Step 3C: Normalize the values on the "roulette wheel" to be between zero and one.

Step 3D: Choose random numbers ($R_1$) between 0.0 and 1.0 to select an individual parent chromosome $N_{parent}$.
Step 3E: If $N_{parent} \leq N_{chrom}$ go to Step 3D.

**Step 4. Crossover Process:**
Step 4A: Select a random number ($R_2$) for mating two parent chromosomes.
Step 4B: If $R_2$ is between 0.6 and 1.0 then combine the two parents to generate two offsprings and go to step 4C. Else, transfer the chromosome with no crossover.
Step 4C: Repeat steps 4A to 4B for all chromosomes.

**Step 5. Mutation Process:**
Step 5A: Select a random number ($R_3$) for mutation of one chromosome.
Step 5B: If $R_3$ is between 0.01 and 0.1 then apply the mutation process at a random position in the string and go to Step 5C. Else, transfer the chromosome with no mutation.
Step 5C: Repeat Steps 5A to 5B for all chromosomes.

**Step 6. Updating Population:** Replace the old population with the new improved population generated by Steps 2 to 5.

**Step 7. Convergence:** If all chromosomes are the same or the maximum number of iterations have been reached ($N_{iterations} = N^{max}$) print the solution and stop, else go to Step 2.

**Step 8. Final Solution:** The final solution of the genetic placement and sizing of capacitor banks for the distribution system of Fig. E10.1.1 is shown in Table E10.2.2.

# Index


A
Alpha-beta-zero (αβ0) transformation 453–458
Activation energy (see aging) 228, 240, 241
Active power line conditioner (see Compensators) 446
Admittance 263
Aging 227, 240
  activation energy E 228, 240
  additional temperature rise for transformers 231
  additional temperature rise (or loss) versus weighted-harmonic-factor function 239
  aging (decrease of lifetime) due to additional temperature rise 242
Arrhenius plots 241
calculated harmonic losses of single-phase induction machine 234
calculated harmonic losses of three-phase induction machine 235
decrease of lifetime 241
elevated temperature rise 228
equation of aging 240
exponents of weighted-harmonic factors 236
heat flow related to conduction 250
heat flow related to radiation and convection 250
heat flow 256
induction machines 231, 234, 252, 254, 255
k-factor 238
ℓ-factor 238
lifetime 241
limits for harmonic voltages 242
measured temperature increases for transformers 230
reaction-rate equation 240
reduction of lifetime 242
temperature as a function of time 255, 256
thermal aging 240
transformers 230, 253,
weighted-harmonic factors for induction machines 231
weighted-harmonic factors for transformers 229
worst-case conditions 228
Amortisseur 195–197
Artificial intelligence (AI) techniques 404, 407
  artificial neural network (ANN) 404
  drawbacks of AI-based methods 404
  expert systems 407
  fuzzy (see fuzzy set theory) 408
  genetic (see genetic algorithms) 404
  graph search algorithm 410
  particle swarm algorithm 410
  sequential quadratic programming 411
  simulated annealing 407
  tabu search algorithm 411
Average value 18
  nonsinusoidal waveform 18

B
Boltzmann constant 241
Brushless DC machine 10, 15, 25, 48, 197
Broadband power line (BPL) communication 2
Bearing currents 194

C
Capacitance 263
Capacitor 209
  classification of allocation techniques for sinusoidal operation 402
  as harmonic sources 214, 216, 224
  capacitance scanning (see scanning) 217
  cost index 414
  constraints 218, 225, 414
  current constraint 219
  displacement power factor (DPF) 212, 223
  displacement power factor angle φ 210, 223
  distribution shunt capacitor banks 400
  equivalent circuits 221
  for harmonic filtering 214
  for power factor correction (see power factor) 209
  for reactive power compensation 210, 213, 398
  frequency scan 217
  harmonic constraints for capacitors 218–221
  harmonic losses 222, 225
  harmonic resonance (see resonance) 215, 216
  objective function 414
  optimal placement 397
  optimal placement by fuzzy algorithm 408, 411, 419, 424
  optimal placement by genetic algorithm 404
  optimal placement by hybrid genetic-fuzzy algorithm 433
  optimal placement by hybrid MSS-LV 415, 417,
  optimal placement by local variation (LV) 417
  optimal placement by maximum sensitivities selection (MSS) 415
  permissible operating region for capacitors 220
  pole-mounted capacitor banks 401
  power-factor correction 212
  power quality problems associated with capacitors 214
  protection of capacitors 217, 225
  reactive-power compensation 213
  reactive-power constraint 219
  relation between displacement power factor angle φ and firing angle α 212
  relation between displacement power factor and total power factor 212, 223, 224
  series 17, 76
  shunt 397, 401
  sizing of capacitor banks 38
  switching 214
  transients associated with capacitor switching 214
  total power factor (TPF) 212, 223
  total power factor angle θ 211
  voltage constraint 219
C-message 20
Compensators 444



ISBN 978-0-12-369536-9
© Elsevier Inc.
All rights reserved.

active power line conditioner (APLC) 446
custom power devices (compensation-custom power devices) 445, 446
custom power devices (network-reconfiguration devices) 446
FACTS (see flexible AC transmission systems) 2, 443
series compensators 445, 459
shunt compensators 445, 457
phase shifters 444
Compressed-air storage facility 348
Computer-aided testing (CAT) 90–97
computer-aided testing of electrical apparatus program (CATEA) 128
Converters 41
shunt 457
six-pulse 50
twelve-pulse 41, 49
Corona 306
audible noise 311
barometric pressure 308
critical disruptive voltage 308
discharge 307
economic considerations 312
effects 305, 310
electron avalanche 307
frequency distribution 312
frequency spectra 311
in transmission lines 306
factors influencing generation 308
mechanism 306
minimization 310
negative effects 308
NOx generation 311
onset of corona 308
ozone generation 311
radio interference (RI) 311
solutions for the minimization 310
television interference (TVI) 311
Custom power devices (see Compensators) 445

D
DC bias (see geomagnetic disturbance) 9, 83, 324
Dedicated line 37, 48
Demand-side management 332
Derating 40, 60–64, 89–97, 99, 100
definition 40
measurement 60–64, 89–97
Describing function 68
Distortion 8
Distortion power (D) 22
Distortion index 22
Distributed generation (DG) 314
cogeneration 314
frequency control 314
voltage control 314
Disturbances 1
Distribution 263
Distribution feeder 41
Transformer with DC bias 324

E
Earth-surface potential (see geomagnetic disturbances) 82
Electromagnetic field (EMF) 2, 305
biological effects 308
electric field strength 305, 339
environmental concerns 310
generation of EMFs 305
magnetic field strength 306, 339
maximum surface gradient 339
minimization 310
mitigation 312
negative effects on people and animals 308
passive shielding 308
reducing the effects 307
solutions for the minimization 310
Electromagnetic phenomena 5
Electron volt (eV) 241, 254
Electrostatic discharge phenomena (ESD) 3
Emergency standby power 344
Energy storage 100, 336
superconducting coil 100
compressed-air storage facility 348
hydro pumped-storage plant 336, 337
flywheel storage plant 346
supercapacitor storage plant 202
Error calculation 101
maximum error analysis 318–325
Expert systems 407

F
Feeder 302
flower configuration 303
radial configuration 302
ring configuration 303
Ferroresonance phenomenon 75
avoidance of ferroresonance 78
calculation of ferroresonant currents 75, 79, 80
chaotic behavior 78, 80
definition 75
ferroresonant circuit 75
single-pole switching 76
susceptibility 78
transformer connection 76
resonance (see resonance phenomenon) 75
ways to avoid ferroresonance 78
$F_{HL}$-factor 63
sensitivity 63, 64
Fields
transformer 74
Filters 359
active 375
block diagram of active filters 382
classification of filters 361
classification of active filters 375
classification of hybrid filters 378
classification of passive filters 362, 364, 370, 373
compensation signals 390
composite filter 370
control of filters 383
correction of negative- and zero-sequence components 384
current-divider transfer functions 364
DC bus energy balance 383, 391
derivation of reference signal 385
derivation of compensating signal 388
design 41, 49–51
distortion identification techniques 382, 383
filter placement 41, 49, 51
first-order high-pass 365
first-order damped high-pass 366
flicker 384
generation of compensation signal 391
high-power active 378
hybrid 378
hybrid passive 373
hybrid of passive and active 392
impedance-based blocking 390
impedance-based compensation 390
impedance transfer functions 363
instantaneous power 389
inverter 382
inverter controller 382
limitations of passive power filters 371
low-power active 377
medium-power active 378
passive 362, 370
parallel resonance 20
potentials of passive power filters 371
reactive-power control 384
series resonance 20
second-order band-pass 367
second-order damped band-pass 369
sensors and transformers 382
supply current distortion 390
synchronizer 383
reference following techniques 391
three-phase four-wire passive filter 373
three-phase three-wire passive filter 372
transfer function 363
types of nonlinear loads 359
voltage-divider transfer functions 364





voltage sag and voltage swell 384
waveform compensation 385, 387
Flexible AC transmission system (FACTS) 2, 443, 444
combined shunt-series FACTS controllers 445
static synchronous series compensator (SSSC) 445
series FACTS controllers 445
shunt FACTS controllers 445
STATCOM 445, 464
Flicker 2, 12, 464
Flux distribution 113, 160
induction machine 113–117
permanent-magnet machine 163, 172
switched-reluctance machine 176
synchronous machine 160–162, 178
flux-density measurement 132
Form factor (FF) 19
Force calculation 89, 100, 114, 115, 175–178
magnetic 89, 100
Fourier analysis 198
program 89–97
Frequency control 314–316
Frequency variation 339–341
Fuel cell 26, 48, 344
Fuzzy set theory 408
alpha-cut process 422
defuzzification 409
for optimal capacitor placement in presence of harmonics 397, 413, 430–435
for optimal capacitor placement with sinusoidal operation 411
fuzzy approach for capacitor bank placement 419
fuzzification 421
fuzzy expert system 410, 424, 429
fuzzy fitness (suitability) functions 430
fuzzy inference 409
fuzzy logic operators 409
fuzzy sets 408
implication 409
membership function 408

G
Gear box 349
Generation 147, 261
cogeneration 314
distributed 314
Genetic algorithms 404, 425, 430
Chromosomes 405
convergence criterion 406
crossover process 432
evaluation (fitness) function 430
for optimal capacitor placement in presence of harmonics 411, 425, 427, 429–435
for optimal capacitor placement with sinusoidal operation 406, 425
genetic operators 426, 431
genetic parameters 406
genetic representation 405
initialization 405
mutation process 428
reproduction process 432
Geomagnetic disturbances (storms) 81
aurora australis 81
aurora borealis 81
calculation of GIC 9, 83
DC bias 9, 82
earth-surface potential (ESP) 82
effects 82
geomagnetically induced current (GIC) 9, 81
GIC in transformers 81
mitigation techniques 84
modeling 83
origins 82
power system effects 82
sun-spot cycles 82
transformers with DC bias Current 9, 83, 324
Graph search algorithm 410
Grounding 84
choice of grounded 84
connection to earth 89
equipment grounding 88
grounded system 84, 85
multiple faults 85
service continuity 84
static grounding 88
system grounding 84
ungrounded system 84
Guidelines 29

H
Harmonics 13
admittance matrix (see harmonic power flow) 263
cancellation 36
characteristic 17
cost of harmonics 244
current calculation 37–43
domain simulation 35
even 13, 121
even space harmonics 135
factor 19
flicker 12, 464
form factor (FF) 19
frequency conversion 188
frequency variations 12, 198, 314, 339
harmonic domain simulation 35
harmonic factor (HF) 19
harmonic filter 40
harmonic power 56
interaction of space and time harmonics 134
interharmonic 17, 37
lowest order harmonic (LOH) 19
modeling harmonic sources 34, 36
negative sequence 17
noninteger 17, 37
noninteger space harmonics 135
notching 11
odd 13
order 13
positive sequence 17
propagation 5, 87
resonance (see resonance) 49–51, 75, 95, 215, 224, 399, 400
simulation techniques 35
space 17, 120
spatial 17
subharmonic 17, 48
THD (see total harmonic distortion) 19
time 17, 122
time-domain simulation 35
time-varying nature of harmonics 12, 17, 79, 244
transients 4
triplen 14, 121
uncharacteristic 17
unpredictable events 2
voltage calculation 37–43
weighted-harmonic factors (see aging) 236
zero sequence 17
Harmonic power flow (HPF) 277, 297
accuracy of decoupled HPF 287, 293
algorithm 279–281, 285
assembly of equations 279
bus admittance matrix 278
classification of HPF techniques 278
classification of time harmonics 278
current balance at fundamental frequency 280
current balance at harmonic frequency 281
correction bus vector 287
decoupled HPF 287, 288
fast HPF 289
fuzzy HPF 290
harmonic (bus) admittance matrix 278, 286
harmonic frequencies 278
harmonic Jacobian entry formulae 284, 285
harmonic Jacobian matrix 287, 298
harmonic power definitions 278
linear bus 279
mismatch vector 282, 286
modeling of nonlinear loads (see loads) 279, 286
modeling of linear loads 279

modified fast decoupled HPF 290
modular HPF 292
nonlinear bus 279, 296
negative sequence 17
Newton-Raphson approach 281–286
phase shift 57
probabilistic HPF 290
spatial 17
space 17
weak power system 296
zero sequence 17
Heuristic method 403
Heat flow 250
conduction 250–252
convection 250–252
radiation 250–252
High-voltage DC (HVDC) transmission 2
Hunting 155
Hybrid MSS-LV algorithm 417

I
Imbalance 462
Impedance 263
Inductance 263
Induction machine 109
additional temperature rise due to harmonics (see aging) 238
aging (see aging) 227
asynchronous torques 135
auxiliary winding 130
classification 144
control 146, 254
conventional harmonic model 141
critical speeds 147
current-source-fed induction motor 133, 148
double-squirrel cage circuit 144, 145
doubly fed induction generator 345
dynamic rotor eccentricity 143
equivalent circuit 111
(E/f) control 146, 254
leakage flux loss 142
flux distribution 113
forward rotating fundamental mmf 121
forward rotating harmonic mmf 123
fundamental slip 111, 124
fundamental torque 111, 123, 148
fractional horsepower 129
harmonic current 149
harmonic (equivalent circuit) model 123
harmonic slip 124, 125, 126
harmonic torque 123
harmonics in stator teeth and yokes 130
harmonic voltage 149
interaction of time and space harmonics 134
interharmonic torque 132, 148
iron-core loss resistance 130
linear (sinusoidal) model 111
main-phase winding 130
magnetic fields 113
magnetizing impedance 129
measurements 127
measured harmonic losses (see aging) 235
noninteger space harmonics 135
nonlinear circuit parameters 128
nonlinear harmonic models 141
operation modes (see operating modes of rotating machines) 245
overvoltage 112, 146
overfrequency 147
permanent-split-capacitor (PSC) 128
phasor diagram 145
reduction of harmonic torque 249, 255
reflected harmonic slip 125–127
rotating magnetomotive (mmf) force 135
rotor core loss 141
rotor eccentricity 143
rotor impedance 129
search coil 131
single phase 128
sinusoidal equivalent circuit 110
spatial (space) harmonics 120
spectral-based harmonic model 142, 143
stability, steady-state 118, 142, 145
starting current 117
starting performance 117
starting torque 117
static rotor eccentricity 143
stator yoke (backiron) 130
stator impedance 129
stator teeth 130
single-phase 127
subharmonic torque 132–134, 148
synchronous torques 135
temperature-rise calculation 252
three-phase 111
three-phase machine operated on single-phase system 144
time harmonics 122
turns ratio 130
underfrequency 146
undervoltage 112, 146
torque, three-phase 118
(V/f) control 146, 254
unstable operation 118
voltage-source-fed induction motor 132, 149
voltage stress 148, 149
weighted-harmonic factors (see aging) 228
winding failures 136, 148, 149
winding stress 137, 148, 149
winding switching 119
Inductor 98
Inverter
current-controlled voltage-source inverter 27, 166, 202, 350
current-source inverters (CSI) 96
paralleling with power system 169
phasor diagram of inverter 165
pulse-width-modulated (PWM) PWM inverters 96, 137, 139
six-step inverter 25, 94
voltage-source inverter (VSI) 15, 16, 27, 166, 344, 346
Islanding 329
intentional islanding 329–334
definition of problem 330
solution approach 331
I·T product 21

J
Jacobian matrix 275, 282, 297, 298
fundamental Jacobian matrix 275
harmonic Jacobian matrix 282, 297, 298

K
K-factor 62, 63, 99, 100
sensitivity 63
Kelvin 241

L
LabVIEW 326
Lanchester-Betz equation 350
Lifetime
rated 241
reduction (see aging) 227
Lightning 5, 85, 87
insulator flashover 87
PSpice solution 87
arrester operation 87
PSpice solution 88
strike 5
surge 149
Local variation (LV) 417
Load flow (see power flow) 270
Loads 263, 359
linear loads 263
modeling linear loads at harmonic frequencies 279
nonlinear loads (see nonlinear loads) 263, 359
Load point 302
Load sharing 340, 341
Losses
breakdown 112
conventional approach ($P_{Loss} = P_{in} - P_{out}$) 93, 323
direct loss measurement 93
harmonic 56
indirect loss measurement 60
maximum error analysis 92
new approach ($p_{cu} = i_2'(v_1 - v_2')$ and $p_{fe} = v_1 (i_1 - i_2')$) 323

M
Magnetic field strength 306
calculation 58, 81
Magnetic force calculation 89
Magnetics 58
major loop 58
minor loop 58
Measurement 11, 13–16, 89–97, 127–132, 230, 231, 235, 237, 318–325
accuracy 92
computer sampling 130
errors 92
current 130
flux density 130
uncertainty 102
voltage 130
Manufacturing regulations 3
Mathematica solutions 79, 137–141, 314–316
MATLAB solutions 79, 137–141, 314–316
Maximum sensitivities selection (MSS) 415, 429
convergence 417
MMS algorithm 415
sensitivities functions 415
Motoring 147

N
National Electrical Code (NEC) 88
Newton-Raphson (see Power flow) 271
Nonlinear Loads 359
current-source (current-fed or current-stiff) nonlinear loads 360
voltage-source (voltage-fed or voltage-stiff) nonlinear loads 361
frequency spectrum of an unbalanced, three-wire three-phase nonlinear load 386
harmonic modeling of nonlinear loads 279
modeling linear loads at harmonic frequencies (see loads) 263, 279, 359
Nonperiodic events 303
$NO_x$ generation 312
Nuclear electromagnetic pulse (NEMP) 3, 81

O
Operating modes of rotating machines 245
intermittent 247
short term 246
steady-state 246
steady-state with short term 247
steady-state with intermittent 247
Optocoupler 91

P
Park (dq0) transformation 158, 451
Partial differential equation 256
Peak-power tracker 337, 343
Particle swarm algorithm 410
Permanent-magnet machine 170, 172
cogging torque 170–172
Permanent-magnet material 173
neodymium-iron-boron (NdFeB) 173
coercivity 173
residual flux density 173
Permeability 76
free-space 81, 101
relative 99
recoil 171–174
Phase-lock loop (PLL) circuit 456
Phasor diagram 164
piston compressor 248
pole transformer 98
Photovoltaic power plant 314, 347
frequency control 314
voltage control 314
Point of common coupling (PCC) 41, 49, 51
Polymer Electrolyte Membrane (PEM) 26
Positive-sequence voltage detector (PSVD) 457
Possible voltage spectra 243, 244, 254
Power 60, 211
active 60, 211
apparent 22
average 60, 211
distortion 22, 211
harmonic 56
instantaneous 60
reactive 211
Power factor 48
benefits of power-factor correction 212
displacement power factor (DPF) 48, 51, 210, 223
power-factor correction 209
total power factor (TPF) 211, 223
Power filters (see filters) 359
Power flow 261
admittance (bus) matrix 263–267, 271, 276, 294
algorithm 274, 276
backward substitution 268, 269
bus voltage vector 272
distribution 263
formation of table of factors 269
forward substitution 268, 269
fundamental power flow 270
generation 261
harmonic (see harmonic power flow) 277
interconnected (mesh) power systems 271
inverse of a matrix 277
Jacobian entry formulas 274–276
Jacobian matrix 269, 277
linear load 263
load (PQ) bus 271
matrix multiplication 267
mismatch power 273, 277
Newton-Raphson 271
Newton-Raphson algorithm 274, 276
nonlinear bus (see harmonic power flow) 280
nonlinear load 263
nonsingular 277
PQ bus 271
PV bus 271
power system 261
radial power systems 270
singularity 266, 277
subtransmission 262
swing bus 271
table of factors 269, 294
Taylor series expansion 272, 273
transformers 261
transmission 262
triangular factorization 267
voltage control 294
voltage controlled (PV) bus 271
weak power system 294
Power line communication 305
Power quality 1
automatic disconnect 336
backup power system 335
batteries 335, 343
causes 1
CBEMA voltage-tolerance curve 334, 344
classification 3
DC offset 8
definition 1
Diesel-generator set 335, 344
direction of harmonic power flow 317
electric noise
emergency power system 335, 344
energy-storage methods 336
flicker 12
fluctuation 12
flywheels 335, 346
formulation 13
fuel cells 335, 344
frequency control 340
frequency regulation 335
voltage control 340
frequency regulation 335
guidelines 29
hydro pumped-storage plant 336
imbalance 8, 9, 45–47, 81–84, 143, 144, 167, 462

improvement techniques 36
interharmonics 11, 17, 20, 37–39, 304
interruption 6
ITIC voltage-tolerance curve 334, 344
lightning 5, 87
load sharing 340
load shedding 336
long-duration variation 7
matching of renewable sources with energy storage 336
nonperiodic event 303
notching 11
overvoltage 8, 400
peak-power tracker 337, 343
power-frequency variation 12
recommendations 29–32
ride-through capability 334
ripple factor (RF) 19
sags 6
SEMI F47 curve 334, 335, 344
single-time event 303
spikes 2
standards 29
standby power system 335
subharmonics 48
supercapacitors 335
sustained interruption 8
swells 7
switching surges 6
short-duration variation 4
tools for detecting poor power quality 316
transients 4
undervoltage 8
unpredictable events 2
voltage fluctuation 12
voltage imbalance 8, 462
voltage pick-up 339
voltage regulation 334
waveform distortion 8
Power system capacity 398
Power system 198, 261
automatic disconnect 336
frequency control 200, 314–316
frequency regulation 335
frequency variation 339
intentional islanding 329–334
interconnected 329
intermittent power plants 336
islanding operation 199
load change 198–200
load sharing 316, 340, 341
load shedding 336
reclosing 169
redundant 329
ride-htrough capability 335
self-healing 329
sequence components 200
sequence matrices 200
short-circuit 200
short-circuit apparent power 37–34
short-circuit current 37–43
steady-state frequency variation 198–200
voltage control 314
voltage regulation 334
voltage tolerance curve 334
Programmable logic controller (PLC) 326, 443
Protection devices (PD) 302
Proximity effect 57
PSpice solutions 5, 10, 11, 15, 23–29, 87, 88, 137–141, 212, 223
Pulse-width-modulated (PWM) (see inverter) 27
PWM inverters (see inverter) 27

Q
Quality (see power quality) 1
Q-factor 368

R
Reactor 101
interphase 101
Real power capability (RPC) 61
Reactance 263
Reclosing 169
Rectifiers
diode rectifier 24
duty cycle/ratio δ 223
firing angle α 212
full-wave 94
notching 11
resonant 95
silicon-controlled rectifiers (SCRs) 13, 23, 359
six-step/pulse 25, 94, 101
three-phase 23, 24, 37–47, 94, 95, 102, 202
thyristor or SCR 23, 24, 37–47, 102
twelve-pulse 49
Reduction in apparent power rating (RAPR) 61
Reduction of harmonic torques 249, 255
Relay 304
frequency rate of change 304
harmonics 304
interharmonics 11, 17, 20, 37–39, 304
operating time increase 304
overcurrent 304
underfrequency 304
set point 304
Reliability, Relaying and Security 301, 339
calculation of reliability indices 302, 339
customer-oriented system indices 301
degradation of reliability and security due to poor power quality 303
demand side management 332
economical evaluation of reliability 301
error analysis 318
fast interrupting switches (FIS) 327
fault-current limiters (FCL) 327, 328, 343
harmonics and interharmonics affecting relays 304
intentional islanding (see islanding) 329
load-point reliability indices 301
load-oriented system indices 301
overcurrent relays 304
programmable logic converter (PLC) 326
power line communication 305
reliability indices 301
supervisory control and data acquisition (SCADA) 326
tools for improving reliability/security 32336
uncertainty analysis 326, 341, 342
under-frequency relays 304
Reluctance machine 176
switched-reluctance machine 175, 176
Renewable plants 100, 201, 336–338, 340, 343, 344, 346, 348, 349
Resistance 263
Resonance phenomenon 49–51, 75, 95, 215, 399
definition 75
ferroresonance (see ferroresonance phenomenon) 75
parallel 20, 216, 224
resonant circuit 48–51, 75–80, 368, 399, 400
resonant current 57–80
resonant rectifier 95
series 20, 216, 224
solutions to resonance problems 78, 198, 217, 224, 314
subsynchronous resonance 17
Ripple factor 19
Root-mean-squared (rms) value 18
nonsinusoidal waveform 13, 18
sinusoidal waveform 2

S
Sampling techniques
channel 89–97
direct memory access (DMA) 89–97
interpolation 89–97
parallel 89–07
series 89–97
throughput rate 89–97
Quick BASIC 89–97
Saturation 56, 184
influence 127–132
SCADA 226
Scanning 218





capacitance scanning 218
frequency scanning 218
Security (see reliability, relaying and security) 301
Shaft flux 194
Shunt capacitor banks 397
benefits of reactive power compensation 398
common types of distribution 400
constraints 414
drawbacks of reactive power compensation 399
objective function 414
optimal placement 413
reactive power compensation 398
Simulated annealing 407
Single-time event 303
Skin Effect 56
Stability 118, 145, 146, 199, 200
Standards 3, 29–34
EN 61000 33
IEC 30, 32
IEC 61000 32, 33
IEEE 31
IEEE-519 32, 41–43, 48–51
Superconductor 100
coil 100
Susceptance 263
Synchronous machine 155
abc reference system 169, 187
amortisseur 169
asymmetric load 183
balanced three-phase short circuit 169, 178, 195
bearing currents 194
consumer reference frame 164
breadth factor 168
cross coupling 167
current densities 175
current-source fed machine 180
current spectrum 182
cylindrical-rotor machine 164, 167
damper bar currents 169
damper winding 169
delta winding connection 191
design guidelines 175
displaced stator windings 195
distribution factor 168
dq0 reference system 169
electrical equations 156
equivalent circuit 159, 163
eccentricities of rotor (dynamic, static) 192
field winding current 169
flux distribution 160
forces during short circuit 178
frequency conversion 188
generator reference frame 164
harmonic equivalent circuit 177, 182, 186
imbalance 184
line-to-line short circuit 169, 195, 200
line-to neutral short circuit 169, 196
magnetic field (for calculation of either $L_d$ or $X_d$) 161
magnetic field (for calculation of either $L_q$ or $X_q$) 161
magnetic field (for calculation of either $L'_d$ or $X'_d$) 162
magnetic field (full-load) 162
magnetic field (no-load) 161
magnetic field (permanent-magnet machine) 163
magnetic field (steady-state short-circuit) 161
magnetic field (subtransient short-circuit) 178
magnetic saturation 158
mechanical equations 157
maximum flux densities 175
Maxwell stress 177
model applied to power flow 178
motor reference frame 164
negative–sequence reactance 179
non-salient pole machine 164, 167, 195
nonlinear load 174, 184, 201
operation modes (see operating modes of rotating machines) 245
out-of-phase synchronization 169, 196
permanent-magnet machines 170, 172
phasor diagram 164, 165, 195
pitch factor 168
positive-sequence reactance 179
power quality 190
reclosing 169
reduction of harmonic torques 249, 255
relation between induced and terminal voltages 175
round-rotor machine 164, 195
rotor winding 168
salient-pole machine 165, 169, 195
saturation 184, 189
shaft flux 194
sinusoidal dq0 modeling 158
sinusoidal state-space modeling 156
subtransient operation 158
stability 118, 169
stacking factor 175
starting performance 197
stator winding 168
steady-state operation/analysis 158, 195
subtransient reactance 163
synchronizing and damping torques 169, 196
synchronous reactance 167
switching substations (SS) 303
terminals 168
two displaced stator windings 196
torque 157, 169, 195, 197
transient operation 158
transient reactance 161
unbalanced load 169
voltage ripple 170
voltage-source fed machine 180
voltage stress 202, 203
winding forces 177
zero-sequence reactance 179
Storage plants 100, 201
battery 343
compressed-air 348, 349
Diesel generator 344
flywheel 346
fuel cell 344
hydro (pumped-hydro) 336, 337
supercapacitor 201
superconducting coil (magnetic storage) 100
Switches 327
Fast-interrupting switch (FIS) 327
fault-current limiter (FCL) 327, 328, 343

T
Tabu search algorithm 411
Telephone influence factor (TIF) 20
Telephone form factor (TFF) 21
Temperature rise calculation 250
Thermal network 250
Torque 111
fundamental 111, 123
starting 117
transient 169
harmonic torque 123, 249
torque pulsations 249
reduction of harmonic torques 249
Total demand distortion (TDD) 20
Total harmonic distortion (THD) 19
equation of THD 19
sensitivity of THD 19, 20
suitability of THD 19, 20
Total interharmonic distortion (TIHD) 20
Total subharmonic distortion (TSHD) 20
Transformations 451
αβo transformation 453
αβ0 transformation (for sinusoidal system supplying a linear load) 454
αβ0 transformation (for sinusoidal system supplying a nonlinear load) 455
αβ0 transformation (for unbalanced system supplying a linear load) 455
abc transformation 453, 455
dqo (Park) transformation 451
Transformer 261
additional temperature rise due to harmonics (see aging) 238
aging (see aging) 242

autotransformer 83
derating 40, 60, 64, 89, 99, 100
dedicated transformer 37
delta-delta 90
delta-wye 14, 42, 43, 44, 77, 92, 102, 319, 322, 349
delta-wye ungrounded 44, 91, 92, 322
delta-wye grounded 102, 319
delta-zigzag 45–47, 101
direct-loss measurement 93, 101, 319, 323
eddy-current losses 57
earth-surface potentials 82
equipment for tests 93–96
ferroresonance (see ferroresonance phenomenon) 75
$F_{HL}$-factor 63
flux distribution 74
geomagnetic effects 81
half-cycle saturation 9, 82
harmonic losses 56
hysteresis losses 57
iron-core loss 57
K-factor 62, 99
loss measurement (direct method) 60
loss measurement (indirect method) 60
measurement errors of powers 323, 341
modeling (combined frequency- and time-domain) 55
modeling (equivalent circuit) 56
modeling (frequency-domain model) 66, 67, 72
modeling (general harmonic model) 65
modeling (harmonic-domain model) 64
modeling (finite-difference, finite-element models) 73
modeling (nonlinear harmonic model) 64, 66, 68
modeling (sinusoidal linear model) 55
modeling (state-space formulation) 70
modeling (time-domain harmonic model) 66, 67
modeling (time-domain model) 66, 70, 72
modeling (transient model) 70
pole transformer 73, 98
proximity effect 57
reduction of apparent power rating (RAPR) 62
real power capability (RPC) 62
resonance (see resonance phenomenon) 49–51, 75, 95, 215
saturation 56, 64, 75
sinusoidal model 55
skin effect 56
sun-spot cycles 82
weighted-harmonic factors (see aging) 228
wye-delta 14, 42, 43, 44, 77, 92, 102, 319, 322, 349
wye-wye ungrounded 90, 91
wye-wye grounded 320
wye grounded-wye grounded 321
Transmission 262, 310
audible noise 311
new design 310
transmission line 310
visual impact 311
Subtransmission 262

**U**

Unbalanced 8, 9, 45–47, 81–84, 143, 144, 167, 462
Unified power quality conditioner (UPQC) 443, 447
compensation devices 444
control (dqo) 451
control (instantaneous power) 453, 456, 458
control of DC voltage 453
control of series converter 452
control of shunt converter 452
control system 450
conventional compensation devices 444
DC capacitor 453
functions of UPQC 447
left-shunt UPQC 447
operation 448
operation (unbalanced and distorted system voltage and load current) 455
operation (unbalanced system voltages and load current) 449
pattern of reference signals 451
performance 460
performance (compensation of flicker) 464
performance (compensation of voltage imbalance) 462
performance (compensation of voltage harmonics) 462
performance (current compensation) 462
performance (damping of harmonic oscillations) 462
performance (dynamic performance) 462
phase-lock-loop (PLL) 456
positive-sequence voltage detector (PSVD) 457
right-shunt UPQC 447
structure 447
series converter 459
shunt converter 457
Uncertainty 102, 341–343
Uninterruptible power supplies (UPS) 3

**V**

Variable-frequency converter (VFC) 136
Variable-frequency drive (VFD) 136
Variable-speed drive 25, 26
Variable-speed generator 25
Voltage regulation 334
V·T product 21

**W**

Waveform compensation (see filters) 384
Waveform distortion 8
Weighting function 415
Weighted-harmonic factor 228
Wind-power plant 16, 26, 145, 172–174, 345
direct-drive permanent-magnet generator 170
low-speed generator 171
frequency control 314, 341
voltage control 314, 341
doubly excited induction generator 345
Wind turbine 350
torque 118
Winding
field 169
rotor 169
stator 168
two displaced stator 196
winding stress 136, 137–141, 148, 149, 202
winding switching 119
Wye transformer configurations
wye-delta 14, 42, 43, 44, 77, 92, 102, 319, 322, 349
wye-wye ungrounded 90, 91
wye-wye grounded 320
wye grounded-wye grounded 321

**X**

X-ray generation 314

**Y**

Y transformer configurations
Y-Δ 14, 42, 43, 44, 77, 92, 102, 319, 322, 349
Y-Y ungrounded 90, 91
Y-Y grounded 320
Y grounded-Y grounded 321

**Z**

Zigzag transformer connection 45–47, 101

Electrical Engineering / Power Resources / Engineering General

# Power Quality in Power Systems and Electrical Machines

Ewald F. Fuchs, *University of Colorado*, Boulder, USA
Mohammad A.S. Masoum, *Curtin University of Technology*, Perth, Western Australia

An outstanding resource for professionals and students in understanding and resolving Power Quality Issues!

*Power Quality in Power Systems and Electrical Machines* provides a comprehensive reference for understanding the causes, effects, modeling, measurement and resolution of power quality issues. This extensive volume covers power quality problems including nonsinusoidal wave shapes, voltage outages, harmonic losses, origins of single-time events such as voltage dips, voltage reductions and outages, along with techniques to mitigate these problems.

## Key Features

- Provides both theoretical and practical insight into power quality problems of machines and systems
- Includes application examples implemented in SPICE, Mathematica and MATLAB
- Numerous end-of-chapter problems
- Analytical as well as measuring techniques are applied to power quality problems as they occur in existing systems
- Provides extensive references (700+)
- Suitable for use as an advanced undergraduate/graduate course textbook as well as reference for professionals

**Ewald F. Fuchs** is Professor of Electrical and Computer Engineering at the *University of Colorado* at Boulder. He received his Dipl.-Ing. [illegible] from the *University of Stuttgart*, Germany in electrical engineering, and his PhD from the *University of Colorado* in 1970. He has published 91 refereed journal articles and 84 refereed [illegible] papers in the areas of power quality, energy conversion, power systems and renewable [illegible] Fuchs serves as an Associate Editor for the *International Journal of Electrical Power and* [illegible] ACTAPress/IASTED (International Association of Science and Technology Development) [illegible] Canada. He is an IEEE Fellow and reviewer for IEEE and the British IEE, and is a member [illegible] national technical (conference) committees.

**Mohammad A. S. Masoum** is a faculty member (Associate Professor), and discipline leader for Power Systems Engineering at the Department of Electrical and Computer Engineering, *Curtin University of Technology*, Perth,
Australia. Dr. Masoum has published three books (in Persian) and over 100 refereed papers including 40 journal articles in the areas of power quality, energy conversion, power systems and renewable energy.

Dr. Masoum received his BSc, MSc and PhD degrees in Electrical and Computer Engineering from the *University of Colorado* in 1983, 1985 and 1991, respectively. He is a reviewer and Senior Member of IEEE.

## Related Titles

*Power Electronics Handbook Second Edition: Devices, Circuits and Applications*, Muhammad H. Rashid (ed.), 2006 ISBN: 9780120884797

ISBN: 978-0-12-369536-9
90000
9 780123 695369

ELSEVIER

ACADEMIC PRESS
An imprint of Elsevier
books.elsevier.com